Transactions of the ASME

Technical Editor, **L. B. FREUND**

APPLIED MECHANICS DIVISION

Chairman, **CHARLES R. STEELE**
Secretary, **J. D. ACHENBACH**
Associate Editors, **S. T. ARIARATNAM**
T. BELYTSCHKO
D. B. BOGY
M. M. CARROLL
R. J. CLIFTON
L. B. FREUND
MAURICE HOLT
W. D. IWAN
W. G. KNAUSS
A. S. KOBAYASHI
L. E. MALVERN
R. P. NORDGREN
R. H. PLAUT
R. T. SHIELD
C. T. SUN
J. S. WALKER
G. A. WEMPNER
S. E. WIDNALL

BOARD ON COMMUNICATIONS
Chairman and Vice-President
M. J. RABINS

Members-at-Large
W. BEGELL
W. G. GOTTENBERG
H. C. REEDER
D. KOENIG
M. KUTZ
F. LANDIS
J. W. LOCKE
J. E. ORTLOFF
C. PHILLIPS
K. REID

President, **FRANK M. SCOTT**
Exec. Dir.
PAUL ALLMENDINGER
Treasurer, **ROBERT A. BENNETT**

PUBLISHING STAFF
Mng. Dir., Pub., **J. J. FREY**
Dep. Mng. Dir., Pub.
JOS. SANSONE
Managing Editor,
CORNELIA MONAHAN
Production Editor, **SUZANNE MAGIDA**

The Journal of Applied Mechanics (ISSN 0021-8936) is published quarterly for $72 per year by The American Society of Mechanical Engineers, 345 East 47th Street, New York, NY 10017. Second class postage paid at New York, NY and additional mailing offices. POSTMASTER: Send address changes to The Journal of Applied Mechanics, c/o THE AMERICAN SOCIETY OF MECHANICAL ENGINEERS, P.O. Box 3199, Grand Central Station, New York, NY 10163. **CHANGES OF ADDRESS** must be received at Society headquarters seven weeks before they are to be effective. Please send old label and new address.

PRICES: To members, $36.00, annually; to nonmembers, $90.00. Single copies, $24.00 each. Add $6.00 for postage to countries outside the United States and Canada.

STATEMENT from By-Laws. The Society shall not be responsible for statements or opinions advanced in papers or . . . printed in its publications (B7.1, Par. 3).

COPYRIGHT © 1983 by the American Society of Mechanical Engineers. Reprints from this publication may be made on condition that full credit be given the TRANSACTIONS OF THE ASME, JOURNAL OF APPLIED MECHANICS, and the author, and date of publication be stated.

INDEXED by the Engineering Index, Inc.

Journal of Applied Mechanics

Published Quarterly by The American Society of Mechanical Engineers

VOLUME 50 • NUMBER 4*b* • DECEMBER 1983

919 Preface

TECHNICAL PAPERS

921 Crystal Plasticity
R. J. Asaro

935 Shell Instability
C. D. Babcock

941 Dynamic Plasticity
R. J. Clifton

953 Random Vibration: A Survey of Recent Developments
S. H. Crandall and W. Q. Zhu

963 Experimental Methods in Applied Mechanics
I. M. Daniel

977 Contact-Line Problems in Fluid Mechanics
S. H. Davis

983 Hydrodynamic Stability
R. C. DiPrima and J. T. Stuart

992 Stress Intensity Factors
F. Erdogan

1003 On the Foundations of Biomechanics
Y. C. Fung

1010 Continuum Thermodynamics
P. Germain, Q. S. Nguyen, and P. Suquet

1021 Strange Attractors and Chaos in Nonlinear Mechanics
P. J. Holmes and F. C. Moon

1033 A Precis of Developments in Computational Methods for Transient Analysis
T. J. R. Hughes and T. Belytschko

1042 Fundamentals of the Phenomenological Theory of Nonlinear Fracture Mechanics
J. W. Hutchinson

1052 The Evolution of Computational Methods in Aerodynamics
A. Jameson

1071 Multibody Dynamics
T. R. Kane and D. A. Levinson

1079 Deterministic and Stochastic Aspects of Turbulence
J. Laufer

1086 Stability of Dynamic Systems
H. H. E. Leipholz

1097 Turbulence Modeling
J. L. Lumley

1104 Boundary-Layer Interaction Theory
A. F. Messiter

1114 On Finite Plastic Flow of Crystalline Solids and Geomaterials
S. Nemat-Nasser

1127 The History of the Soliton
A. C. Newell

1139 On Structural Optimization
N. Olhoff and J. E. Taylor

1152 Elastic Waves in Solids
Y. H. Pao

1165 Analysis of Circular Cylindrical Shells
J. L. Sanders, Jr.

1171 Equilibrium Solutions in Finite Elasticity
R. T. Shield

1181 Recent Progress in Rheology
R. I. Tanner

1191 Quantitative Ultrasonic Nondestructive Evaluation Methods
R. B. Thompson

1202 The Overall Elastic Response of Composite Materials
J. R. Willis

1210 The Generalized Finite Element Method-State of the Art and Future Directions
O. C. Zienkiewicz

Downloaded 04 May 2010 to 171.66.16.34. Redistribution subject to ASME license or copyright; see http://www.asme.org/terms/Terms_Use.cfm

Preface

This special issue celebrates 50 years of publication of the ASME JOURNAL OF APPLIED MECHANICS. The first issue of the Journal, dated January–March 1933, appeared in the Transactions of the American Society of Mechanical Engineers under the title *Applied Mechanics*, contributions of the ASME Applied Mechanics Division. The issue did not have the usual preface by the Editors, which perhaps indicates that the reasons for initiating the new Journal were thought to be obvious to the members of the Applied Mechanics Division, who then already numbered more than two thousand. Instead, the first page featured an article entitled "Progress in Applied Mechanics," with contributions by S. P. Timoshenko (Theory of Elasticity and Stress Analysis), J. P. den Hartog (Rigid Body Dynamics), R. E. Peterson (Mechanics of Materials), O. G. Tietjens (Hydrodynamics and Aerodynamics), G. B. Karelitz and L. M. Tichvinsky (Lubrication), and J. A. Goff (Thermodynamics). The authors critically reviewed recent publications, and they discussed significant contributions to national and international conferences that had been held during the one or two years prior to 1933. This first article, which contained 62 references, covered altogether four pages in the Journal. Four regular papers were also published: on self-induced vibrations, fatigue, turbulence, and stress analysis, respectively.

After this auspicious start the Journal went into hibernation, apparently due to financial difficulties of ASME. It was not until 1935 that a second issue was published. From then on, the Journal did, however, appear quarterly and it flourished to become one of the most prestigious in the field, a distinction that it has now maintained for many years. A detailed chronicle and an account of the evolution of the editorial arrangements of the Journal between its inception and 1977 have been given in "Brief History of the Applied Mechanics Division of ASME" by P. M. Naghdi, which was prepared at the occasion of the 50th Anniversary of the Applied Mechanics Division, and published in the JOURNAL OF APPLIED MECHANICS (Vol. 46, 1979, pp. 723–749).

Progress in applied mechanics has been remarkable over the last 50 years, and the JOURNAL OF APPLIED MECHANICS has served as a major stimulus by publishing significant contributions to the field. This Anniversary Issue is an attempt to highlight some of the progress that has been achieved in recent years. Some of the topics are the same as in 1933, others were not developed until much later, some not until recently. Obviously the Issue cannot be comprehensive, but the 29 papers which follow are intended to be representative of the research areas covered by the Journal.

The idea for the Anniversary Issue was suggested in 1981 by C. S. Hsu, then Technical Editor of the JOURNAL OF APPLIED MECHANICS. In November 1981 the Executive Committee of the Applied Mechanics Division established an Editorial Committee composed of Technical Editors of the Journal (past and present) and Chairmen of the Publication Committee (present and incoming). The Members of the Committee are: D. C. Drucker, P. G. Hodge, C. S. Hsu, J. Kestin, P. C. Paslay, C. R. Steele, and J. D. Achenbach (Chairman). L. B. Freund joined the Committee after his appointment to the position of Technical Editor of the Journal in 1982.

The topics were selected by the Editorial Committee after lengthy deliberations. The authors were asked to discuss the state of the art, to review the most significant results of the last 10–15 years, and to highlight interesting recent results. In order to make coverage as broad as possible in a single volume, it was necessary to ask the authors to conform to length constraints.

The Anniversary Issue is now before you as a collection of excellent papers. It is hoped that the papers will be of interest not only to the broad membership of the Applied Mechanics Division, but to anyone who has an interest in the field. The diversity of topics and individual approaches, yes, even the regrettable omissions that will be noted, befit the vibrancy of the field and illustrate its continued vitality.

For the Editorial Committee,

J. D. Achenbach, Chairman

Copyright © 1983 by ASME
Downloaded 02 May 2010 to 171.66.16.250. Redistribution subject to ASME license or copyright; see http://www.asme.org/terms/Terms_Use.cfm

Crystal Plasticity

R. J. Asaro
Division of Engineering,
Brown University,
Providence, R.I. 02912

Significant progress has been made during the past decade in incorporating micromechanics in continuum descriptions of inelastic deformation. This has led to the development of a rather comprehensive constitutive theory for rate-dependent and idealized rate-independent crystalline materials that deform plastically by crystalline slip. This theory is reviewed in some detail and examples are presented which illustrate how complex slip phenomena involving localized plastic flow and nonuniform crystallographic texture can be analyzed. The paper concludes by suggesting that it is now possible to develop accurate models for rate-dependent polycrystals undergoing arbitrarily large strains. Such models would have as principal aims the prediction of texture development and the rigorous assessment of such anisotropy on constitutive behavior. An example of how this would be of immediate value in analyzing strain-hardening behavior of metal polycrystals at large strains is provided.

1 Introduction

This paper has four main objectives. The first is to provide a very brief overview of some important aspects of crystalline plasticity, especially of features that are important for the development of large strain-continuum constitutive laws. The second is to illustrate how these features can be included in a continuum framework. In meeting these objectives our attention is nearly confined to describing the kinematics of crystalline slip; a somewhat detailed overview of dislocation mechanics as it relates to constitutive laws can be found in other recent reviews [1, 2]. The third goal is to show that, when some of the salient micromechanical features are included in continuum analyses of large strain plasticity of crystalline solids, accurate and perhaps surprisingly detailed descriptions of complex slip phenomena are obtained. Examples are given of nonuniform deformation in crystals which illustrate the vital role played by crystal lattice kinematics and, in particular, of the development of crystallographic texture. The final objective is to suggest how these analyses could be extended to develop models for large strain, rate-dependent, polycrystalline behavior. There is indeed a clear and strong impetus for this which is illustrated in connection with strain-hardening phenomena in metals at large strains. Essentially what is proposed as a useful direction for future research is the development of a large strain theory and suitable models for polycrystals that would extend those originally proposed by G. I. Taylor in 1938 [3] to describe deformation texture. As discussed in Section 4, the theory required to accomplish this would have to be rate-dependent so that lattice kinematics is described unambiguously.

The detailed plan of the paper is as follows. In Section 2 the basic kinematics of crystalline slip is cast in a rigorous framework and constitutive laws are presented for rate-independent and rate-dependent crystalline materials. The kinematical structure here falls within the framework laid out by Hill and Rice [3] and is confined to deformation by crystallographic dislocation slip alone; in the present paper we do not consider deformation by twinning, diffusion, or grain boundary sliding, for example. The constitutive theory is placed within a more general plasticity framework in Section 2. In Section 3 a set of complex slip phenomena known to be very important in the large strain deformation of single crystals and of individual grains of polycrystals is analyzed. The need for brevity demands that this be done using the rate-independent version of the theory although the examples are also used to highlight some inherent limitations of rate independence in accounting for what are obviously dominant lattice kinematical effects. References to recent rate-dependent analyses that overcome these fundamental problems of the rate-independent theory are provided. The success the analysis of Section 3 has in describing slip phenomena and the effects of nonuniform crystallographic texture on localized deformation should provide encouragement for a successful extension of the theory to the large strain deformation of polycrystals. In Section 4 this extension is proposed.

Standard notations are used throughout. Matrices and tensors, the rank and order of which are indicated in the text, are written in boldface type. The summation convention is used for Latin indices but summations over crystallographic slip systems are indicated explicitly. For brevity dots and double dots are used to indicate the following products:

$$\mathbf{P}\cdot\mathbf{n} = P_{ij}n_j,\ \mathbf{P}:\mathbf{D} = P_{ij}D_{ji}$$

and

$$\mathfrak{L}:\mathbf{P} = \mathfrak{L}_{ijkl}P_{lk},\ \boldsymbol{\sigma}\cdot\mathbf{P} = \sigma_{ij}P_{jk}$$

Other special symbols are defined in the text as needed.

Contributed by the Applied Mechanics Division for publication in the JOURNAL OF APPLIED MECHANICS.

Discussion on this paper should be addressed to the Editorial Department, ASME, United Engineering Center, 345 East 47th Street, New York, N.Y. 10017, and will be accepted until two months after final publication of the paper itself in the JOURNAL OF APPLIED MECHANICS. Manuscript received by ASME Applied Mechanics Division, April, 1983.

Copyright © 1983 by ASME
Downloaded 02 May 2010 to 171.66.16.250. Redistribution subject to ASME license or copyright; see http://www.asme.org/terms/Terms_Use.cfm

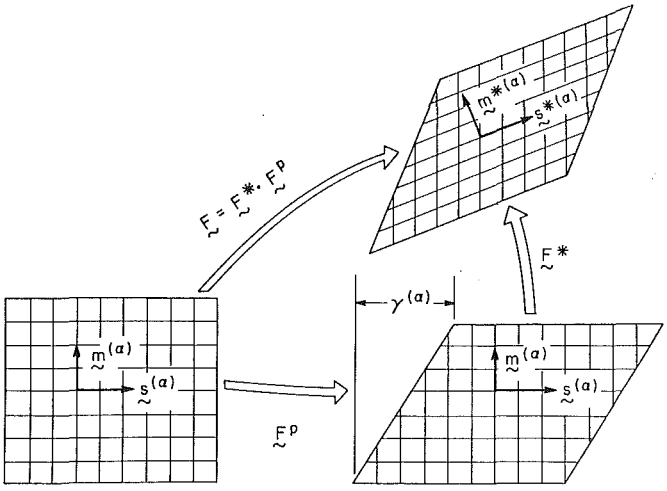


Fig. 1 Kinematics of elastic-plastic deformation of crystalline solid deforming by crystallographic slip

2 Constitutive Laws

2.1 Kinematics. A comprehensive kinematical theory for the mechanics of elastic-plastic deformation of crystals is now well established, at least when crystallographic slip is the sole cause of inelastic deformation. The development traces its origins to the pioneering work of Taylor [3] and to the precise mathematical expression of the physical concepts by Hill [5] and Hill and Rice [4]. In the following summary we will closely follow the procedures and the specific kinematical representation used by Asaro and Rice [6] and more recently by Peirce, Asaro, and Needleman [7, 8]. This particular scheme is chosen because of its clarity and utility in the analysis of boundary value problems.

A basic tenet of all the cited analyses is that material flows through the crystal lattice via dislocation motion as proposed by Taylor [3], whereas the lattice itself, with the material embedded on it, undergoes elastic deformations and rotations. The picture for this as shown by Asaro and Rice [6] and Peirce et al. [7] is given in Fig. 1. If $\mathbf{F}^P$ is the part of the total deformation gradient due solely to slip then the total deformation gradient, $\mathbf{F}$, is given by

$$\mathbf{F} = \mathbf{F}^* \cdot \mathbf{F}^P. \tag{2.1}$$

$\mathbf{F}^*$ is the lattice contribution to $\mathbf{F}$ and is associated with stretching and rotation of the lattice. The deformation gradient remaining after elastic unloading *and upon returning the lattice to its orientation in the reference state is* $\mathbf{F}^{*-1} \cdot \mathbf{F} = \mathbf{F}^P$. Of course, in real processes removal of the loads alone will not return the lattice to its original state and thus what remains as a residual $\mathbf{F}$ after slip is more than just $\mathbf{F}^P$; the lattice may be permanently reoriented (but undeformed) for example, as well as placed in a state of residual deformation.

As the crystal deforms and rotates, lattice vectors stretch and rotate, i.e., they convect with the lattice. The slip direction and other vectors lying in the slip plane can be taken to be such vectors. When this is done, the slip direction $\mathbf{s}^{(\alpha)}$ of slip system α is given in the deformed configuration by

$$\mathbf{s}^{*(\alpha)} = \mathbf{F}^* \cdot \mathbf{s}^{(\alpha)}. \tag{2.2}$$

The normal to the slip plane however, since it is normal to all vectors in the slip plane, is the reciprocal base vector corresponding to $\mathbf{m}^{(\alpha)}$ or

$$\mathbf{m}^{*(\alpha)} = \mathbf{m}^{(\alpha)} \cdot \mathbf{F}^{*-1}. \tag{2.3}$$

$\mathbf{s}^{(\alpha)}$ and $\mathbf{m}^{(\alpha)}$ are taken to be unit vectors that define the slip system α in the reference state. $\mathbf{s}^{*(\alpha)}$ and $\mathbf{m}^{*(\alpha)}$ are not in general unit vectors, but remain orthogonal since $\mathbf{s}^{*(\alpha)} \cdot \mathbf{m}^{*(\alpha)} = \mathbf{s}^{(\alpha)} \cdot \mathbf{m}^{(\alpha)} = 0$.

The velocity gradient in the current state is given by a standard formula:

$$\mathbf{L} = \dot{\mathbf{F}} \cdot \mathbf{F}^{-1} = \dot{\mathbf{F}}^* \cdot \mathbf{F}^{*-1} + \mathbf{F}^* \cdot \dot{\mathbf{F}}^P \cdot \mathbf{F}^{P-1} \cdot \mathbf{F}^{*-1} \tag{2.4}$$

where $\mathbf{L}$ can also be expressed as

$$\mathbf{L} = \mathbf{D} + \boldsymbol{\Omega}. \tag{2.5}$$

$\mathbf{D}$ and $\boldsymbol{\Omega}$ are the symmetric rate of stretching and spin tensors, respectively; in terms of the velocity $\mathbf{v}$ and spatial coordinates $\mathbf{x}$ their components are given by

$$D_{ij} = 1/2(\partial v_i/\partial x_j + \partial v_j/\partial x_i) \tag{2.6}$$

and

$$\Omega_{ij} = 1/2(\partial v_i/\partial x_j - \partial v_j/\partial x_i). \tag{2.7}$$

$\mathbf{D}$ and $\boldsymbol{\Omega}$ may be decomposed from (2.4) into plastic parts ($\mathbf{D}^P$, $\boldsymbol{\Omega}^P$) and lattice parts ($\mathbf{D}^*$ and $\boldsymbol{\Omega}^*$) as follows:

$$\mathbf{D} = \mathbf{D}^* + \mathbf{D}^P, \ \boldsymbol{\Omega} = \boldsymbol{\Omega}^* + \boldsymbol{\Omega}^P \tag{2.8}$$

where

$$\mathbf{D}^P + \boldsymbol{\Omega}^P = \mathbf{F}^* \cdot \dot{\mathbf{F}}^P \cdot \mathbf{F}^{P-1} \cdot \mathbf{F}^{*-1}. \tag{2.9}$$

Since in our present discussion plastic deformation occurs by dislocation slip, we find in the current state that

$$\mathbf{D}^P + \boldsymbol{\Omega}^P = \sum_{\alpha=1}^{n} \dot{\gamma}^{(\alpha)} \mathbf{s}^{*(\alpha)} \mathbf{m}^{*(\alpha)} \tag{2.10}$$

where $\dot{\gamma}^{(\alpha)}$ is the slipping rate of the α slip system and is defined relative to the reference state lattice, i.e., $\dot{\gamma}^{(\alpha)}$ are *defined* so that

$$\dot{\mathbf{F}}^P \cdot \mathbf{F}^{P-1} = \sum_{\alpha=1}^{n} \dot{\gamma}^{(\alpha)} \mathbf{s}^{(\alpha)} \mathbf{m}^{(\alpha)}.$$

In (2.10) and in what follows the sum ranges over all slip systems that participate in the deformation increment.

Finally, we note that the plastic parts of the rate of stretching and the rate of spin are given by the symmetric and skew parts of (2.10). It is convenient to introduce for each slip system the tensors $\mathbf{P}^{(\alpha)}$ and $\mathbf{W}^{(\alpha)}$ defined as

$$\mathbf{P}^{(\alpha)} = 1/2(\mathbf{s}^{*(\alpha)} \mathbf{m}^{*(\alpha)} + \mathbf{m}^{*(\alpha)} \mathbf{s}^{*(\alpha)}) \tag{2.11}$$

and

$$\mathbf{W}^{(\alpha)} = 1/2(\mathbf{s}^{*(\alpha)} \mathbf{m}^{*(\alpha)} - \mathbf{m}^{*(\alpha)} \mathbf{s}^{*(\alpha)}). \tag{2.12}$$

Then, from (2.10)

$$\mathbf{D}^P = \sum_{\alpha=1}^{n} \mathbf{P}^{(\alpha)} \dot{\gamma}^{(\alpha)} \tag{2.13}$$

and

$$\boldsymbol{\Omega}^P = \sum_{\alpha=1}^{n} \mathbf{W}^{(\alpha)} \dot{\gamma}^{(\alpha)}. \tag{2.14}$$

2.2 Constitutive Laws. We will assume that the crystal's elasticity is unaffected by slip, then following Hill and Rice [4] the elastic law takes the form

$$\overset{\nabla}{\tau}{}^* = \underset{\sim}{\mathcal{L}} : \mathbf{D}^* \tag{2.15}$$

where $\underset{\sim}{\mathcal{L}}$ is the tensor of elastic moduli and $\overset{\nabla}{\tau}{}^*$ is the Jaumann rate of Kirchoff stress. We will for the present discussion consider $\underset{\sim}{\mathcal{L}}$ to be derivable from a potential (free energy) function so that it possesses symmetry in the leading and trailing indices. Here the superscript * signifies that the derivative is of the stress components formed on axes that rotate with the *lattice* and so according to the standard formula,

Downloaded 02 May 2010 to 171.66.16.250. Redistribution subject to ASME license or copyright; see http://www.asme.org/terms/Terms_Use.cfm

$$\overset{\nabla}{\tau}{}^{*} = \dot{\tau} - \Omega^{*}\cdot\tau + \tau\cdot\Omega^{*} \tag{2.16}$$

where $\dot{\tau}$ is the material rate of Kirchoff stress. This, in turn, is defined as $\rho_0/\rho\sigma$ where σ is Cauchy stress and ρ_0 and ρ are the mass densities in the reference and current states. To formulate constitutive laws for the material we introduce the Jaumann stress rate on axes that rotate with the material,

$$\overset{\nabla}{\tau} = \dot{\tau} - \Omega\cdot\tau + \Omega\cdot\tau \tag{2.17}$$

and note by using (2.14) that the difference between these two stress rates is

$$\overset{\nabla}{\tau}{}^{*} - \overset{\nabla}{\tau} = \sum_{\alpha=1}^{n} \beta^{(\alpha)}\dot{\gamma}^{(\alpha)} \tag{2.18}$$

where

$$\beta^{(\alpha)} = \mathbf{W}^{(\alpha)}\cdot\tau - \tau\cdot\mathbf{W}^{(\alpha)}. \tag{2.19}$$

By combining (2.13), (2.14), (2.15), and (2.19) we obtain the constitutive law

$$\overset{\nabla}{\tau} = \underset{\sim}{\mathcal{L}}:\mathbf{D} - \sum_{\alpha=1}^{n} [\underset{\sim}{\mathcal{L}}:\mathbf{P}^{(\alpha)} + \beta^{(\alpha)}]\dot{\gamma}^{(\alpha)} \tag{2.20}$$

where it remains to specify the shearing rates $\dot{\gamma}^{(\alpha)}$ in terms of stress or stress rate.

Now before proceeding with the development of the $\dot{\gamma}$'s for rate-independent and then rate-dependent materials we introduce a particular definition of the so-called resolved shear stress, or *Schmid stress* for a slip system. Essentially this is a component of shear stress resolved in the slip plane and in the slip direction and thus is the component of stress that produces forces on dislocations causing them to slip. With this in mind it should be noted that this stress is caused not only by macroscopically applied loads but also by elastic interactions with other dislocations or misfitting defects. Asaro and Rice [6] have discussed various ways this definition can be made but, as noted by Rice [11], there is one particular definition that we call the Schmid stress with which basic notions such as the existence of plastic potentials and normality structure to flow laws (when these exist) are most concisely phrased. This is the Schmid stress, $\tau^{(\alpha)}$, defined to be work conjugate to the $\dot{\gamma}^{(\alpha)}$ such that $\tau^{(\alpha)}\dot{\gamma}^{(\alpha)}$ is precisely the rate of working due to slip on system α per unit *reference* volume. Then from the general expression for this rate of working,

$$\tau:\mathbf{D}^{P} = \sum_{\alpha=1}^{n} \tau:\mathbf{P}^{(\alpha)}\dot{\gamma}^{(\alpha)} \tag{2.21}$$

we identify

$$\tau^{(\alpha)} = \mathbf{P}^{(\alpha)}:\tau. \tag{2.22}$$

For rate-independent materials, flow laws (as prescribed later) adapted from the well-known Schmid law of a "critical resolved shear stress" connect the rate of slipping on each slip system to the rates of change of the $\tau^{(\beta)}$. Some useful expressions for $\dot{\tau}^{(\alpha)}$ are given in the following. For rate-dependent materials, simple kinetic laws for dislocation motion, again adapted from Schmid's law, generally relate the slipping rates on each slip system to the resolved shear stress itself. When the stress dependence of the slip rates in both cases involves only $\tau^{(\alpha)}$, and precisely the $\tau^{(\alpha)}$ as defined, normality rules can be shown to result. This essential structure for both time-dependent and independent constitutive laws has been discussed at length by Hill [9], Rice [10, 11], and Hill and Rice [12]. Because of its obvious importance for future developments of constitutive models for polycrystalline flow a very brief statement of normality rules for crystals is given in the next section. The promised expressions for $\dot{\tau}^{(\alpha)}$ are however given first.

It is important to note that since the $\mathbf{P}^{(\alpha)}$ depend on lattice orientation and stress state, they change during a program of loading and straining – if the material stresses were cycled for instance, so that plastic flow occurred and the lattice rotated relative to the material before the stresses were returned to their original values, the $\mathbf{P}^{(\alpha)}$ would undergo a permanent change. A general expression for $\dot{\tau}^{(\alpha)}$ can then be given in terms of the material time derivatives of $\mathbf{P}^{(\alpha)}$ and τ

$$\dot{\tau}^{(\alpha)} = \dot{\mathbf{P}}^{(\alpha)}:\tau + \mathbf{P}^{(\alpha)}:\dot{\tau} \tag{2.23}$$

or from either of the two corotational derivatives introduced previously, namely,

$$\dot{\tau}^{(\alpha)} = \overset{\nabla}{\mathbf{P}}{}^{*}{}^{(\alpha)}:\tau + \mathbf{P}^{(\alpha)}:\overset{\nabla}{\tau}{}^{*} \tag{2.24}$$

and

$$\dot{\tau}^{(\alpha)} = \overset{\nabla}{\mathbf{P}}{}^{(\alpha)}:\mathrm{z} + \mathbf{P}^{(\alpha)}:\overset{\nabla}{\tau}. \tag{2.25}$$

Now it is easy to verify that, when the deformation is only elastic,

$$\overset{\nabla}{\mathbf{P}}{}^{*}{}^{(\alpha)}:\tau = \beta^{(\alpha)}:\mathbf{D}^{*} \tag{2.26}$$

and that $\dot{\tau}^{(\alpha)}$ may also be computed from

$$\dot{\tau}^{(\alpha)} = \mathbf{P}^{(\alpha)}:\overset{\nabla}{\tau}{}^{*} + \beta^{(\alpha)}:\mathbf{D}^{*} \tag{2.27}$$

or, after using (2.15), from

$$\dot{\tau}^{(\alpha)} = (\mathbf{P}^{(\alpha)}:\underset{\sim}{\mathcal{L}} + \beta^{(\alpha)}):\mathbf{D}^{*}. \tag{2.28}$$

The last relation will be useful in what follows for understanding the nature of the normality rules that follow from the Schmid stress.

2.3 Normality Rules and Plastic Potentials. In this section a very brief discussion is given of the origins of normality and the kinetic restrictions that lead to the existence of plastic potentials. As mentioned earlier, a concise and elegant framework for this has been given by Hill and Rice [12] and what follows is a short summary of their results. Where appropriate, however, certain quantities are identified using the specific kinematical description given in Sections 2.1 and 2.2 and this should provide a helpful link for the reader in making contact with the Hill and Rice work.

Inelastic materials are considered that are capable of exhibiting purely elastic response at any stage in the deformation history. For rate-independent, elastic-plastic materials such a purely elastic response results when stress variations are directed and terminate within the current yield surface, the existence of which would also be assumed. For rate-dependent materials, on the other hand, the response may be purely elastic only when the stress variations are very rapid compared to the fastest rates at which inelastic slip processes can respond. The scope of this framework would seem to encompass a wide range of crystallographic slip processes occurring at quasi-static strain rates and perhaps even at strain rates of up to 10^3.

Now again following Hill and Rice [12], let $\mathbf{e}$ denote any objective, symmetric strain tensor and let $\mathbf{t}$ be its work conjugate (symmetric) stress defined in the manner laid out by Hill [13]. As in (2.21) then, $\tau:d\mathbf{e}$ is an increment of work per unit reference volume, that is, per unit volume in the reference state from where $\mathbf{e}$ is measured. If $\mathbf{e}$ is taken to be the Green strain, for example,

$$\mathbf{e}^{G} = 1/2(\mathbf{F}^{T}\cdot\mathbf{F} - \mathbf{I}),$$

and then $\mathbf{t}$ is the Piola-Kirchoff stress

$$\mathbf{t}^{G} = \mathbf{F}^{-1}\cdot\tau\cdot\mathbf{F}^{-1T}.$$

To draw a correspondence with the specific kinematical schemes of Sections 2.1 and 2.2 it is useful to also consider the logarithmic strain measure defined as

$$\mathbf{e}^{0} = ln(\mathbf{\Lambda}) = (\mathbf{\Lambda} - \mathbf{I}) - \frac{1}{2}(\mathbf{\Lambda} - \mathbf{I})^{2} + \ldots$$

Downloaded 02 May 2010 to 171.66.16.250. Redistribution subject to ASME license or copyright; see http://www.asme.org/terms/Terms_Use.cfm

(provided no principal stretch exceeds 2) where the stretch tensor $\mathbf{\Lambda}$ is defined by writing $\mathbf{F} = \mathbf{R}\cdot\mathbf{\Lambda}$ where $\mathbf{R}$ is a pure rotation. Hill [14] has shown, with a derivation not reproduced here, that the objective conjugate stress to this measure can be expressed as

$$\mathbf{t}^0 = |\mathbf{F}|\mathbf{R}^T\cdot\boldsymbol{\sigma}\cdot\mathbf{R} + \mathcal{O}(e^2)$$

where $\boldsymbol{\sigma}$ is the Cauchy stress. Then if the current state and reference states are taken to be coincident, all stress measures equal $\boldsymbol{\sigma}$, and all strain rates equal $\mathbf{D}$ and $\overset{\nabla}{t}{}^0 = \overset{\nabla}{\tau}$.

The inelasticity in our restricted class of solids is thought to occur as a result of a (enormously complex) set of microstructural rearrangements, e.g., as a result of the incremental motion of large numbers of dislocation segments. At each stage the current dislocated state of the material is denoted symbolically by H and the properties of the solid are a functional of this prior history. Furthermore if the material's response is assumed to be of Green type in the sense that a potential (i.e., free energy) exists for all dislocated states, then the following can be taken to hold for any purely *elastic* strain variation $\delta\mathbf{e}$ at fixed H ($dH \neq 0$ implies dislocation slips and the accumulation of plastic strain)

$$\mathbf{t}:\delta\mathbf{e} = \delta\phi(\mathbf{e}, H) \tag{2.29}$$

and

$$\mathbf{t} = \frac{\partial\phi}{\partial\mathbf{e}} = \mathbf{t}(\mathbf{e}, H). \tag{2.30}$$

In the foregoing we use the symbolism introduced by Hill and Rice [12] that variations indicated by a δ are purely elastic; this, of course, means that $\delta H = 0$. The free energy function $\phi(\mathbf{e}, H)$ depends on the dislocated state through the self and interaction energies of the assumed internal variables, e.g., the dislocation segments. A dual potential can be introduced via the Legendre transformation

$$\psi = \mathbf{t}:\mathbf{e} - \phi \tag{2.31}$$

and as before, for a purely elastic variation, we find

$$\mathbf{e}:\delta\mathbf{t} = \delta\psi(\mathbf{e}, H) \tag{2.32}$$

and

$$\mathbf{e} = \frac{\partial\psi}{\partial\mathbf{t}}. \tag{2.33}$$

At this point we reintroduce the fourth-order tensor of elastic moduli $\underset{\sim}{\mathcal{L}}$ and its inverse $\underset{\sim}{\mathcal{L}}^{-1}$ here defined for the pair $(\mathbf{t}, \mathbf{e})$. If $d\mathbf{e}$ is an arbitrary strain variation, $\underset{\sim}{\mathcal{L}}:d\mathbf{e}$ is the stress increment that *would* result if the response *were* purely elastic. When the response is elastic-plastic, however, $d\mathbf{t}$ is the actual stress increment, and the difference

$$d^P\mathbf{t} = d\mathbf{t} - \underset{\sim}{\mathcal{L}}:d\mathbf{e} = d\mathbf{t} - \frac{\partial\mathbf{t}}{\partial\mathbf{e}}:d\mathbf{e} \tag{2.34}$$

is what Hill and Rice have called the "plastic" part of the increment. In the same manner, $\underset{\sim}{\mathcal{L}}^{-1}:d\mathbf{t}$ is the strain increment that *would* result from purely elastic response and the difference

$$d^P\mathbf{e} = d\mathbf{e} - \underset{\sim}{\mathcal{L}}^{-1}:d\mathbf{t} = d\mathbf{e} - \frac{\partial\mathbf{e}}{\partial\mathbf{t}}:d\mathbf{t} \tag{2.35}$$

is the "plastic part." These two plastic quantities are related by the elastic moduli

$$d^P\mathbf{t} = -\underset{\sim}{\mathcal{L}}:d^P\mathbf{e} \quad \text{and} \quad d^P\mathbf{e} = -\underset{\sim}{\mathcal{L}}^{-1}:d^P\mathbf{t}. \tag{2.36}$$

It is observed from (2.34) and (2.35) that for a rate-independent material $d^P\mathbf{t}$ is the residual change (decrement) in stress after an infinitesimal cycle of $\mathbf{e}$ during which inelastic straining occurs, whereas $d^P\mathbf{e}$ is the residual increment of plastic strain during an infinitesimal loading-unloading cycle of $\mathbf{t}$.

The "plastic parts" as defined in the foregoing can be easily identified for the specific kinematical representation given in Section 2.1 and Section 2.2. If t denotes time, dt a time increment, we identify $d\mathbf{t}$ and $d\mathbf{e}$ as

$$d\mathbf{t} \Leftrightarrow \overset{\nabla}{\tau}\, dt \tag{2.37$_1$}$$

and

$$d\mathbf{e} \Leftrightarrow \mathbf{D}\, dt \tag{2.37$_2$}$$

then examining (2.20) we identify

$$d^P\mathbf{t} \Leftrightarrow (\overset{\nabla}{\tau}\, dt)^P = -\sum_{\alpha=1}^{n} \{\underset{\sim}{\mathcal{L}}:\mathbf{P}^{(\alpha)} + \boldsymbol{\beta}^{(\alpha)}\} d\gamma^{(\alpha)} \tag{2.38$_1$}$$

and

$$d^P\mathbf{e} \Leftrightarrow (\mathbf{D}dt)^P = \sum_{\alpha=1}^{n} \{\mathbf{P}^{(\alpha)} + \underset{\sim}{\mathcal{L}}^{-1}:\boldsymbol{\beta}^{(\alpha)}\} d\gamma^{(\alpha)} \tag{2.38$_2$}$$

where $d\gamma^{(\alpha)} = \dot{\gamma}^{(\alpha)}\, dt$.

It is informative to identify these "plastic parts" explicitly since it is the plastic increment $(\mathbf{D}dt)^P$ which can be shown, with appropriate kinetic assumptions, to be normal to the yield surface in stress space and not

$$\mathbf{D}^P dt \left(= \sum_{\alpha=1}^{n} P^{(\alpha)} d\gamma^{(\alpha)}\right)$$

defined earlier in (2.8), (2.10), and (2.13).

The plastic parts of the increments in free energies are similarly defined by Hill and Rice [12] as

$$d^P\phi = \phi(\mathbf{e}, H + dH) - \phi(\mathbf{e}, H) \tag{2.39}$$

and

$$d^P\psi = \psi(\mathbf{t}, H + dH) - \psi(\mathbf{t}, H). \tag{2.40}$$

Furthermore as pointed out by them, the potentials, ϕ and ψ, and thus the increments, can be evaluated at any $\mathbf{e}$ or $\mathbf{t}$ where ϕ and H are defined. Then if $d^P\phi$ and $d^P\psi$ are differentiated with respect to $\mathbf{e}$ and $\mathbf{t}$, respectively, we find from (2.30) and (2.33) that

$$\frac{\partial}{\partial\mathbf{e}}(d^P\phi) = \mathbf{t}(\mathbf{e}, H + dH) - \mathbf{t}(\mathbf{e}, H) = d^P\mathbf{t} \tag{2.41}$$

and

$$\frac{\partial}{\partial\mathbf{t}}(d^P\psi) = \mathbf{e}(\mathbf{t}, H + dH) - \mathbf{e}(\mathbf{t}, H) = d^P\mathbf{e} \tag{2.42}$$

which effectively shows that the plastic variations in the potentials serve as potentials for the plastic parts of variations in stress and strain. To identify these latter potentials and demonstrate the fundamental role played by the Schmid stress we first examine the question of normality. This is done with respect to conjugte variables.

Normality for Rate-Independent Materials. At each history a yield surface is supposed to exist in either $\mathbf{t}$ or $\mathbf{e}$ space. Confining our attention to $\mathbf{t}$ space, suppose the current stress is at a point on the yield surface where dH occurs producing a plastic increment $d^P\mathbf{e}$. If $\delta\mathbf{t}$ represents *any* stress increment beginning at this stress point but directed *inside*, and if

$$\delta\mathbf{t}:d^P\mathbf{e} < 0 \tag{2.43}$$

for all such $\delta\mathbf{t}$'s, then the strain increment will be said to be normal. Further implications regarding the behavior of the potential ϕ itself are seen by studying the Il'yushin inequality for a strain cycle involving an infinitesimal plastic strain increment, viz,

$$\oint \mathbf{t}:d\mathbf{e} \geq 0. \tag{2.44}$$

Downloaded 02 May 2010 to 171.66.16.250. Redistribution subject to ASME license or copyright; see http://www.asme.org/terms/Terms_Use.cfm

The integral is taken about a strain cycle beginning at a point within the yield surface and the inequality holds if plastic strain occurs. To evaluate this integral, carry out the three segment cycle suggested by Hill and Rice: (*a*) from an arbitrary point interior to the yield surface at strain $\mathbf{e}_o$, load (elastically) to the yield point at strain $\mathbf{e}_y$; (*b*) load elastic-plastically to the strain $\mathbf{e}_y + d\mathbf{e}_y$ (on the subsequent yield surface characterized by $H + dH$), and unload elastically within the *new elastic domain* back to $\mathbf{e}_y$; and finally (*c*) unload back to $\mathbf{e}_o$ elastically. The final segment can be taken along the same path in (*a*) because of the assumed path independence within elastic domains. Segment (*b*) contributes a second-order effect and thus may be ignored. Furthermore by appealing to (2.30) we note that along segment (*a*) $\mathbf{t} = \mathbf{t}(\mathbf{e}, H)$ while along (*b*) with the same end points, $\mathbf{t} = \mathbf{t}(\mathbf{e}, H + dH)$. It is evident then that by using (2.41),

$$\oint \mathbf{t}:d\mathbf{e} = \int_{\mathbf{e}_o}^{\mathbf{e}_y} \{\mathbf{t}(\mathbf{e}, H) - \mathbf{t}(\mathbf{e}, H+dH)\}:\delta\mathbf{e} =$$

$$-\int_{\mathbf{e}_o}^{\mathbf{e}_y} d^P\mathbf{t}:\delta\mathbf{e} = -\int_{\mathbf{e}_o}^{\mathbf{e}_y} \frac{\partial}{\partial\mathbf{e}}(d^P\phi):\delta\mathbf{e} = d^P\phi\Big|_{\mathbf{e}_y}^{\mathbf{e}_o}. \tag{2.45}$$

The Il'yushin postulate when applied to such cycles thus states that

$$d^P\phi\Big|_{\mathbf{e}_y}^{\mathbf{e}_o} \geq 0. \tag{2.46}$$

To see how this singles out the Schmid stress in connection with normality, consider the following heuristic construct. If ϕ *is the* isothermal Hemholtz free energy per unit reference volume, $d^P\phi$ is its change at *fixed overall strain* due to the occurrence of slips $d\gamma^{(\alpha)}$. If $\tau^{(\alpha)}$ is the *net* Schmid stress produced by applied loads *and interactions with the dislocated state* (characterized by H) then

$$\sum_{\alpha=1}^{n} \tau^{(\alpha)} d\gamma^{(\alpha)}$$

is the work done through the slips and

$$-\sum_{\alpha=1}^{n} \tau^{(\alpha)} d\gamma^{(\alpha)}$$

is the change in ϕ. Of course this is equivalent to identifying $\tau^{(\alpha)}$ as the thermodynamic force acting on a set of internal variables whose infinitesimal variations are identified with the $d\gamma^{(\alpha)}$'s which, incidentally, is an alternative starting point for defining $\tau^{(\alpha)}$ (Rice [11] in fact starts from that point). Then combining (2.44) and (2.46) the Il'yushin postulate applied to such cycles becomes for the case of crystallographic slip

$$\oint \mathbf{t}:d\mathbf{e} = \sum_{\alpha=1}^{n} (\tau_y^{(\alpha)} - \tau^{(\alpha)})\, d\gamma^{(\alpha)} \geq 0. \tag{2.47}$$

where τ_y is evaluated at $\mathbf{e}_y$ on the yield surface and $\tau^{(\alpha)}$ at *any* point within the surface. In fact (2.43) implies that if $d\gamma^{(\alpha)} > 0$, for example, $\delta\tau^{(\alpha)} < 0$, for any $\delta\mathbf{t}$ variation emanating from a yield point since, by (2.28) and the fact that $\delta\mathbf{t} = \underset{\sim}{\mathfrak{L}}:\delta\mathbf{e}$ for elastic variations,

$$\delta\mathbf{t}:d^P\mathbf{e} = \sum_{\alpha=1}^{n} \{\mathbf{P}^{(\alpha)}:\underset{\sim}{\mathfrak{L}} + \boldsymbol{\beta}^{(\alpha)}\}:\delta\mathbf{e}\; d\gamma^{(\alpha)} = \sum_{\alpha=1}^{n} \delta\tau^{(\alpha)} d\gamma^{(\alpha)} < 0 \tag{2.48}$$

at least whenever at least one $d\gamma^{(\alpha)} \neq 0$; in deriving (2.48) we note that $\delta\mathbf{e} = \mathbf{D}^* dt$ for this purely elastic variation. If the flow laws or hardening rules are such that each pair $\delta\tau^{(\alpha)} d\gamma^{(\alpha)} < 0$ when $\dot{\tau}^{(\alpha)}$ is *changed elastically*, normality follows. This is true when the yield surface is smooth or when the stress point is at a corner made up of intersecting yield planes.

Rate-Dependent Materials. Still following Hill and Rice, we consider materials that exhibit elastic response to sufficiently rapid loading or straining and take a constitutive law in the form

$$\frac{d^P\mathbf{e}}{dt} = \frac{d\mathbf{e}}{dt} - \mathfrak{L}^{-1}:\frac{d\mathbf{t}}{dt} \tag{2.49}$$

Here $d^P\mathbf{e}/dt$ is thought to depend on the current state of stress and dislocated state but instantaneous stress changes are met with the assumed purely elastic response. Thus it is possible to examine variations of the type $\delta\mathbf{t}:d^P\mathbf{e}/dt$ and if this is a perfect differential, say

$$\delta\mathbf{t}:\frac{d^P\mathbf{e}}{dt} = \delta\Gamma(\mathbf{t}, H) \tag{2.50}$$

then

$$\frac{d^P\mathbf{e}}{dt} = \frac{\partial\Gamma}{\partial\mathbf{t}} \tag{2.51}$$

and a flow potential exists. For the present case of crystallographic slip we take $\delta\mathbf{t}$ to be $\underset{\sim}{\mathfrak{L}}:\mathbf{D}^*\delta t = \underset{\sim}{\mathfrak{L}}:\delta\mathbf{e}$ and use the identity (2.38_2) for $d^P\mathbf{e}$ to obtain

$$\sum_{\alpha=1}^{n} \{\mathbf{P}^{(\alpha)}:\underset{\sim}{\mathfrak{L}} + \boldsymbol{\beta}^{(\alpha)}\}\delta\mathbf{e}\frac{d\gamma^{(\alpha)}}{dt} \tag{2.52}$$

which can be rewritten as

$$\sum_{\alpha=1}^{n} \delta\tau^{(\alpha)} \frac{d\gamma^{(\alpha)}}{dt} \tag{2.53}$$

Now, as Rice [10, 11] has suggested, if the kinetic laws for $d\gamma^{(\alpha)}/dt$ are stress-dependent only through the associated conjugate force $\tau^{(\alpha)}$, equation (2.53) is a perfect differential and a flow potential and normality again result.

2.4 Hardening Laws for Rate-Independent Materials. In this section hardening laws are formulated in accordance with the normality rules described in the preceding section. This is done using the kinematical representation introduced in Sections 2.1 and 2.2. Two quantities for each slip system are first defined:

$$\boldsymbol{\lambda}^{(\alpha)} = \mathbf{P}^{(\alpha)}:\underset{\sim}{\mathfrak{L}} + \boldsymbol{\beta}^{(\alpha)} \tag{2.54}$$

and

$$\boldsymbol{\mu}^{(\alpha)} = \mathbf{P}^{(\alpha)} + \underset{\sim}{\mathfrak{L}}^{-1}:\boldsymbol{\beta}^{(\alpha)} = \underset{\sim}{\mathfrak{L}}^{-1}:\boldsymbol{\lambda}^{(\alpha)} \tag{2.55}$$

Consistent with the normality structure just described we state that plastic flow occurs on slip system α when $\tau^{(\alpha)}$ reaches a critical value $\tau_c^{(\alpha)}$. For those so-called "critical systems" where $\tau^{(\alpha)} = \tau_c^{(\alpha)}$

$$\dot{\tau}^{(\alpha)} = \dot{\tau}_c^{(\alpha)} = \sum_{\beta=1}^{n} h_{\alpha\beta}\dot{\gamma}^{(\beta)} \quad \text{if } \dot{\gamma}^{(\alpha)} > 0 \tag{2.56}$$

which maintains $\tau^{(\alpha)}$ at the current yield value.

If the system becomes inactive

$$\dot{\tau}^{(\alpha)} \leq \dot{\tau}_c^{(\alpha)} = \sum_{\beta=1}^{n} h_{\alpha\beta}\dot{\gamma}^{(\beta)} \quad \text{with } \dot{\gamma}^{(\alpha)} = 0. \tag{2.57}$$

For noncritical systems there is only the inequality

$$\tau^{(\alpha)} < \tau_c^{(\alpha)} \quad \text{with } \dot{\gamma}^{(\alpha)} = 0. \tag{2.58}$$

The $h_{\alpha\beta}$ are the slip-plane hardening rates; the diagonal terms represent "self-hardening" on a slip system whereas the off-diagonal terms represent coupled or "latent hardening." The effect of latent hardening is described in Section 2.6 where some of its implications are compared to experiments.

Downloaded 02 May 2010 to 171.66.16.250. Redistribution subject to ASME license or copyright; see http://www.asme.org/terms/Terms_Use.cfm

When these relations are combined with (2.54), (2.55), and (2.28), the hardening laws take the form

$$\boldsymbol{\lambda}^{(\alpha)}:\mathbf{D}^* = \boldsymbol{\mu}^{(\alpha)}:\overset{\nabla}{\boldsymbol{\tau}}{}^* = \sum_{\beta=1}^{n} h_{\alpha\beta}\dot{\gamma}^{(\beta)}, \quad \dot{\gamma}^{(\alpha)} > 0 \tag{2.59}$$

and

$$\boldsymbol{\lambda}^{(\alpha)}:\mathbf{D}^* = \boldsymbol{\mu}^{(\alpha)}:\overset{\nabla}{\boldsymbol{\tau}}{}^* \leq \sum_{\beta=1}^{n} h_{\alpha\beta}\dot{\gamma}^{(\beta)}, \quad \dot{\gamma}^{(\beta)} > 0 \tag{2.60}$$

In terms of the total material deformation rate **D** we find after using (2.8)

$$\boldsymbol{\lambda}^{(\alpha)}:\mathbf{D} = \sum_{\beta=1}^{n} g_{\alpha\beta}\dot{\gamma}^{(\beta)}, \quad \dot{\gamma}^{(\beta)} > 0 \tag{2.61}$$

$$\boldsymbol{\lambda}^{(\alpha)}:\mathbf{D} \leq \sum_{\beta=1}^{n} g_{\alpha\beta}\dot{\gamma}^{(\beta)}, \quad \dot{\gamma}^{(\alpha)} = 0 \tag{2.62}$$

or in terms of the material Jaumann rates $\overset{\nabla}{\boldsymbol{\tau}}$

$$\boldsymbol{\mu}^{(\alpha)}:\overset{\nabla}{\boldsymbol{\tau}} = \sum_{\beta=1}^{n} k_{\alpha\beta}\dot{\gamma}^{(\beta)}, \quad \dot{\gamma}^{(\alpha)} > 0 \tag{2.63}$$

$$\boldsymbol{\mu}^{(\alpha)}:\overset{\nabla}{\boldsymbol{\tau}} \leq \sum_{\beta=1}^{n} k_{\alpha\beta}\dot{\gamma}^{(\beta)}, \quad \dot{\gamma}^{(\alpha)} > 0. \tag{2.64}$$

The matrices **g** and **k** were introduced in this context by Hill and Rice [4] and for the specific kinematical description used here the elements are given by

$$g_{\alpha\beta} = h_{\alpha\beta} + \boldsymbol{\lambda}^{(\alpha)}:\mathbf{P}^{(\beta)} \tag{2.65}$$

and

$$k_{\alpha\beta} = h_{\alpha\beta} - \boldsymbol{\mu}^{(\alpha)}:\boldsymbol{\beta}^{(\beta)}. \tag{2.66}$$

These two matrices play a particularly significant role regarding "slip mode" uniqueness as shown by Hill and Rice. The details are not reproduced here but their main result, which takes the form of sufficiency conditions, is simply stated: when the **D**'s are fully specified the specification of the $\dot{\gamma}^{(\alpha)}$'s is unique if **g** is positive-definite; if the stress rates are instead specified, in our case the $\overset{\nabla}{\boldsymbol{\tau}}$'s, uniqueness is guaranteed if **k** is positive-definite. It should be noted that the restrictions placed on material properties such as latent hardening to insure uniqueness of the slip mode are rather severe and in fact too restrictive to include the full range of experimentally observed behavior. This will be discussed a bit further in connection with a specific model study later.

If, however, **g** can be inverted (2.61) yields

$$\dot{\gamma}^{(\alpha)} = \sum_{\beta=1}^{n} g^{-1}_{\alpha\beta}\boldsymbol{\lambda}^{(\beta)}:\mathbf{D} \tag{2.67}$$

and

$$\overset{\nabla}{\boldsymbol{\tau}} = \mathbf{C}:\mathbf{D} \tag{2.68}$$

with

$$\mathbf{C} = \underset{\sim}{\mathcal{L}} - \sum_{\alpha=1}^{n}\sum_{\beta=1}^{n} \boldsymbol{\lambda}^{(\alpha)} g^{-1}_{\alpha\beta}\boldsymbol{\lambda}^{(\alpha)}. \tag{2.69}$$

2.5 Kinetic Laws for Rate-Dependent Materials. The formulation of suitable kinetic laws for dislocation motion has received much attention and suitable reviews of the subject are available. For the present we will confine our attention to isothermal behavior and to quasi-static strain rates.

The specific law we adopt here for purposes of subsequent calculatoin is the simple power law used earlier by Hutchinson [15] for polycrystalline creep and by Pan and Rice [16] to describe the influence of rate sensitivity on yield vertex behavior in single crystals, viz,

$$\dot{\gamma}^{(\alpha)} = \dot{a}^{(\alpha)}\left(\frac{\tau^{(\alpha)}}{g^{(\alpha)}}\right)\left|\frac{\tau^{(\alpha)}}{g^{(\alpha)}}\right|^{(1/m)-1}. \tag{2.70}$$

Strain hardening is described by the evolution of the functions $g^{(\alpha)}$ which describe the current strain-hardened state. For example, Pan and Rice [16] propose the hardening law

$$\dot{g}^{(\alpha)} = \sum_{\beta=1}^{n} h_{\alpha\beta}\dot{\gamma}^{(\beta)} \tag{2.71}$$

where the $h_{\alpha\beta}$ are again slip-plane hardening moduli. As in the rate-independent theory, $h_{\alpha\alpha}$ represent self-hardening where $h_{\alpha\beta}\,(\alpha \neq \beta)$ are the latent hardening rates. $\dot{a}^{(\alpha)}$ has the simple interpretation of being reference strain rate on system α so that, for example, if $\dot{\gamma}^{(\alpha)} = \dot{a}^{(\alpha)}$ throughout the deformation history, $\tau^{(\alpha)} = g_0^{(\alpha)} + \int \dot{g}^{(\alpha)}\,dt$ where the integral is, of course, path dependent. In practice the $g^{(\alpha)}$ functions would be fit to τ versus γ curves obtained from single crystal deformed so that only one slip system was active, i.e., in a mode of "single slip;" the latent hardening rates are more

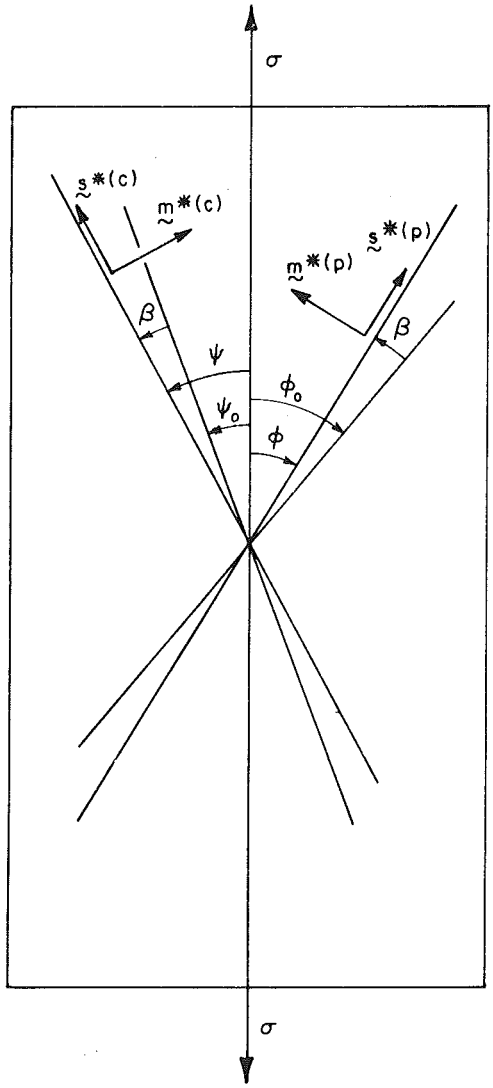


Fig. 2 Planar model for a single crystal subjected to tension. The crystal initially undergoes primarily single slip on the "primary" system labeled (p). Lattice rotations occur, designated by β, such that s(p) rotates toward the tensile axis which eventually causes the conjugate system to become active.

Downloaded 02 May 2010 to 171.66.16.250. Redistribution subject to ASME license or copyright; see http://www.asme.org/terms/Terms_Use.cfm

difficult to directly measure and are instead typically inferred via the effects they have on "overshoot" behavior as described in the next section.

In rate-dependent formulations of this type, there is no explicit yielding; all systems are active with the rate of shearing determined by (2.70). However, in practice, for values of $m \leq 0.02$ which incorporates a wide range of metal strain-rate sensitivities, "yielding" would appear to occur abruptly as $\tau^{(\alpha)}$ approaches the current value of $g^{(\alpha)}$; when $\tau^{(\alpha)} < g^{(\alpha)}$ the corresponding $\dot{\gamma}^{(\alpha)}$ is exceedingly small. Furthermore, using (2.70) in its present form does not require defining $(\mathbf{s}^{(\alpha)}, \mathbf{m}^{(\alpha)})$ and $(\mathbf{s}^{(\alpha)}, -\mathbf{m}^{(\alpha)})$ as different systems since negative $\dot{\gamma}^{(\alpha)}$'s are allowed. When this is done, however, the hardening law (2.71) would need to be altered so that inadvertent strain-softening effects are excluded. If Bauschanger effects were excluded outright, $\dot{\gamma}^{(\beta)}$ could be replaced with its absolute magnitude to yield an acceptable hardening law.

2.6 Latent Hardening. The slip-plane hardening rates $h_{\alpha\beta}$ introduced in (2.56) and (2.71) play a vital role in determining the character of the governing equations and therefore the patterns of deformation that develop at large strains. In addition, the level of latent hardening is of paramount importance in deciding whether or not the slip mode is unique in the rate-independent idealization of crystalline slip. The discussion, in fact, will show that the range of latent hardening observed in metals is such that uniqueness is perhaps only rarely guaranteed in a rate-independent model and is so only for simple crystal geometries involving relatively few slip systems. This would seem to place a severe limitation on the use of rate-independent theories since, as the examples given in Section 3 will show, large strain-deformation behavior in crystals depends intimately on lattice kinematics and therefore on the slip mode.

There are two methods which have appeared in the literature for estimating latent hardening. These have been reviewed recently by Peirce, Asaro, and Needleman [7], and Asaro [2] and so only a brief summary is given here. The first method involves deforming large crystals oriented for single slip and then cutting from them smaller specimens oriented for *single* slip on previously latent systems. The yield stress on the latent system is then compared to the flow stress of the original, or "primary," system. A second method is illustrated in Fig. 2. It is well known that when a single crystal is deformed in tension in single slip the lattice rotates relative to the loading axis such that the slip direction rotates *toward* the loading axis. The model sketched in Fig. 2 is meant to represent a cubic metal such as a face-centered or body-centered cubic metal and indicates that after a finite amount of slip on one system a second slip system eventually becomes equally stressed. This is known as the "conjugate" system. If slip is rate-independent and the hardening is isotropic such that all the $h_{\alpha\beta}$ are equal, we expect the conjugate system to yield when it becomes symmetrically oriented with respect to the primary system about the tensile axis. If the latent hardening rate of the conjugate slip system is larger than the self-hardening rate of the primary system, the lattice rotation "overshoots" the symmetry position until the resolved stress on the conjugate system exceeds that on the primary and conjugate slip begins. Measurements of the amount of overshoot therefore provide a means of estimating latent hardening levels. The two methods just described do not in general yield identical estimates of latent hardening. For one thing the strain path histories accumulated during the two tests are quite different and it is almost assured that the $h_{\alpha\beta}$ will be strongly path-dependent. For cases where loading produces multiple slip, estimates based on overshoot may be more representative and so we close this section with a brief discussion of overshoot observations and predictions.

Overshoot angles of between 0 and 4 deg have been commonly reported whereas there are cases of where secondary (i.e., conjugate) slip has been reported to begin even before symmetry positions are reached. Kocks [17] has reviewed much of this data and has summarized it by estimating that the ratio of latent hardening to self-hardening rates is between 1 to 1.4. For systems that share the same plane, this ratio is closer to 1 whereas for systems with intersecting planes the ratio is generally larger than unity. What is then important is that the hardening law used fits this range of observation. In the remainder of this section several hardening laws proposed in the literature are summarized and the implications they have for overshoot are explored in one particular case for rate-dependent and rate-independent materials.

As discussed by Peirce et al. [7], most of the hardening laws proposed to date process the symmetry $h_{\alpha\beta} = h_{\beta\alpha}$. For example, Hutchinson [18], Asaro [2], and Peirce et al. [7] have used the simple form

$$h_{\alpha\beta} = h_1 + (h - h_1)\delta_{\alpha\beta}. \tag{2.72}$$

This may be further simplified by setting $h_1 = qh$ where q is constant; the experimental range of q as suggested by Kocks [17] is then $1 \leq q \leq 1.4$. Symmetry of the $h_{\alpha\beta}$, however, generally implies a lack of symmetry in the matrix $\mathbf{g}$ and in the constitutive matrix $\mathbf{C}$. Symmetry in the matrix $\mathbf{C}$ allows the governing equations to be cast in variational form which is, in the rate-independent theory, very useful analytically. For example, in finite element calculations of the type performed by Peirce et al. [7] symmetry in $\mathbf{C}$ leads to symmetry in the global stiffness matrix. In addition, the variational structure imparted allows questions of uniqueness and bifurcation in boundary value problems to be addressed within the framework laid out by Hill [19]. Havner and Shalaby [20] recognized advantages of such symmetry and proposed a hardening law of the form

$$h_{\alpha\beta} = \mathcal{H}_{\alpha\beta} + \mathbf{P}^{(\alpha)} : \boldsymbol{\beta}^{(\beta)} \tag{2.73}$$

where in their "simple theory" $\mathcal{H}_{\alpha\beta}$ is taken to be symmetric and all the elements equal to $\mathcal{H}$. This law leads to very strong latent hardening via the coupling of the off-diagonal elements to stress through the $\boldsymbol{\beta}$'s which was used by them to describe overshoot. Peirce et al. [7] used a law with the form

$$h_{\alpha\beta} = \mathcal{H}_{\alpha\beta} + 1/2[\mathbf{P}^{(\alpha)} : \boldsymbol{\beta}^{(\beta)} - \boldsymbol{\beta}^{(\alpha)} : \mathbf{P}^{(\beta)}] \tag{2.74}$$

with $\mathcal{H}_{\alpha\beta} = \mathcal{H}_{\beta\alpha}$ but with the off-diagonal elements different than the diagonal elements; specifically they set

$$\mathcal{H}_{\alpha\beta} = q\mathcal{H} + (1 - q)\ \mathcal{H}\ \delta_{\alpha\beta} \tag{2.75}$$

as suggested in the foregoing. In the rate-dependent formulation of the type just described, on the other hand, the variational structure that follows from a symmetric $\mathbf{C}$ is not directly applicable and so it is just as convenient to simply specify the $h_{\alpha\beta}$ directly.

Peirce et al. [7] have carried out overshoot calculations using the plane model shown earlier in Fig. 2 for both rate-dependent and rate-independent calculations. In both cases the self-hardening rates took the form

$$h(\gamma) = h_0\ \mathrm{sech}^2 \left| \frac{h_0 \gamma}{\tau_s - \tau_0} \right| \tag{2.76}$$

where h_0 is the initial hardening rate, τ_0 is the yield stress, and γ is the cumulative shear strain on both slip systems, i.e.,

$$\gamma = \sum_{\beta=1}^{2} |\gamma^{(\alpha)}|.$$

This hardening rule describes a material that saturates at large strains as the flow stress approaches τ_s. In the rate-dependent case τ_0 is equal to $g^{(\alpha)}(0)$.

Downloaded 02 May 2010 to 171.66.16.250. Redistribution subject to ASME license or copyright; see http://www.asme.org/terms/Terms_Use.cfm

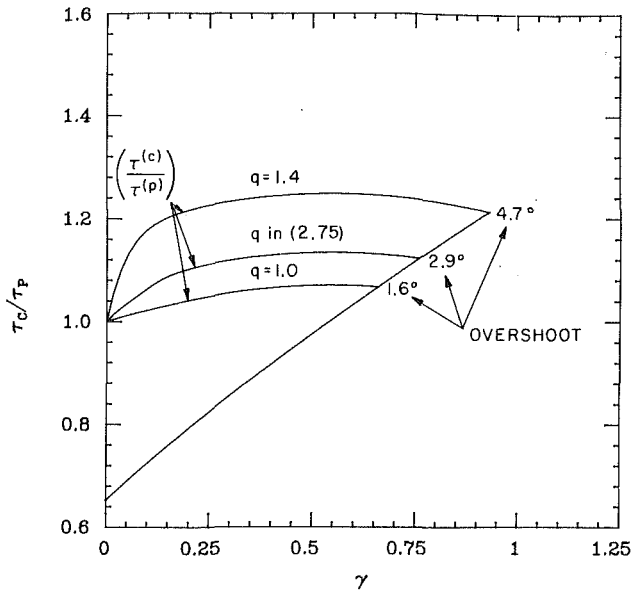


Fig. 3 This figure corresponds to simulations of single slip "overshoot" using the model of Fig. 2 for a rate-independent crystal. Various levels of latent hardening are indicated by the three values for q as explained in the text. The figure is taken from Peirce et al. [7].

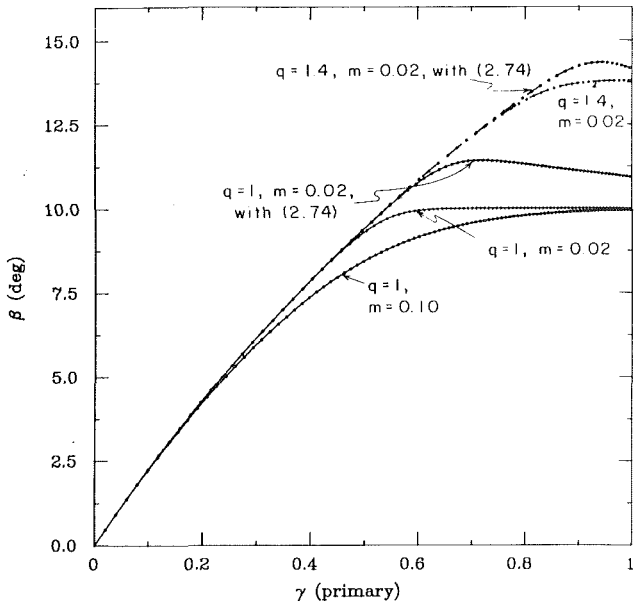


Fig. 4 Lattice rotation, β, and "overshooting" simulated using the planar model of Fig. 2 for a crystal deformed in tension. The crystal is rate-dependent and various strain-rate sensitivities, m, and levels of latent hardening, q, are indicated (taken from Peirce et al. [8]).

The calculations were performed for a rigid-plastic idealization of the crystal since the elasticity has a negligible effect on the lattice rotation. Kinematics links the angle of rotation β directly to the slip; at any stage for instance

$$\tan\beta = F^P_{12}/F^P_{22} \tag{2.77}$$

where $\mathbf{F}^P$ is the plastic part of the deformation gradient. The integration procedure is rather straightforward [2] and the results are shown in Figs. 3 and 4.

For the rate-independent crystal the hardening law given by (2.74) was used with

$$\mathcal{H}_{\alpha\beta} = qh + (1-q)\ h\ \delta_{\alpha\beta}. \tag{2.78}$$

q was varied between 1 and 1.4. As noted by Peirce et al. [7] the stress terms in (2.74) have the effect of contributing to latent hardening and overshoot. On the ordinate of Fig. 3 is plotted the ratio of the shear stresses on the conjugate and primary systems. The curves marked $(\tau^{(c)}/\tau^{(p)})$ are the ratios of the yield stresses plotted as functions of shear strain on the primary system. Note that even for $q=1$ the curve rises due to the aforementioned stress terms. The other line is the ratio of the resolved shear stresses generated on the slip systems by the tensile stress and it is presumed that when these two ratios are equal conjugate slip begins. At this point the net lattice rotation ceases due to conjugate slipping. The overshoot angles are listed on the figure where it is seen that the range of $1 \leq q \leq 1.4$ certainly does encompass the range of overshoot previously quoted.

For the rate-dependent calculation the hardening law was taken as (2.72) with $h(\gamma)$ again given by (2.76). The results, taken from the work of Peirce et al. [8], are shown in Fig. 4. In the figure, angle β is shown plotted as a function of the primary shear strain, γ; note that $\beta = 10$ deg corresponds to reaching a symmetric orientation.

When $q=1$ and the strain-rate sensitivity given by $m = 0.02$, the lattice rotation is such that $\beta \to 10$ deg and holds constant. In this case conjugate shearing comes on rather abruptly when the symmetry position is reached. When q is larger, e.g., $q=1.4$, overshoot of up to ~ 4 deg is evident as in the rate-independent case. One striking difference between the rate-independent and rate-dependent formulations is exemplified by the case where $q=1$ and $m=0.1$; a rather rate-sensitive case. Here the premature deviations from the curve for $q=1$ and $m=0.02$ are caused by earlier conjugate slip, that is, the flow law given by (2.70) allows conjugate slip to occur at a noticeable rate at resolved shear stress levels below that on the primary. Instances of such "undershooting" have indeed been observed in the literature. In fact, if q were larger than unity, initial undershoot would be followed by overshooting – again this type of behavior has been commonly observed.

Our tentative conclusion then is that levels of latent hardening ratios of 1-1.4 seem to account for a good deal of the observed data. Of course, the actual history of such ratios is undoubtedly quite complex so that even this rather approximate description can only be interpreted as an averaged effect on the hardening.

3 Analysis of Nonuniform Slip Phenomena in Single Crystals

An inevitable outcome of large strain plasticity in ductile solids is that homogeneous patterns of plastic flow break down into patterns characterized by nonuniform and highly localized plastic flow. The subject of localized deformation has received a good deal of attention during the past 10 years, largely because of the fundamental role it plays in limiting ductility and causing fracture. Analysis of localized deformation at large strains have shown the material's response is highly sensitive to constitutive description. For example, the existence of yield vertexes in rate-independent theories has been shown to promote bifurcations of a homogeneous deformation pattern into modes characterized by localized shear bands [21, 22]. An example of this for a single crystal is given in the following. Deviations from plastic normality, even when they are of such small magnitudes that are difficult to experimentally detect, likewise have been shown to promote the localization of plastic flow [6, 23].

There are, however, many other forms of nonuniform inelastic flow in crystalline materials, some catastrophic in their effects on ductility and others not, which are as yet unexplainied but clearly have important implications for the eventual development of large strain constitutive laws for

Downloaded 02 May 2010 to 171.66.16.250. Redistribution subject to ASME license or copyright; see http://www.asme.org/terms/Terms_Use.cfm

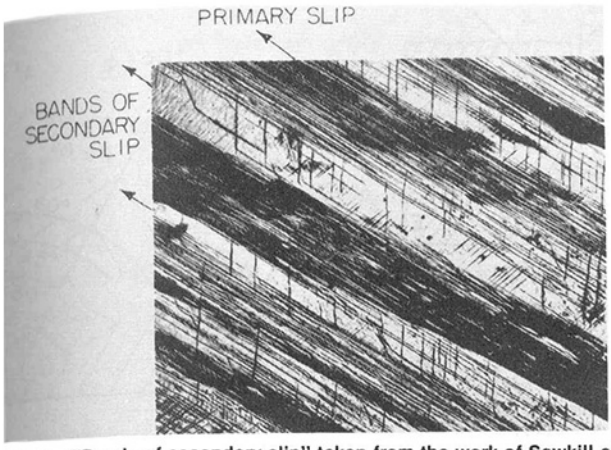


Fig. 5 "Bands of secondary slip" taken from the work of Sawkill and Honeycombe [24]



Fig. 6 An example of a discontinuous slip mode with the grains of polycrystalline aluminum, taken from Boas and Ogilvie [26]. The grain appears to break up into "patches," each characterized by a different mode of slip.

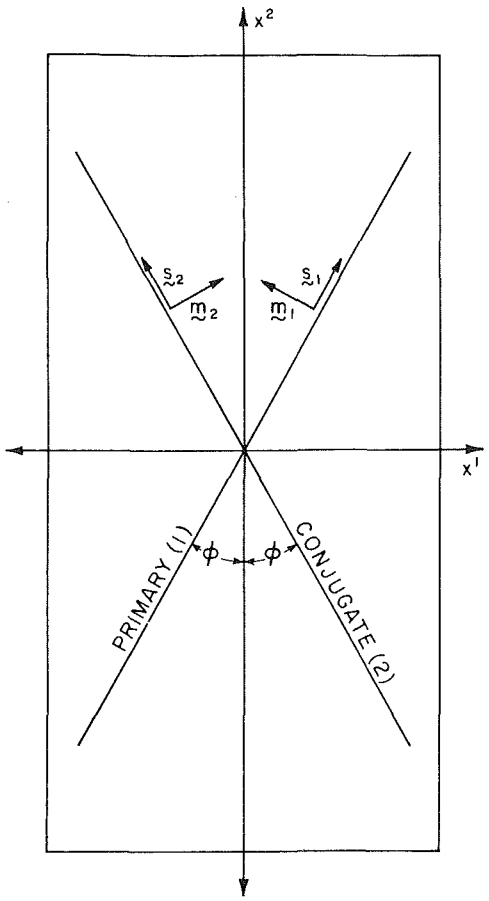


Fig. 7 Planar model for a single crystal subjected to tension. The crystal is presumed to undergo a primarily double mode of slip on the primary and conjugate slip systems.

polycrystals as well as single crystals. A case in point is illustrated in Fig. 5 which is taken from the work of Sawkill and Honeycombe [24]. As described by them, the (homogeneous) gage section of the crystal developed bands closely aligned with one slip system that were characterized by concentrated slip on other systems. These bands were referred to as "bands of secondary slip" and are kinematically quite different than the shear bands discussed by Chang and Asaro [25] and Peirce et al. [7, 8] in that they do not tend to accumulate very large strains. They do cause very significant lattice rotations and thus contribute to the development of nonuniform "texturing" of the crystal's gage section.

Another example of nonuniform slip is shown in Fig. 6 which is taken from the work of Boas and Olgivie [26]. In this case it is apparent that the *slip mode* within the individual grains of the polycrystal is nonuniform. The grains break up into what Peirce et al. [7] have called "patches," which are contiguous regions in which the slip modes are different. Since lattice rotation depends on the slip mode, the crystallographic orientation of neighboring patches becomes different which again leads to a nonuniform texture.

The development of nonuniform texture strongly affects the constitutive properties of the crystal. For one thing the kinematics of slip is changed to the point where it may no longer be sensible to refer to the specimen as a single crystal. The kinematics of slip is altered so that in some cases intensely localized deformation results. A case in point is the formation of shear bands resulting from "geometrical softening" or textural softening of the lattice studied by Chang and Asaro [25] and Peirce et al. [7]. In other cases macroscopically homogeneous deformation is promoted. For example, there are numerous examples of "contained bands" of localized deformation in both polycrystals and single crystals. By this is meant bands that are apparently constrained against propagating throughout the specimen's gage section. Peirce et al. [8] have illustrated how the orientation discontinuities associated with patchy slip in single crystals can prevent shear bands from propagating across patch boundaries. It is possible that similar geometric constraints act in polycrystals, but this has yet to be explored in sufficient depth.

We explore several examples of nonuniform flow in this section using the simple crystal model shown in Fig. 7 and the constitutive description just outlined.

In the interest of brevity, our attention is confined to rate-independent models; the reader is directed to other work for a discussion of rate dependence.

3.1 A Crystal Model. Since the kinematics of *nonuniform lattice rotation* require more than one slip system, complex slip phenomena described in the preceding section invariably occur when the slip mode is multiple slip. A simple plane model of a crystal undergoing a symmetric mode of primary-conjugate slip in tension is shown in Fig. 7. This model has been successfully used to describe the behavior of single crystals of common face-centered-cubic and body-centered-cubic models [2, 7]. As discussed in Section 2.4, crystals deformed in single slip undergo lattice rotations that eventually bring a second, i.e., the conjugate, slip system into a more or less symmetric orientation about the tensile axis with respect to the primary slip system. At this stage the deformation mode is predominantly double slip and the model geometry becomes applicable. There is, however, an im-

Downloaded 02 May 2010 to 171.66.16.250. Redistribution subject to ASME license or copyright; see http://www.asme.org/terms/Terms_Use.cfm

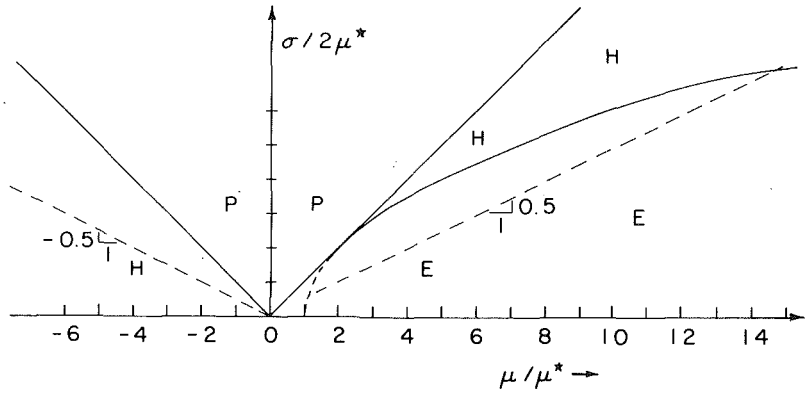


Fig. 8 Regimes of elliptic (*E*), parabolic (*P*), and hyperbolic (*H*) behavior of the equations governing the rate-independent crystal model shown in Fig. 7 (taken from Peirce et al. [8])

portant proviso: although at any stage in a program of homogeneous deformation the model geometry makes both slip systems critical, there is still the question of what will be the slip mode in the next increment of loading. If the slip mode is nonunique, as it may well be in the rate-independent idealization, then so is the rotation of the lattice relative to the material. The description of texturing is therefore nonunique and a proper description of slip phenomena becomes impossible. In the next section a bifurcation analysis is presented which is based on an assumed mode of double slip of a rate-independent crystal. This analysis is very helpful in uncovering the origins of the sort of nonuniform slip phenomena described in the foregoing. However, as noted by Asaro [2] and more specifically by Peirce et al. [8] the kinematic uncertainties of rate independence preclude a full analysis, at least if a reasonably complete set of material parameters is used. To gain some specific understanding of this, the slip-mode uniqueness question for the model of Fig. 7 is examined first. This is done using the sufficiency conditions given by Hill and Rice [4].

For reasons to be explained in the next section, it is instructive to take the elasticity of the model crystal shown in Fig. 7 to be isotropic and incompressible. In this case the matrice elements of $\mathbf{g}$ and $\mathbf{k}$ take the form

$$\mathbf{g}_{\alpha\beta} = h_{\alpha\beta} - (\sigma/2)\cos 2\phi + G, \ \alpha = \beta \tag{3.1$_1$}$$

$$\mathbf{g}_{\alpha\beta} = h_{\alpha\beta} + (\sigma/2)\cos 2\phi - G\cos 4\phi, \ \alpha \neq \beta \tag{3.1$_2$}$$

and

$$k_{\alpha\beta} = h_{\alpha\beta} + (\sigma/2)\cos 2\phi + \mathcal{O}(\sigma^2/G), \ \alpha = \beta \tag{3.2$_1$}$$

$$k_{\alpha\beta} = h_{\alpha\beta} - (\sigma/2)\cos 2\phi + \mathcal{O}(\sigma^2/G), \ \alpha = \beta \tag{3.2$_2$}$$

We also recall that when the deformation rates are specified, slip-mode uniqueness is guaranteed if $\mathbf{g}$ is positive-definite; when the $\overset{\nabla}{\tau}$'s are specified uniqueness follows when $\mathbf{k}$ is positive-definite.

If the degenerate case of $\phi = \pi/4$ is excluded, it is clear that so long as σ and the $h_{\alpha\beta}$ are much less than G, $\mathbf{g}$ is positive-definite. The situation is quite different when the stress rates are specified as noted by Pan and Rice [16]. If, for example, we take $h_{11} = h_{22} = h$ and $h_{12} = h_{21} = h_1$ as the model's orthotropic symmetry might imply we find that $\mathbf{k}$ is positive-definite if and only if

$$h - h_1 + \sigma\cos 2\phi > 0 \tag{3.3}$$

or if we set $h_1 = qh$ as in the discussion of Section 2.6, if

$$(\sigma/h)\cos 2\phi > (1-q). \tag{3.4}$$

In Section 2.4, it was noted that experimental observations easily incorporate the range $1 \leq q \leq 1.4$ for latent hardening. If q is set at 1.4 and ϕ at 30 deg to model on face-centered-cubic crystal as in Asaro [2] and Peirce et al. [7, 8] the inequality (3.4) becomes $\sigma/h > 0.8$ or, since the resolved shear stress on either slip system is $\tau = \sigma/2 \sin 2\phi = 0.43\,\sigma$, $\tau/h > 0.346$. There are numerous cases where this inequality would fail – in fact it would fail during the first 1 percent strain of almost any ductile metal single crystal. If $\phi > \pi/4$, $\cos 2\phi < 0$ and uniqueness requires $q < 1$ which is effectively ruled out by experiment. When more realistic models for crystals are examined, e.g., with 12 slip systems for face-centered-cubic crystals, uniqueness is even more difficult to guarantee in either case, and the range of possible geometries and strain hardening required to do so is too restrictive to include real materials. This, incidentally, has been one of the major difficulties in the prediction of deformation texture in polycrystals. Nonetheless, considerable progress can be made using the rate-independent model. The reader is referred to the work of Peirce et al. [8] for a discussion of their rate-dependent formulation which overcomes these limitations and allows the complete range of material properties to be included.

3.2 Bifurcation Phenomena and Slip Patterns. When the crystal's elasticity is taken as isotropic and incompressible, the crystal model falls into the class of plane orthotropic incompressible solids studied by Biot [27] and Hill and Hutchinson [28]. In particular, the rather comprehensive bifurcation analysis presented by Hill and Hutchinson [28] applies. The constitutive laws take the form

$$\overset{\nabla}{\sigma}_{22} - \overset{\nabla}{\sigma}_{11} = 2\mu^*(D_{22} - D_{11}) \tag{3.5}$$

$$\overset{\nabla}{\sigma}_{12} = 2\mu\, D_{12} \tag{3.6}$$

with the condition of incompressibility expressed as

$$D_{11} + D_{22} = 0. \tag{3.7}$$

The two instantaneous moduli μ and μ^* are defined so that μ governs shear parallel to the x_1, x_2 coordinate axes and μ governs shear at 45 deg to them. With this in mind it is clear that when $\phi = \pi/4$, μ is essentially the elastic modulus since simple shearing on the slip systems does not produce shear parallel to the x_1, x_2 coordinate axes. When ϕ differs from $\pi/4$ shear involves plastic straining and the material's stiffness rapidly decreases. This is equivalent to the formation of a yield vertex and development of vertex softening.

The moduli μ and μ^* are (see Asaro [2] or Peirce et al.)

$$\mu^* = \frac{Gh^*(1+q)}{h^*(1+q) + 2G\sin^2 2\phi^*} \tag{3.8}$$

and

$$\mu = \frac{G(h^*(1-q) + \sigma\cos 2\phi^*) - \sigma^2/2}{h^*(1-q) + 2G\cos^2 2\phi^* - \sigma\cos 2\phi^*} \tag{3.9}$$

Downloaded 02 May 2010 to 171.66.16.250. Redistribution subject to ASME license or copyright; see http://www.asme.org/terms/Terms_Use.cfm

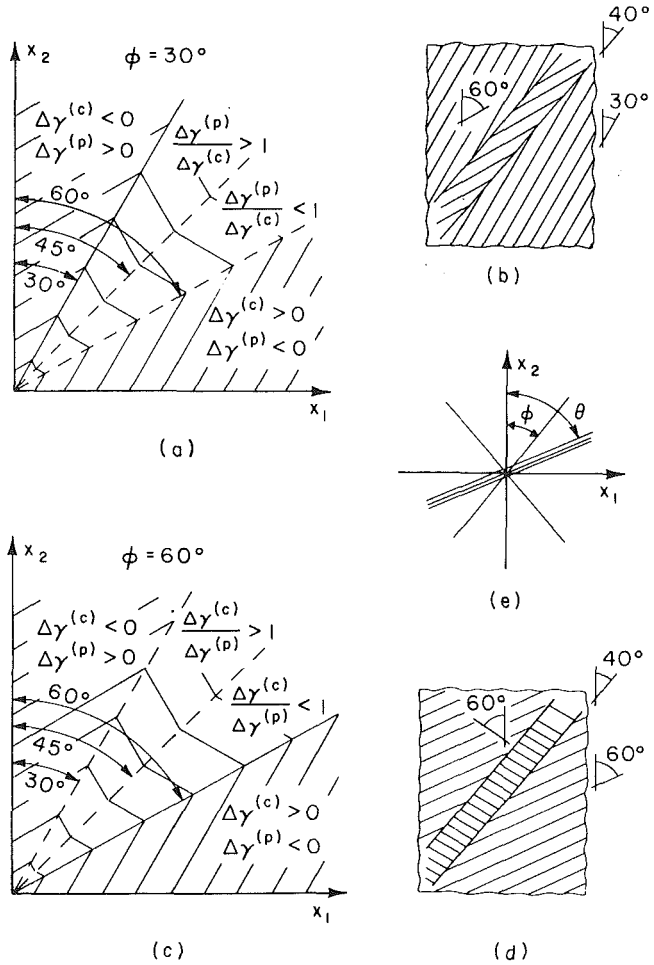


Fig. 9 Slip patterns and loading regimes for the localized bands of slip described in the text (taken from the work of Peirce et al. [8])

where the moduli $h_{\alpha\beta}$ are taken so that $h_{11} = h_{22} = h$ and $h_{12} = h_{21} = h_1 = qh$. h^* and ϕ^* are elastically altered quantities,

$$h^*\left(\frac{ds^*}{ds}\right) = h \tag{3.10}$$

and

$$\lambda^{*2}\tan\phi^* = \tan\phi \tag{3.11}$$

where ds^*/ds is the elastic stretch ratio of either slip direction and λ^* is the elastic stretch ratio along the tensile axis. For practical purposes (i.e., when σ/G, $h/G << 1$) the elastic terms can be set aside and then

$$\mu^* = \frac{h(1+q)}{2\sin^2 2\phi} \tag{3.12}$$

and

$$\mu = \frac{h(1-q)+\sigma\cos 2\phi}{2\cos^2 2\phi}. \tag{3.13}$$

In what follows we examine the conditions that allow the deformation mode to bifurcate into bands of localized deformation. As shown by Hill and Hutchinson [28] for a band to form with unit normal **n** continuing equilibrium and compatability require that

$$(\mu - 1/2\sigma)n_1^4 + 2(2\mu^* - \mu)n_1^2 n_2^2 + (\mu + 1/2\sigma)n_2^4 = 0. \tag{3.14}$$

The governing equations are elliptic, parabolic, or hyperbolic depending on whether there are 0, 2, or 4 real solutions for n_2/n_1. Figures 8 and 9, taken from the recent work of Peirce et al. [8], summarize the bifurcation results and the kinematics of the localized bands that form. The coordinates in Fig. 8 are given by

$$\mu/\mu^* = \frac{[(1-q)+(\tau/h)\cot 2\phi]\tan^2 2\phi}{(1+q)} \tag{3.15}$$

and

$$\mu/2\mu^* = \frac{(\tau/h)\sin 2\phi}{(1+q)} \tag{3.16}$$

where we note $\sigma/2\mu^* > 0$ so long as h and q are positive.

When this model is applied to face-centered-cubic crystals undergoing tension, ϕ is set equal to 30 deg. Now as pointed out by Peirce et al. [8], if $q = 1$, $(\sigma/2\mu^*)/(\mu/\mu^*) = 0.5$ and the trajectory is along the line of slope 0.5 indicated in Fig. 8. When this line intersects the *E-H* boundary there are two *coincident* sets of real characteristics; the angles θ_1 and θ_2 that make the tensile axis are in the range 38–40 deg. What is also apparent from Fig. 8 is that the ratio of σ/h (generally referred by its inverse h/σ) at this point is *positive* and equal to approximately $(h/\sigma)_{crit} \approx 0.04$. This indicates, as noted earlier, that localized flow is possible in defect-free crystals with *positive strain hardening* and that strain softening is not necessary. At other values of q, say in the range $0 \le q \le 2$, the results are quite similar with h/σ in the range $0.03 \le (h/\sigma)_{crit} \le 0.06$.

Figure 9 indicates that the bands just described involve predominantly shear on the slip system to which they are nearly parallel; this is referred to as the primary slip system. In general if the bands are taken to be a simple shearing mode, and are inclined by the angle θ to the tensile axis, the ratio of excess straining on the primary to that on the congugate system is

$$\frac{\Delta\gamma^{(p)}}{\Delta\gamma^{(c)}} = \frac{\sin 2(\theta+\phi)}{\sin 2(\theta-\phi)}. \tag{3.17}$$

On the other hand, it is also possible to show that the net *lattice* spin rate in the band is

$$\Omega_{12}^* = 1/2\left(1 - \frac{\cos 2\theta}{\cos 2\phi}\right)\dot{\gamma} \tag{3.18}$$

where $\dot{\gamma}$ is the net shearing rate in the band. If $\theta \approx 40$ deg with $\phi \approx 30$ deg, $\Omega_{12}^* > 0$ and lattice tends to rotate *away* from the tensile axis. This has the effect of increasing the Schmid stress on the primary system and promoting additional slip. In other words as the slip direction rotates from an initial angle of 30 deg *toward* the maximum shear stress 45 deg orientation, the dominant slip system becomes "geometrically softened." This is an example of a textural softening effect that leads to highly localized and potentially unstable flow.

When $\phi = 60$ deg in this model a rather different nonuniform mode appears. If we again take $q = 1$ for illustration we find $\mu/\mu^* < 0$, $(\sigma/2\mu^*)/(\mu/\mu^*) = -0.05$, and the trajectory is along the line of slope -0.05 in the hyperbolic regime. Now during a typical program of straining the magnitude of μ/μ^* increases and Peirce et al. [8] have shown that as $\mu/\mu^* \to -\infty$, $\theta_1 \to 45$deg and $\theta_2 \to 60$ deg; when $\mu/\mu^* > -2.0$, $\theta_1 < 30$ deg and $\theta_2 > 60$ deg. Figure 9 shows, therefore, that the first bands to appear, which are characterized by active loading on both systems, have orientations 30 deg $\le \theta \le$ 45 deg and are dominated by conjugate slip. The lattice rotations specified by (3.18) would in this case indicate that eventually the conjugate system becomes geometrically hardened (after an initial softening) whereas the Schmid stress on the primary system becomes negligible and may indeed vanish. Thus this mode will not tend to accumulate arbitrarily large strains.

The slip patterns expected from these two modes are sketched in Fig. 9. The shear band modes predicted when $\phi =$ 30 deg are known to compare to shear bands found ex-

Downloaded 02 May 2010 to 171.66.16.250. Redistribution subject to ASME license or copyright; see http://www.asme.org/terms/Terms_Use.cfm

perimentally in face-centered-cubic crystals. Lattice rotations that produce geometrical or textural softening have been documented [25, 2]. For the modes corresponding to "bands of secondary slip" the comparison is only qualitative at present, but the slip pattern does resemble that shown earlier in Fig. 5.

One of the more striking aspects of the phenomena just described is their dependence on lattice kinematics. The development of texture and the softening or hardening associated with it depends on the precise specification of the slip mode. If this is not uniquely specified a detailed analysis becomes impossible. As pointed out in Section 2.6, slip-mode uniqueness is generally difficult to guarantee when a full range of material properties are used and for this reason it appears that a full analysis of slip phenomena in crystals undergoing multiple slip will not be possible within a rate-independent framework. Peirce et al. [8] have now extended the theory to incorporate rate-dependent material behavior and have carried out finite element calculations of nonuniform and localized flow in single crystals. The reader is directed to their work for further details.

4 A Direction for Future Research

One of the more important outstanding problem areas in crystalline plasticity is the development of models for large strain deformation of polycrystals. The need for this has been made clear in recent years, especially in connection with studies of nonuniform and unstable deformation. For example, the softening effects produced by yield vertexes in rate-independent plasticity in response to nonproportional stressing have been shown to promote localized plastic flow in cases where homogeneous flow would otherwise be expected [21, 2, 23]. It is well known that micromechanical models for crystalline slip such as presented in the previous sections lead to vertex structure for polycrystals even at small strains [9, 18]. What has not been explored in near sufficient detail, however, are the very important effects of deformation-induced anisotropy on material stiffness at large strains. A promising, albeit challenging, direction, therefore, is the extension of the micromechanical theory outlined in the foregoing to a description of polycrystalline plasticity at large strains. A vital feature of such models should be the description of deformation-induced anisotropy, and ultimately a proper description of phenomena occurring at grain boundaries.

One important cause of anisotropy is the formation of crystallographic texture. In his now classic treatment of axisymmetric tension in face-centered-cubic polycrystals, Taylor [3] described how the slip-induced rotation of the lattice within the grains caused a $<111>-<100>$ "fiber" texture to develop in aggregates with an initially *uniform* array of grain orientations. That is, the grains in an initially isotropic aggregate tend to take on crystallographic orientations that align either a $<111>$ or $<100>$ type crystallographic direction with the tensile axis. Taylor's original analysis has been the inspiration and conceptual foundation of a broad range of further experimental and theoretical study of texture in metal polycrystals [29]. Nearly all of the work, however, has been confined to small strains and thus provides only suggestions of the vital influences texture has on material behavior at large strains. What is suggested, on the other hand, appears of sufficient importance to warrant a considerable new effort. In closing, an example of some intriguing and evidently important strain-hardening phenomenology is outlined.

Effect of Texture on Strain Hardening. As mentioned in the foregoing, there is a widespread interest in documenting and describing material strain-hardening at large strains. For this purpose experimental techniques such as wire drawing and torsion testing are commonly used to avoid the inherent instabilities of simple tension tests [30]. What is commonly observed, however, is that the flow stresses and strain-hardening rates measured in torsion are much less than those extracted from tension tests. Examples of this have recently been given by Shrivastava et al. [31] who suggest that deformation texture accounts for a good part of the observed effect.

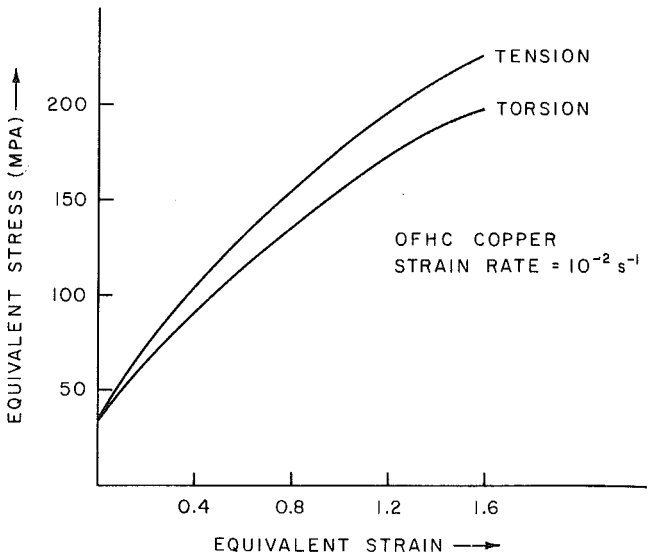


Fig. 10 Strain-hardening curves for copper as extracted from separate torsion and tension tests. The curves are taken from the paper by Shrivastava et al. [31] who conclude that torsion is characterized by a lower strain-hardening rate than tension.

Figure 10 shows a comparison of strain-hardenig curves for single-phase polycrystalline copper taken from the work of Shrivastava et al. [31]. The curves are compared in the basis of equivalent stress versus what they define as equivalent strain. The equivalent stress is defined as

$$\sigma_{eq} = \sqrt{3J_2} \tag{4.1}$$

where J_2 is the second invariant of deviatoric Cauchy stress. Equivalent strain was computed by integrating the expression for the increment in equivalent strain, defined as in (4.1) but multiplied by a factor of 2/3 with the invariant of strain deviator replacing J_2, along the entire strain path. In this way Shrivastava et al. [31] established a correspondence between torsion and simple shear in that $\epsilon_{eq} = \gamma\sqrt{3}$ in both cases. For the tension test they took $\epsilon_{eq} = ln\ \lambda_1$ where λ_1 is the stretch along the tensile axis. The difference between the tension and torsion strain-hardening curves shown for this example is representative for a wide range of face-centered-cubic metals. Furthermore, although it may be argued that presenting data in terms of these particular equivalent quantities is arbitrary, the effect illustrated is qualitatively common to other strain measures.

Shrivastava et al. [31] suggest that the role of texture may be seen as follows. For an isotropic face-centered-cubic polycrystal deformed in axisymmetric tension, Taylor [3] had shown that the average ratio of cumulative shear-strain increments on the active slip systems to the increment of principal tensile strain was approximately 3.06. Taylor's model was rigid plastic and based on the assumption that all grains were subject to the *same axisymmetric strain increment*. This latter aspect of the model is often overlooked, by the way. The procedure of imposing axisymmetric strain increments to simulate a tension test requires justification, and in Taylor's specific calculation, this was provided by the additional assumption of initial isotropy of the aggregate.

Downloaded 02 May 2010 to 171.66.16.250. Redistribution subject to ASME license or copyright; see http://www.asme.org/terms/Terms_Use.cfm

Taylor's calculations were confined to a neighborhood around initial yield and indicated only the initial trends in grain rotation and texture development. The result of his analysis is that if τ_c is the slip-plane yield stress, common to all slip systems, the tensile yield stress is $\sigma = 3.06\ \tau_c$. With the adopted definition of equivalent stress this yields $\sigma_{eq}^{yT} = 3.06\ \tau_c$. Bishop and Hill [32] later extended the Taylor model to yielding of polycrystals comprised of rigid-plastic grains subjected to multiaxial loading and found that for initially isotropic face-centered-cubic polycrystals the yield strength in shear was approximately $1.65\ \tau_c$. Again with the definition of equivalent stress adopted in the foregoing, this means that $\sigma_{eq}^{ys} = 1.65\sqrt{3}\ \tau_c = 2.86\ \tau_c$. Thus with the understanding that these models yield upper-bound approximations to the actual yield strengths, the yield strength in torsion is expected to be some 6.5 percent lower than in tension.

Now the numbers 3.06 and 1.65 have come to be known in the metallurgical literature as average Taylor factors. They are computed for each grain by imposing the aggregate strain and determining the active slip systems and the amounts of shear on each of them in accordance with isotropic hardening and Taylor's [3] minimum work principal or equivalently Bishop and Hill's [32] maximum work postulate. For axisymmetric tension, for example, the Taylor factor equals 3.674 for a face-centered-cubic grain aligned with a $<111>$ direction along the tensile axis and 2.449 for a grain aligned along a $<100>$ direction. To the extent that the aggregate remains transversely isotropic it is found that the fiber texture described earlier tends to increase the average value of this factor above the isotropic aggregate value of 3.06 thereby causing a textural hardening. Another way of appreciating this is by noting that the so-called Taylor factor represents the ratio of the cumulative shear-strain increment on the active slip systems to the maximum principal strain increment produced by the slips. Qualitatively, then, the lower the value of the Taylor factor the less total slip is required to produce the imposed strain increment. When the strain hardening is approximately isotropic a similar comment may be made concerning the strain-hardening increment, $d\tau_c$. The situation is somewhat different for torsion.

At finite strains the texture developed in torsion can be described as composed of three principal comonents which involve placing {111}, {112}, or {101}-type crystal planes in the plane of shear and, respectively, $<112>$, $<111>$, or $<110>$-type directions parallel to radial directions. Citing Shrivastava et al. [31], this has the effect of slightly reducing the average Taylor factor from the Bishop and Hill value of 1.65 which leads to a textural softening. Furthermore a qualitative study of the slip mode in these two cases indicates that in tension, the strong $<111>$ texture component in materials like copper involves the activation of possibly six slip systems (as judged within the rate-independent theory) while in torsion the stronger {111} component described in the foregoing would involve only one slip system. For the other texture components the situation is similar in that tension involves slip on many systems while in torsion only one or two are active. The point here is made most effectively by calling to mind the discussion of Section 2.6 on latent hardening and by extrapolating our discussion a bit beyond the Taylor model.

Taylor's calculatons were based on the assumption of isotropic hardening i.e., $q = 1$ (cf Section 2.6). Experimental observations suggest that q is larger than 1 for systems whose slip planes intersect. Thus the operation of six or eight systems in the case of axisymmetric tension should involve a greater increment in strain hardening (i.e., the increase in τ_c) for a given cumulative shear strain than for the corresponding case in torsion. Thus there are two effects proposed here, both strongly kinematical in nature: the first is that simple shear (identified with torsion) has a lower net Taylor factor than axisymmetric tension, which means that for a given increment of equivalent strain, a smaller increment in cumulative glide strain is required; the second is simple shear involves the operation of fewer intersecting slip systems and should accordingly be characterized by a reduced overall strain-hardening rate.

There is little value in pursuing this speculative line much further in the context of small strain-rate-independent models such as the Taylor model. For one thing, the kinematical nonuniqueness associated with rate independence renders clear cut analyses of texture development itself impossible, especially when realistic descriptions of latent hardening are included. In addition, there are other cautions concerning the interpretation of experimental data that must be born-in mind in pursuing future study. For example, the preceding discussion has been concerned with the possible, or perhaps likely, role of deformation-induced crystallographic texture. There is also the matter of texturing of the material itself, involving inter alia the elongating and flattening of grains. In a rate-dependent formulation the slip mode is unique but dependent on stress state. Gross alterations in grain shape would affect the manner in which neighboring grains interact and thereby affect the slip modes. Similar complications arise no doubt from very fine grain size. Neither of these have as yet been included in polycrystalline models.

Polycrystalline models developed to data fall within two broad categories. First is the Taylor isostrain type as extended by Bishop and Hill [32] for rate-independent materials and by Hutchinson [15] for rate-dependent (but small strain) creep. The second is the class of self-consistent models, in particular as proposed by Hill [33], and again used by Hutchinson [15] for time-dependent materials deforming by steady-state power law creep. In either case rate dependence and the slip-mode uniqueness it imparts would appear to be vital to produce a well-posed kinematical structure so that texture evolution may be unambiguously predicted. In addition, the models used to study texture development should not be based on a priori prescribed strain increments as in the Taylor model. Typical (homogeneous) deformation processes would specify some of the strain rates and other (nonconjugate) stress rates. For example, a model for a simiple tension test might specify the axial strain rate, possibly the *orientation* of the principal tensile fiber, and vanishing transverse stresses. Models of this type could be used, for example, to assess the effects of tension on the development of textural softening in shear, on whether this leads to significantly reduced softening with respect to nonproportional stressing, and if this would promote unstable or localized flow. In this regard we note that Dillamore and coworkers [34] have reported experimental evidence that localized shear bands in polycrystals are characterized by textural softening.

Acknowledgments

This manuscript was prepared with the support of the Brown University Materials Research Laboratory funded by the U. S. National Science Foundation. The collaboration and many fruitful discussions I have had with A. Needleman and J. R. Rice dealing with the mechanics of crystals are also gratefully acknowledged.

References

1 Argon, A. S., ed., *Constitutive Equations in Plasticity*, MIT Press, Cambridge, Mass., 1975.

2 Asaro, R. J., "Micromechanics of Crystals and Polycrystals," in *Advances in Applied Mechanics*, Vol. 23, Academic Press, in press.

3 Taylor, G. I., "Plastic Strain in Metals," *J. Inst. Metals*, Vol. 62, 1938, pp. 307-324.

Downloaded 02 May 2010 to 171.66.16.250. Redistribution subject to ASME license or copyright; see http://www.asme.org/terms/Terms_Use.cfm

4 Hill, R., and Rice, J. R., "Constitutive Analysis of Elastic-Plastic Crystals at Arbitrary Strain," *J. Mech. Phys. Solids*, Vol. 20, 1972, pp. 401-413.

5 Hill, R., "Generalized Constitutive Relations for Incremental Deformation of Metal Crystals by Multislip," *J. Mech. Phys. Solids*, Vol. 14, 1966, pp. 95-102.

6 Asaro, R. J., and Rice, J. R., "Strain Localization in Ductile Single Crystals," *J. Mech. Phys. Solids*, Vol. 25, 1977, pp. 309-338.

7 Peirce, D., Asaro, R. J., and Needleman, A., "An Analysis of Nonuniform and Localized Deformation in Ductile Single Crystals," *Acta Metall.*, Vol. 30, 1982, pp. 1087-1119.

8 Peirce, D., Asaro, R. J., and Needleman, A., "Material Rate Dependence and Localized Deformation in Crystalline Solids," in press.

9 Hill, R., "The Essential Structure of Constitutive Laws for Metal Composites and Polycrystals," *J. Mech. Phys. Solids*, Vol. 15, 1966, pp. 79-95.

10 Rice, J. R., "On the Structure of Stress-Strain Relations for Time-Dependent Plastic Deformation in Metals," ASME JOURNAL OF APPLIED MECHANICS, Vol. 37, 1970, pp. 728-737.

11 Rice, J. R., "Inelastic Constitutive Relations for Solids: An Internal-Variable Theory and its Application to Metal Plasticity," *J. Mech. Phys. Solids*, Vol. 19, 1971, pp. 433-455.

12 Hill, R., and Rice, J. R., "Elastic Potentials and the Structure of Inelastic Constitutive Laws," *SIAM, J. Appl. Math.*, Vol. 25, 1973, pp. 448-461.

13 Hill, R., "On Constitutive Inequalities for Simple Materials," *J. Mech. Phys. Solids*, Vol. 16, 1968, pp. 229-242; pp. 315-322.

14 Hill, R., "Aspects of Invariance in Solid Mechanics," in *Advances in Applied Mechanics*, Vol. 18, 1978, pp. 1-75.

15 Hutchinson, J. W., "Bounds and Self-Consistent Estimates for Creep of Polycrystalline Materials," *Proc. Roy. Soc.*, Series, A, Vol. 348, 1976, pp. 101-127.

16 Pan, J. and Rice, J. R., unpublished research, Brown University, 1981.

17 Kocks, U. F., "The Relation Between Polycrystalline Deformation and Single-Crystal Deformation," *Metall. Trans.* Vol. 1, 1970, pp. 1121-1142.

18 Hutchinson, J. W., "Elastic-Plastic Behavior of Polycrystalline Metals and Composites," *Proc. Roy. Soc.*, Series A, Vol. 319, 1976, pp. 247-272.

19 Hill, R., "A General Tehory of Uniqueness and Stability in Elastic-Plastic Solids," *J. Mech. Phys. Solids*, Vol. 6, 1958, pp. 236-249.

20 Havner, K. S., and Shalaby, A. H., "A Single Mathematical Theory of Finite Distortional Latent Hardening in Single Crystals," *Proc. Roy. Soc.*, Series A, Vol. 358, 1977, pp. 47-70.

21 Rice, J. R., "The Localization of Plastic Deformation," in *Proceedings of 14th International Congress of Theoretical and Applied Mechanics*, I, North-Holland, 1977.

22 Hutchinson, J. W., and Tvergaard, V., "Surface Instabilities on Statistically Strained Plastic Solids," *Int. J. of the Mech. Sci.*, Vol. 22, 1980, pp. 339-354.

23 Needleman, A., and Rice, J. R., "Limits to Ductility Set by Plastic Flow Localization," in *Mechanics of Sheet Metal Forming*, Koistinen, D. P., and Wang, N. M., eds., Plenum Press, New York, 1978, pp. 237-

24 Sawkill, J., and Honeycombe, R. W. K., "Strain Hardening in Face-Centered Cubic Metals Crystals," *Acta Metal.*, Vol. 2, 1954, pp. 854-864.

25 Chang, Y. W., and Asaro, R. J., "An Experimental Study of Shear Localization in Aluminum-Copper Single Crystals," *Acta Metal.*, Vol. 29, 1981, pp. 241-257.

26 Boas, W., and Ogilvie, G. J., "The Plastic Deformation of a Crystal in a Polycrystalline Aggregate," *Acta Metall.*, Vol. 2, 1954, pp. 655-659.

27 Biot, M., *Mechanics of Incremental Deformations*, Wiley, New York, 1965.

28 Hill, R., and Hutchinson, J. W., "Bifurcation Phenomena in Plane Strain Tension Test," *J. Mech. Phys. Solids*, Vol. 23, 1975, pp. 239-264.

29 Gil Sevillano, J., van Houtte, P., and Aernoudt, E., "Large Strain Work Hardening and Textures," *Progress in Materials Science*, Vol. 25, 1980, pp. 69-412.

30 Hecker, S. S., Stout, M. G., and Eash, D. T., "Experiments on Plastic Deformation at Finite Strains," in *Plasticity of Metals at Finite Strain*, Lee, E. H., and Mallett, R. L., eds., Stanford Univ. Publ., 1982, pp. 162-205.

31 Shrivastava, S. C., Jonas, J. J., and Canova, G., "Equivalent Strain in Large Deformation Torsion Testing: Theoretical and Practical Considerations," *J. Mech. Phys. Solids*, Vol. 30, 1982, pp. 75-90.

32 Bishop, J. F. W., and Hill, R., "A Theoretical Derivation of the Plastic Properties of a Polycrystalline Face-Centered Metal," *Philos. Mag.*, Vol. 42, 1951, pp. 414-427.

33 Hill, R., "A Self-Consistent Mechanics of Composite Materials," *J. Mech. Phys. Solids*, Vol. 13, 1965, pp. 213-222.

34 Dillamore, I. L., Roberts, J. G., and Bush, A. C., "Occurrence of Shear Bands in Heavily Rolled Cubic Metals," *J. Metal Sci.*, Vol. 13, 1979, pp. 73-77.

Downloaded 02 May 2010 to 171.66.16.250. Redistribution subject to ASME license or copyright; see http://www.asme.org/terms/Terms_Use.cfm

Shell Stability

C. D. Babcock
Graduate Aeronautical Laboratories,
California Institute of Technology,
Pasadena, Calif. 91109
Mem. ASME

Recent advances in shell buckling research are reviewed. Five separate subject areas are covered: elastic postbuckling behavior and imperfection sensitivity, plastic buckling, dynamic buckling, experiments and computations. Recent history of the research is presented emphasizing important advances in understanding. Areas of needed research and current trends are pointed out.

1 Introduction

A recent review of buckling problems began with the statement that "Everybody loves a buckling problem" [1]. Certainly from the number of papers (and reviews) published on the subject, this statement cannot be doubted. If the subject is enlarged to include all shell problems, Sechler [2] has provided us with a quantitative measure of the written work on this subject (Fig. 1). Extrapolation of his results to the 50th year of the JOURNAL OF APPLIED MECHANICS would indicate that 1220 papers on shells were written this year. This might be an overestimation, but is probably within a factor of two or three. Carrying out the extrapolation to the 100th anniversary would show a production rate of 53,600 papers per year.

It was perhaps this type of extrapolation that led the JOURNAL OF APPLIED MECHANICS [3] in 1962 to make the editorial decision to "exlcude" full-length papers on ". . . shell solutions found by employing routine procedures for small displacements. . . ," "eigenvalue problems of . . . buckling requiring little extension of established mathematical methods," and "computer solutions to problems (no matter how interesting) made tractable solely by . . . computing machines . . . ." Fortunately, these exclusions did not have much effect, because if they had, much of what I have reviewed would not have been written.

Editors aside, there is another class of people who would prefer to avoid buckling problems: those who actually experience them in practice. Figure 2 shows the results of a buckling failure of a buoyancy tank for an offshore platform jacket [4]. Sixteen of these tanks (and a few other jacket parts) collapsed during an attempted installation of the jacket in 1974. Failures of this type occur rather regularly but they represent an extremely small number as compared to buckling critical structures that do not fail. However, in an increasingly industrialized society that is becoming ever more material cost conscious, the number of buckling critical structures is rapidly increasing. This, and the challenge of buckling problems is what drives the paper barrage.

What has the research community produced in understanding and useful results over the last 20 years or so? This reviewer approaches the task of answering this question with some trepidation, especially when realizing that the appropriate design equations for preventing the failure shown

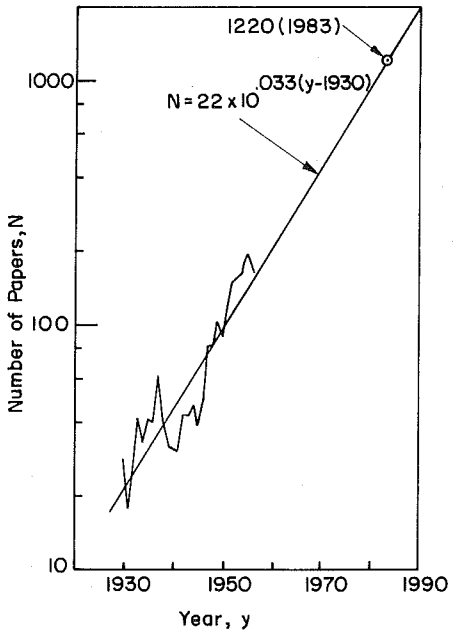


Fig. 1 Shell papers written as a function of year [2]

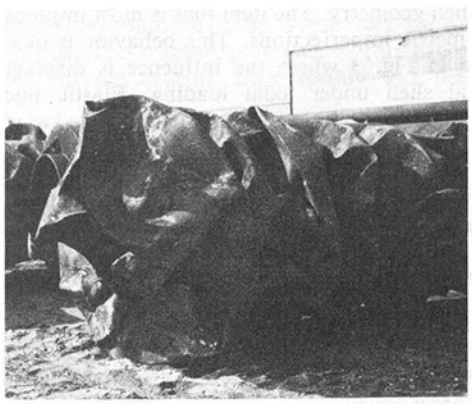


Fig. 2 Buckled buoyancy tank [4]

Contributed by the Applied Mechanics Division for publication in the JOURNAL OF APPLIED MECHANICS.

Discussion on this paper should be addressed to the Editorial Department, ASME, United Engineering Center, 345 East 47th Street, New York, N.Y. 10017, and will be accepted until two months after final publication of the paper itself in the JOURNAL OF APPLIED MECHANICS. Manuscript received by ASME Applied Mechanics Division, April, 1983.

Copyright © 1983 by ASME
Downloaded 02 May 2010 to 171.66.16.250. Redistribution subject to ASME license or copyright; see http://www.asme.org/terms/Terms_Use.cfm

in Fig. 2 were developed long ago. It is apparent that there have been great advances in the understanding of buckling problems. Equally apparent is the fact that this knowledge and understanding has become a self-perpetuating monster which awaits a modern day Timoshenko to tame it and place it in the service of the practicing engineer.

This review has been broken down into five subsections covering elastic postbuckling behavior and imperfection sensitivity, plastic buckling, dynamic buckling, experiments, and computations. Each of these subjects has been the object of many reviews and I will concentrate on extremely brief histories, important advances, and personally biased conclusions. Most reference works are drawn from the American and Western European literature.

2 Elastic Postbuckling and Imperfection Sensitivity

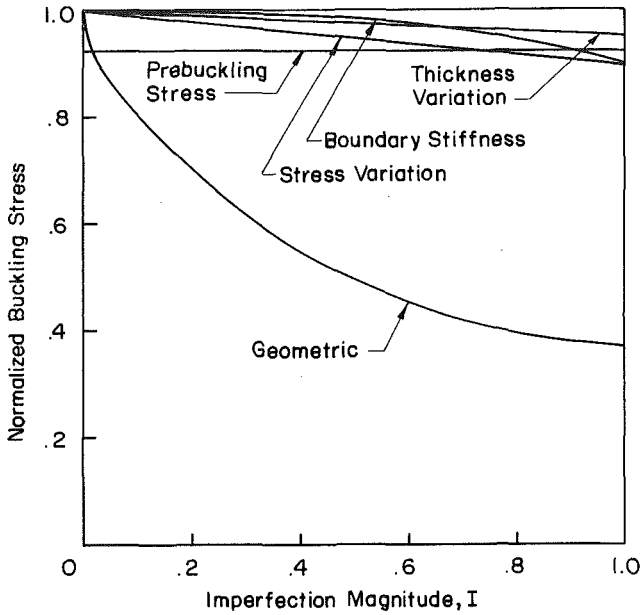
This subject is one that has been the object of much research and many reviews in the past 20 years. It is even difficult reviewing the reviews since so many have been written. Rather than doing this, I will attempt to give an extremely brief history of the subject, point out a number of review works, and end with a few observations.

Elastic postbuckling behavior of shell structures was rather strikingly introduced by Karman, Tsien, and Dunn [5–7] in the early 40s. Koiter [8] was able to connect the initial postbuckling behavior with the imperfections sensitivity and showed that the analysis can be accomplished in an elegant asymptotic manner. This type of analysis has been used to examine a large number of problems. The analysis has also been developed in quite general terms. Survey articles have been written by Hutchinson and Koiter [9], Budiansky and Hutchinson [1, 10], Tvergaard [11], and Citerley [12]. The general theory has been further developed by Sewell [13], Thompson [14], and Budiansky [15]. The four survey papers referenced in the foregoing contain almost 800 references which indicates the extent of the work on this one subject and the impossibility of adequately reviewing the work.

This great volume of work has firmly established the imperfection sensitivity of some shell/load combinations and developed analysis procedures to examine other problems. This certainly has been one of the great successes in mechanics research, but unfortunately one that has had little effect on engineering practices. This might be considered a somewhat controversial or even inappropriate statement in a survey paper and I would welcome examples that would show it to be incorrect. But let me examine the lessons learned from imperfection sensitivity.

Some shell structures when subjected to certain loads buckle at stresses lower that those predicted. The reason for this discrepancy is manifold; such items as nonuniform shell thickness, nonuniform loading, inaccurately modeled boundary conditions, influence of prebuckling deformations (nonmembrane prebuckling stresses), and deviations from the perfect shell geometry. The item that is most important is the last, geometric imperfections. This behavior is qualitatively displayed in Fig. 3 where the influence is displayed for a cylindrical shell under axial loading. Elastic buckling is assumed. The horizontal axis is artificially scaled to reflect the author's guess as to reasonable magnitudes of the "imperfections." This figure should be convincing that the geometric imperfection is the most important factor.

A quantitative measure of the sensitivity of the system to certain geometric imperfections can be calculated. This sensitivity to imperfections is reflected in the magnitude of the "knockdown" factor[1] chosen by the engineer when predicting



Imperfection	Value	Ref
Geometric	$\delta/t = .2$	16
Stress Variation	$\sigma = \sigma_o \pm 0.10\sigma_o$	17
Boundary Stiffness	$N_{xy} = \frac{kEA\eta^2}{R} v$ $\frac{1}{k} = 0 \rightarrow 3$	18
Thickness Variation	$t = t_o \pm 0.05t_o$	
Prebuckling Stress	$u = v = w = \beta = 0$	19

R = Shell Radius
δ = Imperfection Amplitude
t = Shell Thickness
σ_o = Applied Axial stress
u,v,w,β = Axial, Circumferential and Radial Displacements Meridional Rotation
N_{xy} = Inplane Shear Resultant
E = Young's Modulus
A = End Ring Area
n = Number of Circumferential Waves

Fig. 3 Effect of "imperfections" on critical stress-cylindrical shell under axial load

the expected buckling load. The imperfection sensitivity plays no direct role in the process of deciding on this factor but is included indirectly in experimental data used in the choice of a value. Unfortunately, very little has been accomplished in improving this situation. Budiansky and Hutchinson [16] looked at the cylindrical shell under axial compression and showed that for an axisymmetric imperfection the postbuckling behavior becomes stable for a knockdown factor less than about one-third. Unfortunately the observed radius-to-thickness dependence of this factor did not come out of the analysis. Citerley [20] relates shell manufacturing tolerance guidelines to imperfection sensitivity analysis and recommended knockdown factors. He finds inconsistencies in the recommendations and states that improved prediction procedures will depend on establishing appropriate imperfections for use in "qualified" numerical procedures. Elishakoff [21] pursues the concept of reliability using the Monte Carlo method. Again the problem of suitable initial imperfections arises. Arbocz and Babcock [22–25] have engaged in a lengthy program to use laboratory scale shells to establish the validity of methods to predict "knockdown" factors. Arbocz at Delft [26] and Signer at Technion have established a data bank of shell imperfections with the goal of providing a data base for design imperfections. A preliminary procedure to use this type of data and a hierarchy of analysis procedures was proposed by Arbocz and Babcock [27], but this procedure is still a straw man. Another attempt to get imperfection sensitivity analysis into design practice was carried out by Cohen who implemented the so-called "*b*

[1] The "knockdown" factor is the reduction factor used to determine the expected buckling load based on a calculated buckling load not accounting for imperfections. It can vary from 1.0 to as low as 0.1.

Downloaded 02 May 2010 to 171.66.16.250. Redistribution subject to ASME license or copyright; see http://www.asme.org/terms/Terms_Use.cfm

factor'' calculation into his series of shell-of-revolution codes [28]. This code has been used in research endeavors but has not been used in actual design to my knowledge.

The mechanics research over the past 40 years has produced a great deal of understanding about elastic postbuckling and imperfection sensitivity. There still exist a large number of technically important problems to tackle, particularly in structures that exhibit coincident or nearly coincident buckling loads. Unfortunately, all of this understanding has had little impact on the manner in which buckling-critical shells are currently designed. The actual design problem seems to rapidly get bogged down in details that cannot be easily accommodated by the asymptotic approach. An attempt to improve on this situation, by wedding the asymptotic approach with the finite element method, was initiated [29] but it has not been further pursued. Another ''interim'' approach was proposed [30] which used an effective axisymmetric imperfection along with a probability based ''knockdown'' factor. The further development of these procedures which exploit the present understanding of the problem is a task that badly needs the attention of the research community.

3 Dynamic Buckling

Dynamic buckling is generally meant to describe the buckling of structures under transient loads. It is obvious that all loads are transient. The experimentalist implicitly assumes that if the experiment is to be ''static,'' the loads are applied on a time scale that is large compared to the ''buckling time.'' However, in many applications (impact, earthquake, blast, gust, maneuvering), this is not the case and the complete dynamic problem must be addressed.

Over the past 20 years there have been many studies on shell structures subjected to transient loadings which, if applied statically, would lead to a buckling failure. The common types of loading that are analyzed are the step and impulse loads. Budiansky and Hutchinson [31–33] have provided the most general results for these loads when applied to imperfection sensitive shell/load combinations. The results are quite general, but the analysis is restricted to simple structures and loads so that the mathematics reduces to a few degrees of freedom. The equations can then be handled either algebraically or studied numerically.

Budiansky [32] addresses the problem of dynamic buckling resulting from a Mathieu-type instability. Special cases of this type have been treated [34–36] but the analysis of Budiansky is carried out in some generality. The results must be used with some caution since damping can play an important role in this problem and shells generally have many possible modes of buckling. In addition, very few experiments exist that are useful in deciding the robustness of the results. The importance of the analysis actually lies in the elucidation of phenomena that one may encounter in direct numerical approaches to the dynamic buckling problem.

The problem becomes much more complex when the solution must be obtained numerically as shown by Almroth, Meller, and Brogan [37]. Even for the problem of a homogeneous shell with cutouts, the computer time may become prohibitive.

In carrying out a numerical dynamic buckling anlaysis, the time-dependent solution must be obtianed for a succession of loads. From these results, the ''dynamic buckling load'' is deduced by using some measure of the transient response and observing its behavior as a function of the load. The confusion arising from the calculation of buckling loads stems from the necessity of using this procedure. This also makes the connection with the static buckling load somewhat tenuous.

An alternative to a complete numerical solution of the dynamic buckling problem is to treat the problem as a transient dynamic problem (linear or nonlinear) and then assume that at any instant of time the stresses in the shell are static. One then performs a bifurcation analysis using as the prebuckling state the calculated stresses or some manipulation of them. This ''freezing in time'' technique is commonly used in practice for complex structures but has received little attention by the research community. An exception is Akkas [38] who treats the shallow spherical cap in this manner.

The justification for this dynamic buckling calculation has not been presented in general terms. It is obvious that the analyst assumes that there exists a large separation in the time scales: loading characteristic time versus buckling time. The technique is analogous to the ''local buckling'' approach in static buckling of shells where the prebuckling stress (which is variable in space) is replaced by a uniform stress state for the buckling calculation. However, in this case, the procedure has been justified by many example calculations and experiments. It would seem that the time-scale problem could be treated in some generality, at least for simple shell/load combinations. An experimental approach for a rather complicated problem met with some success [39].

This has been a brief review of a very complex and often misunderstood problem. Fortunately, the nature of the dynamic buckling problem (i.e., an unacceptably large response under a transient load) has been clarified by a number of analytical and numerical studies. General results for dynamic buckling loads have been presented for special shell/load combinations that are imperfection sensitive. For problems that must be treated entirely numerically, the present procedures are not satisfactory. Since the ''freezing in time'' technique is commonly used, it is important to establish the criteria and associated error inherent in its implementation.

4 Plastic Buckling

Most shell structures undergo plastic deformation during a buckling test or accident. This occurs since shells usually have very little postbuckling load-carrying capability and in many tests and applications the situation is more or less load-controlled. The plastic deformation is the result of the postbuckling deformation and may not be associated with the initial buckling or the near postbuckling deformation. From an analysis standpoint, this allows the prediction of buckling using the assumption of elastic material behavior.

If the prebuckling loading results in plastic flow of the material, then buckling prediction not only has the usual computational problems but fundamental ones associated with the material model. Plastic buckling problems are not unique to shell stability and, in fact, have been addressed by practicing engineers for many years as related to column buckling. For the column, the problem was largely addressed by conducting many tests and drawing educated curves through the data. The curves approached the Euler limit for large slenderness ratios and the yield load for small slenderness ratios. The mechanics impact in this procedure was important but not crucial, since testing was feasible and prudent.

The mechanics of plastic column buckling was not resolved until 1947 [40] long after suitable design procedures had been adopted. The problem of shell stability is much more complicated since the stress is not one-dimensional and the mode is not well defined. The usual approach in industrial practice to determine the plastic buckling load [41, 42] is to carry out an elastic analysis and then either modify the elastic modulus using a combination of the tangent modulus and the secant modulus or use a capacity reduction factor based on test data. The manipulations of the modulus are based on analysis of particular cases but the technique is applied to loads and structures for which a suitable analysis does not exist.

Downloaded 02 May 2010 to 171.66.16.250. Redistribution subject to ASME license or copyright; see http://www.asme.org/terms/Terms_Use.cfm

Despite this lack of impact on industrial practice, the mechanics community has not been silent. In fact, over a period of 20 years the theoretical basis for plastic bifurcation has been clarified, postbuckling and imperfection sensitivity analysis carried out, and plastic buckling analysis implemented in some shell buckling numerical codes.

This history has been documented in a number of recent papers. Hill's work on the theoretical foundation of plastic bifurcation, carried out some 20 years ago, is reported in his recent paper [43]. Hutchinson [44, 45] presents extensive work which includes a number of plastic buckling examples ranging from simple models to shell structures. Problems of postbuckling and imperfection sensitivity are emphasized in this work. Plastic postbuckling is also treated by Needleman and Tvergaard [46]. The computer implementation of plastic buckling analysis is reviewed by Bushnell [47]. This reference also gives a large number of plastic buckling problems analyzed by Bushnell. Sewell [48] surveys plastic buckling problems and discusses a number of examples. He presents an organized reference list on plastic buckling which contains over 600 entries.

What can be said about all of the mechanics work that has been carried out on the problems of plastic buckling? I believe that probably the most important advancement is that the theoretical foundation of the bifurcation theory has been adequately laid. The postbuckling problem and the associated imperfection sensitivity has been extensively studied.

This work has clarified to a great extent the behavior found in experimental results. It has also been successful in isolating a fundamental aspect of plastic buckling (i.e., the details of the plastic material behavior can influence the analysis results). The nicest example of this is the cruciform column [49]. In this problem the results from the deformation theory of plasticity and those from the J_2 flow theory show considerable difference. It has been shown, however, that for this particular problem the theories can give similar results if initial imperfections are introduced. Whether these results can be generalized remains a question.

There still exists a need to clarify the problems associated with the plastic material models. This need is accentuated when dealing with cyclic plasticity which leads to buckling. While the situation may be quite clear to the mechanics researcher, the uncertainty that it creates for the engineer with a problem easily discourages the use of recent research results. There also exists a need to develop more universal design approaches which do not treat the plastic buckling simply as a reduction in capacity of the elastic buckling load.

5 Experiments

Only in recent years has it been acceptable to review experimental work on shell buckling. For many years the data from experiments/tests have been the subject of papers discussing design practices or correlations studies. However, only recently has the experimental work itself, not the results, been the subject of the reviews.

Babcock [50] reviewed techniques that mostly applied to research-type experiments. Singer [51] extended this to include a review of many experiments/tests carried out in the last 10 years and initiated a discussion of the motivation for carrying out experimental work. Sechler [52] wrote in a similar vein as he discussed the philosophy of experimental research. Singer recently updated his review [53] and also discussed specifically shell buckling research in Israel [54]. Miller [55] reviewed buckling tests on "fabricated" steel cylindrical shells which have been carried out in the U.S., and Valsgard, and Foss reviewed the work at Det Norske Veritas which has been very active in shell buckling research in the last 10 years [56].

From reading these reviews, and some of the papers that they reference, one is struck by a number of thoughts. First, as pointed out by Singer, the idea that one should measure the shape of the test specimen before carrying out the buckling test seems to have gained fairly wide acceptance. There have even been a number of attempts to assess the importance of the measured imperfections using a numerical solution. Unfortunately, these analyses have not met with much success. It appears to me that unless better use can be made of the imperfection data immediately by the experimenter, the motivation for taking the data will rapidly die out. This is particularly true of tests carried out to meet an immediate industry need.

Second, the testing that is being carried out to meet industry need (i.e., proof tests, code verifications, etc.) has not always been utilized by the research community to advance its understanding. For instance, the term "fabricated" shell has been increasingly used to describe large welded steel specimens used in buckling tests. I must assume that all other shell specimens are "unfabricated" or "not fabricated." On a more serious note, it is important to quantify the notion of "fabricated" and to establish the quality of the shell or the results of the manufacturing technique in a more scientific manner. It is difficult to believe that a model of a welded stiffened shell made in a random shop is of the same quality as the full-scale specimen until the quality can be accurately related to the knockdown factor (capacity reduction factor). It is feasible to do this if the test is carried out carefully and the analysis tools currently available are used to their fullest extent.

Third, there appears to be a great deal of testwork carried out, particularly for industrial needs, that uses poorly designed specimens. In many instances this results in a buckling mode (such as rib crippling) that can be either calculated or determined by much simpler, and much less expensive, test procedures. The large amount of money going into complicated shell buckling tests could be more effectively used if test specimens and the structures they represent were more optimally designed.

Fourth, there does not seem to be a great deal of fundamental experimental research being carried out in shell buckling. Some research groups continue to pursue fundamental questions that will hopefully lead to better designed shell structures. However, much work is going on that either fails to relate to analysis or uses analysis very poorly in designing specimens and qualifying test setups. This neglect may relegate much modern test work to the same graveyard used for the cellophane test specimens of the 30s. It would be unfortunate if in 10 years, when some other reviewer looks over the progress that has been made, very little of a fundamental nature is found.

6 Computations

By far the greatest advance in the last 20 years in shell stability has been the ability to solve the shell equations numerically. I will not dwell on the techniques developed, but only report on what has been accomplished. Other reviews in this volume deal with the advances in computational mechanics. Two problems dominated the early work in computational buckling problems. These were the spherical cap under uniform pressure load [57–60] and the cylindrical shell under uniform axial load [61, 19]. The first involves a highly nonlinear axisymmetric prebuckling solution followed by a linear eigenvalue problem. The cylinder problem has a closed-form prebuckling state followed by a linear eigenvalue problem. Out of these problems grew the general shell-of-revolution computer codes, which today are the most useful numerical tools in shell buckling problems [62–65]. This resulted since these analyses are actually one-dimensional

Downloaded 02 May 2010 to 171.66.16.250. Redistribution subject to ASME license or copyright; see http://www.asme.org/terms/Terms_Use.cfm

problems and can be solved quickly, inexpensively, and accurately.

In addition to the special purpose (i.e., buckling) computer codes, there exist a sizable number of general-purpose structural analysis codes which are capable of handling nonlinear collapse and bifurcation buckling for shells of revolution. To the buckling community these are not as important as one developed specifically for this problem. Bushnell has been the most active worker in this field and has summarized many of his experiences in a recent report [66]. This volume also contains a review of shell buckling problems and an extensive reference list. The report is almost 800 pages in length and it is impossible to adequately summarize his results. Suffice it to say that if the buckling problem faced by a designer is a shell-of-revolution under axially symmetric loads (or can be adequately approximated as such) there are highly developed computational methods available, and a great deal of experience has been accumulated by analysts, if not by designers.

The situation is not so rosy for two-dimensional discretizations of shell buckling problems. Here again, both general-purpose codes and special-purpose shell codes have been developed to handle the nonlinear-prebuckling analysis, the nonlinear collapse problem, and the linearized eigenvalue problem. A well-known special purpose code, STAGS, [67] has been exercised rather extensively for these types of problems.

The main obstacle to wider use in engineering practice of two-dimensional codes is still the large amount of computer time necessary for general loading on general shells. This is particularly true when the collapse or bifurcation modes are not apparent and may involve wave lengths much shorter than the dimensions of the shell structure being analyzed. To circumvent this problem some numerical work has been carried out to determine the accuracy of using a bifurcation solution with a linear prebuckling stress state as an approximation to the full-fledged analysis, [68]. Intuitive rules for situations when this is correct have been advanced, but more specific guidelines are needed. Analysts have been amazingly silent on this problem which is of great practical importance.

When the buckling problem justifies carrying out the complete nonlinear anlaysis, an extremely good comparison with experiments can be obtained. This is demonstrated in the case of elastic buckling of an axially loaded cylinder with cutouts as long as the cutout is the dominant "imperfection" [69, 70]. For buckling in the plastic range of the material, excellent results for a ring-stiffened cylinder under bending and axial compression is obtained with and without cutouts [71, 72].

This very brief review of the most revolutionary change in shell stability analysis can hardly do justice to the subject. However, its intent is only to point out the state of the art and the research subjects introduced by computational shell stability analysis. Several important conclusions stand out.

Shell of revolution buckling problems under axisymmetric loads have been effectively resolved by the development of reliable computer codes based on a one-dimensional discretization of the problem. Two-dimensional nonlinear shell buckling problems continue to be out of the reach of day-to-day analysis due to computational costs. The reduction of costs can be accomplished by either faster machines or clever techniques. There is no doubt that computation will become less expensive, but the development of approximate techniques should be pursued. For problems where the important details of the shell/load combination can be modeled and the system is imperfection insensitive for one reason or another, excellent agreement between computational results and experimental results can be obtained.

7 Conclusion

This review concentrated on five areas of shell stability which I thought focused on the majority of research efforts over the last 20 years. Many interesting and important problems within each area remain to be addressed. Among those of current interest are mode interaction problems, localization of buckling patterns, contact buckling problems, nondestructive buckling tests, and propagating buckling. Even the five areas that were included could only be treated superficially and I chose to concentrate on discussion and thoughts about current trends and future problems. This is a risky business at best, but one that is important for the research community to address. Like all fields of mechanics, the directions of research in shell stability are continually rebounding between basic understanding and practical application. This review is only one biased opinion on the proper trajectory.

Acknowledgment

The author would like to dedicate this work to Ernest E. Sechler, Professor, Colleague, and Friend whose influence on this review should be evident to those who knew him.

I would also like to acknowledge the assistance of his colleagues and the staff at the Graduate Aeronautical Laboratories, California Institute of Technology in carrying out and reporting shell buckling research over the past 25 years.

References

1 Budiansky, B., and Hutchinson, J. W., "Buckling: Progress and Challenge," *Trends in Solid Mechanics* 1979, Proceedings of the Symposium Dedicated to the 65th Birthday of W. T. Koiter, Delft University of Technology June 13–15, 1979, Besseling, J. F., and van der Heijden, A. M. A., eds., Delft University Press, 1979, pp. 93–116.

2 Sechler, E. E., "The Historical Development of Shell Research and Design," *Thin-Shell Strucutres, Theory, Experiments and Design*, Fung, Y. C., and Sechler, E. E., eds., Prentice-Hall, Englewood Cliffs, N.J., 1974, pp. 3–25.

3 ASME JOURNAL OF APPLIED MECHANICS, Vol. 29, No. 1, 1962.

4 Cottrill, A., "Crumpled Frigg Jacket Begins to Recover Its Lost Buoyancy," *Offshore Engineer*, May 1975, p. 32.

5 Karman, Th. von, and Tsien, H. S., "The Buckling of Spherical Shells by External Pressure," *Journal of Aerospace Sciences*, Vol. 7, 1939, pp. 43–50.

6 Karman, Th. von, Dunn, L. G., and Tsien, H. S., "The Influence of Curvature on the Buckling Characteristics of Structures," *Journal of Aerospace Sciences*, Vol. 7, 1940, p. 276.

7 Karman, Th. von, and Tsien, H. S., "The Buckling of Thin Cylindrical Shells Under Axial Compression," *Journal of Aerospace Sciences*, Vol. 8, 1941, p. 303.

8 Koiter, W. T., "Over de Stabiliteit van het Elastisck Evenwicht (On the Stability of Elastic Equilibrium)," Thesis, Delft, H. J. Paris, Amsterdam, 1945. English translation issued as NASA TT F-10, 1967.

9 Hutchinson, J. W., and Koiter, W. T., "Postbuckling Theory," ASME *Applied Mechanics Reviews*, Vol. 23, No. 12, 1970, pp. 1353–1366.

10 Budiansky, B., and Hutchinson, J. W., "A Survey of Some Buckling Problems," *AIAA Journal*, Vol. 4, No. 9, Sept. 1966, p. 1505.

11 Tvergaard, V., "Buckling Behaviour of Plate and Shell Structures," *Theoretical and Applied Mechanics*, W. T. Koiter, ed., North-Holland, 1976, pp. 233–247.

12 Citerley, R. L., "Imperfection Sensitivity and Post-Buckling Behavior of Shells," *Pressure Vessels and Piping: Design Technology - 1982 A Decade of Progress*, Zamrik, S. Y., and Dietrich, D., eds., ASME, New York, pp. 27–45.

13 Sewell, M. J., "A General Theory of Equilibrium Paths Through Critical Points, I, II.," *Proc. Roy. Soc.*, London, Series A, Vol. 306, 1968, pp. 201–223, pp. 225–238.

14 Thompson, J. M. T., "A General Theory for the Equilibrium and Stability of Discrete Conservative Systems," *Zeit. fur Math. und Physik*, Vol. 20, 1969, pp. 797–846.

15 Budiansky, B., "Theory of Buckling and Post-Buckling Behavior of Elastic Structures," *Advances in Applied Mechanics*, Vol. 14, Academic Press, New York, 1974, pp. 1–65.

16 Budiansky, B., and Hutchinson, J. W., "Buckling of Circular Cylindrical Shells Under Axial Compression," *Contributions to the Theory of Aircraft Structures*, Delft University Press, Rotterdam, 1972, pp. 239–259.

17 Bijlaard, P. P., and Gallagher, R. H., "Elastic Instability of a Cylindrical Shell Under Arbitrary Circumferential Variation of Axial Stress," *Journal of the Aerospace Sciences*, Nov. 1960, pp. 854–859.

18 Kobayashi, S., "The Influence of the Boundary Conditions on the Buckling Load of Cylindrical Shells Under Axial Compression," *Journal of the*

Downloaded 02 May 2010 to 171.66.16.250. Redistribution subject to ASME license or copyright; see http://www.asme.org/terms/Terms_Use.cfm

Japan Society for Aeronautical and Space Sciences, Vol. 16, No. 170, 1963, p. 74.

19 Almroth, B. O., "Influence of Edge Conditions on the Stability of Axially Compressed Cylindrical Shells," NASA CR-161, Feb. 1965.

20 Citerley, R. L., "The Use of Manufacturing Tolerances in Imperfection Analysis of Shells," *Pressure Vessel Design - PVP*, Vol. 57, Widera, G. E. O., ed., ASME, New York, pp. 49–66.

21 Elishakoff, I., "How to Introduce the Imperfection Sensitivity Concept Into Design," *The Buckling of Structures in Theory and Practice*, Thompson, J. M. T., and Hunt, G. W., eds., Cambridge University Press, Cambridge, 1983. *Proceedings of the IUTAM Symposium, University College*, London, Aug. 1982.

22 Arbocz, J., and Babcock, C. D., "Effect of General Imperfections on the Buckling of Cylindrical Shells," ASME JOURNAL OF APPLIED MECHANICS, Mar. 1969, pp. 28–38.

23 Arbocz, J., and Babcock, C. D., "Prediction of Buckling Loads Based on Experimentally Measured Initial Imperfections," *Buckling of Structures*, IUTAM Symposium, Cambridge/USA, 1974, Budiansky, B., ed., Springer-Verlag, Berlin, 1976, pp. 291–311.

24 Arbocz, J., and Babcock, C. D., "Utilization of Stags to Determine Knockdown Factors From Measured Initial Imperfections," Report LR-275, Delft University of Technology, Department of Aerospace Engineering, Delft, The Netherlands, 1978.

25 Arbocz, J., "Spell Stability Analysis: Theory and Practice," *The Buckling of Structures in Theory and Practice*, Thompson, J. M. T., and Hunt, G. W., eds., Cambridge University Press, Cambridge, 1983. *Proceedings of the IUTAM Symposium, University College*, London, Aug. 1982.

26 Arbocz, J., and Abramovich, H., "The Initial Imperfection Data Bank at the Delft University of Technology, Part I," Report LR-290, Delft University of Technology, Department of Aerospace Engineering, Delft, The Netherlands, 1979.

27 Arbocz, J., and Babcock, C. D., "The Buckling Analysis of Imperfection Sensitive Shell Structures," NASA Contractor Report 3310, Aug. 1980.

28 Cohen, A. G., "Computer Analysis of Imperfection Sensitivity of Ring-Stiffened Orthotropic Shells of Revolution," *AIAA Journal*, Vol. 9, 1971, pp. 1032–1039.

29 Haftka, R. T., Mallett, R. H., and Nachbar, W., "Adaptation of Koiter's Method of Finite Element Analysis of Snap-Through Buckling Behavior," *International Journal of Solids and Structures*, Vol. 7, 1971, pp. 1427–1445.

30 Almroth, B. O., Burns, A. B., and Pittner, E. V., "Design Criteria for Axially Loaded Cylindrical Shells," *Journal of Spacecraft and Rockets*, Vol. 7, No. 6, 1970, pp. 714–720.

31 Budiansky, B., and Hutchinson, J. W., "Dynamic Buckling of Imperfection-Sensitive Structures," *Proceedings of the Eleventh International Congress of Applied Mechanics*, Munich, Germany, Goler, H., ed., Springer-Verlag, Berlin, 1964, pp. 636–651.

32 Budiansky, B., "Dynamic Buckling of Elastic Structures: Criteria and Estimates," *Dynamic Stability of Structures, Proceedings of an International Conference held at Northwestern University*, Evanston, Ill., Oct. 18–20, 1965, Herrmann, G., ed., Pergamon Press, Oxford, 1966, pp. 83–106.

33 Hutchinson, J. W., and Budiansky, B., "Dynamic Buckling Estimates," *AIAA Journal*, Vol. 4, No. 3, Mar. 1966, pp. 525–530.

34 Goodier, J. N., and McIvor, I. K., "The Elastic Cylindrical Shell Under Nearly Uniform Radial Impulse," ASME JOURNAL OF APPLIED MECHANICS, Vol. 31, 1964.

35 Tamura, Y. S., and Babcock, C. D., "Dynamic Buckling of Cylindrical Shells Under Step Loading," ASME JOURNAL OF APPLIED MECHANICS, Vol. 42, 1975, pp. 190–194.

36 Danielson, D. A., "Dynamic Buckling Loads of Imperfection-Sensitive Structures From Perturbation Procedures," *AIAA Journal*, Vol. 7, No. 8, Aug. 1969, pp. 1506–1510.

37 Almroth, B. O., Meller, E., and Brogan, F. A., "Computer Solutions for Static and Dynamic Buckling of Shells," *Buckling of Structures*, IUTAM Symposium, Cambridge/USA, 1974. Budiansky, B., ed., Springer-Verlag, Berlin, 1976, pp. 52–66.

38 Akkas, N., "Asymmetric Buckling Behavior of Spherical Caps Under Uniform Step Pressures," ASME JOURNAL OF APPLIED MECHANICS, Vol. 39, 1972, pp. 293–294.

39 Shih, C.-F., and Babcock, C. D., "Scale Model Buckling Tests of a Fluid Filled Tank Under Harmonic Excitation," Century 2 Pressure Vessel & Piping Conference, San Francisco, Calif., Aug. 12–15, 1980, ASME 80-C2/PVP-66.

40 Shanley, F. R., "Inelastic Column Theory," *Journal of Aerospace Sciences*, Vol. 14, 1947, pp. 261–267.

41 "Buckling of Thin-Walled Circular Cylinders," NASA Space Vehicle Design Criteria, NASA SP-8007, Aug. 1968.

42 Miller, C. D., "Code Case N-284, ASME Boiler and Pressure Vessel Code, 1980 Code Cases," *Nuclear Components*, ASME, New York, July 1980, pp. 633–656.

43 Hill, R., "Aspects of Invariance in Solid Mechanics," *Aspects in Applied Mechanics*, Vol. 18, 1978, pp. 1–75.

44 Hutchinson, J. W., "Plastic Buckling," *Advances in Applied Mechanics*, Vol. 14, 1974, pp. 67–143.

45 Hutchinson, J. W., "Post-Bifurcation Behavior in the Plastic Range," *Journal of Mechanics and Physics of Solids*, Vol. 21, 1973, pp. 163–190.

46 Needleman, A., and Tvergaard, V., "Aspects of Plastic Postbuckling Behavior," Hopkins, H. G., and Sewell, M. J., eds., Pergamon Press, Oxford, 1982, pp. 453–498.

47 Bushnell, D., "Plastic Buckling," *Pressure Vessels and Piping: Design Technology - 1982, A decade of Progress*, Zamrik, S. Y., and Dietrich, D., eds., ASME, New York, 1982.

48 Sewell, M. J., "A Survey of Plastic Buckling," Study No. 6, Solid Mechanics Division, University of Waterloo, Waterloo, Ontario, Canada, Ariarathnam, S. T., et al. eds., 1972, pp. 85–197.

49 Hutchinson, J. W., and Budiansky, B. W., "Analytical and Numerical Study of the Effects of Initial Imperfections on the Inelastic Buckling of a Cruciform Column," *Buckling of Structures*, IUTAM Symposium, Cambridge/USA, 1974; Budiansky, B., ed., Springer-Verlag, Berlin, 1976, pp. 98–105.

50 Babcock, C. D., "Experiments in Shell Buckling," *Thin-Shell Structures, Theory, Experiments and Design*, Fung, Y. C., and Sechler, E. E., eds., Prentice-Hall, Englewood Cliffs, N.J., 1974, pp. 345–369.

51 Singer, J., "Buckling Experiments on Shells—A Review of Recent Developments," Paper presented at Euromech Colloquium No. 128 "Stability, Buckling, and Postbuckling Behavior, Foundation and Analysis," Delft, March 31–April 2, 1980. Also, TAE Report 403, Dept. of Aeronautical Engineering, Technion, Israel Inst. of Technology, Apr. 1980.

52 Sechler, E. E., "The Role of Experimentation in Shell Research," *Mechanics Today*, Vol. 5, Nemat-Nasser, S., ed., Pergamon Press, 1980, pp. 439–449.

53 Singer, J., "The Status of Experimental Buckling Investigations of Shells," *Buckling of Shells*. Proceedings of a State-of-the-Art Colloquium. Ramm, E., ed., Springer, Berlin, 1982, pp. 501–533.

54 Singer, J., "Shell Buckling Research in Israel and its Application to Offshore Structures,"

55 Miller, C. D., "Summary of Buckling Tests on Fabricated Steel Cylindrical Shells in USA," *Offshore Structures Engineering III, Buckling of Shells in Offshore Structures*, Harding, J. E., Dowling, P. J., and Agelidis, N., eds., Gulf, Houston, 1982, pp. 429–473.

56 Valsgard, S., and Foss, G., "Buckling Research in Det Norske Veritas," *Offshore Structures Engineering III, Buckling of Shells in Offshore Structures*, Harding, J. E., Dowling, P. J., and Agelidis, N., eds., Gulf, Houston, 1982, pp. 491–549.

57 Reiss, E. L., Greenberg, H. J., and Keller, H. B., "Nonlinear Deflections of Shallow Spherical Shells," *Journal of Aerospace Sciences*, Vol. 24, 1957, pp. 533–543.

58 Budiansky, B., "Buckling of Clamped Shallow Spherical Shells," *Proc. IUTAM Symp. on the Theory of Thin Elastic Shells*, Delft, Netherlands, Koiter, W. T., ed., 1959, pp. 64–94.

59 Huang, N. C., "Unsymmetrical Buckling of Thin Shallow Spherical Shells," ASME JOURNAL OF APPLIED MECHANICS, Vol. 31, 1964, pp. 447–457.

60 Kaplan, A., "Buckling of Spherical Shells," *Thin-Shell Structures Theory, Experiment, and Design*, Fung, Y. C., and Sechler, E. E., eds., Prentice-Hall, Englewood Cliffs, N.J., 1974, pp. 247–288.

61 Stein, M., "The Influence of Prebuckling Deformations and Stresses on the Buckling of Perfect Cylinders," Report No. TR-190, National Aeronautics and Space Administration, Feb. 1965.

62 Kalnins, A., "Analysis of Shells of Revolution Subjected to Symmetrical and Nonsymmetrical Loads," ASME JOURNAL OF APPLIED MECHANICS, Vol. 31, 1964, pp. 467–476.

63 Cohen, G. A., "Computer Analysis of Asymmetric Buckling of Ring-Stiffened Orthotropic Shells of Revolution," *AIAA Journal*, Vol. 6, 1968, p. 141.

64 Almroth, B. O., and Bushnell, D., "Computer Analysis of Various Shells of Revolution," *AIAA Journal*, Vol. 6, 1968, p. 1848.

65 Bushnell, D., "Analysis of Buckling and Vibration of Ring-Stiffened, Segmented Shells of Revolution," *International Journal for Solids and Structures*, Vol. 6, 1970, pp. 157–181.

66 Bushnell, D., "Computerized Buckling Analysis of Shells," AFWAL-TR-83-3049, Dec. 1981, Wright-Patterson Air Force Base, Ohio.

67 Almroth, B. O., and Brogan, F. A., "The STAGS Computer Codes," NASA CR 2950, Feb. 1978.

68 Almroth, B. O., and Brogan, F. A., "Bifurcation Buckling as an Approximation of the Collapse Load for General Shells," *AIAA Journal*, Vol. 10, No. 4, 1972, pp. 463–467.

69 Almroth, B. O., and Holmes, A. M. C., "Buckling of Shells With Cutouts, Experiment and Analysis," *International Journal for Solids and Structures*, Vol. 8, 1972, pp. 1057–1071.

70 Almroth, B. O., Brogan, F. A., and Marlowe, M. B., "Stability of Cylinders With Circular Cutouts," *AIAA Journal*, Vol. 11, Nov. 1973, pp. 1582–1584.

71 Bushnell, D., and Meller, E., "Elastic-Plastic Collapse of Nonuniformly Axially Compressed Ring-Stiffened Cylindrical Shells with Reinforced Openings," 4th National Congress on PVP Technology, June 18–24, 1983, Portland, Ore.

72 Baker, W. E., Bennett, J. G., and Babcock, C. D., "Experimental Buckling Investigation of Ring-Stiffened Cylindrical Shells Under Unsymmetrical Axial Loads," 4th National Congress on PVP Technology, June 18–24, 1983, Portland, Ore.

Downloaded 02 May 2010 to 171.66.16.250. Redistribution subject to ASME license or copyright; see http://www.asme.org/terms/Terms_Use.cfm

Dynamic Plasticity

R. J. Clifton
Division of Engineering,
Brown University,
Providence, R.I. 02912
Mem. ASME

Recent advances in the understanding of the dynamic plastic response of crystalline solids are discussed. At the level of individual dislocations progress is being made on measurements of dislocation mobility at high stress levels and on elastodynamics solutions for transient dislocation motions. More progress is required on the understanding of changes in mobile dislocation density during dynamic plastic deformation. Widespread use of the Kolsky (or split-Hopkinson) bar has resulted in a reasonably clear picture of the dependence of flow stress on plastic strain rate for polycrystalline metals deformed at strain rates up to $10^3 s^{-1}$. Influences of strain-rate history, temperature, and pressure require further investigation. At strain rates of approximately $10^3 s^{-1}$ to $10^5 s^{-1}$ there is increasing evidence of a marked increase in flow stress with increasing strain rate. Pressure-shear plate impact experiments appear to be attractive for studying plastic response in this high strain-rate regime. Differences, if any, between stress-path effects at quasi-static strain rates and at strain rates of $10^3 s^{-1}$ and higher remain poorly understood. Larger-than-predicted precursor decay observed in plate impact experiments on single crystals remains unresolved and of continuing fundamental interest; however, the importance of precursor decay measurements in determining dynamic plastic response appears to be diminishing because surface effects and limitations on the resolution of wave-front profiles represent serious constraints on the inferences that can be drawn from precursor decay measurements. Modeling of dynamic plastic response of polycrystals in terms of the response of slip systems is in an early stage of development. Kinematics of finite deformation by crystalline slip and consistent averaging techniques for modeling polycrystalline response are understood reasonably well. Increased emphasis on the understanding of the dynamic plastic response of single crystals and on the influence of microstructure appear desirable for sustained progress. Physically based models of wide applicability are required.

Introduction

Dynamic plasticity is the subject that relates the dynamic response of plastically deforming solids and structures to the imposed loading conditions. It involves both the prediction of dynamic structural response based on applicable constitutive models for the plastic behavior of the constituent materials and the determination of such constitutive models from dynamic experiments. This determination of acceptable constitutive equations is difficult because of the lack of a physical theory of plasticity that would provide the form of such equations and because the interpretation of the dynamic experiments often requires the use of the constitutive equations that are to be determined from the experiments. Progress requires interplay between theory and experiment and between macroscopic and microscopic viewpoints. Contributions from the applied mechanics community are particularly important to advances over this wide range of inquiry.

Early contributions to the understanding of stress waves in plastically deforming metals have been reviewed by Hopkins [1]. The state of understanding at the beginning of the 1970s can be obtained from articles by Herrmann [2] and Clifton [3]. A recent update has been provided by Nicholas [4]. Duffy [5] has surveyed experimental results on the plastic response of materials at the high shear-strain rates, say $10^2 s^{-1}$ and higher, which are of interest in dynamic plasticity. Davison and Graham [6] have reviewed shock wave experiments that contribute to the understanding of dynamic plastic response at high pressures, say greater than 1GPa, and high strain rates. Combined, these articles provide a good overview of the plastic response of metals to dynamic loads. The viewpoint is primarily that of macroscopic continuum mechanics, although reference is made to underlying dislocation mechanisms that are responsible for the plastic flow.

In this state-of-the-art paper an attempt is made to begin at the scale of dislocations and to trace developments in investigations that are intended to provide insight into the mechanisms of dynamic plastic deformation. Issues to be considered include the mobility of dislocations in crystals,

Contributed by the Applied Mechanics Division for publication in the JOURNAL OF APPLIED MECHANICS.
Discussion on this paper should be addressed to the Editorial Department, ASME, United Engineering Center, 345 East 47th Street, New York, N.Y. 10017, and will be accepted until two months after final publication of the paper itself in the JOURNAL OF APPLIED MECHANICS. Manuscript received by ASME Applied Mechanics Division, June, 1983.

Copyright © 1983 by ASME
Downloaded 02 May 2010 to 171.66.16.250. Redistribution subject to ASME license or copyright; see http://www.asme.org/terms/Terms_Use.cfm

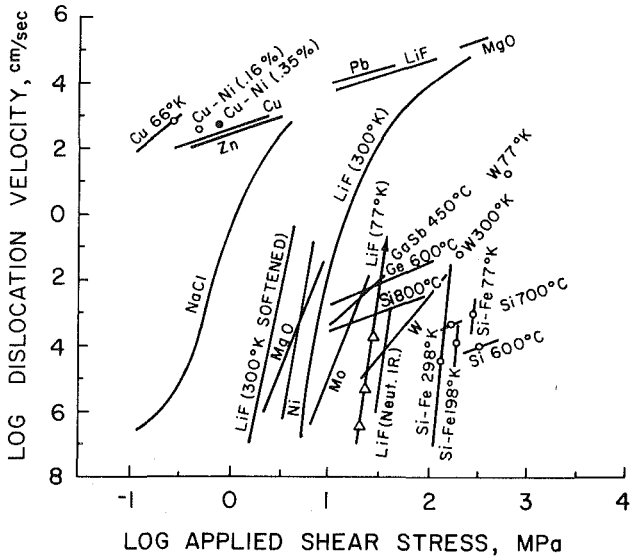


Fig. 1 Dislocation mobility in various materials (from [11])

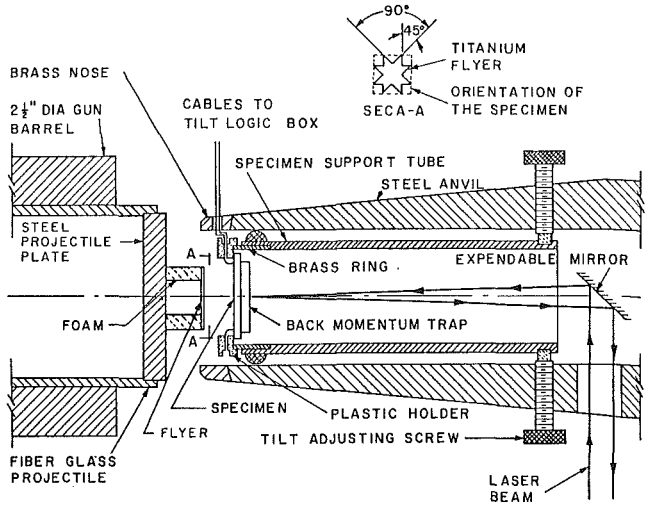


Fig. 2 Schematic of the plate impact experiment for determining dislocation mobility (from [10])

changes in dislocation density, a transition in the rate-controlling mechanism of plastic flow at high strain rates, the effects of high pressure, and the effects of complex stress paths. Understanding of these issues is incomplete. Hopefully, addressing them here will hasten their further understanding.

Dislocation Mobility

Fundamental to the development of constitutive equations for dynamic plasticity is the relation between the resolved shear stress τ on a crystallographic slip plane and the velocity v_d of dislocations moving on that slip plane. To determine this relation Johnston and Gilman [7] introduced the so-called "direct dislocation velocity measurement" experiment in which a single crystal is stressed by a square stress pulse of amplitude τ and duration Δt. Dislocation configurations are observed before and after the pulse is applied and the average dislocation velocity is computed from $v_d = \Delta x/\Delta t$ where Δx is the distance moved by the dislocations. A summary of results by many investigators is shown in Fig. 1. The curves indicate two regimes: (*i*) a low stress regime in which the dislocation velocity increases strongly with the applied shear stress and (*ii*) a high stress regime in which the dislocation velocity is proportional to the applied shear stress. The existence of the latter regime is becoming more evident as additional experimental results are obtained in this regime. In the former regime the rate-controlling mechanism is understood to be the thermally activated motion of dislocations past barriers such as impurities and intersecting dislocations. For this mechanism the dislocation velocity increases essentially exponentially with increases in the resolved shear stress. In regime (*ii*) the stress amplitudes are understood to be large enough for the barriers to be overcome easily so that the rate-controlling mechanism becomes the resistance of the clear lattice to the glide of dislocations. At stress levels that are high enough to overcome the so-called Peierels barrier associated with the periodic structure of the lattice, and low enough to cause dislocation velocities that are sufficiently below elastic wave speeds for relativistic effects to be unimportant, the resolved shear stress and the dislocation velocity satisfy a linear viscous drag relation

$$\tau b = B v_d \tag{1}$$

where b, the Burgers vector, is a lattice dimension corresponding to the displacement discontinuity of the dislocation and B is a drag coefficient.

The drag coefficient B has been obtained from direct dislocation velocity measurement experiments employing longitudinal stress pulses in bars [7], torsional pulses in bars [8], and compressive pulses in plates [9, 10]. Data at the highest stress levels and highest dislocation velocities shown in Fig. 1 have been obtained in the plate impact configuration introduced by Kumar and Clifton [10]. In this configuration, shown in Fig. 2, a square single crystal specimen is impacted by a thin flyer plate. Impact faces are flat and parallel. Impact occurs in vacuum. An elastic compressive pulse propagates through the specimen and the impedance-matched momentum trap. This pulse, reflected from the stress-free rear surface of the momentum trap as a tensile pulse, separates the unbonded momentum trap from the specimen. The specimen remains at rest and nominally unstressed except for unloading waves emanating from the periphery of the flyer. Because of the eight-pointed star shape of the flyer these waves are confined largely to corridors outside of a central octagonal region of the crystal. Subsequent impacts are avoided by using an anvil to stop the projectile. As a result, the central region of the specimen is subjected to a single, nearly square pulse with a duration Δt equal to the round trip transit time (0.15–0.3 μsec) for longitudinal elastic waves propagating through the thickness of the flyer. The stress amplitude (50–500 MPa) of the pulses is computed from the measured projectile velocity using elastic wave theory. Detailed wave profiles are obtained by using a Michelson interferometer to monitor the motion of the rear surface of the momentum trap.

After the experiment the specimen is removed and etched to reveal dislocations. Glide bands of closely spaced dislocations are observed on active slip planes. These glide bands correspond to slipped regions that are approximately circular in shape. The average dislocation velocity is then estimated from $v_d = \Delta x/\Delta t$ where Δx is the radius of the circular regions of slip. For annealed, high purity (99.999 percent) LiF crystals with low initial dislocation density (approximately 5×10^4 cm^{-2}) the dislocation velocity is approximately proportional to the resolved shear stress with a drag coefficient $B \simeq 3 \times 10^{-5}$ N s/m^2. This value, obtained for dislocation velocities in the range from 0.3–0.8 kms^{-1}, compares favorably with the value obtained for similar crystals in a different plate impact experiment [9] that resulted in dislocation velocities of $\simeq$ 0.1 kms^{-1}. Furthermore, comparable values of the drag coefficient are obtained in ultrasonic attenuation studies at dislocation velocities that are, say, four orders of magnitude smaller than those occurring in the plate impact experiments [15]. Thus it appears

Downloaded 02 May 2010 to 171.66.16.250. Redistribution subject to ASME license or copyright; see http://www.asme.org/terms/Terms_Use.cfm

that in this high purity, low-dislocation density material the linear viscous drag model (1) provides a good description of the relationship between the drag force τb and the dislocation velocity for a wide range of dislocation velocities—up to at least one-fourth the elastic shear wave speed. Much less complete results obtained for high purity MgO single crystals indicate similar response with $B \simeq 5 \times 10^{-5}$ Ns/m^2 [11]. These values of B are comparable to those obtained by Vreeland and coworkers at dislocation velocities less than 0.1 km/s in fcc metals and hcp metals [8, 12, 13]. Overall, it appears that (1) with B of the order of 5×10^{-5} Ns/m^2 at room temperature, is quite a satisfactory relationship for describing dislocation mobility in many materials when the dislocation motion is controlled by the intrinsic resistance of the lattice.

Phonon viscosity associated with the interaction of dislocations with thermal phonons is viewed as the mechanism mainly responsible for the drag force Bv_d at room temperature [14]. The estimated value of B based on phonon viscosity is [14]

$$B \simeq \frac{bw}{10c} \tag{2}$$

where c is an elastic wave speed and w is the thermal energy density, which is approximately $3K\theta/a^3$ where K is Boltzmann's constant, θ is the absolute temperature, and a^3 is the volume per atom. For LiF at room temperature the value for B computed from (2) is approximately 1×10^{-5} Ns/m^2 whereas the value obtained from (1) for direct dislocation velocity measurement experiments and for ultrasonic attenuation experiments [15] is approximately 3×10^{-5} Ns/m^2.

Differences between the values of B obtained from experiments and the predicted values (2) appear to be due to additional mechanisms of resistance to dislocation motion that are not considered in deriving (2). Phonon scattering is estimated [14] to provide a contribution to the drag coefficient that is comparable to that given by (2). Residual stresses due to other defects tend to reduce the average dislocation velocity with the result that the value for B computed from (1) is larger than the value that is predicted without consideration of residual stresses. Inertial resistance to dislocation motion has been estimated by means of continuum elastodynamics solutions for dislocations that jump to a constant velocity and maintain this velocity thereafter. The drag coefficient due to these continuum drag effects has been computed for screw dislocations by Eshelby [16],

$$B^c_{\text{screw}} \simeq \frac{\mu b}{4\pi t c_2^2} \quad (\text{for } v_d < 0.4c_2) \tag{3a}$$

and for edge dislocations by Clifton and Markenscoff [17]

$$B^c_{\text{edge}} \simeq \frac{\mu b(1+(c_2/c_1)^4)}{4\pi t c_2^2} \quad (\text{for } v_d < 0.4c_2). \tag{3b}$$

The quantities c_1 and c_2 in (3) are, respectively, the elastic longitudinal wave speed and the elastic shear wave speed; t is time measured from the time when the dislocation began to move; μ is the elastic shear modulus. For times t greater than, say 0.1 ns, the inertial drag (3) estimated from continuum elastodynamics solutions is negligible relative to the drag (2). Thus, on the time scale of the plate impact experiments and the ultrasonic attenuation experiments it appears that the drag associated with the transient motion of dislocations is negligible. Consequently, in high-purity, low-dislocation density materials, the motion of dislocations at moderate dislocation velocities appears to be governed by the linear viscous drag model (1) with a drag coefficient B attributable to lattice dynamics processes.

Macroscopic Plastic Flow

For homogeneous macroscopic plastic straining of a single crystal the plastic strain rate tensor is (e.g., [18])

$$\dot{E}^p = \sum_{k=1}^{n} \dot{\gamma}^p_k (\mathbf{m}^k \otimes \mathbf{n}^k)_s \tag{4}$$

where n is the number of slip systems and $\dot{\gamma}^p_k$ is the rate of shearing on the kth slip system, which has the slip direction $\mathbf{m}^k$ and the slip plane normal $\mathbf{n}^k$; $(\mathbf{m}^k \otimes \mathbf{n}^k)_s$ denotes the symmetric part of the tensor defined by the tensor product $(\mathbf{m}^k \otimes \mathbf{n}^k)$. The rate of shearing $\dot{\gamma}^p_k$ is given by

$$\dot{\gamma}^p_k = b^k N^k \bar{v}^k_d \tag{5}$$

where b^k is the Burgers vector, N^k is the dislocation line length per unit volume, and $\bar{v}^k_d$ is the average dislocation velocity; all quantities are for the kth slip system. Equations (4) and (5) would provide a constitutive equation for plastic flow if the quantities N^k and $\bar{v}^k_d$ could be computed from a given history of the imposed macroscopic stresses. So far, fully satisfactory means of doing this have not been established; however, progress has been made.

In particular, Rice [19] has provided a thermodynamics argument that can be used to establish the inequality

$$\tau^k b^k v^k_d \geq 0 \tag{6}$$

where τ^k is the nonsingular, local resolved shear stress due to all sources of stress except for the dislocation itself and v^k_d is the corresponding velocity for the glide motion of the dislocation. Requiring (6) to hold for all local states of stress one can conclude that near $\tau^k = 0$ the dislocation velocity must depend on the local stress state primarily through the value of τ^k. That is, for example, in a Taylor's expansion of v^k_d in terms of components of the stress tensor T only the combination of components corresponding to $\tau^k = \mathbf{m}^k \cdot T\mathbf{n}^k$ can appear as a linear term in an expansion that converges near $\tau^k = 0$. While this does not preclude the dependence of v^k_d on other components of the stress tensor it appears reasonable to expect that the main features of plastic response can be characterized by taking

$$v^k_d = f(\tau^k). \tag{7}$$

Since the dislocation mobility in high-purity, low-dislocation density materials is apparently described quite well by (1), it appears that the relationship (7) between local values of dislocation velocity and resolved shear stress is described adequately over wide ranges of resolved shear stress by taking $f(\tau^k) = \tau^k b^k / B$.

One of the difficulties in modeling macroscopic plastic flow lies in making the step from the local relationship (7) for dislocation mobility to the determination of the average dislocation velocity $\bar{v}^k_d$ in terms of the macroscopic applied stress and appropriate measures of the current configuration of dislocations and other defects. Another difficulty is the calculation of the evolution of the dislocation density N^k for a given loading history. These are complicated matters and little progress has been made.

When applied stress levels are low relative to the stress levels due to impurities, vacancies, and other dislocations, these inhomogeneities serve as barriers to the motion of dislocations. Then, the average velocity $\bar{v}^k_d$ is related more to the time that the dislocation is stopped at obstacles, than to the time for the glide of dislocations between obstacles. Thus, at such low levels of applied stress the relationship (7) is of little significance in the determination of $\bar{v}^k_d$. Instead, the average velocity $\bar{v}^k_d$ is determined by the spacing between obstacles and the frequency of successful attempts to cross these obstacles. Application of activation rate theory to the

Downloaded 02 May 2010 to 171.66.16.250. Redistribution subject to ASME license or copyright; see http://www.asme.org/terms/Terms_Use.cfm

calculation of the frequency ω of successful crossings gives the Arrhenius relation

$$\omega = \omega_0[\exp(-\Delta G^+/K\theta) - \exp(-\Delta G^-/K\theta)] \tag{8}$$

where ω_0 is the attempt frequency, K is Boltzmann's constant, θ is the absolute temperature, and ΔG^+, ΔG^- are the barriers in Gibbs free energy that are to be overcome by thermal motion in crossing the obstacle in, respectively, the direction assisted by the applied stress and the direction opposed by the applied stress. The activation energies ΔG are often modeled simply as square potentials for which $\Delta G^+ = (\tau_b - \tau^k)V$, and $\Delta G^- = (\tau_b + \tau^k)V$ where τ_b is the height of the stress barrier, τ^k is the resolved shear stress corresponding to the applied macroscopic stress state and V is a barrier parameter called the activation volume. Substitution of these expressions in (8) gives

$$\omega = \bar{\omega}_0 \sinh(\bar{\tau}^k/\tau_0) \tag{9}$$

where $\tau_0 = K\theta/V$ and $\bar{\omega}_0 = 2\omega_0 \exp(-\tau_b/\tau_0)$.

For barriers of uniform height τ_b and uniform spacing d, the averaging dislocation velocity can be written as $v = d/(t_w + t_g)$ where $t_w = 1/\omega$ is the wait time at the obstacle and $t_g = d/f(\tau^k)$ is the glide time between obstacles. From (9) this relation becomes

$$v_d^k = \frac{\sinh(\bar{\tau}^k/\tau_0) f(\bar{\tau}^k)}{\sinh(\bar{\tau}^k/\tau_0) + f(\bar{\tau}^k)/(\bar{\omega}_0 d)}. \tag{10}$$

The relationship between the resolved shear stress $\bar{\tau}^k$ and the plastic shear strain rate for single slip given by (5) and (10) is essentially the same as that shown by the solid lines in Fig. 7. Dislocation density is assumed to be constant. The transition strain rate $\dot{\gamma}_c$ is defined as the strain rate at which $t_w = t_g$. At this strain rate the stress is $\bar{\tau}^k = \bar{\tau}_c^k$ where $\bar{\tau}_c^k$ is obtained from

$$\sinh(\bar{\tau}_c^k/\tau_0) = f(\bar{\tau}_c^k)/(\bar{\omega}_0 d). \tag{11}$$

At strain rates above $\dot{\gamma}_c$ the flow stress becomes proportional to the strain rate whereas at strain rates below $\dot{\gamma}_c$ the flow stress varies essentially linearly with the logarithm of strain rate. Evidence of such a transition in material response at high strain rates will be examined in the next section.

The dislocation density N^k in (5) increases due to the multiplication of dislocations, the expansion of dislocation loops, and the nucleation of dislocations at defects. It decreases due to the annihilation of dislocations when, for example, screw dislocations of opposite sign become near each other. Plate impact experiments that are designed to allow examination of dislocation configurations after passage of a known stress pulse through a crystal are useful in examining changes in dislocation density due to stress pulse loading. In experiments on high-purity annealed LiF, Kumar and Clifton [10] showed that dislocation density increases through the formation of glide bands; dislocation density increases are greatest near the front and rear surface of the specimen. Similar results were obtained by Vorthman [20] for similar crystals impacted at higher impact velocities. These results are interpreted as indicating that heterogeneous nucleation at impurities in the crystals is not an important mechanism of dislocation generation in these crystals. However, such heterogeneous nucleation appears to be evident in similar plate impact experiments on (99.99 percent) MgO crystals [12]. The dominant dislocation generation in all these experiments is the generation at the contact faces between the flyer plate and the specimen and between the specimen and a momentum trap placed at the rear surface of the specimen. Such generation of dislocations at surfaces has not been considered in most investigations, although it is being considered as a possible contributor to the larger-than-predicted decay of the elastic precursor in plate impact experiments on single crystals [21]. An empirical relation commonly used to represent the dislocation density is

$$N^k = \left[N_m^k + M(\gamma^p)^k\right] \exp(-\phi(\gamma^p)^k) \tag{12}$$

where N_m^k is the initial mobile dislocation density for the kth slip system, M is a multiplication coefficient, and ϕ is an annihilation coefficient.

Equations (4), (5), (10), and (11) are indicative of the constitutive equations used for modeling the dynamic plastic response of single crystals. The barrier stress τ_b^k is normally taken to be an increasing function of $(\gamma^p)^k$ in order to incorporate strain hardening. The drag coefficient is sometimes taken to have the form $B = B_0/[1 - (v_d^k/c_2)^2]^{1/2}$, where B_0 is a constant. The latter form is used to make the elastic shear wave speed a limiting velocity for dislocations in accord with the result [17] that the continuum drag force for the transient motion of both edge and screw dislocations in isotropic elastic materials becomes infinite for dislocations that start from rest and jump to dislocation velocities $v_d = c_2$.

Wave profiles for copper single crystals impacted along <100> have been calculated using such constitutive equations, without barriers and without dislocation annihilation [22]. Values of N_m^k and M, which appear reasonable physically, and which provide satisfactory agreement between computed and observed wave profiles over much of the profile, result in a spike at the wave front that has not been observed in the experiments. Improvement in both the recording of wave-front profiles and in the modeling of the dynamic plastic response appear to be required if computed and observed profiles are to be reconciled.

Modeling of plastic response can be extended to the case of polycrystals by defining the macroscopic plastic strain rate tensor $\dot{E}^p$ through (Rice [18])

$$\Sigma : \dot{E}^p = \frac{1}{V} \sum_{k=1}^{n} \int_{C^k} \bar{\tau}^k b^k v_d^k dl^k \tag{13}$$

where the two dots denotes the inner product of two tensors and Σ is an arbitrary constant stress tensor such that $\Sigma\mathbf{n}$ is the traction applied to an elemental volume V with exterior normal $\mathbf{n}$. The resolved shear stress $\bar{\tau}^k$ corresponds to the value computed from the traction $\Sigma\mathbf{n}$, assuming that all dislocations remain fixed as $\Sigma\mathbf{n}$ is applied. All dislocation lines, with line elements dl^k, in the volume V constitute the contour C^k for the kth slip system. If the stress tensor for the αth crystal is uniform throughout the crystal, then (13) can be rewritten as

$$\Sigma : \dot{E}^p = \sum_{\alpha=1}^{m} \frac{V_\alpha}{V} \bar{T}_\alpha : \dot{E}_{c\alpha}^p \tag{14}$$

where (V_α/V) is the volume fraction of the αth crystal, which has a plastic strain rate $\dot{E}_{c\alpha}^p$. Such uniformity of stress is expected if the m crystals that comprise the elemental volume V are sufficiently small to justify use of Eshelby's result [23] that the stress in a small elliptical inclusion in an unbounded elastic matrix is uniform when uniform stresses are imposed at infinity. In either formulation (13) or (14) the difficulty in computing the macroscopic plastic strain rate $\dot{E}^p$ is that the actual resolved shear stress in each crystal is required in order to compute either v_d^k or $\dot{E}_{c\alpha}^p$. Modeling of the polycrystal so that stresses in single crystals are computed can be accomplished by introducing a so-called self-consistent slip model in which each crystal is viewed as an inclusion in a surrounding matrix. Self-consistency is imposed by requiring tractions and displacement to be continuous across the surface of the inclusion. Such self-consistent slip models, introduced initially for rate-independent material response [24–26] have been extended to the case of steady state creep of time-dependent materials [27]. However, these models have not yet been used for dynamic plasticity calculations. Instead,

Downloaded 02 May 2010 to 171.66.16.250. Redistribution subject to ASME license or copyright; see http://www.asme.org/terms/Terms_Use.cfm

equation (13) has been used to establish the existence of a flow potential $\Omega(\sigma_{ij};\ \xi_\alpha)$ where ξ_α is a vector that characterizes the current structure of dislocations and defects and σ_{ij} are the components of the macroscopic stress tensor. The existence of such a potential follows from (13) by identifying $\dot{E}^p$ with the strain rate $\dot{E}^P(\Sigma)$ due to the macroscopic stress tensor Σ. Then, considering differentials of the stress state Σ, at fixed structure, gives

$$\Sigma : \dot{E}^p(\Sigma) = \frac{1}{V}\sum_{k=1}^{n}\int_{C_k} d\tau^k b^k v_d^k(\tau^k)\,dl^k \tag{15}$$

where $d\tau^k = d\bar{\tau}^k$ is the corresponding change in the resolved shear stress at fixed structure. Because integration of the right side of (15) from one stress state to another is path-independent, integration of the left side is also path-independent. Consequently, the components of the plastic strain rate can be represented in the form [18]

$$\dot{E}^p_{ij}(\sigma_{ij};\ \xi_\alpha) = \frac{\partial\Omega(\sigma_{ij};\ \xi_\alpha)}{\partial\sigma_{ij}} \tag{16}$$

where $\Omega(\sigma_{ij};\ \xi_\alpha)$ is a flow potential corresponding to the current structure of dislocations and defects. For v_d^k a monotonically increasing function of τ^k the surface Ω = const. is a smooth, convex surface in stress space [18]. Macroscopic constitutive equations for dynamic plastic flow of polycrystals are generally taken in the form (16) with empirical functions $\Omega(\sigma_{ij};\ \xi_\alpha)$ and differential equations for determining the evolution of the vector ξ_α. Examples are given subsequently in connection with the calculation of wave profiles due to pressure-shear impact of plates.

Kolsky Bar Experiments

The primary experiment for obtaining the plastic response of materials at strain rates of 10^2-10^4 s^{-1} is one in which a short specimen sandwiched between two long elastic bars is subjected to loading by an approximately square stress pulse that is generated in one of the elastic bars called the transmitter bar. As this pulse interacts with the specimen, it becomes partially reflected into the transmitter and partially transmitted to the other elastic bar called the anvil bar. After a few reverberations of the wave front along the length of the specimen the stress and strain-rate in the specimen are expected to become nominally homogeneous. The stress in this state can be obtained by monitoring the transmitted wave in the anvil whereas the strain rate can be obtained from monitoring the incident and reflected waves in the transmitter. In introducing this configuration Kolsky [28] brought in the concepts of (*i*) making the specimen short relative to the length of the pulse in order to obtain nominally homogeneous states of stress in the specimen, as in quasi-static experiments; and (*ii*) making the elastic bars long relative to the length of the pulse in order to obtain the stress and average strain rate in the specimen before waves reflected from the remote ends of the transmitter and anvil bars arrive at the locations where the wave profiles are monitored. Implementation of the first concept avoids the iterative process of determining the nonlinear response of a material from the comparison of theoretical and experimental wave profiles where the former profiles must be calculated from the material's unknown nonlinear response. Implementation of the second concept eliminates unwanted effects due to the inertia of testing machines and load cells.

Kolsky [28] used a configuration in which compressional waves in bars were used to subject cylindrical specimens to nominal stress states of uniaxial compression. This configuration continues to be used although in much recent research and in most new research facilities a torsional wave configuration [29] similar to that shown in Fig. 3 is used.

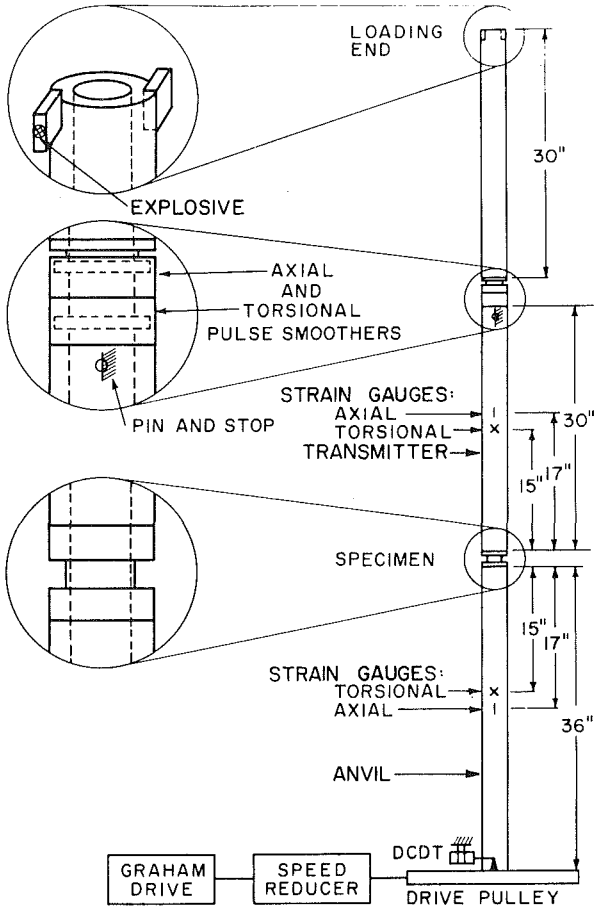


Fig. 3 Schematic of torsional Kolsky bar (from [29])

Originally the torsional configuration was introduced to eliminate unwanted effects of lateral inertia of the specimen and end friction that are present in compression experiments. Both of these effects tend to cause measured values of the flow stress to be larger than they would be in an idealized simple compression experiment in which the axial compressive stress is the only nonzero stress component. However, comparisons of stress-strain curves from the two types of Kolsky bars indicate that the effects of lateral inertia and end friction are essentially insignificant (less than 5 percent, say) as long as the ends are lubricated, and the length-diameter ratio of the specimen is kept within limits (0.5–1.0, say) in the compression experiments [30]. These comparisons are based on plots of the second invariant of the stress deviator tensor versus the second invariant of the strain tensor; for compression and torsion this corresponds, respectively, to plotting $\sigma/\sqrt{3}$ versus $\sqrt{3}\epsilon$ and τ versus γ where $(\sigma,\ \epsilon)$ are the axial compressive stress and strain and $(\tau,\ \gamma)$ are the torsional shear stress and strain. Comparisons are made in strain regimes where elastic strains are negligible, yet finite strain effects can be neglected.

Continuing preference for the torsional configuration is based not so much on concern for the validity of dynamic stress-strain curves obtained in the compressive configuration as it is on other attractive features of the torsional configuration. These features include: nondispersive elastic waves in the transmitter and anvil bars, shorter rise times for the incident pulses, convenience in applying changes in strain rate, and the suitability of the geometry for investigating the development of bands of localized shearing deformation. The principal disadvantage of the torsional configuration is the additional machining of the specimen that is required in order

Downloaded 02 May 2010 to 171.66.16.250. Redistribution subject to ASME license or copyright; see http://www.asme.org/terms/Terms_Use.cfm

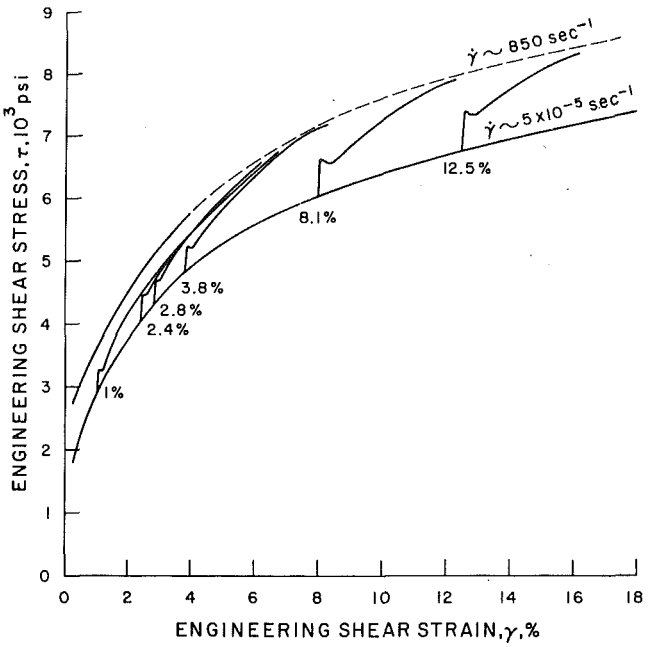


Fig. 4 Behavior of 1100-0 aluminum due to a jump in shear strain rate (from [29])

to obtain a geometry for which the imposed torques can be transferred between the specimen and the two elastic bars. Generation of the incident pulse is also more difficult in the torsional configuration.

Representative quasi-static and dynamic stress-strain curves obtained in the torsional configuration of Fig. 3 are shown in Fig. 4. Three types of curves are shown corresponding to three types of loading: quasi-static loading, dynamic loading at constant strain rate, and quasi-static loading to a strain γ_s, followed by dynamic loading at constant strain rate. The latter strain-rate jump experiments are generally viewed as particularly important in determining constitutive relations for dynamic plasticity because configurations are expected not to change significantly during the rise time of the jump in strain rate. Consequently, the stress jump is expected to be a direct measure of the change in flow stress with changes in strain rate at fixed dislocation structures. Whether or not the expectation of negligible change in dislocation structures is realized in experiments has not been established. Nevertheless it appears reasonable to expect that if the rise time is sufficiently short for the plastic strain produced during the jump to be small relative to the plastic strain produced prior to the jump, then the experiment can be interpreted as a probe of the material's response for the dislocation structures that existed prior to the jump. The jump in stress $\Delta\tau$ associated with the jump in strain rate is used to calculate the strain rate sensitivity parameter $\partial ln\dot{\gamma}^p/\partial\tau \simeq \Delta ln\dot{\gamma}^p/\Delta\tau$. For stress states in which the resolved shear stresses are sufficiently large for the frequency of jumps of dislocations past obstacles to be governed by ΔG^+ (i.e., $\Delta G^+ >> \Delta G^-$ in (8)), but small enough for viscous drag to be unimportant as a rate-controlling mechanism, this parameter becomes

$$\frac{\partial ln\dot{\gamma}^p}{\partial\tau} = \frac{1}{K\theta}\frac{\partial\Delta G^+}{\partial\tau} \equiv \frac{V}{K\theta} \tag{17}$$

where V is the activation volume. Equation (17) is consistent with the results of many experiments involving strain-rate jumps from $10^{-3}s^{-1}$ to $10^3 s^{-1}$ at temperatures between, say, $-100°C$ and $300°C$ (e.g. [5]). The activation volume in (17) depends on the previous deformation history and, to a lesser extent, on the stress jump [5]. Satisfactory correlation of experimental results with models of the form (17) suggests that the thermally activated motion of dislocations past obstacles is the rate-controlling mechanism for the metals studied, over the strain-rate and temperature ranges cited.

Pressure-Shear Experiments

One means for studying the plastic response of materials at strain rates greater than those attained in Kolsky bar experiments is to use the pressure-shear impact configuration shown in Fig. 5 [31]. A thin specimen (e.g., 0.2–0.4 mm thick) is sandwiched between two hard plates that remain elastic throughout the experiment. The flyer, specimen, and anvil plates are aligned to be parallel, but inclined relative to the direction of approach. Rotation of the projectile is prevented by a keyway in the barrel and a key on a plate at the rear of the projectile. Parallelity of the impacting faces is maintained to better than 1×10^{-3} radians, as monitored by the times at which four electrically isolated, voltage-based pins at the periphery of the specimen are contacted by the flyer plate. Impact occurs in vacuum (e.g., 60μm Hg). Shear traction is transmitted across interfaces between the various plates by means of dry friction. The possibility of slip between the contacting surfaces is reduced by leaving the surfaces rough (0.3 μm) although the surfaces are lapped flat to approximately one wavelength of light over the diameter.

The stress wave transmitted through the specimen is monitored at the rear surface of the anvil plate by means of a normal velocity interferometer (NVI) and a transverse displacement interferometer (TDI) [32]. Only the motion during the time before unloading waves arrive from lateral boundaries is of interest. During this time the waves propagating in the three plates can be analyzed as plane waves propagating in the direction perpendicular to the impact face. Linear elastic wave theory is used to describe the wave propagation in the anvil and flyer plates. As in the Kolsky bar

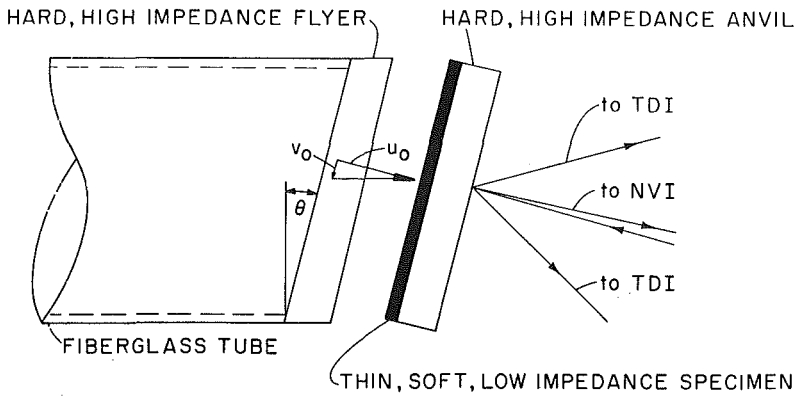


Fig. 5 Schematic of high strain rate pressure-shear experiment (from [31])

Downloaded 02 May 2010 to 171.66.16.250. Redistribution subject to ASME license or copyright; see http://www.asme.org/terms/Terms_Use.cfm

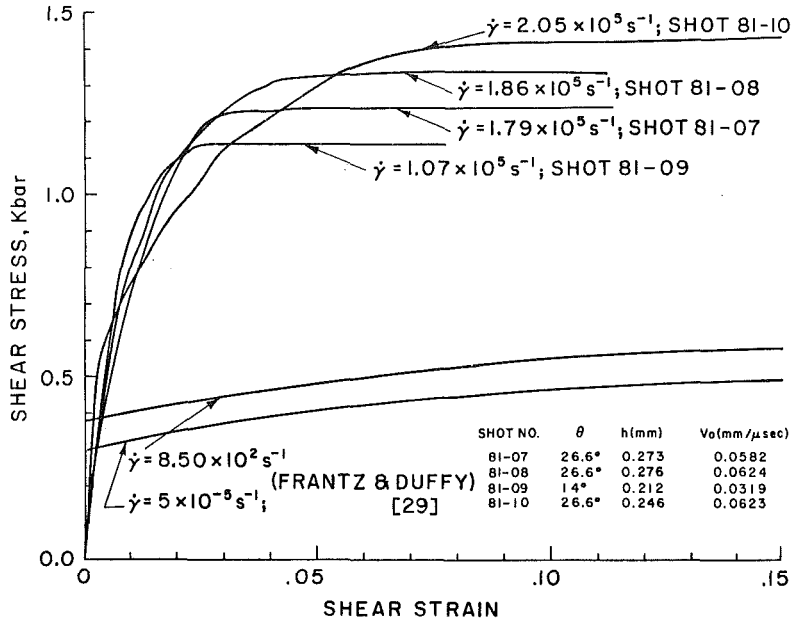


Fig. 6 Dynamic stress-strain curves for 1100-0 aluminum (from [31]) (hydrostatic pressure is approximately 2.8 GPa for the pressure-shear experiments)

experiments the time of interest in the experiment begins after the waves in the specimen have reflected from its faces several times so that a nominally homogeneous states of stress is established in the specimen. Then, the nominal longitudinal and shear strain rates in the specimen are

$$\dot{\epsilon} = \frac{u_0 - u_{fs}}{h} \tag{18a}$$

$$\dot{\gamma} = \frac{v_0 - v_{fs}}{h} \tag{18b}$$

where u_0, and v_0 are the normal and in-plane components of the flyer velocity, and u_{fs}, and v_{fs} are the normal and in-plane components of the velocity of the rear surface of the anvil plate; h is the specimen thickness. The normal and shear tractions at the rear surface of the specimen are

$$\sigma = \frac{1}{2} \rho c_1 u_{fs} \tag{19a}$$

$$\tau = \frac{1}{2} \rho c_2 v_{fs} \tag{19b}$$

where ρ, c_1, c_2, are, respectively, the mass density, the elastic longitudinal wave speed, and the elastic shear wave speed for the anvil. Because of the specimen's elastic stiffness to volume changes, the longitudinal stress increases with each wave reflection until, after a few reflections, the difference between the longitudinal components of particle velocity at the two faces of the specimen becomes negligible so that $u_{fs} \to u_0$ and $\dot{\epsilon} \to 0$. Furthermore, since the longitudinal wave speed is greater than the shear wave speed this state of constant volume, which corresponds to a constant state of hydrostatic pressure, is reached before a nominally homogeneous state of shear stress is established in the specimen. Thus, during the time of interest for studying the plastic response in shear the hydrostatic pressure is essentially constant. Numerical simulation of the experiment indicates that the value of the hydrostatic pressure is approximately equal to the value of the normal stress σ obtained from (19*a*) as $u_{fs} \to u_0$ [31].

A dynamic stress-strain curve for shearing deformation is obtained by plotting the shear stress τ from (19*b*) versus the shear strain γ obtained from the integration of (18*b*). Representative dynamic stress-strain curves for annealed 1100-0 aluminum are shown in Fig. 6. The steeply rising parts of the curves should be disregarded because the corresponding deformation occurs before nominally homogeneous states of stress are established. After the rise time, the strain rate and the flow stress become essentially contstant. The shear strain rates for the experiments shown vary from approximately $1 \times 10^5\ s^{-1}$ to $2 \times 10^5\ s^{-1}$. These strain rates are approximately two orders of magnitude larger than are obtained in conventional Kolsky bar experiments. The flow stress increases strongly with increasing strain rate over the range of strain rates shown. Stress levels are much higher than those shown for dynamic torsion tests at strain rates of $0.85 \times 10^3\ s^{-1}$ [29]. The stress-strain curves at the lower strain rates in Fig. 6 have been shifted to the left by approximately a 1.5 percent shear strain to provide more direct comparison with the curves obtained from pressure-shear experiments in which the longitudinal compressive wave causes an additional effective shear strain of approximately 1.5 percent.

The increase in flow stress between the torsion experiments and the pressure-shear experiments appears to be due primarily to the increase in strain rate, not to the hydrostatic pressure that is present in the pressure-shear experiments and not in the torsion experiments. The relative importance of the effects of strain rate and pressure are examined in pressure-shear experiments by varying the angle θ and the projectile velocity V_0; constant pressure (shear strain rate) and varying shear strain rate (pressure) is obtained by keeping the normal component (in-plane component) of the projectile velocity constant while the other component is varied. Systematic variation of pressure and shear strain rate in a series of 27 experiments on 1100-0 aluminum indicated that the effect of hydrostatic pressure was statistically insignificant [31].

A simple analysis of the effect of hydrostatic pressure on the flow stress has been given for different mechanisms of plastic flow by considering the pressure sensitivity of the various quantities in (1) and (8) [33]. For dislocation motion governed by phonon viscosity the fractional change in flow stress due to a change in pressure δp can be written as

$$\frac{\delta \tau}{\tau} \simeq \left[-\frac{1}{2} \frac{d\mu}{dp} + \frac{7(1-2\nu)}{4(1+\nu)} \right] \frac{\delta p}{\mu} \tag{20a}$$

where μ is the shear modulus and ν is Poisson's ratio. For

Downloaded 02 May 2010 to 171.66.16.250. Redistribution subject to ASME license or copyright; see http://www.asme.org/terms/Terms_Use.cfm

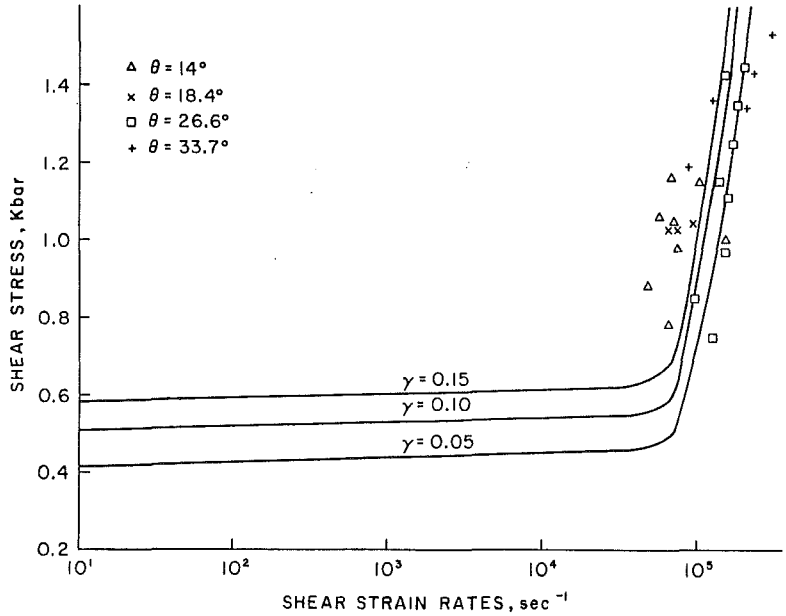


Fig. 7 Dependence of the flow stress on the shear strain rate for 1100-0 aluminum (from [31])

dislocation motion governed by the time required for thermally activated motion of dislocations past obstacles the corresponding expression is

$$\frac{\delta\tau}{\tau} \simeq \left\{ \frac{\tau_b}{\tau}\frac{d\mu}{dp} - \frac{3(1-2\nu)}{2(1+\nu)}\left(\frac{\tau_b}{\tau}-1\right) + \frac{\partial\tau/\partial ln\dot{\gamma}^p}{\tau}\left[\frac{1-2\nu}{4(1+\nu)} - \frac{1}{2}\frac{d\mu}{dp}\right]\right\}\frac{\delta p}{\mu} \qquad (20b)$$

where τ_b is the stress barrier in (9). For aluminum ($\nu = 1/3$, $\mu = 27.4$ GPa, $d\mu/dp \simeq 17/8$) the fractional change in flow stress due to a pressure increase of 1 GPa would be -2.3 percent according to (20*a*) and $+10$ percent to $+20$ percent according to (20*b*) (with $(\tau_b/\tau) \simeq 1.5$–2.3 and $(\partial\tau/\partial ln\,\dot{\gamma}^p)/\tau \simeq 0.02$). Thus, equation (20*b*) predicts a significant positive effect of pressure on flow stress for straining at low strain rates where thermally activated motion of dislocations is rate-controlling and a small, possibly negative, effect of pressure on flow stress at very high strain rates where phonon viscosity may be rate controlling. Furthermore, from (20*b*) the pressure sensitivity decreases at high strain rates as $\tau \to \tau_b$. Although these results and the validity of (20) have not been established by systematic investigation, the apparent lack of pressure sensitivity in the pressure-shear experiments and the significant positive pressure sensitivity observed at low strain rates (e.g., [39]) suggest that the predictions of (20) are at least qualitatively correct for small changes in pressure (i.e., $\delta p << \mu$).

The dependence of the flow stress on the plastic shear strain rate is shown in Fig. 7 for 1100-0 aluminum. The straight lines are based on results of quasi-static torsion experiments at strain rates of approximately $10^{-3}s^{-1}$ and torsional Kolsky bar experiments at strain rates of approximately $10^{3}s^{-1}$. Data points at strain rates of approximately $10^{5}s^{-1}$ are from pressure-shear experiments; each point corresponds to the flow stress and the strain rate for the plateau region of a dynamic stress-strain curve of the form shown in Fig. 6. Different points correspond to different pressures and different shear strains as well as different shear strain rates. However, the previously mentioned lack of the dependence of flow stress on pressure, and the lack of significant dependence of flow stress on plastic strain, as indicated by the plateau region of the stress-strain curves in Fig. 6, suggest that the flow stress depends primarily on strain rate at these high strain rates. Although there is considerable scatter in the data it is evident that the flow stress is markedly higher than would be obtained by extrapolation of the lines that characterize the material's response at strain rates below $10^{-3}s^{-1}$. Furthermore, the values of the shear stress exceed the values of τ_b that characterize the barrier height in the modeling of the temperature and strain rate sensitivity of the material at strain rates of $10^{3}s^{-1}$ and less. For example, for the case (equation (9)) of an activation energy that is linear in the applied stress, Lindholm [34] reports a barrier height $\tau_b \simeq 85$ MPa for a plastic strain $\gamma^p \simeq 0.17$. At higher stress levels and lower temperatures the barrier height extrapolates to 135 MPa at the same plastic strain. Since the measured values exceed these estimates of barrier height it appears that the barriers are overcome without thermal activation for the upper range of shear stresses attained in the pressure-shear experiments.

If thermal activation is not required for dislocation motion at the stress levels of the pressure-shear experiments, then it is expected that the average dislocation velocity is limited by the intrinsic resistance of the clear lattice to the motion of dislocations. From (5) and (7) the form of the relationship between the plastic shear strain rate $\dot{\gamma}^p$ and the shear stress is

$$\dot{\gamma}^p = \frac{b^2 N_m}{\beta B}\tau \qquad (22)$$

when dislocation velocity is proportional to the local resolved shear stress. The dislocation density N_m in (22) is the total mobile dislocation density on all slip systems. The effects of multiple slip systems in each crystal and different orientations of the crystals that comprise the polycrystalline aggregate are accounted for by the dimensionless parameter β. For randomly oriented, face-centered cubic crystals with the same mobile dislocation density on all slip systems the calculated value of β is 2.97 [35], based on Taylor's assumption [36] of uniform plastic straining in all crystals. From (22), applied to the data point ($\dot{\gamma}^p = 3.1 \times 10^{5}s^{-1}$, $\tau = 153$ MPa), the calculated value of N_m for $b = 2.86 \times 10^{-10}$ m, $B = 5 \times 10^{-11}$ MPas is $N_m = 3.7 \times 10^{8}$ cm^{-2}. The dislocation velocity corresponding to the shear stress $\tau = 153$ MPA is $v_d = 0.88$ dm s^{-1}, which is approximately 25 percent of the

Downloaded 02 May 2010 to 171.66.16.250. Redistribution subject to ASME license or copyright; see http://www.asme.org/terms/Terms_Use.cfm

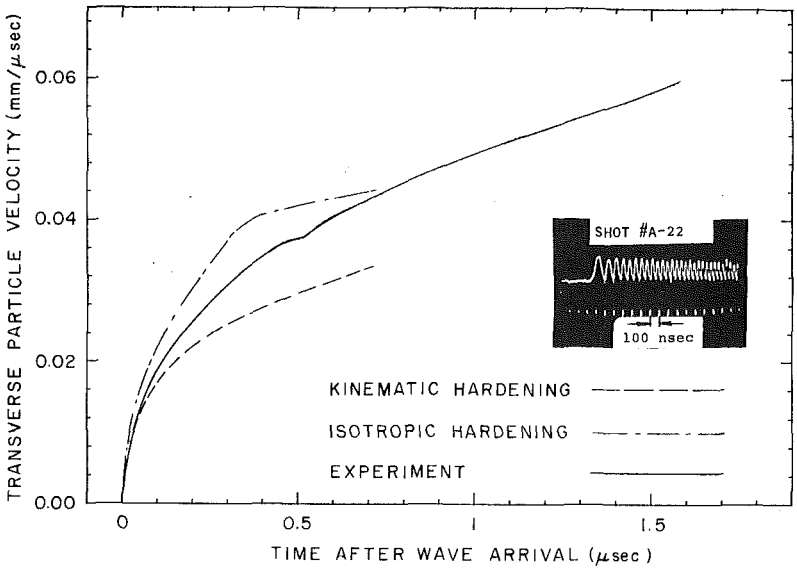


Fig. 8 Transverse velocity-time profiles at the rear surface of an alpha-titanium specimen subjected to symmetric pressure-shear impact (from [37]). $V_0 = 0.208 \times 10^3 \text{ms}^{-1}$, $\theta = 26.6$ deg, thickness = 4.6 mm.

elastic shear wave speed. At these dislocation velocities a relativistic correlation of the drag coefficient is unnecessary so that the assumed linear relationship between dislocation velocity and resolved shear stress appears to be reasonable. The calculated mobile dislocation density also appears to be reasonable in the sense that it is less than total dislocation densities reported for plastic strains of the order obtained in these experiments. Furthermore, the mobile dislocation density calculated from (22) for $(\dot{\gamma}^p, \tau)$ values obtained in the pressure-shear experiments decreases with decreasing strain-rate, reaching a value of approximately $N_m = 2.4 \times 10^8$ cm^{-2} at a strain rate $\dot{\gamma}^p = 1 \times 10^5 \text{s}^{-1}$. This trend is analogous to that reported by Shioiri et al. [37] who inferred mobile dislocation densities from measurements of the attenuation of ultrasonic waves during, and following, deformation of a specimen in a Kolsky bar experiment. For high-purity polycrystalline copper they obtained a change in mobile dislocation density from 4.0×10^7 cm^{-2} to 2.3×10^7 cm^{-2} for a change in strain rate from 83 s^{-1} to 32 s^{-1}. The experiments of Shioiri et al. [37] are discussed further in the next section.

Another aspect of dynamic plasticity that can be addressed by means of pressure-shear experiments is the plastic response of materials subjected to loading histories for which the stress trajectories are not radial lines in stress space. These paths arise in pressure-shear impact because longitudinal compressive waves propagate at higher speeds than shear waves. Consequently, the waves generated at impact cause a material element to follow a nonproportional loading path consisting of compression when the longitudinal wave arrives followed by shear when the shear wave arrives. Understanding plastic response for such paths is important in the formulation of constitutive equations that are applicable for combined states of stress and complex loading histories.

Loading path effects, as well as the effects of pressure and high shear strain rates have been studied in so-called symmetric impact pressure-shear experiments. The configuration for these experiments is the same as that shown in Fig. 5 except that the thin specimen is removed and the two remaining plates are made from the material whose plastic response is to be studied. Gilat [38] has used this configuration to make a systematic study of the response of 6061-T6 aluminum and commercially pure alpha-titanium. The velocity and angle of impact were varied to assess the relative importance of pressure and shear strain rate on the flow stress. Velocity-time profiles at the rear surface of the target plate were computed by solving the corresponding mixed initial and boundary value problem, using elementary constitutive models of the material's response. These profiles were compared with measured profiles as shown, for example, for the transverse velocity in Fig. 8.

Several general conclusions can be drawn from such comparisons. First, the transverse velocity of the rear surface is more sensitive to the modeling of the plastic response of the material than is the longitudinal velocity; hence, comparisons of histories of transverse velocity are particularly useful in determining the applicability of proposed constitutive models. Second, the effect of hydrostatic pressure appears to be small; for example, varying the angle θ from 9.5 deg to 33.8 deg has, at most, a small effect on differences between measured profiles and computed profiles where the latter are obtained using constitutive equations that do not inlcude an effect due to hydrostatic pressure. Third, the transverse velocity profile spreads with distance of propagation, causing a reduction in the nominal shear strain rate; consequently, the measured wave profiles are influenced more strongly by the material's response at lower strain rates than those obtained when high strain rates are maintained by shearing the specimen between two hard plates as shown in Fig. 5. Nevertheless, the regions of high strain rates near the impact face has sufficient influence on the remote velocity-time profiles that good agreement between computed and measured velocity-time profiles can be obtained only by using a constitutive model that includes a strong increase in the flow stress at strain rates greater than approximately 10^4s^{-1}—analgous to that shown in Fig. 7 for 1100-0 aluminum.

Reflection of the incident waves from the traction-free rear surface of the target plate is strongly dependent on the effects of stress path on plastic response. Gilat [38] compared experimental results with predictions based on elastic/viscoplastic models of the form

$$\dot{\epsilon}_{ij}^p = \phi(\bar{\tau}, \bar{\gamma}^p) \frac{\partial f}{\partial \sigma_{ij}} \tag{23}$$

where $\phi = (2\dot{\epsilon}_{ij}^p \dot{\epsilon}_{ij}^p)^{1/2}$ is the equivalent plastic strain rate, and $\bar{\gamma}^p$ is the equivalent plastic strain obtained by integration of $\dot{\bar{\gamma}}^p = \phi$. The effective shear stress $\bar{\tau}$ was taken to have the value of the plastic potential f. Two flow potentials were used:

Downloaded 02 May 2010 to 171.66.16.250. Redistribution subject to ASME license or copyright; see http://www.asme.org/terms/Terms_Use.cfm

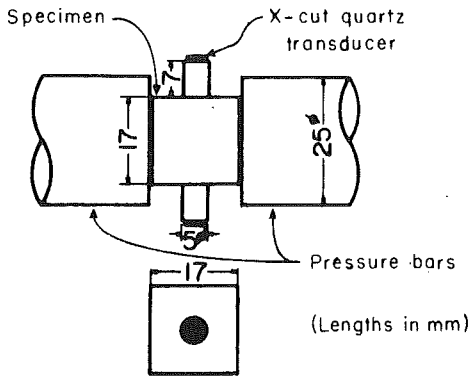


Fig. 9 Schematic of experiment for ultrasonic probing of specimen being deformed at high strain rates (from [36])

$$f(\sigma_{ij}) = (\tfrac{1}{2}s_{ij}s_{ij})^{\frac{1}{2}} \text{ (isotropic hardening)} \tag{24a}$$

$$f(\sigma_{ij},\alpha_{ij}) = [\tfrac{1}{2}(s_{ij}-\alpha_{ij})(s_{ij}-\alpha_{ij})]^{\frac{1}{2}} \text{ (kinematic hardening)} \tag{24b}$$

where s_{ij} denotes the components of the deviatoric stress tensor and α_{ij} denotes the coordinates of the center of a yield surface that translates in the direction of $\dot{\epsilon}_{ij}$ according to $\dot{\alpha}_{ij} = \eta(\bar{\gamma}^p)\dot{\epsilon}^p_{ij}$ where $\eta(\bar{\gamma}^p)$ is determined by unloading at various stages of, for example, a simple shear experiment in order to determine the extent of the elastic region. The summation convention of summation over repeated indices is used in (24) and throughout. The plastic strain rate function $\phi(\bar{\tau},\bar{\gamma}^p)$ characterizes the material's response in simple shear. Its value during such an experiment is equal to the current value of the plastic shear strain rate. It vanishes inside the respective yield surfaces defined by

$$\tfrac{1}{2}(s_{ij}s_{ij}) = k^2(\bar{\gamma}^p) \quad \text{(isotropic hardening)} \tag{26a}$$

$$\tfrac{1}{2}(s_{ij}-\alpha_{ij})(s_{ij}-\alpha_{ij}) = k_0^2 \quad \text{(kinematic hardening)} \tag{26b}$$

where $k(\bar{\gamma}^p)$ is the quasi-static flow stress in pure shear at a plastic shear strain $\bar{\gamma}^p$, and k_0 is the initial yield stress in shear. For these models the transverse velocity predicted at the free surface is, as shown in Fig. 8, less for kinematic hardening than for isotropic hardening; such a difference was observed in all symmetric impact experiments. Lower values of transverse velocity are predicted for the kinematic hardening model because of greater renewed plastic straining after the longitudinal wave reflects from the free surface. No clear advantage of one model over the other is evident from the comparisons due to uncertainty in the function $\phi(\bar{\tau},\bar{\gamma}^p)$ which would allow the computed wave profiles for either the isotropic or kinematic hardening models to be shifted nearer to the measured profiles. Better determination of $\phi(\bar{\tau},\bar{\gamma}^p)$, especially for the small plastic strains that occur in symmetric impact experiments, as well as greater variation in loading paths would be helpful in improved modeling of dynamic plastic response for complex loading paths.

Ultrasonic Attenuation Experiments

Ultrasonic waves propagating in a crystalline solid are attenuated by their interaction with dislocations, impurities, and other defects. The attenuation due to mobile dislocations can be separated from the attenuation due to other defects by a differential technique in which the attenuation during plastic deformation is compared with that before and after the plastic deformation occurs. A configuration developed by Shioiri et al. [37] for applying such a technique to plastic deformation at strain rates of approximately $10^2 s^{-1}$ is shown in Fig. 9. The specimen is deformed in a compressional Kolsky bar experiment. Simultaneously, ultrasonic waves

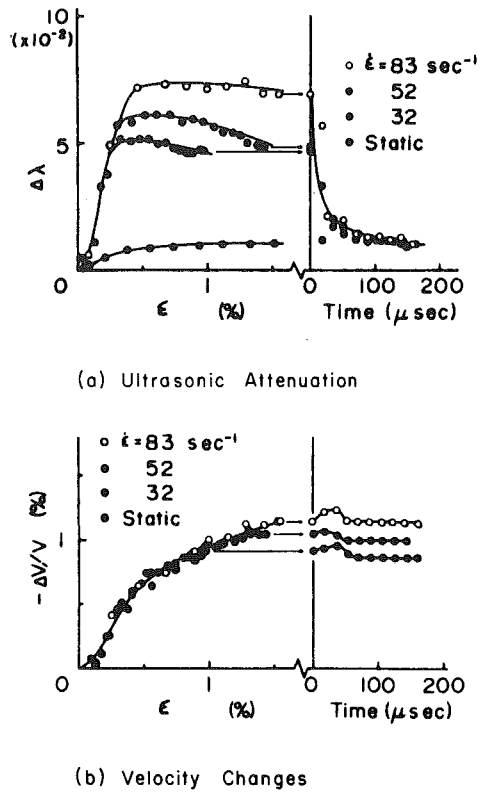


Fig. 10 Ultrasonic attenuation and wave speed changes during and after dynamic plastic deformation (from [36])

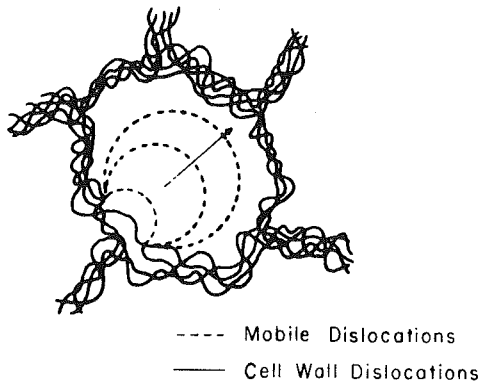


Fig. 11 Dislocation cell structure (from [36])

(approx. 10 MHz) are propagated through the specimen at right angles to the axis of compression. As the specimen is deformed there is an increase $\Delta\lambda$ in the attenuation of the pulse and a decrease Δv in its velocity of propagation. Changes in attenuation and in the relative velocity are monitored at regular intervals before, during, and following the loading by the compressive pulse used in the Kolsky bar experiment. Results are shown in Fig. 10 for a polycrystalline, annealed [OFHC] copper specimen [37]. The attenuation during plastic deformation increases with increasing strain rate whereas the corresponding wave velocity is independent of the strain rate. After the specimen is unloaded, the attenuation decreases to approximately the values that are obtained for quasi-static deformation to the same total plastic strain. The velocity change $\Delta v/v$ is essentially unchanged by unloading.

These results are interpreted by Shioiri et al. [37] within the framework of the Granato-Lücke theory [39] for the in-

Downloaded 02 May 2010 to 171.66.16.250. Redistribution subject to ASME license or copyright; see http://www.asme.org/terms/Terms_Use.cfm

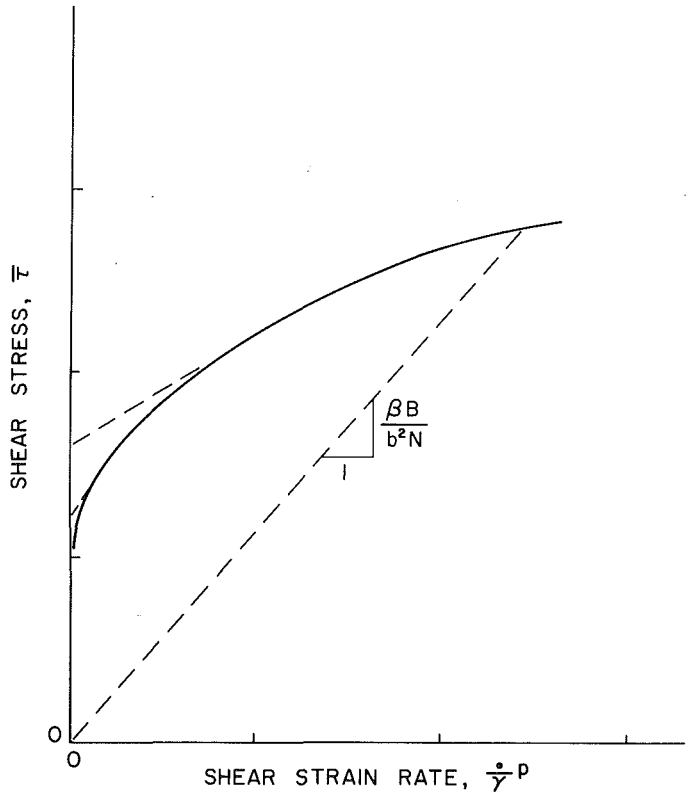


Fig. 12 Schematic dependence of shear stress on plastic shear strain rate at high strain rates

teraction of pinned dislocations with a harmonic stress wave. Dislocations are viewed as consisting of tangled cell wall dislocations and relatively free mobile dislocations moving through the open regions between cell walls as shown in Fig. 11. The strain rate-sensitive part of the change in attenuation is viewed as indicative of the change in mobile dislocation density whereas the strain rate-insensitive change in wave speed is viewed as indicative of the increased density of cell wall dislocations as the deformation proceeds. From the theory [39] and assumed linear variation of the dislocation velocity with resolved shear stress, Shioiri et al. [37] obtain the estimates of mobile dislocation density reported in the previous section. In addition, they estimate the density of cell wall dislocations to be approximately 50 times higher than the mobile dislocation density. Cell wall structures analogous to those shown schematically in Fig. 11 have been observed in copper and aluminum [41, 42].

Concluding Remarks

The overall picture of dynamic plastic deformation that appears to be emerging is one in which dislocation mobility is inhibited by the extrinsic resistance of obstacles at low stress levels and by the intrinsic resistance of the lattice at high stress levels; high strain rates are accommodated largely by increases in the mobile dislocation density. Plots of flow stress versus strain rate on a linear scale appear to have the form shown in Fig. 12. Over the limited range of strain rates that are obtained in a particular type of high strain rate experiment the relationship between flow stress and strain rate often appears to be linear with a positive intercept on the τ-axis [43]. Such a relationship is generally reported as indicative of a viscous drag mechanism. The slope of the line is viewed as indicative of the coefficient $\beta B/(b^2 N)$ in (22) and the intercept on the τ-axis is viewed as a stress barrier that must be overcome before the viscous drag mechanism becomes rate-controlling. An alternative interpretation that appears to be more compatible with the results of experiments at widely different strain rates and with predicted effects of residual stress fields on dislocation velocity is that the experimental results are described by (22), with the mobile dislocation density increasing with increasing shear stress of shear strain rate. The principal objection to the former interpretation is that the intercept on the τ-axis appears to be significantly higher for a series of experiments at very high strain rates than for a series at strain rates that are an order of magnitude lower; thus, the intercept does not appear to be a fundamental property of the material or its initial state of residual stress. Furthermore, because the resolved shear stress due to the residual stress field has an average value of zero, its net effect on the average dislocation velocity is of second order in the difference between the applied shear stress and the residual shear stress. The resulting form of the predicted τ versus $\dot{\gamma}^p$ relation, at constant dislocation density, does not have an intercept on the τ-axis at stress levels that are large relative to the so-called Peierels stress required for the initiation of dislocation motion in a clear lattice. The alternative of interpreting the experimental results in terms of the form (22), possibly with an additional factor in the denominator to account for fluctuations in dislocation density and residual stresses as described in [33], is supported by reported changes in mobile dislocation density with changes in strain rate [37].

Although the emphasis in this paper is on continuum descriptions of dynamic plastic deformation due to dislocation motion there are developments in the dynamics of discrete dislocations that should be mentioned. One such development, due to Callias and Markenscoff [44], is the presentation of a method for obtaining the near-field asymptotic expansion for an accelerating dislocation. Denoting distance from the moving dislocation by ϵ they obtain, in addition to the $(1/\epsilon)$ singular terms that are present in the steady-state solution, terms that are proportional to the

Downloaded 02 May 2010 to 171.66.16.250. Redistribution subject to ASME license or copyright; see http://www.asme.org/terms/Terms_Use.cfm

crack-tip acceleration and that have a $ln\epsilon$ singularity. Knowledge of the logarithmic singular terms is essential for the evaluation of the fields radiated by arbitrarily moving dislocations. Another development of interest is the result [17] that an elastodynamics analysis of the waves radiated by discrete dislocations set in motion by an elastic plane wave gives a slightly different expression for the decay of the plane wave than is obtained from a continuum description. The difference in the two expressions arises because in the elastodynamics analysis dislocations moving toward the front of the plane wave have a greater effect on the decay of its amplitude than those moving away from the wave front. Such an effect is not present in the continuum description where, according to (5), a change in the sign of the dislocation velocity combined with a change in the sign of the Burgers vector leaves the plastic strain rate unchanged. This discrepancy between the interpretation of dynamic plastic deformation by means of a continuum description and a discrete dislocation description is cited as a reminder that the constitutive modeling used in dynamic plasticity is based on quasi-static modeling of the response of an elemental volume. Differences between the two descriptions are not expected to be significant except in special cases where a large fraction of the dislocations are propagating at high speeds and in the same direction.

Finally, there are other important aspects of dynamic plasticity that have not been addressed here. Obvious omissions include the formation of shear bands, structural dynamics, and computational methods for dynamic plasticity. Each of these areas is an area of major research activity which would be a suitable choice for a review article of length comparable to this one.

Acknowledgments

Preparation of this article has been supported by the Brown University Materials Research Laboratory funded by NSF. Research of the author and his collaborators that is described here has been supported by NSF, ARO, and the Brown NSF/MRL.

References

1 Hopkins, H. G., "Dynamic Anelastic Deformation of Metals," ASME *Applied Mechanics Reviews*, Vol. 14, 1961, pp. 417-431.

2 Herrmann, W., "Nonlinear Stress Waves in Metals," *Wave Propagation in Solids*, Miklowitz, J., ed., ASME, New York, 1969, pp. 129-183.

3 Clifton, R. J., "Plastic Waves: Theory and Experiment," *Mechanics Today*, Vol. 1, Nemat-Nasser, S., ed., Pergamon, 1973, pp. 102-167.

4 Nicholas, T., "Elastic-Plastic Stress Waves," *Impact Dynamics*, Zukas, J. A., Nicholas, T., Swift, H. F., Greszczuk, L. B., and Curran, D. R., eds., Wiley, New York, 1982, pp. 95-153.

5 Duffy, J., "The Dynamic Plastic Deformation of Metals: A Review," Air Force Wright Aeronautical Laboratories Technical Report No. AFWAL-TR-82-4024, 1982.

6 Davison, L., and Graham, R. A., "Shock Compression of Solids," *Physics Reports*, Vol. 55, 1979, pp. 255-379.

7 Johnston, W. G., and Gilman, J. J., "Dislocation Velocities, Dislocation Densities, and Plastic Flow in Lithium Fluoride Crystals," *J. Appl. Phys.*, Vol. 30, 1959, pp. 129-144.

8 Pope, D. P., Vreeland, T., Jr., and Wood, D. S., "Mobility of Edge Dislocations in the Basal Slip System of Zinc," *J. Appl. Phys.*, Vol. 38, 1967, pp. 4011-4018.

9 Flinn, J. E., and Tinder, R. F., "Dislocation Mobility Observations in LiF Monocrystals after Impact Loading," *Scripta Metallurgica*, Vol. 8, 1974, pp. 689-694.

10 Kumar, P., and Clifton, R. J., "Dislocation Motion and Generation in LiF Single Crystals Subjected to Plate Impact," *J. Appl. Phys.*, Vol. 50, 1979, pp. 4747-4762.

11 Kim, K. S., and Clifton, R. J., "Dislocation Motion in MgO Crystals Under Plate Impact," to appear in *Journal of Materials Engineering*.

12 Greenman, W. F., Vreeland, T., Jr., and Wood, D. S., "Dislocation Mobility in Copper," *J. Appl. Phys.*, Vol. 38, 1967, pp. 3595-3603.

13 Gorman, J. A., Woods, D. S., and Vreeland, T., Jr., "Mobility of Dislocations in Aluminum," *J. Appl. Phys.*, Vol. 40, 1969, pp. 833-841.

14 Hirth, J. P., and Lothe, J., *Theory of Dislocations*, McGraw-Hill, New York, 1968, pp. 193-196.

15 Fanti, F., Holder, J., and Granato, A. V., "Viscous Drag on Dislocations in LiF and NaCl," *J. Accoust. Soc. Am.*, Vol. 45, 1969, pp. 1356-1366.

16 Eshelby, J. D., "The Equation of Motion of a Dislocation," *Phys. Rev.*, Vol. 90, 1953, pp. 248-255.

17 Clifton, R. J., and Markenscoff, X., "Elastic Precursor Decay and Radiation from Nonuniformly Moving Dislocations," *J. Mech. Phys. Solids*, Vol. 29, 1981, pp. 227-251.

18 Rice, J. R., "On the Structure of Stress-Strain Relations for Time-Dependent Plastic Deformation in Metals," ASME JOURNAL OF APPLIED MECHANICS, Vol. 37, 1970, pp. 728-737.

19 Rice, J. R., "Continuum Mechanics and Thermodynamics of Plasticity in Relation of Microscale Deformation Mechanisms," *Constitutive Equations in Plasticity*, Argon, A. S., ed., M.I.T. Press, Cambridge Mass., 1975, pp. 23-79.

20 Vorthman, J. E., and Duvall, G. E., "Dislocations in Shocked and Recovered LiF," *J. Appl. Phys.*, Vol. 53, 1982, pp. 3607-3615.

21 Meir, G., "Surface Damage Effects on Precursor Decay in High Purity LiF," Sc.M. Thesis, Brown University, Providence, R.I., 1982.

22 Herrmann, W., Hicks, D. L., and Young, E. G., "Attenuation of Elastic-Plastic Stress Waves," *Shock Waves and the Mechanical Properties of Solids*, Burke, J. J., and Weiss, V., eds., Syracuse University Press, Syracuse, N.Y. 1971, pp. 23-63.

23 Eshelby, J. D., "Elastic Inclusions and Inhomogeneities," *Progress in Applied Mechanics Vol. II*, 1961, pp. 87-139.

24 Kroner, E., "Zar Plastischen Verformung des Vielkristalls," *Acta Met.*, Vol. 9, 1961, pp. 155-161.

25 Budiansky, B., and Wu, T. T., "Theoretical Prediction of Plastic Strains of Polycrystals," *Proc. 4th U.S. National Congr. Appl. Mech.*, 1962, pp. 1175-1185.

26 Hill, R., "Continuum Micro-Mechanics of Elastoplastic Polycrystals," *J. Mech. Phys. Solids*, Vol. 13, 1965, pp. 89-101.

27 Hutchinson, J. W., "Bounds and Self-Consistent Estimates for Creep of Polycrystalline Materials," *Proc. R. Soc. Lond.*, Series A, Vol. 348, 1976, pp. 101-127.

28 Kolsky, H., "An Investigation of the Mechanical Properties of Materials at Very High Rates of Loading," *Proc. Phys. Soc. London*, Series *B*, Vol. 62, 1949, pp. 676-700.

29 Frantz, R. A., Jr., and Duffy, J., "The Dynamic Stress-Strain Behavior in Torsion of 1100-0 Aluminum Subjected to a Sharp Increase in Strain Rate," ASME JOURNAL OF APPLIED MECHANICS, Vol. 39, 1972, pp. 939-945.

30 Lindholm, U. S., "Some Experiments With the Split Hopkinson Bar," *J. Mech. Phys. Solids*, Vol. 12, 1964, pp. 317-335.

31 Li, C. H., "A Pressure-Shear Experiment for Studying the Dynamic Plastic Response of Metals at Shear Strain Rates of $10^5 s^{-1}$," Ph.D. Thesis, Brown University, Providence, R.I., 1982.

32 Kim, K. S., Clifton, R. J., and Kumar, P., "A Combined Normal and Transverse Displacement Interferometer With an Application to Impact of *Y*-Cut Quartz," *J. Appl. Phys.*, Vol. 48, 1977, pp. 4132-4139.

33 Clifton, R. J., Gilat, A., and Li, C. H., "Dynamic Plastic Response of Metals under Pressure-Shear Impact," *Material Behavior Under High Stress and Ultrahigh Loading Rates*, Mescall, J., and Weiss, V., eds., Syracuse University Press, Syracuse, N.Y., 1983.

34 Lindholm, U. S., "Deformation Maps in the Region of High Dislocation Velocity," *High Velocity Deformation of Solids*, Kawata, K., and Shioiri, J., eds., Springer-Verlag, New York, 1978, pp. 26-35.

35 Yang, J. P., "Calculation of Visco-Plastic Response of Polycrystals from Slip Theory for FCC Crystals," Sc.M. Thesis, Brown University, Providence, R.I., 1983.

36 Taylor, G. I., "Plastic Strain in Metals," *J. Inst. Metals*, Vol. 62, 1938, pp. 307-324.

37 Shioiri, J., Satoh, K., and Nishimura, K., "Experimental Studies on the Behavior of Dislocations in Copper at High Rates of Strain," *High Velocity Deformation of Solids*, Kawata, K., and Shioiri, J., eds., Springer-Verlag, New York, 1978, pp. 50-66.

38 Gilat, A., "An Experimental Investigation of Pressure-Shear Waves in 6061-T6 Aluminum and Alpha-Titanium," Ph.D. thesis, Brown University, Providence, R.I., 1982.

39 Granato, A., and Lücke, K., "Theory of Mechanical Damping due to Dislocations," *J. Appl. Phys.*, Vol. 27, 1956, pp. 583-593.

40 Yoshida, S., and Oguchi, A., "Influence of High Hydrostatic Pressure on the Flow Stress of Aluminum Polycrystals," *Trans. Japan Inst. Metals*, Vol. 11, 1970, pp. 424-430.

41 Edington, J. W., "The Influence of Strain Rate on the Mechanical Properties and Dislocation Substructures in Deformed Copper Single Crystals," *Phil. Mag.*, Vol. 19, 1969, pp. 1189-1206.

42 Chiem, C. K., and Duffy, J., "Strain Rate History Effects and Observation of Dislocation Substructure in Aluminum Single Crystals Following Dynamic Deformation," *Mat. Sci. and Eng.*, Vol. 57, 1983, pp. 233-247.

43 Klahn, D., Mukherjee, A. K., and Dorn, J. E., "Strain-Rate Effects," *Second Int. Conf. on the Strength of Metals and Alloys*, ASM 3, 1970, pp. 951-982.

44 Callias, C., and Markenscoff, X., "Singular Asymptotics of Integrals and the Near-Field Radiated from Nonuniformly Moving Dislocations," manuscript submitted for publication.

Downloaded 02 May 2010 to 171.66.16.250. Redistribution subject to ASME license or copyright; see http://www.asme.org/terms/Terms_Use.cfm

S. H. Crandall
Ford Professor of Engineering,
Massachusetts Institute
of Technology,
Cambridge, Mass. 02139
Fellow ASME

W. Q. Zhu[1]
Visiting Scientist,
Massachusetts Institute
of Technology,
Cambridge, Mass. 02139

Random Vibration: A Survey of Recent Developments

A general overview of the problems, methods, and results achieved in random vibration since its inception as a technical discipline nearly 30 years ago is given with particular emphasis on developments during the past 15 years. Research areas of current interest include development of improved probabilistic models for sources of random excitation, development of more effective random response prediction procedures for nonlinear systems and systems with parametric excitation, development of improved procedures for estimating reliability of systems undergoing random vibration, and development of improved techniques for identification of system parameters from measurements made during random vibration.

Introduction

Random vibration is the name given to the body of theory associated with dynamic systems responding to random excitations. The ultimate purpose of the theory is to provide a sound basis for improving the reliability of structures, vehicles, and equipment that must withstand randomly fluctuating loads. Within the general framework of random vibration theory, three principal problems can be identified depending on whether attention is focused on the response, the excitation, or the dynamic system. Most commonly the system and its excitation are taken to be known and the problem is to predict statistical information about the dynamic response or the reliability of the system. The inverse problem of characterizing the excitation where the system and its response are known is called the measurement problem. Associated with this are the statistical operations performed on the measurements (referred to as data processing) and the problem of constructing useful probabilistic models to represent the random processes and random fields under investigation. Finally there is the diagnostic or identification problem in which information about the dynamic system is sought based on knowledge of the random excitation and its response.

In retrospect, the first investigation of dynamic response to random excitation was Einstein's pioneering study of Brownian motion in 1905 ([72] of [16]). The words "random vibrations" were first used in the title of a technical paper by Lord Raleigh in 1919 ([3] of [18]) to describe an acoustical problem equivalent to the random walk in a plane. The present usage of the term random vibration arose in the middle 1950s in connection with three aerospace problems: buffeting of aircraft by atmospheric turbulence, acoustic fatigue of aircraft panels due to jet noise, and the reliability of payloads in rocket-propelled vehicles. The common factor in all three problems was the random nature of the excitation. The procedures developed to solve these problems [1] were largely based on existing theories of statistical mechanics, communication noise, and fluid turbulence (Wax, [184] of [16]). Initially, most of the work was based on linear models. In the middle 1960s many investigators turned their attention to random vibration of nonlinear systems and to problems involving random parametric excitation. Random data processing was primarily performed by analog instruments until about 1970 when efficient digital data-processing instruments, triggered by the fast Fourier transform (FFT) breakthrough, became available. Random vibration theory was first applied to vehicles (aerospace vehicles, ships, trucks, trains, etc.) and then to nominally stationary structures such as tall buildings subject to random wind and earthquake loadings, off-shore structures subject to random wave loadings, and heat exchanger tubes subject to turbulent external flows.

During the development of random vibration theory, many books and survey papers have been written. Introductions to random vibration theory are provided by Crandall and Mark [2], by Robson [3], by Bolotin [4], and by Newland [5]. The books by Lin [6] and by Bolotin [7] give deeper and more systematic descriptions of random vibration theory with emphasis on structural engineering. Further discussions of particular topics in random vibration are contained in the collections edited by Crandall [1] and in the proceedings of two IUTAM Symposiums [13, 14]. Random data processing with engineering applications is described in some depth in the books by Bendat and Piersol [8, 9]. Theoretical treatments of stochastic differential equations and stochastic stability (closely related to random vibration theory) are provided by Jazwinski [10], by Arnold [11], and by Khasminskii [12]. The results of the first decade of development of random vibration theory are described in survey papers by Crandall [15, 16]. Further developments in random vibration theory since 1966 are surveyed by Vanmarcke [19]. Special topics reviewed include random vibration of nonlinear systems [17, 18,

[1] Present address: Department of Mechanics, Zhejiang University, Hangzhou, People's Republic of China.

Contributed by the Applied Mechanics Division for publication in the JOURNAL OF APPLIED MECHANICS.

Discussion on this paper should be addressed to the Editorial Department, ASME, United Engineering Center, 345 East 47th Street, New York, N.Y. 10017, and will be accepted until two months after final publication of the paper itself in the JOURNAL OF APPLIED MECHANICS. Manuscript received by ASME Applied Mechanics Division, April, 1983.

Copyright © 1983 by ASME
Downloaded 02 May 2010 to 171.66.16.250. Redistribution subject to ASME license or copyright; see http://www.asme.org/terms/Terms_Use.cfm

20–22], random parametric vibration [23, 24], random vibration of one and two-dimensional structures [25], and modern spectrum analysis [26].

The present paper gives a general description of the important concepts, problems, and methods of random vibration, and a survey of the most significant results in the field, especially those achieved in the last 15 years. Efforts also have been made to try to indicate directions for future work.

Random Processes and Random Fields

As a technical discipline random vibration is a combination of structural dynamics and probability theory. The key concepts from probability theory are those of random processes and random fields which are used as models for excitation and response time histories. A random process is an infinite population or ensemble whose samples are functions of a single variable (usually time) together with information concerning relative probabilities of sample values. A random field [27] is a similar ensemble whose samples are functions of more than one variable (usually time and space). In principle, random processes and random fields can be described completely in terms of infinite sequences of joint probability distributions of successively higher order, or in terms of infinite sequences of moment functions or cumulant functions. In practice, it is customary to deal with very incomplete descriptions; e.g., first and second-order probability distributions only, or with a limited number of statistical averages based on these two distributions.

For many applications it is acceptable to assume a kind of uniformity for the random process or random field under consideration that is expressed by the designations *stationary* in time and *homogeneous* in space. A stationary process is one whose probability distributions across the ensemble are invariant with respect to translations of the origin of time. Similarly a random field is homogeneous with respect to a particular spatial coordinate if its probability distributions are invariant with respect to translations of the origin along the axis of that coordinate.

The common statistical averages are the mean and mean square, which depend on the first-order probability distribution, and the correlation function, which depends on the second-order probability distribution. If $f(\mathbf{x}, t)$ is a random field, the space-time correlation function is the ensemble average of the product $f(\mathbf{x}_1, t_1) f(\mathbf{x}_2, t_2)$. In general this is a function of the two locations and the two times. If the field is stationary then the correlation no longer depends on the two times separately but only on their difference $\tau = t_2 - t_1$. The Fourier transform of the space-time correlation function of a stationary field with respect to the time lag τ is called the space-time cross-spectral density function which is a function of the two locations and a frequency variable. When only a single time history is involved the correlation function for a random process $x(t)$ is the ensemble average of the product $x(t_1)x(t_2)$. This (auto)correlation function R_x depends only on the the time lag $\tau = t_2 - t_1$ if the process is stationary. The Fourier transform of the correlation with respect to τ is called the (auto)spectral density function W_x which is a function of a single frequency variable f. The mean square $<x^2>$ of the stationary random process is given by the value of $R_x(\tau)$ when τ is zero or by the total area under the spectrum

$$<x^2> = \int_0^\infty W_x(f)\,df \tag{1}$$

The importance of the correlation and spectral density functions is because they provide average amplitude and frequency information about the sample histories and that (*i*) they can be measured with available data-processing techniques; (*ii*) they are closed with respect to linear time-invariant operations in the sense that if these statistics are known for the excitation, then it is possible to obtain the corresponding statistics for the response of a linear time-invariant dynamic system; and (*iii*) they often provide adequate information about the response for making engineering decisions concerning the severity of the vibration and the reliability of the system.

Nonstationary random processes and fields are more awkward to deal with at every step: measurement, response prediction, and drawing conclusions about reliability. A nonstationary process can sometimes be modeled as a stationary random process modulated by a deterministic amplitude variation [7] or as a nonstationary shot noise [6]. Since the correlation function of a nonstationary process involves two independent time arguments the ordinary spectral density function for stationary processes loses its significance. Some of the manipulative advantages of a spectrum can be retained by introducing a generalized spectral density defined by a double Fourier transform [6, 8]. An evolutionary spectrum was proposed by Priestley ([28–30] of [19]) to describe relatively slow changes of the frequency content of nonstationary processes. Two time-dependent spectra, the physical spectrum and the instantaneous spectrum, were introduced by Mark ([31] of [19]).

Another classification of random processes and fields can be made according to the influence of the past on the present probability distributions. There are processes with no memory at all; i.e., their present distributions are totally independent of the past, and there are processes whose present distributions are completely determined by the distributions at any single time in the past. An important example of the former class is white noise which is a stationary random process having uniform spectral density for all frequencies. Its correlation function is proportional to the Dirac delta function; i.e., it has no correlation with the past, no matter how recent. Such a process is an idealized concept that cannot be physically realized (the mean square of a white noise process is infinite) but it is a useful model for stationary processes with short correlation times in the same sense that ideal point loads are useful in the theory of elasticity.

A process whose present probability distribution depends on that at only one previous time is aclled a Markov process. The structure of a Markov process is completely determined for all future times by the distribution at some initial time and by a transition probability density function. The importance of Markov processes resides in the fact that when the excitation of a dynamic system (linear or nonlinear) is ideal white noise, the response is a Markov process, and a formal technique exists to obtain a partial differential equation satisfied by the transition probability density function of the process.

An important special class of random process (and fields) are the normal or Gaussian processes. These are processes whose probability distributions of all orders are completely determined by knowledge of the mean value for all times t and knowledge of the correlation function for all pairs of times t_1 and t_2. The importance of normal processes is because (*i*) they are closed with respect to linear time-invariant operations in the sense that if the excitation of a linear time-invariant system is a normal process, then so is the response process, and (*ii*) many real phenomena can be satisfactorily modeled by normal processes. A rationalization for the latter statement can be based on the central limit theorem which states that when a process is the sum of a very large number of small independent random processes it approaches a normal process as the number of independent constituents increases without limit.

Downloaded 02 May 2010 to 171.66.16.250. Redistribution subject to ASME license or copyright; see http://www.asme.org/terms/Terms_Use.cfm

Sources of Random Excitation

Random loading on a dynamic system can be modeled by a random process when it is applied at a single location or by a random field when it is applied as a distributed loading over a given length or given area of the system. In many cases it is assumed that the excitation is stationary and normal. This simplifies the problem of measuring the appropriate parameters to characterize the excitation and the problem of predicting the response and judging the reliability. Similar measurements made over a range of conditions together with physically based scaling laws sometimes provide a means for extrapolating the excitation parameters to estimate the levels of excitation that will occur under conditions beyond the range of previous experience. This procedure, however, has its limitations. One of the more important areas of future development of random vibration theory is the construction of improved models for random excitations.

In many cases the excitation is clearly nonstationary over a long period of time although for short intervals, which are still long compared to the response times of the dynamic system, the excitation appears to be stationary. A random process (or field) of this sort is called quasi-stationary [7] and may be described by a short-term (local) behavior and a long-term (global) behavior. For example, the short-term behavior of a quasi-stationary random process might be described by a spectral density function whose parameters were slowly varying functions of time. The long-term behavior might then be described by a joint probability distribution for the slowly varying parameters in the spectral density function. Several proposals for quantifying quasi-stationary or quasi-homogeneous random processes and random fields have been put forth. This is indicated in the brief descriptions of random excitations which follow. Because of the difficulty of making extensive measurements of random fields, simplifying assumptions are often built in to the models employed. For example, in cases of moving random loads due to turbulent flow about a vehicle it may be assumed, as in Taylor's hypothesis, that a "frozen" turbulence pattern is convected past the vehicle. In random fields with two space dimensions the fluctuations in one direction may be neglected, or it may be assumed that the randomness is isotropic so that measurements along any one direction can be used to infer the complete two-dimensional behavior.

Atmospheric Turbulence. Gust loading due to atmospheric turbulence can be a major design load for large commercial airplanes. It is commonly assumed that the vertical turbulent velocity component can be represented as a quasi-stationary normal process [29]. The short-term behavior is described by a spectral density function in which the RMS turbulent velocity is a slowly varying parameter whose long-term behavior is described by a probability density function. The assumption that the turbulent velocity pattern has no spanwise variation and is frozen as it is convected past the airplane, permits calculating the gust loads and the airplane response by using appropriate aerodynamic theory. A more elaborate model for gust loading (see G. Coupry in [13]) includes spanwise fluctuations by assuming the turbulence to be isotropic in the horizontal plane. The short-time behavior of the quasi-stationary random turbulent field is described by a cross-spectral density function derived from the isotropy assumption. The long-time behavior is described by a probability density function for the RMS turbulent velocity which appears as a scale factor in the cross-spectrum. The long-term fluctuations in atmospheric turbulence may also be described by means of an evolutionary spectrum ([28] of [19]).

Turbulence in Wind. The turbulent component of the wind in the planetary boundary layer has an RMS level that is usually between 5–25 percent of the average wind velocity. When the wind strikes a structure the fluctuating velocity component causes a fluctuating drag force which may excite an appreciable dynamic response in a flexible tower or antenna. The turbulent component of the wind can be modeled as a quasi-stationary and quasi-homogeneous random field whose short-term behavior is described by a cross-spectral density function. Davenport [30] has proposed a spectral density function for the turbulent velocity at a single point and a coherence function that decays exponentially with separation and frequency to describe the spatial correlation. For recent publications on wind turbulence and the response of structures to it, see the survey by Johns [31].

Jet Noise. Large gas turbine jets and the jets produced by rocket engines generate intense levels of random acoustic noise. The random pressure fluctuations radiated acoustically to nearby panels on the vehicle may cause local fatigue failures (so-called acoustic fatigue [32]) and provide a distributed excitation over the surface of the vehicle that may excite structural vibrations of the vehicle and may be transmitted as acoustic noise within the vehicle. An important characteristic of the random field of pressure acting on the vehicle is the fact that the random fluctuations are convected past the surface at a relative velocity that is the vector difference between the sound velocity and the vehicle velocity. Another characteristic of jet noise is the extremely wide band of frequencies over which its intensity is distributed. Whereas the major contribution to many mechanical random loading processes (e.g., ocean waves, natural winds, earthquakes, etc.) is limited to a band of frequencies that encompasses about one decade, the spectrum of a large rocket jet shows substantial contributions over a band of frequencies that extends over three decades. The structure of the near field of jet noise is sufficiently complicated that it is generally necessary to resort to detailed measurements in particular configurations [33].

Turbulent Boundary Layer. The random pressure fluctuations in the turbulent boundary layer on the skin of a vehicle can be an important source of excitation. For supersonic flight vehicles the fluctuating pressures are sufficiently large as to constitute a significant input to the fatigue problem of the skin panels and to generate intense levels of noise and vibration within the vehicle. For underwater vehicles the boundary layer pressure fluctuations are generally not large enough to impose significant structural loadings but the noise generated may create problems for a vehicle trying to operate detection equipment while underway. Boundary layer pressure fluctuations on a panel are usually modeled by a random field characterized by a convected pattern of fairly coherent loading. The convective velocity in the boundary layer is of the order of 60–80 percent of the free stream velocity. See [34] for an up-to-date discussion of the measurements made and the models used to describe turbulent boundary layers.

Road and Track Roughness. Random irregularities in the surface of a road or track generate dynamic loads in the vehicles passing over them. Depending on the application, these loads may cause passenger discomfort, or may cause derailment or otherwise threaten the integrity of the vehicle structure. The elevation profile of a road is transformed into a time history of loading for the wheel of a vehicle that traverses the road at a given speed. Auto and cross- correlations for the loads at all wheels can be determined if the path and speed of the vehicle are known and if the spatial cross-correlation function of the road surface is known. At the present state of the art one-dimensional measurements are usually made along straight line paths. The resulting profiles can be

Downloaded 02 May 2010 to 171.66.16.250. Redistribution subject to ASME license or copyright; see http://www.asme.org/terms/Terms_Use.cfm

modeled by locally homogeneous random processes described by wave-number spectral density functions [35]. A two-dimensional random field model can be generated from this data if the assumption of spatial isotropy is made [36]. Vertical measurements along a pair of railroad tracks provide spectra for profile and cross-level and horizontal measurements provide spectra for alignment and gage. It is generally assumed that these four processes are independent [44].

Ocean Waves. Storm waves at sea constitute major loadings for ships and off-shore platforms. The elevation of the sea surface can be modeled as a two-dimensional quasi-homogeneous, quasi-stationary random field. It is customary to describe the surface in terms of straight-crested progressive wave patterns of given amplitude and frequency. In deterministic analysis a single fixed wave pattern is assumed for a sea state characterized by a significant wave height and wave period. A (linear or nonlinear) wave theory is used to define the corresponding fluid motion in the neighborhood of the ship or platform under consideration and a (linear or nonlinear) hydrodynamic law is used to determine the loading on the structure [37]. In random analysis the sea surface is considered to be a superposition of straight-crested waves of various amplitudes and frequencies as described by a spectral density function of wave heights. All wave components may be assumed to advance in the same direction, or in different directions as described by a directional wave spectrum [37]. The commonly used spectral models have parameters that depend on the sea state so that the long-term behavior of the field is described by a joint probability distribution of significant wave height and wave period [38]. Considerable current effort is being directed toward obtaining improved measurements of directional spectra and long-term distributions.

Earthquake Ground Motions. For many buildings, dams, bridges, and elevated highways a major design loading is that due to an anticipated earthquake. A number of probabilistic factors enter into the estimation of the location, intensity, and frequency of occurrence of earthquakes ([89, 156] of [16]; [4] of [19]). Earthquake ground motions involve triaxial accelerations at each point in the affected area. An important characteristic of the motion is its nonstationary nature. The strong motion phase of an earthquake seldom lasts longer than half a minute. In building codes it is common to specify design ground motions in terms of a single-degree-of-freedom "response spectrum." This simplifies the design of structures that can be modeled as a single-degree-of-freedom system but introduces ambiguity into the design of more complex systems. Recently, rational procedures for predicting response statistics of multidegree-of-freedom systems from excitations described by response spectra have been proposed by Vanmarcke [66] and by Der Kiureghian [54]. In research investigations ground motions have been modeled by "equivalent" stationary random processes, by stationary random processes modulated by deterministic envelope functions, and by other representations of nonstationary processes. In most work a uniform ground motion is assigned to the entire foundation. Array measurements to determine the nature of the ground motion random field are just beginning to be made [55].

Prediction of Random Response

Solving the random vibration response problem consists of determining probabilistic or statistical information about the dynamic response of a mechanical system from similar information about the excitation. The problem can be categorized according to the information sought and given, according to whether the system is linear or nonlinear, whether the excitation is external or parametric, whether the excitation (and also the response) is a single random process, a finite number of discrete processes, or a continuously distributed random field, and whether the response is stationary or nonstationary. Solution methods can be categorized according to whether they are exact or approximate. The class of problems for which exact solution procedures are known is quite limited. In principle, second-order statistics for the response of linear time-invariant systems can always be obtained if corresponding second-order statistics for the excitation are known. In practice, this may become intractable if the system is very complex or if the response is nonstationary. In principle, a linear partial differential equation for the response transition probably density function can always be obtained when the response is a Markov process. In practice, exact solutions of the partial differential equation are available in only a few special cases. Here we divide our discussion into three parts according to the type of dynamic system: linear time-invariant systems, nonlinear systems, and parametrically excited systems.

Linear, Time-Invariant Systems. Consider a single input-single output stable linear time-invariant dynamic system with a frequency response function $H(f)$. If the excitation is a stationary random process with mean value m_e and spectral density $W_e(f)$, then the mean value and spectral density of the stationary response are [2]

$$m_r = H(0)m_e$$
$$W_r(f) = |H(f)|^2 W_e(f) \tag{2}$$

independently of the probability distributions involved. If the excitation is a normal process then so is the response and the In this case a number of additional response properties useful in reliability studies, such as the average rate of crossing a fixed level, the distribution of maxima, and the distribution of the envelope are available [2] based on the work of S. O. Rice ([151] of [16]). These results extend formally to multiple input-multiple output systems [6], via matrices of frequency responses and matrices of excitation and response spectra including auto and cross- spectral density functions for finite numbers of inputs and outputs, and via space integrals of frequency influence functions and space-time cross-spectral density functions for random fields of input and output. Decomposition of the excitation and response into natural-mode components permits representing the response space-time cross-spectrum as a sum over all pairs of modes of modal cross-spectra. This modal sum has been widely used [7, 25] to obtain the spatial distribution of the mean-square response of structures.

When the number of modes involved is large the modal sum calculations become prohibitive. Estimates can be obtained by using asymptotic approximations [7, 25] or by using statistical energy analysis [39]. In the former, the asymptotic behavior of the natural modes and natural frequencies [7] is used along with such devices as replacing the discrete sum by a continuous integral to approximate the required modal sum. In the latter, crude estimates are obtained by analyzing power flow and energy storage in the structure based on estimates of how the energy is partitioned among modes. Usually the only specific information about the modes that is required is the average density of their natural frequencies along the frequency axis.

For structures with little modal overlap (light damping) the modal cross-correlations can be neglected in comparison with the modal autocorrelations. This greatly reduces the labor involved in evaluating the modal sums. The distribution of mean-square velocity response in uniform structures with little modal overlap when excited by stationary wide-band

Downloaded 02 May 2010 to 171.66.16.250. Redistribution subject to ASME license or copyright; see http://www.asme.org/terms/Terms_Use.cfm

random forces applied at isolated points, has several interesting features. When the number of excited resonances increases the mean-square velocity response tends to a uniform level over most of the structure independently of the boundary conditions. If the structure has some degree of symmetry (e.g., rectangular, circular, or equilateral triangular plates) there are narrow lanes or localized zones of intensified response which stand out from the substantially uniform response field [25]. The magnitude of the relative intensification of response in these lanes and zones is generally not sensitive to the excitation bandwidth but the intensification factor for the driving point of a square plate excited at its center increases without limit as the excitation bandwidth is increased (See Crandall and Zhu in [14]). There appear to be a number of interesting phenomena worthy of further research associated with the random response of systems in which the number of responding modes is so large that simplifying asymptotic trends are observed.

The response of a linear time-invariant system will be nonstationary if the excitation is nonstationary (which includes the transient periods associated with starting or stopping a stationary excitation). Even with stationary excitation the response can be nonstationary if the system has no damping, or is unstable. The first and second-order statistics for the response of a linear time-invariant system can in principle be obtained from those of the excitation [6, 8] although the labor involved is an order of magnitude greater than that for the stationary case. Double time integrations of the correlation functions or double frequency integrations of the generalized spectra are required to obtain mean-square responses. Nonstationary input-output relations have been given for Mark's instantaneous spectrum ([31] of [19]). Recently the stochastic averaging method (see section Approximate Methods for Nonlinear Systems) has been applied (see P. D. Spanos in [14]) to obtain approximate response statistics when the excitation was modeled (*i*) by an evolutionary process and, (*ii*) by a modulated stationary process. Additional references to material on nonstationary response can be found in [6, 16, 19].

Nonlinear Systems. In the past two decades considerable effort has been extended in developing techniques to predict the response of nonlinear dynamic systems to random excitation [16–22]. When the excitation is a white noise process (or a field of independent white noises) the response is a Markov process. The transition probability density function, which together with an initial distribution (or distributions) completely describes the response, satisfies a linear partial differential equation known as the Fokker-Planck-Kolmogorov (FPK) equation. See Fuller ([30] of [20]) for a good historical account of this equation. The (variable) coefficients in the FPK equation can be derived from the nonlinear equations of motion of the dynamic system. Two procedures have been developed for this. In the first procedure ([183] of [16]), favored by physicists and engineers, the drift and diffusion coefficients are obtained by limit operations (see Appendixes in Fuller [30] of [20], and in Crandall [16] of [23]) applied directly to the equations of motion. In the second procedure [10], favored by mathematicians, the equations of motion are replaced by an "equivalent" set of Itô-equations according to certain translation rules and the drift and diffusion coefficients obtained by formal operations on the coefficients of the Itô-equations. The two procedures are operationally parallel for external excitation but differ for parametric excitation. The resulting FPK equation is the same in every case. There was a period of confusion and controversy ([80] of [16]) between the two procedures before the translation rules were clarified by Wong and Zakai (p. 125 of [10]).

The difference between the two approaches arises because of the pathological properties of white noise and Markov processes. A special stochastic calculus is required for a mathematically rigorous treatment of these extreme concepts. Physically realizable excitations and responses on the other hand are mathematically well behaved. In random vibration analysis, real excitations with short correlation times are replaced by white noise models in the expectation that the Markov response to the white noise will be easy to obtain and will provide a useful approximation to the real response. The statistical properties of the Markov process are given by the FPK equation, which is itself a well-behaved partial differential equation expressed in terms of the usual differential calculus. Its drift and diffusion coefficients can be obtained by ordinary limiting processes from the equations of motion provided that the excitation is treated as having small but finite correlation time (i.e., physically realizable) until the final step when the correlation time is allowed to approach zero. In this way approximations to the statistical properties of the real response process are obtained without ever dealing with the pathological properties of a Markov process. The Itô calculus (p. 112 of [10]) was developed in 1944 as a rigorous procedure for integrating and differentiating stochastic processes of the Markov type. It unfortunately was not designed to insure that the stochastic differential equations for the limiting Markov process would have the same format as the equations of motion for a smooth response whose broad-band excitation tended toward white noise. It does however provide drift and diffusion coefficients in a simple manner from a stochastic differential equation for a Markov process. In 1966 an alternative stochastic calculus of comparable rigor was devised by Stratonovich (p. 116 of [10]). This calculus does have the property that the stochastic differential equation for the Markov process has exactly the same format as the equations of motion for less pathological processes. The rules for obtaining the drift and diffusion coefficients from Stratonovich equations are slightly more complicated than those for Itô equations.

When the time derivative in the FPK equation is set equal to zero, the equation describes the first-order probability distribution for the stationary response. This distribution is readily obtained for a limited class of vibratory systems with nonlinear restoring forces and special forms of nonlinear damping. See Fuller ([30] of [20]) and Caughey [17]. The class of systems involved is that in which there is equipartition of energy among the various degrees of freedom. Systems with only a single degree of freedom are automatically included. The exact mean-square response and average frequency provided by the first-order distribution have been widely used as a basis for comparison with results of various approximate procedures. The time-dependent solution to the FPK equation, i.e., the transition probability density function, has been obtained for linear time-invariant systems by Wang and Uhlenbeck ([183] of [16]) and only a very few nonlinear systems [17, 20].

For the response to be approximated by a Markov process it is necessary that the excitations be approximated by white noises. This restriction can be in principle be removed, at the price of increasing the complication of the system, by introducing linear filters between the white-noise excitations and the system. The filters serve to produce realistic excitation spectra for the nonlinear system while the white-noise excitations driving the filters guarantee that the response of the extended system is a Markov process (of higher order) for which an extended FPK equation can be written. This strategy has often been suggested but it has apparently never been implemented for nonlinear response problems.

Approximate Methods for Nonlinear Systems. A great

Downloaded 02 May 2010 to 171.66.16.250. Redistribution subject to ASME license or copyright; see http://www.asme.org/terms/Terms_Use.cfm

many approximate procedures for estimating nonlinear response statistics have been proposed. Most of the known techniques for deterministic excitation have been extended to apply to random excitation. Approximation methods have been based directly on the system equations of motion or indirectly on the associated FPK equation. Perhaps the two most broadly applicable procedures are statistical linearization and numerical simulation. The statistical or equivalent linearization method [18, 19, 21, 22] is an extension to random excitation of the Krylov and Bogoliubov equivalent linearization method (the describing function method of control theory) for deterministic excitation. It was independently introduced by Booton, Kazakov, and Caughey [18]. Nonlinear stiffness and damping elements in the vibratory system are replaced by optimal linear elements obtained by minimizing the mean-square discrepancy between the nonlinear and linear equations. The procedure is one of the simplest to implement. It applies to systems with many degrees of freedom and can be adapted to nonstationary as well as stationary excitation. Although rationalizations for the procedure usually appeal to a small nonlinearity argument it fortuitously turns out that the error in mean-square response remains quite modest even for large nonlinearities ([10] of [21]; [56]).

Numerical simulation or the Monte Carlo method [7, 22] consists of generating a large number n of sample excitations, computing the corresponding response samples, and processing them to obtain the desired response statistics. The procedure is in principle very general, applicable to stationary or nonstationary response of systems of any degree of complication (that can be modeled in a digital or analog computer). The main drawback of the method is cost. The statistical uncertainty in the response statistics decreases in proportion to $n^{-1/2}$ while the cost increases essentially in proportion to n. To gain one additional significant figure in a result requires a hundredfold increase in cost. Spanos [22] has estimated that, for cases where both statistical linearization and numerical simulation can be applied, the computational efficiency of the former will be of the order of 100 to 1000 times better than the latter. In applications where no exact solution is available numerical simulation is often used as a basis for assessing the accuracy of other approximate methods.

A set of differential equations for various statistical moments of the response, as functions of time, can be obtained by multiplying the FPK equation by suitable functions and integrating over the probability space. Equivalent sets of equations can be derived directly from the dynamic equations of motions or the equivalent Itô equations. The response problem is thus reduced to a set of coupled ordinary differential equations. For linear systems the set of equations closes in the sense that for some finite n there is a set of n independent equations in which only n unknown moments appear. For nonlinear systems the set of equations forms an infinite hierarchy: there are always more unknown moments than equations. Approximate solutions have been proposed based on ad-hoc closure assumptions: certain higher order moments are neglected or assumed to be related to lower order moments in the same way that moments of Gaussian processes are related [7, 20, 23]. A non-Gaussian closure method, based on constructing an approximate representation of the systems probability density function with n adjustable parameters and using n independent moment equations to determine the parameters, was proposed by Dashevskii and Liptser ([1] of [57]). The method gives good results in some cases ([16] of [24]) but is apparently not a very robust procedure [57].

The designation "stochastic averaging" has been applied to a class of procedures in which rapid fluctuations are averaged to provide simpler equations for slowly fluctuating quantities. The procedure is a nontrivial extension of the Krylov-Bogoliubov averaging method for deterministic excitations since it involves accounting for the averaged effect of a random excitation multiplied by a correlated response. We describe three stochastic averaging methods. The first, introduced by Stratonovich [40] and rigorously justified by Khasminskii [41] and by Papanicolaou and Kohler [42], applies to narrow-band responses which are represented as sinusoidal oscillations with slowly varying amplitude and phase. Approximate equations for the slowly varying quantities are obtained by time-averaging the rapid fluctuations. In the second method the drift and diffusion coefficients in the FKP equation are averaged with respect to time. The mathematical basis for this method is contained in a theorem by Khasminskii [43]. In the third method the response variables are divided into rapidly varying quantities and slowly varying quantities and approximate equations for the latter are obtained by averaging the rapid fluctuations of the former. The basis for this is also due to Khasminskii ([103] of [28]). For a single-degree-of-freedom oscillator the rapidly varying quantity is the displacement and the slowly varying quantity is the energy envelope (See Dimentberg [28], Roberts [14], Spanos [14], and Zhu [14]). Stochastic averaging methods have been extensively applied to nonlinear and parametric excitation problems [7, 13, 14, 20, 23, 24, 28].

When the amount of nonlinearity in a system is controlled by a small parameter ϵ then the perturbation method may be used. The solution is sought in terms of a power series in ϵ and the successive terms evaluated as linear responses to nonlinear functions of the preceding terms. This classical approach for deterministic nonlinear problems was extended to random vibration problems by Crandall ([49] of [16]). In practice the calculations are seldom carried beyond the first perturbation. The perturbation series is often an asymptotic series so that higher order perturbations improve the approximation for small ϵ at the expense of worsening it for large ϵ.

A variety of approximate methods have been proposed to solve the FPK equation corresponding to broad-band excitation of a nonlinear dynamic system. In principle the time-varying solution can be expressed as a sum of eigenfunctions in state space decaying at time rates proportional to the corresponding eigenvalues. The eigenvalue problem with variable coefficients can be solved approximately by iteration methods, perturbation methods, and various numerical procedures [17, 20]. All of the methods investigated so far appear to involve prodigious amounts of labor.

A continuing research goal is to find an efficient procedure for predicting nonlinear random response statistics that can be applied to multidegree-of-freedom systems. Possibly the most important goal for further research is to develop improved procedures for obtaining second-order statistics (spectra and correlation functions) for the stationary response of a nonlinear system. At present the only practical methods available for estimating these functions are statistical linearization and numerical simulation. Spectra obtained by statistical linearization are always for equivalent linear systems and therefore incapable of displaying the effects of nonlinearity upon spectra. Spectra obtained by Monte Carlo methods can in principle be as accurate as desired. High cost has however limited investigation by this approach.

The procedures developed so far have been applied to a wide range of nonlinear problems. One of the most-studied systems is the Duffing oscillator. In addition to the usual statistics that follow from the stationary joint distribution of displacement and velocity ([48] of [16]), a few inherently nonlinear aspects of the response have been investigated. Using a combined perturbation and linearization procedure, Dienes [17] showed that the response spectrum has two peaks,

Downloaded 02 May 2010 to 171.66.16.250. Redistribution subject to ASME license or copyright; see http://www.asme.org/terms/Terms_Use.cfm

a large one near the natural frequency and a small one near the third harmonic. When the Duffing oscillator is excited by narrow-band random excitation there can be a range of input center frequencies for which there are two stable stationary responses just as there is for sinusoidal excitation. This was demonstrated independently by Lyon ([121] of [16]) and by Dimentberg [28] using statistical linearization, and by Bolotin [7] using the method of moments. The jump phenomenon, as the response passes from one stationary level to the other, has been studied by Dimentberg [28]. Another widely studied system is the Van der Pol oscillator. Stratonovich [40] showed that the addition of small random excitation had the effect of decreasing the mean value of the limit cycle amplitude while increasing the mean square of the amplitude. Faulty analyses leading to an opposite conclusion were given independently by Caughey and Piszczek, as was pointed out by Ariaratnam (p. 192 of [13]). Additional research is required to further clarify the nature of random vibration in the presence of such nonlinear phenomena as jumps and limit cycles.

An important practical application of random vibration of nonlinear systems is in research on structural response to earthquake excitations. The nonlinearity enters through plastic deformation of the structural elements and joints. This kind of history-dependent restoring force is awkward to model. Clever techniques for representing hysteretic behavior by means of auxiliary differential equations have been developed by Wen [58]. The earthquake response problem is further complicated by the nonstationary nature of the excitation. A number of approximate procedures including statistical linearization and stochastic averaging have been applied [18, 19, 21, 22].

Parametric Excitation. A vibratory system in which the effective stiffness and/or damping parameters are forced to vary with time is said to be parametrically excited. The most important property of such systems is that for periodic parametric excitation there are ranges of excitation amplitude and frequency for which the response remains bounded (stable) and ranges for which the response grows without limit (unstable). There has been considerable interest in studying the behavior of these systems under random parametric excitation [23, 24]. Most investigations (even for deterministic excitation) have been directed toward delineating the boundaries between stable and unstable response without attempting to characterize the response in any futher detail.

A central problem with random response concerns how stability is to be defined for analytical purposes and how it is to be recognized in experimental observations of response. Kozin ([1] of [23]) points out that for each of the several deterministic stability definitions there are at least three corresponding random definitions depending on whether convergence occurs in probability, in the mean of order p, or in the almost sure sense. He has also addressed ([147] of [23]) the problem of deciding stability on the basis of observed data (see also [7]).

The principal procedures that have been developed for studying random parametric excitation are moment methods and methods based on a Lyapunov function [7, 23]. In the former, a set of ordinary differential equations is obtained for certain response moments and the system stability decided on the basis of the stability of the moments. In the latter, use is made of an energy-like non-negative function V of the response and the system stability decided on the basis of the sign of $d/dt <V>$. In implementing these approaches it is often necessary to incorporate one or more of the approximate procedures described in the preceding section; e.g., linearization, averaging, moment closure, etc. Results of a wide variety of methods have been compared with each other and with experiment [7, 23]. Much effort has also gone into developing a mathematical theory for the case where the parametric excitation consists of white noises and the response is a Markov process. This work generally makes use of stochastic calculus (either that of Itô or that of Stratonovich) and is described in the books on stochastic stability by Kushner ([14], p. 141 of [10]) and Khasminskii [41].

An interesting problem which has attracted many contributions [23] is that of the inverted pendulum. The statically unstable upright position of the pendulum can be stabilized by a single frequency vertical oscillation of the point of support provided that its amplitude is sufficiently large. Two such stabilizing parametric excitations when superposed may cause a loss of stability if their frequencies are close together, or if one frequency is nearly twice the other. There has been considerable speculation as to whether the upright position could be stabilized by a stationary random process with a continuous spectrum and, if so, whether it is necessary to filter out low frequencies. Analog computer simulations by Mitchell ([60] of [23]) using band-limited white noise with the lowest 10 percent of the spectrum removed indicated stability for pendulums with damping greater than a critical value. These results were modeled reasonably well in an analysis by Howe ([59] of [23]) that uses a spectrum that includes these low frequencies but for which the stability threshold depends on both the intensity and the upper roll-off frequency of the excitation as well as the damping and other pendulum parameters.

When a nonlinear system is parametrically excited, the stability of the equilibrium position can usually be decided on the basis of a linearized approximation to the equations of motion. If the equilibrium is unstable, the linearized equations predict unbounded growth of the solutions. In a nonlinear system, however, solution trajectories escaping from an unstable equilibrium often end up in bounded limit cycles. Recently Zhu [14] considered a single-degree-of-freedom oscillator with nonlinear stiffness, nonlinear damping, and nonlinear inertia whose equilibrium was unstable when subjected to white-noise parametric excitation. Using the third form of stochastic averaging, he showed that when the destabilizing excitation was applied to the stiffness parameter, the response process would be limited by sufficiently strong nonlinearities in any one of the three following cases: (*i*) nonlinear stiffness with linear damping and inertia; (*ii*) nonlinear damping with linear stiffness and inertia, (*iii*) nonlinear inertia with linear stiffness and damping. When the destabilizing excitation was applied to the damping parameter, however, the response could be limited in cases (*ii*) and (*iii*), but it could not be limited by any form of stiffness nonlinearity coupled to linear damping and inertia.

Reliability

The major use of response statistics is as data on which decisions concerning safety and reliability are made. In many cases empirical rules based simply on RMS response levels are applied. If, however, a well-defined failure model is available it may be possible to continue the chain of probabilistic reasoning and derive statistical or probabilistic measures of the safety. The most common measure in use today is the reliability function $R(T)$ which is the probability of nonfailure after a life of duration T. There has been active theoretical development of two failure models under random vibration: (*i*) failure occurs the first time a particular response quantity oversteps a threshold, as when a vibrating relay contact first touches the frame and shorts out; and (*ii*) failure occurs due to an accumulation of many small damages inflicted throughout the life of the system, as occurs in wear and fatigue.

The first passage problem has a simple answer [2] if the response is stationary and its average crossing rate is known

Downloaded 02 May 2010 to 171.66.16.250. Redistribution subject to ASME license or copyright; see http://www.asme.org/terms/Terms_Use.cfm

and it is assumed that crossings of the threshold are sufficiently rare as to constitute a process of Poisson. In this case the reliability function is a simple exponential decay. Under weaker assumptions the problem becomes much more difficult. For an oscillator excited by white noise the problem reduces to solving a partial differential equation of FPK type with an absorbing boundary condition. A wide variety of approximate solution techniques have been applied. Surveys of results are available for linear oscillators [19, 45] and for nonlinear oscillators [46]. Comparison of analytical predictions with measurements on a cantilever beam undergoing random vibration are reported in [47].

Fatigue failure is a very much more complicated mechanism. Although the general nature of crack initiation, crack growth and final fracture of metal specimens under fluctuating loads is known, there is a large scatter in fatigue lives of identical specimens tested under identical laboratory conditions with identical deterministic load histories. The additional scatter introduced by stationary random load histories is often small in comparison. Most engineering design (see, for example [38]) is based on a highly idealized model in which each cycle of a narrow-band random stress history is assigned a nominal fractional damage obtained from life tests at constant amplitudes. The mean and variance of the sum of the elementary damages accumulated in a given time, is estimated [2] from the probability distribution of peaks in the random stress history. Failure is predicted to occur when the accumulated fractional damage sum reaches unity. The corresponding probability distribution of the time of failure and the reliability are discussed in [7]. The simple cumulative damage law used here does not model reality in that it is indifferent to the order in which cycles of different stress amplitude are applied, whereas the results of many tests indicate that the sequence in which different stress levels are applied can have considerable effect on fatigue life. In spite of this the discrepancies between life predictions for narrow-band random stress histories and test results are not excessive [48]. The general philosophy of this approach has been extended to wider band random stress histories by introducing more sophisticated techniques for counting elementary damage events; e.g., rainflow counting [49]. More elaborate models for fatigue under random loading have recently been proposed [50, 51].

Data Processing

The transformation of raw time histories from vibration transducers into statistical or probabilistic functions is called data processing. The most common statistical functions in random vibration are spectral densities and correlations but in addition probability density functions, coherence functions, and cepstrum functions are required in particular applications. Essentially all random signal measurements made with commercial data-processing instrumentation are interpreted on the basis of the assumption that the data record operated on is a segment of a sample from a stationary process. There has been a remarkable development of data-processing equipment during the past 30 years. Spectral analyzers, for example, evolved from analog instruments which measured one frequency at a time, to instruments with automatic frequency sweep which could complete a spectrum in under half an hour, to "real-time" analyzers that combined digital time-compression techniques with analog analyzers, to completely digital instruments that made use of either the FFT or digital filters. Single-channel units have given way to two-channel units with a wide variety of processing options available at the push of a button.

The importance of spectral analysis is due to the simplicity of the frequency domain description of linear time-invariant system dynamics and the corresponding ease of interpretation of spectral descriptions of excitations and responses. The theory of spectral density measurement has been widely discussed (Vol. 2 of [1]; [10] of [16]; [8, 52]). There is a fundamental trade-off between the frequency resolution of the measurement and its statistical uncertainty which must be carefully considered when measuring records of limited duration. It is not possible to obtain both high resolution and low statistical uncertainty without having very long records. Applications of spectral analysis are described in [9, 52]. Recent developments in spectral analysis [26] have been aimed at improving spectral resolution by using nonlinear data-adaptive procedures. Examples of these are the maximum entropy and maximum likelihood methods. The central idea of the former is that the correlations, for time lags too large to permit estimation of the correlation from the data sample, are not simply neglected but are extrapolated on the basis that the spectral estimate should be the most random (i.e., have maximum entropy) consistent with the estimated correlations for the time lags available. The maximum likelihood spectral estimate can be considered to result from solving an optimal filtering problem in which the power within a narrow band about the signal frequency of interest is passed while minimizing the interference from other spectral components. These nonlinear methods require more extensive calculations than the classical linear procedures but they achieve sharper resolution from a limited duration sample. A maximum entropy spectrum has better frequency resolution at the price of greater statistical uncertainty in comparison with the corresponding maximum likelihood spectrum [24].

Correlation functions contain, in principle, the same statistical information presented in a time domain as the corresponding spectra display in the frequency domain. In some applications the time-domain presentation is more convenient, e.g., measurement of time delays, determination of transmission paths, detection and recovery of signals in noise, etc. Correlation measurement techniques are described in ([10] of [16]) and [8]. Applications are discussed in [9]. It is interesting that prior to 1965 when the FFT algorithm was discovered by Cooley and Tukey ([9] of [5]), the digital processing procedure of choice for obtaining a spectrum ([10] of [16]) was first to evaluate the corresponding correlation and then Fourier transform it, whereas today the opposite procedure is more common. Spectra are computed first and then if correlations are desired they are obtained by Fourier transforming the corresponding spectra.

Probability density functions are usually measured to provide a probabilistic measure of the signal amplitude. They may also be used to detect nonlinear effects or to distinguish between random or sinusoidal signals. Analog and digital measurement techniques are described in [8].

Coherence functions are essentially normalized magnitudes of (complex valued) cross spectra considered as functions of frequency. They are commonly available as supplementary outputs in two-channel spectral analyzers. Coherence functions between excitation and response process are used to detect extraneous noise in experimental measurements and to test the linearity of the dynamic system. See [9] for applications.

The term cepstrum analysis is applied to a family of data-processing procedures whose common feature is that a logarithm of a spectral density is Fourier transformed. The transformed domain is called the quefrency domain. The words cepstrum and quefrency are transformations of the words spectrum and frequency in which the letters of the first syllables are rearranged. In cepstrum analysis there also arise the terms gamnitude and saphe (derived from magnitude and phase) and lifter and rahmonic (derived from filter and harmonic). The point of this play on words is that when a spectrum is the product of two frequency functions as in

Downloaded 02 May 2010 to 171.66.16.250. Redistribution subject to ASME license or copyright; see http://www.asme.org/terms/Terms_Use.cfm

equation (2) its logarithm is the sum of two contributions whose effects may sometimes be separated in the quefrency domain. Cepstrum analysis has been applied to seismic and underwater signals containing echoes, and to harmonics and side bands produced by gear boxes and other rotating machines. It may be used simply to identify certain components of a signal or may be used to reconstruct the signal with one component deleted. See [53] for a description of cepstrum analysis techniques.

System Identification

The process of using excitation and response data to deduce properties of the dynamic system is called system identification. In most cases a specific form of system representation with unknown parameters is selected a priori so that the process is actually one of parameter identification. For example, the parameters may be the stiffness, damping, and inertia parameters in a differential equation model of the system, or they may be the poles and zeros of a transfer function description of the system. In practical applications to linear time-invariant vibratory systems the most common parameters are the natural frequencies, damping ratios, and mode shapes of the natural modes. The estimation of these quantities from test data is called modal analysis. There has been a burst of activity in this area [59] spurred on by the availability of spectral analyzers connected to minicomputers. For the most part modal analysis is performed with deterministic excitations; e.g., one or more shakers driven at a common frequency might be used or an instrumented impact hammer might be used.

When the excitation and response are stationary random processes, then according to equation (2) the quotient of their spectral densities provides the amplitude, but not the phase, of a linear system frequency response function. This is sufficient, however, to provide estimates of the natural frequencies and damping ratios. If the cross-spectrum between excitation and response is measured along with the spectral density of the excitation, then the system frequency response is, in principle, completely determined [3]. Corresponding statements apply to correlation functions and system impulse response functions with multiplication in the frequency domain replaced by convolution in the time domain. If the excitation is not available for measurement but is assumed to be broad-band with substantially flat spectrum over the frequency range of interest then it is possible to estimate natural frequencies and damping ratios by only measuring the response spectral density. Natural mode shapes may also be estimated by using two or more response transducers and measuring response cross-spectra as well as autospectra. This procedure has been successfully implemented to estimate modal parameters for large structures such as bridges and tall buildings [60] where the broad-band excitation is provided by the natural noise of the ambient environment: microseismic activity, wind, traffic, etc. It has also been extended to nonstationary random excitation as provided by earthquakes [61]. In a recent application [62] the maximum entropy method of spectral estimation was used to obtain an improved estimate of the damping ratio of an offshore platform.

An alternative procedure for utilizing unmeasured broad-band random excitation is the random decrement signature method proposed by H. A. Cole, Jr. in 1968 [63]. The randomdec signature of a stationary random signal, associated with a particular signal value, is the average waveform of a large number of separate segments of the signal, all of which are triggered to begin at instants when the signal passes through the assigned value. It has been heuristically argued that the randomdec signature of the response of a dynamic system is equivalent to the free decay response of that system. As such it has been used to estimate natural frequencies and damping ratios of vibratory systems. Recently it was shown that the randomdec signature of a stationary random process is (to within a constant of proportionality) a statistical estimate of the autocorrelation function of the process [63]. For a lightly damped single-degree-of-freedom vibratory system the autocorrelation function of the response to broadband excitation is only an approximation to a free decay response. The approximation, however, becomes exact in the limit as the excitation approaches white noise. The randomdec method has been incorporated into a time domain modal analysis technique [64].

Much of the practical work on system identification under random vibration has not been based on the formal procedures of classical statistics; e.g., questions of bias, statistical reliability, quality of estimates, etc., are seldom addressed. The most widely applicable classical method of parameter identification is the maximum likelihood method. In outline a likelihood function is constructed from the observed data and the desired parameters so that it is essentially the probability density function for the observations. The estimated parameter values are then those that maximize the likelihood function. The procedure is flexible and gives asymptotically unbiased minimum variance estimates of the desired parameters. It does, however, require extensive calculation. See [65] for a survey. A limited information maximum likelihood method based on field data was employed by Shinozika, Imai, Enami, and Takemura [13] to identify aerodynamic parameters for a suspension bridge. An analog simulation study showed the procedure to be superior to the ordinary least squares method. The forms of maximum likelihood estimates of system parameters for linear and nonlinear systems subjected to white-noise excitations were given by Kozin [14]. He gave a rigorous explanation for the commonly experienced fact that for a linear oscillator the stiffness estimate has smaller relative error than the damping estimate. Finally, under system identification, mention should be made of the theoretical investigations of Dimentberg [28] addressed to such qualitative problems as determining from the response process of a nonlinear oscillator whether the system was self-excited, externally excited, or parametrically excited.

References

1 Crandall, S. H., ed., *Random Vibration*, The MIT Press, Cambridge, Mass., Vol. 1, 1958; Vol. 2, 1963.

2 Crandall, S. H., and Mark, W. D., *Random Vibration in Mechanical Systems*, Academic Press, New York, 1963.

3 Robson, J. D., *An Introduction to Random Vibration*, Edinburgh Univ. Press, 1963.

4 Bolotin, V. V., *Statistical Methods in Structural Mechanics*, Holden-Day, San Francisco, 1969.

5 Newland, D. E., *An Introduction to Random Vibration and Spectral Analysis*, Longmans, London, 1975.

6 Lin, Y. K., *Probabilistic Theory of Structural Dynamics*, McGraw-Hill, New York, 1967.

7 Bolotin, V. V., *Random Vibration in Elastic Systems*, Nauka, Moscow, 1979 (in Russian).

8 Bendat, J. S., and Piersol, A. G., *Random Data: Analysis and Measurement Procedures*, Wiley-Interscience, New York, 1971.

9 Bendat, J. S., and Piersol, A. G., *Engineering Applications of Correlation and Spectral Analysis*, Wiley, New York, 1980.

10 Jazwinski, A. H., *Stochastic Processes and Filtering Theory*, Academic Press, New York, 1970.

11 Arnold, L., *Stochastic Differential Equations: Theory and Applications*, Wiley, New York, 1974.

12 Khasminskii, R. Z., *Stochastic Stability of Differential Equations*, Sijthoff & Norrdhoff, Alphen aan den Rijn, The Netherlands, 1980.

13 Clarkson, B. L., ed., *Stochastic Problems in Dynamics*, Pitman, London, 1977.

14 *Proc. IUTAM Symp. on Random Vibration*, held in Frankfurt on Oder, Nov. 1-5, 1982, to appear.

Downloaded 02 May 2010 to 171.66.16.250. Redistribution subject to ASME license or copyright; see http://www.asme.org/terms/Terms_Use.cfm

15 Crandall, S. H., "Random Vibration," *Appl. Mechs. Revs.*, Vol. 12, 1959, pp. 739–742.

16 Crandall, S. H., "Random Vibration," in *Applied Mechanics Surveys*, Abramson, H. N., Liebowitz, H., Crowley, J. M., and Juhasz, S., eds., Sparton Books, Washington, D.C., 1966, pp. 681–689.

17 Caughey, T. K., "Nonlinear Theory of Random Vibrations, in *Advances in Applied Mechanics*, Vol. 11, Academic Press, New York, 1971, pp. 209–253.

18 Crandall, S. H., "Nonlinear Problems in Random Vibration," in *Internationale Konferenz uber Nichtlinear Schwingungen*, Band II, 1, Abh. Akad, Wissensch. DDR, Berlin, 1977, pp. 215–224.

19 Vanmarcke, E. H., "Some Recent Developments in Random Vibration," *Appl. Mechs. Revs.*, Vol. 32, 1979, pp. 1197–1202.

20 Roberts, J. B., "Response of Nonlinear Mechanical Systems to Random Excitation, Part 1: Markov Method," *Shock and Vibration Digest*, Vol. 13, 1981, pp. 17–28.

21 Roberts, J. B., "Response of Nonlinear Mechanical Systems to Random Excitation, Part 2: Equivalent Linearization and Other Methods," *Shock and Vibration Digest*, Vol. 13, 1981, pp. 15–29.

22 Spanos, P. D., "Stochastic Linearization in Structural Dynamics," *Appl. Mechs. Revs.*, Vol. 34, 1981, pp. 1–8.

23 Ibrahim, R. I., and Roberts, J. W., "Parametric Vibration, Part 5: Stochastic Problems," *Shock and Vibration Digest*, Vol. 10, 1978, pp. 17–38.

24 Ibrahim, R. I., and Roberts, J. W., "Parametric Vibration, Part 6: Stochastic Problems," *Shock and Vibration Digest*, Vol. 13, 1981, pp. 23–25.

25 Crandall, S. H., "Random Vibration of One- and Two-Dimensional Structures," in *Developments in Statistics*, Krishnaiah, P. R., ed., Vol. 2, Academic Press, New York, 1979, pp. 1–82.

26 Kay, S. M., and Marple, S. L., Jr., "Spectrum Analysis — A Modern Perspective," *Proc. IEEE*, Vol. 69, 1981, pp. 1380–1419.

27 Vanmarcke, E. H., *Random Fields: Analysis and Synthesis*, The MIT Press, Cambridge, Mass., 1983.

28 Dimentberg, M. F., *Nonlinear Stochastic Problems of Mechanical Vibrations*, Nauka, Moscow, 1980 (in Russian).

29 Hoblit, F. M., Paul, N., Shelton, J. D., and Ashford, F. E., "Development of a Power-Spectral Gust Design Procedure for Civil Aircraft," FAA Report No. ADS-53, Jan. 1966 (AD 651152).

30 Davenport, A. G., and Novak, M., "Vibration of Structures Induced By Wind," *Shock and Vibration Handbook*, Harris, C. M. and Crede, C. E., eds., McGraw-Hill, New York, 1976, Chapter 29, pp. 21–43.

31 Johns, D. J., "Wind Excited Behaviour of Structures, Part 3," *Shock and Vibration Digest*, Vol. 14, 1982, pp. 23–38.

32 Richards, E. J., and Mead, D. J., eds., *Noise and Acoustic Fatigue in Aeronautics*, Wiley, New York, 1968.

33 Belcher, P. M., "Selected Topics From the Structural Acoustics Program for the B-1 Aircraft," *Shock and Vibration Bull.*, Vol. 49, 1979, pp. 55–68.

34 Blake, W. K., *The Mechanisms of Flow-Induced Sound and Vibration*, Addison-Wesley, Reading, Mass., 1983.

35 Dodds, C. J., and Robson, J. D., "The Description of Road Surface Roughness," *J. Sound and Vibration*, Vol. 31, 1973, pp. 1975–1983.

36 Kamash, K. M., and Robson, J. D., "The Application of Isotropy in Road Surface Modelling," *J. Sound and Vibration*, Vol. 57, 1978, pp. 89–100.

37 Price, W. G., and Bishop, R. E. D., *Probabilistic Theory of Ship Dynamics*, Chapman and Hall, London, 1974.

38 Kinra, R. K., and Marshall, P. W., "Fatigue Analysis of the Cognac Platform," *Offshore Technology Conference Proceedings*, OTC 3378, 1979.

39 Lyon, R. H., *Statistical Energy Analysis of Dynamical Systems*, The MIT Press, Cambridge, Mass., 1975.

40 Stratonowich, R. L., *Topics in the Theory of Random Noise*, Vol. 2, Gordon and Breach, New York, 1967.

41 Khasminski, R. Z., "A Limit Theorem for the Solutions of Differential Equations With Random Right-Hand Sides," *Theory of Probability & Applications*, Vol. 11, 1966, pp. 390–405.

42 Papanicolaou, G. C., and Kohler, W., "Asymptotic Theory of Mixing Stochastic Ordinary Differential Equations," *Comm. on Pure and Appl. Math.*, Vol. 27, 1974, pp. 614–668.

43 Khasminski, R. Z., "Principle of Averaging for Parabolic and Elliptic Differential Equations and for Markov Processes With Small Diffusion," *Theory of Probability & Applications*, Vol. 8, 1963, pp. 1–21.

44 Corbin, J. C., "Statistical Characterization of Track Geometry," FRA/ORD Report 80/22.1, Mar. 1980 (PB81-17920).

45 Crandall, S. H., "First-Crossing Probabilities of the Linear Oscillator," *J. Sound and Vibration*, Vol. 12, 1970, pp. 285–299.

46 Roberts, J. B., First-Passage Time for Oscillators With Nonlinear Restoring Forces," *J. Sound and Vibration*, Vol. 56, 1978, pp. 71–86.

47 Roberts, J. B., and Yousri, S. N., "An Experimental Study of First-Passage Failure of a Randomly Excited Structure," ASME JOURNAL OF APPLIED MECHANICS, Vol. 45, 1978, pp. 917–922.

48 Pook, L. P., and Greenan, A. F., The Effect of Narrow-Band Random Loading on the High Cycle Fatigue Strength of Edge-Cracked Mild Steel Plates," *Int. J. Fatigue*, Vol. 1, 1979, pp. 17–22.

49 Downing, S. D., and Socie, D. F., "Simple Rainflow Counting Algorithms," *Int. J. Fatigue*, Vol. 4, 1982, pp. 31–40.

50 Oh, K. P., "The Prediction of Fatigue Life Under Random Loading: A Diffusion Model," *Int. J. Fatigue*, Vol. 2, 1980, pp. 99–104.

51 Bogdanoff, J. L., and Kozin, F., "On a New Cumulative Damage Model for Fatigue," *Proc. Ann. Reliability & Maintainability Symposium 1981*, pp. 9–17.

52 Jenkins, G., and Watts, D., *Spectral Analysis and Its Applications*, Holden-Day, San Francisco, 1969.

53 Childers, D. G., Skinner, D. P., and Kemerait, R. C., "The Cepstrum: A Guide to Processing," *IEEE Proc.*, Vol. 65, 1977, pp. 1428–1443.

54 Der Kiureghian, A., "A Response Spectrum Method for Random Vibration Analysis of MDF Systems, Earthquake Eng. and Struct. Dyn., Vol. 9, 1981, pp. 419–435.

55 Bolt, B. A., Tsai, Y. B., Yeh, K., and Hsu, M. K., "Earthquake Strong Motions Recorded by a Large Near-Source Array of Digital Seismographs," *Earthquake Eng. and Struct. Dyn.*, Vol. 10, 1982, pp. 561–573.

56 Crandall, S. H., "Heuristic and Equivalent Linearization Techniques for Random Vibration of Nonlinear Oscillators," *Proc. VIII Int. Conf. Nonlinear Oscillations*, Prague, 1979, pp. 211–226.

57 Crandall, S. H., "Non-Gaussian Closure Techniques for Stationary Random Vibration," *Proc. IX Int. Conf. Nonlinear Oscillations*, held in Kiev, Aug. 30–Sept. 5, 1981, to appear.

58 Baber, T. T., and Wen, Y.-K., "Random Vibration of Hysteretic, Degrading Systems," *J. Eng. Mechs. Div. ASCE*, Vol. 107, EM6, 1981, pp. 1069–1087.

59 *Proc. 1st Intl. Modal Analysis Conference*, Union College, Schenectady, N.Y., 1982.

60 Udwadia, F. E., and Trifunac, M. D., "Ambient Vibration Tests of Full-Scale Structures," in *Proc. 5th World Conf. Earthquake Eng.*, Rome, 1973, pp. 1430–1439.

61 Beck, J. L., and Jennings, P. C., "Structural Identification Using Linear Models and Earthquake Records," *Earthquake Eng. and Struct. Dyn.*, Vol. 8, 1980, pp. 145–160.

62 Briggs, M. J., and Vandiver, J. K., "Multichannel Maximum Entropy Method of Spectral Analysis Applied to Offshore Platforms," *Offshore Technology Conference Proceedings*, OTC 4286, 1982.

63 Vandiver, J. K., Dunwoody, A. B., Campbell, R. B., and Cook, M. F., "A Mathematical Basis for the Random Decrement Vibration Signature Analysis Technique," ASME *Journal of Mechanical Design*, Vol. 104, 1982, pp. 307–313.

64 Ibrahim, S. R., and Mikulcik, E. C., "A Method for the Direct Identification of Vibration Parameters from Free Responses," *Shock and Vibration Bull.*, Vol. 47, 1977, pp. 183–198.

65 Gersch, W., "Parameter Identification: Stochastic Process Techniques," *Shock and Vibration Digest*, Vol. 7, 1975, pp. 71–86.

66 Vanmarcke, E. H., "Structural Response to Earthquakes," in *Seismic Risk and Engineering Decisions*, Lomnitz, C., and Rosenblueth, E., eds., Elsevier, Amsterdam, 1976, Chapter 8.

Downloaded 02 May 2010 to 171.66.16.250. Redistribution subject to ASME license or copyright; see http://www.asme.org/terms/Terms_Use.cfm

Experimental Methods in Applied Mechanics

I. M. Daniel
Department of Mechanical Engineering,
Illinois Institute of Technology,
Chicago, Ill. 60616

An overview is presented of recent developments and the current status of several experimental mechanics methods, i.e., strain gages, moiré, photoelasticity, and interferometry. Examples of applications of these methods are given. Progress has been noted in all aspects, including methodology, data acquisition instrumentation, data processing, and range of applications. The trend is to tackle more difficult problems and to take full advantage of technological advances.

1 Introduction

The rapid progress in computer technology, both hardware and software, and the development of powerful numerical methods of analysis have cast some doubt on the value of experimental analysis. This development did in fact influence the emphasis, direction, and applications of experimental analysis. However, it created many new challenges and opportunities. Experimental techniques received a tremendous impetus from the availability of new sophisticated instrumentation for data acquisition and processing, which has created new approaches, such as hybrid analytical/experimental methods.

Experimental methods are an essential tool in the study of applied mechanics and an indispensable companion to analytical methods. They are necessary in providing realistic material parameter inputs in the analysis and they are very useful in checking the validity of assumptions and hypotheses used in analysis. The value of the experimental approach increases with the complexity of loading conditions, structure geometry, and material response. In the case of failure analysis the need for experimentation is even greater since existing failure theories are not always capable of predicting strength and fatigue life under a variety of loading and environmental conditions. Specific applications of experimental methods to mechanics include the following:

1. Characterization of material response, especially nonlinear, and inelastic, such as, plastic, viscoelastic, viscoplastic, anisotropic, dynamic, and finite-deformation response.

2. Stress analysis. Strain distributions are obtained experimentally, and stress distributions are determined from these by using appropriate constitutive relations for the material.

3. Fracture characterization, including identification of fracture mechanisms, modes, initiation, and propagation.

4. Assessment of structural integrity and reliability using nondestructive techniques.

5. Life prediction through accelerated testing.

A variety of experimental methods are used for the various applications mentioned before. Most of these deal with measurement of material deformation. Some employ modeling procedures and others are applied directly to the prototype structure. Some give point-per-point information and others give full-field representations. The most commonly used methods in the last decade are:

1. Strain gages.

2. Moiré methods.

3. Photoelastic methods. These include two and three-dimensional, static and dynamic, photoelastic techniques; photoviscoelastic and photoplastic techniques; anisotropic photoelasticity; and birefringent coatings.

4. Holographic and interferometric methods.

5. Nondestructive evaluation methods.

This paper describes the state of the art of these methods, highlights some important developments in the recent past, and discusses current trends in methodology and applications.

2 Strain Gages

Electrical resistance strain gage techniques are the most widely used in industrial and research laboratories for both general purpose stress analysis and transducer applications. Etched foil strain gages, first introduced in the mid-1950s, are available today in a variety of configurations and sizes (ranging in gage length from 0.20 mm to 102 mm), resistances (from 50 to 1000 Ohms), and made of various alloys having the desired properties for particular applications. Gage construction, and backing and bonding materials have been improved to allow applications in extreme environments. Typical foil gages can be used over a temperature range of $-100°C$ to $400°C$ for elongations up to 5 percent. Special

Contributed by the Applied Mechanics Division for publication in the JOURNAL OF APPLIED MECHANICS.
Discussion on this paper should be addressed to the Editorial Department, ASME, United Engineering Center, 345 East 47th Street, New York, N.Y. 10017, and will be accepted until two months after final publication of the paper itself in the JOURNAL OF APPLIED MECHANICS. Manuscript received by ASME Applied Mechanics Division, April, 1983.

Copyright © 1983 by ASME
Downloaded 02 May 2010 to 171.66.16.250. Redistribution subject to ASME license or copyright; see http://www.asme.org/terms/Terms_Use.cfm

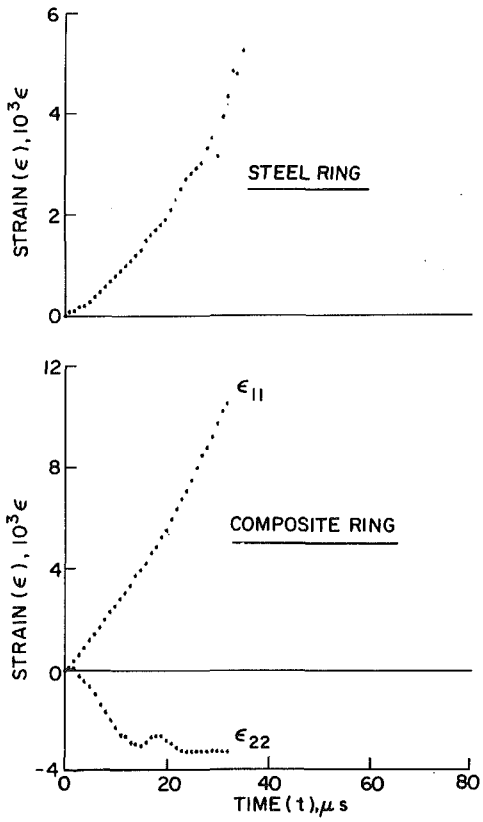


Fig. 1 Strain records in steel ring and SP288/AS [0_6] graphite/epoxy ring under dynamic loading

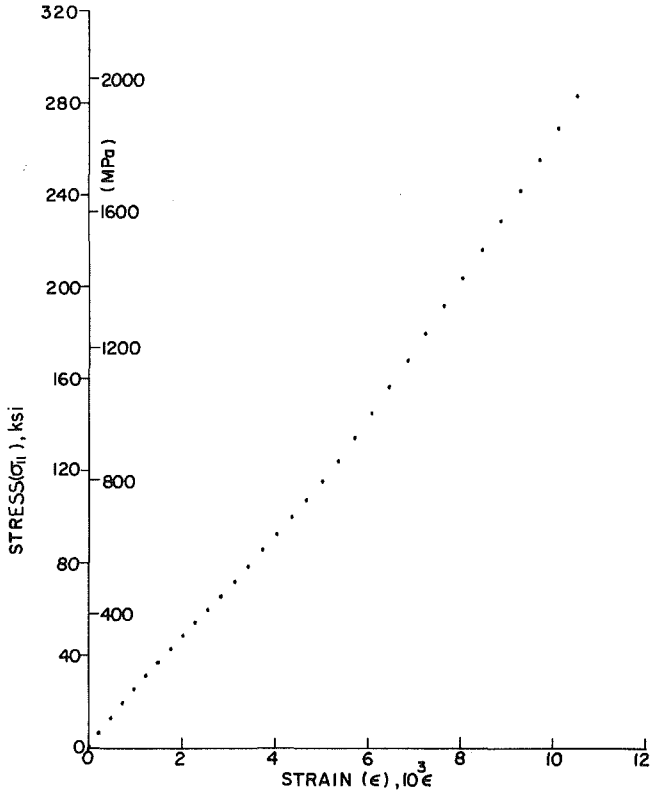


Fig. 2 Stress-strain curve for dynamically loaded [0_6] SP288/AS graphite/epoxy ring

gages, such as weldable gages, have been developed for even more extreme temperature environments, for higher elongations, and for recording fatigue damage.

Although no major developments have occurred in the basic strain gage methodology, the greatest impetus has come from the rapid development of microprocessor-based instrumentation for multichannel rapid data acquisition and on-line processing. Signal conditioning of the gage signals, which used to require manual adjustments of the balance and excitation voltages in the Wheatstone bridge, and gage calibration are automatically handled by appropriate microcomputer software. Transient digital recording instrumentation allows the application of strain gages to dynamic phenomena where records are obtained at sampling rates of one point per μsec or faster.

New applications abound. They include stress analysis of the hot section of a jet engine, monitoring of the buildup of residual stresses in composites, and material characterization at high strain rates. Techniques have been developed for embedding strain gages between the various piles during the fabrication process of a laminated composite for measuring subsurface strains under static loading, impact, and curing conditions [1, 2]. In the area of material characterization at high strain rates, a method was described where a thin ring specimen instrumented with strain gages is loaded with a dynamic internal pressure pulse [3]. The dynamic pressure is measured by means of a calibrated steel ring instrumented with strain gages. Strains in the calibration and test rings are recorded with a digital processing oscilloscope. The equation of motion is solved numerically and the data processed by the microcomputer attached to the oscilloscope. Typical strain records for a graphite/epoxy composite specimen are shown in Fig. 1. Data processing includes a number of smoothing and approximate differentiation operations. Results are obtained and plotted in the form of a dynamic stress-strain curve, such as the one for a graphite/epoxy specimen shown in Fig. 2.

3 Moiré Methods

3.1 Introduction. The moiré effect results when two similar systems of lines, dots, or other regular features are superimposed. The resulting moiré patterns are directly related to the relative displacements of the two systems. In the most common applications, moiré fringe patterns are formed by the itnerference of two arrays of equidistant lines or gratings. One of these, the model grating, is used to track the deformation of the specimen surface. It can be applied to the specimen surface by photoprinting, bonding, etching, ruling, transfer, or projection techniques. The second grating, the master or reference grating, remains undeformed and is superimposed on the model grating to produce the moiré fringe patterns. The method yields full-field information of in-plane or out-of-plane displacements. Being strictly geometric in nature, it is independent of the inelasticity or anisotropy of the material studied. An extensive literature survey is given in a recent review article on the moiré method [4].

The formation of moiré fringes between coarse gratings can be explained as a mechanical interference using geometrical optics and rectilinear light propagation, whereas in the case of high-frequency gratings, the phenomenon can only be described by physical optics in terms of diffraction and interference of coherent light components.

The sensitivity of the moiré method depends on the density of the gratings used and on the magnitude of deformation. A great deal of the work to date deals with coarse gratings of up to 40 lines per mm (1000 l/in), a practical upper limit until recently. Fringe interpolation and multiplication techniques have been developed for enhancing the sensitivity of the method when using coarse gratings[5–9]. However, the greatest progress in sensitivity enhancement occurred with

Downloaded 02 May 2010 to 171.66.16.250. Redistribution subject to ASME license or copyright; see http://www.asme.org/terms/Terms_Use.cfm

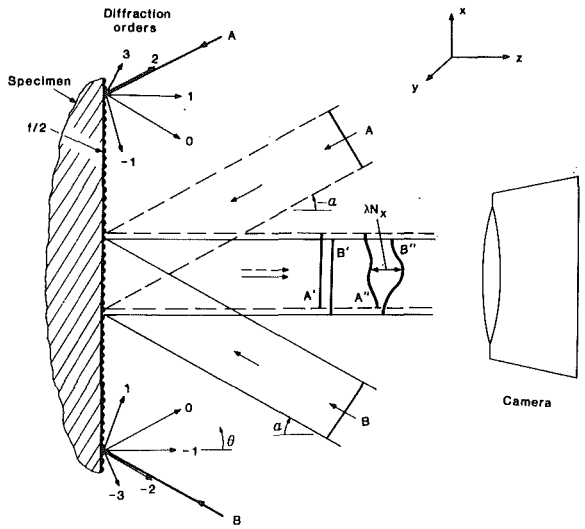


Fig. 3 Basic scheme for moiré interferometry (courtesy D. Post [11])

new developments in moiré interferometry using high frequency gratings of up to the theoretical limit of approximately 4000 lines/mm (101,600 lines/in)[10, 11].

The application of moiré techniques in general consists of three basic steps: (1) application of model grating, (2) recording of moiré data in the form of fringe patterns, or deformed grids, and (3) analysis of moiré data.

3.2 Application of Grating. In conventional practice gratings of up to 40 lines/mm (1000 lines/in.) are applied to the specimen surface by photographic, etching, transfer, or bonding techniques. The specimen surface is normally prepared with a smooth and partially reflective substrate. Film gratings can be bonded to this reflective surface or photoprinted onto this surface by the photoresist process.

In the case of moiré interferometry a new effective and highly accurate technique has been described for producing specimen gratings of frequencies up to the theoretical limit of 4,000 l/mm (101, 600 l/in.) [11]. The gratings are phase-type diffraction coatings approximately 0.025 mm (0.001 in.) thick. They are formed by squeezing an adhesive in liquid form between the specimen and a specially prepared mold, allowing the adhesive to cure and harden, and removing the mold. The mold is a processed photographic plate that has been exposed to two symmetrically disposed collimated coherent beams producing a virtual grating of the desired frequency. When the plate is developed, bleached, and dried, the emulsion gelatin shrinks nonuniformly and assumes a corrugated form of the same frequency as the virtual grating. This corrugated surface can be mirrorized by vacuum-depositing a thin aluminum coating which can be transferred to the specimen grating.

3.3 Recording the Moiré Data. The simplest method used in conventional practice with coarse gratings is to place the master or reference grating in front of the specimen and photograph the fringe pattern. This technique can be applied under static and dynamic loading. In the case of fringe multiplication techniques, the deformations of a coarse specimen grating are photographed directly with a special camera on high resolution plates. These plates are subsequently analyzed on an optical bench by interfering them with high-frequency gratings.

In the case of moiré interferometry, the specimen with a grating of frequency $f/2$ is illuminated by two mutually coherent beams A and B inclined at angles α and $-\alpha$ with the normal to the specimen surface (Fig. 3) [11]. The angle α is selected to produce a virtual reference grating of frequency f given by

$$f = \frac{2\sin\alpha}{\lambda}$$

where λ is the wavelength of the light used. Each one of the incident beams A and B is diffracted into several discrete beams of different diffraction orders. The diffracted beams of order one emerge normal to the specimen surface resulting into two diffracted beams A' and B' as shown in Fig. 3. When the specimen is loaded, the specimen grating is distorted and the diffracted wavefronts become warped as A'' and $B.''$ Their mutual interference produces a moiré pattern that is a contour map of wavefront separation λn_x, where n_x is the fringe order. The camera collects these two beams and displays the interference pattern.

3.4 Analysis of Moiré Data. In the in-plane displacement application, moiré fringes represent loci of points having the same component of displacement normal to the reference grating. Thus, moiré fringes are families of curves of equal displacement components.

The in-plane displacement components are related as follows to the fringe orders obtained from gratings normal to the x and y-axes:

$$u = \frac{n_x}{f}; \quad v = \frac{n_y}{f}$$

Strains are obtained by using the appropriate strain-displacement relations, which require differentiation of the displacement components. Displacement gradients are obtained by graphical, optical (mechanical), or numerical differentiation techniques. Regardless of the technique used, strain computation is subject to some errors because it relies on differentiation of experimental data.

3.5 Applications. The moiré method has been applied to the study of deformation for a variety of types of material response. Figure 4 illustrates an application of conventional moiré techniques to the study of wave propagation in an explosively loaded rock specimen [12]. Both model and reference gratings had a density of 40 lines/mm (1000 lines/in.) and the dynamic fringe pattern was recorded with a high-speed camera at a rate of one million frames per sec.

Figure 5 shows the application of fringe multiplication techniques to the study of deformations around a hole in a uniaxially loaded glass/epoxy composite laminate [13]. Here a grid of 20 dots/mm (500 dots/in.) was photoprinted on the specimen surface. This grid was photographed at various load levels on high resolution plates which were subsequently analyzed with a 200 lines/mm (5000 lines/in.) grating for a ten-fold multiplication. The moiré patterns were analyzed by graphical differentiation of displacement curves. More specific applications of moiré to composite materials are described in a recent monograph [14].

An application of moiré interferometry with a grating frequency approaching the theoretical limit of $2/\lambda$ is illustrated in Fig. 6 [10, 11]. Beams of 488 nm wavelength from an argon laser were used at an angle $\alpha = 77.4$ deg to produce a virtual grating of 4000 l/mm (101,600 l/in.). The specimen was an acrylic plate with a hole having a grating of 2000 l/mm (50,800 l/in.).

Another application of moiré interferometry is illustrated in Fig. 7 [15]. In-plane displacement fields are revealed around fatigue cracks in aluminum alloys. The patterns corresponding to moiré with 2400 l/mm (60,960 l/in.) represent both u and v displacement fields around the crack tips.

An embedded grid method has been introduced for measuring large three-dimensional deformations around a

Downloaded 02 May 2010 to 171.66.16.250. Redistribution subject to ASME license or copyright; see http://www.asme.org/terms/Terms_Use.cfm

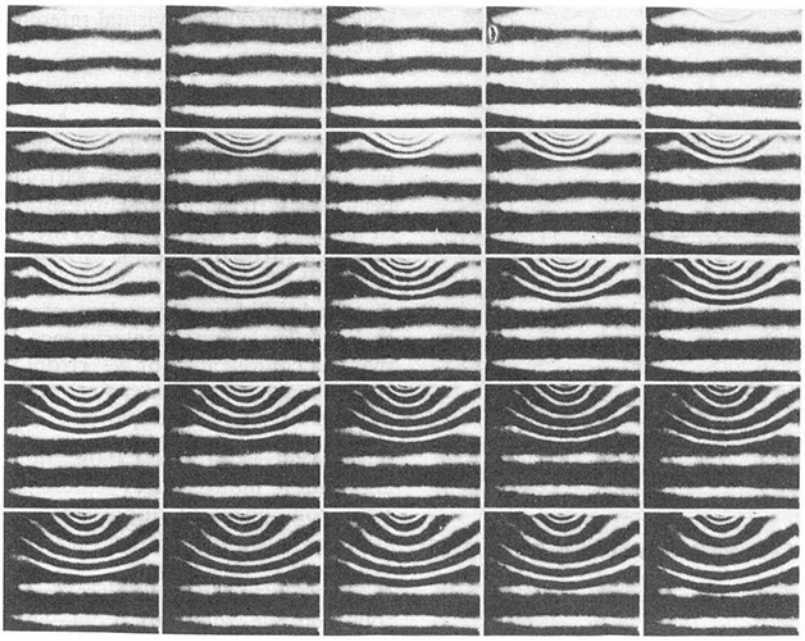


Fig. 4 Moiré fringe patterns corresponding to vertical displacements in marble specimen loaded explosively on the edge. (Camera speed: 1,004,500 frames per sec; grating: 40 lines per mm, 1,000 lines per in.).

crack and for determining the through-the-thickness distributions of stress-intensity factors [16].

Other applications of moiré Methods have been published in the areas of fracture mechanics, biomechanics, high temperature deformation, residual stresses, and adhesive and welded joints.

4 Photoelastic Methods

4.1 Introduction. Photoelasticity in general is based on the stress-optic law which relates the state of stress in a transparent material and the stress-induced optical anisotropy. The latter, known as birefringence, is a change in indices of refraction and is usually expressed in terms of the number of wavelengths of relative retardation of light propagating through the material along two principal directions. The method is a full-field method for determination of the state of stress under a variety of conditions: two and three-dimensional, static and dynamic, elastic and inelastic, isotropic and anisotropic. Like other experimental methods, it has been influenced by the development of numerical methods, and it has been enhanced by the availability of new materials and advanced instrumentation. Systems utilizing vidicon and digital cameras and computer processing of photoelastic data are gathering momentum.

4.2 Three-Dimensional Photoelasticity. After experiencing some temporary decline with the advent of finite-element methods, the three-dimensional photoelastic method is reasserting itself as a powerful method of stress analysis. In the method of "stress freezing" the stresses are "frozen in" when the three-dimensional model is loaded at a critical temperature [17]. Subsequently slices and subslices are removed from the model and analyzed in the polariscope. With the development of more easily castable and machinable epoxies the method is cost-effective for many industrial applications. A new technique using gamma rays to freeze in the stresses at room temperature has been introduced to overcome potential problems with high deformations at the elevated temperature of normal stress freezing [18].

Stress freezing and slicing techniques are used effectively in fracture mechanics to obtain flaw shapes and distributions of

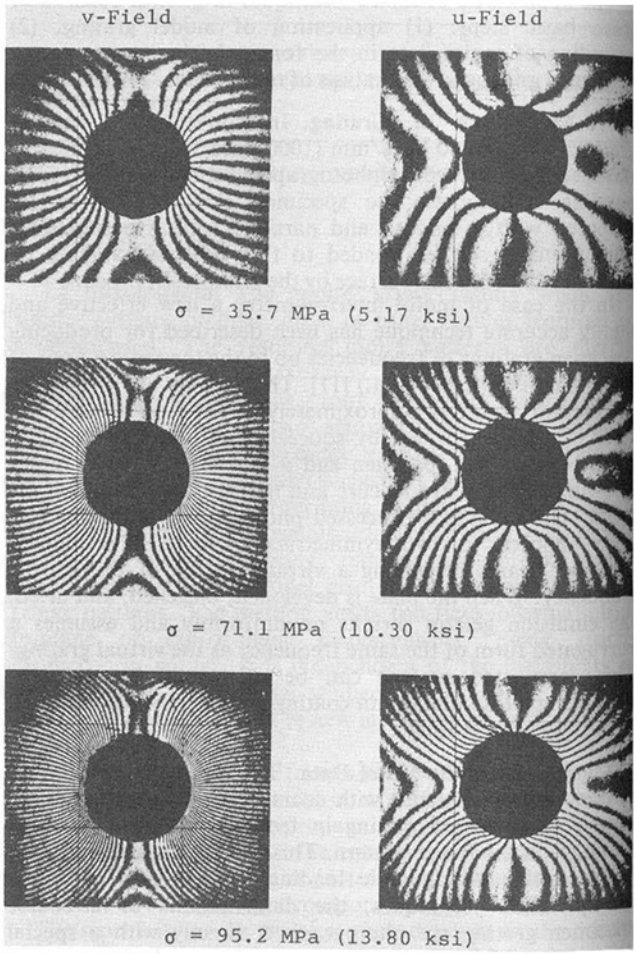


Fig. 5 Moiré fringe patterns for vertical and horizontal displacements around hole of $[0/\pm 45/\overline{90}]_S$ glass/epoxy laminate under uniaxial loading. (Model grating: 20 dots/mm; fringe multiplication factor: 10)

stress-intensity factors in cracked bodies [19]. In applying the method, starter cracks are grown in three-dimensional photoelastic models under monotonic loading above the

Downloaded 02 May 2010 to 171.66.16.250. Redistribution subject to ASME license or copyright; see http://www.asme.org/terms/Terms_Use.cfm

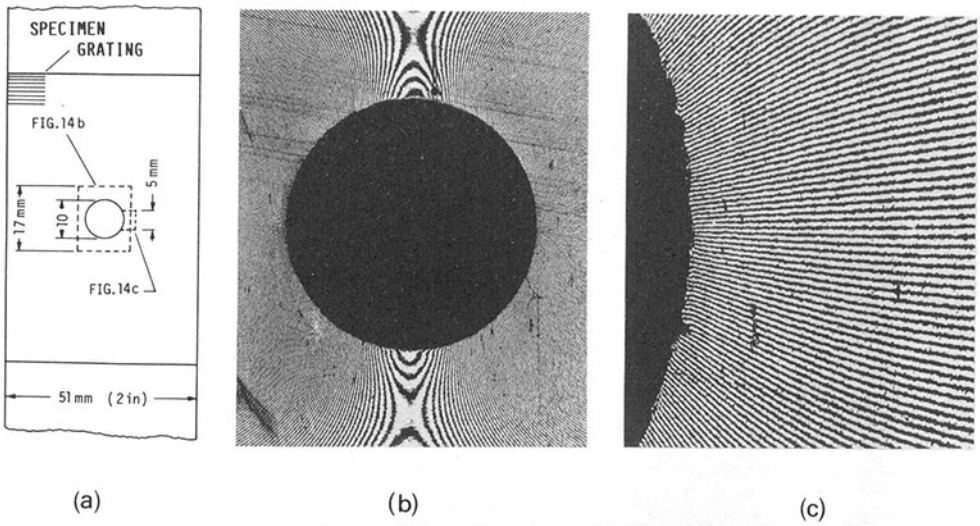


Fig. 6 Application of moiré interferometry near the theoretical limit of sensitivity; grating frequency $f = 4000$ l/mm (courtest D. Post [11])

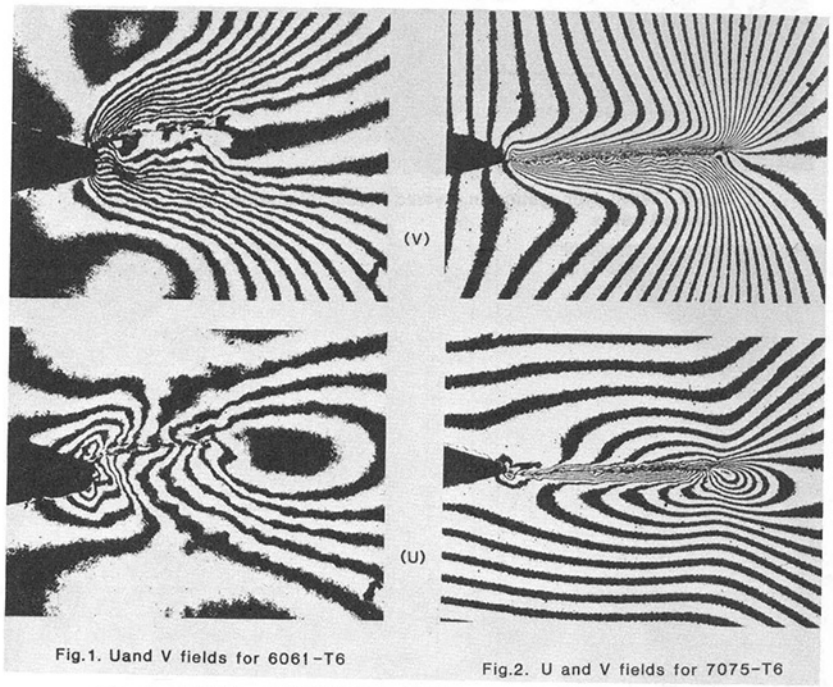


Fig. 7 In-plane displacement fields around fatigue cracks in aluminum alloys; grating frequency $f = 2400$ l/mm (courtesy D. Post [15])

critical temperature. The loads are reduced when the cracks are extended to several times the starter crack size. After stress freezing, thin slices are removed along the flaw boundary and analyzed. Cracks grown in this manner have been found to be virtually identical to those grown under fatigue loading in steel models of a reactor vessel nozzle-corner. The method is especially useful for the case of nonself-similar, subcritical, fatigue crack growth where neither the flaw shapes nor stress-intensity factor distributions may be known a priori.

The objection to loading the model at an elevated temperature and destroying it is overcome by the use of scattered-light photoelasticity, a nondestructive technique. The method has been known for many years but it received a great impetus with the development of lasers [20]. It can be applied to static and dynamic problems. Another similar approach is the optical slicing method where a slice of the model between two parallel sheets of light is analyzed [21].

Nondestructive stress analysis can also be conducted in many cases by transmission photoelasticity by analyzing the integrated effects along the path of light through a three-dimensional model. The theoretical foundations as well as many applications of integrated photoelasticity have been described in a recent book [22].

4.3 Dynamic Photoelasticity. A review of recording methods and data-analysis procedures was described in a recent article [23]. The method is applicable to all areas of estastodynamics, i.e., stress-wave propagation, vibration and impact, quasi-static transients, and fracture propagation.

The most difficult aspect of dynamic photoelasticity is recording the transient isochromatic fringe patterns. Typical velocities of fringes for Homalite-100 range up to 2500 ms^{-1}. Recording methods used to date include the high-speed framing camera, the spark-gap camera (Cranz-Schardin),

Downloaded 02 May 2010 to 171.66.16.250. Redistribution subject to ASME license or copyright; see http://www.asme.org/terms/Terms_Use.cfm

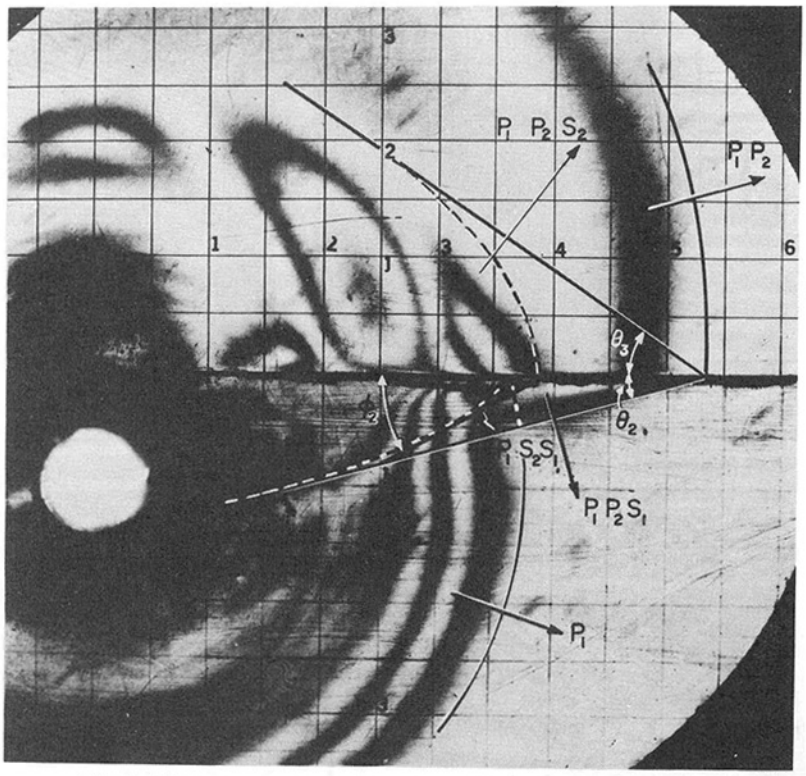


Fig. 8 Wave propagation in layered model illustrating reflected and refracted waves

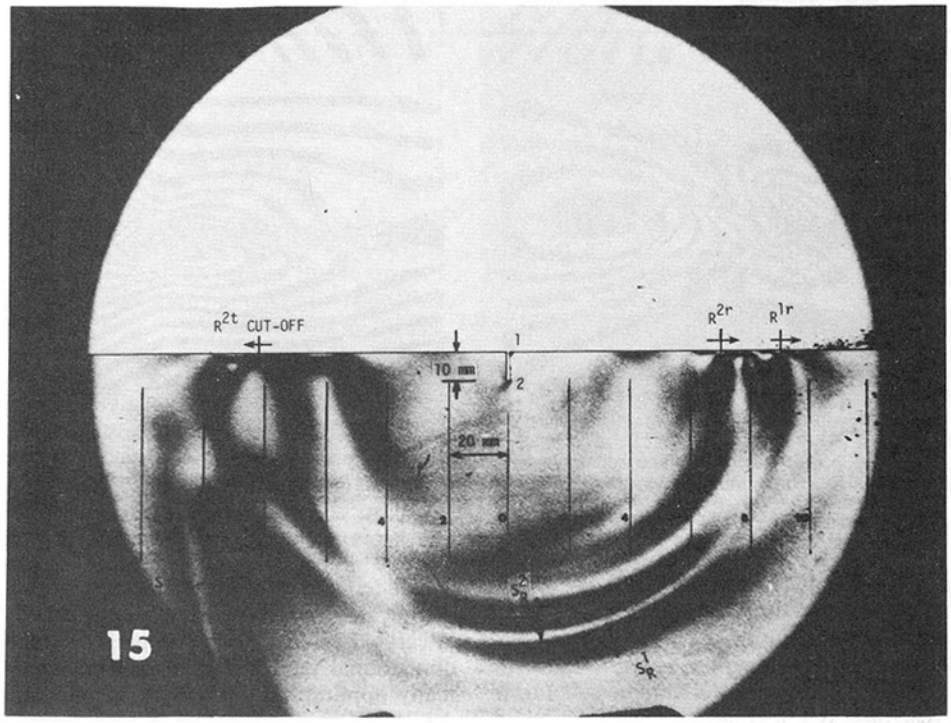


Fig. 9 Reflected, transmitted, and mode-converted waves following interaction of Rayleigh wave with slot (courtesy C. P. Burger [27])

modulated pulsed laser, and stop-action single-pulse or strobe systems. High-speed framing cameras use a rotating prism or mirror and operate in the range of 100,000 to 2,000,000 frames per sec. However, the writing time is short and the total number of frames is usually less than 100. They require high-intensity light sources, usually provided with overdriven flash lamps, pulsed ruby lasers, or argon gas bombs. The Cranz-Schardin camera has been applied to a variety of dynamic photoelastic applications such as wave propagation, fracture, and impact [24]. Framing rates from 20,000 to 800,000 frames per sec can be achieved, with the interframe time adjustable from frame to frame. The pulsed ruby laser is ideal as a light source for dynamic photoelasticity. Sequentially pulsed systems have been synchronized with a high-speed framing camera [25]. Hybrid Cranz-Schardin-laser systems have also been developed.

Downloaded 02 May 2010 to 171.66.16.250. Redistribution subject to ASME license or copyright; see http://www.asme.org/terms/Terms_Use.cfm

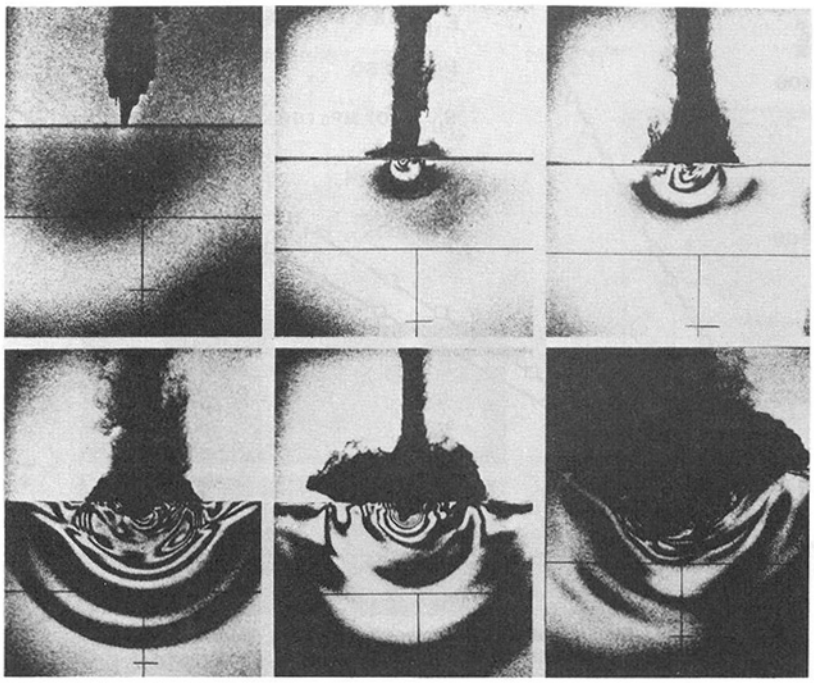


Fig. 10 Sequence of isochromatic fringe patterns for water jet impact on CR-39 specimen at a velocity of 900 ms $^{-1}$

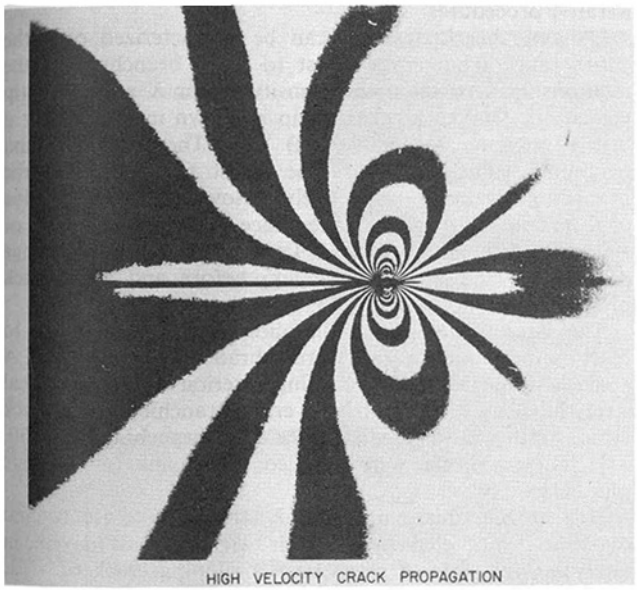


Fig. 11 Isochromatic fringe pattern around tip of a high-velocity crack in Homalite-100; crack velocity $\dot{a} = 380$ ms $^{-1}$ (courtesy J. W. Dally [29] and Photomechanics Laboratory - University of Maryland)

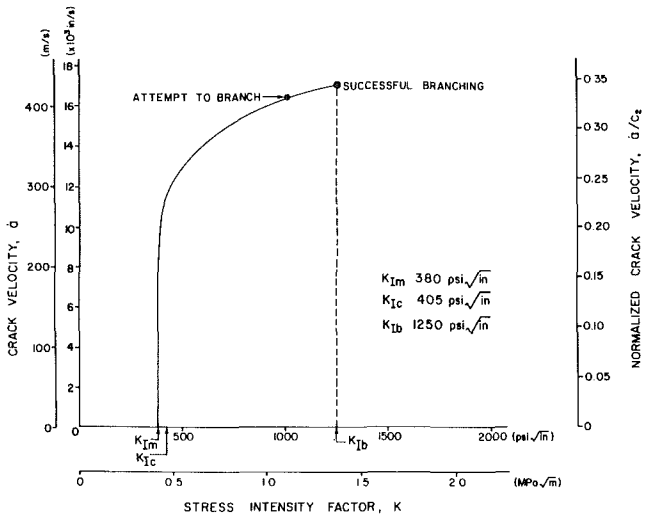


Fig. 12 Crack velocity as a function of the instantaneous stress-intensity factor for Homalite-100 (courtesy J. W. Dally [29])

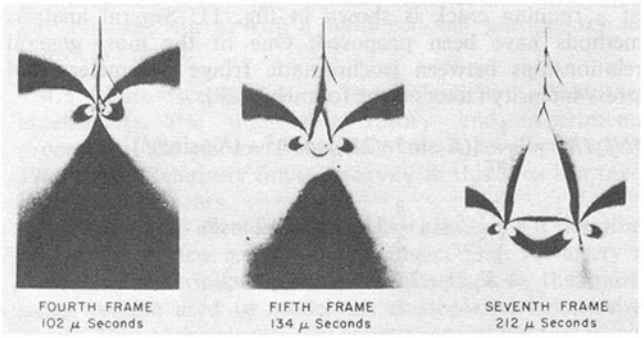


Fig. 13 Typical crack branching dynamic photoelastic fringe patterns in Homalite-100 single-edge-notched specimen (courtesy A. S. Kobayashi [30])

Data analysis is based on a dynamic version of the stress-optic law. Stress separation is possible in special cases, such as free or rigid boundaries, axisymmetric problems, and pure shear wave propagation.

Dynamic photoelasticity has been applied to a variety of problems in many fields such as wave propagation, fracture mechanics, jet cutting, and flaw detection.

An example of wave propagation in layered media is illustrated in Fig. 8 [26]. The model consisted of two photoelastic layers with an impedance ratio of 2:1. Figure 8 is one of a sequence of frames obtained with a Cranz-Schardin camera operated at a speed of 187,000 frames per sec. The fringe pattern shows the incident (P_1) and refracted (P_1P_2) dilatational waves, and reflected and refracted shear head-waves ($P_1P_2S_1$ and $P_1P_2S_2$).

Dynamic photoelasticity can help visualize the interaction of elastic waves with defects and thus aids in the development and understanding of ultrasonic nondestructive flaw

Downloaded 02 May 2010 to 171.66.16.250. Redistribution subject to ASME license or copyright; see http://www.asme.org/terms/Terms_Use.cfm

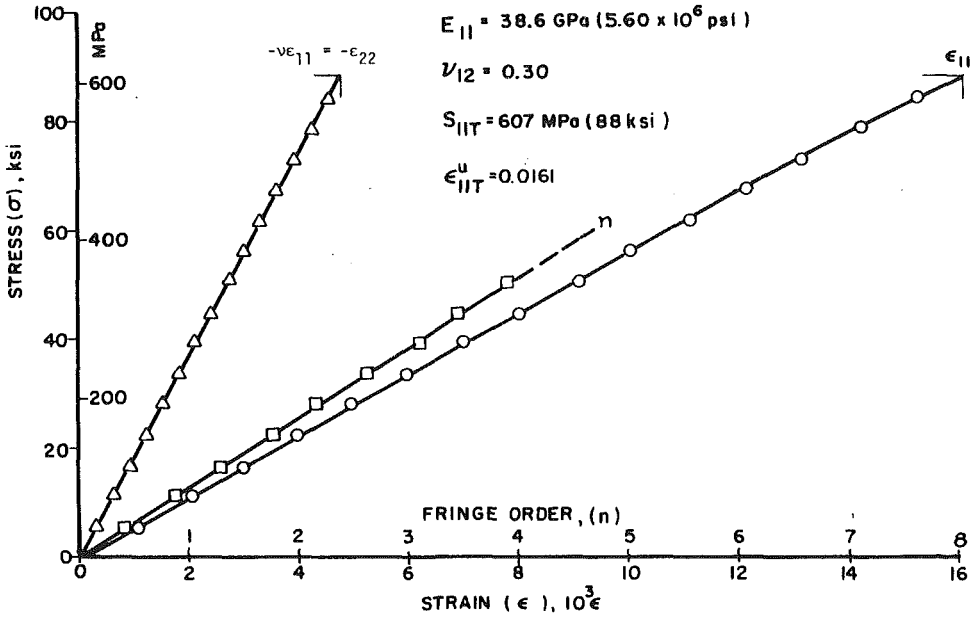


Fig. 14 Stress-strain and stress-birefringence curves for $[0_{30}]$ glass/epoxy composite (style 3733 glass; Maraset 658/558 epoxy)

detection. Figure 9 shows an example of the interaction between Rayleigh waves and cracks on the surface of a half plane [27]. Reflected, transmitted, and mode-converted waves are identified. It is shown how the frequency spectrum of the transmitted wave can be used to determine the depth of surface cracks.

The mechanics of fracture by water jet impact were studied photoelastically [28]. A device was used for explosively propelling water jets at speeds up to 2800 ms^{-1}. The jet impact on transparent photoelastic specimens was studied with dynamic photoelasticity, using a spark-gap camera at a rate of 180,000 frames per sec. Fringe patterns in the vicinity of the impact were also recorded with a pulsed ruby laser (Fig. 10) [28]. A water jet is impacting a Columbia Resin specimen at a speed of 900 ms^{-1}. The fringe patterns show the pressure buildup, wave propagation, and crater formation.

One of the most important applications of dynamic photoelasticity is fracture [29]. The dynamic fracture behavior of brittle polymers can be characterized by developing a relation between the instantaneous stress-intensity factor and the crack-tip velocity. Since the state of stress near the crack tip is related to the fringe pattern, it is possible to determine the stress-intensity factor in terms of fringe pattern parameters. A typical fringe pattern near the tip of a running crack is shown in Fig. 11. Several analysis methods have been proposed. One of the most general relationships between isochromatic fringe parameters and stress-intensity factors is the following [29]:

$$(Nf_\sigma/h)^2 = \frac{1}{2\pi r}[(K_I\sin\theta + 2K_{II}\cos\theta)^2 + (K_{II}\sin\theta)^2]$$

$$+ \frac{2\sigma_{ox}}{\sqrt{2\pi r}}\sin\frac{\theta}{2}[K_I\sin\theta(1+2\cos\theta) + K_{II}(1+2\cos^2\theta+\cos\theta)] + \sigma_{ox}^2$$

where,

N = fringe order
f_σ = material fringe value
h = specimen thickness
r = radial distance to point in question
θ = angle from crack axis to point in question
K_I, K_{II} = mode *I* and mode *II* stress-intensity factors
σ_{ox} = far-field stress along crack direction

This equation is solved for the unknowns K_I, K_{II}, and σ_{ox} by applying it at several data points and using numerical iterative procedures.

Dynamic brittle fracture can be characterized over the entire range from crack arrest to crack branching by the relationship between stress-intensity factor K and crack-tip velocity $\dot{a}$. One such relationship is shown in Fig. 12 for a brittle polyester (Homalite-100) [29]. The minimum and maximum values of K are the arrest toughness and the branching toughness, respectively. Below the minimum value of K no crack propagation takes place. At the highest value of K crack branching occurs. Typical isochromatic fringe patterns around a running crack, before and after crack branching are shown in Fig. 13.

The latest developments in photoelastic applications to fracture mechanics deal with crack branching and curving. A recently proposed crack branching criterion requires a critical stress-intensity factor to trigger crack branching and a crack curving criterion for predicting the crack branching angle [30, 31]. These criteria were verified by means of dynamic photoelasticity.

Hybrid techniques employing dynamic photoelasticity and dynamic finite element methods are used effectively in analyzing the state of stress near a running crack tip [32]. Dynamic photoelasticity is also used as a means of verifying dynamic finite element codes in wave propagation and fracture mechanics.

4.4 Anisotropic Photoelasticity. This method, also known as photoorthotropic elasticity, applies transmission photoelastic techniques to stress analysis of birefringent fibrous composite materials. These materials are glass-fiber-reinforced plastics with the matrix and the fibers having the same index of refraction. These transparent composites are treated as homogeneous materials with anisotropic elastic and optical properties. In the general case the birefringence tensor N_{ij} is related to the stress tensor σ_{kl} by means of the stress-optic law:

$$N_{ij} = B_{ijkl}\sigma_{kl}$$

where B_{ijkl} is the fringe value tensor. For orthotropic materials under plane stress conditions the stress-optic law takes the following form:

Downloaded 02 May 2010 to 171.66.16.250. Redistribution subject to ASME license or copyright; see http://www.asme.org/terms/Terms_Use.cfm

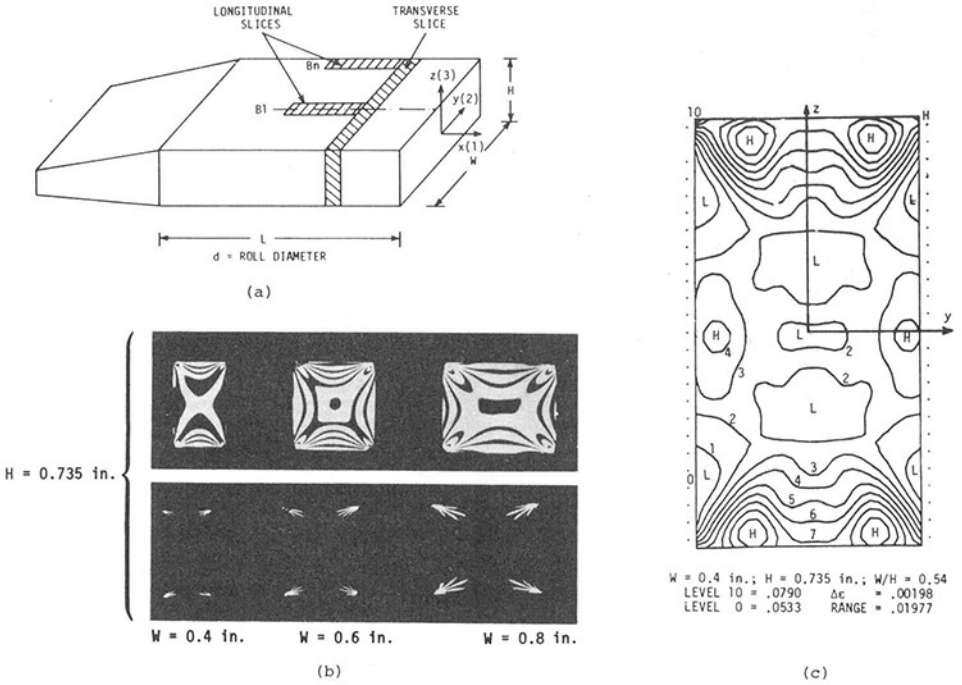


Fig. 15 Application of photoplasticity to rolled slabs. (*a*) Billet geometry; (*b*) fringe patterns in transverse slices of three models; (c) topographical map of longitudinal strain at a transverse cross section (courtesy C. P. Burger [37]).

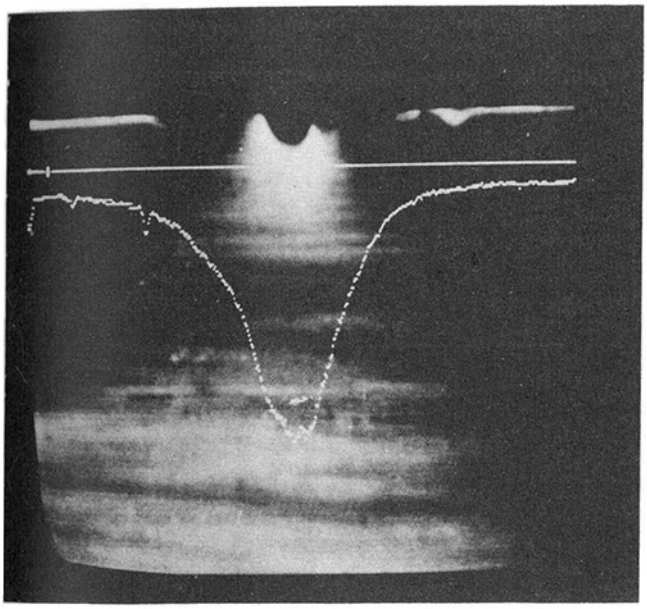


Fig. 16 Variation of light intensity across section in a birefringent composite plate under a concentrated load (courtesy A. S. Voloshin and C. P. Burger [34])

$$\begin{bmatrix} N_{11} \\ N_{22} \\ N_{12} \end{bmatrix} = \begin{bmatrix} B_{11} & B_{12} & 0 \\ B_{21} & B_{22} & 0 \\ 0 & 0 & B_{66} \end{bmatrix} \begin{bmatrix} \sigma_{11} \\ \sigma_{22} \\ \sigma_{12} \end{bmatrix}$$

In terms of relative birefringence the stress-optic law takes the form:

$$N = \left[\left(\frac{\sigma_{11}}{2f_{11}} - \frac{\sigma_{22}}{2f_{22}} \right)^2 + \left(\frac{2\sigma_{12}}{f_{12}} \right)^2 \right]^{\frac{1}{2}}$$

The latest advances in this area are the development of fabrication procedures for multidirectional laminates and digital image analysis procedures for analyzing low levels of birefringence [33, 34]. Typical stress-strain and stress-birefringence curves for a unidirectional glass/epoxy are shown in Fig. 14.

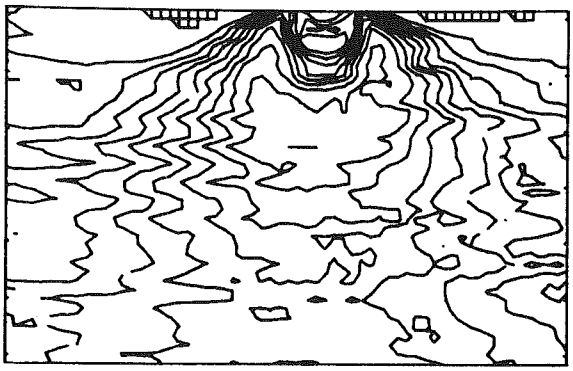


Fig. 17 Birefringence map for composite plate under concentrated load (courtesy A. S. Voloshin and C. P. Burger [34])

4.5 Photoviscoelasticity; Photoplasticity; Photothermoelasticity. The underlying theory and experimental procedures for photoviscoelasticity were developed in the 1960s [35]. Relatively limited activity in this area has taken place in recent years.

The historical development of photoplasticity is described in a recent review article on the subject [36]. A variety of polymeric materials exhibiting birefringence in the plastic range can be used to model the elastoplastic behavior of metals. One of the most useful applications of photoplasticity is the modeling of large three-dimensional strains encountered in metal-forming processes. Photoplastic studies have been conducted with upset forged rings and rolled slabs [37]. Model billets shaped as in Fig. 15(*a*), were rolled and then sliced as shown in Fig. 15(*b*). A topographical map of the longitudinal strain ϵ_x is shown in Fig. 15(*c*) for one case.

Downloaded 02 May 2010 to 171.66.16.250. Redistribution subject to ASME license or copyright; see http://www.asme.org/terms/Terms_Use.cfm

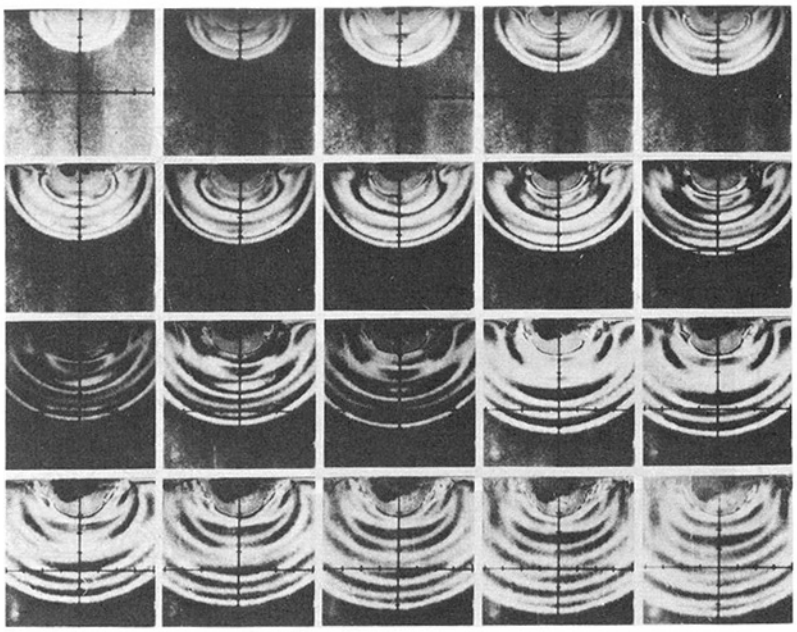


Fig. 18 Isochromatic fringe patterns in photoelastic coating on marble specimen under explosive loading (camera speed: 500,000 frames per sec)

A review of photothermoelastic modeling techniques describes applications to shrinkage stresses, stresses caused by steady-state temperature gradients, and transient thermal stresses [38].

4.6 Half-Fringe Photoelasticity. Classical photoelasticity makes use of polymeric materials with high birefringence. The relatively high loads applied and the low modulus of these materials sometimes result in nonlinear behavior and cause distortions in the similitude relations between model and prototype. Reducing the loads or using high-modulus, low-sensitivity materials results in low-level birefringence. Elaborate fringe multiplication techniques have been used for sensitivity enhancement.

With the development of digital image analysis procedures a new field, known as "half-fringe photoelasticity," has emerged [39]. The technique brings together on-line, digital-image-processing procedures with photoelasticity. It is based on a digital gray-level analyzer and picture-processing system. The intensity field of a half-fringe light-field photoelastic pattern can be divided into 256 levels from "light" to "dark" for an equivalent fringe multiplication of 512 times.

The potential of the method is great and the number of applications is increasing. They include the determination of stress-intensity factors for near-surface cracks in glass, which correlate well with results from geometrically similar polyester models with very low loads [40], and application to composite materials using anisotropic birefringent composites [34]. The light intensity and birefringence map for a concentrated load on a plate of such a material are shown in Figs. 16 and 17 [34]. Other applications of half-fringe photoelasticity under study include dynamic problems, adhesive joints, interlaminar stresses, and photoelastic coatings using very thin layers of low-modulus coating.

4.7 Birefringent Coatings. While photoelastic model analysis is an effective means for measuring stresses, its application is limited to problems that can be studied by means of transparent models. Birefringent or photoelastic coatings on the other hand can be readily applied to opaque prototype structures. The method consists of bonding a thin sheet of photoelastic material to the surface of the specimen,

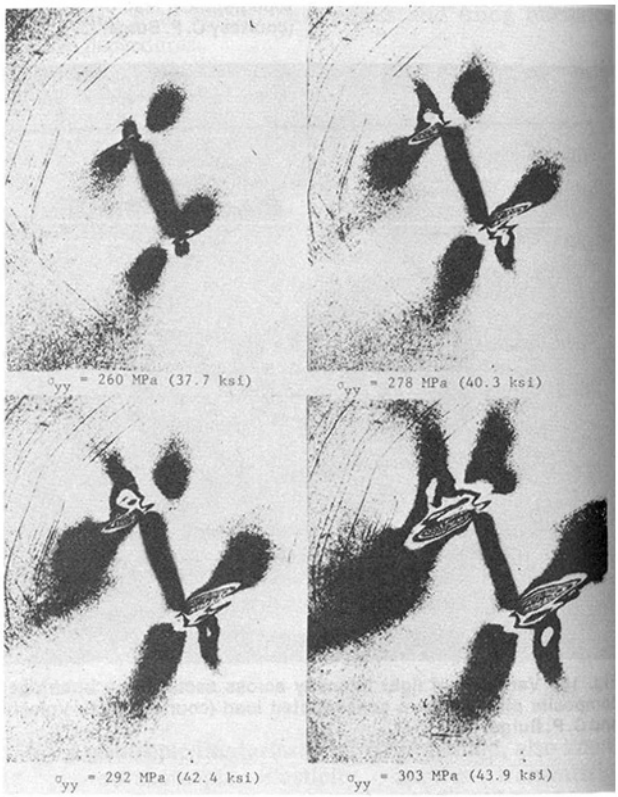
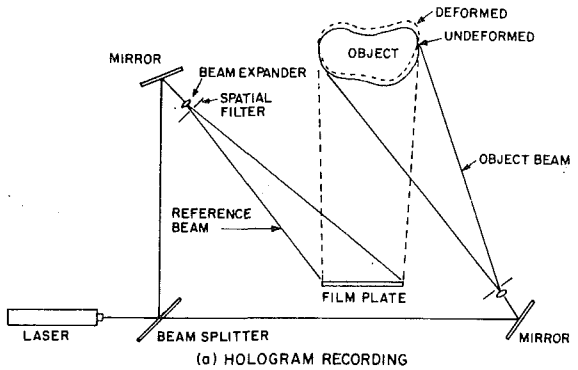


Fig. 19 Isochromatic fringe patterns in photoelastic coating around 1.27 cm (0.5 in.) crack in $[0/\pm 45/90]_S$ graphite/epoxy specimen under biaxial loading. $\sigma_{yy} = 2.03\sigma_{xx}$ at 30 deg with crack direction.

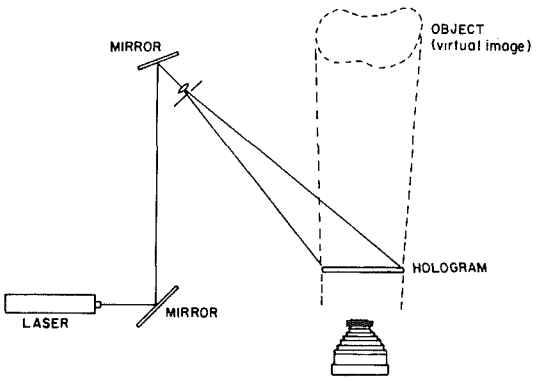
such that the bonded interface is reflective. When the specimen is loaded, the surface strains are transmitted to the coating and produce a fringe pattern which is recorded and analyzed by means of a reflection polariscope.

The method in general and its specific applications to composite materials have been reviewed in two monographs [41, 14]. The method gives full-field information on the surface strains of the structure, whether elastic, viscoelastic,

Downloaded 02 May 2010 to 171.66.16.250. Redistribution subject to ASME license or copyright; see http://www.asme.org/terms/Terms_Use.cfm



(a) HOLOGRAM RECORDING



(b) RECONSTRUCTION

Fig. 20 Holographic processes

or plastic. Applications of the method are wide ranging. Wave and fracture propagation in rock media has been studied by means of photoelastic coatings [12]. Isochromatic fringe patterns illustrating wave propagation in an explosively loaded marble slab are shown in Fig. 18. Photoelastic coatings are also a sensitive means for identifying fracture mechanisms, and studying fracture initiation and propagation in composite materials with stress concentrations. This type of application is illustrated in Fig. 19 for the case of biaxial loading of a quasi-isotropic graphite/epoxy plate with a crack [42]. The specimen was loaded under a 2:1 biaxial tensile loading producing an appreciable shear stress component in addition to the normal stress components normal and parallel to the crack. The fringe pattern shows that, in addition to the primary fracture propagation normal to the initial crack, there is crack extension along the original crack direction in the subsurface plies and additional crack propagation normal to the extended subsurface crack.

5 Interferometric Methods

5.1 Holographic Interferometry. Holography is an optical method based on the optical interference produced by superposition of coherent light waves reflected from the object under consideration (object beam) and those of a coherent reference beam. The laser is an ideal source of coherent monochromatic light. A typical arrangement for the holographic processes of construction and reconstruction is shown in Fig. 20. The interference of the object and reference beams impinging on the film plate produces a pattern containing both amplitude and phase information (hologram). In the reconstruction process, light refracted through the hologram contains the same intensity and phase characteristics as those of the original object.

In holographic interferometry, two holograms of the test object are recorded on the same photographic plate with an

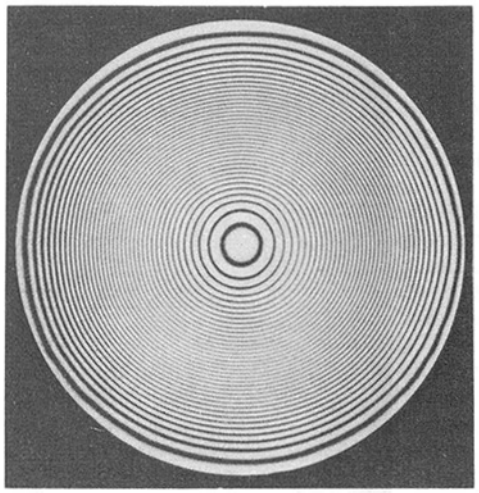


Fig. 21 Holographic fringe pattern of transverse deflection of a clamped circular unidirectional boron/epoxy plate under uniform pressure (courtesy R. E. Rowlands)

alteration of the object surface occurring between the two exposures. The surface of the test object can be altered in several ways, including mechanical loading, pressurization, thermal loading, and vibration. Upon reconstruction, a fringe pattern is obtained depicting contours of displacement. Each fringe represents a relative displacement with respect to its neighboring fringe of approximately one-half the wavelength of light.

An improved technique with many advantages is image-plane holography. The light waves emanating from the object are collected by an imaging lens and the film plate is placed near the image plane.

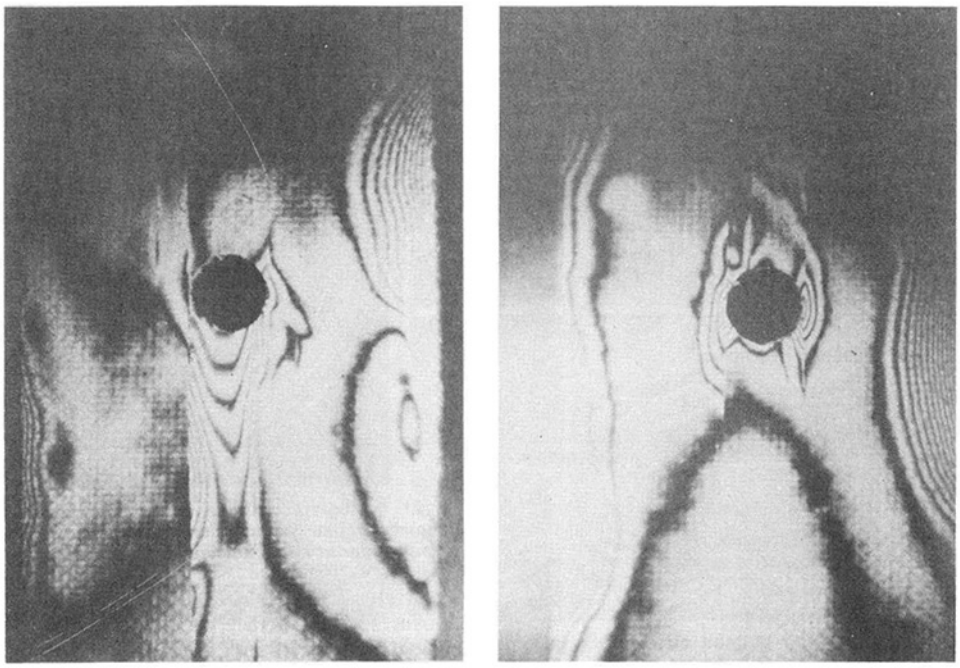
Holographic techniques commonly used in experimental mechanics fall into four basic categories:

1. Double-exposure holographic interferometry;
2. Real-time holographic interferometry;
3. Time-average or vibration holographic interferometry;
4. Dynamic double-exposure pulsed holographic interferometry.

Since conventional holographic techniques are best suited for measuring out-of-plane displacements, many applications deal with flexure and vibration of plates. A holograpic fringe pattern depicting the deflection of a clamped composite plate under uniform pressure is shown in Fig. 21. Another important application of holographic interferometry is the nondestructive evaluation (NDE) of material integrity. The technique relies on the fact that if the state of stress in the component is changed, the surface displacements will be altered locally around surface or near-surface defects. This alteration is manifested as a local anomaly in the overall fringe pattern. This nondestructive evaluation is carried out either by double-exposure or real-time holography. Figure 22 shows an example of the application of holography to the detection of fatigue-induced damage growing around a circular hole in a graphite/epoxy plate. The holographic fringe patterns were induced thermally by using a radiant heat source.

Recent technological advances such as the thermoplastic film holographic camera have overcome one of the major difficulties of holographic NDE by reducing the development of holograms to a three-second process. The holograms are erasable and reusable. This device coupled with a closed circuit TV camera allows for easy observation and continuous recording of fringe patterns in real time. Recent and current efforts are directed at automated fringe readout and processing.

Downloaded 02 May 2010 to 171.66.16.250. Redistribution subject to ASME license or copyright; see http://www.asme.org/terms/Terms_Use.cfm



(a) (b)

Fig. 22 Thermally induced holographic fringe patterns in fatigue loaded $[(0/\pm 45/90)_s]_2$ graphite/epoxy specimen with circular hole (courtesy G. P. Sendeckyj)

5.2 Photoelastic Holography. This method of analysis uses transparent birefringent models with coherent optics, and thus combines features of photoelasticity and holography [43]. For a birefringent model two wave fronts are produced for each exposure corresponding to the two principal optical (stress) directions. When two exposures are taken at two load levels, four wave fronts are recorded on the hologram. In addition to the classical isochromatic and isoclinic fringe patterns, holographic interferometry provides fringe patterns related to the absolute retardation (i.e., σ_1 and σ_2 separately), isopachics (i.e., lines of constant $\sigma_1 + \sigma_2$), and combined isochromatics and isopachics.

5.3 Holographic moiré. The holographic moire method combines features of the moiré method and holographic interferometry [44]. In conventional holographic interferometry, the observed phenomenon is a function of the object deformation and the manner in which it is illuminated and observed. However, the information obtained is not always in a convenient form for processing. The amount and diversity of information are increased by modifying one or more of the optical components of the system. Thus, it is possible to obtain separately the components of displacement, displacement derivatives, and surface contours. Techniques such as translation and/or rotation of the holographic plate, rotation of the object and/or reference beam, and optical filtering have been introduced.

5.4 Speckle Interferometry. Speckle interferometry makes use of the speckle pattern produced on the surface of an object illuminated by coherent light. It has many characteristics of holographic interferometry, however, it is less sensitive than that. The technique has several advantages over conventional interferometry, namely: (1) the setup is relatively simple; (2) mechanical and environmental stability are not critical; (3) it is less demanding in coherence length of light; (4) sensitivity can be controlled over a wider range; (5) it is less demanding in film resolution; (6) the fringes always localize on the specimen surface; and (7) displacement derivatives can be obtained directly.

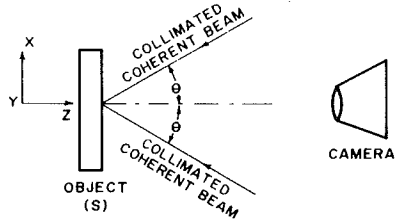


Fig. 23 Schematic diagram of the dual beam method for measuring in-plane displacements (Y. Y. Hung[45])

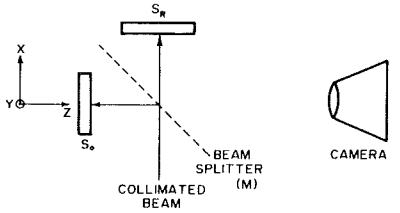


Fig. 24 Schematic diagram of the dual beam method for measuring out-of-plane displacements (Y. Y. Hung[45])

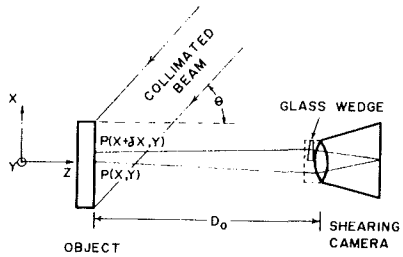


Fig. 25 Schematic diagram for measuring displacement derivatives with a shearing camera (Y. Y. Hung [45])

The deformation measurement techniques fall into two categories: speckle interferometry for measuring surface displacements and speckle-shearing interferometry for measuring derivatives of displacements. A review of these methods is given in a chapter of a recent book on speckle metrology [45].

Downloaded 02 May 2010 to 171.66.16.250. Redistribution subject to ASME license or copyright; see http://www.asme.org/terms/Terms_Use.cfm

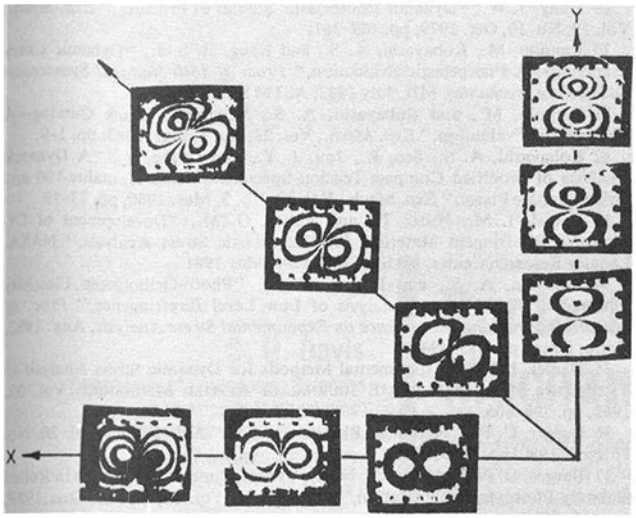


Fig. 26 Fringe patterns filtered from a sheared speckle interferogram of a centrally loaded rectangular plate. (Fringes depict deflection derivatives with varying sensitivity along various directions; Hung et al. [46].)

Two versions of speckle interferometry have been described: the dual beam method, and the single beam method. In the former, the object is illuminated by two collimated coherent beams equally inclined from the normal (Fig. 23). With this arrangement the two speckle wave fronts, one from each beam, impinge on the photographic film of the camera and produce a speckle pattern. When the object is deformed, a relative phase change is produced between the two wavefronts. For the arrangement shown, the relative phase change is due only to in-plane displacements in the x-direction given by

$$\Delta(x, y) = [(4\pi/\lambda)\sin\theta]u$$

where $\Delta(x, y)$ is the relative phase change; λ is the wavelength of light; θ is the angle of illumination; and u is the displacement component in the x-direction. Using a real-time or a double-exposure technique a fringe pattern contouring $\Delta(x, y)$ is obtained.

Out-of-plane displacements are measured using the setup shown in Fig. 24, where S_o is the object and S_R is a reference surface. Both S_o and S_R are illuminated and imaged simultaneously by the camera. When S_o is deformed, the relative phase change of the two speckle fronts is due only to the out-of-plane displacement w.

It is also possible to obtain in-plane displacements with single-beam illumination by using a Fourier filtering technique.

Displacement derivatives can be obtained directly by speckle-shearing interferometry. The method uses an image-shearing camera illustrated in Fig. 25. One-half of the camera lens is covered by a thin glass wedge. The two images focused by the two halves of the lens are sheared with respect to each other, in the x-direction for the setup shown. The fringe pattern obtained by double exposure is a linear function of the displacement derivatives in the x and z-directions.

Speckle shearing can also be obtained by intensional misfocusing. The processed photographic plate can be Fourier-filtered to yield displacement derivatives along any desired direction and with variable sensitivity [46]. The fringe patterns of Fig. 26, obtained from a single photographic plate (specklegram), depict derivatives of deflections of a centrally loaded clamped plate, along the various directions selected during the filtering process.

6 Other Methods

Space limitations do not permit a survey of many other methods of experimental mechanics, although many important developments have occurred in other areas. The optical method of caustics, for example, have been actively pursued and applied successfully to fracture mechanics. The method is well suited for analyzing stress singularities at crack tips, and has been applied to the determination of stress-intensity factors under biaxial stress conditions.

Residual stresses, especially near the surface of heat-treated metals, have been analyzed using X-ray diffraction techniques and ultrasonic surface waves. Acoustoelasticity, analogous to photoelasticity, has been discussed as a means of stress analysis in opaque bodies. Acoustic holography has been developed as an extension of optical holography.

Nondestructive evaluation of material integrity relies heavily on ultrasonics and X-radiography. New techniques and instrumentation, and new data-processing methods are being introduced in this field. Acoustic emission techniques have also undergone considerable development, with attempts to correlate frequency and amplitude distributions of the acoustic emission output with microscopic deformation and fracture phenomena in the material.

7 Conclusion

An overview was presented of the development and status of several experimental mechanics methods, i.e., strain gages, moiré, photoelasticity, and interferometry. Considerable progress has been made in all aspects, experimental methodology, data acquisition instrumentation, and data processing. In the application area the emphasis is shifting toward the more challenging problems of inelastic and nonlinear material characterization, fracture and damage mechanics, nondestructive evaluation, and accelerated testing for reliability determination and life prediction. The availability of advanced instrumentation and computers allows the acquisition of a great deal more data than ever before in a shorter period of time, requiring more advanced treatment of these data. The interaction between theory and experiment is becoming stronger as new hybrid analytical-experimental approaches are introduced.

References

1 Daniel, I. M., Mullineaux, J. L., Ahimaz, F. J., and Liber, T., "The Embedded Strain Gage Technique for Testing Boron/Epoxy Composites," *Composite Materials: Testing and Design*, ASTM STP 497, 1972, pp. 257–272.

2 Daniel, I. M., Liber, T., and LaBedz, R. H., "Wave Propagation in Transversely Impacted Composite Laminates," *Experimental Mechanics*, Vol. 19, No. 1, Jan. 1979, pp. 9–16.

3 Daniel, I. M., LaBedz, R. H., and Liber, T., "New Method for Testing Composites at Very High Strain Rates," *Exp. Mech.*, Vol. 21, No. 2, Feb. 1981, pp. 71–77.

4 Sciammarella, C. A., "The Moiré Method—A Review," *Exp. Mech.*, Vol. 22, No. 11, Nov. 1982, pp. 418–433.

5 Sciammarella, C. A., "Techniques of Fringe Interpolation in Moiré Patterns," *Exp. Mech.*, Vol. 7, No. 11, 1967, pp. 19A–30A.

6 Chiang, F. P., Parks, V. J., and Durelli, A. J., "Moiré-Fringe Interpolation and Multiplication by Fringe Shifting," *Exp. Mech.*, Vol. 8, No. 12, 1968, pp. 554–560.

7 Post, D., "Analysis of Moiré Fringe Multiplication Phenomena," *Applied Optics*, Vol. 6, No. 11, 1967, pp. 1938–1942.

8 Post, D., "New Optical Methods of Moiré Fringe Multiplication," *Exp. Mech.*, Vol. 8, No. 2, 1968, pp. 63–68.

9 Hung, Y. Y., Durelli, A. J., and Hovanesian, J. D., "An Improved Moiré-Fringe Multiplication Technique," *Proc. of 1982 Joint Conf. on Experimental Mechanics*, Society for Experimental Stress Analysis/Japan Society of Mechanical Engineering, May 1982, Hawaii, pp. 167–174.

10 Weissman, E. M., and Post, D., "Moiré Interferometry Near the Theoretical Limit," *Applied Optics*, Vol. 21, No. 9, May 1982, pp. 1621–1623.

11 Post, D., "Developments in Moiré Interferometry," *Optical Engineering*, Vol. 21, No. 3, May/June 1982, pp. 458–467.

12 Daniel, I. M., and Rowlands, R. E., "On Wave and Fracture Propagation in Rock Media," *Exp. Mech.*, Vol. 15, No. 12, Dec. 1975, pp. 445–457.

13 Daniel, I. M., Rowlands, R. E., and Post, D., "Strain Analysis of Composites by Moiré Methods," *Exp. Mech.*, Vol. 13, No. 6, June 1973, pp. 246–252.

Downloaded 02 May 2010 to 171.66.16.250. Redistribution subject to ASME license or copyright; see http://www.asme.org/terms/Terms_Use.cfm

14 Whitney, J. M., Daniel, I. M., and Pipes, R. B., *Experimental Mechanics of Fiber Reinforced Composite Materials*, Society for Experimental Stress Analysis Monograph, Brookfield Center, 1982.

15 Post, D., Czarnek, R., and Smith, C. W., "Patterns of u and v Displacements Around Cracks in Aluminum by Moiré Interferometry," presented at *International Conf. on Application of Fracture Mechanics to Materials and Structures*, Freiburg, Germany, June 1983.

16 Obata, M., Shimada, H., Otani, K., "Study on Three-Dimensional Distributions of Stress Intensity Factors by the Embedded Fine Dyeing Grid Method," *Proc. of 1982 Joint Conf. on Experimental Mechanics*, Society for Experimental Stress Analysis/Japan Society of Mechanical Engineering, May 1982, Hawaii, pp. 83–88.

17 Cernosek, J., "Three-Dimensional Photoelasticity by Stress Freezing," *Exp. Mech.*, Vol. 20, No. 12, Dec. 1980, pp. 417–426.

18 Takahashi, S., "A Survey of Recent Experimental Mechanics in Japan," *Proc. of Joint Conf. on Exp. Mech.*, Society for Experimental Stress Analysis/Japan Society of Mechanical Engineers, May 1982, Hawaii, pp. 1–11.

19 Smith, C. W., "Photoelasticity in Fracture Mechanics," *Exp. Mech.*, Vol. 20, No. 11, Nov. 1980, pp. 390–396.

20 Swinson, W. F., Turner, J. L., and Ranson, W. F., "Designing With Scattered-Light Photoelasticity," *Exp. Mech.*, Vol. 20, No. 11, Nov. 1980, pp. 397–402.

21 Desailly, R., and Lagarde, A., "The Application of a New Non-destructive Optical Slicing Procedure to Problems in Three-Dimensional Photoelasticity," *Proc. 1982 Joint Conf. on Exp. Mechanics*, Society for Experimental Stress Analysis/Japan Society of Mechanical Engineers, May 1982, Hawaii, pp. 520–526.

22 Aben, H., *Integrated Photoelasticity*, McGraw-Hill, New York, 1978.

23 Dally, J. W., "An Introduction to Dynamic Photoelasticity," *Exp. Mech.*, Vol. 20, No. 12, Dec. 1980, pp. 409–416.

24 Riley, W. F., and Dally, J. W., "Recording Dynamic Fringe Patterns With a Cranz-Schardin Camera," *Exp. Mech.*, Vol. 9, No. 8, Aug. 1969, pp. 27N–33N.

25 Rowlands, R. E., Taylor, C. E., and Daniel, I. M., "A Multiple-Pulse Ruby Laser System for Dynamic Photomechanics. Applications to Transmitted and Scattered-Light Photoelasticity," *Exp. Mech.*, Vol. 9, No. 9, Sept. 1969, pp. 385–393.

26 Daniel, I. M., and Marino, R. L., "Wave Propagation in Layered Model due to Point-Source Loading in Low-Impedance Medium," *Exp. Mech.*, Vol. 22, No. 5, May 1971, pp. 210–216.

27 Burger, C. P., Testa, A., and Singh, A., "Dynamic Photoelasticity as an Aid in Developing New Ultrasonic Test Methods," *Exp. Mech.*, Vol. 11, No. 4, Apr. 1982, pp. 147–154.

28 Daniel, I. M., "Experimental Studies of Water Jet Impact on Rock and Rocklike Materials," *Proc. of Third International Symposium on Jet Cutting Technology*, BHRA, Paper B3, Chicago, May 1976.

29 Dally, J. W., "Dynamic Photoelastic Studies of Fracture," *Exp. Mech.*, Vol. 19, No. 10, Oct. 1979, pp. 349–361.

30 Ramulu, M., Kobayashi, A. S., and Kang, B. S.-J., "Dynamic Crack Branching—A Photoelastic Evaluation," *Proc. of 15th National Symposium on Fracture Mechanics*, MD, July 1982; ASTM STP . . . , 1983.

31 Ramulu, M., and Kobayashi, A. S., "Dynamic Crack Curving—A Photoelastic Evaluation," *Exp. Mech.*, Vol. 23, No. 1, Mar. 1983, pp. 1–9.

32 Kobayashi, A. S., Seo, K., Jou, J. Y., and Urabe, Y., "A Dynamic Analysis of Modified Compact-Tension Specimens Using Homalite-100 and Polycarbonate Plates," *Exp. Mech.*, Vol. 20, No. 3, Mar. 1980, pp. 73–79.

33 Daniel, I. M., Niiro, T., and Koller, G. M., "Development of Orthotropic Birefringent Materials for Photoelastic Stress Analysis," NASA-Langley Research Center, NASA CR-165709, May 1981.

34 Voloshin, A. S., and Burger, C. P., "Photo-Orthotropic Elasticity Through a Digital Image Analysis of Low Level Birefringence," *Proc. of Seventh International Conference on Experimental Stress Analysis*, Aug. 1982, Haifa, Israel, pp. 483–494.

35 Daniel, I. M., "Experimental Methods for Dynamic Stress Analysis in Viscoelastic Materials," ASME JOURNAL OF APPLIED MECHANICS, Vol. 32, 1965, pp. 598–606.

36 Burger, C. P., "Nonlinear Photomechanics," *Exp. Mech.*, Vol. 20, No. 11, Nov. 1980, pp. 381–389.

37 Burger, C. P., and Gomide, H. A., "Three-Dimentional Strains in Rolled Slabs By Photoplastic Simulation," *Exp. Mech.*, Vol. 22, No. 12, Dec. 1982, pp. 441–447.

38 Burger, C. P., "Thermal Modeling," *Exp. Mech.*, Vol. 15, No. 11, Nov. 1975, pp. 430–441.

39 Voloshin, A. S., and Burger, C. P., "Half-Fringe Photoelasticity: A New Approach to Whole Field Stress Analysis," to be published in *Exp. Mech.*

40 Burger, C. P., Kar, R., and Voloshin, A., "Half-Fringe Photoelasticity Applied to K-Determination for Cracks in Glass," presented at 1983 Spring Meeting of SESA, May 1983, Cleveland, Ohio.

41 Zandman, F., Redner, S., and Dally, J. W., *Photoelastic Coatings*, SESA Monograph No. 3, Iowa State University Press, Ames, Iowa, 1977.

42 Daniel, I. M., "Biaxial Testing of Graphite/Epoxy Laminates With Cracks," *Test Methods and Design Allowables for Fibrous Composites*, Chamis, C. C., ed., ASTM STP 734, 1981, pp. 109–128.

43 Sanford, R. J., "Photoelastic Holography—A Modern Tool for Stress Analysis," *Exp. Mech.*, Vol. 20, No. 12, Dec. 1980, pp. 427–436.

44 Sciammarella, C. A., "Holographic Moiré, an Optical Tool for the Determination of Displacements, Strains, Contours, and Slopes of Surfaces," *Optical Eng.*, Vol. 21, No. 3, May/June 1982, pp. 447–457.

45 Hung, Y. Y., "Displacement and Strain Measurement," *Speckle Metrology*, Erf, R. K., ed., Academic Press, New York, 1978, pp. 51–71.

46 Hung, Y. Y., Daniel, I. M., and Rowlands, R. E., "Full-Field Optical Strain Measurement Having Post-Recording Sensitivity and Direction Selectivity," *Exp. Mech.*, Vol. 18, No. 2, Feb. 1978, pp. 56–60.

Downloaded 02 May 2010 to 171.66.16.250. Redistribution subject to ASME license or copyright; see http://www.asme.org/terms/Terms_Use.cfm

S. H. Davis
Department of Engineering Sciences
and Applied Mathematics,
The Technological Institute,
Northwestern University,
Evanston, Ill. 60201

Contact-Line Problems in Fluid Mechanics

The types of contact-line problems that arise in fluid-dynamical applications are described and classified. Examples of each type are discussed in terms of the boundary conditions that are used and the singular nature of the solutions that emerge.

1 Introduction

Consider two fluid phases separated by a thin interfacial region as shown in Fig. 1. It is conventional [1] to treat such a system by a model in which the interfacial region is replaced by an interface, which is a mathematical dividing surface of zero thickness, plus two continuum fluids having uniform properties right up to the interface. The "error" made in such a replacement is accounted for by endowing the interface [1, 2] with surface excess properties such as mass density γ and surface tension σ. Thus, the interface is a two-dimensional continuum possessing its own material properties and coupled to the three-dimensional fluids in which it is embedded. The mass/momentum/energy balances of the interface are then partial differential equations that serve as boundary conditions (jump conditions) on the fields describing the fluid mechanics.

Consider now the intersection of an interfacial region with a solid surface as shown in Fig. 2. Again, the interfacial region is replaced by an interface, the solid-fluid interfacial regions are replaced by solid-fluid boundaries, and the three-phase region is replaced by a contact line, the intersection of the fluid-fluid interface with the solid.

The usual situation in fluid mechanics is that interfaces are free boundaries since their positions are a priori unknown. The contact lines have positions a priori unknown so that there are "nested" free boundaries. Furthermore, these free boundaries are not passive; they have localized properties that can drive the motions of the bulk fluids.

In the present paper we will classify the types of contact-line problems that arise in fluid mechanics and sketch examples of the various cases. The intention is to give a flavor of the issues that arise. We shall show the types of boundary-value problems that occur, the novel boundary conditions that are posed, and discuss the interesting singular behaviors that occur at contact lines.

2 Formulation of the Interface Conditions

In order to simplify the *presentation* we develop only the two-dimensional system where the velocity $\mathbf{v}=(u,v)$ corresponds to the coordinates (x,y) as shown in Fig. 3. For convenience we call one fluid a liquid and one a gas even though the liquid-liquid case is not excluded. We assume that

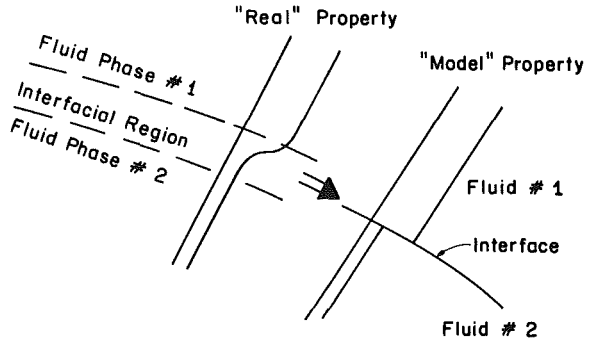


Fig. 1 A sketch of the symbolic replacement of a real two-phase system by a model involving an interface

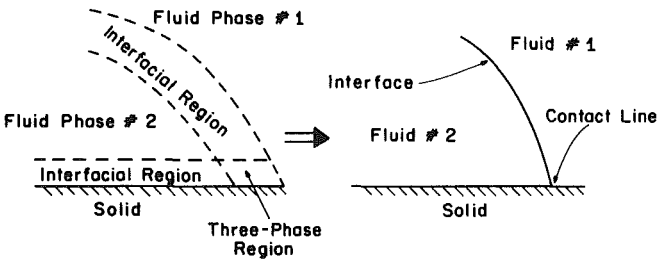


Fig. 2 A sketch of the symbolic replacement of a real three-phase system by a model involving an interface and a contact line

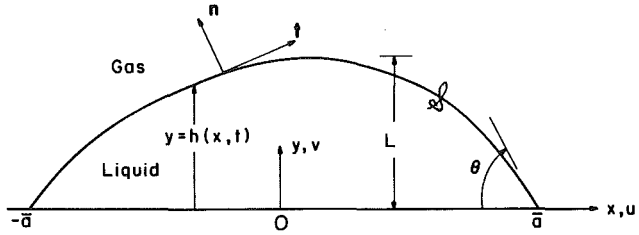


Fig. 3 A sketch of a liquid drop on a solid

Contributed by the Applied Mechanics Division for publication in the JOURNAL OF APPLIED MECHANICS.
Discussion on this paper should be addressed to the Editorial Department, ASME, United Engineering Center, 345 East 47th Street, New York, N.Y. 10017, and will be accepted until two months after final publication of the paper itself in the JOURNAL OF APPLIED MECHANICS. Manuscript received by ASME Applied Mechanics Division, March, 1983.

Copyright © 1983 by ASME
Downloaded 02 May 2010 to 171.66.16.250. Redistribution subject to ASME license or copyright; see http://www.asme.org/terms/Terms_Use.cfm

the liquid and gas are both Newtonian fluids with constant density.

Each bulk fluid satisfies the Navier-Stokes equations

$$\rho(\mathbf{v}_t + \mathbf{v}\cdot\nabla\mathbf{v}) = -\nabla p + \mu\nabla\cdot\underline{\mathbf{S}} + \rho\mathbf{f}, \tag{1a}$$

$$\underline{\mathbf{S}} = \nabla\mathbf{v} + (\nabla\mathbf{v})^T \tag{1b}$$

and the equation of continuity

$$\nabla\cdot\mathbf{v} = 0 \tag{1c}$$

where $\mu\underline{\mathbf{S}}$ is the viscous-stress tensor, $\mathbf{f}$ is the body force per unit mass, μ and ρ denote the viscosity and density of the fluids, superscript T denotes transpose, and subscripts denote partial differentiation. The pressure is p and time is t.

The interface $\mathcal{S}$ of Fig. 3 is given by

$$\mathcal{S}: y = h(x,t) \tag{2}$$

and we define the unit normal $\mathbf{n}$ (pointing out of the liquid) and unit tangent $\mathbf{t}$ by

$$\mathbf{n} = (1+h_x^2)^{-1/2}(-h_x, 1)\ , \tag{3a}$$

$$\mathbf{t} = (1+h_x^2)^{-1/2}(1, h_x)\ . \tag{3b}$$

We define the jump at $\mathcal{S}$ of a quantity Q by

$$[\![Q]\!] = Q_L(x,h,t) - Q_G(x,h,t) \tag{4}$$

where here subscripts L and G denote limits taken, respectively, from the liquid and gas sides of $\mathcal{S}$.

We assume that no mass is transported across $\mathcal{S}$ so that $\mathcal{S}$ is a bounding surface,

$$v = h_t + uh_x \quad \text{on} \quad y = h \tag{5}$$

where (u,v) denotes the velocity in either the liquid or gas.

If both fluids are viscous, then

$$[\![\mathbf{v}\cdot\mathbf{t}]\!] = 0 \quad \text{on} \quad y = h. \tag{6}$$

If either (or both) fluid is inviscid, then this no-slip condition is abandoned.

The force balance on $\mathcal{S}$ has two components. The normal component is

$$-[\![p]\!] + [\![\mu\underline{\mathbf{S}}\cdot\mathbf{n}\cdot\mathbf{n}]\!] = \sigma(1+h_x^2)^{-3/2}h_{xx} \tag{7}$$

where the right-hand side represents the surface tension σ times twice the mean curvature of $\mathcal{S}$. In writing equation (7) we have taken the excess surface mass to be zero. Hence, the interface has a negligible excess inertia and body force.

In the case of fluid statics, $\underline{\mathbf{S}} = \underline{\mathbf{0}}$, equation (7) states that the pressure excess on the concave side of a static meniscus is equal to surface tension times the curvature. If σ is large enough, then this static balance, giving a constant-curvature interface, is a good approximation even in dynamical contexts; this is likewise true in three-dimensional cases.

The force balance on $\mathcal{S}$ has a tangential component of the form

$$[\![\mu\underline{\mathbf{S}}\cdot\mathbf{n}\cdot\mathbf{t}]\!] = (\mathbf{t}\cdot\nabla)\sigma. \tag{8}$$

The surface tension σ generally depends on scalar fields such as the local temperature T or the surface concentration Γ of surface-active material. One then requires an equation of state

$$\sigma = \sigma(\Gamma, T) \tag{9}$$

where in general $\partial\sigma/\partial\Gamma < 0$ and $\partial\sigma/\partial T < 0$. This reduction in surface tension, coupled with the balance (8) of shear stress with surface-tension gradient, gives rise to what is sometimes called a Marangoni effect; surface tension differences on $\mathcal{S}$ can drive bulk motions.

If the material on $\mathcal{S}$ is insoluble, the mass of surfactant on $\mathcal{S}$ is conserved. If this material is soluble, its concentration C in the fluids obeys a mass-balance equation and a state equation relating Γ to C.

If the surface tension depends on T, then the temperature distributions in the fluids are governed by an energy equation.

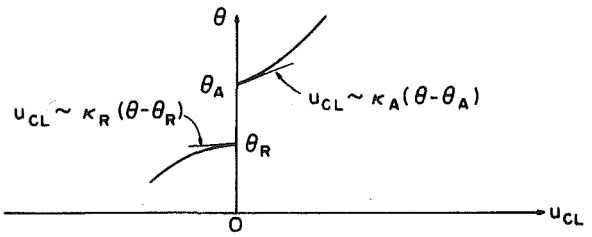


Fig. 4 A sketch of typical measured contact angles θ versus the contact-line speed u_{CL}. The advancing angle is θ_A and the receding angle is θ_R. κ_R^{-1} and κ_A^{-1} are the local slopes of the measured values.

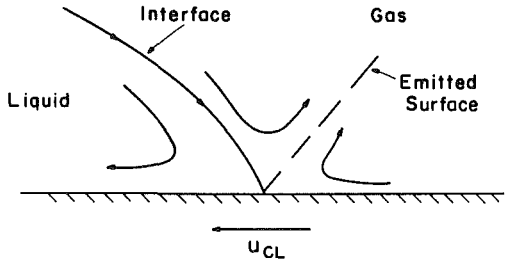


Fig. 5 A sketch of the local flow field near a moving contact line

3 Formulation of Contact-Line Conditions

Figure 3 shows a configuration in which contact lines are present at $x = \pm\tilde{a}$. Since equation (7) is a differential equation of second order in x, a well-posed boundary-value problem requires conditions at the "edges" of $\mathcal{S}$, i.e., at the contact lines.

The contact-line position $x = \tilde{a}$ is defined by

$$h(\tilde{a},t) = 0 \tag{10a}$$

while the contact angle θ (measured through the liquid) is defined by

$$h_x(\tilde{a},t) = -\tan\theta. \tag{10b}$$

Usually, one cannot prescribe the contact-line position $\tilde{a}$; rather, it is natural to prescribe a relation between θ and the speed u_{CL} of the contact line. Measurements of contact angles θ in liquid-gas-solid systems typically have the form shown in Fig. 4. Here u_{CL} is taken as positive if liquid advances over solid and displaces gas; u_{CL} is taken as negative if liquid recedes and is displaced by gas. The limiting static case gives static angles θ_A and θ_R. The existence of the interval $[\theta_R, \theta_A]$, much larger than the error in the experimental measurements, is called contact-angle hysteresis. The implication in Fig. 4 is that any angle θ in the range $[\theta_R, \theta_A]$ corresponds to a static equilibrium. Thus, static menisci of liquids of a given volume are not unique.

Moving contact lines require a further modeling assumption. Dussan V. and Davis [3] show that if the fluids at the interface migrate toward the contact line as shown in Fig. 5 and if the no-slip boundary condition is applied on all fluid-solid interfaces, then the local flow field is as shown. (Here the coordinate system moves with the contact line so that the solid moves past the observer at speed $|u_{CL}|$.) The material at the contact line has multiple indentities (e.g., gas and solid) that later split into multiple points. This trajectory splitting leads to fluid stresses at a distance r from the contact line that behave like r^{-1} and so to forces that behave like $\ln r$. This singularity precludes the prediction of spreading rates of the liquid or even global interface shapes (if σ is large). The analysis of Dussan V. and Davis [3] has led to the use of the inclusion of effective or apparent slip on the solid-fluid interfaces near the contact line. Any such slip model that gives

Downloaded 02 May 2010 to 171.66.16.250. Redistribution subject to ASME license or copyright; see http://www.asme.org/terms/Terms_Use.cfm

perfect slip[1] at the contact line will relieve the force singularity. Dussan V. [4] discusses the relation between experimental observation and such physical modeling.

Various types of slip models can be posed. Two types are generally used. There are "fixed interval" slip models [5, 6] of the type

$$u = u_{CL}, \quad |x - \bar{a}(t)| > \beta'$$
$$u = u_s(x), \quad |x - \bar{a}(t)| \le \beta' \tag{11}$$

where $u_s(\bar{a}+\beta') = u_{CL}$ and $u_s(\bar{a}) = 0$ and there are the Navier slip models [6-8] of the type

$$u = \beta' \underline{\mathbf{S}} \cdot \mathbf{n} \cdot \mathbf{t} \tag{12}$$

where $\mu \underline{\mathbf{S}} \cdot \mathbf{n} \cdot \mathbf{t}$ is the shear stress on the solid. Note that the slip coefficients β' in equations (11) and (12) have different meanings.

Dussan V. [5] has examined the problem of an infinite plate plunged through an interface into an infinite pool of liquid and has shown that a whole class of fixed-interval models yields the same outer flow, although the flows in the immediate neighborhood of the contact line are different. Hocking [7] has examined a wedge (sector) flow and mutual displacement in a channel and has shown that the imposition of a Navier slip model does in fact give perfect slip at the contact line so that again there is a sensibly fixed interval slip model that only affects the local flow and not the outer flow.

Before we turn to concrete examples of contact-line problems let us discuss some general points. In the general formulation of contact-line problems there are two principal parameters. There is the capillary number Ca,

$$Ca = \frac{\hat{u}_s \mu}{\sigma} \tag{13}$$

where $\hat{u}_s$ is a velocity scale that measures the speed of the fluid near the contact line. $Ca \to \infty$ ($\sigma \to 0$) is a singular limit of equation (7) so that surface-tension effects are confined to a thin boundary layer near the contact line. Thus, if $Ca >> 1$, then surface-tension effects and contact-line effects are relatively unimportant since viscous deformation of the interface is large. If $Ca << 1$, the interface is nearly a static meniscus whose shape is defined by a contact-angle condition. However, the contact angle is strongly affected by the local dynamics (including slip and local viscous flow). Hence, small changes in the conditions at the contact line can lead to large changes of the interfacial shape.

If effective slip is used to model moving contact lines, then the dimensional slip length β' gives rise to a second principal parameter,

$$\beta = \beta'/L \tag{14}$$

where L is a length scale of the gross system. The slip parameter β is presumably small even though the limit $\beta \to 0$ is a singular limit (since $\beta = 0$ recovers the force singularity). A common case, then, for moving-contact-line problems is that both Ca and β are present as small parameters.

There are several mathematical types of contact lines that arise; it is useful to classify these here. A contact line may be *stationary* or it may be *moving*. A contact line may constitute a *free* boundary (its position is unknown a priori) or a *fixed* boundary (its position is known a priori). Hence, we shall refer to four types of problems: *stationary-fixed*, *stationary-free*, *moving-fixed*, and *moving-free*. As we shall see, under certain circumstances one type can convert into another type.

We turn now to concrete examples that illustrate the general features of boundary-value problems that contain contact lines.

[1] The phrase "perfect slip" means that the fluid on the solid-fluid interfaces at the contact line move with speed $|u_{CL}|$.

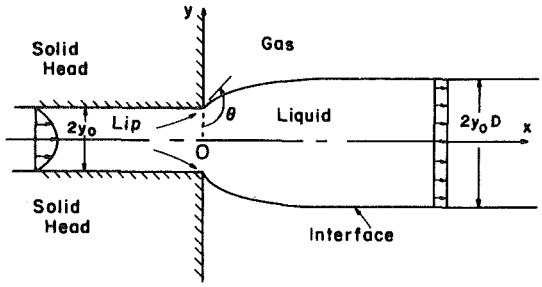


Fig. 6 A sketch of a two-dimensional die-swell configuration

4 Contact-Line Problems

(a) **Die Swell.** A viscous liquid is extruded from an orifice of a long two-dimensional channel and into the surrounding air as shown in Fig. 6. The interface is shown leaving the sharp lip and approaching a plane jet for large x. Body forces, air drag, and inertia are ignored.

The swell ratio D is defined as the final width (as $x \to \infty$) divided by the initial width $2y_0$ (at $x = 0$). Experiments [9] give $D \approx 1.13$ for an axisymmetric jet when the Reynolds number Re is small.

If one supposes that the interface leaves the lip as shown in Fig. 6, then the die-swell problem qualifies as the "simplest" type of contact-line problem, the stationary-fixed case.

Local analysis of the Stokes flow near the contact line [10] shows that the discontinuous change at $x = 0$ from the no-slip to the zero-shear-stress boundary condition leads to pressure and velocity gradients being singular like $r^{-1/2}$. Thus, the forces are finite.

There is a limiting case for $Ca \to 0$, which according to boundary condition (7), has planar interfaces at $y = h = \pm y_0$. This is Richardson's [11] stick-slip problem in which the gas is supposed to have negligible density and viscosity. The stress singularity is present and this precludes [11] a regular perturbation technique in powers of Ca from yielding a "rational" prediction of the swelling ratio. This conclusion is based on Michael's [10] observation that the normal stress on the interface at the contact line is regular only for the interface angle $\theta = \pi/2$; see Fig. 6. This singularity likewise troubles the numerical solution of die-swell configurations [12]. Much of the interest in this problem arises from the fact that the lip singularity dominates the local flow near the lip and that this region gives birth to the die swell. However, the fact that the singularity is integrable leads one to suppose that its influence is only local.

Let us presume that the die-swell problem, as posed, has been satisfactorily solved. This does *not* mean that the problem is complete since characteristics of Fig. 4 demand a *compatibility condition*. If one takes the foregoing solution and evaluates the angle θ of Fig. 6, one must have [13] both $\theta \le \theta_A$ and $\theta + \pi/2 \ge \theta_R$ for the solution to correspond to a stationary contact line. This prescription is consistent with the view [13] that the contact angle θ at a sharp corner is the limiting case for a rounded corner with the contact angle in the range $[\theta_R, \theta_A]$.

If $\theta > \theta_A$, then the liquid will spread on the solid head until it reaches a position $y = y^* > y_0$ for which $\theta = \theta_A$. The spreading is a dynamical process (discussed in the following in §4c) under which the contact line belongs to the moving-free category. The final angle of spread would depend on whether the contact line only advances or advances and then recedes. Thus, depending on the history of the local motion, a variety of "spread" die-swell configurations would be possible [14].

(b) **Gas Bubble Rising in a Liquid.** Gas bubbles rising in liquid can be analyzed for Stokes flow and small capillary

Downloaded 02 May 2010 to 171.66.16.250. Redistribution subject to ASME license or copyright; see http://www.asme.org/terms/Terms_Use.cfm

number. The drag predicted for such spherical bubbles is one-third smaller than that for the equivalent rigid sphere, the difference being attributable to the mobility of the liquid-gas interface. Measurements [15], however, show that small bubbles have terminal velocities equal to those of solid spheres whereas large bubbles have terminal velocities equal to those of spheres with mobile interfaces. Moreover, the correlations for terminal speed involve both bubble diameter and surface tension.

The accepted explanation [16] lies with surface-active material in the liquid, adsorbing onto the bubble interface and being swept to the rear of the bubble. The surface tension is then lowered as by equation (9) for isothermal conditions, and a surface-tension gradient is created that (through equation (8)) counteracts the surface flow through a Marangoni effect. If the surfactant is nearly insoluble and sufficiently compressed at the rear of the bubble, an effectively stagnant cap is produced on which the liquid satisfies the no-slip condition. On the remainder of the bubble, the shear stress is continuous across the interface. Small bubbles are essentially fully capped while large bubbles have tiny caps.

The edge of the cap is (for vanishing solubility) effectively a stationary-free contact line, its position determined [17] by a physicochemical balance between the collapse pressure of the surfactant and the flow. Such a theory has been developed by Savic [16] and Davis and Acrivos [17] for $Ca=0$, creeping liquid flow, and convectively dominated mass transport for insoluble surfactants. This mathematical problem posed severe numerical difficulties [17] due to the $r^{-1/2}$ singularity in stresses at the cap edge; this singularity is seen explicitly in the exact solution generated by Sadhal and Johnson [18]. Both the pressure and the viscous normal stress are singular although the full normal stress is regular [19] consistent with a passive enclosed gas having constant pressure and the local analysis of Michael [10].

(c) Spreading of Liquid Drops on a Horizontal Plate. A small liquid drop is placed on a solid horizontal plate as shown in Fig. 7. The liquid spreads, displaces the neighboring gas, and ultimately achieves an equilibrium configuration with contact angle $\theta=\theta_A$. For drops small enough to ignore gravity, the spreading occurs through two simultaneous processes. (*i*) If at time $t=0$, the contact angle were $\theta=\theta_A$, spreading would occur whenever the bulk drop is not in an equilibrium configuration. Thus, the anomaly in capillary pressure would drive a bulk motion. (*ii*) If at time $t=0$, $\theta>\theta_A$ then, as shown in Fig. 4, the contact-line speed $u_{CL}>0$ and the drop is "pulled" along. The actual spread process combines the two preceding effects.

Dynamical spreading involves moving-free contact lines. Effective slip is applied on the liquid/solid interface. Greenspan [8] and Greenspan and McCay [20] use a modified Navier slip model where $\beta'(x)=\beta' h(x,t)$. They examine thin spreading drops using lubrication theory measured by a lubrication parameter A (equivalent to an aspect ratio). They examine $A\to 0$ with Ca, $\beta=0(1)$, and obtain for two-dimensional drops a system that governs the drop shape h and the contact line position $\tilde{a}$,

$$Ca\,\frac{\partial h}{\partial t}+\frac{\partial}{\partial x}\left\{(\beta h+h^3)\,\frac{\partial^3 h}{\partial x^3}\right\}=0 \qquad (15a)$$

with

$$\frac{d\tilde{a}}{dt}=\mp\,\frac{\partial h}{\partial x}-\theta_A \quad \text{on } x=\pm\tilde{a}(t) \qquad (15b)$$

subject to the volume constraint that

$$\int_{-\tilde{a}(t)}^{\tilde{a}(t)} h\,dx=\frac{2}{3}. \qquad (15c)$$

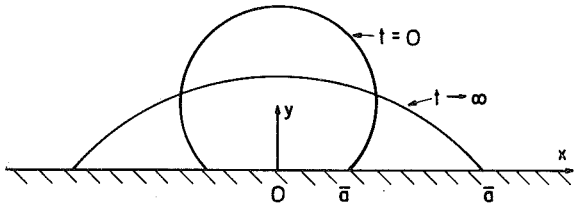


Fig. 7 A sketch of a spreading liquid drop on a solid indicating initial and final shapes

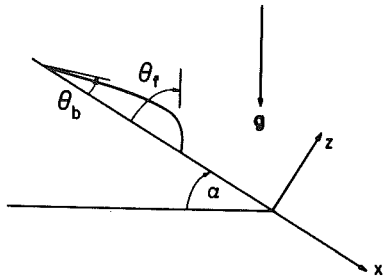


Fig. 8 A sketch of a two-dimensional liquid drop moving down an inclined plane

Numerical methods [20] are used to obtain spreading rates while asymptotics is used in limiting cases.

For $\beta=0(1)$, the limit $Ca\to 0$ is uniform [8] in that corrections to the equilibrium shape and contact angle are $O(Ca|ln\beta|)$.

For $\beta\to 0$ and $Ca=O(1/|ln\beta|)$ analyses in wedges, capillaries, and slots [5–7] indicate that matched asymptotic expansions yield an inner region (near the contact line) where slip is important and the thermostatic contact angle determines a local wedge flow. The outer region depends on the geometry of the drop. The two expansions match asymptotically and result in the outer flow seeing an intermediate contact angle θ_I that Kafka and Dussan V. [21] argue is geometry independent. Given that Ca is so small, θ_I and θ do not differ greatly.

For $\beta\to 0$, $Ca=O(1/|ln\beta|)$, the region near the contact line has a double structure. Hocking and Rivers [22] find that the two regions have sizes $O(\beta)$ and $O(|ln\beta|)$. In the middle region, interfacial deformation can be large and θ_I and θ may differ greatly.

(d) Spreading of Liquid Layers on a Tilted Plate. A two-dimensional liquid drop is placed on a horizontal plane and spreads to an equilibrium configuration as discussed in §4*c*. The contact lines are straight and parallel. Now the plate is tilted so that the drop remains two-dimensional and moves down the plate under the influence of gravity. Hocking [23] has used a Navier slip model and analyzed the motion of the drop when $\kappa_A^{-1}=\kappa_R^{-1}=0$ so that from Fig. 4 the contact angles are velocity independent; the foreward angle is θ_A and the rearward angle is θ_R. Hocking uses lubrication theory to determine the motion and interface shape.

A three-dimensional liquid drop is placed in a horizontal plane and spreads to an equilibrium configuration as discussed in §4*c*. The contact line is circular. Now the plate is tilted an angle α to the horizontal. If it maintains an equilibrium configuration as shown in Fig. 8 then, due to gravity, the observed contact angle θ_f in the front exceeds the observed contact angle θ_b in the back and both angles are in the range $[\theta_R,\theta_A]$.

Dussan V. [24] investigates the configuration of the drop (and its subsequent motion) at its critical tilt angle α_c for which $\alpha<\alpha_c$ yields a static state and $\alpha>\alpha_c$ causes the drop to roll down the plate. The key to the analysis is the observation

Downloaded 02 May 2010 to 171.66.16.250. Redistribution subject to ASME license or copyright; see http://www.asme.org/terms/Terms_Use.cfm

that contact-angle hysteresis requires the contact line to evolve into the shape shown in Fig. 9. Here the front is advancing so that $\theta_f > \theta_A$ at point a. The angle continuously decreases until points b where $\theta = \theta_A$. The segments bc are stationary straight lines down the plate along which the contact angle continuously decreases to $\theta = \theta_R$ at points c. The rear of the drop is receding so that the contact angle continuously decreases from $\theta = \theta_R$ at c to $\theta = \theta_b < \theta_R$ at the point d. Thus, the segments bab and cdc are moving-free contact lines and segments bc are stationary-free contact lines. The points b and c are themselves stationary-free transition points; their positions are unknown although their contact angles are known. Dussan V. [24] uses lubrication theory to determine the largest drop that can remain stationary at a given angle α and analyzes the subsequent slow motion within the moving drop.

(e) **Dynamic Instabilities of Rivulets.** A rivulet is a narrow stream of liquid flowing down a solid surface and sharing an interface with the surrounding gas. The flow within the rivulet is driven by the component of gravity along the solid surface as shown in Fig. 10.

There is a simple solution for rivulet flows called the straight rivulet [25] in which the interface is a cylindrical meniscus, the contact lines are straight, parallel, and stationary, and the bulk flow is unidirectional and parallel. Rivulets exhibit a wide range of instabilities [26, 27] including breakup into droplets, nonlinear surface waves, meandering, and transition to turbulence. These instabilities are accompanied by moving-free contact lines.

If the straight rivulet is disturbed, then the interface position, contact-line position, and contact angle are now given by $y = h_0(z) + h'(x,z,t)$, $z = \tilde{a}_0 + \tilde{a}'(x,t)$, and $\theta = \theta_0 + \theta'(x,t)$, respectively. The contact-line conditions (10*a*,*b*) then involve the three disturbance quantities h', $\tilde{a}'$, and θ'. The characteristic of Fig. 4 is also needed. If we write this as

$$\theta = G(u_{CL}), \tag{16}$$

then $G'(0)$ does not exist. Hence, systems that display contact-angle hysteresis do not have a well-defined linearized stability theories and must be treated by other means. If the hysteresis of equation (16) is *absent* so that

$$\theta - \theta_0 \sim g u_{CL} + O(u_{CL}) \tag{17}$$

as $u_{CL} \to 0$, then equations (10*a*), (10*b*), and (17) can be combined [28] to obtain the linearized contact-line boundary condition

$$\frac{\partial h'}{\partial z} - k_1 h' = k_2 g \frac{\partial h'}{\partial t} \quad \text{at} \quad z = \tilde{a}_0 \tag{18}$$

where k_1 and k_2 are positive constants. Thus, in the absence of hysteresis, moving-free contact lines induce linear time-dependent boundary conditions of the third kind. With hysteresis, these boundary conditions would also be nonlinear. Davis [28] and Weiland and Davis [29] show that the gross instability characteristic of rivulets are very sensitive to contact-line boundary conditions.

5 Conclusions

In the previous discussion we have sketched several simple model problems that serve to illustrate the character of interfacial fluid-mechanics problems having contact lines.

The interfaces are free boundaries whose positions are usually unknown a priori. The "end points" of these free boundaries are contact lines whose positions are usually unknown a priori. The "end points" of these contact lines are transition points whose positions are usually unknown a priori.

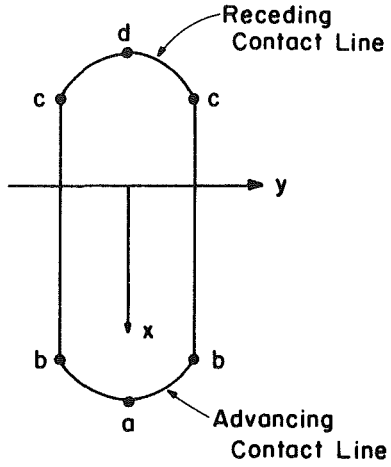


Fig. 9 A sketch of the contact-line shape of a three-dimensional liquid drop in its critical configuration

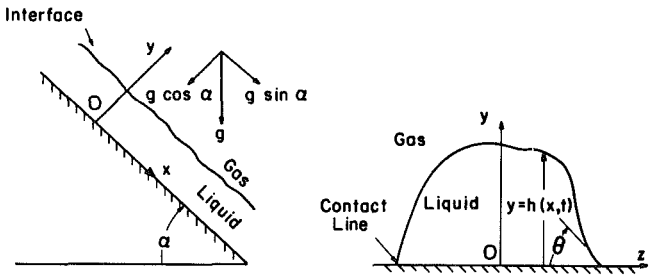


Fig. 10 A sketch of a three-dimensional liquid rivulet on an inclined plane

Contact lines can control the interfacial behavior of the system under study. They are often the site of singularities whose careful treatment is required to determine the behavior of the system. Modeling assumptions are often necessary to relieve the singular nature of the solutions near the contact lines.

The boundary conditions at moving contact lines are generally both nonlinear and time-dependent. The nonlinearities arise from both the kinematical (free-boundary) nature of the contact line and the dynamical (contact-angle hysteresis) nature of the conditions imposed.

Acknowledgments

The author is grateful for the suggestions made on a draft of this manuscript by Professors E. B. Dussan V., G. M. Homsy, S. Rosenblat and W. W. Schultz. This work was supported by the National Science Foundation, Fluid Mechanics Program.

References

1 Gibbs, J. W., "On the Equilibrium of Heterogeneous Substances," *The Collected Works of J. Willard Gibbs*, Vol. 1, 1948, pp. 55–353.

2 Rowlinson, J. S., and Widom, B., *Molecular Theory of Capillarity*, Oxford Science Publications, Clarendon Press, 1982.

3 Dussan V., E. B., and Davis, S. H., "On the Motion of a Fluid-Fluid Interface Along a Solid Surface," *Journal of Fluid Mechanics*, Part 1, 1974, Vol. 65, pp. 71–95.

4 Dussan V., E. B., "The Moving Contact Line," in *Waves on Fluid Interfaces*, Meyer, R. E., ed., Symposium at Mathematics Research Center, University of Wisconsin, October 1982.

5 Dussan V., E. B., "The Moving Contact Line: The Slip Boundary Condition," *Journal of Fluid Mechanics*, Part 4, Vol. 77, 1976, pp. 665–684.

6 Huh, C., and Mason, S. G., "The Steady Movement of a Liquid Meniscus in a Capillary Tube," *Journal of Fluid Mechanics*, Part 3, Vol. 81, 1977, pp. 401–419.

Downloaded 02 May 2010 to 171.66.16.250. Redistribution subject to ASME license or copyright; see http://www.asme.org/terms/Terms_Use.cfm

7 Hocking, L. M., "A Moving Fluid Interface. Part 2. The Removal of the Force Singularity by a Slip Flow," *Journal of Fluid Mechanics*, Part 2, Vol. 79, 1977, pp. 209–229.

8 Greenspan, H. P., "On the Motion of a Small Viscous Droplet That Wets a Surface," *Journal of Fluid Mechanics*, Part 1, Vol. 84, 1978, pp. 125–143.

9 Goren, S. L., and Wronski, S., "The Shape of Low-Speed Capillary Jets of Newtonian Liquids," *Journal of Fluid Mechanics*, Part 1, Vol. 25, 1966, pp. 185–198.

10 Michael, D. H., "The Separation of a Viscous Liquid at a Straight Edge," *Mathematika*, Vol. 5, 1958, pp. 82–84.

11 Richardson, S., "A Stick-Slip Problem Related to the Motion of a Free Jet at Low Reynolds Numbers," *Proceedings of the Cambridge Philosophical Society*, Vol. 67, 1970, pp. 477–489.

12 Nickell, R. E., Tanner, R. I., and Caswell, B., "The Solution of Viscous Incompressible Jet and Free-Surface Flows Using Finite-Element Methods," *Journal of Fluid Mechanics*, Part 1, Vol. 65, 1974, pp. 189–206.

13 Coghill, W. H., and Anderson, C. O., "Certain Interfacial Tension Equilibria Important in Flotation," *United States Bureau of Mines Technical Paper* 262, 1923.

14 Jean, M., and Pritchard, W. G., "The Flow of Fluids from Nozzles at Small Reynolds Numbers," *Proceedings of the Royal Society*, London, Series A, Vol. 370, 1980, pp. 61–72.

15 Bond, W. N., and Newton, D. A., "Bubbles, Drops, and Stokes' Law," *Philosophical Magazine*, Vol. 5, 1928, pp. 794–800.

16 Savic, P., "Circulation and Distortion of Liquid Drops Falling Through a Viscous Medium," National Research Council of Canada, Division of Mechanical Engineering Report MT-22, 1953.

17 Davis, R. E., and Acrivos, A., "The Influence of Surfactants on the Creeping Motion of Bubbles," *Chemical Engineering Science*, Vol. 21, 1966, pp. 681–685.

18 Sadhal, S. S., and Johnson, R. E., "Stokes Flow Past Bubbles and Drops Partially Coated With Thin Films. Part 1. Stagnant Cap of Surfactant Film—Exact Solution," *Journal of Fluid Mechanics*, Vol. 126, 1983, pp. 237–250.

19 Sadhal, S. S., Private communication, 1983.

20 Greenspan, H. P., and McCay, B. M., "On the Wetting of a Surface by a Very Viscous Fluid," *Studies in Applied Mathematics*, Vol. 64, 1981, pp. 95–112.

21 Kafka, F. Y., and Dussan V., E. B., "On the Interpretation of Dynamic Contact Angles in Capillaries," *Journal of Fluid Mechanics*, Part 3, Vol. 95, 1979, pp. 539–565.

22 Hocking, L. M., and Rivers, A. D., "The Spreading of a Drop by Capillary Action," *Journal of Fluid Mechanics*, Vol. 121, 1972, pp. 425–442.

23 Hocking, L. M., "Sliding and Spreading of Thin Two-Dimensional Drops," *Quarterly Journal of Mechanics and Applied Mathematics*, Vol. 34, 1981, pp. 37–55.

24 Dussan, V., E. B., "On the Ability of Drops and Bubbles to Stick to Nonhorizontal Surfaces of Solids," *Journal of Fluid Mechanics*, 1983, to appear.

25 Towell, G. D., and Rothfeld, L. B., "Hydrodynamics of Rivulet Flows," *American Institute of Chemical Engineering Journal*, Vol. 12, 1966, pp. 972–980.

26 Kern, J., "Zur Hydrodynamik der Rinnsale," *Verfahrenstechnik*, Vol. 3, 1969, pp. 425–430.

27 Kern, J., "Stabilitätsprobleme der Rinnsalströmung" *Verfahrenstechnik*, Vol. 5, 1971, pp. 289–294.

28 Davis, S. H., "Moving Contact Lines and Rivulet Instabilities. Part 1. The Static Rivulet," *Journal of Fluid Mechanics*, Vol. 98, 1980, pp. 225–242.

29 Weiland, R. H., and Davis, S. H., "Moving Contact Lines and Rivulet Instabilities. Part 2. Long Waves on Flat Rivulets," *Journal of Fluid Mechanics*, Vol. 107, 1981, pp. 261–280.

Downloaded 02 May 2010 to 171.66.16.250. Redistribution subject to ASME license or copyright; see http://www.asme.org/terms/Terms_Use.cfm

R. C. DiPrima
Department of Mathematical Sciences,
Rensselaer Polytechnic Institute,
Troy, N.Y. 12181
Mem. ASME

J. T. Stuart
Department of Mathematics,
Imperial College
London SW7 2BZ, England

Hydrodynamic Stability

Theoretical and experimental developments for the stability and transition of plane Poiseuille flow and for Couette flow between rotating concentric cylinders are reviewed. The paper concludes with brief comments on the stability of Hagen-Poiseuille flow in a pipe and brief comments on the stability of slowly varying flows.

1 Introduction

In this review we consider the problem of stability and transition for viscous incompressible flow. We concentrate on two classic problems with which we can illustrate many aspects of the theoretical and experimental progress of the last 25 years. Stability and transition for plane Poiseuille flow are discussed in Section 2 and for Couette flow between rotating concentric cylinders in Section 3. The concluding Section 4 contains some brief comments on the stability of slowly varying flows, especially the boundary layer, the stability of time periodic flows, and the stability of Hagen-Poiseuille flow in a pipe.

In this brief review it is not possible to discuss many other interesting topics, such as Bénard convection, effects of interfacial forces, baroclinic instability, the compressible boundary layer, Görtler vortices, and related mathematical areas such as bifurcation theory, energy methods, solitons, strange attractors, and chaos. We call the reader's attention to several recent monographs which provide useful accounts of various portions of the field: (*i*) *Stability of Fluid Motions I, II* by Joseph [1], especially for energy methods and bifurcation theory; *Hydrodynamic Instabilities and the Transition to Turbulence*, edited by Swinney and Gollub [2], especially for bifurcation theory, strange attractors, and transition to chaos; and *Hydrodynamic Stability* by Drazin and Reid [3], especially for linear stability theory and the asymptotic solution of the Orr-Sommerfeld equation. Other topics are also discussed in these volumes. For example, there are interesting articles in the monograph edited by Swinney and Gollub on Rayleigh-Bénard convection by F. H. Busse, on shear flow instabilities by S. A. Maslowe, and on instabilities in geophysical fluid dynamics by D. J. Tritton and P. A. Davies. The reader is referred also to Pedlosky [4] for a discussion of instabilities in geophysical fluid dynamics.

Suppose that we have an exact or approximate steady flow solution of the Navier-Stokes equations. Associated with this flow there is a characteristic velocity U_0 and a characteristic length l. We define the Reynolds number $R = U_0 l/\nu$, where ν is the kinematic viscosity. If this steady flow is slightly perturbed, then the linearized disturbance equations and associated boundary conditions are homogeneous and admit solutions proportional to $\exp(\sigma t)$, where t is the time. The flow is linearly unstable if there exist solutions of the disturbance equations such that $Re(\sigma) > 0$.

The complex growth rate σ is the solution of an eigenvalue problem; it depends on R, possibly other parameters describing the basic flow and geometry, and on parameters describing the disturbance. For example, suppose that we have a two-dimensional problem in which the basic steady flow is a function of y and is in the x direction, $-\infty < x < \infty$. (It is not important for the present discussion, but we assume that all variables have been made dimensionless in an appropriate manner.) Then we may choose disturbances that are periodic in x and z and discuss the single Fourier mode proportional to $\exp(\sigma t + i\alpha x + i\beta z)$ for α and β real and positive. If the geometry and basic flow are fixed except for the Reynolds number, then $\sigma = \sigma(R, \alpha, \beta)$. The condition that the eigenvalue σ with the largest real part has $Re(\sigma) = 0$ defines a neutral (or marginal) surface $R(\alpha, \beta)$. The minimum of $R(\alpha, \beta)$ over all $\alpha > 0$ and $\beta > 0$ determines a critical value of R, say R_c, and corresponding values of α, β, and $Im(\sigma)$. The basic flow is stable to such small disturbances if $R < R_c$; but for $R > R_c$ there exist values of α and β (normal modes) such that there is at least one eignevalue σ with $Re(\sigma) > 0$. Accounts of linear stability theory into the 1950s can be found in the monographs by Lin [5] and Chandrasekhar [6], and in the book edited by Rosenhead [7, Chapter IX]. With the availability of high-speed electronic computers and the development of mathematical software for dealing with complicated systems of differential equations the mathematical solution of a linear eigenvalue problem associated with a system of ordinary differential equations is today a routine, though often lengthy, task especially if there are several parameters in the problem.

In this review we concentrate on developments in nonlinear hydrodynamic stability theory stemming from the early ideas of Landau [8] and the work of Malkus and Veronis [9], Stuart [10, 11], and Watson [12]. We first restrict our attention to two-dimensional disturbances that are periodic in x with period $2\pi/\alpha_c$. As R is increased from $R < R_c$ to $R > R_c$, an infinitesimal Fourier mode proportional to $\exp(i\alpha_c x)$ will grow exponentially with time according to linear theory. As

Contributed by the Applied Mechanics Division for publication in the JOURNAL OF APPLIED MECHANICS.

Discussion on this paper should be addressed to the Editorial Department, ASME, United Engineering Center, 345 East 47th Street, New York, N.Y. 10017, and will be accepted until two months after final publication of the paper itself in the JOURNAL OF APPLIED MECHANICS. Manuscript received by ASME Applied Mechanics Division, June, 1983.

Copyright © 1983 by ASME
Downloaded 02 May 2010 to 171.66.16.250. Redistribution subject to ASME license or copyright; see http://www.asme.org/terms/Terms_Use.cfm

the disturbance grows the nonlinear terms will become important. Their immediate effect is to force the first harmonic $[\exp(i2\alpha_c x)]$ of the fundamental mode, to generate a mean motion in the x direction, and to alter the spatial structure (in y) of the fundamental mode. If $A(t)$ is the amplitude of the fundamental mode, then for $|R-R_c|$ small, or equivalently $|Re(\sigma_r)|$ small, A satisfies the amplitude equation

$$dA/dt = \sigma A + kA|A|^2 + 0(A^5). \tag{1.1}$$

In general σ, k, and A are complex. The parameter σ is the eigenvalue of the linear stability problem and $Re(\sigma) \sim R - R_c$ as $R \to R_c$. The parameter k is calculated as part of the expansion procedure. It embodies the nonlinear effects mentioned in the foregoing. Notice that the linear stability result, $A \sim \exp(\sigma t)$, is recovered from equation (1.1) if the nonlinear terms are neglected. For a detailed discussion of the derivation of equation (1.1) from the underlying physical ideas, see the cited papers by Stuart and Watson, or the monograph by Eckhaus [13]. We also call attention to the brief, and relatively elementary, discussion of bifurcation theory and hydrodynamic stability problems using center manifold theory by Richtmyer [14, Chapter 29].

Suppose for the moment that σ is a real simple eigenvalue and that k is real, as is the case for the Taylor vortex problem discussed in Section 3. Equation (1.1) is the classic equation for the pitchfork bifurcation. If $k < 0$, then the solution $A = 0$ is unstable for $\sigma > 0$ and $A^2 \to (-\sigma/k)^{1/2}$ as $t \to \infty$. We refer to this transition to a new steady state solution as a supercritical equilibrium. On the other hand, if $k < 0$ and $\sigma < 0$, then the zero solution is stable for $A^2(0) < -\sigma/k$ but is unstable if $A^2(0) > -\sigma/k$. We refer to this instability as a subcritical instability. In the case of a supercritical equilibrium ($R > R_c$) the nonlinear terms bring an exponentially growing disturbance to a new equilibrium state; in the case of a subcritical instability ($R < R_c$) the nonlinear terms are destabilizing and produce growth if the amplitude lies above a threshold, which tends to zero as $R \to R_c$.

Now suppose that σ and k are complex and that σ is simple as is the case for plane Poiseuille flow which is discussed in Section 2. In this case we have a pair of simple complex conjugate eigenvalues that cross into the right half-plane as R increases past R_c and a classic Hopf bifurcation. If $k_r < 0$, then for $R > R_c$ the instability of the solution $A \equiv 0$ leads to a time periodic orbit with $|A(t)|^2 \to (-\sigma_r/k_r)^{1/2}$ as $t \to \infty$. If $k_r > 0$, then again for $R < R_c$ we have a subcritical instability of the zero solution if $|A(0)|^2 > -\sigma_r/k_r$.

Finally, notice that if $|A|^2 = 0(\sigma_r)$ then the first and second terms on the right side of equation (1.1) are of the same order of magnitude, while the term $0(A^5)$ is of higher order and negligible. Thus truncation at cubic order is self-consistent.

Equation (1.1) is only valid for the development of a disturbance that is periodic in x with a wave number α. If we assume that the neutral curve $R(\alpha)$ has a parabolic shape in the neighborhood of the minimum point (α_c, R_c), then it is possible, by the method of multiple scales, to derive an equation for the amplitude A of a modulated wave (or wave packet) centered on α_c that varies slowly in space (x) and in time. In terms of the original variables x and t, the amplitude equation derived by Stewartson and Stuart [15] takes the form

$$\frac{\partial A}{\partial t} - a_2 \frac{\partial^2 A}{\partial X^2} = \sigma A + kA|A|^2. \tag{1.2}$$

Here $X = x - c_g t$, where the group velocity c_g and the constant a_2 are given by

$$c_g = i\left(\frac{\partial \sigma}{\partial \alpha}\right)_{\alpha_c, R_c}, \quad a_2 = -\frac{1}{2}\left(\frac{\partial^2 \sigma}{\partial \alpha^2}\right)_{\alpha_c, R_c}. \tag{1.3}$$

Equation (1.2) is discussed in Section 2, but we note here that if we denote the scale of σ_r by ϵ and let $\tau = \epsilon t$, $\xi = \epsilon^{1/2} X$, and $A = \epsilon^{1/2} A_1$ and substitute in equation (1.2) all terms will be 0(1) provided that $a_2 = 0(1)$ and $k = 0(1)$. Thus, $A = \epsilon^{1/2} A_1[\epsilon t, \epsilon^{1/2}(x - c_g t)]$. Equation (1.2) was also derived using a different approach by Eckhaus, DiPrima, and Segel [16] and for the case of Bénard convection by Newell and Whitehead [17], and Segel [18]. For the generalization of equation (1.2) for three-dimensional disturbances see Davey, Hocking, and Stewartson [19].

Equations (1.1) and (1.2) and their generalizations for three-dimensional disturbances for simultaneously competing modes and to quintic order, form the basis for much of the theoretical work in nonlinear hydrodynamic stability during the last 25 years. In applications the computations required to determine the necessary constants, especially if there are several competing modes, can be significant. Also, all the properties of the nonlinear partial differential equation (1.2) are not yet understood. We now discuss these theoretical developments in association with experiments for two classic problems.

2 Plane Poiseuille Flow

This flow is often regarded as a prototype for the problem of instability of flows of boundary-layer type, although there are differences arising from its being truly a parallel flow, whereas boundary layers usually develop in space. Thus plane Poiseuille flow has been used as a "testing ground" for methods over the last few decades with, relatively recently, adequate comparison with experiment becoming possible. In the course of this work the concept of a threshold amplitude for instability has become established, for regions of Reynolds number, wave number, and frequency for which a theory of small perturbations predicts decay. This is perhaps the central result of these activities hitherto, but much remains to be done.

We take axes x in the direction of flow, y normal to the confining planes ($y = \pm 1$), and z along the span. The corresponding components of velocity are u, v, and w, the pressure p and time t. If $2h$ is the dimensional distance between the planes, U_0 is the maximum velocity in the laminar case, and ν is the kinematic viscosity, lengths are scaled on h, velocity components on U_0, pressure on ρU_0^2 (where ρ is the density) and time on h/U_0. Then the Reynolds number is $U_0 h/\nu = R$, and the basic flow is given by

$$\bar{u} = 1 - y^2, \bar{v} = \bar{w} \equiv 0, \frac{\partial \bar{p}}{\partial x} = \frac{-2}{R}. \tag{2.1}$$

We wish to study the possibility of an instability of this flow, with respect to perturbations that are periodic in x and z, but oscillatory and growing exponentially in time. For modes of small amplitude this implies a behavior with a perturbation proportional to

$$\exp\{i(\alpha x + \beta z - \alpha c t)\}, \tag{2.2}$$

where α and β are real, and c is complex ($c = c_r + ic_i$). (In comparison with Section 1, $\sigma = -i\alpha c$).

A situation with c real would then correspond to a neutral boundary or surface between damped and amplified oscillations. We note in passing that, in comparison with experiment, it is more appropriate to consider α complex, β real, and $\alpha c = \omega$ a real frequency; oscillations then grow spatially in the flow direction. However, for present descriptive purposes, it may be sufficient to remain with the classical situation of α, β real, and c complex.

If we consider small perturbations from the laminar flow, we can show that the govening differential system is

$$(\bar{u} - c)[\psi'' - (\alpha^2 + \beta^2)\psi] - \bar{u}''\psi + \frac{i}{\alpha R}[\psi^{IV} - 2(\alpha^2 + \beta^2)\psi'' + (\alpha^2 + \beta^2)^2 \psi] = 0, \tag{2.3}$$

$$\psi = \psi' = 0, y = \pm 1,$$

Downloaded 02 May 2010 to 171.66.16.250. Redistribution subject to ASME license or copyright; see http://www.asme.org/terms/Terms_Use.cfm

and where dashes denote y derivatives. The velocity and pressure fields can be expressed in terms of ψ. Problem (2.3) implies an eigenvalue relations of the form

$$F(\alpha^2+\beta^2, \alpha R, c)=0. \tag{2.4}$$

In general, this must be obtained as a result of computer calculations (Thomas [20], Orszag [21], and Davey [22]), although (for large Reynolds numbers) several valuable analytical representations are known in the form of "uniform approximations" (Lakin, Ng, and Reid [23]) and "triple-deck" approximations (Hall and Smith [24]). Central to these calculations is the phase-shifting mechanism between the velocity components, whereby a Reynolds stress is developed to promote instability.

The upshot of this work is the fact that, for Reynolds numbers above about 5772, there is a band of both wave numbers, α and β, for which c_i is positive. The implication is that such wavy perturbations of the form (2.2) grow exponentially with time, thereby indicating an instability. (A transformation due to Gaster [25], using the group velocity, c_g, transform this result to spatial growth, $\alpha_i < 0$, where $-\alpha_i c_g = \alpha c_i$ approximately). At large Reynolds numbers, the range of unstable wave numbers becomes vanishingly small, a feature very clearly demonstrated by use of the triple-deck and related techniques (Hall and Smith [24]), although presaged by the seminal work of Heisenberg (see Chapter 9 of Reference [7]). An account of much of this work, though not including any treatment of triple decks, has been given recently by Drazin and Reid [3].

Long after the work of Heisenberg, Lin [26], and Meksyn [27] had shown that a linearized instability mechanism was possible in plane Poiseuille flow, detailed experimental work of Nishioka, Iida, and Ichikawa [28] showed that an instability band of wave numbers does exist if the Reynolds number is high enough. Indeed, the experimental data of Nishioka et al. shows respectably good agreement with the theoretical predictions for infinitesimal disturbances.

The central difficulty to which these results lead, is that early experiments of Davies and White [29] indicate that *turbulence* can exist at much lower Reynolds numbers, of the order of 1000 or 2500. What is the origin of such turbulence? It is clearly not the phenomenon associated with infinitesimal perturbations as outlined in the foregoing, since the disparity between the appropriate Reynolds numbers is too great. A resolution of this dilemma is afforded by the inclusion of nonlinearities into the theory, in the sense of finite, and not infinitesimal, fluctuating amplitudes of velocity and pressure. We turn now to a discussion of such effects.

The Orr-Sommerfeld equation (2.3) arises from the discussion of infinitesimal perturbations of the form (2.2), when superimposed on a basic field (2.1). But the Navier-Stokes equations of fluid motion are nonlinear, so that harmonics of (2.2) are produced, together with a rectified perturbation field to constitute a modification of the given mean flow (2.1). Such processes are ignored in the derivation of (2.3) and, although we oversimplify the description of the matter, we observe that terms proportional to $\psi|\psi|^2$ have been ignored in (2.3).

Nonlinear effects can be brought into theoretical play as follows: instead of (2.2) we consider a spatially periodic perturbation in x and z, known as weakly nonlinear, whose fundamental node has the form

$$A(t)\psi(y)\exp\{i(\alpha x+\beta z-\alpha c_r t)\}. \tag{2.5}$$

Here the exponential growth factor of (2.2), namely exp $\{\alpha c_i t\}$, is replaced by the complex amplitude function $A(t)$. Provided the growth rate, αc_i, is small, and provided certain other conditions are met, it can be shown by detailed analysis of the fundamental (2.5), harmonic and rectified fields, that $A(t)$ satisfies the following amplitude equation:

$$\frac{dA}{dt}=\alpha c_i A+kA|A|^2. \tag{2.6}$$

All terms in (2.6) are of order $(\alpha c_i)^{3/2}$, and terms neglected are of order $(\alpha c_i)^{5/2}$.

The importance of this equation in the context of plane Poiseuille flow lies in the signs and magnitude of the two parameters, namely αc_i and k. The former is naturally the growth rate determined by (2.4), whereas the complex number k is obtained from a succession of forced linear calculations involving the harmonic and rectified fields. The *critical* Reynolds number, $R = R_c$, below which αc_i is negative and above which αc_i is positive, is known to be about $R_c = 5772$, as mentioned earlier; the corresponding critical wave numbers are $\alpha_c = 1.02$ approximately and $\beta \equiv 0$. In the neighborhood of these critical Reynolds and wave numbers, it is known from calculations of Reynolds and Potter (30) and Pekeris and Shkoller (31) that the real part of k, namely k_r, is positive. Thus we infer that nonlinearities are destabilizing.

Now consider a perturbation for $R < R_c$ (but with the overriding requirement that αc_i be small); it is possible for A to be independent of t and to be given by

$$|A|^2=|A_e|^2=-\alpha c_i/k_r, \tag{2.7}$$

with a corresponding phase function of the form exp $\{i\gamma\}$. This amplitude $|A_e|$ is a threshold, above which a perturbation of the form (2.5) amplifies and below which it decays. The time-dependent solution of (2.6) is

$$|A|^2=\frac{|A_e|^2 e^{2\alpha c_i t}}{C+e^{2\alpha c_i t}}. \tag{2.7}$$

With $R < R_c$ ($\alpha c_i < 0$), $|A|^2$ tends to $|A_e|^2$ as $t \to -\infty$. This represents an equilibrium amplitude state, but it is a *threshold* state because perturbations of slightly greater amplitude are amplified, while those of a lesser amplitude decay; futhermore, on the decaying branch, the solution tends to zero like $C^{-1}|A_e|^2 e^{2\alpha c_i t}$ when $t \to +\infty$, with C as a positive arbitrary constant.

Thus, we reach the conclusion that there is a *subcritical* instability mechanism, operative at Reynolds numbers below critical, provided the amplitude of the velocity perturbation lies above the threshold value. This idea had been current in the theoretical literature since about 1951 (Meksyn and Stuart [32], Grohne [33], Stuart [10], Watson [12], Reynolds and Potter [30], Pekeris and Shkoller [31], and Itoh [34]), but was finally exposed as an experimental phenomenon by the work of Nishioka, Iida, and Ichikaya [28] in 1975. They showed how, at a Reynolds number of 5000, the threshold amplitude depends on the frequency of oscillation. Reasonable agreement was obtained with calculations of Itoh [34] while, more recently, Zhou [35] obtained still better agreement. Sen and Venkateswarlu [36] have expressed concern, however, since there is some disagreement between their theoretical results and those of Zhou, who utilized an iteration method with an artificial Reynolds stress.

Encouraging as these results are in general, they do not take the Reynolds number, above which finite-amplitude oscillations can exist, down to the lower levels (of order 2500) of Davies and White's experiments. There are, fortunately, other pieces of theoretical work which do given a pointer to the origins of turbulence at Reynolds numbers as low as 2500. One set of papers, namely those of Meksyn and Stuart [32], Grohne [33], and others, use as a basis the so-called mean-field equations. Here the fundamental oscillation and the rectified (or mean) field are included in the calculations, but not the harmonics, so that a particular truncated set of equations is treated. The result of such calculations is a relationship between critical Reynolds number (R_{cA}) and threshold amplitude, $|A_e|$, in that R_{cA} falls as $|A_e|$ rises. Typically, a root-mean square velocity fluctuation of about 8 percent corresponds to a value of R_{cA} of about 2500–3000.

Downloaded 02 May 2010 to 171.66.16.250. Redistribution subject to ASME license or copyright; see http://www.asme.org/terms/Terms_Use.cfm

More recently, Herbert [37], Orszag and Kells [38], Orszag and Patera [39], and Dhanak [40] have taken this work further, and in a more rational way, by inclusion of the harmonics. Herbert uses a Galerkin method, while Orszag and his colleagues use a spectral method. Herbert has shown that two-dimensional finite-amplitude equilibrium solutions do exist at Reynolds numbers as low as 2500–3000, and this has later been confirmed by Orszag and his colleagues. Moreover, Orszag and Patera have shown that these two-dimensional equilibrium solutions are unstable against three-dimensional perturbations. A crucial role is played in this three-dimensional instability by the stretching and tilting of vortex filaments, so that localized shear layers emerge, from which higher-frequency velocity fluctuations are shed. This may be termed a secondary instability. The role of vortex-stretching in the production of local shear layers has been recognized experimentally at least since 1962, when Klebanoff, Tidstrom, and Sargent [41] showed the occurrence of regions of high shear in association with longitudinal vortex filaments. Later experiments of Kovasznay, Komoda, and Vasudeva [42] confirmed and extended our understanding of this phenomenon and stimulated a mathematical theory of this phenomenon due to Stuart [43]. Later work has been done by Ellingsen and Palm [44], and by Wray and Hussaini [45]. An experimental investigation of secondary instability in plane Poiseuille flow was undertaken by Nishioka, Asai and Iida [46], and they have shown the validity of the ideas mentioned in the foregoing in plane Poiseuille flow.

Extensions of the theory of weakly nonlinear waves have been made to allow for amplitude modulation, in which the amplitude function A depends not only on time, but also on a variable $X = x - c_g t$, where c_g is the group velocity of the carrier wave. For two-dimensional modulated waves, equation (2.6) is replaced by

$$\frac{\partial A}{\partial t} - a_2 \frac{\partial^2 A}{\partial X^2} = \alpha c_i A + kA\,|A|^2. \tag{2.8}$$

If the perturbations are three-dimensional it is explicitly necessary to include a perturbation pressure field, rather akin to that in Reynolds' lubrication theory, but here in association with the Reynolds stress. (This need is avoided in the two-dimensional case by use of a stream function). The concept of a pressure eigenfunction was noted by Eagles [47], who followed earlier discussions of pressure fields by Stuart [10, 11]. Thus, Davey, Hocking, and Stewartson [19] derived a system of two coupled partial differential equations consisting of a generalized form of (2.8) and an associated Poisson equation for a "pressure function." The functions depend on t, X, and the spanwise variable and the Poisson equation contains a term involving the spanwise spatial derivative of $|A|^2$.

Many studies have been made of (2.8), including those of Hocking and Stewartson [48], which show that the solution stemming from Gaussion initial conditions becomes singular at a finite time, at least within certain parameter ranges. Moreover, it is known that a mechanism for instability of a given periodic solution, the Eckhaus or Benjamin-Feir side-band mechanism, is governed by this equation [49].

One further theoretical development, which may point the way to influences at work in experiment, concerns the role of perturbations (or imperfections) imposed from the boundary. Hall [50] treated the effects of deflections on one wall, with frequency and wave number that are close to those occurring in a Tollmien-Schlichting wave. Thus there is a resonance effect, and the strength of the Tollmien-Schlichting wave is enhanced, and can occur even for Reynolds numbers below the "critical" value, in accordance with concepts of imperfect bifurcations. The perturbation that Hall treated needs to move with the natural speed of wave propagation, which is substantially less than the maximum flow velocity. Thus it seems unlikely that his work could be used to model a forced perturbation on a boundary layer, travelling with the free stream (maximum) speed.

In contrast, Dhanak [40] has considered imposed three-dimensional perturbations to plane Poiseuille flow and, in particular, he shows that a perturbation of spanwise wave number 2β can resonate with, and promote the growth of, a perturbation of wave number β, thus with twice the wavelength. These perturbations imposed at the wall are standing waves, with no propagation, and are thus more characteristic of disturbances which could be imposed from a free stream on a boundary layer. Far more work is needed on the matter of mode stimulus and selection, especially in a three-dimensional situation.

3 Flow Between Rotating Cylinders

We consider viscous incompressible flow between two rotating concentric cylinders. We denote the radii and angular velocities of the inner and outer cylinders by a, b, and Ω_1, Ω_2, respectively, and the length of the cylinders by h. We let $d = b - a$ and define the parameters

$$\eta = a/b,\ \mu = \Omega_2/\Omega_1,\ \Gamma = h/d,\ R = \Omega_1 a d/\nu, \tag{3.1}$$

where ν is the kinematic viscosity and R is a Reynolds number.

Much theoretical work is concerned with the case of infinite aspect ratio, $\Gamma = \infty$, although Γ is finite in experiments. For the moment we assume that Γ is infinite but describe finite length effects later. Then an exact steady solution of the Navier-Stokes equations is Couette flow. With the usual notation (r, ϑ, z) for cylindrical coordinates we have

$$u_r = u_z = 0,\ u_\vartheta = V(r) = Ar + B/r,\ \partial p/\partial r = \rho v^2/r, \tag{3.2}$$

where ρ is the density, $A = -\Omega_1(\eta^2 - \mu)/(1 - \eta^2)$, and $B = \Omega_1 a^2(1 - \mu)/(1 - \eta^2)$.

For all of the discussion in this section we will set $\mu = 0$, so the outer cylinder is at rest. As R is increased with η near 1, the following sequence of events can occur:

(1) There is a critical value of R, say $R_c(\eta)$, such that for $R < R_c$ Couette flow is stable to infinitesimal disturbances that are periodic in the azimuthal coordinate ϑ and axial coordinate z (Taylor [51]). Moreover, R_c corresponds to an axisymmetric disturbance with an axial wave number $\lambda_c(\eta)$ and the growth rate σ is real. If λ is scaled on the gap width d, then $\lambda_c \cong \pi$.

(2) The instability of Couette flow for, say $\lambda = \lambda_c$, and R slightly greater than R_c leads to a steady axisymmetric flow that is periodic in z with cells bounded by planes perpendicular to the axis - Taylor vortex flow [11, 52]. This corresponds to σ real, k real, and $k < 0$ in equation (1.1) and arises from a steady bifurcation of Couette flow.

(3) There exists a second critical value of R, say $R_c'(\eta)$, such that for $R > R_c'$ the Taylor vortex flow is unstable with the instability leading to a wavy vortex flow (Davey, DiPrima, and Stuart [53]). This equilibrium flow is periodic in ϑ and in z, is periodic in time, and corresponds to a wave traveling in the azimuthal direction. The boundaries between adjacent cells are not plane but are wavy surfaces. For the instability of Taylor vortex flow we have σ and k complex in equation (1.1) and $k_r < 0$; the bifurcation is of Hopf type. For η near 1, $R_c'(\eta)$ is very close to $R_c(\eta)$. While $R_c'(\eta)$ corresponds to an azimuthal wave number one, wavy vortices with a higher number of waves usually emerge for $R > R_c'(\eta)$.

The theoretical results described by the sequence (1), (2), and (3) are in reasonable qualitative and quantitative agreement with a number of experimental observations including those of Taylor [51]. These, and related matters

Downloaded 02 May 2010 to 171.66.16.250. Redistribution subject to ASME license or copyright; see http://www.asme.org/terms/Terms_Use.cfm

described in this section, are discussed in some detail and many additional references are given in a survey paper by DiPrima and Swinney (see [2]). As R is increased to values much greater than R_c we turn to experimental observations, and in particular to those of Fenstermacher, Swinney, and Gollub [54] which also are summarized by DiPrima and Swinney (see [2]). The geometrical parameters are $\Gamma = 20$ and $\eta = 0.877$ and observations are based on measurements of the power spectrum of the radial component of velocity using Laser Doppler techniques.

(4) A time-periodic wavy vortex flow with four waves in the azimuthal direction and 17 cells in the axial direction is observed for $R/R_c < 10.1$. A second fundamental frequency appears in the power spectrum at $R/R_c = 10.1$ and persists until $R/R_c = 19.3$. The quasiperiodic flow corresponds to a modulated wavy vortex flow (Swift, Gorman, and Swinney [55]).

(5) At $R/R_c \cong 12$ there is the first indication of chaos through the appearance of a weak broad component in the power spectrum.

(6) The second frequency disappears at $R/R_c = 19.3$ and the first frequency at $R/R_c = 21.9$ while the broad band remains. This indicates chaotic motion, although observations show a continued spatial Taylor vortex structure.

For different values of η and Γ and/or spatial states the transitions may be different, as is noted in DiPrima and Swinney [2] and where experimental observations by others are summarized. For example, in an apparatus with $\eta = 0.875$ Walden and Donnelly [56] found the reemerging of a spectral component for $28 < R/R_c < 36$ and $\Gamma > 25$. However, there is general agreement on the following qualitative picture as R increases: steady bifurcation of Couette flow to Taylor vortex flow; Hopf bifurcation of Taylor vortex flow to wavy vortex flow; transition of wavy vortex flow to a quasiperiodic wavy vortex flow; appearance of weak chaotic motions; but it should be remembered that there can be variations on this theme.

We now comment on several different aspects of the transitions and flow patterns.

Nonuniqueness. In an important paper, Coles [57] reported on experimental observations showing that not only is the wavy vortex flow not a unique function of the Reynolds number, but that at a fixed Reynolds number a remarkable number of different states is possible. Indeed, for an apparatus with $\eta = 0.877$ and $\Gamma = 27.9$ and for the outer cylinder at rest, he found as many as 20 different stable states at the same Reynolds number with the number of axial vortices between 18–32 and the number of azimuthal waves from 3–7. These states were reached by different operating conditions.

A similar phenomenon occurs in the steady axisymmetric Taylor vortex flow regime. We call attention to the recent experiments of Benjamin and Mullin [58] with an apparatus for which $\eta = 0.6$ and $\Gamma = 12.61$. For $\mu = 0$ and $R = 359$ they found 20 stable steady Taylor vortex flows for which they published photographic evidence, with five of these flows realizable in two different ways. They also point out that there must be at least 39 steady Taylor vortex flows with the other 19 being unstable. For some of the flows it was necessary to vary Γ as well as the acceleration rate in reaching the final values of Γ and R.

These results demonstrate the caution that must be taken in interpreting experimental observations and theoretical calculations. For example, the determination of R_c' for the onset of wavy vortex motion will depend not only on η for fixed Γ but also on the number of Taylor cells, and similarly transitions from wavy vortex flow to modulated wavy vortex flow, and then to chaos, may depend not only on Γ and η but also the wavy vortex state. While the first flow state is not unique for a given geometry and Reynolds number, there is no reason to believe that a properly posed initial value problem will not have a unique solution, at least in the absence of chaos. The stable steady solutions will have different domains of attraction from all possible initial states, with a few states having (probably) much larger domains of attractions. This is not inconsistent with Coles' [57] concept of a mean state or the repeatability of instabilities and transitions as R is slowly increased from $R < R_c$ to $R >> R_c$. We will return to these questions later, but now turn to other matters.

Chaos. The theoretical techniques ($\Gamma = \infty$) discussed in the Introduction, and which have been successful in the calculation of a Taylor vortex flow, of its instability, and of a wavy vortex flow for R near R_c, depend on expansions in a small parameter, namely the appropriate growth rate. As a consequence these techniques may not be satisfactory for $R >> R_c$. However, Richtmyer [59] has extended the analysis of reference [53] for the instability of the Taylor vortex flow and the development of wavy vortex flows. The latter work led to a six-dimensional manifold spanned by the eigenfunctions associated with disturbances proportional to $\exp(\pm i\lambda z)$ and $\exp(\pm i\lambda z \pm im\vartheta)$ for fixed λ and m. Richtmyer has considered a ten-dimensional manifold for the modes $\exp(\pm i\lambda z)$, $\exp(\pm i\lambda z \pm i\vartheta)$ and $\exp(\pm i\lambda z \pm i2\vartheta)$ with $\eta = 0.9512$, and a fourteen-dimensional manifold with the additional modes $\exp(\pm i\lambda z \pm i3\vartheta)$ for $\eta = 0.6$. Although $R >> R_c$, and for $\eta = 0.9512$ the amplitude equations are taken to quintic order, he does not find evidence of a transition to a quasiperiodic wavy vortex flow.

Yahata in a series of papers (see [60, 61], and the references given there) has studied the transition to chaos for $\Gamma = \infty$ and the value of η and flow state corresponding to the experiments of Fenstermacher et al. [54]. He uses truncated Fourier-Galerkin series to define a system of ordinary nonlinear differential equations for the evaluation of the time-dependent amplitude coefficients in this series. His axisymmetric and nonaxisymmetric Fourier modes are in phase in the axial direction, so his analysis does not represent a wavy vortex flow; however, for very large R the boundaries between cells do appear to be planes (point (6)). With only a few Fourier modes, Yahata finds several results that are in surprisingly good qualitative agreement with several of the observations noted in points (4), (5), and (6). However, if more Fourier modes were chosen, it is possible that the results would be quite different.

We call attention to the fundamental question of modeling the behavior of solutions of the Navier Stokes equations for all time using finite dimensional Fourier-Galerkin models. It is known that as the dimensionality of the model is changed, the qualitative and quantitative behavior of the solution may change drastically. For relevant work on this matter see the papers by Manley and Treve [62] and Foias and Treve [63] and their references.

Radius Ratio Effects. Calculations ($\Gamma = \infty$) show that $R_c(\eta)$ varies continuously with η as η decreases from one (small gap limit) toward zero. A table of values of $R_c\ (d/a)^{1/2}$ for values of η between 0.1 and 1 is given in DiPrima and Swinney (see [2]). The situation is quite different for $R_c'(\eta)$. Jones [64] has used Fourier series in the axial variable and Tchebycheff polynomials radially, with collocation to calculate the Taylor vortices, and then to study their stability. For η near one his results are consistent with those of references [53] and [47]. However, he also finds (*i*) that for $R > R_c'(\eta)$ disturbances with azimuthal wave numbers $m > 1$ have larger growth rates than for $m = 1$; and (*ii*) that $R_c'(\eta) - R_c(\eta)$ initially increases slowly as η decreases, but such that the graph of R_c' versus η

Downloaded 02 May 2010 to 171.66.16.250. Redistribution subject to ASME license or copyright; see http://www.asme.org/terms/Terms_Use.cfm

has a vertical tangent at $\eta \cong 0.75$ and turns backward [Fig. 3 of [64]]. For $\eta < 0.75$ he finds no instability of the Taylor vortex flow for $Ta = 2R^2 (1-\eta)/(1+\eta) < 12{,}500$. The latter results have been confirmed qualitatively by Ng, Eagles, and DiPrima (work in progress) using the amplitude equations given in references [53] and [47]. However, we note that Richtmyer [59] finds for $\eta = 0.6$ an instability of the Taylor vortex flow for R somewhere in the range 11.2 R_c to 15.8 R_c with the disturbance having three waves in the azimuthal direction. These values of R are much larger than those of Jones and indeed may be too large for the results to be significant. On the other hand, Richtmyer's value of $R_c'(\eta = 0.6)$ is in accordance with some experimental observations, which show $R_c'(1/2)/R_c(1/2) \sim 10$ or more. Also experimenters have called attention to a precipitous increase in $R_c'(\eta)$ for decreasing η between 0.8 and 0.7. We mention only the work of Debler, Füner, and Schaaf [65], Zarti, Jones, and Mobbs [66], and Cole [67, 68]. We also note that it is not always clear what type of instability of the Taylor vortex flow is being observed or measured for these lower values of η.

It is interesting that Coles [[57], p. 401] in a discussion of the tangential instability of the Taylor vortex flow suggested that such an instability may not occur for $\eta < 0.714$. His argument is based on a criterion for wave motions in rotating fluids and involves approximations, but the conclusion is in surprisingly good qualitative agreement with the theoretical calculations and observations for $\eta \sim 0.7$.

Finite Length Effects. We first discuss the axisymmetric problem. If the cylinders are of finite length, the flow is three-dimensional for any value of R even if small, with a weak circulatory motion in the r-z plane, and an azimuthal component that is nearly Couette flow except near the ends of the cylinders. For finite value of Γ (say $\Gamma > 10$), and as R is increased, there is a smooth development of the circulatory motions until near R_c ($\Gamma = \infty$) there is a very rapid, but smooth transition, to a Taylor vortex flow over most of the length of the cylinders. The interesting numerical calculations of Alziary de Roquefort and Grillaud (69) verify such a picture, while experimenters have noted "ghost" vortices for $R < R_c$.

Mathematically, finite length effects change a pitchfork bifurcation into a smooth transition. Thus there is no true R_c for Γ finite, but nevertheless it is still useful to speak of an R_c (Γ) associated with the development of a classical Taylor vortex flow over most of the length of the cylinders. For example, for finite values of Γ (> 10) the mean torque on the inner cylinder with $R > R_c$ is adequately predicted by the case $\Gamma = \infty$. Cole [70] has shown experimentally that the value of R at which fully developed Taylor vortex flow is observed is rather insensitive to annulus length. In contrast he finds that the value of R at which a wavy vortex flow develops *is* very dependent on Γ, as well as on η. Values of $\Gamma > 40$ are required for the observed values of R_c' to be within a few percent of the calculated value for $\Gamma = \infty$.

Of special interest are the experimental observations for cylinders of very short aspect ratio with $\eta = 0.615$ by Benjamin [71]. We designate as a primary flow the flow that develops naturally as R is increased from very small values for fixed Γ. A secondary flow is one that can also exist for a fixed Γ and same range of R, but is not stable for R sufficiently small. By varying both Γ and R he obtained transitions from four-cell secondary flows to two-cell primary flows for $\Gamma < 3.6$ and from two-cell secondary flows to four-cell primary flows for $\Gamma > 3.72$. For $3.6 < \Gamma < 3.72$ there is a cusped curve in the R-Γ plane corresponding to a hysteresis effect in the transition from the primary cellular pattern to a secondary cellular pattern and the reverse. These results have been extended to other transitions (4 to 6 cell, 6 to 8, 8 to 10, and 10 to 12) by Mullin [72] on an apparatus with $\eta = 0.6$ (also see Mullin, Pfister, and Lorenzen [73] for the 4–6 transition). His observations are in general agreement with those of Benjamin but show other interesting variations.

Mullin and Benjamin [74] have also considered the transition to wavy vortex flow in the apparatus with $\eta = 0.615$ and with $0 < \Gamma < 5.45$. They find that the transition is strongly dependent on the initial axisymmetric state and on Γ, and that there is a hysteresis effect.

Such observations and those mentioned earlier on nonuniqueness emphasize that end effects play a more significant role than the mere smoothing of a pitchfork bifurcation (see [58] and [72]). But also state selection depends not ony on the radius ratio and aspect ratio, but also on the initial state. And if there is not already sufficient complexity we call attention to a paper by Ahlers, Cannell, and Lerma [75] in which a wavy vortex flow with an azimuthal wave number 3/2 is observed for much of the azimuthal range.

It is not surprising that analytical and computational work on end effects has not kept pace with the experimental observations. All mathematical models have used artificial boundary conditions at the ends of the cylinders in order to obtain a tractable and relevant mathematical problem. The situation in which the end plates also move with the velocity of Couette flow has been studied by Blennerhassett and Hall [76], Hall [77], Stuart and DiPrima [78], and Shearer and Walton [79]. One interesting aspect of this analysis is the existence of transcritical bifurcations corresponding to quadratic terms in an amplitude equation such as equation (1.1) (See Hall [77]) for the analysis of the nonlinear amplitude equations and the different possible flows.)

Schaeffer [80] has developed a model with the following artificial end boundary conditions in terms of a parameter α, $0 \le \alpha \le 1$:

$$(1-\alpha)\partial u_r/\partial n + \alpha u_r = 0,\ (1-\alpha)\partial u_\vartheta/\partial n + \alpha u_\vartheta = 0,$$
$$u_z = 0 \tag{3.3}$$

where $\partial/\partial n$ is the outward normal derivative. If $\alpha = 0$ we have an artificial problem, for which Couette flow is an exact solution, but true boundary conditions for rigid stationary ends correspond to $\alpha = 1$. The $\alpha = 0$ problem is tractable and it is hoped that a perturbation analysis for α small will be relevant to the true situation $\alpha = 1$: for $\alpha = 0$ and with η fixed, the linear stability problem can be easily solved for $2m$-cell dsturbances to obtain a graph of R_c versus Γ for each m. The neutral curves for $2m$ and $(2m+2)$-cell disturbances intersect at (R_m^*, Γ^*). In the neighborhood of the intersection the nonlinear interaction of a disturbance pair can be studied by perturbing from $\alpha = 0$. The model proposed by Schaeffer has cubic nonlinearities for the amplitude. While he does not calculate the coefficients in his amplitude equations, he does show that his model has the possibility of predicting behavior such as was observed by Benjamin [71]. However, it is important to note that for the transitions between two and four cells ($m = 1$), quadratic terms must appear in the nonlinear amplitude equations for the modes; and thus the Schaeffer model is not applicable to Benjamin's experiments. This was noted by Hall [81] who used the boundary conditions (3.3) in reformulating the two and four-cell interaction. Hall also calculated the coefficients in the amplitude equations for the small-gap case ($\eta \to 1$) and found a number of features, but not all, in qualitative agreement with the observations of Benjamin. It is recognized by Hall, Schaeffer, and others that conditions (3.3) are used at $\alpha = 1$ so as to compare with experiments, even though an expansion for small α is used.

Of special interest is the work of Hall [82] for the case $m = 2$, for which there is a four and six-cell interaction, and the amplitude equations have cubic nonlinearities. For this case Hall finds for $\eta = 0.626$ an upside-down version of the cusp described by Benjamin for the two-cell four-cell interaction.

Downloaded 02 May 2010 to 171.66.16.250. Redistribution subject to ASME license or copyright; see http://www.asme.org/terms/Terms_Use.cfm

This was found experimentally by Mullin [72], lending credence to the analytical efforts.

Finally, we mention the calculations of Andreichikov [83] and of Frank and Meyer-Spasche [84] with $\eta = 0.5$ for two-cell and four-cell flows with artificial *periodic* boundary conditions in the axial coordinate.

Two Mathematical Matters. (*a*) Again we consider the case $\Gamma = \infty$. In work on the stability of Couette flow to an axisymmetric disturbance with given axial wave number it is usually assumed that as R increases the first eigenvalue σ that crosses from the left half to the right half of the complex plane is simple and crosses on the real axis. This is the so-called "principle of exchange of stabilities." This important assumption is required, for example, in the proof of the existence of the Taylor vortex flow (Velte [85]). Yih [86] has given an intricate argument suggesting that not only the first but *all* the eigenvalues σ are real for all $R > 0$, if the cylinders rotate in the same direction or the outer cylinder is at rest. However, in computational work in progress Hall and DiPrima have found complex conjugate eigenvalues corresponding to decaying disturbances. Their results do not contradict the principle of exchange of stabilities, but they do suggest that the argument of reference [86] is not valid. A proof of the principle of exchange of stabilities is thus still required if, as in widely believed, the result is valid.

(*b*) Let $R'_{cm}(\eta)$ denote the critical Reynolds number for the instability of Taylor vortex flow to a disturbance with azimuthal wave number m. As we have noted $R'_c = R_{c1}$ for the interactions of a Taylor vortex flow with a nonaxisymmetric mode with m given. For η near one it is known that $R'_{c1} < R'_{c2} < R'_{c3} < R'_{c4}$ are grouped very closely. Since for $R > R'_{c4}$ (say) modes with $m > 1$ may have greater growth rates than for $m = 1$, it is not easy to decide on the preferred value of m for the emergent wavy vortices. Torque calculations by Eagles [87] for different wavy vortex flows and comparison with experimental measurements for $\eta = 0.95$ suggest some preference for $m = 4$. An analysis involving nonlinear interactions with several nonaxisymmetric modes with different azimuthal wave numbers is needed to provide useful information on the wave-number selection process.

Some progress in this direction has been made by Richtmyer [59], who has considered the interaction of an axisymmetric mode with two nonaxisymmetric modes of $m = 1$ and 2, respectively. For $\eta = 0.9512$ he finds a transition from Taylor vortex flow to a wavy vortex flow at R'_{c1} with $m = 1$. This flow is stable only for a short range of R, beyond which the flow with $m = 2$ is stable. However, the results do not provide a transition from the flow with $m = 1$ to that with $m = 2$.

4 Concluding Remarks

In the studies outlined in Sections 2 and 3, two classical problems have been described, mainly from a theoretical point of view, but with some reference to comparison with experiment. The mechanisms by which instability is promoted differ in the two cases, being centrifugal in rotating-cylinder flows (Section 3) but deriving from a Reynolds stress in plane Poiseuille flow (Section 2). The former case (Section 3) is characteristic of flows where a body force is present, and there are some connections with buoyancy driven thermal convection. On the other hand, the Reynolds-stress driven instability is the common feature of instabilities in aerodynamical boundary layers, although boundary-layer growth is involved in those situations.

There is, however, one further important class of flows, namely those that are stable according to linearized instability theory, and for which there is no commonly accepted mechanism for instability. Two flows of this kind are plane Couette flow and Hagen-Poiseuille flow in a pipe of circular cross section. On the other hand, it is known experimentally that, in pipe flow, turbulence can occur at Reynolds numbers as low as 2000 or thereabouts (Ekman, Taylor, see reference [88], p. 321). Moreover, Coles [89], Wygnanski and his coworkers ([90] and references given there), Teitgen [91], and others have shown that such pipe-flow turbulence often occurs in the form of slugs or puffs interspersed with regions of laminar flow. Various attempts have been made to give an explanation of the occurrence of turbulence or, more simply, to devise a mechanism for instability. We now mention some of these attempts.

(*i*) Tatsumi [92] showed that the basic developing flow in the entry length of a pipe is unstable to linearized perturbations at or above a Reynolds number of 10^4. This may be relevant for some experiments but, if the instability is to persist into the region of fully developed flow, some nonlinear or other influence would be needed.

(*ii*) Davey [93] considered the instability of flow in a slightly elliptical pipe, and showed that the ellipticity is destabilizing. He did not, however, establish that instability would occur, since he did not study the higher-order terms.

(*iii*) Davey and Nguyen [94], Itoh [95], and Davey [96] have developed a nonlinear theory, which shows that nonlinear terms *may* be destabilizing for small amplitudes. However, their work is inconclusive, and no threshold amplitude has been calculated. Recent unpublished work of Sen and his colleagues takes this idea further for both axisymmetric and nonaxisymmetric modes.

(*iv*) Stuart [97] has shown that vorticity fluctuations of long wave length are concentrated spatially by a "negative" diffusion phenomenon, thus countering the natural decay.

(*v*) Smith and Bodonyi [98] have studied amplitude-dependent, nonaxisymmetric neutral modes, in which the critical layer is of the nonlinear type envisaged by Benney an Bergeron (see [98]) and by Davis (see [98]). They provide powerful analytical-numerical evidence that neutral modes $\exp(in\vartheta)$ can exist for an azimuthal wave number $n = 1$, where ϑ is the azimuthal angle.

Of the mechanisms detailed in the foregoing, the last, that of Smith and Bodonyi seems extremely promising, although it has not yet provided an instability by showing that the neutral modes calculated represent a threshold.

For plane Couette flow, work related to (*iii*) has been done by Ellingsen, Gjevik, and Palm [99]. In summary, we may perhaps say that the development of a thoroughly satisfactory nonlinear theory of instability and transition for Hagen-Poiseuille flow and for plane Couette flow provides one of the biggest challenges in our subject.

Finally, we need to comment on the fact that many flows are not truly parallel, or rectilinear, or circular; a flow in a boundary-layer or in a lubricating film develops and changes in the flow direction. Two parameters at least are available, one representing the overall change in the flow, and the other the rate of change. We note the following points: (*i*) One method of treating problems where both such effects are small has been given by DiPrima and Stuart [100]. (*ii*) When the overall change is not small, but the rate of change is small, as in boundary layers, the WKBJ method is appropriate, as was shown by Gaster [101], Bouthier [102], and others. (*iii*) The triple-deck method (and n-tuple extensions) can be used to evaluate stability properties on and near the upper and lower branches of the neutral curve (Smith [103]).

Downloaded 02 May 2010 to 171.66.16.250. Redistribution subject to ASME license or copyright; see http://www.asme.org/terms/Terms_Use.cfm

Problems concerning flows that are time-dependent have some features in common with steady flows that develop in space. Significant progress has been made by Hall [104–106], both by a method derived from that of [100] and by powerful use of Floquet theory for time periodic problems [107]. Also see the paper by Von Kerczek and Davis [108] and the review article by Davis [109] on the stability of time-periodic flows.

Acknowledgments

The work of R.C.D. was partially supported by the U.S. Army Research Office while he was a visitor at Imperial College in Autumn 1982. He was also a Guggenheim Fellow and a Visiting Fellow with support from the British Science and Engineering Research Council and the U.S. National Science Foundation.

Because of the brevity of this review it has not been possible to reference all the significant contributions. However, such work is described in the papers and monographs mentioned here.

References

1 Joseph, D. D., *Stability of Fluids Motions I and II*, Springer, Tracts in Natural Philosophy, Vols. 27 and 28, Springer, Berlin, Heidelberg, New York, 1976.

2 Swinney, H. L., and Gollub, J. P., *Hydrodynamic Instabilities and the Transition to Turbulence*, Topics in Applied Physics, Vol. 45, Springer, Berlin, Heidelberg, New York, 1981.

3 Drazin, P. G., and Reid, W. H., *Hydrodynamic Stability*, Cambridge University Press, Cambridge, 1981.

4 Pedlosky, J., *Geophysical Fluid Dynamics*, Springer, Berlin, Heidelberg, New York, 1979.

5 Lin, C. C., *The Theory of Hydrodynamic Stability*, Cambridge University Press, Cambridge, 1955.

6 Chandrasekhar, S., *Hydrodynamic and Hydromagnetic Stability*, Clarendon Press, Oxford, 1961.

7 Rosenhead, L., ed., *Laminar Boundary Layers*, Clarendon Press, Oxford, 1963.

8 Landau, L. D., "On the Problem of Turbulence," *Akademiaa Nauk SSSR*, Dokaldy, Vol. 44, 1944, pp. 311–314.

9 Malkus, W. V. R., and Veronis, G., "Finite-Amplitude Cellular Convection," *Journal of Fluid Mechanics*, Vol. 4, 1958, pp. 225–260.

10 Stuart, J. T., "On the Non-Linear Mechanics of Wave Disturbances in Stable and Unstable Parallel Flows. Part 1. The Basic Behavior in Plane Poiseuille Flow," *Journal of Fluid Mechanics*, Vol. 9, 1960, pp. 353–370.

11 Stuart, J. T., "On the Non-Linear Mechanics of Hydrodynamic Stability," *Journal of Fluid Mechanics*, Vol. 4, 1958, pp. 1–21.

12 Watson, J., "On the Non-Linear Mechanics of Wave Disturbances in Stable and Unstable Parallel Flows. Part 2. The Development of a Solution for Plane Poiseuille Flow and for Plane Couette Flow," *Journal of Fluid Mechanics*, Vol. 9, 1960, pp. 371–389.

13 Eckhaus, W., *Studies in Non-Linear Stability Theory*, Springer, Tracts in Natural Philosophy, Vol. 6, Springer, Berlin, Heidelberg, New York, 1965.

14 Richtmyer, R. D., *Principles of Advanced Mathematical Physics*, Vol. 2, Springer, Berlin, Heidelberg, New York, 1981.

15 Stewartson, K., and Stuart, J. T., "A Non-Linear Instability Theory for a Wave System in Plane Poiseuille Flow," *Journal of Fluid Mechanics*, Vol. 48, 1971, pp. 529–545.

16 Eckhaus, W., DiPrima, R. C., and Segel, L. A., "Non-Linear Wave-Number Interaction in Near-Critical Two-Dimensional Flows," *Journal of Fluid Mechanics*, Vol. 49, 1971, pp. 705–744.

17 Newell, A. C., and Whitehead, J. A., "Infinite Bandwidth, Finite Amplitude Convection," *Journal of Fluid Mechanics*, Vol. 38, 1969, pp. 279–303.

18 Segel, L. A., "Distant Side-Walls Cause Slow Amplitude Modulation of Cellular Convection," *Journal of Fluid Mechanics*, Vol. 38, 1969, pp. 203–224.

19 Davey, A., Hocking, L. M., and Stewartson, K., "On the Nonlinear Evolution of Three-Dimensional Disturbances in Plane Poiseuille Flow," *Journal of Fluid Mechanics*, Vol. 63, 1974, pp. 529–536.

20 Thomas, L. H., "The Stability of Plane Poiseuille Flow," *Physical Review*, Vol. 91, 1953, pp. 780–783.

21 Orszag, S. A., "Accurate Solution of the Orr-Sommerfeld Stability Equation," *Journal of Fluid Mechanics*, Vol. 50, 1971, pp. 689–703.

22 Davey, A., "A Simple Numerical Method for Solving Orr-Sommerfeld Problems," *Quarterly Journal of Mechanics and Applied Mathematics*, Vol. 26, 1973, pp. 401–411.

23 Lakin, W. D., Ng, B. S., and Reid, W. H., "Approximations to the Eigenvalue Relation for the Orr-Sommerfeld Problem," *Philosophical Transactions of the Royal Society of London*, Vol. 289, 1978, pp. 347–371.

24 Hall, P., and Smith, F. T., "A Suggested Mechanism for Nonlinear Wall Roughness Effects on High Reynolds Number Flow Stability," *Studies in Applied Mathematics*, Vol. 66, 1982, pp. 241–265.

25 Gaster, M., "A Note on the Relation Between Temporally-Increasing and Spatially-Increasing Disturbances in Hydrodynamic Stability," *Journal of Fluid Mechanics*, Vol. 14, 1962, pp. 222–224.

26 Lin, C. C., "On the Stability of Two-Dimensional Parallel Flows: Part I General Theory, Part II Stability in an Inviscid Theory, and Part III Stability in an Viscous Fluid," *Quarterly of Applied Mathematics*, Vol. 3, 1945, pp. 117–142; 218–234; and 277–301.

27 Meksyn, D., "Fluid Motion Between Parallel Planes," *Proceedings of the Royal Society of London*, Series *A*, Vol. 186, 1946, pp. 391–409.

28 Nishioka, M., Iida, S., and Ichikawa, Y., "An Experimental Investigation of the Stability of Plane Poiseuille Flow," *Journal of Fluid Mechanics*, Vol. 72, 1975, pp. 731–751.

29 Davies, S. J., and White, C. M., "An Experimental Study of the Flow of Water in Pipes of Rectangular Section," *Proceedings of the Royal Society of London*, Series *A*, Vol. 119, 1928, pp. 92–107.

30 Reynolds, W. C., and Potter, M. C., "Finite-Amplitude Instability of Parallel Shear Flows," *Journal of Fluid Mechanics*, Vol. 27, 1967, pp. 465–492.

31 Pekeris, C. L., and Shkoller, B., "Stability of Plane Poiseuille Flow to Periodic Disturbances of Finite Amplitude in the Vicinity of the Neutral Curve," *Journal of Fluid Mechanics*, Vol. 29, 1967, pp. 31–38.

32 Meksyn, D., and Stuart, J. T., "Stability of Viscous Motion Between Parallel Planes for Finite Disturbances," Proceedings of the Royal Society of London, Series *A*, Vol. 208, 1951, pp. 517–526.

33 Grohne, D., "Die Stablität der ebenen Kanalströmung gegenüber dreidimensionalen Störungen von endlicher Amplitude," AVA Gottingen Report 69-A-30, 1969.

34 Itoh, M., "Spatial Growth of Finite Wave Disturbances in Parallel and Nearly Parallel Flows. Part 1. The Theoretical Analysis and the Numerical Results for Plane Poiseuille Flow," *Transactions of the Japan Society for Aeronautical and Space Sciences*, Vol. 17, 1974, pp. 160–174.

35 Zhou, H., "On the Nonlinear Theory of Stability of Plane Poiseuille Flow in the Subcritical Range," *Proceedings of the Royal Society of London*, Series *A*, Vol. 381, 1982, pp. 407–418.

36 Sen, P. K., and Venkateswarlu, D., "On the Stability of Plane Poiseuille Flow to Finite-Amplitude Disturbances, Considering the Higher Order Landau Coefficients," *Journal of Fluid Mechanics*, Vol. 133, 1983, pp. 179–206.

37 Herbert, T., "Finite Amplitude Stability of Plane Poiseuille Flow," *Laminar-Turbulent Transition*, AGARD Conference Proceedings No. 224, 1977, pp. 3.1–3.10; and "On Perturbation Methods in Nonlinear Stability Theory," *Journal of Fluid Mechanics*, Vol. 126, 1983, pp. 167–186.

38 Orszag, S. A., and Kells, L. C., "Transition to Turbulence in Plane Poiseuille and Plane Couette Flow," *Journal of Fluid Mechanics*, Vol. 96, 1980, pp. 159–205.

39 Orszag, S. A., and Patera, A. T., "Subcritical Transition to Turbulence in Planar Shear Flows," *Transition and Turbulence*, Meyer, R. E., ed., 1981, pp. 127–146, Academic Press, New York; and "Secondary Instability of Wall-Bounded Shear Flows," *Journal of Fluid Mechanics*, Vol. 128, 1983, pp. 347–385.

40 Dhanak, M. R., "On Certain Aspects of Three-Dimensional Instability of Parallel Flows," *Proceedings of the Royal Society of London*, Series *A*, Vol. 385, 1983, pp. 53–84.

41 Klebanoff, P. S., Tidstrom, K. D., and Sargent, L. M., "The Three-Dimensional Nature of Boundary-Layer Instability," *Journal of Fluid Mechanics*, Vol. 12, 1962, pp. 1–34.

42 Kovasznay, L. S. G., Komoda, H., and Vasudeva, B. R., "Detailed Flow Field in Transition," Proceedings of the 1962 Heat Transfer and Fluid Mechanics Institute, Ehlers, F. E., Kauzlarich, J. J., Sleicher, C. A., Jr., and Street, R. E., eds., Stanford University Press, Stanford, Calif.

43 Stuart, J. T., "The Production of Intense Shear Layers by Vortex Stretching and Convection," AGARD, Report 514, 1965.

44 Ellingsen, T., and Palm, E., "Stability of Linear Flow," *The Physics of Fluids*, Vol. 18, 1975, pp. 487–488.

45 Wray, A., and Hussaini, M. Y., "Numerical Experiments in Boundary Layer Stability," ICASE Report No. 80-3, Jan. 22, 1980; and AIAA Paper No. 80-0275, AIAA 18th Aerospace Sciences Meeting, Pasadena, Calif., Jan., 1980.

46 Nishioka, M., Asai, M., and Iida, S., "Wall Phenomena in the Final Stage of Transition to Turbulence," *Transition and Turbulence*, Meyer, R. E., ed., Academic Press, New York. 1981, pp. 113–126.

47 Eagles, P. M., "On Stability of Taylor Vortices by Fifth-Order Amplitude Expansions," *Journal of Fluid Mechanics*, Vol. 49, 1971, pp. 529–550.

48 Hocking, L. M., and Stewartson, K., "On the Nonlinear Response of a Marginally Unstable Plane Parallel Flow to a Two-Dimensional Disturbance," *Proceedings of the Royal Society of London*, Series *A*, Vol. 326, 1972, pp. 289–313.

49 Stuart, J. T., and DiPrima, R. C., "The Eckhaus and Benjamin-Feir Resonance Mechanisms," *Proceedings of the Royal Society*, Series *A*, Vol. 362, 1978, pp. 27–41.

50 Hall, P., "Effect of External Forcing on the Stability of Plane Poiseuille Flow," *Proceedings of the Royal Society of London*, Series *A*, Vol. 359, 1978, pp. 453–478.

51 Taylor, G. I., "Stability of a Viscous Liquid Contained Between Two Rotating Cylinders," *Philosophical Transactions of the Royal Society of London*, Vol. *A*233, 1923, pp. 289–343.

52 Davey, A., "The Growth of Taylor Vortices in Flow Between Rotating Cylinders," *Journal of Fluid Mechanics*, Vol. 14, 1962, pp. 336–368.

Downloaded 02 May 2010 to 171.66.16.250. Redistribution subject to ASME license or copyright; see http://www.asme.org/terms/Terms_Use.cfm

53 Davey, A., DiPrima, R. C., and Stuart, J. T., "On the Instability of Taylor Vortices," *Journal of Fluid Mechanics*, Vol. 31, 1968, pp. 17–52.

54 Fenstermacher, P. R., Swinney, H. L., and Gollub, J. R., "Dynamical Instabilities and the Transition to Chaotic Taylor Vortex Flow," *Journal of Fluid Mechanics*, Vol. 94, 1979, pp. 103–128.

55 Swift, J. B., Gorman, M., and Swinney, H. L., "Modulated Wavy Vortex Flow in Laboratory and Rotating Reference Frames," *Physics Letters*, Vol. 87*A*, 1982, pp. 457–460.

56 Walden, R. W., and Donnelly, R. J., "Reemergent Order of Chaotic Circular Couette Flow," *Physical Review Letters*, Vol. 42, 1979, pp. 301–304.

57 Coles, D., "Transition in Circular Couette Flow," *Journal of Fluid Mechanics*, Vol. 21, 1965, pp. 385–425.

58 Benjamin, T. B., and Mullin, T., "Notes on the Multiplicity of Flows in the Taylor Experiment," *Journal of Fluid Mechanics*, Vol. 121, 1982, pp. 219–230.

59 Richtmyer, R. D., "A Method for the Calculation of Invariant Manifolds in Hydrodynamic Stability Problems," NCAR/TN-176+STR, Boulder, Colo. 1981.

60 Yahata, H., "Temporal Development of the Taylor Vortices in a Rotating Fluid. IV," *Progress of Theoretical Physics*, Vol. 66, 1981, pp. 879–891.

61 Yahata, H., "Temporal Development of the Taylor Vortices in a Rotating Fluid. V," *Progress of Theoretical Physics*, Vol. 69, 1983, pp. 396–402.

62 Manley, O. P., an Treve, Y. M., "Minimum Number of Modes in Approximate Solutions to Equations of Hydrodynamics," *Physics Letters*, Vol. 82*A*, 1981, pp. 88–90.

63 Foias, C., and Treve, Y. M., "Minimum Number of Modes for the Approximation of the Solutions of the Navier-Stokes Equations in Two and Three Dimensions," *Physics Letters*, Vol. 85*A*, 1981, pp. 35–37.

64 Jones, C., "Nonlinear Taylor Vortices and Their Stability," *Journal of Fluid Mechanics*, Vol. 102, 1981, pp. 249–261.

65 Debler, W., Funer, E., and Schaaf, B., "Torque and Flow Patterns in Supercritical Circular Couette Flow," *Proceedings of the Twelfth International Congress of Applied Mechanics*, Hetenyi, M., and Vicenti, W. G., eds., Springer, Berlin, Heidelberg, New York, 1969, pp. 158–178.

66 Zarti, A. S., Jones, C. D., and Mobbs, F. R., "Influence of Cylinder Radius Ratio on the Variation of Critical Taylor Number with Eccentricity Ratio," *Superlaminar Flow in Bearings, Proceedings of 2nd Leeds-Lyon Symposium on Tribology*, Dowson, D., Godet, M., and Taylor, C. M., eds., Mechanical Engineering Publications, London, 1975, pp. 23–27.

67 Cole, J. A., "Wavy Vortex Onset and Cylinder Radius Ratio," *1981 Taylor Vortex Flow Working Party*, Astill, K., ed., Tufts University, Medford, Mass.

68 Cole, J. A., "The Effect of Cylinder Radius Ratio on Wavy Vortex Onset," *1983 Taylor Vortex Flow Working Party*, Cognet, G., ed., Nancy, France.

69 Alziary de Roquefort, T., and Grillaud, G., "Computation of Taylor Vortex Flow by a Transient Implicit Method," *Computers and Fluids*, Vol. 6, 1978, pp. 259–269.

70 Cole, J. A., "Taylor-Vortex Instability and Annulus-Length Effects," *Journal of Fluid Mechanics*, Vol. 75, 1976, pp. 1–15.

71 Benjamin, T. B., "Bifurcation Phenomena in Steady Flows of a Viscous Fluid," *Proceedings of the Royal Society of London*, Series *A*, Vol. 359, 1978, pp. 27–43.

72 Mullin, T., "Mutations of Steady Cellular Flows in the Taylor Experiment," *Journal of Fluid Mechanics*, Vol. 121, 1982, pp. 207–218.

73 Mullin, T., Pfister, G., and Lorenzen, A., "New Observation on Hystersis Effects in Taylor-Couette Flow," *Physics of Fluids*, Vol. 25, 1982, pp. 1134–1136.

74 Mullin, T., and Benjamin, T. B., "Transition to Oscillatory Motion in the Taylor Experiment," *Nature*, Vol. 288, 1980, pp. 567–569.

75 Ahlers, G., Connell, D. S., and Lerma, M. A. D., "Fractional Mode Numbers in Wavy Taylor Vortex Flow," *Physical Review Letters*, Vol. 49, 1982, pp. 368–371.

76 Blennerhassett, P. J., and Hall, P., "Centrifugal Instabilities of Circumferential Flows in Finite Cylinders: Linear Theory," *Proceedings of the Royal Soceity of London*, Series *A*, Vol. 365, 1979, pp. 191–207.

77 Hall, P., "Centrifugal Instabilities of Circumferential Flows in Finite Cylinders: Nonlinear Theory," *Proceedings of the Royal Society of London*, Series *A*, Vol. 372, 1980, pp. 317–356.

78 Stuart, J. T., and DiPrima, R. C., "On the Mathematics of Taylor-Vortex Flows in Cylinders of Finite Length," *Proceedings of the Royal Society of London*, Series *A*, Vol. 372, 1980, pp. 357–365.

79 Shearer, M., and Walton, I. C., "On Bifurcation and Symmetry in Bénard Convection and Taylor Vortices," *Studies in Applied Mathematics*, Vol. 65, 1981, pp. 85–93.

80 Schaeffer, D. G., "Qualitative Analysis of a Model for Boundary Effects in the Taylor Problem," *Mathematical Proceedings of the Cambridge Philosophical Society*, Vol. 87, 1980, pp. 307–337.

81 Hall, P., "Centrifugal Instabilities in Finite Containers: A Periodic Model," *Journal of Fluid Mechanics*, Vol. 99, 1980, pp. 575–596.

82 Hall, P., "Centrifugal Instabilities of Circumferential Flows in Finite Cylinders: The Wide Gap Problem," *Proceedings of the Royal Society of London*, Series *A*, Vol. 384, 1982, pp. 359–379.

83 Andreichikov, I. P., "Branching of Secondary Modes in the Flow between Rotating Cylinders," *Fluid Dynamics*, Vol. 12, 1977, pp. 38–43.

84 Frank, G., and Meyer-Spasche, R., "Computation of Transitions in Taylor Vortex Flows," *Journal of Applied Mathematics and Physics (ZAMP)*, Vol. 32, 1981, pp. 710–720.

85 Velte, W., "Stabilität und Verzweigung Statiionärer Losungen der Navier-Stokesschen Gleichungen beim Taylorproblem," *Archive for Rational Mechanics and Analysis*, Vol. 22, 1966, pp. 1–14.

86 Yih, C. S., "Spectral Theory of Taylor Vortices Part I Structures of Unstable Modes and Part II Proof of Nonoscillation," *Archive for Rational Mechanics and Analysis*, Vol. 46, 1972, pp. 218–240 and Vol. 47, 1972, pp. 288–300.

87 Eagles, P. M., "On the Torque of Wavy Vortices," *Journal of Fluid Mechanics*, Vol. 62, 1974, pp. 1–9.

88 Goldstein, S., ed., *Modern Developments in Fluid Dynamics*, Vol. 1, 1938, Clarendon Press, Oxford.

89 Coles, D., "Interfaces and Intermittency in Turbulent Shear Flow," *Mecanique de la Turbulence*, 1962, C. N. R. S., Paris, pp. 229–248.

90 Rubin, Y., Wygnanski, I., and Haritonidis, J. H., "Further Observations on Transition in a Pipe," *Laminar Turbulent Transition*, Eppler, R., and Fasel, H., eds., 1980, Springer, Berlin, Heidelberg, New York, pp. 17–26.

91 Teitgen, R., "Laminar-Turbulent Transition in Pipe Flow: Development and Structure of the Turbulent Slug," *Laminar-Turbulent Transition*, Eppler, R., and Fasel, H., eds., 1980, Springer, Berlin, Heidelberg, New York, pp. 27–36.

92 Tatsumi, T., "Stability of the Laminar Inlet-Flow Prior to the Formation of Poiseuille Regime, I," *Journal of the Physical Society of Japan*, Vol. 7, 1952, pp. 489–502.

93 Davey, A., "On the Stability of Flow in an Elliptic Pipe Which is Nearly Circular," *Journal of Fluid Mechanics*, Vol. 87, 1978, pp. 233–241.

94 Davey, A., and Nguyen, H. P. F., "Finite-Amplitude Stability of Pipe Flow," *Journal of Fluid Mechanics*, Vol. 45, 1971, pp. 701–720.

95 Itoh, N., "Nonlinear Stability of Parallel Flows With Subcritical Reynolds Numbers. Part 1. An Asymptotic Theory Valid for Small Amplitude Disturbances and Part 2. Stability of Pipe Poiseuille Flow to Finite Axisymmetric Disturbances," *Journal of Fluid Mechanics*, Vol. 82, 1977, pp. 455–467 and pp. 469–479.

96 Davey, A., "On Itoh's Finite Amplitude Stability Theory for Pipe Flow," *Journal of Fluid Mechanics*, Vol. 86, 1978, pp. 695–703.

97 Stuart, J. T., "Instability and Transition in Pipes and Channels," *Transition and Turbulence*, Meyer, R. E., ed., 1981, Academic Press, New York, pp. 77–94.

98 Smith, F. T., and Bodonyi, R. J., "Amplitude-Dependent Neutral Modes in the Hagen-Poiseuille Flow Through a Circular Pipe," *Proceedings of the Royal Society of London*, Series *A*, Vol. 384, 1982, pp. 463–489.

99 Ellingsen, T., Gjevik, B., and Palm, E., "On the Non-Linear Stability of Plane Couette Flow," *Journal of Fluid Mechanics*, Vol. 40, 1970, pp. 97–112.

100 DiPrima, R. C., and Stuart, J. T., "The Nonlinear Calculation of Taylor-Vortex Flow Between Eccentric Rotating Cylinders," *Journal of Fluid Mechanics*, Vol. 67, 1975, pp. 85–111 and "Non-Local Effects in the Stability of Flow Between Eccentric Rotating Cylinders," *Journal of Fluid Mechanics*, Vol. 54, 1972, pp. 393–415.

101 Gaster, M., "On the Effects of Boundary-Layer Growth on Flow Stability," *Journal of Fluid Mechanics*, Vol. 66, 1974, pp. 465–480.

102 Bouthier, M., "Stabilité Linéaire des Écoulements Presque Parallèles, Partie I and Partie II La Couche Limite de Blasius," *Journal of Mécanique*, Vol. 11, 1972, pp. 599–621 and Vol. 12, 1973, pp. 75–95.

103 Smith, F. T., "On the Non-Parallel Flow Stability of the Blasius Boundary Layer," *Proceedings of the Royal Society of London*, Series *A*, Vol. 366, 1979, pp. 91–109; and "Nonlinear Stability of Boundary Layers for Disturbances of Various Sizes," *Proceedings of the Royal Society of London*, Series *A*, Vol. 368, 1979, pp. 573–589.

104 Hall, P., "The Stability of Unsteady Cylinder Flows," *Journal of Fluid Mechanics*, Vol. 67, 1975, pp. 29–63.

105 Hall, P., "The Linear Stability of Flat Stokes Layers," *Proceedings of the Royal Society of London*, Series *A*, Vol. 359, 1978, pp. 151–166.

106 Hall, P., "On the Nonlinear Stability of Slowly Varying Time-Dependent Viscous Flows," *Journal of Fluid Mechanics*, Vol. 126, 1983, pp. 357–368.

107 Seminara, G., and Hall, P., "Centrifugal Instability of a Stokes Layer: Linear Theory," *Proceedings of the Royal Society of London*, Series *A*, Vol, 350, 1976, pp. 299–316.

108 Von Kerczek, C., and Davis, S., "Linear Stability Theory of Oscillatory Stokes Layers," *Journal of Fluid Mechanics*, Vol. 62, 1974, pp. 753–773.

109 Davis, S., "The Stability of Time-Periodic Flows," *Annual Review of Fluid Mechanics*, Vol. 8, 1976, pp. 57–74.

Downloaded 02 May 2010 to 171.66.16.250. Redistribution subject to ASME license or copyright; see http://www.asme.org/terms/Terms_Use.cfm

Stress Intensity Factors

F. Erdogan
Department of Mechanical Engineering and Mechanics, Lehigh University, Bethlehem, Pa. 18015
Mem. ASME

In this paper the concept of the stress intensity factor, the underlying mechanics problem leading to its emergence, and its physical relevance, particularly its relation to fracture mechanics are discussed, the reasons as to why it has become nearly an indispensable tool for studying such important phenomena as brittle fracture and fatigue or corrosion fatigue crack propagation in structural solids are considered, a brief discussion of some of the important methods of solution of elastic crack problems is given, and a number of related special mechanics problems are described.

1 Introduction

From the elasticity solutions of problems involving stress concentrations it is known that the maximum stress becomes unbounded as the notch root radius tends to zero. In this case it is said that the (theoretical) stress state at the notch root is singular and the asymptotic examination would show that the magnitude of the stresses are of the form $\sigma_{ij} \sim k/r^{\alpha}$, $(0<\alpha<1)$, where r is the distance from notch root and k is a constant. It is seen that the two constants α (the power) and k(the strength) fully describe the nature of stress singularity at the notch root. In the special case when the notch becomes a crack (i.e., when the local wedge angle becomes 2π), the strength of the stress singularity k is known as the stress intensity factor. As it stands, the concept is really useless on two grounds: (*a*) in practice the notch root radius cannot be zero, and (*b*) due to local inelastic deformations or yielding there would always be some stress relaxation and redistribution eliminating the possibility of infinite stress. These shaky foundations to some extent explains the reasons for the slow acceptance of the stress intensity factor as a physically relevant parameter when it was introduced in the 1950s. The concept, however, is closely associated with the phenomenon of brittle fracture and, despite its peculiar dimension ($Nm^{3/2}$) for a primary correlation parameter of a very important physical phenomenon, it seems to have found almost universal acceptance and very wide usage. It is the purpose of this paper to trace the evolution of the stress intensity factor, to show its relation to fracture mechanics, and to briefly discuss the concept and its applications in the broader context of problems in solid mechanics.

2 Development of the Concept

The origin of fracture mechanics goes back to Griffith's work on the fracture of glass (see Chapters 1-3 in [1]). The basic idea of Griffith's theory is that, similar to liquids, the surface of a solid possesses surface tension, and that when a crack in the solid propagates, the increase in the externally added or internally released energy is balanced by the increase in the surface tension energy. In an elastic solid such as that considered by Griffith if U and V, respectively, refer to the work of the external forces and the elastic energy and if γ refers to the specific surface tension energy of the solid, then Griffith's energy balance theory may be expressed as

$$\frac{d}{dA}(U-V)=\gamma \tag{1}$$

where A is the surface area of the crack. For example, by using the solution [1]

$$\sigma_{yy}(x,0)=\frac{\sigma_0|x|}{(x^2-a^2)^{1/2}},\ \sigma_{xy}(x,0)=0,\ (|x|>a), \tag{2}$$

$$v(x,0)=\frac{1+\kappa}{4\mu}\sigma_0(a^2-x^2)^{1/2},\ (|x|<a) \tag{3}$$

for an infinite plane that is under uniform tension σ_0 in y direction and which contains a through crack of length $2a$ along the x axis, it may be shown that for the fixed grip case (more specifically, if the crack is introduced after loading and then fixing the grips) the total strain energy (per unit thickness) is

$$V=\frac{1}{2}\frac{\sigma_0^2}{E}v_0-\frac{1+\kappa}{8\mu}\pi\sigma_0^2a^2, \tag{4}$$

where v_0 is the total volume (per unit thickness), μ is the shear modulus, and $\kappa=4-3\nu$ for plane strain and $\kappa=(3-\nu)/(1+\nu)$ for plane stress, ν being the Poisson's ratio. If we now observe that for the fixed grip case $dU=0$ and $dA=4da$ (where da is the extension of the crack at each end), from (1) and (4) it follows that

$$\frac{1+\kappa}{8\mu}\pi\sigma_0^2a=2\gamma. \tag{5}$$

Note that $(1+\kappa)/8\mu$ is $1/E$ for the plane stress and $(1-\nu^2)/E$ for the plane strain case. In the case of crack extension under "fixed load" both dU and dV increase and it can be shown that $d(U-V)/dA$ is still given by (5). Aside from the minor error pointed out by Sack and Orowan (see, for example, [2]), equation (5) is essentially the energy balance equation ob-

Contributed by the Applied Mechanics Division for publication in the JOURNAL OF APPLIED MECHANICS.
Discussion on this paper should be addressed to the Editorial Department, ASME, United Engineering Center, 345 East 47th Street, New York, N.Y. 10017, and will be accepted until two months after final publication of the paper itself in the JOURNAL OF APPLIED MECHANICS. Manuscript received by ASME Applied Mechanics Division, April, 1983.

Copyright © 1983 by ASME
Downloaded 02 May 2010 to 171.66.16.250. Redistribution subject to ASME license or copyright; see http://www.asme.org/terms/Terms_Use.cfm

tained by Griffith. In (5) the left-hand side is the energy available for fracture and the right-hand side represents the resistance of the solid to fracture propagation.

The next important development on the subject was Sneddon's work on the plane and the axisymmetric crack problems [2]. By using Westergaard's solution [3] for the plane-strain crack problem, and by solving the (axisymmetric) penny-shaped crack problem through the use of Hankel transforms, Sneddon obtained the correct asymptotic behavior of stresses in the small neighborhood of the crack front and showed that the asymptotic expressions for the components of the stress in the two cases differ only by a numerical factor $(2/\pi)$. For the case of an infinite elastic solid under uniform axial tension σ_0 and containing a penny-shaped crack of radius a he also obtained the following energy balance equation

$$\frac{1-\nu^2}{E}\,\frac{4}{\pi}\,\sigma_0{}^2 a = 2\gamma, \tag{6}$$

which differs from (the plane-strain version of) (5) only by a factor $(2/\pi)^2$. However, by (incorrectly) stating that $\sigma_{\theta\theta}$ in the penny-shaped crack has no analogue in the plane-strain case, he failed to recognize the importance of his finding and did not generalize his results. As pointed out later by Irwin [4], in the penny-shaped crack problem the stress state around the crack front is, of course, one of plane strain, and the isolation of the "numerical factor" referred to by Sneddon is the key to generalizing the crack problems. It should be pointed out that the energy balance relation (1) is only a necessary condition for crack growth. From the physical meaning of the terms in (1) it is clear that the stability of (quasi-static) fracture propagation may be determined from

$$\frac{d}{dA}\left[\frac{d}{dA}(U-V)-\gamma\right]\begin{cases} >0: & \text{unstable fracture,} \\ <0: & \text{stable fracture,} \\ =0: & \text{neutral equilibrium.} \end{cases} \tag{7}$$

Since the practical fracture resistance of structural solids was observed to be orders of magnitude higher than the corresponding surface tension energy γ, Griffith's work was more or less ignored by the engineering community until the late 1940s. The revival of the theory came about after the X-ray work indicated that even in materials that were fracturing in "purely brittle" manner, there were extensive plastic deformations on the fracture surfaces. This led Irwin and Orowan (independently) to propose that in the energy balance theory the rate of plastic work at the crack front should also be considered as a disipative energy component (see, for example, [4] for related references). In the early 1950s Irwin made two important contributions. First, he observed that in a fracturing elastic solid if the characteristic size of the zone of large plastic deformations or energy dissipation around the crack front is very small compared to the length parameter of the crack, then it is reasonable to assume that the energy $(U-V)$ "pumped" into the fracture zone will come from the elastic bulk of the solid and therefore will not be critically dependent on the details of the stress state very near the crack front, and the stress state in the elastic bulk of the solid will not differ from a purely elastic crack solution to any significant extent. The importance of this observation lies in the fact that one may now be justified in calculating the energy $(U-V)$ available for fracture from a purely elastic solution.

Irwin's second important contribution was his recognition of the universality of the asymptotic stress and displacement fields around the crack tip of his interpretation of the fixed-grip strain energy release rate (which involves the strain energy distribution in the entire solid) in terms of the rate of

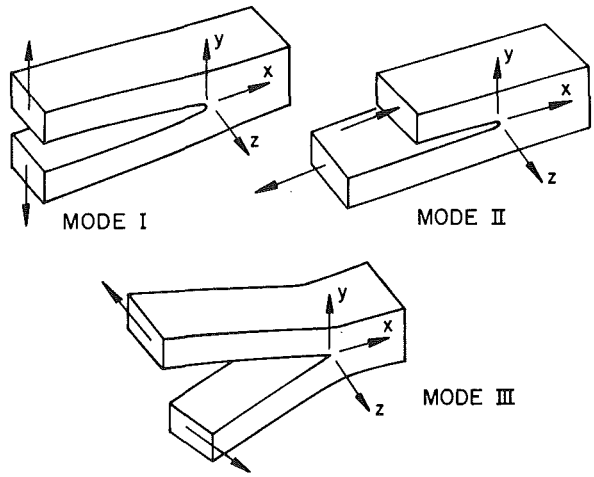


Fig. 1 Modes *I*, *II*, and *III* crack surface displacements

crack closure energy that can be calculated by using the asymptotic expressions for the crack surface displacements and the corresponding "cleavage" stresses only. He introduced a constant $\mathcal{G}$ (after Griffith) and observed that the symmetric crack solutions given by Westergaard and Sneddon may be generalized to include asymptotic expressions for all crack problems having the plane of the crack as the plane of symmetry and for small values of the distance r from the crack tip the cleavage stress and the crack surface displacement in the plane of the crack may be expressed as (see, for example, equation (2) and (3), where $r = |x-a|$)

$$\sigma_{yy} \cong \left(\frac{8\mu}{1+\kappa}\,\frac{\mathcal{G}}{\pi}\right)^{1/2} \frac{1}{\sqrt{2r}},\quad v \cong 2\left(\frac{1+\kappa}{8\mu}\,\frac{\mathcal{G}}{\pi}\right)^{1/2}\sqrt{2r}. \tag{8}$$

For a small crack extension da he then proceeded to calculate the strain energy release through the crack-closure energy as follows (see (1))

$$d(U-V) = 2\int_0^{da} \frac{1}{2}\,\sigma_{yy}(r)\,v(da-r)\,dr = \mathcal{G}\,da, \tag{9}$$

or

$$\frac{d}{da}(U-V) = \mathcal{G}. \tag{10}$$

Thus, from (10) and (8) it is seen that the energy available for fracture per unit crack extension may be directly related to the coefficient of the singular term in the expression of the stress state at the crack tip. Irwin called the coefficient $(8\mu/1+\kappa\,\mathcal{G}/\pi)^{1/2}$ which appears in the asymptotic expression of the stress (see (8)) the "stress intensity factor."

Subsequently, by using Westergaard's solution Irwin showed that the stress and displacement states in the close neighborhood of the smooth internal boundary of a plane crack in a linearly elastic solid under most general loading conditions may be expressed in terms of three stress intensity factors k_1, k_2, and k_3 associated with the symmetric opening, in-plane or forward shear, and antiplane shear modes of deformation, respectively (see Fig. 1). These asymptotic stress and displacement components may be expressed as follows [5], [1]:

$$\sigma_{xx} \cong \frac{k_1}{\sqrt{2r}}\cos\frac{\theta}{2}\left(1-\sin\frac{\theta}{2}\sin\frac{3\theta}{2}\right) - \frac{k_2}{\sqrt{2r}}\sin\frac{\theta}{2}\left(2+\cos\frac{\theta}{2}\cos\frac{3\theta}{2}\right),$$

Downloaded 02 May 2010 to 171.66.16.250. Redistribution subject to ASME license or copyright; see http://www.asme.org/terms/Terms_Use.cfm

$$\sigma_{yy} \cong \frac{k_1}{\sqrt{2r}}\cos\frac{\theta}{2}\left(1+\sin\frac{\theta}{2}\sin\frac{3\theta}{2}\right) + \frac{k_2}{\sqrt{2r}}\sin\frac{\theta}{2}\cos\frac{\theta}{2}\cos\frac{3\theta}{2},$$

$$\sigma_{xy} \cong \frac{k_1}{\sqrt{2r}}\cos\frac{\theta}{2}\sin\frac{\theta}{2}\cos\frac{3\theta}{2} + \frac{k_2}{\sqrt{2r}}\cos\frac{\theta}{2}\left(1-\sin\frac{\theta}{2}\sin\frac{3\theta}{2}\right),$$

$$\sigma_{zz} \cong \begin{cases} 0, \text{ for plane stress,} \\ \nu(\sigma_{xx}+\sigma_{yy}), \text{ for plane strain,} \end{cases} \quad (11a\text{–}d)$$

$$u \cong \frac{k_1}{8\mu}\sqrt{2r}\left[(2\kappa-1)\cos\frac{\theta}{2}-\cos\frac{3\theta}{2}\right] + \frac{k_2}{8\mu}\sqrt{2r}\left[(2\kappa+3)\sin\frac{\theta}{2}+\sin\frac{3\theta}{2}\right],$$

$$v \cong \frac{k_1}{8\mu}\sqrt{2r}\left[(2\kappa+1)\sin\frac{\theta}{2}-\sin\frac{3\theta}{2}\right] - \frac{k_2}{8\mu}\sqrt{2r}\left[(2\kappa-3)\cos\frac{\theta}{2}+\cos\frac{3\theta}{2}\right], \quad (12a, b)$$

$$\sigma_{xz} \cong -\frac{k_3}{\sqrt{2r}}\sin\frac{\theta}{2},$$

$$\sigma_{yz} \cong \frac{k_3}{\sqrt{2r}}\cos\frac{\theta}{2}, \quad (13a, b)$$

$$w \cong \frac{k_3}{\mu}\sqrt{2r}\sin\frac{\theta}{2}, \quad (14)$$

where xz is the plane of the crack, the axis z is tangent to the crack border, and r, θ are the polar coordinates in the xy plane (Fig. 1). The asymptotic expressions (11a–c) were also obtained by Williams from an eigenfunction expansion of the Airy stress function for a plane with a semi-infinite crack [6]. Perhaps the simplest way of obtaining the equations (11–14) would be to use the complex potentials (Kolosov functions in the in-plane and an analytic function in the antiplane problem) and to observe that the crack tip is a branch point (of power 1/2) [1].

From (8) and (11b) it is seen that the strain energy release rate $\mathcal{G}$ defined by (10) is related to the Mode I stress intensity factor k_1 as follows:

$$k_1 = \left(\frac{8\mu}{1+\kappa}\frac{\mathcal{G}}{\pi}\right)^{1/2}, \quad \text{or} \quad \mathcal{G} = \frac{1+\kappa}{8\mu}k_1 2\pi. \quad (15)$$

If the elasticity solution of the crack problem is available, the stress intensity factors may be evaluated at any point on the crack border from the asymptotic behavior of the stresses (in the plane of the crack) or crack surface displacements by using the expressions (11)–(14) for $\theta=0$ or $\theta=\pi$. In general let the crack locally occupy the $x-z$ plane, the $x-y$ plane be perpendicular to the crack border (which may be a smooth curved line) at the point of interest, the x coordinate of the point on the crack border be a, and z axis be parallel to the tangent of the crack border (e.g., Fig. 1 with $x-a$ replacing x). Then the following expressions may be obtained from (11)–(14) which may be quite useful to calculate the stress intensity factors once the elasticity solution of the problem is found:

$$k_1 = \lim_{x\to a}\sqrt{2(x-a)}\,\sigma_{yy}(x,0,0) = \frac{2\mu}{1+\kappa}\lim_{x\to a}\frac{1}{\sqrt{2(a-x)}}[v(x,+0,0)-v(x,-0,0)] = \frac{2\mu}{\kappa+1}\lim_{x\to a}\sqrt{2(a-x)}\,\frac{\partial}{\partial x}[v(x,+0,0)-v(x,-0,0)], \quad (16)$$

$$k_2 = \lim_{x\to a}\sqrt{2(x-a)}\,\sigma_{xy}(x,0,0) = \frac{2\mu}{1+\kappa}\lim_{x\to a}\frac{1}{\sqrt{2(a-x)}}[u(x,+0,0)-u(x,-0,0)] = \frac{2\mu}{1+\kappa}\lim_{x\to a}\sqrt{2(a-x)}\,\frac{\partial}{\partial x}[u(x,+0,0)-u(x,-0,0)], \quad (17)$$

$$k_3 = \lim_{x\to a}\sqrt{2(x-a)}\,\sigma_{yz}(x,0,0) = \mu\lim_{x\to a}\frac{1}{\sqrt{2(a-x)}}[w(x,+0,0)-w(x,-0,0)] = \mu\lim_{x\to a}\sqrt{2(a-x)}\,\frac{\partial}{\partial x}[w(x,+0,0)-w(x,-0,0)]. \quad (18)$$

It should be pointed out that the foregoing results refer to a quasi-static problem in which the crack border in the neighborhood of the point of interest is surrounded by a linearly elastic, isotropic, and homogeneous medium. Consideration of such factors as material anisotropy, nonhomogeneity, and nonlinearity, and dynamic (or inertia) effects would clearly influence the asymptotic expressions given by (11)–(14). In the most general crack problem for linear materials the asymptotic expressions for stresses and displacements near the crack border have the following form:

$$\sigma_{ij} \cong \frac{k_1(t)}{r^\alpha}f_{ij}^1(\theta, c_k) + \frac{k_2(t)}{r^\alpha}f_{ij}^2(\theta, c_k), \quad 0<\alpha<1, (i,j=x,y), \quad (19)$$

$$u_i \cong \frac{1}{E^*}k_1(t)r^{1-\alpha}F_i^1(\theta, c_k) \quad (19)$$

$$+ \frac{1}{E^*}k_2(t)r^{1-\alpha}F_i^2(\theta, c_k), (i=x,y), \quad (20)$$

$$\sigma_{iz} \cong \frac{k_3(t)}{r^\beta}f_{iz}^3(\theta, c_k), 0<\beta<1, (i=x,y), \quad (21)$$

$$w \cong \frac{1}{\mu^*}k_3(t)r^{1-\beta}F_3(\theta, c_k), \quad (22)$$

where the notation is the same as (11)–(14) and Fig. 1, E^* and μ^* are normalizing material constants (having the dimension of shear modulus), c_k, (k = 1, 2, . . .) represent dimensionless material constants, and f_{ij}^k and F_i^k are (known) bounded functions with symmetry properties in θ similar to the corresponding functions in (11)–(14). In dynamic problems the stress intensity factors k_i are functions of time t. The powers of stress singularity α and β differ from 1/2 only in nonhomogeneous and certain homogeneous anisotropic (e.g., cylindrically anisotropic) materials. In such cases α and β are generally not equal. In the general problem described by (19)–(22) the stress intensity factors may again be defined and calculated in terms of the corresponding stress or displacement component in the plane of the crack. For example, for Mode I type of loading (Fig. 1(a)) we have

$$k_1(t) = \frac{1}{f_{yy}^1(0, c_k)}\lim_{r\to 0} r^\alpha \sigma_{yy}(r,0,0,t). \quad (23)$$

The important cases for which the asymptotic expressions are different from (11)–(14) will briefly be discussed in a subsequent section.

Downloaded 02 May 2010 to 171.66.16.250. Redistribution subject to ASME license or copyright; see http://www.asme.org/terms/Terms_Use.cfm

3 Practical Applications: Fracture Mechanics

The development of the concept of stress intensity factor outlined in the preceding section as a measure of the severity of the flow geometry and the intensity of the applied loads is based entirely on the notions of continuum solid mechanics. To make it an effective tool in studying the mechanical failure of the flaw geometry and the intensity of the applied loads is based entirely on the notions of continuum solid mechanics. material's resistance to fracture also needs to be developed. As pointed out in the preceding section, Irwin and Orowan observed that in essentially elastic structures undergoing fracture, the main component of energy dissipation is due to the plastic deformations in the material near the advancing crack front and the contribution of the surface tension energy proposed by Griffith is relatively insignificant. If one gets entangled in the microscopic and microstructural aspects of the range of phenomena culminating in the rupture separation of the material, the problem is hopelessly complicated. The question needs to be viewed again from the perspective of continuum solid mechanics.

In the type of "brittle" or "low energy" fracture under consideration it was observed that the plastic deformations are confined to a small region around the crack front. To establish a simple "fracture criterion," one may thus assume that (*a*) the characteristic size of the "energy dissipation" or "fracture process" zone around the growing crack front is "small" compared to the length parameter of the crack, and (*b*) the size and shape of the dissipation zone remain relatively constant as the crack extends. Based on these assumptions one may then make the hypothesis that, in solids undergoing essentially brittle fracture, under given environmental conditions, the resistance of the material to fracture, more precisely, the energy needed to create a unit fracture surface is a material constant. In Mode *I* fracture, from (10) we recall that the energy available for unit fracture surface is $\mathcal{G}$ (which is now referred to as $\mathcal{G}_I$ for Mode *I*). Correspondingly Irwin designated the material's critical resistance parameter by $\mathcal{G}_{IC}$ which he called the "fracture toughness" of the material. $\mathcal{G}_{IC}$ is also known as the "specific fracture energy" or the "critical strain energy release rate." Referring to (15), it is now seen that (under Mode *I* conditions) the necessary condition for fracture may be expressed as

$$\mathcal{G}_I = \frac{1+\kappa}{8\mu} k_1^2 \pi = \mathcal{G}_{IC}, \tag{24}$$

and, since $\mathcal{G}_{IC}$ is constant, $\partial \mathcal{G}_I / \partial a$ determines the fracture stability, where a is a length parameter characterizing the fracture area (see equations (7) and (10)).

Mainly because of the validity of the hypothesis regarding the fracture toughness $\mathcal{G}_{IC}$ being practically constant, in applications the simple fracture criterion expressed by (24) has been extremely successful. The parameter $\mathcal{G}_{IC}$ is determined experimentally by following certain procedures established by the American Society for Testing Materials (see, for example, [7, 8]). From (24) one may see that the next step in the evolution of a fracture criterion applicable to structures that behave in a brittle manner was inevitable.[1] Since $\mathcal{G}_{IC}$ is a measured constant and k_1 is the only calculated quantity, it was natural to reduce the criterion to a simpler form by defining the critical value of the stress intensity factor as the material constant. At this point also a slight change in notation took place as a result of absorbing the coefficient π in (24) into (the definition of) the stress intensity factor, namely $\pi k_1^2 = K_I^2$, K_I being the new stress intensity factor. Referring to (16)–(18) the definition of Modes *I*, *II*, and *III* stress intensity factors becomes[2]

$$K_I = \lim_{x \to a} \sqrt{2\pi(x-a)}\, \sigma_{yy}(x, 0, 0), \text{ etc.} \tag{25}$$

The corresponding critical value of K_I which represents the fracture resistance of the material and which is obtained from standardized experiments is denoted by K_{IC} and is called the "critical stress intensity factor." Note that K_{IC} is related to the fracture toughness $\mathcal{G}_{IC}$ by

$$K_{IC} = \left(\frac{8\mu}{1+\kappa} \mathcal{G}_{IC} \right)^{1/2}, \tag{26}$$

and the fracture criterion (24) becomes

$$K_I = K_{IC}. \tag{27}$$

Again, since K_{IC} is constant, for unstable fracture one must have $\partial K_I / \partial a > 0$, a being a length parameter of the crack. An additional change in terminology seems to be referring to K_{IC} as the "fracture toughness" of the material. This improper usage, too, appears to be embedded permanently in the fracture literature.

In the continuum solid mechanics approach to fracture discussed in this paper it is implicitly assumed that the material contains some macroscopic flaws which may act as fracture nuclei and the medium is a homogeneous continuum or consists of homogeneous continua in the sense that the size of the macroscopic flaws is large compared with the characteristic microstructural dimension of the material. The problem is then to study the effect of the applied loads, the flaw geometry, and the environmental conditions on the fracture of the solid. This particular field of study which evolved from Griffith's work has come to be known as "fracture mechanics." Specifically, if the conditions leading to the simple fracture criterion (27) are satisfied the field is sometimes referred as the "linear elastic fracture mechanics" (LEFM).

In addition to the direct application of (27) to static or quasi-static fracture problems, it is also used (by properly modifying K_I and K_{IC}) in such other problems as impact loading and dynamic fracture propagation. In impact loading, K_{IC} is simply replaced by K_{ID} which is obtained from standardized impact tests [8]. In dynamic crack propagation problems, K_I can be, in most cases, calculated as a function of time and is still the most effective factor representing the crack-structure geometry and the applied load. In this case, however, there seem to be serious unresolved questions regarding the corresponding strength characterization of the material.

Among many uses of the stress intensity factors in fracture mechanics, perhaps its most effective applications may be found in the study of the so-called subcritical crack propagation phenomena (i.e., the phenomena for which the

[1] The terminology "brittle" is generally used to denote a certain mechanical behavior of structural materials with regard to failure associated with low energy absorption. In fracture mechanics sometimes it is used (particularly by purists) only in connection with the ideal case in which there is no inelastic deformations near the crack tip. For this reason some investigators have used the term "quasi-brittle fracture" to denote those phenomena in actual structures which, despite considerable energy absorption due to plastic deformations near the crack front, remain essentially elastic and fails in an unstable manner. The current usage of "brittle fracture" appears to be the latter and no longer any distinction seems to be needed.

[2] The change came about from the desire to simplify the expression for $\mathcal{G}$. For example, in the case of plane problems $\mathcal{G}_I$ becomes $\pi k_1^2 / E_1 = K_I^2 / E_1$, ($E_1 = E$ for plane stress, $E_1 = E/(1-\nu^2)$ for plane strain). This, of course, introduces the awkward and unnecessary constant $\sqrt{\pi}$ into the elasticity solutions. In the infinite plate solution, for instance, given by (2) and (3) the asymptotic stress state is $\sigma_{yy} \cong \sigma_0 \sqrt{a} / \sqrt{2(x-a)}$, by (11*b*) giving $k_1 = \sigma_0 \sqrt{a}$. The new definition requires that the asymptotic expression be written as $\sigma_{yy} \cong \sigma_0 \sqrt{\pi a} / \sqrt{2\pi(x-a)}$ giving $K_1 = \sigma_0 \sqrt{\pi a}$. Considering the fact that the stress intensity factor is by far the most widely used fracture mechanics parameter, this artificial change seems to be hardly necessary. However, K_I, K_{II}, and K_{III} are now the standard notation used by the practicing engineers. The necessity of using $\sqrt{\pi}$ in theoretical work is generally removed by introducing a normalizing load or stress and treating k_1, k_2, and k_3 defined by (11)–(14) as dimensionless stress intensity ratios.

Downloaded 02 May 2010 to 171.66.16.250. Redistribution subject to ASME license or copyright; see http://www.asme.org/terms/Terms_Use.cfm

maximum K_I value derived from the peak load is below K_{IC}). In practice there are two groups of such important problems. The first is the basically time-independent fatigue crack growth process in structural components under cyclic loading. In this case the length parameter a characterizing fracture area is assumed to be a function of the load cycle n and the related mechanics problem is the determination of this function under given environmental and loading conditions. The second is primarily the time-dependent crack growth phenomenon under sustained loads. As typical examples for such problems one may mention the crack propagation in metal alloys under a corrosive environment (known as the stress corrosion cracking), the so-called static fatigue in ceramics under adverse environments (e.g., humidity), and (under some unusual conditions) the creep crack growth. In this case the mechanics problem is to determine the crack size a as a function of time.

The analysis of experimental results show that by far the most dominant single parameter that influences the crack propagation rate da/dn (in fatigue) or da/dt (in corrosion) is the stress intensity factor K_I, specifically, the amplitude ΔK_I for fatigue and $(K_I)_{\max}$ for static or corrosion crack growth.[3] This is not surprising because generally in such problems the plastic zone size around the crack tip is relatively small and the stress and deformation states are controlled by the stress intensity factor.

In fatigue problems the crack propagation rate is generally expressed as

$$\frac{da}{dn} = F(\Delta K_I, C_i) \tag{28}$$

where F is a known function and $C_1, C_2, \ldots$, represent the material constants and secondary factors which may influence the phenomenon. The following simplified version of (28) is widely used in practice and, in most cases, seems to be highly adequate:

$$\frac{da}{dn} = C(\Delta K_I)^{\alpha}, \tag{29}$$

where for a given material the constants C and α are determined from simple standard experiments. Aside from the environment-related parameters, the constants that are most often considered in the macroscopic crack growth model (28) are the mean-to-amplitude stress intensity factor ratio, a critical K_I value K_c representing fracture resistance of the material under a single application of the load, and the "threshold" value ΔK_T of the stress intensity amplitude below which no (observable) crack propagation may take place. For example, a model such as

$$\frac{da}{dn} = \frac{C(1+\beta)^{\alpha_1}(\Delta K_I - \Delta K_T)^{\alpha_2}}{K_C - (1+\beta)\Delta K_I}, \quad \beta = \frac{K_{I\max} + K_{I\min}}{K_{I\max} - K_{I\min}} \tag{30}$$

gives a typical sigmoidal curve (in log (da/dn) versus log(ΔK_I) plane) observed experimentally and can be made to represent the process in a very wide range (e.g., from 10^{-8} to 10^{-2} in./cycle) by properly determining the constants C, α_1, and α_2, and by characterizing the material with regard to K_C and ΔK_T. It has been suggested that ΔK_T may be related to the fatigue endurance limit S_e of the material. An approximate relationship between ΔK_T and S_e may be established by approximating the (dominant) natural microstructural flaw of the characteristic size $2a$ by a penny-shaped crack and by assuming that S_e is the stress amplitude. From the penny-shaped crack solution it then follows that

$$\Delta K_T = \frac{2}{\pi} S_e \sqrt{\pi a}. \tag{31}$$

Even though there have been some efforts (largely by material scientists) to "prove" the validity of the power relationship given by (29) (particularly for $\alpha = 4$) through microstructural considerations, the fatigue crack propagation models remain to be mostly empirical, nonetheless very highly effective (see [9] for a summary of the early efforts). The models do, however, have certain rationale and may qualitatively be related to certain microstructural phenomena (see, for example, Chapter 5 in [1]).

The models for the crack growth rate in materials exposed to an adverse environment and subjected to sustained loads are too largely empirical and are also of the form

$$\frac{da}{dt} = f(K_I, B_i) \tag{32}$$

where $B_1, B_2, \ldots$, represent the secondary factors (e.g., in addition to the material constants, K_{IC} and K_{ISCC}, the stress corrosion cracking threshold, in corrosion, and the activation energy and the gas constant in glasses). Whereas most corrosion models are power laws of the form (29), expressions such as

$$\frac{da}{dt} = v_0 \exp[(CK_I - E_0)/RT] \tag{33}$$

seem to model the crack growth process in most ceramics more effectively (see, for example [8, 10]). In (33) v_0 and C are material constants determined from standard experiments and E_0, R, T, respectively, are the activation energy, the gas constant, and the absolute temperature.

Needless to say, in many applications fatigue and corrosion may together be responsible for crack propagation. Such coupled effects may be modeled by considering the details of the load time profile, primarily the frequency and the waveform. These models, however, do not have the same simplicity and the universal appeal as the corresponding fatigue models (see, for example, [11], [12], and [8] for modeling, review, and applications).

In connection with the application of the stress intensity factors one often encounters references to a K-dominated domain or K-dominated phenomena. Considered judiciously this can be an extremely useful tool to study the nature of certain inelastic phenomena around propagating cracks. This way the domain is rendered infinite, the crack semi-infinite, and the phenomenon self-similar, simplifying the problem quite considerably. However, if one wants to draw quantitative conclusions based on such studies one should first specify as to what is meant by a K-dominated region and then be aware of the fact that the "reach" of such a region heavily depends on the nature of the applied loads and the structure-crack geometry. Table 1, for example, shows some results calculated from (2) where σ_{yy} is the actual stress and $\sigma_{yy}{}^a$ is the asymptotic approximation given by

$$\sigma_{yy}{}^a = \frac{k_1}{\sqrt{2(x-a)}}, \quad k_1 = \sigma_0 \sqrt{a}. \tag{34}$$

It may be seen that there is no definitely discernible "circle" distinguishing a K-dominated domain, and selection of such a circle largely depends on one's purpose and on the degree of accuracy required of the underlying discussions.

The last remark regarding the practical applications of the stress intensity factors concerns the so-called mixed-mode case (that is, the case for which in addition to K_I, K_{II} and K_{III} are also nonzero). From the fracture criterion

$$\mathcal{G} = \frac{\partial}{\partial A}(U - V) = \gamma_F \tag{35}$$

[3] It is in the nature of the subcritical crack growth phenomenon that in isotropic materials the crack generally orients itself in a plane perpendicular to the local maximum tensile stress. Consequently, the crack usually tends to follow a path for which $K_{II} = 0$. Most subcritical crack propagation models are, therefore, based on the Mode I stress intensity factor K_I.

Downloaded 02 May 2010 to 171.66.16.250. Redistribution subject to ASME license or copyright; see http://www.asme.org/terms/Terms_Use.cfm

Table 1 Actual and asymptotic stresses around the crack tip in a uniformly loaded plate

x/a	1.005	1.01	1.04	1.08	1.12	1.16	1.20	1.30	1.40	1.6
σ_{yy}/σ_0	10.037	7.124	3.641	2.648	2.221	1.973	1.809	1.565	1.429	1.281
$\sigma_{yy}{}^a/\sigma_0$	10.000	7.071	3.535	2.500	2.041	1.768	1.581	1.291	1.118	0.913
$\frac{\sigma_{yy}-\sigma_{yy}{}^a}{\sigma_{yy}}$	0.0037	0.0074	0.029	0.056	0.081	0.104	0.126	0.175	0.218	0.287

it is seen that the new incremental crack surface dA would be in the plane corresponding to maximum available energy $\mathcal{G}$ provided the medium is isotropic with regard to its fracture resistance (or fracture energy) γ_F. Assuming that $\mathcal{G}$ can be calculated (exactly or in some approximate way) in terms of the local stress intensity factors, this reasoning may be sufficient to determine the crack path as well as the critical level of the applied loads. However, as in all composite materials, if γ_F is a function of the local polar angle θ at the crack tip, then the crack would grow in the direction θ corresponding to the (absolute) maximum of $\mathcal{G}(\theta)/\gamma_F(\theta)$ in $-\pi<\theta<\pi$. In highly oriented materials with a well-defined weak cleavage plane (e.g., in layered composites), usually $\mathcal{G}/\gamma_F$ is maximum for $\theta=0$. In this case calculation of $\mathcal{G}$ must also include the contributions from the shear modes which are designated as $\mathcal{G}_{II}$ and $\mathcal{G}_{III}$ and may be evaluated from integrals similar to (9) by using the complementary stress and displacement pairs (σ_{xy}, u) and (σ_{yz}, w). In isotropic materials we thus have

$$\mathcal{G}_I=\frac{1+\kappa}{8\mu}K_I{}^2,\ \mathcal{G}_{II}=\frac{1+\kappa}{8\mu}K_{II}{}^2,\ \mathcal{G}_{III}=\frac{1}{2\mu}K_{III}{}^2,$$

$$\mathcal{G}=\mathcal{G}_I+\mathcal{G}_{II}+\mathcal{G}_{III}. \tag{36}$$

Aside from the fracture of oriented materials, as a very practical example for the application of $\mathcal{G}$ one may mention the delamination fatigue crack propagation in layered composites and in adhesively bonded joints where the stress state is one of mixed mode and K_I is no longer an effective correlation parameter.

4 Methods of Solution

In this section we discuss very briefly some of the important methods of solution of crack problems leading to the calculation of the stress intensity factors. A fairly thorough description of the techniques used in solving elastostatic crack problems may be found in [13] (see, also Chapters 1–3 in [1]).

4.1 Complex Potentials. Applicable to only two-dimensional problems, the complex potentials were first introduced by Goursat to represent the biharmonic function. Their applications to problems in elasticity were then elaborately developed by a school of Georgian mathematicians led by Muskhelishvili [14]. The description of the method and many of its applications to crack problems may be found in [14]. Expressing the displacements in terms of two holomorphic functions ϕ and ψ as

$$2\mu(u+iv)=\kappa\,\phi(z)-z\,\bar{\phi}'(\bar{z})-\bar{\psi}(\bar{z}) \tag{37}$$

and observing that in the mixed boundary value problem which represents the plane containing a number of cracks along (a_k, b_k), $(k = 1, 2, \ldots)$, a_k and b_k are branch points, the complex potentials, for example, in the neighborhood of the end point $z=b_k$ may be expressed as

$$\phi'(z)=\frac{F_{1k}(z)}{(z-b_k)^{1/2}}+G_{1k}(z),\ \psi'(z)=\frac{F_{2k}(z)}{(z-b_k)^{1/2}}+G_{2k}(z), \tag{38}$$

where the functions F_{jk} and G_{jk}, $(j = 1, 2)$ are holomorphic near and at b_k. It can further be shown that the asymptotic stress distribution (11) directly follows from (38) and the stress intensity factors may be determined from (see, for example, [1] Chapters 2 and 3)

$$k_1-ik_2=\lim_{z\to b_k}2\sqrt{2(z-b_k)}\,\phi'(z). \tag{39}$$

Similarly, in antiplane shear problems it may easily be shown that

$$w=Re[\Omega(z)],\ \Omega'(z)=\frac{f_1(z)}{(z-b_k)^{1/2}}+f_2(z),$$

$$k_3=i\,\mu\lim_{z\to b_k}\sqrt{2(z-b_k)}\,\Omega'(z) \tag{40}$$

where f_1 and f_2 are holomorphic near and at b_k. The holomorphic functions ϕ', ψ' and Ω' are determined by solving the related Reimann-Hilbert problems which follow from the mixed boundary conditions.

The method of complex potentials provides perhaps the simplest and most rigorous method for solving the crack problems and for analyzing the singular behavior of the solution. The serious shortcoming of the method is that it is restricted to two-dimensional elastostatic problems for (generally) infinite domains. The technique used by Westergaard [3] is a special case of the method of complex potentials.

There are a number of techniques used in the solution of two-dimensional crack problems which are also based on the application of complex potentials. Among these we may mention the method of conformal-mapping, Laurent series expansion, boundary collocation method, and certain applications of the Wiener-Hopf method [13].

4.2 Integral Transforms. The integral transforms is one of the most widely used methods in the formulation of the boundary value problems in mechanics. If the problem is a mixed boundary value problem the formulation would invariably lead to a pair of dual integral equations. Specifically, the crack problems for an elastic plane or an infinite strip containing a line crack, plane infinite wedge with a radial crack, and an elastic cylinder with an infinite or finite radius containing an axisymmetric crack may easily be reduced to dual integral equations by using Fourier, Mellin, and Hankel transforms, respectively. The dual integral equations may then be reduced to an Abel's (integral) equation which may in turn be either solved in closed form or reduced to a Fredholm integral equation. The literature on this subject is rather extensive. Description of various integral transforms and many of their applications to crack problems may be found in [15] (see, also Chapter 6 in [13] for further applications and references).

4.3 Singular Integral Equations. Dual integral equations, dual series equations, or dual series-integral equations arising from the formulation of the crack problems may be reduced to a singular integral equation (with a Cauchy-type singularity) in a straightforward manner. The crack problems can also be formulated in terms of a (system of) singular integral equation(s) directly by using the related Green's functions (e.g., dislocation and concentrated load solutions) and the technique of superposition. The method has clear advantages in problems involving unusual stress singularities (see the simple example given in Section 5.2 of this paper). It also lends itself to relatively simple numerical treatment.

Downloaded 02 May 2010 to 171.66.16.250. Redistribution subject to ASME license or copyright; see http://www.asme.org/terms/Terms_Use.cfm

Consider, for example, the elastic half plane $y>0$ subject to

$$\sigma_{xy}(x,0)=0, \frac{1+\kappa}{4\mu}\sigma_{yy}(x,0)=f(x), \ -\infty<x\infty. \tag{41}$$

Defining

$$\frac{\partial}{\partial x}v(x,0)=g(x), (-\infty<x<\infty), \tag{42}$$

it may easily be shown that

$$g(x)=-\frac{1}{\pi}\int_{-\infty}^{\infty}\frac{f(t)}{t-x}dt, \ -\infty<x<\infty. \tag{43}$$

Hilbert inversion of (43) is

$$f(x)=\frac{1}{\pi}\int_{-\infty}^{\infty}\frac{g(t)}{t-x}dt, \ -\infty<x<\infty. \tag{44}$$

Consider now the problem for an infinite plane containing a line crack along the x axis. Let the (known self-equilibrating) normal tractions $f(x)$ acting on the crack surfaces be the only external loads acting on the plane and the necessary change in variable be made so that the crack occupies $(-1<x<1, y=0)$. Equation (44) is then valid for the problem. In particular, by observing that $g(x)=0$ for $|x|>1$ and $f(x)$ is known for $|x|<1$, (44) becomes

$$f(x)=\frac{1}{\pi}\int_{-1}^{1}\frac{g(t)}{t-x}dt, \ -1<x<1 \tag{45}$$

giving the integral equation to determine the unknown function $g(t)$, $(-1<t<1)$. The condition of single-valuedness of the displacement v requires that (see (42))

$$\int_{-1}^{1}g(x)dx=0. \tag{46}$$

Equation (45) can, of course, be solved by using the function theoretic method [14]. One may also write the solution of (45) by inspection, if one considers the following properties of the Chebyshev polynomials [16]:

$$\frac{1}{\pi}\int_{-1}^{1}\frac{T_n(t)\,dt}{(t-x)\sqrt{1-t^2}}=\begin{cases}0, n=0, \ |x|<1,\\ U_{n-1}(x), n>0, \ |x|<1,\\ -\dfrac{(x-\sqrt{x^2-1})^n}{\sqrt{x^2-1}}, \ |x|>1,\end{cases} \tag{47}$$

$$T_n(x)=\cos n\theta, U_n(x)=\sin(n+1)\theta/\sin\theta, x=\cos\theta, \ |x|<1. \tag{48}$$

Noting that the fundamental solution of the singular integral equation (45) is $(1-x^2)^{-1/2}$, $g(x)$ may be expressed as

$$g(x)=G(x)/\sqrt{1-x^2}, \ |x|<1. \tag{49}$$

If we now express the bounded functions $f(x)$ and $G(t)$ by

$$f(x)=\sum_{0}^{\infty}A_kU_k(x), G(t)=\sum_{0}^{\infty}B_nT_n(t) \tag{50}$$

from (45) and (47) it follows that

$$B_0=0, B_n=A_{n-1}, n=1,2,\ldots \tag{51}$$

The orthogonality relation

$$\frac{1}{\pi}\int_{-1}^{1}\frac{T_n(x)T_k(x)}{\sqrt{1-x^2}}dx=\begin{cases}0, n\neq k,\\ 1, n=k=0\\ 1/2, n=k>0,\end{cases} \tag{52}$$

and $T_0(x)=1$ insure that the single-valuedness condition (46) is identically satisfied. By using (47) and (41) for $|x|>0$, σ_{yy} may then be obtained as follows:

$$\frac{1+\kappa}{4\mu}\sigma_{yy}(x,0)=f(x)$$

$$=-\sum_{n=1}^{\infty}A_{n-1}\frac{(x-\sqrt{x^2-1})^n}{\sqrt{x^2-1}}, \ |x|>1. \tag{53}$$

Note that the function $(x^2-1)^{1/2}$ changes sign as x goes over the branch cut. For example, if $\sigma_{yy}(x,0)=-\sigma_0$, $(|x|<1)$ is the input, then from (50) it follows that $A_0=-\sigma_0(1+\kappa)/4\mu$, $A_k=0$, $(k>0)$ and with $a=1$ (53) reduces to the known solution (2).

In problems involving complex geometries and loading conditions, and having cracks embedded in homogeneous media, the governing system of singular integral equations may invariably be expressed in the following form

$$\frac{1}{\pi}\int_{-1}^{1}\sum_{j=1}^{n}\left[\frac{a_{ij}}{t-x}+k_{ij}(x,t)\right]g_j(t)\,dt$$

$$=f_i(x), \ |x|<1, (i=1,\ldots,n), \tag{54}$$

$$\int_{-1}^{1}g_i(t)\,dt=0, (i=1,\ldots,n), \tag{55}$$

where the constants a_{ij}, the kernels k_{ij}, and the input functions f_i, $(i,j=1,\ldots,n)$ are known. By using the simple technique described in the foregoing, the reduction of the system of integral equations (54) to a linear system of algebraic equations is relatively straightforward.

Perhaps a much simpler method of treating the singular integral equations numerically is the following. By substituting from (49) into (45) and by using again certain properties of Chebyshev polynomials [16] (see, also, Chapter 7 in [13]) it can be shown that

$$\frac{1}{\pi}\int_{-1}^{1}\frac{G(t)\,dt}{(t-x_i)\sqrt{1-t^2}}=\frac{1}{n}\sum_{k=1}^{n}\frac{G(t_k)}{t_k-x_i}, (i=1,\ldots,n-1),$$

$$T_n(t_k)=0, (k=1,\ldots,n),$$

$$U_{n-1}(x_i)=0, (i=1,\ldots,n-1), \tag{56}$$

provided the bounded function $G(t)$ can be represented by a polynomial of degree less than $2n$. Equations (45) and (46) may thus be reduced to a system of linear algebraic equations for the unknowns $G(t_k)$, $(k=1,\ldots,n)$ as follows:

$$f(x_i)\cong\frac{1}{n}\sum_{k=1}^{n}\frac{G(t_k)}{t_k-x_i}, (i=1,\ldots,n-1),$$

$$\int_{-1}^{1}\frac{G(t)}{\sqrt{1-t^2}}dt\cong\frac{\pi}{n}\sum_{k=1}^{n}G(t_k)=0. \tag{57}$$

Again, the extension of the technique to more complicated systems of singular integral equations is rather straightforward. From (15), (42), and (49) it is seen that $G(+1)$ and $G(-1)$ are directly related to the stress intensity factors at the crack tips.

Downloaded 02 May 2010 to 171.66.16.250. Redistribution subject to ASME license or copyright; see http://www.asme.org/terms/Terms_Use.cfm

4.4 The Alternating Method. The method is also known as Schwarz algorithm or successive approximations. It is developed for regions with several contours (e.g., a crack and a bounding surface) and is based on the idea that by solving the problem successively for the region with one contour at a time and varying (or correcting) the boundary conditions at each step, a useful approximate solution may be obtained after a sufficient number of steps (see, for example, Chapter 4 in [13] for applications and references).

4.5 Finite Element Method. For apparent reasons this is one of the most widely used methods in practice to calculate the stress intensity factors. In the so-called indirect method the stress intensity factor is obtained through extrapolation of or curve fitting to the values of a stress or a displacement component calculated at certain interior locations. In the direct method, special crack-tip elements are used and the stress intensity factors are directly calculated. The special elements developed for this purpose seem to be quite numerous among which one may mention the circular core element, the enriched element, the singular triangle, the quarter-point element, and specialized hybrid elements. In all these techniques the basic idea is to design the elements adjacent to the crack tip in such a way that the displacements are forced to vary according to the asymptotic distributions given by (12). The properly calculated local amplitudes would then give k_1 and k_2. Needless to say the literature on the subject is quite extensive. The review of the method with some applications may be found in Chapters 8 and 9 of [13].

There are, of course, other methods to solve the crack problems and to determine the stress intensity factors among which one may mention the methods of weight functions, boundary integral equations, curvilinear coordinates, and finite differences. One may also note that in certain problems such experimental techniques as the method of caustics and photoelasticity may prove to be quite effective in estimating the stress intensity factors. In particular, the three-dimensional photoelasticity (using frozen fringe technique) could be very useful in studying cracked structural components with a complex geometry.

5 Special Problems

In this section we briefly discuss the stress intensity factors in connection with certain special problems, again related to the fracture of solids.

5.1 Crack Problems in Elastodynamics. These are the problems in which, because of the high rates of loading or high crack velocities, it becomes necessary to take into account the inertia effects in formulating and solving the problem. These problems may generally be considered in two broad categories, namely that of stationary and propagating cracks. Conceptually the stationary crack problems are by far the simpler of the two. They require the solution of the wave equations in a solid containing a crack and subjected to certain initial, and boundary conditions. The basic feature of the stationary crack solutions is that the asymptotic behavior of the elastodynamic stress and displacement fields, too, are given by (11)–(14) with the only difference that the stress intensity factors now are functions of time. Variety of plane and axisymmetric crack problems have been solved under time-harmonic or standing waves and under impact type of loading. A rather fundamental result found for the impact problem is that for small values of time the time dependence of the stress intensity factors is parabolic [17, 18]. For example, in an infinite medium (under plane strain or antiplane shear conditions) containing a semi-infinite crack along the negative x axis and subjected to the following step loadings

$$\sigma_{yy}(x, 0, t) = -\sigma_0 H(t),\ \sigma_{xy}(x, 0, t) = -\tau_1 H(t),$$

or

$$\sigma_{yz}(x, 0, t) = -\tau_2 H(t),\ x<0,\ t>0, \tag{58}$$

the stress intensity factors are found to be [18]

$$k_1(t) = \frac{2\sqrt{2}}{\pi}\frac{c_R}{\sqrt{c_1 c_2}}\sigma_0\sqrt{c_2 t},\ k_2(t) = \frac{2\sqrt{2}}{\pi}\frac{c_R}{c_2}\tau_1\sqrt{c_2 t},$$

$$k_3(t) = \frac{2\sqrt{2}}{\pi}\tau_2\sqrt{c_2 t}, \tag{59}$$

where c_R, c_1, and c_2 are, respectively, the Rayleigh, the dilatational, and the shear wave velocities.

In the case of a finite crack, because of the arrival of the scattered Rayleigh and P waves from the opposite crack tip, generally the stress intensity factor versus time relations would contain discontinuous slopes [17]. For the incident wave front parallel to the crack, the dynamic "overshoot" is approximately 30 percent. An extensive review of the solutions of stationary crack problems obtained by analytical as well as the finite element and finite difference methods may be found in [18].

The second group of crack problems in elastodynamics concerns the propagating cracks. In this case the complexity of the problem lies largely in its physical description rather than the underlying mathematics. In running crack problems the length parameter representing the fracture surface is an additional unknown function. Theoretically the condition to account for this unknown is a fracture criterion which must be satisfied under dynamic conditions. In this case, too, the energy balance theory appears to provide a physically sound criterion if a continuum approach is followed to treat the problem. This requires that the basic energy balance relation (1) be modified as follows:

$$\dot{U} - \dot{V} - \dot{T} = \dot{D} \tag{60}$$

where $\dot{U}$, $\dot{V}$, $\dot{T}$, and $\dot{D}$ are, respectively, the rate of external work, strain energy, kinetic energy, and dissipative energy (which may include plastic work, surface tension, and other dissipative forms). The main difficulty in elastodynamic crack propagation problems lies in the characterization of the material with regard to its dynamic fracture resistance $\dot{D}$ which, apparently is not simply a velocity-dependent quantity.

The analytical research in the field is concentrated on the behavior of the stress and deformation states around the crack tip and on the solution of running crack problems to calculate the energy available for fracture, which is the left-hand side of (60). To solve these problems a crack velocity rather than a fracture criterion is generally assumed beforehand. A review of the basic results, a summary of most of the available solutions, and extensive references may be found in [19], [20], and [18], respectively.

The essential difference between the asymptotic fields obtained from the stationary and running cracks is in the angular distribution of stresses and displacements around the crack tip. For the running cracks the in-plane stress components, for example, have the form [20]

$$\sigma_{ij} \cong \frac{K_I(t)}{\sqrt{2\pi r}}F_{ij}^{I}(\theta, v) + \frac{K_{II}(t)}{\sqrt{2\pi r}}F_{ij}^{II}(\theta, v),\ (i, j) = (x, y) \tag{61}$$

where (r, θ) are again local polar coordinates. The bounded functions F_{ij}^{I} and F_{ij}^{II} (which for a stationary crack are identical to those given in (11)) are relatively complicated functions of θ and the crack velocity v as well as the

Downloaded 02 May 2010 to 171.66.16.250. Redistribution subject to ASME license or copyright; see http://www.asme.org/terms/Terms_Use.cfm

characteristic wave speeds c_1 and c_2. An interesting result found from the running crack solutions is that the functions F_{ij}^k depend on the instantaneous value of v only and is unaffected by the crack acceleration or deceleration [20].

From the viewpoint of applications, an important result found from the solution of running cracks is the fact that the energy available for fracture, $U^{\cdot} - V^{\cdot} - T^{\cdot}$ (in the entire solid) may be interpreted in terms of the rate of the crack closure energy and can be calculated from the stress intensity factors (see [19], [20], and Chapter 5 of [1] for alternate viewpoints leading to the same result). Thus, for example, for a crack propagating at an instantaneous velocity v under Mode *I* plane strain conditions it is found that [20]

$$U^{\cdot} - V^{\cdot} - T^{\cdot} = \frac{1+\nu}{E}\frac{v^3\sqrt{1-v^2/c_1^2}}{c_2^2 R}K_I^2, \tag{62}$$

$$R = 4\sqrt{(1-v^2/c_1^2)(1-v^2/c_2^2)} - (2-v^2/c_2^2)^2.$$

Some of the techniques regarding the application of the finite element method to running cracks and solutions of some specific problems may be found in [21].

5.2 Nonhomogeneous Materials. In studying the failure problems in fiber-reinforced, layered, particulate, and other composites the type of approach one may have to follow would generally depend on the size of flaws relative to the length parameters of the constituent materials. If the flaw size is of the same order or smaller than the characteristic length parameters of the composite medium, then the problem must be treated as one of nonhomogeneous elastic medium with isotropic constituents. On the other hand, if the flaw is large compared to the local length parameters of the medium and if the medium has an ordered structure, then the problem may be treated as one of anisotropic medium with a macroscopic flaw. In both cases the flaws are usually fatigue-sharpened imperfections and, for purposes of failure analysis, are treated as cracks.

In nonhomogeneous elasticity problems, as long as the crack remains fully embedded in a homogeneous constituent, neither the singular behavior of the results nor the method of solution would be different from those of the elastic crack problems in homogeneous isotropic materials. However, if the crack intersects the bimaterial boundary the singular behavior of the stress state may be quite different than the isotropic results. As a very simple example consider the antiplane shear (Mode *III*) problem for two bonded elastic half planes with shear moduli μ_1 and μ_2. Let the material 1 contain a crack of length b which is perpendicular to and touches the interface. Assume that the self-equilibrating crack surface shear traction $\tau_{yz}(x, 0) = g(x)$, $(0<x<b)$ is the only external load acting on the medium. By using the integral transforms the problem may be formulated and reduced to the following integral equation in a relatively straightforward manner:

$$\frac{1}{\pi}\int_0^b \left(\frac{1}{t-x}+\frac{\lambda}{t+x}\right)f(t)\,dt = \frac{2}{\mu_1}g(x),\ 0<x<b, \tag{63}$$

$$\int_0^b f(t)\,dt = 0,\ \lambda = (\mu_1-\mu_2)/(\mu_1+\mu_2), \tag{64}$$

$$f(x) = \frac{\partial}{\partial x}[w_1(x,+0) - w_1(x,-0)]. \tag{65}$$

Note that in (63) the second term in the kernel becomes unbounded as x and t tend to the end point zero and, since its degree is the same as the Cauchy kernel, namely x^{-1}, it is also expected to contribute to the singular behavior of the solution. Let us assume that the solution of (63) is of the form

$$f(x) = F(x)(b-x)^{\alpha}x^{\beta},\ 0<x<b,\ -1<Re(\alpha,\beta)<0, \tag{66}$$

where $F(x)$ is a bounded function, and define

$$\phi(z) = \frac{1}{\pi}\int_0^b \frac{f(t)}{t-z}dt. \tag{67}$$

Substituting from (66) into (67), the following asymptotic relations may be obtained [16]

$$\frac{1}{\pi}\int_0^b \frac{f(t)}{t-x}dt = \frac{1}{2}[\phi^+(x)+\phi^-(x)] = -F(0)b^{\alpha}\cot\pi\beta\, x^{\beta} + F(b)b^{\beta}\cot\pi\alpha(b-x)^{\alpha} + G_1(x),$$

$$\frac{1}{\pi}\int_0^b \frac{f(t)}{t+x}dt = \phi(-x) = -F(0)b^{\alpha}\frac{1}{\sin\pi\beta}x^{\beta} + G_2(x),\ 0<x<b, \tag{68a, b}$$

where G_1 and G_2 are bounded functions. If we now substitute from (68) into (63), multiply both sides first by $(b-x)^{-\alpha}$, and let $x\to b$, then by $x^{-\beta}$ and let $x\to 0$, we obtain the following characteristic equations to determine α and β:

$$\cot\pi\alpha = 0,\ \cos\pi\beta = -\lambda,\ (-1<Re(\alpha,\beta)<0) \tag{69a, b}$$

giving $\alpha = -1/2$, $\beta = -|\cos^{-1}(-\lambda)|/\pi$. It is seen that we have $-1<\beta<-1/2$ for $\mu_1>\mu_2$ and $-1/2<\beta<0$ for $\mu_1<\mu_2$, that is, depending on the stiffness ratio, the power of singularity may be stronger or weaker than the homogeneous case.

The formulation of the problem also gives the cleavage shear in medium 2 as follows:

$$\tau_{yz}^2(x,0) = \frac{\mu_1\mu_2}{\mu_1+\mu_2}\frac{1}{\pi}\int_0^b \frac{f(t)}{t-x}dt,\ -\infty<x<0. \tag{70}$$

If we now observe that $x<0$ is outside the branch cut and $\sin\pi\beta = -\sqrt{1-\lambda^2}$, $\tau_{yz}^2(x,0)$ may be expressed as

$$\tau_{yz}^2(x,0) = \frac{\sqrt{\mu_1\mu_2}}{2\sqrt{b}}F(0)(-x)^{\beta}+0(1),\ x<0,\ (-1<\beta<0). \tag{71}$$

Stress singularities of powers other than $-1/2$ as in (71) are often encountered in crack problems for nonhomogeneous materials. In such cases the coefficient in the singular term may still be defined as the "stress intensity factor." For example, in the problem under consideration, from (71) the Mode *III* stress intensity factor at the crack tip $x=0$ may be defined as

$$k_3(0) = \lim_{x\to 0}(-x)^{-\beta}\tau_{yz}^2(x,0) = \frac{\sqrt{\mu_1\mu_2}}{2\sqrt{b}}F(0). \tag{72}$$

The general method for treating the crack problems with such unconventional singularities, fairly extensive references, and the description of numerical techniques (based on Gauss-Jacobi type integration formulas) for solving the related integral equations with generalized Cauchy kernels such as (63) may be found in [16]. One should note that if the crack is embedded into a nonhomogeneous medium with smoothly varying elastic properties the square root nature of the stress singularity seems to remain unchanged. As indicated by the simple example given in this section, a discontinuity in the elastic constants would cause a change in the $-1/2$ singularity. At this point the effect of simply a discontinuous slope in the elastic constants on the stress singularity does not seem to have been investigated.

5.3 Anisotropic Materials. For rectilinearly anisotropic homogeneous materials containing a macroscopic crack the results do not seem to contain any surprises. The square root singularity is maintained and generally the problem may be formulated and solved by following the same methods used for the isotropic materials (see, for example, Chapter 2 in [1]).

Downloaded 02 May 2010 to 171.66.16.250. Redistribution subject to ASME license or copyright; see http://www.asme.org/terms/Terms_Use.cfm

However, unconventional singularities may exist in cylindrically anisotropic materials if the crack tip is at the axis of anisotropy [22].

5.4 Three-Dimensional Surface Crack. In three-dimensional problems for homogeneous elastic solids that contain a fully embedded crack bounded by a smooth plane curve, the difficulties appear to be computational rather than conceptual. Modes *I*, *II*, *III* stress states and the corresponding stress intensity factors are well understood from the closed-form solutions of internal or external cracks with an elliptic periphery (see, for example, Chapter 2 in [1]). Particularly for finite domains, the analytical treatment of the problem is difficult and the reliable solutions seem to be mostly that of finite elements. For the internal cracks the unresolved theoretical questions concern the nature of the solution for nonplanar cracks and cracks with "kinked" boundaries. These are, of course, also critical questions in surface cracks where additional complications arise from the existence of the traction-free boundary.

In three-dimensional surface cracks the problem of somewhat more practical and of a great deal of theoretical interest is the nature of stress singularity at the point of intersection of the crack boundary and the free surface of the solid. The problem does not appear to lend itself to rigorous analytical treatment through either a direct asymptotic analysis or function-theoretic methods (via the related integral equations) as was done, for example, in [6] and [14] for plane problems. The problem was considered by Benthem for an elastic half space $z>0$ which contains a semi-infinite crack along the quarter plane $y=0$, $x>0$ (see [23] for the results and references to other studies). Using the spherical coordinates (r, θ, ϕ) Benthem assumed an asymptotic stress field of the form

$$\sigma_{ij}=r^{\lambda}f_{ij}(\lambda, \theta, \phi), (i, j=x, y, z) \tag{73}$$

where the condition of boundedness of strain energy requires that the acceptable eigenvalues λ_n be greater than $-3/2$. He further assumed the functions f_{ij} to be separable. The main difficulty in this problem is that the boundary conditions cannot be satisfied exactly by the resulting solutions and, therefore, the characteristic equation giving the eigenvalues λ_n has to be obtained by writing the determinant of an infinite system equal to zero. In his first paper Benthem solved the problem by truncating the system. In his second paper he used a finite difference scheme to calculate the eigenvalues (in order to independently verify his earlier results and to allay doubts about the separability of the solution[4]). Benthem's results appear to be sufficiently accurate and show that for $0\le\nu\le0.5$ the power of stress singularity λ_1 (the dominant acceptable eigenvalue) varies as $-0.5\le\lambda_1\le-0.3318$ for the symmetric or Mode *I* loading and as $-0.5\ge\lambda_1\ge-0.6462$ for the antisymmetric (i.e., for Modes *II* and *III* loading. Thus the stress intensity factors along the z axis defined on the basis of $-1/2$ power singularity would have the behavior $k_1\to0$, $k_2\to\infty$ and $k_3\to\infty$ for $z\to0$.

In addition to finite elements, the alternating method has been used to obtain the stress intensity factors in three-dimensional crack problems involving stress-free boundaries [13]. However, a neat analytical formulation of the problem suitable for a relatively clean method of solution still seems to be missing.

5.5 Plates and Shells. In plate and shell structures containing a through crack, if the crack length is relatively large compared to the thickness, then the essentially three-dimensional crack problem may be simplified considerably by using a bending theory of plates or shells. In plates, membrane and bending problems may be treated separately. Because of curvature the shell problem is coupled. Depending on the nature of the theory, the thickness distribution of the stress intensity factors is predetermined (e.g., in the simpler theories used in most solutions it is linear in z). Most of the existing solutions are based on either the "classical" theory (in which the transverse shear and the twisting moment are combined on the boundary, including the crack surface, through a Kirchhoff-type assumption) or Reissner's transverse shear theory. The asymptotic results at the crack tip obtained from the latter are identical to the in-plane and antiplane elasticity solutions given by (11)–(14), whereas there are some discrepancies between the classical results and (11)–(14). Also, as in the three-dimensional surface crack problems, if Reissner's theory is used, the Mode *I* solution can be separated by properly decomposing the external loads with respect to the plane of the crack. Again, as in three-dimensional problems, Modes *II* and *III* are always coupled regardless of the nature of the skew-symmetric external loads. For example, tensile membrane loads perpendicular to the crack gives only Mode *I* stress state with $k_1\neq0$, $k_2=k_3=0$. On the other hand, membrane shear loading of the plate or the shell would give Mode *III* as well as Mode *II* stress states with $k_1=0$, $k_2\neq0$, $k_3\neq0$. The description and the solution of the general problem for shells containing a crack and relevant references may be found in [24].

6 Further Remarks

In a general sense the stress intensity factor is the counterpart of stress concentration factor in notched solids. In the case of notches it is known that the maximum stress at the notch root is given by

$$\sigma=K\sigma_0=\frac{A}{\sqrt{\rho}}\sigma_0, \tag{74}$$

where K is the (dimensionless) stress concentration factor, A is a constant, ρ is the notch root radius, and σ_0 is a nominal stress representing the magnitude of external loads. Note that as $\rho\to0$, σ tends to infinity. In this limiting case near the notch root, the stress may be expressed as

$$\sigma\cong\frac{k}{r^{\alpha}}, \tag{75}$$

where $0<\alpha<1/2$ for $\pi<\theta<2\pi$ (θ being the wedge angle around the apex), k is a constant, and r is the distance from the notch root. Clearly, at the notch root the stress is singular and one may again interpret k as a "stress intensity factor." Even though in homogeneous materials α is always real, in nonhomogeneous wedges α can be complex.

Finally, it should be noted that the contact problems involving elastic solids with sharp corners may be formulated in terms of integral equations that are essentially the same as those obtained from the crack problems, the end points (or the boundary) of the contact area are points of stress singularity, and again the stress state at these locations can be described in terms of a power α of stress singularity and a "stress intensity factor" k.

References

1 Liebowitz, H., ed., *Fracture*, Vol. 2, Academic Press, New York, 1968.

2 Sneddon, I. N., "The Distribution of Stress in the Neighborhood of a Crack in an Elastic Solid," *Proc. Roy. Soc. London*, Series *A*, Vol. 187, 1946, pp. 229–260.

[4] Generally, the results have also been confirmed by Bazant's work who used the method of finite element [23].

Downloaded 02 May 2010 to 171.66.16.250. Redistribution subject to ASME license or copyright; see http://www.asme.org/terms/Terms_Use.cfm

3 Westergaard, H. M., "Bearing Pressures and Cracks," JOURNAL OF APPLIED MECHANICS, Vol. 61, 1939, pp. A49–53.

4 Irwin, G. R., "Analysis of Stresses and Strains Near the End of a Crack Traversing a Plate," JOURNAL OF APPLIED MECHANICS, Vol. 24, 1957, pp. 361–364.

5 Irwin, G. R., "Fracture Mechanics," *Structural Mechanics*, Goodier, J. N., and Hoff, N. J., eds., Pergamon Press, New York, 1960, pp. 557–591.

6 Williams, M. L., "On the Stress Distribution at the Base of a Stationary Crack," ASME JOURNAL OF APPLIED MECHANICS, Vol. 24, 1957, pp. 109–114.

7 Brown Jr., W. F., ed., *Review of Developments in Plane Strain Fracture Toughness Testing*, ASTM STP 463, 1970.

8 Rolfe, S. T., and Barsom, J. M., *Fracture and Fatigue Control in Structures*, Prentice Hall, Englewood Cliffs, N.J., 1977.

9 Paris, P. C., and Erdogan, F., "A Critical Analysis of Crack Propagation Laws," ASME *Journal of Basic Engineering*, Vol. 85, 1963, pp. 528–534.

10 Bradt, R. C., Hasselman, D. P. H., and Lange, F. F., eds., *Fracture Mechanics of Ceramics*, Vols. 1 and 2, Plenum Press, New York, 1973.

11 Fong, J. T., ed., *Fatigue Mechanisms*, ASTM STP 675, 1979.

12 Curran, R. M., ed., *ASME-MPC Symposium on Creep Fatigue Interaction*, MPC-3, ASME, New York, 1976.

13 Sih, G. C., ed., *Methods of Analysis and Solutions of Crack Problems*, Noordhoff, Leyden, 1973.

14 Muskhelishvili, I. N., *Some Basic Problems of the Mathematical Theory of Elasticity*, P. Noordhoff Ltd., Groningen-Holland, 1953.

15 Sneddon, I. N., and Lowengrub, M., *Crack Problems in the Classical Theory of Elasticity*, Wiley, New York, 1969.

16 Erdogan, F., "Mixed Boundary Value Problems in Mechanics," *Mechanics Today*, Nemat-Nasser, S., ed., Vol. 4, Pergamon Press, New York, pp. 1–81.

17 Thau, S. A., and Lu, Tsin-Hwei, "Transient Stress Intensity Factors for a Finite Crack in an Elastic Solid Caused by a Dilatational Wave," *Int. J. Solids Structures*, Vol. 7, 1971, pp. 731–750.

18 Sih, G. C., ed., *Elastodynamic Crack Problems*, Noordhoff, Leyden, 1977.

19 Achenbach, J. D., *Dynamic Effects in Brittle Fracture, Mechanics Today*, Nemat-Nasser, S., ed., Vol. 1, Pergamon Press, New York, 1–57.

20 Freund, L. B., "The Analysis of Elastodynamic Crack Tip Stress Fields," *Mechanics Today*, Nemat-Nasser, S., ed., Vol. 3, Pergamon Press, 1976, pp. 55–91.

21 Perrone, N., and Atluri, S. N., eds., *Nonlinear and Dynamic Fracture Mechanics*, AMD-Vol. 35, ASME, New York, 1979.

22 Delale, F., Erdogan, F., and Boduroglu, H., "Stress Singularities at the Vertex of a Cylindrically Anisotropic Wedge," *Int. J. of Fracture*, Vol. 19, 1982, pp. 247–256.

23 Benthem, J. P., "The Quarter-Infinite Crack in a Half Space; Alternative and Additional Solutions," *Int. J. Solids Structures*, Vol. 16, 1980, pp. 119–130.

24 Yahsi, O. S., and Erdogan, F., "A Cylindrical Shell With an Arbitrarily Oriented Crack," *Int. J. Solids, Structures*, Vol. 19, 1983.

Downloaded 02 May 2010 to 171.66.16.250. Redistribution subject to ASME license or copyright; see http://www.asme.org/terms/Terms_Use.cfm

On the Foundations of Biomechanics

Y. C. Fung
Department of Applied Mechanics and Engineering Science, University of California, San Diego
La Jolla, Calif. 92093
Fellow ASME

After a brief survey of the present status of the vast field, a more concentrated review is presented on some issues concerning the foundations of biomechanics. The mechanical properties of living tissues, or their mathematical expressions, i.e., the constitutive equations, are discussed in some detail. Future prospects are considered. The expanding domain of biomechanics is surveyed, and new guideposts – the recently published books, are listed.

Introduction

The field of biomechanics received vigorous cultivation and development in recent times. Fifteen or 20 years ago there were only a few authors writing occasional papers on the subject. Now many journals and books on the subject are published every year. When the U.S. National Committee for Biomechanics was formed in the Spring of 1982, its membership included 20 professional societies in this country. Examples are ASME, ASCE, AIChE, Biomedical Engineering Society, Orthopedic Research Society, Alliance of Engineering in Medicine and Biology, American Orthopedics Society for Sports Medicine, American Physical Society, American Physiological Society, American Society for Artificial Internal Organs, American Society of Biomechanics, American Society for Engineering Education, Microcirculatory Society, Society of Automotive Engineers, and Society of Rheology. Each of these societies has members interested in biomechanics, and considers biomechanics its business. The breadth of this field is thus very clear. The vitality is evident. Expectation for useful applications in the future is high. The National Committee hopes to speak for the common interest of all the member societies.

Biomechanics is mechanics applied to biology. Therefore, it is applied mechanics. But it is also biology, medicine, surgery, physical education, sports, rehabilitation, prosthesis, robots, health-related industrial problems, automobile and aircraft safety, trauma, manned space flight, etc. These fields have problems to be solved: they enrich mechanics, they define the structure of boundary-value problems, and they mold trends of research.

Twenty years ago, we could claim a rich heritage in biomechanics from such classical works as Giovanni Borelli's analysis of animal locomotion, Leonhard Euler's analysis of pulse waves, Thomas Young's analysis of hearing, vision, and blood flow, Jean Poiseuille's experiments on flow of blood in cylindrical tubes, Herrmann von Helmholtz's theory of sensation of tone and colors, the theories and experiments of pulse wave propagation by Diederik Korteweg, Horace Lamb, Otto Frank, John Womersley, Donald MacDonald, and Michael Taylor, and simulation of the heart by Balthasar van der Pol (see Bibliography in reference [18]). But in most of these papers blood is treated as water (i.e., Newtonian) and tissues are treated as solids obeying Hooke's law of elasticity. It is not that the savants did not know better, but data on mechanical properties of biological tissues did not exist.

Now the mechanical properties of living tissues are studied in laboratories all over the world, and the constitutive equations are gradually becoming known. Biomechanics can now approach its problems realistically.

But biomechancis deals with living materials, and living materials have a major property that has no counterpart in all of the materials in other branches of engineering: namely, the capability to grow and to resorb. Living tissues can change their dimensions, or, sometimes, mechanical properties. These changes are often regulated by stresses, as well as by biochemical processes. The effect is that the strain and stress fields in a living organism can change with time. This marvelous property, which is essential to life, does confuse mechanics. Because of this effect, we cannot be certain about the residual stresses in organs (i.e., the stresses that remain when all the external loads are removed). Unless a new principle is found, which tells us how residual stresses in tissues of an organ can be found, we will not be able to determine the stress distribution in organs. The searching of such a principle is a topic of the supreme interest.

The field of biomechanics is vast. Every direction you look, you will find basic problems and possible new applications. From the point of view of mechanics, we may list the issues of biomechanics as follows:

Biomechanics of the Future

Foundation

Structure of materials of living organisms.
Constitutive equations.
New concepts and methods: Growth and repair, strength and tolerance, new mathematical approach, new instruments.

Contributed by the Applied Mechanics Division for publication in the JOURNAL OF APPLIED MECHANICS.
Discussion on this paper should be addressed to the Editorial Department, ASME United Engineering Center, 345 East 47th Street, New York, N.Y. 10017, and will be accepted until two months after final publication of the paper itself in the JOURNAL OF APPLIED MECHANICS. Manuscript received by ASME Applied Mechanics Division, February, 1983.

Copyright © 1983 by ASME
Downloaded 02 May 2010 to 171.66.16.250. Redistribution subject to ASME license or copyright; see http://www.asme.org/terms/Terms_Use.cfm

Applications

Biomechanics in diagnosis.
Biomechanics in treatment.
Health and fun: sports, body development, longevity, rehabilitation.
Important problems of society: Such as safety in war and peace, highway and air traffic, survival and response to environmental changes.

Industrial problems:

Biomechanical engineering
Genetic engineering
Prosthetic devices, medical and surgical instruments.

Agriculture:

Plants, fruits, preservation, shipping.

Forestry
Animal husbandry, veterinary medicine.

Organ Systems of Man, Animals, or Plants

Circulatory and lymphatic
Respiratory
Musculoskeletal
Digestive
Urinary
Nervous
Endocrine
Sensory
Reproductive
Whole body integration

I say that this is a list for the future because at the present time only a few items have received sufficient attention. While some areas are well cultivated, others are still barren. But the vastness of the field is clear. The division of foundations from applications is somewhat arbitrary. One cannot solve any applied problems without dealing with fundamental issues. And the foundations are constantly changing as the domain of application expends. Finally, all issues of foundations and applications can be grouped under various organ systems. Each organ is different, but they all share the same fundamental issues.

It would be far beyond my ability to review the whole field. Even within the few areas I know a little about it would not be useful to cover too many topics because it would necessarily be too brief and shallow. Therefore, in the following I will discuss only a few issues on foundations.

2 Identification of Constitutive Equations of Biological Materials

Biomechanics cannot be developed without the constitutive equations of the materials. Identification of the constitutive equations of living tissues has been a major activity in recent years; and it is one of considerable achievement. The mechanical properties of living tissues are rather different from those of the familiar engineering materials. A few concrete examples will illustrate the situation:

Blood. Blood is an incompressible non-Newtonian fluid in ordinary circumstances. If blood is tested in a Couette viscometer or a cone-plate viscometer, it is found that in steady flow the coefficient of viscosity is higher if the shear gradient is smaller. The shear stress τ is related to the shear strain rate $\dot{\gamma}$. The relationship is approximated by Casson's equation [10]

$$\sqrt{\tau}=\sqrt{\tau_y}+\sqrt{\eta\dot{\gamma}} \tag{1}$$

where τ_y and η are constants. τ_y has the significance of a yield stress. η is called Casson's coefficient of viscosity. This relation reflects the deformability of red blood cells in shear flow, and the ability of red cells to stick to each other and from a spatial structure when the shear gradient decreases.

Generalizing equation (1) to a stress-strain law, we may write [18]

$$\sigma_{ij} = -p\delta_{ij} + 2\mu\,(J_2)V_{ij} \tag{2}$$

where σ_{ij} is the stress tensor, V_{ij} is the strain rate tensor, p is the pressure, δ_{ij} is the Kronecker delta, and μ is a function of the strain rate invariant J_2:

$$\mu(J_2) = [(\eta^2 J_2)^{1/4} + 2^{-1/2}\tau_y^{1/2}]^2 J_2^{-1/2}. \tag{3}$$

where J_2 is related to V_{ij} and the velocity vector v_i as follows:

$$J_2 = \frac{1}{2}\,V_{ij}V_{ij}, \quad V_{ij} = \frac{1}{2}\,(v_{i,j} + v_{j,i}) \tag{4}$$

If τ_y is taken to be a yield stress literally, then these equations must be supplemented by a yield rule, and an elastic stress-strain relationship below yielding. But it is quite possible that the concept of yielding is only a mathematical idealization, and the real process is much more complex. Equation (2) does not account for the normal stress due to shear, nor other viscoelastic features of blood which exist but whose significance has not yet been demonstrated.

Red Blood Cells. Red blood cells are very thin-walled shells filled with hemoglobin solution which in normal blood is a Newtonian fluid with a viscosity of about 6 cp. In flowing through capillary blood vessels the red cells are severely deformed. When stationary, however, the cells assume a regular shape of a biconcave circular disk (a circular disk with a reduced thickness at the center). Human red cells have an average diameter of about 7.8 μm, a thickness of about 2 μm, and a wall (cell membrane) thickness of about 0.005 μm.

Theoretically, a thin-walled biconcave disk cannot sustain a finite transmural pressure if the bending rigidity of the wall can be neglected. Since the cell membrane is very thin, the transmural pressure must vanish and the membrane unstressed in biconcave configuration. (See reference [18] for details and bibliography.) A liquid filled biconcave disk can be deformed into a large variety of other shapes through isometric transformation. Such a transformation changes one surface into another surface without tearing and without stretching; hence without strain, and without stress. Thus the red cells may be considered as having been designed (by having a biconcave disk as its natural shape) to withstand a variety of large deformations without inducing any membrane stresses. This remarkable flexibility without being stressed may be the secret of the durability of the red cells in their strenuous courses through the microcirculation.

By testing red blood cells in the *off-design* conditions which cause membrane strains and stresses, one can determine the mechanical properties of the cell membrane. Through many years of research (see references [18] and [16] for bibliography) we know that red blood cell membranes are deformable, can be stretched uniaxially several hundred percent, but its area cannot be changed more than 3 or 4 percent without beaking it. The constitutive equations for the cell membrane may be written as follows [18, modified from Evans and Skalak, 16]:

$$N_1 = K(\lambda_1\lambda_2 - 1) + \mu(\lambda_1^2 - \lambda_2^2) \tag{5a}$$

$$N_2 = K(\lambda_1\lambda_2 - 1) + \mu(\lambda_1^2 - \lambda_2^2) \tag{5b}$$

in which N_1, N_2 represent the principal stress resultants in the cell membrane, λ_1, λ_2 are the principal stretch ratios, K is an elastic modulus for cell membrane area change, and μ is an elastic modulus relating shear stress and shear strain. The

Downloaded 02 May 2010 to 171.66.16.250. Redistribution subject to ASME license or copyright; see http://www.asme.org/terms/Terms_Use.cfm

unique feature of red cell membrane is that K is about four orders of magnitude larger than μ:

$$K \sim 10^4 \mu \tag{6}$$

Blood Vessels. All living tissues work in normal in vivo condition at stress levels far below their ultimate strength. In pathology or strength studies (as in problem of human tolerance to car crash) one must study yielding, tearing, fracture, strength, and failure. In the study of physiology one may limit oneself to lower stress levels. Tissues are more thoroughly studied in physiological condition, and the following remarks are limited to this range.

All living tissues are pseudoelastic; that is, they are not elastic, but under periodic loading, a steady-state stress-strain relationship exists that is not very sensitive to strain rate. The loading and unloading branches can be treated separately, and a pseudoelastic potential can be introduced to describe the stress-strain relationship in either loading or unloading. The elastic potential $\rho_0 W$ is a function of the Green's strain components E_{ij}. The partial derivative of $\rho_0 W$ with respect to E_{ij} gives the corresponding stress S_{ij} (Kirchhoff stress). W is defined for unit mass of the vessel wall, ρ_0 is the density in the initial state, hence $\rho_0 W$ is the strain energy per unit initial volume. For arteries and veins subjected to stresses and strains in the physiological range, the pseudostrain energy functions are of the form [22]

$$\rho_0 W^{(2)} = C \exp\left[a_1 E_1^2 + a_2 E_2^2 + 2a_4 E_1 E_2\right] \tag{7}$$

Here the superscript (2) over $\rho_0 W$ signifies that this is a two-dimensional approximation, treating the arterial wall as a membrane, ignoring the radial stress, with subscript 1 referring to the circumferential direction, and 2 referring to the longitudinal direction. Comparison of equation (7) with other proposed strain energy functions such as polynomials is discussed in detail in [22]. A polynomial strain energy function proposed by patel and Vaishnav ([43]) is especially well known.

Skin. The skin is an anisotropic material. Treated as a membrane, the two-dimensional pseudostrain energy function for the skin in the physiological range of stresses and strains [35, 51] is

$$\rho_0 W^{(2)} = \frac{1}{2}\left[\alpha_1 E_1^2 + 2\alpha_4 E_1 E_2 + \alpha_2 E_2^2\right]$$

$$+ \frac{1}{2} C \exp\left[a_1 E_1^2 + a_2 E_2^2 + 2a_4 E_1 E_2 + E_1 E_2(\beta_1 E_1 + \beta_2 E_2)\right], \tag{8}$$

where C, a's, α's, and β's are constants. The β terms may be omitted without significant sacrifice of accuracy.

Bone. The bone functions at a strain so small that the classical linearized theory of elasticity is sufficiently accurate for most problems concerning stress distribution. But the structure of the bone is very complex, and the mechanical property is nonhomogeneous. Hence the identification of mechanical property with bone structure remains a challenging problem. Recent advances in this regard have been very impressive. Combining a detailed study of morphology, material testing, and finite elements method, Hayes and other authors have made close correlation between bone structure and mechanical properties. See literature cited in [13, 18, 24].

Cartilage. Cartilages have remarkable mechanical properties which make joints function marvelously. It has unique lubrication qualities. Savio Woo and others have clarified the constitutive equation of cartilage. Van Mow and others have studied cartilage as a two-phase material (solid phase and liquid phase), thereby successfully explaining its mechancial and lubricative behavior. See references in [18].

Other Biological Tissues – Muscles. In the foregoing we presented some typical constitutive equations of biomaterials. These examples convey the impression that biomaterials are complex; but there is also a unifying simplicity. For example, most of the soft tissues are exponentially stiffening. For certain purpose of biomechanical analysis it is sufficient to know these general features. For other purposes, especially for clinical application, it is necessary to know the details of the mechanical properties.

Of all the constitutive equations in biomechanics, that of the muscle must be one of the most important. Without a constitutive equation for the active contraction of the heart muscle we cannot build a rigorous theory of cardiology. Without the constitutive equations for the vascular smooth muscle, we cannot develop a mathematical theory of circulatory regulation and control. Similarly, for theories of other internal organs we need the constitutive equations of their smooth muscles. Yet reliable constitutive equations for these muscles are not yet available! There is a huge literature, a large number of investigators, a lot of controversy, but no unchallenged success. See, for example, [4, 5, 18]. Hence, looking toward the future, I would say that the clarification of the constitutive equations of the muscles is the key to future development of biomechanics.

3 Understanding Mechanical Properties of Organs

The unique mechanical properties of living tissues demand an explanation. A scientific explanation not only satisfies intellectual curiosity, but it also suggests applications and brings the knowledge closer to practical utility.

One direction of research in this regard is to study the ultrastructure of the tissues, and try to put together a theory of the mechanical properties on its basis. One of the most spectacular successes in this direction is the "sliding-element" theory of contraction of the skeletal muscle, conceived and published almost simultaneous by two Huxley's, Andrew F. and Hugh E. [31, 32]. Other successes, less spectacular, appear frequently, and they add to our understanding of the living tissues.

Another direction of research is to study the mechanical properties of the organ, as opposed to the individual tissues that make up the organ. For physiology it is the mechanical properties of the organ that is needed. Here the scale of things is either microscopic or macroscopic.

The great variety of things in the biological world is a source of pleasure to biomechanical investigators. The search for common features that are shared by things very different in appearance or composition is important, because they unify and simplify our understanding of nature. The search for constitutive equations is of this nature. But sometimes things appear similar but behave differently. The understanding or explanation of these differences is equally important. For example, all blood vessels serve the same purpose: They carry blood to where it is needed. Under the microscope the structures of systemic and pulmonary vessels are similar. Yet mechanicaly all blood vessels do not behave the same way, as the following summary shows:

(*a*) Aorta, arteries, veins of systemic circulation:

The stress-strain relationship is nonlinear. When the stress is low the vessel is very compliant. Compliance decreases with increasing stress. Stress grows exponentially with increasing strains.

Downloaded 02 May 2010 to 171.66.16.250. Redistribution subject to ASME license or copyright; see http://www.asme.org/terms/Terms_Use.cfm

(*b*) Pulmonary arteries and veins:

The pressure-diameter relationship is almost linear. The stress-strain relationship is, therefore, also almost linear.

(*c*) Capillary blood vessels in the mesentery, kidney, and most tissues:

Essentially rigid. Little measurable change in diameter when blood pressure varies in physiological range.

(*d*) Pulmonary capillaries:

Very compliant. Diameter increases linearly with increasing blood pressure when blood pressure is larger than the alveolar gas pressure.

(*e*) Systemic vessels, such as vena cava, brachial artery, etc., readily collapse when blood pressure falls below the external pressure.

(*f*) In an inflated lung, pulmonary vessels, including all veins and venules, do not collapse when local blood pressure falls below alveolar gas pressure external to the vessels.

All these apparently diverse properties can be explained on the basis of the support the vessels receive from the surrounding tissues. For example, to explain item (*a*), we note that peripheral vessels, when isolated and surrounded by fluid, reveal large compliance at low stress level because elastin and smooth muscles are very compliant and collagen fibrils are coiled and do not take up much stress. At higher stress levels the collagen fibers are gradually straightened and take up more and more of the load. If we roughly characterize the normal stress S in the vessel wall as equal to the number, per unit cross sectional area, N, of fibers that are stretched and carrying a force, f; then $S = Nf$. In a blood vessel, the stress increases exponentially with increasing strain $E_{\theta\theta}$. This is consistent with the assumption that the collagen fibers are recruited (strengthened) at a rate proportional to the number of existing straightened fibers:

$$\frac{d(Nf)}{dE_{\theta\theta}} = a_1(Nf) + a_2 \tag{9}$$

where a_1, a_2 are constants. More exactly, if the strain energy depends on a quadratic function of strain

$$Q = a_1 E_{\theta\theta}^2 + a_2 E_{zz}^2 + 2a_4 E_{\theta\theta} E_{zz} \tag{10}$$

and if the rate of change of strain energy is equal to the current value of the strain energy, so that

$$\frac{d\rho_0 W^{(2)}}{dQ} = \rho_0 W^{(2)}, \tag{11}$$

then an integration yields

$$\rho_0 W^{(2)} = ce^Q \tag{12}$$

which is exactly equation (7). This derivation is given in reference [18, p. 282]. It interprets item (*a*) in the foregoing.

Pulmonary blood vessels, however, are embedded in the lung tissue. Interalveolar septa are integrally attached to the blood vessel wall. In an inflated lung, these interalveolar septa are stretched so that the tissue is in tension. They are also acted on by surface tension due to the liquid-gas interface. Thus, the blood vessels are embedded in an elastic medium in tension. The linear behavior listed under item (*b*) is a result of this embedding. Experimental results show that this is true even for arterioles and venules whose diameter are much smaller than the diameter of the pulmonary alveoli. The reason is that each of these small vessels is tethered by three interalveolar septa, spaced roughly 120 deg apart, keeping the vessel open even when the local blood pressure falls below the alveolar gas pressure. This explains both items (*b*) and (*f*).

Similarly, the difference between the capillary blood vessels of the mesentery etc. (item (*c*)) and those of the lung (item (*d*)) is caused by the embedding of the vessels in a solid gel in the mesentery etc., whereas in the lung the pulmonary capillaries are exposed to gas on the outer wall, which offers little structural support.

Finally, the stability features named in items (*e*) and (*f*) can be explained by the lack of support from surrounding tissues in the case of vena cava, and the embedding in the case of pulmonary veins and venules.

This discussion brings out the fact that the mechanical properties of blood vessels depend not only on the material of the blood vessel wall, but also on the tissues surrounding the vessel, much as the behavior of an individual in the society depends on the environment.

This feature is pretty evident once it is pointed out. But it is a fact to remember when we consider the mechanical behavior of organs. It is important also to the analysis of the material properties in terms of the fine structure of the material. For example, collagen and elastin fibrils are curved. In a stress field tension in these fibers depends on the support they receive from the embedding medium: the ground substances. We can infer further, for example, that emphysema of the lung, a disease characterized by the degeneration of the alveolar walls, can be caused by changes of either collagen or elastin, or of the ground substances; such as proteglycans. If we knew exactly which one was the principal culprit we would be closer to finding a cure for the emphysema.

4 Collection of the Needed Data

The truly great task facing biomechanics now and in the future is to systematically collect the needed data on morphology, material properties, and functions. Knowing the principles is not enough, we must have a data base. Otherwise everything is fuzzy. Engineers are very proud of parameter survey, studying trends by varying parameters; but to survey parameters forever is very tiring, and cannot come to grips with real problems.

To name an example, let us consider the problem of blood flow. To analyze blood flow in any organ, we must know the size of the vessels, the way the circuit is put together, and the mechanical properties of every vessel in the system. But such a set of data did not exist for any organ of any animal for a long time. Only recently has a program for collecting such a set of data for the lungs of the cat been completed [57–59]. With this data a theoretical analysis of the blood flow through the lungs of the cat was done for the first time [60] with reasonable details and without having to resort to fictitious geometry and elasticity. The results can then be used to compare with the results of physiological experiments either to evaluate the theory, or to investigate other factors such as the nervous control, drug effects, etc. When a theory is well established, then it can be used clinically with confidence with the needed versatility.

Nobody objects to the collection of data. The question is who is going to do it. In the field of biomechanics, past exprience shows that the biomechanics research worker have to do it. They would have to be good anatomists, histologist, physiologists, in addition to being good applied mathematicians and experts in applied mechanics. Many have succeeded well, and made invaluable contributions. They deserve to be acclaimed, and encouraged to go further.

5 The Expanding Domain of Biomechanics

In recent years fine work appeared again and agian to expand the domain of biomechanics further and further. One of the earliest books published in this area is Donald MacDonald's book on blood flow in arteries, 1960 [38], which

Downloaded 02 May 2010 to 171.66.16.250. Redistribution subject to ASME license or copyright; see http://www.asme.org/terms/Terms_Use.cfm

summarizes extensive work by Womersley, Taylor, and others. Then Alan Burton's textbook *Physiology and Biophysics of Circulation*, 1965 [7] appeared, which exerted a considerable influence on medical education in America. The third edition of Robert Rushmer's *Cardiovascular Dynamics* appeared in 1970 [47]. These books were not written in the style of applied mechanics, because too little was known at the time to pursue the subject logically as the method of applied mechanics would have demanded. But they followed the reasoning of mechanics, and introducd refreshing simplicity and logic into complex subject of physiology. In 1968 Wetterer and Kenner's book *Grundlagen der Dynamik des Arterienpulses* [53] appeared. In 1972, D. H. Bergel edited a collective work of 21 authors entitled *Cardiovascular Fluid Dynamics* [3], and Fung, Perrone, and Anliker edited a volume entitled *Biomechanics: Its Foundations and Objectives*, a collection of 23 chapters by 28 authors [21]. These volumes hold mechanics as the main line of inquiry. The last mentioned reference, as its subtitle indicates, aims particularly at stating the objectives and clarifying the foundations of the subject. About the same time there followed a rapid succession of other books. In 1972 Middleman's book *Transport Phenomena in Cardiovascular System* [40] was published. In 1973 Lightfoot's *Transport Phenomena and Living Systems* [36] appeared. They emphasize mass transfer as well as momentum transfer. In 1978, a major work by Caro, Pedley, Schroter, and Seed, *The Mechanics of the Circulation* [8], was published, to be followed by Pedley's *The Fluid Mechanics of Large Blood Vessels* 1980, [45], Patel and Vaishnav's *Basic Hemodynamics and Its Role in Disease Processes*, 1980, [42], and Poorinya and Kasyanov's *Biomechanics of Large Blood Vessels of Man*, (*Biomechanika Kropnich Krovenosnich Sosoodov Cheloveka*), 1980 [46]. These books are based ona a large number of published papers. They attest to a high state of development in the field of cardiovascular mechanics. But, as we have remarked earlier, much of the basic data on blood vessel morphology and rheology are missing, and the theory remains nonspecific; no detailed prediction of the macro and microcirculation in any specific organ is possible without additional collection of data. That is why I said before that a systematic collection of basic data is an essential taak for the future.

Flow of blood in microblood vessels is called microcirculation. Microcirculation is characterized by several characteristics: (1) The vessels are so small that their diameters are comparable with the dimensions of the red blood cells. Hence blood must be treated as a fluid containing a concentrated suspension of highly flexible particles. (2) The blood vessel walls are leaky to gases, water, ions, and proteins. Mass transfer between blood and cells of the body takes place across the walls of the capillary blood vessels. (3) The smooth muscles of the smallest arteries and arterioles are most effective in controlling the diameters of these vessels. Because of the smallness of these vessels, diameter change affects pressure drop significantly. (Remember Poiseuille's formula: for a given flow, the pressure drop varies as $(\text{diameter})^{-4}$.) Hence the arterioles control the blood pressure of the body. (4) In many vital organs, a phenomenon of the autoregulation exists. If the systemic blood pressure increases, the diameter of the arterioles decreases. Conversely, if the systemic blood pressure decreases, the arterioles dilate. In this way the pressure field of the microcirculation is kept more or less constant in spite of wide fluctuations of systemic blood pressure.

These features of microcirculation have attracted many applied mathematicians and applied mechanicians. Burton, Lighthill, Fung, Skalak, Evans, Chien, Gross, Bassingthwaighte, Oka, Goldsmith, Sutera, Hochmuth, Salathe, Weinbaum, and many others contributed to this field. References [7, 9, 14, 27, 33] are collections of papers presented at meetings and conferences. The journal *Microvascular Research* is devoted exclusively to this subject. The book by Caro et al. [8] and Fung [20] contain systematic presentations on mechanics of microcirculation, the latter especially on pulmonary microcirculation.

Biorheology is the science of deformation and flow of biological materials. It lies at the foundation of biomechanics. In recent years the one person who has contributed most in promoting biorheology is Alfred L. Copley. Al is an M.D. and an artist. He is equally proud of his painting as of his hemorheology. In the 1960's he organized a number of international meetings on hemorheology, published several books on the subject [11, 12], and the journals *Hemorheology, Biorheology*, and *Clinical Hemorheology*. Other prominent authors in hemorheology are Dintenfass [14, 15] and Whitmore [54]. On the rheology of connective tissues, Hartmann [29] edited the proceedings of a conference *Biopolymere und Biomechanik von Bindegewebssystemen*. On biorheology in general, we must mention Frey-Wyssling's *Deformation and Flow of Biological Systems*, 1952 [17], Scott Blair's *An Introduction to Biorheology*, 1974 [48], and Syoten Oka's *Rheology-Biorheology*, 1974 [41]. Oka's book, in particular, is an excellent textbook. His new book, *Cardiovascular Hemorheology*, 1981 [41*a*], presents hemorheology beautifully and concisely.

More recently, a book by Evans and Skalak [16], *Mechanics and Thermodynamics of Membranes*, offers a thorough treatment of the mechanics of the red blood cell membrane. A text by Y. C. Fung [18], *Biomechanics: Mechanical Properties of Living Tissues*, presents a broad discussion of all aspects of biorheology: fluids, solid, muscles, bone, and microcirculation.

A book by Yamada, *Strength of Biological Materials* [56] stands out in its presentation of the strength data of biological tissues of the Japanese people. There is no book giving the corresponding data for other races. Strength is, of course, of great importance to trauma, emergency medicine, head injury, bone fracture, damage to internal organs due to imapct, surgery, etc. A large collection of data related to the tolerance limits of human organs to automobile collision exists in scattered literature. A selected bibliography is given in Fung's *Biodynamics* [19].

Locomotion and sports forever hold attention of man, and we have in recent years many journals and books published on this subject. James Hay's *The Biomechanics of Sports Techniques* [30] is an extremely interesting book. McNeil Alexander's *Animal Mechanics* [1] is very well done. Alexander and Goldspink's *Mechanics and Energetics of Animal Locomotion* [2] is also rich in material. But the true classics are James Gray's *Animal Locomotion* [25, 26] and Weis-Fogh's studies of locust flight [52], a summary of which is given in reference [37]. They are observational biology at its best.

A modern era for mathematical investigation of swimming and flying began with G. I. Taylor's investigations of the swimming of microscopic organisms [49, 50], and the literature is greatly enriched by the contributions and books by Lighthill, *Mathematical Biofluiddynamics* [37], and Wu et al., *Swimming and Flying in Nature* [55].

Another remarkable area of development is orthopedics and rehabilitation. The value of biomechanics to practical clinical applications in this area is well recognized by physicians and surgeons, and the strength of the teams working in this field is attested by the thousands of people participating in the annual meetings of the Orthopedics Research Society. Papers on joints, bone, cartilage, musculoskeletal system, low back pain, scoliosis, trauma, surgery, and artificial limbs occupy major parts of the

Downloaded 02 May 2010 to 171.66.16.250. Redistribution subject to ASME license or copyright; see http://www.asme.org/terms/Terms_Use.cfm

Journal of Biomechanics and the ASME *Journal of Biomechanical Engineering*.

Fine work on the bone has a long history. One of the celebrated hypothesis that changes in structure and shape of bone is stress modulated is known as Wolff's law (1884). The story went that in 1866 G. H. Meyer presented a paper on the structure of spongeous (cancellous) bone to a meeting in Zurich at which Professor C. Culmann was present. Culmann had just published a book on graphical statics. He pointed out that Meyer's line drawings resembled very much the stress trajectories (lines of principal stresses) of a cantilever beam loaded at the end. In a paper published in 1867 [39] Meyer reported that Culmann had asked one of his students to draw up the stress trajectories in a cranelike curved beam loaded in a fashion similar to the human femur. This drawing became the famous Culmann's crane. Wolff seized on Culmann's crane and formulated his "law" which states that there is a complete correspondence between the bone structure and the stress trajectories. This law cannot be taken too seriously, but it served as the starting point for many new theories later. One of the best books representing research along this line is Pauwel's *Biomechanics of the Locomotor Apparatus*, [44] which is a collection of the author's contributions of a lifetime. Typical newer multiauthored publications are Ghista's *Osteoarthromechanics* and ASME's AMD-45, *Mechanical Properties of Bone*, edited by S. C. Cowin [13].

Vigorous development on biomechanics is taking place in all parts of the world. The Soviet Union's journal, *Mechanika Polymerov* (recently changed to *Mechanika Kompositnich Materialov*), published by Latvin SSR Academy of Science in Riga, regularly publishes biomechanics papers. Bulgaria Academy of Science publishes the series *Biomechanika* and proceedings of a number of international meetings on biomechanics held in Bulgaria.The proceedings of the first Soviet Union Congress on biomechanics in Riga, 1975, lists many hundreds of papers. Brankov's book *Osnovi Biomechaniki* (*Basic Biomechanics*) [6], Knets, Pfafrod, and Saulogozis's *Deformation and Failure of Solid Biological Tissues* [34], and Poorinya and Kasyanov's *Biomechanics of Large Blood Vessels of Man* [46] are high quality publications. The last book contains a great many numerical tables on the variation of mechanical properties of blood vessels with age. Many papers are coming out also in Japanese, Chinese, and other languages.

This brief survey, citing some of the books that serve as landmarks in the field of biomechanics, is sufficient to demonstrate the breadth and depth of the field, and the vigorous development that is taking place; but is certainly inadequate to serve as a literature survey, or as a record of the most original publications. In my own effort to make the entire field available to graduate students (Fung, *Biodynamics*: *Circulation, Respiration, Fluid Balance, Locomotion, Strength and Growth* [19, 20]) I needed 800 pages.

6 In Search of New Principles

Biomechanics obeys all the rules of mechanics. In a sense, biomechanics merely extends classical applied mechanics to deal with a group of difficult problems involving materials with peculiar constitutive equations, large deformation, and complex boundary conditions. But the real activity in the field is the searching of new principles – new biological principles on how living organisms work. Biomechanics participates in the broad field of biology because many principles cannot be clarified without a thorough understanding of the mechanics involved. For example, atherosclerosis is a serious concern to many people. We would like to know what causes atherosclerosis and how to deal with it. In spite of a tremendous effort in research and many claims to the contrary, atherosclerosis remains a problem and a mystery. To advance further biomechanics is needed. The point is that atherogenesis cannot be understood without a thorough understanding of blood flow and its control.

Mechanics of living organs is intimately tied up with biological principles. For example, we know that growth and resorption of bone and soft tissues are to some extent modulated by the stresses in the tissues. To calculate the stress distribution in a structure in response to external loads is a familiar problem in mechanics. But in dealing with biological situation new questions arise: In the case of bone and joints, there are many muscles acting on the structure. These muscles form a highly redundant system. How can we evaluate the forces in these muscles? To do this evaluation we need a biological principle. Take another example of the blood vessel. Arteries are not stress-free in vivo. To compute stress distribution in arteries we must know the initial stresses in them (i.e., the stresses that remain when the internal and external pressures are equalized and the longitudinal tension is reduced to zero.) What principle governs the distribution of the initial stresses? Since initial stresses can be easily changed by growth or resorption of cells, the question cannot be answered by mechanics principles alone. Some biological principles, unknown at present, must be found to solve the stress distribution problem. Some suggestions have been made, see e.g., Fung [20, Chapter 2], but proofs are needed.

7 Perspective of the Future

It is safe to predict that biomechanics will continue to develop until its potential to medicine and biology is fully realized. Understanding physiology is a big attraction in itself. Predicting the consequences of artificial interventions will be a legitimate objective of this science. Developing methods of preserving and improving health will benefit man. To achieve these and other objectives, systematic collection of the needed data if of utmost importance. Orderly development can come only if an adequate data base is in existence.

References

1 Alexander, R. M., *Animal Mechanics*, University of Washington Press, 1968.

2 Alexander, R. M., and Goldspink, G., *Mechanics and Energetics of Animal Locomotion*, Chapman & Hall, London, 1977.

3 Bergel, D. H., *Cardiovascular Fluid Dynamics*, Vols. 1 and 2, Academic Press, New York, 1972.

4 Berne, R. M., and Sperelakis, N., eds., *Handbook of Physiology, Sec. 2, Cardiovascular System, Vol. 1, The Heart*, American Physiological Society, Bethsda, Md., 1980.

5 Bohr, D. F., Somlyo, A. P., and Sparks, H. V., Jr., eds., *Handbook of Physiology, Sec 2, The Cardiovascular System, Vol. 2. Vascular Smooth Muscle*, American Physiological Society, Bethesda, Md., 1979.

6 Brankov, George *Osnovi Biomechaniki. (Basic Biomechanics)*, Izdatelstvo "MIR," Moscow, 1981.

7 Burton, A. C., *Physiology and Biophysics of the Circulation*, Year Book Medical Publishers, Chicago, 1965.

8 Caro, C., Pedley, T. J., Schroter, R. C., and Seed, W. A., *The Mechanics of the Circulation*, Oxford University Press, Oxford, 1978.

9 Cokelet, G. R., Meiselman, H. J., and Brooks, D., eds., *Erthrocyte Mechanics and Blood Flow*, Alan Liss, New York, 1980.

10 Cokelet, G. R., Merrill, E. W., Gilliland, E. R., Shin, H., Britten, A., and Wells, R. E., "The Rheology of Human Blood—Measurement Near and at Zero Shear Rate," *Trans. Soc. Rheology*, Vol. 7, 1963, pp. 303–317.

11 Copley, A. L., and Stainsby, G., *Flow Properties of Blood and Other Biological Systems*, Pergamon Press, New York, 1960.

12 Copley, A. L., ed., *Symposium on Biorheology*, Interscience, New York, 1965.

13 Cowin, S. C., ed., *Mechanical Properties of Bone*, American Society of Mechanical Engineers, New York, 1981.

14 Dintenfass, L., *Blood Microrheology: Viscosity Factors in Blood Flow, Ischemia and Thrombosis*, Butterworths, London, 1971.

15 Dintenfass, L., *Rheology of Blood in Diagnostic and Preventative Medicine*, Butterworths, London, 1976.

16 Evans, E. A., and Skalak, R., *Mechanics and Thermodynamics of Biomembranes*, CRC Press, Boca Raton, Fla., 1980.

17 Frey-Wyssling, A., *Deformation and Flow of Biological Systems*, North Holland Pub., Amsterdam, 1952.

Downloaded 02 May 2010 to 171.66.16.250. Redistribution subject to ASME license or copyright; see http://www.asme.org/terms/Terms_Use.cfm

18 Fung, Y. C., *Biomechanics: Mechanical Properties of Living Tissues*, Springer Verlag, New York, 1981.

19 Fung, Y. C., *Biodynamics: Respiration, Fluid Balance, Locomotion, Stress Distribution, Strength and Growth*, Springer Verlag, New York, in press.

20 Fung, Y. C., *Biodynamics: Circulation*, Springer Verlag, New York, in press.

21 Fung, Y. C., Perrone, N., and Anliker, M. *Biomechanics: Its Foundations and Objectives*, Prentice-Hall, Englewood Cliffs, N.J., 1972.

22 Fung, Y. C., Fronek, K., and Patitucci, P., "On Pseudo-Elasticity of Arteries and the Choice of its Mathematical Expression," *Am. J. of Physiol.*, Vol. 237, No. 5, 1979, pp. H620–H631.

23 Fung, Y. C., Sobin, S. S., Tremer, H., Yen, M.R.T., and Ho, H. H., "Patency and Compliance of Pulmonary Viens When Airway Pressure Exceeds Blood Pressure," *J. Applied Physio.*, in press.

24 Ghista, D. N., *Osteoarthromechanics*, McGraw-Hill, New York, 1982.

25 Gray, J., *How Animals Move*, Cambridge Univ. Press, 1953.

26 Gray, J., *Animal Locomotion*, Weindenfeld an Nicolson, London, 1969.

27 Grayson, J., and Zingg, W., eds., *Microcirculation, Vols. 1 & 2*, Plenum Press, New York, 1976.

28 Gross, J. F., and Popel, A., eds., *Mathematics of Microcirculation Phenomena*, Raven Press, New York, 1980.

29 Hartmann, F., ed., *Biopolymere und Biomechanik von Bindegewebssystemen*, Springer-Verlag, Heidelberg, 1974.

30 Hay, J. G., *The Biomechanics of Sports Techniques, 2nd ed.*, Prentice-Hall, Englewood Cliffs, N.J., 1978.

31 Huxley, A. F., "Muscle Structure and Theories of Contraction," *Prog. in Biophys. & Biophys. Chem.*, Vol. 7, 1957, pp. 255–318.

32 Huxley, H. E., "The Double Array of Filaments in Cross-Striated Muscle," *J. Physios. Biochem. Cytol.*, Vol. 3, 1957, pp. 631–643.

33 Kaley, G., and Altura, B. M., eds., *Microcirculation*, Vols. 1 & 2, University Park, Baltimore, Md., 1977.

34 Knets, E. V., Pfafrod, G. O., and Saulgozis, U. J., *Deformation and Failure of Solid Biological Tissues (Deformerovanie e Razryshenie Tverdi Biologichskeh Tkanee)*, Riga, "Zenatne," 1980.

35 Lanir, Y., and Fung, Y. C., "Two-Dimensional Mechanical Properties of Rabbit Skin. I. Experimental System. II. Experimental Results, *J. Biomech.*, Vol. 7, 1974, pp. 29–34, and pp. 171–182.

36 Lightfoot, E. N., *Transport Phenomena and Living Systems*, Wiley, New York, 1974.

37 Lighthill, J., *Mathematical Biofluiddynamics*, Society for Industrial and Applied Mathematics, Philadelphia, Pa., 1975.

38 McDonald, D. A., *Blood Flow in Arteries*, Williams & Wilkins, Baltimore, Md., 1st ed. 1960, 2nd ed., 1974.

39 Meyer, G. H., "Die Architektur der Spongiosa," *Archiv Fur Anatomie, Phsiologie und wissenschaftliche Medizin*, Vol. 34, 1867, pp. 615–628.

40 Middleman, S., *Transport Phenomean in the Cardiovascular System*, Wiley, New York, 1972.

41 Oka, Syoten, *Rheology-Biorheology* (In Japanese), Syokabo, Tokyo, 1974.

41*a* Oka, Syoten, *Cardiovascular Hemorheology*, Cambridge Univ. Press, 1981.

42 Patel, D. J., and Vaishnav, R. N., *Basic Hemodynamics and Its Role in Disease Process*, University Park Press, Baltimore, Md., 1980.

43 Patel, D. J., and Vaishnav, R. N., "The Rheology of Large Blood Vessels," In *Cardiovascular Fluid Dynamics*, Vol. 2, Bergel, D. H., Academic Press, New York, Ch. 11, 1972, pp. 2–65.

44 Pauwels, F., *Biomechanics of the Locomotor Apparatus*, (Translated from the German by P. Maquet and R. Furlong), Springer Verlag, New York, 1980.

45 Pedley, T. J., *The Fluid Mechanics of Large Blood Vessels*, Cambridge University Press, London, 1980.

46 Poorinya, B. A., and Kasayanov, V. A., *Biomechanika Kropinch Krovenosnich Sosoodov Cheloveka (Biomechanics of Large Blood Vessels of Man)*, Riga "Zenatne," 1980.

47 Rushmer, R. F., *Cardiovascular Dynamics*, Saunders, Philadelphis, 1st. ed., 1955, 2nd, ed. 1961, 3rd, ed., 1970.

48 Scott Blair, G. W., *An Introduction to Biorheology*, Elsevier, Amsterdam, 1974.

49 Taylor, G. I., "Analysis of Swimming Microscopic Organisms," *Proc. Roy. Soc., London, Series A*, Vol. 209, 1951, pp. 447–461.

50 Taylor, G. I., Analysis of the Swimming of Long and Narrow Animals, *Proc. Roy. Soc. London, Series A*, 1952, pp. 158–183.

51 Tong, P., and Fung, Y. C., "The Stress-Strain Relationship for the Skin," *J. P. Biomech.*, Vol. 9, 1976, pp. 649–657.

52 Weis-Fogh, T., Biology and Physics of Locult Flight. II. Flight Performance of Desert Locust (Schistocera Gregaria)," *Philosophical Transactions Roy. Soc. London Series B*, Vol. 239, 1956, pp. 459–510. VIII. Lift and Metabolic Rate of Flying Locusts, *J. Experimental Biology*, Vol. 41, 1964, pp. 257–271.

53 Wetterer, E., and Kenner, T., *Grundlagen der Dynamik des Arterienpulses*, Springer Verlag, Berling, Heidelberg, 1968.

54 Whitmore, R. L., *Rheology of the Circulation*, Pergamon Press, Oxford, 1968.

55 Wu, T. V.-T., Brokaw, C. J., and Brennen, C., *Swimming and Flying in Nature*, Vols. 1 and 2, Plenum Press, New York, 1975.

56 Yamada, H., *Strength of Biological Materials*, ed., Evans, F. G., Williams & Wilkins, Baltimore, Md., 1970.

57 Yen, M. R. T., and Foppiano, L., "Elasticity of Small Pulmonary Veins in the Cat," ASME *J. Biomechanical Eng.*, Vol. 103, 1981, pp. 38–42.

58 Yen, R. T., Fung, Y. C., and Bingham, N., "Elasticity of Small Pulmonary Arteries in the Cat," ASME *J. Biomechanical Eng.*, Vol. 102, 1980, pp. 170–177.

59 Yen, R. T., Zhuang, F. Y., Fung, Y. C., Ho, H. H., Tremer, H., and Sobin, S. S., "The Morphological Structure of the Cat's Pulmonary Veins," *J. Appl. Physiol.*, in press.

60 Zhuang, F. Y., Fung, Y. C., and Yen, R. T., "Analysis of Blood Flow in Cat's Lung With Detailed Anatomical and Elasticity Data," accepted by *J. Appl. Physiology*, in press.

Downloaded 02 May 2010 to 171.66.16.250. Redistribution subject to ASME license or copyright; see http://www.asme.org/terms/Terms_Use.cfm

P. Germain
Laboratoire de Mécanique Théorique,
P. et M. Curie,
Paris, France 75005

Q. S. Nguyen
Laboratoire de Mécanique
des Solides,
Ecole Polytechnique,
91120 Palaiseau, France

P. Suquet
Laboratoire de Mécanique Théorique,
P. et M. Curie,
Paris, France 75005

Continuum Thermodynamics

Introduction

Fifty years ago, the term "continuum mechanics" was not widely used. A significant emphasis on continuum mechanics could be found in the postwar literature with Rivlin's and Truesdell's pioneering works. A few years later, it became clear to most scientists involved in this new field that thermodynamics should play a central role in continuum mechanics. If one may say that the importance of continuum mechanics significantly increased during the 1950s, one may assert that it is during the 1960s that continuum thermodynamics began to be a popular topic attracting the attention of numerous people.

Quite a number of great scientists had already introduced "continuum thermodynamics" in their work without using the word: for instance, Lord Rayleigh for viscous flows and Lord Kelvin for the thermoelectric effect. Special mention should be made of Duhem's work [1] which demonstrated a very clear view of the role of thermodynamics in continuum physics. At the time, his main ideas did not receive the attention they deserved. They are nevertheless present in Jouguet's and Roy's works. Other examples may be given in the field of chemistry: de Donder's work and the fundamental results of Onsager and Casimir provided the foundations on which the thermodynamics of irreversible processes (TIP) was built. The expansion of continuum thermodynamics in the 1960s is evidenced not only through the number of situations that have been considered but also by the widespread desire to deal with the field in its full generality, to exhibit the basic assumptions as well as the significance of the concepts involved, and hopefully, to derive methods that could be applied to any physical situation.

The expansion of continuum thermodynamics has raised many controversies during the last 20 years; they still persist at the present time[1]. A first line of thought, referred to as "rational thermodynamics," asserts that the introduction of thermodynamical concepts into the field of moving continuous media requires a complete rethinking and reformulation of classical thermodynamics which is primarily concerned with systems in equilibrium. A second line of thought maintains that the concepts should not be drastically changed. The former criticizes the lack of ambition and of intrepidity of the latter; it prefers to think of "entropy" and of "absolute temperature" as basic concepts similar to that of "forces" in dynamics. The second argues that these concepts have no physical content outside equilibrium and its neighborhood. Such important questions will receive some attention in the present paper but we will not take side in the controversy. It is, in our opinion, a new example of the diversity of preferences: on the one hand, the need for a clear and rigorous mathematical formulation, and on the other hand the desire to remain in close contact with physical reality. We prefer to emphasize what we consider to be the main objective of continuum thermodynamics, i.e., *the construction of models*[2] that *are as simple as possible and which can*:

(*i*) explain the qualitative behavior of various experimentally observed phenomena;

(*ii*) give rise to a quantitative evaluation which may be compared to measurements;

(*iii*) allow one to formulate well-posed mathematical problems and to study the solutions together with their evolution and stability for varying data.

To conclude this introduction we will briefly describe the main parts of the paper. The first section is devoted to the

Contributed by the Applied Mechanics Division for publication in the JOURNAL OF APPLIED MECHANICS.

Discussion on this paper should be addressed to the Editorial Department, ASME, United Engineering Center, 345 East 47th Street, New York, N.Y. 10017, and will be accepted until two months after final publication of the paper itself in the JOURNAL OF APPLIED MECHANICS. Manuscript received by ASME Applied Mechanics Division, March, 1983.

[1] See for instance the recent discussions in the *Bulletin of the Institute of Mathematics and Applications*. References to these discussions are given in [2].

[2] We emphasize that we are concerned with *models*; we do not claim for them a universal validity.

Copyright © 1983 by ASME
Downloaded 02 May 2010 to 171.66.16.250. Redistribution subject to ASME license or copyright; see http://www.asme.org/terms/Terms_Use.cfm

basic equations. Section *II* is concerned with the concepts connected with the generalization of the second law. It will provide the opportunity to mention a few important questions and answers formulated in the spirit of rational thermodynamics. Section *III* describes the method of the "local accompanying equilibrium state" (l.a.s.) which will be used later in its most convenient version, i.e., when the constitutive equations may be obtained from two scalar valued convex functions: a thermodynamical potential and a pseudopotential of the dissipations. Some classical applications, mainly in solid mechanics, are given in Section *IV*. The concept of global state variables is introduced in Section *V*, and its interest is illustrated in relevant examples. Section *VI*, which is devoted to homogenization[3] and thermodynamics, provides some insight into the consistency of the l.a.s. model and into its physical interpretation by exhibiting the relations between descriptions at the microlevel and at the macrolevel. Finally, a few elements of bifurcation and stability theory are given in Section *VII*. They show that the model emphasized in this paper provides a first significant contribution toward what was called the third main objective.

I Basic Equations of Thermodynamics

1 A Few Remarks About Classical Thermodynamics. Classical thermodynamics is concerned with systems in equilibrium which usually may be characterized by a finite number of scalar quantities which define the state Σ of the system. Any thermodynamical property of the system is by definition represented by a function defined on the space V of states.

Classical thermodynamics exhibits properties that can be associated with any thermodynamical system as consequences of a few statements or laws: the empirical temperature θ by the "zeroth" law; by the first law, the internal energy E and the heat received by the system in a transformation or process between two states after interaction with the surroundings. *Reversible processes* may be represented by an arc drawn on V and all the thermodynamical functions attached to any point Σ of this arc have their usual physical significance. Consequently, the differential dE of E is the sum of two differential forms, the elementary work and the elementary heat received by the system during an elementary reversible process.

The second law has received a remarkably large number of forms, and discussions still continue to decide which one of these forms is optimal. Carathéodory's formulation rests on a statement of "inaccessibility" by adiabatic processes. It is then possible to prove that there exists a universal (absolute) temperature T and a universal entropy S such that $T\,dS$ is the elementary heat received in a reversible process. Moreover, for an adiabatic process $\Sigma_1 \rightarrow \Sigma_2$, it may be shown that $S(\Sigma_2) \geq S(\Sigma_1)$.

Some people say that classical thermodynamics has to be called *thermostatics* because it deals only with equilibrium states. Others disagree, noting that time is in fact implied in most of its classical definitions; namely it is true that the statement "such a system is in equilibrium" and the choice of the variables that characterize its state Σ depend on the characteristic time which is of interest for the observer. The work thermostatics is adequate if one restricts its use to case where *all* the properties associated with a state Σ of V—like E, S, and T for instance—have their full physical significance. The following example which gives a first idea of what will be called *internal variables* shows the nuance that may be introduced. Take a system [3] whose states Σ may be defined by E and deformation variables X_i. A continuous process (with time) may have an image on V—it is possible to define $E(t)$, $X_i(t)$, and then $S(t)$. Generally, the function $S(\Sigma)$ will have no significance for such a process. But it may happen that this same process may be considered as a reversible one, when V is embedded in a "larger" space $\hat{V}$. The process may be looked upon as a thermodynamic one on V and as a thermostatic one on $\hat{V}$. Internal energy has the same significance (although different analytic expressions) in V and in $\hat{V}$; entropy may be defined only in $\hat{V}$, and $\hat{S}(\hat{\Sigma})$ has nothing to do with $S(\Sigma)$.

[3] Homogenization is the modeling of a heterogeneous system by a continuum.

2 Basic Equations. We consider now a continuous material system Ω in motion with respect to an inertial frame R. The *basic equations* express the laws that fully describe the physical system independently of the special properties of the material. They always include the conservation laws of mass, momentum, and energy and when only thermomechanical interactions are involved, as is usual in classical continuum mechanics, these conservation laws are the basic equations. A conservation law is symbolically written for any subdomain D of Ω as:

$$\frac{d}{dt}\int_D \mathfrak{A}\, dv + \int_{\partial D} J_A\, d\sigma - \int_D \varphi_A\, dv = 0 \tag{1}$$

As is well known, [4], for a three-dimensional domain:

A is the quantity (a vector or a scalar) that is conserved per unit mass and $\mathfrak{A} = \rho A$ the quantity per unit volume; d/dt or $\dot{(\ )}$ means the material derivative;

J_A is the *associated flux* (per unit area and per unit time);

φ_A is the *supply* (per unit volume and per unit time) that represents the action of the surroundings of Ω ($\varphi_A = \rho S_A$);

As a consequence:

J_A is linear in n (outer unit normal to ∂D), $J_A = j_A \cdot n$, j_A being the associated flux tensor or vector;

At each point of Ω, the following equation holds:

$$\rho \dot{A} + \operatorname{div} j_A - \varphi_A = 0 \tag{2}$$

At each point of a surface of discontinuity inside Ω, a jump relation may be written.

The conservation of energy is the natural extension of the first law of thermostatics; differences are replaced by material derivatives, work by power, heat by heat rate and kinetic energy is taken into account. The material derivative of the kinetic energy of D may be eliminated by application to the real motion of the virtual power statement and, consequently, the power $P_{(e)}$ of external forces on D disappears. Heat rate on D may be assumed (as $P_{(e)}$) to be the result of an associated flux J_Q and of a supply φ_Q. Finally, the equation (2) for energy may be replaced by:

$$\rho \dot{e} = \epsilon_{(i)} + \operatorname{div} j_Q + \varphi_Q, \tag{3}$$

where e is the internal energy per unit mass, $\epsilon_{(i)}$ the opposite of the power of internal forces (per unit volume) or the *energy (per unit volume) due to internal forces*. In (3) all the quantities involved are objective or frame indifferent.

(*i*) In *classical continuum mechanics* for an Eulerian representation

$$j_Q = -q, \quad \varphi_Q = r, \quad \epsilon_{(i)} = tr(\sigma \cdot D) \tag{4}$$

with D, the strain rate tensor or the symmetric part of the velocity gradient, and the conservation laws are symbolically written:

	$\mathfrak{A} = \rho A$	j_A	$\varphi_A = \rho S_A$
Mass	ρ	0	0
Momentum	ρv	$-\sigma$	f
Energy	$\rho\left(e + \frac{1}{2}v^2\right)$	$q - \sigma.v$	$f.v + r$

Downloaded 02 May 2010 to 171.66.16.250. Redistribution subject to ASME license or copyright; see http://www.asme.org/terms/Terms_Use.cfm

In a Lagrangian representation (x_i orthonormal Eulerian variables, $\hat{x}_\alpha$ orthonormal Lagrangian variables), the motion is described by:

$$x_i = \phi_i(\hat{x}_\alpha, t) \quad i, \alpha = 1, 2, 3 \tag{5}$$

A conservation law is written on a fixed domain in the reference configuration $\hat{R}$: A, S_A can again be used; but mass-density $\hat{\rho}$ (mass per unit volume of $\hat{R}$), quantities per unit volume of $\hat{R}$, flux vector or tensor $\hat{j}_A$ have to be changed in order to obtain an equation similar to (2). Similarly, in the Lagrangian version of (3), one has to write:

$$\hat{\epsilon}_{(i)} = tr(t \,.\, \dot{L}), \quad \rho^{-1}\epsilon_{(i)} = \hat{\rho}^{-1}\hat{\epsilon}_{(i)} \tag{6}$$

with t the (second) Piola-Kirchhoff stress tensor and L the Green-Lagrange strain tensor.

(*ii*) When electromagnetic interactions have to be taken into account, one must include in the conservation laws the electromagnetic effects in the flux and supplies of momentum and energy, but also include among the basic equations the Maxwell equations, see for instance [5][4].

(*iii*) *Mixture of fluids* is another example which requires a refined description. Let us introduce a *balance equation*, similar to the conservation law (1) but including a production term on the right-hand side:

$$\frac{d}{dt}\int_D \mathfrak{B}\, dv + \int_{\partial D} j_B \,.\, n\, d - \int_D \varphi_B\, dv = \int_D \mathfrak{B}^*\, dv \tag{7}$$

The supply φ_B comes from the surroundings of Ω; on the contrary $\mathfrak{B}^* = \rho B^*$ is produced inside the system, and $\mathfrak{B}^*$ is the rate of production per unit mass. The equations of balance of each constituent ($\lambda = 1,2 \ldots \nu$) of the mixture are symbolically written (no summation with respect to λ):

$\mathfrak{B} = \rho B$	j_B	φ_B	$\mathfrak{B}^* = \rho B^*$
ρ^λ	0	0	τ^λ
$\rho^\lambda v^\lambda$	$-\sigma^\lambda$	f^λ	m^λ
$\rho^\lambda\left[e^\lambda + \frac{1}{2}(v^\lambda)^2\right]$	$q^\lambda - \sigma^\lambda \,.\, v^\lambda$	$r^\lambda + f^\lambda \,.\, v^\lambda$	l^λ

Conservation laws for the mixture as a whole implies:

$$\sum_{\lambda=1}^{\nu} \tau^\lambda = 0, \quad \sum_{\lambda=1}^{\nu} m^\lambda = 0, \quad \sum_{\lambda=1}^{\nu} l^\lambda = 0 \tag{8}$$

These global conservations may be written as previously with the following definitions:

$$\left.\begin{aligned} &\rho = \sum_{\lambda=1}^{\nu}\rho^\lambda, \quad \rho_v = \sum_{\lambda=1}^{\nu}\rho^\lambda v^\lambda, \quad u^\lambda = v^\lambda - v, \\ &\rho e = \sum_{\lambda=1}^{\nu}\rho^\lambda\left[e^\lambda + \frac{1}{2}(u^\lambda)^2\right], \quad \sigma = \sum_{\lambda=1}^{\nu}(\sigma^\lambda - \rho^\lambda u^\lambda \otimes u^\lambda) \\ &q = \sum_{\lambda=1}^{\nu}\left\{q^\lambda + \rho^\lambda\left[e^\lambda + \frac{1}{2}(u^\lambda)^2\right]u^\lambda - \sigma^\lambda \,.\, u^\lambda\right\} \end{aligned}\right\} \tag{9}$$

In particular (3) has to be written with $\varphi_Q = r = \Sigma_{\lambda=1}^{\nu}(r^\lambda + f^\lambda u^\lambda)$.

The u^λ are the diffusion velocities. If there are p chemical independent reactions with Λ^k, $k = 1,2 \ldots p$, their reaction rate densities, if $\gamma^{\lambda,k}$ is the stoichiometric coefficient of constituent λ (molecular weight M_λ) in the reaction k, then

$$\tau^\lambda = \sum_{k=1}^{p}(\gamma^{\lambda,k} M_\lambda \mu)\ \Lambda^k \tag{10}$$

[4] This paper shows the usefulness of the method of virtual power in dealing with such complicated situations.

with 16μ the mass of the oxygen atom. Then the p rate densities Λ^k determine the ν mass production terms τ^λ.

What are the basic equations for a mixture? *Various answers are possible.* There is general agreement to accept the existence of *one* empirical temperature θ valid for the mixture and for all constituents; then it is natural to write only the global conservation law of energy. A first choice is to keep as basic equations the following $4\nu + 1$ scalar valued equations:

$$\left.\begin{aligned} &\dot{\rho}^\lambda + \rho^\lambda \operatorname{div} v^\lambda = \tau^\lambda \\ &\rho^\lambda \dot{v}^\lambda - \operatorname{div}\sigma^\lambda = m^\lambda + f^\lambda \\ &\rho\,\dot{e} = tr\{\sigma \,.\, D\} - \operatorname{div} q + r \end{aligned}\right\} \tag{11}$$

Another less refined but more classical choice is to take as basic equations the $\nu + 4$ equations written in (11) after replacing the ν momentum equations $(11)_2$ by the global momentum equation.

3 Constitutive Equations. When the basic equations have been chosen, one must analyze the quantities involved. Among these quantities, one has to identify those which will be chosen as *principal unknowns* (p.u.). Then in order to solve the problem, the *complementary unknowns* (c.u.) must be expressed through laws that describe the properties of the material: these laws are the constitutive equations. This can be explained by some examples.

In *classical continuum mechanics*, one may choose as the *principal unknowns* (p.u.) one of the following set according to the selected representation:

$$\left.\begin{aligned} &[\rho(x_k, t), \quad v_i(x_k, t), \quad \theta(x_k, t)] \text{ or} \\ &[\rho(\hat{x}_\alpha, t), \quad \phi_i(\hat{x}_\alpha, t), \quad \theta(\hat{x}, t)] \end{aligned}\right\} \tag{12}$$

The auxiliary unknowns[5] (a.u.) are the quantities that can be directly computed from the (p.u.): acceleration $\dot{v}$, deformation gradient F, strain rate tensor. . . Looking at the basic equations, one sees that the *complementary unknowns* (c.u.) are:

$$[e, \sigma, q] \quad \text{or} \quad [e, t, \hat{q}] \tag{13}$$

These (c.u.) —say C— must be expressed in terms of the (p.u.) by the constitutive functions that must fulfill some very well-known requirements: causality, localization, objectivity or material frame indifference[6], and material symmetry.

If one writes symbolically:

$$C(\hat{x}_\alpha, t) = \underset{t' \le t}{\mathfrak{F}}\left\{\Phi(\hat{x}_\alpha, t'), \theta(\hat{x}_\alpha, t'); \hat{x}_\alpha\right\} \tag{14}$$

$\mathfrak{F}$ is a casual functional which depends on the history of the system up to (and including) time t. Note that the basic equations impose no further restriction on F: whatever be the values of the (p.u.), whatever be F, one can always check the equations by a convenient choice of the supplies f and r.

For a mixture of fluids ruled by the $(4\nu + 1)$ basic equations (11) the (p.u.) will be:

$$\rho^\lambda(x_k, t), \quad v_i^\lambda(x_k, t), \quad \theta(x_k, t) \tag{15}$$

and, the (c.u.) are:

$$e, \sigma^\lambda, q, m^\lambda, \Lambda^k; \quad \lambda = (1,2 \ldots \nu), \quad k = (1,2 \ldots \rho) \tag{16}$$

If the mixture is described by the less refined description with $\nu + 4$ equations, the (p.u.) and the (c.u.) will be, respectively:

[5] As ρ may be directly computed from the ϕ_i or from the v_i, it is generally considered as an auxiliary unknown; in such a case mass conservation is not counted among the basic equations.

[6] Frame indifference of the constitutive equations is not always accepted in its full generality—see for instance [2]. Let us emphasize that the *models* considered in the present paper rest effectively on this *working assumption*. Experimental studies show that this working assumption may be used safely in most of the applications met by engineers.

Downloaded 02 May 2010 to 171.66.16.250. Redistribution subject to ASME license or copyright; see http://www.asme.org/terms/Terms_Use.cfm

$$\rho^\lambda,\ v_i,\ \theta;\quad e,\ u^\lambda,\ \sigma,\ q,\ \Lambda^k \tag{17}$$

In each case the constitutive equations must relate the (c.u.) to the (p.u.) by functions or functionals that fulfill the aforementioned requirements.

II Entropy, Absolute Temperature, and Fundamental Inequality

Continuum thermodynamics impose new important restrictions on constitutive equations when a suitable generalization of the second law is formulated. The main objective of continuum thermodynamics is to provide a method to write constitutive equations that fulfill these new restrictions.

One may look at this generalization of the second law from many different points of view. In the following subsections, we will consider first the case where entropy and absolute temperature are more or less considered as primitive concepts, then the case when only entropy is a primitive concept, and finally we consider attempts to start without such assumptions.

1 Clausius Duhem Inequality. The First Version of Rational Thermodynamics. In classical continuum mechanics, any time that specific entropy s and absolute temperature T have been defined or are considered as primitive concepts, everybody agrees to write the rate of production of entropy σ^* in the form:

$$\rho T\sigma^* = \epsilon_{(i)} + \rho(T\dot{s} - \dot{e}) - q\,.\,\nabla(\log T) \tag{18}$$

when $\epsilon_{(i)}$ has been defined in (4). Note that no *supply is involved* in (18). Clausius Duhem inequality, which is an expression of the second law, says that σ^* and then the right-hand side of (18) is *non-negative*.

The first version of rational thermodynamics [6], considers s and T as primitive concepts. An admissible process is a solution of the basic equations when constitutive laws are taken into account, for which the Clausius Duhem inequality holds. For instance, for simple materials, the (c.u.) are w, s, σ, q ($w = e - Ts$ is the free energy) and are expressed as functionals:

$$C = \underset{t'\le t}{\mathfrak{F}}\left\{F(\hat{x}_\alpha, t),\quad T(\hat{x}_\alpha, t'),\quad g(\hat{x}_\alpha, t');\quad \hat{x}_\alpha\right\} \tag{19}$$

where $g = \nabla T$. In order to discover the restrictions imposed on admissible processes, the expressions (19) are introduced in (18). Assuming that the F's are Frechet-differentiable, that their arguments F, T, and g have time derivatives (at least right derivatives) and noting that, at each t, the values of these derivatives may be chosen independently, one shows that the coefficients of these derivatives in the right-hand side of (18) must be zero. This analysis provides the necessary and sufficient conditions for a process to be admissible.

We must content ourselves here with this general outline which has been applied successfully with care and rigor to various cases. General properties have been proved and classical thermostatics results recovered by an asymptotic analysis. Such rigorous achievements must be put on the credit side of this well-founded mathematical theory.

2 The Entropy Balance Assumptions. Following Müller [7, 8] one may assume only that s—but not T—is a primitive quantity which fulfills a balance equation like (7) with $B = s$, $B^* = \sigma^*$. More precisely one assumes that

(a) the rate of entropy production σ^* is non-negative for admissible thermodynamical processes;

(b) the associated entropic flux j_s, like s, is a constitutive quantity;

(c) the supply φ_s is linear with respect to the other supplies with coefficients that are constitutive quantities;

(d) the normal component of the entropy flux across a surface of discontinuity Σ satisfies a conventional continuity requirement. For instance, if [.] denotes the jump of a quantity and if the system is at rest $[\ j_s\,.\,\mathbf{n}\ ] = 0$ if $[\ \theta\ ] = 0$.

From these quite natural assumptions, it is possible to prove in many cases the existence of the absolute temperature, to find the precise expression of j_s and φ_s as well as the restrictions on the constitutive equations.

The method to derive these results implies two steps. The first step is to write that the entropy production σ^* cannot be negative for fields constrained by the condition that they are solutions of the basic equation. Liu has shown that one can get rid of these constraints by the use of Lagrange multipliers which are new unknown constitutive quantities[7]. One then gets an expression for σ^* which must be non-negative whatever by the (p.u.). Taking account now of the assumed constitutive equations, the expression of σ^* involves linearly a number of derivatives of the constitutive variables, whose coefficients must vanish, because at each t the values of these derivatives may be chosen independently. The second step is to use the preceding condition (d) which allows one to exhibit the universal character of some quantities and their physical significance by looking at the simple case of equilibrium.

We must refer to the literature for the details of this rigorous and quite interesting method; we will only comment on some applications.

In thermoelasticity [9] the application of the first step leads to:

$$\dot{s} = \Lambda(\theta)[\dot{e} - \rho^{-1}\ tr\ \{t\,.\,\dot{L}\}],$$

$$j_s = \Lambda(\theta)q,\quad \frac{d\Lambda}{d\theta}q\,.\,\nabla\theta \ge 0;$$

here $\Lambda(\theta)$ is the only Lagrange multiplier which is not zero. The second step leads to the conclusion that Λ is a *universal function* which is easily identified with T^{-1}. All the classical results are recovered.

An instructive application concerns a mixture of inviscid fluids. *The analysis and the results depend on the basic equations chosen* (see *I*.2). If one takes (11), it is convenient to choose as constitutive quantities:

$$e_I,\ \sigma^\lambda = -p^\lambda,\ q_I,\ m_I^\lambda = m^\lambda - \tau^\lambda v$$

instead of (16), with "intrinsic" integral energy e_I and heat flux q_I defined by:

$$\rho\, e_I = \sum_{\lambda=1}^{\nu}\rho^\lambda e^\lambda,\ q_I = q - \sum_{\lambda=1}^{\nu}\frac{1}{2}\rho^\lambda\ (u^\lambda)^2\ u^\lambda.$$

After the first step, one gets the equation that gives $\rho\, ds$ in terms of $d(\rho\ e_I)$ and $d\ \rho^\lambda$ and the equations that give the entropy flux j_s in terms of q and u^λ as well as the supplies φ_s in terms of f^λ and r. But, Lagrange multipliers remain in the coefficients of these equation. Now the second step, when condition (d) is conveniently formulated for an impermeable or semipermeable wall for a constituent shows that, again, the multiplier of the energy equation may be identified with T^{-1}, and that another quantity has to be continuous for each fluid, a result that leads to the introduction of the chemical potentials μ_I^λ. Let us write some of the results:

[7] In most cases, it may be proved that they do not depend on the supplies.

Downloaded 02 May 2010 to 171.66.16.250. Redistribution subject to ASME license or copyright; see http://www.asme.org/terms/Terms_Use.cfm

$$
\left.
\begin{aligned}
d(\rho e_I) &= T d(\rho s) + \sum_{\rho=1}^{\nu} \mu_I^{\lambda} d\rho^{\lambda}, \\
\rho(e_I - Ts) &= \sum_{\rho=1}^{\nu} \rho^{\lambda}\, \mu_I^{\lambda} - p \\
T j_s &= q_I - \sum_{\lambda=1}^{\nu} \rho^{\lambda} \mu_I^{\lambda} u^{\lambda}, \\
T \varphi_s &= r - \sum_{\lambda=1}^{\nu} \rho^{\lambda}\, u^{\lambda} \cdot f^{\lambda}, \quad p = \sum_{\lambda=1}^{\nu} p^{\lambda}
\end{aligned}
\right\} \tag{20}
$$

These results are very remarkable: Gibbs equation for the mixture $(20)_1$ and Gibbs-Duhem equation $(20)_2$ have been proved, correct expressions for j_s and φ_s have been found. In the residual inequalities appear all the dissipative mechanisms producing entropy: heat conduction, chemical reactions, momentum, and thermal diffusion. This is the starting point of a complete "rational thermodynamics" of fluid mixtures developed by Müller.

A last example, again due to Müller [10], concerns a single inviscid fluid whose constitutive equations depend on the constitutive variables ρ, θ, $\dot{\theta}$, $\nabla\theta$. It is found that:

$$j_s = \Lambda(\theta, \dot{\theta}) q, \quad \varphi_s = \Lambda(\theta, \dot{\theta}) r.$$

Moreover $\Lambda(\theta, \dot{\theta})$ is a *universal function*, the *coldness*, whose equilibrium value reduces to $\Lambda(\theta, 0) = T^{-1}(\theta)$. This example is quite instructive: *the absolute temperature concept and the Gibbs equation in its classical form are only valid for equilibrium.*

3 A Challenge to Mathematicians? What we have called the "first" rational thermodynamics considers entropy and absolute temperature as primitive concepts. With Müller, only entropy was assumed, and it was proved in many interesting cases that an absolute temperature may be defined. The last step would be to justify the existence of both concepts on the basis of a statement comparable to the Caratheodory "inaccessibility" axiom for thermostatics. Müller has again considered the question in the frame of thermoelasticity and gave a precise formulation of the challenge: roughly speaking one has to find a statement that ensures the existence of certain quantities (entropy flux and supply, Lagrange multiplier) such that a precise inequality holds for any solution of the equations of motion [9].

4 Alternative Versions of Rational Thermodynamics. Recent attempts to develop further the axiomatic basis of thermodynamics must be mentioned [11], although it is impossible to give them the developments they deserve.

The basic ingredients are the concepts of "state" and "process," like in the Noll's new conception of continuum mechanics. Each process P associates to a state σ one another state $P\sigma$ and to each pair of processes corresponds, when it can be defined, the resulting process of the pair. For the statement of the laws of thermodynamics, the concept of an "action" $a(P, \sigma)$ is introduced in order to render precise and general the idea of "an integral along a process." It assigns to each pair (P, σ) a number (the supply of a in going from σ to $P\sigma$) with the requirements of continuity with respect to σ and additivity with respect to resulting processes. An action has the *conservation property* (alternatively *Clausius property*) at σ, if for every "nearly cyclic" process P starting at σ (and arriving inside an η-neighborhood of σ): $|a(P, \sigma)| < \eta$ or $a(P, \sigma) < \eta$. In any branch of thermodynamics, one must introduce an action $\hat{\epsilon}$ which has the conservation property for at least one state (first law) and an action $\hat{s}$ which has the Clausius property for at least one state (second law). That provides us with a quite reduced requirement. But in fact it may be proved (on some natural assumptions) that $\hat{\epsilon}(P, \sigma)$ has a potential $e(\sigma)$ and that $\hat{s}(P, \sigma)$ has an "upper potential" $s(\sigma)$. Of course $e(\sigma)$ is the internal energy and $s(\sigma)$ the entropy.

This abstract frame must be fitted in each branch of continuum mechanics by prescribing how a state and a process are defined by giving some constitutive functions of the state and by introducing the two actions $\hat{\epsilon}$ and $\hat{s}$. For instance, for an elastic element, σ is defined by a triplet, essentially the present values of the deformation gradient, of the internal energy and of the temperature gradient. The constitutive functions are the temperature, the stress tensor, and the heat flux vector. The processes are defined by the functions of time that appear in equations ruling the derivatives of the triplet—for instance div $j_Q + \varphi_Q$ in (3) *which is here considered as a part of the definition of the process*. For an element with fading memory, a state is defined by the previous triplet *and* by their past history up to, but not including, the present time. This new thermodynamics is also able to include the theory of plasticity [12]. It appears then as a method for reorganizing the results of a given theory into a unified and rigorous scheme which permits us to derive general properties and the thermodynamical restrictions on response functions, more than a guide to discover a convenient schematization in a new field.

A recent paper [13] leads to a definition of the action $\hat{s}$ which is more closely related to the earlier considerations of Clausius, Kelvin, and Planck. It provides us with a new and interesting way to introduce absolute temperature and entropy in thermodynamics.

III The Local Accompanying State Model (l.a.s.)

The model described in the following is in essence very well known and is developed and commented on in various books [14, 15] and papers [16], most of them dealing with the so-called thermodynamics of irreversible processes (TIP). Nevertheless, its mathematical and physical consistency has been recently largely improved; it is then worthwhile to recall quickly some of its main features.

1 Internal Variables, Thermodynamical Potential, and Equations of State. As was mentioned in *II*.1, reversible processes in thermostatics correspond to a time scale such that the internal energy and the deformation variables are adequate to define at each time the state of the system, and these variables may be independently controlled by the observer. If the time of evolution one wants to consider is shorter, it is often possible to extend the previous space into a larger one in which processes can be described by the classical methods of thermostatics. The additional variables that have to be introduced, the *internal variables*, characterize quite generally *dissipative mechanisms*; they may change without changes in the surroundings, and usually the observer is not able to control their value.

Let us present, somewhat formally, how the model works. Having in mind a continuum, one uses quantities defined on each particle: specific internal energy e, variables that describe the deformation in the adopted—possibly generalized [5]—kinematical description $\chi = (\chi_1, \ldots, \chi_n)$, internal variables[8] $\alpha = (\alpha_1, \ldots, \alpha_p)$. The main assumption is that one may attach to any particle a thermostatic system (of unit mass) defined by (e, χ, α), which is significant for the physical description of the particle. For this "accompanying" system, the Gibbs equation may be written:

[8] One does not specify here the tensorial character of the χ and of the α. For simplicity they will be considered as scalars.

Downloaded 02 May 2010 to 171.66.16.250. Redistribution subject to ASME license or copyright; see http://www.asme.org/terms/Terms_Use.cfm

$$T^a\, ds^a = d\, e - \sum_{i=1}^{n} \eta_i^a d\, \chi_i + \sum_{k=1}^{p} A_k^a d\, \alpha_k \tag{21}$$

Generally, the superscript a will be omitted: then $T = T^a$, $s = s^a$ are, respectively, an absolute temperature and a specific entropy which may be used for the description of the particle. The conditions under which such an interpretation may be physically reasonable will be discussed in the following.

Then if one writes $e(s, \chi, \alpha)$ the specific internal energy (alternatively $w(T, \chi, \alpha)$ the specific free energy), one may express T, η, A (alternatively s, χ, A) as functions of s, χ, α (alternatively T, χ, α). These equations are the *equations of state* of the material. *Generally*, in account of the thermodynamic stability requirements, $e(s, \chi, \alpha) = e(\tilde{\chi})$ is a convex lower semicontinuous function of its arguments; one says also a *convex closed* function in order to recall that the epigraph of e (i.e., the domain $z \geq e(\tilde{\chi})$ in the space $\tilde{\chi}, z$) is a convex closed set. Then one may apply all the concepts introduced in convex analysis [4]. The dual function $e^*(T, \eta, -A) = e^*(\tilde{\eta})$ of e, obtained by a *Legendre-Fenchel transformation*, may be used in order to write the equations of state in an equivalent way; subgradients may be introduced if e or e^* are not differentiable. With the notation:

$$(\tilde{\chi}, \tilde{\eta}) = T\, s + \sum_{i=1}^{n} \eta_i \chi_i + \sum_{k=1}^{p} (-A_k)\, \alpha_k \tag{22}$$

one may say that $\tilde{\chi}, \tilde{\eta}$ are connected by the equations of state if one of the following three equivalent statements holds:

$$e(\tilde{\chi}) + e^*(\tilde{\eta}) - (\tilde{\chi}, \tilde{\eta}) = 0, \quad \tilde{\eta} \in \partial\, e(\tilde{\chi}), \quad \tilde{\chi} \in \partial\, e^*(\tilde{\eta}) \tag{23}$$

By definition, if the left-hand side of $(23)_1$ is not zero, it is positive. Other thermodynamical potentials, i.e., functions from which the equations of state may be written with gradients (or subgradients), may be built from $e(\tilde{\chi})$ by a *partial Legendre-Fenchel transformation*; that is precisely the case for the specific free energy.

2 Production Rate of Entropy and Dissipation. Complementary Constitutive Equations. Let us assume, as usual in classical continuum mechanics, that the entropy balance equation can be written with $T j_s = q$, $T \varphi_s = r$, i.e., that Clausius Duhem inequality (18) holds. From (21) one may write:

$$\left.\begin{aligned} &\dot{e} = \rho\, T\, \dot{s} + \epsilon^r_{(i)}; \\ &\epsilon^r_{(i)} = \sum_{i=1}^{n} \eta_i\, \dot{\tilde{\chi}}_i - \sum_{k=1}^{p} A_k \dot{\alpha}_k = (\eta, \dot{\chi}) - (A, \dot{\alpha}) \end{aligned}\right\} \tag{24}$$

Then (18) may be written:

$$\epsilon_{(i)} - \epsilon^r_{(i)} - q\, .\, \nabla\, (\mathrm{Log}\, T) = \rho\, T\, \sigma^* = d \tag{25}$$

One calls d the *dissipation* (per unit volume), $d_1 = \epsilon_{(i)} - \epsilon^r_{(i)}$ the *intrinsic dissipation*, $d_2 = d - d_1$ the *thermal dissipation*. By construction $\epsilon_{(i)}$, the opposite of internal power in the *real* evolution, involves the (generalized) strain rates which appear in the chosen kinematical description. One may prove in most cases that they may be chosen as derivatives of generalized strains (as for instance in (6)) and we may assume that the χ_i introduced in the foregoing are precisely the (generalized) strains. As a consequence $\epsilon^r_{(i)}$ which is analogous to $\epsilon_{(i)}$ in the associated artificial reversible evolution of the accompanying state is, like $\epsilon_{(i)}$, linear in the $\dot{\chi}_i$. Consequently (25) may be written:

$$d = (\eta^{an}, \dot{\chi}) + (A, \dot{\alpha}) - q\, .\, \nabla(\mathrm{Log}\, T) \tag{26}$$

Then d has the familiar expression,

$$d = \sum_{\mu=1}^{m} Y_\mu X_\mu = (Y, X) \tag{27}$$

where the Y_μ stand for the "fluxes" $(\dot{\chi}, \dot{\alpha}, q)$ an X_μ for the "forces" $(\eta^{an}, A, -\nabla(\mathrm{Log}\, T))$.

Going back to *I*.3, it is easily recognized that in the l.a.s. model *the constitutive equations are given by the equations of state and by the complementary constitutive equations which express for instance the* η^{an}, $\dot{\alpha}$ *and* q *in terms of* $\dot{\chi}$, A, *and* $\nabla(Log\, T)$ or more generally, which relate the Y and the X.

When the preceding classical assumptions for j_s and φ_s are not valid, the crucial point is to first derive the convenient expressions for these quantities, and consequently for the dissipation d, in a way which is consistent with the chosen basic equations. In each case, ad-hoc methods, which rest on physical reasoning, are adopted; one then must be careful to fulfill the consistency requirements, for instance to exclude the outside supplies from the expression of d. In some cases, as said before (*II*.2), the analysis of Müller provides a systematic method to answer these questions. The next three subsections are devoted to the formulation of the complementary equations (c.c.e.).

3 Classical Model of TIP. TIP originated from the decisive contributions of Onsager and Casimir and is presented in many books authored by Meixner and Reik, Prigogine, de Groot and Mazur [14], Woods [3], and many others. Quite interesting, stimulating and also critical discussions may be found in [10] about the statistical foundations, the various branches of physics where it may be applied, and the impressive set of experiments that support the validity of the Onsager-Casimir reciprocity relations (OCRR) which is the basic tool of TIP. These relations say that, when the "fluxes" Y and the "forces" X are linearly related, the c.c.e. may be written:

$$X_i = \sum_{j=1}^{M} L_{ij}\, Y_j \tag{28}$$

where the matrix L_{ij} is *symmetric, non-negative*[9] and may depend on the thermodynamical variables, and especially on T and χ_i. Other restrictions arise from the tensorial character of the Y and the X, the frame invariance and the material symmetry.

Such a result requires a proper choice between the Y and the X in the right-hand side of (27). In a specific situation ad-hoc considerations give the answer and no difficulty arises. For instance, strain rates, heat flux vector, and rates of progress of chemical reactions have to be listed among the Y. A rigorous recipe [3] may be given if one accepts to introduce the concept of a "microscopic time reversal" (mtr) for which $Y \to -Y$, $X \to +X$ (it corresponds to a time interval smaller than the collision time). One can write (28) if the linearly related Y and X have a definite parity under mtr. Conjugate linear transformations $Y \to Y'$, $X \to X'$ may be applied, provided $(Y', X') = (Y, X)$. The OCRR may also be generalized when the Y and the X are not dependent but satisfy some linear constraints [17].

4 The Pseudopotential of Dissipation Model or Standard Model. In TIP, one may write (28)

$$X_i = \frac{\partial \varphi}{\partial Y_i}, \quad \varphi = \frac{1}{2} \sum_{i=1}^{m} \sum_{j=1}^{m} L_{ij}\, Y_i\, Y_j \tag{29}$$

where $\varphi(Y)$ is a quadratic non-negative form. *The standard model presented now is a generalization of* (29), *when* $\varphi(Y)$ *is assumed to be a non-negative convex closed function such that* $\varphi(0) = 0$.

This assumption leads to thermodynamical admissible process because d is consequently non-negative. This pseudopotential (p.p.) $\varphi(Y)$ may, in some cases, depend on

[9] Then d is necessarily non-negative.

Downloaded 02 May 2010 to 171.66.16.250. Redistribution subject to ASME license or copyright; see http://www.asme.org/terms/Terms_Use.cfm

the thermodynamical variables that have to be considered as parameters.

Needless to say, other p.p. may be introduced, as mentioned for the thermodynamical potentials in *III*.1, by a complete Legendre-Fenchel transformation which leads to $\varphi^*(X)$, again a convex closed p.p., or by a partial Legendre-Fenchel transformation which leads to a saddle (convex-concave) p.p.. General formulations of the c.c.e. may be written in a similar way to those in (23) given for the equations of state. In conclusions, for such a model, all *the constitutive equations of the material can be recast in two non-negative convex closed functions, the potential e and the pseudopotential* φ.

The present formulation is essentially due to Moreau [18], see also [4, 19]. It is impossible here to give an account of all the contributions which have been useful to prepare this formulation. Plasticity theory, with its normality rule, played an important role in order to focus attention on the importance of convexity. A decisive step must be attributed to Ziegler [20] when he recognized the role of "dissipation functions."

5 General Formulation of c.c.e. Although the p.p. model can be used to describe a great variety of physical situations, it does not possess a universal validity. Quite a general formulation may be proposed by assuming that the X and Y are functionally related with, possibly, the thermodynamical variables as parameters. For instance, for a dissipation like (26)

$$\eta^{an},\ \dot{\alpha},\ q = \mathfrak{F}\ (\dot{\chi},\ A,\ \nabla\ (\text{Log}\ T);\ T,\ \chi,\ \alpha) \tag{30}$$

The function $\mathfrak{F}$ must satisfy the causality, the objectivity and the material symmetry requirements, and must also lead to a solution of the basic equations, supplemented by (30) and the equations of state, for which d is never negative, a condition that was automatically fulfilled in the standard model.

6 Physical Significance of the l.a.s. Model. It is already known that any rheological model composed of springs, dashpots, and gliders is a standard model [21]. Considerations on rheological models throw some light on the understanding of two important questions concerning the l.a.s. method: what is the significance of the thermodynamic potential e? How is it possible to select the internal variables α?

In order to simplify, one will assume that the χ variables reduce to ϵ, strain tensor in small perturbation theory, and that the system has only elastic stresses ($\eta = \sigma$, $\eta^{an} = 0$). In essence, the l.a.s. method assumes that a particle in the usual macroscopic description (M.D.) represents in fact a microscopic structure or cell which is itself a continuum in the microscopic description (m.d.). Then e, local value in M.D., can be looked upon as the *global* internal energy of the corresponding cell in m.d. (per unit mass). Similarly ϵ, local strain in M.D., can be looked upon as the *global* geometrical description of the cell. Keeping e and ϵ constant means that the cell, from a thermodynamical point of view, is isolated. This cell may be highly heterogeneous and various physical dissipative mechanisms may be involved in the evolution, each of them being described by an internal variable α. If one wants to keep only a finite number of α, one must take into consideration the characteristic time of the macroscopic evolution, i.e., of the macroscopic strain rates, say $\tau_M = \epsilon\ .\ \dot{\epsilon}^{-1}$, and the characteristic value of the bound of macroscopic stresses, say σ_M. The dissipative mechanisms characterized by a relaxation time (like for viscosity) of the same order than τ_M must be kept. The rate-independent mechanisms (like for plasticity) whose yield limits are below σ_M must be kept. If one α has a relaxation time much greater than τ_M or a yield limit much greater than σ_M, its value is considered as frozen and it plays no role in the l.a.s. method. The α which have relaxation times much shorter than τ_M do not appear either because they are considered to have the equilibrium values, they reach, when *the whole system has been considered isolated with e,* ϵ, *and all the others* α *frozen.* Then, the definition of the system associated with a particle, i.e., the choice of the $\alpha_1 \ldots \alpha_p$ depends on the degree of the refinement which seems suitable; it is not a well-defined entity. *Consequently* T^a, s^a, η_i^a, A_k^a *in (21) depend on the choice of the* α *which have been kept.* In particular, in the l.a.s. model, absolute temperature and specific entropy are not uniquely defined and have only a relative significance. When one writes $T = T^a$ and $s = s^a$ as was done in the foregoing, one assumes that these ad-hoc definitions may correctly represent what may be called temperature[10] and entropy in a system in motion, which is not in thermostatic equilibrium [16].

7 Comparison and Connection With the Models of Rational Thermodynamics. In such a comparison with the l.a.s. models, the models of rational thermodynamics present some points of superiority from the point of view of rigor while the l.a.s. method seems to be more efficient. Rational thermodynamics does not assume the validity of Gibb's equation which becomes a theorem; such an assumption is essential in any l.a.s. model, which consequently claims to be only valid for systems *near equilibrium.* Rational thermodynamics must start with specific classes of material whose constitutive equations obey precise requirements; an l.a.s. model prefers, as it is traditional in classical thermodynamics, to leave things more open, and to start only with the thermodynamical description of the l.a.s. which may be used for quite different dissipative mechanisms. But in a specific field—say for instance viscoelasticity or mixture of fluids—final results are quite comparable, when internal parameters have been, formally at least, eliminated, although those deriving from rational thermodynamics are usually more general [16].

But the flexibility of the l.a.s. method is probably its main advantage along with the simplicity of the formulation of the constitutive equations, especially for standard materials. It may be adapted to many field of application; it remains open to further improvements of its physical significance and of its mathematical consistency. It provides constitutive laws simple enough to allow for quite interesting mathematical studies and numerical analysis of the mechanical systems to which it may be applied. These points which have been described in the foregoing as *main objectives* of continuum thermodynamics will be briefly illustrated in the following sections.

IV Applications

The present section is restricted to four examples related to isothermal solid mechanics in the frame of small perturbation theory[11]. The thermal dissipation is neglected. When it is not, if intrinsic and thermal dissipation are uncoupled, the generalized Fourier's law for a standard model is:

$$q = -\frac{\partial \varphi_{th}}{\partial \xi},\quad \xi = \nabla\ (\text{Log}\ T) \tag{31}$$

where $\varphi_{th}(\xi)$ is a convex non-negative function with $\varphi_{th}(0) = 0$. It reduces to the usual Fourier law for small deviations from a fixed T_0. One will deal also only with materials with *elastic stresses* ($\sigma^{an} = 0$).

1 Plasticity With Hardening. The internal variables α and their conjugates A will be chosen as:

$$\alpha = (\epsilon^p,\ \beta,\ p),\quad A = (\sigma,\ B,\ R) \tag{32}$$

[10] Other choices are possible in the frame of the l.a.s. model. For instance, Meixner assumes that $s = s^a$ but $T \neq T^a$, [10].

[11] For application to finite-deformation theory of plasticity, see Mandel's paper "Thermodynamics and Plasticity" in [10]. See also Sidoroff [17].

Downloaded 02 May 2010 to 171.66.16.250. Redistribution subject to ASME license or copyright; see http://www.asme.org/terms/Terms_Use.cfm

and the free energy will be written:

$$\rho\, w = \frac{1}{2}\,(\epsilon-\epsilon^p)\,a(\epsilon-\epsilon^p)+k(\beta)+h(p) \tag{33}$$

Here, a is a fourth-order tensor (a_{ijlm}), ϵ^p the plastic strain, β and p, respectively, a tensorial (symmetric) and a scalar parameter that describe the hardening effect, $k(\beta)$ and $h(p)$ two scalar-valued functions. The equations of state are:

$$\sigma = a(\epsilon-\epsilon^p), \quad B = -\frac{dk}{d\beta} = -k'(\beta),$$

$$R = -\frac{dh}{dp} = -h'(p) \tag{34}$$

and the dissipation is:

$$d = (\sigma,\ \dot{\epsilon}^p) + (B,\dot{\beta}) + (R,\ \dot{p}) \tag{35}$$

In the A space, a convex domain P is introduced, with K_0 a constant:

$$P: J(\sigma+B)+R-K_0 \le 0, J(\tau) = \sqrt{\tau^D_{ij}\,\tau^D_{ij}} \tag{36}$$

with τ^D the deviatoric part of τ. The c.c.e. are defined by the p.p. $\varphi^*(A)$:

$$\varphi^* = I_p(A) \tag{37}$$

with I_P the indicator function of P, i.e., the (generalized) closed convex function which is zero in P and $+\infty$ outside P. The c.c.e. may then be written:

$$\dot{\epsilon}^p = \dot{\beta} = \lambda\frac{\sigma^D+B^D}{J(\sigma+B)},\ \dot{p} = \lambda\ (\lambda \ge 0) \tag{38}$$

It is easily seen that β may be identified with ϵ^p, and p with the cumulated plastic strain since:

$$\dot{p} = \sqrt{\dot{\epsilon}^p\,\dot{\epsilon}^p} \tag{39}$$

If $k(\beta)$ is a constant, one gets the model of isotropic hardening: the domain P of elasticity keeps a constant center, but its size is modified with the evolution. If $R(p)$ is a constant, one gets a model of *kinematic hardening*: the size and the shape of P remain unchanged, but its center may move with the evolution; linear kinematic hardening (Prager) is obtained with a quadratic $k(\beta)$.

2 Viscoplasticity. A class of rate-dependent viscoplastic materials may be defined by the previous formulas (32)–(36), with a p.p. $\varphi^*(A)$ of the Norton-Hoff type (Friaa [22]):

$$(n+1)\ \varphi^*(A) = \mu\left\{j_p(A)\right\}^{n+1} \tag{40}$$

where j_p is the gauge function of the convex domain P, for instance to be specific, the domain defined by (36). Again, β may be identified with ϵ^p, equation (39) holds and:

$$\dot{\epsilon}^p = \frac{\mu}{K_0}\left(\frac{J(\sigma+B)+R}{K_0}\right)^n \frac{\sigma^D+B^D}{J(\sigma+B)} \tag{41}$$

The previous result (38) is recovered for $n \to +\infty$.

3 Cyclic Plasticity. Experimental data show that the previous model (41) is not satisfactory for cyclic loadings. Chaboche [23] obtained a good agreement with experiments with a suitable modification. Instead of (40), let us take a p.p. which will depend on the thermodynamical variables:

$$\varphi^*(A;\alpha) = \frac{\mu}{n+1} \times\left\{\frac{2(J(+B)+R)+\eta[(B,B)-(k'(\beta),\ k'(\beta))]}{K_0}\right\}^{n+1} \tag{42}$$

The term added in the right-hand side of (42) vanishes in a real evolution according to (34). Previous (38), (39), and (41) are still valid but now:

$$\dot{\beta} = \dot{\epsilon}^p + \eta\, B\, \dot{p} \tag{43}$$

The new term in the right-hand side of (43) is precisely the term introduced in Chaboche's theory which allows it to fit the experimental data.

4 Damage of Ductile Materials. Ductile fracture in metals involve considerable damage at crack tips, via nucleation and growth of voids initiated by inclusions. For the sake of simplicity, damage and hardening will be assumed isotropic and described by two scalar-valued variables D and p. Then, one takes:

$$\alpha = (\epsilon^p,\ D,\ p), \quad A = (\sigma,\ Y,\ R) \tag{44}$$

and for the free energy, a suitable modification of (33)

$$\rho\, w = \frac{1}{2}\,(\epsilon-\epsilon^p)\,a(\epsilon-\epsilon^p)+m(D)+h(p) \tag{45}$$

One will take a p.p. $\varphi^*(A)$ associated to a domain P which depends on the mean stress (J defined by (36)):

$$P: J(\sigma)+R+Y\,g(\sigma_m) \le 0,\ 3\ \sigma_m = tr\{\sigma\} \tag{46}$$

If $\dot{\epsilon}^p$ and $\dot{\epsilon}^{pD}$ are the mean part and the deviatoric part of the plastic strain rate $\dot{\epsilon}^p$, then the c.c.e. may be written:

$$\dot{\epsilon}^p D = \lambda\frac{\sigma^D}{J(\sigma)},\ \dot{\epsilon}^p_m = \lambda\ Y\,g'(\sigma_m), \quad \dot{D} = g(\sigma_m), \quad \dot{p} = \lambda \tag{47}$$

Following Rousselier [24], one can derive the form of $g(\sigma_m)$, if one assumes first that D is related to the volume fraction of the growing microscopic voids, (i.e., D is a function of ρ) second that change of volume due to elastic strains may be neglected in the equation of continuity, i.e., $\dot{\rho}+3\ \rho\dot{\epsilon}^p_m = 0$. Then, according to (47):

$$g(\sigma_m)\,g'^{-1}(\sigma_m) = -3\ \rho\ Y\,D'(\rho) \tag{48}$$

But $Y = -m'(D)$ is also a function of ρ, and both sides have to be assumed to equal a constant. Looking at $(47)_2$ *the rate of extension of the damage is proportional to the exponential of triaxiality*. That is the result obtained by Rice-Tracey through a direct investigation of growth of cavities in ductile metals submitted to high stress triaxiality.

V Global Analysis in Continuum Thermodynamics

So far one has considered the thermodynamical description of the particle or of the "microscopic" cell which is schematized by this particle. One will now consider what are the thermodynamical concepts which have to be used for a system, like a structure. The present section shows that one *must* in some cases introduce some global variables, and that this introduction is quite useful, if not necessary, for a thermodynamical description of a structure.

Geometrically, Ω is the bounded domain of the structure in the x_i space[12], $\partial\Omega$ its boundary. The material is assumed to have elastic stresses ($\sigma^{an} = 0$). Evolutions are sufficiently slow to be quasi-static. Body forces are neglected; given loads [F^d per unit area] are applied on the part $\partial\Omega_F$, and displacements [u^d] are imposed on the complementary part $\partial\Omega_u$. Small perturbations are assumed. The system is assumed to be thermally isolated.

1 A First Example From Fracture Mechanics. Let us consider the propagation of a linear crack of length $l(t)$ in a solid undergoing two-dimensional deformation (plane strain, plain stress, antiplane shear). Assuming no surface contribution to energy or entropy on the crack, then the internal energy $E(\Omega)$ of the system is:

$$E = \int_\Omega \rho e\, d\Omega \tag{49}$$

[12] The x_i are orthonormal coordinates; a comma is used for a partial derivative.

Downloaded 02 May 2010 to 171.66.16.250. Redistribution subject to ASME license or copyright; see http://www.asme.org/terms/Terms_Use.cfm

The energy balance leads to a quantity H which represents the heat source produced at the crack tip of the moving crack [25]: if Γ denotes a closed curve surrounding the crack tip and n the external normal, one obtains:

$$\left.\begin{aligned} H &= \lim_{\Gamma \to 0} \int_\Gamma q \,.\, n \, d\Gamma = J_0 \, \dot{l}_0 \\ J_0 &= \lim_{\Gamma \to 0} \int_\Gamma (\rho \, e \, n_1 - n \,.\, \sigma \,.\, u_{,1}) \, d\Gamma; \end{aligned}\right\} \quad (50)$$

The quantity J_0 appears as a crack tip force due to thermomechanical singularities at A. The heat source H appears in the expression of σ^* (through the term $T_A^{-1}H$) and then this source is a hot one. Moreover in the dissipation d, appears the term $J_0 \, \dot{l}$. One may get a model of the propagation law of the crack, by giving a p.p. $\varphi^*(J_0)$:

$$\dot{l} \in \partial \, \varphi^*(J_0) \quad (51)$$

Griffith's criterion corresponds quite clearly to $\varphi^*(J_0) = I_\gamma(J_0)$, where I_γ is the indicator function of the convex domain $J_0 \leq \gamma$.

This example shows that introduction of the global variable l and of the global function E may be quite useful.

2 Global Variables and Global Potentials. If one wants to introduce a global thermodynamical *potential* for the structure, one is led to consider *fields* of local variables as new global variables; such a field is then usually defined by a density in a volume, on a surface or along a line and will be denoted by a bold letter. The evolutions are assumed to be isothermal.

If the fields $\mathbf{F}^d$, $\mathbf{u}^d$, $\boldsymbol{\alpha}$ are given, the stresses and strains in Ω may be found by solving a problem of equilibrium as in elasticity. For instance the displacement field $\mathbf{u}$ is the kinematically admissible field $\mathbf{u}'$ for which:

$$W'(\mathbf{u}':\mathbf{F}^d,\mathbf{u}^d,\boldsymbol{\alpha}) = \int_\Omega \rho \, w(\epsilon(u'), \alpha) \, d\Omega - \int_{\partial\Omega_F} F^d \,.\, u' \, da \quad (52)$$

reaches its minimum value. The value of this minimum is by definition the *thermodynamical potential* for the variables $\mathbf{F}^d$, $\mathbf{u}^d$, $\boldsymbol{\alpha}$:

$$W(\mathbf{F}^d,\mathbf{u}^d,\boldsymbol{\alpha}) \quad (53)$$

It is possible to prove that:

$$\frac{dW}{dt} = \int_\Omega -A \,.\, \dot{\alpha} \, d\Omega + \int_{\partial\Omega} (u \,.\, \dot{F}^d + \sigma \,.\, n \,.\, \dot{u}^d) \, da$$

in such a way that $\mathbf{A}$, the conjugate variable of $\boldsymbol{\alpha}$, is effectively the field of A in Ω. Moreover the conjugate variable of $\mathbf{F}^d$ is the displacement field on $\partial\Omega_F$, and the conjugate field of $\mathbf{u}^d$ is the field of traction $\sigma \,.\, n$ on $\partial\Omega_d$. The analysis of the dissipation leads to a similar result and, for instance, in the example of *II*.4 related to damage mechanics one may write:

$$d = \mathbf{A} \,.\, \dot{\boldsymbol{\alpha}} = \int_\Omega ((\sigma, \dot{\epsilon}^p) + Y \, \dot{D} + R \, \dot{p}) \, d\Omega; \quad (54)$$

then $\boldsymbol{\sigma}$, $\mathbf{Y}$, $\mathbf{R}$ may be considered as the variables conjugate (with respect to the dissipation) to the variables $\dot{\epsilon}^p$, $\dot{\mathbf{D}}$, $\dot{\mathbf{p}}$. For a standard material, a global p.p. may be introduced:

$$\Phi(\dot{\alpha}) = \int_\Omega \varphi(\dot{\alpha}) \, d\Omega, \quad \Phi^*(\mathbf{A}) = \int_\Omega \varphi^*(A) \, d\Omega \quad (55)$$

The introduction of global concepts is important not only to use a more compact notation but for many other reasons. A few of them may be mentioned:

1. In global potentials like (53) or (55) only the fields that are important for the analysis of the structure are kept;

2. It provides a quite useful framework to discuss physical situations like friction, adhesion, unilateral contact, and elastically supported boundary (see for instance [26]);

3. It exhibits the consistency of thermodynamical concepts defined at the level of the particle with the thermodynamical concepts defined on the whole structure. This question will be considered again in Section *VI*.

If the evolutions are not assumed to be isothermal, the fields s and T have to be introduced

For instance, in the situation considered above in Section *V*.1, one may introduce, like in *V*.2, the potential of the structure of the field variables $\mathbf{F}^d$, $\mathbf{u}^d$, $\boldsymbol{\alpha}$, $\mathbf{s}$, and of l, say the global internal energy:

$$E(\mathbf{F}^d,\mathbf{u}^d,\boldsymbol{\alpha},\mathbf{s},l) \quad (56)$$

It may then be proved [25] that J_0 defined by $(50)_2$ is also the conjugate variable of l for this potential:

$$J_0 = -\frac{\partial E}{\partial l}(\mathbf{F}^d, \mathbf{u}^d, \boldsymbol{\alpha}, \mathbf{s}, l) \quad (57)$$

Then, as it is the case for internal variables, the thermomechanical force at the crack tip is at the same time the conjugate of l with respect to the thermodynamical potential, and the conjugate of l with respect to the dissipation, see (51) and (57).

The introduction of global variables is even more necessary when one deals with a three-dimensional crack extension: the crack front curve C is a global variable. In the thermodynamical analysis there appear the normal crack extension velocity field $\mathbf{V}$ along the curve C and its conjugate force density field $\mathbf{J}_0$ along the same curve.

VI Continuum Thermodynamics and Homogenization

The object of the present section is to bring more precisions to the considerations given previously in *III*.6. Homogenization refers to a method by which it is possible and reasonable, in an asymptotic sense, to substitute for a highly heterogeneous medium (at a microscopic level), a homogeneous continuum model (at the macroscopic level) [26, 27]. It will appear that some local variables in the macroscopic description are in fact related to global variables at the microscopic level.

To be specific, one will be concerned with materials that admit elastic stresses ($\sigma^{an} = 0$) and thermodynamic potentials, $e(\epsilon, \alpha, s)$, internal energy or $w(\epsilon, \alpha, \theta)$, free energy; θ is the absolute microscopic temperature. Then the equations of state may be written, for instance:

$$\sigma = \rho \frac{\partial w}{\partial \epsilon}, \quad s = -\frac{\partial w}{\partial \theta}, \quad A = -\rho \frac{\partial w}{\partial \alpha} \quad (58)$$

Noting $\xi = \nabla(\text{Log } \theta)$, generalized Fourier's law (see *IV*.1) will be assumed:

$$q = -k(\xi) \quad (59)$$

1 Preliminary Concepts and Notation. In the discussion of overall properties of heterogeneous media, it is essential to define a volume element that is small enough to allow us to distinguish the microscopic heterogeneities, yet large enough to represent the overall behavior of the heterogeneous medium. Such a volume element V is called the representative volume element (r.v.e.), (for periodic composite it is simply the elementary cell). Most of the macroscopic quantities (M.Q.) are the average on the r.v.e. of the microscopic quantities (m.q.), eventually extended in the case of holes or rigid inclusions. More precisely with ρ, σ, ϵ, e, w, s, ξ, q we associate $\bar{\rho}$, $\bar{\sigma}$, $\bar{\epsilon}$, $\bar{e}$, $\bar{w}$, $\bar{s}$, $\bar{\xi}$, $\bar{q}$ defined by:

Downloaded 02 May 2010 to 171.66.16.250. Redistribution subject to ASME license or copyright; see http://www.asme.org/terms/Terms_Use.cfm

$$\left.\begin{aligned} &\bar{\rho}=\langle\rho\rangle,\ \bar{\sigma}=\langle\sigma\rangle,\ \bar{\epsilon}=\langle\epsilon\rangle,\ \bar{q}=\langle q\rangle,\ \bar{\xi}=\langle\xi\rangle \\ &\bar{\rho}\,\bar{s}=\langle\rho\, s\rangle,\ \bar{\rho}\,\bar{e}=\langle\rho\, e\rangle,\ \bar{\rho}\,\bar{w}=\langle\rho\, w\rangle \end{aligned}\right\} \quad (60)$$

where

$$\langle f\rangle=\frac{1}{|V|}\int_V f(y)\,dy \quad (61)$$

y refers to the microscopic set of coordinates (local coordinates in the r.v.e. V), while x denotes the macroscopic coordinates.

Conversely, starting with the (M.Q.) $\bar{\sigma}$, $\bar{\epsilon}$, $\bar{q}$, $\bar{\xi}$, the definition of suitable corresponding (m.q.) σ, ϵ, q, ξ requires a *localization process*. Such a definition must obviously satisfy not only the corresponding conditions (60), but also the localization conditions. When a r.v.e. is chosen, suitable boundary conditions have to be prescribed. The set of boundary conditions must satisfy some requirements.

(*i*) It must allow us to define a *localization process*: any macroscopic state variables $\bar{\sigma}$, $\bar{\epsilon}$, $\bar{w}$, $\bar{\xi}$ being given, we must be able to find the m.q. σ, ϵ, w, ξ implied by the M.Q. ones, by mean of the microscopic constitutive laws, of the boundary conditions and of the equations of microscopic equilibrium:

$$\operatorname{div}_y \sigma=0,\quad \operatorname{div}_y q=0 \quad \text{(inertia effects on the microscale can be neglected).} \quad (62)$$

(*ii*) For mechanical reasons, Hill's macrohomogeneity condition must be fulfilled by all fields σ^*, ϵ^*, q^*, ξ^*:

$$\bar{\sigma}^*\bar{\epsilon}^*=\langle\sigma^*\epsilon^*\rangle,\quad \bar{q}^*\bar{\xi}^*=\langle q^*\xi^*\rangle \quad (63)$$

As examples, let us mention [26].

(*1*) *Localization in Periodic (or Quasi-Periodic) Structure.* It is the theory of homogenization developed in some books [27] and in many papers, which appears to have numerous practical applications in various fields of mechanics. The cell V is such that by periodicity it generates the whole geometry (V is a special polyedron) and the boundary conditions on ∂V are simply that σ, ϵ, q, ξ take equal values on opposite sides of ∂V, a necessary condition resulting from the periodicity.

(*2*) *Hill-Mandel Stress-Flux Localization Process.* Boundary conditions on V are $\sigma\,.\,n=\bar{\sigma}\,.\,n$, $q\,.\,n=\bar{q}\,.\,n$.

(*3*) *Hill-Mandel Displacement-Temperature Localization Process.* The boundary conditions express that displacement u and $\log\theta$ are the traces on ∂V of linear functions of y in V, $u=\bar{\epsilon}\,.\,y$, $\log\theta=\bar{\xi}\,.\,y$.

A homogenization theory proceeds as follows: starting with the M.Q., using a localization process, knowing all the laws that connect the m.q., we get these quantities and we deduce the corresponding laws that connect the M.Q. This is the scheme that will be applied to thermodynamics in the following subsections.

2 Systems in Equilibrium (Thermostatics). One starts with $\bar{\epsilon}$, T, α where T is the temperature in the macroscopic description, and $\alpha(x,y)$ the field of internal variables will be considered as parameters. As a consequence of the equilibrium assumption, one will assume that T and θ may be practically equal (but not ∇T and $\nabla\theta$ because the latter may exhibit very high spatial oscillations due to the heterogeneities). It is possible to find σ, ϵ, q, ξ as functions of E, T, α, and $\bar{\xi}$ by solving in the cell V, the equations (62) supplemented by the conditions $(60)_3$ and $(60)_5$, the constitutive laws (58) and (59) and the localization boundary conditions. For a given localization process, this solution is unique. If then one computes $\bar{\sigma}$, $\bar{e}$, $\bar{s}$, $\bar{w}$, and $\bar{q}$ by (61), it may be *proved* that:

$$\left.\begin{aligned} &\bar{\sigma}=\bar{\rho}\frac{\partial\bar{w}}{\partial\bar{\epsilon}}(\bar{\epsilon},T,\alpha)=\bar{\rho}\frac{\partial\bar{e}}{\partial\bar{\epsilon}}(\bar{\epsilon},s,\alpha) \\ &\bar{s}=-\frac{\partial\bar{w}}{\partial T},\quad T=\frac{\partial\bar{e}}{\partial\bar{s}} \end{aligned}\right\} \quad (64)$$

thus usual state laws are valid in the macroscopic description. Moreover (64) gives the stress-strain relation of the homogenized material, and similarly it is possible to find the generalized Fourier law for this material which gives $\bar{q}$ as a function of $\bar{\xi}$.

For instance, for a periodic structure whose constituents are linearly thermoelastic, the free energy may be written:

$$2\,\rho\,w(\epsilon,\theta)=(\epsilon-\lambda\theta)\,a(\epsilon-\lambda\theta)-(\lambda\, a\lambda)\,\theta^2-\beta\,\theta^2 \quad (65)$$

where a is a fourth-order tensor, λ a second-order tensor, β a scalar, all of them being functions of x and y. It is then possible to prove that the homogenized body is itself thermoelastic and that $2\,\bar{\rho}\,\bar{w}(E,T)$ has an expression similar to the right-hand side of (65), with coefficients a^{hom}, λ^{hom}, β^{hom} functions of x only which may be uniquely computed with the mean value operator $\langle\ \rangle$ when a finite number of boundary problems have been solved on the cell V.

3 Thermodynamical Evolutions Very Close to Equilibrium. The precise hypothesis is now that the characteristic time τ_M of the macroscopic evolution is large as compared to any time of propagation inside the cell.

If one admits that the first and second principles may be written with m.q.:

$$\rho\,\dot{e}-(\sigma,\dot{\epsilon})+\operatorname{div} q=0,\ \rho\,\theta\,\dot{s}+\operatorname{div} q-q.\xi\geq 0$$

then it is possible to prove that the corresponding laws are still valid for the corresponding M.Q. and that at each time t equations (64) hold. This means that the thermostatic description and Gibb's equation are valid for the homogenized material, if they are assumed to be valid for the constituents.

4 Nonequilibrium Evolutions and Local Equilibrium State. If the temperature θ cannot be assumed to be nearly uniform in the cell V or if the characteristic time in the cell is of the same order as τ_M, the previous analysis fails. In particular, equations (62) are no longer valid since inertia effect with small wavelengths must be taken into account.

At each time t, one may apply to a cell the artificial process described in *III*.6 for which the cell is isolated. As was said in the foregoing, $\bar{e}$, $\bar{\epsilon}$, and some of the α have to be kept constant; those α, say α', which have relaxation time shorter than τ_M are functions of time t, like all the other quantities defined on the cell. One has to study a dynamical evolution toward equilibrium in order to get the m.q. that characterize this equilibrium. For instance, if the set of α' is empty, one has to study a dynamical thermoelastic evolution toward equilibrium. Then one gets the microscopic local accompanying state. The l.a.s. defined in *III*, and especially in *III*.6, is obtained when applying to this microscopic state the technique of homogenization like in *VII*.3.

The anaysis of this section is surely not a decisive justification of the model described in *III* and applied in *IV* and *V*. But it strengthens the interpretation given in *III*.6 and gives an interesting contribution to prove at least the consistency of the model and, simultaneously, a new example of the usefulness of the method of homogenization and localization in order to study highly heterogeneous media.

VII Bifurcation and Stability

In this last very brief section, we want to cite a few general results concerning the stability of the evolutions of systems of

Downloaded 02 May 2010 to 171.66.16.250. Redistribution subject to ASME license or copyright; see http://www.asme.org/terms/Terms_Use.cfm

standard materials (*III*.4). For the sake of simplicity one will assume that the thermal dissipation is negligible (adiabatic or isothermal evolutions).

1 Convexity and Stability. If the material is elastic (no dissipation), the solution of an equilibrium problem corresponds to the minimum of the deformation energy $W'(\mathbf{u}, \mathbf{F}^d, \mathbf{u}^d)$ on the set of the kinematically admissible displacements. On an equilibrium path, the first variation of W must be zero and it has been proved that if the second variation is positive, then the system is stable and no bifurcation is possible:

$$W'_{,\mathbf{u}^2}(\mathbf{u}, \mathbf{F}^d, \mathbf{u}^d).\delta\mathbf{u}^2 > 0 \tag{66}$$

Inequality (66) expresses the local and strict convexity of the thermodynamic potential on the equilibrium path. This theorem is also valid for finite deformation.

This known result may be generalized to most thermoelastic and viscoelastic systems. For example, the Kelvin-Voigt material [28]. *Joint, strict convexity of the thermodynamic potential and of the p.p. potential ensure in general the stability* of an equilibrium.

This result generalizes directly, but significantly, those of Prigogine and his coworkers who have emphasized in the frame of TIP [15] the importance of monotonicity of the force-flux relation:

$$(A_1(\dot{\alpha}_1) - A_2(\dot{\alpha}_2)) \cdot (\dot{\alpha}_1 - \dot{\alpha}_2) \geq 0 \tag{67}$$

which expresses simply the convexity of the p.p. potential $\varphi(\dot{\alpha})$.

2 Special Case of Systems for Which p.p. $\varphi^*(A)$ is the Indicator Function of a Convex Domain. As is well known and as was mentioned previously, such cases appear in plasticity theory and in brittle fracture mechanics. The p.p. $\varphi(\dot{\alpha})$ is a positively homogeneous function of degree 1 and $\varphi^*(A)$ is the indicator function I_p of a convex, closed domain P. As seen in Section *V*.2 or *V*.3, such a system has a global potential W and a global p.p. ϕ^*:

$$W = W(\mathbf{F}^d, \mathbf{u}^d, \boldsymbol{\alpha}),\ \mathbf{A} = -\frac{\partial W}{\partial \boldsymbol{\alpha}},\ \phi^* = \phi^*(\mathbf{A}) \tag{68}$$

and the corresponding c.c.e.:

$$\dot{\boldsymbol{\alpha}} \in \partial\phi^*(\mathbf{A}) \tag{69}$$

is equivalent to Hill's maximum dissipation, i.e., for any A^* in P:

$$(\mathbf{A} - \mathbf{A}^*) \cdot \dot{\boldsymbol{\alpha}} \geq 0.$$

The evolution of the system is obtained by solving (68) and (69) with initial condition $\boldsymbol{\alpha}(0)$.

Here again, the positivity of the second derivative $W_{,\alpha^2}$ plays an important role in bifurcation and stability analysis. Following Hill, by studying the incremental response when $\varphi(\dot{\alpha})$ does not depend on the actual state [29], one obtains:

$$\left.\begin{array}{l} W_{,\alpha^2} \text{ strictly positive on } \partial I_p(A) \Rightarrow \text{stability} \\ W_{,\alpha^2} \text{ strictly positive on } \overline{\overline{\partial I_p}}(A) \Rightarrow \text{nonbifurcation} \end{array}\right\} \tag{70}$$

where $\partial I_p(A)$ is the normal cone and $\overline{\overline{\partial I_p}}(A)$ the subspace generated by vectors of the normal cone.

These criteria have been applied successfully to various problems of solid mechanics: plastic buckling, stability of interacting cracks in brittle fracture, etc. . .

Conclusion

We have tried to exhibit some of the most significant lines of research which have appeared in literature during the last 15–20 years in the field of continuum thermodynamics. Nevertheless, continuum thermodynamics is still in the process of full expansion. Progress may be expected in the next few years in many directions: the improvement of the formulation of basic statements and of the methods in order to give to this field a better mathematical consistency, a deepening of the physical interpretations and significance, and the ability to provide powerful tools to extend the scientific study of many fields, especially in solid mechanics.

References

1 Duhem, P., *Traité d'Energétique*, Gautheir-Villars, Paris, 1911.

2 Woods, L. C., "Thermodynamics Inequalities in Continuum Mechanics," *IMA Journal of Appl. Math.*, Vol. 29, 1982, pp. 221–246.

3 Woods, L. C., *The Thermodynamics of Fluid Systems*, Clarendon Press, Oxford, 1975.

4 Germain, P., *Cours de Mécanique des Milieux Continus*, Masson & Cie, Paris, 1973.

5 Maugin, G., "The Method of Virtual Power in Continuum Mechanics, Application to Coupled Fields," *Acta Machanica*, Vol. 35, 1980, pp. 1–70.

6 Coleman, B. D., "Thermodynamics of Material With Memory," *Arch. Rat. Mech. Anal.*, Vol. 17, 1964, pp. 1–46.

7 Müller, I., "Thermodynamics of Mixture of Fluids," *Journal de Mécanique*, Vol. 14, 1975, pp. 267–303.

8 Müller, I., "Rational Thermodynamics of Mixture of Fluids, Thermodynamics and Constitutive Equations," CIME, Noto, 1982.

9 Müller, I., "Entropy in Non-Equilibrium. A Challenge to Mathematicians," *Trends of Applications of Pure Math. to Mechanics*, Vol. II, Pittmann, London, 1979, pp. 281–295.

10 *Foundations of Continuum Thermodynamics*, Domingos, J. J. D., Nina, M. R., and Whitelaw, J .H., eds., MacMillan, London, 1974.

11 Coleman, B. D., and Owen, D. R., "A Mathematical Foundation for Thermodynamics," *Arch. Rat. Mech. Anal.*, Vol. 54, 1974, pp. 1–104.

12 Coleman, B. D., and Owen, D. R., "On the Thermodynamics of Elastic Plastic Materials With Temperature Dependent Moduli and Yield Stresses," *Arch. Rat. Mech. Anal.*, Vol. 70, 1979, pp. 339–354.

13 Coleman, B. D., Owen, D. R., and Serrin, J., "The Second Law of Thermodynamics for Systems With Approximate Cycles," *Arch. Rat. Mech. Anal.*, Vol. 77, 1982, pp. 103–142.

14 De Groot, S. R., and Mazur, P., *Nonequilibrium Thermodynamics*, North-Holland, 1962.

15 Glansdorff, P., and Prigogine, I., *Structure, Stability and Fluctuations*, Wiley Interscience, New York, 1971.

16 Bataille, J., and Kestin, J., "Irreversible Processes and Physical Interpretation of Rational Thermodynamics," *J. Non Equil. Thermodyn.*, Vol. 4, 1979, pp. 229–258.

17 Sidoroff, F., "Variables Internes en Viscoélasticité et en Plasticité," Thèse, Université Pierre et Marie Curie, Paris, 1976.

18 Moreau, J. J., "Sur les Lois de Frottement, de Viscosité et de Plasticité," *C. R. Acad. Sc.*, Paris, Vol. 271, 1970, pp. 608–611.

19 Halphen, B., and Nguyen, Q. S., "Sur les Matériaux Standards Généralisés," *J. de Mécanique*, Vol. 14, 1975, pp. 39–63.

20 Ziegler, H., "Some Extremum Principles in Irreversible Thermodynamics With Application to Continuum Mechanics," *Progress in Solid Mechanics*, Vol. IV, 1963, pp. 93–193.

21 Mandel, J., "Equations de Comportement d'un Système Élastoplastique Dont l'Écrouissage est dû à des Constraintes Résiduelles," *C. R. Acad. Sc.*, Vol. 284, *A*, 1977, pp. 257–260.

22 Friaâ, A., "Le Matériau de Norton-Hoff Généralisé," These, Université Pierre et Marie Curie, Paris, 1978.

23 Chaboche, J. L., "Description Thermodynamique et Phénoménologique de la Viscoplasticité Cyclique Avec Endommagement," Thèse, Université Pierre et Marie Curie, Paris, 1978.

24 Rousselier, G., "Finite-Deformation Constitutive Relations Including Ductile Fracture Damage," *IUTAM Symp.*, Three-dimensional Const. Rel. and Ductile Fracture, North-Holland, 1981, pp. 331–355.

25 Nguyen, Q. S., "A Thermodynamic Description of the Running Crack Problem," *IUTAM Symp.*, Three-dimensional Const. Rel. and Ductile Fracture, North-Holland, 1981, pp. 315–330.

26 Suquet, P., "Plasticité et Homogénéisation," Thèse, Universite Pierre et Marie Curie, Paris, 1982.

27 Sanchez-Palencia, E., *Nonhomogeneous Media and Vibration Theory*, Lecture notes in Physics, Springer-Verlag, 1980.

28 Potier-Ferry, M., "On the Mathematical Foundations of Elastic Stability," *Arch. Rat. Mech. Anal.*, Vol. 78, 1982, pp. 55–72.

29 Nguyen, Q. S., "Bifurcation et Stabilité des Systèmes Irréversibles Obéissant au Principe de Dissipation Maximale," to be published in *J. de Mécanique*.

Downloaded 02 May 2010 to 171.66.16.250. Redistribution subject to ASME license or copyright; see http://www.asme.org/terms/Terms_Use.cfm

P. J. Holmes
Associate Professor of
Theoretical and Applied Mechanics,
Director of
Center for Applied Mathematics.

F. C. Moon
Professor and Chairman of
the Department of Theoretical
and Applied Mechanics.

Cornell University
Ithaca, N.Y. 14853

Strange Attractors and Chaos in Nonlinear Mechanics

We review several examples of nonlinear mechanical and electrical systems and related mathematical models that display chaotic dynamics or strange attractors. Some simple mathematical models—iterated piecewise linear mappings—are introduced to explain and illustrate the concepts of sensitive dependence on initial conditions and chaos. In particular, we describe the role of homoclinic orbits and the horseshoe map in the generation of chaos, and indicate how the existence of such features can be detected in specific nonlinear differential equations.

Introduction

In the past decade clues to the emergence of randomlike motions in deterministic dynamical systems have been uncovered by new topological methods in mathematics. At the same time experimental measurements and numerical simulation have provided supporting evidence to the mathematical analysis which show that many physical systems may exhibit chaotic behavior without random inputs. The term "chaos" is generally used to distinguish such behavior from a true random process. The systems include mechanical devices with nonlinear springs and multiple equilibrium states, nonlinear circuits, convective flows, aeroelastic systems, and electromagnetomechanical systems, including feedback control devices. These chaotic motions have been called *strange attractors* to distinguish them from classic limit cycle and forced periodic motions. Central to an understanding of these motions is the concept of maps. For continuous motions, this amounts to discrete time sampling of the motion in phase space. A particular map that is common to all strange attractor systems is the horseshoe map. Chaotic motions are also related to classic bifurcation theory in dynamical systems. A common feature of a chaotic system is a succession of bifurcations to higher and higher subharmonics as a parameter is varied. In some simple systems this occurs as a sequence of period doubling bifurcations with a limit point beyond which strange attractors occur (see eg. Feigenbaum [1]).

Infinite sequences of bifurcations to incommensurate periodic motions had been suggested as a route to turbulence in fluids by Landau (cf. Hopf [2]), but Ruelle and Takens [3] were the first to suggest that strange attractors could arise after a finite sequence of bifurcations and might provide models for turbulent motions. In spite of intense activity in this area, however, the connections between the equations of classical fluid mechanics and strange attractors remain unclear and in this paper we will concentrate on models of simpler problems that arise in solid mechanics, dynamics and control theory.

Amongst the important problems to be studied in this area in the future are criteria for determining when a system may become chaotic and analytical methods to predict the spectral properties of the motion. Experimental techniques are also needed to determine if a given chaotic motion belongs to a system with random inputs or to a deterministic one with a strange attractor. Some striking progress has been made in this area recently (cf. Takens [4]).

A Simple Example

In this paper we restrict ourselves to ordinary differential equations and mappings, although many of the ideas generalize, for example, to the partial differential equations of continuum mechanics. Before giving specific examples of chaotic systems of differential equations, we describe a simple one-dimensional map (or first-order difference equation) which introduces many of the important ideas. We define unfamiliar terms as we go along, italicizing them.

Given an initial condition $x=x_0$, our task is to describe the solution or *orbit* based at x_0. Since the map or vector field of the equation are given *deterministic* functions, this is, in principle, possible. However, our first example of a one-dimensional mapping shows that, while any solution can be completely described, *this is sometimes possible only when the initial state is known to infinite accuracy*, and thus in practice the solution might as well become random after a finite time.

Consider the iterated mapping

$$x \to f(x) = \begin{cases} 2x & ; 0 \le x < \tfrac{1}{2} \\ 2x-1; & \tfrac{1}{2} < x \le 1 \end{cases}, \qquad (1)$$

where x is a variable in the closed unit interval $I=[0,1] \subset R$; see Fig. 1. It is easy to see that any point x_0 lying in I will generate an *orbit* $\{x_0, x_1, x_2 \ldots\} = \{x_j\}_{j=0}^{\infty}$, under iteration of f, i.e., $x_{j+1}=f(x_j)$. We also write the orbit $\{f^j(x_0)\}_{j=0}^{\infty}$, where the superscript j denotes j-fold com-

Contributed by the Applied Mechanics Division for publication in the JOURNAL OF APPLIED MECHANICS.

Discussion on this paper should be addressed to the Editorial Department, ASME United Engineering Center, 345 East 47th Street, New York, N.Y. 10017, and will be accepted until two months after final publication of the paper itself in the JOURNAL OF APPLIED MECHANICS. Manuscript received by the ASME Applied Mechanics Division, March 1983.

Copyright © 1983 by ASME
Downloaded 02 May 2010 to 171.66.16.250. Redistribution subject to ASME license or copyright; see http://www.asme.org/terms/Terms_Use.cfm

position of f. Since f is not defined for $x=1/2$, orbits that land there are declared to stop.

Now f clearly has two *fixed points*, 0 and 1, for which $x=f(x)$. Also it can be shown that f has a countable infinity of periodic orbits and that f displays extreme sensitivity to initial conditions. To see this, and to get a complete description of all the orbits of f, we use *symbolic dynamics*. Denote the subintervals [0, 1/2) and (1/2, 1] by I_0 and I_1 (Fig. 1), and assign a (possibly infinite) symbol sequence $a(x)=\{a_j(x)\}$ to each point $x\epsilon I$ by the rule

$$a_j(x)=\left\{\begin{array}{l}0 \text{ if } f^j(x)\epsilon I_0\\ 1 \text{ if } f^j(x)\epsilon I_1\end{array}\right\} \tag{2}$$

(the sequence terminates (is finite) if $f^j(x)=1/2$ for some j). The sequence $a(x)$ is simply the binary expansion of the number x, and, from (2), the action of f on I is modeled by dropping the leading symbol and shifting all others one place to the left. To illustrate we have marked the leading three symbols for points x in eight subintervals each of length 1/8 in., Fig. 1. The reader can easily check that points x in "101" lie in I_1, $f(x)\epsilon I_0$ and $f^2(x)\epsilon I_1$, etc. We cannot specify where $f^3(x)$ is without a finer subdivision, and herein lies the chaos: if the initial point x is known only to finite accuracy, say N places of the expansion, then we cannot say where $f^N(x)$ lies. *Iteration of f is accompanied by a loss of information*; moreover, two points lying within 2^{-N} of one another can lie on orbits that completely differ after N iterates. In fact almost all orbits locally separate exponentially fast: f displays *sensitive dependence on initial conditions.*

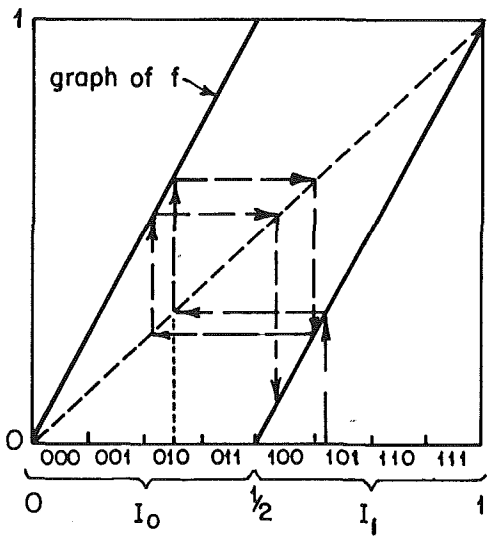


Fig. 1 Bilinear map of equation (1)

Even worse, there is an exact correspondence between a completely random process, coin tossing, and the orbits of f, since *any* sequence of 0's (heads) and 1's (tails) corresponds to an orbit $\{f^n(x)\}_{n=0}^{\infty}$. Once the information given in the initial condition is dissipated, we might as well be coin tossing!

We can clearly write a (countably) infinite set of periodic sequences, 000..., 111..., 0101..., 001001..., 011011..., etc., and can thus conclude that f has countably many periodic orbits. Since $|f'|>1$, all such orbits are unstable and "typical" orbits of f, as in coin tossing, are drawn from the uncountably infinite set of nonperiodic sequences and the orbits corresponding to them.

This piecewise linear map may seem a special example but it is, in fact, similar to a one-dimensional map obtained from careful numerical and geometrical study of the flow of the Lorenz equation [5] derived by truncating the equations for convection in a two-dimensional layer heated from the following:

$$\begin{aligned}\dot{x}&=\sigma(y-x)\\ \dot{y}&=\rho x-y-xz\\ \dot{z}&=-\beta z+xy\end{aligned} \tag{3}$$

For the parameter values $\sigma=10$, $\rho=28$, $\beta=8/3$ (studied by Lorenz) there are three fixed points, all of them unstable saddles, but it is possible to find an ellipsoidal region D into which all solutions ultimately enter and in which they remain

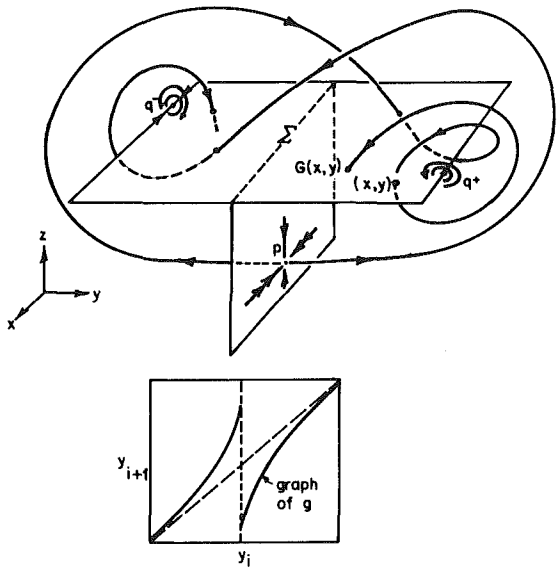


Fig. 2(*a*) Three equilibrium points and trajectories in the phase space of the Lorenz flow (3); and (*b*) A one-dimensional map based on equation (3) (see text)

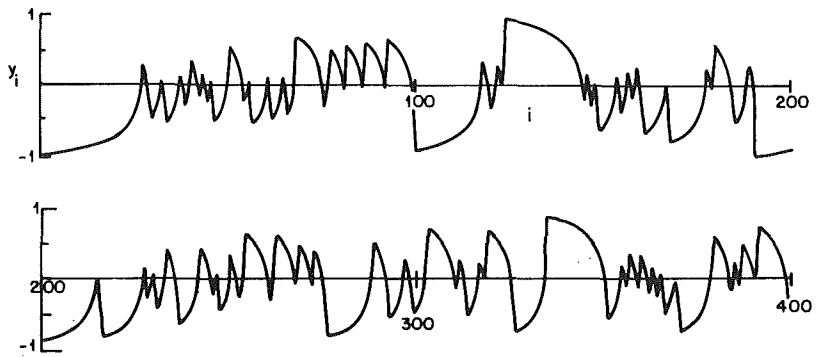


Fig. 3 First 400 iterates of the orbit of g (Fig. 2(*b*)) based on the Lorenz equations (3)

Downloaded 02 May 2010 to 171.66.16.250. Redistribution subject to ASME license or copyright; see http://www.asme.org/terms/Terms_Use.cfm

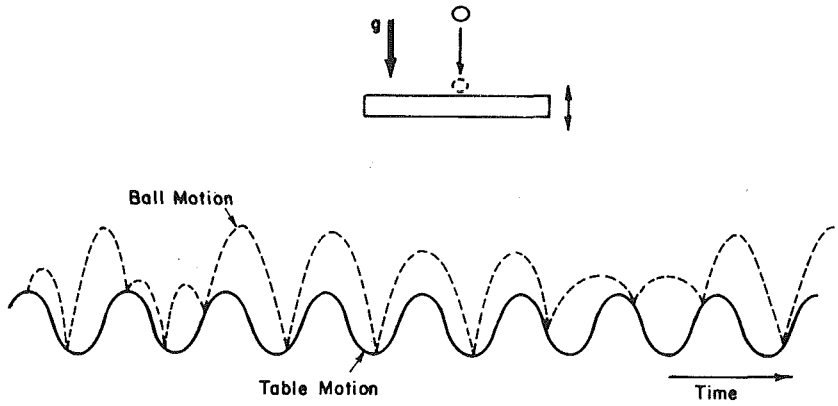


Fig. 4 Multiple impacts of a ball bouncing on a vibrating table

trapped. Moreover, the flow of (3) contracts volumes, for the trace of the Jacobian $\partial\dot{x}/\partial x + \partial\dot{y}/\partial y + \partial\dot{z}/\partial z = -(\sigma+\beta+1)$ is negative. It follows that there is an *attracting set* A inside D that captures all solutions starting nearby. A is the best understood example of a *strange attractor*: an attracting set that is not a fixed point nor a periodic orbit, and for which almost all solutions display sensitive dependence on initial conditions. Thus an orbit asymptotic to a strange attractor A rapidly approaches the subset $A \subset D$ but thereafter wanders erratically about the "surface" of A.

Figure 2 shows a schematic picture of the Lorenz flow and the corresponding one-dimensional map. Note the similarity to the map f of Fig. 1. Roughly speaking, the map g is obtained from the flow by recording the value of one component of the solution (a nonlinear combination of x and y) whenever the z component passes down through the plane $z=\rho-1$ on which the points $q^{\pm}$ lie. For more details, see [6, 7] or the book of Sparrow [8]. In Fig. 3 we show a record of 400 iterates of such a map, to illustrate the nature of the chaotic orbits.

Poincaré Maps

The preceding example introduces an important concept: the *Poincaré map*. Associated with any differential equation that has periodic or recurrent orbits, we have such a map. To define it, we select a *cross section* Σ transverse to the vector field, and pierced by a periodic orbit at a point p. Continuous dependence of solutions on initial data implies that the bundle of solutions originating on Σ near p will follow around and return to p. Thus each point $x_0 \in \Sigma$ near p has an image $x(t_0;x_0) \in \Sigma$, where $x(t;x_0)$ is the solution based at x_0 and t_0 is the return time. The map $P: x_0 \to x(t_0;x_0)$ is the Poincaré map; see Fig. 2. Here the map should really be two-dimensional, and we have projected out one dimension to obtain g.

Another use of Poincaré maps is in forced oscillations. Suppose we have a forced system of differential equations

$$\dot{\mathbf{x}} = f(\mathbf{x},t); \quad \mathbf{x} \in \mathbb{R}^n, \tag{4}$$

where $\mathbf{f}$ is T-periodic in time. To construct a Poincaré map we imagine a particular solution $\mathbf{x}(t;x_0)$ which satisfies an initial condition $\mathbf{x}(0)=x_0$. Then we stroboscopically choose points with values at times $t=nT$, where n is an integer, to obtain the sequence $\{x_n \equiv x(nT;x_0)$. The Poincare map is the given by the rule

$$x_{n+1} = P(x_n) \tag{5}$$

In general, fixed points of P correspond to T-periodic orbits. Cycles of period k $\{x_0, \ldots x_{k-1}; x_k = x_0\}$ correspond to subharmonics of order k, and stability types of orbits also correspond.

The use of the Poincaré map reduces the dimension of the system by one, which is often helpful, and in general the theory of such *discrete dynamical systems* or maps is more highly developed than that of flows, and easier to apply. A typical analysis of a chaotic nonlinear system, then, often starts with *numerical* integration and definition of a Poincaré map, followed by the extraction of relevant *qualitative* features and analysis of the resulting geometrically defined system.

The space available here precludes a detailed review of the differentiable dynamical and global analytical methods used in the study of chaotic equations and maps. The reader wishing to delve further might start with the books of Chillingworth [9] and Guckenheimer and Holmes [10]. Rather than attempt a comprehensive outline of unfamiliar topological notions, in this paper we have concentrated on a few specific examples of differential equations and maps whose solutions behave chaotically. In this way we hope to provide some feeling for the subject and its importance without burdening the reader with overmuch mathematics.

Strange Attractors in Physical Models

There appear to be wide classes of differential or difference equations (maps) that have chaotic solutions. Of particular interest are those that purport to model physical phenomena. The Lorenz equations (3), which attempt to model atmospheric dynamics, have already been mentioned. However the parameter values for which chaotic solutions are found for these equations are not in the range of their physical validity.

Enumerated in the following are examples of mechanical systems, electrical circuits, rotary magnetomechanical devices, feedback controlled devices, and chemical systems, for which a closer connection between the physical system and model exist. Our aim here is to provide a "rogues gallery" of examples before returning to discuss the mathematical aspects of their analysis.

Mechanical Systems

Strange attractor solutions for a periodically forced buckled beam were first studied by Holmes [11] who employed both analysis and analog simulation. Later, experiments were performed [12, 13], which supported the mathematical analysis of a strange attractor. Planar motion of a buckled spherical pendulum has also exhibited chaotic behavior (Moon [14]). These phenomena have been characterized as multiequilibrium problems in which the solution jumps erratically from phase space orbits about one equilibrium point to orbits about another. However, several mechanical vibration problems involving one equilibrium point have recently been found to exhibit chaotic vibrations. These include multiple impacts of a mass on an oscillating table (Holmes [15]), Fig. 4, and vibrations of a bilinear spring

Downloaded 02 May 2010 to 171.66.16.250. Redistribution subject to ASME license or copyright; see http://www.asme.org/terms/Terms_Use.cfm

such as the beam in Fig. 5 with bilinear boundary conditions (Shaw and Holmes [16], Moon and Shaw [17], and Thompson and Ghaffari [61]). The latter problem has also been studied experimentally.

Recently Dowell [18] has found chaotic limit cycle behavior in the aeroelastic problem of flow over a buckled plate (Fig. 6). Using two, four, and six-mode digital simulation, he has computed Poincaré maps that exhibit properties characteristic of strange attractors.

The Buckled Beam – An Experimental Case Study

A physical or intuitive understanding of how chaotic motions may occur in a deterministic system is perhaps best obtained from the simple example of the vibration of a system with two stable equilibria as shown in Fig. 7, or two potential energy wells. Such a potential results from the postbuckling of a column under dead loads or under magnetic forces. In the example shown in Fig. 7, two magnets are moved toward the free end of a ferromagnetic cantilevered beam until the straight position becomes unstable. The magnets in effect change the undeformed position from a potential energy well to a energy hill. In a phase space diagram, the undamped, unforced system exhibits a saddle point at the origin and two centers or stable equilibria surrounded by a figure-eight separatrix. Chaotic motion occurs when damping and periodic forcing are added (Fig. 8). The resulting single mode equation is a form of Duffing's equation which, in non-dimensional form, becomes

$$\ddot{A}+\delta\dot{A}-A+A^3=f\cos\omega t, \tag{6}$$

where $A(t)$ is the amplitude of the first bending mode of the beam.

For small forcing amplitude the stable motion is a periodic orbit about one of the equilibria $A=\pm 1$. However, as the mean radius of this orbit approaches the mean radius of the separatrix, the orbit can jump across the potential hill into the neighboring potential wall. Experimental data shown in Fig. 8 illustrate this jumping from motion about one equilibrium point to another. What makes this behavior so unusual is that the jumping seems to take place randomly. Somewhat as in the simple piecewise linear map f, arbitrary sequences of oscillations about the left (0) or the right (1) equilibrium apparently occur. In fact a spectral analysis of the motion using a Fast Fourier algorithm on discrete time sampled data shows a broad-band distribution of subharmonics below the forcing and small-amplitude natural frequencies (Fig. 9).

However what really provides the "proof test" for experimental observation of strange attractor is the measurement of Poincaré maps, which provide a "foot print" of the strange attractor on which the motion is riding. To obtain an experimental Poincaré map, one measures the displacement and velocity pair $[A(t_n), \dot{A}(t_n)] \equiv \{r_n\}$ at times that are synchronous with a particular phase of the periodic forcing function. The set of points $\{r_n\}$ are either plotted sequentially on a storage oscilloscope or stored in a computer and displayed later on a plotter. An example of such a plot is shown in Fig. 10.

What is remarkable about these experimental maps is that they appear to be invariant in time as long as the original chaotic motion is not disturbed in any way. Thus while the time traces show no order, the Poincaré maps show a complicated but repeatable structure. The "parallel" sets of points are thought to have the character of Cantor sets, as in

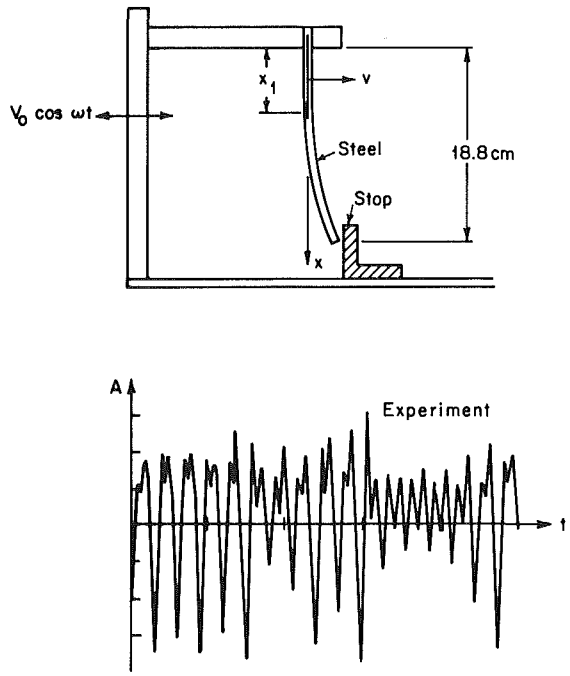


Fig. 5 Chaotic vibrations of a beam with nonlinear boundary conditions (from Moon and Shaw [17])

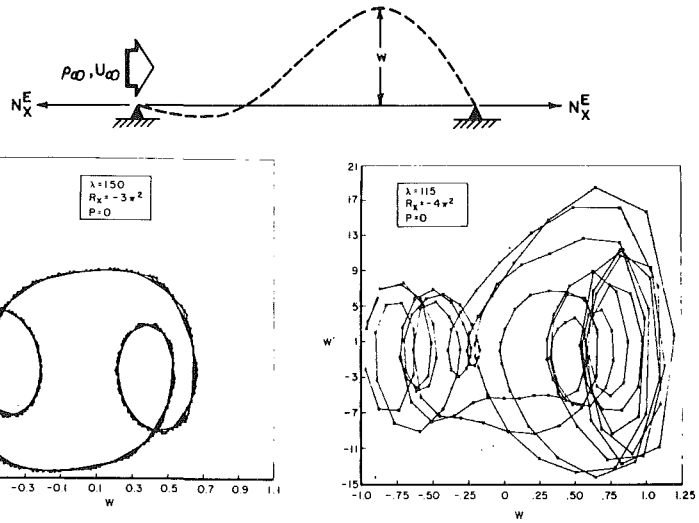


Fig. 6 Flow of fluid over a buckled plate (top); phase plane portrait of periodic limit cycle oscillations (bottom left); phase plane portrait of chaotic oscillations (bottom right) (from Dowell [18] Fig. 6)

Downloaded 02 May 2010 to 171.66.16.250. Redistribution subject to ASME license or copyright; see http://www.asme.org/terms/Terms_Use.cfm

the horseshoe map, described in the following. The orbit is apparently asymptotic to a strange attractor.

A two degree of freedom extension of the planar buckled beam has also been found to exhibit chaotic motion (Moon, [14]). This model is essentially a spherical pendulum with a ferromagnetic mass. Again, magnets below the mass can create multiple equilibrium positions and forced motion of the clamped end of the pendulum provides a periodic input to the system. The differential equation for this system takes the form

$$\ddot{x}+\gamma\dot{x}-\tfrac{1}{2}(1-x^2)x+\beta y^2 x=f_2 \tag{7}$$

$$\ddot{y}+\delta\dot{y}+\alpha(1+\epsilon y^2)y+\beta x^2 y=f_0+f_1\cos\omega t \tag{8}$$

Electrical Circuits

There are an increasing number of numerical simulations and experimental studies of chaotic motions in nonlinear electrical circuits. These studies are of importance to mechanics since their mathematical models often have analogs in mechanical systems. The most extensive work in this field has been done by Ueda and coworkers [19–22] who have used analog and digital simulation techniques. For example Ueda has examined the forced chaotic oscillations of a nonlinear inductance modeled by the equation [19],

$$\ddot{x}+k\dot{x}+x^3=B\cos t, \tag{9}$$

which is a special case of the Duffing's equation. Using Poincaré maps, Ueda has published extensive data on the effect of the damping and forcing amplitude on the transitions into and out of chaos as well as the effects of these parameters on the spectral characteristics of the chaotic vibration. Ueda, Doumoto, and Suehiro [20] also have found chaotic solutions in numerical simulations of the nonlinear Mathieu equation

$$\ddot{x}+k\dot{x}+(a+2b\cos 2t)x+x^3=0. \tag{10}$$

Another problem studied by Ueda is a negative resistor oscillator shown in Fig. 11. The equation for this system is [21],

$$\ddot{x}+(\dot{x}^2-1)\dot{x}+x^3=B\cos\omega t, \tag{11}$$

(a modified Duffing-Van der Pol equation). Using this example, Ueda has demonstrated the difference between *almost periodic* oscillations and strange attractors. The Poincaré map of an almost periodic oscillation has a single simple closed curve for the attracting set in contrast to the accumulating Cantor set like curves characteristic of strange attractors. (Almost periodic flow takes place on the surface of a torus in the three-dimensional $(x, \dot{x}, t)$ phase space of (11).)

A class of problems unique to electrical circuits is a second-order circuit with time delay. Ueda and Nanahara [22] have found chaotic motion in such a system which models a phase-locked feedback loop with time delays.

Period doubling bifurcations and chaotic oscillations have been observed in a circuit with a nonlinear capacitor by Lindsay [23]. The circuit had a varactor diode with a capacitance voltage relation of the form

$$C=C_0(1+\alpha V)^{-\gamma}, \tag{12}$$

where experimentally $\gamma\cong 0.44$. The equations for this system take the form

$$\frac{d}{dt}C(V)V=I$$

$$L\frac{dI}{dt}=-RI-V+V_0\sin\omega t. \tag{13}$$

A similar study of a nonlinear capacitor (a silicon varactor diode) in a harmonically forced series LRC circuit was published by Testa, Perez, and Jefferies [24]. They observed subharmonic bifurcations up to $f/32$. Their experiments were conducted at a base frequency of around 93 kHz. They also obtained the now classic Feigenbaum number [1] corresponding to the critical values of V_0 at which subharmonics appear

$$\frac{V_n-V_{n-1}}{V_{n+1}-V_n}\cong 4.669$$

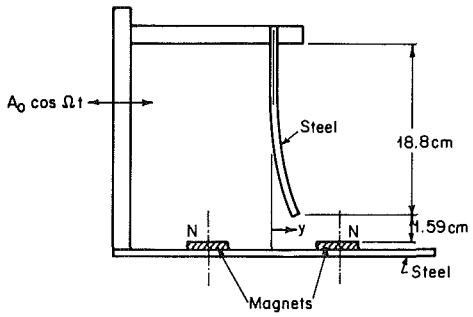


Fig. 7 Experimental apparatus of a buckled beam and two magnets (from Moon and Holmes [12], Moon [13])

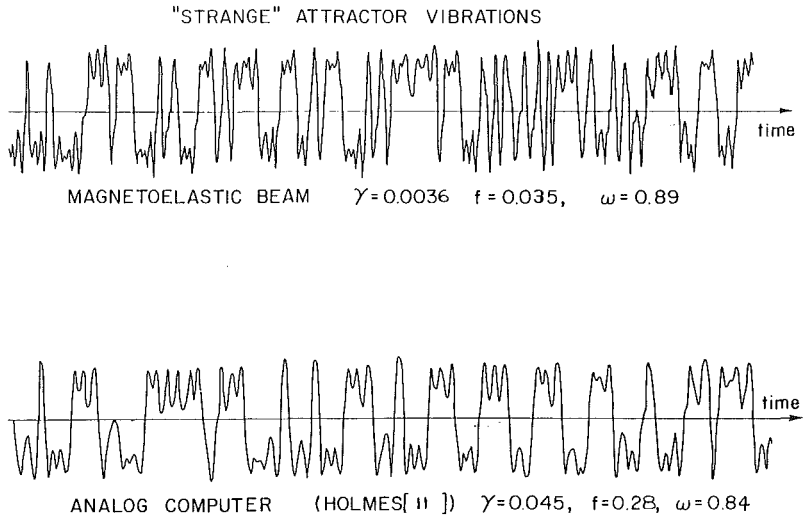


Fig. 8 Chaotic vibrations of a buckled beam experimental data (top), analog computer (bottom) (from Moon and Holmes [12])

Downloaded 02 May 2010 to 171.66.16.250. Redistribution subject to ASME license or copyright; see http://www.asme.org/terms/Terms_Use.cfm

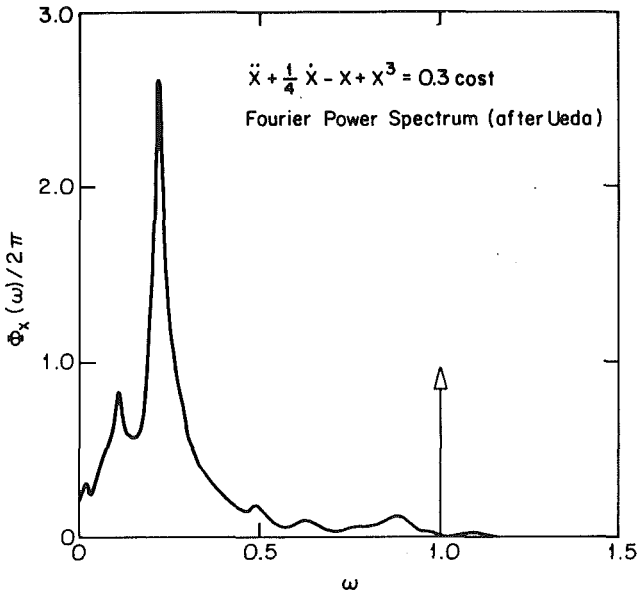


Fig. 9 Fourier spectrum of experimental data

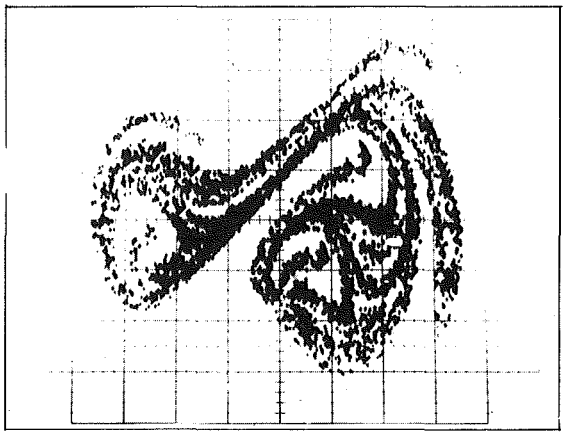


Fig. 10 Experimental Poincare map for chaotic vibrations of a buckled beam

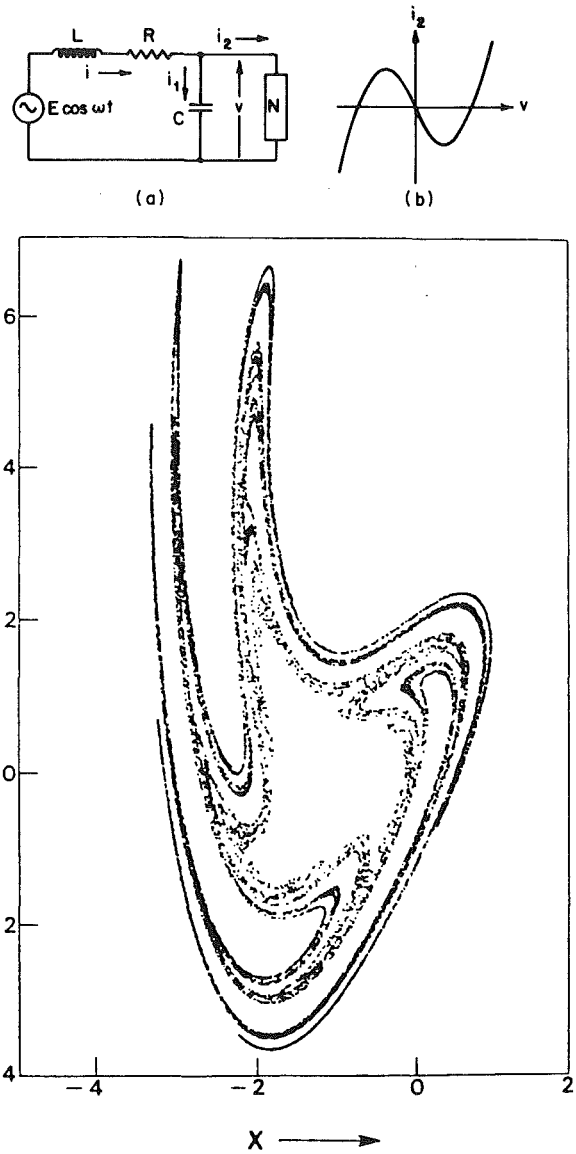


Fig. 11 Circuit diagram with nonlinear negative resister element (top); Poincare map of chaotic oscillations of circuit-numerical simulation (from Ueda [21])

Another example of a harmonically forced nonlinear circuit is a bilinear capacitor studied by Robinson [25]. The bilinear capacitors are created by junction field-effect transistors, which switch linear capacitors into and out of the circuit, depending on the circuit voltage.

Autonomous chaotic oscillations have been observed by Gollub, Romer, and Socalar [26] using a tunnel diode circuit shown in Fig. 12. The current-voltage characteristic of this device has a hysteretic behavior. The dynamics were simulated with bilinear circuit elements. These authors used experimentally determined Lyapunov exponents, discussed in the next section, as a measure of chaos.

Dynamos

A physical system which has received considerable attention has been the dynamics of a rotating disk in a magnetic field. This example is similar to the Lorenz equations in that it is a third-order set of differential equations with product or squared variable nonlinearities. The example is shown in Fig. 13 and the equations governing the rotation Ω and the currents I_1, I_2 are of the form, [27],

$$J\dot{\Omega} = -k\Omega - \mu_2 I_1(I_1 + I_2) + T$$
$$L_1\dot{I}_1 = -RI_1 - R_3 I_2 + \mu_1 \Omega I_1 \qquad (15)$$
$$L_2\dot{I}_2 = -R_2 I_2 + \mu_2 \Omega I_1.$$

This magnetomechanical system is of more interest to geophysists than to electrical engineers since it is one of the mathematical models used to explain the reversals of the Earth's magnetic field. A two-disk dynamo was first proposed by Rikitake [28] in 1958 and by Cook and Roberts [29] in 1970, and numerical simulation showed nonperiodic behavior. The single-disk dynamo previously described has been shown to exhibit strange attractor dynamics by Robbins [27] in which the current exhibits reversals in time of the type shown in Fig. 14. The equations have much in common with the Lorenz system (3): see Chillingworth and Holmes [30].

This magnetomechanical example leads one to suspect that strange attractor vibrations might be possible in turbine generator systems, especially when torsional flexibilities are considered. However this important application has not yet been explored.

Magnetic Torque on a Magnet

Another magnetomechanical device with stochastic dynamics is the torsional oscillations of a compass needle in

Downloaded 02 May 2010 to 171.66.16.250. Redistribution subject to ASME license or copyright; see http://www.asme.org/terms/Terms_Use.cfm

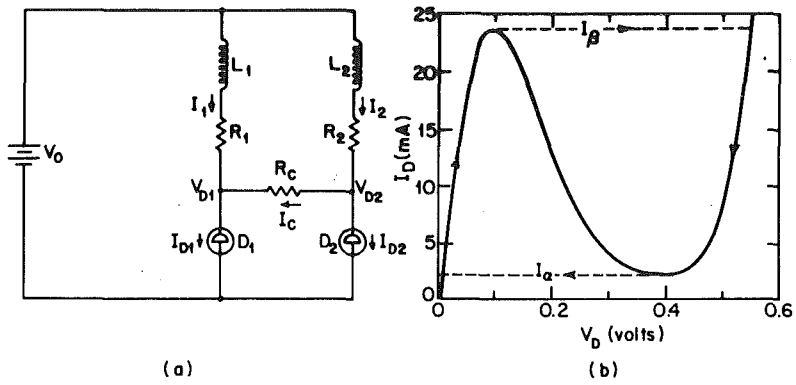


Fig. 12 Tunnel diode oscillator circuit (left) and current-voltage characteristic of the tunnel diode (right) (from Gollub et al. [26])

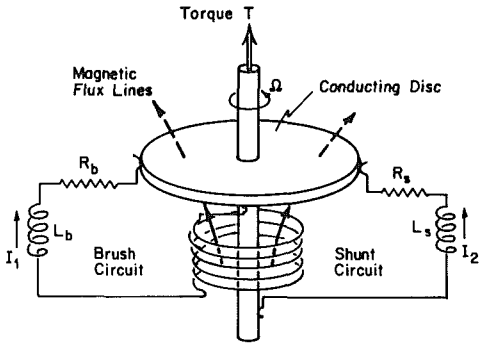


Fig. 13 Rotating dynamo and circuits

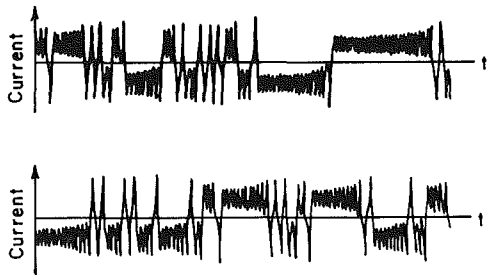


Fig. 14 Chaotic current oscillations in the coil under constant torque (from Robbins [27])

an oscillating or rotating magnetic field (Croquette and Poitou [31]). Damping was minimized in this experiment, so that the problem closely resembles a *Hamiltonian system*. The equation of motion takes the form

$$J\ddot{\theta} = -\mu[\sin(\theta-\omega t)+\sin(\theta+\omega t)], \tag{16}$$

where J is the rotary moment of inertia of the compass and μ is proportional to the product of the maximum field strength and magnetic moment of the compass. Croquette and Poitou observed period doubling bifurcations in this system. In such Hamiltonian systems the occurrence of chaotic orbits is often called *stochasticity* in the literature. A problem that exhibits stochasticity is that of an electron or charged particle in a field of electromagnetic waves (See eg. Chirikov [32]). The equation of motion in one dimension is given by

$$\ddot{x}+\nu\dot{x}=k\sum_{-N}^{N}\sin 2\pi(x-nt). \tag{17}$$

When $N\to\infty$, this equation can be shown to reduce to a set of difference equations

$$\begin{aligned} x_n &= x_{n-1}+V_n \\ V_n &= (1-\nu)V_{n-1}+k\sin 2x_{n-1}. \end{aligned} \tag{18}$$

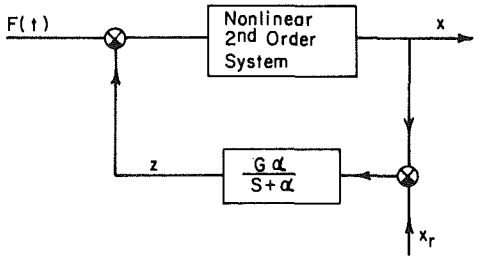


Fig. 15 Schematic of a nonlinear oscillator with linear feedback loop

This map is dissipative for $0<\nu\leq 1$. Numerical simulation of these equations by Jensen and Oberman [33], have shown strange attractor behavior of the solutions. Equation (18), in slightly different coordinates, also models the dynamics of a ball bouncing on a massive sinusoidally vibrating table and chaotic solutions (horseshoes; see the following) have been proved to occur in it (Holmes [15]). Discrete systems or maps such as (18) have also been derived for mechanical impact processes by Hsu [34, 35] who has studied bifurcations of periodic orbits for them, but has not extensively examined chaotic solutions.

Feedback Control Systems

The study of chaos in feedback control systems has received only recent attention (see e.g. [36, 37]). One goal of such research is to understand under what condition noisy solutions can occur in feedback-controlled mechanical devices. The feedback-controlled positioning device described in the following provides an example.

Imagine a mechanical device with multiple equilibrium positions in the absence of feedback. A control force is added to move the system from one position to another. One system that has three stable equilibrium positions is shown in Fig. 15 and is described by the following equation:

$$\begin{aligned} \ddot{x}+\delta\dot{x}+K(x)x &= -z+F(t) \\ \dot{z}+\alpha z &= \alpha G[x-x_r(t)]. \end{aligned} \tag{19}$$

This represents a mechanical oscillator with linear damping δ, nonlinear spring constant $K(x)$, and a linear feedback loop with a time constant $1/\alpha$ and gain parameter G. $F(t)$ represents an external force and $x_r(t)$ represents the desired position history of the device. A specific example with three stable equilibrium positions has the nonlinear function

$$K(x)=\frac{1}{B}(x^2-1)(x^2-B), \quad B>1, \tag{20}$$

where $x=0$, $\pm\sqrt{B}$ are stable equilibria when $G=0$, and $x=\pm 1$ are saddle points. For certain design parameters (δ, α,

Downloaded 02 May 2010 to 171.66.16.250. Redistribution subject to ASME license or copyright; see http://www.asme.org/terms/Terms_Use.cfm

G, B) the system will move from one equilibrium point to another under a given input command $x_r(t)$. However, under a different set of parameters the system may exhibit stable limit cycles and even chaotic behavior. Limit cycle behavior of such systems is well known. In this case for $F=x_r=0$, the origin of the phase space will become an unstable spiral type saddle at a particular value of gain G. Using fourth-order Runge-Kutta difference equations to simulate this system, we have observed chaotic solutions as shown in Fig. 16. The Fourier spectrum of this motion is shown in Fig. 17. The character of these solutions did not change with a decrease of step size. However, the solutions were sensitive to initial conditions as is characteristic of other strange attractor systems.

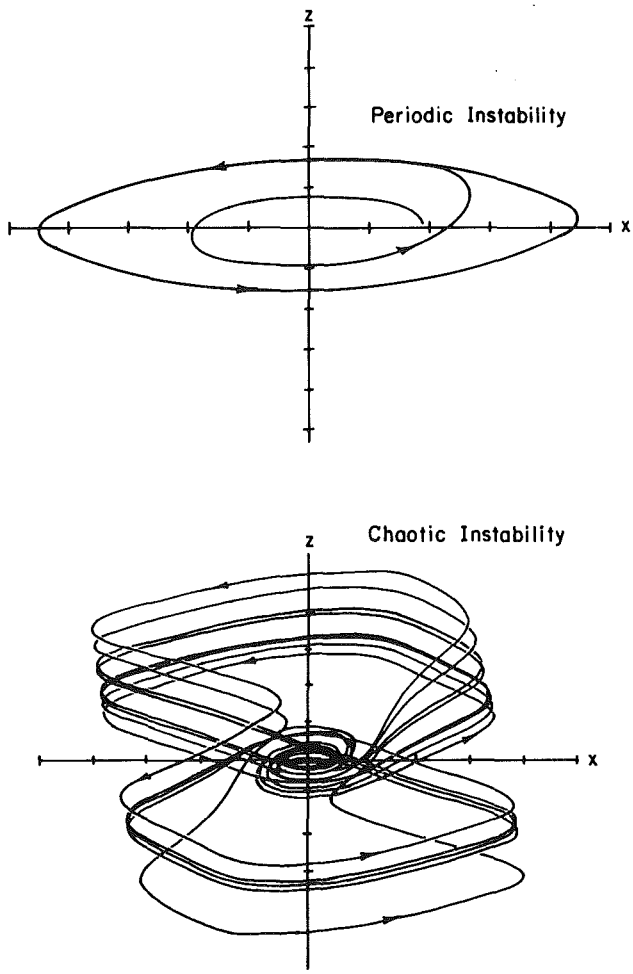


Fig. 16 Phase plane portraits of chaotic dynamics of a multiple equilibria oscillator with feedback (Fig. 15)

Ueda, Doumoto, and Nobumoto [37] have examined chaotic motion in a similar third-order system with nonlinear feedback:

$$\ddot{x}+\mu(z-1)x+x=0$$

$$\tau\dot{z}+z=x^2 \tag{21}$$

This example is similar to the van der Pol oscillator with feedback delay τ. The case $\tau=0$, retrieves the classic van der Pol case. Ueda et al. obtain similar trajectories to those in Fig. 16 as well as a broad spectrum of frequencies in their numerical solution.

Chemical Chaos

Rossler [38] has observed chaotic dynamics in a small reactor-diffusion system. Another example has been demonstrated by Schreiber, Kubicek, and Marik [39] who considered two coupled stirred cell reactors in which two chemicals of concentrations (x_1, y_1) react in one cell and interact with chemicals in a neighboring cell with concentrations (x_2, y_2). The set of governing equations was similar to that used by Rossler [38],

$$\begin{aligned}
\dot{x}_1 &= A-(B+1)x_1+x_1^2y_1+D_1(x_2-x_1)\\
\dot{y}_1 &= Bx_1-x_1^2y_1+D_2(y_2-y_1)\\
\dot{x}_2 &= A-(B+1)x_2+x_2^2y_2+D_1(x_1-x_2)\\
\dot{y}_2 &= Bx_2-x_2^2y_2+D_2(y_1-y_2)
\end{aligned} \tag{22}$$

The interaction between cells was accomplished by flow of liquid between reactors while concentrations of reactants in the inlet stream were held constant. Periodic and chaotic oscillations in concentration were observed within the cells and in the outlet stream.

These systems are analogous to coupled nonlinear spring-mass systems in mechanical vibration such as the one discussed earlier [14], equations (7) and (8).

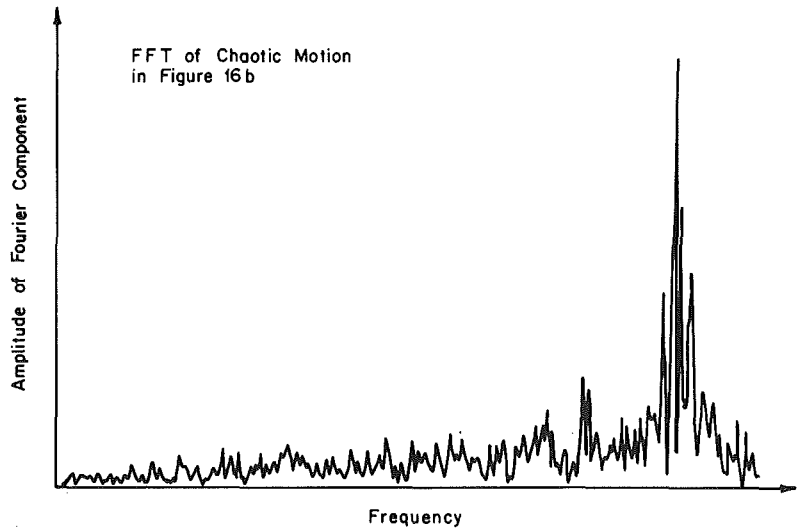


Fig. 17 Frequency spectrum of chaotic motions of single loop feedback system in Figs. 15 and 16

Downloaded 02 May 2010 to 171.66.16.250. Redistribution subject to ASME license or copyright; see http://www.asme.org/terms/Terms_Use.cfm

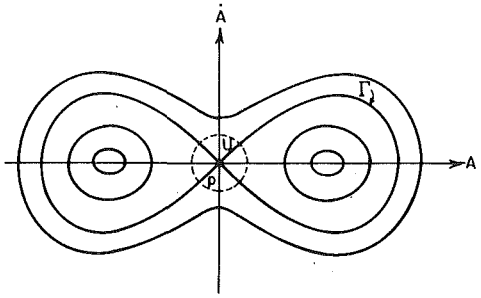


Fig. 18 Phase plane level curves and separatrix of Hamiltonian of Duffing's equation (equation (6), $\delta = f = 0$)

Analytical Methods

We now turn to a brief review of some methods applicable to the analysis of nonlinear differential equations and maps. There are two main approaches open to us, *local analysis*, in which we study small amplitude solutions that bifurcate from a known equilibrium or periodic solution as it becomes unstable, and *global methods*. The former methods are derived from the work of Liapunov and others and are relatively well known, although recent advances in invariant (center) manifold, normal form methods, and computational techniques have rendered them much more powerful. Roughly speaking, these methods enable one to describe the qualitative behavior of solutions near degenerate *nonhyperbolic*, fixed points for which the linearized system has eigenvalues with zero real parts (for differential equations) or unit modulus (for maps). (*Hyperbolic* fixed points have eigenvalues with nonzero real parts and the linearized system suffices to determine behavior near them. Such methods are treated at length in the texts of Marsden-McCracken [40], Guckenheimer and Holmes [10], and Hassard et al. [41]. There are strong connections between such local theories and classical bifurcation theory of equilibrium solutions, as discussed by Iooss and Joseph [42] or Chow and Hale [43]. However, while local methods are useful in describing the details of the bifurcations leading to chaos and strange attractors, the structure of strange attractors is essentially a global question and for the remainder of this section we will concentrate on global methods.

As the Lorenz example of Fig. 2 shows, the essence of an attracting set with sensitive dependence on initial conditions consists in a local expansion that drives nearby solutions apart (usually exponentially fast), followed by a folding or cutting and reinjection of solutions, so that they do not escape but remain trapped in some bounded region. It is usually easy to establish local expansion by linear analysis near a saddle point for example, but showing that nonlinear terms cause the growing solution to turn back and reenter the neighborhood of the saddle is much more difficult. As an example, we will sketch how this is done for the Duffing equation.

For zero external force and damping ($f = \delta = 0$), equation (6) reduces to an integrable Hamiltonian system, its orbits being the level curves of

$$H(A,\dot{A}) = \frac{1}{2}\dot{A}^2 - \frac{1}{2}A^2 + \frac{1}{4}A^4, \qquad (23)$$

sketched in Fig. 18. We especially note the figure-eight double-saddle-connection or *homoclinic orbit* Γ, points on which limit as $t \to \pm\infty$ on the saddle point p. When a small time-periodic force $f \cos t$ is applied, solutions starting in U near p still flow around close to Γ, but on their return to U they can pass either to the left or to the right of p (p has, in fact now become a small $2\pi/\omega$-periodic saddle-type orbit). Of course, they do not have a free choice, their fate is completely determined by the initial condition and the phase of the force

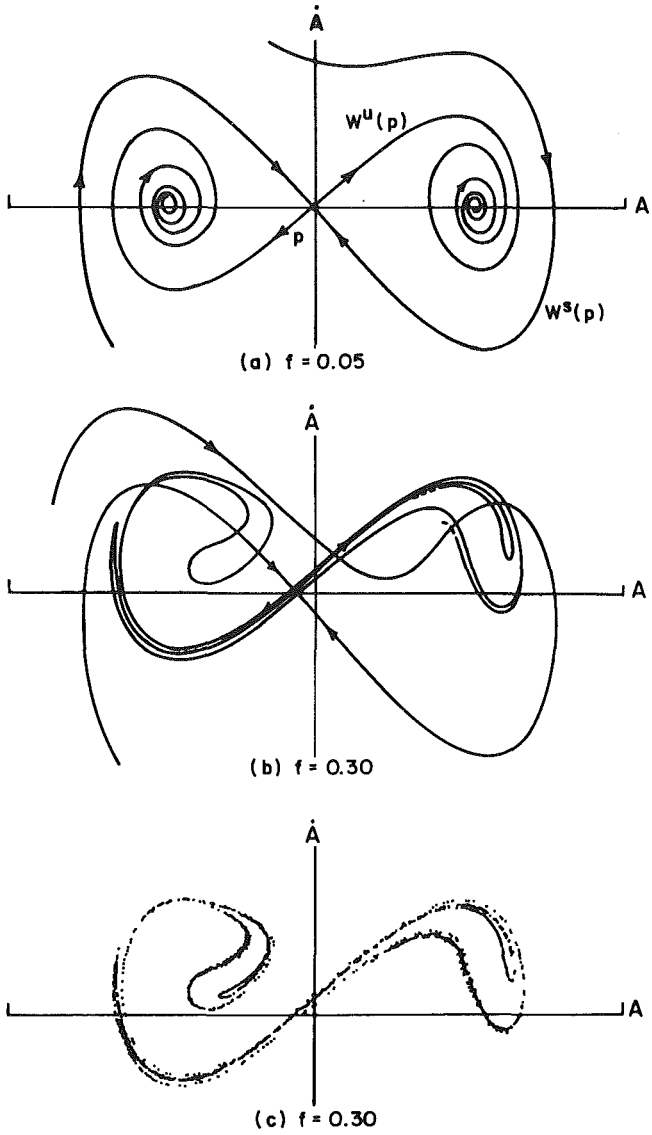


Fig. 19 Poincare maps for Duffing's equation $\delta = 0.25$, $\omega = 1.0$. (*a*) invariant manifolds of *P*; (*b*) invariant manifolds of *P*; and (c) a single orbit presumably asymptotic to the strange attractor (numerical integration).

function, but as in the one-dimensional example, the reliability of our predictions depends on the accuracy of our initial data.

While increase in the force, f, promotes such chaotic orbits, increases in damping, δ, clearly tend to simplify the flow in that, if δ is large enough relative to f, almost all orbits will decay to simple periodic oscillations near the equilibria at $(A, \dot{A}) = (\pm 1, 0)$. We are led to conjecture a *critical ratio* f/δ, above which chaotic orbits can be expected to occur. A *necessary* (but not sufficient) condition can be obtained using *Melnikov* theory [44], developed by Holmes and others [45, 46], which makes use of perturbation calculations based on the homoclinic orbit Γ. To see how this works we consider the Poincaré map of equation (6), and in particular the *stable and unstable manifolds* of the saddle point p (although p becomes a periodic orbit for $f = 0$, it is still fixed point for the map P). The stable manifold $W^s(p)$ is the set of points $x \in R^2$ which are asymptotic to p under forward iteration of P: $\lim_{n\to\infty} P^n(x) = p$. The unstable manifold is the set asympotic to p under backward iteration. The Melnikov theory enables us to determine when these manifolds first intersect. When they do, complicated invariant sets, Smale horseshoes, [47] burst into

Downloaded 02 May 2010 to 171.66.16.250. Redistribution subject to ASME license or copyright; see http://www.asme.org/terms/Terms_Use.cfm

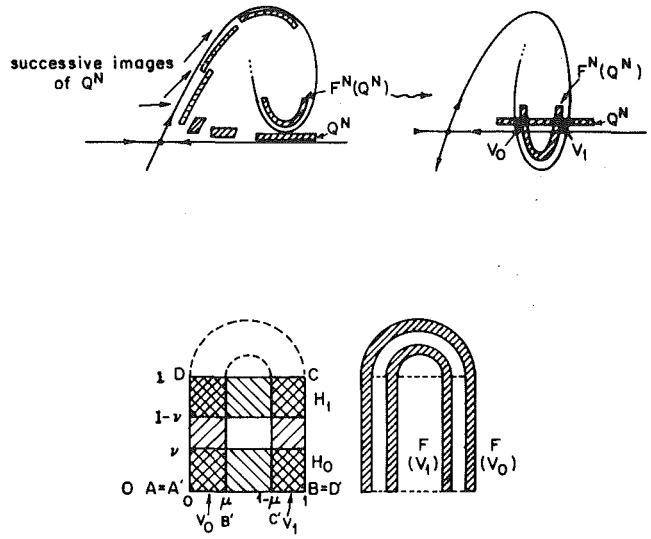


Fig. 20 *(a)* **The creation of horseshoes in a homoclinic bifurcation and** *(b)* **The piecewise linear horseshoe**

existence in infinite sets of bifurcations. We show numerical results due to Ueda which illustrate this in Fig. 19, and in Fig. 20 we show how the approach and ultimate intersection of the manifolds as f increases for fixed δ leads to the existence of a horseshoe in some iterate of the map, P^N. Once such intersections or *homoclinic* points exist, a small "rectangular" region Q^N can be found such that the horseshoe shaped image $P^N(Q^N)$ intersects Q^N in two "vertical" strips V_0 and V_1.

The Melnikov calculation requires only a simple integration along the unperturbed orbits and thus conditions necessary for the existence of strange attractors can be established analytically in many cases, see [10, 45-46] for details.

We are therefore led to study maps F defined on a square Q such that $F(Q)$ intersects Q in two disjoint strips. Here we consider a simple piecewise linear mapping which retains all the important qualitative features of the nonlinear map P^N near the homoclinic point q. Our exposition is adapted from Chillingworth [9], following the original work of Smale [47]. We take the unit square $Q=[0,1]\times[0,1]$ and consider the map F: $Q\to\mathbb{R}^2$ defined such that the images of two horizontal strips H_i are two vertical strips V_i, as shown in Fig. 20(*a*). We assume that F is linear on H_0 and H_1, and has derivatives

$$DF(p)=\begin{bmatrix}\mu & 0\\ 0 & 1/\nu\end{bmatrix},\ p\in H_0;\quad 0<\mu<\nu<1$$

$$DF(p)=\begin{bmatrix}-\mu & 1\\ 0 & -1/\nu\end{bmatrix},p\in H_1 \tag{24}$$

and that $F([0,1]\mathbf{x}(\nu, 1-\nu))$ lies outside Q.

The *nonwandering set* Λ_v of points which remain in Q for all backward iterates of F is given by

$$\Lambda_v=\bigcap_{k\geq 0} F^k(Q)=Q\cap F(Q)\cap F^2(Q)\cap\ \ldots \tag{25}$$

$Q\cap F(Q)$ is just the pair of vertical strips $V_0\cup V_1$ of Fig. 20(*a*). The image of each of these itself intersects Q in a pair of strips. It is easy to verify that

$$\bigcap_{k=0}^{n} F^k(Q)$$

consists of 2^n vertical strips each of width μ^n, so that in the limit one obtains an uncountable set of vertical lines. Hence $\Lambda_v=C_v\mathbf{x}[0,1]$, where C_v is the *Cantor set* obtained by removing the middle fraction $\delta_v=(1-2\mu)$ of the horizontal interval [0,1], followed by the middle δ_v of the remaining closed intervals, ad infinitum. Similarly one finds that Λ_h, the set of points remaining in Q for all forward iterates of F, is given by $\Lambda_h=[0,1]\mathbf{x}C_h$, where C_h is the middle $\delta_h=(1-2\nu)$ Cantor set of the vertical interval. Thus the nonwandering set of points which *never* leave Q is given by $\Lambda=\Lambda_h\cap\Lambda_v=C_h\mathbf{x}C_v$, and is itself a Cantor set.

We can label each of the points $p\in\Lambda$ with a doubly infinite symbol sequence $\{a_n(p)\}=\{\ldots a_{-2}(p)a_{-1}(p)\cdot a_0(p)a_1(p)a_2(p)\ldots\}$ as follows. The forward going sequence $a_0a_1a_2\ldots$ locates p in one of the horizontal lines of Λ_h and the backward going sequence $a_{-1}a_{-2}\ldots$ locates p in one of the vertical lines of Λ_v. For example $a_0=0$ if $p\in H_0$ and $a_0=1$ if $p\in H_1$. It can be shown that there is precisely one such symbol sequence for each point in Λ. Moreover, the sequences can be chosen to reflect the dynamics of F restricted to Λ by requiring that $a_n(F(p))=a_{n+1}(p)$, so that iteration of F corresponds to shifting the sequence to the left, as in the example f described in the foregoing. However, now we have *doubly* infinite sequences, since unlike our one-dimensional example F is an *invertible* map. But just as before we obtain infinite sets of periodic and nonperiodic orbits by enumerating the symbol sequences.

In this way we obtain a set of chaotic orbits similar to those of the piecewise linear map f. However, these sets are not attracting, but rather behave like chaotic saddle points. Thus, while they promote sensitive dependence on initial conditions, almost all orbits ultimately escape from them and then perhaps settle down to a stable periodic orbit (stable orbits can coexist with the horseshoe since we have only considered the image under F of a specially chosen domain of the state space). However, any such stable periodic orbits may have arbitrarily long periods, and hence may appear as erratic as the nonperiodic motions [45].

Returning to Figs. 19 and 20, the reader can see that the invariant set

$$\Lambda^N=\bigcap_{n=-\infty}^{\infty} P^N(Q^N)$$

is empty for small f, and is a full horseshoe for large f. Infinitely many bifurcations evidently occur as the tangency is approached. Calculations with model problems and perturbation theory for the Duffing problem [45] show that stable periodic orbits of long periods are created in any neighborhood of homoclinic points. These sinks repeatedly double their periods as the homoclinic bifurcation point is approached and ultimately vanish into the horseshoes. However, more delicate computations due to Newhouse [48] show that, for typical invertible maps, *infinitely* many such stable periodic orbits can coexist for sets of parameter values near those at which homoclinic bifurcations occur. In these situations, while the attracting set contains horseshoes, it also contains infinitely many sinks which have "sneaked in" and hence is not indecomposable. It is still unknown whether there are parameter values for which all the sinks in one region have "sneaked out" again, without new ones being created in other regions, although there are such results for one-dimensional maps [49].

Another way of describing the complicated structure of the attracting set for the Duffing system is to note that it is *nonhyperbolic*. Just as fixed points and periodic orbits can be hyperbolic (and hence stable to small perturbations), so can more complicated attracting sets. The theory of hyperbolic attractors is quite complete and they can be analysed nicely (Chillingworth [9], Newhouse [48]). To verify that an invariant set A is hyperbolic we must show that the linearized map DF uniformly contracts tangent vectors in one direction E^s_x at every point $x\epsilon A$ and uniformly expands tangent vectors in a second, transverse direction E^u_x. The stable and unstable tangent spaces must fit together in a continuous manner, so that, for the nonlinear problem, one obtains a foliation of a neighborhood of the attractor by one-dimensional leaves of

Downloaded 02 May 2010 to 171.66.16.250. Redistribution subject to ASME license or copyright; see http://www.asme.org/terms/Terms_Use.cfm

the stable manifold of points $x \in A$. For the Duffing problem this is impossible; since the stable manifold $W^s(p)$ winds around in a complicated fashion so that, even if $W^s(p)$ is not itself tangent to $W^u(p)$ anywhere, nevertheless any locally "parallel" foliation including $W^s(p)$ must be tangent to $W^u(p)$ at some point. Thus we cannot project along the stable direction to obtain a one-dimensional map as in the Lorenz equations.

A good measure of the hyperbolicity of an attracting set is provided by Liapunov or characteristic exponents [10] which measure the average expansion and contraction rates of the flow or map linearized along typical orbits. Such exponents can be computed numerically quite easily [50]. We refer to them again in the following section.

Another way in which chaotic solutions and horseshoes can be found in specific differential equations is by the local analysis of multiply degenerate bifurcating equilibria. If, for example, in a two parameter problem the parameters are adjusted so that the equilibrium becomes unstable to an oscillatory and a steady mode simultaneously (combined flutter and divergence, in aeronautical parlance) then the periodic mode can feed energy to the steady mode and cause erratic oscillations much as in the externally forced Duffing equation; see [51, 52, 10].

Criteria for Chaos

Two examples of chaos criteria based on mathematical analysis are those derived from Melnikov theory for periodically forced oscillators [10, 11, 45] and Zaslavskii's criterion for the two-dimensional map (18), [53]. The former has already been outlined.

A heuristic semianalytical criteria for strange attractors has been proposed by Moon [13] for the forced Duffing's equation with three equilibrium positions, which is similar in spirit to one proposed by Chirikov (see the following). Moon imagines that for small f and δ, the motion takes place in a potential well and is periodic. If the amplitude of this periodic motion gets too large, the particle can jump out of this well and oscillate about all three equilibrium points. He proposes a critical velocity which is close to the maximum velocity on the separatrix of the unforced, undamped system. The criterion agrees reasonably well with experimental observation [13].

For the two-dimensional map (18), Zaslavskii has found that when $0 < \nu < 1$, and k is small, (dissipative case) all orbits are attracted to stable fixed points but when $k > 1$, strange attractor solutions appear (see Jensen and Oberman [33]). These orbits appear before the "large" horseshoes found by Holmes [15] for $k > 5/2$ and $\nu \cong 0$.

Another chaos criteria for maps which has been used by Rechester and White [54], is the Liapunov exponent

$$\lambda = \lim_{T \to \infty} \frac{1}{T} \sum_{t=0}^{T} ln \left| \frac{dF(x_t)}{dx} \right| \tag{26}$$

for the map

$$x_{t+1} = F(x_t; \alpha), \tag{27}$$

where $\lambda < 0$ for a periodic attractor, and $\lambda > 0$ for a strange attractor. The interpretation of this criterion is that when $\lambda > 0$, nearby orbits diverge. This criterion has been used experimentally by Gollub et al. [26].

Chirikov [32] has developed a criterion for chaos or stochasticity in a forced nonlinear Hamiltonian system of the form

$$\ddot{x} + x^3 = f_1 \cos(\omega_1 t + \phi_1) + f_2 \cos(\omega_2 t + \phi_2) \tag{28}$$

Local chaotic motions have been found in the neighborhood where the nonlinear resonant frequency is equal to the forcing frequencies ω_1, ω_2. As f_1, f_2 are increased the regions of local chaotic solutions grow. Chirikov proposed that the critical values of f_1, f_2 for global chaos are found when the local regions begin to overlap. This criterion seems to give predictions that are the right order of magnitude. Greene [55] and others have worked on finer criteria for the break up of invariant curves in the two-dimensional area preserving Poincaré maps for such systems and more recently the renormalization approach used by Feigenbaum [1] has been successfully applied to study the quasiperiodic motions occurring on such tori and how the tori break up [56, 57].

It should be noted however that such "Hamiltonian" chaos is not a strange attractor, though Ueda [19] has added damping to the preceding system of equations and has found chaotic bevavior. One of the goals of current research efforts in nonlinear dynamics is to understand the transition and the connection between chaotic strange attractor vibrations in dissipative systems and stochastic solutions in Hamiltonian systems. Certainly homoclinic orbits and horseshoes play an important role in both. The Melnikov perturbation theory provides a useful method in this area.

Conclusions

In this paper we have demonstrated by means of several examples that apparently simple sets of third-order and time-dependent or coupled second-order deterministic differential equations can display extremely complicated, chaotic solutions. We have chosen our examples mainly from the dynamics of simple mechanical and electrical systems, but many other applications arise in fluid mechanics, physics, chemistry, and the other sciences. See [58–60] for a representative range of papers. In the past 5–10 years the results of abstract mathematical research in dynamical systems have been applied to such problems, and many new computational and analytical tools have been developed in the process. However, much remains to be done, both in the mathematical analysis of nonhyperbolic sets containing horseshoes, and in the study of specific equations and maps for which naive applications of perturbation theory fail. (In most practical problems, one's parameters are neither small nor in front of the right terms!) An area of special concern for engineering applications is that of predicting the statistics of a chaotic motion from the topological structure of the attracting set. While there are some results for abstract hyperbolic attractors [10, 48], almost nothing is known about "realistic" problems such as the Duffing equation.

References

1 Feigenbaum, M. J., "Quantitative Universality for a Class of Nonlinear Transformations," *J. Stat. Phys.*, Vol. 19, 1978, pp. 25–52.

2 Hopf, E., "A Mathematical Example Displaying Features of Turbulence," *Comm. Pure. Appl. Math.*, Vol. 1, 1948, pp. 303–322.

3 Ruelle, D., and Takens, F., "On the Nature of Turbulence," *Comm. Math. Phys.*, Vol. 20, pp. 167–192; Vol. 23, pp. 343–344.

4 Takens, F., "Detecting Strange Attractors in Turbulence," *Dynamical Systems and Turbulence*, 1980, Rand, D. A., and Young, L.-S., eds., pp. 366–381; *Springer Lecture Notes in Mathematics*, Vol. 898, Springer Verlag, New York, Heidelberg, Berlin.

5 Lorenz, E. N., "Deterministic Non-Periodic Flow," *J. Atmospheric Sciences*, Vol. 20, 1963, pp. 130–141.

6 Guckenheimer, J., "A Strange Strange Attractor," *The Hopf Bifurcation and Its Applications*, 1976, Marsden, J. E., and McCracken, M., eds., Springer Verlag, New York, Heidelberg, Berlin, pp. 368–381.

7 Williams, R. F., "The Structure of Lorenz Attractors," *Publ. Math. I.H.E.S.*, Vol. 50, 1979, pp. 101–152.

8 Sparrow, C., *The Lorenz Equations*, 1982, Springer Verlag, New York, Heidelberg, Berlin.

9 Chillingworth, D. R. J., *Differentiable Topology With a View to Applications*, Pitman, London, 1976.

10 Guckenheimer, J., and Holmes, P. J., *Nonlinear Oscillations, Dynamical Systems and Bifurcations of Vector Fields*, 1983, Springer Verlag, New York, Heidelberg, Berlin.

11 Holmes, P. J., "A Nonlinear Oscillator With a Strange Attractor," *Phil. Trans. Roy. Soc. A*, Vol. 292, 1979, pp. 419–448.

Downloaded 02 May 2010 to 171.66.16.250. Redistribution subject to ASME license or copyright; see http://www.asme.org/terms/Terms_Use.cfm

12 Moon, F. C., and Holmes, P. J., "A Magnetoelastic Strange Attractor," *J. Sound Vib.*, Vol. 65, No. 2, 1979, pp. 275-296; Moon, F. C., and Holmes, P. J., "A Magnetoelastic Strange Attractor," *J. Sound Vib.*, Vol. 69, No. 2, p. 339.

13 Moon, F. C., "Experiments on Chaotic Motions of a Forced Nonlinear Oscillator: Strange Attractors," ASME JOURNAL OF APPLIED MECHANICS, Vol. 47, 1980, pp. 638-44.

14 Moon, F. C., "Experimental Models for Strange Attractor Vibration in Elastic Systems," *New Approaches to Nonlinear Problems in Dynamics*, Holmes, P. J., ed., 1980, pp. 487-495.

15 Holmes, P. J., "The Dynamics of Repeated Impacts With a Sinusoidally Vibrating Table," *J. Sound Vib.*, Vol. 84, 1982, pp. 173-189.

16 Shaw, S. W., and Holmes, P. J., "A Periodically Forced Piecewise Linear Oscillator," *J. Sound Vib.*, 1983, in press.

17 Moon, F. C., and Shaw, S. W., "Chaotic Vibration of a Beam With Nonlinear Boundary Conditions," to appear in *J. Nonlinear Mechanics*, 1983.

18 Dowell, E. H., "Flutter of a Buckled Plate as an Example of Chaotic Motion of a Deterministic Autonomous System," *J. Sound Vib.*, Vol. 85, No. 3, 1982, pp. 333-344.

19 Ueda, Y., "Randomly Transitional Phenomena in the System Governed by Duffing's Equation," *J. Statistical Physics*, Vol. 20, 1979, pp. 181-196.

20 Ueda, Y., Doumoto, H., and Suehiro, Y., "Randomly Transitional Phenomena in the System Governed by Mathieu's Equation With Nonlinear Restoring Term," Report of Electric and Electronic Communication in Japan, Nov. 1978, NLP-24.

21 Ueda, Y., and Akamatsu, N., "Chaotically Transitional Phenomena in the Forced Negative Resistance Oscillator," *Proc. IEEE ISCA8 '80*, 1980. Also *IEEE Trans. Circuits and Systems*, Vol. CAS-28, No. 3, Mar. 1981.

22 Ueda, Y., and Nanahara, T., "Computer Experiments on the Solutions of Nonlinear Differential-difference Equations—For the Phase-locked loop With Time Delay," Report of Electric and Electronic Communication, Nov. 1978, NLP 78-20.

23 Linsay, P. S., "Period Doubling and Chaotic Behavior in a Driven, Anharmonic Oscillator," *Phys. Rev. Let.*, Vol. 47, No. 19, 1981, pp. 1349-1352.

24 Testa, J., Perez, J., and Jeffries, C., "Evidence of Universal Chaotic Behavior of a Driven Nonlinear Oscillator," *Phys. Rev. Let.*, Vol. 48, 1982, p. 714.

25 Robinson, F. N. H., "An Experimental Study of the Catastrophic Behavior of a Non-Linear Differential Equation," preprint of Clarendon Laboratory, 1982.

26 Gollub, J. P., Romer, E. J., and Socalar, J. E., "Trajectory Divergence for Coupled Relaxation Oscillators: Measurements and Models," *J. Statistical Physics*, Vol. 23, No. 3, 1980.

27 Robbins, K. A., "A New Approach to Subcritical Instability and Turbulent Transitions in a Simple Dynamo," *Math. Proc. Camb. Phil. Soc.*, Vol. 82, 1977, pp. 309-325.

28 Rikitake, T., "Oscillations of a System of Disc Dynamos," *Proc. Caomb. Phil. Soc.*, Vol. 54, 1958, pp. 89-105.

29 Cook, A. E., and Roberts, P. H., "The Rikitake Two-Disc Dynamo System," *Proc. Comb. Phil. Soc.*, Vol. 68, 1970, pp. 547-569.

30 Chillingworth, D. R. J., and Holmes, P. J., "Dynamical Systems and Models for Reversals of the Earth's Magnetic Field," *Mathematical Geology*, Vol. 12, 1980, pp. 41-59.

31 Croquette, V., and Poitou, C., "Cascade of Period Doubling Bifurcations and Large Stochasticity in the Motions of a Compass," *J. Physique-Lettres*, Vol. 42, 1981, pp. L537-L539.

32 Chirikov, B. V., "A Universal Instability of Many Dimensional Oscillator Systems," *Physics Reports*, Vol. 52, 1979, pp. 263-379.

33 Jensen, R. V., and Oberman, C. P., "Statistical Properties of Chaotic Dynamical Systems Which Exhibit Strange Attractors," Princeton Plasma Physics Lab Report PPPL-1780, July 1981.

34 Hsu, C. S., Yee, H. C., and Cheng, W. H., "Steady-State Response of a Nonlinear System Under Impulsive Periodic Parameteric Excitation," *J. Sound and Vibration*, Vol. 50, 1977, pp. 95-116.

35 Hsu, C. S., "On Nonlinear Parametric Excitation Problems," *Advances in Applied Mechanics*, Vol. 17, 1977, pp. 245-301.

36 Sparrow, C. T., "Chaos in a Three-Dimensional Single Loop Feedback System With a Piecewise Linear Feedback Function," *J. Math. Anal. and Appl.*, Vol. 83, 1981, pp. 275-291.

37 Ueda, Y., Doumoto, H., and Nobumoto, K., "An Example of Random Oscillations in Three-Order Self-Restoring System," *Proc. Electric and Electronic Communication Joint Meeting*, at Kansai District in Japan, October 1978.

38 Rössler, O. E., "Chemical Turbulence: Chaos in a Small Reaction-Diffusion System," *Naturforsch*, Vol. 31a, 1976, pp. 1168-1172.

39 Schreiber, I., Kubicek, M., and Marak, M., "On Coupled Cells," *New Approaches to Nonlinear Problems in Dynamics*, Holmes, P. J., ed., SIAM, Philadelphia, 1980, pp. 496-508.

40 Marsden, J. E., and McCracken, M., *The Hopf Bifurcation and Its Applications*, Springer-Verlag, New York, Heidelberg, Berlin, 1976.

41 Hassard, B. D., Kazarinoff, N. D., and Wan, Y-H., *Theory and Applications of the Hopf Bifurcation*, Cambridge University Press, Cambridge, United Kingdom, 1980.

42 Iooss, G., and Joseph, D. D., *Elementary Stability and Bifurcation Theory*, Springer-Verlag, New York, 1981.

43 Chow, S. W., and Hale, J. K., *Methods of Bifurcation Theory*, Springer-Verlag, New York, Heidelberg, Berlin, 1982.

44 Melnikov, V. K., "On the Stability of the Center for Time Periodic Perturbations," *Trans. Moscow Math. Soc.*, Vol. 12, 1963, pp. 1-57.

45 Greenspan, B. D., and Holmes, P. J., "Homoclinic Orbits, Subharmonics and Global Bifurcations in Forced Oscillations," to appear in *Nonlinear Dynamics and Turbulence*, Barenblatt, G., Iooss, G., and Joseph, D. D., eds., 1982.

46 Holmes, P. J., and Marsden, J. E., "Horseshoes in Perturbations of Hamiltonians With Two Degrees of Freedom," *Comm. Math. Phys.*, Vol. 82, 1982a, pp. 523-544.

47 Smale, S., "Diffeomorphisms With Many Periodic Points," *Differential and Combinational Topology*, Cairns, S. S., ed., 1963, pp. 63-80.

48 Newhouse, S. E., "Lectures on Dynamical Systems," *Dynamical Systems*, CIME Lectures Bressanone, Italy, June 1978, pp. 1-114. Progress in Mathematics No. 8, Birkhauser Boston, Inc.

49 Collet, P., and Eckmann, J-P., "Iterated Maps on the Interval as Dynamical Systems," *Progress in Physics*, Vol. 1, 1980.

50 Feit, S. D., "Characteristic Exponents and Strange Attractors," *Comm. Math. Phys.*, Vol. 61, 1978, pp. 249-260.

51 Holmes, P. J., "Center Manifolds, Normal Forms and Bifurcations of Vector Fields With Application to Coupling Between Periodic and Steady Motions," *Physica 2D*, 1981a, pp. 449-481.

52 Guckenheimer, J., "On a Codimensional Two Bifurcation," *Dynamical Systems and Turbulence*, Rand, D. A., and Young, L.-S., eds., 1981, pp. 99-142. Also Springer Lecture Notes in Mathematics, Vol. 898, Springer-Verlag, New York, Heidelberg, Berlin.

53 Zaslavskii, G. M., *Phys. Lett.*, Vol. 69*A*, 1978, p. 145.

54 Rechester, A. B., and White, R. B., "Statistical Description of an Attractor," Princeton Plasma Physics Lab Report, PAPL-1821, July 1981.

55 Greene, J. M., "Method for Determining a Stochastic Transition," *J. Math. Phys.*, Vol. 20, No. 6, 1980, pp. 1183-1201.

56 Shenker, S. J., and Kadanoff, L. P., "Critical Behavior of a KAM Surface: Empirical Results," preprint, University of Chicago, 1982.

57 Ostlund, S., Rand, D. A., Sethna, J., and Siggia, E., "Universal Properties of the Transition from Quasi-Periodicity to Chaos in Dissipative Systems," preprint, Mathematics Institute, University of Warwick, United Kingdom, 1982.

58 Gurel, O., and Rossler, O. E., eds., "Bifurcation Theory and Applications in Scientific Disciplines," *Ann. NY Acad. Sci.*, Vol. 316, NY Acad. Sci., New York, 1979.

59 Helleman, R. H. G., ed., "Nonlinear Dynamics," *Ann. NY Acad. Sci.*, Vol. 357, NY Acad. Sci., New York, 1980.

60 Campbell, D. K., Feigenbaum, M. J., Rose, H. A., and Scott, A. C., eds., "Order in Chaos," *Proceedings of a Conference Held at Los Alamos National Lab*, May 1982, to appear.

61 Thompson, J. M. T., and Ghaffari, R., "Chaos After Period-Doubling Bifurcations in the Resonance of an Impact Oscillator," *Phys. Let.*, Vol. 91A, No. 1, 1982, pp. 5-8.

Downloaded 02 May 2010 to 171.66.16.250. Redistribution subject to ASME license or copyright; see http://www.asme.org/terms/Terms_Use.cfm

T. J. R. Hughes
Professor of Mechanical Engineering,
Division of Applied Mechanics,
Durand Building,
Stanford University,
Stanford, Calif. 94305
Mem. ASME

T. Belytschko
Professor of Civil and
Nuclear Engineering
Department of Civil Engineering,
Northwestern University,
Evanston, Ill.
Fellow, ASME

A Précis of Developments in Computational Methods for Transient Analysis

Recent developments in computational transient analysis methodology are described. Emphasis is placed on fundamental properties of some of the most widely used algorithms, the techniques used to analyze their behavior, and newer procedures that attain greater computational efficiency.

1 Introduction

A great deal of progress has been made in recent years in the development and understanding of computational methods for transient analysis, especially those pertaining to finite element spatial discretizations (i.e., "semidiscretizations"). Until about 15 years ago only the simplest algorithms were used and the behavior of these algorithms was not even fully understood. A number of analytical studies performed during the interim have clarified the situation considerably. During this same period several new types of algorithms have appeared and attracted a great deal of research interest. Improved performance and greater computational efficiency have been simultaneously achieved in the process.

In this paper we present a very brief overview of some of the recent developments in the field. For expository purposes we restrict our presentation primarily to linear symmetric equation systems. Nevertheless the subject matter finds its greatest application in the analysis of nonlinear problems. Methods that, for all practical purposes, are limited to linear systems, such as modal response analysis, are not dealt with herein; neither are methods of solving algebraic equation systems. We begin in Section 2 by introducing a family of one-step methods for first-order systems that arise in heat conduction. This enables the presentation of some fundamental concepts in the simplest possible circumstances. In Section 3 we consider second-order systems such as the semidiscrete equations of motion. The Newmark family of methods is described and a summary of its accuracy and stability behavior is presented. Throughout Sections 2 and 3 the modal (also called spectral or Fourier) method of analyzing algorithms is emphasized. In addition, an example of the energy method of stability analysis is given in Section 3 because of its importance in the analysis of some of the newer methods mentioned subsequently. In Section 4 linear multistep methods are described. This class of methods has been the most widely studied and contains the most often used algorithms. It is noted that the well-known step-by-step integration algorithms of structural dynamics fall within a subclass of linear multistep methods and a brief resume of their comparative performance is presented. Brief mention is made in Section 5 of the stabilty behavior of nonlinear and nonsymmetric systems. The understanding of these types of systems is less complete than for linear symmetric systems. In Sections 6 and 7 partitioning methods and operator splitting methods are discussed. These classes of methods have had the most significant impact on increasing the computational efficiency of transient analysis procedures. Current research activity is focused on these areas and will likely remain so for the foreseeable future. Concluding remarks are made in Section 8.

For a broader and more detailed presentation of the state of the art in computational transient analysis, and further references to the literature, the interested reader is urged to consult [*B*3].

2 First-Order Symmetric Systems

Semidiscrete Heat Equation. The semidiscrete heat equation is

$$\mathbf{M}\dot{\mathbf{d}} + \mathbf{K}\mathbf{d} = \mathbf{F} \tag{2.1}$$

where $\mathbf{M}$ is the capacity matrix, $\mathbf{K}$ is the conductivity matrix, $\mathbf{F}$ is the heat supply vector, $\mathbf{d}$ is the temperature vector, and $\dot{\mathbf{d}}$ is the time (t) derivative of $\mathbf{d}$. The matrices $\mathbf{M}$ and $\mathbf{K}$ are assumed symmetric, $\mathbf{M}$ is positive-definite, and $\mathbf{K}$ is positive-semidefinite. The heat supply is a prescribed function of t. We write $\mathbf{F} = \mathbf{F}(t)$ for $t \in [0, T]$. Equation (2.1) is to be thought of as a coupled system of n_{eq} ordinary differential equations.

The initial-value problem consists of finding a function $\mathbf{d} = \mathbf{d}(t)$ satisfying (2.1) and the initial condition

$$\mathbf{d}(0) = \mathbf{D}_0 \tag{2.2}$$

where $\mathbf{D}_0$ is given.

Contributed by the Applied Mechanics Division for publication in the JOURNAL OF APPLIED MECHANICS.

Discussion on this paper should be addressed to the Editorial Department, ASME, United Engineering Center, 345 East 47th Street, New York, N.Y. 10017, and will be accepted until two months after final publication of the paper itself in the JOURNAL OF APPLIED MECHANICS. Manuscript received by ASME Applied Mechanics Division, April, 1983.

Copyright © 1983 by ASME
Downloaded 02 May 2010 to 171.66.16.250. Redistribution subject to ASME license or copyright; see http://www.asme.org/terms/Terms_Use.cfm

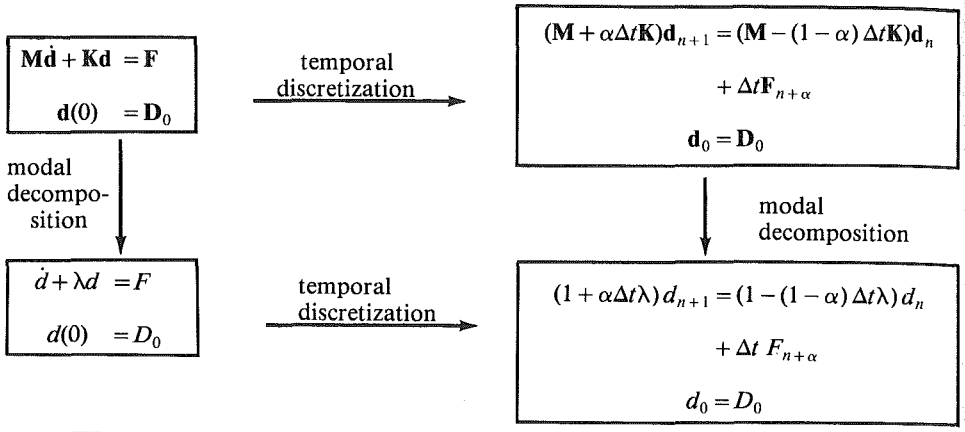
One-Step Algorithms for the Semidiscrete Heat Equation: Generalized Trapezoidal Method. Perhaps the most well-known and commonly used algorithms for solving (2.1) are members of the so-called *generalized trapezoidal family of methods* which consists of the following equations:

$$\mathbf{M}\mathbf{v}_{n+1} + \mathbf{K}\mathbf{d}_{n+1} = \mathbf{F}_{n+1} \tag{2.3}$$

$$\mathbf{d}_{n+1} = \mathbf{d}_n + \Delta t \mathbf{v}_{n+\alpha} \tag{2.4}$$

$$\mathbf{v}_{n+\alpha} = (1-\alpha)\mathbf{v}_n + \alpha \mathbf{v}_{n+1} \tag{2.5}$$

where $\mathbf{d}_n$ and $\mathbf{v}_n$ are the approximations to $\mathbf{d}(t_n)$ and $\mathbf{v}(t_n)$, respectively; $\mathbf{F}_{n+1} = \mathbf{F}(t_{n+1})$; Δt is the time step, assumed constant in the present circumstances; and α is a parameter, taken to be in the interval [0, 1].



Some well-known members of the generalized trapezoidal family are identified in the following table.

α	Method
0	forward differences; forward Euler
1/2	trapezoidal rule; midpoint rule; Crank-Nicolson
2/3	Galerkin
1	backward differences; backward Euler

In the case of $\alpha = 0$, the method is said to be *explicit*. The value of explicit methods may be seen from (2.3)–(2.5) if $\mathbf{M}$ is assumed "lumped" (i.e., diagonal). In this case the solution may be advanced without the necessity of equation solving.

If $\alpha \neq 0$, the method is said to be *implicit*. In these cases a system of equations, with coefficient matrix $(\mathbf{M} + \alpha\Delta t\, \mathbf{K})$, needs to be solved at each step because $\mathbf{K}$ will not be diagonal in practice.

The primary requirement of the preceding algorithms is convergence. An algorithm is called *convergent* if for t_n fixed and $\Delta t = t_n/n$, $\mathbf{d}_n \to \mathbf{d}(t_n)$ as $\Delta t \to 0$. To establish the convergence of an algorithm, two additional notions must be considered; *stability* and *consistency*. Once stability and consistency are verified, convergence is automatic. In addition, one is obviously concerned with the accuracy of an algorithm, especially the rate of convergence, and allied topics such as the behavior of the (spurious) higher modes.

Modal Analysis. There are several techniques that can be employed to study the characteristics of an algorithm. In the present context the most revealing approach appears to be modal analysis (sometimes called spectral, or Fourier, analysis). Assuming $\mathbf{M}$ and $\mathbf{K}$ are symmetric and positive-definite, the properties of the eigenproblem related to (2.1), namely

$$(\mathbf{K} - \lambda_l \mathbf{M})\psi_l = \mathbf{0}, \quad l \in \{1, 2, \ldots, n_{\text{eq}}\} \tag{2.6}$$

where

$$0 < \lambda_1 \leq \lambda_2 \leq \ldots \leq \lambda_{n_{\text{eq}}} \tag{2.7}$$

and

$$\psi_l^T \mathbf{M}\, \psi_m = \delta_{lm} \quad \text{(orthornormality)} \tag{2.8}$$

in which δ_{lm} is the Kronecker delta, enables the decomposition of the system of ordinary differential equations (i.e., (2.1)) and the generalized trapezoidal algorithm (i.e., (2.3)–(2.5)) into systems of uncoupled, single-degree-of-freedom (SDOF) equations. This process is summarized in the commutative diagram in the following where, for notational simplicity, the lth modal subscript has been omitted in the SDOF equations. Analysis of the entire system thus reduces to consideration of a typical SDOF model equation.

Stability. The appropriate notion of stability emanates from the homogeneous form of the temporally discrete SDOF equation. In this case,

$$d_{n+1} = A\, d_n \tag{2.9}$$

where $A = (1 - (1 - \alpha)\Delta t\, \lambda) / (1 + \alpha \Delta t\, \lambda)$ is the *amplification factor*. Stability requires that $|A| < 1$ for each modal equation. An algorithm for which stability imposes a time-step restriction is called *conditionally stable*. An algorithm for which there is no time-step restriction imposed by stability is called *unconditionally stable*. The stability conditions that ensue are summarized as follows:

unconditional stability: $\alpha \geq 1/2$ (2.10)

conditional stability: $\alpha < 1/2, \quad \Delta t < 2/[(1-2\alpha)\lambda_{n_{\text{eq}}}]$ (2.11)

where $\lambda_{n_{\text{eq}}}$ is the maximum eigenvalue. If (2.1) emanates from a finite element discretization, then $\lambda_{n_{\text{eq}}}$ may be conservatively bounded by the maximum eigenvalue of the individual elements [*H*13, *I*1].

Consistency and Convergence. The temporally-discrete model problem may be written in the form

$$d_{n+1} - A d_n - L_n = 0 \tag{2.12}$$

where $L_n = \Delta t F_{n+\alpha}/(1 + \alpha\Delta t\lambda)$. If d_n and d_{n+1} are replaced by the corresponding exact values, an expression of the form

$$d(t_{n+1}) - A d(t_n) - L_n = \tau(t_n) \tag{2.13}$$

is obtained where $\tau(t_n)$ is called the *local truncation error*. If $|\tau(t)| \leq c\Delta t^{k+1}$, for all $t \in [0, T]$, where c is a constant independent of Δt, and $k > 0$, the algorithm defined by (2.12) is called *consistent*. Stability and consistency imply convergence. Furthermore, it can be shown that the solution error, $e(t_n) = d(t_n) - d_n$, where t_n is fixed, approaches zero with order Δt^k. Hence k is referred to as the *order of accuracy* or *rate of convergence*. The generalized trapezoidal methods are consistent, with $k = 1$ for all $\alpha \in [0, 1]$, except $\alpha = 1/2$, in which case $k = 2$. Thus the trapezoidal rule ($\alpha = 1/2$) is the only member of the family of methods that is second-order accurate.

Downloaded 02 May 2010 to 171.66.16.250. Redistribution subject to ASME license or copyright; see http://www.asme.org/terms/Terms_Use.cfm

3 Second-Order Symmetric Systems

Semidiscrete Equation of Motion. The semidiscrete equation of motion is

$$\mathbf{M}\ddot{\mathbf{d}}+\mathbf{C}\dot{\mathbf{d}}+\mathbf{K}\mathbf{d}=\mathbf{F} \tag{3.1}$$

where $\mathbf{M}$ is the mass matrix, $\mathbf{C}$ is the viscous damping matrix, $\mathbf{K}$ is the stiffness matrix, $\mathbf{F}$ is the vector of applied forces, and $\mathbf{d}$, $\dot{\mathbf{d}}$, and $\ddot{\mathbf{d}}$ are the displacement, velocity, and acceleration vectors, respectively. We take $\mathbf{M}$, $\mathbf{C}$, and $\mathbf{K}$ to be symmetric, $\mathbf{M}$ is positive-definite, and $\mathbf{C}$ and $\mathbf{K}$ are positive-semidefinite.

The initial-value problem for (3.1) consists of finding a displacement, $\mathbf{d} = \mathbf{d}(t)$, satisfying (3.1) and the given initial data:

$$\mathbf{d}(0)=\mathbf{D}_0 \tag{3.2}$$

$$\dot{\mathbf{d}}(0)=\mathbf{V}_0 \tag{3.3}$$

One-Step Algorithms for the Semidiscrete Equation of Motion: Newmark Method. Perhaps the most widely used family of direct methods for solving (3.1)-(3.3) is the Newmark family [*N*1], which consists of the following equations:

$$\mathbf{M}\,\mathbf{a}_{n+1}+\mathbf{C}\,\mathbf{v}_{n+1}+\mathbf{K}\,\mathbf{d}_{n+1}=\mathbf{F}_{n+1} \tag{3.4}$$

$$\mathbf{d}_{n+1}=\mathbf{d}_n+\Delta t\mathbf{v}_n+\frac{\Delta t^2}{2}\{(1-2\beta)\mathbf{a}_n+2\beta\mathbf{a}_{n+1}\} \tag{3.5}$$

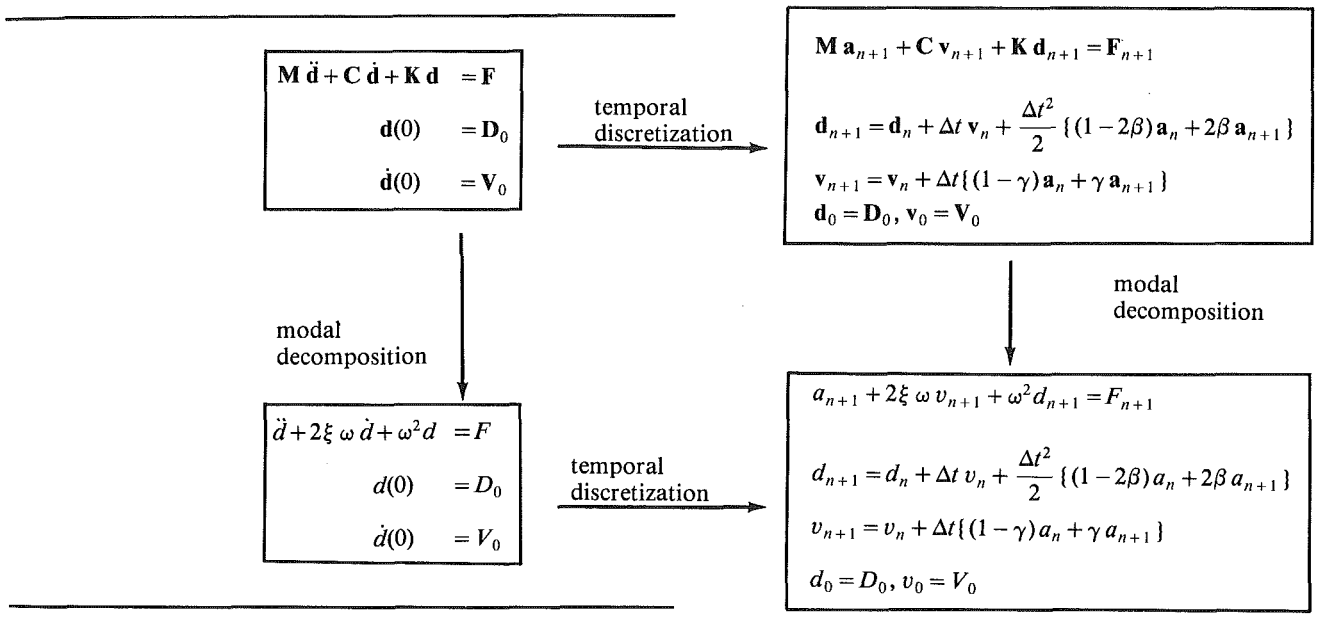
$$\mathbf{v}_{n+1}=\mathbf{v}_n+\Delta t\{(1-\gamma)\mathbf{a}_n+\gamma\mathbf{a}_{n+1}\} \tag{3.6}$$

where $\mathbf{d}_n$, $\mathbf{v}_n$, and $\mathbf{a}_n$ are the approximations of $\mathbf{d}(t_n)$, $\dot{\mathbf{d}}(t_n)$, and $\ddot{\mathbf{d}}(t_n)$, respectively. Equation (3.4) is simply the equation of motion in terms of the approximate solution, and (3.5) and (3.6) are finite difference formulas describing the evolution of the approximate solution. The parameters β and γ determine the stability and accuracy characteristics of the algorithm under consideration. Equations (3.4)-(3.6) may be thought of as three equations for determining the three unknowns $\mathbf{d}_{n+1}$, $\mathbf{v}_{n+1}$, and $\mathbf{a}_{n+1}$, it being assumed that $\mathbf{d}_n$, $\mathbf{v}_n$, and $\mathbf{a}_n$ are known from the previous step's calculations. The Newmark family contains as special cases many well-known and widely used methods.

The convergence analysis of the Newmark family of methods is similar to the convergence analysis given in the preceding section. The main steps are: (*i*) reduction to an SDOF model problem; (*ii*) a suitable notion of stability is defined and shown to hold under certain circumstances; (*iii*) the local truncation error is determined, from which the order of accuracy is obtained; and (*iv*) the latter two conditions are used to prove convergence for the SDOF problem. Some assumption on the form of $\mathbf{C}$ is necessary to perform the modal reduction. For example, if "Rayleigh damping" is assumed, that is

$$\mathbf{C}=a\,\mathbf{M}+b\,\mathbf{K} \tag{3.7}$$

then the symmetry and positive-definiteness of $\mathbf{M}$ and $\mathbf{K}$ enable the decomposition indicated in the following commutative diagram, where ω is the undamped frequency of vibration and $\xi = (a/\omega + b\,\omega)/2$ is the damping ratio.



The SDOF model problem can be recast in a first-order form analogous to equation (2.12):

$$\mathbf{y}_{n+1}=\mathbf{A}\,\mathbf{y}_n+\mathbf{L}_n \tag{3.8}$$

where $\mathbf{A}$ is the *amplification matrix* and

Table 1 Properties of well-known members of the Newmark family of methods

Method	Type	β	γ	Stability condition(2)	Order of Accuracy(3)
Average acceleration (trapezoidal rule)	Implicit	1/4	1/2	Unconditional	2
Linear acceleration	Implicit	1/6	1/2	$\Omega_{crit}=2\sqrt{3}\simeq 3.464$	2
Fox-Goodwin (royal road)	Implicit	1/12	1/2	$\Omega_{crit}=\sqrt{6}\simeq 2.449$	2(4)
Central difference	Explicit(1)	0	1/2	$\Omega_{crit}=2$	2

Notes: (1) Strictly speaking, $\mathbf{M}$ and $\mathbf{C}$ need to be diagonal for the central-difference method to be explicit.
(2) Stability is based on the undamped case in which $\xi = 0$.
(3) Second-order accuracy is achieved if and only if $\gamma = 1/2$.
(4) Fourth-order accuracy is achieved for the Fox-Goodwin method if $\mathbf{C} = \mathbf{0}$.

Downloaded 02 May 2010 to 171.66.16.250. Redistribution subject to ASME license or copyright; see http://www.asme.org/terms/Terms_Use.cfm

$$\mathbf{y}_n = \begin{Bmatrix} d_n \\ v_n \end{Bmatrix} \tag{3.9}$$

The complete analysis of the algorithm reduces to consideration of (3.8). In particular, stability is determined by the spectral properties of **A**. A summary of stability conditions for the Newmark method follows [*G*3, *H*3, *K*1].

Unconditional

$$2\beta \geq \gamma \geq 1/2 \tag{3.10}$$

Conditional

$$\gamma \geq 1/2 \tag{3.11}$$

$$\beta < \gamma/2 \tag{3.12}$$

$$\omega \Delta t \leq \Omega_{\text{crit}} \tag{3.13}$$

where

$$\Omega_{\text{crit}} = \frac{\xi(\gamma - 1/2) + [\gamma/2 - \beta + \xi^2(\gamma - 1/2)^2]^{1/2}}{(\gamma/2 - \beta)} \tag{3.14}$$

The stability conditions must be satisfied for each mode in the system. Consequently, the highest natural frequency, $\omega_{n_{\text{eq}}}$, is critical and therefore must satisfy (3.13). If (3.1) arises from a finite element discretization, $\omega_{n_{\text{eq}}}$ may be bounded by the maximum frequency of the individual elements [*H*13, *I*1]. Note that if $\gamma = 1/2$ viscous damping has *no* effect on stability. Furthermore, when $\gamma > 1/2$, the effect of viscous damping is to *increase* the critical time step of conditionally stable Newmark methods. Thus the undamped critical sampling frequency serves as a conservative value when an estimate of the modal damping coefficient is not available. (Recall that, in the case of Rayleigh damping, ξ is determined by ω.)

Stability and other properties are summarized in Table 1. Observe that the critical time-step restrictions for the linear acceleration and Fox-Goodwin methods are not substantially greater than for the central difference method. Under the circumstances which render the central difference method explicit, it generally results in considerable savings in computer cost when compared with the linear acceleration and Fox-Goodwin methods. The average-acceleration method is one of the most effective and popular implicit techniques for structural dynamcis problems.

Because the higher modes of semidiscrete structural equations are artifacts of the discretization process and not representative of the behavior of the governing partial differential equations, it is generally viewed as desirable, and often is considered absolutely necessary, to have some form of algorithmic damping present to remove the participation of the high-frequency modal components. At the same time it is required to maintain good accuracy in the important lower modes. In terms of the Newmark method, $\gamma > \frac{1}{2}$ is necessary to introduce high-frequency dissipation. Unfortunately, this adversely affects accuracy in the low modes. For this reason there has been considerable research into the development of alternative methods for algorithmically damping the higher modes.

Stability by the Energy Method. In cases where modal analysis is difficult to execute, such as in partitioned or split-operator approaches (see Sections 6 and 7), the energy method is often useful [*R*1]. An alternative derivation of the stability of Newmark's algorithm by way of the energy method proceeds as follows [*H*12].

To simplify the subsequent writing, it is helpful to introduce the jump (undivided forward difference) and mean value operators, [ ] and < >, respectively, which are defined by $[\mathbf{x}_n] = \mathbf{x}_{n+1} - \mathbf{x}_n$ and $<\mathbf{x}_n> = (\mathbf{x}_{n+1} + \mathbf{x}_n)/2$. The notation $\|\cdot\|$ is used to denote any vector norm. A vector-valued sequence, x_n, $n = 0, 1, 2, \ldots$, will be said to be *bounded* if $\|\mathbf{x}_n\| \leq c$, $n = 0, 1, 2, \ldots$, where c is a non-negative constant.

Equations (3.4)–(3.6) may be combined to form the following identify:

$$\mathbf{a}_{n+1}{}^T\mathbf{A}\,\mathbf{a}_{n+1} + \mathbf{v}_{n+1}{}^T\mathbf{K}\,\mathbf{v}_{n+1} = \mathbf{a}_n^T\mathbf{A}\,\mathbf{a}_n + \mathbf{v}_n{}^T\mathbf{K}\,\mathbf{v}_n - (2\gamma - 1)[\mathbf{a}_n]^T\mathbf{B}[\mathbf{a}_n] - 2\Delta t <\mathbf{a}_n>^T\mathbf{C}<\mathbf{a}_n> \tag{3.15}$$

where

$$\mathbf{B} = \mathbf{M} + \Delta t(\gamma - 1/2)\mathbf{C} + \Delta t^2(\beta - \gamma/2)\mathbf{K} \tag{3.16}$$

$$\mathbf{A} = \mathbf{B} + \Delta t(\gamma - 1/2)\mathbf{C} \tag{3.17}$$

(There should be no confusion over the present definition of the matrix **A**, and earlier use for denoting an amplification matrix.) If $\gamma \geq 1/2$ and **B** is positive-definite, then from (3.15) it follows that $\mathbf{a}_n$ and $\mathbf{v}_n$ are bounded. If $\mathbf{K}^{-1}$ exists, then it can be shown that $\mathbf{d}_n$ is also bounded. Thus it remains only to ascertain under what conditions **B** is positive-definite to completely determine the stability characteristics of the Newmark algorithms. The results are identical to those presented previously.

Equation (3.15) is called a *discrete conservation law*, whereas omitting the last two terms on the right-hand side results in a *discrete decay inequality*. It may be easily shown that any spectrally stable method possesses a discrete conservation law or decay inequality [*C*1].

4 Linear Multistep (LMS) Methods

LMS Methods for First-Order Equations. Consider a system of first-order, linear, ordinary differential equations

$$\dot{\mathbf{y}} = \mathbf{f}(\mathbf{y},t) = \mathbf{G}\,\mathbf{y} + \mathbf{H}(t) \tag{4.1}$$

where **G** is a given constant matrix and **H** is a given vector-valued function of t. A *k-step linear multistep method for* (4.1) is defined by the following expression:

$$\sum_{i=0}^{k} \{\alpha_i \mathbf{y}_{n+1-i} + \Delta t\ \beta_i \mathbf{f}(\mathbf{y}_{n+1-i}, t_{n+1-i})\} = \mathbf{0} \tag{4.2}$$

The α_i's and β_i's are parameters that define the method. Note that the word "linear" in "linear multistep method" has noting to do with the linearity of (4.1). Indeed, equation (4.2) is perfectly well defined for a nonlinear function $\mathbf{f}(\mathbf{y}, t)$. Rather, the linearity pertains to the form of (4.2). An excellent reference for LMS methods of this type is Gear [*G*1]. An LMS method is called *explicit* if $\beta_0 = 0$, otherwise it is called *implicit*. It is called a backward-difference method if $\beta_i = 0$ for all $i \geq 1$. An example of a one-step LMS method of first-order type is the generalized trapezoidal family discussed in Section 2 for which $\alpha_0 = -\alpha_1 = 1$, $\beta_0 = -\alpha$, and $\beta_1 = \alpha - 1$. Recall that $\alpha = 0$ defines an explicit method, and $\alpha = 1$, a backward-difference method. The greater the number of steps involved in the definition of an LMS method, the greater the "historical data pool," which must be stored in computing—a practical disadvantage. The semidiscrete heat equation and equation of motion can be put in first-order form. Many algorithms of practical interest take the form (4.2). The analysis of LMS methods may be performed using modal techniques as described previously. Stability is generally phrased in terms of the roots of the polynomial associated to (4.2), namely

$$\sum_{i=0}^{k} (\alpha_i + \Delta t\ \lambda\ \beta_i)\,\zeta^{n+1-i} = 0 \tag{4.3}$$

where λ is an eigenvalue of **G**. An LMS method of the form

Downloaded 02 May 2010 to 171.66.16.250. Redistribution subject to ASME license or copyright; see http://www.asme.org/terms/Terms_Use.cfm

(4.2) is said to be *absolutely stable*, at a fixed $\lambda\Delta t$, if all ζ satisfying (4.3) are such that $|\zeta| \leq 1$. The *region of absolute stability* of an LMS method is the set of $\lambda\Delta t \in \mathbb{C}$at which it is absolutely stable. An LMS method is A - *stable* if solutions of the SDOF analog of (4.2) $\rightarrow 0$ as $n \rightarrow \infty$ when Re $\lambda < 0$. Physically speaking, an A - stable alrogithm is one that produces solutions that decay to zero whenever the corresponding exact solutions decay to zero. Clearly, if an algorithm is A - stable then the region of absolute stability contains the left half-plane of $\mathbb{C}$ The condition of A - stability places no limitation on the size of Δt, consequently it is closely related to what we termed unconditional stability in Sections 1 and 2. The only difference is that spectral stability allows eigenvalues of unit modulus that potentially could conserve a solution rather than contract it to zero. It should be apparent that A - stable algorithms are important for many physical problem classes. However, within the class of LMS methods, the subclass of A - stable methods is severely delimited. This is the content of a celibrated theorem due to Dahlquist [*D*1], which states that:

1 An explicit A - stable LMS method does not exist.

2 A third-order accurate A - stable LMS method does not exist.

3 The second-order accurate A - stable LMS method with the smallest error constant[1] is the trapezoidal rule.

The upshot of this theorem is that if we seek an A-stable LMS method that possesses some special feature (such as high-frequency numerical dissipation), we necessarily entail some loss of accuracy with respect to the trapezoidal rule. Since the spectrum of the **G** - matrix for the equation of motion falls within the left-half complex plane and, in the undamped case, falls on the imaginary axis, it would appear that the trapezoidal rule is the canonical A - stable LMS method for structural dynamics. The widespread use and popularity of the trapezoidal rule in this context appears to confirm this observation. However, there are other useful A - stable LMS methods for structural dynamics; for example, Park's method [*P*1]. Many structural dynamics algorithms do not fall within the class of first-order LMS methods considered so far. The Newmark family of methods may be mentioned in this regard. Another class of LMS methods for second-order equations will be described subsequently which contains the Newmark family among others.

Since A - stable LMS methods are at most second-order accurate, the question arises "Is there some weakened notion of A - stability that pertains to a physically relevant class of problems and allows for the development of higher-order accurate methods?" An affirmative answer is provided by the concept of stiff stability proposed by Gear [*G*1]. A method is said to be *stiffly stable* if it is absolutely stable in the region of the $\lambda\Delta t$ - plane defined by Re $(\lambda\Delta t) < -\delta$, where δ is a positive constant. Gear has developed a family of k-step, kth-order accurate LMS methods which are stiffly stable for $k = 2, 3, \ldots, 6$. Each method is a backward-difference LMS method. The second-order method is, in addition, A-stable, however, it is significantly less accurate than the trapezoidal rule. For $k \geq 3$, the regions of instability include portions of the imaginary axis. Consequently, these stiffly stable algorithms also appear inappropriate for typical structural dynamics applications. Because the region of stability of each of the methods, $k = 2, 3, \ldots, 6$, includes the negative real axis, one would anticipate good behavior in application to problems of heat conduction.

Park [*P*1] has developed a second-order accurate, A - stable algorithm, which retains good accuracy in the low frequencies and strong dissipative characteristics in the high frequencies, by combining Gear's two-step and three-step stiffly stable algorithms.

LMS Methods for Second-Order Equations. Consider a system of second-order, linear, ordinary differential equations written in the form:

$$\ddot{\mathbf{y}} = \mathbf{f}(\mathbf{y},\dot{\mathbf{y}},t) = \mathbf{G}_0\mathbf{y} + \mathbf{G}_1\dot{\mathbf{y}} + \mathbf{H}(t) \tag{4.4}$$

where $\mathbf{G}_0$ and $\mathbf{G}_1$ are given constant matrices. A *k-step LMS method* for (4.4) is given by (Geradin [*G*2]):

$$\sum_{i=0}^{k} \{\alpha_i \mathbf{y}_{n+1-i} + \Delta t\, \beta_i \mathbf{G}_1 \mathbf{y}_{n+1-i} + \Delta t^2 \gamma_i [\mathbf{G}_0 \mathbf{y}_{n+1-i} + \mathbf{H}(t_{n+1-i})]\} = \mathbf{0} \tag{4.5}$$

The method is defined by the values of α_i, β_i, and γ_i, $i = 0, 1, \ldots, k$. An LMS method of this type is called *explicit* if β_0 and $\gamma_0 = 0$. (If $\mathbf{G}_1 = \mathbf{0}$, then clearly only γ_0 need be zero.) The method is a *backward-difference method* if β_i and $\gamma_i = 0$, $i \geq 1$. (Likewise, if $\mathbf{G}_1 = \mathbf{0}$, only the γ_i's, $i \geq 1$, need be zero.) The equation of motion may be put in the form of (4.4) simply by multiplying through by $\mathbf{M}^{-1}$. Observe that with $\mathbf{y} = \mathbf{d}$, equation (4.5) is a displacement difference-equation form of the algorithm. The commonly used algorithms of structural dynamics can all be put into this form, although very few are naturally cast this way.

In the sense of an LMS method for second-order systems, Newmark's method is a two-step method. LMS methods applied to the first-order form of the equations of motion may likewise be recast as second-order-type LMS methods (e.g., Park's method).

The stability properties of second-order-type LMS methods may be investigated in similar fashion to first-order LMS methods. Briefly, modal reduction may be employed which, for the equation of motion, leads to the following polynomial

$$\sum_{i=0}^{k} (\alpha_i + 2\xi\omega\Delta t\, \beta_i + (\omega\Delta t)^2 \gamma_i)\, \zeta^{n+1-i} = 0. \tag{4.6}$$

An analog of Dahlquist's theorem also holds for LMS methods for second-order equations.

Other Algorithms Commonly Used in Structural Dynamics.

(*a*) *Houbolt's Method.* Houbolt's method [*H*6] was one of the earliest employed in structural dynamics computations. It has many features in common with Park's method. However, Park's method is significantly more accurate and thus Houbolt's method is now more of historical interest.

(*b*) *Collocation Methods.* Collocation methods generalize and combine aspects of the Newmark method and Wilson - θ method. A systematic analysis of collocation is contained in Hilber and Hughes [*H*4].

(*c*) *α-Method.* Numerical damping cannot be introduced in the Newmark method without degrading the order of accuracy. To improve on this situation, Hilber, Hughes, and Taylor [*H*5] introduced the α - method.

The aforementioned methods have the following features in common: They are implicit, unconditionally stable, second-order accurate, and dissipative. All are capable of sufficiently damping out the high modes. The Houbolt method affects the low modes much too strongly, both from the point of view of damping and phase error. Park's method possesses good low-mode damping properties, however its phase error is higher than the collocation schemes and α - methods. The collocation schemes damp the low modes too strongly. On balance the α - methods and Park's method perform best. (The recently introduced Bossak's method [*A*1] seems comparable in

[1] The error constant is the coefficient of Δt^{k+1} in the local truncation error.

Downloaded 02 May 2010 to 171.66.16.250. Redistribution subject to ASME license or copyright; see http://www.asme.org/terms/Terms_Use.cfm

performance to the α - methods, however, this evaluation is tentative as practical experience is apparently still limited.)

Another important measure of the performance of unconditionally stable algorithms is called "overshoot," a tendency to violently oscillate for a short time due to certain initial conditions, or discontinuous loading. Collocation schemes have been shown to behave pathologically with respect to overshoot, whereas the other algorithms considered tend to perform acceptably. A discussion of this phenomenon and numerical results are presented in [*H*4].

5 Remarks on the Stability of Nonlinear Symmetric Systems and Nonsymmetric Systems

Algorithms for nonlinear symmetric and nonsymmetric systems are more difficult to analyze than linear symmetric systems. A brief summary of what is known about this important subject follows:

Nonlinear Symmetric Systems. Linearized stability [*H*8] is without doubt the most widely used stability concept in nonlinear analysis. One must realize, however, that it provides only necessary conditions for stability (they may not be sufficient) and so it must be judiciously combined with insight for success in practice. Based on practical experiences, the following observations may be made regarding linearized stability analyses: (*i*) the time-step restriction for explicit schemes is sufficient; (*ii*) if the nonlinear response is accurately discretized by the time step chosen, the stability conditions are also sufficient for implicit schemes; and (*iii*) if the nonlinear response is *not* accurately discretized, biased accumulation of truncation errors can occur and may cause pathological growth of the discrete solution (See [*H*7] for examples and references to further discussion). This is in contrast to the linear regime in which spectral notions of stability imply that a conservation law or decay inequality limits the growth of solutions. Thus the issue has been raised whether or not the notion of linearized stability is adequate for general nonlinear analysis. Stronger notions may be employed, but require different classes of algorithms than those that are now widely used. One such algorithm is based on a modification to the trapezoidal rule for nonlinear applications and results in physically appropriate energy growth characteristics [*H*9]. In particular, when external forces are absent, *energy is identically conserved in nonlinear elastodynamics*, a property shared by the exact continuum equations. As a consequence, *unconditional stability is automatically attained*. For another method of this kind see Haug et al. [*H*1].

In the context of nonlinear first-order systems energy analyses have been used successfully on the generalized trapezoidal and midpoint families [*H*8].

Nonsymmetric Systems. Systems of this type arise, for example, in modeling fluid subdomains. It is difficult to obtain practically useful stability results even in the linear case. However, the energy approach has been used successfully for some basic algorithms [*H*8]. For the most part, von Neumann-type finite difference analyses [*R*1] of model problems are employed. The extrapolation of results of this kind to complicated cases encountered in practice is ad hoc and consequently much additional research is warranted.

6 Partitioning Methods

Methods that combine the attractive features of explicit and implicit time integrators often provide substantial benefits in solving engineering problems. One class of combined schemes is partitioned methods, where different time integrators are used on different parts of the system. These methods are most easily introduced in the context of first-order semidiscretizations, equation (2.1). Consider the integrator (2.3)–(2.5) and partition the nodal variables into two parts, A and B,

$$\mathbf{d} = \begin{Bmatrix} \mathbf{d}^A \\ \mathbf{d}^B \end{Bmatrix} \tag{6.1}$$

The parameter α for partitions A and B will be denoted by α^A and α^B. If $\mathbf{M}$ is diagonal, and if $\mathbf{M}$ and $\mathbf{K}$ are partitioned compatibly with $\mathbf{d}$, the equations for the system can be written as

$$\begin{bmatrix} \mathbf{M}^A + \alpha^A \Delta t\, \mathbf{K}^A & \alpha^B \Delta t\, \mathbf{K}^{AB} \\ \alpha^A \Delta t (\mathbf{K}^{AB})^T & \mathbf{M}^B + \alpha^B \Delta t\, \mathbf{K}^B \end{bmatrix} \begin{Bmatrix} \mathbf{d}^A_{n+1} \\ \mathbf{d}^B_{n+1} \end{Bmatrix} = \mathbf{M}\, \mathbf{d}_n$$

$$+ \Delta t \begin{Bmatrix} \alpha^A \mathbf{F}^A_{n+1} + (1-\alpha^A) & (\mathbf{F}^A_n - \mathbf{r}^A_n) \\ \alpha^B \mathbf{F}^B_{n+1} + (1-\alpha^B) & (\mathbf{F}^B_n - \mathbf{r}^B_n) \end{Bmatrix} \tag{6.2a}$$

$$\mathbf{r} = \mathbf{K}\, \mathbf{d} \tag{6.2b}$$

Various classes of *nodal* partitions can now be constructed by using particular values for α^A and α^B. If $\alpha^A = 0$ and $\alpha^B > 0$, the preceding algorithm is an explicit-implicit partition such as presented in [*B*4, *B*5]. If an unconditionally stable integrator is used for B, i.e., $\alpha^B \geq 1/2$, then stability is insured if

$$\lambda_{\max} \leq \max_e \lambda^e_{\max} \text{ where } e \in S^{\bar{A}} \tag{6.3}$$

and $S^{\bar{A}}$ is the set of all elements with at least one node in A. Note that the stability limit is independent of the frequency content of B. Hence, if a mesh contains a subdomain of stiff elements, it is advantageous to integrate this subdomain implicitly. The stable time step is set by the highest frequency of the elements in the remainder of the mesh, so it will be larger than the explicit time step for the entire mesh. In addition to permitting a larger time step, the partitioned method leads to a smaller system of equations and a smaller bandwidth, which often enables it to substantially exceed the speed of explicit or implicit integration for such problems.

Equation (6.2*a*) is somewhat awkward in practice because the matrix on the left-hand side is not symmetric. However, if the explicit subdomain A is updated first, the equations for subdomain B are symmetric as seen in the following

$$(\mathbf{M}^B + \alpha^B\, \Delta t\, \mathbf{K}^B)\, \mathbf{d}^B_{n+1} = \mathbf{M}^B\, \mathbf{d}^B_n + \Delta t[\alpha^B \mathbf{F}^B_{n+1} + (1-\alpha^B)\, (\mathbf{F}^B_n - \mathbf{r}^B_n)] \tag{6.4}$$

If α^A and α^B are both greater than zero in equation (6.1), the partition is implicit-implicit. These partitions are primarily of interest in applications where two implicit software packages are used to solve a coupled problem or where different implicit solution algorithms are used in the two subdomains. In an implicit-implicit partition, neither A nor B can be updated without an extrapolation of the interface values that are coupled by $\mathbf{K}^{AB}$ in equation (6.2). The stability of the procedure depends on the character of the extrapolation; Park [*P*2] has developed a stable extrapolation for the trapezoidal rule and the linear equations of motion.

Because subdomains A and B are updated alternatively rather than simultaneously in implicit-implicit partitions, they are also known as staggered-solution procedures [*F*1].

An alternative method of partitioning is to identify the elements with different integrators, hence the name *element* partition [*H*12]. In this method, $\mathbf{K}$ is split additively by

$$\mathbf{K}^I = \mathop{\mathbf{A}}_e \mathbf{K}^e, \quad e \in S^I$$
$$\mathbf{K}^E = \mathop{\mathbf{A}}_e \mathbf{K}^e, \quad e \in S^E \tag{6.5}$$

Downloaded 02 May 2010 to 171.66.16.250. Redistribution subject to ASME license or copyright; see http://www.asme.org/terms/Terms_Use.cfm

where $\mathbf{A}$ is the assembly operator and S^I and S^E are the element numbers of the implicit and explicit groups, respectively. As shown in [*H*12], the method is most effective when the integration formulas, equation (6.1), are put in a predictor-corrector form

$$\tilde{\mathbf{d}}_{n+1} = \mathbf{d}_n + (1-\alpha)\,\Delta t \mathbf{v}_n \tag{6.6a}$$

$$\mathbf{d}_{n+1} = \tilde{\mathbf{d}}_{n+1} + \alpha \Delta t \mathbf{v}_{n+1} \tag{6.6b}$$

The equations for updating $\mathbf{d}_{n+1}$ can then be written directly in the form

$$(\mathbf{M} + \alpha \Delta t \mathbf{K}^I)\,\mathbf{d}_{n+1} = (\mathbf{M} - \alpha \Delta t \mathbf{K}^E)\,\tilde{\mathbf{d}}_{n+1} + \alpha \Delta t \mathbf{F}_{n+1} \tag{6.7}$$

In this form of the element partition, the values of α for the explicit and implicit partitions are equal and the explicit and implicit character of the integration formula is accomplished through the structure of $\mathbf{K}^I$: any element included in $\mathbf{K}^I$ is integrated implicitly.

While the system of equations to be solved in this case are of order n_{eq}, if a skyline solution procedure is used, the computational effort only depends on the size of the implicit subdomain, since the left-hand side of equation (6.7) is strictly diagonal on the explicit portion. The stability conditions are similar to (6.3):

$$\lambda_{\max} \leq \max_e (\lambda^e_{\max}),\ e \in S^E \tag{6.8}$$

Thus the element partition has the stability characteristics and computational advantages of nodal partitions, but it is more easily implemented. However, the method is inapplicable to coupling different programs.

The recognition that the stability of a partitioned procedure is governed strictly by the stability limits of the explicitly integrated portion can also be exploited in nonlinear problems by integrating part of the response explicitly, part implicitly; this is called implicit-explicit operator splitting [*H*13]. As an illustration of this procedure, consider the case where the response of an element can be decomposed as follows:

$$\mathbf{r} = \mathbf{K}\,\mathbf{d} + \mathbf{N} \tag{6.9}$$

where $\mathbf{N}$ is the nonlinear portion of the response. Because it is advantageous to triangulate the coefficient matrix only once at the beginning of the solution process, if $\mathbf{K}^I$ is assembled from the linear stiffnesses in equation (6.9), then subsuming $\mathbf{N}$ into $\mathbf{F}$ and applying equation (6.7) yields a procedure in which $\mathbf{N}$ is treated explicitly. Procedures of this type have applications in elastoplastic analysis and to nearly-incompressible media.

Another class of procedures for dealing with problems containing large differences in characteristic time are subcycling procedures [*B*1, *B*6] or time-step mesh partitions. In these procedures, different time steps are used in different parts of the mesh. For example, consider the nodal partition, equation (6.1), and let subdomains A and B be integrated with time steps $m\Delta t$ and Δt, respectively.

For this purpose the integrator is written as

$$\mathbf{d}_{N+1} = \mathbf{d}_N + \mathbf{W}^1_N \mathbf{v}_N + \mathbf{W}^2_N \mathbf{v}_{N+1} \tag{6.11}$$

where

for $N \neq ml$

$$\mathbf{W}^1_N = \Delta t \begin{bmatrix} \mathbf{0} & \mathbf{0} \\ \mathbf{0} & (1-\alpha^B)\mathbf{I} \end{bmatrix} \quad \mathbf{W}^2_N = \Delta t \begin{bmatrix} \mathbf{0} & \mathbf{0} \\ \mathbf{0} & \alpha^B \mathbf{I} \end{bmatrix} \tag{6.12a}$$

for $N = ml$

$$\mathbf{W}^1_N = \Delta t \begin{bmatrix} m(1-\alpha^A)\mathbf{I} & \mathbf{0} \\ \mathbf{0} & (1-\alpha^B)\mathbf{I} \end{bmatrix} \quad \mathbf{W}^2_N = \Delta t \begin{bmatrix} m\alpha^A \mathbf{I} & \mathbf{0} \\ \mathbf{0} & \alpha^B \mathbf{I} \end{bmatrix} \tag{6.12b}$$

The $\mathbf{W}$ matrices are partitioned like $\mathbf{d}$. In this algorithm the solution is advanced $m-1$ times with a time step Δt on nodes in B, and in every mth cycle, the nodes in A and B are advanced with the time step $m\Delta t$ and Δt, respectively. Whether the nodes are integrated implicitly or explicitly is determined by the choice of the parameters α^A and α^B. Thus the following integration procedures result from the foregoing

m	α^A	α^B	integration procedure
1	0	>0	explicit-implicit
>1	0	0	explicit with explicit subcycling
1	>0	>0	implicit-implicit
>1	>0	0	implicit with explicit subcycling
>1	>0	>0	implicit with implicit subcycling

The equations for an explicit partition with explicit subcycling are given in the following

for $N \neq ml$

$$\mathbf{M}^B \mathbf{d}^B_{N+1} = \mathbf{M}^B \mathbf{d}^B_N - \Delta t\,(\mathbf{F}^B_N - \mathbf{r}^B_N) \tag{6.13}$$

for $N = ml$

$$\mathbf{M}\ \mathbf{d}_{N+1} = \mathbf{M}\ \mathbf{d}_N - \Delta t \left\{ \begin{matrix} m\mathbf{F}^A \\ \mathbf{F}^B \end{matrix} \right\}_N - \left\{ \begin{matrix} m\mathbf{r}^A \\ \mathbf{r}^B \end{matrix} \right\}_N \tag{6.14}$$

Thus it is only necessary to update the nodes in A for the $m-1$ cycles of the small time step and to update both sets of nodes every mth cycle by using the foregoing. Stability of this procedure for each node appears to depend only on the spectral character of the elements connected to the node, so that the stable time step can be chosen by

$$m\Delta t < \frac{2}{\lambda_{A^{(e)}}},\ \lambda_A = \max_e \lambda^e_{\max} \quad \text{for} \quad e \in S^A \tag{6.15}$$

$$\Delta t < \frac{2}{\lambda_{B^{(e)}}},\ \lambda_B = \max_e \lambda^e_{\max} \quad \text{for} \quad e \in S^{\bar{B}} \tag{6.16}$$

where S^A is the set of all elements with all nodes in A and $S^{\bar{B}}$ is the set of all elements with at least one node in B [*B*7]. Therefore the time steps in each subdomain can be chosen to be near the stability limit. Although this development is given in terms of two partitions for convenience, in applications it is common to use anywhere from 2 to 20 partitions and the time step in each part of the mesh can be taken close to the stability limit to achieve great efficiency.

7 Operator Splitting Methods

In operator splitting methods, an implicit integrator is generally chosen as a starting point and the operator, namely the left-hand side of equation (6.7), is split so that the solution of equations is avoided or the system to be solved is reduced in size. The motivation for this procedure is to retain the stability of the implicit integrator and achieve the computational efficiency of an explicit integrator.

Split operator methods have been developed extensively in finite differences. In many cases, these developments have exploited the data structure of finite difference methods, that is, the fact that the node number locates the node within the mesh.

As an example of this class of methods, consider the method of Saul'yev [*S*1] applied to the one-dimensional diffusion equation

$$\rho\, \dot{u} = k\, u_{,xx} \tag{7.1}$$

In applying this method, the implicit formula is applied to part of the right-hand side as follows:

$$\rho \frac{u^J_{n+1} - u^J_n}{\Delta t} = \frac{k}{\Delta x^2}\,(u^{J+1}_n - u^J_n - u^J_{n+1} + u^{J-1}_{n+1}) \tag{7.2}$$

Downloaded 02 May 2010 to 171.66.16.250. Redistribution subject to ASME license or copyright; see http://www.asme.org/terms/Terms_Use.cfm

Solving for u_{n+1}^J we obtain

$$u_{n+1}^J(1+r) = u_n^J + r(u_n^{J+1} - u_n^J + u_{n+1}^{J-1}) \tag{7.3}$$

$$r = \frac{k\,\Delta t}{\rho\,\Delta x^2} \tag{7.4}$$

Thus if the nodes are numbered in sequence from left to right and the computation proceeds from left to right, the right-hand side of the preceding equation is always known, and no equations need be solved. In a similar manner an equation can be developed that is explicit in going from right to left. Probably the best-known method of this type is that of Du Fort-Frankel [*A*2]. Typically, unconditional stability is achieved, however, consistency becomes conditional; for example, in Saul'yev's method consistency requires that Δt must go to zero faster than Δx. This shortcoming needs to be overcome for methods of this type to be practically useful.

A finite element form of this procedure has been given by Trujillo [*T*1]. The matrix $\mathbf{K}$ is split into upper and lower triangular matrices

$$\mathbf{K} = \mathbf{K}_L + \mathbf{K}_U, \quad \mathbf{K}_L = \mathbf{K}_U^T \tag{7.5}$$

and the vector $\mathbf{d}$ is updated by

$$(\mathbf{M} + \Delta t/2\mathbf{K}_L)\,\mathbf{d}_{n+\frac{1}{2}} = (\mathbf{M} - \Delta t/2\mathbf{K}_U)\,\mathbf{d}_n + \frac{\Delta t}{2}\mathbf{F}_n \tag{7.6}$$

$$(\mathbf{M} + \Delta t/2\mathbf{K}_U)\,\mathbf{d}_{n+1} = (\mathbf{M} - \Delta t/2\mathbf{K}_L)\,\mathbf{d}_{n+\frac{1}{2}} + \frac{\Delta t}{2}\mathbf{F}_n \tag{7.7}$$

The coefficient matrices in (7.6) and (7.7) are triangular (assuming $\mathbf{M}$ diagonal) and thus, no factorizations need be performed. For a one-dimensional mesh of linear elements with nodes numbered in sequence, and Δt replaced by $\Delta t/2$, equation (7.6) is identical to (7.2). However, an interesting feature of Trujillo's method is that it retains its stability regardless of the numbering of the nodes. It is also interesting to observe that the Trujillo method is similar to Gauss-Seidel iteration, consisting essentially of two iterations, except that in the latter the diagonal is subsumed in $\mathbf{K}_L$ whereas in equation (7.5) the diagonal is split equally between the upper and lower triangular portions of the matrix. Trujillo's method can also be cast as a matrix partition method. Thus there is often little or no distinction between partitioned and split-operator methods.

Trujillo has also presented a form of his method applicable to structural dynamics problems [*T*1]. In this case, the method can also be made unconditionally stable, but its accuracy is quite poor due to the conditional consistency problem cited earlier. For example, in [*M*1] it is shown that regardless of the time increment Δt, the wave apparently advances only one spatial node per time step, so that the dispersive errors in higher frequencies are extremely severe. Park [*P*3] has made modifications and extensions of these methods in attempting to improve their accuracy.

The finite difference literature abounds with other split operator methods such as the method of lines and alternating direction methods [*D*2, *P*4]. Some of these have been cast in a finite element format, for example [*H*2] gives a finite element, alternating direction method, but some of the geometrical limitations of finite difference methods remain.

A promising avenue in finite elements is to devise splitting methods that take advantage of the finite element data structure. A method of this type has been devised by Hughes and coworkers [*H*10, *H*11, *H*14]. This method makes a product approximation of the element summation (assembly) operation so that the inversion of the coefficient matrix is replaced by the sequential inversions of the element matrices. To outline the essential features of this method, consider the following form of the semidiscrete equations where α is taken to be 1/2:

$$(\mathbf{I} + \mu\,\mathbf{M}^{-1}\mathbf{K})\,\mathbf{d}_{n+1} = \mathbf{g}, \quad \mu = \frac{1}{2}\,\Delta t \tag{7.8a}$$

$$\mathbf{g} = \mathbf{d}_n + \frac{1}{2}\,\Delta t\,\mathbf{M}^{-1}(\mathbf{F}_{n+1} + \mathbf{F}_n - \mathbf{r}_n) \tag{7.8b}$$

which is obtained by premultiplying (6.7) by $\mathbf{M}^{-1}$. The matrix $\mathbf{K}$ is now replaced by its element constituents, equation (6.5), and the resulting sum is approximated as follows

$$\mathbf{I} + \mu\,\mathbf{M}^{-1}\sum_e \mathbf{K}^e \cong \prod_e (\mathbf{I} + \mu\,\mathbf{M}^{-1}\mathbf{K}^e) \tag{7.9}$$

where Π is the product operator. If $\mathbf{G}^e$ is defined by

$$\mathbf{G}^e = \mathbf{I} + \mu\,\mathbf{M}^{-1}\mathbf{K}^e \tag{7.10}$$

then an approximation of (7.8*a*) is given by

$$\Big(\prod_e \mathbf{G}^e\Big)\hat{\mathbf{d}}_{n+1} = \mathbf{g} \tag{7.11}$$

The foregoing can be replaced by a sequence of equations

$$\mathbf{d}_{[0]} = \mathbf{g} \tag{7.12a}$$

$$\mathbf{G}^e\mathbf{d}_{[e]} = \mathbf{d}_{[e-1]} e = 1,2,\ldots,n_{el} \tag{7.12b}$$

where n_{el} is the number of elements. Since $\mathbf{G}^e$ is the sum of the unit matrix and $\mu\mathbf{M}^{-1}\mathbf{K}^e$, only the portion of $\mathbf{G}^e$ that is associated with the rows and columns of $\mathbf{K}^e$ need be solved, so if $\mathbf{K}^e$ is $n_{ee} \times n_{ee}$, equation (7.12) requires the solution of n_{el} equation systems of order n_{ee}. It has recently been shown that the size of the system to be solved can be reduced significantly for the class of uniform gradient and strain elements [*B*2]. Note that only implicit elements are included in the sweep. We wish to reiterate that (7.9)–(7.12) is only intended to convey the essential feature of the method and is not to be construed as a practically useful method in itself. In [*H*10] it is shown how to retain the symmetry of the element coefficient array, unlike (7.10), and how to guarantee unconditional stability. Second-order accuracy with respect to Δt can also be achieved by reversing the order of element sweeps every other time step; however, the problem of conditional consistency adversely affects accuracy. Ortiz et al. [*O*1] experienced the same problems with their generalization of [*H*10] to the equations of motion. To circumvent this problem, the $\hat{\mathbf{d}}_{n+1}$ obtained in (7.11) is viewed as an approximation to $\mathbf{d}_{n+1}$ defined by the globally implicit algorithm (7.8). Iterative strategies are then combined with element sweeps until the solution converges to that of (7.8). In this way the full accuracy and stability of the globally implicit algorithm is inherited by the element-by-element algorithm. See [*H*11, *H*14] for further details.

The potential of this method is most pronounced in three-dimensional problems, where the bandwidth of $\mathbf{K}$ is quite large. The element-by-element implicit algorithm is independent of bandwidth, so for an $N \times N \times N$ mesh, the number of multiplications is of order N^3. On the other hand, triangulation requires $0(N^7)$ multiplications, backsubstitution $0(N^5)$. Thus it is apparent that for large three-dimensional problems, particularly nonlinear problems, where frequent retriangulations are necessary, the element-by-element method has significant potential.

8 Concluding Remarks

The understanding of time integration methods for semidiscrete systems has deepened considerably in recent years. At the same time a variety of new approaches have been developed which provide significantly more economical calculations. In this paper we have briefly summarized some fundamental results and some of the new concepts in computational transient analysis.

Downloaded 02 May 2010 to 171.66.16.250. Redistribution subject to ASME license or copyright; see http://www.asme.org/terms/Terms_Use.cfm

Nevertheless, effective engineering analysis of many important problems is still often stymied by the large cost of time integration of computer models. This is particularly critical in nonlinear problems, where the sensitivities and idiosyncracies of nonlinear phenomena require numerous analyses before the results of the computations can be brought to bear on the design process. Thus, additional improvements in the reliability and efficiency of time intergration procedures are urgently needed.

Furthermore, as can be concluded from this paper, many open questions remain in the fundamental theory of time integration procedures. Particularly noteworthy are topics such as the stability and convergence of time integrators for nonlinear problems and nonsymmetric operators, and the effective exploitation of new concepts such as operator splitting and subcycling. Progress in these areas should provide substantial benefits in the speed and reliability of transient response computations.

Acknowledgments

The second author was supported by Air Force Office of Scientific Research Grant F49620-82-K0013.

References

*A*1 Adams, D. D., and Wood, W. L., "Comparison of Two 'α-methods' for the Numerical Integration of Vibration Equations," Department of Mathematics, University of Reading, 1982.

*A*2 Ames, W. F., *Numerical Methods for Partial Differential Equations*, 2nd ed., Academic Press, New York, 1977.

*B*1 Belytschko, T., "Partitioned and Adaptive Algorithms for Explicit Time Integration," in *Nonlinear Finite Element Analysis in Structural Mechanics*, Wunderlich, W., et al., eds., Springer-Verlag, 1980, pp. 572–584.

*B*2 Belytschko, T., "A Split Operator Method for Transient Problems," *SMIRT*, Vol. 6, Chicago, Aug. 1983.

*B*3 Belytschko, T., and Hughes, T. J. R., eds., *Computational Methods in Transient Analysis*, North-Holland, Amsterdam, 1983.

*B*4 Belytschko, T., and Mullen, R., "Mesh Partitions of Explicit-Implicit Time Integration," *Formulations and Computational Algorithms in Finite Element Analysis*, Bathe, K. J., Oden, J. T., and Wunderlich, W., eds., MIT Press, Cambridge, Mass., 1976, pp. 673–690.

*B*5 Belytschko, T., and Mullen, R., "Stability of Explicit-Implicit Mesh Partitions in Time Integration," *International Journal of Numerical Methods in Engineering*, Vol. 12, 1978, pp. 1575–1586.

*B*6 Belytschko, T., Yen, H. J., and Mullen, R., "Mixed Methods for Time Integration," *Computer Methods in Applied Mechanics and Engineering*, Vol. 17/18, 1979, pp. 259–275.

*B*7 Belytschko, T., Liu, W. K., and Smolinski, P., "Computational Methods for Analysis of Transient Response," *Proc. 4th ASCE Engineering Mechanics Specialty Conference*, Purdue, Ind., May 1983.

*C*1 Chorin, A. J., Hughes, T. J. R., McCracken, M. F., and Marsden, J. E., "Product Formulas and Numerical Algorithms," *Communications on Pure and Applied Mathematics*, Vol. XXXI, 1978, pp. 205–256.

*D*1 Dahlquist, G., "A Special Stability Problem for Linear Multistep Methods, *BIT*, Vol. 3, 1963, pp. 27–43.

*D*2 Douglas, J., and Rachford, H. H., "On the Numerical Solution of Heat Conduction Problems in Two and Three Space Variables," *Trans. American Math. Soc.*, Vol. 82, 1956, p. 421.

*F*1 Felippa, C. A., and Park, K. C., "Staggered Solution Transient Analysis Procedures for Coupled Mechanical Systems: Formulation," *Computer Methods in Applied Mechanics and Engineering*, Vol. 24, 1980, pp. 61–111.

*G*1 Gear, C. W., *Numerical Initial Value Problems in Ordinary Differential Equations*, Prentice-Hall, Englewood Cliffs, N.J., 1971.

*G*2 Geradin, M., "A Classification and Discussion of Integration Operators for Transient Structural Response," AIAA Paper 74-105, presented at AIAA 12th Aerospace Sciences Meeting, Washington, D.C., Jan. 30–Feb. 1, 1974.

*G*3 Goudreau G. L., and Taylor, R. L., "Evalaution of Numerical Methods in Elastodynamics," *Journal of Computer Methods in Applied Mechanics and Engineering*, Vol. 2, 1973, pp. 69–97.

*H*1 Haug, E., Nguyen, Q. S., and de Rouvray, A. L., "An Improved Energy Conserving Implicit Time Integration Algorithm for Nonlinear Dynamic Structural Analysis," *Transactions of the 4th International Conference on Structural Mechanics in Reactor Technology*, San Francisco, Aug. 1977.

*H*2 Hayes, L., "Implementation of Finite Element Alternating-Direction Methods on Nonrectangular Regions," *International Journal for Numerical Methods in Engineering*, Vol. 16, 1980, pp. 35–50.

*H*3 Hilber, H. M., "Analysis and Design of Numerical Integration Methods in Structural Dynamics," EERC Report No. 76-29, Earthquake Engineering Research Center, University of California, Berkeley, Calif., Nov. 1976.

*H*4 Hilber, H. M., and Hughes, T. J. R., "Collocation, Dissipation and 'Overshoot' for Time Integration Schemes in Structural Dynamics," *Earthquake Engineering and Structural Dynamics*, Vol. 6, 1978, pp. 99–118.

*H*5 Hilber, H. M., Hughes, T. J. R., and Taylor, R. L., "Improved Numerical Dissipation for Time Integration Algorithms in Structural Dynamics," *Earthquake Engineering and Structural Dynamics*, Vol. 5, 1977, pp. 283–292.

*H*6 Houbolt, J. C., "A Recurrence Matrix Solution for the Dynamic Response of Elastic Aircraft," *Journal of the Aeronautical Sciences*, Vol. 17, 1950, pp. 540–550.

*H*7 Hughes, T. J. R., "Stability, Convergence and Growth and Decay of Energy of the Average Acceleration Method in Nonlinear Structural Dynamics," *Computers and Structures*, Vol. 6, 1976, p. 313–324.

*H*8 Hughes, T. J. R., "Analysis of Transient Algorithms With Particular Reference to Stability Behavior," Chapter 2 in reference B3.

*H*9 Hughes, T. J. R., Caughey, T. K., and Liu, W. K., "Finite Element Methods for Nonlinear Elastodynamics Which Conserve Energy," *Journal of Applied Mechanics*, Vol. 45, 1978, pp. 366–370.

*H*10 Hughes, T. J. R., Levit, I., and Winget, J., "Unconditionally Stable Element-by-Element Implicit Algorithm for Heat Conduction Analysis," *Journal of the Engineering Mechanics Division*, ASCE, Vol. 109, No. 2, April 1983, pp. 576–585.

*H*11 Hughes, T. J. R., Levit, I., and Winget, J., "An Element-by-Element Solution Algorithm for Problems of Structural and Solid Mechanics," *Computer Methods in Applied Mechanics and Engineering*, Vol. 36, No. 2, 1983, pp. 241–254.

*H*12 Hughes, T. J. R., and Liu, W. K., "Implicit-Explicit Finite Element in Transient Analysis: Stability Theory," ASME JOURNAL OF APPLIED MECHANICS, Vol. 45, 1978, pp. 371–374.

*H*13 Hughes, T. J. R., Pister, K. S., and Taylor, R. L., "Implicit-Explicit Finite Elements in Nonlinear Transient Analysis," *Computer Methods in Applied Mechanics and Engineering*, Vol. 17/18, 1979, pp. 159–182.

*H*14 Hughes, T. J. R., Winget, J., Levit, I., and Tezduyar, T. E., "New Alternating Direction Procedures in Finite Element Analysis Based upon EBE Approximate Factorizations," in *Recent Developments in Computer Methods for Nonlinear Solid and Structural Mechanics*, Perrone, N., and Atluri, S., eds., ASME, New York, June 1983. pp. 75–109.

*I*1 Irons, B. M., "Applications of a Theorem on Eigenvalues to Finite Element Problems," (CR/132/70) University of Wales, Department of Civil Engineering, Swansea, 1970.

*K*1 Krieg, R. D., and Key, S. W., "Transient Shell Response by Numerical Time Integration," *International Journal for Numerical Methods in Engineering*, Vol. 7, 1973, pp. 273–286.

*M*1 Mullen, R., and Belytschko, T., "An Analysis of an Unconditionally Stable Explicit Method," to appear in *Computers and Structures*.

*N*1 Newmark, N. M., "A Method of Computation for Structural Dynamics," *Journal of the Engineering Mechanics Division*, ASCE, 1954, pp. 67–94.

*O*1 Ortiz, M., Pinsky, P. M., and Taylor, R. L., "Unconditionally Stable Element-by-element Algorithms for Dynamic Problems," *Computer Methods in Applied Mechanics and Engineering*, Vol. 36, No. 2, 1983, pp. 223–239.

*P*1 Park, K. C., "Evaluating Time Integration Methods for Nonlinear Dynamic Analysis," in *Finite Element Analysis of Transient Non-linear Behavior*, Belytschko, T., Osias, J. R., and Marcal, P. V., eds., Applied Mechanics Symposia Series, ASME, New York, 1975.

*P*2 Park, K. C., "Partitioned Transient Analysis Procedures for Coupled-Field Problems: Stability Analysis," ASME JOURNAL OF APPLIED MECHANICS, Vol. 47, 1980, pp. 370–376.

*P*3 Park, K. C., "An Improved Semi-Implicit Method for Structural Dynamic Analysis," ASME JOURNAL OF APPLIED MECHANICS, Vol. 49, 1982, pp. 589–593.

*P*4 Peaceman, D. W., and Rachford, H. H., "The Numerical Solution of Parabolic and Elliptic Differential Equations," *SIAM Journal*, Vol. 3, 1955, pp. 28–41.

*R*1 Richtmyer, D., and Morton, K. W., *Difference Methods for Initial-Value Problems*, 2nd Ed., Interscience, New York, 1967.

*S*1 Saul'yev, V. K., *Integration of Equations of the Parabolic Type by the Method of Nets*, Pergamon Press, 1964.

*T*1 Trujillo, D. M., "An Unconditionally Stable Explicit Algorithm for Finite Element Heat Conduction Analysis," *Nuclear Engineering and Design*, Vol. 32, 1975, pp. 110–120.

*T*2 Trujillo, D. H., "An Unconditionally Stable Explicit Algorithm for Structural Dynamics," *Int. Journal for Numerical Methods in Engineering*, Vol. 11, 1977, pp. 1579–1592.

Downloaded 02 May 2010 to 171.66.16.250. Redistribution subject to ASME license or copyright; see http://www.asme.org/terms/Terms_Use.cfm

J. W. Hutchinson
Division of Applied Sciences,
Harvard University,
Cambridge, Mass. 02138
Fellow ASME

Fundamentals of the Phenomenological Theory of Nonlinear Fracture Mechanics

An introduction to the theoretical foundations of the phenomenological theory of nonlinear fracture mechanics is given. Following an outline of the full range of objectives of nonlinear fracture mechanics, the paper focuses on the phenomenological, or semiempirical, approach to the initiation of crack growth and the subsequent quasi-static crack growth and loss of stability under monotonic load histories.

1 Objectives of Nonlinear Fracture Mechanics

An individual from applied mechanics who is a newcomer to fracture mechanics is naturally predisposed to regard the subject as a means of analyzing flawed, or cracked, structural components. By contrast, his colleague from materials science is more likely to view fracture mechanics as a means of characterizing, or ordering, the fracture resistance of materials. Both aspects have provided, and continue to provide, impetus for development of the subject. The success of fracture mechanics is derived in part from the union of these two purposes. Measured fracture parameters not only serve to order the resistance of materials to fracture, but they can also be employed directly in the analysis of structural integrity in the presence of flaws. It is important for the newcomer to the subject to bear these dual purposes in mind since otherwise he or she might regard as undue, the emphasis placed on either test specimens, on the one hand, or crack solutions, on the other.

Nonlinear fracture mechanics is largely concerned with inelastic effects. Some inelasticity is almost always present in the vicinity of a stressed crack tip. Depending on material and conditions, the inelasticity can take various forms, including rate-independent plasticity, creep, and phase change. When the zone of inelasticity is small enough, solutions from linear elasticity can be used to analyze, or, more precisely, to correlate, data from test specimens. This data can, in turn, be used in conjunction with other linearly elastic crack solutions to predict failure of cracked structural components. Linear-elastic fracture mechanics has found extensive applications to high-strength, relatively brittle materials such as metals used in the aerospace industry and ceramics. For certain fracture phenomena, such as fatigue crack growth and corrosion cracking, the zone of inelasticity is often small enough to use linear-elastic fracture mechanics even in more ductile materials. However, the more ductile a material, the more likely that the inelastic zone will not be small enough at the point of fracture to justify the use of solutions based on linear elasticity. For example, components and test specimens of practical dimensions, which are made of many of the more common low-to-intermediate-strength structural metals, become fully plastic before a crack starts to advance under monotonic loadings. Under these circumstances it is essential to use solutions to crack problems based on a theory of plasticity.

Nonlinear fracture mechanics encompasses a semiempirical approach, which for the most part is an extension of linear-elastic fracture mechanics to account for large-scale inelastic effects, and a more basic approach whose aim is to predict (as opposed to correlate) fracture conditions by accounting for mechanisms of separation at the microscopic level. In the semiempirical, or phenomenological, approach crack solutions are used to correlate fracture conditions at the tip of a crack in a structural component to corresponding near-tip conditions in a previously tested specimen. It is the semiempirical approach whose foundations will be discussed in this paper. Furthermore, attention will be directed exclusively to the initiation of growth of a preexisting crack and its subsequent quasi-static advance in bodies of rate-independent materials subject to monotonic loading. While this is the most fully developed topic in nonlinear fracture mechanics, a number of other problem areas are currently under intensive investigation. These include creep crack growth, dynamic crack propagation and arrest, low-cycle fatigue cracking, and high-temperature creep-fatigue cracking. In addition, more fundamental work than that to be described in this paper is progressing on stable crack growth.

The more basic problem of relating fracture parameters to microstructural separation processes has received relatively less attention than the semiempirical approach. Nevertheless, important qualitative understanding has been gained from models for crack initiation due to both cleavage in the brittle range of behavior and hole growth in the ductile range. In addition, some progress has been made in relating high-temperature crack growth to rates of grain boundary

Contributed by the Applied Mechanics Division for publication in the JOURNAL OF APPLIED MECHANICS.

Discussion on this paper should be addressed to the Editorial Department, ASME, United Engineering Center, 345 East 47th Street, New York, N.Y. 10017, and will be accepted until two months after final publication of the paper itself in the JOURNAL OF APPLIED MECHANICS. Manuscript received by ASME Applied Mechanics Division, April, 1983.

Copyright © 1983 by ASME
Downloaded 02 May 2010 to 171.66.16.250. Redistribution subject to ASME license or copyright; see http://www.asme.org/terms/Terms_Use.cfm

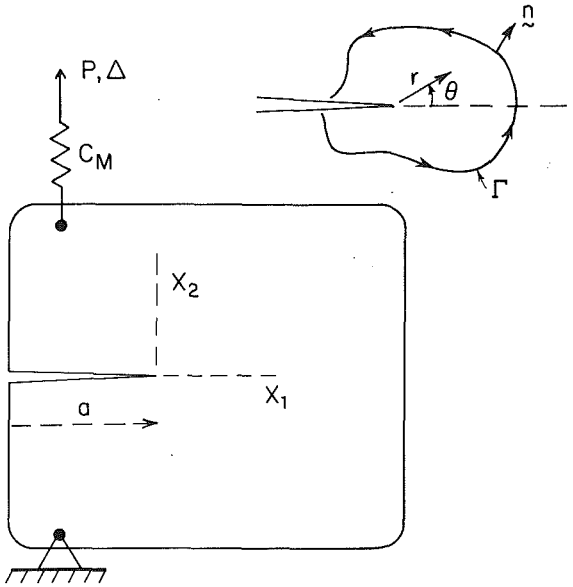


Fig. 1 Conventions for a cracked body in mode I

cavitation in polycrystalline materials. These and other challenging problems in the same category seem ripe for new advances.

2 Background From Linear Fracture Mechanics

The aspects of nonlinear fracture mechanics to be discussed in this paper are largely direct generalizations of concepts and results from linear-elastic fracture mechanics. For the purpose of making contact with the linear theory, we start with a brief synopsis of results from that theory which can be found in any text on the subject.

For an isotropic, linearly elastic solid under conditions of plane strain or plane stress the stress and strain fields at the crack tip always have a singularity of order $r^{-1/2}$. With the conventions shown in Fig. 1, the general form of the stress and strain singularity fields is

$$\sigma_{ij} = \frac{K}{\sqrt{2\pi r}}\tilde{\sigma}_{ij}(\theta)$$

$$\epsilon_{ij} = \frac{K}{\sqrt{2\pi r}}\tilde{\epsilon}_{ij}(\theta) \tag{1}$$

where the amplitude of the singularity, K, is called the stress intensity factor. Fields that are symmetric with respect to the plane of the crack ($x_2 = 0$) are termed mode I, while antisymmetrical fields are termed mode II. For a given mode, the θ-variations, $\tilde{\sigma}$ and $\tilde{\epsilon}$, are fixed. It is standard practice to normalize the singular fields of the linear theory by requiring $\tilde{\sigma}_{22}(\theta=0)=1$ in mode I and $\tilde{\sigma}_{12}(\theta=0)=1$ in mode II. The θ-variations of the in-plane stress components are the same for plane stress and plane strain, but the strains depend on which condition is in effect. The stress intensity factor K depends linearly on the applied load and is a function of the crack length and other geometric parameters characterizing the body. Catalogues of results for stress intensity factors are available for a wide variety of geometries.

The stress intensity factor provides a measure of the level of deformation in the vicinity of the crack tip. Its use to characterize the onset or continuation of crack growth in a real material, which may undergo plasticity, creep, or other inelastic deformation in the most highly stressed region at the tip, relies on satisfaction of a condition known as *small-scale yielding*. In other words, this condition requires that the zone of inelasticity, whatever its source, be contained well within the region over which the singularity fields (1) provide a good approximation to the full linear elasticity solution. Small-scale yielding assures that all the pertinent information related to the geometry and loads applied to the cracked body are communicated to the crack tip only through K for a given mode of loading.

The critical stress intensity factor, K_c, associated with the onset of crack growth under monotonic loading depends on the material, its temperature, and possibly on its chemical environment. It also depends on the mode of loading and on whether plane stress or plane strain, or a set of conditions in between, pertain. The critical value of K for any given set of conditions must be obtained by experiment using a calibrated, precracked test specimen which meets the restrictions of small-scale yielding at the onset of fracture. The critical stress intensity factor in mode I, plane-strain conditions is designated as K_{Ic} and is called the *fracture toughness* of the material at the particular temperature.

A by-product of nonlinear fracture mechanics has been a quantitative clarification of small-scale yielding, but insight into this condition was already available through a combination of test and theory prior to the development of the nonlinear theory [1]. Rough sketches of the boundary of the plastic zone in small-scale yielding are shown in Fig. 2 for mode I. The material is assumed to be elastic-perfectly plastic with a tensile yeild stress σ_0 and a Mises yield surface. The zone size is proportional to K^2. With r_p as the (approximate) distance to the boundary ahead of the crack tip,

$$r_p = \frac{1}{3\pi}\left(\frac{K}{\sigma_0}\right)^2 \quad \text{for plane strain}$$

$$r_p = \frac{1}{\pi}\left(\frac{K}{\sigma_0}\right)^2 \quad \text{for plane stress} \tag{2}$$

The standards of the American Society for Testing and Materials (ASTM) for a valid K_{Ic} test [1] were arrived at by extensive testing using several types of specimens. For a compact tensile specimen, whose plane view is similar to the cracked body shown in Fig. 1, the standard requires that the uncracked ligament and the crack length itself be not less than $25r_p$ at the point of fracture. To ensure plane-strain conditions along most of the crack edge except near the faces, it is also required that the specimen thickness be at least $25r_p$. As a rule of thumb, small-scale yielding will be in force at the onset of crack growth if the applied load is less than half the limit load, modeling the cracked body as elastic-perfectly plastic with yield stress σ_0. For high-strength, relatively brittle metal alloys, values of r_p at fracture initiation in the range 0.1 to 1 mm are typical in plane strain. Thus a specimen with crack lengths on the order of 2.5 to 25 mm will suffice to ensure small-scale yielding. Similarly, many applications involving crack-like flaws in structural components of high-strength alloys will fall within the small-scale yielding range.

The utility of linear-elastic fracture mechanics is substantially diminished for applications and testing involving low and intermediate-strength metals with good ductility. For an intermediate-strength steel used in pressure containment vessels, r_p at fracture initiation under monotonic loads can be as large as 10 mm. A valid K_{Ic} test would therefore require a test specimen the size of a filing cabinet. While such specimens have indeed been produced and tested for some special applications, they are generally prohibitively expensive and too difficult to test. Fracture toughness testing on its own had provided ample motivation for the development of nonlinear fracture mechanics.

Depending on material properties, specimen geometry, and loading compliance, the crack may or may not run dynamically once the critical intensity factor is attained. Certain specimens permit the experimental determination of K versus crack advance Δa under stable quasi-static growth

Downloaded 02 May 2010 to 171.66.16.250. Redistribution subject to ASME license or copyright; see http://www.asme.org/terms/Terms_Use.cfm

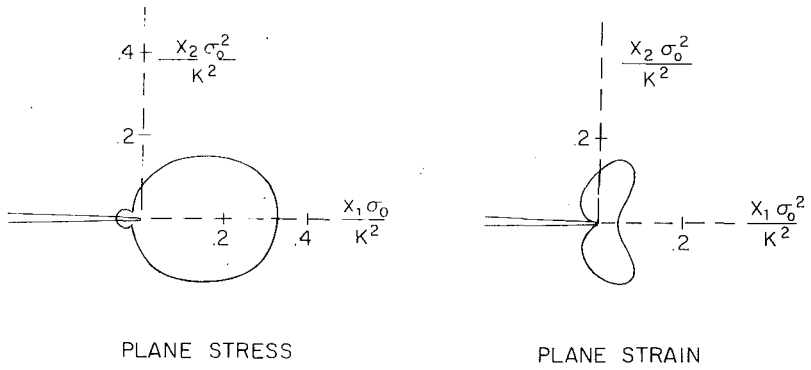


Fig. 2 Boundaries of the plastic zone in small-scale yielding for an elastic-perfectly plastic solid yielding according to the Mises criterion

conditions. A highly brittle material will undergo crack advance under essentially constant K, as depicted in Fig. 3, while a more ductile material with tearing resistance requires an incremental increase in K for each increment of crack advance. The measured curve of K_R versus Δa is called the *resistance curve* of the material. Like K_c itself, the resistance curve is a strong function of whether plane stress or plane strain is in effect, and it only has meaning under small-scale yielding. Given the crack has extended quasi-statically an amount Δa to the current crack length a, the condition for continued crack advance is $K = K_R(\Delta a)$, where K is the applied stress intensity factor. The crack poised for growth is stable (i.e., will not run dynamically) if a small increment of crack advance with the prescribed loading held fixed results in $dK < dK_R$, i.e., if

$$\left(\frac{\partial K}{\partial a}\right)_L < \left(\frac{dK_R}{d\Delta a}\right) \tag{3}$$

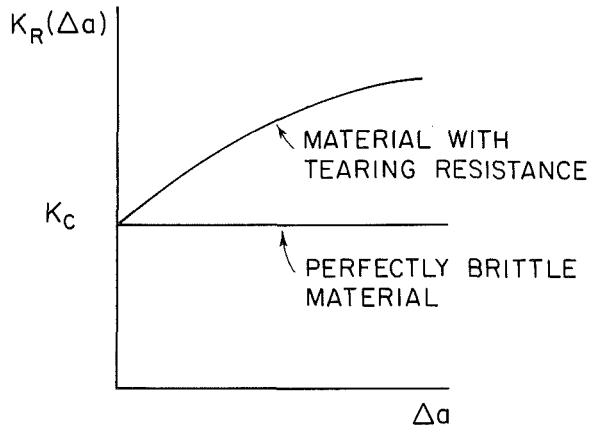


Fig. 3 Small-scale yielding resistance curves

where L denotes the appropriate loading parameter. The body of Fig. 1 represents a cracked component or specimen subject to a generalized load P acting through a generalized spring with compliance C_M. The spring can represent the compliance of a testing machine or the compliance of the portion of the structure communicating the load to the cracked component. While K at a given P does not depend on the spring compliance, $(\partial K/\Delta a)_L$ is a strong function of C_M if Δ is prescribed, thereby influencing the stability of crack advance.

Within the context of the linear theory of elasticity, there is an important connection between the stress intensity factor and the rate of change of the potential energy of the system (cracked body, spring, and loading system) with respect to crack advance. In mode *I* (or mode *II*) the rate of decrease of the potential energy of a system such as that in Fig. 1 per unit crack advance per unit thickness is

$$\mathcal{G} = \frac{1-\nu^2}{E}K^2 \quad \text{(plane strain)}$$

$$= \frac{1}{E}K^2 \quad \text{(plane stress)} \tag{4}$$

where E is Young's modulus and ν is Poisson's ratio. At a given current load level, the energy release rate is independent of C_M and is the same whether the load or the displacement is prescribed to be fixed during the increment of crack advance.

Griffith's original treatment of the onset of crack advance was couched in terms of an energy balance by requiring $\mathcal{G}$ to be equal to $\mathcal{G}_c$, the energy absorbed in the process of creating a unit area of separated surfaces. In small-scale yielding, the energy-based approach and stress intensity approach are mathematically equivalent for crack initiation because of the connection (4). The energy-based interpretation is still preferred in some quarters, particularly in the materials science community. In spite of the appeal of energy arguments, Irwin and others involved in the early development of fracture mechanics saw that for many purposes the intensity-based approach was more flexible and permitted application of the theory beyond what could be rationalized by energy arguments. Examples within linear-elastic fracture mechanics include fatigue crack propagation and creep cracking in brittle materials. The theory of nonlinear fracture mechancis which will be discussed in the following is strictly based on intensity arguments.

In the introduction to the foundations of nonlinear fracture mechanics, which follows, we have not attempted to provide a comprehensive guide to the literature. Instead, we have tried for the most part to give relatively recent articles which will enable the reader to trace backward to earlier contributions.

3 The *J*-Integral and Crack-Tip Fields for Plastically Deforming Solids

The unifying theoretical idea behind nonlinear fracture mechanics for rate-independent materials under monotonic loading is the *J*-integral [2]. A small-strain deformation theory of plasticity (i.e., a small-strain, nonlinearly elastic material) is assumed as the material model. The strain energy density of the material is $W(\epsilon)$ with stress given by

$$\sigma_{ij} = \partial W/\partial \epsilon_{ij} \tag{5}$$

A cracked body such as that in Fig. 1 is considered to be in plane stress or plane strain with the crack lying along the x_1-axis. With Γ as any contour encircling the tip of the crack in a counterclockwise direction, the path-independent line integral expression for J is

$$J = \int_\Gamma (Wn_1 - \sigma_{ij} n_j u_{i,1}) ds \tag{6}$$

Downloaded 02 May 2010 to 171.66.16.250. Redistribution subject to ASME license or copyright; see http://www.asme.org/terms/Terms_Use.cfm

where **u** is the displacement vector, s is the arc length along the contour, and **n** is the outward unit normal to Γ. For the fictitious nonlinearly elastic solid, J is the energy release rate. It reduces to $\mathcal{G}$ for a linearly elastic material. The significance of the energy release rate for the fictitious material will be discussed later. From a physical point of view, the more important role of J is as a measure of the intensity of the near-tip deformation and this will now be addressed.

By taking Γ as a circular contour centered at the tip and by using path independence to shrink the contour down to the tip, one concludes that if J is nonzero then the integrand in (6) should have a r^{-1} singularity. That is,

$$r(Wn_1 - \sigma_{ij}n_j u_{i,1}) = f(\theta) \quad \text{as} \quad r \to 0 \tag{7}$$

and, thus,

$$J = \int_{-\pi}^{\pi} f(\theta)d\theta \tag{8}$$

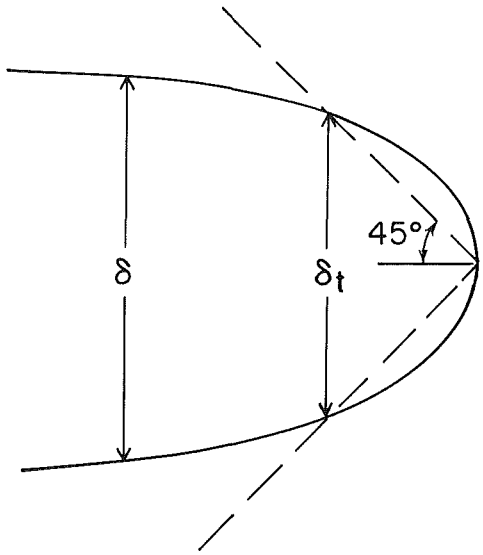


Fig. 4 Crack opening for a hardening material

This relation already suggests an intimate relation between J and the near-tip deformation. A more explicit connection is revealed if a power-law relation between stress and strain is assumed.

A widely used uniaxial stress-strain relation is the Ramberg-Osgood form

$$\epsilon/\epsilon_0 = \sigma/\sigma_0 + \alpha(\sigma/\sigma_0)^n \tag{9}$$

where σ_0 is an effective yield stress, $\epsilon_0 = \sigma_0/E$ is the associated elastic strain with E as Young's modulus, and where α and n are parameters chosen to fit data. Typical n-values range from 3 to 5 for materials with high hardening to as large as 20 for light hardening. Asymptotically, as the crack tip is approached, the contributions to the strains that depend linearly on stress are negligible compared to the power-law terms. The pure-law relation from (9) is

$$\epsilon/\epsilon_0 = \alpha(\sigma/\sigma_0)^n \tag{10}$$

If J_2 deformation theory is used to generalize (10) to multiaxial states, then

$$\frac{\epsilon_{ij}}{\epsilon_0} = \frac{3}{2}\alpha\left(\frac{\sigma_e}{\sigma_0}\right)^{n-1}\frac{s_{ij}}{\sigma_0}, \quad \sigma_e = \left(\frac{3}{2}s_{ij}s_{ij}\right)^{1/2} \tag{11}$$

where **s** is the stress deviator. For the power-law material the r^{-1} singularity in W implies a $r^{-1/(n+1)}$ singularity in the stresses, a $r^{-n/(n+1)}$ singularity in the strains, and a $r^{1/(n+1)}$ variation in the displacements. The near-tip singularity fields can be written as

$$\sigma_{ij} = \sigma_0\left(\frac{J}{\alpha\sigma_0\epsilon_0 I_n r}\right)^{\frac{1}{n+1}}\tilde{\sigma}_{ij}(\theta,n) \tag{12a}$$

$$\epsilon_{ij} = \alpha\epsilon_0\left(\frac{J}{\alpha\sigma_0\epsilon_0 I_n r}\right)^{\frac{n}{n+1}}\tilde{\epsilon}_{ij}(\theta,n) \tag{12b}$$

$$u_i - \hat{u}_i = \frac{J}{I_n\sigma_0}\left(\frac{\alpha\sigma_0\epsilon_0 I_n r}{J}\right)^{\frac{1}{n+1}}\tilde{u}_i(\theta,n) \tag{12c}$$

Details of these fields are given in [3–5]. The dimensionless θ-variations $\tilde{\sigma}$, $\tilde{\epsilon}$, and $\tilde{\mathbf{u}}$ depend on the mode, on n, and on whether plane strain or plane stress is assumed, as does the normalizing constant I_n. These variations must be normalized

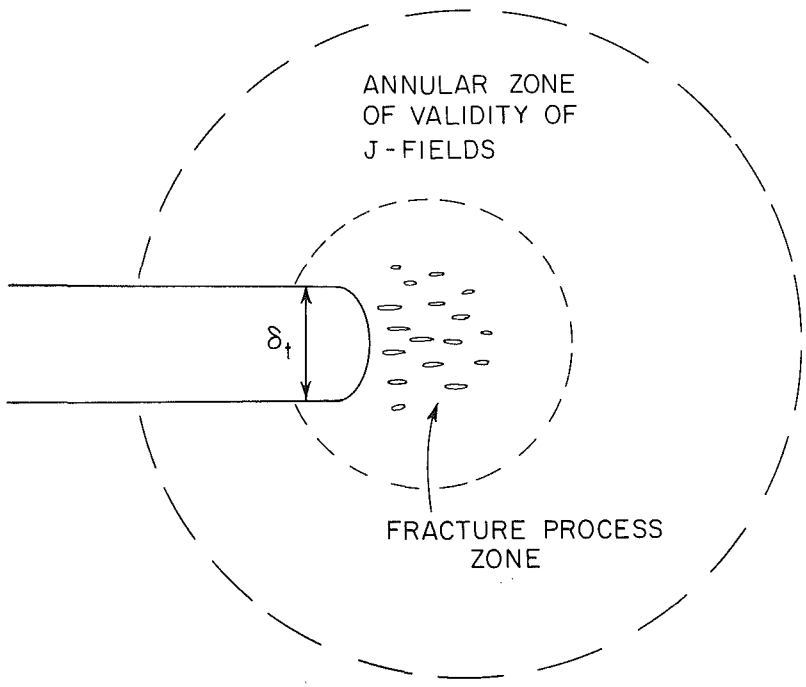


Fig. 5 Schematic of near-tip behavior under J-dominance conditions

Downloaded 02 May 2010 to 171.66.16.250. Redistribution subject to ASME license or copyright; see http://www.asme.org/terms/Terms_Use.cfm

in some manner, and in [3] and [5] the maximum value of $\tilde{\sigma}_e \equiv (3\tilde{s}_{ij}\tilde{s}_{ij}/2)^{1/2}$ is set at unity. The contribution $\hat{\mathbf{u}}$ allows for a possible translation of the crack tip itself.

Later, ways will be discussed for calculating or estimating how J depends on the geometry and loading of the cracked body. It is clear from (12) that J can be regarded as a measure of the intensity of the crack-tip singularity fields. However, before it can be assumed that J can be used to correlate the initiation of crack growth in true elastic-plastic solids, one must be sure that the following two conditions are met. First, the deformation theory of plasticity must be an adequate model of the small-strain behavior of real elastic-plastic materials under the monotonic loads being considered. Second, the regions in which finite strain effects are important and in which the microscopic processes occur must each be contained well within the region of the small-strain solution dominated by the singularity fields. This second condition is sometimes called J-dominance and is analogous to the small-scale yielding requirement for linear fracture mechanics.

The first condition is at issue in any application of a deformation theory of plasticity. Any solution based on the J_2 deformation theory of plasticity coincides exactly with a solution to the J_2 flow (incremental) theory of plasticity if proportional loading (i.e., stress components changing in fixed proportion to one another) occurs everywhere. The singular fields (12) by themselves satisfy this condition exactly. In other words, the crack-tip singularity fields are also solutions to the corresponding J_2 flow theory equations, and J as it appears in (12) could serve as the amplitude of the singular fields, independent of its line integral definition in (6). While the full solution for a body of material characterized by the Ramberg-Osgood tensile relation (9) will not generally satisfy proportional loading exactly, most problems with a single, monotonically applied load do come sufficiently close to meeting proportionality to justify use of deformation theory. Many investigators have demonstrated that the line integral defined in (6) is approximately independent of path when finite element solutions of crack problems are obtained using an incremental theory of plasticity, even though its strict path independence is tied to its deformation theory definition. Moreover, the J-values themselves are accurately approximated by the corresponding deformation theory solutions. It is fair to say that the use of deformation theory solutions to stationary crack problems for monotonic loading is generally accepted for the purpose of evaluating J.

4 J-Dominance in Plane Strain

The requirements connected with the second condition mentioned in the foregoing are more complicated. Most efforts to assess J-dominance have focused on plane-strain configurations under mode I conditions since this combination is generally the most critical in that it leads to the lowest values of J_c (or K_c). Plane strain, mode I will be considered next.

In the discussion that follows the crack-opening displacement plays an important role. The separation of the two crack faces, $\delta = u_2(x_1, 0^+) - u_2(x_1, 0^-)$, varies like $(-x_1)^{1/(n+1)}$ as the tip is approached according to the singularity fields (12) of the small-strain theory. An effective crack-tip opening displacement δ_t can be defined as the separation where the 45 deg lines intercept the crack faces as in Fig. 4. The result is [6]

$$\delta_t = d(\alpha\epsilon_0, n)\frac{J}{\sigma_0} \tag{13}$$

with values of d ranging from about 0.8 for large n to about 0.3 for $n=3$, with a very weak dependence on $\alpha\epsilon_0$. The crack-tip opening displacement provides a measure of the size of the zone in which finite strains are important. Finite element studies based on finite strain incremental plasticity formulations [7, 8] have been performed for the plane-strain small-scale yielding problem. For distances from the tip that are greater than 2 or 3 times δ_t, the deviations from small-strain theory becomes unimportant.

Let R denote the "radius" of the zone of dominance of the singularity fields (12), i.e., the characteristic size of the region in which the singularity fields provide a good approximation to the complete small-strain deformation theory solution. As depicted in Fig. 5, one condition for J-dominance is

$$R > 3\delta_t \tag{14}$$

A second condition is that R be greater than the *fracture process zone* in which the microscopic separation processes occur. The predominant ductile fracture mechanism is void nucleation, growth, and coalescence. Since hole growth is itself a finite strain process, the fracture process zone for this mechanism is roughly comparable to the zone of finite strains, and therefore (14) again serves to ensure $J-$dominance. If failure due to shear localization intervenes, or if it actually precipitates hole nucleation and growth, then the fracture process zone may be somewhat larger than $3\delta_t$. When the separation process is cleavage, the size of the fracture process zone appears to be set by the grain size in many materials with the zone extending from 2 to 10 grain diameters from the tip. This sets a constraint on R for J-dominance under cleavage conditions which usually renders (14) superfluous.

The characteristic size R of the zone of dominance of the singularity fields (12) depends strongly on geometry and hardening. The geometry dependence is especially strong for low-hardening materials (high n) for reasons that will now be discussed.

The mathematical character of the equations governing behavior near the crack tip changes in the limit $n \to \infty$ corresponding to perfect plasticity. For finite n the governing equations are elliptic, and sufficiently near the tip the singularity fields necessarily do provide an asymptotic representation to the complete small-strain solution. In the perfect plasticity limit the equations are hyperbolic and there no longer exists a unique near-tip solution independent of specimen geometry [9]. The limit of the singularity fields (12) as $n \to \infty$ is just one possible near-tip solution. A unique near-tip field tied to J, or any other single parameter, necessarily involves the assumption of hardening. Certain problems do appear to have approximately the same perfectly plastic near-tip fields as those associated with the limit of (12) as $n \to \infty$. Important examples are the small-scale yielding problem itself and the fully plastic bend or compact tension configurations (see Fig. 6). In each of these problems, as well as in the limit of the singularity field (12) as $n \to \infty$, there is a significant elevation of the normal stress ahead of the tip to a level approximately 2.5 times the tensile yield stress σ_0. This high triaxiality largely accounts for the fact that the critical intensity factor (K_{Ic}) associated with mode I, plane-strain conditions is lower than that associated with other possible combinations. The small-scale yielding problem is generally taken as the basic reference configuration since K_{Ic} is determined under this condition. On the other hand, it has long been recognized [9] that a very different near-tip field occurs in a perfectly plastic plane-strain strip with a centered crack pulled to full yield in tension (Fig. 6). In this case the normal stress ahead of the tip is only slightly above σ_0 and the deformation is confined to shear bands extending from the crack tip to the edges of the strip.

Precise estimates of R are difficult to make. Numerical solutions in small-scale yielding indicate that the singularity fields (12) provide a fairly good approximation out to a distance ahead of the tip of roughly

Downloaded 02 May 2010 to 171.66.16.250. Redistribution subject to ASME license or copyright; see http://www.asme.org/terms/Terms_Use.cfm

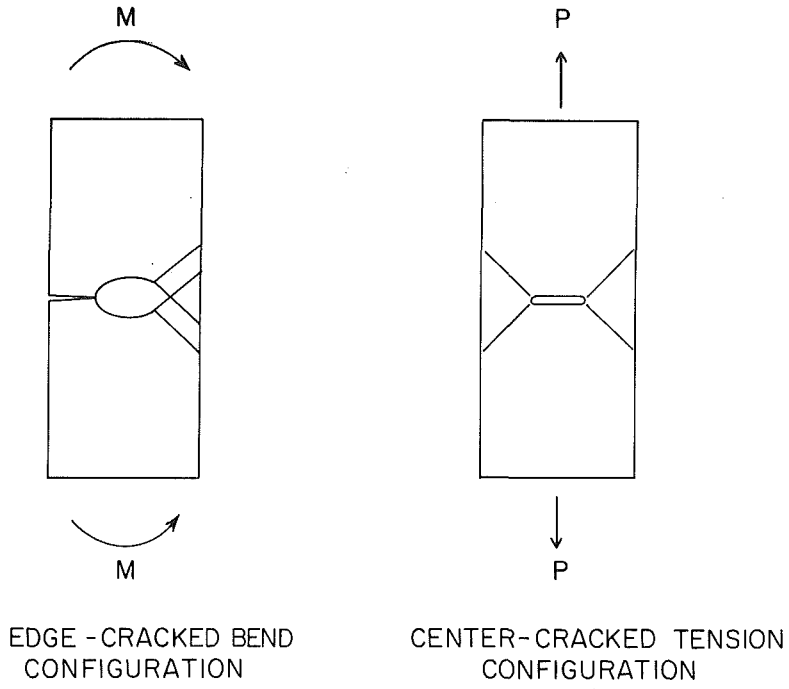


Fig. 6 Plane-strain fully plastic deformation modes

$$R = \left(\frac{1}{5} \quad \text{to} \quad \frac{1}{4}\right) r_p \tag{15}$$

with relatively little dependence on hardening. Under fully plastic conditions, when the plastic zone has reached across the entire uncracked ligament, R for the center-cracked configuration and for the bend configuration, is some fraction of the uncracked ligament b. For the bend configuration (and the compact tension specimen) numerical studies [10] suggest

$$R \cong 0.07b \tag{16}$$

and, again, for essentially all hardening levels including perfect plasticity. The center-cracked tensile configuration has a much smaller zone of dominance which becomes vanishingly small as $n \to \infty$. For light to medium hardening, i.e., $n \cong 10$) it appears that [11], very roughly,

$$R \cong 0.01b \tag{17}$$

Now we return to the issue of J-dominance as specified by (14) for ductile fracture. For low to moderate strain hardening, $\delta_t \cong 0.6J/\sigma_0$. For small-scale yielding, it is readily verified using (2), (15), and $J = (1-\nu^2)\, K^2/\mathrm{E}$ that (14) is always satisfied. For bend-type configurations the condition for J-dominance under fully plastic conditions obtained by combining (16) and (14) is

$$b > 25J/\sigma_0 \tag{18}$$

For the center-cracked tensile configuration the condition for light to moderate hardening from (17) and (14) is

$$b > 175J/\sigma_0 \tag{19}$$

Further work defining J-dominance conditions remains to be done. Moreover, analogous specifications for plane-stress conditions have not been obtained.

5 J_{Ic} Testing

Interaction among application, experiment, and theory has long been a hallmark of fracture mechanics. No sooner was the J-integral put forward than it was exploited in fracture toughness testing [12], and this in turn provided more impetus for theoretical developments. As already mentioned, there was strong motivation to carry out fracture toughness tests on small specimens of low and intermediate-strength materials with no restriction to small-scale yielding.

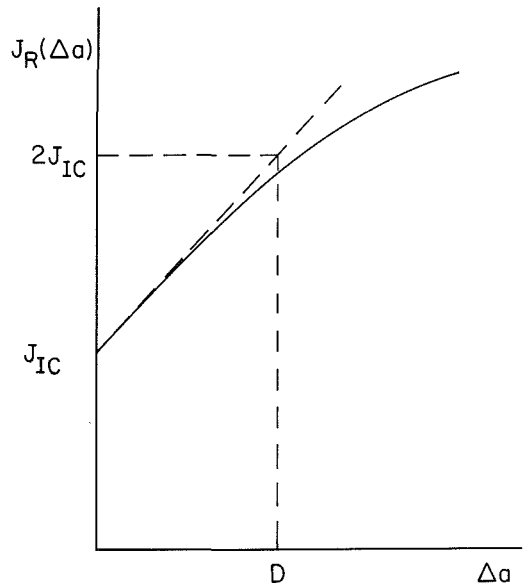


Fig. 7 Resistance curve under J-controlled growth conditions

Testing for J_{Ic} is an art in itself which has advanced significantly from its beginnings [13], and we will not attempt to go into the subtleties of the method here. In principle, the procedure is analogous to K_{Ic} testing. One chooses a plane-strain, mode I specimen that will meet the J-dominance condition, and one experimentally determines the critical value of J, J_{Ic}, at which the initiation of crack growth occurs. When the method was first being developed, it was essential to establish the equivalence of fracture toughness determination by any such J-test with that of valid K_{Ic} test. In small-scale yielding $J = \mathcal{G} = (1-\nu^2)K^2/\mathrm{E}$, and thus it was essential to verify that

Downloaded 02 May 2010 to 171.66.16.250. Redistribution subject to ASME license or copyright; see http://www.asme.org/terms/Terms_Use.cfm

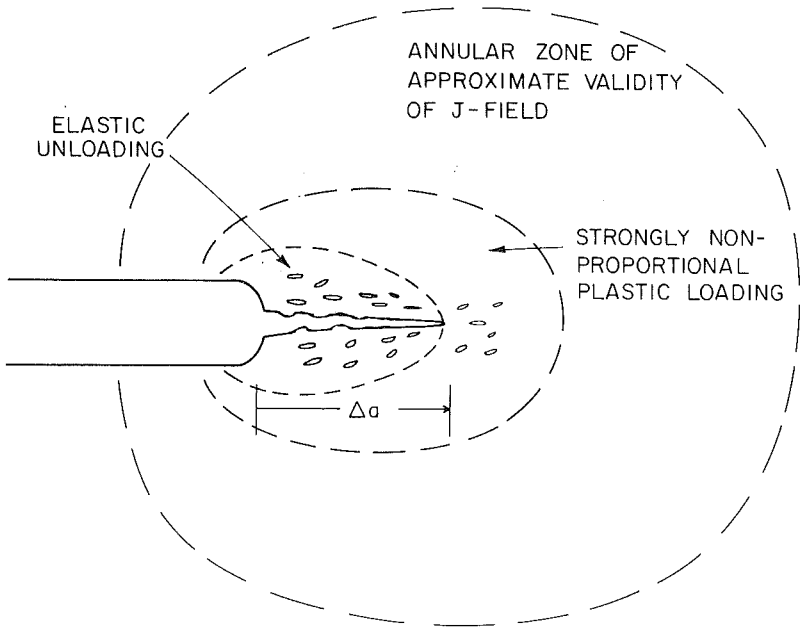


Fig. 8 Schematic of near-tip behavior under J-controlled growth conditions

$$J_{Ic} = (1 - \nu^2)K_{Ic}^2/E \tag{20}$$

This basic relation has been verified for a wide variety of metals using different specimen geometries and sizes with J_{Ic} being determined under conditions ranging from intermediate-scale yielding to full yielding. The determination of J_{Ic}, and of K_{Ic}, involves a somewhat arbitrary decision as to what constitutes the onset of crack growth since this is not necessarily a dramatic event especially in tough materials, as will be discussed further in the following.

The condition (18) for J-dominance in bend-type configurations under fully plastic yielding was first verified experimentally by noting that departures from (20) begin to appear when (18) is violated at initiation. Note that (18) is approximately equivalent to $b > 40\delta_t$. Condition (19) for the center-cracked configuration is clearly much more restrictive and should only be regarded as a rough estimate since relatively few fully plastic J_{Ic}-tests have been conducted using this configuration. Tests conducted under conditions in which (19) is violated all seem to give J_c values that are larger than J_{Ic}, sometimes by as much as a factor of two. All indications are that the mode I plane-strain, J-dominance condition is the most critical leading to the smallest J_c. Obviously, this conclusion must he used with care.

6 J as Energy Release Rate for the Fictitious Nonlinearly Elastic Body

Curiously, the fact that J is the deformation-theory energy release rate is of more mathematical consequence than physical. For this reason, we deliberately delayed discussion of J as the energy release rate until after we had spelled out its role as an intensity measure.

Let $PE(a)$ denote potential energy of the sytem in Fig. 1, i.e., the sum of the strain energy in the nonlinearly elastic body and in the generalized spring, assuming the total displacement Δ is prescribed. An alternative expression to the line integral (6) definition of J is [2]

$$J = -\frac{dPE}{da} \tag{21}$$

generalizing the definition of $\mathcal{G}$ for linear-elastic materials. It is clear from its line integral definition that J depends only on the current deformation state in the cracked body. In particular, it is independent of the compliance C_M of the loading system. Counterintuitive though it may seem, the energy release rate of the specimen itself at a given current load level is the same whether the load ($C_M \to \infty$) or the displacement ($C_M = 0$) is held constant during the increment of crack advance.

Tempting though it may be, to think of the criterion for initiation of crack growth based on J as an extension of Griffith's energy-balance criterion, it is nevertheless incorrect to do so. This is not to say that an energy balance does not exist, just that it cannot be based on the deformation theory J. Crack advance in an elastic-plastic material invariably involves elastic unloading and distinctly nonproportional loading in the vicinity of the crack tip, and neither is adequately modeled by deformation theory. Efforts to develop an energy-based criterion for crack initiation and advance have been fraught with difficulty, and so far, at least, no general theory along these lines has achieved acceptance.

The energy-based definition of J (21) has been used to derive some very useful formulas for J which permit its determination directly from the experimental load-deflection record for a cracked specimen. An example is the deeply cracked bend configuration subject to a moment per unit thickness M. With Ω as the rotation through which M works minus the corresponding rotation in the absence of the crack, the expression for J derived in [14] is

$$J = \frac{2}{b}\int_0^{\Omega} M d\Omega \tag{22}$$

where b is the length of the ligament ahead of the crack. This formula, and modifications of it, are only accurate for cracks that extend at least halfway through the specimen. Nevertheless, the existence of such a formula means that a detailed theoretical analysis of the specimen is not required in order to run a J_{Ic}-test.

7 Basic Solutions to Nonlinear Crack Problems and J-Estimation Formulas

Applications of nonlinear fracture mechanics requires the

Downloaded 02 May 2010 to 171.66.16.250. Redistribution subject to ASME license or copyright; see http://www.asme.org/terms/Terms_Use.cfm

availability of solutions to elastic-plastic crack problems that relate J to load and crack geometry. Because such solutions depend on details of the stress-strain behavior, the task of compiling nonlinear crack solutions is inherently more involved than what has been done for linear-elastic crack problems [15–17]. Finite element methods have been used successfully for solving certain problems, but these numerical solutions are difficult to transfer from one configuration or material to another.

Simple solutions are now available to some basic nonlinear crack problems for the small-strain, deformation-theory material with the pure power-law stress-strain behavior (10) and (11). If P is the load parameter, the solution to any power-law problem necessarily has the property that the stresses and strains are everywhere proportional to P and P^n, respectively, and J is proportional to P^{n+1}. Furthermore, the stress components at every point increase in fixed proportion with increasing P so that the solutions are also rigorous solutions to J_2 flow (incremental) theory. The solutions make contact with limit analysis in that the limit load P_0 of the perfectly plastic cracked body ($n \to \infty$) serves as a useful reference load. A typical solution to a pure power-law crack problem gives

$$\frac{J}{\alpha\sigma_0\epsilon_0 a} = \left(\frac{P}{P_0}\right)^{n+1} h(n, \text{geometry}) \tag{23}$$

where h is a dimensionless function of n and of dimensionless groups of geometric parameters. For most cases, h must be computed numerically; but once computed it can be catalogued, as has been done for a number of basic configurations [18].

Approximate, but highly accurate, solutions have been obtained for two of the most basic nonlinear crack problems, a crack in plane strain and a penny-shaped crack in an infinite body of the power-law material. For a crack of length $2a$ parallel to the x_1 axis and subject to the remote in-plane stress $\sigma_{22} = \sigma$, the plane-strain solution is [19]

$$\frac{J}{\alpha\sigma_0\epsilon_0 a} = \pi\sqrt{n}\left(\frac{\sqrt{3}\sigma}{2\sigma_0}\right)^{n+1} \tag{24}$$

An estimation method has been developed for generating approximate, but reasonably accurate, solutions to elastic-plastic crack problems by combining the linear-elastic solution with the power-law solution [18]. Since the power-law solution provides an accurate estimate under fully plastic yielding, it can be combined with the linear solution to interpolate over the entire range of behavior from small-scale to fully plastic yielding. To illustrate the method consider the crack of length $2a$ in plane strain in an infinite block of material characterized by the Ramberg-Osgood tensile relation (9). The block is subject to an in-plane stress $\sigma_{22} = \sigma$ remote from the crack. In its crudest form, the estimation formula is just the linear combination of the linear and power-law formulas for J comprised to be consistent with (9), i.e.,

$$J = (1-\nu^2)\frac{\pi a}{E}\sigma^2 + \alpha\sigma_0\epsilon_0 a\sqrt{n}\pi\left(\frac{\sqrt{3}\sigma}{2\sigma_0}\right)^{n+1} \tag{25}$$

This formula is clearly asymptotically correct for large and small σ. Improvements in accuracy in the range of intermediate-scale yielding are obtained by the introduction of a crack-length adjustment in the elastic contribution as discussed in [18].

8 *J*-Controlled Crack Growth

Under certain restrictions, small amounts of crack growth can be correlated in large-scale yielding using J in a way that generalizes the resistance curve analysis of small-scale yielding based on K. It is now common practice to use the formula

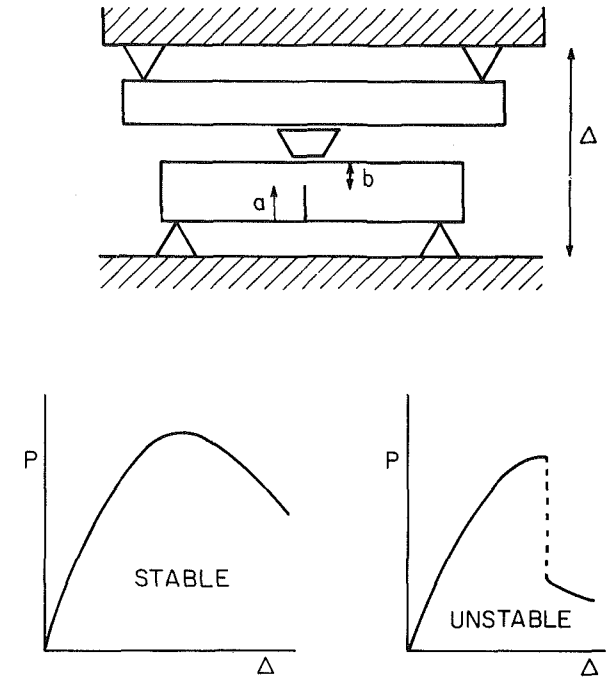


Fig. 9 Cracked specimen in a compliant loading system. Overall load-deflection behavior in presence of stable or unstable crack advance

(22), or an appropriate modification of it, to generate test data for J versus small amounts of crack advance Δa in the form of a J-resistance curve such as that depicted in Fig. 7. Several techniques are available for accurately measuring crack advance, and the observed apparent crack advance associated with crack-tip blunting has been subtracted in Fig. 7. In a typical tough, intermediate-strength steel, the amount of crack advance associated with a doubling of J above J_{Ic} (i.e., $\Delta a \cong D$ in Fig. 7) may be as little as 1 or 2 mm. For many tough materials, resistance curves have been recorded with J-values attaining 5 to 10 times J_{Ic} with J still increasing.

Initially, the J_R-curve was used only as a means of better determining J_{Ic} by using the curve to extrapolate back to $\Delta a = 0$. But it soon became clear that the J_R-curve could be regarded as a material-based curve, in the same sense that the K_R-curve is in small-scale yielding, at least under certain restrictions. Since large increases of J above J_{Ic} are possible in materials with a high tearing resistance, there are considerable practical consequences to design and structural flaw analysis of allowing for small amounts of stable crack growth. Consequently, this subject is being pursued actively in Europe, Japan, the United Kingdom, and the United States [20, 21].

As has already been emphasized, deformation theory on which the J-integral is based does not model elastic unloading or distinctly nonproportional plastic loading, and both effects are present near the crack tip when crack advance occurs. The argument for J-controlled growth requires that the region of elastic unloading and distinct nonproportional loading be contained within the J-dominance zone of the deformation-theory solution. In other words, J will still provide a unique measure for correlating near-tip fracture events if the region within which deformation theory breaks down is well within the zone of dominance. The two conditions for J-controlled growth (in addition to condition (14)) are

$$\Delta a < R \tag{26}$$

and

$$D \equiv J_R \Big/ \left(\frac{dJ_R}{d\Delta a}\right) < R \tag{27}$$

Downloaded 02 May 2010 to 171.66.16.250. Redistribution subject to ASME license or copyright; see http://www.asme.org/terms/Terms_Use.cfm

The first of these ensures that the crack advance and associated unloading all take place within the zone characterized uniquely by J, as depicted in Fig. 8. The second is less obvious. As discussed in [22], D is a rough estimate of the size of the region at the tip within which distinctly nonproportional plastic loading occurs. Both conditions should only be regarded as crude statements of the actual conditions in the sense that the numerical coefficients multiplying Δa and D must be of order unity but not necessarily unity itself.

Under fully yielded conditions R is some fraction of the uncracked ligament b. For the bend configuration with $R = 0.07b$, equation (27) can be written as

$$\omega \equiv \frac{b}{J_R}\frac{dJ_R}{d\Delta a} > 14 \tag{28}$$

while (26) becomes $\Delta a < 0.07b$. Tests on bend and compact tension specimens of varying sizes and uncracked ligament lengths suggest that (28) is too restrictive for this configuration, and that perhaps $\omega > 5$ to 7 is more realistic. Furthermore, with this condition met, the J_R-curves appear to be geometry-independent for crack advance to as much as about $0.1b$. A modified J-like measure has been proposed [23] which appears promising in its ability to extend the range of the correlation to larger amounts of crack advance. This modified J makes use of the deformation theory J and reduces to it for a stationary crack. Whether it will prove to have general utility for growing cracks still remains to be seen.

9 Stability of J-Controlled Crack Growth

Substantial extra load-carrying capacity is gained if small amounts of crack advance are permitted in materials with high tearing resistance. If crack-growth initiation is permitted, the important issue then centers on the stability of crack growth. A large-scale yielding stability analysis based on the experimental resistance curve, $J_R(\Delta a)$, has been proposed and developed in [24] and exploited for design in [25]. The approach assumes J-controlled growth is in force, uses J as the intensity measure, and is otherwise similar in spirit to the K-based stability analysis in small-scale yielding.

To illustrate this approach consider the plane-strain, cracked bend bar of Fig. 9 loaded in series with a linear spring whose compliance is C_M. The total load point displacement Δ is imagined to be imposed on the system. If the crack has advanced stably by an amount Δa and is poised for further advance, then

$$J = J_R(\Delta a) \tag{29}$$

where J is regarded as the "applied" J associated with the current crack length and load carried by the bend bar. Stability of the crack under prescribed Δ requires that

$$\left(\frac{dJ}{da}\right)_\Delta < \frac{dJ_R}{d\Delta a} \tag{30}$$

in direct analog with the corresponding small-scale yielding condition (3). This condition ensures that any sufficiently small accidental advance of the crack due to some disturbance will result in a J-value that falls below that required for continued advance. Conversely, the crack is expected to start running dynamically when (30) is first violated.

A complete analysis of the bend bar of Fig. 9 is possible. In the case where the material is elastic-perfectly plastic and the bar is deeply cracked ($a/b \geq 1$) and fully yielded, the deformation theory analysis [22, 24] gives

$$\left(\frac{dJ}{da}\right)_\Delta = \frac{4P^2}{b^2}(C_{nc} + C_M) - J \tag{31}$$

Here P is the limit load per unit thickness of the cracked bar and C_{nc} is the elastic compliance of the uncracked bar by itself. The compliance of the loading system C_M strongly enters into the stability condition. Under dead load ($C_M \to \infty$) the fully yielded, perfectly plastic bend bar is necessarily unstable.

Nondimensional measures of the driving force for instability, dJ/da, and the tearing resistance, $dJ_R/d\Delta a$, were introduced in [24] according to

$$T = \frac{E}{\sigma_0^2}\left(\frac{dJ}{da}\right)_\Delta \quad \text{and} \quad T_R = \frac{E}{\sigma_0^2}\left(\frac{dJ_R}{d\Delta a}\right) \tag{32}$$

where σ_0 is some appropriate tensile yield stress when the material has a hardening capacity. In terms of the nondimensional quantities, the range of stability is

$$T < T_R \tag{33}$$

In [26] a test series was conducted using a system like that in Fig. 9. A sequence of identical specimens in series with springs of differing compliance were tested, and the validity of the stability condition was checked. The material was a

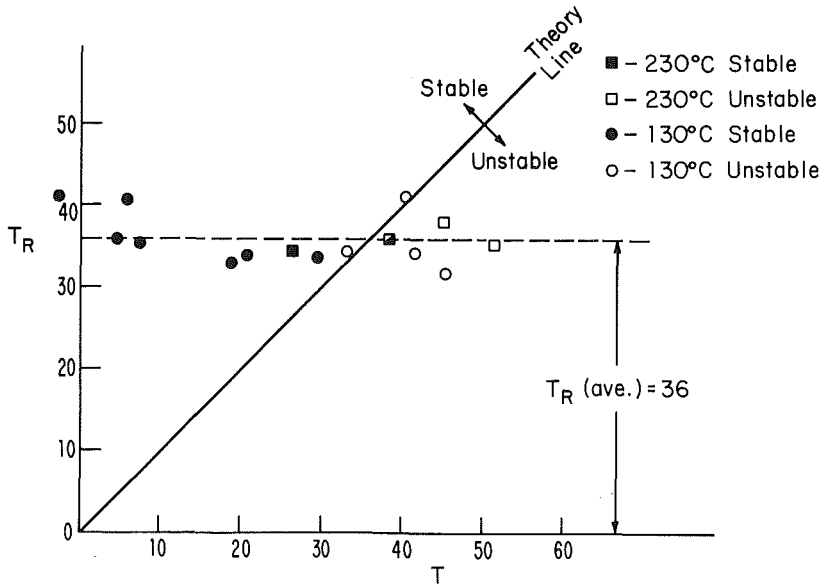


Fig. 10 Experimental data of Paris et al. (1979) showing stable or unstable crack advance

Downloaded 02 May 2010 to 171.66.16.250. Redistribution subject to ASME license or copyright; see http://www.asme.org/terms/Terms_Use.cfm

moderately high-strength steel characterized by $D \cong 1.2$ mm and $T_R \cong 36$ just following initiation. In the tests, attention was focused on the stability of crack advance at, or just following, initiation so that the first condition (26) required for J-controlled growth was certainly met. Furthermore, crack advance did occur under fully yielded, or nearly fully yielded, conditions, and the second condition (28) was also met with $\omega = 15$. The test point for each specimen is plotted in Fig. 9 as the values (T, T_R) at initiation. The solid points indicate specimens for which the crack advanced stably, while the open points designate specimens that experienced dynamic crack advance. The transition to instability occurs near $T = T_R = 36$.

Resistance curves are now generated almost routinely and data for a fairly wide variety of materials at temperatures of application are beginning to accumulate. Tough steels with high tearing resistance can have T_R-values in the range from 100 to 200 for crack advances of several millimeters or more. To put this into some perspective, the T-value for a plane-strain crack in an infinite block of fully yielded power-law material from (24) with $\alpha = 1$ is

$$T = \pi\sqrt{n}(\epsilon^\infty/\epsilon_0)^{\frac{n+1}{n}} \tag{34}$$

For a strain-hardening exponent associated with a typical intermediate strength steel ($n = 5$ to 10), T will not exceed 100 until the applied strain reaches about 10 times the initial yield strain. Of course, in general, T is a strong function of geometry and of loading compliance and therein lies the potential for sound design against unstable crack advance.

Acknowledgment

This review draws on a booklet *A Course on Nonlinear Fracture Mechanics* issued by the Solid Mechanics Department of the Technical University of Denmark, and on a general lecture delivered at the Seventh Canadian Congress of Applied Mechanics, Sherbrooke, Quebec. The work was supported in part by the National Science Foundation under Grant MEA-82-13925, and by the Division of Applied Sciences, Harvard University.

References

1 Srawley, J. E., and Brown, W. F., *Fracture Toughness Testing Methods*, ASTM STP 381, 1965, pp. 133–196.

2 Rice, J. R., "A Path-Independent Integral and the Approximate Analysis of Strain Concentration by Notches and Cracks," ASME JOURNAL OF APPLIED MECHANICS, Vol. 35, 1968, pp. 379–386.

3 Hutchinson, J. W., "Singular Behavior at the End of A Tensile Crack in a Hardening Material," JOURNAL OF MECHANICS AND PHYSICS OF SOLIDS, Vol. 16, 1968, pp. 13–31.

4 Rice, J. R., and Rosengren, G. F., "Plane-Strain Deformation Near a Crack Tip in a Power-Law Hardening Material," JOURNAL OF MECHANICS AND PHYSICS OF SOLIDS, Vol. 16, 1968, pp. 1–12.

5 Shih, C. F., "Small Scale Yielding Analysis of Mixed Mode Plane Strain Crack Problems," ASTM STP 560, 1974, pp. 187–210.

6 Shih, C. F., "Relationship Between the J-Integral and the Crack Opening Displacement for Stationary and Extending Cracks," JOURNAL OF MECHANICS AND PHYSICS OF SOLIDS, Vol. 29, 1981, pp. 305–326.

7 McMeeking, R. M., "Finite Deformation Analysis of Crack Tip Opening in Elastic-Plastic Materials and Implications for Fracture," *Journal of Mechanics and Physics of Solids*, Vol. 25, 1977, pp. 357–381.

8 Rice, J. R., McMeeking, R. M., Parks, D. M., and Sorensen, E. P., "Recent Finite Element Studies in Plasticity and Fracture Mechanics," *Computer Methods in Applied Mechanics and Engineering*, Vol. 17/18, 1979, pp. 411–442.

9 McClintock, F. A., "Plasticity Aspects of Fracture," in *Fracture: An Advanced Treatise* , Vol. 3, Liebowitz, H., ed., Academic Press, New York, 1971, pp. 47–225.

10 Shih, C. F., and German, M. D., "Requirements for a One Parameter Characterization of Crack Tip Fields by the HRR Singularity," *International Journal of Fracture*, Vol. 17, 1981, p. 27.

11 McMeeking, R. M., and Parks, D. M., "On Criteria for J Dominance of Crack Tip Fields in Large Scale Yielding," ASTM STP 668, 1979, pp. 175–194.

12 Begley, J. A., and Landes, J. D., "The J Integral as a Fracture Criterion," *Fracture Toughness*, ASTM STP 514, 1972, pp. 1–23.

13 Landes, J. D., Begley, J. A., and Clarke, G. A., eds., *Elastic-Plastic Fracture*, ASTM STP 668, 1979.

14 Rice, J. R., Paris, P. C., and Merkle, J. G., "Some Further Results on J-Integral Analysis and Estimates," in *Progess in Flaw Growth and Fracture Toughness Testing*, ASTM STP 536, 1973, pp. 231–245.

15 Tada, H., Paris, P. C., and Irwin, G. R., *The Stress Analysis of Cracks Handbook*, Del Research Corporation, Hellertown, Pa., 1973.

16 Rooke, D. P., and Cartwright, J. C., *Compendium of Stress Intensity Factors*, Her Majesty's Stationery Office, London, 1976.

17 Sih, G. C., *Handbook of Stress Intensity Factors*, Institute of Fracture and Solid Mechanics, Lehigh University, Bethlehem, Pa., 1973.

18 Kumar, V., German, M. D., and Shih, C. F., *An Engineering Approach for Elastic-Plastic Fracture Analysis*, Electric Power Research Institute, Inc., 1981.

19 He, M. Y., and Hutchinson, J. W., "The Penny-Shaped Crack and the Plane Strain Crack in an Infinite Body of Power-Law Material," ASME JOURNAL OF APPLIED MECHANICS, Vol. 48, 1981, pp. 830–840.

20 Paris, P. C., ed., *Fracture Mechanics*, ASTM STP 700, 1980.

21 Radon, J. C., ed., *Fracture and Fatigue*, Pergamon Press, 1980.

22 Hutchinson, J. W., and Paris, P. C., "Stability Analysis of J Controlled Crack Growth," ASTM STP 668, 1979, pp. 37–64.

23 Ernst, H. A., "Material Resistance and Instability Beyond J Controlled Crack Growth," to be published in ASTM STP 803.

24 Paris, P. C., Tada, H., Zahoor, A., and Ernst, H., "Instability of the Tearing Mode of Elastic-Plastic Crack Growth," ASTM STP 668, 1979, pp. 5–36.

25 Paris, P. C., "Analysis and Applications With Plastic Tearing Instability," to be published in ASTM STP 803.

26 Paris, P. C., Tada, H., Zahoor, A., and Ernst, H., "An Initial Experimental Investigation of the Tearing Instability," ASTM STP 668, 1979, pp. 251–265.

Downloaded 02 May 2010 to 171.66.16.250. Redistribution subject to ASME license or copyright; see http://www.asme.org/terms/Terms_Use.cfm

The Evolution of Computational Methods in Aerodynamics

A. Jameson
Department of Mechanical and Aerospace Engineering, Princeton University, Princeton, N.J. 08544

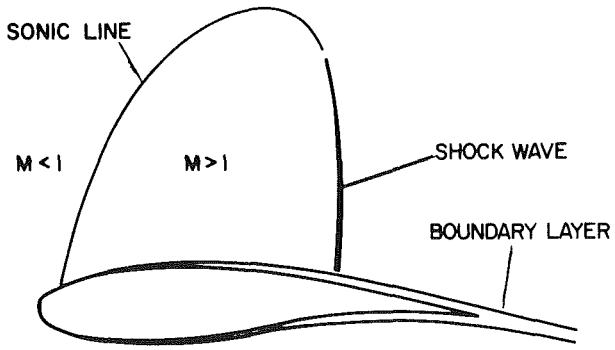
This paper surveys the evolution of computational methods in aerodynamics. Improvements in high-speed electronic computers have made it feasible to attempt numerical calculations of progressively more complex mathematical models of aerodynamic flows. Numerical approximation methods for a hierarchy of models are examined in ascending order of complexity, ranging from the linearized potential flow equation to the Reynolds averaged Navier Stokes equations, with the inclusion of some previously unpublished material on implicit and multigrid methods for the Euler equations. It is concluded that the solution to the Euler equations for inviscid flow past a complete aircraft is a presently attainable objective, while the solution to the Reynolds averaged Navier Stokes equations is a possibility clearly visible on the horizon.

1 Introduction

Computational fluid dynamics has penetrated into a broad variety of fields, including airplane design, car design, studies of blood flow, studies of oil recovery, oceanography, meteorology, and astrophysics. In this paper I will examine the impact computational aerodynamics has on airplane design.

Prior to 1960, computational methods were hardly used in aerodynamic analysis, although they were already widely used for structural analysis. The NACA 6 series of airfoils had been developed during the 1940s, using hand computation to perform the Theodorsen method for conformal mapping [1]. The primary tool for the development of aerodynamic configurations was the wind tunnel. Shapes were tested and modifications selected in the light of pressure and force measurements together with flow visualization techniques. In much the same way that Michelangelo, della Porta, and Fontana could design the dome of St. Peters through a good physical understanding of load paths, so could experienced aerodynamicists arrive at efficient shapes through testing guided by good physical insight. Notable examples of the power of this method include the achievement of the Wright brothers in leaving the ground (after first building a wind tunnel), and more recently Whitcomb's discovery of the area rule for transonic flow, followed by his development of aft-loaded supercritical airfoils and winglets [2–4]. The process was expensive. More than 20,000 hours of wind tunnel testing were expended in the development of some modern designs, such as the F 111 or Boeing 747.

By 1960 it began to be recognized that computers had become powerful enough to make it worthwhile to attempt



TRANSONIC FLOW PAST AN AIRFOIL
Fig. 1.1

calculations of aerodynamic properties of least isolated components of an airplane. Efficient flight can be achieved only by establishing highly coherent flows. Consequently there are many important applications where it is not necessary to solve the full Navier Stokes equations, and useful predictions can be made with simplified mathematical models. Since the work of Prandtl, it has been recognized that in flows at the large Reynolds numbers typical in most flight regimes, viscous effects are important chiefly in thin shear layers adjacent to the surface. While these boundary layers play a critical role in determining whether the flow will separate, and how much circulation will be generated around a lifting surface, the equations of inviscid flow are a good approximation in the bulk of the flow field. The Reynolds numbers for a large airplane (of the order of 30 million) are such that laminar flow in the boundary layer becomes unstable, with the result that the flow will be turbulent over most of the surface of the airplane.

On the other hand, many useful predictions can be made under the assumption that the flow is inviscid. It then follows from Kelvin's Theorem that in the absence of discontinuities

Contributed by the Applied Mechanics Division for publication in the JOURNAL OF APPLIED MECHANICS.
Discussion on this paper should be addressed to the Editorial Department, ASME, United Engineering Center, 345 East 47th Street, New York, N.Y. 10017, and will be accepted until two months after final publication of the paper itself in the JOURNAL OF APPLIED MECHANICS. Manuscript received by ASME Applied Mechanics Division, June, 1983.

Copyright © 1983 by ASME
Downloaded 02 May 2010 to 171.66.16.250. Redistribution subject to ASME license or copyright; see http://www.asme.org/terms/Terms_Use.cfm

an initially irrotational flow remains irrotational. This allows us to simplify the equations further by representing the velocity as the gradient of a potential. Initial attempts concentrated on incompressible potential flows. During the 1960s the boundary integral method was developed into a powerful tool for the analysis of flows over complex configurations.

In the 1970s the battleground of computational aerodynamics switched to the prediction of transonic flows. The reason for this is that to a first approximation, cruising efficiency is proportional to

$$M\,L/D$$

where M is the Mach number (speed divided by the speed of sound), L is the lift, and D is the drag. As long as the speed is well below the speed of sound, the lift to drag ratio does not vary much with speed, so it pays to increase the speed until the effects of compressibility start to cause a radical change in the flow. This occurs when embedded pockets of supersonic flow appear, generally terminating in shock waves. A typical transonic flow pattern over a wing is illustrated in Fig. 1.1. As the Mach number is increased the shock waves become strong enough to cause a sharp increase in drag, and finally the pressure rise through the shock waves becomes so large that the boundary layer separates. An unsteady buffeting flow may then develop. This causes violent vibrations that cannot be tolerated even by the pilots of military aircraft. The most efficient cruising speed is usually in the transonic regime just at the onset of drag rise, and the prediction of aerodynamic properties in steady transonic flow has therefore been the key challenge. Unsteady flow is inherent in certain other modes of flight (the flight of bats, insects, and helicopters, for example), but for airplanes it is important primarily for the analysis of extreme situations such as wing flutter.[1]

Following a review of the mathematical models appropriate to different situations, methods for solving the corresponding equations will be examined in ascending order of complexity, including some unpublished material on implicit and multigrid methods for solving the Euler equations. There follows a brief discussion of the treatment of viscous effects, and finally a discussion of the question of designing shapes intended to have desirable aerodynamic properties.

2 Choice of a Mathematical Model

The equations for flow of a gas in thermodynamic equilibrium are the Navier Stokes equations. Let ρ, u, v, e, and p be the density, Cartesian velocity components, total energy per unit volume, and pressure, and let x and y be Cartesian Coordinates. Then for a two-dimensional flow these equations can be written as

$$\frac{\partial w}{\partial t}+\frac{\partial f}{\partial x}+\frac{\partial g}{\partial y}=\frac{\partial R}{\partial x}+\frac{\partial S}{\partial y} \tag{2.1}$$

where w is the vector of dependent variables, and f and g are the convective flux vectors

$$w=\begin{bmatrix}\rho\\ \rho u\\ \rho v\\ e\end{bmatrix}\quad f=\begin{bmatrix}\rho u\\ \rho u^2+p\\ \rho vu\\ (e+p)u\end{bmatrix}\quad g=\begin{bmatrix}\rho v\\ \rho vu\\ \rho v^2+p\\ (e+p)v\end{bmatrix} \tag{2.2}$$

The flux vectors for the viscous terms are

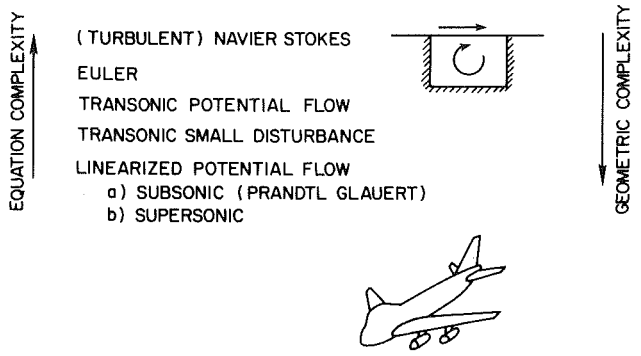


Fig. 2.1 Hierarchy of mathematical models

$$R=\begin{bmatrix}0\\ \tau_{xx}\\ \tau_{xy}\\ u\tau_{xx}+v\tau_{xy}\end{bmatrix}\quad S=\begin{bmatrix}0\\ \tau_{xy}\\ \tau_{yy}\\ u\tau_{xy}+v\tau_{yy}\end{bmatrix} \tag{2.3}$$

Here the viscous stresses are

$$\tau_{xx}=2\mu\,u_x-\frac{2\mu}{3}(u_x+v_y),\ \tau_{yy}=2\mu\,v_y-\frac{2\mu}{3}(u_x+v_y)$$
$$\tau_{xy}=\mu(u_y+v_x) \tag{2.4}$$

where μ is the coefficient of viscosity. The computational requirements for the simulation of turbulent flow have been estimated by Chapman [5]. They are clearly beyond the reach of current computers.

The first level of approximation is to resort to time averaging of rapidly fluctuating components. This yields the Reynolds equations, which require a turbulence model for closure. Since a universally satisfactory turbulence model has yet to be found, current turbulence models have to be tailored to the particular flow. The Reynolds equations can be solved with computers of the class of the Cray 1 or Cyber 205, at least for two-dimensional flows, such as flows over airfoils.

The next level of approximation is to eliminate viscosity. Equations (2.1) then reduce to the Euler equations

$$\frac{\partial w}{\partial t}+\frac{\partial f}{\partial x}+\frac{\partial g}{\partial y}=0 \tag{2.5}$$

It is quite feasible to solve three-dimensional flows with this model, as will be discussed.

If we assume the flow to be irrotational we can introduce a velocity potential ϕ, and set

$$u=\phi_x,\quad v=\phi_y.$$

The Euler equations (2.5) now reduce to the potential flow equation

$$\frac{\partial}{\partial x}(\rho\phi_x)+\frac{\partial}{\partial y}(\rho\phi_y)=0 \tag{2.6}$$

or in quasilinear form

$$(a^2-u^2)\phi_{xx}-2uv\,\phi_{xy}+(a^2-v^2)\phi_{yy}=0 \tag{2.7}$$

where a is the speed of sound. This is given by

$$a^2=\frac{\gamma p}{\rho} \tag{2.8}$$

where γ is the ratio of specific heats. According to Crocco's theorem, vorticity in a steady flow is associated with entropy production through the relation

$$\mathbf{q}\times\zeta+T\cdot\nabla S=0$$

[1] Aircraft manufacturers frequently assign the responsibility for unsteady flow analysis to their structures departments.

Downloaded 02 May 2010 to 171.66.16.250. Redistribution subject to ASME license or copyright; see http://www.asme.org/terms/Terms_Use.cfm

where $\mathbf{q}$ and ζ are the velocity and vorticity vectors, T is the temperature and S is the entropy. Thus the introduction of a potential is consistent with the assumption of isentropic flow. Then if M_∞ is the free stream Mach number

$$p = \frac{\rho^\gamma}{\gamma M_\infty^2}, \quad \rho = (M_\infty^2 a^2)^{1/\gamma - 1} \tag{2.9}$$

The potential flow equation cannot exactly model shock waves, through which entropy is produced. Weak solutions admitting isentropic jumps that conserve mass but not momentum are a good approximation to shock waves, however, as long as the shock waves are quite weak (with a Mach number < 1.3 for the normal velocity component upstream of the shock wave). Stronger shock waves tend to separate the flow, with the result that the inviscid approximation is no longer adequate. Thus this model is well balanced, and it has proved extremely useful for estimating the cruising performance of transport aircraft.

If one assumes small disturbances and a Mach number close to unity, the potential equation can be reduced to the transonic small disturbance equation. A typical form is

$$(1 - M_\infty^2 - (\gamma + 1) M_\infty^2 \phi_x)\phi_{xx} + \phi_{yy} = 0 \tag{2.10}$$

Finally, if the free-stream Mach number is not close to unity, the potential flow equation can be linearized as

$$(1 - M_\infty^2)\phi_{xx} + \phi_{yy} = 0 \tag{2.11}$$

Considering the limits on the available computing power, and the cost of calculations, one has to make a trade-off between the complexity of the mathematical model and the complexity of the geometric configuration that can be treated. This is illustrated in Fig. 2.1. The linearized potential equation has been routinely solved for complete configurations since the early 1970s. A solution to the Navier Stokes equations for a turbulent flow can at best be attempted for something like a rectangular cavity with one moving wall. This trade-off calls for a judgment both of the suitability of the model for a particular application, and of the feasibility of the calculation. Discretization of the three-dimensional nonlinear potential flow equation using curvilinear coordinates, for example, requires about 500 operations per mesh point. A flow over a swept wing can be quite well represented with a mesh containing 100,000 points, and the resulting nonlinear equations can be solved in about 200 cycles. The Control Data 6600, which was introduced in 1964, is capable of sustaining a rate of about 1 million operations per second, and could perform such a calculation in about 10,000 seconds. The first computer program to solve the potential flow equation for a swept wing (FLO 22, written by Jameson and Caughey) did not become operational until 1976. I believe that this long delay was partly caused by a failure in the aeronautical community to recognize that such calculations were possible, with a consequent reluctance to devote the necessary effort and to make available the necessary resources.

3 Boundary Integral Methods

The first major success in computational aerodynamics was the development of boundary integral methods for the solution of the subsonic linearized potential flow equation (2.11). This can be reduced to Laplace's equation by stretching the x coordinate. Then, according to potential theory, the general solution can be represented in terms of a distribution of sources or doublets, or both sources and doublets, over the boundary surface. The boundary condition is that the velocity component normal to the surface is zero. Assuming, for example, a source distribution of strength $\sigma(Q)$ at the point of Q of a surface S, this leads to the integral equation

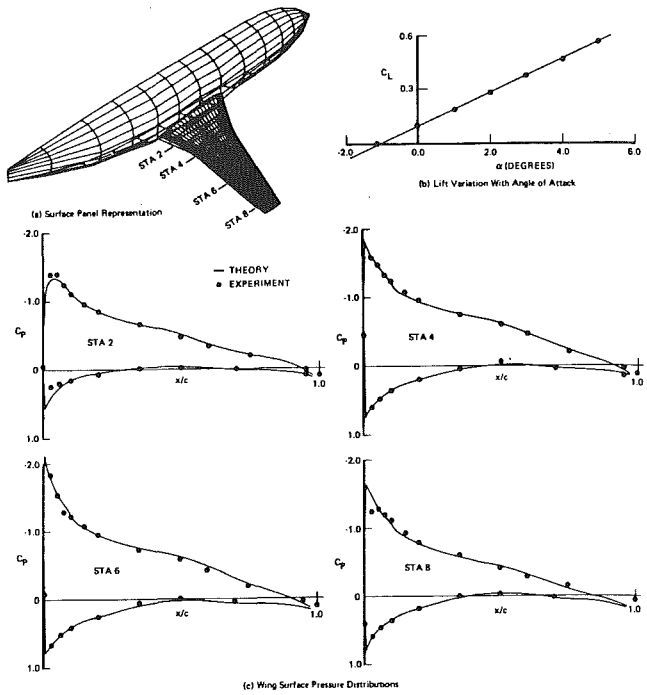


Fig. 3.1 Result of a panel method calculation for a Boeing 737 wing body model at low mach number. —Calculated result; • test data

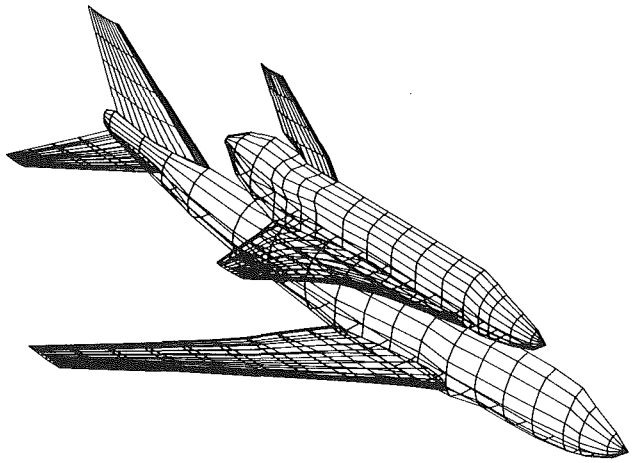


Fig. 3.2 Boeing 747 with space shuttle

$$2\pi\sigma_P - \iint_S \sigma(Q)\ \mathbf{n}_P \cdot \nabla_P \left(\frac{1}{r}\right) = 0 \tag{3.1}$$

where P is the point of evaluation, and r is the distance from P to Q. A similar equation can be found for a doublet distribution and it usually pays to use a combination. Equation (3.1) can be reduced to a set of algebraic equations by dividing the surface into quadrilateral panels, assuming a constant source strength on each panel, and satisfying the condition of zero normal velocity at the center of each panel. This leads to N equations for the source strengths on N panels. The first such method was introduced by Hess and Smith in 1962 [6]. The method was extended to lifting flows, together with the inclusion of doublet distributions, by Rubbert and Saaris [7]. Subsequently higher order panel methods (as these methods are generally called in the aircraft industry) have been introduced. A recent review has been given by Hunt [8]. An example of a calculation by a panel method is shown in Fig. 3.1.[2] The results are displayed in terms of the pressure coefficient defined as

[2] Supplied by Paul Rubbert, the Boeing Company.

Downloaded 02 May 2010 to 171.66.16.250. Redistribution subject to ASME license or copyright; see http://www.asme.org/terms/Terms_Use.cfm

$$c_p = \frac{p - p_\infty}{\frac{1}{2}\rho_\infty {q_\infty}^2}$$

Figure 3.2[3] illustrates the kind of geometric configuration that can be treated by panel methods.

In comparison with field methods which solve for the unknowns in the entire domain, panel methods have the advantage that the dimensionality is reduced. Consider a three-dimensional flow field on an $n \times n \times n$ grid. This would be reduced to the solution of the source or doublet strengths on $N = 0(n^2)$ panels. Since, however, every panel influences every other panel, the resulting equations have a dense matrix, and $0(N^3) = 0(n^6)$ operations are required for an exact solution. If one directly discretizes the equations for the three-dimensional domain the number of unknowns is n^3, but the equations are sparse, and can be solved with $0(n)$ iterations, or even with a number of iterations independent of n if a multigrid method is used. Although the field methods appear to be potentially more efficient, the boundary integral method has the advantage that it is comparatively easy to divide a complex surface into panels, whereas the problem of dividing a three-dimensional domain into hexahedral or tetrahedral cells remains a source of extreme difficulty. Panel methods thus continue to be widely used both for the solution of flows at low Mach numbers for which compressibility effects are unimportant, and also to calculate supersonic flows at high Mach numbers (9), for which the linearized equation (2.11) is again a good approximation.

4 The Transonic Potential Flow Equation

(a) Upwind Differencing. When the potential flow equation (2.6) is used to predict transonic flows, the difficulty arises that the solution is invariant under a reversal of the velocity vector ($u = -\phi_x$, $v = -\phi_y$). Consider a transonic flow past an ellipse with a compression shock wave. Then there is a corresponding solution with an expansion shock wave (see Figs. 4.1(*a*, *b*)). In fact a central difference scheme would preserve fore and aft symmetry, leading to a solution of the type illustrated in Fig. 4.1(*c*). In 1970 there appeared the landmark paper of Murman and Cole [10]. This demonstrated a simple way to obtain physically relevant solutions of the transonic small disturbance equation (2.10). Writing this equation as

$$A\ \phi_{xx} + \phi_{yy} = 0 \tag{4.1}$$

where A is the nonlinear coefficient in (2.10), they proposed the use of central differencing if $A > 0$ (subsonic flow), but upwind differencing for ϕ_{xx} if $A < 0$ (supersonic flow), as illustrated in Fig. 4.2. The equations were then solved by a line relaxation scheme, in which the unknowns were determined simultaneously on each successive vertical line, marching in the streamwise direction. The scheme amounted to a combination of a relaxation method for the subsonic zone, in which the equation is elliptic, with an implicit scheme for the wave equation in the supersonic zone. This idea can be generalized to the quasilinear potential flow equation (2.7) by writing the equations at each point in a coordinate system locally aligned with the flow. Equation (2.7) becomes

$$(a^2 - q^2)\phi_{ss} + a^2\phi_{nn} = 0$$

where

$$\phi_{ss} = \frac{u^2}{q^2}\ \phi_{xx} + \frac{2uv}{q^2}\ \phi_{xy} + \frac{v^2}{q^2}\ \phi_{yy}$$

[3] Supplied by Allen Chen, the Boeing Company.

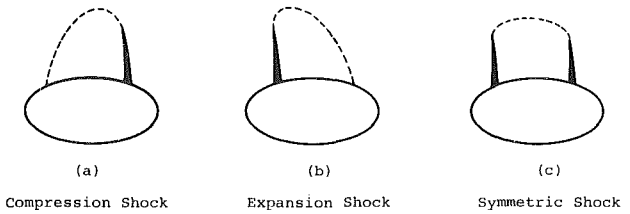


Fig. 4.1 Alternative solutions for an ellipse

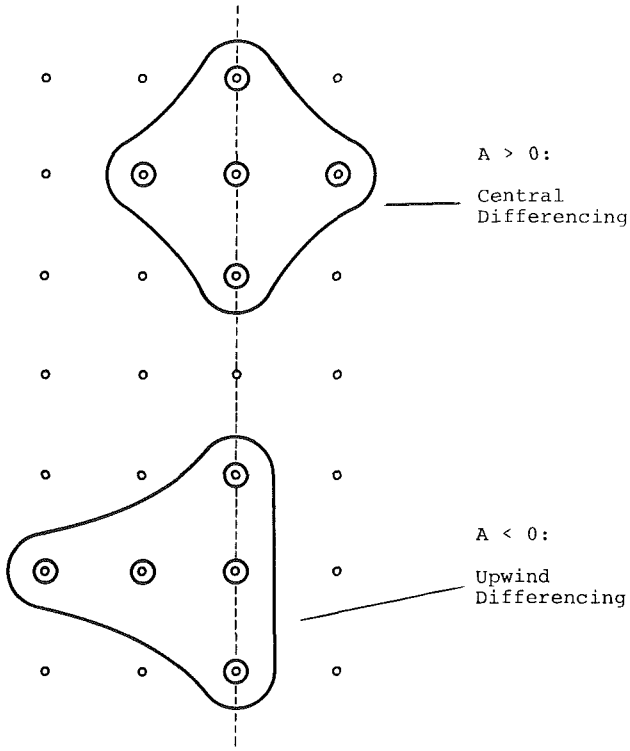


Fig. 4.2 Murman-Cole difference scheme: $A\ \phi_{xx} + \phi_{yy} = 0$

$$\phi_{nn} = \frac{v^2}{q^2}\ \phi_{xx} - \frac{2uv}{q^2}\ \phi_{xy} + \frac{u^2}{q^2}\ \phi_{yy}$$

Then upwind differencing is used for all second derivatives contributing to ϕ_{ss} if $q > a$. This leads to Jameson's rotated difference scheme [11] (see also Albone [12]). A convergent iterative scheme can be derived by regarding the iterations as time steps in an artificial time coordinate. The principal part of the equivalent time-dependent equation has the form

$$(M^2 - 1)\phi_{ss} - \phi_{nn} + 2\alpha\phi_{st} + 2\beta\phi_{nt} = 0$$

Introducing a new time coordinate

$$T = t - \frac{\alpha s}{M^2 - 1} + \beta n$$

this becomes

$$(M^2 - 1)\phi_{ss} - \phi_{nn} - \left[\frac{\alpha^2}{M^2 - 1} - \beta^2\right]\phi_{TT} = 0$$

If the flow is locally supersonic T is spacelike, and either s or n is timelike. Since s is the timelike direction in the steady state problem, the time-dependent problem is compatible with the steady state problem only if

$$\alpha^2 > \beta^2(M^2 - 1)$$

This generally requires the explicit addition of a term in ϕ_{st}.

In his paper of 1973 Murman recognized that the switch in the difference scheme could violate the conservation form of

Downloaded 02 May 2010 to 171.66.16.250. Redistribution subject to ASME license or copyright; see http://www.asme.org/terms/Terms_Use.cfm

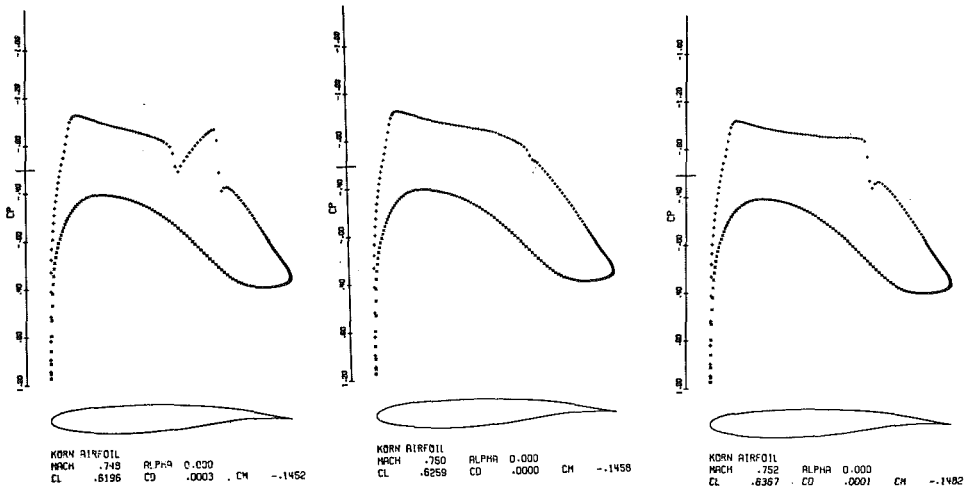


Fig. 4.3 Sensitivity of shock-free transonic flow: verification of the Morawetz theorem

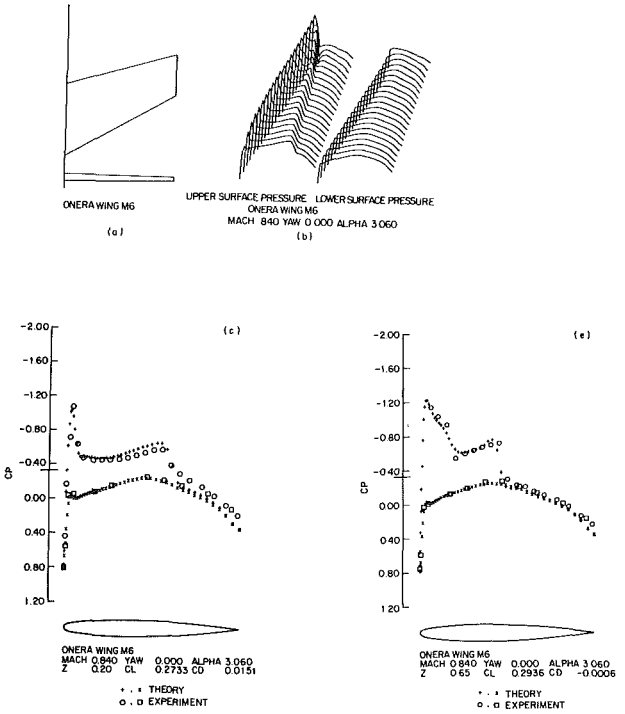


Fig. 4.4

the equations, leading to shock jumps that violated the conservation of mass [13]. This difficulty can be corrected by reformulating the switch to upwind differencing by the introduction of artificial viscosity. The dominant discretization error in the upwind difference formula for ϕ_{xx} is $-\Delta x\, \phi_{xxx}$, for example, and terms of this nature can be added explicitly in conservation form, leading to special transition operators across the sonic line. Jameson showed that an appropriate form of artificial viscosity for the potential flow equation (2.6) is a difference approximation to

$$\Delta x \frac{\partial}{\partial x} \mu |u| \rho_x + \Delta y \frac{\partial}{\partial y} \mu |v| \rho_y$$

where Δx and Δy are the mesh widths, and μ is a switch function

$$\mu = \max\left\{0, 1 - \frac{1}{M^2}\right\}$$

which cuts off the viscosity in the subsonic zone [14]. It was subsequently realized by several authors that a term of this kind can be added simply by biasing the density in an upwind direction [15–17]. This has facilitated the development of discretizations on arbitrary subdivisions of the domain into hexahedra or tetrahedra.

Consistent with the assumption of isentropic flow, it is not possible to conserve both mass and momentum through a discontinuity. The conservative scheme assures a model of a shock wave in which mass, but not momentum, is conserved. There is a school of thought that it is better to use a nonconservative scheme, because a shock wave can be more closely simulated by an isentropic jump if some mass production is permitted [18], and in fact nonconservative schemes are preferred by many practicing engineers.

It also turns out that the switch in the Murman Cole scheme is not fool proof, and can admit stationary expansion shocks in a one-dimensional flow [19]. This difficulty can be overcome by modifying the transition operators (Osher [20], Goorjian [21]).

***(b)* Treatment of Complex Geometric Configurations.** An effective approach to the treatment of two-dimensional flows over complex profiles is to map the exterior domain conformally onto the unit disk [10]. Equation (2.6) is then written in polar coordinates as

$$\frac{\partial}{\partial \theta}\left(\frac{\rho}{r}\phi_\theta\right) + \frac{\partial}{\partial r}(r\rho\phi_r) = 0 \tag{4.2}$$

where the modulus h of the mapping function enters only in the calculation of the density from the velocity

$$\mathbf{q} = \frac{\nabla \phi}{h} \tag{4.3}$$

This procedure is very accurate. Figure 4.3 shows a numerical verification of Morawetz' theorem that a shock-free transonic flow is an isolated point, and that arbitrary small changes in boundary conditions will lead to the appearance of shock waves [22]. These calculations were performed by the author's code FLO 6.

Applications to complex three-dimensional configurations require a more flexible method of discretization, such as that provided by the finite element method. Jameson and Caughey proposed a scheme using isoparametric bilinear or trilinear elements [23, 24]. The discrete equations can most conveniently be derived from the Bateman variational principle. This states that the integral

$$I = \int\int p\, dxdy$$

Downloaded 02 May 2010 to 171.66.16.250. Redistribution subject to ASME license or copyright; see http://www.asme.org/terms/Terms_Use.cfm

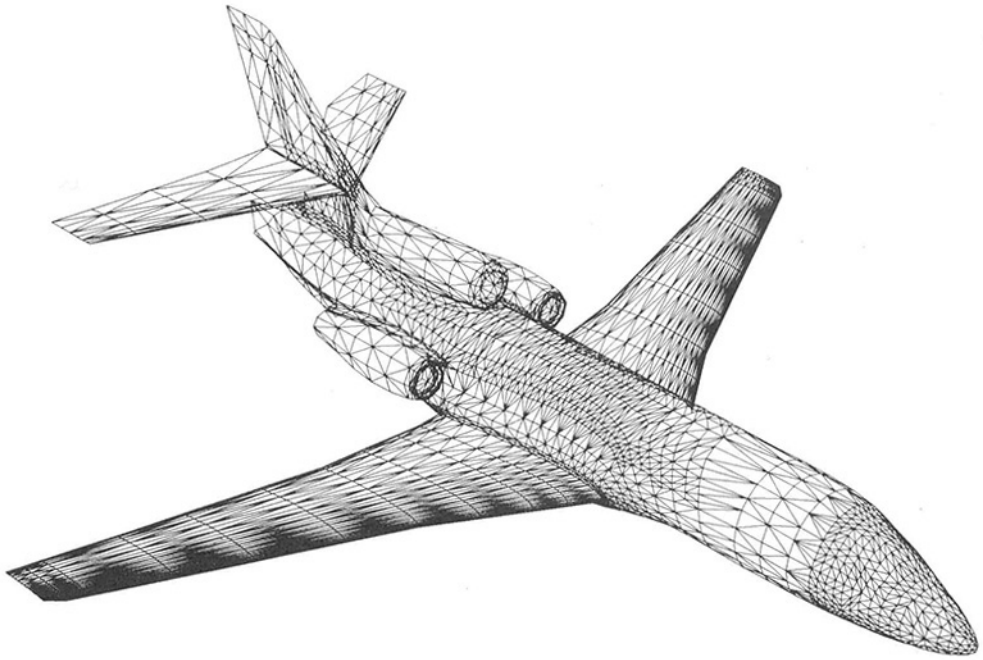


Fig. 4.5(*a*) Mesh for Falcon 50

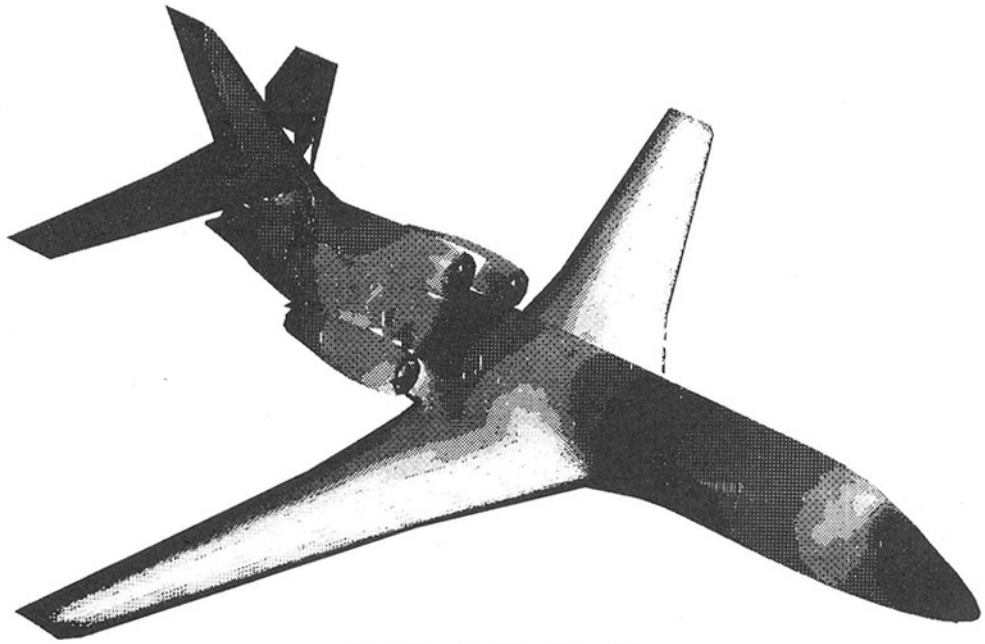


Fig. 4.5(*b*) Result for Falcon 50

Fig. 4.5

is stationary in two-dimensional potential flow. It follows from equations (2.9) that

$$\frac{\partial p}{\partial u} = -\rho u, \quad \frac{\partial p}{\partial v} = -\rho v$$

whence in potential flow

$$\delta I = -\iint (\rho u \delta\phi_x + \rho v \delta\phi_y)\, dxdy$$

and equation (2.8) is recovered on integrating by parts and allowing arbitrary variations $\delta\phi$. In the scheme of Jameson and Caughey I is approximated as

$$I = \sum p_k V_k$$

where p_k is the pressure at the center of the kth cell and V_k is its area (or volume), and the discrete equations are obtained by setting the derivative of I with respect to the nodal values of potential to zero. Artificial viscosity is added to give an upwind bias in the supersonic zone, and an iterative scheme is derived by embedding the steady state equation in an artificial time-dependent equation. Several widely used codes (FLO 27, FLO 28, FLO 30) have been developed using this scheme. Figure 4.4 shows a result for a swept wing.

Downloaded 02 May 2010 to 171.66.16.250. Redistribution subject to ASME license or copyright; see http://www.asme.org/terms/Terms_Use.cfm

An alternative approach to the treatment of complex configurations has been developed by Bristeau, Pironneau, Glowinski, Periaux, Perrier, and Poirier [25]. Their method uses a least square formulation of the problem, together with an iterative scheme derived with the aid of optimal control theory. The method could be used in conjunction with a subdivision into either quadrilaterals or triangles, but in practice triangulations have been used.

The simplest conceivable least squares formulation calls for the minimization of the objective function

$$I=\int_S \psi^2\, dS$$

where ψ is the residual of equation (2.6), and S is the domain of the calculation. The resulting minimization problem could be solved by a steepest descent method in which the potential is repeatedly modified by a correction $\delta\phi$ proportional to $-\partial I/\partial\phi$. Such a method would be very slow. In fact it simulates a time-dependent equation of the form

$$\phi_t=-L^*\, L\, \phi$$

where L is the differential operator in equation (2.6), and L^* is its adjoint.

Much faster convergence can be obtained by the introduction of a more sophisticated objective function

$$I=\int_S \nabla\psi^2\, dS$$

where the auxiliary function ψ is calculated from

$$\nabla^2\psi=\nabla\cdot\rho\nabla\phi$$

Let g be the value of $\partial\phi/\partial n$ specified on the boundary C of the domain. Then this equation can be replaced by the corresponding variational form

$$\int_S \nabla\ \psi\cdot\nabla v dS=\int_S \rho\ \nabla\ \phi\cdot\nabla v dS-\int_C gv ds$$

which must be satisfied by ψ for all differentiable test functions v. This formulation, which is equivalent to the use of an H^{-1} norm in Sobolev space, reduces the calculation of the potential to the solution of an optimal control problem, with ϕ as the control function and ψ as the state function. It leads to an iterative scheme that calls for solutions of Poisson equations twice in each cycle. A further improvement can be realized by the use of a conjugate gradient method instead of a simple steepest descent method.

The least squares method in its basic form allows expansion shocks. In early formulations these were eliminated by penalty functions. Subsequently it was found best to use upwind biasing of the density. The method has been extended at Avions Marcel Dassault to the treatment of extremely complex three-dimensional configurations, using a subdivision of the domain into tetrahedra. Figure 4.5[4] shows a result for the Falcon 50 executive jet. The numbers displayed are the calculated Mach numbers in the surface elements.

(c) Convergence Acceleration. Transonic flow calculations by relaxation methods generally require a very large number of iterations to converge (of the order of 500–2000). This inhibited the more widespread use of these methods, particularly for thee-dimensional calculations, and stimulated numerous efforts to find more rapidly convergent methods. The two most effective approaches have been approximate factorization of the difference operator, and acceleration by the use ofmultiple grids.

Let the difference equations be written as

$$L\ \phi=0 \tag{4.4}$$

where L is a nonlinear difference operator and ϕ is the solution vector. Then a typical iterative scheme can be written as

$$N\ \delta\phi+L\phi^n=0 \tag{4.5}$$

where $\delta\phi$ is the correction, and N is a linear operator that can be inverted relatively cheaply, and should approximate L (in the linear case the error is reduced at each cycle by $I-N^{-1}L$). In an approximate factorization method N is formed as a product

$$N=N_1N_2\ldots N_q$$

of easily invertible operators. Jameson, Ballhaus, and Albert found [26] that a good choice for the small disturbance equation (4.1) is

$$(\alpha-AD_x^-)\,(\alpha D_x^- -\mathrm{D}_y^+ D_y^-)\delta\phi+\alpha L\phi^n=0$$

where D_x^+ and D_x^- are forward and backward difference operators, and

$$D_x^- = \begin{cases} D_x^+ & \text{if } A>0 \\ D_x^- & \text{if } A<0 \end{cases}$$

Very efficient schemes of this type have been developed for the transonic potential flow equation by Holst [17, 27] and Baker [28].

The multigrid method was first proposed by Fedorenko [29], and some promising results for the small disturbance equation were obtained by Brandt and South [30]. The idea is to use corrections calculated on a sequence of successively coarser grids to improve the solution on a fine grid. Consider a linear problem and let

$$L_h\ \phi_h=0 \tag{4.6}$$

be the discrete equations for a mesh with a spacing proportional to h. Let u_h be an estimate of ϕ_h, and let v_h be a correction that should reduce $L_h(u_h+v_h)$ to zero. Then instead one can write an equation for v on a mesh with twice as large a spacing:

$$L_{2h}v_{2h}+Q_{2h}^h L_h u_h=0 \tag{4.7}$$

where Q_{2h}^h is a collection operator that forms a weighted average of the residuals on the fine grid in the neighborhood of each mesh point of the coarse grid. The correction is finally interpolated back to the fine grid:

$$u_h^{\text{new}}=u_h+P_h^{2h}v_{2h} \tag{4.8}$$

where P_h^{2h} is an interpolation operator. Corrections to the solution of equation (4.7) can in turn be calculated on a still coarser grid, and so on. The same basic iterative scheme can be used on all the grids in the sequence. It has been proved that solutions to elliptic problems with N unknowns can be obtained in $0(N)$ operations by the use of multiple grids [31]. A condition for the successful use of multiple grids is that before passing to a coarser grid, the high-frequency error modes should be reduced to the point that the remaining error can be properly resolved on the coarser grid.

The method can be reformulated for a nonlinear problem by explicitly introducing the solution vector u_{2h} on the coarse grid. An updated solution vector $\tilde{u}_{2h}$ is then calculated from the equation

$$L_{2h}\ \tilde{u}_{2h}+Q_{2h}^h\ L_h\ u_h-L_{2h}\ u_h=0$$

Here the difference between the collected residuals from neighboring points on the fine grid and the residual calculated on the coarse grid appears as a forcing function. The correction $\tilde{u}_{2h}-u_{2h}$ is then interpolated back to the fine grid.

Early attempts to solve transonic flow problems by

[4] Supplied by Pierre Perrier, Avions Marcel Dassault.

Downloaded 02 May 2010 to 171.66.16.250. Redistribution subject to ASME license or copyright; see http://www.asme.org/terms/Terms_Use.cfm

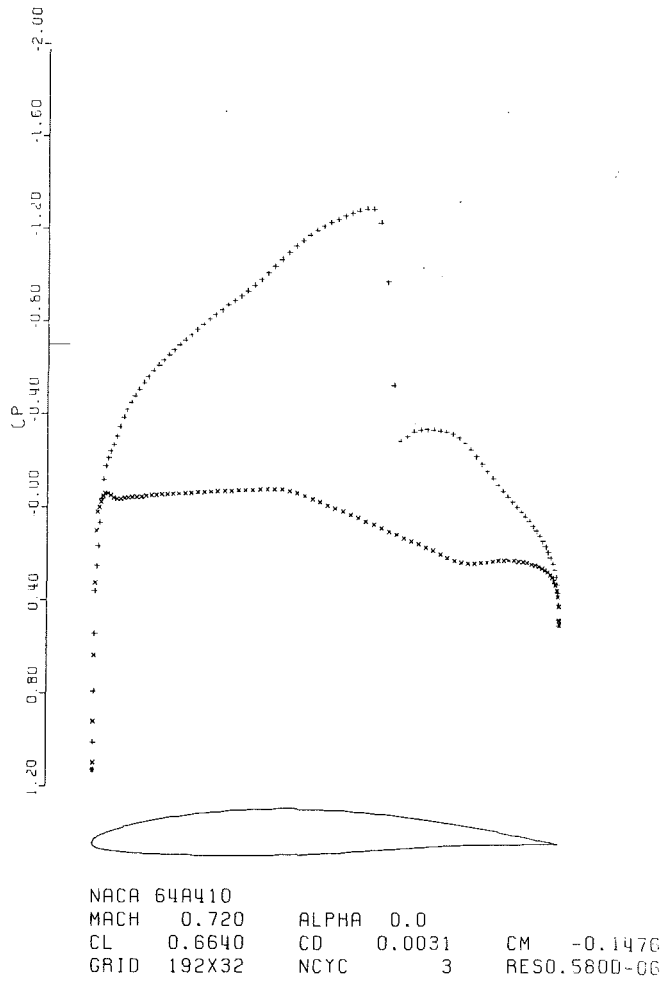


Fig. 4.6 Transonic flow solution obtained with three multigrid cycles

multigrid methods produced schemes that were not at all reliable. Sometimes they would converge rapidly, and at other times they would enter into limit cycles or even diverge. The multigrid alternating direction scheme introduced by Jameson [32] has proved robust. This scheme uses a generalized alternating direction method to drive the multigrid iteration. The ADI scheme differs from the standard ADI scheme in replacing the scalar parameter by a difference operator (which also operates on the residuals). The purpose of this is to retain a well-posed problem in the supersonic zone. The most efficient strategy seems to be a simple V cycle in which 1 ADI Iteration is performed on each grid until the coarsest grid is reached, and then 1 ADI iteration on each grid on the way back up to the fine grid. Figure 4.6 shows the result of a transonic flow calculation by this method. A solution on a 192×32 grid accurate to four figures was obtained by 3 V cycles on a 48×8 grid, followed by 3 V cycles on a 96×16 grid and 3 V cycles on the 192×32 grid. The total calculation is equivalent to 4 V cycles on the 192×32 grid. It seems likely that this must be close to the lower bound for the number of operations required to solve 6144 simultaneous nonlinear equations.

Caughey has succeeded in developing a multigrid method for three-dimensional transonic flow calculations, using the finite volume method for space discretization [33]. In his scheme, line relaxation in alternate chordwise and normal directions is used to drive the multigrid iteration.

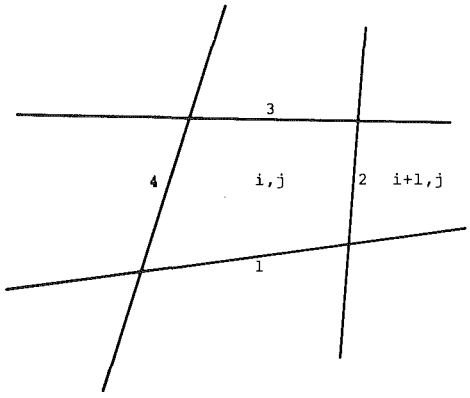


Fig. 5.1 Finite volume scheme

5 Solution of the Euler Equations

(a) **Formulation.** The results of potential flow calculations have proved accurate enough to be used as the basis of the wing design of the latest generation of transport aircraft, such as the Boeing 767 and Airbus A 310. Nevertheless, the assumption of potential flow is not strictly correct when shock waves are present, and this inconsistency must set a limit to the accuracy that could be obtained even if the discretization errors were entirely eliminated. To provide a correct description of inviscid transonic flow we must solve the Euler equations. The widespread use of Euler codes has so far been impeded by large numerical errors (leading, for example, to generation of spurious vorticity), and excessively slow convergence (often no convergence). Recent developments promise to correct this situation.

The emphasis here will be on the calculation of steady state solutions. While other iterative methods can be conceived, most of the methods so far developed are based on the concept of integrating the equations in time until they reach a steady state. An exterior problem can reach a steady state as a result of the propagation of disturbances away to infinity. This explusion mechanism is effective as long as outgoing disturbances are not too strongly reflected back into the interior, and boundary conditions must therefore be treated with care. Since the time-dependent terms are used merely as a device for generating an iterative scheme, they may be modified to increase the rate of convergence. The time-dependent formulation is similar in principle to the Jacobi method. When applied to Laplace's equation, for example, the Jacobi method is equivalent to integrating the heat equation

$$\phi_t = \phi_{xx} + \phi_{yy}$$

until it reaches a steady state.

An advantage of the time-dependent formulation is that it brings the problem within the framework of the mathematical theory of difference methods for hyperbolic equations. Stemming from the early work of Courant, Von Neumann, and Lax, this theory is by now highly developed [34–38]. It was shown by Lax that the correct jump conditions across a discontinuity can be obtained by writing the equations as conservation laws, and preserving this form in the difference approximation [34, 36]. Thus if the Euler equations are expressed in the form (2.5), shock waves can be properly captured by the difference scheme. A stability theory for the initial boundary value problem has been formulated and refined by Kreiss, Gustaffson, and Sundstrom [39–41], and the application of this theory has been worked out for a variety of discretization schemes [42]. Procedures have also been developed for the construction of boundary conditions designed to allow outgoing waves to pass through the outer

Downloaded 02 May 2010 to 171.66.16.250. Redistribution subject to ASME license or copyright; see http://www.asme.org/terms/Terms_Use.cfm

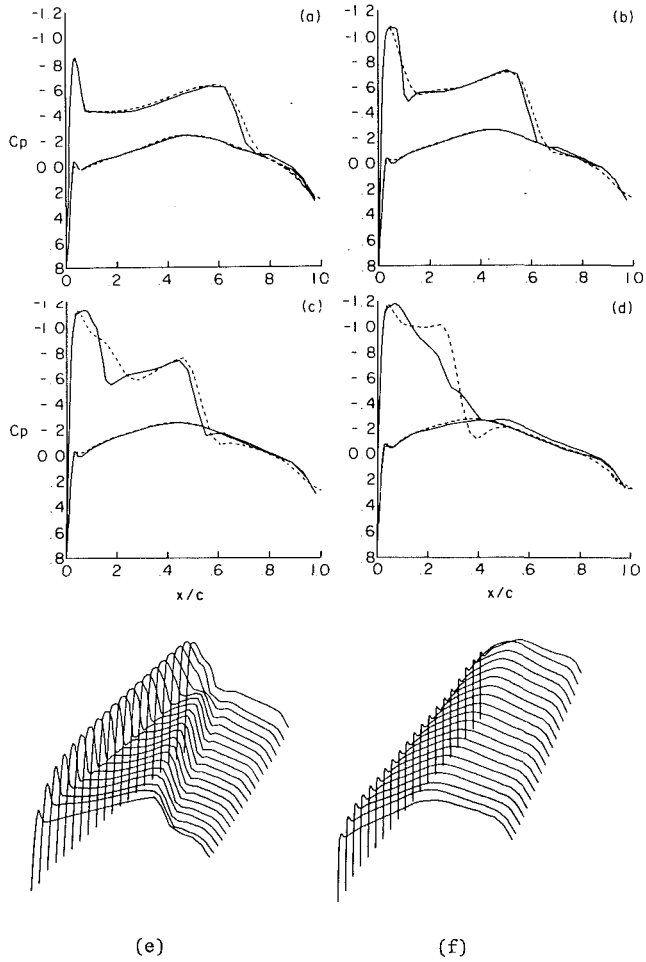


Fig. 5.2 Comparison of Euler and potential flow solutions. ONERA M6 Wing, Mach 0.840, α3.06 deg, 128 × 16 × 32 grid. (a) 1/8 span station; (b) 3/8 span station; (c) 5/8 span station, (d) 7/8 span station; (e) upper surface pressure distribution of Euler solution; (f) lower surface pressure distribution of Euler solution. ——Euler ----------potential flow.

boundary [43–44]. The availability of this body of theory provides a solid foundation for the development of codes to treat practical aerodynamic problems.

A special case occurs when the flow is everywhere supersonic. The steady state equations then constitute a hyperbolic system in which the streamwise coordinate plays the role of the timelike variable, and the entire flow field can be calculated in a single sweep, marching downstream [45, 46].

(b) Modification of the Equations for Faster Convergence. Aside from trying to construct the most efficient possible numerical scheme, it is natural to consider the possibility of modifying the Euler equations to increase the rate of convergence to a steady state. Three main approaches have been tried. The first is to use locally varying time steps, such that the difference scheme operates everywhere in the flow field at its stability limit. This procedure has been widely used, and it ensures that disturbances will be propagated to the outer boundary in a fixed number of steps, proportional to the number of mesh intervals between the body and the outer boundary. Depending on the construction of the difference scheme, the final steady state may or may not be altered by the use of locally varying time steps.

The second idea is based on the observation that the total enthalpy H is constant in a steady flow. If we set $H = H_\infty$ everywhere in the flow field throughout the evolution, the equations remain hyperbolic. Then it is no longer necessary to integrate the energy equation, since p can be recovered from the known values of ρ, q, H. The use of this model has been advocated by Veuillot and Viviand [47].

A third idea, proposed by Jameson [48], is to add forcing terms proportional to the difference between H and H_∞. This is motivated by the observation that in a subsonic potential flow

$$\phi_t + H = H_\infty$$

Thus the addition to the Euler equations of terms proportional to $H - H_\infty$ can play a role similar to the addition of a damping term ϕ_t to the potential flow equation.

(c) Explicit Schemes. The first Euler code to gain acceptance for the prediction of transonic flows was the code developed by Magnus and Yoshihara for the calculation of two-dimensional flows past airfoils [49]. They used a Lax Wendroff difference scheme with added artificial viscosity. The code required many thousands of iterations to approach a steady state, and with the computers available in the late 1960s and early 1970s, it was too expensive to be used routinely.

The work of MacCormack had a major impact. In 1968 he devised his famous two stage scheme [50]. To solve the one-dimensional system

$$\frac{\partial w}{\partial f} + \frac{\partial}{\partial x} f(w) = 0 \tag{5.1}$$

the scheme advances from time level n to time level $n+1$ by setting

$$\tilde{w} = w^n - \Delta t\, D_x^+ f(w^n)$$

and

$$w^{n+1} = w^n - \frac{\Delta t}{2}\left[D_x^+ f(w^n) + D_x^- f(\tilde{w})\right] \tag{5.2}$$

Here the superscripts denote the time level, and D_x^- and D_x^- are forward-backward difference operators approximating $\partial/\partial x$:

$$D_x^+ f_i = \frac{f_{i+1} - f_i}{\Delta x}, D_x^- f_i = \frac{f_i - f_{i-1}}{\Delta x}.$$

The value at the end of the time step is first predicted using forward differences, and then the predicted value is used in the calculation of the final corrected value w^{n+1} by a formula that is centered about the middle of the time step. This is the simplest known two-level difference scheme which is both stable and second-order accurate. MacCormack and Paullay also introduced the idea of deriving approximations to the Euler equations (2.5) from the integral form

$$\frac{\partial}{\partial t}(Vw) + \oint [f(w)\,dy + g(w)\,dx] = 0 \tag{5.3}$$

where V is the cell area and the integral is around the cell boundary [51, 52].

Many codes were written using these ideas, for example, the code of Rizzi and Schmidt [53].

Lerat has considered the general class of two level explicit difference schemes with nine point support [54]. He has shown that spurious entropy production and preshock oscillations can be reduced by controlling the higher order terms in the discretization error.

A disadvantage of the MacCormack scheme for steady state calculations is that the steady state that will be reached depends on the time step, as can be seen by setting $w^{n+1} = w^n$ in equation (5.2). This suggests the desirability of separating the space and time discretization procedures, the so-called method of lines. This procedure is adopted in the scheme proposed by Jameson, Schmidt, and Turkel, which begins by deriving a discrete approximation to the integral form (5.3) of

Downloaded 02 May 2010 to 171.66.16.250. Redistribution subject to ASME license or copyright; see http://www.asme.org/terms/Terms_Use.cfm

the Euler equations. Values of the flow variables are associated with each cell, as illustrated in Fig. 5.1. The rate of convection across side k of a cell is

$$Q_k = \Delta y_k u_k - \Delta x_k v_k \tag{5.4}$$

where the increments Δx, Δy have appropriate signs. Then the balance of, say, the x momentum component, is represented by

$$\frac{d}{dt}(V\rho u) + \sum_{k=1}^{4} [Q_k (\rho u)_k + \Delta y_k p_k] = 0. \tag{5.5}$$

Each quantity such as u_2 or $(\rho u)_2$ is evaluated as the average of the values in the cells on the two sides of the face

$$(\rho u)_2 = \frac{1}{2}[(\rho u)_{i,j} + (\rho u)_{i+1,j}]$$

for example. The use of centered differences ensures that the scheme is second-order accurate if the mesh is sufficiently smooth. It is necessary, however, to inhibit odd and even point decoupling in the solution by adding a dissipative term. Accordingly equation (5.4) is augmented by the addition of fourth differences of the dependent variables. Since these terms are of third order, they do not compromise the second-order accuracy of the scheme. To capture shock waves without any substantial preshock oscillation, it is necessary to add a further dissipative term which is of order one in the neighborhood of the shock wave. This additional dissipation is formed by adding second differences of the dependent variables, with a coefficient proportional to the second difference of the pressure

$$V_{i,j} = \frac{|p_{i+1,j} - 2p_{i,j} + p_{i-1,j}|}{|p_{i+1,j}| + 2|p_{i,j}| + |p_{i-1,j}|}$$

This coefficient is of second order in smooth regions of the flow, with the result that the dissipative terms remain of third order.

The difference equations now have the form

$$\frac{dw}{dt} + R(w) = 0 \tag{5.6}$$

where $R(w)$ is the residual of the difference equations. This may be split into convective and dissipative parts $P(w)$ and $D(w)$, where $P(w)$ is the convective operator defined by equation (5.5) and $D(w)$ is the dissipative operator. Schemes for the solutions of systems or ordinary differential equations such as (5.6) have been the subject of exhaustive investigation [56, 57]. In steady state calculations the primary objective is to devise schemes that allow a large time step. If one restricts the choice to explicit schemes, the multistage Runge Kutta schemes are well adapted to this requirement. Since the order of accuracy of the time integration is secondary, it is sufficient to consider a restricted class of simple multistage schemes. The k stage scheme in this class is

$$\begin{aligned} w^{(0)} &= w^n \\ w^{(1)} &= w^{(0)} - \alpha_1 \Delta t R^{(0)} \\ &\cdots \\ w^{(k-1)} &= w^{(0)} - \alpha_{k-1} \Delta t R^{(k-2)} \\ w^k &= w^{(0)} - \Delta t R^{(k-1)} \\ w^{n+1} &= w^k \end{aligned} \tag{5.7}$$

where w^n and w^{n+1} are the values at the beginning and end of the nth time step, and in the $(q+1)$th stage $R^{(q)} = P(w^{(q)}) + D(w^{(q)})$. These schemes will be second-order accurate in time if $\alpha_{k-1} = 1/2$. The standard four-stage scheme has the coefficients

$$\alpha_1 = 1/4,\ \alpha_2 = 1/3,\ \alpha_3 = 1/2$$

This scheme is fourth-order accurate in time for a linear problem.

A useful insight into the behavior of the scheme can be gained considering the model problem

$$u_t + u_x + \mu \Delta x^3 u_{xxxx} = 0 \tag{5.8}$$

In the absence of the third-order dissipative term this equation describes the propagation of a disturbance without distortion at unit speed. With centered differences

$$\Delta t\, R(u)_i = \frac{\lambda}{2}(u_{i+1} - u_{i-1}) + \lambda\mu(u_{i+2} - 4u_{i+1} + 6u_i - 4u_{i-1} + u_{i-2})$$

where $\lambda = \Delta t/\Delta x$ is the Courant number.

If we consider the effect on a Fourier mode e^{ipx}, we obtain the Fourier symbol of $R(u)$ as

$$z = \lambda i \sin\xi + 4\lambda\mu(1 - \cos\xi)^2$$

where $\xi = p\Delta x$. In the complex plane z describes an oval path as ξ ranges from $-\pi$ to π. The amplification factor of the standard four-stage scheme over one time step is

$$g(z) = 1 - z + \frac{z^2}{2} - \frac{z^3}{6} + \frac{z^4}{24}$$

The stability region is given by those values of z for which $|g(z)| \le 1$. This region intercepts the imaginary axis at a height of $2\sqrt{2}$, establishing the Courant number limit as $2\sqrt{2}$ in the absence of dissipation.

The computational requirements of the scheme defined by equation (5.8) can be substantially reduced by freezing the dissipative part of the residual at the value $D(w^{(0)})$ in all stages of the scheme, so that in the $(q+1)$th stage

$$R^{(q)} = P(w^{(q)}) + D(w^{(0)}) \tag{5.9}$$

This incurs only a slight reduction in the stability limit on the time step.

Figure 5.2 shows a comparison between the Euler solution computed by this method, and the potential flow solution computed by the finite volume method of Jameson and Caughey, for the ONERA M6 wing at Mach 0.840 and an angle of attack of 3.06 deg. Both calculations were performed on the same grid, which contained 65536 cells. The Euler calculation was run 200 cycles. Using the Cray 1, this required 7 minutes. The agreement between the two results reinforces our confidence in both methods.

(*d*) Implicit Schemes. An obvious way to accelerate convergence to a steady state is to increase the time step. The time step of an explicit scheme is limited by the Courant Friedrichs Lewy condition, that the region of dependence of the difference scheme must at least contain the region of dependence of the differential equation. This motivates the introduction of implicit schemes.

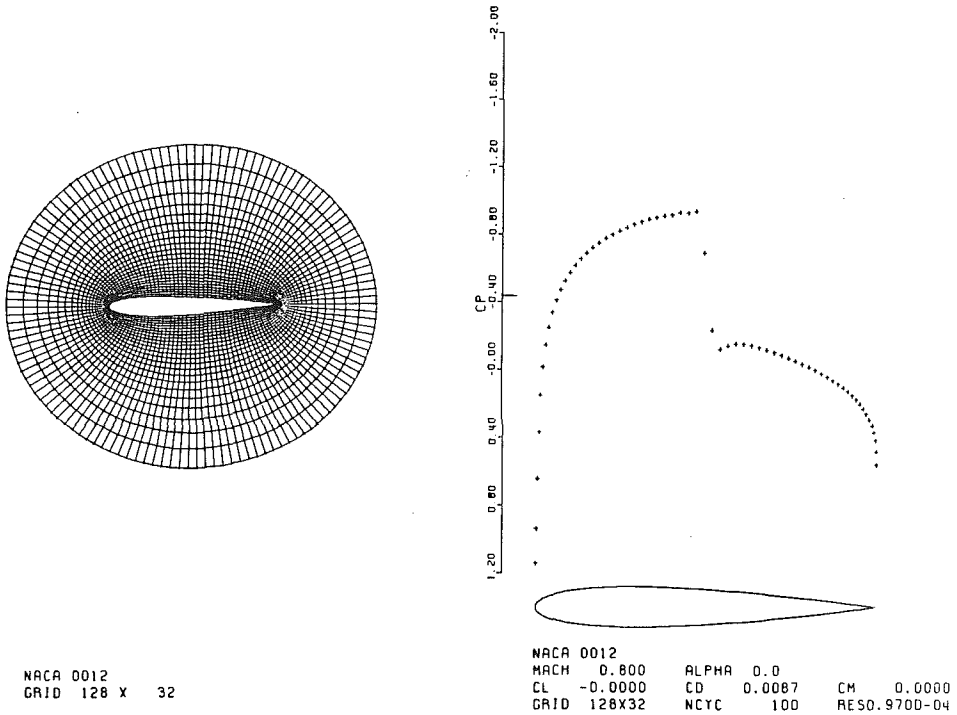
The celebrated paper of Beam and Warming gives an elegant formulation of implicit schemes for nonlinear hyperbolic equations [58]. A prototype implicit scheme for a system of equations such as the Euler equations (2.5), can be formulated as

$$w^{n+1} = w^n - \beta\,\Delta t[D_x f(w^n) + D_y g(w^n)] - (1-\beta)\,\Delta t\,[D_x f(w^{n+1}) + D_y g(w^{n+1})] \tag{5.10}$$

where D_x and D_y are difference operators approximating $\partial/\partial x$ and $\partial/\partial y$. The scheme is second-order accurate in time if $\beta = 1/2$, and in the linear scalar case it will be unconditionally stable for all $\Delta t > 0$ if $\beta \ge 1/2$. In this form the scheme is too expensive, since it calls for the solution of coupled nonlinear equations at each time step. Let the Jacobian matrices be

$$A = \frac{\partial f}{\partial w}, \quad B = \frac{\partial g}{\partial w} \tag{5.11}$$

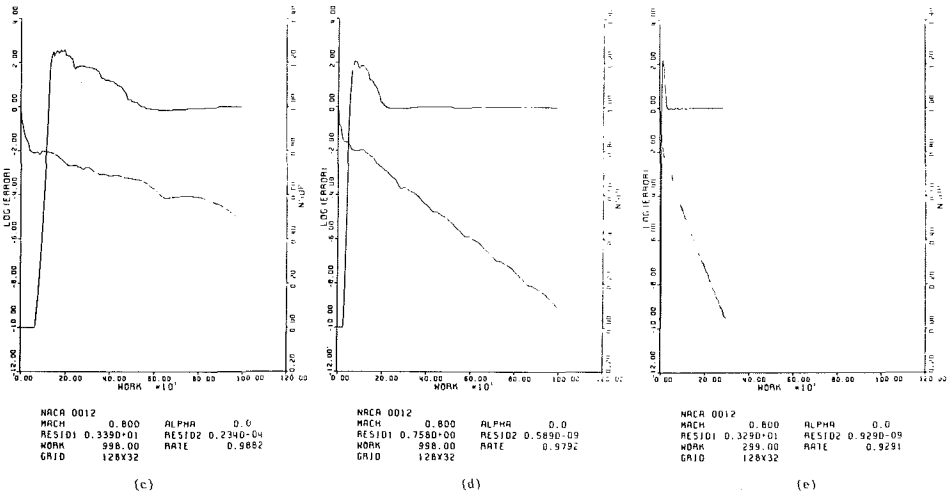
Downloaded 02 May 2010 to 171.66.16.250. Redistribution subject to ASME license or copyright; see http://www.asme.org/terms/Terms_Use.cfm



(a) (b)

Grid

Solution
(obtained by the multigrid scheme)



(c) (d) (e)

Convergence Rate of the 4 Stage Explicit Scheme

Convergence Rate of the 4 Stage Implicit Scheme

Convergence Rate of the 4 Stage Multigrid Scheme

Fig. 5.3 Convergence rates for different schemes to solve the Euler equations. NACA 0012, Mach 0.800, α0 deg. Lower curves: convergence of error. Upper curves: buildup of supersonic zone.

and let the correction be

$$\delta w = w^{n+1} - w^n$$

The scheme can be linearized by setting

$$f(w^{n+1}) = f(w^n) + A\delta w + 0(\|\delta w\|^2)$$

$$g(w^{n+1}) = g(w^n) + B\delta w + 0(\|\delta w\|^2)$$

and dropping the terms of the second and higher order. This yields

$$[I + \beta\Delta t(D_x A + D_y B)]\delta w + \Delta t\, R = 0 \qquad (5.12)$$

where R is the residual

$$R = D_x\, f(w^n) + D_y\, g(w^n)$$

If $\beta = 1/2$ the scheme remains second-order accurate because $\|\delta w\| = 0(\Delta t)$, with the consequence that the neglected terms are $0(\Delta t^2)$. Note also that if $\beta = 1$ the scheme reduces to a Newton iteration in the limit $\Delta t \to \infty$. The Newton iteration has been the subject of experimentation [59]. Written for an $n \times n$ mesh, equation (5.12) has a block tridiagonal form, requiring $0(n^4)$ operations for inversion. Because of this rapid growth of the operation count with n, the Newton method

Downloaded 02 May 2010 to 171.66.16.250. Redistribution subject to ASME license or copyright; see http://www.asme.org/terms/Terms_Use.cfm

thus appears to be uncompetitive except on very coarse meshes.

Beam and Warming derive a relatively inexpensive scheme by replacing the operator on the left side of equation (5.12) by a product of two one-dimensional operators:

$$(I+\beta\Delta t D_x A)\,(I+\beta\Delta t D_y B)\;\delta\, w+\Delta t\, R=0 \qquad (5.13)$$

Equation (5.13) can be inverted in two steps as

$$(I+\beta\Delta t D_x A)\;\delta w^* + \Delta t\, R=0$$

$$(I+\beta\Delta t D_y B)\;\delta w=\delta w^*$$

and the operation count is now $0(n^2)$. Equation (5.13) remains second-order accurate if $\beta = 1/2$, and unconditionally stable for the linear scalar case if $\beta \geq 1/2$. It also has the desirable feature for steady state calculations that steady state is independent of Δt. The corresponding scheme in three dimensions is unstable.

This reduction of an implicit scheme to an alternating direction scheme was originally introduced by Mitchell and Gourlay [60]. Briley and MacDonald have also developed an equivalent alternating direction procedure for solving nonlinear hyerbolic equations [61]. The alternating direction method has been used for transonic flow calculations by Steger and Pulliam [62].

An alternative reduction is to replace the operator on the left-hand side of equation (5.12) by a product of factors with upwind and downwind differencing, leading to an LU implicit scheme [63]. Care must then be taken to ensure the operators in the two factors have, respectively, positive and negative eigenvalues. This scheme has been used to calculate transonic flows through cascades by Buratynski and Caughey [64].

Another approach to increasing the time step has recently been explored by the author [65]. This is to replace the residual at each point by a weighted average of residuals at neighboring points. Consider the multistage scheme described by equation (5.7). In the one-dimensional case one might replace the residual R_i by the average

$$\bar{R}_i=\epsilon\, R_{i-1}+(1-2\epsilon)R_i+\epsilon\, R_{i+1}$$

at each stage of the scheme. This smooths the residuals and also increases the support of the scheme, thus relaxing the restriction on the time step imposed by the Courant Friedrichs Lewy condition. If $\epsilon \geq 1/4$, however, there are Fourier modes such that $\bar{R}_i = 0$ when $R_i \neq 0$. To avoid this restriction it is better to perform the averaging implicitly by setting

$$-\epsilon\bar{R}_{i-1}+(1+2\epsilon)\bar{R}_i-\epsilon\bar{R}_{i+1}=R_i \qquad (5.14)$$

If we assume an infinite interval, this equation can be explicitly inverted to give

$$\bar{R}_i=\frac{1-r}{1+r}\{R_i+r(R_{i+1}+R_{i-1})+r^2(R_{i+2}+R_{i-2})\ldots\}$$

where $\epsilon = r/(1-r)^2$, $r < 1$. Thus the scheme has infinite support, with a decay factor r. The Fourier symbol for the model problem (5.8) is now divided by the factor $1 + 2\,\epsilon(1-\cos\xi)$, and stability can be obtained for any Courant λ provided that the smoothing parameter ϵ satisfies

$$\epsilon\geq\frac{1}{4}\left[\left(\frac{\lambda}{\lambda^*}\right)^2-1\right]$$

where λ^* is the Courant number limit of the unsmoothed scheme.

It turns out that it is sufficient to apply the smoothing only at alternate stages, provided that the smoothing parameter ϵ is sufficiently increased. If the total number of stages is even, smoothing should be applied at stages 2, 4, 6. . . , and if it is odd it should be applied at stages 1, 3, 5. . . . In the two-dimensional case smoothing is applied in product form:

$$(1-\epsilon\delta_x{}^2)(1-\epsilon\delta_y{}^2)\bar{R}=R$$

where δ_x^2 and δ_y^2 are second difference operators in the x and y directions.

The smoothed multistage scheme is in use in a code currently being developed by Baker and Jameson to calculate the flow past a wing-body-fin-tail combination [65]. The best rate of convergence is obtained with a Courant number of about 9.

Two other interesting formulations of implicit schemes have been proposed by MacCormack [66], and Lerat and Sidès [67]. MacCormack adds implicit stages requiring bidiagonal inversions to his explicit scheme. If the stages are reordered and the two implicit stages combined, it is equivalent in the scalar case to residual averaging. Lerat and Sidès consider a general class of implicit schemes using nine-point support in two-dimensions. Their choice of parameters again leads to a form of residual averaging.

***(e)* Multigrid Schemes for the Euler Equations.** While the available theorems in the theory of multigrid methods generally assume ellipticity, it seems that it ought to be possible to accelerate the evolution of a hyperbolic system to a steady state by using large time steps on coarse grids, so that disturbances are more rapidly expelled through the outer boundary. The interpolation of corrections back to the fine grid will introduce errors, however, which cannot be rapidly expelled from the fine grid, and ought to be locally damped, if a fast rate of convergence is to be attained. Thus it remains important that the driving scheme should have the property of rapidly damping out high-frequency modes.

In a novel multigrid scheme proposed by Ni [68], the flow variables are stored at mesh nodes, and the rates of change of mass, momentum, and energy in each mesh cell are estimated from the flux integral (5.3). The corresponding change δw_0 in the solution at the cell center is then distributed unequally between the nodes at its four corners by the rule

$$\delta w_c=\frac{1}{4}\,(\delta w_0 \pm A\;\delta w_0 \pm B\delta w_0)$$

where δw_c is the correction at a corner, and A and B are the Jacobian matrices (5.11). The signs are varied in such a way that the accumulated correction at each mode corresponds to the first two terms of a Taylor series in time, like a Lax Wendroff scheme. As it stands, this scheme does not damp odd and even point oscillations. Ni introduces artificial viscosity by adding a further correction proportional to the difference between the value at each corner and the average of the values at the four corners of the cell. Residuals on the coarse grid are formed by taking weighted averages of the corrections at neighboring nodes of the fine grid, and corrections are then assigned to the corners of coarse grid cells by the same distribution rule. When several grid levels are used, the distribution rule is applied once on each grid down to the coarsest grid, and the corrections are then interpolated back to the fine grid.

Using three or four grid levels, Ni obtained a rate of convergence, measured by the mean error reduction per multigrid cycle, of about 0.95. This leads to a fairly well-converged solution in 100–200 cycles. The accuracy of the results, which can be obtained by the algorithm in its published form, however, appears to be limited by the action of the artificial viscosity, which introduces an error of first order.

The multistage scheme described in Section 5(*c*) forms the basis of a multigrid method recently introduced by Jameson [69]. Auxiliary meshes are introduced by doubling the mesh spacing, and values of the flow variables are transferred to a coarser grid by the rule

$$w_{2h}^{(0)}=\sum\; V_h\; w_h / V_{2h}$$

Downloaded 02 May 2010 to 171.66.16.250. Redistribution subject to ASME license or copyright; see http://www.asme.org/terms/Terms_Use.cfm

where the subscripts denote values of the mesh spacing parameter, V is the cell area, and the sum is over the four cells on the fine grid composing each cell on the coarse grid. This rule conserves mass, momentum, and energy. A forcing function is then defined as

$$P_{2h} = \sum R_h(w_h) - R_{2h}(w_{2h}^{(0)}) \tag{5.15}$$

where R is the residual of the difference scheme. To update the solution on a coarse grid the multistage scheme (5.7) is now reformulated as

$$\begin{aligned} w_{2h}^{(1)} &= w_{2h}^{(0)} - \alpha_1 \Delta t (R_{2h}^{(0)} + P_{2h}) \\ &\cdots \\ w_{2h}^{(q+1)} &= w_{2h}^{(0)} - \alpha_q \Delta t (R_{2h}^{(q)} + P_{2h}) \\ &\cdots \end{aligned} \tag{5.16}$$

where $R^{(q)}$ is defined by equation (5.9). In the first stage of the scheme, the addition of P_{2h} cancels $R_{2h}(w_{2h}^{(0)})$ and replaces it by $\Sigma R_h(w_h)$, with the result that the evolution on the coarse grid is driven by the residuals on the fine grid. This process is repeated on successively coarser grids. Finally the correction calculated on each grid is passed back to the next finer grid by bilinear interpolation.

In the multigrid mode it is more important to improve the damping of high-frequency modes than it is to increase the time step. Using the four-stage scheme with a single evaluation of the dissipative terms, as defined by equations (5.7) and (5.9), a good choice of the coefficients is

$$\alpha_1 = 0.25, \quad \alpha_2 = 0.5, \quad \alpha_3 = 0.55$$

With a time step such that the Courant number $\lambda = 2.0$, and the viscosity coefficient μ set equal to 1/32, the use of these coefficients results in an amplification factor g for the model problem (5.8) which is no greater than 0.35 for all frequencies in the range $1.0 \le \xi \le \pi$.

In the solution of the Euler equations for two-dimensional flow, it has been found that a rate of convergence of about 0.85 per multigrid cycle (measured over 100 cycles) can be attained for subsonic flow, and about 0.9 for transonic flow. Figure 5.3 shows a comparison of the convergence rate realized for a transonic flow calculation using:

(*a*) the four-stage explicit scheme;
(*b*) the four-stage scheme with implicit residual averaging;
(*c*) the four-stage scheme with multiple grids.

The calculation is of the flow past a nonlifting NACA 0012 airfoil at Mach 0.80, using a 128 × 32 grid. For each case the figure shows two curves. One is the decay of the logarithm of the error (measured by the root mean square rate of change of density). The other is the buildup of the number of points in the supersonic zone, which is a useful measure of the global convergence of the flow field. With the multigrid scheme the flow is fully converged in less than 100 cycles. Using a Cray 1 computer, a calculation with 100 cycles takes about 15 seconds. If the same calculation were performed with a CDC 7600, the time would be about 2 minutes. As recently as 1981 it required 1–3 hours to calculate an Euler solution for a two-dimensional flow by the best available method, using a CDC 7600 [70].

(*f*) Upwind Differencing, Flux Vector Splitting, and Flux Corrected Transport. It is not easy to simulate a propagating discontinuity by a numerical method. The simplest model of convection is provided by the one-dimensional wave equation

$$u_t + u_x = 0$$

This equation can be approximated by the one-sided scheme

$$u_i^{n+1} = u_i^n - \lambda(u_i^n - u_{i-1}^n)$$

where λ is the Courant number $\Delta t/\Delta x$. This scheme is stable for $0 \le \lambda \le 1$, and it is appealing for two reasons:

(1) It simulates the physical process of wave propagation by looking backward along the direction of propagation: if $\lambda = 1$, it exactly represents propagation along characteristics.

(2) It has the property of preserving the monoticity of an initially monotone profile: this excludes the possibililty of generating an overshoot behind a shock wave.

These observations have motivated numerous studies of one-sided schemes, dating back to the early work of Courant, Isaacson, and Rees [71]. There has recently been a revival of interest in the use of one-sided differencing for compressible flow calculations, beginning with the nonconservative λ scheme of Moretti [45], and the conservative scheme of Steger and Warming [72]. Monotonicity preserving schemes are unfortunately at best first-order accurate [73], and stable one-sided schemes are no more than second-order accurate [74]. It is also necessary to allow for the fact that in the case of the general one-dimensional system of hyperbolic equations (5.1), signals travel in both directions.

One way of generalizing one-sided differencing to a system of equations is the flux vector splitting method proposed by Steger and Warming [72]. Considering the system (5.1), let the flux f be divided into two parts f^+ and f^-, such that all the eigenvalues of $\partial f^+/\partial w$ are nonnegative, and the eigenvalues of $\partial f^-/\partial w$ are nonpositive. Then equation (5.1) is replaced by

$$w^{n+1} = w^n - \Delta t[D_x^- f^+(w) + D_x^+ f^-(w)] \tag{5.17}$$

where D_x^* and D_x^- are forward and backward difference operators approximating $\partial/\partial x$.

The splitting is not unique. The flux vector $f(w)$ of the Euler equations has the property that

$$f(w) = Aw$$

where $A = \partial f/\partial w$. A can be represented as $T\Lambda T^{-1}$, where the columns of T are the eigenvectors of A, and Λ is a diagonal matrix containing its eigenvalues. Steger and Warming proposed the splitting

$$f^+(w) = A^+ w, \quad f^-(w) = A^- w$$

where

$$A^+ = T\Lambda^+ T^{-1}, \quad A^- = T\Lambda^- T^{-1}$$

and Λ^+ and Λ^- contain the positive and negative eigenvalues of A. This splitting is discontinuous across the sonic line. Van Leer has proposed a splitting that preserves smoothness [75].

An alternative formulation was proposed by Godunov [72]. Suppose that (5.1) is approximated by

$$w_i^{n+1} = w_i^n - \frac{\Delta t}{\Delta x}(F_{i+1/2} - F_{i-1/2}) \tag{5.18}$$

where the numerical flux function $F_{i+1/2} = F(w_i, w_{i+1})$ is an approximation to the flux across the cell boundary $x_{i+1/2}$. This function must satisfy the consistency condition $F(w, w) = F(w)$. In the Godunov scheme $F_{i+1/2}$ is taken to be the flux value arising at $x_{i+1/2}$ in the exact solution of the initial value problem defined by piecewise constant data between each cell boundary. This simulates both the motion of shocks and expansion fans, but it is expensive. A number of simpler schemes, designed to distinguish between the influence of forward and backward moving waves have recently been developed. These flux-difference splitting schemes replace the exact solution of the Riemann problem with an approximate solution. Examples are the schemes of Engquist and Osher [74], Roe [76, 77], and Lombard, Oliger, and Yang [78]. These ideas have been unified in recent papers by Van Leer

Downloaded 02 May 2010 to 171.66.16.250. Redistribution subject to ASME license or copyright; see http://www.asme.org/terms/Terms_Use.cfm

[79], and Harten, Lax, and Van Leer [80]. Harten has also proposed the concept of total variation stable schemes, designed to assure that the total variation

$$\sum_i |w_{i+1}^n - w_i^n|$$

remains bounded [81].

Another way of reducing preshock oscillations was proposed by Boris and Book [82], and refined by Zalesak [83]. Boris and Book gave the name flux-corrected transport to their concept. Consider the difference scheme (5.18), or a corresponding multistage scheme. Let $F_{i+1/2}^H$ be a numerical flux function such that the difference scheme has a high order of accuracy, but may be prone to preshock oscillations. Also let $F_{i+1/2}^L$ be a low-order numerical flux function such that the scheme is monotone, or at least resistant to oscillations. $F_{i+1/2}^L$ might be generated, for example, by adding a dissipative flux to $F_{i+1/2}^H$. Then set

$$\tilde{w}_i = w_i^n - \frac{\Delta t}{\Delta x}(F_{i+1/2}^L - F_{i-1/2}^L)$$

and

$$w_i^{n+1} = \tilde{w}_i - \frac{\Delta t}{\Delta x}(A_{i+1/2} - A_{i-1/2})$$

where $A_{i+1/2}$ is the antidiffusive flux

$$A_{i+1/2} = \omega(F_{i+1/2}^H - F_{i+1/2}^L), \quad 0 \le \omega \le 1.$$

If the parameter $\omega = 1$, the high order scheme is recovered. Logic is included in the code to select the largest possible value of ω such that no new maximum or minimum is generated in the profile.

There is no doubt that these more elaborate schemes can improve the resolution of shock waves and contact discontinuities in one-dimensional unsteady flows. Provided, however, that a dissipative scheme is used, preshock overshoots are generally less severe in steady state calculations, because oscillations generated during the transient phase tend to be damped out in the final steady state. For steady multidimensional flows past complex configurations, it is not yet established whether the improvement realizable by splitting or flux-corrected transport justifies the extra complexity of these schemes. An opposing view is that shock waves and contact discontinuities should be explicitly fit into the calculation as interior boundaries, obviating the need to use a difference scheme in conservation form [45]. A promising alternative approach is adaptive refinement of the grid in regions containing severe gradients [84].

6 Viscous Flow Calculations

(a) Boundary Layer Corrections. While it is true that the viscous effects are relatively unimportant outside the boundary layer, the presence of the boundary layer can have a drastic influence on the pattern of the global flow. This will be the case, for example, in the event that the flow separates. The boundary layer can also cause global changes in a lifting flow by changing the circulation. These effects are particularly pronounced in transonic flows. The presence of a boundary layer can cause the location of the shock wave on the upper surface of the wing to shift 20 percent of the chord.

While we must generally account for the presence of the boundary layer, the accuracy attainable in solutions of the Navier Stokes equations for complete flow fields is severely limited by the extreme disparity between the length scales of the viscous effects, and those of the gross patterns of the global flow. This has encouraged the use of methods in which the equations of viscous flow are solved only in the boundary layer, and the external flow is treated as inviscid. These zonal methods can give very accurate results in many cases of practical concern to the aircraft designer. The underlying ideas have been comprehensively reviewed in recent papers by Lock and Firmin [85], Le Balleur [86], and Melnik [87].

The general features of a zonal method are illustrated in Fig. 6.1. In the outer region the real viscous flow is approximated by an equivalent inviscid flow, which is to be matched to the inner viscous flow by an appropriate selection of boundary conditions. In most of the boundary layer, the viscous flow equations may consistently be approximated by the boundary layer equations. This is sufficient in regions of weak interaction, in which the viscous effect on the pressure is small. There are, however, regions of strong interaction in which the classical boundary layer formulation fails, because of the appearance of strong normal pressure gradients across the boundary layer. Coupling conditions for the interaction between the inner viscous flow and the outer inviscid flow can be derived from an asymptotic analysis in which the Reynolds number is assumed to become very large. The two solutions could be patched at the outer edge of the boundary layer. It is often more convenient, however, to allow the equivalent inviscid flow to overlap the inner viscous region.

A complete analysis of the viscous flow over an airfoil should include the following principal effects:

(1) The displacement effect of the boundary layer over the airfoil;

(2) The displacement effect of the wake;

(3) The wake curvature effect induced by the momentum defect in the wake;

(4) The interaction of the boundary layer with the trailing edge;

(5) The interaction of the boundary layer with shock waves.

The first three of these are weak interactions, and the last two are strong interactions.

The displacement effect is caused by the outward displacement of the streamlines which result from the reduced mass flow in the boundary layer. This effect can be modeled by adding an equivalent thickness to the body, equal to the displacement thickness of the boundary layer, and applying the flow tangency condition at the surface of the modified body. An alternative formulation, discussed, for example, by Lighthill, is to extend the equivalent inviscid flow to the real body, and to apply a transpiration boundary condition [88]. This condition can be derived by considering the defect equation for the difference between the inviscid and viscous flows [85, 86]. By integrating the continuity equation across the boundary layer, and assuming that the inviscid and viscous flows match at the edge of the boundary layer, we find that

$$(\rho_i v_i)\Big|_{\text{wall}} = \frac{d}{ds}\int_0^\delta (\rho_i u_i - \rho u)\, dn \tag{6.1}$$

where s and n are the streamwise and normal directions, δ is the boundary layer thickness, and the subscript i denotes the inviscid flow. This is the boundary condition that is now applied in the calculation of the equivalent inviscid flow. We can write it as

$$(\rho v)\Big|_{\text{wall}} = \frac{dQ}{ds} \tag{6.2}$$

where Q is the mass flux defect defined by the integral in

Downloaded 02 May 2010 to 171.66.16.250. Redistribution subject to ASME license or copyright; see http://www.asme.org/terms/Terms_Use.cfm

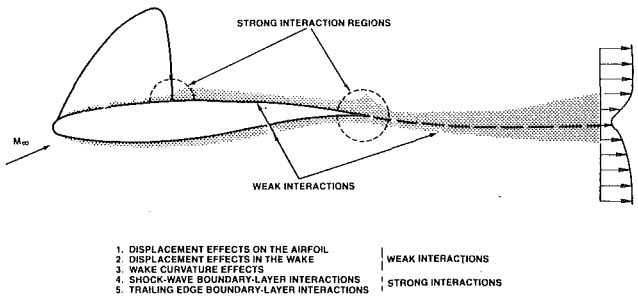


Fig. 6.1 Viscid-inviscid interactions on airfoils

equation (6.1). If the outer inviscid flow is represented by the Euler equations, similar defect equations for the momentum and energy provide the additional boundary conditions that are needed to solve the Euler equations [89]. The displacement effect is usually more pronounced on the upper surface than it is on the lower surface. This leads to an equivalent decambering of the airfoil which acts to reduce the lift.

There is also a displacement effect due to the wake behind the airfoil. The matching condition for the wake displacement effect is

$$[v]_{\text{wake}} = \frac{1}{\rho_w}\frac{dQ_w}{ds} \tag{6.3}$$

where $[v]$ is the jump in the normal velocity across the wake, ρ_w is the average of the densities in the inviscid flow on the two sides of the wake, and Q_w is the total mass flux defect in the wake. The main result of the wake displacmeent effect is a reduction in the pressure near the trailing edge, and a corresponding increase in the drag.

The curvature of the wake induces an additional reduction of the lift. Because there is a momentum defect in the wake, it acts like a jet flap with a negative momentum coefficient. The wake can only be deflected toward the direction of the outer stream through the action of a normal pressure gradient, with the result that the pressure at the trailing edge is larger on the upper surface than it is on the lower surface, and the Kutta condition for the equivalent inviscid flow must be modified to allow for this difference in the pressures. The matching condition for the wake curvature effect is

$$[p]_{\text{wake}} = C_w \kappa_w \tag{6.4}$$

where $[p]$ is the jump in pressure across the wake, C_w is the total momentum defect in the wake, and κ_w is the wake curvature. The magnitude of the wake curvature effect is formally of the same order as that of the displacement effect.

The analysis of the flow in regions of strong interaction is more complicated because of the breakdown of the boundary layer approximation. In the region of the trailing edge the flow in the boundary layer accelerates, and the boundary layer thickness decreases, because the retardation of the flow by skin friction suddenly ceases. Melnik has developed a consistent model of the strong interaction of an unseparated turbulent boundary layer with a cusped trailing edge, under the assumption that the Reynolds number is large [87]. As the flow passes through a shock wave, the sharp pressure rise at the foot of the shock wave causes a steep thickening of the boundary layer. As long as the shock wave is not too strong, it turns out, however, that the growth of the boundary layer thickness through the shock wave is quite well predicted by boundary layer theory, although the local details of the flow are not accurately modeled. Consequently the coupling condition (6.1) can still be used to obtain the global flow.

The coupled viscous and inviscid equations are solved iteratively. The simplest procedure is a direct one. The inviscid flow is first solved without a boundary layer, and the boundary layer is calculated using the wall pressure from the

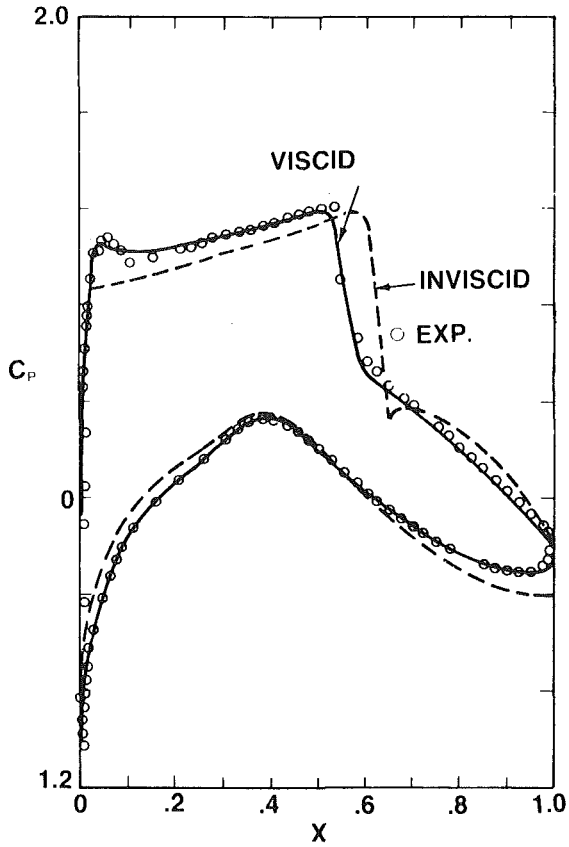


Fig. 6.2 Comparisons between the viscid and inviscid solutions and experimental data. RAE 2822 Airfoil, Mach 0.725, CL0.743.

inviscid solution as a boundary condition. The inviscid flow is then recalculated with a boundary condition that accounts for the presence of the boundary layer, and the process is repeated until the solution converges. A linearized analysis of the procedure indicates that it will generally be necessary to underrelax the changes in the boundary conditions, and that it will become unstable near a separation point [85, 90].

This difficulty has led to the introduction of semi-inverse methods in which the transpiration boundary condition is prescribed in both the inviscid flow calculation and the boundary layer calculation [90, 91]. The inviscid flow calculation provides an estimate $u_{e,I}$ of the speed at the edge of the boundary layer. An inverse boundary layer method is used to calculate a corresponding estimate $u_{e,V}$ of the speed at the edge of the boundary layer from the boundary layer equations. In Carter's method [90], the equivalent mass flux defect Q appearing in the transpiration boundary condition (6.2) is then multiplied by the correction factor

$$1 + \omega\left(\frac{u_{e,V}}{u_{e,I}} - 1\right)$$

where ω is a fixed relaxation factor, and the process is repeated. Le Balleur uses a more complicated correction formula with a locally varying relaxation factor [91]. These methods converge for flows containing separated regions.

The method of Bauer, Garabedian, Korn, and Jameson was the first to incorporate boundary layer corrections into the calculation of transonic potential flow [92]. This method only accounted for displacement effects on the airfoil, and modeled the wake as a parallel semi-infinite strip. Nevertheless, this simple model substantially improved the agreement with experimental data. More complete theoretical models including effects due to the wake thickness and curvature have been developed by Collyer and Lock [93], Le

Downloaded 02 May 2010 to 171.66.16.250. Redistribution subject to ASME license or copyright; see http://www.asme.org/terms/Terms_Use.cfm

Balleur [94], and Melnik, Chow, Mead, and Jameson [95]. Recently Whitfield, Thomas, Jameson, and Schmidt have developed a method based on the use of the Euler equations for the inviscid flow [96]. Figure 6.2 shows the result of a calculation by the method of Melnik, Chow, Mead, and Jameson. It can be seen that the inclusion of the boundary layer correction shifts the inviscid result into close agreement with the experimental data.

(*b*) Reynolds-Averaged Navier Stokes Equations. The simulation of attached flows by zonal methods now rests on a firm theoretical foundation, and has reached a high level of sophistication in practice. The treatment of three-dimensional flows is presently limited by a lack of available boundary layer codes for general configurations. During the last few years there has also emerged the possibility of simulating flows with small separated regions by zonal methods. In cases of massive flow separation, where the flow is often observed to be unsteady, adequate zonal models have yet to be developed. Zonal methods also have the disadvantage that extensions to more general configurations require a separate asymptotic analysis of each component region, such as the corner between a wing and a nacelle pylon, with the result that they can become unmanageable as the complexity of the configuration is increased.

For these reasons a continuing body of research is directed at the global solution of the Reynolds-averaged Navier Stokes equations. The hope is that it will be possible to develop a fairly universal method, which will be able to predict separated flows where the present zonal methods fail, in particular, separated flows that are two-dimensional and unsteady, and three-dimensional separated flows, both steady and unsteady. The present state of the art has been very thoroughly reviewed by Mehta and Lomax [97]. During the past decade the Navier Stokes equations have been the subject of exploratory investigations aimed at establishing the feasibility of their solution, but the methods so far developed have been too expensive to permit their use in a routine production mode.

The principal requirements for a satisfactory solution of the Reynolds-averaged Navier Stokes equations are:

(1) the reduction of the discretization errors to a level such that any numerically introduced dissipative terms are much smaller than the real viscous terms;

(2) the closure of the equations by a turbulence model, which accurately represents the turbulent stresses.

The problem of sufficiently reducing the numerical errors is particularly severe in regions of strong interaction, such as the foot of a shock wave, where it may not be possible to attain a high order of accuracy in the difference approximation. The use of a fine-enough mesh to overcome this problem has so far been impeded by a lack of powerful enough computers.

The development of the necessary numerical methods is already quite well advanced. The methods described in the preceding section can generally be carried over to the Navier Stokes equations. MacCormack has extended both his explicit scheme and his new implicit scheme to the treatment of viscous flows [98, 66]. Deiwert has used MacCormack's explicit scheme in his path-finding calculations of viscous flows over airfoils [99], and Shang and Hankey have recently used the same scheme to calculate the flow past a hypersonic cruiser [100]. Beam and Warming have also made a corresponding extension of their alternating direction implicit scheme to treat viscous flows [101].

Rapid developments in the speed and memory of computers are steadily improving the prospect of useful simulations of the Reynolds-averaged Navier Stokes equations. In the opinion of Mehta and Lomax, the development of reliable turbulence models is now the crucial pacing item [97]. No single turbulence model has been found, which can be used in the simulation of a variety of flows. At the present time not much is known about the behavior of turbulence in separated regions [102], and this has impeded the development of turbulence models for complex three-dimensional flows. It appears that near term improvements in the computational simulation of turbulent flow will probably depend heavily on experimental inputs and checks.

7 The Design Problem

What the designer really needs is a method of determining slopes that will have the desired aerodynamic properties. The mere ability to predict the flow over a given shape is not enough for this purpose, since it does not provide any guidance on how to change the shape if the flow is unsatisfactory. The designer generally has an idea of the kind of pressure distribution that will lead to the desired performance. Thus it is useful to consider the problem of calculating the shape that will lead to a given pressure distribution. Such a shape does not necessarily exist, unless the pressure distribution satisfies certain constraints, and the problem must therefore be very carefully formulated.

Lighthill solved the design problem for airfoils in incompressible flow by conformally mapping the profile to a unit circle [103]. The speed over the surface of the profile is

$$q = \phi_\theta / h \tag{6.1}$$

where ϕ is the potential for the flow past a circle, and h is the modulus of the mapping function. The solution for ϕ is known for incompressible flow. Let q_T be the target surface speed. Then the surface value of h can be obtained by setting $q = q_T$ in equation (6.1), and since the mapping function is analytic, it is uniquely determined by the value of h on the boundary. A solution exists for a given speed at infinity only if

$$\frac{1}{2\pi} \oint q d\theta = q_\infty .$$

There are additional constraints on q if the profile is required to be closed. A computer code embodying this method was developed by James [104].

The method has been extended to the case of compressible flow by McFadden [105]. Starting with a given shape, and a corresponding mapping function, the potential can be determined by equation (2.6) or (2.7). Then a new mapping function is determined from equation (6.1), and the process is repeated. McFadden gives a proof that the iterations will converge in subsonic flow, and extends the method of transonic flow through the introduction of artificial viscosity to suppress shock waves, which would cause the updated mapping function to be discontinuous.

This difficulty can also be overcome by smoothing the changes in the mapping function. This method is used in the code SYN4, written for Grumman by the author in 1980. It allows the recovery of smooth profiles that generate flows containing shock waves, and it has been used to design improved blade sections for propellers [106].

Another way to formulate the problem of designing a profile for a given pressure distribution is to integrate the corresponding surface speed to obtain the surface potential. Equation (2.6) or (2.7) is then solved with a Dirichlet boundary condition, and a shape correction is determined from the calculated normal velocity through the surface. This scheme was first tried by Tranen [107]. Volpe has shown how to allow for the constraints that must be satisfied by the pressure distribution if a solution is to exist [108].

Downloaded 02 May 2010 to 171.66.16.250. Redistribution subject to ASME license or copyright; see http://www.asme.org/terms/Terms_Use.cfm

The same idea has been used by Henne for three-dimensional design calculations [109]. Another three-dimensional design method has been proposed by Garabedian and McFadden [110]. In their scheme the surface is treated by a free boundary which is shifted by a time-dependent equation in such a way that the flow evolves toward the specified pressure distribution.

The hodograph method offers an alternative approach to the design of airfoils in transonic flows. Garabedian and Korn have achieved a striking success in the design of airfoils to produce shock-free transonic flows by the method of complex characteristics [111, 112].

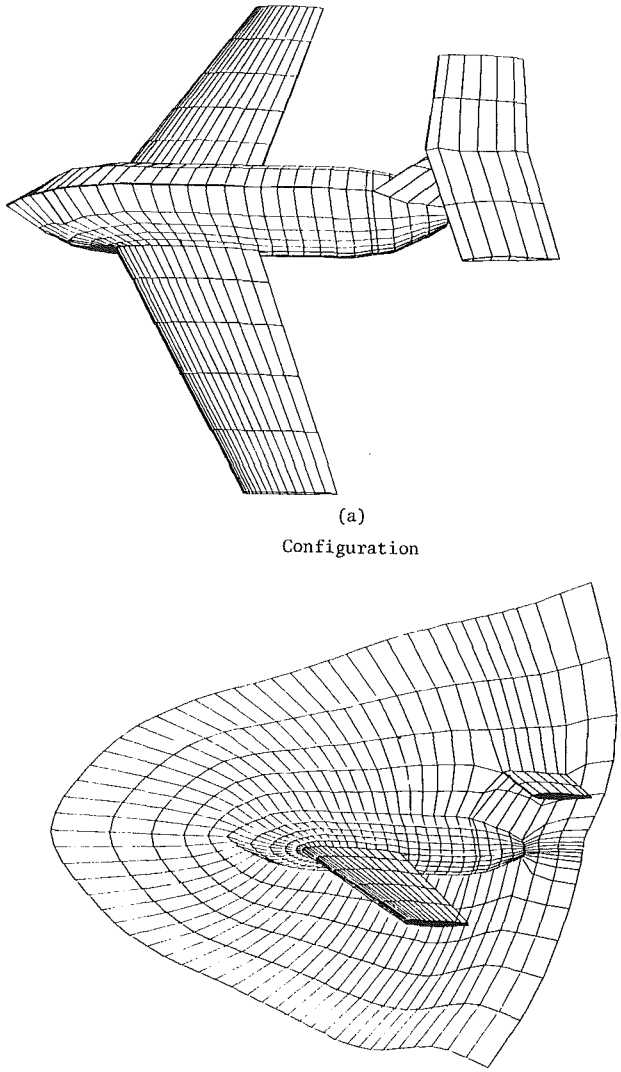
Hicks and Vanderplats have suggested the possibility of meeting desired design objectives by using constrained optimization. The configuration is specified by a set of parameters, and any suitable code for flow analysis is used to evaluate the aerodynamic characteristics. The optimization method then selects values of these parameters that maximize some criterion of merit, such as the lift-to-drag ratio [113]. This is the ultimate method, which in principle, allows the designer to specify any reasonable design objectives. The method becomes extremely expensive, however, as the number of parameters is increased, and its successful application in practice calls for great skill in choosing the parameterizations.

8 Conclusion

This is a view from the trenches, of one who has been closely involved in the day-to-day development of codes for the prediction of aerodynamic flows past real configurations. While bearing in mind the broader perspective of the mathematical theory of computational methods, I have tried to show how the choice of mathematical models and selection of numerical methods has been motivated by the needs of the aircraft designer. For a more Olympian view, less concerned with the immediate difficulties of constructing stable and accurate approximations to the differential equations and boundary conditions, the reader may wish to consult the recent papers of Chapman [5], and Kutler [114], who both make projections of trends and pacing items. A perspective analysis of the impact of computational methods on aerodynamic design is contained in a review by Ballhaus [115]. An historical perspective, including various personal reminiscences, may be found in Hall's appealing survey paper [116].

With the advent of a new generation of computers it will be entirely feasible to calculate solutions of the Euler equations for a complete aircraft. A code to solve the Euler equations for wing-body-tail-fin combinations is already operational [65]. The kind of configuration that can be treated is illustrated in Fig. 8.1. The Cray 2, for example, is projected to be at least six times faster than the Cray 1, and will have 256 million words of memory. When a Cray 1 is used to perform calculations with the four-stage scheme described in Section 5(*c*), three-dimensional Euler solutions on a 25,000 point mesh can be advanced 200 steps in 150 seconds. Assuming that the multigrid acceleration procedure described in Section 5(*e*) is introduced, 200 steps should be ample for convergence. Using a grid with one million points, it should therefore be possible to calculate a solution in 20 minutes or less with a Cray 2. One million grid points should be enough for a reasonably accurate representation of an airplance, and the corresponding memory requirement, of the order of 40 million words, would not tax the new machines.

We can also anticipate the routine calculation of unsteady flows for the determination of structural loads. Looking further ahead, we can see on the horizon the increasingly real possibility of simulating the flow past a complete aircraft with the Reynolds-averaged Navier Stokes equations.



(a)
Configuration

(b)
Grid

Fig. 7.1 Transonic glider

Acknowledgment

I have had invaluable help from my friends in preparing this paper. I am particularly indebted to Robert Melnik for discussions of the problems of viscous flow calculations, and to Tim Baker for his assistance in correcting the complete manuscript.

References

1 Theodorsen, Theodore, "Theory of Wing Sections of Arbitrary Shape," NACA TR 411, 1931.

2 Whitcomb, R. T., "A Study of the Zero Lift Drag-Rise Characteristics of Wing-Body Combinations Near the Speed of Sound," NACA TR 1273, 1956.

3 Whitcomb, R. T., "Review of NASA Supercritical Airfoils," 9th ICAS Congress, Haifa, Paper 74-10, 1974.

4 Whitcomb, R. T., "A Design Approach and Selected Wind Tunnel Results at High Subsonic Speeds for Wing-Tip Mounted Winglets," NASA TN D8260, 1976.

5 Chapman, D. R., "Computational Aerodynamics Development and Outlook," Dryden Lecture, 1979, *AIAA Journal*, Vol. 17, 1979, pp. 1293–1313.

6 Hess, J. L., and Smith, A. M. O., "Calculation of Non-Lifting Potential Flow About Arbitrary Three-Dimensional Bodies," Douglas Aircraft Report, ES 40622, 1962.

Downloaded 02 May 2010 to 171.66.16.250. Redistribution subject to ASME license or copyright; see http://www.asme.org/terms/Terms_Use.cfm

7 Rubbert, P. E., and Saaris, G. R., "A General Three Dimensional Potential Flow Method Applied to V/STOL Aerodynamics," SAE Paper 680304, 1968.

8 Hunt, B., "The Mathematical Basis and Numerical Principles of the Boundary Integral Method for Incompressible Potential Flow Over 3-D Aerodynamic Configurations, Numerical Methods in Fluid Dynamics," by Hunt, B., ed., Academic Press, New York, 1980, pp. 49–135.

9 Woodward, F. A., "An Improved Method for Aerodynamic Analysis of Wing-Body-Tail Configurations in Subsonic and Supersonic Flow," NASA CR 2228, 1973.

10 Murman, E. M., and Cole, J. D., "Calculation of Plane Steady Transonic Flows," *AIAA Journal*, Vol. 9, 1971, pp. 114–121.

11 Jameson, Antony, "Iterative Solution of Transonic Flows Over Airfoils and Wings, Including Flows at Mach 1," *Comm. Pure. Appl. Math.*, Vol. 27, 1974, pp. 283–309.

12 Albone, C. M., "A Finite Difference Scheme for Computing Supercritical Flows in Arbitrary Coordinate Systems," RAE Report 74090, 1974.

13 Murman, E. M., "Analysis of Embedded Shock Waves Calculated by Relaxation Methods," *AIAA Journal*.

14 Jameson, Antony, "Transonic Potential Flow Calculations in Conservation Form," *Proc. AIAA 2nd Computational Fluid Dynamics Conference*, Hartford, Conn., 1975, pp. 148–161.

15 Eberle, A., "A Finite Volume Method for Calculating Transonic Potential Flow Around Wings From the Minimum Pressure Integral," NASA TM 75324, translated from MBB UFE 1407(0), 1978.

16 Hafez, M., South, J. C., and Murman, E. M., "Artificial Compressibility Method for Numerical Solutions of Transonic Full Potential Equation," *AIAA Journal*, Vol. 17, 1979, pp. 838–844.

17 Holst, T. L., and Ballhaus, W. F., "Fast Conservative Schemes for the Full Potential Equation Applied to Transonic Flows," *AIAA Journal*, Vol. 17, 1979, pp. 145–152.

18 Lock, R. C., "A Modification to the Method of Garabedian and Korn," *Proc. GAMM Workshop on Numerical Methods for the Computation of Inviscid Transonic Flows With Shock Waves*, Stockholm, 1979, Rizzi, A., and Viviand, H., eds., Vieweg, 1981, pp. 116–124.

19 Jameson, Antony, "Numerical Solution of Nonlinear Partial Differential Equations of Mixed Type," *Proc. SYNSPADE 1975*, Hubbard, B., ed., Academic Press, New York, 1976, pp. 275–320.

20 Engquist, B., and Osher, S., "Stable and Entropy Satisfying Approximations for Transonic Flow Calculations," *Math. Comp.*, Vol. 34, 1980, pp. 45–75.

21 Goorjian, P., Meagher, M., and Van Buskirk, R., "Implicit Monotone Algorithms for the Small-Disturbance and Full Potential Equations Applied to Transonic Flows," AIAA Paper 0371, 1983.

22 Morawetz, C. S., "On the Non-Existence of Continuous Transonic Flow Past Profiles," *Comm. Pure. Appl. Math.*, Vol. 9, 1956, pp. 45–68.

23 Jameson, Antony, and Caughey, D. A., "A Finite Volume Method for Transonic Potential Flow Calculations," Proc. *AIAA 3rd Computational Fluid Dynamics Conference*, Albuquerque, N. Mex., 1977, pp. 35–54.

24 Jameson, Antony, "Remarks on the Calculation of Transonic Potential Flow by a Finite Volume Method," *Proc. IMA Conference on Numerical Methods in Applied Fluid Dynamics*, Reading, 1978, Hunt, B., ed., Academic Press, New York, 1980, pp. 363–386.

25 Bristeau, M. O., Pironneau, O., Glowinski, R., Periaux, J., Perrier, P., and Poirier, G., "Application of Optimal Control and Finite Element Methods to the Calculation of Transonic Flows and Incompressible Viscous Flows," *Proc. IMA Conference on Numerical Methods in Applied Fluid Dynamics*, Reading 1978, Hunt, B., ed., Academic Press, New York, 1980, pp. 203–312.

26 Ballhaus, W. F., Jameson, A., and Albert, J., "Implicit Approximate Factorization Schemes for Steady Transonic Flow Problems," *AIAA Journal*, Vol. 16, 1978, pp. 573–579.

27 Holst, T. L., and Thomas, S. D., "Numerical Solution of Transonic Wing Flow Fields," AIAA Paper 82-0105, 1982.

28 Baker, T. J., "Approximate Factorization Methods," *Proc. IMA Conference on Numerical Methods in Aeronautical Fluid Dynamics*, Reading, 1981, Roe, P. L., ed., Academic Press, New York, 1982, pp. 115–141.

29 Fedorenko, R. P., "The Speed of Convergence of One Iterative Process," *USSR Comp. Math. and Math. Phys.*, Vol. 4, 1964, pp. 227–235.

30 South, J. C., and Brandt, A., "Application of a Multi-Level Grid Method to Transonic Flow Calculations," *Proc. of Workshop on Transonic Flow Problems in Turbomachinery*, Monterey, 1976, Adamson, T. C., and Platzer, M. F., eds., Hemisphere, 1977.

31 Hackbusch, W., "On the Multi-Grid Method Applied to Difference Equations," *Computing*, Vol. 20, 1978, pp. 291–306.

32 Jameson, Antony, "Acceleration of Transonic Potential Flow Calculations on Arbitrary Meshes by the Multiple Grid Method," *Proc. AIAA 4th Computational Fluid Dynamics Conference*, Williamsburg, 1979, pp. 122–146.

33 Caughey, D. A., "Multigrid Calculation of Three-Dimensional Transonic Potential Flows," AIAA Paper 83-0374, 1983.

34 Lax, P. D., "Weak Solutions of Nonlinear Hyperbolic Equations and Their Numerical Computation," *Comm. Pure Appl. Math.*, Vol. 7, 1954, pp. 159–193.

35 Lax, P. D., and Richtmyer, R. D., "Survey of the Stability of Linear Finite Difference Equations," *Comm. Pure. Appl. Math.*, Vol. 9, 1956, pp. 267–293.

36 Lax, Peter, and Wendroff, Burton, "Systems of Conservation Laws," *Comm. Pure. Appl. Math.*, Vol. 13, 1960, pp. 217–237.

37 Lax, Peter, and Wendroff, Burton, "Difference Schemes for Hyperbolic Equations With High Order of Accuracy," *Comm. Pure. Appl. Math.*, Vol. 17, 1964, pp. 381–398.

38 Richtmyer, R. D., and Morton, K. W., *Finite Difference Methods for Initial Value Problems*, InterScience, New York, 1967.

39 Kriess, H. O., "Stability Theory of Difference Approximations for Mixed Initial Boundary Value Problems," *I. Math. Comp.*, Vol. 22, 1968, pp. 703–714.

40 Gustaffson, B., Kreiss, H. O., and Sundstrom, A., "Stability Theory of Difference Approximations for Mixed Initial Boundary Value Problems," *II, Math. Comp.*, Vol. 26, 1972, pp. 649–686.

41 Gustaffson, B., "The Convergence Rate for Difference Approximations to Mixed Initial Boundary Value Problems," *Math. Comp.*, Vol. 29, 1975, pp. 396–406.

42 Gustaffson, B., and Oliger, J., "Stable Boundary Discretizations for a Class of Time Discretizations of $u_t = AD_0 u_x$," Uppsala University Computer Science Report 87, 1980.

43 Engquist, B., and Majda, A., "Absorbing Boundary Conditions for the Numerical Simulation of Waves," *Math. Comp.*, Vol. 31, 1977, pp. 629–651.

44 Bayliss, A., and Turkel, E., "Far Field Boundary Conditions for Compressible Flows," *Proc. Symposium on Numerical Boundary Condition Procedures*, NASA CP 2201, 1981.

45 Moretti, Gino, "Calculations of Three Dimensional Inviscid Supersonic Flows," NASA CR 3573, 1982.

46 Arlinger, B. G., "Computation of Supersonic Flow Around Three Dimensional Wings," *Proc. 13th ICAS Congress*, Seattle, 1982, Vol. 2, pp. 224–232.

47 Veuillot, J. P., and Viviand, H., "Methodes Pseudo-Instationnaire pour le Calcul d'Ecoulements Transsoniques," ONERA Publication 1978-4, 1978.

48 Jameson, Antony, "Steady-State Solution of the Euler Equations for Transonic Flow," *Proc. Symposium on Transonic Shock, and Multidimensional Flows*, Madison, 1980, Meyer, ed., Academic Press, New York.

49 Magnus, R., and Yoshihara, H., "Inviscid Transonic Flow Over Airfoils," *AIAA Journal*, Vol. 8, 1970, pp. 2157–2162.

50 MacCormack, R. W., "The Effect of Viscosity in Hyper-Velocity Impact Cratering," AIAA Paper 69-354, 1969.

51 MacCormack, R. W., and Paullay, A. J., "Computational Efficiency Achieved by Time Splitting of Finite Difference Operators," AIAA Paper 72-154, 1972.

52 MacCormack, R. W., and Paullay, A. J., "The Influence of the Computational Mesh on Accuracy for Initial Value Problems With Discontinuous or Nonunique Solutions," *Computers and Fluids*, Vol. 2, 1974, pp. 339–360.

53 Rizzi, A. W., and Schmidt, W., "Finite Volume Method for Rotational Transonic Flow Problems," *Proc. 2nd GAMM Conference on Numerical Methods in Fluid Mechanics*, Hirschel, E. H., and Geller, W., eds., GAMM, 1977, pp. 152–161.

54 Lerat, A., and Sidès, J., "A New Finite Volume Method for the Euler Equations With Applications to Transonic Flows," *Proc. IMA Conference on Numerical Methods in Aeronautical Fluid Dynamics*, Reading, 1981, Roe, P. L., ed., Academic Press, New York, 1982, pp. 245–288.

55 Jameson, A., Schmidt, W., and Turkel, E., "Numerical Solution of the Euler Equations by Finite Volume Methods Using Runge-Kutta Time Stepping Schemes," AIAA Paper 81-1259, 1981.

56 Stetter, H. J., "Analysis of Discretization Methods for Ordinary Differential Equations," Springer, 1973.

57 Van der Houwen, P. J., "Construction of Integration Formulas for Ordinary Differential Equations," North Holland, 1977.

58 Beam, R. W., and Warming, R. F., "An Implicit Finite Difference Algorithm for Hyperbolic System in Conservation Form," *J. Comp. Phys.*, Vol. 23, 1976, pp. 87–110.

59 Rizzi, A., and Sköllermo, G., "Semi-Direct Solution to Steady Transonic Flow by Newton's Method," *Proc. 7th International Conference on Numerical Methods in Fluid Dynamics*, Stanford, 1980, Reynolds, W. C., and MacCormack, R. W., eds., Springer, 1981, pp. 349–353.

60 Gourlay, A. R., and Mitchell, A. R., "A Stable Implicit Difference Method for Hyperbolic Systems in Two Space Variables," *Numer. Math.*, Vol. 8, 1966, pp. 367–375.

61 Briley, W. R., and MacDonald, H., "Solution of the Three Dimensional Compressible Navier Stokes Equations by an Implicit Technique," *Proc. 4th International Conference on Numerical Methods in Fluid Dynamics*, 1974.

62 Steger, J. L., "Implicit Finite Difference Simulation of Flow About Arbitrary Two-Dimensional Geometries," *J. Comp. Phys.*, Vol. 16, 1978, pp. 679–686.

63 Jameson, A., and Turkel, E., "Implicit Schemes and LU Decompositions," *Math. Comp.*, Vol. 37, 1981, pp. 385–397.

64 Buratynski, E. K., "A Lower-Upper Factored Implicit Scheme for the Numerical Solution of the Euler Equations Applied to Arbitrary Cascades," Cornell University Thesis, Ithaca, N. Y., 1983.

65 Jameson, Antony, and Baker, T. J., "Solution of the Euler Equations for Complex Configurations," AIAA Paper 83-1929.

66 MacCormack, R. W., "A Numerical Method for Solving the Equations of Compressible Viscous Flows," AIAA Paper 81-110.

67 Lerat, A., Sidès, J., and Daru, V., "An Implicit Finite Volume Scheme for Solving the Euler Equations," *Proc. 8th International Conference on*

Downloaded 02 May 2010 to 171.66.16.250. Redistribution subject to ASME license or copyright; see http://www.asme.org/terms/Terms_Use.cfm

Numerical Methods in Fluid Dynamics, Aachen, 1982, Krause, E., ed., Springer, 1982, pp. 343-349.

68 Ni, R. H., "A Multiple Grid Scheme for Solving the Euler Equations," *Proc. AIAA 5th Computational Fluid Dynamics Conference*, Palo Alto, Calif., 1981, pp. 257-264.

69 Jameson, Antony, "Solution of the Euler Equations for Two Dimensional Transonic Flow by a Multigrid Method," presented at the International Multigrid Conference, Copper Mountain, 1983.

70 Hall, M. G., "Advances and Shortcomings in the Calculation of Inviscid Flows With Shock Waves," *Proc. IMA Conference on Numerical Methods in Aeronautical Fluid Dynamics*, Reading, 1981, Roe, P. L., ed., Academic Press, New York, 1982, pp. 33-60.

71 Courant, R., Isaacson, E., and Rees, M., "On the Solution of Nonlinear Hyperbolic Differential Equations," *Comm. Pure. Appl. Math.*, Vol. 5, 1952, pp. 243-255.

72 Steger, J. L., and Warming, R. F., "Flux Vector Splitting of the Inviscid Gas Dynamics Equations With Applications to Finite Difference Methods," *J. Comp. Phys.*, Vol. 40, 1981, pp. 263-293.

73 Godunov, S. K., "A Difference Method for the Numerical Calculation of Discontinuous Solutions of Hydrodynamic Equations," *Mat. Sbornik*, Vol. 47, 1959, pp. 271-306, translated as JPRS 7225 by U. S. Dept. of Commerce, 1960.

74 Engquist, Bjorn, and Osher, Stanley, "One-Sided Difference Approximations for Nonlinear Conservation Laws," *Math. Comp.*, Vol. 36, 1981, pp. 321-351.

75 Van Leer, Bram., "Flux Vector Splitting for the Euler Equations," *Proc. 8th International Conference on Numerical Methods in Fluid Dynamics Aachen*, 1982, Krause, E., ed., Springer, 1982, pp. 507-512.

76 Roe, P. L., "The Use of the Riemann Problem in Finite Difference Schemes," *Proc. 7th International Conference on Numerical Methods in Fluid Dynamics*, Stanford, 1980, Reynolds, W. C., and MacCormack, R. W., eds., Springer, 1981, pp. 354-359.

77 Roe, P. L., "Numerical Modelling of Shock Waves and Other Discontinuities," *Proc. IMA Conference on Numerical Methods in Aeronautical Fluid Dynamics*, Reading, 1981, Roe, P. L., ed., Academic Press, New York, 1982, pp. 211-243.

78 Lombard, G. K., Obiger, J., and Yang, J. Y., "A Natural Conservative Flux Difference Splitting for the Hyperbolic Equations of Gas Dynamics," AIAA Paper 82-0976, 1982.

79 Van Leer, Bram, "On the Relation Between the Upwind Differencing Schemes of Godunov, Engquist-Osher, and Roe," ICASE Report 81-11, 1981.

80 Harten, Amiram, Lax, Peter, and Van Leer, Bram, "On Upstream Differencing and Godunov-Type Schemes for Hyperbolic Conservation Laws," *SIAM Review*, Vol. 25, 1983, pp. 35-61.

81 Harten, Amiram, "On a Class of High Resolution Total Variation Stable Finite Difference Schemes," New York University Report DOE/ER/03077-176, 1982.

82 Boris, J. P., and Book, D. L., "Flux Corrected Transport, 1, SHASTA, A Fluid Transport Algorithm That Works," *J. Comp. Phys.*, Vol. 11, pp. 38-69.

83 Zalesak, Stephen, "Fully Multidimensional Flux Corrected Transport Algorithm for Fluids," *J. Comp. Phys.*, Vol. 31, 1979, pp. 335-362.

84 Harten, A., and Hyman, J., "Self-Adjusting Grid Methods for One Dimensional Hyperbolic Conservation Laws," Los Alamos National Laboratory Report, LA 9105, 1982.

85 Lock, R. C., and Firmin, M. C. P., "Survey of Techniques for Estimating Viscous Effects in External Aerodynamics," *Proc. IMA Conference on Numerical Methods in Aeronautical Fluid Dynamics*, Reading, 1980, Roe, P. L., ed., Academic Press, New York, 1982, pp. 337-430.

86 Le Balleur, J. C., "Numerical Viscid-Inviscid Interaction in Steady and Unsteady Flows," *Proc. 2nd Symposium on Numerical and Physical Aspects of Aerodynamic Flows*, Long Beach, Calif., 1983.

87 Melnik, R. E., "Turbulent Interactions on Airfoils at Transonic Speeds—Recent Developments," *Proc. AGARD Conference on Computation of Viscous-Inviscid Iteractions*, Colorado Springs, 1980, AGARD CP 291, Paper No. 10.

88 Lighthill, M. J., "On Displacement Thickness," *J. Fluid Mechanics*, Vol. 4, 1958, pp. 383-392.

89 Johnston, W., and Sockol, P., "Matching Procedure for Viscous-Inviscid Interactive Calculations," *AIAA Journal*, Vol. 17, 1979, pp. 661-663.

90 Carter, J. E., "A New Boundary Layer Inviscid Interation Technique for Separated Flow," *Proc. AIAA 4th Computational Fluid Dynamics Conference*, Williamsburg, 1979.

91 Le Balleur, J. C., Peyret, R., and Viviand, H., "Numerical Studies in High Reynolds Number Aerodynamics," *Computers and Fluids*, Vol. 8, 1980.

92 Bauer, F., Garabedian, P. R., Korn, D. G., and Jameson, A., *Supercritical Wing Sections II*," Springer Verlag, 1975.

93 Collyer, M. R., and Lock, R. C., "Prediction of Viscous Effects in Steady Transonic Flow Past an Aerofoil," *Aeronautical Quarterly*, Vol. 30, 1979.

94 Le Balleur, J. C., "Strong Matching Methods for Computing Transonic Viscous Flow Including Wakes and Separations—Lifting Airfoils," *La Recherche Aerospatiale*, Vol. 3, 1981.

95 Melnik, R. E., Chow, R. R., Mead, H. R., and Jameson, A., "A Multigrid Method for the Computation of Viscid/Inviscid Interaction on Airfoils," AIAA Paper 83-0234, 1983.

96 Whitfield, D. L., Thomas, J. L., Jameson, A., and Schmidt, W., "Computation of Transonic Viscous Inviscid Interacting Flow," *Proc. 2nd Symposium on Numerical and Physical Aspects of Aerodynamic Flows*, Long Beach, Calif., 1983.

97 Mehta, Unmeel, and Lomax, Harvard, "Reynolds Averaged Navier Stokes Computations of Transonic Flow—the State of the Art," *Proc. Transonic Perspectives Symposium*, Moffat Field, 1979, Nixon, D., ed., *AIAA*, 1981, pp. 297-375.

98 MacCormack, R. W., and Baldwin, B. S., "A Numerical Method for Solving the Navier Stokes Equations With Application to Shock Boundary Layer Interactions," AIAA Paper 75-1, 1975.

99 Deiwert, G. S., "Numerical Simulation of High Reynolds Number Transonic Flows," *AIAA Journal*, Vol. 13, 1975, pp. 1354-1359.

100 Shang, J. S., and Hankey, W. L., "Computation of Flow Past a Hypersonic Cruiser," *Proc. 2nd Symposium on Numerical and Physical Aspects of Aerodynamic Flows*, Long Beach, Calif., 1983.

101 Beam, R., and Warming, R. F., "An Implicit Factored Scheme for the Compressible Navier Stokes Equations," *AIAA Journal*, Vol. 16, pp. 393-402.

102 Bradshaw, P., "Structure of Turbulence in Complex Flows," AGARD LS 94, 1978.

103 Lighthill, M. J., "A New Method of Two Dimensional Aerodynamic Design," ARC, Rand M 2112, 1945.

104 James, R. M., "A New Look at Incompressible Airfoil Theory," McDonnell Douglas Report J 0198, 1971.

105 McFadden, G. B., "An Artificial Viscosity Method for the Design of Supercritical Airfoils," New York University Thesis, 1979.

106 Taverna, Frank, "Advanced Airfoil Design for General Aviation Propellers," AIAA Paper 83-1791, 1983.

107 Tranen, J. L., "A Rapid Computer Aided Transonic Airfoil Design Method," AIAA Paper 74-501, 1974.

108 Volpe, G., and Melnik, R. E., "The Role of Constraints in the Inverse Design Problem for Transonic Airfoils," AIAA Paper 81-1233, 1981.

109 Henne, P. A., "An Inverse Transonic Wing Design Method," AIAA Paper 80-0330, 1980.

110 Garabedian, P., and McFadden, G., "Computational Fluid Dynamics of Airfoils and Wings," *Proc. of Symposium on Transonic, Shock, and Multidimensional Flows*," Madison, 1981, Meyer, R., ed., Academic Press, New York, 1982, pp. 1-16.

111 Garabedian, P. R., and Korn, D. G., "Numerical Design of Transonic Airfoils," *Proc. SYNSPADE 1970*, Hubbard, B., ed., Academic Press, New York, 1971, pp. 253-271.

112 Bauer, F., Garabedian, P., and Korn, D., "Supercritical Wing Sections," Springer, 1972.

113 Hicks, R. M., and Henne, P. A., "Wing Design by Numerical Optimization," AIAA Paper 79-0080, 1979.

114 Kutler, Paul, "A Perspective of Theoretical and Applied Computational Fluid Dynamics," AIAA Paper 83-0037, 1983.

115 Ballhaus, W. F., "Computational Aerodynamics and Design," *Proc. 8th International Conference on Numerical Methods in Fluid Dynamics*, Aachen, 1982, Krause, E., ed., Springer, 1982, pp. 1-20.

116 Hall, M. G., "Computational Fluid Dynamics—A Revolutionary Force in Aerodynamics," *Proc. AIAA 5th Computational Fluid Dynamics Conference*, Palo Alto, Calif., 1981, pp. 176-188.

Downloaded 02 May 2010 to 171.66.16.250. Redistribution subject to ASME license or copyright; see http://www.asme.org/terms/Terms_Use.cfm

T. R. Kane
Professor of Applied Mechanics,
Stanford University,
Stanford, Calif. 94305
Fellow ASME

D. A. Levinson
Senior Scientist,
Lockheed Palo Alto
Research Laboratory,
Palo Alto, Calif. 94304
Mem. ASME

Multibody Dynamics

Figure 1 is a schematic representation of the Stanford Arm, a robotic manipulator consisting of six connected bodies, $A, \ldots, F$, capable of moving relative to each other, and Fig. 2 shows plots of associated generalized coordinates, $q_1, \ldots, q_6$, as functions of time. These curves could not have been produced 50 years ago, for their construction involves solving simultaneously 12 first-order nonlinear differential equations, an undertaking that is carried out routinely today, but that could not be accomplished prior to the advent of electronic computers. This is an important realization, for the possibility of solving large systems of nonlinear differential equations has had a profound impact on the field of dynamics, an impact that has manifested itself most notably in widespread attempts to develop so-called multibody (or n-body) computer programs, that is, programs intended to simultaneously generate (numerically) and solve equations of motion for user-specified arrangements of connected bodies. Indeed, the subject of multibody dynamics has formed the basis for symposia [e.g., 1], and the literature in this field is so extensive as to preclude comprehensive, detailed review. (Long lists of references can be found in [2-4].) However, one can identify in this literature certain major concerns, and one can propose ways to address these. It is the purpose of the present paper to do both.

Multibody program development has proceeded simultaneously in essentially three fields, namely spacecraft dynamics, machine design, and robotics, with relatively little interdisciplinary interaction. In the field of spacecraft dynamics, the first paper describing a quite general multibody program, published by Hooker and Margulies [5] in 1965, involved an algorithm based on Newton-Euler equations. The following year, Roberson and Wittenburg [6] reported on a similar effort, and a host of additional papers [e.g., 7-25] soon followed. Most of these works were based either on Newton-Euler equations [e.g., 7, 8, 10, 11, 13, 14, 16, 18, 19, 22, 25], Lagrange's equations [e.g., 9, 12, 15, 21, 24], or a combination of these [e.g., 20, 23].

The authors of the papers just cited were confronted by serious difficulties intrinsic to the use of Newton-Euler or Lagrange equations. When relying on the former, they were burdened, in the formulation of algorithms, by the extensive effort required to eliminate nonworking constraint forces; when appealing to the latter, thus being relieved of this burden, they had to face new problems, such as those pointed out by Keat [9], who says, "The Lagrange approach . . . has several disadvantages. The manual labor needed to derive and

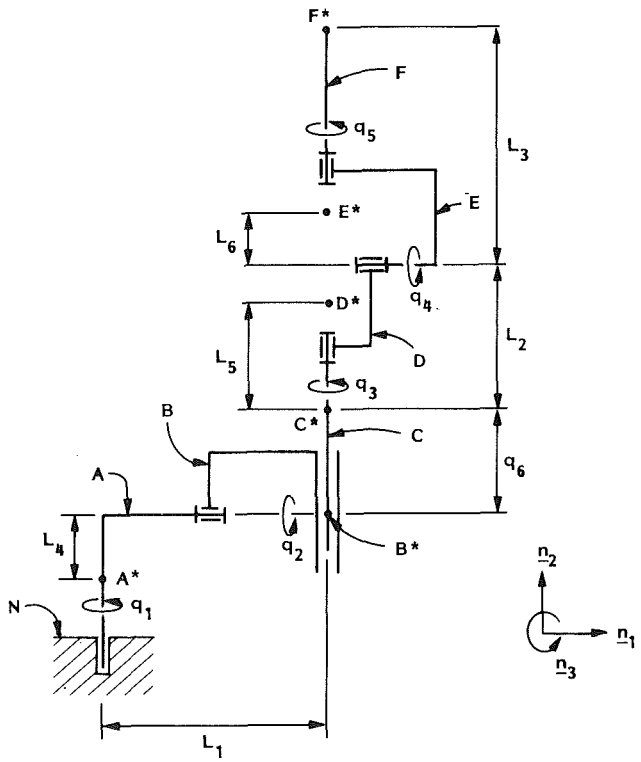


Fig. 1 Schematic representation of Stanford Arm

Contributed by the Applied Mechanics Division for publication in the JOURNAL OF APPLIED MECHANICS.
Discussion on this paper should be addressed to the Editorial Department, ASME, United Engineering Center, 345 East 47th Street, New York, N.Y. 10017, and will be accepted until two months after final publication of the paper itself in the JOURNAL OF APPLIED MECHANICS. Manuscript received by ASME Applied Mechanics Division, February, 1983.

Copyright © 1983 by ASME
Downloaded 02 May 2010 to 171.66.16.250. Redistribution subject to ASME license or copyright; see http://www.asme.org/terms/Terms_Use.cfm

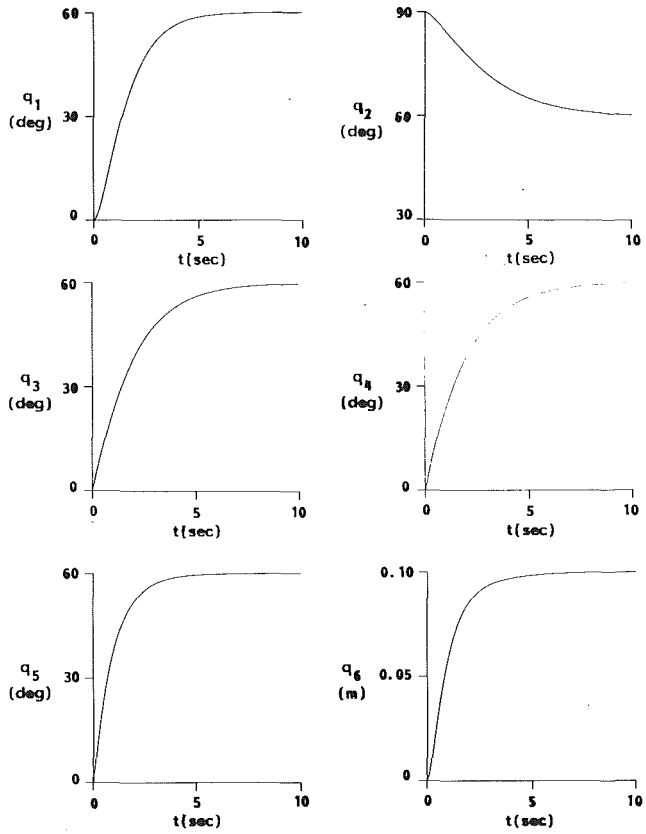


Fig. 2 Time histories of generalized coordinates

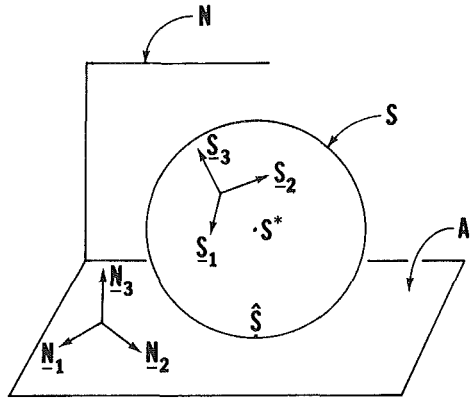


Fig. 3 Sphere on horizontal plane

differentiate the kinetic energy expression can be time consuming and difficult to accomplish without error. The resulting equations are difficult to modify after they have been developed, and the significance of individual terms is often obscure. In satellite problems, the resulting rotation equations often are less convenient than those obtained by angular momentum techniques. The generalized forces of rotation are not merely torque vector components resolved on an orthogonal frame, and the possibility of simplifying the rotation equations by using internal torques is precluded. Assuming that attitude is specified by Euler angles, the dynamics equations are made cumbersome by the presence of trigonometric functions of these angles." These obstacles are not overcome by the use of a computer; indeed they can encumber a computer program to such an extent that the program's utility may be outweighed by its unwieldiness. As a case in point, the voluminous user's manual [24] accompanying the Lagrange-based DISCOS multibody program contains a disclaimer stating that, "DISCOS . . . is not an easy program to understand and effectively apply . . . . The user is expected to have an extensive working knowledge of rigid and flexible-body dynamics, finite-element techniques, numerical methods, and frequency-domain analysis."

In the relevant machine design literature [e.g., 26–33], where the use of Lagrange's equations predominates [e.g., 26–30, 32, 33], constraints give rise to special concerns, for machines tend to possess relatively few degrees of freedom while being composed of relatively many connected bodies, which means that one must confront what has come to be known as the problem of closed loops. To come to grips with this, most authors have resorted to the use of Lagrange multipliers, which entails the introduction and subsequent elimination of quantities not of interest in their own right.

In the literature on robotics [e.g., 34–42], one finds that most multibody programs are based on Newton-Euler [e.g., 35, 37, 39, 42] or Lagrange [e.g., 34, 38, 42] equations. Here, an important consideration is the speed with which forces and torques can be evaluated, and simulations of motions performed, for this can bear crucially on the operation of a robotic device. Awareness of this problem comes into evidence in nearly every paper dealing with the dynamics of robots.

What the literature reveals very clearly is that the following issue is of major concern: Which method of dynamics provides the best basis for the solution of multibody dynamics problems? We believe that we can deal with this question most incisively by considering a particular problem in detail, rather than by undertaking a discussion in general terms, but here we are confronted by a dilemma. The question under consideration arises first and foremost because of the complexity of multibody dynamics problems, and this very complexity renders any truly representative example unsuitable for detailed treatment within the confines of a journal article. The discussion of an unrepresentatively simple and pleasingly transparent problem, on the other hand, can demean the issues to be faced, potentially to the extent of creating the false impression that the issues are trivial. Counting on our readers' perspicacity in this regard, we shall consider an example that, while simple enough to be manageable, permits us to draw inferences that are pivotal in connection with the complex problems ultimately of interest.

In what follows, we focus attention on the *labor* that must be expended in formulating equations of motion and on the *form* assumed by these equations. The latter determines the number of operations required for a numerical solution of the equations, while the former has a direct bearing on the expenditure of analysts' time or, when a symbol manipulation computer program is brought into play, on the associated expenditure of computer time. The method employed to formulate equations of motion has a decisive effect on both.

The burdens associated with eliminating nonworking constraint forces when one uses Newton-Euler equations are well known, for they manifest themselves, albeit harmlessly, even in connection with relatively simple textbook problems. On the other hand, serious shortcomings of the widely used Lagrange equations do not come to light until one attempts to attack a sufficiently complex problem. Similarly, the difficulties inherent in virtual work methods, which are currently in extensive use, become apparent only when one tries to employ these methods in nontrivial situations. Therefore, we forego further discussion of the Newton-Euler equations, and devote the remainder of this paper to contrasting the classical Lagrangian result [43],

$$\frac{d}{dt}\frac{\partial T}{\partial \dot{q}_r} - \frac{\partial T}{\partial q_r} = Q_r + \sum_{s=1}^{m} \lambda_s A_{sr} \quad (r = 1, \ldots, n) \qquad (1)$$

Downloaded 02 May 2010 to 171.66.16.250. Redistribution subject to ASME license or copyright; see http://www.asme.org/terms/Terms_Use.cfm

and various virtual work principles, on the one hand, with four interpretations of the equations [44]

$$F_r + F_r^* = 0 \quad (r = 1, \ldots, n-m) \tag{2}$$

on the other hand. Equations (2) represent an generalization of equations (1), and, like equations (1), apply to both holonomic and nonholonomic systems.

Turning to the specific example to be discussed in detail, we direct attention to Fig. 3, which shows a sphere S of radius R and mass M moving in contact with a horizontal plane A that is fixed in a Newtonian reference frame N. The mass center of S is presumed to coincide with S^*, the geometric center of S, but, rather than having equal moments of inertia about all lines passing through S^*, S has central principal moments of inertia I_1, I_2, I_3; the associated principal axes are parallel to unit vectors $\mathbf{S}_1$, $\mathbf{S}_2$, $\mathbf{S}_3$, respectively. Finally, $\mathbf{N}_1$, $\mathbf{N}_2$, $\mathbf{N}_3$ are mutually perpendicular unit vectors fixed in N, with $\mathbf{N}_3$ pointing vertically upward.

Considering, for the time being, solely motions during which S slides on A subject to the laws of Coulomb friction, let us examine what is involved in the numerical simulation of such motions.

To use equations (1) for the formulation of differential equations of motion, one must introduce five generalized coordinates. The first three may be taken to be orientation angles q_1, q_2, q_3 generated by aligning $\mathbf{S}_1$, $\mathbf{S}_2$, $\mathbf{S}_3$ with $\mathbf{N}_1$, $\mathbf{N}_2$, $\mathbf{N}_3$, respectively, and then subjecting S to successive rotations characterized by the vectors $q_1\mathbf{S}_1$, $q_2\mathbf{S}_2$, $q_3\mathbf{S}_3$; the two remaining generalized coordinates, q_4 and q_5, are defined conveniently as $\mathbf{p} \cdot \mathbf{N}_1$ and $\mathbf{p} \cdot \mathbf{N}_2$, respectively, where $\mathbf{p}$ is the position vector from a point fixed in A to the point S^*. And, after defining ω_i as $\omega_i \triangleq \boldsymbol{\omega} \cdot \mathbf{S}_i$ $(i = 1, 2, 3)$, where $\boldsymbol{\omega}$ denotes the angular velocity of S in N, and introducing ω_4 and ω_5 as $\omega_4 \triangleq \dot{q}_4$ and $\omega_5 \triangleq \dot{q}_5$, one can write the kinematical differential equations

$$\dot{q}_1 = (\omega_1 c_3 - \omega_2 s_3)/c_2 \tag{3}$$

$$\dot{q}_2 = \omega_1 s_3 + \omega_2 c_3 \tag{4}$$

$$\dot{q}_3 = (-\omega_1 c_3 + \omega_2 s_3) s_2/c_2 + \omega_3 \tag{5}$$

$$\dot{q}_4 = \omega_4 \tag{6}$$

$$\dot{q}_5 = \omega_5 \tag{7}$$

where s_i and c_i denote $\sin q_i$ and $\cos q_i$ $(i = 1, 2, 3)$, respectively, and express T, the kinetic energy of S in N, as

$$T = \frac{1}{2}[I_1\omega_1^2 + I_2\omega_2^2 + I_3\omega_3^2 + M(\omega_4^2 + \omega_5^2)] \tag{8}$$

Next, one must form the partial derivatives $\partial T/\partial \dot{q}_r$ $(r = 1, \ldots, 5)$, obtaining

$$\frac{\partial T}{\partial \dot{q}_1} = I_1\omega_1 c_2 c_3 - I_2\omega_2 c_2 s_3 + I_3\omega_3 s_2 \tag{9}$$

$$\frac{\partial T}{\partial \dot{q}_2} = I_1\omega_1 s_3 + I_2\omega_2 c_3, \quad \frac{\partial T}{\partial \dot{q}_3} = I_3\omega_3 \tag{10}$$

$$\frac{\partial T}{\partial \dot{q}_4} = M\omega_4, \quad \frac{\partial T}{\partial \dot{q}_5} = M\omega_5 \tag{11}$$

as well as the partial derivatives $\partial T/\partial q_r$ $(r = 1, \ldots, 5)$, given by

$$\frac{\partial T}{\partial q_1} = 0, \quad \frac{\partial T}{\partial q_2} = (-I_1\omega_1 s_2 c_3 + I_2\omega_2 s_2 s_3 + I_3\omega_3 c_2)\dot{q}_1 \tag{12}$$

$$\frac{\partial T}{\partial q_3} = I_1\omega_1(-c_2 s_3 \dot{q}_1 + c_3\dot{q}_2) - I_2\omega_2(c_2 c_3 \dot{q}_1 + s_3\dot{q}_2) \tag{13}$$

$$\frac{\partial T}{\partial q_4} = \frac{\partial T}{\partial q_5} = 0 \tag{14}$$

Furtheremore, it is necessary to make use of the fact that the generalized forces $Q_1, \ldots, Q_5$ appearing in equation (1) can be written

$$Q_1 = RP_2, \quad Q_2 = -Rc_1P_1, \quad Q_3 = R(s_1c_2P_1 + s_2P_2) \tag{15}$$

$$Q_4 = P_1, \quad Q_5 = P_2 \tag{16}$$

where P_1 and P_2 are scalars such that the friction force exerted by A on S is given by $P_1\mathbf{N}_1 + P_2\mathbf{N}_2$, and to observe that, since no nonholonomic constraints come into play during sliding, the right-hand members of equations (1) consist solely of Q_r $(r = 1, \ldots, 5)$. Thereupon, one can complete the formulation of dynamical differential equations of motion by substituting from equations (9)–(16) into equations (1), which leads to

$$I_1c_2c_3\dot{\omega}_1 - I_2c_2s_3\dot{\omega}_2 + I_3s_2\dot{\omega}_3 = I_1\omega_1(s_2c_3\dot{q}_2 + c_2s_3\dot{q}_3) - I_2\omega_2(s_2s_3\dot{q}_2 - c_2c_3\dot{q}_3) - I_3\omega_3c_2\dot{q}_2 + RP_2 \tag{17}$$

$$I_1s_3\dot{\omega}_1 + I_2c_3\dot{\omega}_2 = -I_1\omega_1c_3(s_2\dot{q}_1 + \dot{q}_3) + I_2\omega_2s_3(s_2\dot{q}_1 + s_3\dot{q}_3) + I_3\omega_3c_2\dot{q}_1 - Rc_1P_1 \tag{18}$$

$$I_3\dot{\omega}_3 = I_1\omega_1(-c_2s_3\dot{q}_1 + c_3\dot{q}_2) - I_2\omega_2(c_2c_3\dot{q}_1 + s_3\dot{q}_2) + R(s_1c_2P_1 + s_2P_2) \tag{19}$$

$$M\dot{\omega}_4 = P_1, \quad M\dot{\omega}_5 + P_2. \tag{20}$$

When basing the formulation of dynamical equations of motion on equations (2), one begins by designating generalized speeds. Since the labor performed in deriving equations (17)–(20) from equations (1), and that entailed in deducing the corresponding equations from equations (2), can be compared most easily by using as generalized speeds the quantities $\dot{q}_r$ $(r = 1, \ldots, 5)$, we do this for now, and note that, concomitantly, $\boldsymbol{\Omega}_r$ $(r = 1, \ldots, 5)$, the partial angular velocities of S in N, and $\mathbf{V}_r$ $(r = 1, \ldots, 5)$, the partial velocities of S^* in N, found simply by inspecting precisely the angular velocity and velocity expressions previously used to form T, may be written

$$\boldsymbol{\Omega}_1 = c_2c_3\mathbf{S}_1 - c_2s_3\mathbf{S}_2 + s_2\mathbf{S}_3 \tag{21}$$

$$\boldsymbol{\Omega}_2 = s_3\mathbf{S}_1 + c_3\mathbf{S}_2, \quad \boldsymbol{\Omega}_3 = \mathbf{S}_3, \quad \boldsymbol{\Omega}_4 = \boldsymbol{\Omega}_5 = 0 \tag{22}$$

$$\mathbf{V}_1 = \mathbf{V}_2 = \mathbf{V}_3 = 0, \quad \mathbf{V}_4 = \mathbf{N}_1, \quad \mathbf{V}_5 = \mathbf{N}_2 \tag{23}$$

These are used to form expressions for the generalized inertia forces F_r^* $(r = 1, \ldots, 5)$ in accordance with the relationship

$$F_r^* = \boldsymbol{\Omega}_r \cdot \mathbf{T}^* - M\mathbf{V}_r \cdot \mathbf{a} \quad (r = 1, \ldots, 5) \tag{24}$$

where $\mathbf{T}^*$, the inertia torque for S in N, is given by

$$\mathbf{T}^* = [(I_2 - I_3)\omega_2\omega_3 - I_1\dot{\omega}_1]\mathbf{S}_1 + [(I_3 - I_1)\omega_3\omega_1 - I_2\dot{\omega}_2]\mathbf{S}_2 + [(I_1 - I_2)\omega_1\omega_2 - I_3\dot{\omega}_3]\mathbf{S}_3 \tag{25}$$

while $\mathbf{a}$, the acceleration of S^* in N, can be written

$$\mathbf{a} = \ddot{q}_4\mathbf{N}_1 + \ddot{q}_5\mathbf{N}_2 \tag{26}$$

Expressions for F_r $(r = 1, \ldots, 5)$, the generalized active forces appearing in equations (2), are derived from the relationships

$$F_r = \hat{\mathbf{V}}_r \cdot (P_1\mathbf{N}_1 + P_2\mathbf{N}_2) \quad (r = 1, \ldots, 5) \tag{27}$$

where $\hat{\mathbf{V}}_1, \ldots, \hat{\mathbf{V}}_5$ are the partial velocities of the point $\hat{S}$ of S that is in contact with A, that is,

$$\hat{\mathbf{V}}_1 = R\mathbf{N}_2, \quad \hat{\mathbf{V}}_2 = -Rc_1\mathbf{N}_1, \quad \hat{\mathbf{V}}_3 = R(s_1c_2\mathbf{N}_1 + s_2\mathbf{N}_2) \tag{28}$$

$$\hat{\mathbf{V}}_4 = \mathbf{N}_1, \quad \hat{\mathbf{V}}_5 = \mathbf{N}_2 \tag{29}$$

Substitution from equations (25) and (26) into equations (24), and from equations (28) and (29) into equations (27), followed by use of equations (2), leads to

$$I_1c_2c_3\dot{\omega}_1 - I_2c_2s_3\dot{\omega}_2 + I_3s_2\dot{\omega}_3 = (I_1 - I_2)s_2\omega_1\omega_2 + [(I_2 - I_3)c_3\omega_2 + (I_1 - I_3)s_3\omega_1]c_2\omega_3 + RP_2 \tag{30}$$

Downloaded 02 May 2010 to 171.66.16.250. Redistribution subject to ASME license or copyright; see http://www.asme.org/terms/Terms_Use.cfm

$$I_1 s_3 \dot{\omega}_1 + I_2 c_3 \dot{\omega}_2 = [(I_2 - I_3) s_3 \omega_2 + (I_3 - I_1) c_3 \omega_1] \omega_3 - R c_1 P_1 \quad (31)$$

$$I_3 \dot{\omega}_3 = (I_1 - I_2) \omega_1 \omega_2 + R (s_1 c_2 P_1 + s_2 P_2) \quad (32)$$

$$M \dot{\omega}_4 = P_1, \quad M \dot{\omega}_5 = P_2 \quad (33)$$

The left-hand members of equations (30)–(33) are identical to those of equations (17)–(20), respectively, and the right-hand members of equations (17)–(20) reduce to those of equations (30)–(33), respectively, when $\dot{q}_1$, $\dot{q}_2$, and $\dot{q}_3$ are eliminated from equations (17)–(20) by making use of equations (3)–(5). We shall comment on the forms of the right-hand sides of equations (17)–(19), on the one hand, and equations (30)–(32), on the other hand, after assessing the relative amounts of labor expended in forming the two sets of equations.

The derivation of equations (17)–(20) involves 15 differentiations, namely the 10 partial differentiations represented by equations (9)–(14) plus the time-differentiation of each of equations (9)–(11). The corresponding task associated with equations (30)–(33) is the evaluation of the 10 dot-products in equations (24). Clearly, the latter process is less laborious than the former. However, the use of equations (2) entails working with an acceleration vector that is not needed in connection with equations (1). In the present example, this imposes no burden; in general, the worst that can happen is that one must perform time differentiations of available velocity vectors, a task that need not be any more laborious than that of squaring the same velocity vectors for use in forming T. Hence, one may expect, in general, to expend considerably less effort when using equations (2) to formulate dynamical equations of motion than when calling on equations (1) for this purpose.

Now a few words about the difference in the forms of the expressions appearing in right-hand sides of equations (17)–(19) and equations (30)–(32). To evaluate these expressions for a given instant of time, which one must do many times during the course of a numerical solution of the equations, one needs to perform 44 multiplications and 15 additions in the case of equations (17)–(19), but only 22 multiplications and 13 additions when working with equations (30)–(32). Obviously, therefore, the latter set of equations is preferable to the former. Now, as was pointed out previously, use of equations (3)–(5) makes it possible to transform equations (17)–(19) into equations (30)–(32). But an analyst who has not seen equations (30)–(32) would have no motivation for such an undertaking and would certainly expend additional effort in carrying it out. Thus, it may be concluded that use of equations (2) not only is less laborious than is that of equations (1), but leads to equations having a superior form for purposes of numerical integration.

As we shall now demonstrate by working with equations (2) and taking certain generalized speeds to be quantities other than time-derivatives of generalized coordinates, equations (30)–(33) can be replaced with equations still better suited for numerical integration. Specifically, if generalized speeds u_r ($r = 1, \ldots, 5$) are defined as $u_r \triangleq \omega_r$ ($r = 1, 2, 3$), $u_4 \triangleq \dot{q}_4$, and $u_5 \triangleq \dot{q}_5$, then equations (21) and (22) give way to

$$\boldsymbol{\Omega}_1 = \mathbf{S}_1, \quad \boldsymbol{\Omega}_2 = \mathbf{S}_2, \quad \boldsymbol{\Omega}_3 = \mathbf{S}_3, \quad \boldsymbol{\Omega}_4 = \boldsymbol{\Omega}_5 = 0 \quad (34)$$

Equations (23)–(27) and (29) remain applicable, but equations (28) are replaced with

$$\begin{aligned} \hat{\mathbf{V}}_1 &= R(-C_{21}\mathbf{N}_1 + C_{11}\mathbf{N}_2) \\ \hat{\mathbf{V}}_2 &= R(-C_{22}\mathbf{N}_1 + C_{12}\mathbf{N}_2) \\ \hat{\mathbf{V}}_3 &= R(-C_{23}\mathbf{N}_1 + C_{13}\mathbf{N}_2) \end{aligned} \quad (35)$$

where C_{ij}, defined as $C_{ij} \triangleq \mathbf{N}_i \cdot \mathbf{S}_j$ ($i = 1, 2; j = 1, 2, 3$), are given by

$$C_{11} = c_2 c_3, \quad C_{12} = -c_2 s_3, \quad C_{13} = s_2 \quad (36)$$

$$C_{21} = s_1 s_2 c_3 + s_3 c_1, \quad C_{22} = -s_1 s_2 s_3 + c_3 c_1, \quad C_{23} = -s_1 c_2 \quad (37)$$

Hence, after forming F_r^* ($r = 1, 2, 3$) with the aid of equations (24)–(26), (34), and (23), and using equations (27), (35), and (29) to construct F_r ($r = 1, 2, 3$), one finds that equations (2) lead to the following replacements for equations (30)–(32):

$$\dot{\omega}_1 = [(I_2 - I_3)\omega_2 \omega_3 - R(C_{21}P_1 - C_{11}P_2)]/I_1 \quad (38)$$

$$\dot{\omega}_2 = [(I_3 - I_1)\omega_3 \omega_1 - R(C_{22}P_1 - C_{12}P_2)]/I_2 \quad (39)$$

$$\dot{\omega}_3 = [(I_1 - I_2)\omega_1 \omega_2 - R(C_{23}P_1 - C_{13}P_2)]/I_3 \quad (40)$$

The advantage of these equations over equations (30)–(32) is that they are *uncoupled* in $\dot{\omega}_1$, $\dot{\omega}_2$, $\dot{\omega}_3$, and are, therefore, ideally suited to being integrated simultaneously with the kinematical equations, equations (3)–(7), and the remaining dynamical equations, equations (33). By way of contrast, to integrate equations (30)–(32) simultaneously with equations (3)–(7) and (33), one must either first employ analytical methods to solve equations (30) and (31) for $\dot{\omega}_1$ and $\dot{\omega}_2$, or resort to numerical means to effect such a solution at every time-step of a numerical integration of the equations. Both courses of action lead to simulation algorithms inferior to one based on equations (38)–(40).

It should now be evident that equations (1) suffer from a fundamental flaw: they do not permit one to work sufficiently directly with dependent variables other than generalized coordinates, or, to put it another way, with generalized speeds other than time derivatives of generalized coordinates. The Boltzmann-Hamel equations [45, 46], sometimes referred to as Lagrange's quasi-coordinate equations, represent an early attempt to remedy this defect, but this endeavor can hardly be regarded as having been successful when one considers what is involved in writing these equations. To do so for the system at hand, one begins by solving equations (3)–(7) for $\omega_1, \ldots, \omega_5$, which yields

$$\omega_1 = c_2 c_3 \dot{q}_1 + s_3 \dot{q}_2, \quad \omega_2 = -c_2 s_3 \dot{q}_1 + c_3 \dot{q}_2, \quad \omega_3 = s_2 \dot{q}_1 + \dot{q}_3 \quad (41)$$

$$\omega_4 = \dot{q}_4, \quad \omega_5 = \dot{q}_5 \quad (42)$$

Next, one compares equations (41) and (42) with

$$\omega_j = \sum_{i=1}^{5} \alpha_{ij} \dot{q}_i \quad (j = 1, \ldots, 5) \quad (43)$$

to identify the 25 quantities α_{ij} ($i, j = 1, \ldots, 5$) obtaining

$$\alpha_{11} = c_2 c_3, \quad \alpha_{21} = s_3, \quad \alpha_{31} = \alpha_{41} = \alpha_{51} = 0 \quad (44)$$

$$\alpha_{12} = -c_2 s_3, \quad \alpha_{22} = c_3, \quad \alpha_{32} = \alpha_{42} = \alpha_{52} = 0 \quad (45)$$

$$\alpha_{13} = s_2, \quad \alpha_{23} = 0, \quad \alpha_{33} = 1, \quad \alpha_{43} = \alpha_{53} = 0 \quad (46)$$

$$\alpha_{14} = \alpha_{24} = \alpha_{34} = 0, \quad \alpha_{44} = 1, \quad \alpha_{54} = 0 \quad (47)$$

$$\alpha_{15} = \alpha_{25} = \alpha_{35} = \alpha_{45} = 0, \quad \alpha_{55} = 1 \quad (48)$$

and, similarly, finds β_{ij} ($i, j = 1, \ldots, 5$) by comparing equations (3)–(7) with

$$\dot{q}_i = \sum_{j=1}^{5} \beta_{ij} \omega_j \quad (i = 1, \ldots, 5) \quad (49)$$

which leads to

$$\beta_{11} = c_3/c_2, \quad \beta_{12} = -s_3/c_2, \quad \beta_{13} = \beta_{14} = \beta_{15} = 0 \quad (50)$$

$$\beta_{21} = s_3, \quad \beta_{22} = c_3, \quad \beta_{23} = \beta_{24} = \beta_{25} = 0 \quad (51)$$

$$\beta_{31} = -c_3 s_2/c_2, \quad \beta_{32} = s_3 s_2/c_2, \quad \beta_{33} = 1, \quad \beta_{34} = \beta_{35} = 0 \quad (52)$$

$$\beta_{41} = \beta_{42} = \beta_{43} = 0, \quad \beta_{44} = 1, \quad \beta_{45} = 0 \quad (53)$$

$$\beta_{51} = \beta_{52} = \beta_{53} = \beta_{54} = 0, \quad \beta_{55} = 1 \quad (54)$$

Downloaded 02 May 2010 to 171.66.16.250. Redistribution subject to ASME license or copyright; see http://www.asme.org/terms/Terms_Use.cfm

Now one forms 125 quantities γ_{ijk} $(i, j, k = 1, \ldots, 5)$ as

$$\gamma_{ijk} = \sum_{r=1}^{5} \sum_{s=1}^{5} \beta_{ri}\beta_{sk}\left(\frac{\partial \alpha_{rj}}{\partial q_s} - \frac{\partial \alpha_{sj}}{\partial q_r}\right) \quad (i, j, k = 1, \ldots, 5) \tag{55}$$

For example, with $i = 1, j = 2, k = 3$, this yields

$$\gamma_{123} = \sum_{r=1}^{5} \sum_{s=1}^{5} \beta_{r1}\beta_{s3}\left(\frac{\partial \alpha_{r2}}{\partial q_s} - \frac{\partial \alpha_{s2}}{\partial q_r}\right) \tag{56}$$

or, in view of equations (50)–(54),

$$\gamma_{123} = (c_3/c_2)\left(\frac{\partial \alpha_{12}}{\partial q_3} - \frac{\partial \alpha_{32}}{\partial q_1}\right) + s_3\left(\frac{\partial \alpha_{22}}{\partial q_3} - \frac{\partial \alpha_{32}}{\partial q_2}\right) \tag{57}$$

so that, referring to equations (44)–(48), one finally arrives at

$$\gamma_{123} = (c_3/c_2)(-c_2c_3) + s_3(-s_3) = -1 \tag{58}$$

After performing similar operations 124 more times, one then writes T as in equation (8) and forms δ_i and ϵ_i $(i = 1, \ldots, 5)$ as

$$\delta_i = \sum_{j=1}^{5} \beta_{ji}\frac{\partial T}{\partial q_j}, \quad \epsilon_i = \frac{\partial T}{\partial \omega_i} \quad (i = 1, \ldots, 5) \tag{59}$$

which leads one, in the present case, to

$$\delta_i = 0 \quad (i = 1, \ldots, 5) \tag{60}$$

$$\epsilon_i = I_i\omega_i \quad (i = 1,2,3), \quad \epsilon_i = M\omega_i \quad (i = 4,5) \tag{61}$$

and this brings one into position to write dynamical equations of motion by substituting into the Boltzmann-Hamel equations,

$$\dot{\epsilon}_i + \sum_{j=1}^{5} \sum_{k=1}^{5} \gamma_{ijk}\omega_k\epsilon_j - \delta_i = \sum_{j=1}^{5} \beta_{ji}Q_j \quad (i = 1, \ldots, 5) \tag{62}$$

where Q_j $(j = 1, \ldots, 5)$ are given by equations (15). The resulting equations turn out to be precisely equations (38)–(40) and equations (33), but the labor expended to arrive at these via equations (62) can only be regarded as excessive when compared to that associated with the use of equations (2).

Whittaker [43, pp. 43–44] mentions a variant of equations (62) (applicable to a body with a fixed point) that leads to equations (38)–(40) considerably more directly than do equations (62), namely

$$\frac{d}{dt}\frac{\partial T}{\partial \omega_1} - \omega_3\frac{\partial T}{\partial \omega_2} + \omega_2\frac{\partial T}{\partial \omega_3} - \delta_1 = \sum_{j=1}^{5} \beta_{j1}Q_j \tag{63}$$

$$\frac{d}{dt}\frac{\partial T}{\partial \omega_2} - \omega_1\frac{\partial T}{\partial \omega_3} + \omega_3\frac{\partial T}{\partial \omega_1} - \delta_2 = \sum_{j=1}^{5} \beta_{j2}Q_j \tag{64}$$

$$\frac{d}{dt}\frac{\partial T}{\partial \omega_3} - \omega_2\frac{\partial T}{\partial \omega_1} + \omega_1\frac{\partial T}{\partial \omega_2} - \delta_3 = \sum_{j=1}^{5} \beta_{j3}Q_j \tag{65}$$

But even this alternative does not free one from the burden of having to form fifteen β's, and it fails to provide a basis for writing the remaining two dynamical equations of motion. We conclude that the best way to reap the benefits of working with $\omega_1, \ldots, \omega_5$ so as to generate equations (38)–(40) and equations (33) is to use equations (2).

Both equations (1) and equations (2) apply to systems subject to simple nonholonomic constraints, that is, constraints such that m nonintegrable differential equations of the form

$$\sum_{r=1}^{n} A_{sr}\dot{q}_r + B_s = 0 \quad (s = 1, \ldots, m) \tag{66}$$

are satisfied throughout all motions. For example, two such equations come into play when the sphere S and the plane A are so rough that S rolls on A without slipping, these equations being

$$-Rc_1\dot{q}_2 + Rs_1c_2\dot{q}_3 + \dot{q}_4 = 0 \tag{67}$$

and

$$R\dot{q}_1 + Rs_2\dot{q}_3 + \dot{q}_5 = 0 \tag{68}$$

which means that [see equations (66)]

$$A_{11} = 0, \quad A_{12} = -Rc_1, \quad A_{13} = Rs_1c_2, \quad A_{14} = 1, \quad A_{15} = 0 \tag{69}$$

$$A_{21} = R, \quad A_{22} = 0, \quad A_{23} = Rs_2, \quad A_{24} = 0, \quad A_{25} = 1 \tag{70}$$

and

$$B_1 = B_2 = 0 \tag{71}$$

Under these circumstances, equations (3)–(5) remain applicable; equations (6) and (7) are replaced, respectively, with

$$\dot{q}_4 = R(c_1\dot{q}_2 - s_1c_2\dot{q}_3) \tag{72}$$

and

$$\dot{q}_5 = -R(\dot{q}_1 + s_2\dot{q}_3) \tag{73}$$

which are simply alternate forms of equations (67) and (68), respectively; and the dynamical equations one obtains with the aid of equations (1) differ from their earlier counterparts, equations (17)–(20), only in that P_1 and P_2 are replaced by the Lagrange multipliers λ_1 and λ_2, respectively, while $\dot{\omega}_4$ and $\dot{\omega}_5$ give way to $\ddot{q}_4$ and $\ddot{q}_5$, respectively. However, the replacement of P_1 and P_2 with λ_1 and λ_2 is no mere formality. When one uses equations (17)–(20) to deal with motions of sliding, one can express P_1 and P_2 explicitly in terms of $q_1, \ldots, q_5$ and $\omega_1, \ldots, \omega_5$ by invoking the laws of Coulomb friction, which require that

$$P_1 = \frac{-\mu Mgv_1}{(v_1^2 + v_2^2)^{1/2}}, \quad P_2 = \frac{-\mu Mgv_2}{(v_1^2 + v_2^2)^{1/2}} \tag{74}$$

where v_1 and v_2 are defined as

$$v_1 \triangleq \omega_4 - R(\omega_1C_{21} + \omega_2C_{22} + \omega_3C_{23}) \tag{75}$$

$$v_2 \triangleq \omega_5 + R(\omega_1C_{11} + \omega_2C_{12} + \omega_3C_{13}) \tag{76}$$

while μ denotes the coefficient of kinetic friction, and g is the local gravitational acceleration. The multipliers λ_1 and λ_2 [or P_1 and P_2, when one uses equations (17)–(20) to deal with rolling], on the other hand, cannot be expressed in this fashion, for when S is rolling on A, nothing is known a priori about the magnitude or direction of the friction force exerted by A on S. To overcome this difficulty, one can begin by eliminating λ_1 and λ_2 (or P_1 and P_2) from equations (17)–(19) with the aid of equations (20), obtaining,

$$I_1c_2c_3\dot{\omega}_1 - I_2c_2s_3\dot{\omega}_2 + I_3s_2\dot{\omega}_3 = I_1\omega_1(s_2c_3\dot{q}_2 + c_2s_3\dot{q}_3) - I_2\omega_2(s_2s_3\dot{q}_2 - c_2c_3\dot{q}_3) - I_3\omega_3c_2\dot{q}_2 + RM\ddot{q}_5 \tag{77}$$

$$I_1s_3\dot{\omega}_1 + I_2c_3\dot{\omega}_2 = -I_1\omega_1c_3(s_2\dot{q}_1 + \dot{q}_3) + I_2\omega_2s_3(s_2\dot{q}_1 + \dot{q}_3) + I_3\omega_3c_2\dot{q}_1 - RMc_1\ddot{q}_4 \tag{78}$$

$$I_3\dot{\omega}_3 = I_1\omega_1(-c_2s_3\dot{q}_1 + c_3\dot{q}_2) - I_2\omega_2(c_2c_3\dot{q}_1 + s_3\dot{q}_2) + RM(s_1c_2\ddot{q}_4 + s_2\ddot{q}_5) \tag{79}$$

But now one is forced to construct two additional equations to restore the balance between the number (five) of unknown functions (ω_1, ω_2, ω_3, q_4, q_5) and the number (three) of equations [equations (77)–(79)] as yet available for the determination of these functions. The simplest way to generate the required two additional equations is to exploit the fact that during rolling, the acceleration of S^* in N is given both by

$$\mathbf{a} = R\dot{\boldsymbol{\omega}} \times \mathbf{N}_3 \tag{80}$$

where $\dot{\boldsymbol{\omega}}$ denotes the time derivative of $\boldsymbol{\omega}$ in N, and by

Downloaded 02 May 2010 to 171.66.16.250. Redistribution subject to ASME license or copyright; see http://www.asme.org/terms/Terms_Use.cfm

$$\mathbf{a} = \ddot{q}_4 \mathbf{N}_1 + \ddot{q}_5 \mathbf{N}_2 \tag{81}$$

so that

$$\ddot{q}_4 = \mathbf{a} \cdot \mathbf{N}_1 = R\dot{\omega} \times \mathbf{N}_3 \cdot \mathbf{N}_1 = R\dot{\omega} \cdot \mathbf{N}_2 \tag{82}$$

or, equivalently,

$$\ddot{q}_4 = R(\dot{\omega}_1 C_{21} + \dot{\omega}_2 C_{22} + \dot{\omega}_3 C_{23}) \tag{83}$$

and, similarly,

$$\ddot{q}_5 = \mathbf{a} \cdot \mathbf{N}_2 = -R\dot{\omega} \cdot \mathbf{N}_1 = -R(\dot{\omega}_1 C_{11} + \dot{\omega}_2 C_{12} + \dot{\omega}_3 C_{13}) \tag{84}$$

Equations (77)–(79), (83), and (84) suffice for the determination of ω_1, ω_2, ω_3, q_4, and q_5.

In the present context, a significant difference between equations (1) and (2) comes to light when the latter are used to formulate dynamical equations compatible with the nonholonomic constraint conditions expressed by equations (67) and (68) or, equivalently, equations (72) and (73). For, with the aid of equations (72) and (73) one can write for $\mathbf{v}$, the velocity of S^* in N,

$$\mathbf{v} = R[(c_1 \dot{q}_2 - s_1 c_2 \dot{q}_3)\mathbf{N}_1 - (\dot{q}_1 + s_2 \dot{q}_3)\mathbf{N}_2] \tag{85}$$

Hence, if $\dot{q}_r$ ($r = 1, \ldots, 5$) are once again chosen as generalized speeds, and $\dot{q}_1$, $\dot{q}_2$, $\dot{q}_3$ are regarded as independent of each other, but $\dot{q}_4$ and $\dot{q}_5$ are treated as dependent on $\dot{q}_1$, $\dot{q}_2$, $\dot{q}_3$ in accordance with equations (72) and (73), then $\mathbf{\Omega}_r$ ($r = 1, 2, 3$), here called nonholonomic partial angular velocities of S in A, and $\mathbf{V}_r$ ($r = 1, 2, 3$), the corresponding nonholonomic partial velocities of S^* in A, become

$$\mathbf{\Omega}_1 = c_2 c_3 \mathbf{S}_1 - c_2 s_3 \mathbf{S}_2 + s_2 \mathbf{S}_3, \quad \mathbf{\Omega}_2 = s_3 \mathbf{S}_1 + c_3 \mathbf{S}_2, \quad \mathbf{\Omega}_3 = \mathbf{S}_3 \tag{86}$$

and [see equation (85)]

$$\mathbf{V}_1 = -R\mathbf{N}_2, \quad \mathbf{V}_2 = Rc_1 \mathbf{N}_1, \quad \mathbf{V}_3 = -R(s_1 c_2 \mathbf{N}_1 + s_2 \mathbf{N}_2) \tag{87}$$

Furthermore, $\hat{\mathbf{V}}_r$ ($r = 1, 2, 3$), the associated nonholonomic partial velocities of point $\hat{S}$, all vanish, because the velocity of $\hat{S}$ is equal to zero when S rolls on A without slipping. Consequently, forming F_r^* and F_r ($r = 1, 2, 3$) in accordance with equations (24) and (27), respectively, and substituting the results into equations (2), one arrives at equations (77)–(79) *without having had to take any steps* analogous to those previously required to eliminate λ_1 and λ_2. This is true in general: equations (2) render Lagrange multipliers unnecessary for the purpose of formulating dynamical differential equations of motion of nonholonomic systems.

The benefits associated with using equations (2) in conjunction with *generalized speeds chosen optimally* are just as great in connection with nonholonomic as with holonomic systems. For example, letting ω_r ($r = 1, 2, 3$) be (the only) generalized speeds, we find with the aid of equations (2) that motions of rolling of S on A are governed by the beautifully symmetric set of equations

$$[I_1 + MR^2(1 - C_{31}^2)]\dot{\omega}_1 - MR^2 C_{31}(C_{32}\dot{\omega}_2 + C_{33}\dot{\omega}_3) = (I_2 - I_3)\omega_2 \omega_3 \tag{88}$$

$$[I_2 + MR^2(1 - C_{32}^2)]\dot{\omega}_2 - MR^2 C_{32}(C_{33}\dot{\omega}_3 + C_{31}\dot{\omega}_1) = (I_3 - I_1)\omega_3 \omega_1 \tag{89}$$

$$[I_3 + MR^2(1 - C_{33}^2)]\dot{\omega}_3 - MR^2 C_{33}(C_{31}\dot{\omega}_1 + C_{32}\dot{\omega}_2) = (I_1 - I_2)\omega_1 \omega_2 \tag{90}$$

These equations were generated with less labor, and can be solved more easily, than the ones associated with eliminating $\ddot{q}_4$ and $\ddot{q}_5$ from equations (77)–(79) with the aid of equations (83) and (84), which is what one is forced to do when starting with equations (1).

The full power of equations (2) manifests itself most strikingly when these equations are used to attack truly complex problems. For instance, D. Rosenthal and M. Sherman, of Symbolic Dynamics Co., recently used equations (2) as the starting point for constructing a computer program intended to simulate motions of systems consisting of rigid bodies connected to each other so as to form a "tree." The program formulates explicitly, and solves numerically, equations of motion, requiring the user to do no more than to supply data characterizing the system and the initial conditions of interest to him. Applied to the Mariner Venus/Mercury 1973 spacecraft, a system modeled as 10 rigid bodies possessing 17 degrees of freedom, this program, when executed on a VAX 11/780 computer, requires less than 2000 CPU sec to formulate, in literal form, the 34 first-order nonlinear differential equations governing general motions of the spacecraft, and it consumes less than 300 CPU sec in simulating 1 sec of motion. So far as we know, there does not exist at present any other program capable of formulating equations of motion in literal form for systems of this complexity. Moreover, after having produced literal equations for a given system, this program requires only about one-fourth as much CPU time to simulate motions of the system as does the fastest conventional multibody program known to us. Huston, et al. [17, 36, 40, 41, 47–50] have employed equations (2) in the development of multibody programs that have been successfully applied to the solution of problems in such diverse areas as spacecraft dynamics, machine design, robotics, and human body motion.

Two classes of problems of current interest are those giving rise to the need to formulate *linearized equations* of motion of complex systems, say for purposes of stability analysis or control system design, and of systems involving "*closed loops*," such as the one depicted in Fig. 4, where a planar linkage is shown attached to a flying rigid body. Equations (2) can serve one well in both contexts. To generate with the aid of equations (2) dynamical equations linear in one or more of the generalized coordinates and associated generalized speeds, one proceeds as follows: Develop complete, nonlinear expressions for angular velocities and for velocities of rigid body mass centers and points of application of forces, and use these to determine partial angular velocities and partial velocities by inspection. Next, linearize all nonholonomic constraint equations, angular velocities, velocities, partial angular velocities, and partial velocities and, with their aid, construct generalized active forces F_r and generalized inertia forces F_r^* ($r = 1, \ldots, n - m$) in the usual way, but linearize at every stage of this process. Finally, substitute into equations (2) to obtain the desired equations. In general, this process is far less arduous than that of first formulating fully nonlinear equations and then dropping terms of second and higher degree, which is essentially what one is forced to do when starting with equations (1). As for systems containing closed loops, these can be treated conveniently as pseudononholonomic; that is, one can introduce in connection with each closed loop a number of extraneous generalized coordinates and an equal number of extraneous generalized speeds, write constraint equations governing the generalized coordinates, differentiate these equations with respect to time to obtain equations necessarily linear in the generalized speeds, solve these for the extraneous generalized speeds in terms of independent generalized speeds, and then use equations (2) as when dealing with a simple nonholonomic system, thus being freed of the burden associated with eliminating Lagrange multipliers or constraint forces.

Now let us examine the relationship between equations (2) and expressions of the laws of dynamics in the form

$$\sum_{i=1}^{\nu} (\mathbf{F}_i - m_i \mathbf{a}_i) \cdot \delta \mathbf{z}_i = 0 \tag{91}$$

Downloaded 02 May 2010 to 171.66.16.250. Redistribution subject to ASME license or copyright; see http://www.asme.org/terms/Terms_Use.cfm

where $\mathbf{F}_i$ is the resultant of all contact and/or distance forces acting on a particle P_i of mass m_i; $\mathbf{a}_i$ is the acceleration of P_i in a Newtonian reference frame N, ν is the number of particles comprising a system S, and $\delta\mathbf{z}_i$ is a quantity the definition of which is generally accompanied by the word "virtual," as in "virtual displacement" or "virtual velocity." As will be shown presently, it is precisely the matter of defining $\delta\mathbf{z}_i$ that lies at the heart of the relationship between equations (2) and equation (91). First, however, it is important to draw attention to the fact that, since

$$\mathbf{F}_i - m_i\mathbf{a}_i = 0 \quad (i = 1, \ldots, \nu) \tag{92}$$

in accordance with Newton's Second Law, equation (91) is a valid relationship, *no matter what one says* about $\delta\mathbf{z}_i$ ($i = 1, \ldots, \nu$). Why, then, does it matter how $\delta\mathbf{z}_i$ is defined? The answer is that if, and only if, $\delta\mathbf{z}_i$ is chosen properly, then certain forces that contribute to $\mathbf{F}_i$, namely forces often called "nonworking constraint forces," make no contributions to the equations ultimately derived from equation (91), and this is, of course, a state of afffairs much to be desired. Now, in the attempt to reach this goal, it is traditional to resort to a purely verbal (rather than mathematical) definition of $\delta\mathbf{z}_i$, invoking terminology such as "compatibility with constraints," infinitestimal displacements," "small, imagined displacements," and so forth and, when interpreted suitably, the resulting definition indeed accomplishes the intended purpose. But it can hardly be gainsaid that maximum clarity is guaranteed by defining $\delta\mathbf{z}_i$ *mathematically* in terms of more fundamental quantities. The partial velocities used in conjunction with equations (2) make it possible to do this, because they are, themselves, quantities defined with great precision [and they are easily formed in practice, as in equations (23), (28), (29), and (87).] Specifically, suppose that the configuration of S in N depends on n generalized coordinates; let S be subject to constraints such that m equations having the form of equations (66) must be satisfied throughout every motion of S in N; introduce n generalized speeds $u_1, \ldots, u_n$, and let $\mathbf{v}_r^{Pi}$ be the partial velocity of P_i associated with u_r ($i = 1, \ldots, \nu$; $r = 1, \ldots, n - m$); finally, let ζ_r ($r = 1, \ldots, n - m$) denote *any* $n - m$ quantities having the same dimensions as $u_r t$ ($r = 1, \ldots, n - m$), respectively, where t denotes the time. What is customarily called " a set of virtual displacements compatible with the constraints" then is nothing more or less than $\delta\mathbf{z}_i$ defined as[1]

$$\delta\mathbf{z}_i \triangleq \sum_{r=1}^{n-m} \mathbf{v}_r^{Pi}\zeta_r \quad (i = 1, \ldots, \nu) \tag{93}$$

(Note that there is no implication here that anything is small or infinitesimal.) Moreover, when one recalls that the generalized active forces F_r ($r = 1, \ldots, n - m$) and generalized inertia forces F_r^* ($r = 1, \ldots, n - m$) which appear in equations (2) are defined as

$$F_r \triangleq \sum_{i=1}^{\nu} \mathbf{v}_r^{Pi} \cdot \mathbf{F}_i, \quad F_r^* \triangleq -\sum_{i=1}^{\nu} m_i \mathbf{v}_r^{Pi} \cdot \mathbf{a}_i \tag{94}$$

then one can see that substitution from equations (93) into equation (91) leads directly to

$$\sum_{r=1}^{n-m} (F_r + F_r^*)\zeta_r = 0 \tag{95}$$

[1] With equal precision, one can define $\delta\rho$, a virtual rotation of a rigid body B belonging to S, as

$$\delta\rho \triangleq \sum_{r=1}^{n-m} \Omega_r \zeta_r,$$

where Ω_r ($r = 1, \ldots, n - m$) are partial angular velocities of B in N.

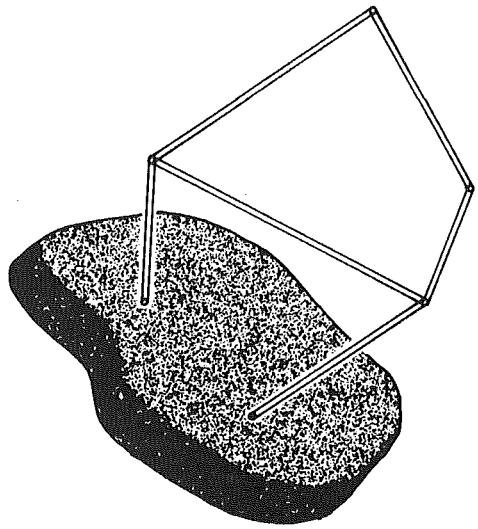


Fig. 4 Planar linkage attached to flying rigid body

and this, in turn, leads to equations (2), for ζ_r ($r = 1, \ldots, n-m$) were defined as *any* $n - m$ quantities having suitable dimensions, so that it is permissible to set all but one of them equal to zero, and to do this, in turn, with each one. Hence, when $\delta\mathbf{z}_i$ is defined as in equations (93), then equation (91) and equations (2) become equivalent statements [and equation (91) expresses what is known variously as the Principle of Virtual Work, D'Alembert's Principle, or Jourdain's Principle, the last appellation being appropriate when u_r differs from $\dot{q}_r$ for one or more values of r]. The following conclusion thus emerges: At best, that is, when $\delta\mathbf{z}_i$ ($i = 1, \ldots, \nu$) are chosen properly, equation (91) leads to exactly the same dynamical equations of motion as do equations (2), and no savings in labor are realized by using equation (91) rather than equations (2). To insure that $\delta\mathbf{z}_i$ ($i = 1, \ldots, \nu$) are chosen so as to bring about elimination of all nonworking constraint forces, one can appeal to equations (93). But to use these equations, one must form $\mathbf{v}_r^{Pi}$ ($i = 1, \ldots, \nu$; $r = 1, \ldots, n - m$) and, having done so, one will always find it more expedient to proceed directly to the formation of F_r and F_r^* in accordance with equations (94), and then to appeal to equations (2), than to make use of equation (91), for the latter course of action entails the necessity of taking the additional step that brings one from equation (95) to equations (2). Consequently, for the formulation of equations of motion, the use of principles represented by equation (91) is contraindicated, at least for systems possessing a finite number of degrees of freedom. But this is not to say that there is a conflict between equations (2) and equation (91). On the contrary, equations (2) simply fulfill the promises made by the advocates of equation (91).

In conclusion, the following matter derserves consideration. While it is highly likely that a computer must be employed to deal with any given multibody dynamics problem, it is by no means true that it is always best to use a general purpose multibody computer program to carry out the requisite calculations. Indeed, in many situations the opposite is true: it is better to use equations (2) to formulate an *explicit* computational algorithm for the problem at hand than it is to attempt to work with an available multibody program. For example, the plots in Fig. 1. were generated by means of a computer program based on explicit equations of motion written for the Stanford Arm with the aid of equations (2), and the number of multiplications and additions required for the evaluation of the joint force and five joint torques was thus reduced to fewer than half the number needed when a multibody program based on equations (1) was used for the same purpose.

Downloaded 02 May 2010 to 171.66.16.250. Redistribution subject to ASME license or copyright; see http://www.asme.org/terms/Terms_Use.cfm

References

1 Magnus, K., *Dynamics of Multibody Systems*, Springer-Verlag, Berlin, 1978.

2 Jerkovsky, W., "The Structure of Multibody Dynamics Equations," *Journal of Guidance and Control*, Vol. 1, No. 3, May-June 1978, pp. 173-182.

3 Paul, B., "Analytical Dynamics of Mechanisms—A Computer Oriented Overview," *Mechanism and Machine Theory*, Vol. 10, 1975, pp. 481-507.

4 Wittenburg, J., *Dynamics of Systems of Rigid Bodies*, Stuttgart, 1977, pp. 221-222.

5 Hooker, W. W., and Margulies, G., "The Dynamical Attitude Equations for an *n*-Body Satellite," *The Journal of the Astronautical Sciences*, Vol. XII, No. 4, 1965, pp. 123-128.

6 Roberson, Robert E., and Wittenburg, Jens, "A Dynamical Formalism for an Arbitrary Number of Interconnected Rigid Bodies, With Reference to the Problem of Satellite Attitude Control," *Proceedings of the Third Congress of the International Federation of Automatic Control*, London, Paper 46.D, June 24, 1966.

7 Russell, W. J., "On the Formulation of Equations of Rotational Motion for an *N*-Body Spacecraft," Aerospace Corporation, Report No. TR-0200(4133)-2, Feb. 14, 1969.

8 Hooker, W. W., "A Set of *r* Dynamical Attitude Equations for an Arbitrary *n*-Body Satellite Having *r* Rotational Degrees of Freedom," *AIAA Journal*, Vol. 8, No. 7, July 1970, pp. 1204-1207.

9 Keat, James E., "Dynamical Equations of Nonrigid Satellites," *AIAA Journal*, Vol. 8, No. 7, July 1970, pp. 1344-1345.

10 Fleischer, Gerald E., "Multi-Rigid-Body Attitude Dynamics Simulation," JPL Technical Report 32-1516, Feb. 15, 1971.

11 Likins, Peter W., and Fleischer, Gerald E., "Large-Deformation Modal Coordinates for Nonrigid Vehicle Dynamics," JPL Technical Report 32-1565, Nov. 1, 1972.

12 Boland, Ph., Samin, J. C., and Willems, P. Y., "On the Stability of Interconnected Rigid Bodies," *Ingenieur-Archiv*, Vol. 42, 1973, pp. 360-370.

13 Likins, Peter W., "Dynamic Analysis of a System of Hinge-Connected Rigid Bodies with Nonrigid Appendages," *International Journal of Solids and Structures*, Vol. 9, 1973, pp. 1473-1487.

14 Likins, Peter W., "Hybrid-Coordinate Spacecraft Dynamics Using Large-Deformation Modal Coordinates," *Astronautica Acta*, Vol. 18, No. 5, 1973, pp. 331-348.

15 Boland, P., Samin, J. C., and Willems, P. Y., "Stability Analysis of Interconected Deformable Bodies in a Topological Tree," *AIAA Journal*, Vol. 12, No. 8, Aug. 1974, pp. 1025-1030.

16 Frisch, Harold P., "A Vector-Dyadic Development of the Equations of Motion for *N*-Coupled Rigid Bodies and Point Masses," NASA TN D-7767, Oct. 1974.

17 Huston, R. L., and Passerello, C. E., "On the Dynamics of Chain Systems," ASME Paper 74-WA/Aut-11, 1974.

18 Ho, J. Y. L., Hooker, W. W., Margulies, G., and Winarske, T. P., "Remote Manipulator System Simulation, Vol. 1: Dynamics and Technical Description," Lockheed Palo Alto Research Laboratory, Palo Alto, Calif. LMSC-D403329, Oct. 1974.

19 Larson, V., "State Equations for an *n*-Body Spacecraft," *The Journal of the Astronautical Sciences*, Vol. XXII, No. 1, July-Sept. 1974, pp. 21-35.

20 Hooker, W. W., "Equations of Motion for Interconnected Rigid and Elastic Bodies," *Celestial Mechanics*, Vol. 11, No. 3, May 1975, pp. 337-359.

21 Boland, Ph., Samin, J. Cl., and Willems, P. Y., "Stability Analysis of Interconnected Deformable Bodies with Closed-Loop Configuration," *AIAA Journal*, Vol. 13, No. 7, July 1975, pp. 864-867.

22 Frisch, Harold P., "A Vector-Dyadic Development of the Equations of Motion for *N*-Coupled Flexible Bodies and Point Masses," NASA TN D-8047, Aug. 1975.

23 Ho, J. Y. L., "Direct Path Method for Flexible Multibody Spacecraft Dynamics," *Journal of Spacecraft and Rockets*, Vol. 14, Feb. 1977, pp. 102-110.

24 Bodley, Carl S., Devers, A. Darrell, Park, A. Colton, and Frisch, Harold P., "A Digital Computer Program for the Dynamic Interaction Simulation of Controls and Structure (DISCOS)," Vol. I, NASA Technical Paper 1219, May 1978.

25 Hughes, P. C., "Dynamics of a Chain of Flexible Bodies," *The Journal of the Astronautical Sciences*, Vol. XXVII, No. 4, Oct.-Dec. 1979, pp. 359-380.

26 Chace, M. A., "Analysis of the Time-Dependence of Multi-Freedom Mechanical Systems in Relative Coordinates," ASME *Journal of Engineering for Industry*, Vol. 89, 1967, pp. 119-125.

27 Uicker, J. J., Jr., "Dynamic Force Analysis of Spatial Linkages," ASME JOURNAL OF APPLIED MECHANICS, Vol. 34, 1967, pp. 418-424.

28 Uicker, J. J., Jr., "Dynamic Behavior of Spatial Linkages," ASME *Journal of Engineering for Industry*, Vol. 91, No. 1, Feb. 1969, pp. 251-265.

29 Chace, M. A., and Bayazitoglu, Y. O., "Development and Application of a Generalized d'Alembert Force for Multifreedom Mechanical Systems," ASME *Journal of Engineering for Industry*, Vol. 93, 1971, pp. 317-327.

30 Bayazitoglu, Y. O., and Chace, M. A., "Methods for Automated Dynamic Analysis of Discrete Mechanical Systems," ASME JOURNAL OF APPLIED MECHANICS, Vol. 40, 1973, pp. 809-811.

31 Gupta, V. K., "Dynamic Analysis of Multi-Rigid-Body Systems," ASME *Journal of Engineering for Industry*, Vol. 9, 1974, pp. 886-892.

32 Dubowsky, S., and Matuuk, J., "The Dynamic Analysis of Elastic Spatial Mechanisms," *Proceedings of the Fourth World Congress on the Theory of Machines and Mechanisms*, University of Newcastle upon Tyne, England, Sept. 8-12, 1975, pp. 927-932.

33 Paul, B., "Dynamic Analysis of Machinery via Program DYMAC," Society of Automotive Engineers, International Automotive Engineering Congress and Exposition, Detroit, Feb. 28-Mar. 4, 1977, Paper No. 770049.

34 Bejczy, A. K., "Robot Arm Dynamics and Control," JPL Technical Memorandum 33-669, Feb. 15, 1974.

35 Langrana, N. A., and Bartel, D. L., "An Automated Method for Dynamic Analysis of Spatial Linkages for Biomedical Applications," ASME *Journal of Engineering for Industry*, Vol. 97, 1975, pp. 566-574.

36 Huston, R. L., Passerello, C. E., and Harlow, M. W., "Dynamics of Multirigid-Body Systems," ASME JOURNAL OF APPLIED MECHANICS, Vol. 45, 1978, pp. 889-894.

37 Vukabratovic, M., "Dynamics of Active Articulated Mechanisms and Synthesis of Artificial Motion," *Mechanism and Machine Theory*, Vol. 13, No. 1, 1978, pp. 1-56.

38 Hollerbach, John M., "A Recursive Lagrangian Formulation of Manipulator Dynamics and a Comparative Study of Dynamics Formulation Complexity," *IEEE Transactions on Systems, Man, and Cybernetics*, Vol. SMC-10, No. 11, Nov. 1980, pp. 730-736.

39 Luh, J. Y. S., Walker, M. W., and Paul, R. P. C., "On-Line Computational Scheme for Mechanical Manipulators," ASME *Journal of Dynamic Systems, Measurement, and Control*, Vol. 102, 1980, pp. 69-76.

40 Huston, Ronald L., Passerello, Chris E., "Multibody Structrual Dynamics Including Translation Between the Bodies," *Computers and Structures*, Vol. 12, No. 5, 1980, pp. 713-720.

41 Huston, Ronald L., "Multi-Body Dynamics Including the Effects of Flexibility and Compliance," *Computers and Structures*, Vol. 14, No. 5-6, 1981, pp. 443-451.

42 Silver, William M., "On the Equivalence of Lagrangian and Newton-Euler Dynamics for Manipulators," *The International Journal of Robotics Research*, Vol. 1, No. 2, Summer 1982, pp. 60-70.

43 Whittaker, E. J., *A Treatise on the Analytical Dynamics of Particles and Rigid Bodies*, 4th Ed., Dover, New York, 1937, p. 215.

44 Kane, T. R., Likins, P. W., and Levinson, D. A., *Spacecraft Dynamics*, McGraw-Hill, New York, 1983, p. 275.

45 Boltzmann, L., "Uber die Form der Lagrangeschen Gleichungen fur Nichtholonome, Generalisierte Koordinaten," *Sitzungsberichte der Mathematisch-Naturwissenschaftlichen Klasse der Kaiserlichen Akademie der Wissenschaften*, Vol. 61, 1902, pp. 1603-1614.

46 Hamel, G., "Die Lagrange-Eulerschen Gleichungen der Mechanik," *Zeitschrift fur Mathematik und Physik*, Vol. 50, 1904, pp. 1-57.

47 Huston, R. L., and Passerello, C. E., "On the Dynamics of a Human Body Model," *Journal of Biomechanics*, Vol. 4, 1971, pp. 369-378.

48 Huston, Ronald L., Hessel, Richard E., and Winget, James M., "Dynamics of a Crash Victim—A Finite Segment Model," *AIAA Journal*, Vol. 14, No. 2, 1976, pp. 173-178.

49 Huston, R. L., Passerello, C. E., Hessel, R. E., and Harlow, M. W., "On Human Body Dynamics," *Annals of Biomedical Engineering*, Vol. 4, 1976, pp. 25-43.

50 Huston, R. L., and Passerello, C., "On Multi-Rigid-Body System Dynamics," *Computers and Structures*, Vol. 10, 1979, pp. 439-446.

Downloaded 02 May 2010 to 171.66.16.250. Redistribution subject to ASME license or copyright; see http://www.asme.org/terms/Terms_Use.cfm

Deterministic and Stochastic Aspects of Turbulence

J. Laufer[1]
Department of Aerospace Engineering,
University of Southern California,
Los Angeles, Calif. 90089-1454

The recent active interest in the deterministic aspects of turbulent flows, referred to as coherent structures is discussed and justified. It is shown that this line of experimental research has yielded some important new results, and has provided new insight to the stochastic character of the flow as well as added new directions for further experimental and theoretical inquiry.

1 Introduction

The historical development of difficult problems in physics is known to be cyclic in character: as a promising new theory or a new experimental technique is developed, it generates great interest, it becomes fashionable; however, when it appears obvious after some time that the utility of the new approach has been exhausted, interest in it diminishes until a new method of attack is proposed. So it has happened to the turbulence problem: it has had its share of fashions in the past 60 years. In the 1920s and early 1930s the various phenomenological theories – especially the momentum and vorticity transport theories – were popular; in the 1930s and 1940s the statistical theory of homogeneous turbulence occupied researchers' attention; later the turbulent kinetic energy balance was the subject of most of the experimental work and eventually, became the basis for turbulence modeling. Finally, in the late 1960s and 1970s, the so-called coherent or large-scale structures were discovered and since then a considerable number of researchers in turbulence devote their time to studying these structures.

Is such a large commitment justified? Will it lead to a better understanding of turbulence? It is, of course, difficult to give a definitive answer at this stage; one should view the study of the coherent structures as another cycle in the evolution of the turbulence problem which, in all likelihood, will provide additional understanding but not a complete solution.

In this short paper, an attempt is made, first, to present the new developments related to the coherent structures in a proper perspective; second, to describe some of the significant new results; and finally, to discuss new trends.

2 General Remarks

Until recently, it was an accepted procedure that the time-averaged Reynolds equations and their higher moments were the starting point of any theory of turbulence. This approach is quite understandable, since one is interested mainly in average values of the various flow quantities: values that the solution of these equations could give, provided some additional closure assumptions are made. For instance, Prandtl introduced the momentum transfer theory, in which he expresses the Reynolds stresses in terms of his well-known mixing length hypothesis using the Boussinesq gradient diffusion model. Taylor, on the other hand, proposed a vorticity transfer theory in which the effect of the pressure fluctuations are implicitly taken into account. Von Karman criticizes both of these theories using the argument that in any turbulent flow a proper balance must exist between the turbulent energy production and viscous dissipation. "Hence, it is extremely unlikely that the mechanism of the turbulence should be determined by equations in which the influence of the viscosity terms vanishes with increasing Reynolds number" [1]. He proceeded to state that the mean turbulent kinetic energy or the mean square vorticity equations "are the fundamental equations of a satisfactory theory of turbulence." This point of view prevailed for some 40 years. In fact, the majority of the turbulence modeling methods of today are based on these equations.

Recent experimental evidence suggests a different situation: the dissipative small-scale motions do not play an important role in the dynamics of the flow development (except near a solid surface, of course). This does not mean that energy dissipation is negligible; rather, that *the turbulent energy balance is a constraint but not the driving mechanism of the turbulent transport.*

It is becoming quite clear in working with the Reynolds equations that too much information is lost in the averaging process and the closure problem makes the solution difficult, if not impossible. Consequently, one is forced to start with the full, time-dependent Navier Stokes equations. The question then arises, at what stage or in which manner should one introduce the methods of stochastic theory? The study of the large-scale structures should be helpful in pointing to an answer to this question in the following sense. Viewing turbulence in terms of a completely random motion is found to be inappropriate. Apparently, the degree of *spatial randomness is scale-dependent.* Only fluid elements smaller than a certain length dimension – determined by a local Reynolds number – seem to be spatially random; the larger scale structures appear to be what one might describe as spatially

[1] Deceased.

Contributed by the Applied Mechanics Division for publication in the JOURNAL OF APPLIED MECHANICS.

Discussion on this paper should be addressed to the Editorial Department, ASME United Engineering Center, 345 East 47th Street, New York, N.Y. 10017, and will be accepted until two months after final publication of the paper itself in the JOURNAL OF APPLIED MECHANICS. Manuscript received by ASME Applied Mechanics Division, April, 1983.

Copyright © 1983 by ASME
Downloaded 02 May 2010 to 171.66.16.250. Redistribution subject to ASME license or copyright; see http://www.asme.org/terms/Terms_Use.cfm

quasi-deterministic. That is to say, on the average, they have similar geometric shapes, determined by a given flow configuration and they have similar temporal behavior; any variation in their "signal pattern" at a fixed point is due primarily to phase fluctuations rather than spatial randomness. There is strong evidence that these large, coherent structures are responsible for the efficient transport of various fluid properties across a shear layer. Thus, the experimental methods used for their detection and the study of their dynamic behavior should help clarify the stochastic processes taking place in the flow, as well as to better understand the turbulent transport mechanism itself.

Considerable literature is available on coherent structures (see for instance the recent review article of Cantwell [2]). The pioneering works of Kline and his group [3], of Brown and Roshko [4], and Winant and Browand [5] are well documented. In examining subsequent developments, one may distinguish two main directions of inquiry: the first recognizes the fact that in many situations the origin of a typical large-scale structure can be traced upstream to the initial instability of the flow and, therefore, this line of inquiry concentrates on the early development of the shear layer; the second considers the turbulent shear layer in its later development, usually referred to as its fully developed sate and attempts to detect and to study the various quasi-deterministic structures there. In the following sections these two types of inquiries are examined in more detail.

3 The Initial Development of a Shear Layer

As mentioned earlier, a great deal of attention has been recently placed on the early stages of the flow development. In the past, this region was usually referred to as the transition stage and was treated separately from the "fully developed" turbulent one. This separation contains the implicit assumption that, the "fully developed" turbulence is independent of the initial conditions. Indeed, as far as the averaged quantities are concerned, measurements show self-preservation in most simple geometry flows, implying that these mean values scale with certain *local* characteristic quantities. A more careful examination of the measurements, however, indicates that in most cases the scaling parameters are, in fact, affected by the initial conditions. Furthermore, it has been noted that in some flow configurations (in free shear layers, for instance) the coherent structures in the fully turbulent region bear surprising resemblance to those found in the transition zone; indeed, the origin of these structures can be traced back to the instability modes of the initial shear layers. Herein lies the renewed interest in the initial development of turbulence.

One common feature of these experimental studies is the utilization of artificial perturbations near the origin of the shear layer to control the initial conditions. The technique is, of course, not new: it was first used by Schubauer and Skramstad in their classical work on laminar boundary layer stability [6]. The idea is based on the fact that in its natural state, the shear layer is perturbed by a wide spectrum of disturbances influencing its later development. As a consequence, instabilities of various frequencies arise, phase fluctuations develop, and these factors make the interpretation of the measurements obtained in the later stages of the flow development quite difficult. In fact, they produce in some cases (in the mixing layer, for instance) different results in different facilities.

The reason for the fixed-frequency artificial perturbation was to control the initial conditions by making the imposed amplitude small, but much larger, than the naturally present disturbances. This technique proved to be extremely helpful especially in free shear flows; i.e., mixing layers, jets, and wakes. They will be discussed separately.

(a) The Two-Dimensional Mixing Layer. Although the shear layer that develops due to the mixing of two parallel uniform streams has no geometric length scale, in an actual realization it starts with a finite thickness due to the presence of a "splitter plate" that separates the streams before mixing. This thickness is in fact quite important: it imposes a Reynolds number dependence on the initial conditions and determines the length scale of the flow. Specifically, this scale prescribes the length of the most unstable wave of the shear layer and this wave and its subharmonics dominate the subsequent development of the layer. Qualitatively speaking this occurs as follows: the vorticity carried by the instability wave tends to concentrate into lumps of vorticity as the wave amplitude increases. These vortices interact with each other entraining fluid into the layer in the process. The dynamics of this interaction is believed to be the key to the understanding of the flow development. In general the interaction occurs randomly in space rendering its study by stationary probes difficult. However, the use of the artificial perturbations tends to localize the interactions.

The first study utilizing forcing in a two-dimensional mixing layer was made by Sato [7]. Since that work, a number of papers have appeared on the subject, perhaps the most comprehensive being that of Ho and Huang [8]. It is not the intention here to give a detailed account of these efforts, but rather to focus on the results concerning the large-scale structures.

The most striking result of these experiments is the fact that the shear layer could be made surprisingly organized by a proper choice of the perturbation frequency. That is to say, the temporal and spatial fluctuations of the coherent structures could be decreased considerably. Furthermore, the spreading rate of the layer could be altered by changing the frequency of the perturbations. As a consequence, some general statements about the spreading, entrainment, and transport mechanism could be made. The experimental observations lead to the conclusion that these processes are generated by an instability related to the inductive property of these vortex structures. The induced field depends on the vortex strength of each structure and on its relative spatial position which in turn can be manipulated by the artificial disturbances. Thus by artificially varying the induced fields of each structure, their interaction can be influenced and simultaneously, the entrainment of irrotational fluid into and transport of momentum across the layer is affected. It should be emphasized that the induction-driven transport process is quite different in principle from the gradient diffusion type. In the latter case the process is related to local conditions, that is, to the local mean velocity or vorticity gradient that is assumed a priori. The induction-driven transport, on the other hand, is generated by a long-range effect and the mean velocity is the result of the process.

The induced field causes another, more subtle effect: it influences the initial conditions of the flow. This means, that because of the elliptic nature of the problem the conditions at the origin cannot be prescribed since they are affected by the unsteady flow downstream. There is insufficient quantitative data available to ascertain the importance of this "feedback" effect. Ho and Huang describe it as a mechanism that "fine-tunes" the mixing layer at specific frequencies [8].

Laufer and Zhang (9) have speculated about the feedback and about the subsequent flow development. The initial shear layer in the form of a vortex sheet is inviscidly unstable. The initial instability is well understood and is completely determined in terms of the initial perturbation amplitudes. In a physical realization these amplitudes are not constant. In other words, the strength of the vortex sheet at the origin (that is, at the trailing edge of the splitter plate) varies with time due to perturbations arriving from the upstream and from the

Downloaded 02 May 2010 to 171.66.16.250. Redistribution subject to ASME license or copyright; see http://www.asme.org/terms/Terms_Use.cfm

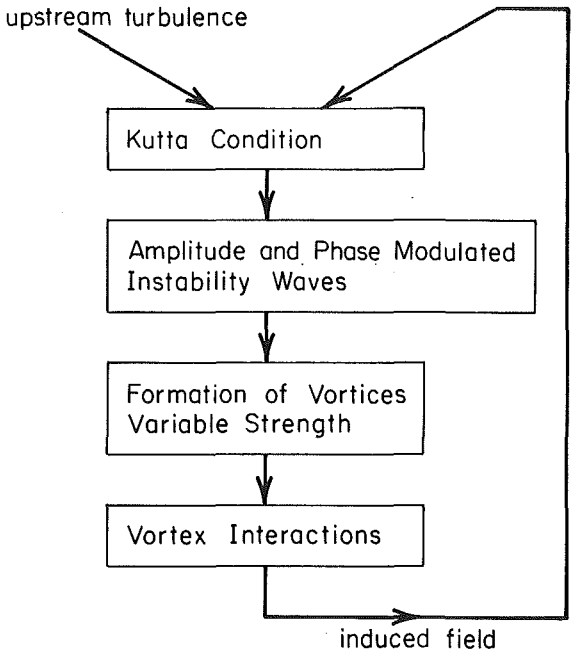


Fig. 1 A schematic diagram of the feed-back mechanism

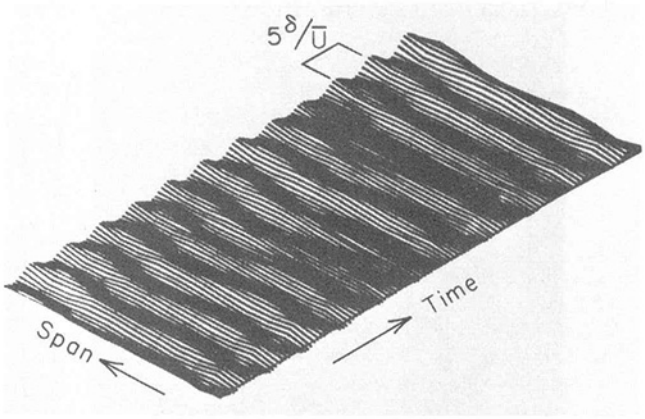


Fig. 2 Instantaneous velocity surfaces as a function of span and time; is the local vorticity thickness and U is the average velocity.

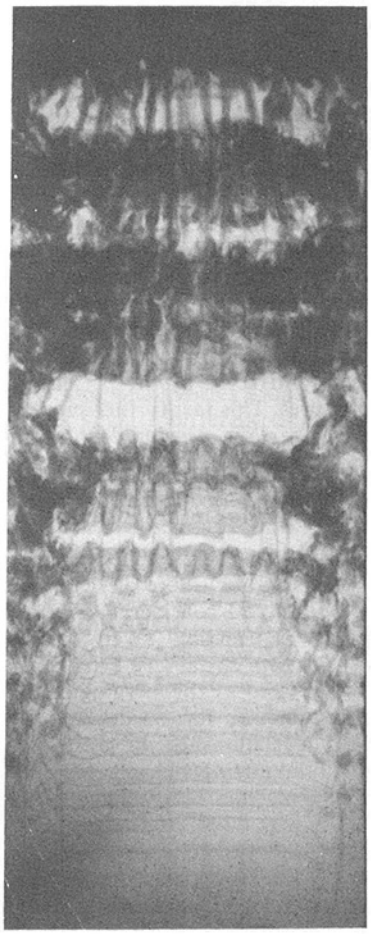


Fig. 3 Visualization of a two-dimensional mixing layer in plan view [12]. Flow toward the top. Courtesy of Professor A. Roshko, California Institute of Technology.

downstream directions. This variation is believed to come about as follows: the perturbations alter the flow at the trailing edge; in order for the Kutta condition to be satisfied at each instant, the vorticity that is being supplied to the vortex sheet at the origin varies with time. This variation due to upstream perturbations, or to feed back from downstream, becomes greatly amplified in the unstable sheet, hence, the observed amplitude and phase modulation in the initial shear layer [10]. Subsequently, when the sheet breaks up into lumps of vorticity in the nonlinear regime, these lumps will have varying strengths, generating varying induced fields that in turn causes a variation in the interaction between them. Figure 1 shows a schematic diagram of this process. Thus, according to this qualitative picture, *the random element enters the problem already at the origin of the flow*. However, the stochasticity here primarily affects the large-scale structures: it causes phase variations along their fronts in the spanwise direction and causes spatial variation in the location of pairings. It is this type of random behavior that can be minimized by imposing a fixed-frequency, fixed-amplitude perturbation at the origin. A typical example of the phase fluctuations is shown in Fig. 2 obtained by Browand [11]. Instantaneous velocity surfaces are illustrated as a function of span and time.

In addition to the two-dimensional, large-scale vortex structures, other organized vortices have also been observed. The most revealing pictures have been taken by Breidenthal [12]. In particular, soon after the large two-dimensional vortices are generated, weaker, "wiggle" shaped vortices appear. They seem to be superimposed on the large structures in a complex geometric pattern with a characteristic transverse scale. Their origin is not understood. It is possible that three-dimensional disturbances originating from the side-wall boundary layers, or from upstream, initiate a spatial perturbation or "kink" on the primary vortices and thereafter they take on the observed patterns through self-induction (Fig. 3).

Hopfinger and Browand [13] have shown experimentally in a rotating flow that isolated kinks propagate along vortex cores as solitary waves. They suggested that solitary vortex waves may be important in other turbulent flows. Aref and Flinchem [14] have independently investigated this possibility numerically. They place three randomly chosen solitons on the primary vortex filament. These solitons decay and produce a quasi-periodic wave train that is amplified by the imposed shear flow. The resulting distortions of the vortex core have an appearance very similar to Breidenthal's observations (Figs. 3 and 4).

The presence of these vortex wiggles are significant because they are believed to be the precursors to transition, that is, to the appearance of small-scale random motions in the flow. Just exactly how this "breakdown" happens is still a matter of conjecture. It is likely that it is caused by a high strain rate occurring in the flow. Ho and Huang [15] noted, for instance,

Downloaded 02 May 2010 to 171.66.16.250. Redistribution subject to ASME license or copyright; see http://www.asme.org/terms/Terms_Use.cfm

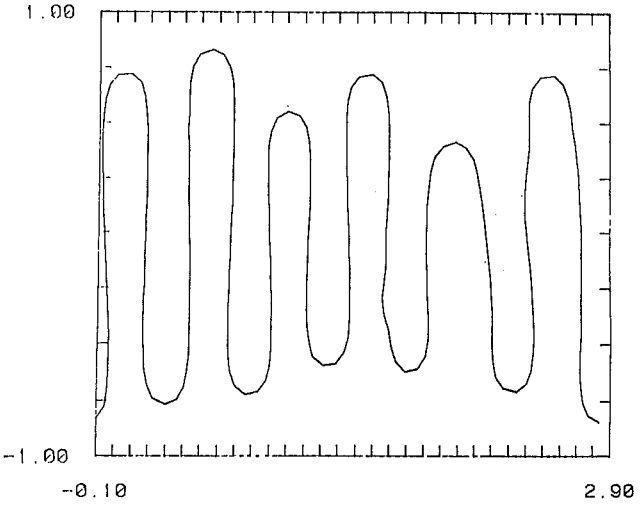


Fig. 4 Distortion of a vortex filament due to self-induction and straining [14]. Abcissa is the spanwise direction. Scale is arbitrary.

that the breakdown is always associated with a vortex pairing event (provided the local Reynolds number is high enough). It is also possible that local vorticity production is so intense, due to the straining of streamwise vorticity, that the curved sections or "pin heads" of the vortex filaments may break up into individual, small vortex loops, thus initiating the small scale random motion. (More will be said about this in the following section.) According to Breidenthal's pictures, this happens all along a primary vortex structure and not at a local region as in the case of turbulent spot formation in the boundary layer. It is also significant that the rate of spreading is not significantly affected by the presence of the random small-scale structures. This fact further supports the view that the *dynamics of the flow development in the mixing layer depends primarily on the large-scale structures*. A more detailed discussion on this point can be found in a recent paper by Browand and Ho [16].

(*b*) Jets and Wakes. The complicated geometry of these flows presents considerably more difficulties than the plane mixing layer. One has to consider two regions that are intimately related: the mixing layer that develops after separation with its own instability behavior, and the "bell-shaped" layer generated by the merging of the mixing layers which is also unstable. So far, no detailed experiments exist examining the interrelationships of these two flow regions, although some initial attempts have been made [17]. For this reason, the comments that follow have to be taken as tentative.

The problem has two characteristic length scales: a geometric one, D (jet width or diameter for jets and body dimension for wakes) and an intrinsic one, λ_0 (the initial instability wave length after separation).

If one assumes that the vortex frequencies and their position relative to each other are determined by the linear instability characteristics of the two types of shear layers (a reasonable supposition based on observations), one may expect the following picture of the flow development in the circular jet, for example. The initial shear layer has at least two modes of instability with nearly the same amplification rates: a symmetric and a first-order spiral mode [18]. Experience has shown that provided the upstream disturbance level in the facility is small and the jet velocity low, the shear layer generates mainly axially symmetric instability waves that develop into vortex rings with a separation distance equal to λ_0. (The bell-shaped profile, on the other hand has only a spiral mode instability [19].) The vortex rings coalesce as they move downstream and develop azimuthal instabilities. The coalescence is both amplitude and frequency-modulated by the spiral instabilities produced downstream primarily by the bell-shaped profiles. Simultaneously, the spiral instability frequency is affected by the frequencies of the axisymmetric modes. Thus, the vortex structures are the result of both local instabilities and long-range-induced effects: initially they are ring shaped (in a "clean" facility) and further downstream, spiral shaped. The detection or visualization of the downstream structures is difficult, especially at higher velocities because of the large phase fluctuations and the presence of the spatially random small-scale turbulence.

Similar to the three-dimensional waves in the mixing layer, one observes azimuthal instabilities in the circular jet. The three time sequence photographs clearly show this in Fig. 5 [20]). Using a hydrogen bubble technique, the first picture shows the bubbles concentrated in segments of a circular loop of the order of the nozzle diameter showing the primary vortex ring. Because of a secondary instability [21], smaller loops develop (Fig. 5(*b*) that subsequently break off and become randomized presumably within the primary vortex structure (Fig. 5(*c*). Thus, the process of randomization is similar to that proposed for the mixing layer, only the geometry is different.

A similar situation is expected to occur in two-dimensional jets and wakes except that since the instability modes are different, the shape, sense of rotation, and spatial distribution of the primary vortex structures are different.

Considerably more work has to be done to understand the interaction between the initial mixing layer and the bell-shaped layer. It is most likely that their strength, relative spatial position, and development occurring in the fully developed region of the flow will depend on this interaction. Some important process in this direction has been made recently by Wygnanski and Champagne studying a two-dimensional wake [22].

(*c*) Boundary Layers. The stability and transition of a Blasius layer has been the subject of renewed intensive work in the past few years. Again, it is not the intention here to review these important contributions, but to focus on the deterministic and stochastic character of this flow regime on the basis of the available information.

The classical Orr-Sommerfeld formulation of the stability problem is, of course, deterministic and its solution well substantiated by experiments. However, it does not consider the absolute amplitudes and three-dimensional aspects of the perturbations, both of which are known to be essential to the transition phenomenon. In fact, even in the "cleanest" experimental conditions, transition is always observed in the presence of three-dimensional disturbances that are known to have vorticity components in the mean flow direction. There is still some question exactly how these disturbances get into the boundary layer and in particular, how they develop a characteristic lateral wave length. Here again the possibility of a soliton interaction generating a lateral wave train on the primary vortex core is attractive (13). Specifically if a "local kink" develops (due to a localized free-stream vorticity disturbance or to the side-wall turbulent boundary layer) on the primary Tollmien-Schlichting waves, the "kink" generates lateral waves with a certain wave length. In the boundary layer case this wave length is comparable to that of the primary wave. It is quite feasible that the stretching of these vortex lines in the flow direction is the precondition of the transition process. In formulating the mathematical problem, it is necessary, according to this picture, to include in the boundary condition an appropriate three-dimensional vorticity disturbance in addition to the usual two-dimensional convective wave perturbations. A possible sequence of events is as follows: simultaneously with the amplification of the

Downloaded 02 May 2010 to 171.66.16.250. Redistribution subject to ASME license or copyright; see http://www.asme.org/terms/Terms_Use.cfm

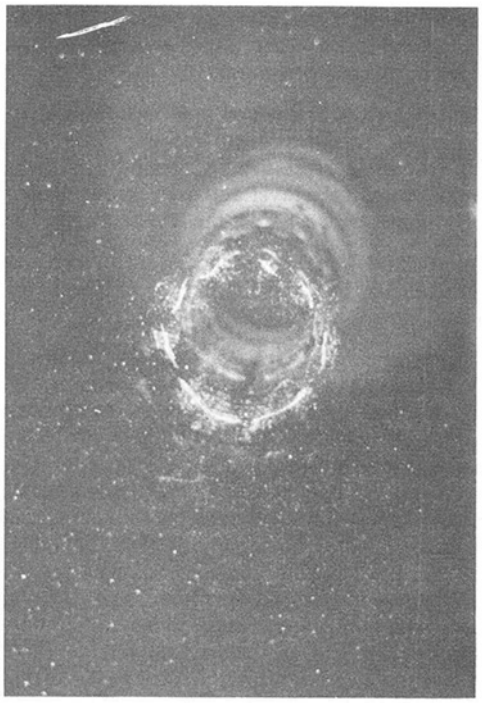


Fig. 5(a) $x = 1.75\,D$

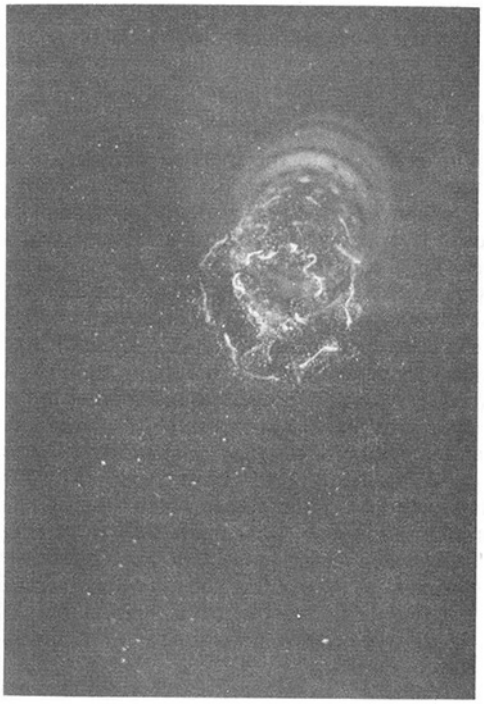


Fig. 5(b) $x = 2.75\,D$

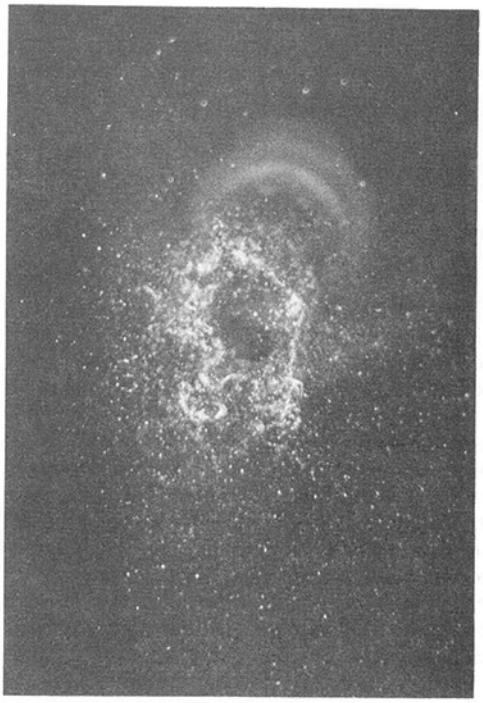


Fig. 5(c) $x = 3.3\,D$

Fig. 5 Visualization of a circular jet at three axial stations

primary Tollmien-Schlichting waves, spanwise wavy perturbations develop on them. (These are beautifully illustrated by the experiments of Wortmann [28].) Due to the straining of the mean flow, the vortices are stretched in the flow direction, and lifted away from the solid boundary until a characteristic hairpin shape develops at the head of the vortex loop. Wortmann's pictures indicate that similar events occur, but slightly delayed, at various heights in the boundary layer causing a "tile-roof" arrangement. Presumably, self-induction and vortex-image effects play an essential role here. The actual vortex-line breakup is not understood. Perhaps, one should consider the problem in terms of the stability of a curved vortex filament in a straining motion. In particular, if the vorticity production due to stretching becomes locally larger than the vorticity diffusion, it is feasible that the "pin heads" break off into small vortex loops which are distorted and carried off in slightly different directions by the local instantaneous velocity, hence, the start of the stochastic process and of the so-called "turbulent spot." Obviously, the preceding scenario is highly speculative and should serve only as a guide for further experimentation. The three essential points here are: (1) the need for inclusion of an arbitrary, three-dimensional vorticity disturbance in the initial condition of the stability problem; (2) the self-induction mechanism is an important factor in the initiation and spreading of turbulence; and (3) there is apparently a basic difference in the transition process between free shear layers and the boundary layers. In the former case the primary vortex structures remain essentially undistorted and the three-dimensional smaller vortices carried by the primary one have a much smaller wave length and breakdown almost simultaneously all along the primary wave. In the latter case, the primary vortex itself becomes laterally distorted with a wave length comparable to its own and transition (or a turbulent spot) develops locally.

4 The Fully Developed Shear Layer

The notion of large-scale structures in fully developed, high Reynolds number shear layers is a classical one. It was discussed and its importance emphasized in some detail by Townsend [24]. However, in this classical context, the spatial extent of these structures was defined in terms of the integral correlation length. The averaging process involved in determining this length is not based on any pattern recognition or sampling technique. As a result, it represented at best a smeared out image of a large number of structures in various stages of their lifetime, at worst, no identifiable structure at all. The deterministic aspects of these structures, such as the two-dimensional vortices in the mixing layer and the streamwise streaks in the viscous sublayer, have been first recognized not from correlation measurements but with the

Downloaded 02 May 2010 to 171.66.16.250. Redistribution subject to ASME license or copyright; see http://www.asme.org/terms/Terms_Use.cfm

help of flow visualization techniques [3, 4]. Only instantaneous glimpses of a sufficiently large portion of the flow field enabled one to distinguish between individual structures and at subsequent time increments, to observe their development.

There are two important questions that arise in connection with these quasi-deterministic structures: (1) what is their asymptotic behavior at high Reynolds number and (2) what are appropriate statistical methods for their detection and study.

The first question is especially appropriate for the two-dimensional mixing layer. Can the vortices remain two-dimensional in the limit of very large Reynolds number? Evidence indicates an affirmative answer, provided the disturbances in the uniform streams are not overwhelmingly large. Velocity cross-correlations between two points separated along the span of the layer attain an asymptotic form when the separation distance between points is scaled with the local shear layer thickness [25]. Browand and Ho have shown that the two-dimensional vortices reform some distance downstream [16] after being destroyed by a honeycomb placed in the mixing layer.

In general one finds that in turbulent free shear layers the Reynolds number is not a controlling parameter as far as the flow development is concerned; it enters the problem primarily through its influence on the initial conditions of the flow. This fact was well recognized by Townsend some 30 years ago [24]. It also implies that the shape and behavior of the large-scale structures are asymptotically Reynolds number independent.

With reference to turbulent boundary layers, no general statement can be made at this time concerning the large-scale structures at high Reynolds numbers, since to the knowledge of this author, no experiments are available in that range. It is most likely, however, that the large three-dimensional structures, as well as the longitudinal streaks in the viscous layer that receive a lot of attention in relatively low Reynolds number flows play similar roles at large Reynolds numbers. The behavior and interaction of these structures is still very little understood and, in fact, no significant new results can be reported, since the recent exhaustive review of Cantwell [1].

With reference to the second question posed in the foregoing, it is much more difficult to give a completely satisfactory answer. The detection of a large-scale structure by its very nature is somewhat arbitrary. Since the instantaneous signature of each individual structure is slightly different as it passes by a detector, an appropriate statistical method has to be devised for its detection and for determining its character. The method and the resulting conditionally averaged structure signature is not unique. Such techniques have been criticized in the past for this reason [26]. However, it has to be remembered that such experiments are exploratory in nature and seeks certain features of the large-scale structures, such as shape, velocity, and vorticity content, to explore their dynamic roles. Experience shows that with careful choice of a detection scheme, different experimentors arrive at similar conclusions. An excellent discussion concerning various pattern recognition schemes is given by Blackwelder [27]. Many of the pitfalls associated with detection techniques can be avoided by using the orthogonal decomposition technique of Lumley [28], however, the amount of data required is prodigious.

5 Concluding Remarks

In recent years a great deal of effort has been focused on the study of the large-scale motions in turbulent flows. This concentrated work has been worthwhile: it has produced some important new results, has clarified some vague concepts and finally, has provided new directions for continued research.

The main results can be summarized as follows:

(1) The large-scale structures play an essential role in the development of turbulent shear flows. This is especially evident in free shear layers where their induced fields govern the spreading rate of the layer and are responsible for most of the momentum transport across the layer.

(2) The turbulent energy balance is seen to be a constraint of the turbulent transport process and not its driving mechanism.

(3) The experimental results strongly suggest that the method of finding a solution to the *averaged* governing equations is unproductive if one seeks to understand the governing dynamics of the flow. Exactly how to handle this analytically is still unresolved. One school of thought attempts to formulate the problem in terms of nonlinear, higher order instabilities. Kelly's subharmonic resonance theory for the mixing layer is one example [29]. The difficulty of these approaches is the fact that when considering the stability of the mean velocity, the velocity profile is itself the result of the instability modes imposed. These ideas could, however, be helpful in providing some partial answers to the problem. Another approach recognizes the fact that vorticity is the fundamental dynamic quantity of the stability and turbulence problems, and its point of departure is the unsteady vorticity equation that lends itself to a Lagrangian description; a useful property when studying shear layers. In a recent article, Saffman [30] discusses the difficulties encountered with this line of inquiry. Nevertheless, this approach is believed to be worthwhile to pursue.

(4) With reference to the classical question of how does stochasticity enter a problem formulated in terms of deterministic equations, the experiments provide some useful directions. It appears that it enters at least two ways: (*a*) "artifically," one must provide an arbitrary three-dimensional disturbance as an initial condition to model realistic flow situations. Such a disturbance might be introduced at the start of the flow development or in the case of a boundary layer at the solid surface as well; (*b*) these perturbations serve to generate lateral instabilities in the primary vortex structures that are the precursor to the eventual small-scale randomization of the flow; (*c*) this latter randomization is, of course, the central problem of transition. It is suggested here that random motion comes about when high straining rates stretch the vortex filaments to such an extent that they break into small vortex loops that are convected away in various directions depending on the local instantaneous velocity. Obviously, this picture is highly speculative, but hopefully, it will suggest new directions to investigate the breakdown.

Acknowledgment

The author wishes to thank his friends and colleagues for the many helpful and productive discussions they had together, in particular Professors R. F. Blackwelder, F. K. Browand, C. M. Ho, P. Huerre, and I. Wygnanski.

The support of AFOSR under Contract Number F49620-82-K-0019 is gratefully acknowledged.

References

1 von Karman, Th., "The Fundamentals of the Statistical Theory of Turbulence," *J. of the Aeronautical Sc.*, Vol. 4, 1937, p. 236.

Downloaded 02 May 2010 to 171.66.16.250. Redistribution subject to ASME license or copyright; see http://www.asme.org/terms/Terms_Use.cfm

2 Cantwell, B. J., "Organized Motion in Turbulent Flow," *Ann. Rev. Fluid Mech.*, Vol. 13, 1981, pp. 457-515.

3 Kline, S. J., and Runstadler, P. W., "Some Preliminary Results of Visual Studies of the Wall Layers of the Turbulent Boundary Layer," ASME Vol. 2, 1959, pp. 166-170.

4 Brown, G., and Roshko, A., "On Density Effects and Large Structure in Turbulent Mixing Layers," *J. F. M.*, Vol. 64, 1974, pp. 775-816.

5 Winant, C. D., and Browand, F. K., "Vortex Pairing: A Mechanism of Turbulent Mixing Growth at Moderate Reynolds Number," *J. F. M.*, Vol. 63, 1974, pp. 237-255.

6 Schubauer, G. B., and Skramstad, H. K., "Laminar Boundary Layer Oscillations and Transition on a Flat Plate," NACA Report No. 909, 1948.

7 Sato, H., "Further Investigation on the Transition of Two-Dimensional Separated Layer at Subsonic Speeds," *J. of the Physical Soc. of Japan*, Vol. 14, No. 12, 1959, pp. 1797-1810.

8 Ho, C.-M., and Huang, L.-S., Subharmonics and Vortex Merging in Mixing Layers, *J. F. M.*, Vol. 119, pp. 443-473.

9 Laufer, J., and Zhang, J. X., "Unsteady Aspects of a Low Mach Number Jet," *Phys. of Fluids*, to be published.

10 Laufer, J., and Monkewitz, P., "On Turbulent Jet Flows: A New Perspective," AIAA Paper No. 80-0962, Hartford, Conn., 1980.

11 Browand, F. K., private communication.

12 Breidenthal, R., "Structure in Turbulent Mixing Layers and Wakes Using a Chemical Reaction," *J. F. M.*, Vol. 109, 1981, pp. 1-24.

13 Hopfinger, E. J., and Browand, F. K., "Vortex Solitary Waves in a Rotating Turbulent Flow," *Nature*, Vol. 295, No. 5848, 1982, pp. 393-395.

14 Aref, H., and Flinchem, E. P., "Dynamics of a Vortex Filament in a Shear Flow," Brown University, Div. of Eng., preprint, 1983.

15 Ho, C.-M., and Huang, L.-S., "Transition in Plane Shear Layers," to be submitted.

16 Browand, F. K., and Ho., C.-M., "The Mixing Layer: An Example of Quasi Two-Dimensional Turbulence," *J. de Mecanique*, to be published.

17 Drubka, R. E., "Instabilities in Near Field of Turbulent Jets and Their Dependence on Initial Conditions and Reynolds Number," Ph.D. Thesis, 1981.

18 Michalke, A., "Instabilität eines Kompressibelen runden Freistrahls unter Berücksichtigung des Einflusses der Strahlgrenzschichtdicke," *Z. Flugwiss*, Vol. 19, 1971, pp. 319-238.

19 Crighton, D. G., "Basic Principles of Aerodynamic Noise Generation," *Prog. Aerospace Sci.*, Vol. 16, No. 1, 1975, p. 87.

20 Browand, F. K., and Laufer, J., "The Role of Large Scale Structures in the Initial Development of Circular Jets, Turbulence in Liquids, Univ. of Missouri-Rolla, Science Press, 1975, pp. 333-342.

21 Widnall, S. E., Bliss, D. B., and Tsai, C-Y., "The Instability of Short Waves on a Vortex Ring," *J. F. M.*, Vol. 66, 1974, pp. 35-47.

22 Wygnanski, I., and Champagne, F. H., private communication.

23 Wortmann, F. X., "The Incompressible Fluid Motion Downstream of Two-Dimensional Tollmien-Schlichting Waves," AGARD-DP-224, 1977, p. 12.

24 Townsend, A. A., *Structure of Turbulent Shear Flows*, Cambridge Univ. Press, 1956.

25 Browand, F. K. and Troutt, T. R., "A Note on Spanwise Structure in the Two-Dimensional Mixing Layer," *J. F. M.*, Vol. 97, 1980, pp. 771-781.

26 Lumley, J. L., *Coherent Structures in Turbulence Transition and Turbulence*, Meyer, R. E., ed., Academic Press, New York, 1981, pp. 215-242.

27 Blackwelder, R., "On the Role of Phase Information in Conditional Sampling," *Phys. of Fluids*, Vol. 20, 1977, pp. S232-242.

28 Lumley, J. L., "The Structure of Inhomogeneous Turbulent Flows," *Atmospheric Turbulence and Radio Wave Propagation*, Yaglom and Tatarskii, eds., NAUKA, Moscow, 1967, pp. 166-178.

29 Kelly, R. E., "On the Resonant Interaction of Neutral Disturbances in Two Inviscid Shear Flows," *J. F. M.*, Vol. 31, 1968, pp. 789-799.

30 Saffman, P. G., *Vortex Interactions and Coherent Structures in Turbulence, Transition and Turbulence*, Meyer, R. E., ed., Academic Press, New York, 1981, pp. 149-166.

Downloaded 02 May 2010 to 171.66.16.250. Redistribution subject to ASME license or copyright; see http://www.asme.org/terms/Terms_Use.cfm

Stability of Dynamic Systems

H. H. E. Leipholz
Professor,
Departments of Civil and
Mechanical Engineering,
University of Waterloo,
Waterloo, Ontario, Canada, N2L 3G1
Mem. ASME

It is shown how stability theory of dynamic systems, emerging from various beginnings strewn over the realm of mechanics, developed into a unified, comprehensive theory for ***dynamic systems with a finite number of degrees of freedom.*** *It is then demonstrated, how such theory could be adapted over the last five decades to the specific nature of stability problems involving continuous elastic systems. The need for such adaption is stressed by pointing to systems with follower forces. The difficulties arising from the fact that continuous systems are* ***systems with an infinite number of degrees of freedom*** *are emphasized, and an adequate approach to a unified stability theory including also continuous systems is outlined.*

Introduction

Stability theory is a discipline in mathematical physics, which over the last 50 years, has experienced a dramatic development toward a certain degree of perfection. The germs of stability theory and those of the likewise important spectral theory of differential operators were laid by L. Euler in 1744 when he considered the eigenvalue problem of column buckling. Another direction to stability theory was introduced by J. L. Lagrange in 1788 through his investigations of the vibrations of a dynamical system with a finite number of degrees of freedom and the stability of such motions about an equilibrium position. Ideas of that kind were extended to cover not only the stability of motions resulting from the perturbation of steady motions (E. J. Routh, 1884), but also the stability of motions in general (M. A. Lyapunov, 1892). A third trend in stability theory was initiated by H. Poincaré in 1881 as a result of his investigations of orbital stability. This stability concept was introduced in the context of periodic motions and led to the notion of the index of a singular point and of a closed orbit (Poincare, 1892), which has experienced a revival in modern works on dynamic systems [1]. Also, I. Bendixon (1901) has made important contributions to this facet of stability theory, which stressed the topological aspects of stability in the phase space and led to a rigorous definition of dynamical systems by G. D. Birkhoff in 1927.

The impressive result of a development covering half a century and arriving at a modern version is that there now exists a comprehensive theory encompassing various aspects of stability, like those mentioned before, based on the concept of the dynamic system, using the qualitative behavior of solutions to differential equations and, more generally, topological and functional analytical methods for the treatment of operator equations.

One important step toward enforcing the uniformity of stability theory of mechanical objects was taken by H. Ziegler [2] when he popularized the possibility, and for certain problems, the need to also consider elastic structures as dynamic systems. In this way, stability problems of such systems were treated by methods developed in the realm of dynamics, while, unfortunately, the dominating genius of Euler had persuaded his contemporaries and following generations, to consider stability problems of such structures as belonging to statics. However, the discovery of structures subjected to follower forces by E. L. Nicolai in 1928 made the restrictiveness of Euler's static approach to stability obvious. Hence, efforts were made to reconsider the stability of sturctures as the stability of motions of these structures either about their trivial equilibrium position or about other prescribed motions considered to be the "unperturbed" ones. Since the notion of "structures with follower forces" had a very deep effect on driving the domain of structural stability toward a unified theory of stability, thus leading to its coalescence with ideas on topological equivalence of differential equations and their trajectories in the phase space due to A. Andronov and L. S. Pontrjagin (1937), structures with follower forces will play an important role in the following.

The subsequent exposition will dwell on the foundations of a unified stability theory of dynamic systems displaying at the same time the various aspects that such a theory assumes when referred to the different practical problems to which it may be applied.

Dynamic Systems

In classical mechanics, a dynamic system would be defined, for example by L. A. Pars [3], as a system described by N equations of motion

$$m_s\ddot{x}_s = X_s + \sum_{r=1}^{L} \lambda_r A_{rs}, \quad s = 1,2, \ldots, N,$$

and L equations of constraint

$$\sum_{s=1}^{N} A_{rs}\dot{x}_s + A_r = 0, \quad r = 1,2, \ldots, L,$$

where the X_s are given forces and the A_{rs}, A_r, given functions

Contributed by the Applied Mechanics Division for publication in the JOURNAL OF APPLIED MECHANICS.
Discussion on this paper should be addressed to the Editorial Department, ASME, United Engineering Center, 345 East 47th Street, New York, N.Y. 10017, and will be accepted until two months after final publication of the paper itself in the JOURNAL OF APPLIED MECHANICS. Manuscript received by ASME Applied Mechanics Division, March, 1983.

Copyright © 1983 by ASME
Downloaded 02 May 2010 to 171.66.16.250. Redistribution subject to ASME license or copyright; see http://www.asme.org/terms/Terms_Use.cfm

in C^1 and domain $(x_1,x_2, \ldots, X_N,t)$. These $N + L$ equations determine the variables $x_1,x_2, \ldots, X_N,\lambda_1,\lambda_2, \ldots, \lambda_L$ as functions of t, while the system is said to have $k = N - L$ degrees of freedom.

In modern mechanics, a more abstract definition of a dynamic system as a "flow" is adopted; see for example, R. Abraham and J. E. Marsden [4]. Stressing the abstractness of the concept has the advantage of making it applicable to a broad variety of systems. In this way, systems also defined by means of partial differential equations, i.e., continuous systems, can be included. Such systems are of course of great practical importance.

From the many versions of definitions that exist in the literature for a dynamic systems, the following will be presented here: A dynamic system, also called a flow, is a continuous mapping Φ: $\kappa \times R \rightarrow \kappa$, where κ is a metric space and R denotes the real line. The mapping Φ is supposed to satisfy two properties:

(*i*) (Identity property) $\Phi(x,0) = \Phi^0 = x$ for all x in κ.

(*ii*) (Group property) $\Phi(\Phi(x,t),s) = \Phi^s\Phi^t = \Phi(x,t+s) = \Phi^{t+s}$ for all x in κ and t,s in R

If property (*ii*) is defined only for $t,s \geq 0$, one speaks of a semiflow.

While Φ is the *flow* (motion), the graph of Φ, say, (t,Φ) is the *trajectory*. The projection of the trajectory onto κ, i.e., $\gamma(x) = \{\Phi(x,t): t \in R\}$, is called the *orbit*.

In the course of abstraction, one would tend to study the common morphology of classes of objects and operations performed on them. This leads finally to concepts like categories and functions. It is well foreseeable that a development of this kind will also happen in stability theory. On such a level of treatment, one is able to clearly see the bare essence of the stability concept. One gains in this way a sound foundation, on which one can subsequently build *that* specific version of stability theory that may eventually be required for a certain practical application.

Here, such a general, abstract perception of stability will be described as follows: Consider a subset S of a metric space X. Let $s_i \in S$ and $x \in X$. Then,

$$\mathcal{S}_i(s_i, \delta) = \{x: d(s_i, x) < \delta\}$$

is the sphere in X around point s_i in S with the radius δ, while d denotes the distance between points s_i and x in the sense of the metric of X.

Consider a mapping Φ on S as a motion. Applying the mapping Φ on S repeatedly in order to obtain Φ: $S \rightarrow S^1$, Φ: $S^1 \rightarrow S^2$, etc., where S^1, S^2, etc. are images of S, S^1, etc., respectively, in X. Then, $\Phi \cdot \Phi \ldots \Phi = \Phi^k$: $S \rightarrow S^k$. The S^k, $k = 1,2,3, \ldots$, are the various states of the motion of the reference set S.

Let the mapping Φ be the identity mapping. Then, $S^k \equiv S$ for every k, and the reference state S can be considered to be the "state of equilibrium." Around S create the subset $N \subset X$ be setting $N = \cup_i \mathcal{S}_i$. Assume another subset $T \subset N \subset X$. Assume a mapping ψ to be applied on T generating by successive mapping the sets T^1, T^2, T^3, $\ldots$ T^k, $\ldots$, . If for any k, $T^k \subset N$, the state of equilibrium S is said to be stable against a perturbation leading from S to T.

Adopting a more general approach, consider the two subsets $S \subset X$ and $T \subset X$. Apply the mapping Φ on S and a mapping ψ on T. Mapping repeatedly, the sets S^1, S^2, $\ldots$, S^k and T^1, T^2, $\ldots$, T^k are obtained, which can be viewed as elements of *trajectories*. Construct the subspace $\mathcal{N}^k = \cup_i \mathcal{S}_i^k$, where

$$\mathcal{S}_i^k(s_i^k, \delta) = \{x: \quad d(s_i^k, x) < \delta\}$$

are spheres around the points s_i^k of subset S^k. If for any k, $T^k \subset N^k$, it is said that there is *trajectorial stability*. One may also say that the trajectory $\{S^1, S^2, \ldots, S^k, \ldots\}$ is stable against the perturbation caused by switching from S to T and from mapping Φ to mapping ψ.

Another kind of stability is established, if the subspace $\mathfrak{N} = \cup_i N^i$, $i = 1,2, \ldots, k, \ldots$, is introduced. If for any k, $T^k \subset \mathfrak{N}$, *orbital stability* for the trajectories $\{S^1, S^2, \ldots, S^k, \ldots\}$ and $\{T^1, T^2, \ldots, T^k, \ldots\}$ is said to prevail.

It is easy to realize that if the mapping Φ is, as mentioned before, the *identify mapping*, which maps S into itself so that the trajectory $\{S^1, S^2, \ldots, S^k, \ldots\}$ degenerates into an equilibrium state, the trajectorial stability with regard to S and $\{T^1, T^2, \ldots, T^k, \ldots\}$ becomes orbital stability.

The preceding description of stability has on the one hand revealed that stability investigation is in essence a *qualitative* one. On the other hand, it has shown what the mere ingredients of stability are: There has to be an *object* (set of objects) subjected to an *operator* that causes a *reference flow*. This flow gives rise to *trajectories*. A trajectory carries a system of *neighborhoods* along. There will be a *perturbation causing a perturbed flow*. Decision on *stability* is being made by considering a certain *topological relation* between reference flow and perturbed flow, using the system of neighborhood.

Such basic discussion of stability makes the very topological nature of stability obvious and also shows that there is much latitude in assigning a factual meaning to these ingredients of the stability notion.

A special kind of flow is determined by (*i*) a system of *ordinary differential equations*, which for the sake of generality may be nonautonomous, and (*ii*) a related initial value problem.

Consider the system $\ddot{\mathbf{x}} = \mathbf{F}(\mathbf{x}, \dot{\mathbf{x}}, t)$, a Newtonian system, where $\mathbf{F} = (F_1, F_2, \ldots, F_n)$ is a matrix of forces and $\mathbf{x} = (x_1, x_2, \ldots, x_n)$ is the coordinate vector. Setting $x_k = y_{2k-1}$, $\dot{x}_k = y_{2k}$, $\ddot{x}_R = \dot{y}_{2k}$, one arrives at the first-order system

$$\dot{y}_{2k-i} = y_{2k},$$
$$\dot{y}_{2k} = F_k(\mathbf{y},t), \quad k = 1,2, \ldots, n,$$

where

$$\mathbf{y} = (x_1 = y_1, \dot{x}_1 = y_2, x_2 = y_3,$$
$$\dot{x}_2 = y_4, \ldots x_n = y_{2n-1}, \dot{x}_n = y_{2n}).$$

Since the transformation of a Newtonian system into a first-order system is always possible, it is no restriction of generality if, subsequently, exclusively first-order systems will be considered. For the sake of simplification of the representation let the system and its initial condition be written as

$$\dot{\mathbf{y}} = \mathbf{F}(\mathbf{y},t), \quad \mathbf{y}(0) = \mathbf{y}^0. \tag{1}$$

Let the norm be given as

$$\|\mathbf{y}(t)\| = \sum_{i=1}^{2n} |y_i(t)|, \tag{2}$$

which is no restriction of generality, as in a finite-dimensional space all norms are equivalent.

The solution to (1) is

$$\mathbf{y}(t) = \mathbf{y}^0 + \int_0^t \mathbf{F}(\mathbf{y}(s),s)ds \equiv \boldsymbol{\phi}(t). \tag{3}$$

This solution exists and is unique under appropriate conditions for $\mathbf{F}$: Let $\mathbf{F}$ be such that $F_k \in (C, \text{Lip})$. Then,

$$\|\mathbf{F}\| \leq m \text{ and } \|\mathbf{F}(\mathbf{y}^1, t) - \mathbf{F}(\mathbf{y}^2, t)\| \leq k\|\mathbf{y}^1 - \mathbf{y}^2\|.$$

Hence,

$$\|\boldsymbol{\phi}^1 - \boldsymbol{\phi}^2\| = \left\| \int_0^t [\mathbf{F}(\mathbf{y}^1(s),s) - \mathbf{F}(y^2(s),s)]ds \right\| \leq tk\|\mathbf{y}^1 - \mathbf{y}^2\|. \tag{4}$$

Downloaded 02 May 2010 to 171.66.16.250. Redistribution subject to ASME license or copyright; see http://www.asme.org/terms/Terms_Use.cfm

Relationship (4) proves that for $tk < \alpha < 1$, operator ϕ is a contraction operator which guarantees existence and uniqueness of solutions to (1).

Moreover, solutions to (1) represent a flow: To recognize this fact, introduce for operator ϕ defined in (3) the notation

$$\phi(t) \equiv \Phi^t(\mathbf{y}^0) \tag{5}$$

Since $\phi(0) = \mathbf{y}^0$ follows from (3), one can deduce from (5) the existence of a *unit operator*

$$\phi(0) \equiv \Phi^0(\mathbf{y}^0) \equiv \mathbf{y}^0. \tag{6}$$

Hence, from (5) and (6) follows $\phi(t) = \Phi^t(\Phi^0(\mathbf{y}^0)) \equiv \Phi^t(\mathbf{y}^0)$.

Consider the relationship

$$\phi(t+s) = \mathbf{y}^0 + \int_0^{t+s} \mathbf{F}(\mathbf{y}(\xi),\xi)d\xi$$

$$= \left[\mathbf{y}^0 + \int_0^t \mathbf{F}(\mathbf{y}(\xi),\xi)d\xi\right] + \int_t^s \mathbf{F}(\mathbf{y}(\xi),\xi)d\xi. \tag{7}$$

Yet

$$\left[\mathbf{y}^0 + \int_0^t \mathbf{F}(\mathbf{y}(\xi),\xi)d\xi\right] = \mathbf{y}(t).$$

Therefore, also

$$\phi(t+s) = \mathbf{y}(t) + \int_t^s \mathbf{F}(\mathbf{y}(\xi),\xi)d\xi \equiv \Phi^s(\mathbf{y}^t). \tag{8}$$

But, $\phi(t+s) \equiv \Phi^{t+s}$, and $\mathbf{y}^t \equiv \phi^t \equiv \Phi^t$. Hence, from (8),

$$\Phi^{t+s} = \Phi^s(\Phi^t) \tag{9}$$

for solutions to (1).

Since operator $\phi(t)$ is a continuous one, and since it satisfies through (6) and (9) the basic properties of a flow (i.e., identity and group property), the solutions $\mathbf{y}(t)$ to (1) represent a flow.

The conclusion is that the initial value problem of a first-order differential equation system leads under appropriate circumstances to a flow.

There are numerous realizations of a flow. Yet, the initial value problem of a first-order differential equation system was the most obvious and basic example, which was encountered in the course of developing Newtonian mechanics. It should therefore to be no surprise that stability theory had its beginnings when the stability of solutions to ordinary differential equations was investigated. This fact will be pursued further in the next section.

Stability of Dynamic Systems With a Finite Number of Degrees of Freedom

Although we will deal in this section mathematically with a first-order system of differential equations, one should keep in mind that such a system is supposed to represent *the motion of a mechanical object with a finite number of degrees of freedom*. In this way, one is able-to identify, what will be said here, with the facts obtained in the course of the historical development of *mechanics*.

Early attempts on stability followed from J. L. Lagrange's investigations (1762–65) of small vibrations of a system with a finite number of degrees of freedom. In a more general sense, such small vibrations originated from the so-called *variational equations* introduced by H. Poincare (1892).

Consider a first-order system $\dot{\mathbf{y}}(t) = \mathbf{F}(\mathbf{y},t)$. Besides $\mathbf{y}$, the system may have another solution $\mathbf{z} = \mathbf{y} + \eta$, where η is the variation of $\mathbf{y}$. Substituting in the system $\mathbf{z}$ for $\mathbf{y}$ yields

$$\dot{\mathbf{y}} + \dot{\eta} = \mathbf{F}(\mathbf{y}+\eta,t) = \mathbf{F}(\mathbf{y},t) + \frac{\partial \mathbf{F}}{\partial \mathbf{y}}\eta + \ldots,$$

from which follows in the first approximation

$$\dot{\eta} = \frac{\partial \mathbf{F}}{\partial \mathbf{y}}\eta, \quad \text{i.e.,} \quad \dot{\eta}_i = \frac{\partial F_i}{\partial y_j}\eta_j, \quad i,j = 1,2,\ldots,n.$$

These are the linearized variational equations, which for $(\partial F_i/\partial y_j) \equiv \mathbf{A}(t)$ read

$$\dot{\eta} = \mathbf{A}(t)\eta. \tag{10}$$

The solution of (10) is $\eta(t) = \psi(t)\mathbf{c}$, where $\mathbf{c}$ is an appropriate constant vector. Since also $\eta(t_0) = \psi(t_0)\mathbf{c}$ must hold for an initial time t_0, one has $\psi^{-1}(t_0)\eta(t_0) = \mathbf{c}$. Therefore,

$$\eta(t) = \psi(t)\psi^{-1}(t_0)\eta(t_0) = \Omega(t)\eta(t_0). \tag{11}$$

where $\Omega(t) = \psi(t)\psi^{-1}(t_0)$, and $\eta(t_0)$ is the vector of initial values.

One arrives at *small vibrations*, if A is a matrix with *constant* coefficients. Then, $\eta = A\eta$, $\eta = \Omega\eta_0$, and $\dot{\Omega} = A\,\Omega$. Thus, $\Omega = e^{At}$. The resolvent matrix $\Omega = e^{At}$ involves coefficients $\omega_{ij} = \sum_{\sigma=1}^{n} \alpha_{ij}^{(\sigma)} e^{\lambda_\sigma t}$, where $\alpha^\sigma{}_{ij} = \alpha_{ij}^{(\sigma)} P^{(\sigma)}(t)$ (with $\alpha_{ij}^{(\sigma)} = \text{const.}$, $P^{(\sigma)}(t) = $ polynomial in t), $\sigma =$ ordinal number of the eigenvalue λ_σ of matrix A.

A fairly well-established stability theory for these small vibrations has been developed based on a condition ascribed to J. L. Lagrange that for stability, $\|\eta\|$ should be bounded. This is certainly the case if $\|\Omega\|$ is bounded. From

$$\|\Omega\| \leqq \sum_{i,j} |\omega_{ij}|$$

follows that $\|\Omega\|$ is bounded if $|\omega_{ij}|$ is bounded, which on its part is bounded if $|\alpha_{ij}^{(\sigma)}(t)e^{\lambda_\sigma t}|$ is bounded. For the latter to happen, it is sufficient that the real parts of all λ_σ be negative.

Since the λ_σ are the roots of an algebraic equation, say, the characteristic equation following from $\det(A - \lambda_\sigma E) = 0$ (E = unit matrix), the stability problem becomes indirectly an algebraic problem: This is the problem of determining under which condition an algebraic equation has roots with negative real parts and only such roots. It was A. Hurwitz (1895), who solved this problem, thus establishing an indirect criterion for the stability of small vibrations.

Another interesting case is the one, when a certain λ_σ is zero. If at the same time the corresponding $P^{(\sigma)}(t)$ degenerates to a constant, which happens if the defect of $A - \lambda_\sigma E$ is equal to the multiplicity of that eigenvalue $\lambda_\sigma = 0$, then, stability is not effected, see [5]. Yet, realizing that one is actually dealing with a variational system as an approximation to a truly nonlinear system, the case of $\lambda_\sigma = 0$ is in fact a *critical case*. It was this case, which enforced further development of the stability theory of dynamic systems by M. A. Lyapunov, who took it upon himself to investigate for the critical case the influence on stability of nonlinear terms in nonabbreviated variational equations.

Complementing attempts by A. Sommerfeld (1877), M. A. Lyapunov established in the first place an adequate and rigorous stability condition, as follows: "Let $\mathbf{y}^{(1)}$, $\mathbf{y}^{(2)}$ be two solutions of the dynamic system $\dot{\mathbf{y}} = F(\mathbf{y},t)$ which do exist for $t \leq t_0$ and which satisfy the initial conditions $\mathbf{y}^{(1)}(t_0) \equiv \mathbf{y}_{(1)}^{(0)}$, $\mathbf{y}^{(2)}(t_0) \equiv \mathbf{y}_{(2)}^{(0)}$. Let the positive quantity ϵ be given. If another positive quantity $\delta(\epsilon,t_0)$ can be found so that for $\|\mathbf{y}^{(1)}(t_0) - y^2(t_0)\| < \delta$ the condition $\|\mathbf{y}^{(1)}(t) - \mathbf{y}^{(2)}(t)\| < \epsilon$ holds for all $t \geq t_0$, then, the solution $\mathbf{y}^{(1)}$ (considered as the unperturbed one) is said to be stable with respect to the solution $\mathbf{y}^{(2)}$ (considered as the perturbed one)."

This definition can be made compatible with the earlier mentioned stability definition of A. Sommerfeld, if one presupposes in addition, continuous dependence of the solutions $\mathbf{y}(t)$ on their initial values $\mathbf{y}(t_0)$. Then, it follows that the measure of perturbation ϵ of the solutions decreases continuously and tends toward zero as the perturbation δ of the initial values tends toward zero.

Downloaded 02 May 2010 to 171.66.16.250. Redistribution subject to ASME license or copyright; see http://www.asme.org/terms/Terms_Use.cfm

It is interesting to note, that for small vibrations, the Lagrangian stability definition based on the boundedness of $\| \eta \|$, also actually satisfies Lyapunov's stability definition: As shown earlier, $\eta(t) = \Omega(t)\eta(t_0)$. Hence, $\|\eta^{(1)}(t) - \eta^{(2)}(t)\| \leq \| \Omega(t)[\eta^{(1)}(t_0) - \eta^{(2)}(t_0)] \| \leq \|\Omega\| \, \| \eta^{(1)}(t_0) - \eta^{(2)}(t_0)\|$. Yet, in the case of a vibration, $\|\Omega\| \leq k$, where k is an appropriate constant. Let $\|\eta^{(1)}(t_0) - \eta^{(2)}(t_0)\| < \delta$ hold. Then, obviously, $\|\eta^{(1)}(t) - \eta^{(2)}(t)\| \leq k\delta = \epsilon$. That is stability in the sense of Lyapunov, and even stronger: by virtue of the relationship $\epsilon = k\delta$, there is continuous dependence of ϵ on δ. Hence, the perturbation of the solution $\eta^{(1)}$ tends toward zero, if the perturbation δ of the initial value $\eta^{(1)}(t_0)$ so does.

Recall, that $\mathbf{y}(t)$ was supposed to be a solution, say, the unperturbed one, of $\dot{\mathbf{y}}(t) = \mathbf{F}(\mathbf{y},t)$. Consider $\mathbf{z}(t) = \mathbf{y}(t) + \eta(t)$ to be a perturbed solution satisfying $\dot{\mathbf{z}}(t) = \mathbf{F}(\mathbf{z},t)$. Consider the variation $\dot{\eta}(t) = \mathbf{z}(t) - \mathbf{y}(t)$. Hence, also $\dot{\eta}(t) = \mathbf{F}(\mathbf{z},t) - \mathbf{F}(\mathbf{y},t) = \mathbf{H}(\eta,t)$.

Having transformed the original stability problem of $\eta(t)$ in this way, it can now be reinterpreted as the stability of the zero solution $\eta \equiv \mathbf{0}$, while the perturbed solution is $\eta(t) \neq \mathbf{0}$. For stability of the zero-solution, one has to require that for a given ϵ, a δ exists so that if $\|\eta(t_0)\| < \delta$, the condition $\|\eta(t)\| < \epsilon$ is satisfied for any $t \geq t_0$.

Instead of investigating the behavior of the trajectory, let the orbit of $\eta(t)$ be investigated in a vector space V_{2n} spanned by a set of $\eta_1, \eta_2, \ldots, \eta_{2n}$ axes, in which $\bar{\eta} = (\eta_1(t), \ldots, \eta_{2n}(t))$, the projection of η along the t-axis onto the vector space, is for any fixed value of t, a point in this space. In this way, a geometric interpretation of stability is possible: Let $\mathcal{S}(\mathbf{0},\delta)$ and $\mathcal{S}(\mathbf{0},\epsilon)$ be spheres in the vector space V_{2n} with centers in $\mathbf{0}$ and radii δ and ϵ. If for $\bar{\eta}(t_0)$ in $\mathcal{S}(\mathbf{0},\delta)$, the subsequent image points $\bar{\eta}(t)$ of the orbit in V_{2n} remain for all $t \geq t_0$ in $\mathcal{S}(\mathbf{0},\epsilon)$, then, the "equilibrium position" $\mathbf{0}$ in the vector space is said to be stable.

To assess the behavior of the orbit of $\eta(t)$, M. A. Lyapunov introduced a test function $L = W(\eta_i) - c = 0$ in V_{2n}, $c =$ positive const., of which he assumed that for an infinite sequence of value of $c \epsilon R^{(+)}$, ($R^{(+)}$ = positive real line), the corresponding sequence of L would pass through any point in the vector space and that for $c \to 0$, L would shrink into the $\mathbf{0}$-point. This requirement can for example be met by choosing W as a function that becomes positive definite within a sufficiently large sphere $\mathcal{S}(\mathbf{0},\rho)$, $\rho > \max(\epsilon,\delta)$, around point $\mathbf{0}$. Due to the property attributed to L, it can be asserted that any point of the orbit is located at a certain time on one of the L-functions. If in addition it is assumed that

$$\frac{dL}{dt} = \dot{L} = \frac{\partial W}{\partial \eta_i}\dot{\eta}_i = \frac{\partial W}{\partial \eta_i}H_i = \text{grad } W \cdot \mathbf{H} \leq 0,$$

then, the orbit remains either permanently on a certain L-function for $\dot{L} = 0$ or traverses it from the outside toward the inside for $\dot{L} < 0$. Let for example $\dot{L} < 0$ at any time. Then, the point $\bar{\eta}(t_0)$ is within the sphere $\mathcal{S}(\mathbf{0},\rho)$ and therefore momentarily on a closed surface around point $\mathbf{0}$, since W is supposed to be positive definite in this sphere. Due to $\dot{L} < 0$, the orbit will proceed from this surface to the next one which is *inside* of the first one, and so on. Thus, the orbit will remain at any time at least within the sphere $\mathcal{S}(\mathbf{0},\rho)$. Consequently, point $\mathbf{0}$ is stable.

One easily realizes that the original stability conditions of M. A. Lyapunov can be generalized. That is best understood if one interprets his theory in geometric terms as a special case of a broader theory: Consider for the sake of simplicity a space of only two dimensions, say, V_2. In V_2, a set of arbitrary curves is supposed to exist whose arbitrariness is however limited by the following assumptions: The set consists of simple, smooth curves $L = W(\eta) - c = 0$. While $c \to 0$, the set is supposed to cover, as sequence of nested curves, continuously the whole space V_2. The curves are required to shrink for $c = 0$ into $\mathbf{0}$ or at least toward a "double curve," bounding in V_2 a domain that contains $\mathbf{0}$, has an infinitesimal small "volume," and is completely contained in a strip of bounded width perpendicular to one of the axes in V_2.

Let the individual curve of such a set be called a "multicline," due to its smoothness, the quantity $\dot{L} = (\partial L/\partial \dot{\eta}_i) H_i$ exist at any point of the curve, prescribing at such individual point of the curve the slope of the η-orbit with respect to the curve. Since the set of L-curves covers V_2, there is at any point of V_2 a value of $\dot{L}$. By means of these $\dot{L}$ values, a "topography" is prescribed on V_2. This topography decides the way in which the η-orbit will "flow" through V_2 starting at an initial point $\eta(t_0)$. Thus, the topography induced on V_2 by means of $\dot{L}$ and the L-set will reveal the extent to which the point $\mathbf{0}$ may be stable. It appears to be obvious that a "lense" of positive $\dot{L}$ points on V_2, which is bounded by a closed curve carrying $\dot{L} = 0$ values (see hatched area in Fig. 1), leads to a statement like $|\eta_2| < k$ at any time $t \geq t_0$. That is indeed a kind of conditional stability of $\mathbf{0}$. The final conclusion is that a set of *closed* L-curves surrounding $\mathbf{0}$, and a V_2-topography following from the condition "$\dot{L} \leq 0$ throughout V_2" (i.e., a *Lyapunov*-topography) is only one of many other choices which one can make to assess stability of $\mathbf{0}$.

Indeed, the L-surfaces in V_{2n} may form a set of nested cylinders which have however projections that are closed around point $\mathbf{0}$ in a subspace of V_{2n}. Then, the L-surfaces are not truly positive definite in V_{2n}, and stability of $\mathbf{0}$, if at all, can only be asserted with respect to the said subspace of V_{2n}, i.e., in a conditional way. Also, as stated in the foregoing, the requirement that $\dot{L}$ is sign-definite throughout V_{2n} can be relaxed. Modern developments of stability theory along such lines do in fact already exist; see for example investigations by A. Olas (1980) in [6] and by H. Leipholz (1980) in [7]. A. Olas has, for example, substituted Lyapunov's requirement that $\dot{L} \leq 0$, by the weaker requirement

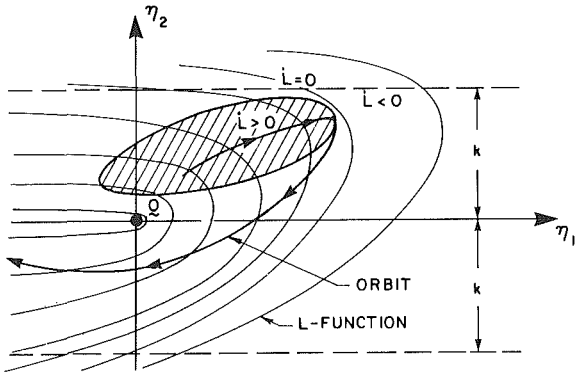
$$\int_{t_0}^{t} L(\tau,\eta)d\tau \leq 0,$$

which does not exclude the possibility that $\dot{L} > 0$ holds in some subset of the neighborhood of point $\mathbf{0}$. On his part, H. Leipholz has replaced the Lyapunov condition for L by a "growth condition" for $\dot{L}$ which reads

$$\int_{t_0}^{t} \frac{\partial L}{\partial \eta_i} H_i d\tau < \epsilon(1-\gamma); \quad \epsilon = \text{small, positive}; \quad \gamma < 1.$$

This condition is even weaker than the one by A. Olas.

A difficult problem has all along been: how to find an appropriate Lyapunov function L, which is positive definite and satisfies the condition $\dot{L} \leq 0$. If the dynamic system is



CONDITIONAL STABILITY : $|\eta_2| < k$ FOR THE ORBIT SHOWN

Fig. 1 *L*-function topography in the phase space

Downloaded 02 May 2010 to 171.66.16.250. Redistribution subject to ASME license or copyright; see http://www.asme.org/terms/Terms_Use.cfm

linear and the corresponding system of differential equations has constant coefficients, a Lyapunov function can be constructed systematically. This is also true under appropriate assumptions for a linear system, perturbed by nonlinear terms, as shown by W. Hahn (1967), see [8]. Another interesting method to construct Lyapunov functions for certain linear, nonautomous or nonlinear differential equations has been proposed by P. J. Ponzo (1965), [9], and generalized by R. J. Charron (1982), [10]. But, in spite of any such attempts, the problem has not been solved summarily. Yet, this may not even be necessary any more, if one replaces the specific kind of L-functions required by Lyapunov by the less restrictive L-functions proposed earlier in this paper and called "multiclines." It should be possible to find such functions with much less difficulties than the actual functions proposed by M. A. Lyapunov. Once the multiclines have been chosen, one can determine the topography on V_{2n} by calculating the distribution of the $\dot{L}$ values on V_{2n}. This topography decides on the stability of point **0**.

Instead of generalizing the L-function concept, one may, on the other hand, specialize it. This can easily be done in the case of conservative dynamic systems. For such systems, the energy may be a positive definitie function and can serve in a natural way as an L-function. It was E. J. Routh who proposed to use the energy of a dynamic system to assess the stability of an unperturbed (reference) motion against perturbations. There is no difficulty to show that the theory he developed fits completely into the more general theory established by M. A. Lyapunov, if one interprets the Hamiltonian $\mathcal{H}$ of the conservative system as an L-function. Since $\mathcal{H}$ is a first integral of the system, condition $\dot{\mathcal{H}} = 0$ follows immediately, thus, making the choice of $\mathcal{H}$ as an L-function very appropriate. Stability is decided on by requiring that $\mathcal{H}$ be positive definite. In the light of these findings, it becomes clear that Routh's theory has no importance of its own and can be viewed as a special case of Lyapunov's theory. Yet, from the historical point of view, it still makes sense to refer to E. J. Routh, since one learns through his work, as one of many other examples, how the human mind felt its way through the stability problem, before reaching sufficient clarity about this subject.

The definition of Lyapunov for stability requires that a comparison between the unperturbed motion $\mathbf{y}^{(1)}(t)$ and the perturbed one, say, $\mathbf{y}^{(2)}(t)$, is to be made at equal moments of time for both motions, i.e., $\|\mathbf{y}^{(1)}(t) - \mathbf{y}^{(2)}(t)\| < \epsilon$ for any $t \geq t_0$ must hold for stability. This condition is in many cases too demanding and does indeed exclude a number of phenomena from the class of stable motions, which most people would regard as stable. As J. J. Stoker [11] pointed out, a way out of this dilema is to follow H. Poincare's proposal and to adopt the notion of *orbital* stability.

To deal with orbital stability, time should be excluded from one's considerations. This can be done by projecting the trajectories of a flow parallel to the time axis (R-axis), onto the metric space κ, thus, generating in κ the orbits of the motion. There is orbital stability of a reference motion (unperturbed motion), if the orbit of a perturbed motion remains in a prescribed neighborhood of the orbit of the reference motion. As pointed out earlier, orbital stability comes naturally into play if one deals with the stability of a state of equilibrium. This is true, even if one would use the terminology of Lyapunov's method, i.e., requiring for stability of point **0** that $\|\eta(t)\| < \epsilon$ for all $t \geq t_0$, because this is equivalent to the *orbit* η remaining in a prescribed sphere $S(\mathbf{0},\epsilon)$, where the term sphere is to be used in the broadcast sense, including also a square, a cube, etc. These facts have been stressed to make it apparent that the various notions of stability, although seemingly different at a first glance, are actually closely related and in a sense, variations of one and the same theme.

Dealing with stability of a dynamic system described by a system of differential equations, the orbits are curves in a V_{2n} -space. Since one can assume that the differential equation system is of the first order, these orbits are first integrals of that system.

Let the system by given as $\dot{\mathbf{y}}(t) = \mathbf{F}(\mathbf{y})$, i.e., as an autonomous one. The singular points (points of "equilibrium") follow from condition $\mathbf{F}(\mathbf{y}) = 0$. The result may be a set of points $\mathbf{y}_s$. To study the stability of these points, set $\mathbf{y} = \mathbf{Y}_s + \eta$ and use $\mathbf{y}$, thus specified, in the first-order system. The result are variational equations of the kind

$$\dot{\eta} = \frac{\partial \mathbf{F}}{\partial \mathbf{y}} \eta + \text{higher order terms.} \tag{12}$$

If the singular points are *simple*, i.e., if not all of the $\partial \mathbf{F}/\partial \mathbf{y}$ are zero, one may use the linear equations $\dot{\eta} = (\partial \mathbf{F}/\partial \mathbf{y})\eta$ to determine the trace of a perturbed orbit around a simple singular point. If all $\partial \mathbf{F}/\partial \mathbf{y}$ vanish, the singular point for which that happens is nonsimple. Then, one must work with nonlinear variational equations taking higher order terms in equation (12) into account. These nonlinear equations may subsequently be used for the tracing of the perturbed motion's orbit.

Depending on the trace of the perturbed orbit, the singular points may be centers, nodes, saddles, etc., and they indicate in a well-established way whether the respective singular point is stable or not.

One of the problems, faced is how to determine the trace of the orbits, following from $\dot{\eta}_i(t) = H_i(\eta)$, around the singular point. Since stability theory can in this context be interpreted as a kind of "qualitative theory" of the solutions to differential equations, and since a qualitative theory is meant to provide information with a little effort as possible towards actually solving the differential equations, one could certainly try to apply Lyapunov's method to the stability of the singular point in question. In this case, one chooses the said function $L = W(\eta) - c = 0$ and determines the slope $\dot{L} = (\partial W/\partial \eta_i) H_i$ with which the orbit crosses L. If L can be found to be positive definite and $\dot{L} \leq 0$, around the singular point, one can conclude on stability without actually drawing the orbit. Such a procedure would indeed satisfy the characteristics of a qualitative approach to the largest extent. In many cases, it may be difficult to find such a positive definite function L. Then, one may choose a more arbitrary net of L-functions, and may use $\dot{L} = (\partial W/\partial \eta_i)H_i$ together with $\partial \eta_i/\partial t = H_i$ for an approximate, graphical determination of the orbit. In the extreme case, let $L = W^*(\eta) - c$, where W^* is the solution of $\partial W/\partial \eta_i = \text{const.}\ (H_i^{-1})$. Then, L is an "isocline," and one is back in well-known territory of graphic treatment of differential equations. From this point of view, one can assess Lyapunov's theory as the last stage in the following development: (*i*) choose isoclines; determine the orbit of a perturbed motion; infer on stability of the singular point; (*ii*) choose appropriate, yet arbitrary curves $L = W(\eta) - c$, which are neither isoclines nor Lyapunov functions, and use the relations

$$\frac{dL}{dt} = \frac{\partial W}{\partial \eta_i} H_i, \quad \frac{d\eta_i}{dt} = H_i(\eta),$$

to draw the orbit of a perturbed motion; infer on stability of the singular point; (*iii*) choose especially positive definite L-functions and use these, together with relationship $\dot{L} = (\partial W/\partial \eta_i)H_i$, for concluding on stability of the singular point without even drawing the orbit of a perturbed motion. At stage (*iii*) one has reached Lyapunov's approach to stability which now appears to be a sophisticated version of a "graphical integration" of the differential equation yielding the orbit of a perturbed motion.

Assume critical points in the phase space and orbits around

Downloaded 02 May 2010 to 171.66.16.250. Redistribution subject to ASME license or copyright; see http://www.asme.org/terms/Terms_Use.cfm

these critical points have been determined. Assume further, that the system of differential equations involves a set of parameters λ_r^0, $r = 1,2, \ldots, l$. It will now be shown that, in varying these parameters, one can influence the nature of the critical points and thus the stability behavior of the dynamic system. The phenomenon of the system's reaction to parameter changes is called "structural stability." Structural stability embraces a vast field of stability problems, specifically in structural engineering. For example, Euler's fundamental problem of column buckling deals with structural stability, the parameter causing instability being the compressive load.

Including the parameters in one's investigations, the first-order, differential equation system reads $\dot{y}_i = F_i(y_i, \lambda_r^{(0)}, t)$, $i = 1,2, \ldots, 2n$, $r = 1,2, \ldots, l$, yielding the solutions $y_i = y_i(\lambda_r^{(0)}, t)$. A perturbation of the parameters leads to the perturbed solutions $y_i^{(p)} = y_i(\lambda_r^{(0)} + \beta_r, t) = y_i(\lambda_r^{(0)}, t) + \beta_r (\partial y_i/\partial \lambda_r)_{\lambda_r = \lambda_r^{(0)}}$, where the β_r are the parameter variations. The perturbed solutions satisfy the conditions

$$\dot{y}_i^{(p)} = \dot{y}_i(\lambda_r^{(0)}, t) + \frac{d}{dt}\left[\left(\frac{\partial y_i}{\partial \lambda_r}\right)_{\lambda_r = \lambda_r^{(0)}} \beta_r\right]$$

and

$$\dot{y}_i^{(p)} = F_i(y_k^{(p)}, \lambda_r^{(0)} + \beta_r, t) = F_i\left[y_k(\lambda_r^{(0)}, t) + \left(\frac{\partial y_k}{\partial \lambda_r}\right)_{\lambda_r = \lambda_r^{(0)}} \beta_r, \lambda_r^{(0)} + \beta_r, t\right].$$

Thus,

$$\frac{d}{dt}\left[\left(\frac{\partial y_i}{\partial \lambda_r}\right)_{\lambda_r = \lambda_r^{(0)}} \beta_r\right] = \left(\frac{\partial F_i}{\partial \lambda_k}\right)_{\substack{\lambda_r = \lambda_r^{(0)} \\ y_k = y_k(\lambda_r^{(0)}, t)}} \left(\frac{\partial y_k}{\partial \lambda_r}\right)_{\lambda_r = \lambda_r^{(0)}} \beta_r + \left(\frac{\partial F_i}{\partial \lambda_r}\right)_{\substack{\lambda_r = \lambda_r^{(0)} \\ y_k = y_k(\lambda_r^{(0)}, t)}} \beta_r,$$

which follows from a Taylor expansion of the right-hand side of the differential equation. Cancelling the common factor β_r and introducing the *sensitivity* $s_{ir} = (\partial y_i/\partial \lambda_r)_{\lambda_r = \lambda_r^{(0)}}$, one arrives at the *sensitivity equations*

$$\dot{s}_{ir} = \left(\frac{\partial F_i}{\partial \lambda_k}\right)_{\substack{\lambda_r = \lambda_r^{(0)} \\ y_k = y_k(\lambda_r^{(0)}, t)}} s_{kr} + \left(\frac{\partial F_i}{\partial \lambda_r}\right)_{\substack{\lambda_r = \lambda_r^{(0)} \\ y_k = y_k(\lambda_r^{(0)}, t)}}. \tag{13}$$

These equations, another kind of variational equations, yield the sensitivity s_{ir} as their solutions. There is stability against parameter perturbation, if $| s_{ir} | < \epsilon$, where ϵ is a small, prescribed quantity.

In problems of structural analysis, y_i is for example the deflection of a structure at a certain point, λ_r a load, and $y_i = y_i(\lambda_r)$ the well-known load-deflection curve. Indeed, if that curve has a load maximum at which $\partial y_i/\partial \lambda_r = \infty$, instability, for example snap-through, occurs. Hence,

$| \partial y_i/\partial \lambda_r | < \epsilon < \infty$ is stability, $| \partial y_i/\partial \lambda_r | = \infty$ is instability.

In the general case, s_{ir} follows from a set of first-order differential equations. However, one is entitled to eliminate the influence of time on the sensitivity by setting $\dot{s}_{ir} = 0$. The justification is that the moment of time at which $s_{ir} = \infty$ causes instability is completely arbitrary, as there is no specification on how to count time in the context of parameter sensitivity. Therefore, modifying equations (13) into $(\partial F_i/\partial y_k)s_{kr} + (\partial F_i/\partial \lambda_r) = 0$, one obtains for the sensitivity

$$s_{ir} = \Delta_r^{(i)}/\Delta, \quad \text{where } \Delta = \det(\partial F_i/\partial y_k),$$

and $\Delta_r^{(i)}$ is the determinant that follows from Δ by replacing respective columns of this determinant by the column vectors $(-\partial F_i/\partial \lambda_r)$.

One realizes that $s_{ir} = \infty$, i.e., instability, follows for $\Delta = 0$. This condition yields λ_{crit}, which is the critical value of the control parameter which causes instability, i.e., for example, snap through. It may be interesting to mention that $s_{ir} = (\partial y_i/\partial \lambda_r)$ can also interpreted as the "deformation velocity" of the phase diagram in the phase space. When this velocity becomes infinite, critical points in the phase diagram collapse, coalesce with others, and formerly stable points become unstable. A description of such phenomena can be found in [12]. An abstract, mathematical description of structural stability is given in [13].

It appears to be the case that from Lyapunov stability, involving perturbation of initial values of the system, stability branches out to structural stability involving parameter perturbation. Also, one may feel that one has switched from Lyapunov's stability condition to another one given by $| s_{ir} | < \infty$. This is actually not true. The consistency of the stability theory is not at stake at all: For example, consider initial conditions as parameters. Let $\dot{\eta}_i = A\eta_i$ be the system of variational equations following from the perturbation of initial conditions. The solution of that system is $\eta = e^{At}$, and stability is decided on by the behavior of the eigenvalues of martix A. Now, return to the original equation $\dot{\mathbf{y}} = \mathbf{F}(\mathbf{y}, t)$ describing the dynamic system. Obviously, $\mathbf{y} = \mathbf{y}(\mathbf{y}^{(0)}, t)$, where $\mathbf{y}^{(0)}$ is the vector of initial conditions. In deriving those sensitivity equations for which the initial conditions are taken as parameters, one obtains

$$\frac{d}{dt}\left[\frac{\partial y_i}{\partial y_r^{(0)}}\right] = \frac{\partial F_i}{\partial y_k}\frac{\partial y_k}{\partial y_r^{(0)}} + \frac{\partial F_i}{\partial y_r^{(0)}}, \quad \frac{\partial F_i}{\partial y_r^{(0)}} = \frac{\partial F_i}{\partial y_k}\frac{\partial y_k}{\partial y_r^{(0)}}.$$

Hence,

$$\dot{s}_{ir} = 2As_{ir}, \quad s_{ir} = e^{2At},$$

since $(\partial F_i/\partial y_k) = (a_{ik}) \equiv A$. Thus, the condition $| s_{ir} | \to \infty$ indicating instability, comes again about by the eigenvalues of the same matrix A as in the foregoing. This fact confirms that using either Poincare's variational equations or sensitivity equations for a stability investigation is, for the case considered, equivalent.

For Lyapunov stability, one requires $| \mathbf{y}^{(1)}(\mathbf{y}_{(1)}^{(0)}, t) - \mathbf{y}^{(2)}(\mathbf{y}_{(2)}^{(0)}, t) | < \epsilon$ for two trajectories $\mathbf{y}^{(1)}$ and $\mathbf{y}^{(2)}$ obtained from different initial conditions $\mathbf{y}_{(1)}^{(0)}$ and $\mathbf{y}_{(2)}^{(0)}$. This condition can be substituted by $| \mathbf{y}^{(1)} - \mathbf{y}^{(2)} | < | \mathbf{y}_{(1)}^{(0)} - \mathbf{y}_{(2)}^{(0)} | p$, where p is a sufficiently small positive quantity. Hence, also

$$\left| \frac{\mathbf{y}^{(1)} - \mathbf{y}^{(2)}}{\mathbf{y}_{(1)}^{(0)} - \mathbf{y}_{(2)}^{(0)}} \right| < p, \quad \left| \frac{\partial y_i}{\partial y_k^{(0)}} \right| < p, \text{ respectively.}$$

Considering $y_k^{(0)} \equiv \lambda_k$ as a parameter, one has actually $| \partial y_i/\partial \lambda_k | = | s_{ik} | < p$, which shows that also the two seemingly different stability conditions can be made equivalent.

In the spirt of such drive towards a uniform stability theory, two recent developments may be mentioned. First, it could be shown that in the case of creep stability, time may be interpreted as a destabilizing structural parameter [14]. Second, based on this assumption, creep stability could then be classified as structural stability of nonconservative, nonautonomous dynamic systems in the phase space, using the concept of sensitivity against parameter perturbations as the means for an evaluation of stability [15].

Stability of Continuous Dynamic Systems.

Stability theory for continuous, elastic systems used to deal (and still does to a large extent) with the stability of the *equilibrium position* of such systems, using *statics* to determine so called *buckling laods*. This theory is an extensive

Downloaded 02 May 2010 to 171.66.16.250. Redistribution subject to ASME license or copyright; see http://www.asme.org/terms/Terms_Use.cfm

one; names like L. Euler (1757), G. Dirichlet (1846), A. G. Greenhill (1881), G. H. Bryan (1888), E. Trefftz (1930), S. Timoshenko (1936), W. T. Koiter (1945), and others are attached to it. Due to its specific nature as a static theory, it appeared to be an individual branch of stability theory existing independently beside the stability theory for dynamic systems. There were of course early attempts, for example, by A. Sommerfeld (1905), to fit stability problems of continuous, elastic systems into the general stability theory of dynamic systems by considering the small vibrations about the equilibrium positions of the continuous, elastic systems. However, these investigations showed that increasing the compressive load meant decreasing the vibration frequency until the buckling load was reached at zero frequency, i.e., at a nontrivial equilibrium position. Hence, one concluded that a dynamic approach to stability was redundant and that the stability of continuous elastic systems should indeed be dealt with by means of statics. Such a conclusion is unfortunately only partly correct. It holds true, if the system is a *conservative* one. The first researcher to realize that one might easily be confronted with a nonconservative problem for which the conclusion may not hold any more, was probably E. L. Nikolai (1927), who dealt with twisted bars. In such a case, the torque turns out to be a *follower force*, which is not derivable from a potential. Then, it can happen that no nontrivial equilibrium position of the bar exists, which means that stability is lost by flutter. The corresponding flutter load cannot be detected by means of statics, and a dynamic approach to stability is then inevitable. Therefore, the need to also consider a continuous, elastic system in a general loading case as a dynamic system, and to apply to it a dynamic method to decide on stability, was for the first time expressed very definitely by H. Ziegler (1952). His critical review of stability criteria [16] marks a turning point in the history of general stability theory, as it initiates a development that led to the inclusion of the stability theory for continuous, elastic systems in a unified dynamic theory. This development took place, of course, in close connection with investigations devoted to the stability of systems with follower forces. Some names related with this topic are V. V. Bolotin [17], H. Ziegler [2], H. Leipholz [7, 18], and K. Huseyin [19].

It should be mentioned here, that another loading case, say, a loading consisting of harmonic forces, requires again a dynamic approach to stability. For problems of that kind, the term "dynamic stability" has been introduced. Yet, in some early attempts to tackle dynamic stability, for example by N. J. Hoff, B. Budiansky, and E. Mettler [20], the true nature of the problem had been simplified by replacing the actually continuous systems by corresponding approximate systems with a finite number of degrees of freedom. This is still partly the case in the basic work of V. V. Bolotin [21] on dynamic stability. As a result of such simplification, the actual difficulties and specific features of the stability of *dynamic*, continuous, elastic systems came to light only later.

To also apply the dynamic version of stability theory to continuous, elastic systems, it had to be shown first that they can be viewed as dynamic systems in that abstract sense which had been introduced earlier. This has been done for example by J. K. Hale (1969). An even broader definition of a continuous dynamic system was given by R. J. Knops and E. W. Wilkes [22].

Having classified certain continuous systems as dynamic systems, the immediate reaction must be to apply the well-developed stability theory that exists for dynamic systems with a finite number of degrees of freedom to continuous dynamic systems as well. However, that is not so simple. Continuous systems, possessing an infinite number of degrees of freedom, have their pecularities. It was therefore an essential development of modern stability theory, when Lyapunov's method was adjusted for an application to continuous systems. One of the first researchers contributing successfully to this process was A. A. Movchan (1959).

While it was relatively simple to treat the stability of a rod using Lyapunov's theory, since a rod is a *one-dimensional* continuous system, the true difficulties came to light when considering for example a two-dimensional system like a rectangular plate. This was done by H. Leipholz in [23]: Let the characteristics of the plate be its deflection $w(x,y)$ and the derivatives $\dot{w}$, w_x, w_y, w_{xx}, w_{xy}, and w_{yy} of the deflection representing velocities, slopes and curvatures. The most obvious choice for a Lyapunov functional in the case of a plate subjected to conservative, compressive forces is the Hamiltonian $\mathcal{H} = 1/2 \int_S \{\mu h \dot{w}^2 + D[w_{xx}^2 + 2w_{xx}w_{yy} + w_{yy}^2 + 2(1-\nu)(w_{xy}^2 - w_{xx}w_{yy}) - q/D(l-x)w_x^2]\}dS$, where q are distributed, compressive forces acting parallel to the plate's side of length l. One is used to consider that value of q, which makes $\mathcal{H}$ lose its positive definiteness, to be the buckling load causing instability. Hence, one tends to claim stability when q is smaller than the buckling load and $\mathcal{H}$ is therefore still positive definite. But, one must realize, that $\mathcal{H}$ can never be truly positive definite in the space of the characteristics, since $\mathcal{H}$ does not include the deflection w and the slope w_y. Therefore, one must work with $\mathcal{H}$ actually in a subspace only, which one obtains from the space of the characteristics by means of appropriate projections. As a result, one can at best claim conditional stability. The way in which stability would prevail if q were a value below the so-called buckling load, thus, making $\mathcal{H}$ positive definite, must be derived in terms of an appropriate norm from the expression representing $\mathcal{H}$. One may, for example, find $\int_S (w_x^2 + w_y^2)dS < \epsilon$ being satisfied at all times, which would indicate permanent smallness of the slopes in the mean square: a very weak stability statement, indeed! For stability one would certainly expect smallness of the deflections at any point of the plate's surface. To show that this condition might be satisfied, one had to carry out several transformations, using a series of inequalities. For these inequalities to hold true, one is, however, forced to lower the stability limit gradually *below* the value corresponding to the classical buckling load of a plate. Only for such a lower value of q could one then expect a stability behavior of the plate which appears to be the common one. But, with this finding, one has reached an important point of understanding the stability behavior of continuous, elastic systems: The Lyapunov functional yields always a *specific* norm measuring a specific stability behavior only. Since one is working for a continuous system in the space of the characteristics, which has infinite dimensions, norms are not equivalent any more to each other as in a finite dimensional Euclidean space. Hence, it sometimes takes a great effort (depending on the boundary conditions of the continuous system) to change from a stability norm prescribed by the Lyapunov functional to a more practical norm appropriate for design purposes. And this changing over from one norm to the other may be accompanied by a sacrifice in the magnitude of the stability limit. These facts, mentioned so far, may also explain the difficulties to meet the classical buckling load experimentally. Discrepancies between predicted values for the buckling load and measured ones may not only result from imperfections and interactions with testing equipment, but may be due to an erroneous calculation of the buckling load. How questionable the classical energy approach to plate buckling may be, has for example been emphasized by H. Leipholz [24]. The final conclusion must be that dealing with the stability of continuous systems via Lyapunov's method requires a thorough application of topology and functional analysis, as shown in the already mentioned reference [23].

As long as the systems are conservative, the Hamiltonian is readily available as a Lyapunov functional. The situation becomes more difficult, if the continuous system is subjected

Downloaded 02 May 2010 to 171.66.16.250. Redistribution subject to ASME license or copyright; see http://www.asme.org/terms/Terms_Use.cfm

to follower forces and therefore becomes nonconservative. Then, the choice of an appropriate Lyapunov functional is not obvious any more. P. C. Parks [25] suggested a method to derive suitable functionals. His method is actually an analog in the realm of partial differential equations to the one proposed by P. J. Ponzo for ordinary differential equations. H. Leipholz [26] has applied the properly modified Lyapunov approach to the stability investigation of a number of continuous, elastic systems subjected to follower forces establishing a well defined methodology.

Another important step toward the use of Lyapunov's theory in the context of continuous systems was made by replacing the energy functional, which in the nonconservative case is not time invariant any more, by other functionals that are time invariant in spite of the presence of follower forces. Such functionals come about by switching from Hilbert spaces with the usual "scalar product" of forces and displacements to more general spaces in which products of adequately chosen differential operators are introduced [27]. In this way, energy-wise nonconservative systems may become "conservative of the second kind," the lacking self-adjointness of their boundary-value problems being substituted by a "generalized self-adjointness." Functionals created by means of such "generalized semiscalar products" may serve as Lyapunov functionals as well as a basis for stationarity principles. However, in some cases, the sign definiteness of the functionals may be lost. Yet, as H. Leipholz has shown [28], the functionals are still applicable, if one is ready to switch from common norms to indefinite norms like the one introduced by H. Minkowski.

Lyapunov's approach to stability is an impressive one, and the results obtained cover the stability of a system in a general sense and not just the stability of a particular motion of the system. Yet, despite this advantage, the method yields sufficient conditions for stability only. Therefore, the stability limits obtained are not always sharp ones, sufficiently close to the real ones, which should be known for the sake of an economical design. Hence, another method has been developed for the calculation of continuous system's stability limits using functional analysis and specifically the spectral theory of self-adjoint and nonself-adjoint operators. The introduction and justification of such methods can be seen as a major event in the drive to expand stability theory into the realm of dynamic systems with an infinite number of degrees of freedom.

For a derivation of the basic equtions, one may fall back on general principles, including well-known extremum principles. These may then be used for an application of so-called "direct methods." It is a welcome by-product of the aforementioned method to have contributed to a clarification of what the relationship between principles like virtual work, Hamilton, etc., are, and what the domains of applicability of corresponding methods like Galerkin, Ritz, etc., actually might be [20]. Not suprisingly, the principle of virtual work turns out to be the most fundamental one, easily allowing the inclusion of nonconservative forces' effects. The other principles can be derived from the principle of virtual work by equivalence operations, using from case to case additional, simplifying, but at the same time, restricting assumptions. Hence, Galerkin's method is correspondingly the most general one, requiring yet that its coordinate functions satisfy *all* the boundary and the initial conditions imposed on the dynamic system. To preserve the well-known advantage of Ritz's method, that only geometric boundary conditions have to be met by the coordinate functions, additional terms can be added to the principle of virtual work, which compensate for the violation of the dynamic boundary conditions. This has been shown in [29] and put to practice in [30].

Assuming in the following for the sake of simplicity that the variations satisfy *all* conditions of the system, one has as a starting point for example the relationship

$$\int_\Omega \{D_{0,t}[w(\mathbf{x},t)] + D_{1,\mathbf{x}}[w(\mathbf{x},t)] + q(\mathbf{x},t)D_{2,\mathbf{x}}[w(\mathbf{x},t)]\}\delta w d\Omega = 0,$$

where D_0, D_1, and D_2 are linear differential operators acting on t or $\mathbf{x}$, respectively. Moreover, w is the system's characteristic (for example, deflection), $\mathbf{x}$ is the vector of spatial coordinates, t is the time, q is a structural parameter (for example, load), and Ω is an appropriate domain of integration. A basic idea (L. W. Kantorovich, 1933) is to replace w by the series $w(\mathbf{x},t) = \Sigma f_i(t)\phi_i(x)$. The convergence of such a series is justified by expansion theorems provided by functional analysis. The f_i are supposed to satisfy initial or periodicity conditions. The coordinate functions ϕ_i are required to satisfy the boundary conditions of the original problem and must form a *complete* set. A systematic way to generate appropriate coordinate functions consists in solving the auxiliary eigenvalue-boundary value problem $D_{1,\mathbf{x}}[\phi_i] = \lambda_i\phi_i$ for the boundary conditions of the original problem. As one sees, the coordinate functions are then the eigenfunctions, and the λ_i the eigenvalues of operator $D_{1,\mathbf{x}}$. Thus, one is immediately involved, as predicted, in spectral theory, because one has to make sure that $D_{1,\mathbf{x}}$ has a discrete spectrum and yields a complete set of ϕ_i functions.

One may use the series for w in the identity in the foregoing to derive a differential equation of the f_i (t). Since the ϕ_i (x) have been chosen and are known, one is supposed to have obtained a series solution for w, once the f_i have been determined. However, it may be a *weak solution* only, because the series may not satisfy strictly speaking the differential equation of the problem. This may happen as termwise differentiation of the series yields further series that are supposed to represent the derivatives of w, but that may actually not converge.

By using the series for w, the preceding identity changes into

$$\int_\Omega \Big\{\sum_i \phi_i(\mathbf{x})D_{0,t}[f_i(t)] + \sum_i f_i(t)D_{1,\mathbf{x}}[\phi_i(\mathbf{x})] + q(\mathbf{x},t)\sum_i f_i(t)D_{2,\mathbf{x}}[\phi_i(\mathbf{x})]\Big\} \cdot \sum_j \delta f_j(t)\phi_j(\mathbf{x})d\Omega = 0.$$

Observing the arbitrariness of the variations δf_j, one arrives at the system of equations

$$\int_\Omega \Big\{\sum_i [D_{0,t}[f_i(t)]\phi_i(\mathbf{x}) + f_i(t) < D_{1,\mathbf{x}}[\phi_i(\mathbf{x})] + q(\mathbf{x},t)D_{2,\mathbf{x}}[\phi_i(\mathbf{x})] >]\Big\}\phi_j(\mathbf{x})d\Omega = 0.$$

Truncating the series, and integrating termwise, one obtains

$$\sum_i \{a_{ij}D_{0,t}[f_i(t)] + < b_{ij} + Q\Phi(t)c_{ij} > f_i(t)\} = 0, \tag{14}$$

where

$$a_{ij} = \int_\Omega \phi_i\phi_j d\Omega, \quad b_{ij} = \int_\Omega D_1[\phi_i]\phi_j d\Omega,$$

$$Q\Phi(t)c_{ij} = \int_\Omega q\phi_j D_2[\phi_i]d\Omega.$$

Equations (14) represent the system of ordinary differential equations supposed to yield the unknown f_i approximately. If $\Phi(t)$ is a periodic function causing parametric excitation of the

Downloaded 02 May 2010 to 171.66.16.250. Redistribution subject to ASME license or copyright; see http://www.asme.org/terms/Terms_Use.cfm

continuous system, one is faced with the typical set of equations encountered in the context of *dynamic stability*. V. V. Bolotin [21] and E. Mettler [20] have distinguished themselves through investigating such problems and calculating that critical value of the structural parameter Q which causes instability.

A justification of the procedure described in the foregoing must be provided by means of convergence investigations. This has been done to a certain extent in [7].

A slightly different problem arises when the structural parameter q depends on the spatial coordinates only, so that the basic relationship reads

$$\int_\Omega \{D_{0,t}[w(\mathbf{x},t)] + D_{1,\mathbf{x}}[w(\mathbf{x},t)] + q(\mathbf{x})D_{2,\mathbf{x}}[x(\mathbf{x},t)]\}\delta w d\Omega = 0.$$

From the point of view of mechanics, $D_{0,t}$ $[w]$ may represent the inertia forces $D_{1,\mathbf{x}}$ $[w]$ the elastic forces, and $qD_{2,\mathbf{x}}$ $[w]$ the external forces. Operator $D_{1,\mathbf{x}}$ is certainly self-adjoint with respect to the boundary conditions of the continuous system. Operator $D_{2,\mathbf{x}}$ may either be self-adjoint in the case of conservative forces or nonself-adjoint in the case of follower forces.

For a treatment of the problem, one may set again w $(\mathbf{x},t) = \Sigma f_i(t)\phi_i(\mathbf{x})$, where the coordinate functions are obtained as before from $D_{1,\mathbf{x}}[\phi_i] = \lambda_i\phi_i$, applying the boundary conditions of the original problem. Since operator $D_{1,\mathbf{x}}$ is assumed to be self-adjoint, it has a spectrum guaranteeing a complete set of eigenfunctions ϕ_i, and convergence of the series representing w is ensured by a number of expansion theorems available in the literature.

Using the series for w in the preceding equation, one obtains

$$\int_\Omega \left[\sum_i \{\phi_i D_{0,t}[f_i] + f_i D_{1,\mathbf{x}}[\phi_i] + q(\mathbf{x})f_i D_{2,\mathbf{x}}[\phi_i]\}\right]\phi_j d\Omega = 0,$$

and, after having truncated the series,

$$\sum_i \{a_{ij}D_0[f_i] + b_{ij}f_i + Qc_{ij}f_i\} = 0,$$

where $$a_{ij} = \int_\Omega \phi_i\phi_j d\Omega, \quad b_{ij} = \int_\Omega \phi_j D_{1,\mathbf{x}}[\phi_i]d\Omega,$$

$$Qc_{ij} = \int_\Omega q(\mathbf{x})\phi_j D_{2,\mathbf{x}}[\phi_i]d\Omega.$$

Setting $D_0[f_i]/f_i = -\omega^2$ yields

$$\sum_i f_i[-\omega^2 a_{ij} + b_{ij} + Qc_{ij}] = 0.$$

This is a homogeneous equation which renders nontrivial solutions for the f_i at fixed moments of time only when

$$\det(-\omega^2 a_{ij} + b_{ij} + Qc_{ij}) = 0.$$

From this condition, the eigenvalue equation $F(\omega^2, Q) = 0$ is derived, which relates the two eigenvalues of the problem, say, ω^2 and Q, with each other. Much research has been done on this equation and its graphical presentation, i.e., the eigenvalue curve. Since the actually infinite determinant has been truncated, the stability problem has become an algebraic problem.

The trace of the eigenvalue curve determines the stability limit of the system and the mode of instability: divergence or flutter. If the system is conservative, the mode is always divergence, and the static approach to stability is permissible. If the system is nonconservative. The mode can either be divergence (for conservative systems of the second kind), or flutter, or both divergence and flutter. Since flutter instability can be detected by means of dynamics only, it is advisible to deal with nonconservative systems by means of dynamics.

In the cases that dynamics must be applied, further problems do arise because damping will have an effect on stability. Also, the mass distribution will not only have an influence through the weight associated with the mass, but additionally will have a strong effect by making the coefficient in the inertia force term of the problem's differential equation a variable one. In this way, the mass distribution contributes essentially to the degree of optimally of a stability solution. Further information on problems of this kind can be found in [7].

So far, only two parameters, ω^2 and Q, have been taken into account. However, in practice, one may encounter multiple parameters like $\omega^2, Q_1, Q_2, \ldots, Q_n$ due to multiple loading. Then, eigenvalue curves become eigenvalue hypersurfaces. The critical points on these surfaces decide on stability and instability and on the special way in which stability may be lost. Investigations of such topics have for example been carried out by K. Huseyin [19].

In the preceding considerations, no mention was made of the perturbations applied to the continuous system, thus, causing the variational equations to emerge. These equations were used for ensuing stability investigations. However, as much as the capacity of the system to remain stable might be a sturctural property, the potentiality of the system to preserve stability must also depend on the nature of the perturbation. Therefore, let the following problem be investigated:

$$\mu\ddot{w}(\mathbf{x},t) + D[q(\mathbf{x}), w(\mathbf{x},t)] = K(\mathbf{x},t),$$

$$\mathbf{U}[w]_B = 0, \quad w(\mathbf{x},0) = 0, \quad \dot{w}(\mathbf{x}0) = 0,$$

where operator D is supposed to be linear, but nonself-adjoint for the sake of generality. $K(\mathbf{x},t)$ is a perturbation satisfying the conditions

$$\int_0^\infty |\partial K/\partial t| dt < K^*, \quad |K(\mathbf{x},t)| < K^{**} \quad \text{for} \quad t \geq 0.$$

$\mathbf{U}$ is a "vector" of boundary conditions at the boundary B of the system. The initial conditions are assumed to be homogeneous for the sake of simplicity. However, in [31], a reference that serves as a foundation for the following discourse, inhomogeneous initial conditions have also been taken into account

Assuming that $D[q,w] \equiv D_{1,\mathbf{x}}[w] + q(\mathbf{x})D_{2,\mathbf{x}}[w]$, one arrives for $q = 0$ at the problem

$$-\mu\omega^2\phi_i^{(0)} + D_{1,\mathbf{x}}[\phi_i^{(0)}] = 0, \quad \mathbf{U}[\phi_i^{(0)}]_B = 0,$$

which describes the free vibrations of the unloaded, continuous system. Since $D_{1,\mathbf{x}}$ is a sufficiently definite, self-adjoint operator, there exists an inverse

$$D_{1,\mathbf{x}}^{-1} = \int_\Omega G^{(0)}(\mathbf{x},\xi) \ldots \mathbf{d}\Omega,$$

where

$$\sum_k \frac{\phi_k^{(0)}(\mathbf{x})\phi_k^{(0)}(\xi)}{\mu\omega_{k,0}^2} = G^{(0)}(\mathbf{x},\xi),$$

and where $\Sigma_k 1/\mu\omega_{k,0}^2 = S^{(0)}$ is convergent (Mercer's theorem).

Now let $q \neq 0$. Then, one is led to the two adjoint problems

$$-\mu\omega^2\phi_i + D[q,\phi_i] = 0, \quad -\mu\omega^{-2}\psi_i + \tilde{D}[q,\psi_i] = 0,$$

$$\mathbf{U}[\phi_i]_B = 0, \qquad \tilde{U}[\psi_i]_B = 0,$$

where the adjoint operators are defined by means of the relation

$$\int_\Omega \psi_j D[q,\phi_i]d\Omega = \int \phi_i \tilde{D}[q,\psi_j]d\Omega.$$

Downloaded 02 May 2010 to 171.66.16.250. Redistribution subject to ASME license or copyright; see http://www.asme.org/terms/Terms_Use.cfm

The eigenfunctions satisfy the condition $\int_\Omega \psi_j \phi_i d\Omega = \delta_{ji}$ and are supposed to form complete sets of uniformly bounded eigenfunctions. This is true, if the respective differential equations have smooth coefficients and if $0 \leq q < q^*$, where q^* is a sufficiently small upper bound.

For $q \neq 0$, the two adjoint problems in the foregoing can be considered to be the perturbations of the preceding free vibration problem. Then, it can be shown, like in [31], that under fairly general conditions not only $G^{(0)}$ but also

$$G^* = \sum_k \frac{\phi_k(\mathbf{x})\psi_k(\mathbf{x})}{\mu\omega_k^2}$$

exists. By the same token, not only $\sum_k 1/\mu\omega_{k,0}^2 = S^{(0)}$ is convergent, but also $\sum_k 1/\mu\omega_k^2 = S$. All this is again true for $q < q^*$, where q^* can be proved to be the lowest critical load, having thus a relevant and practical meaning.

Applying Laplace transformation to the system's differential equation yields $\mu p^2 \bar{w} + D[q, \bar{w}] = \bar{K}$, where $\bar{w}$ and $\bar{K}$ are the image functions of w and K. Setting $\bar{w} = \sum_k A_k \phi_k$ and $\bar{K} = \sum_k B_k \phi_k$, where $B_k = \int_\Omega \bar{K}\psi_k d\Omega$, one obtains $\bar{w} = \sum_k B_k [\mu(p^2 + \omega_k^2)]^{-1} \phi_k$, $\bar{w} = \sum_k \eta_k(\mathbf{x})[\mu(p^2 + \omega_k^2)]^{-1} \int_\Omega \bar{K}\psi_k(\xi) d\Omega$. Carrying out the inverse Laplace transformation on this relationship yields

$$w(\mathbf{x},t) = \sum_k \int_t \int_\Omega \frac{\phi_k(\mathbf{x})\psi_k(\xi)}{\mu\omega_k} \sin \omega_k (t-\tau) K(\xi,\tau) d\tau d\Omega.$$

Integration by parts on the right-hand side of this equation results in

$$w(\mathbf{x},t) = \sum_k \int_t \int_\Omega \frac{\phi_k(\mathbf{x})\psi_k(\xi)}{\mu\omega_k^2} \cos \omega_k (t-\tau) \frac{\partial K}{\partial \tau} d\tau d\Omega + \sum_k \int_\Omega \frac{\phi_k(\mathbf{x})\psi_k(\xi)}{\mu\omega_k^2} K(\xi,t) d\Omega - \sum_k \int_\Omega \frac{\phi_k(\mathbf{x})\psi_k(\xi)}{\mu\omega_k^2} \cos \omega_k t K(\xi,0) d\Omega. \quad (15)$$

Moreover, in equation (15),

$$\left| \sum_k \int_t \int_\Omega \frac{\phi_k(\mathbf{x})\psi_k(\xi)}{\mu\omega_k^2} \cos \omega_k (t-\tau) \frac{\partial K}{\partial \tau} d\tau d\Omega. \right|$$

$$\leq \sum_k \int_t \int_\Omega \frac{\phi_k(\mathbf{x})\psi_k(\xi)}{\mu\omega_k^2} \left| \cos \omega_k (t-\tau) \right|$$

$$\left| \frac{\partial K}{\partial \tau} \right| d\tau d\Omega \leq \int_t \left| \frac{\partial K}{\partial \tau} \right| d\tau \sum_k \int_\Omega \left| \frac{\phi_k(\mathbf{x})\psi_k(\xi)}{\mu\omega_k^2} \right| d\Omega$$

$$\leq K^* \Omega M \sum_k \frac{1}{\mu\omega_k^2} \leq K^* \Omega M S,$$

which follows from $| \phi_k(\mathbf{x})\psi_k(\xi) | < M$ and other previously made assumptions on K and the series $\sum_k 1/\mu\omega_k^2$. Hence, the said term converges uniformly and absolutely. Thus, summation and integration can be interchanged. The same is true for the other two terms in equation (15). Consequently,

$$w(\mathbf{x},t) = -\int_t \int_\Omega \left[\sum_k \frac{\phi_k(\mathbf{x})\psi_k(\xi)}{\mu\omega_k^2} \cos \omega_k (t-\tau) \right] \frac{\partial K}{\partial \tau} d\tau d\Omega + \int_\Omega \left(\sum_k \frac{\phi_k(\mathbf{x})\psi_k(\xi)}{\mu\omega_k^2} \right) K(\xi,\tau) d\Omega - \int_\Omega \left[\sum_k \frac{\phi_k(\mathbf{x})\psi_k(\xi)}{\mu\omega_k^2} \cos \omega_k t \right] K(\xi,0) d\Omega.$$

Setting

$$G(\mathbf{x},\xi,t,\tau) = \sum_k \frac{\phi_k(\mathbf{x})\psi_k(\xi)}{\mu\omega_k^2} \cos \omega_k (t-\tau),$$

which is permissible, since the series on the right-hand side converges, one has finally

$$w(\mathbf{x},t) = -\int_t \int_\Omega G(\mathbf{x},\xi,t,\tau) \frac{\partial K}{\partial \tau} d\tau d\Omega + \int_\Omega G(\mathbf{x},\xi,t,t) K(\xi,t) d\Omega - \int_\Omega G(\mathbf{x},\xi,t0) K(\xi,0) d\Omega.$$

This expression can be used to assess stability. As one clearly sees, stability depends indeed on the one hand on G, which expresses the structural properties of the system, and on the other hand on K, which represents the perturbation. If the perturbation K satisfies the fairly general conditions mentioned earlier, stability depends fully on G. Via ϕ and ψ, G is a function of q. Hence, if K behaves well, it will be q, exceeding the bound q^*, which destroys stability.

Conclusion

Stability theory of dynamic systems has been developed into a comprehensive, consistent theory over a century, drawing input from various sources. These have been set up without regard to each other, or only loosely related, in various areas of mechanics. The development of the theory consisted in stressing common aspects of the various attempts to deal with stability, and in introducing common concepts as well as a unified methodology. In the domain of the stability of motions of systems with a finite number of degrees of freedom, this trend toward a common theory led very far and to a satisfactory situation.

For the stability of elastic systems, a special approach to stability based on statics has always existed and may remain in use as far as conservative systems are concerned. However, for nonconservative elastic systems, there is definitely the need to fall back on those dynamic methods, which have already been established for an investigation of the stability of motions. In responding to this need, the common features of a unified stability theory have been extended to include the area of stability of *continuous*, elastic systems. Yet, in doing this, it has been recognized that relevant modifications and generalizations of the theory had to be accepted, as the specific nature of the systems, following from their continuity, required on application of topology and functional analysis in the context of stability investigations. Another important result of the application of general methods of stability analysis to continuous elastic systems is that a clarification of the question when to use either static methods of when to choose dynamic methods was possible. The latter is the case if one deals with follower forces.

In the early days of handling systems with follower forces, it has been claimed that the "energy method" is not permissible for such systems. If one takes this statement literally, it is wrong. Correct is, that a method based on a consideration of the kinetic and potential energy only, should not be used for systems carrying follower forces. However, if one used the *total* energy of the system, including the work done by the nonconservative follower forces, then, an energy approach to stability is quite acceptable. This has, for example, been shown in [32].

References

1 Hsu, C. S., "Theory of Index for Dynamical Systems of Order Higher than Two," ASME Journal of Applied Mechanics, Vol. 47, 1980, pp. 421-427.

2 Ziegler, H., *Principles of Structural Stability*, Blaisdell, Waltham, Mass., 1968.

Downloaded 02 May 2010 to 171.66.16.250. Redistribution subject to ASME license or copyright; see http://www.asme.org/terms/Terms_Use.cfm

3 Pars, L. A., *A Treatise on Analytical Dynamics*, Ox Bow Press, Woodbridge, Conn., 1979, pp. 20-27.

4 Abraham, R., and Marsden, J. E., *Foundations of Mechanics*, 2nd Ed., Benjamin/Cummings, Reading, Mass., 1978, pp. 60-69.

5 Leipholz, H., *Stability Theory*, Academic Press, New York, 1970, pp. 21-27.

6 Olas, A., "A Criterion of Stability of the Trivial Solution of a Set of Ordinary Differential Equations," *Bulletin de L'Académie Polonaise des Sciences*, Serie des Sciences Techniques, Vol. XXIX, No. 5-6, 1981, pp. 67-73.

7 Leipholz, H., *Stability of Elastic Systems*, Sijthoff et Noordhoff, Alphen aan den Rijn, The Netherlands, 1980, pp. 85-88.

8 Hahn, W., *Stability of Motion*, Springer-Verlag, New York, 1967, pp. 115-127.

9 Ponzo, P. J., "On the Stability of Certain Nonlinear Differential Equations," *IEEE Trans. Aut. Ctrol.*, Short paper-Vol. *AC*-10, 1965.

10 Charron, R. J., "Routh-Hurwitz Stability Conditions for Ordinary Differential Equations," Thesis, University of Waterloo, 1982.

11 Stoker, J. J., *Stability of Continuous Systems, Dynamic Stability of Structures*, Herrman, G., ed., Pergamon Press, Oxford, 1967, pp. 45-52.

12 Leipholz, H., "Stability Analysis of Nonconservative Systems Via Energy Considerations," *Mechanics Today*, Vol. 5, 1980, pp. 193-214.

13 Peixoto, M. M., "On Structural Stability," *Ann. of Math.*, Vol. 69, 1959, pp. 182-222.

14 Leipholz, H., "An Attempt to Refine Certain Stability Concepts," *Proceedings Fifth Canadian Congress of Applied Mechanics*, Univ. of New Brunswick, Fredericton, N. B., Canada, 1975, G61-G74.

15 Leipholz, H., *Stability of Elastic Systems*, Sijthoff et Noordhoff, Alphen aan den Rijn, The Netherlands, 1980, pp. 43-82.

16 Ziegler, H., "Die Stabilitätskriterien der Elastromechanik," *Ingenieur-Archiv*, Vol. 20, 1951, p. 49.

17 Bolotin, V. V., *Nonconservative Problems of the Theory of Elasticity*, Pergamon Press, Oxford, 1963.

18 Leipholz, H., *Direct Variational Methods and Eigenvalue Problems in Engineering*, Noordhoff, Leyden, 1977.

19 Huseyin, K., *Nonlinear Theory of Elastic Stability*, Noordhoff, Leyden, 1975.

20 Herrmann, G., ed., *Dynamic Stability of Structures*, Pergamon Press, Oxford, 1967, pp. 7-41, pp. 83-106, pp. 169-188.

21 Bolotin, V. V., *The Dynamic Stability of Elastic Systems*, Holden-Day, San Francisco, 1964.

22 Knops, R. J., and Wilkes, E. W., "Theory of Elastic Stability," *Encyclopedia of Physics*, Vol. VIa/3, Mech. of Solids III, Truesdell, C., ed., pp. 125-302.

23 Leipholz, H., "Liapunov Stability of Continuous Elastic Systems and Its Topological Foundations," *Acta Mechanics*, Vol. 45, 1982, pp. 135-162.

24 Leipholz, H., "On The Energy Criterion in the Context of Plate Stability," *Comp. Meth. in Appl. Mech. and Eng.*, Vol. 32, 1982, pp. 401-414.

25 Parks, P. C., *Some Applications of Liapunov Functionals, Instability of Continuous Systems*, Leipholz, H., ed., Springer-Verlag, New York, 1971, pp. 125-131.

26 Leipholz, H., "Liapunov's Second Method and Its Application to Continuous Systems," *SM Archive*, Vol. 1, 1976, pp. 367-444.

27 Leipholz, H., "On Time Invariant Functionals for Certain Mechanical Systems Subject to Follower Forces," *Hadronic Journal*, Vol. 3, 1980, pp. 962-1017.

28 Leipholz, H., "Analysis of Non-Conservative, Nonholonomic Systems," *Proceedings of the XVth ICTAM*, Univ. of Toronto, 1980, pp. 1-11.

29 Leipholz, H., "On Direct Methods in the Calculus of Variations," *Comp. Meth. in Appl. Mech. and Eng.*, Vol. 37, 1983, pp. 57-78.

30 Leipholz, H., and Pfendt, F., "Application of Extended Equations of Galerkin to Stability Problems of Rectangular Plates With Free Edges and Subjected to Uniformly Distributed Follower Forces," *Comp. Meth. in Appl. Mech. and Eng.*, Vol. 37, 1983, pp. 341-365.

31 Leipholz, H., "Assessing Stability of Elastic Systems by Considerating Their Small Vibrations," *Ing. Arch.*, Vol. 53, 1983.

32 Leipholz, H., "On the Application of the Energy Method of the Stability Problem of Nonconservative Mechanical Systems," *Acta Mechanica*, Vol. 28, 1977, pp. 113-138.

Downloaded 02 May 2010 to 171.66.16.250. Redistribution subject to ASME license or copyright; see http://www.asme.org/terms/Terms_Use.cfm

Turbulence Modeling[1]

J. L. Lumley
Department of Mechanical and Aerospace Engineering,
Cornell University,
Ithaca, N.Y. 14853

The historical development of and motivation for turbulence modeling is briefly surveyed. The models of various levels are described, and the performance of second-order models discussed. The various basic constraints to which second-order models are or are not subject are considered, including invariance, material frame indifference, realizability, and the preservation of moment inequalities. Finally, fundamental difficulties that arise in the case of multiple scales are discussed.

Historical Background

The instantaneous velocity field in a turbulent flow is described by the Navier-Stokes equations. Apparently in common with other systems of three or more degrees of freedom [1], these equations are said to possess a strange attractor; that is, with deterministic initial and boundary conditions, the solutions display extremely complex, non-periodic, pseudorandom behavior. Although the details of the solutions are reproducible in exact numerical simulations, they are exquisitely sensitive to minute changes in the initial and boundary conditions, while averages are not, and from a practical point of view we are generally interested only in being able to calculate the averages: average velocity, momentum flux (drag), variances, and so forth. These remarks are equally applicable to turbulence involving active and passive contaminants.

Exact numerical simulation of turbulence at relatively low Reynolds numbers is possible [2]. As the turbulence Reynolds number increases, however, the ratio of the large to small scale increases, rapidly exceeding the storage capacity of the largest computers in the foreseeable future. Exact numerical simulation of the large scales with modeling of the unresolved small scales is possible at these higher Reynolds numbers (large eddy simulation; [3]). If the flow being simulated has a coordinate in which it is statistically invariant, so that averaging can be carried out over that coordinate to obtain the statistical quantities, these approaches are currently just financially accessible for some practical calculations, although they must be regarded as a research tool. If the flow has no coordinate over which it can be averaged, so that many successive runs must be made to obtain an ensemble, the cost is quite out of reach for practical purposes.

The desire to make practical calculations useful in design and planning, the lack of interest in the instantaneous details of the flow, and the impracticality of exact simulation even of the large scales in any event (even more impractical in the past) led very early in the study of turbulence to the development of various models. In the latter part of the nineteenth century, Boussinesq suggested replacing turbulence by a laminar flow with a greatly increased viscosity (termed an eddy viscosity), the value of the viscosity being determined from experiment. Even the average behavior of the turbulent flow and the model flow are somewhat different, of course, since the way in which turbulent eddies transport momentum and other quantities is physically different from the way in which molecular motion transports these quantities. However, the equations conserve mass, momentum, and energy, are calibrated to have correct overall transport of momentum, heat, etc. in benchmark situations, and are realizable; that is, a Newtonian constitutive relation (which is what the assumption of an eddy viscosity amounts to) is thermodynamically consistent, assuring that physically acceptable results will be obtained. The equations may not contain the relevant physical mechanisms, of course; there is no way (other than by crude ad hoc parameterizations) to include the effects of buoyancy in an eddy, viscosity, for example, and without it this apprroach will fail completely in cases in which this effect is important. In cases having physical mechanisms similar to the benchmark case, however, and not too far from the same parameter values, results are obtained that are not grossly in error. In one form or another, this approach is still extensively used today. It is helped by the fact that many flows of practical interest are dominated by the inertia or buoyancy of the mean flow ([4], 1982), and the turbulent transport is a relatively minor part of the picture (Fig. 1). It can be replaced by nearly any other mechanism transporting about the same amount of momentum or heat without changing the mean flow appreciably.

The approach to turbulence in fact has many parallels to the way in which non-Newtonian media have been approached. Here one school has attempted to understand macroscopic behavior of non-Newtonian media by careful examination of the microscopic structure; names such as Einstein, Zimm, Rouse, Peterlin, and Batchelor come to mind. The other school has more or less ignored the microscopic structure, and has sought instead mathematical constraints on the macroscopic behavior, reducing what is not known to a minimal number of unknown functions in-

[1] Supported in part by the U.S. Office of Naval Research under the following programs: Physical Oceanography (Code 422PO), Fluid Dynamics (Code 438), Power (Code 473); in part by the U.S. National Science Foundation under grant no. ATM 79-22006 and CME-79-19817; and in part by the U.S. Air Force Office of Scientific Research.

Contributed by the Applied Mechanics Division for publication in the JOURNAL OF APPLIED MECHANICS.

Discussion on this paper should be addressed to the Editorial Department, ASME, United Engineering Center, 345 East 47th Street, New York, N.Y. 10017, and will be accepted until two months after final publication of the paper itself in the JOURNAL OF APPLIED MECHANICS. Manuscript received by ASME Applied Mechanics Division, March, 1983.

Copyright © 1983 by ASME
Downloaded 02 May 2010 to 171.66.16.250. Redistribution subject to ASME license or copyright; see http://www.asme.org/terms/Terms_Use.cfm

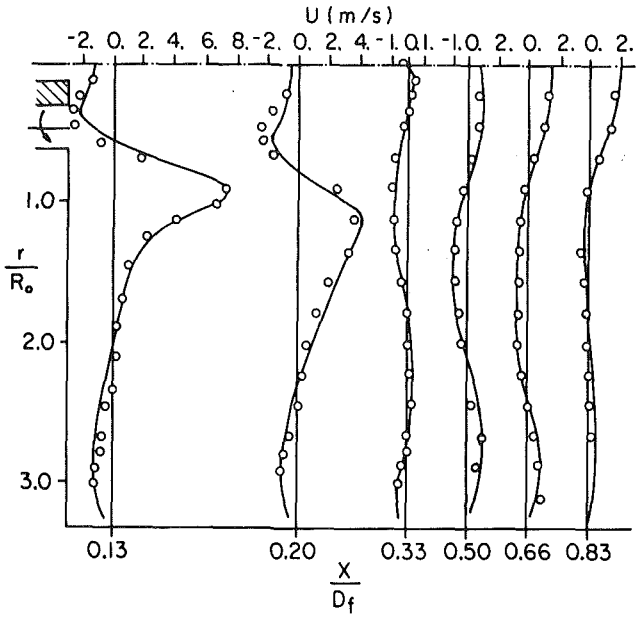


Fig. 1 Velocity profiles in a model combustion chamber calculated by Hutchinson et al. [2] using the k-ϵ model. An experimental situation without combustion was simulated; fluid enters the chamber through the annulus with a swirl component (no center jet). The various recirculation zones are faithfully reproduced by the model. An example of a flow dominated by the mean pressure, in which the details of the turbulent transport are not terribly important.

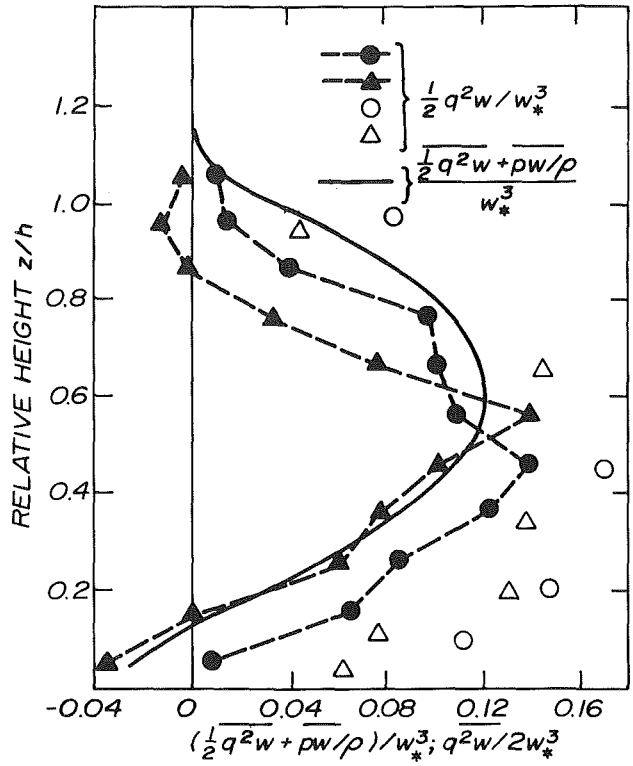


Fig. 2 Predicted vertical fluxes of turbulent energy in a buoyancy-driven mixed layer compared with data from Zeman and Lumley [14]. The full line is the prediction, which includes the pressure transport. The data is that of Willis and Deardorff, Lenschow, Lenschow, and Johnson, and Telford and Warner (see [14] for references). h is the height of the inversion base capping the mixed layer, which is driven by incoming solar radiation heating the ground, which heats the air. w_* is a scaling velocity defined using the surface buoyancy flux and the mixed layer height.

dependent of geometry, which are determined by experiment. Here we may recall Stokes, Navier, Truesdell, Rivlin, Ericksen, Coleman, and Noll.

Turbulence has proceeded in a similar way, with the more respectable school attempting to understand the macroscopic behavior of turbulence by detailed consideration of the physics of the fluctuations. We may mention Taylor, Kolmogorov, Batchelor, Corrsin, Kraichnan, and Edwards, among others. The less respectable school, which attempts to construct macroscopic models on a semiempirical basis, has always been associated with engineering, and more recently with meteorology and oceanography, the consumers: that is, those who have a need to calculate the effects of turbulent flow.

Many turbulent flows have a mechanism too complex to be subsumed under an eddy viscosity. For example, flows in which the turbulence itself is the most important mechanism (as opposed to mean flow inertia, for example), and in which several dynamical effects act at once (say, shear and buoyancy). An example might be turbulent heat transfer on a gas turbine blade, or during an accident in a sodium-cooled nulcear reactor. As a result, there has been a continual effort to construct more elaborate models which contain more of the physics than a simple eddy viscosity. We may mention von Karman, Prandtl, and Taylor before WWII, and Kolmogorov, Chou, Rotta, and Davidov through the mid-sixties (see [5] for references). The modern period begins with Donaldson and Spalding and their students in the late sixties. The early efforts were hobbled by the lack of large-capacity high-speed computers, so that many early ideas could not be implemented.

Modern Models

The first modern approach to modeling preserved the concept of an eddy viscosity, but attempted to predict its value. As is well known in turbulence theory, the eddy viscosity is proportional to the product of a length and velocity scale characteristic of the turbulence [6]. It was an idea of Kolmogorov [7] that turbulence could, to a first approximation, be characterized by a single length l and velocity scale u locally. Hence, Launder and Spalding [8] constructed model transport equations for the mean-square turbulent kinetic energy, which they designated by k, and for the mean turbulent dissipation of kinetic energy per unit mass, ϵ. From these they could obtain the eddy viscosity using the well-known relations $2k = 3u^2$, $\epsilon = u^3/l$ [6]. This model is widely used in practical applications, although it suffers from the limitations mentioned in the foregoing, common to all eddy viscosity formulations. Construction of the model equations necessitated modeling of the turbulent transport both of the turbulent kinetic energy and of the dissipation, and of the production and destruction of the dissipation. While crudely satisfactory in many simple situations, these models leave much to be desired, particularly the equation for ϵ. In fact, a form of this equation is used in all the models we will discuss, and is the weakest point in the technique.

In the k-ϵ models a number of approximate modifications have been introduced to account for the effects of buoyancy, curvature, and so forth on the eddy viscosity (see, for example, [4]). These corrections are adequate in many circumstances, as long as the turbulent transport is not the dominant physical mechanism in the flow, and provided the flow considered is not too distant geometrically or in parameter values from the flow for which the engineering parameterization was calibrated. However, if a correction developed for curved boundary layers is applied in weakly swirling flow (for example), and if it is radial turbulent transport of a scalar that is significant (as in a gas turbine combustor, say), then the correction is inadequate [9].

In an effort to include more physics in the models, Donaldson [10] (see [5, 11, 12]) proposed carrying equations

Downloaded 02 May 2010 to 171.66.16.250. Redistribution subject to ASME license or copyright; see http://www.asme.org/terms/Terms_Use.cfm

for the second moments: the six independent components of $\langle u_i u_j \rangle$ in an isothermal flow, in addition to ϵ (the angle brackets indicate an average which we may take to be over an ensemble of flow with similar average conditions). In an intermediate phase, [13] proposed writing

$$\langle q^2 \rangle D_t \langle u_i u_j \rangle = \langle u_i u_j \rangle D_t \langle q^2 \rangle$$

where D_t is the average substantial derivative following the total velocity; that is, it contains the substantial derivative following the mean velocity and the turbulent transport by the fluctuating velocity. $\langle q^2 \rangle$ is twice the mean turbulent kinetic energy per unit mass. This formulation leads to an algebraic equation for the Reynolds stress tensor $\langle u_i u_j \rangle$ which is dynamically a slight improvement on the eddy viscosity model; this is referred to as the algebraic stress model.

The full second-order models carry prognostic differential equations for all second moments. In the case of, say, a three-dimensional atmospheric flow involving heat and water vapor this would involve 22 differential equations for (in addition to mean velocity, mean temperature, mean humidity, and mean pressure) Reynolds stress, heat flux, moisture flux, temperature-humidity correlation, and so forth. In these equations various terms appear other than the dependent variables (the second moments); in order to close the equations and make them determinate, these terms must be modeled. For example, here is the equation for the Reynolds stress in an isothermal flow:

$$\partial_t \langle u_i u_j \rangle + \partial_k \langle u_i u_j \rangle U_k + \partial_k U_i \langle u_k u_j \rangle + \partial_k U_j \langle u_k u_i \rangle$$
$$+ \partial_k \langle u_i u_j u_k \rangle = -[\langle u_i \partial_j p \rangle + \langle u_j \partial_i p \rangle / \rho + 2\nu \langle \partial_k u_i \partial_k u_j \rangle$$

The terms on the second line must all be modeled: the third moments (which represent turbulent transport of the second moments), the moments involving pressure, and the moments relating to dissipation of turbulent fluctuations by molecular transport. We will not present here details of the various models proposed; these can be found in numerous surveys (e.g., [3]) and critiques [5] and in the original papers. Rather, we will focus on principles and problems that arise.

In addition to the terms previously mentioned, nearly the entirety of the equations for the dissipation of turbulent kinetic energy, temperature variance, and humidity variance must be constructed. There are, of course, many of these terms that must be modeled, and the principles and techniques for constructing the models are far from clear. As a consequence, it is hardly surprising that, when a first-order (eddy viscosity) and a second-order model both work in a given flow, the second-order model usually does not give superior results; presumably enough errors have been made in the construction of the many models to compensate for the more accurate physics contained in the equations. However, there are many situations in which the first-order models do not work at all, in which the second-order models, despite their problems, give very satisfactory results. An example is the atmospheric buoyancy-driven mixed layer (without wind shear), in which second-order models predict moments up to order three within experimental error (Fig. 2) [14–18], while eddy viscosity models are unable to cope.

Third-order models have occasionally been tried (for example, [19]), in which prognostic differential equations are carried for the third moments, and models introduced for higher-order moments. However, the number of independent third moments is considerably larger than the number of independent second moments, and except in very restricted situations, the model becomes too complex for practical use.

Performance of Existing Second-Order Models

Just as in the case of the first-order models, we are dealing with a calibrated surrogate for turbulence, albeit one that contains a little more of the physics. We would thus expect again that the models would work satisfactorily in situations not too far removed geometrically or in parameter values from the benchmark situations used to calibrate the model. To the extent that more physics has been retained, we might expect the range of satisfactory performance to be greater. If the modeled terms behave correctly physically, there does not seem any reason not to hope for a very extensive range of satisfactory performance, supposing that the relevant physical mechanisms have been retained in the equations.

In 1981–82 a competition was held [20] between various methods for calculating isothermal flows of engineering interest. Nearly all the methods in competition were of the type considered here: k-ϵ, algebraic stress, or second order. The conclusion of the judges was that the range of satisfactory performance of the models was rather narrow, and that we should probably expect to use for some time a variety of models optimized for particular geometrical situations and parameter ranges. The judges were split on the likelihood of ultimately improving this situation: the pragmatists felt that there was no objective evidence for putative universality, while the optimists (including the present author) felt that improvement of the physical behavior of the modeled terms held considerable hope. Most of the models have been constructed in a somewhat haphazard manner; as we will see in the following, there are many restrictions that they should satisfy, which are generally violated. Much of the modeling is not based on first principles, but is almost compeltely ad hoc. It seems there is enough room for improvement here to justify a certain optimism.

Many of the initial successes of the models have been in more complex flows, involving heat transfer, buoyancy, and the like. Because the relevant physical mechanisms are included, the behavior of the models is vastly superior to first-order models. Emboldened by these initial successes, the modelers have been somewhat overenthusiastic in promoting their models for increasingly complex situations, without in many cases considering at sufficient depth the exceedingly complex questions that arise. As a consequence, there is currently some disillusionment with the models, a feeling that they embody too many unphysical ad hoc assumptions, and that they are basically unreliable as a result (Wyngaard, private communication). This reaction is probably justified, but it would be a shame if it resulted in a cessation of efforts to put a little more physics and mathematics into the models.

Model Constraints

The form of the modeled terms is clearly subject to many constraints of a mathematical and physical nature. The most obvious is the requirement that the terms have the same tensor structure as the terms they replace, so that they will transform properly in different coordinte systems. In this way, there is some hope that whatever model is constructed may be geometry-independent. This is certainly not sufficient to guarantee this, but without this requirement the matter is hopeless. This type of modeling was referred to as invariant modeling by Donaldson [10].

Certainly to anyone who has worked in continuum mechanics the concept of material indifference would come to mind as a principle that could be applied to help in the construction of models. As used in continuum mechanics, this principle requires that constitutive relations be invariant under abritrary time-dependent rigid rotations and translations. This has been suggested by Speziale [21, 22]. Let me state at the outset that this principle is not applicable to turbulent flows.

Material indifference [23] has been an extremely powerful tool for the construction of constitutive relations; volumes

Downloaded 02 May 2010 to 171.66.16.250. Redistribution subject to ASME license or copyright; see http://www.asme.org/terms/Terms_Use.cfm

have been written about it, and it has acquired the status of dogma in continuum mechanics. I believe that there is currently considerable confusion over whether it is a universal truth or a convenient approximation. We may recall that Truesdell [23] suggested that if the principle began to appear too obvious, we should recall that in it we were requiring of a constitutive relation a type of invariance that the equations of motion did not obey.

I believe it is clear [24] that requiring a constitutive relation to satisfy the principle of material indifference is equivalent to ignoring the inertia of any motions responsible for the development of the stress, since the relation is required to be the same in inertial and noninertial frames. Since all matter has inertia, this means that the principle must be an approximation in any situation in which unresolved motions contribute to the stress. It is, of course, a superb approximation in most situations; for solids and polymer melts the velocities and length scales of the molecular motions are so exceedingly small as to make their inertia completely negligible under all but the most extraordinary conditions. The kinetic theory of gases is a more interesting case; a controversy has existed in the literature over exactly this point, and is as yet unresolved.

At the present time the conclusion appears to be[2] that there is not, within the framework of the statistical mechanics of a dilute gas, in general a clearly defined constitutive relation in the sense of modern continuum mechanics (the present state of the stress depending in a complex way on the history of the deformation), and so the question of whether or not it satisfies the principle of material indifference is formally moot. I believe it is legitimate to speculate on this point, however, since the Newtonian constitutive relation is known empirically to apply with remarkable precision to ordinary flows of dilute gases. I believe it will be found that there is a constitutive relation valid asymptotically in the limit of motions slow and of large scale relative to the molecular motions; I have argued elsewhere [24] that material indifference is satisfied in the same limit. Again, for all ordinary circumstances, the mean free path is small enough so that the effects of inertia are entirely negligible.

In the case of turbulence, of course, the matter is quite different. The motions responsible for the development of the stress (the Reynolds stress) are now not microscopic, but of quite finite amplitude, and definitely subject to inertia. Speziale has argued [22] that the Reynolds stress $\langle u_i u_j \rangle$ must be materially indifferent, since the vectors involved transform correctly under arbitrary time dependent rigid translations and rotations. He has argued further that, since the equations for the Reynolds stress are definitely not materially indifferent, there must then be something wrong with the concept of writing moment equations. This is, of course, not correct. The same argument can be applied to the Navier-Stokes equations: the velocity u_i transforms properly, yet the equation is not materially indifferent. The question addressed by Speziale [22] is whether the representation of the same fixed velocity transforms properly; of course it does—it is a tensor. The stickier problem is whether the turbulent fluctuating velocity remains the same in a rotating frame (with the same mean velocity field and boundary conditions), and of course it does not, which is why the Navier-Stokes equations are not materially indifferent, and the Reynolds stress equations are not either. There is ample experimental evidence (see [25]) that turbulence in a rotating frame is quite distinct from turbulence in a nonrotating frame.

Thus, we must discard material frame indifference as a constraint on the models. There are, however, many other constraints. The most straightforward have to do with symmetry in the various indices and incompressibility (presuming that the flow is incompressible), i.e., that $u_{i,i} = 0$, which requires that all moments formed with $u_{i,i}$ also vanish. There is also the question of correct behavior at large and small Reynolds number, which can often be determined. These are all relatively simple.

There is, in addition to the foregoing, an extremely important and powerful class of constraints which are grouped under the name of realizability [26]; see also [5]. This is the general requirement that the models in the various equations be constructed in such a way that all component energies remain non-negative, that Schwartz's inequality be satisfied for all off-diagonal components of the Reynolds stress tensor, and similar constraints on the heat flux and moisture flux and the variances, if they are involved. In addition, there are numerous inequalities relating moments of different orders which must be satisfied.

Let us discuss first the maintenance of the relations among the various second moments. The basic idea is this: suppose that A must be non-negative; in the equation for A, if A vanishes, $\partial_t A$ must vanish simultaneously to prevent A from becoming negative at the next instant. Now we have several possibilities; if $A = 0$ is a permanent state that will persist until disturbed, then we expect that derivatives of all orders of A will also vanish. On the other hand, if $A = 0$ is a temporary state from which the system will extricate itself without help, then we expect that $\partial^2_t A > 0$. This is not completely convincing, because various other possibilities come to mind—for example, it is really only necessary that $\partial_t A$ be non-negative if $A = 0$. Fortunately Pope (private communication) has shown that, if ρ is a correlation coefficient between any two quantities, then $\partial_t \rho = 0$ if $\rho^2 = 1$; we are able to rephrase most of our conditions as $1 - \rho^2 \geq 0$.

Let us consider the heat flux $\langle \theta u_i \rangle$. Lumley [5] has shown that the satisfaction of Schwarz's inequality for all components of this vector is equivalent to the tensor

$$D_{ij} = (\langle \theta^2 \rangle \langle u_i u_j \rangle - \langle \theta u_i \rangle \langle \theta u_j \rangle)/(\langle \theta^2 \rangle \langle q^2 \rangle - \langle \theta u_p \rangle \langle \theta u_p \rangle)$$

having non-negative eigenvalues. We can introduce a quantity $F_D = 27III_D$; since III_D is the product of the eigenvalues of D_{ij}, F_D will vanish if and only if one of the eigenvalues of D_{ij} vanishes. The factor of 27 is introduced for convenience, so that $0 < F_D < 1$. Hence, we must arrange that $\partial_t F_D = 0$ if $F_D = 0$. Let us now look at the equations in a particularly simple case, a homogeneous flow without mean velocity or mean scalar gradients. The equations for the scalar flux, variance, and Reynolds stress are given by

$$\partial_t \langle \theta u_i \rangle = -\phi^\theta \langle \theta u_i \rangle \epsilon / \langle q^2 \rangle$$

$$\partial_t \langle \theta^2 \rangle = -2\epsilon_\theta$$

$$\partial_t \langle u_i u_j \rangle = -\epsilon \beta b_{ij} - 2\epsilon \delta_{ij}/3$$

$$b_{ij} = \langle u_i u_j \rangle / \langle q^2 \rangle - \delta_{ij}/3$$

The term in ϕ^θ is a model for the pressure-scalar gradient correlation, while the term in β is a model for the pressure-strain rate correlation. We will suppose that β has already been determined from earlier considerations. Our problem is to find a form for ϕ^θ by use of the realizability condition. If we form an equation for F_D we find

$$\partial_t F_D \propto P(2\phi^\theta - 2r - \beta) + Q(\beta - 2)$$

where r is the time scale ratio, $\langle q^2 \rangle \epsilon_\theta / \epsilon \langle \theta^2 \rangle$, and P and Q are complex expressions involving invariants of D_{ij} and b_{ij}. There is a strictly positive coefficient of proportionality which need not concern us. If F_D vanishes, the right-hand side of the equation for F_D must vanish, so that we must have

$$\phi^\theta = r + \beta/2 - Q(\beta - 2)/2P \quad \text{if} \quad F_D = 0$$

[2] C. Truesdell (1982). "Thermodynamics According to the Kinetic Theory of Gases," Public lecture, Cornell University, Friday, Dec. 3, 1982.

Downloaded 02 May 2010 to 171.66.16.250. Redistribution subject to ASME license or copyright; see http://www.asme.org/terms/Terms_Use.cfm

Now we must proceed delicately; if F_D is not zero, how must this expression be modified to give an expression valid for all values of F_D? We first examine P and Q. We can show from the expressions that $Q \geq 0$, and vanishes only if D_{ij} is isotropic or one-dimensional (i.e., - all eigenvalues are equal, or two eigenvalues vanish; this has no relation to the corresponding properties of the velocity field). P, however, although it vanishes in these two cases, vanishes elsewhere also, and is not of a single sign. However, the combination $P + F_D/9 \geq 0$, and vanishes only if D_{ij} is one-dimensional. If the mechanical turbulence is isotropic, $P = Q$. Since $Q + F_D/9 \geq 0$ also, and vanishes only if D_{ij} is one-dimensional, we suggest for arbitrary values of F_D

$$\phi^\theta = r + \beta/2 - (Q + F_D/9)(\beta - 2)/2(P + F_D/9) + HF_D^{1/2}$$

This expression gives a particularly simple form if the mechanical turbulence is isotropic. It is not difficult to show that $(Q + F_D/9)(\beta - 2)$ has the same zeros as $P + F_D/9$ and approaches them at the same rate, so that the ratio is bounded. The selection of the additive term in the square root of F_D requires explanation. We can, of course, add any expression that vanishes as F_D vanishes. If we examine the expression for $\partial_t F_D$, we find that, regardless of our choice of ϕ^θ and β the right-hand side will vanish if D_{ij} is one-dimensional. This is a permanent state which will persist if undisturbed. However, consider a homogeneous turbulence with no mean velocity or temperature gradients, of arbitrary structure, with a heat flux only in the 1 - direction in which, at $t = 0$ we have somehow made $\theta \propto u_1$. A careful analysis of the exact equations indicates that $F_D = 0$, $\partial_t F_D = 0$, but $\partial^2_t F_D > 0$; that is, the turbulence will mix up the field, and destroy the state of perfect correlation. In order to generate a positive second derivative, the right-hand side of the F_D equation must be proportional to the square root of F_D near $F_D = 0$; we take it proportional to the square root everywhere. Finally, the unknown function H can be determined by comparison with experiment. Shih and Lumley, [27] found that $H = 1.1r^2$ if the mechanical turbulence is isotropic. Unfortunately, no experiments exist on relaxation of heat flux in anisotropic homogeneous turbulence.

So far as relations between moments of different orders are concerned, they are myriad. For example, Schwarz's inequality and its variations produce relations of the type $\langle\theta^3\rangle^2 \leq \langle\theta^2\rangle\langle\theta^4\rangle$, $\langle\theta^2\rangle^2 \leq \langle\theta^4\rangle$, . . .but these by no means exhaust the possibilities. Which ones are vital, and how can we be assured that they will be satisfied, particularly if we are not carrying differential equations for moments higher than the second?

Andre et al. [28, 29] have presented a method for dealing with some of the inequalities relating third-order quantities to second. They constructed equations for the third moments, neglecting pressure correlations and viscous terms (which is completely without justification). The resulting differential equations for the third-order quantities are solved as functions of time. Inequalities relating the third order to second-order quantities are derived from Schwarz's inequality, and these inequalities are applied at each time step, the third-order quantities being clipped when they exceed the bounds. Applied to buoyant convection, the results obtained from this method are excellent, fully the equal of those obtained by Zeman and Lumley [14–17] and Lumley [5] who used more physical equations for the third moments. Although it is evident that the rather vestigial equations for the third moments used by Andre et al. [28, 29] give the wrong rates of growth and decay of the third moments due to neglected terms, while the clipping produces discontinuous derivatives, this apparently is far less important to the solution than the fact that the moments remain always within their proper bounds.

A possibly more elegant way out of this difficulty [5] is to write an equation for the probability density (or an equivalent function) of the variables in question; model this equation, being sure that the solution has the properties of a probability density (or equivalent), being sure also that it produces the terms in the second-order equations that have been modeled so as to satisfy realizability, and then obtain from this equation the equations for whatever other moments are necessary. In this way one is assured that all inequalities are automatically satisfied, since the moments come from a possible probability density.

As an example, we can consider [30] the equation for a fluctuating scalar θ in a homogeneous turbulent flow. The most convenient function to work with is the moment generating function, which is the logarithm of the characteristic function (the Fourier transform of the probability density):

$$F = ln\langle G\rangle, \quad G = \exp[ik\theta]$$

If the equation obeyed by θ is

$$\partial_t\theta + \ldots = \gamma\nabla^2\theta$$

(we are suppressing all terms but those of interest), then the equation obeyed by F is

$$\partial_t F + \ldots = k^2\langle G\epsilon_\theta\rangle/\langle G\rangle$$

We could model this term, but it is simpler to introduce a little physics. We know from experiment that homogeneous turbulence in the absence of disturbing influences is approximately Gaussian in the energy containing range. Thus, we want to construct an equation that will relax to Gaussian. A simple equation that relaxes to Gaussian from arbitrary initial conditions is

$$\partial_t F = -k^2(\epsilon_\theta/\langle\theta^2\rangle)\partial^2{}_k F$$

and we will use this right-hand side as a model.

If we now carry out an order of magnitude analysis of the *full* equation (including suppressed terms) for a cumulant of arbitrary order (the nth cumulant is the nth derivative at the origin of F), supposing that the ratio of a turbulence length scale to a length scale characteristic of inhomogeneity is small, we find that the dimensionless cumulants are progressively smaller as the order increases; that is, that the fourth cumulant can be neglected in the equation for the third cumulant, and so forth. We also find that the terms involving the substantial derivatives and the gradients of mean temperature are of higher order in the length scale ratio, and hence may be negelected to lowest order. In this way we obtain an equation for the third moment

$$\langle\theta w\rangle\partial_z\langle\theta^2\rangle = -2\langle\theta^3\rangle\epsilon_\theta/\langle\theta^2\rangle$$

(We have taken a case in which the inhomogeneity is in the z direction). Notice that no new constant has been introduced. This simplified example, of course, is not much use in a practical situation, but the same technique applied to the velocity and scalar flux equations produces expressions for the third moments that are relatively simple, have no additional constants, and give assurance of satisfying all of the required inequalities relating the moments of various orders. In carrying out the order of magnitude analysis different terms must be kept in different situations; if the effects of swirl are dominant, then certain terms in the azimuthal velocity will be of lower order and must be kept [9]; if buoyancy is dominant, certain buoyant terms will remain [5].

Fundamental Restrictions on the Modeling

Pope [31] has pointed out a curious failure of such models as we describe. He considers the case of several passive scalars all having the same diffusivity. Then the equations for the instantaneous values of the scalars are identical, and we can

Downloaded 02 May 2010 to 171.66.16.250. Redistribution subject to ASME license or copyright; see http://www.asme.org/terms/Terms_Use.cfm

recombine the scalars in arbitrary linear combinations to form a new set. He points out that the modeled equations should have this same property: the modeled equation for a member of the new set should be obtainable by simple transformation of the modeled equations for the members of the old set, where all terms should transform in the same way (i.e., all linearly, of quadratically, etc.). Existing models do not; the model presented in the foregoing for ϕ^θ, for example, depended in a complex way on invariants of D_{ij}. If this principle were adhered to, ϕ^θ would have to be constant. This is not too serious, since many authors use a constant value, although it would violate realizability. The equations for the ϵ_θ are more serious; existing equations [32] certainly do not satisfy the principle, and if equations are adopted that do satisfy it, completely unphysical behavior is obtained. Pope also points out that there is no consistent way to define a time scale. For a single scalar, a time scale is defined as $\langle\theta^2\rangle/\epsilon_\theta$. This does not transform in any convenient way.

The source of this perplexing difficulty lies in a basic assumption implcit in the modeling. Effectively we assume in all cases that each variable has a spectrum of universal form that can be characterized completely by the scales of the energy containing range. Suppose that each of the primitive scalars in our example has such a spectrum, but each one has different scales characterizing the energy containing range; this means, in effect, that the peaks of the spectra occur at different wave number, so that the time scales (which reflect approximately the time scale of the mechanical turbulence that is mixing the scalar at the peak wave number) will be different. Now if the scalars are linearly combined in an arbitrary way, the spectra of the resulting scalars will no longer be simple; they will have multiple peaks, and it will not be possible to characterize them by a single set of scales. This is why the modeled equations cannot be transformed in this way: each equation contains a simple estimate of the time scale for the process (say, the relaxation of the heat flux, or the decay of the dissipation), and these time scales cannot be combined in a simple way. ϕ^θ is a dimensionless form of such a scale. In the equation for ϵ_θ a similar scale appears, proportional to $\langle\theta^2\rangle/\epsilon_\theta$; it is the appearance of this scale (which makes the equation quadratic in ϵ_θ) which destroys the transformation property. If the time scales of all the primitive scalars were the same, then the linear recombination would leave all the time scales unchanged, and the equations would transform properly.

This has serious consequences for modeling of many situations. Suppose it is desired, for example, to model the pollution emitted by multiple sources. At a given cross section of the flow, overlapping plumes of different ages arising from different sources will be present, each with its own scales. The spectrum of the pollutant will consequently have multiple peaks, and it will not be possible to characterize it by a single set of scales. In principle, each source could be treated as a different species, and the result combined, but this would complicate the calculation considerably. Again, if we are considering the combined effects of heat and water vapor, they can be lumped together as a density anomaly only with great care, since the sources of each are probably different, and hence the scales.

This problem arises also in purely mechanical flows; for example, a boundary layer in a turbulent stream. The turbulence in the external stream and that in the boundary layer will have quite different scales. There are also situations of a different character in which the spectrum is not an equilibrium spectrum, and hence cannot be characterized by the scales of its energy containing range. In an effort to cope with this difficulty several more complex models have been devised. Launder and Schiestel [33, 34] devised a scheme in which the spectrum is split into a large scale and a small scale part, with different time scales for transfer into the large scale part, and transfer from the large scale part to the small scale part. Bertoglio [35] and Cambon and Jeandel [36] have devised a full spectral model, in which modeling ideas related to those we have discussed are applied directly to the equations for the spectrum, with a different time scale at each wave number. This is, of course, quite complex, and many simplifications are necessary to reduce the computational cost to an acceptable level.

References

1 Lanford, O. E., III, "The Strange Attractor Theory of Turbulence," in *Annual Review of Fluid Mechanics*, Vol. 14, Van Dyke, M., Wehausen, J. V., and Lumley, J. L., eds., Annual Reviews Inc., Palo Alto, Calif., 1982, pp. 347–364.

2 Feiereisen, W. J., Shirani, E., Ferziger, J. H., and Reynolds, W. C., "Direct Simulation of Homogeneous Turbulent Shear Flows on the ILLIAC IV Computer: Applications to Compressible and Incompressible Modeling," in *Third Symposium of Turbulent Shear Flows*, Bradbury, L. J. S., Durst, F., Launder, B. E., Schmidt, F. W., and Whitelaw, J. H., eds., University of California, Davis, Calif., 1981, pp. 19.31–19.37.

3 Reynolds, W. C., "Computation of Turbulent Flows," in *Annual Review of Fluid Mechanics*, Vol. 8, Van Dyke, M., Wehausen, V., and Lumley, J. L., eds., Palo Alto CA: Annual Reviews Inc., Palo Alto, Calif., 1976, pp. 183–208.

4 Rodi, W., "Examples of Turbulence Model Applications," in *Proceedings of Ecole d'Eté d'Analyse Numérique—Modélisation Numérique de la Turbulence*, Clamart, France, 1982.

5 Lumley, J. L., "Computational Modeling of Turbulent Flows," in *Advances in Applied Mechanics*, Vol. 18, Yih, C.-S., ed., Academic Press, New York, 1978, pp. 124–176.

6 Tennekes, H., and Lumley, J. L., *A First Course in Turbulence*, MIT Press, Cambridge, Mass., 1972.

7 Kolmogorov, A. N., "Equation of Turbulent Motion of an Incompressible Fluid," *Izv. Akad. Nauk SSSR, Ser. Fiz.*, Vol. 6, 1942, pp. 56–58.

8 Launder, B. E., and Spalding, D. B., "The Numerical Computation of Turbulent Flows," *Comp. Meths. Appl. Mech. Eng.*, Vol. 3, 1974, p. 269.

9 Lumley, J. L., "Parameterization of Turbulent Transport in Swirling Flows," Sibley School of Mechanical and Aerospace Engineering, Report No. FDA-81-02, Cornell University, Ithaca, N.Y., 1981.

10 Kline, S. J., Morkovin, M. J., Sovran, G., and Cockrell, J. J., eds., *Proc. Comput. Turbulent Boundary Layers-1968 AFOSR-IFP-Stanford Conference*. Thermosciences Division, Stanford University, Stanford, Calif., 1969.

11 Hanjalic, K., and Launder, B. E., "A Reynolds Stress Model of Turbulence and its Application to Thin Shear Flows," *J. Fluid Mech.*, Vol. 52, 1972, pp. 609–638.

12 Launder, B. E., Reece, G. J., and Rodi, W., "Progress in the Development of a Reynolds Stress Turbulent Closure," *J. Fluid Mech.*, Vol. 68, 1975, pp. 537–566.

13 Rodi, W., "The Prediction of Free Turbulent Boundary Layers by Use of a Two-Equation Model of Turbulence," Ph.D. Thesis, Faculty of Engineering, University of London, 1972.

14 Zeman, O., and Lumley, J. L., "Turbulence and Diffusion Modeling in Buoyancy Driven Mixed Layers," in *Proceedings of Third Symposium on Atmospheric Turbulence, Diffusion and Air Quality*, Raleigh, N.C., American Meteorological Society, Boston, Mass., 1976 *a*, pp. 38–45.

15 Zeman, O., and Lumley, J. L., "Modeling Buoyancy-Driven Mixed Layers," *J. Atmos. Sci.*, Vol. 33, No. 10, 1976 *b*, pp. 1974–1988.

16 Zeman, O., and Lumley, J. L., "A Second-Order Model for Buoyancy-Driven Mixed Layers," in *Proceedings*, 9th ICHMT International Seminar "Turbulent Buoyant Convection," Dubrovnik, Washington, DC, Hemisphere Publishing, 1976 *c*, pp. 65–76.

17 Zeman, O., and Lumley, J. L., "Buoyancy Effects in Entraining Turbulent Boundary Layers: a Second-Order Closure Study," in *Turbulent Shear Flows I*, Durst, F., Launder, B. E., Schmidt, F. W., and Whitelaw, J. H., eds., Springer-Verlag, Berlin, Heidelberg, 1979, pp. 295–302.

18 Lumley, J. L., Zeman, O., and Siess, J., "The Influence of Buoyancy on Turbulent Transport, J. Fluid Mech., Vol. 84, 1978, pp. 581–597.

19 André, J.-C., Lacarrère, P., and Traoré, K., "Pressure-Effects on Triple Correlations in Turbulent Convective Flows," in *Third Symposium of Turbulent Shear Flows*, Bradbury, L. J. S., Durst, F., Launder, B. E., Schmidt, F. W., and Whitelaw, J. H., eds., University of California, Davis, Calif., 1981, pp. 9.13–9.18.

20 Kline, S. J., Cantwell, B. J., and Lilley, G. M., The 1980-81 *AFOSR-HTTM-Stanford Conference on Complex Turbulent Flows: Comparison of Computation and Experiment I, II and III*, Thermosciences Division, Mechanical Engineering Department, Stanford University, Stanford, Calif., 1981.

21 Speziale, C. G., "Invariance of Turbulent Closure Models," *Physics of Fluids*, Vol. 22, 1979, pp. 1033–1037.

22 Speziale, C. G., "Closure Relations for the Pressure-Strain Correlation of Turbulence," *Physics of Fluids*, Vol. 23, 1980, pp. 459–463.

Downloaded 02 May 2010 to 171.66.16.250. Redistribution subject to ASME license or copyright; see http://www.asme.org/terms/Terms_Use.cfm

23 Truesdell, C., "The Principles of Continuum Mechanics," *Colloquium Lectures in Pure and Applied Science No. 5*, Socony Mobil Oil Co., Dallas, Texas, 1961.

24 Lumley, J. L., "Toward a Turbulent Constitutive Relation," *J. Fluid Mech.*, Vol. 41, 1970, pp. 413–434.

25 Bardina, J., Ferziger, J. H., and Rogallo, R. S., "Effect of Rotation on Isotropic Turbulence: Computation and Modeling," Submitted to *J. Fluid Mech.*, 1983.

26 Schumann, U., "Realizability of Reynolds Stress Turbulence Models," *Physics of Fluids*, Vol. 20, 1977, pp. 721–725.

27 Shih, T.-H., and Lumley, J. L., "Influence of Time Scale Ratio on Scalar Flux Relaxation: Modeling Sirivat and Warhaft's Homogeneous Passive Scalar Fluctuations," Sibley School of Mechanical and Aerospace Engineering Report No. FDA-81-06, Cornell University, Ithaca, N.Y., 1981.

28 André, J.-C., de Moor, G., Lacarrère, P., and du Vachat, R., "Turbulence Approximation for Inhomogeneous Flows—1. The Clipping Approximation," *J. Atmos. Sci.*, Vol. 33, 1976 *a*, pp. 476–481.

29 André, J.-C., de Moor, G., Lacarrère, P., and du Vachat, R., "Turbulence Approximation for Inhomogeneous Flows—2. The Numerical Simulation of a Penetrative Convection Experiment," *J. Atmos. Sci.*, Vol. 33, 1976 *a*, pp. 482–491.

30 Lumley, J. L, "A New Kind of Realizability in Turbulence Modeling of the Planetary Boundary Layer," in *Workshop on the Planetary Boundary Layer*, Wyngaard, J., ed., American Meteorological Society, Boston, Mass., 1980, pp. 151–181.

31 Pope, S. B., "Consistent Modeling of Scalars in Turbulent Flows," *Physics of Fluids*, Vol. 26, 1983, pp. 404–408.

32 Newman, G. R., Launder, B. E., and Lumley, J. L., "Modeling the Behavior of Homogeneous Scalar Turbulence," *J. Fluid Mech.*, Vol. 111, 1981, pp. 217–232.

33 Launder, B. E., and Schiestel, R., "On the Use of Multiple Time Scales in Turbulent Transport Modelling," *C. R. Hebd. Seances Acad. Si. Ser. A*, France, Vol. 286, No. 16, 1979, pp. 709–712.

34 Launder, B. E., and Schiestel, R., "Application of a Multiscale Transport Model of Turbulence to the Calculation of Free Shear Flows," *C. R. Hebd. Seances Acad. Si. Ser. B*, France, Vol. 288, No. 8, 1979, pp. 127–130.

35 Bertoglio, J.-P., "A Model of Three-Dimensional Transfer in Nonisotropic Homogeneous Turbulence," in *Third Symposium of Turbulent Shear Flows*, Bradbury, L. J. S., Durst, F., Launder, B. E., Schmidt, F. W., and Whitelaw, J. H., eds., University of California, Davis, Calif., 1981, pp. 17.1–17.6

36 Cambon, C., and Jeandel, D., "Approach of Nonisotropic Homogeneous Turbulence Submitted to Mean Velocity Gradients," in *Third Symposium of Turbulent Shear Flows*, Bradbury, L. J. S., Durst, F., Launder, B. E., Schmidt, F. W., and Whitelaw, J. H., University of California, Davis, Calif., 1981, pp. 17.7–17.11.

Downloaded 02 May 2010 to 171.66.16.250. Redistribution subject to ASME license or copyright; see http://www.asme.org/terms/Terms_Use.cfm

Boundary-Layer Interaction Theory

A. F. Messiter
Professor,
Department of Aerospace Engineering,
The University of Michigan,
Ann Arbor, Mich. 48109

Boundary-layer theory for flows at high Reynolds number fails locally in small regions with large gradients, where special solutions are required, with the pressure initially unknown. Examples include the flow near a discontinuity in surface geometry or near a separation point. During the past 15 years, local-interaction problems have been studied extensively for laminar flows, with particular attention to the description and prediction of separation, and a few examples have been worked out for turbulent flows. The basic ideas of asymptotic local-interaction theory are described, and applications are summarized for a variety of flows.

Introduction

Some kind of local boundary-layer interaction occurs in almost every example of fluid motion at high Reynolds number. For illustration, it might be appropriate here to mention the first two papers concerned with flows of this kind in the JOURNAL OF APPLIED MECHANICS. In 1935 Kuethe [1] and von Kármán and Millikan [2] discussed, respectively, the turbulent mixing downstream of a trailing edge or a nozzle exit and the estimation of the maximum lift coefficient of an airfoil. In Kuethe's paper a discontinuity in the transverse velocity component implies, perhaps indirectly, the need for a local correction to the flow description near a sharp trailing edge. Von Kármán and Millikan gave a procedure for predicting incipient separation of a laminar boundary layer near the leading edge of an airfoil. A detailed description of separation, however, again requires a special local solution, and the appearance of a region of separated flow of course has global rather than local effects on the remainder of the flow. It has since become clear that the needed solutions near an edge or a separation point involve a local interaction of the boundary layer and the external flow; an essential feature is the need for calculation of a local pressure perturbation as part of the solution.

In 1969 and 1970, independent studies of laminar separation at supersonic speeds (by Stewartson and Williams and by Neiland) and of incompressible laminar trailing-edge flows (by Stewartson and by Messiter) were published. While there had been a number of precursors, these four papers presented the first complete and systematic analyses explaining the local interaction of the boundary layer and the external flow in small regions where streamwise gradients are large. The general idea is that in such regions most of the boundary layer behaves approximately as an inviscid rotational flow, and is shifted in the transverse direction by the displacement effect of a viscous sublayer, which is required in order that the no-slip boundary condition can be satisfied. The local pressure distribution is not specified in advance, but is determined by the coupling of a boundary-layer solution for the sublayer with a small-disturbance description of the external flow. Thus the usual boundary-layer approximation fails locally. In more precise terms, the derivation of asymptotic solutions to the steady-state Navier-Stokes equations as the Reynolds number tends to infinity now requires three additional limit processes for the description of local changes in the sublayer, the main boundary layer, and the external flow. Solutions are to be carried out in each of these limits, subject to all the proper matching conditions. The analysis of laminar local interactions in terms of such three-tiered asymptotic structures is now commonly referred to, following Stewartson, as "triple-deck theory." The general solution procedure of course follows from the fundamental ideas of singular-perturbation theory, which have been developed in a systematic way primarily since about the beginning of the 1950's (e.g., Lagerstrom and Cole [3]).

The asymptotic local-interaction theory has subsequently been extended to include other geometries, somewhat different types of interaction, low-speed separation, turbulent interactions, etc. Especially noteworthy are Sychev's proposed asymptotic description of bluff-body separation and the many contributions of Stewartson and of Smith in a wide range of flow problems. This work has been reviewed comprehensively in references [4–7] and with emphasis on particular types of flows in references [8–10]. A lucid survey of mathematical aspects has been given in reference [11]. In the present survey, an effort is made to concentrate on the main ideas for a number of applications, rather than to show detailed results. The following sections attempt to identify the major problem areas and to give a largely qualitative summary of selected examples. It is convenient to start by discussing one specific example at some length; the other applications are outlined more briefly. References are given to the earlier reviews, particularly [4–7], which contain extensive bibliographies, rather than to the original papers. A few recent papers not cited elsewhere are also listed here, as references [12–21].

Low-Speed Motions Without Flow Reversal

Interaction at the Trailing Edge of a Flat Plate. Because of the simple geometry and the absence of reversed flow, and

Contributed by the Applied Mechanics Division for publication in the JOURNAL OF APPLIED MECHANICS.
Discussion on this paper should be addressed to the Editorial Department, ASME United Engineering Center, 345 East 47th Street, New York, N.Y. 10017, and will be accepted until two months after final publication of the paper itself in the JOURNAL OF APPLIED MECHANICS. Manuscript received by ASME Applied Mechanics Division, March, 1983.

Copyright © 1983 by ASME
Downloaded 02 May 2010 to 171.66.16.250. Redistribution subject to ASME license or copyright; see http://www.asme.org/terms/Terms_Use.cfm

because the fluid properties are constant, the most straightforward example of fluid motion at high Reynolds number would seem to be the incompressible laminar flow past a flat plate aligned parallel to a uniform stream. The flow is very nearly undisturbed except in thin viscous boundary layers at the surfaces and, for a plate of finite length, in the thin wake directly downstream. Deceleration of the fluid in the boundary layers implies a slight outward displacement of the streamlines, and the external flow is perturbed as if by a very thin body. Immediately downstream of the trailing edge, the merging of the boundary layers from the upper and lower surfaces leads to an acceleration of the fluid near the centerline and therefore now a small local inward displacement of streamlines. This inward displacement actually begins slightly upstream of the trailing edge, and the effect on the external flow is the same as that for a local distribution of sinks in the external potential flow near the edge. The corresponding local pressure perturbation is initially negative, then increases to positive values, and finally decreases again toward zero. These pressure changes also contribute to the velocity changes in the thin viscous shear layers, and so a local interaction occurs between the shear layers and the external flow. The local pressure distribution is not known in advance but is to be calculated as part of the solution.

The nature of the equations required for an asymptotic description of the interaction can be inferred from considerations that are primarily physical. The discontinuous boundary condition at the end of the plate implies large streamwise gradients near the edge. The orders of magnitude of the pressure force and the fluid acceleration are therefore larger than in the upstream boundary layer, and so the flow is approximately inviscid, the vorticity remaining nearly constant along streamlines, except in a thin sublayer. The sublayer then plays the role of a viscous shear layer in an inviscid rotational flow, on a suitably small scale. The streamwise component of the momentum equation for the sublayer must therefore contain the boundary-layer viscous force and the usual acceleration terms, which are nonlinear because the change in velocity for a fluid element is of the same order as its velocity just upstream. Since the pressure force is an essential part of the interaction, it too must be present. The velocity components also, of course, are to satisfy the continuity equation.

In the external potential flow all perturbations are of the same order of magnitude. It can be assumed in advance, and verified later, that the length scale in the streamwise direction is somewhat larger in order of magnitude than the boundary-layer thickness. Throughout the shear layers the streamline curvature is then small enough that the largest term in the perturbation pressure is a function only of the streamwise coordinate. Moreover, the fluid elements with the lowest velocity undergo the largest increase in velocity, so that changes in streamtube width occur primarily in the sublayer. It follows that the pressure and streamline slope obtained as the sublayer coordinate becomes large are nearly the same as seen by the external flow.

Coordinates $\bar{x}$ and $\bar{y}$ are measured, respectively, along and normal to the direction of the undisturbed flow, with the origin at the trailing edge. The corresponding velocity components are $\bar{u}$ and $\bar{v}$, and the pressure is $\bar{p}$. The Reynolds number is $\mathrm{Re} = \rho UL/\mu$, where ρ is the density, U is the velocity of the undisturbed flow, L is the plate length, and μ is the viscosity coefficient; the ratio $\nu = \mu/\rho$ is the kinematic viscosity. Nondimensional boundary-layer coordinates are $X = \bar{x}/L$ and $Y = \mathrm{Re}^{1/2}\bar{y}/L$, and nondimensional velocity components are $u = \bar{u}/U$ and $v = \bar{v}/U$. The nondimensional perturbation pressure is $p = (\bar{p} - \bar{p}_\infty)/\rho U^2$, where $\bar{p}_\infty$ is the pressure in the undisturbed uniform flow.

Ordinary boundary-layer theory is constructed through successive applications of an outer limit, with coordinates fixed relative to the plate length, and an inner limit, with transverse coordinate fixed relative to the boundary-layer thickness. The inner limit is determined by the requirements that viscous forces appear in the momentum equation and that a matching of the inner and outer solutions be possible. The coordinates are $\bar{x}/L$, $\bar{y}/L$ for the outer solution and $\bar{x}/L$, $\mathrm{Re}^{1/4}\bar{y}/L$ for the inner solution. The corresponding asymptotic expansions are parameter expansions presumed valid as the Reynolds number tends to infinity, with one or the other set of coordinates held fixed. Except for some modifications needed when logarithms arise, the terms in the expansions are derived in an alternating sequential fashion: first term outer, first term inner, second term outer, etc. The expansions are properly matched if they agree term-by-term when $\bar{y}/L$ is small and $\mathrm{Re}^{1/2}\bar{y}/L$ is large. This approximation scheme has to be modified near the leading edge, in a very small region with dimensions proportional to the local viscous length, where the full Navier-Stokes equations are required.

For the trailing-edge interaction, the conditions already listed are sufficient, except perhaps for minor omissions, to determine the system of equations for the first approximation and also to fix all the relevant orders of magnitude. The interaction length is found to be $\bar{x}/L = \mathrm{O}(\mathrm{Re}^{-3/8})$, the sublayer thickness is $\bar{y}/L = \mathrm{O}(\mathrm{Re}^{-5/8})$, the pressure perturbation is $p = O(\mathrm{Re}^{-1/4})$, etc. Sublayer coordinates x and y are then defined by $x = \mathrm{Re}^{3/8}\bar{x}/L$ and $y = \mathrm{Re}^{5/8}\bar{y}/L$. Asymptotic representations for the flow properties in the sublayer have the form $u = \mathrm{Re}^{-1/8}\, u_1(x,y) + \ldots$, etc. Differential equations for the sublayer are obtained by taking a limit of the Navier-Stokes equations as $\mathrm{Re} \to \infty$ with x and y held fixed. Local perturbations in the main part of the boundary layer correspond to a limit with x and Y fixed, and perturbations outside the shear layer are found in a limit with x and $\mathrm{Re}^{3/8}\bar{Y}/L$ fixed.

The details of the problem formulation then take the form that has been outlined in the foregoing. The sublayer differential equations are the usual boundary-layer equations, but now in terms of the properly scaled dependent variables as functions of coordinates x and y. The boundary conditions include the no-slip conditions upstream and symmetry conditions downstream of the edge. Upstream of the interaction the solution must approach the first term, as $Y \to 0$, of the Blasius similarity solution for a semi-infinite flat plate. Outside the sublayer the velocity matches with the Blasius solution plus a function of x which represents the small inward displacement of the streamlines. As already anticipated, in the main part of the boundary layer the largest perturbations in pressure and streamline slope are found to be independent of Y. In the external flow the perturbation potential satisfies Laplace's equation in the variables x and $\mathrm{Re}^{3/8}\bar{y}/L$. The solution there has the same form as for the flow past a thin body, and the matching conditions then lead to a relation between the changes in pressure and sublayer displacement thickness. Thus the sublayer perturbations are directly coupled to perturbations in the external flow, the streamlines in the main part of the boundary layer being displaced slightly in the Y-direction, through a distance which is independent of Y in a first approximation. A weak singularity remains as $x \to 0$, where the pressure gradient and streamline curvature become infinite. The singular behavior can be resolved by a study of smaller length scales, but these refinements are not needed for numerical solution of the interaction problem as formulated here.

The solutions further downstream are expressed in terms of coordinate expansions derived by Goldstein. These are intermediate solutions for $\mathrm{Re}^{-1/8} << X << 1$ which give, e.g., $u = \mathrm{O}\,(X^{1/3})$ for $Y = \mathrm{O}\,(X^{1/3})$ and also $p = \mathrm{O}\,(\mathrm{Re}^{-1/2}X^{-2/3})$. In fact, the correct scaling for the interaction could have been inferred from the intermediate solutions, since the interaction

Downloaded 02 May 2010 to 171.66.16.250. Redistribution subject to ASME license or copyright; see http://www.asme.org/terms/Terms_Use.cfm

occurs at values of X such that $|p|$ is no longer small in comparison with u^2.

One of the results obtained by numerical solution is the second term in the drag coefficient $C_D = 1.328\ \mathrm{Re}^{-1/2} + d\mathrm{Re}^{-1/8} + \ldots$, where $d \approx 2.67$. The numerical accuracy of this expression might naturally be questioned because the relevant small parameter is actually $\mathrm{Re}^{-1/8}$. The interaction length and sublayer thickness are, respectively, larger and smaller than the boundary-layer thickness by a factor $O(\mathrm{Re}^{1/8})$, and neglected terms in the expansions of the flow variables are typically smaller only by a factor $O(\mathrm{Re}^{-1/8})$. Clearly $\mathrm{Re}^{-1/8}$ is not really small if, say, $\mathrm{Re} = 10^4$. Nonetheless, the two-term approximation for C_D agrees remarkably well with measured values and with numerical solutions of the full Navier-Stokes equations for Reynolds numbers as low as $\mathrm{Re} = 10$. The wide range of agreement is, of course, fortuitous but also quite encouraging.

Other Interactions at Low Speed. A variety of other interaction problems can be formulated in nearly the same way but with different boundary conditions [4–7]. For a trailing edge with nonzero wedge angle ϵ, the surface slope is no longer small in comparison with typical local streamline slopes when $\epsilon = O(\mathrm{Re}^{-1/4})$. The no-slip condition is then to be satisfied at $|y| = \epsilon \mathrm{Re}^{1/4} |x|$ for $x < 0$. If a flat trailing edge is at an angle of incidence α, near the edge the surface pressure predicted by inviscid-flow theory is $p = O(\alpha |X|^{-1/2})$. For $X = O(\mathrm{Re}^{-3/8})$, this term in the pressure is $O(\mathrm{Re}^{-1/4})$ when $\alpha = O(\mathrm{Re}^{-1/16})$. The requirement that the pressure be continuous at $x = y = 0$ leads to a perturbation in the external flow which contributes a term $\Delta p = O(\mathrm{Re}^{3/8} \alpha |X|^{-1/2})$ to the surface pressure as $|X| \to 0$. The effect is global, since $\Delta p = O(\mathrm{Re}^{-3/8} \alpha)$ elsewhere in the external flow. Interactions at a flat trailing edge have also been studied when the undisturbed uniform streams have different velocities above and below the edge and when a velocity component along the edge is superimposed.

At a convex or concave corner with angle ϵ, the discontinuity in surface slope implies a pressure perturbation $p = O(\epsilon ln |X|)$ in the external potential flow, where X is measured from the corner, and the local interaction removes the singularity. If $\epsilon << \mathrm{Re}^{-1/4}$ the length scales for $\bar{x}$ and $\bar{y}$ are unchanged, but the sublayer momentum equation is linear and an analytical solution can be obtained. Integration of the linearized solution for the pressure gives the pressure distribution for another flow, namely the flow close to a discontinuity in curvature rather than in slope, where the variable term in p is $O(\mathrm{Re}^{-3/8})$ and the sublayer momentum equation is linear. If instead the wall has a short and shallow two-dimensional bump defined by $y = hf(x)$, where x and y are scaled as before the $f \to 0$ sufficiently rapidly as $|x| \to \infty$, the formulation again requires only a change in boundary conditions. The effect of a three-dimensional bump has also been studied. For blowing at a velocity $v_w = O(\mathrm{Re}^{-3/8})$ through a slot of length $\Delta \bar{x} = O(\mathrm{Re}^{-3/8} L)$, the flow disturbances again are described by the local-interaction formulation with modified boundary conditions.

In each of these examples with a second small parameter, the local-interaction formulation contains a parameter of order one, which represents a scaled disturbance strength. That is, the description of the interaction is obtained in the limit as $\mathrm{Re} \to \infty$ with $\epsilon \mathrm{Re}^{1/4}$, $\alpha \mathrm{Re}^{1/16}$, h, or $v_w\ \mathrm{Re}^{3/8}$ held fixed. For each case, there is a maximum value of the parameter above which a solution with attached flow no longer exists. Details and original references for these examples are given in references [4–7].

For unsteady trailing-edge flows, the shedding of vorticity at the edge involves a local interaction [6, 7]. Brown and Daniels have studied a trailing edge undergoing a transverse oscillation with large angular frequency ω and small amplitude αL. The largest term in the surface pressure near the edge, obtained from the potential-flow solution, is $p = O(\alpha k^2 |X|^{1/2} e^{i\omega \bar{t}})$ where $\bar{t}$ is the time and $k = \omega L / U$. In the boundary layer ahead of the trailing-edge region the largest time-dependent term in u is independent of Y, except in the thin Stokes layer where the viscous force is important and $\bar{y} = O\{(\nu/\omega)^{1/2}\}$, i.e., $Y = O(k^{-1/2})$. Near the trailing edge, for $X = O(\mathrm{Re}^{-3/8})$, the Stokes layer has thickness of the same order as the sublayer thickness $Y = O(\mathrm{Re}^{-1/8})$ if $k = O(\mathrm{Re}^{1/4})$. That is, the time derivative appears in the first approximation to the sublayer momentum equation when $k = O(\mathrm{Re}^{1/4})$. With these orders for X and k, the external-flow pressure perturbation given above is of the same order as the trailing-edge pressure perturbation $p = O(\mathrm{Re}^{-1/4})$ when the oscillation has amplitude $\alpha = O(\mathrm{Re}^{-9/16})$. As for steady flow, a higher-order Kutta condition requires the term $p = O(\mathrm{Re}^{-1/4})$ to be continuous at the edge and appears to give a self-consistent local flow description. An added term (const.) $\mathrm{Re}^{-3/8} \alpha k^2 |X|^{-1/2} e^{i\omega \bar{t}}$ then appears in the surface pressure as $X \to 0$, with corresponding changes throughout the external flow and therefore in the circulation.

Linear stability analyses have been carried out in terms of a local boundary-layer interaction by Smith and Bodonyi [7] and by Ryzhov et al. (e.g., references [12–13]). This approach allows a systematic derivation of series expansions, as $\mathrm{Re} \to \infty$, of the frequency for neutral stability. The assumptions that the reduced frequency is again $\omega L / U = O(\mathrm{Re}^{1/4})$ and the length scale is $\Delta \bar{x} = O(\mathrm{Re}^{-3/8} L)$ lead to expansions describing the lower branch of the neutral stability curve for a Blasius boundary layer. The largest terms in frequency and wave number agree with expansions of solutions to the Orr-Sommerfeld equation as $\mathrm{Re} \to \infty$, and the first effects of nonparallel flow arise in higher-order terms. Ryzhov et al. have also studied effects of compressibility and of three-dimensional disturbances. Smith has also formulated the nonlinear stability problem for disturbances in the streamwise velocity component u having amplitude $O(\mathrm{Re}^{-1/8})$. For disturbances with amplitude of a slightly smaller order of magnitude, the linear problem is recovered in a first approximation. The amplitude is then a function of x which satisfies a nonlinear ordinary differential equation of the expected form, obtained by imposing a compatibility condition in a later approximation. For the upper branch of the neutral stability curve a different scaling is implied by the Orr-Sommerfeld solutions as $\mathrm{Re} \to \infty$, and the asymptotic structure is more complicated. Stability of Poiseuille flow in channels and pipes has also been discussed in the context of local interactions.

A somewhat different kind of interaction occurs when there is no external flow [5–7]. A heated vertical plate induces a free-convection boundary layer, with a discontinuous boundary condition at the upper edge. Similarly, if a circular disk rotates about the axis through its center and normal to the disk, the thin viscous layer at the surface has a radial as well as a circumferential velocity component, again with a discontinuous boundary condition at the edge. In each case a jet-like boundary layer, or wall jet, undergoes a local adjustment at, in effect, a trailing edge. As in other interaction problems, the local flow perturbations near the edge are described by boundary-layer equations in a viscous sublayer, and the fluid in the main part of the layer experiences primarily a displacement effect. Now, however, the pressure perturbation in the sublayer arises because of the transverse pressure gradient across the main part of the layer. As a result, the scalings are different. If Re is defined in terms of the appropriate reference velocity, arguments similar to those outlined earlier show that the length of the interaction is $X = O(\mathrm{Re}^{-3/7})$, the sublayer thickness is $Y = O(\mathrm{Re}^{-1/7})$, the pressure perturbation $p = O(\mathrm{Re}^{-2/7})$, etc. The local flow description requires a change only in the pressure-

Downloaded 02 May 2010 to 171.66.16.250. Redistribution subject to ASME license or copyright; see http://www.asme.org/terms/Terms_Use.cfm

displacement relation, with p now proportional to the streamline curvature in the main part of the boundary layer. If $u = U_0(Y)$ is the velocity just upstream of the interaction, the constant of proportionality is the integral of $\rho U_0^2(Y)$ across the layer.

If a Poiseuille flow in a circular tube encounters a slight constriction, the velocity and pressure are again perturbed only locally [6, 7]. As shown by Smith, the disturbances in a core part of the flow are described by inviscid-flow equations, but a low-speed viscous wall layer is required so that the no-slip boundary condition can be satisfied. The reference length and velocity are now the tube radius L and the centerline velocity U. For an axisymmetric constriction defined by $L - \bar{r} = hLF(\bar{x}/L)$, where $\bar{r}$ is the radial coordinate, the wall-layer momentum equation is linear if $h << \mathrm{Re}^{-1/8}$. When $h = O(\mathrm{Re}^{-1/8})$, pressure changes at the constriction are $O(\mathrm{Re}^{-3/8})$ in the wall layer and in the core flow, whereas velocity changes are $O(\mathrm{Re}^{-1/8})$ near the wall and $O(\mathrm{Re}^{-3/8})$ in the core. The matching condition for the velocity perturbation shows that the wall layer has zero displacement effect. The pressure is then found by solution of the boundary-layer equations with the no-slip conditions at the wall and the requirement of zero displacement thickness. Separation can take place on the downstream side of the constriction if $\mathrm{Re}^{1/8} h$ is large enough, but no pressure changes of order $\mathrm{Re}^{-3/8}$ occur upstream. If the constriction is not axisymmetric, so that the tube cross section undergoes a shape change instead of an area change, the differential equations for the wall layer are the three-dimensional boundary-layer equations. For $h = O(\mathrm{Re}^{-1/8})$, the swirl velocity as well as the axial velocity is $O(\mathrm{Re}^{-1/8})$ in the wall layer, and so a strong secondary flow is present.

In a two-dimensional channel, the effects of a symmetric constriction are essentially the same as in a tube. But for an asymmetric constriction the displacement effect is not constrained to be zero and the influence of the constriction does extend upstream. The small streamline curvature in the core flow implies a weak transverse pressure gradient, consistent with a thickening of the wall layer on one side and a thinning on the other side. If the pressure change across the core is of the same order as the pressure change along the wall layers, the interaction has the same character as for a wall jet. This condition corresponds to a special large length scale $O(\mathrm{Re}^{1/7}L)$, with wall-layer thickness $O(\mathrm{Re}^{-2/7}L)$, pressure change $p = O(\mathrm{Re}^{-4/7})$, etc. The two unknown functions of the streamwise coordinate are then the streamline displacement in the core flow and the pressure at one channel surface. These functions are determined by numerical solution of the boundary-layer equations at the two surfaces, subject to the no-slip conditions and the condition that the pressure difference across the channel is proportional to the streamline curvature in the core flow.

Low-Speed Flows With Separation

Bluff-Body Flows. If no separation were to occur, the potential flow past a circular cylinder without circulation would be represented by the superposition of a uniform flow and a doublet, and the drag force would be zero because of the fore and aft symmetry. This is a simple example of "d' Alembert's paradox;" in reality, of course, the flow does separate and a nonzero drag is observed. The velocity potential for attached flow therefore does not appear to give the correct limit of the solution to the Navier-Stokes equations for steady flow as $\mathrm{Re} \to \infty$. A more attractive possibility, which does allow nonzero drag, is the Kirchhoff free-streamline solution, with constant wake pressure equal to the undisturbed pressure. An obvious choice for the location of separation is the one point, at an angle $\theta \approx 55$ deg from the forward stagnation point, for which the separation streamline is predicted to have continuous curvature. If the flow were to separate further upstream, the separation streamline would be found to intersect the body surface. Separation at a point further to the rear would be accompanied by an infinite adverse pressure gradient, which presumably implies earlier occurrence of separation. If the solution for the dividing case is tentatively accepted as the correct limiting solution, it is to be understood as the solution obtained by taking a limit as $\mathrm{Re} \to \infty$ with coordinates held fixed relative to the body diameter. Other limit processes, corresponding to smaller and larger length scales, are needed to describe the flow near the separation point and at large distances.

Velocity profiles in the laminar boundary layer on the forward part of a circular cylinder can be calculated numerically, provided only that a suitable pressure distribution is prescribed. The boundary layer is expected to separate from the surface at the point where the surface shear stress becomes zero; numerical solutions appear to show singular behavior at this point. Goldstein worked out the flow details near the singularity by assuming a locally constant pressure gradient and constructing appropriate coordinate expansions for small upstream distance $|X|$ from the separation point [6, 7]. The surface shear stress decreases as $|X|^{1/2}$, and the streamline slope increases as $|X|^{-1/2}$. Goldstein also showed that similar expansions could not be constructed on the downstream side.

As separation is approached, the growth of the normal velocity component clearly suggests a local interaction with the external flow and therefore a modified local pressure distribution. Stewartson, however, showed that there is no local solution of the "triple-deck" type which approaches the form given by Goldstein for the flow just upstream [6, 7]. The nature of the difficulty was first partially recognized through numerical solutions obtained with some other quantity, such as a guessed displacement thickness or surface shear-stress distribution, prescribed locally instead of the pressure. Messiter and Enlow were able to derive expansions analogous to Goldstein's but with the local pressure given by the Kirchhoff solution, and showed the possibility of constructing self-consistent coordinate expansions downstream as well [5]. The crucial steps, however, were taken by Sychev, who successfully combined the local-interaction description with the Kirchhoff solution [5–7, 10, 11]. If the separation point is shifted downstream from $\theta \approx 55$ deg through a suitable distance that disappears in the limit as $\mathrm{Re} \to \infty$, the resulting adverse pressure gradient becomes just large enough, as separation is approached, to match with the local pressure gradient associated with the interaction.

For a local description of separation, rectangular coordinates $\bar{x}$ and $\bar{y}$ are defined with origin at the separation point and directed, respectively, along the tangent and the normal to the surface. Again $X = \bar{x}/L$ and $Y = \mathrm{Re}^{1/2}\bar{y}/L$, where L is now the cylinder radius. The complex perturbation velocity is approximately $-(p + iv)$, since locally $p \sim 1 - u$. In terms of the complex variable $z = (\bar{x} + i\bar{y})/L$, $0 < \arg z < \pi$, the Kirchhoff solutions as $z \to 0$ have the form $p + iv \sim ic_0 z^{1/2} + \ldots$ where $c_0 = 0$ when $\theta \approx 55$ deg, and c_0 is negative or positive when the separation point is, respectively, further upstream or downstream. For $\arg z = 0$, downstream of separation, $p \sim 0$ and the separation streamline has the form $\bar{y}/L \sim \frac{2}{3}c_0(\bar{x}/L)^{3/2}$. Therefore $c_0 \geq 0$ so that the separation streamline lies outside the cylinder surface $\bar{y}/L - \frac{1}{2}(\bar{x}/L)^2 + \ldots$. For $\arg z = \pi$, upstream of separation, $p = -c_0|\bar{x}/L|^{1/2} + \ldots$ and a positive value of c_0 implies an infinite adverse pressure gradient as $|\bar{x}/L| \to 0$. If separation is to take place through a local interaction of the boundary layer with the external flow, the pressure as $\bar{x}/L \to 0$ must match with a perturbation pressure of the form $p \sim \mathrm{Re}^{-1/4} p_1(x)$ evaluated as $x = \mathrm{Re}^{3/8}\bar{x}/L \to -\infty$. Therefore c_0 $O(\mathrm{Re}^{-1/16})$. The shape of the free streamline at distances $\bar{x} = O(L)$ differs from the shape corresponding to separation

Downloaded 02 May 2010 to 171.66.16.250. Redistribution subject to ASME license or copyright; see http://www.asme.org/terms/Terms_Use.cfm

at $\theta \approx 55$ deg by terms $O(Re^{-1/16})$, and so the separation point is shifted downstream through a distance $O(Re^{-1/16}L)$. The adverse pressure gradient then is present only for a short distance $O(Re^{-1/16}L)$. Furthermore, the first approximation to the boundary-layer behavior near separation is obtained with the transverse pressure gradient equal to zero. In these respects the asymptotic description of separation is quite different from the description anticipated intuitively with a larger region of adverse pressure gradient and with a nonzero local $\partial p/\partial Y$ assumed to play an important role.

The local-interaction problem has the same general form as before, but with some modifications in the boundary and matching conditions. One further assumption concerning the local nature of the reversed flow is also required. Downstream, of course, the fluid from the upstream boundary layer moves away from the surface in a shear layer having thickness $O(Re^{-1/2}L)$. Below this layer is a region of reversed flow, which in the limit is described by inviscid-flow equations. A mixing of these two flows takes place in a thin sublayer containing the separation streamline, and it is assumed that the backflow is just sufficient to provide the mass required for entrainment in this thin mixing layer. There is also a reversed boundary layer along the surface, which experiences a weak favorable pressure gradient, so that no secondary separation occurs. The assumption about the local reversed flow does not seem to imply further specific assumptions about the wake further downstream. A numerical solution was carried out by Smith; among the results is an evidently unique value for the constant $Re^{1/16}c_0$. Another more recent calculation [10] is in substantial agreement with Smith's. While not conclusive, these results do provide a most convincing argument for the existence and also uniqueness of the solution to the problem proposed by Sychev as providing an asymptotic description of separation.

The Kirchhoff free-streamline solution can also be matched with solutions that describe the flow at distances large in comparison with the body dimensions. In reality, of course, transition to turbulence will occur, but the limiting form of the solution for laminar flow nonetheless can be a useful approximation at Reynolds numbers low enough that the motion is still steady. At lower Reynolds numbers it is known from experiment and from numerical solutions of the Navier-Stokes equations that the region of recirculating flow increases in length as Re increases. If this trend continues at high Reynolds numbers, the Kirchhoff wake width, which grows as the square root of the distance downstream, must match with the wake width given by the solution obtained for an appropriate larger length scale. Experimental and numerical evidence also suggests strongly that the drag coefficient should approach a nonzero limit as $Re \to \infty$. The drag force can be equated to the deficit in momentum flux far downstream. At the free streamlines the laminar mixing of the outer flow with the recirculating flow implies thin viscous shear layers with thickness $O[LRe^{-1/2}(\bar{x}/L)^{1/2}]$. If the flow remains steady and these shear layers eventually come together, the fluid outside the separation streamlines continues downstream and the fluid inside is turned back. The momentum deficit downstream of this point is $O(\rho U^2 L)$ if the wake length is $O(L\mathrm{Re})$. The matching requirement gives a corresponding wake width $O(Re^{1/2}L)$.

This description of the limiting form of the laminar wake behind a bluff body was proposed by Roshko and by Sychev in 1967. Sychev assumed further that the recirculating flow is just sufficient to supply the mass needed for entrainment, and also suggested appropriate asymptotic expansions for each of the several important flow regions. Smith elaborated on Sychev's work and showed effects of the $O(Re^{-1/16})$ correction associated with the rearward shift of the separation point from $\theta \approx 55$. He also showed comparisons with experimental results and with numerical solutions of the Navier-Stokes equations at lower Reynolds numbers. For a circular cylinder at $Re = 100$ (based on diameter), predicted values of pressure drag and for pressure at the rear stagnation point were within a few percent of values found from numerical solutions of the full equations.

A possible objection to this wake description arises because of uncertainty about the flow details at "reattachment," when the two separated shear layers come together. Since the dimensions of this region are $O(L)$ and the velocity is $O(U)$, the differential equations in the limit become the inviscid-flow equations. If the flow remains steady, along the centerline a jet-like flow directed toward the body would initially have the same profile, but inverted, as the velocity in the inner parts of the two shear layers. A contradiction follows, since velocities $O(U)$ would persist all the way to the cylinder. Sychev [10] has recently made the interesting observation that the available pressure force is not sufficient to accomplish this turning. By integration over suitable control volumes, he notes that the drag force is equal to twice the integral of the shear stress along one of the separation streamlines. This integral is also equal to the momentum flux in the inner portion of one of the shear layers. The pressure force along the dividing streamlines near reattachment is also equal to the drag. This force is then sufficient only to cancel the momentum flux of the downstream-moving fluid and not to impart an equal and opposite upstream momentum flux. It might follow that there really is no limiting flow as $Re \to \infty$ which is everywhere steady.

Other Flows With Separation. In several of the examples mentioned in the foregoing, separation is first predicted to occur when a scaled disturbance strength reaches a particular value, which can be calculated by numerical solution of the appropriate local-interaction problem. More difficult is the description of the separated flow as the disturbance strength continues to increase [7]. For a symmetric airfoil shape with a sharp trailing edge, Cheng and Smith have proposed a description of the rather complicated manner in which the motion changes continuously from an attached flow to a bluff-body flow as the thickness increases. In the asymmetric case Smith has suggested that separation from one surface at a point near the trailing edge is followed by reattachment just ahead of the edge. Guided by numerical solutions of the local-interaction equations, with the pressure required to be continuous at the edge, he concludes that again a continuous change from attached flow to bluff-body flow is possible, as the angle of attack is increased. For the separated flow over a shallow bump, there appears to be an intermediate range of bump sizes such that a weak square-root singularity is present but is, in fact, removable because of the form of the pressure-displacement relation, by introduction of solutions for suitable small length scales. If the boundary layer is disturbed instead by blowing through a narrow slot, numerical solutions of the local-interaction problem show that the first separation occurs downstream of the slot, whereas for sufficiently strong blowing, separation might be expected to occur ahead of the slot; solutions for intermediate cases are not yet available.

For a circular tube [6, 7] with an axisymmetric constriction defined as before by $L - \bar{r} = hLF(\bar{x}/L)$, velocity and pressure perturbations in the core flow become $O(Re^{-1/4})$ when $h = O(Re^{-1/6})$. The wall layer upstream of the constriction then also has a velocity perturbation $O(Re^{-1/4})$, because of the changes in the core flow, and separation can occur ahead of, as well as at, the constriction. If $h = O(1)$, and if $F(\bar{x}/L) \to 0$ sufficiently rapidly upstream, the first separation occurs at a distance $O(L/n\mathrm{Re})$ upstream. This separation is described by the boundary-layer equations within a distance $O(L)$ from the separation point, with prescribed displacement thickness but unknown pressure. In a limit with the distance from the constriction held fixed, a free streamline appears to originate at the surface infinitely far upstream and reattaches on the

Downloaded 02 May 2010 to 171.66.16.250. Redistribution subject to ASME license or copyright; see http://www.asme.org/terms/Terms_Use.cfm

front of the constriction. The second separation, at the constriction, is of the same type as the bluff-body separation described in the foregoing, followed by a free streamline and eventual reattachment at a distance O(LRe) downstream. At these large distances the flow is fully viscous, and so the reattachment process does not seem to raise the same questions as for bluff-body flows. If the constriction is not axisymmetric, the separation is three-dimensional and the motion is more complicated.

In a two-dimensional channel, as for unseparated flow, the effects of a symmetric constriction are similar to the effects in a tube. For a severe asymmetric constriction, say with length and height both O(L), the first separation occurs at a larger upstream distance O($\mathrm{Re}^{1/7}L$). The reversed flow is confined to a thin layer of width O($\mathrm{Re}^{-2/7}L$) for most of this distance, consistent with the description of interaction given earlier for unseparated flow. The flow on the large length scale does not depend on the nature of the constriction and thus might be called a "free interaction." Numerical solution of the interaction problem suggests a singularity of a form that allows matching with a free-streamline solution for the flow at a distance $\bar{x}=\mathrm{O}(L)$ ahead of the constriction. Separation of a wall jet occurs through a similar free interaction.

If a thin airfoil with a rounded leading edge is placed at a small angle of attack α, the surface shear stress τ_w has a minimum value, so that $d\tau_w/dX=0$, at some point near the edge. Here X is measured along the surface and has been made nondimensional with the leading-edge radius of curvature. If α is large enough that separation occurs, a numerical solution calculated with a prescribed pressure gradient leads to a square-root behavior for τ_w at separation, so that $d\tau_w/dX\rightarrow-\infty$ there. In the dividing case, ordinary boundary-layer theory gives a minimum value $\tau_w=0$, with $\tau_w/(\rho U^2)\sim$(const.)$\mathrm{Re}^{-1/2}|X|$ as the minimum is approached. The local pressure perturbation remains O($\mathrm{Re}^{-1/2}$), and coordinate expansions for $X\rightarrow0$ and $\alpha\rightarrow\alpha_s$, where α_s is the value of α which separation first appears, show that the change in sign of $d\tau_w/dX$ occurs when $X=\mathrm{O}\{|\alpha-\alpha_s|^{1/2}/\alpha_s^{1/2}\}$. A local interaction then is found to occur [6, 7, 14] within a distance $\Delta X=\mathrm{O}(\mathrm{Re}^{-1/5})$ for angles of attack in a range $(\alpha-\alpha_s)/\alpha_s=\mathrm{O}(\mathrm{Re}^{-2/5})$.

The absence of a singularity in $d\tau_w/dX$ at the separation point in this case implies that the velocity in the main part of the boundary layer has the form $u\sim a_2Y^2+\mathrm{O}(Y^6)$ as $Y\rightarrow0$. In the sublayer [14], $u\sim a_2Y^2$ and a second term is linear in Y, with coefficient proportional to the local streamline displacement. A third term satisfies a linear momentum equation which, when solved and combined with the pressure displacement relation outside the boundary layer, leads to an integrodifferential equation for the streamline displacement. Numerical solutions show a very shallow separation bubble for a range of values of $\mathrm{Re}^{2/5}$ $(\alpha-\alpha_s)/\alpha_s$, and no solution exists beyond a critical value of this parameter. Smith [15] has also formulated the corresponding time-dependent problem, and has obtained numerical solutions for larger values of α. As a particular value of the scaled time coordinate is approached, the peak displacement thickness grows indefinitely, and is followed by a waviness which may imply the presence of additional separation bubbles.

For unsteady flows the first complete description of separation in terms of a local interaction was given by Sychev [16]. Unsteady flow over a fixed surface with separation moving upstream at a speed u_w is equivalent to steady flow over a wall moving downstream at speed u_w provided that u_w does not change too rapidly with time. In an adverse pressure gradient the velocity profile for the steady flow will develop a minimum at some point away from the surface, and this minimum velocity will subsequently decrease to zero. Thus separation is associated with the simultaneous vanishing of u and $\partial u/\partial Y$ at a point away from the surface; this is the condition proposed by Moore, Rott, and Sears. Sychev assumes a free-streamline flow as $\mathrm{Re}\rightarrow\infty$, with $\bar{y}/L\sim$ (const.) $(\bar{x}/L)^{3/2}$ at the separation streamline, where $\bar{x}$ is measured from the separation point. A local interaction is expected because $\partial p/\partial X=\mathrm{O}(|X|^{-1/2})$ along the surface just upstream of separation. A first guess for the length scale of the interaction can be found by equating the orders of magnitude of the boundary-layer thickness and the displacement of the free streamline; the result is $X=\mathrm{O}(\mathrm{Re}^{-1/3})$. Sychev has verified this estimate in a more careful way, by a study of coordinate expansions as $X\rightarrow0$ from the upstream side, which also show that the local boundary-layer thickness has increased and is now O($\mathrm{Re}^{-1/2}ln\mathrm{Re}$). Matching of the pressure gives $p=\mathrm{O}(\mathrm{Re}^{-1/6})$ when $X=\mathrm{O}(\mathrm{Re}^{-1/3})$, and as usual it is found that the local flow perturbations are described by inviscid-flow equations in most of the boundary layer. These equations are nonlinear only when $u=\mathrm{O}(\mathrm{Re}^{-1/12})$, for points near the velocity minimum. The solution in this region, after matching requirements are satisfied, expresses the local increase in displacement thickness in terms of the pressure. This effect, calculated from inviscid-flow equations, is now the dominant displacement effect, since the viscous wall layer has a velocity that is not small and it therefore contributes only a higher-order term to the streamline displacement. Substitution in the pressure-displacement relation for the external flow then gives an integrodifferential equation for p.

If the velocity u_w of the downstream-moving wall is small, the interaction length is found to be $X=\mathrm{O}(\mathrm{Re}^{-1/3}u_w^{1/3})$ and the point where $u=\partial u/\partial Y=0$ is close to the surface. A dividing case occurs for $u_w=\mathrm{O}(\mathrm{Re}^{-1/8})$, when viscous effects again enter the problem in a first approximation. In the corresponding unsteady flow over a fixed surface, time derivatives are absent in the first approximation, and so the time enters only as a parameter, provided that the characteristic time ω^{-1} for the variation of u_w satisfies the condition $\omega^{-1}>>\mathrm{Re}^{-1/6}u_w^{2/3}$.

High-Speed Flows

Boundary-layer interactions at supersonic speeds were understood in a qualitative way long before a systematic analytical description became available. As early as 1939, Ferri observed experimentally that an oblique shock wave can be present well ahead of the trailing edge of an airfoil at angle of attack. Soon afterward it was pointed out by Oswatitsch and Wieghardt that a local interaction can occur at supersonic speed because a boundary-layer thickening and a pressure increase reinforce each other. Later experiments included studies of separation caused by compression corners, forward-facing steps, and incident oblique shock waves. As the strength of the disturbance is increased, it was found that the separation point moves rapidly upstream. An initial small pressure rise near separation is then followed by a "plateau" region of nearly constant pressure, as a nearly straight separated shear layer moves away from the surface. Near separation the flow details are almost independent of the manner in which separation is induced, and the interaction has therefore been called a "free interaction." Additional flow changes of course occur close to the disturbance which is responsible for the separation.

Early attempts at calculation of interaction pressures, typically for weakly separated flows, were based on the boundary-layer equations coupled with a pressure-displacement relation for the external flow. These equations, later called "interacting boundary-layer equations," were solved approximately with the help of integral methods. A key additional step was the recognition in the early 1950s, in particular by Lighthill, that the pressure change in a local interaction takes place in an asymptotically short distance, so that viscous forces locally are of lesser importance in most of

Downloaded 02 May 2010 to 171.66.16.250. Redistribution subject to ASME license or copyright; see http://www.asme.org/terms/Terms_Use.cfm

the boundary layer but crucial in a thinner sublayer. A systematic asymptotic representation of supersonic free interaction was first given in 1969 by Stewartson and Williams and by Neiland; numerous extensions have followed, notably by Stewartson et al.

The local flow description for a supersonic interaction is very similar to that for interactions in incompressible flow [4–8]. Within a short distance of separation, viscous forces are important primarily in a thin sublayer where the velocity is small and the temperature and density are nearly constant. In the external flow small perturbations in any of the flow variables are, however, described by the wave equation. For example, in a first approximation a velocity potential ϕ exists and satisfies $(M_\infty{}^2-1)\phi_{\bar{x}\bar{x}}-\phi_{\bar{y}\bar{y}}=0$, where M_∞ is the Mach number in the undisturbed flow. Just outside the boundary layer, as $\bar{y}/L\to 0$ and $\mathrm{Re}^{1/2}\bar{y}/L\to\infty$, the pressure change $p\approx -\phi_{\bar{x}}/U$ is now proportional to the streamline slope $\phi_{\bar{y}}/U$, which in the first approximation, results entirely from the displacement effect of the sublayer. A linear dependence of viscosity on temperature is usually assumed; if the subscript ∞ indicates undisturbed-flow conditions, $\mu/\mu_\infty=CT/T_\infty$. Arguments similar to those used for incompressible flow lead again to the orders of magnitude $\bar{x}/L=\mathrm{O}(\mathrm{Re}^{-1/8})$, $p=(\mathrm{Re}^{-1/4})$, etc., where now $p=(\bar{p}-\bar{p}_\infty)/\rho_\infty U^2$, L is the length of the boundary layer, $\mathrm{Re}=\rho_\infty UL/\mu_\infty$, and $\bar{x}$ is measured from the separation point. Suitable additional factors allow the parameters to be absorbed. For example, $p\sim\lambda^{1/2}(B^2\mathrm{Re}/C)^{-1/4}p_1(x)$, where $B^2=M_\infty{}^2-1$ and $x=\lambda^{5/4}(B^2\mathrm{Re}/C)^{1/8}(T_w/T_\infty)^{-3/2}\bar{x}/L$. The wall temperature is T_w, assumed constant, and for a flat plate $\lambda=0.332$.

With these modifications, the sublayer differential equations to be solved are as before, with the boundary conditions at $y=0$ replaced by $u=v=0$ for all x. The pressure-displacement relation for the external flow is now replaced by a linear relation between the perturbations in pressure and in streamline slope. Downstream a straight constant-pressure shear layer moves away from the surface, with a thinner mixing layer developing about the separation streamline. It is assumed that the low-speed reversed flow between this layer and the surface is just sufficient to provide the mass needed for entrainment in the mixing layer.

Numerical solutions of the free-interaction problem are in qualitative agreement with experimental results. Typically the prediction of separation pressure and plateau pressure appear to be fairly accurate, but the predicted pressure gradient at separation is too low. The difficulty of course is that the flow remains laminar only up to Reynolds numbers somewhat above $\mathrm{Re}=10^5$. Second-order terms in the expansions for u, v, p are smaller only by factors $\mathrm{O}(\mathrm{Re}^{-1/8})$ and errors can therefore be large at $\mathrm{Re}\approx 10^5$. A complete second-order theory has also been worked out, but is found to overcorrect both the pressure and the pressure gradient at separation.

The free-interaction formulation describes separation at a distance l ahead of a disturbance that is strong enough that $\mathrm{Re}^{-1/8}L<<l<<L$. With suitable modification of the boundary conditions, local interactions can be described for weaker disturbances such that the entire interaction takes place within a distance $\mathrm{O}(\mathrm{Re}^{-1/8}L)$. Examples include flow over corners or steps and interactions caused by an incident oblique shock wave or by boundary-layer blowing [4–8].

For a compression or expansion corner with angle $\alpha=\mathrm{O}(\mathrm{Re}^{-1/4})$, the surface boundary conditions for $x>0$ are applied at $y=\mathrm{Re}^{1/4}\alpha x$. Numerical solutions predict separation at specific values of $\alpha\mathrm{Re}^{1/4}$. Extensive studies of compression corners have allowed comparison of the theory with experimental results and with numerical solutions of the full Navier-Stokes equations. Burggraf et al. [8] note that satisfactory agreement is not obtained until the Reynolds number reaches unrealistically large values of about 10^9. Much better agreement at, say, $\mathrm{Re}=10^5$ has been obtained with the "interacting boundary-layer equations," which are asymptotically equivalent to the local-interaction equations, in the sense of providing a composite representation. A three-dimensional ramp problem has also been studied, with surfaces $\bar{y}=\alpha\bar{x}$ for $\bar{z}>0$ and $\bar{y}=-\alpha\bar{x}$ for $\bar{z}<0$.

When the region of separated flow has length $l>>\mathrm{Re}^{-1/8}L$, reattachment of the separated shear layer is accompanied by a turning of the external flow through an angle $\mathrm{O}(\alpha)$ and a pressure rise $\Delta p=\mathrm{O}(\alpha)$, where, in the examples cited in the following, $\mathrm{Re}^{-1/4}<<\alpha<1$. This pressure rise is described in a first approximation by inviscid-flow equations. Along the separated shear layer upstream of reattachment, the flow close to the separation streamline is described in a first approximation as the mixing of a uniform shear flow with fluid at rest. The appropriate self-similar solution gives $u=\mathrm{O}\{(l/L)^{1/3}\}$ at reattachment. Since this velocity is brought to zero at the reattachment stagnation point, the pressure rise is $\Delta p=\mathrm{O}\{(l/L)^{1/3}\}$. Therefore $\alpha=\mathrm{O}\{(l/L)^{1/3}\}$, or $l=\mathrm{O}(\alpha^{3/2}L)$ [5, 8].

For a compression ramp at an angle α such that $\mathrm{Re}^{-1/4}<<\alpha<<1$, the separated shear layer lies at an angle $\mathrm{O}(\mathrm{Re}^{-1/4})$ from the upstream surface and at an angle $\mathrm{O}(\alpha)$ relative to the ramp. Separation therefore occurs at a distance $l=\mathrm{O}(\alpha^{3/2}L)$ upstream. For an incident oblique shock wave with strength Δp such that $\mathrm{Re}^{-1/4}<<\Delta p<<1$, the same general argument predicts that separation occurs at a distance $l=\mathrm{O}\{(\Delta p)^{3/2}L\}$ ahead of the shock wave. For a backward-facing step of height h, the boundary layer separates at the shoulder, and reattachment occurs at a distance l further downstream. Then α is replaced by h/l, and it follows that $l/L=\mathrm{O}\{(h/L)^{3/5}\}$ and $p=\mathrm{O}\{(h/L)^{2/5}\}$.

A detailed description of the recirculating flow, however, with no further assumptions, is still lacking in each of these examples. One of the major difficulties is in understanding what happens to the fluid that is entrained below the separation streamline and is subsequently turned back at reattachment. This is the same difficulty, but on a smaller scale, as encountered far downstream in bluff-body flows.

The form of the free-interaction pressure distribution given previously is incorrect of M_∞ is either too large or too close to one. For an insulated plate at large M_∞, since $T_w/T_\infty=\mathrm{O}(M_\infty{}^2)$, the interaction length and pressure perturbation remain small only if $M_\infty{}^6/\mathrm{Re}\to 0$ as $\mathrm{Re}\to\infty$. Hypersonic-flow solutions have been studied for a cooled wall and in the limit as $\gamma\to 1$, where γ is the ratio of specific heats. If instead M_∞ is near one, the change $M-M_\infty$ in the local Mach number, which is proportional to p, remains small in comparison with $M_\infty-1$ only if $\mathrm{Re}^{-1/5}/(M_\infty^2-1)\to 0$ as $\mathrm{Re}\to\infty$. In the transonic small-disturbance approximation, perturbations in the external flow are described by the nonlinear differential equation $\phi_{\bar{y}\bar{y}}\approx\{(M_\infty{}^2-1)+(\gamma+1)\phi_{\bar{x}}\}\phi_{\bar{x}\bar{x}}$, and pressure changes are of the same order as the two-thirds power of the typical streamline slope. With this modification, the reasoning used before shows, e.g., that the interaction length is $\mathrm{O}(\mathrm{Re}^{-3/10}L)$ and the pressure changes are $\mathrm{O}(\mathrm{Re}^{-1/5})$ when $M_\infty^2-1=\mathrm{O}(\mathrm{Re}^{-1/5})$. If $M-1$ remains positive in the external flow, a free interaction still can occur, with the pressure perturbation now a nonlinear function of the streamline slope. Finally, for subsonic Mach numbers the external flow is described by $(1-M_\infty{}^2)\phi_{\bar{x}\bar{x}}+\phi_{\bar{y}\bar{y}}\approx 0$. The parameters can be absorbed as for supersonic flow, but with $M_\infty{}^2-1$ replaced by $1-M_\infty{}^2$. For flows in which the streamline slope remains small, the solutions for incompressible flow are then applicable for subsonic Mach numbers if the definitions of the variables are changed in this way.

Turbulent Flows

Local interactions of a turbulent boundary layer with the

Downloaded 02 May 2010 to 171.66.16.250. Redistribution subject to ASME license or copyright; see http://www.asme.org/terms/Terms_Use.cfm

external flow have a quite different character because of the two-layer structure of the mean-velocity profile in the undisturbed boundary layer. This structure was originally inferred from a combination of dimensional considerations and experimental observations. Near the surface the important parameters are the friction velocity $u_\tau = (\tau_w/\rho)^{1/2}$, where τ_w is the local wall shear stress, and the viscous length ν/u_τ. It is observed that $u_\tau << \bar{u}_e$ and $\nu/u_\tau << \delta$, where $\bar{u}_e$ is the local external-flow velocity and δ is a local boundary-layer thickness. At a given location the "law of the wall" expresses the mean-flow velocity in the form $\bar{u} = u_\tau f(u_\tau \bar{y}/\nu)$. In most of the boundary layer, however, the viscosity is not directly an important parameter, and the effect of the wall is to provide a retarding shear stress τ_w such that the mean velocity is reduced from the external-flow value by a term proportional to u_τ. For a flat plate, with $\bar{u}_e = U$, the "velocity-defect law" is then $\bar{u} = U - u_\tau F(\bar{y}/\delta)$. In an intermediate range, for small $\bar{y}/\delta$ and large $u_\tau \bar{y}/\nu$, it has been observed that the mean velocity has a logarithmic form $\bar{u} \sim \kappa^{-1} u_\tau ln(u_\tau \bar{y}/\nu)$ where $\kappa \approx 0.41$ is the von Kármán constant. Millikan gave important analytical support for this idea in 1938, noting that the logarithmic profile follows from the requirement that the wall-layer and defect-layer predictions for $\bar{y}\partial\bar{u}/\partial\bar{y}$ be identical in the intermediate range.

It has been pointed out more recently, in the early 1970s, that the two-layer structure might be interpreted as providing an asymptotic flow description for large Reynolds number, such that $u_\tau/\bar{u}_e \to 0$ and $u_\tau \delta/\nu \to \infty$ [9]. The wall-layer representation corresponds to a limit with $u_\tau \bar{y}/\nu$ held fixed and with the assumption $\bar{u} = u_\tau f(u_\tau \bar{y}/\nu) + \ldots$. In this limit the momentum equation expresses a balance between the usual boundary-layer viscous and turbulent shear stresses. In the defect-layer limit, the expansion of $\bar{u}$ is carried out with $\bar{y}/\delta$ fixed, and since $\tau_w/\rho U^2 \to 0$ it is plausible to expect that the shear stress causes only a small change in velocity. For a flat plate, the largest terms in the momentum equation are the linear inertia term $\rho U \bar{u}_{\bar{x}}$ and the term $\tau_{\bar{y}}$ representing the effect of turbulent shear stresses. Here $\tau = -\rho \overline{u'v'}$, where primes denote fluctuating quantities and the bar indicates an average. In carrying out the matching as $\bar{y}/\delta \to 0$ and $u_\tau \bar{y}/\nu \to \infty$, it is convenient to adopt Millikan's choice and consider first $\bar{y}\partial\bar{u}/\partial\bar{y}$. This matching implies the logarithmic intermediate profile and shows that $\bar{u} - U = O(u_\tau)$ in the defect-layer limit. Since intermediate limits give $\tau_{\bar{y}} \sim 0$, it is further implied that $\tau = O(\rho u_\tau^2)$ in the defect layer as well as in the wall layer. It follows from the defect-layer momentum equation that $\delta/L = O(u_\tau/U)$, and matching of $\bar{u}$ gives $\delta/L = O(1/ln\mathrm{Re})$.

This representation of a turbulent boundary layer has provided a starting point for asymptotic studies of several examples of turbulent interactions. The first systematic investigations, by Melnik et al. and by Adamson, Messiter, et al., were concerned with interaction at transonic speeds with a weak normal shock wave [8, 9]. It seems more convenient, however, again to discuss low-speed interactions first.

For a flat plate aligned parallel to the undisturbed stream, rapid changes in the mean velocity occur near the trailing edge. Here the relevant friction velocity u_τ is a constant, equal to the value slightly upstream of the trailing-edge region. Within a very small distance $O(\nu/u_\tau)$ from the edge, both velocity components are $O(u_\tau)$ and the full Navier-Stokes equations are required. As $\bar{x}$ increases, at first the velocity profiles remain nearly the same as the boundary-layer profiles just ahead of the trailing edge, except in a thin sublayer where the mean velocity is increased rapidly by turbulent shear stresses. The variable $\xi = \kappa^{-1} ln(u_\tau \bar{x}/\nu)$ and the nondimensional centerline velocity $\bar{u}_0/u_\tau$ both increase from values of order one to large values close to U/u_τ. Convenient nondimensional sublayer coordinates are ξ and $\eta = \bar{y}/\Delta$, where $\Delta = \Delta(x)$ is a sublayer thickness defined such that turbulent stresses are important when $\eta = O(1)$. Expansions for the flow properties near the centerline are then sought as $u_\tau/U \to 0$ and $\xi \to \infty$ with η held fixed. The matching conditions for large η require that $\bar{u}$ and τ approach the same from as for the profile just ahead of the trailing edge, so that $u \sim \kappa^{-1} u_\tau ln(u_\tau \bar{y}/\nu)$ and $\tau \sim \rho u_\tau^2$ as $\eta \to \infty$. These conditions appear to imply expansions of the form $\bar{u} = \bar{u}_0 + u_\tau f(\eta) + \ldots$ and $\tau = \rho u_\tau^2 g(\eta) + \ldots$. The first approximation to the momentum equation is then $\rho \bar{u}_0 \bar{u}_{\bar{x}} \approx \tau_{\bar{y}}$, which suggests the choice $\Delta = u_\tau \bar{x}/\bar{u}_0$. A complete solution would of course require the choice of a turbulence model to describe τ. The matching condition for $\bar{u}$ is, however, sufficient to give $f(\eta) \sim \kappa^{-1} ln\eta$ as $\eta \to \infty$ and also $\bar{u}_0/u_\tau + \kappa^{-1} ln(\bar{u}_0/u_\tau) = \kappa^{-1} ln(u_\tau \bar{x}/\nu)$. This form for $\bar{u}_0$ was first proposed in reference [17].

This formulation is clearly not complete. It appears necessary next to consider a weak trailing-edge interaction, because of the acceleration of fluid in the sublayer and the resulting displacement effect. When $\bar{x} = O(\delta)$ the self-similar form for $(\bar{u} - \bar{u}_0)/u_\tau$, now with $\eta = (U/u_\tau)(\bar{y}/\bar{x})$, is evidently still correct since the boundary and matching conditions are unchanged. The sublayer thickness is now $O(u_\tau \delta/U)$ and so the continuity equation gives $v = O(u_\tau^2/U^2)$. In the outer part of the layer, for $\bar{x} = O(\delta)$ and $\bar{y} = O(\delta)$, perturbations in u, v, and p are $O(u_\tau^2/U^2)$ and are described in a first approximation by equations for inviscid rotational flow, with the displacement effect of the sublayer entering through the matching condition as $\bar{y}/\delta \to 0$. The solution would then allow a correction to the sublayer solution, probably with special attention required when $\bar{x}/\delta$ and $\bar{y}/\delta$ are both small. These steps have not yet been carried out.

For a flat plate at an angle attack α, the inviscid-flow surface pressure near the trailing edge is, as noted earlier, $p = O(\alpha |X|^{1/2})$ as $X \to 0$. For $\bar{x} = O(\delta)$ and $\bar{y} = O(\delta)$, where $\delta/L = O(u_\tau/U)$, additional flow perturbations are of the same order as the changes due to the streamline displacement predicted by the inviscid-flow solution. These changes in u, v, and p are found to be $O(\alpha u_\tau^{3/2}/U^{3/2})$ and are described by equations for inviscid rotational flow. In contrast to solutions for laminar flow, the transverse pressure gradient must be retained, but the largest pressure perturbations do not depend on the solution in a sublayer. A Kutta condition is imposed by the requirement that the perturbation pressure remain finite as $\bar{x}/\delta \to 0$ and $\bar{y}/\delta \to 0$. The local correction then has a global effect through the change in circulation. Details of this problem have been discussed in a systematic way by Melnik [9], in the context of flow at high subsonic speed near the cusped trailing edge of an airfoil.

Sykes [8] has studied the changes in mean-flow properties of a turbulent boundary layer that encounters a shallow two-dimensional bump having length $O(\delta)$ and height $O(\delta u_\tau^{1/2}/U^{1/2})$. The largest perturbation in pressure is the same as for a uniform potential flow over the bump. In the solution for the wall layer, the surface shear stress τ_w is just replaced by its unknown local values, and matching the velocity u then shows that the largest correction to τ_w is proportional to the change in pressure at the surface. In a sublayer having thickness $O(\delta u_\tau/U)$, as for the trailing-edge problem, the momentum equation contains a term representing the effects of Reynolds stresses, as well as the pressure and inertia terms. The sublayer allows changes in the Reynolds stress from the near-equilibrium values in the wall layer to the values in the outer part of the boundary layer where the dependence on upstream history is strong. Solutions obtained for higher-order terms in τ_w depend on the turbulence model chosen, and Sykes suggests that at least a second-order closure based on the Reynolds-stress transport equations is required.

In a recent study of turbulent wall jets [19], expansions of averaged quantities are carried out in terms of two small parameters, a nondimensional friction velocity, and a non-

Downloaded 02 May 2010 to 171.66.16.250. Redistribution subject to ASME license or copyright; see http://www.asme.org/terms/Terms_Use.cfm

dimensional turbulent diffusivity. The reference value for the diffusivity is $k^2/(\rho\epsilon)$, where k is the turbulent kinetic energy and ϵ is the turbulent dissipation. The continuity and momentum equations are supplemented by differential equations for k and ϵ. Obvious reference lengths are the viscous length ν/u_τ and the initial jet thickness, implying a wall-layer solution and an outer solution that describes a free jet in a first approximation. The two solutions cannot be matched directly, and it is found that two additional limits must be considered. Solutions are obtained for both plane and radial jets.

The two-layer structure in compressible boundary layers introduces an additional complication. The velocity-defect layer has nearly constant density, as does the wall layer. Thus it is plausible to expect incompressible-flow solutions in the defect-layer and wall-layer limits, but with different constant values of the density. Again the solutions are expected to have logarithmic behavior as $\bar{y}/\delta \to 0$ and $u_\tau \bar{y}/\nu_w \to \infty$, where ν_w is the wall value of ν. For an insulated wall or for a wall at constant temperature, it is typically assumed that the temperature is the same quadratic function of velocity as for a laminar boundary layer (the Crocco integral). Since, however, $\tau = -\overline{\rho u' v'}$ (in terms of mass-weighted averages) and neither representation allows a density variation, it might be anticipated that a direct matching is impossible; i.e., there is no overlap domain. This failure can be demonstrated with a mixing-length approximation $\tau = \rho\kappa(\bar{y}\tilde{u}_{\bar{y}})^2$ for $\bar{y} << \delta$, where $\tau = \tau_w + \ldots$ and $\rho T = \rho_\infty T_\infty$. Integration then gives $\tilde{u}$ as a function of $u_\tau ln(\bar{y}/\delta)$. This intermediate solution, obtained for intermediate limits such that $\bar{y}/\delta \to 0$ and $u_\tau \bar{y}/\nu_w \to \infty$, matches with the defect-layer solution as $\bar{y}/\delta \to 0$ and $u_\tau ln(\bar{y}/\delta) \to 0$, and with the wall-layer solution as $u_\tau \bar{y}/\nu_w \to \infty$ and $u_\tau ln(u_\tau \bar{y}/\nu_w) \to 0$. The same general mathematical features also appear in solutions for two-dimensional compressible laminar flow at low Reynolds number past a body such as a circular cylinder. The situation is clarified if the problem is reformulated in terms of a variable $\sigma = u_\tau ln(\bar{y}/\delta)$, where $-A < \sigma < 0$ and $A = u_\tau ln(u_\tau \delta/\nu_w) = O(1)$, with δ obtained from the matching as a function of u_τ and the other parameters. Now the problem is expressed in a more conventional way, in terms of limit-process expansions for σ fixed (intermediate), σ/u_τ fixed (defect layer), and $(\sigma + A)/u_\tau$ fixed (wall layer). A composite solution formed from the intermediate and defect-layer solutions is often interpreted as providing a correlation between velocity profiles for compressible and incompressible flows.

For a range of high subsonic speeds the pressure over an airfoil surface is strongly affected by the presence of a region of supersonic flow terminated by a nearly normal shock wave that extends into a turbulent boundary layer. The flow details near the foot of the shock wave must be described in terms of a local interaction [8, 9]. There are two small parameters, $u_\tau/\tilde{u}_e$ and $M_e^2 - 1 > 0$, where $\tilde{u}_e$ and M_e are local external-flow values just ahead of the shock wave. As $M_e^2 - 1$ increases, the sonic line moves closer to the surface in the boundary layer immediately upstream; the shock wave becomes stronger and can extend further into the boundary layer. Each of the small parameters characterizes a velocity difference, and their ratio $\chi = (M_e^2 - 1)/(u_\tau/\tilde{u}_e)$ plays the role of a similarity parameter.

The pressure rise across the shock wave changes by $O(u_\tau)$ in a distance $\bar{y} = O(\delta)$, so that the transverse pressure gradient is nonzero in a first approximation, and in fact can be regarded as the cause of the interaction. In the limit as $u_\tau/\tilde{u}_e \to 0$ and $M_e^2 - 1 \to 0$ with χ, $\bar{y}/\delta$, and $(M_e^2 - 1)^{-1/2}(\bar{x}/\delta)$ fixed, the first term in the perturbation potential is found to satisfy a modified nonlinear transonic-small-disturbance equation. The displacement effect of thinner layers is of higher order, so that no representation of changes in turbulent stresses is needed for calculation of a first approximation to the pressure distribution. The largest correction to the wall shear stress is again proportional to the first term in the pressure perturbation. It follows that separation will not be predicted in any limit for which the pressure change tends to zero; rather, separation will occur only when $p = O(1)$. Higher-order terms in the wall shear stress require solution of a sublayer momentum equation that expresses a balance between Reynolds-stress, pressure, and inertia terms. This sublayer has been called a "blending layer" or a "Reynolds-stress sublayer."

The asymptotic formulation has also been given for $\chi \to 0$ and for $\chi \to \infty$. In the latter case the shock wave extends very close to the wall and the first term in the perturbation potential, as a function of $(M_e^2 - 1)^{-1/2}(\bar{x}/\delta)$ and $\bar{y}/\delta$, satisfies Laplace's equation in a quarter-plane. Thus, e.g., the surface pressure and shear stress can be expressed analytically, except for rapid initial changes in the gradients at the very beginning of the interaction. Effects of axial symmetry and of wall curvature have also been included. Analogous solutions for supersonic flow over a shallow compression ramp can be derived in various limits by use of the supersonic, hypersonic, and transonic small-disturbance theories.

Concluding Remarks

The asymptotic theory of local boundary-layer interactions is now about 15 years old. Laminar interactions without separation have been studied extensively and are quite thoroughly understood in a very broad range of situations, for steady and unsteady flows, for incompressible and compressible flows, and for external and internal flows with a variety of geometries. Moreover, asymptotic descriptions of separation through a free interaction have been given for supersonic flows and for certain internal flows, and a strong case has been made for linking bluff-body separation with free-streamline theory. Outstanding problem areas, most of which have been mentioned or implied in the preceding sections, fall primarily into two obvious major categories. First, serious gaps still remain in our understanding of laminar separated flows; and, second, only a few examples of turbulent boundary-layer interactions have been studied in a systematic way.

For two-dimensional laminar separated flows, a fully self-consistent description of reattachment and recirculation is still not available. This leaves incomplete the otherwise convincing Sychev proposal for the low-speed wake behind a bluff body, as well as proposed descriptions of separated flow at supersonic speeds and also of separated internal flows. Another question concerns the form of solutions that might exist for intermediate cases between attached flow past a thin body and separated flow past a bluff body. As noted earlier, substantial progress has been made toward closing these gaps. For leading-edge separation, the work of von Kármán and Millikan [2] represents an example of an early calculation method for prediction of incipient laminar separation, but only recently has the first step been taken toward a description of the flow details just after the first appearance of separation. Further study is needed of the time-dependent change from attached to separated flow as the angle of attack is increased. Unsteady separation is now understood in particular examples, and additional applications should also be possible. Finally, and perhaps of greatest importance, asymptotic studies of three-dimensional separation have been limited to the free interaction in a pipe flow and the separation of a vortex sheet from a smooth surface [7].

In most turbulent local interactions the dominant effects occur in a small region where the mean flow is rotational and nearly inviscid. For unseparated flows the most important observation is that a representation of the changes in turbulent stresses is not needed for calculation of the largest perturbations in pressure, or even for the first approximation

Downloaded 02 May 2010 to 171.66.16.250. Redistribution subject to ASME license or copyright; see http://www.asme.org/terms/Terms_Use.cfm

to the changes in the surface shear stress. An exception is the weaker interaction in symmetric flow at a cusped trailing edge, for which the turbulent mixing close to the surface streamline is the dominant effect, and here the term of order one in u does not seem to require a representation of the Reynolds stress. A similar result might be expected for the merging of flows with unequal velocities, as in the work of Kuethe [1]. It should now be possible to complete the formulation of these and other trailing-edge problems in a systematic way, and to carry out solutions for simple representations of the Reynolds stresses. As for laminar motions, it sh ould also be possible to study interactions between a shock wave and a turbulent boundary layer for various geometries. But by far the most serious need at this stage is an asymptotic description of the mean flow near separation. Existing solutions for turbulent interactions without regions of reversed mean flow might seem to suggest that separation is characterized by pressure changes on a scale $O(\delta)$ with changes in Reynolds stresses important only in smaller regions, i.e., for suitable inner limits. A different view of the extent of the interaction has recently been proposed by Sychev and Sychev [10].

There now exists quite a large catalog of local-interaction solutions, showing a variety of effects for a variety of flows. Less has been done, however, toward the incorporation of these local solutions into the overall description of a larger flow field. This step requires suitable numerical techniques. For laminar flows, one procedure uses the interacting boundary-layer equations as a composite set of equations [20], with local scaling chosen to be consistent with the appropriate local-interaction scaling. Calculations of separated flows are probably limited to fairly small regions of reversed flow, and the change in flow direction introduces an additional difficulty in finite-difference marching methods. Burggraf and Duck [21] have avoided this difficulty in calculations of the flow over a shallow two-dimensional bump by a Fourier-transform method. For fully turbulent boundary layers, Melnik et al. [9] have shown a way of properly including trailing-edge effects with the interacting boundary-layer equations in a calculation of the transonic potential flow past an airfoil. These examples all illustrate applications of two-dimensional solutions, whereas interactions of practical interest are often, if not usually, three-dimensional. The extension of existing solutions to a reasonably broad class of three-dimensional flows remains a formidable challenge.

Acknowledgment

The author would like to thank Dr. R. E. Melnik for several helpful conversations during the preparation of this article.

References

1 Kuethe, A. M., "Investigations of the Turbulent Mixing Regions Formed by Jets," ASME JOURNAL OF APPLIED MECHANICS, Vol. 57, 1935, pp. A87–A95.

2 von Kármán, T., and Millikan, C. B., "A Theoretical Investigation of the Maximum-Lift Coefficient," ASME JOURNAL OF APPLIED MECHANICS, Vol. 57, 1935, pp. A21–A27.

3 Lagerstrom, P. A., and Cole, J. D., "Examples Illustrating Expansion Procedures for the Navier-Stokes Equations," *Journal of Rational Mechanics and Analysis*, Vol. 4, 1955, pp. 817–882.

4 Stewartson, K., "Multistructured Boundary Layers on Flat Plates and Related Bodies," *Advances in Applied Mechanics*, Vol. 14, 1974, pp. 145–239.

5 Messiter, A. F., "Boundary-Layer Separation," *Proc. 8th U.S. Natl. Congr. Appl. Mech.*, Western Periodicals, North Hollywood, Calif., 1979, pp. 157–179.

6 Stewartson, K., "D' Alembert's Paradox," *SIAM Review*, Vol. 21, 1981, pp. 308–343.

7 Smith, F. T., "On the High Reynolds Number Theory of Laminar Flows," *IMA J. Appl. Math.*, Vol. 28, 1982, pp. 207–281.

8 Adamson, T. C., Jr., and Messiter, A. F., "Analysis of Two-Dimensional Interactions Between Shock Waves and Boundary Layers," *Annual Review of Fluid Mechanics*, Vol. 12, 1980, pp. 103–138.

9 Melnik, R. E., "Turbulent Interactions on Airfoils at Transonic Speeds—Recent Developments," *AGARD CP-291*, Computation of Viscous-Inviscid Interactions, 1980, Paper No. 10.

10 Sychev, V. V., "Asymptotic Theory of Separation Flows," *Fluid Dynamics*, Vol. 17, 1982, pp. 179–188.

11 Meyer, R. E., "A View of the Triple Deck," *SIAM J. Appl. Math.*, Vol. 43, 1983.

12 Ryzhov, O. S., and Terentev, E. D., "On Unsteady Boundary Layer With Self-Induced Pressure," *J. Appl. Math. Mech.*, Vol. 41. 1977, pp. 1024–1040.

13 Zhuk, V. I., and Ryzhov, O. S., "On the Stability of a Freely Interacting Boundary Layer," *J. Appl. Math. Mech.*, Vol. 45, 1981, pp. 403–410.

14 Ruban, A. I., "Asymptotic Theory of Short Separation Regions on the Leading Edge of a Slender Airfoil," *Fluid Dynamics*, Vol. 17, 1982, pp. 33–41.

15 Smith, F. T., "Concerning Dynamic Stall," *Aeronautical Quarterly*, Vol. 33, 1982, pp. 331–352.

16 Sychev, Vik. V., "Asymptotic Theory of Nonstationary Separation," *Fluid Dynamics*, Vol. 14, 1979, pp. 829–838.

17 Robinson, J. L., "Similarity Solutions in Several Turbulent Shear Flows," National Physical Laboratory Aero Rept. 1242, 1967.

18 Sykes, R. I., "An Asymptotic Theory of Incompressible Turbulent Boundary Layer Flow over a Small Hump," *J. Fluid Mech.*, Vol. 101, 1980, pp. 647–670.

19 Melnik, R. E., and Rubel, A., "Asymptotic Theory of Turbulent Wall Jets," *Second Symposium on Numerical and Physical Aspects of Aerodynamics Flows*, Long Beach, Calif., 1983.

20 Davis, R. T., and Werle, M., "Progress on Interacting Boundary-Layer Computations at High Reynolds Numbers," *Numerical and Physical Aspects of Aerodynamic Flows*, Cebeci, T., ed., Springer-Verlag, 1982, pp. 187–210.

21 Burggraf, O. R., and Duck, P. W., "Spectral Computation of Triple-Deck Flows," *Numerical and Physical Aspects of Aerodynamic Flows*, Cebeci, T., ed., Springer-Verlag, 1982, pp. 145–158.

Downloaded 02 May 2010 to 171.66.16.250. Redistribution subject to ASME license or copyright; see http://www.asme.org/terms/Terms_Use.cfm

On Finite Plastic Flow of Crystalline Solids and Geomaterials

S. Nemat-Nasser
Professor of Civil Engineering and Applied Mathematics, Department of Civil Engineering, The Technological Institute, Northwestern University, Evanston, Ill. 60201
Fellow ASME

Certain fundamentals of finite-deformation elastoplastic flow of crystalline solids and geomaterials are discussed from microscopic and macroscopic phenomenological points of view. In the first case, physically based constitutive relations for microelements are formulated on the basis of slip-induced plastic deformation with due account of possible frictional or pressure dependencies and inelastic volumetric changes. The close relation between the double-slip theory of single crystals and that of granular materials is discussed. The calculation of overall instantaneous moduli in terms of the local quantities for arbitrary strains and rotations is examined, and some recent results for polycrystals and granular materials are reviewed. Then, attention is focused on phenomenological constitutive relations which apply to both metals and geomaterials. Specific results are given for an isotropic-kinematic hardening model, including frictional and plastic dilatancy effects. Finally, certain fundamental thermodynamic aspects of finite-deformation inelasticity are reviewed, emphasizing conditions under which flow potentials exist.

1 Introduction

The plasticity theory aims to quantify and predict the behavior of crystalline solids, particularly metals which, in the microscale and at suitable temperatures, deform dissipatively by essentially rate-independent slip over crystallographic planes, accompanied by reversible elastic lattice distortion. Finite plasticity addresses mechanical processes that involve large plastic deformations. Examples are wire drawing and sheet forming. Included within the range of the theory is the characterization of flow and fracture of geomaterials which fundamentally differ from metals, since frictional effects and inelastic volumetric changes are then the basic concomitants of the process.

The purpose of this paper is to summarize some of the major results in finite plasticity which particularly pertain to polycrystal aggregates, composite elastoplastic materials, granular masses, jointed rocks, and other related technological materials and geomaterials.

The paper is organized in the following manner. Section 2 is devoted to a microscopically based continuum approach, where, guided by observations, we use simple elemental assumptions to characterize microelement constitutive description, and then employ averaging processes to extract the overall response. A main objective here is to bring into focus the interrelation among seemingly different approaches for the formulation of granular flow, the plasticity of single crystals, and the deformation of jointed rocks. Guided by various contributions in these areas, we present a unified constitutive formulation at the microlevel and discuss some of its implications. Another objective of Section 2 is to present a basic result analogous to Eshelby's [1], but for finite strains and rotations, which is necessary for calculating the local microelemental quantities in terms of the overall far-field data. This is then used together with Hill's averaging theorem, [2], to estimate the overall response of a macroelement when arbitrarily large strains and rotations at both the microlevels and macrolevels may be involved. Some very recent interesting results peculiar to finite deformations are mentioned. Section 3 is devoted to phenomenological macroscopic elastoplasticity. Selected constitutive relations that are physically motivated and apply to both metals and geomaterials, at least under certain loading and temperature ranges, are summarized, and an attempt is made to relate their implications as well as their physical bases to the micromechanically based models of Section 2. Such physical considerations provide guidance for avoiding pitfalls which may emerge when simple models well suited for linearized infinitesimal deformation regimes (e.g., Hooke's law and kinematic hardening) are extended for application to finite deformation and rotation regimes, without due regard to the physics of the assumed processes. In Section 4, certain fundamental results that bear on the essential structure of constitutive relations for rate-independent, as well as rate-dependent inelasticity at finite strains, are briefly reviewed. The notions of "normality," "associative flow rule," and "coaxiality" are examined, and the limitations of work and

Contributed by the Applied Mechanics Division for publication in the JOURNAL OF APPLIED MECHANICS.
Discussion on this paper should be addressed to the Editorial Department, ASME, United Engineering Center, 345 East 47th Street, New York, N.Y., 10017, and will be accepted until two months after final publication of the paper itself in the JOURNAL OF APPLIED MECHANICS. Manuscript received by ASME Applied Mechanics Division, May, 1983.

Copyright © 1983 by ASME
Downloaded 02 May 2010 to 171.66.16.250. Redistribution subject to ASME license or copyright; see http://www.asme.org/terms/Terms_Use.cfm

stability postulates in the range of finite deformations are discussed. Some basic kinematical and dynamical results due to Hill [2–5] are summarized in Appendix A.

The reader may find the following related and complementary overview articles of interest, as some attempt has been made to minimize overlap: Havner [6], Hill [5], Nemat-Nasser [7, 8] and Rice [9].

2 Micromechanically Based Finite Plasticity

A representative sample (macroelement) consisting of a suitably large number of microelements is considered. On the macroscopic scale, the sample is viewed to be uniform and subjected to boundary data that are compatible with uniform overall deformation and stress. The resulting overall constitutive relations, therefore, model the mechanical response of continuum material neighborhoods (continuum particles), and may be used in the continuum equations of motion in various initial and boundary-value problems.

2.1 Plasticity of Microelements. On a sufficiently fine microscale, the deformation of crystals and granular masses is not continuous. In crystals, slip over crystallographic planes leads to overall plastic deformation, and in granular materials discrete contacting granules slide and roll relative to each other, producing overall inelasticity. The continuum representation of these processes does account for their discrete nature, but this is done in terms of continuum measures such as the local velocity gradient, the deformation rate tensor, and the spin tensor, taken to be constant throughout the microelement. The kinematics of the microelement is thus described in terms of the *continuum velocity gradient* l_{ij}, consisting of two *accompanying* contributions, l^p_{ij} and l^*_{ij},

$$l_{ij} = l^p_{ij} + l^*_{ij}, \quad i,j = 1,2,3, \tag{2.1}$$

where components with respect to a fixed rectangular Cartesian coordinate system are implied; in the sequel both the direct and index notations will be used.

The contribution l^p_{ij} is called "plastic." It arises from slip on a finite number of slip systems which may or may not involve volumetric strain rates,

$$l^p_{ij} = d^p_{ij} + w^p_{ij} \equiv p^\alpha_{ij}\dot\gamma^\alpha + \omega^\alpha_{ij}\dot\gamma^\alpha \quad (\alpha \text{ summed}), \tag{2.2}$$

where $\dot\gamma^\alpha$ is the rate of slip, $\mathbf{d}^p$ and $\mathbf{w}^p$ are the plastically induced deformation rate and spin tensors, respectively, and

$$p^\alpha_{ij} = r^\alpha_{ij} + \tan\nu_1 n^\alpha_i n^\alpha_j + \tan\nu_2 s^\alpha_i s^\alpha_j + \tan\nu_3 \delta_{ij},$$

$$r^\alpha_{ij} = \frac{1}{2}(s^\alpha_i n^\alpha_j + s^\alpha_j n^\alpha_i), \quad \omega^\alpha_{ij} = \frac{1}{2}(s^\alpha_i n^\alpha_j - s^\alpha_j n^\alpha_i)$$

(α not summed). (2.3)

Here, $\mathbf{n}^\alpha$ and $\mathbf{s}^\alpha$, with components n^α_i and s^α_i, are unit vectors defining the slip plane and the slip direction, respectively; $\boldsymbol{\delta}$, with components δ_{ij}, is the Kronecker delta; and tan ν_1, tan ν_2, and tan ν_3 characterize the associated "plastic" volumetric strain rate per unit rate of slip. Since any three mutually orthogonal unit vectors (**n**, **s**, and **m**) satisfy $n_i n_j + s_i s_j + m_i m_j = \delta_{ij}$, equation (2.2) accounts for rather general plastic volume straining. In (2.2), α is summed over all instantaneously *active* slip systems.

The contribution l^*_{ij} in (2.1) *is an accompanying "accommodating" velocity gradient which renders l_{ij} compatible, and gives rise to stress changes.* For the single crystal, l^*_{ij} corresponds to the elastic lattice distortion accompanying crystallographic slip. For jointed rocks, it represents the elastic distortion of the rock matrix, and in the case of granular materials, l^*_{ij} corresponds to possible elastic distortion of grains, *as well as the change in the orientation of the contact unit normals and hence the "frictional" contact forces.* Therefore, a general[1] class of constitutive behaviors is characterized by assuming that an objective stress rate relates linearly to the symmetric part of l^*_{ij}, i.e.,

$$\overset{\nabla}{\boldsymbol{\tau}}{}^* = \underset{\sim}{\mathcal{L}}{}^\Omega : \mathbf{d}^*, \quad d^*_{ij} = \frac{1}{2}(l^*_{ij} + l^*_{ji}),$$

$$\overset{\nabla}{\boldsymbol{\tau}}{}^* \equiv \dot{\boldsymbol{\tau}}^* - \mathbf{w}^*\boldsymbol{\tau} + \boldsymbol{\tau}\mathbf{w}^*, \quad \mathbf{w}^*_{ij} = \frac{1}{2}(l^*_{ij} - l^*_{ji}). \tag{2.4}$$

Here $\boldsymbol{\tau}$ is the Kirchhoff stress, $\underset{\sim}{\mathcal{L}}{}^\Omega$ is the instantaneous *elastic* modulus tensor of the crystal, Ω, or the rock matrix, and $\dot{\boldsymbol{\tau}}^*$ is defined in terms of the Cauchy stress, $\boldsymbol{\sigma}$, by

$$\dot{\boldsymbol{\tau}}^* = \dot{\boldsymbol{\sigma}} + d^*_{kk}\boldsymbol{\sigma}\ ; \tag{2.5}$$

repeated subscripts are summed, and the components of, say, $\mathbf{w}^*\boldsymbol{\tau}$ are $\mathbf{w}^*_{ik}\tau_{kj}$. For granular materials, $\underset{\sim}{\mathcal{L}}{}^\Omega$ must be interpreted in terms of the granular fabric; see Section 2.4.

Denote by a superimposed ∇, but without an asterisk, the Jaumann rate corotational with the *material*, e.g., for the Kirchhoff stress,

$$\overset{\nabla}{\boldsymbol{\tau}} \equiv \dot{\boldsymbol{\tau}} - \mathbf{w}\boldsymbol{\tau} + \boldsymbol{\tau}\mathbf{w}, \quad w_{ij} = \frac{1}{2}(l_{ij} - l_{ji}),$$

$$\dot{\boldsymbol{\tau}} = \dot{\boldsymbol{\sigma}} + d_{kk}\boldsymbol{\sigma}, \quad d_{ij} = \frac{1}{2}(l_{ij} + l_{ji}). \tag{2.6}$$

From (2.1)–(2.6) it follows that

$$\overset{\nabla}{\boldsymbol{\tau}} = \underset{\sim}{\mathcal{L}}{}^\Omega : \mathbf{d} - \{\underset{\sim}{\mathcal{L}}{}^\Omega : \mathbf{p}^\alpha + \boldsymbol{\omega}^\alpha\boldsymbol{\sigma} - \boldsymbol{\sigma}\boldsymbol{\omega}^\alpha - p^\alpha_{kk}\boldsymbol{\sigma}\}\dot\gamma^\alpha$$

(α summed), (2.7)

where the components of $\underset{\sim}{\mathcal{L}}{}^\Omega : \mathbf{d}$ are $\mathcal{L}^\Omega_{ijkl} d_{kl}$.

We now need to express $\dot\gamma^\alpha$ in terms of the deformation rate $\mathbf{d}$ through relevant local flow relations. A general[1] class of micromaterial responses is encompassed by the relation,

$$\dot\tau^\alpha + \tan\eta_1 \dot\sigma^\alpha + \tan\eta_2 \dot p = h^{\alpha\beta}\dot\gamma^\beta \quad (\beta \text{ summed}), \tag{2.8}$$

where τ^α and σ^α are the shear and normal stresses transmitted across the *active* α-slip system; $p = \sigma_{kk}/3$ is the mean stress; tan η_1 and tan η_2 are material parameters defining the resistance to slip, produced, respectively, by the normal stress and the mean pressure; and $h^{\alpha\beta}$ is the hardening matrix, generally dependent on the plastic deformation history. The parameter tan η_1 represents the coefficient of friction, whereas tan η_2 relates to the possible effect of hydrostatic pressure on the motion of dislocations and hence, slip. For pressure insensitive metals, $\eta_1 = \eta_2 = 0$.

To calculate $\dot\tau^\alpha$ and $\dot\sigma^\alpha$, we must define the rate of change of $\mathbf{n}^\alpha$ and $\mathbf{s}^\alpha$. While various assumptions may be considered (Asaro and Rice [10]),

$$\dot{\mathbf{n}}^\alpha = \mathbf{w}^*\mathbf{n}^\alpha \quad \text{and} \quad \dot{\mathbf{s}}^\alpha = \mathbf{w}^*\mathbf{s}^\alpha, \tag{2.9}$$

suggested by Hill [11] and employed by Asaro [12] and Nemat-Nasser, Mehrabadi, and Iwakuma [13], seem reasonable and appealing.[1] Then (2.8) becomes

$$\overset{\nabla}{\sigma}{}^*_{ij} q^\alpha_{ij} = h^{\alpha\beta}\dot\gamma^\beta \quad (\beta \text{ summed}), \tag{2.10}$$

$$q^\alpha_{ij} = r^\alpha_{ij} + \tan\eta_1 n^\alpha_i n^\alpha_j + \tan\eta_2 \delta_{ij} \quad (\alpha \text{ not summed}). \tag{2.11}$$

The relation (2.10) applies to *active* slip systems only. The system is active when the stress state attains a critical level. Often used models are described by the rule,

$\dot\gamma^\alpha \geq 0$ if $0 < \sigma_{ij} q^\alpha_{ij} = \tau^\alpha_Y$ and

$$\overset{\nabla}{\sigma}{}^*_{ij} q^\alpha_{ij} = h^{\alpha\beta}\dot\gamma^\beta \quad (\beta \text{ summed}), \tag{2.12}$$

where τ^α_Y is the local current "*yield*" stress in shear.

[1] See, however, comments at the end of present section.

Downloaded 02 May 2010 to 171.66.16.250. Redistribution subject to ASME license or copyright; see http://www.asme.org/terms/Terms_Use.cfm

With the aid of (2.10) and (2.4) $\dot{\gamma}^\alpha$ may be (formally) expressed by

$$\dot{\gamma}^\alpha = M^{\alpha\beta}\mathbf{q}^\beta : (\underset{\sim}{\mathcal{L}}^\Omega - \boldsymbol{\sigma}\otimes\boldsymbol{\delta}) : \mathbf{d},$$
$$M^{\alpha\beta} = [h^{\alpha\beta} + \mathbf{q}^\alpha : (\underset{\sim}{\mathcal{L}}^\Omega - \boldsymbol{\sigma}\otimes\boldsymbol{\delta}) : \mathbf{p}^\beta]^{-1}, \tag{2.13}$$

where $\otimes$ denotes the tensor product; i.e., components of $\boldsymbol{\sigma}\otimes\boldsymbol{\delta}$ are $\sigma_{ij}\delta_{kl}$. In some cases, the matrix inside the braces in $(2.13)_2$ may be singular, Hill [11]. However, one may always choose a set of acceptable slip systems. A discussion of this has been given recently by Havner [14] who proposes a criterion based on minimum rate of plastic work.

From (2.13) and (2.7) we obtain a general physically based elastic-plastic rate-constitutive relation for the microelement.

$$\overset{\nabla}{\boldsymbol{\tau}} = \mathbf{L}^\Omega : \mathbf{d}, \tag{2.14}$$

with the *instantaneous elastic-plastic modulus*,

$$\mathbf{L}^\Omega \equiv \underset{\sim}{\mathcal{L}}^\Omega - [\underset{\sim}{\mathcal{L}}^\Omega : \mathbf{p}^\alpha + \boldsymbol{\omega}^\alpha\boldsymbol{\sigma} - \boldsymbol{\sigma}\boldsymbol{\omega}^\alpha - p^\alpha_{mm}\boldsymbol{\sigma}]M^{\alpha\beta}[\mathbf{q}^\beta : (\underset{\sim}{\mathcal{L}}^\Omega - \boldsymbol{\sigma}\otimes\boldsymbol{\delta})]. \tag{2.15}$$

While $\mathbf{L}^\Omega$ is symmetric with respect to the exchange of i and j, and k and l, it is not, in general, symmetric with respect to the exchange of ij and kl. This is true even if parameters ν_1, ν_2, and ν_3, and η_1 and η_2 are all identically zero. In such a case, the nonsymmetry may arise from the presence of terms of the order $\boldsymbol{\sigma}$ in (2.15). Some implications of (2.14) and (2.15) are examined in the following sections.

In many applications, the Cauchy stress is often used instead of the Kirchhoff stress. Since $\boldsymbol{\sigma} = \boldsymbol{\tau}$ (but $\dot{\boldsymbol{\sigma}} \neq \dot{\boldsymbol{\tau}}$) when the current configuration is used as the reference, equations (2.5) and $(2.6)_3$ allow immediate reinterpretation of the results in terms of other stress measures. If we *redefine* the modulus tensor $\underset{\sim}{\mathcal{L}}^\Omega$ in such a manner that $(2.4)_1$ is replaced by

$$\overset{\nabla}{\boldsymbol{\sigma}}^* = \underset{\sim}{\mathcal{L}}^\Omega : \mathbf{d}^*, \tag{2.16}$$

then in place of (2.14) we may use

$$\overset{\nabla}{\boldsymbol{\sigma}} = \mathbf{L}^\Omega : \mathbf{d}, \tag{2.17}$$

where now $\mathbf{L}^\Omega$ is given by

$$\mathbf{L}^\Omega \equiv \underset{\sim}{\mathcal{L}}^\Omega - [\underset{\sim}{\mathcal{L}}^\Omega : \mathbf{p}^\alpha + \boldsymbol{\omega}^\alpha\boldsymbol{\sigma} - \boldsymbol{\sigma}\boldsymbol{\omega}^\alpha][h^{\alpha\beta} + \mathbf{q}^\alpha : \underset{\sim}{\mathcal{L}}^\Omega : \mathbf{p}^\beta]^{-1}\mathbf{q}^\beta : \underset{\sim}{\mathcal{L}}^\Omega. \tag{2.18}$$

At this point, a few comments may be in order.

The constitutive assumption $(2.4)_1$, as well as (2.16), though suitably general for many applications, does disregard possible slip-induced changes in lattice elasticity. It may be modified to include this and other secondary effects, as discussed by Hill and Havner [15] and Hill and Rice [16]. The kinematic assumption (2.9) neglects the influence of lattice distortion on slip orientation. It is useful when elastic distortion is small, but must be modified in more general settings; see, e.g., Asaro and Rice [10]. Finally, while the flow rule (2.8) does embody frictional and certain non-Schmid slip laws, it is by no means completely inclusive; for example, it may not account for cross-slip effects. Therefore, while we have presented results with considerable generality, they are intended more as illustrative than comprehensive.

2.2 Double-Slip Theories. The slip theory of single crystals was pioneered by Taylor and Elam [17], and since then has been explored for both small and finite deformations; see, e.g. Asaro [12], Asaro and Rice [10], Havner [14], Havner and Shalaby [18], Hill [11], Hill and Havner [15], Hill and Rice [16], Kocks [19], Mandel [20], and Zarka [21]. Recently, Asaro [12] has examined the implications of a two-dimensional model of both fcc and bcc single crystals (which deform plastically by double slip), particularly in relation to possible localized deformations. The theory is closely related to the double slip (sliding) model of granular flow originated by Mandel [22] in 1947, and further developed by de Josselin de Jong [23], Spencer [24, 25], and, more recently, Mehrabadi and Cowin [26] and Nemat-Nasser, Mehrabadi, and Iwakuma [13]. The general equations (2.15) include both theories, and point toward further applications and additional results.

To demonstrate the interrelation between these two-dimensional theories, consider a special version of (2.18), formulated by Nemat-Nasser, Mehrabadi, and Iwakuma [13], where only one dilatancy parameter, $\nu = \nu_1$ (i.e., $\nu_2 = \nu_3 = 0$), and one pressure sensitivity parameter, $\eta = \eta_1$ (i.e., $\eta_2 = 0$), are included, the coordinate axes are taken along the principal Cauchy stresses, $\sigma_1 > \sigma_2$, and the slip lines are taken symmetrical with respect to the coordinate axes, at angle $\phi/2 + \pi/4$ with the σ_1-axis. The hardening matrix is assumed symmetric with $h^{11} = h^{22} = h$, and $h^{12} = h^{21} = h_1$. The elasticity tensor, $\underset{\sim}{\mathcal{L}}^\Omega$, is assumed isotropic, $\mathcal{L}^\Omega_{ijkl} = G(\delta_{ik}\delta_{jl} + \delta_{il}\delta_{jk}) + \lambda\delta_{ij}\delta_{kl}$. Then equations (2.17) become

$$\overset{\nabla}{\sigma}_{11} = a_1 d_{11} + a_2 d_{22}, \quad \overset{\nabla}{\sigma}_{22} = b_1 d_{11} + b_2 d_{22},$$
$$\overset{\nabla}{\sigma}_{12} = 2\bar{\mu} d_{12}, \tag{2.19}$$

where

$$\begin{aligned}
a_1 &= K[(2G+\lambda)\mu^* + G(G+\lambda)(1-M)(1-B)],\\
a_2 &= K[\lambda\mu^* + G(G+\lambda)(1-M)(1+B)],\\
b_1 &= K[\lambda\mu^* + G(G+\lambda)(1+M)(1-B)],\\
b_2 &= K[(2G+\lambda)\mu^* + G(G+\lambda)(1+M)(1+B)],\\
\bar{\mu} &= \frac{G[H_1 + \bar{\tau}(M-\sin\phi)(1-B\sin\phi)]}{H_1 + G(M-\sin\phi)(B-\sin\phi)},\\
K &= [\mu^* + G + MB(G+\lambda)]^{-1}, \quad \bar{\tau} = \frac{1}{2}(\sigma_1 - \sigma_2) > 0,\\
M &= \frac{\sin\eta}{\cos(\phi-\eta)}, \quad B = \frac{\sin\nu}{\cos(\phi-\nu)},\\
2H_1 &= (h-h_1)(1-M\sin\phi)(1-B\sin\phi),\\
2\mu^*\cos^2\phi &= (h+h_1)(1-M\sin\phi)(1-B\sin\phi).
\end{aligned} \tag{2.20}$$

Here M and B are the pressure-sensitivity and the dilatancy factors, respectively. When these parameters are nonzero, then $a_2 \neq b_1$ unless $M = B$.

Single Crystals and Incompressible Flow of Granular Materials. To obtain equations for the double-slip theory of single crystals [12], and to show that they closely relate to the double-slip theory of granular materials [22–25], set $M = B = 0$ in equations (2.20), and obtain

$$\overset{\nabla}{\sigma}_{11} - \overset{\nabla}{\sigma}_{22} = \frac{2G(h+h_1)}{(h+h_1) + 2G\cos^2\phi}(d_{11} - d_{22}),$$
$$\overset{\nabla}{\sigma}_{12} = \frac{2G[(h-h_1) - 2\bar{\tau}\sin\phi]}{(h-h_1) + 2G\sin^2\phi} d_{12}. \tag{2.21}$$

When $h = h_1$, the last equation becomes

$$d_{12} = -\frac{\sin\phi}{2\bar{\tau}}\overset{\nabla}{\sigma}_{12} = \frac{\cos 2\hat{\phi}}{2\bar{\tau}}\overset{\nabla}{\sigma}_{12}, \tag{2.22}$$

where $\hat{\phi} = \phi/2 + \pi/4$. The quantity

$$2\bar{\mu} = -\frac{2\bar{\tau}}{\sin\phi} = \frac{2\bar{\tau}}{\cos 2\hat{\phi}} \tag{2.23}$$

may be termed "vertex modulus." It renders the plastic strain rate tensor *noncoaxial* with the stress tensor. It has also been called the "noncoaxiality" parameter. Rudnicki and Rice [27]

Downloaded 02 May 2010 to 171.66.16.250. Redistribution subject to ASME license or copyright; see http://www.asme.org/terms/Terms_Use.cfm

and Stören and Rice [28] interpret $\bar{\mu}$ as the "secant modulus" associated with the *effective* shear stress versus *effective* shear strain curve. Then the vertex modulus always would be positive. However, as is seen from equations $(2.21)_1$ and (2.23), this parameter can be negative. For example, when $h - h_1 \leq 0$, and $\hat{\phi} > \pi/4$ (for bcc models), the vertex modulus would be negative.

Since result (2.23) was inherent in equations first developed by Mandel [22] in 1947 for the flow of granular materials, and since later it was explicitly obtained by Spencer [24], this writer proposes that $\bar{\mu}$ be called the "Mandel-Spencer noncoaxiality modulus." It has been shown by Nemat-Nasser [8, p. 859] that noncoaxiality of this kind emerges naturally in general elastoplasticity, and is associated with plastic strain-rate components which do not contribute to the rate of dissipation, i.e., they are "workless"; see also Spencer [25] and Section 3.2. However, the presence of these terms is essential, if the observed macroscopic instabilities by localized deformations are to be modeled [27-35]. Furthermore, the "noncoaxiality" is a natural consequence of the slip-based physical model of plasticity.

Equations (2.20) also demonstrate the significance of dilatancy and frictional effects. When M and B are unequal, then $a_2 \neq b_1$, and therefore, rate potentials in the sense of Hill [36] do not exist. Note that even when these parameters are zero, the quantities involving the stress σ and spin ω^α in (2.18) may render L^Ω_{ijkl} nonsymmetric with respect to the exchange of ij and kl. Furthermore, equations (2.20) show that, in general, the rate of volumetric strain is coupled with the rate of shearing.

2.3 Overall Response of Aggregates of Microelements. The characterization of the overall properties of a representative macroelement requires: (1) a suitable averaging scheme, compatible with the overall boundary data; and (2) the description of the local quantities for a typical microelement in terms of the far-field macrodata. For small deformation problems, these have been essentially resolved; see Bui [37], Bui, Zaoui, and Zarka [38], Hill [39, 40], Mandel [41], and Rice [42]. In particular, Eshelby's result [1] has been an effective tool for the calculation of the local quantities in terms of the far-field data; see Mura [43] for references.

When strains and rotations are finite, the proper choice of stress and strain measures and their rates requires care, because the macrovariables are no longer necessarily formal volume averages of the corresponding microquantities; even for small deformation, care must be exercised. Furthermore, it is not clear at the outset how the local quantities relate to the overall macrodata.

Hill [2] has shown inter alia that the fixed-axes components of the nominal stress and the deformation gradient, as well as their rates are special, since their unweighted volume averages (over the reference state) depend uniquely on surface data; the same is also true for the Kirchhoff stress. Hill [2] presents a wealth of important information, some of which has been reviewed recently by Havner [6]. Of particular interest here are the averaging properties of the nominal stress rate, $\dot{n}_{ij}$, and the velocity gradient, l_{ij}, both measured with respect to the *current* configuration, i.e.,

$$L_{ij} \equiv <l_{ij}> = \frac{1}{v}\int v_i \nu_j dS, \quad \dot{N}_{ij} \equiv > \dot{n}_{ij} > = \frac{1}{v}\int x_i \dot{t}_j dS,$$
$$\dot{n}_{ij,i} = 0 \quad \text{in} \quad V \quad \text{and} \quad \dot{n}_{ij}\nu_i = \dot{t}_j \quad \text{on} \quad S, \qquad (2.24)$$

where integration is over the current surface with ν as its exterior unit normal, and a comma followed by an index denotes partial differentiation with respect to the corresponding coordinate; in (2.24) and in the sequel, $< \cdots >$ represents the volume average. The self-consistent overall nominal stress rate and the velocity gradient hence are the average quantities $\dot{N}_{ij}$ and L_{ij} which are compatible with boundary data $\dot{t}_j = \dot{N}_{ij}\nu_i$ and $V_i = L_{ij}x_j$, respectively. Since the macroelement is intended to represent a small continuum material neighborhood, the assumption of uniform stress-rate and velocity gradient is appropriate; in (2.24), however, the boundary data need not be uniform.

From

$$\dot{n}_{ij} = \overset{\nabla}{\tau}_{ij} - d_{ik}\sigma_{kj} + w_{jk}\sigma_{ki} \qquad (2.25)$$

and equations (2.14) and (2.15), it follows that

$$\dot{n}_{ij} = \mathfrak{F}^\Omega_{ijkl} l_{kl}, \qquad (2.26)$$

$$\mathfrak{F}^\Omega_{ijkl} = L^\Omega_{ijkl} - \frac{1}{2}(\delta_{ik}\delta_{lm} + \delta_{il}\delta_{km})\sigma_{mj}$$
$$+ \frac{1}{2}(\delta_{jk}\delta_{lm} - \delta_{jl}\delta_{km})\sigma_{mi}. \qquad (2.27)$$

Then, to obtain the overall modulus $\underset{\sim}{\mathfrak{F}}$ in

$$\dot{N}_{ij} = \mathfrak{F}_{ijkl} L_{kl}, \qquad (2.28)$$

we must relate l_{kl} in (2.26) to the overall quantity L_{kl}.

To this end a basic theorem, a counterpart of Eshelby's result, but for finite deformations, is noted (Iwakuma and Nemat-Nasser [44]) as follows.

A Basic Result. Consider an unbounded finitely and uniformly deformed homogeneous elastic-plastic solid with instantaneous rate modulus $\underset{\sim}{\mathfrak{F}}^0$, as in (2.28). Let an ellipsoidal region Ω in this solid undergo a uniform transformation which in the absence of the surrounding material is characterized by the velocity gradient $v^*_{i,j}$. Then, when the operator $\mathfrak{F}^0_{ijkl}\partial^2/\partial x_i \partial x_l$ is elliptic, the resulting velocity gradient in the presence of the constraint imposed by the surrounding material is still uniform and is given by

$$v_{i,j} = -\mathfrak{B}_{ijkl} v^*_{k,l}, \qquad (2.29)$$

where the constant tensor $\underset{\sim}{\mathfrak{B}}$ corresponds to Eshelby's tensor, and can be calculated in terms of $\underset{\sim}{\mathfrak{F}}^0$ and the geometry of Ω; see Iwakuma and Nemat-Nasser [44] for details.

Now, when the overall velocity gradient L_{ij} is prescribed, one can show that the velocity gradient l_{ij}, in a single ellipsoidal region of modulus $\underset{\sim}{\mathfrak{F}}^\Omega$, different from the uniform modulus $\underset{\sim}{\mathfrak{F}}^0$ of its surrounding material, becomes

$$l_{ij} = \mathfrak{A}^\Omega_{ijkl} L_{kl}, \qquad (2.30)$$

where, after Hill [45], $\underset{\sim}{\mathfrak{A}}^\Omega$ is called the concentration tensor [44]. $\underset{\sim}{\mathfrak{A}}^\Omega$ depends on the geometry of Ω, and on moduli $\underset{\sim}{\mathfrak{F}}^0$ and $\underset{\sim}{\mathfrak{F}}^\Omega$; see Iwakuma and Nemat-Nasser [44].

Overall Moduli. When a common $\underset{\sim}{\mathfrak{B}}$, but not a common $\underset{\sim}{\mathfrak{F}}^\Omega$, is used to calculate the concentration tensor $\underset{\sim}{\mathfrak{A}}^\Omega$ for each microelement, the overall modulus tensor $\underset{\sim}{\mathfrak{F}}$ in (2.28) may be estimated by a self-consistent approach. For example, in Hill's method [45], $\underset{\sim}{\mathfrak{A}}^\Omega$ is calculated for a typical ellipsoid embedded in a uniform matrix of the overall (yet unknown) modulus, $\underset{\sim}{\mathfrak{F}}$. Then from $(2.24)_2$, (2.26), and (2.30) one obtains

$$\mathfrak{F}_{ijkl} = <\mathfrak{F}^\Omega_{ijmn}\mathfrak{A}^\Omega_{mnkl}>. \qquad (2.31)$$

Since $\underset{\sim}{\mathfrak{B}}$ is common to all microelements, it follows that $<\mathfrak{A}^\Omega_{ijkl}> = I_{ijkl}$, the identity tensor. Once the operator $\mathfrak{F}_{ijkl}\partial^2/\partial x_i \partial x_l$ ceases to be elliptic, the $\underset{\sim}{\mathfrak{B}}$-tensor can no longer be calculated on the basis of $\underset{\sim}{\mathfrak{F}}$. The overall uniform deformation of the macroelement breaks down into possible localized deformations. Shear bands may form, across which certain components of the overall velocity gradient admit discontinuities; see Hill [46], Hill and Hutchinson [29], Rice [30], and Thomas [47]. The continuity of traction rates across these bands requires that

$$[\![\dot{N}_{ij}]\!]\nu_i = 0, \qquad (2.32)$$

where $[\![\ ]\!]$ denotes the jump, and ν is a unit vector normal to

Downloaded 02 May 2010 to 171.66.16.250. Redistribution subject to ASME license or copyright; see http://www.asme.org/terms/Terms_Use.cfm

the discontinuity plane. Set $[\![L_{kl}]\!] = \eta_k \nu_l$, Hill [46], and for nonzero η (the magnitude of the jump), obtain

$$\det |\mathcal{F}_{ijkl}\nu_i\nu_l| = 0. \tag{2.33}$$

Iwakuma and Nemat-Nasser [44] show that when (2.33) yields real roots for ν, $\mathcal{B}$ cannot be obtained on the basis of $\mathcal{F}$. The self-consistent calculation of the moduli cannot be continued beyond such a state. These authors present several illustrative examples.[2]

The calculation of $\mathcal{B}$ may be based on a modulus $\mathcal{F}^0$ different from $\mathcal{F}$. For small deformation problems, the overall elastic modulus tensor has been used; see Budiansky and Wu [49], Hutchinson [50], and Kröner [51, 52]. The same may be done for finite deformations. Another possibility is to identify $\mathcal{F}^0$ with the overall moduli at a *fixed* state prior to the loss of stability. This and related schemes entail certain arbitrariness, not shared by Hill's self-consistent method; see Hutchinson [50].

Finally, with the aid of the overall nominal stress rate and velocity gradient, other variables are defined. These, in general are *not* necessarily the volume averages of the corresponding local quantities, although, obviously $\mathbf{D} \equiv <\mathbf{d}>$ and $\mathbf{W} \equiv <\mathbf{w}>$ are the overall deformation rate and spin tensors. The matter has been thoroughly discussed by Hill [2] and recently reviewed by Havner [6], so details are not given here. Note that for surface data compatible with the uniform stress and deformation of the macroelement, the stress-power is

$$<\tau_{ij}d_{ij}> \equiv <\tau_{ij}><d_{ij}>, \tag{2.34}$$

exactly.

2.4 Granular Materials. The stress and deformation tensors are continuum concepts, whereas granular materials that support the overall loads through contact friction, have distinct particulate structure. With the aid of the virtual work principle, Christoffersen, Mehrabadi, and Nemat-Nasser [53] have shown that the overall Cauchy stress, $\bar{\sigma}$, can be expressed as

$$\bar{\sigma}_{ij} = \frac{1}{N}\sum_{\alpha=1}^{N} t_{ij}^{\alpha} \equiv <t_{ij}>, \quad t_{ij}^{\alpha} = N f_i^{\alpha} l_j^{\alpha}$$

(α not summed), (2.35)

where N is the number of contacts in volume V (taken as the unit of volume), $\mathbf{f}^{\alpha}$ is the contact force at contact α, and $\mathbf{l}^{\alpha}$ is a vector that connects the centroids of two granules in contact at α; the stress is assumed to be symmetric.

To relate the stress tensor to an overall measure of the microstructure, various assumptions may be used. One reasonable approach is to introduce a "local" stress $\hat{\tau}_{ij}$ (not the Kirchhoff stress of the preceding sections), and set

$$f_i = a\hat{\tau}_{ij}n_j, \tag{2.36}$$

where, for simplicity, the superimposed α is omitted, a is an effective contact area, and $\mathbf{n}$ is the contact unit normal. Based on (2.36), some rather interesting results can be obtained for *spherical* granules (circular cylindrical, in two dimensions). We shall consider this case in the sequel. Then (2.35) and the symmetry of $\bar{\sigma}$ yield

$$\bar{\sigma}_{ij} = \frac{1}{2}<\hat{\tau}_{ik}h_{kj} + \hat{\tau}_{jk}h_{ki}>, \quad <\hat{\tau}_{ik}h_{kj}> = <\hat{\tau}_{jk}h_{ki}>,$$

$$h_{kj} \equiv \epsilon n_k n_j, \quad \epsilon \equiv Nal, \tag{2.37}$$

where $\mathbf{l} = l\mathbf{n}$. If $\hat{\tau}_{ij}$ is assumed uncorrelated with h_{ij}, then $\bar{\sigma}_{ij} = \frac{1}{2}[<\hat{\tau}_{ik}><h_{kj}> + <\hat{\tau}_{jk}><h_{ki}>]$, and if $\hat{\tau}_{ij}$ is symmetric, then $\bar{\sigma}_{ij}$, $<\hat{\tau}_{ij}>$, and $H_{ij} \equiv <h_{ij}>$ are all coaxial; this follows from (2.37). Hence,

$$\bar{\sigma}_{ij} = A_0\delta_{ij} + A_1 H_{ij} + A_2 H_{ik}H_{kj} \tag{2.38}$$

exactly, where A_0, A_1, and A_2 are functions of the basic invariants of $\bar{\sigma}$ and $\mathbf{H}$.

$H_{ij} = <\epsilon n_i n_j>$ is a measure of the microstructure or the fabric of the granular mass. The fabric itself is defined by the distribution of the contacts, contact normals, and the "branch" lengths l. Therefore, in this approach, the notion of "fabric" in granular materials replaces that of "lattice" in crystals. The change in fabric is associated with the change in stress. The "plastic" part, l_{ij}^{p}, of the velocity gradient neither affects the fabric nor introduces any stress changes. Further, the accommodating velocity gradient, l_{ij}^{*}, now is induced solely by the fabric change and is instrumental for stress variations; Nemat-Nasser and Mahrabadi [54].

To complete the theory, we consider two assumptions. First, since $\epsilon = Nal$ is an "effective" fractional number of contacts associated with the small volume al, and since l_{ij}^{p} does not affect fabric and hence ϵ, we set[3]

$$\frac{\dot{\epsilon}}{\epsilon} + d_{kk}^{*} = 0. \tag{2.39}$$

Secondly, we introduce a linear relation between $\mathbf{d}^{*}$ and the Jaumann rate of the local stress $\hat{\tau}$, corotational with the "fabric,"

$$\overset{\nabla}{\hat{\tau}}{}^{*} = \mathbf{L}^0 : \mathbf{d}^{*} \tag{2.40}$$

and obtain

$$\overset{\nabla}{\tau}{}_{ij}^{*} \equiv \overset{\nabla}{t}{}_{ij}^{*} + d_{kk}^{*}t_{ij} = \frac{1}{2}[L_{imkl}^{0}h_{mj} + L_{jmkl}^{0}h_{mi}]d_{kl}^{*}$$

$$\equiv \mathcal{L}_{ijkl}^{\Omega}d_{kl}^{*}. \tag{2.41}$$

This now identifies the modulus tensor $\mathcal{L}^{\Omega}$ in equation (2.4) for granular materials. $\mathcal{L}^{\Omega}$ here involves the fabric measure h_{ij} explicitly. Even when $\mathbf{L}^0$ in (2.41) is an isotropic tensor, the influence of fabric is taken into account through h_{ij}.

Each microelement is a small neighborhood of one *active* contact, and includes only one slip system with unit normal $\mathbf{n}$. The distribution of unit contact normals gives the distribution of the microelements. The unit normals change in the course of deformation in accordance with the kinematical assumption $(2.9)_1$. For cohesionless frictional slip, $h^{\alpha\beta}$ and η_2 in (2.10) and (2.11) vanish, and for each microelement

$$\dot{\gamma} = (\mathbf{q}:\mathcal{L}^{\Omega}:\mathbf{d})/(\mathbf{q}:\mathcal{L}^{\Omega}:\mathbf{p}); \tag{2.42}$$

with $\alpha = 1$, equation (2.7) yields the local rate-constitutive relations. The remaining results in Sections 2.1 and 2.3 apply. In particular, for the evaluation of the concentration tensor, the region Ω may be taken to be a unit sphere, which simplifies some of the calculations.

3 Phenomenological Models

Most phenomenological models of finite plasticity stem from their counterpart in the infinitesimal theory. They involve a *yield function*, f, which marks the boundary of the elastic states in the stress space, and a *potential*, g, for the plastic strain rate, $\mathbf{D}^{p}$. Both f and g depend on the current stress-state and on some measures of the past plastic flow. The *flow rule*,

$$\mathbf{D}^{p} = \lambda\frac{\partial g}{\partial \tau}, \tag{3.1}$$

is called "*associative*" when $g \equiv f$, otherwise it is

[2] Similar results are obtained for the self-consistent calculation of overall instantaneous moduli of finitely deformed elastic-plastic porous solids; see Nemat-Nasser and Iwakuma [48].

[3] Note that $\dot{\epsilon}/\epsilon = \dot{N}/N + \dot{a}/a + \dot{l}/l$, and hence is directly related to the rate of change of contact density and branch length.

Downloaded 02 May 2010 to 171.66.16.250. Redistribution subject to ASME license or copyright; see http://www.asme.org/terms/Terms_Use.cfm

"*nonassociative*"; in (3.1) λ is a scalar parameter, and τ is the macroscopic (overall continuum) Kirchhoff stress. In this section, we use τ, σ, $\mathbf{D}$, and $\mathbf{W}$, respectively, to denote the macroscopic Kirchhoff stress, Cauchy stress, deformation rate tensor, and the spin tensor. These should not be confused with the local quantities of the microscopic models of Section 2, even though the same notation may be involved.

For the continued plastic flow, the stress-state remains on the yield surface, $f=0$, and hence $\dot{f}=0$; this is called the *consistency relation*. Functions f and g need not be smooth. They may involve intersecting surfaces that produce vertices and corners.

Since some phenomenological aspects of finite plasticity have been reviewed recently by Neale [34], we emphasize in the sequel only certain limited topics pertaining to dilatant frictional materials of current interest; for a review, see Mroz [55]. For the sake of conciseness, both isotropic and kinematic hardening are examined at the same time.

Let

$$\mathbf{D}=\mathbf{D}^*+\mathbf{D}^p, \quad \mathbf{W}=\mathbf{W}^*+\mathbf{W}^p, \tag{3.2}$$

where superimposed p denotes the plastically induced, and * the accommodating elastic contribution. Only the latter gives rise to a stress change,

$$\mathring{\tau}^*=\underset{\sim}{\mathcal{L}}:\mathbf{D}^*, \quad \mathring{\tau}^*\equiv\dot{\tau}^*-\mathbf{W}^*\tau+\tau\mathbf{W}^*; \tag{3.3}$$

here $\mathring{\tau}^*$ is the Jaumann rate corotational with the *elastic* distortion[4] and $\underset{\sim}{\mathcal{L}}$ is the instantaneous elastic modulus tensor. From (3.3) it follows that (Nemat-Nasser [8])

$$\mathring{\tau}=\underset{\sim}{\mathcal{L}}:\mathbf{D}-\{\underset{\sim}{\mathcal{L}}:\mathbf{D}^p+\mathbf{W}^p\tau-\tau\mathbf{W}^p-D^p_{kk}\tau\},$$

$$\mathring{\tau}=\dot{\tau}-\mathbf{W}\tau+\tau\mathbf{W}. \tag{3.4}$$

We examine $\mathbf{D}^p$ for a special class of models of material behavior.

3.1 Dilatant Frictional Flow With Isotropic-Kinematic Hardening. Models with isotropic hardening have been proposed to describe finite plastic flows of compressible frictional materials; see Dorris and Nemat-Nasser [56], Nemat-Nasser [57], Nemat-Nasser and Shokooh [58], Rice [30], and Rudnicki and Rice [27]. These authors consider isotropic hardening in terms of the Cauchy stress. Here we generalize their results to include combined isotropic-kinematic hardening; we use the Kirchhoff stress tensor.

Consider the following yield function and flow potential:

$$f\equiv\tau-F(I,\Delta,\gamma): \quad \text{yield function}, \tag{3.5}$$

$$g\equiv\tau+G(I,\Delta,\gamma): \quad \text{flow potential}, \tag{3.6}$$

where

$$\tau^2\equiv\frac{1}{2}(\tau'-\beta):(\tau'-\beta),$$

$$\Delta=\int_0^\theta\frac{\rho_0}{\rho}D^p_{kk}d\theta, \quad \gamma=\int_0^\theta(2\mathbf{D}^{p\prime}:\mathbf{D}^{p\prime})^{1/2}d\theta; \tag{3.7}$$

here β is a deviatoric stress, defining the center of the yield surface; a prime denotes the deviatoric part; $I=\tau_{kk}$; Δ is the total *plastic* volumetric strain measured from a reference state of mass-density ρ_0, ρ being the current density; γ is the total "effective" plastic distortional strain, again measured with respect to the same reference state; and θ is a monotone load parameter which, in a continued plastic flow, may be identified with γ. In place of γ, one may use the total plastic distortional work [58].

The "size" of the yield surface is characterized by F. When $\beta\equiv\mathbf{0}$, the yield surface does not move in the stress space, but only expands: isotropic hardening. With $G\equiv-F$, the associative flow rule results.

Define the unit deviatoric tensor,

$$\mu=\frac{\sqrt{2}}{2}\frac{(\tau'-\beta)}{\tau}, \tag{3.8}$$

and from (3.1)–(3.8) obtain

$$\mathbf{D}^p=\frac{1}{H}\left\{\frac{\mu}{\sqrt{2}}+\frac{\partial G}{\partial I}\delta\right\}\left\{\dot{\tau}-\frac{\partial F}{\partial I}\dot{I}\right\}, \tag{3.9}$$

where H is the (isotropic) hardening parameter,

$$H=3\frac{\rho_0}{\rho}\frac{\partial G}{\partial I}\frac{\partial F}{\partial\Delta}+\frac{\partial F}{\partial\gamma}, \tag{3.10}$$

consisting of two parts, the distortional hardening $\partial F/\partial\gamma$, and the density hardening $3(\rho_0/\rho)(\partial G/\partial I)(\partial F/\partial\Delta)$; Nemat-Nasser and Shokooh [58]; λ in (3.1) equals $\dot{\gamma}$.

The *kinematical* quantity

$$3\frac{\partial G}{\partial I}=\frac{D^p_{kk}}{\dot{\gamma}} \tag{3.11}$$

is the dilatancy parameter; it equals the rate of plastic volumetric strain per unit rate of plastic distortion, and may be positive (expansion), negative (contraction), or zero (no volume change).

The *dynamical* quantity $-\partial F/\partial I$, on the other hand, represents the pressure sensitivity for metals, or the frictional resistance for geomaterials; it is strictly positive.

For the associative flow rule, $-\partial F/\partial I\equiv\partial G/\partial I$. The associative flow rule, therefore, does not seem to be appropriate for dilatant frictional (or pressure-sensitive) materials.

$\partial G/\partial I$ can be expressed in terms of $-\partial F/\partial I$ by equating the total rate of plastic work per unit mass, $\tau:\mathbf{D}^p/\rho_0$, to an estimate of the corresponding rate of dissipation calculated on the basis of some simple micromodeling [56–58]. Indeed, for *isotropic* hardening and since $\lambda=\dot{\gamma}$, we have, from (3.9), $\tau:\mathbf{D}^p=(\tau+I\,\partial G/\partial I)\dot{\gamma}$. Then with internal friction as the only dissipation mechanism, one may assume $\tau:\mathbf{D}^p=\alpha|I\,\partial F/\partial I|\dot{\gamma}$ (for $I<0$ only), where $\alpha>0$ is a parameter depending on the stress state, and obtain

$$-\frac{\partial G}{\partial I}=\alpha\left|\frac{\partial F}{\partial I}\right|+\frac{\tau}{I}. \tag{3.12}$$

Hence, under compression, an initial shearing is always accompanied by an initial densification. As τ increases, $\tau/I<0$ may dominate the frictional term, leading to dilatancy; see Nemat-Nasser et al. [56–58]. A similar estimate may be obtained for, say, porous metals. The rate of the plastic distortional work in the metal matrix must be estimated by some micromodeling, but the procedure remains the same.

The kinematical quantity $\partial G/\partial I$ need not be regarded as a constitutive parameter. It is a strain-rate measure similar to other strain-rate components; Nemat-Nasser [59].

In obtaining (3.9), we have used the consistency condition $\dot{f}=0$. This yields

$$\frac{d\tau}{d\gamma}-\frac{\partial F}{\partial I}\frac{dI}{d\gamma}=H(I,\Delta,\gamma), \tag{3.13}$$

where γ is the "load parameter," and H is defined by (3.10). The differential equation (3.13) defines the "effective" stress τ, in terms of the "effective" strain γ, for given loading paths. From (3.7), $\dot{\tau}=(\tau'-\beta):(\tau'-\beta)^\bullet/2\tau$.

To complete the formulation, the rate of change of β must be prescribed by means of an evolutionary equation. An objective flux of β must be expressed in terms of τ, β, Δ, γ, and $\mathbf{D}^p$. For rate-independent models, one considers the general expression

[4] We use superimposed °, instead of ∇ employed in Section 2, in order to distinguish between Jaumann rates at macrolevels and microlevels.

Downloaded 02 May 2010 to 171.66.16.250. Redistribution subject to ASME license or copyright; see http://www.asme.org/terms/Terms_Use.cfm

$$\overset{\Delta}{\boldsymbol{\beta}} = \underset{\sim}{\mathcal{C}}:\mathbf{D}^p, \quad \underset{\sim}{\mathcal{C}} = \underset{\sim}{\mathcal{C}}(\tau,\boldsymbol{\beta},\Delta,\gamma), \tag{3.14}$$

where superimposed Δ denotes an objective rate.

Since most commonly used stress fluxes equal the Jaumann rate plus terms linear in stress $\boldsymbol{\beta}$ and deformation rate $\mathbf{D}$, once the function $\underset{\sim}{\mathcal{C}}$ is given for one suitable flux, say the Jaumann rate, it can easily be rewritten in terms of other fluxes; see Appendix A. Hence the choice of a suitable flux is only a matter of convenience, and must of course reflect the *physics* of the process. Recently some authors have commented that the Jaumann rate is not suitable and that other rates must be used; see Dienes [60], Johnson and Bammann [61], and Lee, Mallett, and Wertheimer [62]. A glance at (3.14) and equation (A.21) reveals that it is not the Jaumann rate (or any other objective stress rate) that ought to be suspect when strange and unwanted results emerge from an assumed form of the modulus tensor $\underset{\sim}{\mathcal{C}}$, but rather that it is this constitutive form that may not be appropriate in conjunction with the chosen flux for the intended objectives.

Often, direct extension of infinitesimal models, though straightforward, may lead to unwanted conclusions. For example, when the Jaumann rate of, say, Cauchy stress is taken to be an isotropic and linear function of the deformation rate tensor with constant coefficients, i.e.,

$$\mathring{\boldsymbol{\sigma}} = 2\mu_0\mathbf{D} + \lambda_0 D_{kk}\boldsymbol{\delta}, \quad \mu_0 \text{ and } \lambda_0 \text{ constants}, \tag{3.15}$$

then oscillatory stresses emerge for simple shearing. Truesdell [63] suggests this as a possible plasticity model, whereas Dienes [60] seeks to remove it by using the objective stress rate $\mathbf{R}(\mathbf{R}^T\boldsymbol{\sigma}\mathbf{R})^{\bullet}\mathbf{R}^T$ in place of $\mathring{\boldsymbol{\sigma}}$; here $\mathbf{R}$ is the total rotation that takes the Lagrangian triad into the Eulerian one. It is shown in Appendix A that

$$\mathbf{R}(\mathbf{R}^T\boldsymbol{\sigma}\mathbf{R})^{\bullet}\mathbf{R}^T = \mathring{\boldsymbol{\sigma}} + \boldsymbol{\sigma}\boldsymbol{\epsilon} - \boldsymbol{\epsilon}\boldsymbol{\sigma}, \tag{3.16}$$

where $\boldsymbol{\epsilon}$ is an objective strain rate with the following components in the *Eulerian triad*:

$$\epsilon_{(ab)} = \frac{\lambda_{(b)} - \lambda_{(a)}}{\lambda_{(b)} + \lambda_{(a)}} D_{(ab)} \quad (a,b \text{ not summed}); \tag{3.17}$$

here, $\lambda_{(a)}$, $a = 1,2,3$, are the principal stretches, and $D_{(ab)}$ are the components of $\mathbf{D}$ in the *Eulerian triad*. Therefore, replacing $\mathring{\boldsymbol{\sigma}}$ in (3.15) by the right-hand side of (3.16) is equivalent to changing the constitutive assumption (3.15) to

$$\mathring{\boldsymbol{\sigma}} = 2\mu_0\mathbf{D} + \lambda_0 D_{kk}\boldsymbol{\delta} - \boldsymbol{\sigma}\boldsymbol{\epsilon} + \boldsymbol{\epsilon}\boldsymbol{\sigma}, \tag{3.18}$$

still in terms of the Jaumann rate of the Cauchy stress. As pointed out by Onat [64], the oscillatory stress can be removed, if unwanted, by modifications somewhat different from (3.18). The solution is not unique, and each assumption pertains to a *new constitutive model*. The choice must be made on the basis of physical soundness and mathematical simplicity. For kinematic hardening, this is briefly discussed in the next section.

On Micromechanics of Kinematic Hardening. Microheterogeneities associated with second-phase particles, grain boundaries, and other defects serve as strain and stress concentrators. The local (micro) strains and stresses are thus considerably different from their overall (macro) average values. The effect of these local residual stresses and strains on the plastic flow is included through the (macro) hardening parameter $\boldsymbol{\beta}$, a macroscopic "back stress." The evolutionary equation for $\boldsymbol{\beta}$ must, therefore, reflect the evolution of residual stresses and strains. $\boldsymbol{\beta} = \mathbf{0}$ corresponds to a *special* state, where the material is macroscopically plastically isotropic. *Deviations from plastic isotropy may hence be reckoned relative to this special state which presents a natural preferred reference configuration.* Note that this reference state may well be deformed and stressed. The only requirement is that it be plastically isotropic with $\boldsymbol{\beta} = \mathbf{0}$ in that state.

Let $\mathbf{F}$ measure the deformation gradient from the $\boldsymbol{\beta} = \mathbf{0}$ reference state to the current one. By polar decomposition, $\mathbf{F} = \mathbf{R}\mathbf{U}$; see Appendix A. A natural objective flux for $\boldsymbol{\beta}$ is

$$\hat{\boldsymbol{\beta}} \equiv (\mathbf{R}^T\boldsymbol{\beta}\mathbf{R})^{\bullet}. \tag{3.19}$$

It measures the rate of change of the back stress, corotational with the Lagrangian triad relative to the preferred state of zero back stress. Since

$$\overset{\Delta}{\boldsymbol{\beta}} \equiv \mathbf{R}\hat{\boldsymbol{\beta}}\mathbf{R}^T = \overset{\circ}{\boldsymbol{\beta}} + \boldsymbol{\beta}\boldsymbol{\epsilon} - \boldsymbol{\epsilon}\boldsymbol{\beta}, \tag{3.20}$$

where $\boldsymbol{\epsilon}$ is given by (3.17), a constitutive assumption for the stress flux $\overset{\Delta}{\boldsymbol{\beta}}$ also gives the corresponding relations for the Jaumann flux $\overset{\circ}{\boldsymbol{\beta}}$. However, an isotropic relation between, say, $\hat{\mathbf{D}}^{p\prime} = \mathbf{R}^T\mathbf{D}^{p\prime}\mathbf{R}$ and $\hat{\boldsymbol{\beta}}$ does not necessarily result in an isotropic relation between $\overset{\circ}{\boldsymbol{\beta}}$ and $\mathbf{D}^{p\prime}$, although linearity in rates is preserved. Since the $\boldsymbol{\beta} = \mathbf{0}$ state is plastically isotropic, a linear isotropic relation of the kind

$$\hat{\boldsymbol{\beta}} = A\hat{\mathbf{D}}^{p\prime}, \quad A = A(\gamma), \tag{3.21}$$

may well be reasonable, whereas a similar relation between $\overset{\circ}{\boldsymbol{\beta}}$ and $\mathbf{D}^{p\prime}$ is not. Assumption (3.21) leads to

$$\overset{\Delta}{\boldsymbol{\beta}} = \overset{\circ}{\boldsymbol{\beta}} + \boldsymbol{\beta}\boldsymbol{\epsilon} - \boldsymbol{\epsilon}\boldsymbol{\beta} = A\mathbf{D}^{p\prime}. \tag{3.22}$$

Since the Lagrangian triad marks the direction of extreme stretches, the stress flux $\hat{\boldsymbol{\beta}}$ is corotational with such material elements. Hence relations (3.21) and (3.22) are equivalent to the relations proposed by Johnson and Bammann [61] if the reference state is the unstrained one. These authors, however, regard the Jaumann rate to be inappropriate. The relation (3.22), as well as the general linear correspondence between essentially all commonly used stress fluxes (equation (A.21) Appendix A), does not seem to support such a viewpoint.

As in the infinitesimal theory, other assumptions may be used to describe the evolution of the back stress. For example, Tvergaard [65] uses an extension of Ziegler's rule [66] and suggests

$$\overset{\circ}{\boldsymbol{\beta}} = (\boldsymbol{\tau}'\boldsymbol{\beta})\dot{\mu}, \tag{3.23}$$

where $\dot{\mu}$ is a rate parameter. In constitutive assumptions of this kind, care must be exercised to avoid unwanted results. Physically, it might be more appropriate to use $\overset{\Delta}{\boldsymbol{\beta}}$ in place of the Jaumann rate, $\overset{\circ}{\boldsymbol{\beta}}$ in (3.23), although this will introduce complications in the actual calculations, and, in fact, is a different constitutive assumption.

3.2 Plastic Anisotropy, Stress Triaxiality, and the Elastic Moduli.

Plastic Anisotropy. When the dependence of g on stress is through the stress invariants only, the plastic strain rate tensor, $\mathbf{D}^p$, is coaxial with the stress tensor. Kinematic hardening alters this, but $\mathbf{D}^p$ remains normal to the *flow potential surface* (not necessarily coincident with the yield surface).

The micromechanics of plasticity invariably leads to potential surfaces with vertices, in addition to kinematic hardening and the associated Bauschinger effect; Section 2.

The vertex effect may be included by the introduction of the "Mandel-Spencer noncoaxiality modulus," in the manner described by Rudnicki and Rice [27] and Stören and Rice [28]. However, this modulus need not be positive nor stand for a secant-type modulus; Nemat-Nasser [59], and Section 2.2. An interesting interpretation of this modulus emerges from an energy consideration, as follows.

The rate of stress-work, $\boldsymbol{\tau}:\mathbf{D}$, in general, consists of an elastic (reversible) part, $\boldsymbol{\tau}:\mathbf{D}^*$, and a plastic (dissipating) part, $\boldsymbol{\tau}:\mathbf{D}^p$. In an isothermal process, $\boldsymbol{\tau}:\mathbf{D} = \boldsymbol{\tau}:\mathbf{D}^* + \boldsymbol{\tau}:\mathbf{D}^p$ or $\boldsymbol{\tau}:(\mathbf{D} - \mathbf{D}^* - \mathbf{D}^p) = 0$. This must hold for any admissable stress state, so that

$$\mathbf{D} = \mathbf{D}^* + \mathbf{D}^p + \boldsymbol{\Lambda}, \quad \boldsymbol{\tau}:\boldsymbol{\Lambda} = 0. \tag{3.24}$$

Downloaded 02 May 2010 to 171.66.16.250. Redistribution subject to ASME license or copyright; see http://www.asme.org/terms/Terms_Use.cfm

The unknown strain rate $\mathbf{\Lambda}$ is "workless." One solution for (3.24) is, Nemat-Nasser [8],

$$\mathbf{\Lambda} = A\left[\frac{\boldsymbol{\tau}'}{\bar{\tau}}\right]^{\circ}, \quad \bar{\tau} = (\tfrac{1}{2}\boldsymbol{\tau}':\boldsymbol{\tau}')^{1/2}, \tag{3.25}$$

where A is inversely proportional to the Mandel-Spencer noncoaxiality modulus, $\bar{\mu}$, and $^{\circ}$ is the Jaumann rate. This solution, like the J_2 flow potential, does not reflect the stress triaxiality. It is essentially a two-dimensional solution. One may seek a general solution for $\boldsymbol{\tau}:\mathbf{\Lambda} = 0$ for triaxial stress states, but this is rather complicated and will not be pursued here.

Stress Triaxiality. For geomaterials, as well as porous metals, the stress triaxiality becomes rather important. The influence of the intermediate principal stress on the mechanical response of granular materials and rocks has been well established experimentally; see Mogi [67] and Nemat-Nasser [57] who gives additional references. The yield function, f, and the plastic potential, g, may be modified to include the third stress invariant. For example, Dorris and Nemat-Nasser [56] use $f \equiv (1+c(\eta))\tau - F$ and $g \equiv (1+c(\eta))\tau + G$, where $\eta = J_3/J_2^{2/3}$ with J_2 and J_3 denoting the second and third invariants of the deviatoric, say, Kirchhoff stress. Other alternatives have been given in the literature, e.g., Drucker [68]. To maintain simplicity, the choice must be made with some care.

The Elastic Moduli. Strictly speaking, the elastic modulus tensor, $\underset{\sim}{\mathcal{L}}$ in (3.3), must be derived from an elastic potential, Section 4. In practice, however, $\underset{\sim}{\mathcal{L}}$ is often identified with the modulus in linear elasticity. This may be justified on the grounds that the elasticity moduli for metals are several orders of magnitude larger than the yield stress, and therefore, the stress related terms are negligibly small. The argument, however, may not apply to geomaterials, and therefore, care must be exercised to avoid possible pitfalls in relation to oscillatory stresses that may emerge, although in (3.3) only the elastic spins enter into the definition of the Jaumann rate of stress.

4 On the Basic Structure of Finite Deformation Inelastic Constitutive Relations

The essential features of rate-independent and rate-dependent elastic-inelastic constitutive relations have been fairly well understood for infinitesimal deformation regimes; see Bui [37], Hill [40], Mandel [41], Martin [69], and Rice [42]. In particular, conditions for the existence of convex flow potentials (which coincide with the yield surface; rate-independent), extremum principles, and uniqueness have been identified. While some of these results do carry over into finite deformation regimes, albeit with reinterpretation, many do not.

4.1 Internal Variables and Thermodynamics. The characterization of inelasticity in terms of internal state variables has been pioneered by Biot [70] and Meixner [71] for small deformations (see also Kestin and Bataille [72]) and has been extended to finite deformations by Coleman and Gurtin [73], Lubliner [74], Mandel [75], Nemat-Nasser [76], Onat [77], Rice [78], Schapery [79], and Valanis [80]. In this approach the thermodynamic state is defined by a material strain measure, $\mathbf{E}$, the temperature θ, *and* a set of variables collectively denoted by the quantity $\boldsymbol{\xi}$ which defines the microstructure. When $\boldsymbol{\xi}$ is held fixed, the subsequent material response will be purely elastic, as no microstructural changes take place. The variables $\mathbf{E}$ and θ are observable and hence controllable. The history measure $\boldsymbol{\xi}$, on the other hand, is not macroscopically observable, and changes in the course of deformation in response to, and as a consequence of the changes in the observable macroscopic state variables, Nemat-Nasser [76].

Some writers have viewed $\boldsymbol{\xi}$ as a set of variables, say ξ_i, $i = 1, 2, \ldots, N$, which in a certain *average* sense reflect the essential features of the microstructural changes; Nemat-Nasser [76], Schapery [79], and Valanis [80]. Others have associated $\boldsymbol{\xi}$ with specific structural changes occurring at specific sites within the sample; Rice [9, 78]. In this last interpretation, the state functions need not necessarily be differentiable with respect to the history variables, whereas in the former approach differentiability of any needed order is assumed, which consequently may exclude certain inelastic effects. The distinction between the two views, therefore, is not only a formal one, but rather it is substantial. In the present brief account, we regard, in most parts, all state functions as suitably smooth and differentiable with respect to *all* state variables (e.g., $\mathbf{E}$, θ, and $\boldsymbol{\xi}$), and refer the reader to Hill [5], Hill and Rice [81], and Rice [9] for detailed examination of the other viewpoint; see, however, comments under *Normality*. In the sequel, $\boldsymbol{\xi}$ represents N scalars ξ_i which may stand for suitable tensorial quantities.

Potentials. At constant $\boldsymbol{\xi}$, the response is elastic. Let $\phi = \phi(\mathbf{E}, \theta; \boldsymbol{\xi})$ be the Helmholtz free energy, and obtain

$$\mathbf{S} = \frac{\partial \phi}{\partial \mathbf{E}}, \quad \eta = -\frac{\partial \phi}{\partial \theta} \quad \text{at} \quad \boldsymbol{\xi} = \text{constant}, \tag{4.1}$$

where $\mathbf{S}$ is the stress conjugate to the strain measure $\mathbf{E}$, and η is the entropy measured per unit reference volume. The total change in ϕ is

$$\begin{aligned} d\phi &= d^e\phi + d^{in}\phi \\ &\equiv \{\mathbf{S}:d\mathbf{E} - \eta d\theta\} - \mathbf{\Lambda}\cdot d\boldsymbol{\xi}, \quad d^{in}\phi \equiv -\mathbf{\Lambda}\cdot d\boldsymbol{\xi}. \end{aligned} \tag{4.2}$$

The elasticity induced change, $d^e\phi$, is at constant $\boldsymbol{\xi}$, whereas the inelastic change, $d^{in}\phi$, is at constant $\mathbf{E}$ and θ; the notation borrows from Hill and Rice [81]. With ϕ a smooth and differentiable function of *all* its arguments, we have

$$\mathbf{\Lambda} \equiv -\frac{\partial \phi}{\partial \boldsymbol{\xi}} = \mathbf{\Lambda}(\mathbf{E}, \theta; \boldsymbol{\xi}). \tag{4.3}$$

Similarly, (4.1) shows that $\mathbf{S} = \mathbf{S}(\mathbf{E}, \theta; \boldsymbol{\xi})$ and $\eta = \eta(\mathbf{E}, \theta; \boldsymbol{\xi})$.

Let t be a suitable time parameter, and denote by superimposed dot the time rate, e.g., $\dot{\phi} \equiv d\phi/dt$. Then

$$\dot{\mathbf{S}} = \dot{\mathbf{S}}^e + \dot{\mathbf{S}}^{in} = \left\{\underset{\sim}{\mathcal{L}}:\dot{\mathbf{E}} + \frac{\partial \mathbf{S}}{\partial \theta}\dot{\theta}\right\} + \frac{\partial \mathbf{S}}{\partial \xi_i}\dot{\xi}_i \quad (i \text{ summed}), \tag{4.4}$$

where

$$\underset{\sim}{\mathcal{L}} \equiv \frac{\partial^2 \phi}{\partial \mathbf{E} \partial \mathbf{E}} \tag{4.5}$$

is the elastic modulus tensor, measured relative to the reference state for the strain measure $\mathbf{E}$; $\underset{\sim}{\mathcal{L}}$ varies with the strain measure and the ground state; Hill [82].

As observed by Hill and Rice [81], $\dot{\phi}^{in} \equiv d^{in}\phi/dt = (\partial\phi/\partial\xi_i)\,\dot{\xi}_i$, when regarded as a function of $\mathbf{E}$, $\boldsymbol{\xi}$, *and* $\dot{\boldsymbol{\xi}}$, serves as a potential for the inelastic stress rate,

$$\dot{\mathbf{S}}^{in} = \frac{\partial^2 \phi}{\partial \xi_i \partial \mathbf{E}}\dot{\xi}_i = \frac{\partial}{\partial \mathbf{E}}\dot{\phi}^{in}. \tag{4.6}$$

In a similar manner,

$$\dot{\eta} = \dot{\eta}^e + \dot{\eta}^{in}, \quad \dot{\eta}^{in} = -\frac{\partial}{\partial \theta}\dot{\eta}^{in}. \tag{4.7}$$

By a Legendre transformation, the roles of $\mathbf{E}$ and $\mathbf{S}$ can be reversed,

$$\psi = \mathbf{S}:\mathbf{E} - \phi \equiv \psi(\mathbf{S}, \theta; \boldsymbol{\xi}),$$

$$\mathbf{E} = \frac{\partial \psi}{\partial \mathbf{S}}, \quad \eta = \frac{\partial \psi}{\partial \theta}, \quad \mathbf{\Lambda} = \frac{\partial \psi}{\partial \boldsymbol{\xi}}. \tag{4.8}$$

Then, again,

Downloaded 02 May 2010 to 171.66.16.250. Redistribution subject to ASME license or copyright; see http://www.asme.org/terms/Terms_Use.cfm

$$\dot{\mathbf{E}} = \dot{\mathbf{E}}^e + \dot{\mathbf{E}}^{in} = \left\{ \mathfrak{M} : \dot{\mathbf{S}} + \frac{\partial \mathbf{E}}{\partial \theta} \dot{\theta} \right\} + \frac{\partial \mathbf{E}}{\partial \xi_i} \dot{\xi}_i \quad (i \text{ summed}), \tag{4.9}$$

where

$$\mathfrak{M} \equiv \frac{\partial^2 \psi}{\partial \mathbf{S} \partial \mathbf{S}} \tag{4.10}$$

is the elastic compliance tensor, the inverse of $\mathfrak{L}$ in (4.5), and

$$\dot{\mathbf{E}}^{in} = \frac{\partial^2 \psi}{\partial \xi_i \partial \mathbf{S}} \dot{\xi}_i = \frac{\partial}{\partial \mathbf{S}} \dot{\psi}^{in}. \tag{4.11}$$

Observe, from (4.8), that

$$\dot{\psi}^{in} + \dot{\phi}^{in} = 0. \tag{4.12}$$

Potential for Fluxes. Suppose for a class of materials, the "fluxes" $\dot{\xi}_i$ depend only on the "forces" Λ_i, i.e.

$$\dot{\boldsymbol{\xi}} = \mathbf{H}(\Lambda_1, \Lambda_2, \ldots, \Lambda_N) \equiv \mathbf{H}(\boldsymbol{\Lambda}), \tag{4.13}$$

and not explicitly on $\mathbf{E}$ and θ; note the *implicit* dependence.[5] The question is under what conditions would there exist an *integrating factor* $\lambda = \lambda(\boldsymbol{\Lambda})$ (assumed to be positive with no loss in generality) such that

$$\dot{\boldsymbol{\xi}} = \mathbf{H} = \lambda \frac{\partial \Omega}{\partial \boldsymbol{\Lambda}}, \tag{4.14}$$

where $\Omega = \Omega(\boldsymbol{\Lambda})$ is a potential for $\dot{\boldsymbol{\xi}}$'s.

It is clear that if each $\dot{\xi}_i = H_i$ depends only on its own force Λ_i, and on no other forces, then with $\lambda = 1$, $\mathbf{H} \cdot d\boldsymbol{\Lambda} = H_1(\Lambda_1) d\Lambda_1 + H_2(\Lambda_2) d\Lambda_2 + \cdots + H_N(\Lambda_N) d\Lambda_N$ is a perfect differential. This has a number of physical implications. It is the classical hypothesis of the separation of individual processes discussed by W. Thomson in 1882, and restated and used by Li [83] and by Rice [9, 78].

When $\mathbf{H}$'s are *smooth enough* functions of the $\boldsymbol{\Lambda}$'s, and there are only *two* fluxes, $\dot{\xi}_1$ and $\dot{\xi}_2$, with two corresponding forces, Λ_1 and Λ_2, then one can *always* obtain an integrating factor which renders $H_1(\Lambda_1, \Lambda_2) d\Lambda_1 + H_2(\Lambda_1, \Lambda_2) d\Lambda_2$ a perfect differential.

There is a fundamental difference between the *elastically* and *inelastically* induced changes, reckoned in the framework of assumption (4.13). Whereas $\dot{\mathbf{S}}^e$, for example, is linear in the rates $\dot{\mathbf{E}}$ and $\dot{\theta}$, equation (4.4), assumption (4.13) renders $\dot{\mathbf{S}}^{in} = (\partial \mathbf{S} / \partial \xi_i) H_i$ *a function of the state variables* $\mathbf{E}$, θ, and $\boldsymbol{\xi}$, *but not of their rates*. Indeed, since the forces, $\boldsymbol{\Lambda}$, are assumed to depend on the state variables and not on their rates, it follows from (4.13) that

$$\dot{\boldsymbol{\xi}} = \mathbf{H}(\boldsymbol{\Lambda}) \equiv \bar{\mathbf{H}}(\mathbf{E}, \theta, \boldsymbol{\xi}). \tag{4.15}$$

Thus at each point in the state space, the fluxes, $\dot{\boldsymbol{\xi}}$, and all the inelastic rates, e.g., $\dot{\phi}^{in}$, $\dot{\mathbf{S}}^{in}$, and $\dot{\eta}^{in}$, are completely defined, whereas $\dot{\mathbf{E}}$ and $\dot{\theta}$, and hence the elastic changes $\dot{\phi}^e$, $\dot{\mathbf{S}}^e$, and $\dot{\eta}^e$ may be assigned arbitrarily.

One restriction, dictated by the second law [76], is the requirement of non-negative rate of dissipation,

$$\boldsymbol{\Lambda} \cdot \dot{\boldsymbol{\xi}} = \boldsymbol{\Lambda} \cdot \mathbf{H}(\boldsymbol{\Lambda}) \geq 0. \tag{4.16}$$

Thermodynamics places no other restriction on functions $\mathbf{H}(\boldsymbol{\Lambda})$. In general, therefore, there exists no a priori reason for the existence of the potential Ω, as in (4.14). Equation (4.14) is an additional constitutive assumption that delimits the class of considered materials.

In certain cases, and subject to some assumptions, Nemat-Nasser [76], one may use Carathéodory's theorem, Buchdahl [84], or other assumptions [85], to show that the Pfaffian, $\mathbf{H}(\boldsymbol{\Lambda}) \cdot d\boldsymbol{\Lambda}$, has an integrating factor $\lambda(\boldsymbol{\Lambda})$, in the $\boldsymbol{\Lambda}$-space, so that (4.14) applies.

[5] In many applications, the fluxes may well be *explicitly* dependent on the temperature, θ. In cases of this kind, all results presented here remain valid at a *fixed temperature*, except, of course, equation (4.18).

Normality. When the fluxes are given by (4.13), and (4.14) is valid, then the inelastic rates are derivable from a potential. Indeed, since λ and Ω are not explicit functions of $\mathbf{E}$ and θ, one obtains (Mandel [86], Nemat-Nasser [76, 85], and Rice [9, 78])

$$\dot{\mathbf{S}}^{in} = \frac{\partial}{\partial \mathbf{E}} \dot{\phi}^{in} = \frac{\partial}{\mathbf{E}} \left\{ \frac{\partial \phi}{\partial \xi_i} \lambda \frac{\partial \Omega}{\partial \Lambda_i} \right\} = -\lambda \frac{\partial \Lambda_i}{\partial \mathbf{E}} \frac{\partial \Omega}{\partial \Lambda_i} = -\lambda \frac{\partial \bar{\Omega}}{\partial \mathbf{E}}, \tag{4.17}$$

where $\Omega = \Omega(\boldsymbol{\Lambda}(\mathbf{E}, \theta; \boldsymbol{\xi})) \equiv \bar{\Omega}(\mathbf{E}, \theta; \boldsymbol{\xi})$. In a similar way,[5]

$$\dot{\eta}^{in} = \lambda \frac{\partial \bar{\Omega}}{\partial \theta}. \tag{4.18}$$

Also, from (4.11), one obtains

$$\dot{\mathbf{E}}^{in} = \lambda \frac{\partial \hat{\Omega}}{\partial \mathbf{S}}, \tag{4.19}$$

where $\Omega(\boldsymbol{\Lambda}) = \hat{\Omega}(\mathbf{S}, \theta; \boldsymbol{\xi})$ with $\boldsymbol{\Lambda}$ defined by $(4.8)_3$.

It is therefore seen that equation (4.14), with λ and Ω depending explicitly on the forces $\boldsymbol{\Lambda}$ only, immediately translates into the existence of the flow potential and normality for all inelastic rates,[5] i.e., (4.17), (4.18), and (4.19). Hill [2, 5] and Hill and Rice [81] prove that: (1) if such normality applies for any pair of conjugate stress and strain measures, reckoned with respect to a chosen reference state, then it necessarily applies for every pair of conjugate stress and strain measures, reckoned with reference to any ground state; and (2) when normality holds at the local level in a composite of microelements, then it carries over to the overall macroelement. Rice [9] gives many examples for rate-independent and rate-dependent inelastic deformations of crystalline solids, where normality applies. He identifies specific microstructures that give rise to inelasticity, and constructs the associated inelastic strain increment, as well as the corresponding flow potential (which coincides with the yield function), for cases when each local flux depends only on its own conjugate force. The internal variables are not interpreted as average quantities, but rather they are viewed as specific sources of defects. The inelastic changes are defined in a general sense where differentiability with respect to the measures of the structural changes need not exist. For example, $d^{in}\phi \equiv \phi(\mathbf{S}, \theta; \boldsymbol{\xi} + d\boldsymbol{\xi}) - \phi(\mathbf{S}, \theta; \boldsymbol{\xi})$ is the change in the *elastic* potential ϕ associated with a change in the microstructure from that measured by $\boldsymbol{\xi}$ to that measured by $\boldsymbol{\xi} + d\boldsymbol{\xi}$; Hill and Rice [81] use the notation $\mathbf{H}$ (in place of $\boldsymbol{\xi}$) to emphasize the history dependence of the microstructure.

A Minimum Principle. When the strain, $\mathbf{E}$, and temperature, θ, are fixed at their current values, the internal forces gradually relax (rate-dependent regimes) to their equilibrium values. Since $d\Omega$ is a perfect differential, equation (4.14),

$$\Omega(\boldsymbol{\Lambda}) = \int_0^{\boldsymbol{\Lambda}} \frac{\mathbf{H}(\mathbf{x})}{\lambda(\mathbf{x})} d\mathbf{x} \tag{4.20}$$

is independent of the integration path. Choose the radial path, $\mathbf{x} = \boldsymbol{\Lambda}\tau$ with $0 \leq \tau \leq 1$, and from the dissipation inequality (4.16) conclude that Ω attains its minimum at the equilibrium values of $\boldsymbol{\Lambda}$. When fluxes are linearly dependent on the forces, and Onsager's relations hold, Ω becomes proportional to the rate of entropy production. In a nonlinear flux-force relation, however, it is the inelastic potential Ω, and not the rate of entropy production, which attains an extreme value at the equilibrium state; see Edelen [87], Li [83], and Nemat-Nasser [76, 85] and references cited by them.

4.2 Postulates Leading to Normality. There are two postulates, one due to Il'yushin [88], the other due to Drucker

Downloaded 02 May 2010 to 171.66.16.250. Redistribution subject to ASME license or copyright; see http://www.asme.org/terms/Terms_Use.cfm

[89, 90], originally stated for infinitesimal deformation elastoplasticity, which lead to the normality of the plastic strain rate to the flow potential (which coincides with the yield function) at locally smooth parts, and which lead to confine this strain rate within or on the cone of limiting outward normals at vertices.

Il'yushin postulates that in an isothermal cycle of strain the net stress work must be non-negative. Being in terms of work, the statement is invariant with respect to the change in the strain measure and the reference state; at finite strains, Hill [3] has shown that the postulate leads to normality when applied to restricted infinitesimal cycles. Hill and Rice [81] extend this to include finite restricted cycles which contain only infinitesimal additional plastic straining. In this context, the postulate ensures normality, but not necessarily convexity of the yield surface, although lack of vertex convexity is excluded.

When applied to a purely elastic cycle, Il'yushin's postulate leads to the existence of an elastic potential, Hill [3]. Indeed, since for an elastic material the stress is uniquely defined by the current strain, for the stress $\mathbf{S}$ conjugate to the strain $\mathbf{E}$,

$$\oint \mathbf{S}:d\mathbf{E} \geq 0$$

shows that the equality must hold for an elastic cycle, and therefore

$$\mathbf{S}:d\mathbf{E} = d\phi, \quad \mathbf{S} = \frac{\partial \phi}{\partial \mathbf{E}},$$

ϕ being the elastic potential.

Drucker postulates that the net work in applying and removing an incremental load on a given prestressed solid should be non-negative. When applied to finite deformations, the postulate is not measure invariant, since it involves the stress rate in a cycle of stress. This fact has been thoroughly discussed by Hill [3], and restated by others. Indeed, if we confine our attention to infinitesimal loading and unloading from the current elastoplastic state, choose conjugate stress and strain, $\mathbf{S}$ and $\mathbf{E}$, and take the current configuration as the reference, then, to the first order, we have for a rate of loading and unloading,

$$\dot{\mathbf{S}}:\dot{\mathbf{E}} - \dot{\mathbf{S}}:\dot{\mathbf{E}}^e = \dot{\mathbf{S}}:\dot{\mathbf{E}}^p, \tag{4.21}$$

where superimposed e and p denote the elastic and plastic contributions and where it is assumed that the elastic properties are not changed noticeably for infinitesimal loading and unloading. The postulate requires that $\dot{\mathbf{S}}:\dot{\mathbf{E}}^p \geq 0$. Now, with the current state as the reference, all strain rates coincide with the deformation rate tensor, and with the stress flux $\mathring{\mathbf{S}}$ given by equation $(A.21)$ of Appendix A, (4.21) becomes

$$\dot{\mathbf{S}}:\dot{\mathbf{E}}^p = \left\{\mathring{\boldsymbol{\tau}} - \frac{1}{2}[f''(1)+1][\boldsymbol{\sigma}\mathbf{D} + \mathbf{D}\boldsymbol{\sigma}]\right\}:\mathbf{D}^p. \tag{4.22}$$

This clearly depends on the chosen stress flux, i.e., the chosen strain measure. For the logarithmic strain measure, for example, $f''(1) = -1$, and hence, the right-hand side of (4.22) reduces to $\mathring{\boldsymbol{\tau}}:\mathbf{D}^p$. In this connection, Hill observes that if the postulate of non-negative $\dot{\mathbf{S}}:\mathbf{E}^p$ should apply, then it ought to be in conjunction with the logarithmic strain.

4.3 Normality Associative Flow Rule and Coaxiality. In Section 4.1 it is pointed out that flow potentials may exist for a broad class of materials. In Section 3, furthermore, an example of a phenomenological flow potential is given for frictional dilatant materials. Therefore, the presence of friction or pressure sensitivity does not necessarily exclude the existence of a flow potential, although it precludes the coincidence of the flow potential with the yield surface. Indeed, if we consider a typical microelement of Section 2.1, and calculate the rate of dissipation from equations (2.2), (2.3), and (2.11), we obtain even for the special case of $\nu_2 = \nu_3 = \eta_2 = 0$,

$$\boldsymbol{\tau}:\mathbf{d}^p = \boldsymbol{\tau}:\mathbf{p}^\alpha\dot{\gamma}^\alpha = \tau_Y^\alpha\dot{\gamma}^\alpha + (\tan\nu_1 - \tan\eta_1)\sigma^\alpha\dot{\gamma}^\alpha \quad (\alpha \text{ summed}).$$

If $\nu_1 = \eta_1$, then, using an argument similar to that of Bishop and Hill [91] for incompressible, pressure-insensitive metals, one shows normality of $\mathbf{d}^p$ to the yield surface at, e.g., smooth points. This, however, requires that the dilatancy parameter (which may well be negative) equal the friction coefficient (which must be positive). In general, therefore, if a plastic potential should exist for materials of this kind, it would be distinct from the yield surface.

Even when the yield surface and the flow potential coincide, the plastic strain rate tensor need not be coaxial with the stress tensor. This occurs in a natural way at vertices and corners. However, when a smooth yield function is used, the non-coaxiality must be introduced by means of other measures. Two distinct and not necessarily mutually exclusive measures have been discussed in Section 3: (1) kinematic hardening; and (2) the introduction of the Mandel-Spencer noncoaxiality modulus.

There are many problems associated with the departure from the classical normality and the associated flow rules, which have not even been touched on in the literature. Such deviations are the natural consequences of friction and various micro-mechanical effects. Many observed phenomena, e.g. localized deformations, have been explained on the basis of rate-independent theories that deviate from normality and coaxiality. However, essentially no research has been done to explore other consequences of this departure.

Acknowledgment

This work has been supported by the Army Research Office under contract DAAG29-82-K-0147 to Northwestern University.

References

1 Eshelby, J. D., "The Determination of the Elastic Field of an Ellipsoidal Inclusion, and Related Problems," *Proc. Roy. Soc.*, London, Vol. *A*241, 1957, pp. 376–396.

2 Hill, R., "On Constitutive Macro-Variables for Heterogeneous Solids at Finite Strain," *Proc. Roy. Soc.*, London, Vol. *A*326, 1972, pp. 131–147.

3 Hill, R., "On Constitutive Inequalities for Simple Materials. I," *J. Mech. Phys. Solids*, Vol. 16, 1968, pp. 229–242; "II," *J. Mech. Phys. Solids*, Vol. 16, 1968, pp. 315–322.

4 Hill, R., "Constitutive Inequalities for Isotropic Elastic Solids Under Finite Strain," *Proc. Roy. Soc.*, London, Vol. *A*314, 1970, pp. 457–472.

5 Hill, R., "Aspects of Invariance in Solid Mechanics," in *Advances in Applied Mechanics*, Vol. 18, Yih, C.-S., ed., Academic Press, New York, 1978, pp. 1–75.

6 Havner, K. S., "The Theory of Finite Plastic Deformation of Crystalline Solids," in *Mechanics of Solids: The Rodney Hill 60th Anniversary Volume*, Hopkins, H. G., and Sewell, M. J., eds., Pergamon Press, Oxford, 1982, pp. 265–302.

7 Nemat-Nasser, S., "Continuum Bases for Consistent Numerical Formulations of Finite Strains in Elastic and Inelastic Structures," in *Finite Element Analysis of Transient Nonlinear Structural Behavior*, Belytschko, T., Osias, J. R., and Marcal, P. V., eds., AMD-Vol. 14, ASME, New York, 1975, pp. 85–98.

8 Nemat-Nasser, S., "On Finite Deformation Elasto-Plasticity," *Int. J. Solids Structures*, Vol. 18, No. 10, 1982, pp. 857–872.

9 Rice, J. R., "Continuum Mechanics and Thermodynamics of Plasticity in Relation to Microscale Deformation Mechanisms," in *Constitutive Equations in Plasticity*, Argon, A. S., ed., M.I.T. Press, Cambridge, Mass., 1975, Chapter 2, pp. 23–79.

10 Asaro, R. J., and Rice, J. R., "Strain Localization in Ductile Single Crystals," *J. Mech. Phys. Solids*, Vol. 25, 1977, pp. 309–338.

11 Hill, R., "Generalized Constitutive Relations for Incremental Deformation of Metal Crystals by Multislip," *J. Mech. Phys. Solids*, Vol. 14, 1966, pp. 95–102.

Downloaded 02 May 2010 to 171.66.16.250. Redistribution subject to ASME license or copyright; see http://www.asme.org/terms/Terms_Use.cfm

12 Asaro, R. J., "Geometrical Effects in the Inhomogeneous Deformation of Ductile Single Crystals," *Acta Met.*, Vol. 27, 1979, pp. 445–453.

13 Nemat-Nasser, S., Mehrabadi, M. M., and Iwakuma, T., "On Certain Macroscopic and Microscopic Aspects of Plastic Flow of Ductile Materials," in *Three-Dimensional Constitutive Relations and Ductile Fracture*, Proc. IUTAM Symp., Dourdan, France, June 2–5, 1980, Nemat-Nasser, S., ed., North-Holland, 1981, pp. 157–172.

14 Havner, K. S., "Minimum Plastic Work Selects the Highest Symmetry Deformation in Axially-loaded f.c.c. Crystals," *Mechanics of Materials*, Vol. 1, No. 2, 1982, pp. 97–111.

15 Hill, R., and Havner, K. S., "Perspectives in the Mechanics of Elastoplastic Crystals," *J. Mech. Phys. Solids*, Vol. 30, 1982, pp. 5–22.

16 Hill, R., and Rice, J. R., "Constitutive Analysis of Elastic-Plastic Crystals at Arbitrary Strain," *J. Mech. Phys. Solids*, Vol. 20, 1972, pp. 401–413.

17 Taylor, G. I., and Elam, C. F., "The Distortion of an Aluminium Crystal During a Tensile Test," *Proc. Roy. Soc.*, London, Vol. *A*102, 1923, pp. 643–667; "The Distortion of Iron Crystals," *Proc. Roy. Soc.*, London, Vol. *A*112, 1926, pp. 337–361.

18 Havner, K. S., and Shalaby, A. H., "A Simple Mathematical Theory of Finite Distortional Latent Hardening in Single Crystals," *Proc. Roy. Soc.*, London, Vol. *A*358, 1977, pp. 47–70.

19 Kocks, U. F., "The Relation Between Polycrystal Deformation and Single-Crystal Deformation," *Metallurgical Transactions*, Vol. 1, 1970, pp. 1121–1143.

20 Mandel, J., "Généralisation de la Théorie de Plasticité de W. T. Koiter," *Int. J. Solids Structures*, Vol. 1, 1965, pp. 273–295.

21 Zarka, J., "Étude du Comportement des Monocristaux Métalliques. Application à la Traction du Monocristal C.F.C.," *J. de Mécanique*, Vol. 12, 1973, pp. 275–318.

22 Mandel, J., "Sur les Lignes de Glissement et le Calcul des Déplacements dans la Déformation Plastique," *Comptes Rendus de l'Académie des Sciences*, Vol. 225, 1947, pp. 1272–1273.

23 de Josselin de Jong, G., *Statics and Kinematics in the Failable Zone of a Granular Material*, Delft, Uitgeverij, 1959.

24 Spencer, A. J. M., "A Theory of the Kinematics of Ideal Soils Under Plane Strain Conditions," *J. Mech. Phys. Solids*, Vol. 12, 1964, pp. 337–351.

25 Spencer, A. J. M., "Deformation of Ideal Granular Materials," in *Mechanics of Solids, The Rodney Hill 60th Anniversary Volume*, Hopkins, H. G., and Sewell, M. J., eds., Pergamon Press, Oxford, 1982, pp. 607–652.

26 Mehrabadi, M. M., and Cowin, S. C., "Initial Planar Deformation of Dilatant Granular Materials," *J. Mech. Phys. Solids*, Vol. 26, 1978, pp. 269–284.

27 Rudnicki, J. W., and Rice, J. R., "Conditions for the Localization of Deformation in Pressure-sensitive Dilatant Materials," *J. Mech. Phys. Solids*, Vol. 23, 1975, pp. 371–394.

28 Stören, S., and Rice, J. R., "Localized Necking in Thin Sheets," *J. Mech. Phys. Solids*, Vol. 23, 1975, pp. 421–441.

29 Hill, R., and Hutchinson, J. W., "Bifurcation Phenomena in the Plane Tension Test," *J. Mech. Phys. Solids*, Vol. 23, 1975, pp. 239–264.

30 Rice, J. R., "The Localization of Plastic Deformation," in *Proc. of the 14th International Congr. of Theoretical and Appl. Mech.*, Vol. 1, 1976, pp. 207–220.

31 Needleman, A., and Tvergaard, V., "Necking of Biaxially Stretched Elastic Plastic Circular Plates," *J. Mech. Phys. Solids*, Vol. 25, 1977, pp. 159–183.

32 Needleman, A., and Rice, J. R., "Limits to Ductility Set by Plastic Flow Localization," in *Mechanics of Sheet Metal Forming, Material Behavior and Deformation Analysis*, Koistinen, D. P., and Wang, N.-M., eds., Plenum Press, New York, London, 1978, pp. 237–265.

33 Nemat-Nasser, S., Shokooh, A., and Taya, M., "On Localized Deformations in Biaxial Tension," Earthquake Research and Engineering Laboratory Technical Report No. 79-2-13, Department of Civil Engineering, Northwestern University, Evanston, Ill., 1979.

34 Neale, K. W., "Phenomenological Constitutive Laws in Finite Plasticity," *SM Archives*, Vol. 6, No. 1, 1981, pp. 79–128.

35 Iwakuma, T., and Nemat-Nasser, S., "An Analytical Estimate of Shear Band Initiation in a Necked Bar," *Int. J. Solids Structures*, Vol. 18, No. 1, 1982, pp. 69–83.

36 Hill, R., "Some Basic Principles in the Mechanics of Solids Without a Natural Time," *J. Mech. Phys. Solids*, Vol. 7, 1959, pp. 209–225.

37 Bui, H. D., "Evolution de la Frontière du Domaine Élastique des Métaux Avec l'Écrouissage Plastique et Comportement Élastoplastique d'un Agrégat de Cristaux Cubiques," *Mem. Artillerie Franç.: Sci. Tech. Armement*, Vol. 1, 1970, pp. 141–165.

38 Bui, H. D., Zaoui, A., and Zarka, J., "Sur le Comportement Élasto-Plastique et Viscoplastique des Monocristaux et Polycristaux Métalliques de Structure Cubique à Faces Centrées," in *Foundations of Plasticity*, Sawczuk, A., ed., Noordhoff Int., Leyden, 1973, pp. 51–75.

39 Hill, R., "Elastic Properties of Reinforced Solids: Some Theoretical Principles," *J. Mech. Phys. Solids*, Vol. 11, 1963, pp. 357–372.

40 Hill, R., "The Essential Structure of Constitutive Laws for Metal Composites and Polycrystals," *J. Mech. Phys. Solids*, Vol. 15, 1967, pp. 79–95.

41 Mandel, J., "Contribution Théorique à l'Étude de l'Écrouissage et des Lois de l'Écoulement Plastique," in *Proc. 11th Int. Congr. Appl. Mech.*, Springer-Verlag, Berlin, 1966, pp. 502–509.

42 Rice, J. R., "On the Structure of Stress-Strain Relations for Time-dependent Plastic Deformation in Metals," ASME JOURNAL OF APPLIED MECHANICS, Vol. 37, 1970, pp. 728–737.

43 Mura. T., *Micromechanics of Defects in Solids*, Martinus Nijhoff, The Hague, Boston, 1982.

44 Iwakuma, T., and Nemat-Nasser, S., "Finite Elastic-Plastic Deformation of Polycrystalline Metals and Composites," Earthquake Research and Engineering Laboratory Technical Report No. 83-3-51, Department of Civil Engineering, Northwestern University, Evanston, Ill., 1983.

45 Hill, R., "Continuum Micro-mechanics of Elasto-Plastic Polycrystals," *J. Mech. Phys. Solids*, Vol. 13, 1965, pp. 89–101.

46 Hill, R., "Acceleration Waves in Solids," *J. Mech. Phys. Solids*, Vol. 10, 1962, pp. 1–16.

47 Thomas, T. Y., *Plastic Flow and Fracture in Solids*, Academic Press, New York, 1961.

48 Nemat-Nasser, S., and Iwakuma, T., "Finite Elastic-Plastic Deformation of Composites," in *Mechanics of Composite Materials: Recent Advances*, Hashin, Z., and Herakovich, C. T., eds., Pergamon Press, 1983, pp. 47–55.

49 Budiansky, B., and Wu, T. T., "Theoretical Prediction of Plastic Strains of Polycrystals," in *Proc. 4th U.S. National Congress of Applied Mechanics*, 1962, pp. 1175–1185.

50 Hutchinson, J. W., "Elastic-Plastic Behaviour of Polycrystalline Metals and Composites," *Proc. Roy. Soc.*, London, Vol. *A*319, 1970, pp. 247–272.

51 Kröner, E., "Berechnung der Elastischen Konstanten des Vielkristalls aus den Konstanten des Einkristalls," *Z. Phys.*, Vol. 151, 1958, pp. 504–518.

52 Kröner, E., "Zur Plastischen Verformung des Vielkristalls," *Acta Met.*, Vol. 9, 1961, pp. 155–161.

53 Christoffersen, J., Mehrabadi, M. M., and Nemat-Nasser, S., "A Micromechanical Description of Granular Material Behavior," ASME JOURNAL OF APPLIED MECHANICS, Vol. 48, 1981, pp. 339–344.

54 Nemat-Nasser, S., and Mehrabadi, M. M., "Micromechanically Based Rate Constitutive Descriptions for Granular Materials," to appear in *Mechanics of Engineering Materials*, Desai, C. S., and Gallagher, R. H., eds., Wiley, New York.

55 Mröz, Z., "Deformation and Flow of Granular Materials," in *Theoretical and Applied Mechanics*, Rimrott, F. P. J., and Tabarrok, B., eds., North Holland, Amsterdam, 1980, pp. 119–132.

56 Dorris, J. F., and Nemat-Nasser, S., "A Plasticity Model for Flow of Granular Materials Under Triaxial Stress States," *Int. J. Solids Structures*, Vol. 18, No. 6, 1980, pp. 497–531.

57 Nemat-Nasser, S., "On Constitutive Behavior of Fault Materials," in *Solid Earth Geophysics and Geotechnology*, Nemat-Nasser, S., ed., AMD-Vol. 42, ASME, New York, 1980, pp. 31–37.

58 Nemat-Nasser, S., and Shokooh, A., "On Finite Plastic Flows of Compressible Materials With Internal Friction," *Int. J. Solids Structures*, Vol. 16, No. 6, 1980, pp. 495–514.

59 Nemat-Nasser, S., "Reply to Discussion of 'On Finite Plastic Flows of Compressible Materials With Internal Friction', *Int. J. Solids Structures*, Vol. 16, 1980, pp. 495–514, by J. W. Rudnicki," *Int. J. Solids Structures*, Vol. 18, No. 4, 1982, pp. 361–366.

60 Dienes, J. K., "On the Analysis of Rotation and Stress Rate in Deforming Bodies," *Acta Mech.*, Vol. 32, 1979, pp. 217–232.

61 Johnson, G. C., and Bammann, D. J., "A Discussion of Stress Rates in Finite Deformation Problems," Sandia Report No. SAND82-8821, Sandia National Laboratories, Albuquerque, N. Mex., 1982.

62 Lee, E. H., Mallett, R. L., and Wertheimer, T. B., "Stress Analysis for Anisotropic Hardening in Finite-Deformation Plasticity," Interim Technical Report, Metal Forming Report No. 4/82, Department of Mechanical Engineering, Rensselaer Polytechnic Institute, Troy, N.Y., 1982.

63 Truesdell, C., "Hypo-Elastic Shear," *J. of Appl. Physics*, Vol. 27, No. 5, 1956, pp. 441–447.

64 Onat, E. T., "Representation of Inelastic Behavior in the Presence of Anisotropy and of Finite Deformations," in *Recent Advances in Creep and Fracture of Engineering Materials and Structures*, Wilshire, B., and Owen, D. R. J., eds., Pineridge Press, Swansea, U.K., 1982, Chapter 5, pp. 231–264.

65 Tvergaard, V., "Effect of Kinematic Hardening on Localized Necking in Biaxially Stretched Sheets," *Int. J. Mech. Sci.*, Vol. 20, 1978, pp. 651–658.

66 Ziegler, H., "A Modification of Prager's Hardening Rule," *Q. Appl. Math.*, Vol. 17, 1959, pp. 55–65.

67 Mogi, K., "Fracture and Flow of Rocks," *Tectonophysics*, Vol. 13, 1972, pp. 541–568.

68 Drucker, D. C., "Relation of Experiments to Mathematical Theories of Plasticity," ASME JOURNAL OF APPLIED MECHANICS, Vol. 16, 1949, pp. 349–357.

69 Martin, J. B., *Plasticity: Fundamentals and General Results*, M.I.T. Press, Cambridge, Mass., 1975.

70 Biot, M. A., "Theory of Stress-Strain Relations in Anisotropic Viscoelasticity and Relaxation Phenomena," *J. Appl. Physics*, Vol. 25, No. 11, 1954, pp. 1385–1391.

71 Meixner, J., "Thermodynamische Theorie der Elastischen Relaxation," *Z. Naturf.*, Vol. *9a*, 1954, pp. 654–663.

72 Kestin, J., and Bataille, J., "Thermodynamics of Solids," in *Continuum Models of Discrete Systems*, Freudenstadt, Germany, 1979, University of Waterloo Press, 1980, pp. 99–147.

73 Coleman, B. D., and Gurtin, M. E., "Thermodynamics With Internal State Variables," *J. Chem Phys.*, Vol. 47, 1967, pp. 597–613.

Downloaded 02 May 2010 to 171.66.16.250. Redistribution subject to ASME license or copyright; see http://www.asme.org/terms/Terms_Use.cfm

74 Lubliner, J., "On Fading Memory in Materials of Evolutionary Type," *Acta Mech.*, Vol. 8, 1969, pp. 75–81.
75 Mandel, J., "Plasticité et Viscoplasticité," Cours No. 97 au C.I.S.M., Springer Wien, 1971.
76 Nemat-Nasser, S., "On Nonequilibrium Thermodynamics of Continua," in *Mechanics Today*, Vol. 2, Nemat-Nasser, S., ed., Pergamon Press, New York, 1975, Chapter 2, pp. 94–158; "On Nonequilibrium Thermodynamics of Continua: Addendum," in *Mechanics Today*, Vol. 4, Nemat-Nasser, S., ed., Pergamon Press, New York, 1977, Chapter 6, pp. 391–405.
77 Onat, E. T., "The Notion of State and Its Implications in Thermodynamics of Inelastic Solids," in *Proc. IUTAM Symp.*, Vienna, 1966, pp. 421–434.
78 Rice, J. R., "Inelastic Constitutive Relations for Solids: An Internal-Variable Theory and Its Application to Metal Plasticity," *J. Mech. Phys. Solids*, Vol. 19, 1971, pp. 433–455.
79 Schapery, R. A., "A Theory of Non-Linear Thermoviscoelasticity Based on Irreversible Thermodynamics," in *Proc. 5th U.S. National Congress of Applied Mechanics*, 1966, pp. 511–530.
80 Valanis, K. C., "Thermodynamics of Large Viscoelastic Deformations," *J. of Mathematics and Physics*, Vol. 45, No. 2, 1966, pp. 197–212.
81 Hill, R., and Rice, J. R., "Elastic Potentials and the Structure of Inelastic Constitutive Laws," *SIAM J. Appl. Math.*, Vol. 25, No. 3, 1973, pp. 448–461.
82 Hill, R., "On the Elasticity and Stability of Perfect Crystals at Finite Strain," *Math. Proc. Camb. Phil. Soc.*, Vol. 77, 1975, pp. 225–240.
83 Li, J. C. M., "Thermodynamics for Nonequilibrium Systems. The Principle of Macroscopic Separability and the Thermokinetic Potential," *J. Appl. Physics*, Vol. 33, 1962, pp. 616–624,
84 Buchdahl, H. A., *The Concepts of Classical Thermodynamics*, Cambridge University Press, Cambridge, 1966.
85 Nemat-Nasser, S., "On Nonequilibrium Thermodynamics of Viscoelasticity: Inelastic Potentials and Normality Conditions," in *Mechanics of Visco-Elastic Media and Bodies*, Hult, J., ed., Springer-Verlag, Berlin, 1975, pp. 375–391.
86 Mandel, J., "Thermodynamics and Plasticity," in *Proc. Int. Symp. Foundations of Continuum Thermodynamics*, Delgado Domingos, J. J., Nina, M. N. R., and Whitelaw, J. H., eds., MacMillan, London, 1974, pp. 283–304.
87 Edelen, D. G. B., "On the Characterization of Fluxes in Nonlinear Irreversible Thermodynamics," *Int. J. Eng. Sci.*, Vol. 12, 1974, pp. 397–411.
88 Il'yushin, A. A., "On the Postulate of Plasticity," *Prikl. Mat. Mekh.*, Vol. 25, No. 3, 1961, pp. 503–507.
89 Drucker, D. C., "Some Implications of Work Hardening and Ideal Plasticity," *Q. Appl. Math.*, Vol. 7, No. 4, 1950, pp. 411–418.
90 Drucker, D. C., "Stress-Strain-Time Relations and Irreversible Thermodynamics," in *Proc. Int. Symp. on Second-Order Effects in Elasticity, Plasticity and Fluid Dynamics*, Reiner, M., and Abir, D., eds., Pergamon Press, Oxford, 1964, pp. 331–351.
91 Bishop, J. F. W., and Hill, R., "A Theory of the Plastic Distortion of a Polycrystalline Aggregate Under Combined Stresses," *Phil. Mag.*, Series 7, Vol. 42, 1951, pp. 414–427.
92 Truesdell, C., and Noll, W., "The Non-Linear Field Theories of Mechanics," *Handbuch der Physik*, Vol. III/3, Flügge, S., ed., Springer-Verlag, Berlin, 1965.
93 Truesdell, C., and Toupin, R., "The Classical Field Theories," in *Handbuch der Physik*, Vol. III/1, Flugge, S., ed., Springer-Verlag, Berlin, 1960, pp. 226–793.
94 Biot, M. A., *Mechanics of Incremental Deformations*, Wiley, New York, 1965.
95 Cotter, B. A., and Rivlin, R. S., "Tensors Associated With Time-dependent Stress," *Q. Appl. Math.*, Vol. 13, 1955, pp. 177–182.
96 Masur, E. F., "On the Definition of Stress Rate," *Q. Appl. Math.*, Vol. 19, 1961, pp. 160–163.
97 Naghdi, P. M., and Wainwright, W. L., "On the Time Derivative of Tensors in Mechanics of Continua," *Q. Appl. Math.*, Vol. 19, 1961, pp. 95–109.
98 Noll, W., "On the Continuity of the Solid and Fluid States," *J. Rat. Mech. Anal.*, Vol. 4, 1955, pp. 3–81.
99 Oldroyd, J. G., "On the Formulation of Rheological Equations of State," *Proc. Roy. Soc.*, London, Vol. *A*200, 1950, pp. 523–541.
100 Prager, W., "An Elementary Discussion of Definitions of Stress Rate," *Q. Appl. Math.*, Vol. 18, 1961, pp. 403–407.
101 Thomas, T. Y., "Kinematically Preferred Coordinate Systems," *Proc. Nat'l. Acad. Sci. U.S.*, Vol. 41, 1955, pp. 762–770.
102 Truesdell, C., "Corrections and Additions to 'The Mechanical Foundations of Elasticity and Fluid Dynamics'," *J. Rat. Mech. Anal.*, Vol. 2, 1953, pp. 593–616.

APPENDIX *A*

A.1 Kinematics

Let $\mathbf{x} = \mathbf{x}(\mathbf{X})$ or $x_i = x_i(X_A)$, $i, A = 1,2,3$, be a one-to-one mapping of material points from a reference (not necessarily undeformed or unstressed) configuration to the current one; a fixed rectangular Cartesian coordinate system is used. The deformation gradient is $\mathbf{F} = \partial\mathbf{x}/\partial\mathbf{X}$ or $F_{iA} = \partial x_i/\partial X_A$.

By polar decomposition, $\mathbf{F} = \mathbf{RU} = \mathbf{VR}$, $\mathbf{R}^{-1} = \mathbf{R}^T$, $\det \mathbf{R} = +1$, where $\mathbf{U}$ and $\mathbf{V}$ are the right and left-stretch tensors, having the common eigenvalues, $\lambda_{(a)}$ (the principal stretches), and respective eigenvectors $\mathbf{N}^{(a)}$ and $\mathbf{n}^{(a)}$, the orthogonal Lagrangian and Eulerian triads, $a = 1,2,3$. Hence,

$$\mathbf{U}^2 = \mathbf{F}^T\mathbf{F} = \sum_{a=1}^{3} \lambda_{(a)}^2 \mathbf{N}^{(a)} \otimes \mathbf{N}^{(a)},$$

$$\mathbf{V}^2 = \mathbf{F}\mathbf{F}^T = \sum_{a=1}^{3} \lambda_{(a)}^2 \mathbf{n}^{(a)} \otimes \mathbf{n}^{(a)}. \tag{A.1}$$

Various material strain measures have been introduced; see Truesdell and Noll [92] and Truesdell and Toupin [93]. We consider Hill's [2, 3] general strain measure,

$$\mathbf{E} = \sum_{a=1}^{3} f(\lambda_{(a)})\, \mathbf{N}^{(a)} \otimes \mathbf{N}^{(a)},$$

$$f(1) = 0, \quad f'(1) = 1, \text{ and } f(\lambda) \text{ monotone.} \tag{A.2}$$

A subset of this is

$$f(\lambda) = \begin{cases} (\lambda^{2m} - 1)/2m, & m \neq 0 \text{ integer}, \\ \ln\lambda, & m = 0. \end{cases} \tag{A.3}$$

Commonly used strains are: Lagrangian, $\frac{1}{2}(\mathbf{U}^2 - \mathbf{1})$, for $m = 1$; Almansi, $\frac{1}{2}(\mathbf{1} - \mathbf{U}^{-2})$, for $m = -1$; and logarithmic, $\ln\mathbf{U}$, for $m = 0$. An Eulerian strain measure associates with (*A*.2), Nemat-Nasser [8],

$$\mathbf{e} = \sum_{a=1}^{3} f(\lambda_{(a)})\, \mathbf{n}^{(a)} \otimes \mathbf{n}^{(a)} = \mathbf{R}\mathbf{E}\mathbf{R}^T. \tag{A.4}$$

Any member of (*A*.2) serves as a standard. Others are expressible in terms of this chosen norm. Direct differentiation with the aid of the implicit function theorem yields,

$$\bar{f}(\lambda) = \hat{f}(f) = f + mf^2 + \ldots, \; 2m = \bar{f}''(1) - f''(1), \tag{A.5}$$

for any $\bar{f}$ and f associated with strain measures $\bar{\mathbf{E}}$ and $\mathbf{E}$. Hence,

$$\bar{\mathbf{E}} = \mathbf{E} + m\mathbf{E}^2 + \ldots,$$

$$\mathbf{E}^n = \sum_{a=1}^{3} [f(\lambda_{(a)})]^n \mathbf{N}^{(a)} \otimes \mathbf{N}^{(a)}. \tag{A.6}$$

Hill [3] suggests $\ln\mathbf{U}$ as a useful norm in finite deformation plasticity. Another appealing candidate is $\mathbf{U} - \mathbf{1}$, contained in Biot's work [94].

Material time differentiation of (*A*.2) and (*A*.4) yields the corresponding strain rate,

$$\dot{\mathbf{E}} = \sum_{a,b=1}^{3} \{f'(\lambda_{(a)})\, \dot{\lambda}_{(a)}\, \delta_{ab} + [f(\lambda_{(b)}) - f(\lambda_{(a)})]\Omega^L_{(ab)}\}\, \mathbf{N}^{(a)} \otimes \mathbf{N}^{(b)},$$

$$\dot{\mathbf{e}} = \sum_{a,b=1}^{3} \{f'(\lambda_{(a)})\, \dot{\lambda}_{(a)}\, \delta_{ab} + [f(\lambda_{(b)}) - f(\lambda_{(a)})]\Omega^E_{(ab)}\}\, \mathbf{n}^{(a)} \otimes \mathbf{n}^{(b)}, \tag{A.7}$$

where

$$\mathbf{\Omega}^L = \sum_{a,b=1}^{3} \Omega^L_{(ab)}\, \mathbf{N}^{(a)} \otimes \mathbf{N}^{(b)}, \quad \dot{\mathbf{N}}^{(a)} = \mathbf{\Omega}^L \mathbf{N}^{(a)},$$

$$\mathbf{\Omega}^E = \sum_{a,b=1}^{3} \Omega^E_{(ab)}\, \mathbf{n}^{(a)} \otimes \mathbf{n}^{(b)}, \quad \dot{\mathbf{n}}^{(a)} = \mathbf{\Omega}^E \mathbf{n}^{(a)}, \tag{A.8}$$

Downloaded 02 May 2010 to 171.66.16.250. Redistribution subject to ASME license or copyright; see http://www.asme.org/terms/Terms_Use.cfm

are the spins of the Lagrangian and Eulerian triads, respectively.

The velocity gradient, with component $\partial v_i/\partial x_j$ in the fixed frame, is

$$\mathbf{L}=\dot{\mathbf{F}}\mathbf{F}^{-1}=\mathbf{D}+\mathbf{W}=\dot{\mathbf{R}}\mathbf{R}^T+\mathbf{R}\dot{\mathbf{U}}\mathbf{U}^{-1}\mathbf{R}^T, \tag{A.9}$$

$$\dot{\mathbf{R}}=\boldsymbol{\Omega}^R\mathbf{R}, \quad \boldsymbol{\Omega}^R=\sum_{a,b=1}^{3}\Omega^R_{(ab)}\mathbf{n}^{(a)}\otimes\mathbf{n}^{(b)}. \tag{A.10}$$

$\boldsymbol{\Omega}^R$ is the spin of the Lagrangian triad relative to the Eulerian one. $\mathbf{D}$ and $\mathbf{W}$, the symmetric and the antisymmetric parts of $\mathbf{L}$, are the deformation and spin tensors, respectively. Denote the components of $\mathbf{D}$ and $\mathbf{W}$ in the *Eulerian triad* by $D_{(ab)}$ and $W_{(ab)}$, and from (A.9) and (A.10) obtain

$$\Omega^L_{(ab)}=\frac{2\lambda_{(a)}\lambda_{(b)}}{\lambda^2_{(b)}-\lambda^2_{(a)}}D_{(ab)},$$

$$\Omega^R_{(ab)}=\frac{\lambda_{(b)}-\lambda_{(a)}}{\lambda_{(b)}+\lambda_{(a)}}D_{(ab)}+W_{(ab)},$$

$$\Omega^E_{(ab)}=\frac{\lambda^2_{(b)}+\lambda^2_{(a)}}{\lambda^2_{(b)}-\lambda^2_{(a)}}D_{(ab)}+W_{(ab)},$$

$$\text{(no sum on } a, b) \quad a\neq b, \quad \lambda_{(a)}\neq\lambda_{(b)}, \tag{A.11}$$

where $\Omega^L_{(ab)}+\Omega^R_{(ab)}=\Omega^E_{(ab)}$. Let $\dot{E}_{(ab)}$ denote components of $\mathbf{E}$ in the *Lagrangian triad*. Then, in view of (A.11),

$$\dot{\mathbf{E}}_{(aa)}=\lambda_{(a)}f'(\lambda_{(a)})D_{(aa)} \quad \text{(no sum on } a),$$

$$\dot{\mathbf{E}}_{(ab)}=[f(\lambda_{(b)})-f(\lambda_{(a)})]\frac{2\lambda_{(a)}\lambda_{(b)}}{\lambda^2_{(b)}-\lambda^2_{(a)}}D_{(ab)},$$

$$\text{(no sum on } a,b) \quad a\neq b, \quad \lambda_{(a)}\neq\lambda_{(b)}. \tag{A.12}$$

When the current state is used as the reference, equation (A.12) reveals that all strain rate measures of this class reduce to $\mathbf{D}$.

A.2 **Stress Fluxes.** Let $\boldsymbol{\sigma}$ and $\boldsymbol{\tau}$ be the Cauchy and Kirchhoff stresses, $\boldsymbol{\tau}=(\rho_0/\rho)\boldsymbol{\sigma}$, with ρ_0 and ρ the reference and current mass-densities. The quantity $\boldsymbol{\tau}:\mathbf{D}/\rho_0=\boldsymbol{\sigma}:\mathbf{D}/\rho$ is the rate of stress-work per unit mass, invariant with respect to changes in strain measure and the reference state. It serves to generate stress measures conjugate to material strain measures in class (A.2), as well as to others, Hill [2, 3].

To relate various stress fluxes, consider two strain measures, $\bar{\mathbf{E}}$ and $\mathbf{E}$, in class (A.2), and let their conjugate stresses be $\bar{\mathbf{S}}$ and $\mathbf{S}$, respectively. Then

$$\frac{1}{\rho_0}\bar{\mathbf{S}}:\dot{\bar{\mathbf{E}}}=\frac{1}{\rho_0}\mathbf{S}:\dot{\mathbf{E}}. \tag{A.13}$$

Expand both $\mathbf{E}$ and $\bar{\mathbf{E}}$ in terms of, say, $(\mathbf{U}-\mathbf{1})$, as in (A.6), substitute into (A.13), and obtain

$$\dot{\bar{\mathbf{S}}}+\frac{1}{2}\bar{f}''(1)[\bar{\mathbf{S}}\dot{\bar{\mathbf{E}}}+\dot{\bar{\mathbf{E}}}\bar{\mathbf{S}}]+0(\bar{\mathbf{E}}^2)$$

$$=\dot{\mathbf{S}}+\frac{1}{2}f''(1)[\bar{\mathbf{S}}\dot{\bar{\mathbf{E}}}+\dot{\bar{\mathbf{E}}}\bar{\mathbf{S}}]+0(\mathbf{E}^2). \tag{A.14}$$

Time differentiation gives

$$\ddot{\bar{\mathbf{S}}}+\frac{1}{2}\bar{f}''(1)[\bar{\mathbf{S}}\ddot{\bar{\mathbf{E}}}+\ddot{\bar{\mathbf{E}}}\bar{\mathbf{S}}]+0(\bar{\mathbf{E}})$$

$$=\dot{\mathbf{S}}+\frac{1}{2}f''(1)[\mathbf{S}\dot{\mathbf{E}}+\dot{\mathbf{E}}\mathbf{S}]+0(\mathbf{E}). \tag{A.15}$$

When the current state is the reference, all stress measures equal the Cauchy stress $\boldsymbol{\sigma}$, all strain rates reduce to $\mathbf{D}$, and all strain measures vanish. Then,

$$\dot{\bar{\mathbf{S}}}+\frac{1}{2}\bar{f}''(1)[\boldsymbol{\sigma}\mathbf{D}+\mathbf{D}\boldsymbol{\sigma}]=\dot{\mathbf{S}}+\frac{1}{2}f''(1)[\boldsymbol{\sigma}\mathbf{D}+\mathbf{D}\boldsymbol{\sigma}], \tag{A.16}$$

exactly.

The Jaumann rate of the Kirchhoff stress,

$$\mathring{\boldsymbol{\tau}}=\dot{\boldsymbol{\tau}}+\boldsymbol{\tau}\mathbf{W}-\mathbf{W}\boldsymbol{\tau}, \tag{A.17}$$

is associated with the logarithmic strain, $ln\mathbf{U}$, when the current state is the reference, Hill [3]. Indeed, since

$$\boldsymbol{\tau}:\mathbf{D}=(\mathbf{R}^T\boldsymbol{\tau}\mathbf{R}):(\mathbf{R}^T\mathbf{D}\mathbf{R})\equiv\hat{\boldsymbol{\tau}}:\hat{\mathbf{D}}; \tag{A.18}$$

where $\hat{\boldsymbol{\tau}}$ and $\hat{\mathbf{D}}$ are the Kirchhoff stress and the deformation rate tensors, rotated to the *Lagrangian frame*, we have $\dot{\hat{\boldsymbol{\tau}}}=\mathring{\hat{\boldsymbol{\tau}}}$ when current state is the reference; also $\dot{\hat{\boldsymbol{\sigma}}}=\mathring{\hat{\boldsymbol{\sigma}}}$. To see this, calculate $\dot{\hat{\boldsymbol{\tau}}}$ directly, and rotate it back to the current state,

$$\mathbf{R}(\mathbf{R}^T\boldsymbol{\tau}\mathbf{R})^{\cdot}\mathbf{R}^T=\mathbf{R}\dot{\hat{\boldsymbol{\tau}}}\mathbf{R}^T=\dot{\boldsymbol{\tau}}+\boldsymbol{\tau}\boldsymbol{\Omega}^R$$

$$-\boldsymbol{\Omega}^R\boldsymbol{\tau}=\{\dot{\boldsymbol{\tau}}+\boldsymbol{\tau}\mathbf{W}-\mathbf{W}\boldsymbol{\tau}\}+\boldsymbol{\tau}\boldsymbol{\epsilon}-\boldsymbol{\epsilon}\boldsymbol{\tau}, \tag{A.19}$$

where, from (A.11),

$$\boldsymbol{\epsilon}=\sum_{a,b=1}^{3}\frac{\lambda_{(b)}-\lambda_{(a)}}{\lambda_{(b)}+\lambda_{(a)}}D_{(ab)}\mathbf{n}^{(a)}\otimes\mathbf{n}^{(b)} \tag{A.20}$$

which vanishes when the reference state coincides with the current configuration; then $\lambda_{(a)}=1$, $a=1,2,3$.

With reference configuration *distinct* from the current one, the objective stress rate $\mathbf{R}\dot{\hat{\boldsymbol{\tau}}}\mathbf{R}^T$ differs from the Jaumann rate, by terms linear in stress and also in off-diagonal components of $\mathbf{D}$ with respect to the *Eulerian triad*, i.e., $D_{(ab)}$, $a\neq b$.

The stress measure $\hat{\boldsymbol{\tau}}$ is not conjugate to the logarithmic strain $ln\mathbf{U}$, but since to the second order in, say, the Lagrangian strain, $1/2\,(\mathbf{U}^2-\mathbf{1})$, we have $d\,ln\,\mathbf{U}/dt=\hat{\mathbf{D}}$, we may write $\hat{\boldsymbol{\tau}}:\hat{\mathbf{D}}\simeq\hat{\boldsymbol{\tau}}:(d\,ln\,\mathbf{U}/dt)$. Therefore, identifying $\bar{\mathbf{S}}$ with $\hat{\boldsymbol{\tau}}$, (A.16) yields the *exact* relation,

$$\dot{\mathbf{S}}=\mathring{\boldsymbol{\tau}}-\frac{1}{2}[f''(1)+1][\boldsymbol{\sigma}\mathbf{D}+\mathbf{D}\boldsymbol{\sigma}], \tag{A.21}$$

where, for the logarithmic strain, $f''(1)=-1$; this also shows that the Jaumann rate of the Kirchhoff stress is conjugate to the logarithmic strain when the current state is the reference, Hill [3]. A number of objective stress fluxes has been introduced by various authors which relate to (A.21); see, e.g., Cotter and Rivlin [95], Masur [96], Naghdi and Wainwright [97], Noll [98], Oldroyd [99], Prager [100], Thomas [101], and Truesdell [102].

Suppose $\mathbf{L}$ is the instantaneous elastic-plastic modulus tensor associated with the Jaumann flux $\mathring{\boldsymbol{\tau}}$ and with $\mathbf{D}$, i.e.,

$$\mathring{\boldsymbol{\tau}}=\mathbf{L}:\mathbf{D}. \tag{A.22}$$

For any other objective stress flux, say, $\dot{\mathbf{S}}$, equation (A.21) gives the difference, $\dot{\mathbf{S}}-\mathring{\boldsymbol{\tau}}$, to be of the order of stress. This difference is significant when the modulus $\mathbf{L}$ is of the order of stress, as is commonly the case at advanced stages of elastoplastic flow of metals, and as is always the case in the flow of granular materials that support the applied loads by contact friction.

Downloaded 02 May 2010 to 171.66.16.250. Redistribution subject to ASME license or copyright; see http://www.asme.org/terms/Terms_Use.cfm

A. C. Newell
Program in Applied Mathematics,
University of Arizona,
Tucson, Ariz. 85721

The History of the Soliton

(A) John Scott Russell's Discovery

The discovery of the soliton, its remarkable properties, and the incredible richness of structure involved in its mathematical description occurred in two stages and over a period of almost 140 years. The story begins with the observation by John Scott Russell of "the great Wave of Translation." I shall let himself tell of the incident.

> "I believe I shall introduce this phenomenon by describing the circumstances of my own first acquaintance with it. I was observing the motion of a boat which was rapidly drawn along a narrow channel by a pair of horses, when the boat suddenly stopped—not so the mass of water in the channel which it had put in motion; it accumulated round the prow of the vessel in a state of violent agitation, then suddenly leaving it behind, rolled forward with great velocity, assuming the form of a large solitary elevation, a rounded, smooth and well-defined heap of water, which continued its course along the channel apparently without change of form or diminution of speed. I followed it on horseback, and overtook it still rolling on at a rate of some eight or nine miles an hour, preserving its original figure some thirty feed long and a foot to a foot and a half in height. Its height gradually diminished, and after a chase of one or two miles I lost it in the windings of the channel. Such, in the month of August 1834, was my first chance interview with that singular and beautiful phenomenon which I have called the Wave of Translation, a name which it now very generally bears." [1]

If the hallmark of a great scientist is his ability to recognize what is essentially new, and it surely must be one of the key qualities, then Russell must be accorded this appelation. From the very first sighting, he was convinced that what he had observed was a new scientific phenomenon and thereafter he spent a major portion of his professional life carrying out experiments to determine the properties of the great wave.

> "This is a most beautiful and extraordinary phenomenon: the first day I saw it was the happiest day of my life. Nobody had ever had the good fortune to see it before or, at all events, to know what it meant. It is now known as the solitary wave of translation. No one before had fancied a solitary wave as a possible thing. When I described this to Sir John Herschel, he said 'It is merely half of a common wave that has been cut off.' But it is not so, because the common waves go partly above and partly below the surface level; and not only that but its shape is different. Instead of being half a wave it is clearly a whole wave, with this difference, that the whole wave is not above and below the surface alternately but always above it. So much for what a heap of water does: it will not stay where it is but travels to a distance." [2]

He knew that it was a fundamental mode of propagation in the sense that an arbitrary heap of water would disintegrate and resolve itself into a primary and residual wave. He knew that its velocity was proportional to its height and proposed after much experimental work the law $c^2 = g(h + \eta)$ where g, h, and η are gravity, the undisturbed depth, and the maximum height of the wave, as measured from the undisturbed level, respectively. He knew that waves of depression behaved differently than waves of elevation and produced no permanent traveling forms. He knew about the interaction of solitary waves but does not appear to have noticed their soliton quality, a property I will discuss shortly. Indeed, if he had applied the reversibility property of the Euler equations and the fact that two waves would become infinitely separated as $t \to \pm\infty$, he could have inferred this truly remarkable feature. He also knew about the strange and uniquely nonlinear reflection properties of slightly oblique waves.

He also knew how to create them! I was recently privileged to attend a most enjoyable and well-organized conference at Heriot-Watt University celebrating this great man's work on the 100th anniversary of his death. It was a grand occasion, filled with lively talks and stimulating discussions and involving an international array of scientists from at least a dozen different disciplines. The highlight of the meeting was to be the recreation of Russell's experience at the same spot on the Union Canal where the original incident took place. I am not proud to admit that we failed, that with all our combined knowledge and experience, we were not able to improvise the means to create the wave when the engine of the powerful motorboat, which had worked so well in trial runs, failed the day before the event. The man himself used to do it on a regular basis, with a couple of horses, a couple of ropes, an old barge, and a great intuitive understanding of how to transfer the momentum of the boat to the water. Standing on the bank, watching the efforts of swarms of eager young scientists charging along the canal in the role of large horses, one could see many a glass raised in silent respect.

Nevertheless, despite the setback of that day, there is not a soul now living who does not believe in the great wave,

Contributed by the Applied Mechanics Division for publication in the JOURNAL OF APPLIED MECHANICS.
Discussion on this paper should be addressed to the Editorial Department, ASME, United Engineering Center, 345 East 47th Street, New York, N.Y. 10017, and will be accepted until two months after final publication of the paper itself in the JOURNAL OF APPLIED MECHANICS. Manuscript received by ASME Applied Mechanics Division, May, 1983.

Copyright © 1983 by ASME
Downloaded 02 May 2010 to 171.66.16.250. Redistribution subject to ASME license or copyright; see http://www.asme.org/terms/Terms_Use.cfm

because the experiments of Russell have been repeated under carefully controlled circumstances and his predictions verified. It was not always that way, however. At first, Russell's ideas faced great hostility and scepticism from the leading lights in the scientific community of his day. Both Airy and Stokes questioned whether a wave that traveled without change in shape could be totally above the water and attributed the dimunition of amplitude as indicating that the wave was inherently nonpermanent. Russell had suggested (correctly) that this failure was due to friction. In fact, Stokes "proved" in his 1849 paper through the use of a small-amplitude expansion of a sinusoidal wave, that the only permanent wave is basically sinusoidal with the nonlinear terms modifying the shape (the second and higher harmonics) and the speed (it becomes weakly dependent on amplitude). What he had discovered, of course, was the other limit (the modulus of the elliptic function tending to zero rather than one) of the general cnoidal wave solution to the equations of motion. Later on, Stokes was to recognize and admit his errors. It is somewhat ironic that the wave that Stokes discovered (the Stokes wave) is itself unstable when the ratio of depth to wavelength is approximately 1 (this ratio is small for the solitary wave). In deeper water, an almost monochromatic wave train of the type he described breaks up into a series of wave groups.

It was not until the 1870s that Russell's work was finally vindicated and its scientific importance can be measured by the eminence of the men who did the job. Independently, Boussinesq [3] (1872) and Rayleigh (1876) found the hyperbolic secant-squared solution for the free surface. Boussinesq's 1872 paper in fact did a lot more and introduced many of the ideas used nowadays by modern analysts. In particular, he found the conserved density of the third conservation law, a quantity he called the moment of instability. He derived his solution from the approximation to the water wave equations that now bear his name. In this approximation, the motion is still bidirectional (see [57])but the basic idea of the balance between nonlinearity and dispersion is present. It was left to Korteweg and deVries in 1895, who apparently did not know the work of Boussinesq and Rayleigh and who were still trying to answer the objections of Airy and Stokes, to write down the unidirectional equation which now bears their names. (It would appear to have been the thesis project of deVries.)

In this first stage of discovery, the primary thrust was to establish the existence and resilience of the wave. The discovery of its universal nature and its additional properties was to await a new day and an unexpected result from another experiment designed to answer a totally different question.

(*B*) Fermi-Pasta-Ulam (FPU)

The scene now changes. It is almost 60 years later and 6000 miles away. The place is Los Alamos and the principals are Enrico Fermi, John Pasta, and Stan Ulam. The question of interest was: why do solids have finite heat conductivity? The solid is modeled by a one-dimensional lattice, a set of masses coupled by springs. In 1914, Debye had suggested that the finiteness of the thermal conductivity of a lattice is due to the anharmonicty of the nonlinear forces in the springs. If the force is linear (Hooke's law), energy is carried unhindered by the independent fundamental or normal modes of propagation. The effective thermal conductivity is infinite; no thermal gradient is required to push that heat through the lattice from one end to another and no diffusion equation obtains. Debye thought that if the lattice were weakly nonlinear, the normal modes (calculated from the linearized spring) would interact due to the nonlinearity and thereby hinder the propagation of energy. The net effect of many such nonlinear interactions (phonon collisions) would manifest itself in a diffusion equation with a finite transport coefficient. This suggestion motivated Fermi, Pasta, and Ulam (FPU) [5] to undertake a numerical study of the one-dimensional anharmonic lattice on the Maniac I computer at Los Alamos. They argued that a smooth initial state in which all the energy was in the lowest mode or the first few lowest modes would eventually relax to a state of statistical equilibrium due to nonlinear couplings. In that state, the energy would be equidistributed among all modes on the average. The relaxation time would then provide a measure of diffusion coefficient.

The model used by FPU to describe their one-dimensional lattice of length L consists of a row of $N-1$ identical masses each connected to the next and the end ones to fixed boundaries by N nonlinear springs of length h. Those springs when compressed or extended by an amount Δ exert a force

$$F=k(\Delta+\alpha\Delta^2) \tag{1}$$

where k is the linear spring constant and α, taken positive, measures the strength of the nonlinearity. The equations governing the dynamics of this lattice are

$$m_{y_{itt}}=k(y_{i+1}-2y_i+y_{i+1})(1+\alpha(y_{i+1}-y_{i-1})) \qquad i=1,2,\ldots,N-1, \quad y_0=y_N=0, \tag{2}$$

y_i being the displacement of the ith mass from its equilibrium position.

FPU usually took the energy to be in the few lowest modes of the corresponding linear problem. In the linear problem, the energy in each mode would persist unchanged forever and no new mode would be excited. In the nonlinear problem, the energy flows from the low modes to higher ones, and FPU expected this to continue until the energy becomes equidistributed over all modes accommodated in their numerical scheme. With 64 points in x-space, they had 64 different modes over which they hoped to see the energy distributed. The observed evolution could then serve as a model of thermalization for more complicated physical systems.

Now a great surprise was encountered—at least it seemed to surprise everyone who was involved in this problem or heard of it. The energy did not thermalize! In fact, when the energy was initially all in the lowest mode, after flowing back and forth among several low-order modes, it eventually recollected into the lowest mode to within an accuracy of 1 or 2 percent and from there on the process approximately repeated itself. They knew the phenomenon was not an example of Poincaré recurrence, the time for which, in a system of 63 independently moving masses, would be enormous. Rather, the system seemed to behave like a system of linearly coupled harmonic oscillators whose motion on a torus is quasiperiodic. (If the two fundamental frequencies were ω_1, ω_2 and $\omega_1/\omega_2 \simeq m/n$ with m, n integers and relatively prime, then the initial state would recur approximately after a time $2\pi n/\omega_2$). But how could this be? Why didn't the nonlinearity excite all the Fourier modes? Could the answer be that the system, when viewed in the right coordinates, was equivalent to a separable system of harmonic oscillators?

The FPU experiment had failed to produce the expected result and indeed the results it did produce challenged, as did the Michelson-Morley experiment of the previous century, the basic thinking of physicists of the day. Nevertheless, since it was not connected with what was regarded at that time as frontier physics (little has changed in this regard today) it could easily have been dismissed, as it was by many, as an anomalous curiosity. Other promising starts on unexpected nonlinear behavior sputtered out. For example, in 1962 Perring and Skyrme found a two-soliton (two-particle elastic collision) solution for the sine-Gordon equation which they were using as a model for a nonlinear meson field theory.

Downloaded 02 May 2010 to 171.66.16.250. Redistribution subject to ASME license or copyright; see http://www.asme.org/terms/Terms_Use.cfm

These exact solutions, which display a nonlinear superposition principle, could have made contact with the work of Bäcklund and Bianchi who invented in the latter part of the 19th century a general scheme for constructing multisoliton solutions for the sine-Gordon equation which emerges in the theory of surfaces of constant negative curvature. Clearly the equation had very special properties, but Perring and Skyrme did not follow the lead.

Thankfully, the curious results of the FPU experiment were not ignored by all. The moment and opportunity were seized by two applied mathematicians at Princeton University, Martin Kruskal and Norman Zabusky. They set out to understand the abnormal, and in doing so discovered the soliton and a wonderful new world of nonlinear behavior which today has captured the imagination of scientists from every physical discipline and has given a renewed life and richness to many previously discovered mathematical structures.

(C) Kruskal, Zabusky, and the Discovery of the Soliton

Kruskal and Zabusky (KZ) [6-10] approached the FPU problem from the continuum viewpoint. They argued that since the energy was contained in the lowest modes of the system, the displacement of neighboring masses differed by $0(h/L)$, and therefore one could define a continuum displacement $y(x,t)$ where $y(ih,t) \simeq y_i$. Expanding the displacements y_{i+1}, y_{i-1} in a Taylor series, setting $kh^2/m = c^2$, $2\alpha h = \epsilon$, $h^2/12\epsilon = \delta^2$, one finds that equation (2) becomes

$$y_{tt} - c^2 y_{xx} = \epsilon c^2 y_x y_{xx} + \epsilon c^2 \delta^2 y_{xxxx} \tag{3}$$

where terms of order ϵ^2 have been ignored. The parameter ϵ is small. As we will see, it is crucial to retain the second term on the right-hand side, the fourth-order derivative, in the approximation to the second-order difference. Since FPU solved the equations by a centered time difference, it is also strictly necessary to include a y_{tttt} term, but since to a good approximation $y_{tttt} = c^4 y_{xxxx}$ this inclusion will only change the size of δ^2. Because the numerical scheme had to satisfy the Courant-Friedrichs-Lewy condition, the sign of δ^2 is not changed.

How does one analyze (3)? It is clear that for times and distances of order one, the solution behaves as if it satisfies the linear wave equation. An initial profile decomposes into right and left-going components, each of which would travel undisturbed if it were not for the cumulative effects of the nonlinear and dispersive terms on the right-hand side of (3). How does each of these components evolve under these new influences? To see this, KZ looked for solutions of (3) in the form

$$y(x,t) = f(\xi,T) + \epsilon y^{(1)}(x,t) + \ldots . \tag{4}$$

where $\xi = x - ct$, $T = \epsilon t$, and the dependence of f on T describes how the profile $f(\xi,T)$ evolves over long distances and times of order $1/\epsilon$. The equation for $y^{(1)}$ reads,

$$y^{(1)}_{tt} - c^2 y^{(1)}_{xx} = 2cf_{\xi T} + c^2 f_\xi f_{\xi\xi} + c^2\delta^2 f_{\xi\xi\xi\xi}. \tag{5}$$

The solution $y^{(1)}$ will grow linearly with $\xi^- = x + ct$ and the asymptotic series (4) will be rendered nonuniform over long times unless the dependence of f on T is chosen to make the right-hand side of (5) zero. Setting $6q = f_\xi$, $\tau = cT/2$, one finds

$$q_\tau + 6qq_\xi + \delta^2 q_{\xi\xi\xi} = 0, \tag{6}$$

the Korteweg-deVries (KdV) equation. The hyperbolic secant-squared solution ($\delta^2 = 1$) with parameter η,

$$q = 2\eta^2 \operatorname{sech}^2 \eta(\xi - v\tau), \tag{7}$$

the infinite period limit of the cnoidal wave periodic solutions, corresponds to the solitary wave seen by Russell.

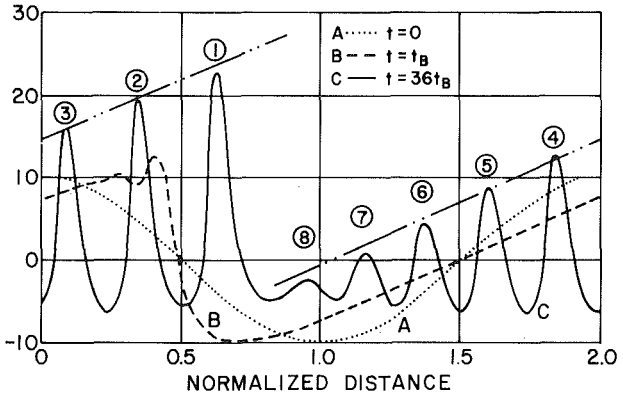


Fig. 1 The temporal development of the wave form $q(\xi)$ (from *Phys. Rev. Lett.*, Vol. 15, 1965, pp. 240-243)

At this point, it should be clear why it was necessary to introduce the second approximation to the finite difference $y_{i+1} - 2y_i + y_{i-1}$. If $\delta^2 = 0$, equation (6) has solutions that develop discontinuities in a finite time. For example, take as an initial condition $q(\xi,0) = 1/6\pi\ a \cos 2\pi\xi$ which corresponds to the initial conditions $y(x,0) = a \sin 2\pi x$, $y_t(x,0) = 0$ (remember, since $y_t(x,0) = 0$, only half the initial profile goes right). The maximum negative slope q_ξ increases monotonically from $-\pi^2 a/3$ at $t = 0$ to $-\infty$ at $t = 1/\pi^2 a\epsilon c$. Thus the naive continuum approximation to (2) breaks down. For δ^2 finite, but small, a different picture emerges. Figure 1, taken from the famous 1965 paper [6] of Zabusky and Kruskal announcing the soliton, shows the results of the KZ numerical experiment in which they use a centered difference, mass and (almost) energy-conserving scheme to solve the KdV equation (6). They used periodic boundary conditions and their starting profile was sinusoidal. Initially the negative slope steepens, then the third derivative term causes fine structure wiggles of (wavelength δ) to appear near and to the left of the maximum of q (see Fig. 1, profile B). In time the wiggles separate forming a train of pulses traveling to the right, with the largest on the right, each pulse seeming to take on a life and identity of its own and having a velocity proportional to its amplitude. These pulses each may be approximately described by the solitary wave solution (7) although strictly this is a solution valid for an isolated pulse on the infinite line. Because of the periodic boundary conditions, the solitary pulses eventually reappear on the left boundary and due to their larger velocity, the larger pulses overtake the smaller ones. At this point, the investigators noticed a remarkable phenomenon. Whereas during the interaction two pulses behaved in a most nonlinear way, afterward they reappeared with the larger one in front, each bearing precisely its former identity (height, width, and velocity). The only evidence of a collision at all was a phase shift whereby the larger one appeared to be ahead of the position it would have been had it traveled alone and the smaller one behind. If the two pulses were almost equal, the interaction seemed to take place by an exchange of identities in which the forward and smaller soliton became taller and narrower when it felt the leading edge of the larger one which then, in turn, took on the identity of the smaller one. If the two pulses were of greatly different amplitudes, the larger one rode over the smaller one in an adiabatic fashion. For amplitude differences in the inbetween range, the interaction was more complicated. In a later analysis of the interaction Lax (1968) verified these observations rigorously.

The pulses were very special indeed. They deserved and got a special name, solitons, a name intended to connote particlelike qualities. After many passes through the grid, the solitons arrive once again at the same relative spatial

Downloaded 02 May 2010 to 171.66.16.250. Redistribution subject to ASME license or copyright; see http://www.asme.org/terms/Terms_Use.cfm

positions, approximately produce the fine structure wiggles and then a gradually decreasing negative slope until the initial sinusoidal shape is almost recovered. This process is the mirror image (in both time and space) of the original break up of the initial shape. The time at which the pulses coalesce is called the recurrence time. The reason for the "almost recurrence" in such a short time is that the initial profile decomposes into relatively few soliton shapes. The approximate recurrence time is the minimum time for pulses with different constant velocities (one can improve the calculation by including the phase shifts) to arrive once again at a common point on a circle of length L. This picture is only an approximation to the exact solution for two reasons. First, as found by later work (circa 1976), for an initial profile that is analytic in ξ, the solution of (6) under periodic boundary conditions may be approximated by the so-called finite-gap potential solution which is given by the second logarithmic derivative of the Riemann Θ function of vector arguments $k_j\xi + \omega_j\tau\, j = 1, \ldots, N$, where N is the number of open gaps (see references [28 or 29]). This is equivalent to saying that for a smooth initial profile most of the energy goes into relatively few soliton states. For large N, the gap widths are exponentially small. If $j = 1$, the Θ function becomes a periodic elliptic function

$$q(\xi,\tau) = \beta + (\alpha-\beta)\,cn^2\left\{\sqrt{\frac{\alpha-\gamma}{2}}\,(\xi - 2(\alpha+\beta+\gamma)\,\tau);m^2\right\}$$

where $m^2 = (\alpha-\beta)/(\alpha-\gamma)$, $\alpha > \beta > \gamma$, and we have taken $\delta^2 = 1$. The infinite period limit, $m^2 \to 1$, is (7) with $\alpha = 2\eta^2$ when we impose the condition that $q \to 0$ at $x = \pm\infty$. Second, whereas the solution is periodic in ξ (because the initial profile is), it is only quasiperiodic in the time τ since the ω_j are not in general commensurate. A measure of the "recurrence" time, therefore, is found by taking rational approximations to the frequencies corresponding to these modes (gaps) containing significant energy. The exactness of the recurrence is then a function of the number of modes included and the chosen accuracy of the rational approximations to the frequencies.

In any event, the strange interaction properties of the solitons together with the almost recurrence property seemed more and more to indicate that, in some sense, the KdV equation was integrable. If this were the case, there should be lots of conserved quantities. However, the connection with Hamiltonian systems was far from uppermost in the minds of the investigators and the motivation for the search for conservation laws came from a different direction. Before I describe that, it is worth noting, as Zabusky has often stressed, the important and seminal role that numerical experimentation played in these discoveries. (I strongly recommend his article [10].) This was the first time in scientific history that investigators had this tremendous new power available to them. Indeed in the last few years we have seen continuing evidence that this mode of research, a combination of analysis and numerical experiment, is becoming increasingly more important in scientific discovery. The strange attractor, a new and fundamental concept in dynamics, and central to our current understanding of certain kinds of turbulence, was also discovered this way.

Now a caveat. The fact that two solitary waves of an equation preserve their form through nonlinear interaction is often taken to be both the acid test for and the definition of the soliton. I want to warn the reader that this condition is only necessary. There are equations (for example; in (54) replace D_x^4 by D_x^8) that admit two-phase solitary wave solutions, and therefore the asymptotic form of each individual solitary wave is preserved through collision, which do not possess all the ingredients for admission to the soliton class. The proper definition of a soliton involves its identification with certain of the scattering data of an eigenvalue problem. We discuss this in Section *E*. Nevertheless, the computational test of colliding two solitary waves together to check their interaction behavior is still a very useful one. A better test is to collide not only a solitary wave with another one but to test its resiliency under interaction with other special but local solutions of the equation. In the case of KdV, one might, for example, collide a solitary wave with a wave of depression.

(*D*) The Conservation Laws and the Miura Transformation

The next step forward in the series of discoveries came about as the result of an attempt to describe the solution to (6) when δ^2 is small by averaging over the wiggly fine structure parts of the solution. This procedure would not be valid for all time of course and certainly things would be modified when the finite structure separated out into the well-defined soliton train of Fig. 1(*c*). Nevertheless, it might allow one to investigate the fascinating reversible-shocklike nature of the portion of the solution where q_ξ is large. By analogy with gas dynamics, therefore, it was important to find conservation laws in order that the jump conditions across the wiggly regions could be calculated. One would need four such pieces of information (the number of characteristic velocities entering or leaving the shock plus the position of the shock itself) as opposed to the usual three of gas dynamics. Two conservation laws

$$q_t + (3q^2 + \delta^2 q_{xx})_x = 0 \tag{8}$$

$$\left(\frac{1}{2}q^2\right)_t + \left(2q^3 + \delta^2\left(qq_{xx} - \frac{1}{2}q_x^2\right)\right)_x = 0 \tag{9}$$

corresponding to conservation of mass and momentum (8) and energy (9) for water waves and to conservation of momentum and energy for the nonlinear spring were already known and Whitham, who had developed a powerful theory for investigating modulated periodic waves about this time, had found a third, the conserved density of which corresponded to Boussinesq's famous moment of instability. Zabusky and Kruskal searched for and found a fourth, and their method of search (finding equations for the coefficients of all terms of degree 4, 5, 6, etc.; degree $q = 1$, degree $\partial/\partial x = 1/2$) indicated that the equations for the coefficients at stage six were overdetermined (as they are thereafter) and, therefore, they were not particularly surprised when they did not find a conservation law at this level. However, they had made an algebraic mistake, and more than a year was to go by before they continued again on this track.

The next surge of momentum came with the arrival of Robert Miura who was asked by Kruskal to get his feet wet by searching for a conservation law at level seven. He found one and then filled in the missing sixth. Eight and nine fell quickly and Kruskal and Miura were fairly certain that there was an infinite number. However, rumors originated from the Courant Institute that nine was the limit (in fact, what investigators there had discovered was what they perceived to be a change in algebraic structure). Miura was therefore challenged to find the tenth. He did it during a two-week vacation in Canada in the summer of 1966. (There is also a rumor that he was seen about this time in Mt. Sinai, carrying all 10.) It was now clear that there was a conservation law at every level. (Each conservation law has the form $\partial U/\partial t + \partial F/\partial x = 0$; U, called the conserved density and F, the corresponding flux, can be assigned a weight by adding the power of q to half the number of $\delta\,\partial/\partial x$ operations in each term in these quantities. For example, q has weight one, $3q^2$ and $\delta^2 q_{xx}$ both have weight two, $2q^3$, $\delta^2 qq_{xx}$, and $\delta^2 q_x^2$ all have weight three and so on. Level then refers to the weight of the conserved density.) How to find them and what kind of

Downloaded 02 May 2010 to 171.66.16.250. Redistribution subject to ASME license or copyright; see http://www.asme.org/terms/Terms_Use.cfm

constraints they would impose on the solution of the KdV equation were thoughts that ran through the minds of the investigators. The original motivation for looking for conservation laws was temporarily put aside. There were suddently too many independent laws and the jump conditions (Rankine-Hugoniot relations) derived from these laws would have to be consistent with each other. Somehow, with all the new discoveries, the question did not seem to be quite as important as before.

For that matter, it is still not understood why a solid has finite heat conductivity!

Miura provided the next key [11]. He had found that the modified Korteweg-deVries equation (MKdV)

$$v_t + 6v^2 v_x + v_{xxx} = 0 \tag{10}$$

also had an apparently infinite string of conservation laws. He observed that they could be matched with their corresponding counterparts in the KdV series by the transformation (which now bears his name)

$$q = v^2 - iv_x. \tag{11}$$

From this point on, we will write x, t for ξ, τ, and take $\delta^2 = 1$. In fact, he showed that

$$q_t + 6qq_x + q_{xxx} = \left(2v - i\frac{\partial}{\partial x}\right)(v_t + 6v^2 v_x + v_{xxx}) \tag{12}$$

and therefore if $v(x,t)$ is a solution of (10), $q(x,t)$ is a solution of (6). Next, since (11) is a Riccati equation, the Miura transformation can be linearized by

$$v(x,t) = -i\frac{\phi_x}{\phi} \tag{13}$$

to the Schrödinger equation with zero energy

$$q = -\frac{\phi_{xx}}{\phi}. \tag{14}$$

Exercising the Galilean invariance of (6) suggests that nothing is changed by adding a constant velocity λ to q whence (14) becomes

$$\phi_{xx} + (\lambda + q(x,t))\phi = 0, \tag{15}$$

the stationary Schrödinger equation with potential $V(x) = -q(x;t)$ and energy $E = \lambda$. (Remark: The time variable in the time-dependent Schrödinger equation has nothing, repeat nothing, to do with the time t in the KdV equation.) The ingredients for what was to become the inverse scattering transform (IST) were now all there. At this stage, both Gardner and Greene had joined in the effort.

Before I relate this part of the story, it is worth describing Gardner's modification of the Miura transformation as it automatically includes λ and gives rise to the important idea that an infinite number of conserved quantities of one equation can be inferred from one conserved quantity of another if their solutions are related through a special kind of transformation (an example of a Bäcklund transformation). Gardner took

$$q = w + i\epsilon w_x + \epsilon^2 w^2 \tag{16}$$

and found the equivalent relation to (12)

$$q_t + 6qq_x + q_{xxx} = \left(1 + 2\epsilon^2 w + i\epsilon\frac{\partial}{\partial x}\right)(w_t + 6(w + \epsilon^2 w^2)w_x + w_{xxx}). \tag{17}$$

Now, linearize (16) with

$$w + \frac{1}{2\epsilon^2} = \frac{i}{\epsilon}\frac{\phi_x}{\phi} \tag{18}$$

whence (16) becomes

$$\phi_{xx} + \left(q + \frac{1}{4\epsilon^2}\right)\phi = 0. \tag{19}$$

Also solve w as function of q and its derivatives as an asymptotic series in ϵ for small ϵ (it turns out that the asymptotic expansion of ϕ for large λ is very important in the theory) and find

$$w = q - i\epsilon q_x - \epsilon^2(q_{xx} + q^2) + \ldots. \tag{20}$$

Since $\int w dx$ is a constant in time when the integral is taken over the infinte line (assuming q and its derivatives approach zero as $x \to \pm\infty$) or the periodic interval, so are $\int q dx$, $\int q^2 dx$ $\int (q^3 - 1/2\ q_x^2) dx$, etc. One can also capture the infinite set of conservation laws for KdV from the first one for the equation $w_t + 6(w + \epsilon^2 w^2)w_x + w_{xxx} = 0$.

(E) The Inverse Scattering Transform (IST) [12]

Given (15) it was now natural to ask: if the potential $-q(x,t)$ evolves according to the KdV equation

$$q_t + 6qq_x + q_{xxx} = 0, \tag{21}$$

how do $\lambda(t)$ and $\phi(x,t)$ evolve? We consider the whole real line $-\infty < x < \infty$, with q and its derivatives vanishing at $\pm\infty$. This can be done by direct computation by substitution of q from (15) into (21). One finds by direct calculation that

$$\lambda_t \phi^2 + (\phi Q_x - \phi_x Q)_x = 0 \tag{22}$$

where $Q = \phi_t + \phi_{xxx} - 3(\lambda - q)\phi_x$. If ϕ vanishes as $x \to \pm\infty$ and is square integrable, then $\lambda_t = 0$. Thus the discrete eigenvalues $\lambda_n < 0$, $n = 1, 2, \ldots N$ of (15) are constants of the motion. From the remaining part of (22) we find,

$$\phi_t + \phi_{xxx} - 3(\lambda - q)\phi_x = C\phi + D\int \frac{dx}{\phi^2} \tag{23}$$

and since ϕ vanishes at $\pm\infty$, $D = 0$. We choose to normalize the bound state eigenfunction ϕ_n so that $\phi_n \sim e^{\sqrt{-\lambda_n}x}$ as $x \to -\infty$. Thus $C_n = 4(-\lambda_n)^{3/2}$ and if $\phi_n \sim b_n(t)e^{-\sqrt{-\lambda_n}x}$ as $x \to +\infty$,

$$b_{nt} = 8(-\lambda_n)^{3/2} b_n \tag{24}$$

and $b_n(t) = b_n(0)e^{8(-\lambda_n)^{3/2}t}$. For $\lambda = \zeta^2 > 0$, a solution of equation (15) for large $|x|$ is a linear combination of $e^{\pm i\zeta x}$. We impose on ϕ the boundary conditions

$$\phi \sim e^{-i\zeta x} + R(\zeta,t)e^{i\zeta x} \quad \text{as} \quad x \to \infty, \tag{25a}$$

$$\sim T(\zeta,t)e^{-i\zeta x}, \quad x \to -\infty. \tag{25b}$$

In the usual quantum mechanical interpretation of (15) the coefficients of unity in (25a) and (implied) zero in (25b) indicate prescribed steady radiation coming from $x = +\infty$ only. The coefficients of transmission $T(\zeta,t)$ and reflection $R(\zeta,t)$ can be shown to satisfy $|T|^2 + |R|^2 = 1$. The spectrum for $\lambda > 0$ is continuous and we may choose λ constant, so that again (23) is valid provided $D = 0$. Because of the way ϕ is normalized at $+\infty$, $C = 4i\zeta^3$. Inserting (25a,b) we find in addition

$$T_t(\zeta,t) = 0, \quad R_t(\zeta,t) = 8i\zeta^3 R(\zeta,t) \tag{26}$$

which means that the transmission coefficient as function of ζ is a constant of the motion and the reflection coefficient $R(\zeta,t)$ evolves by simply changing its phase linearly with time.

It was known from the early 1950s that the potential $-q(x)$ of Schrödinger's equation can be completely recovered from a knowledge of what is called the scattering data,

$$S = \{(\lambda_n, b_n)_1^N; R(\zeta), \zeta \text{ real}\}. \tag{27}$$

From S, the transmission coefficient $T(\zeta)$ can also be found. But if S is known from $q(x,0)$ at $t = 0$, then (24) and (26) allow us to calculate $S(t)$ in a very simple manner. Hence $q(x,t)$ can be reconstructed at any arbitrary time. The prescription for the reconstruction involves a linear integral equation, the Gel'fand-Levitan-Marcenko equation. This and

Downloaded 02 May 2010 to 171.66.16.250. Redistribution subject to ASME license or copyright; see http://www.asme.org/terms/Terms_Use.cfm

many other details can be found in [12]. For now, let us just remark that the general solution of (21) involves several components. The solitons, which propagate with positive velocity, are the physical manifestation of the discrete spectrum, one soliton for each eigenvalue. In isolation (at $t = \pm\infty$), each soliton has a height, width, and speed proportional to $-\lambda_n$, $\sqrt{-\lambda_n}$, and $-\lambda_n$, respectively. Its position at any time can be calculated from b_n. The continuous spectrum gives rise to a component of the solution which, although nonlinear, bears a close resemblance to the solution of the linearized equation (32). The amplitude of the wave group associated with wave number ζ is measured by $|R(\zeta)|$, its position by Arg $R(\zeta)$. The region around $x = 0$ joining these two solution components involves among other things the self-similar solution of (21) and is complicated but it basically plays the role of a nonlinear Airy function. (John Greene liked to attach a moral-religious categorization to the two solution components; the solitons were the soul of the solution while the continuous spectrum gave rise to the mortal flesh. I suppose it depends on your point of view which component deserves to be called good.) If one thinks of the various solution components as normal modes of the nonlinear system and this thinking is useful, then one can single out the soliton mode as special because it is totally new and has no linear analogue.

The essence, then, of the application of IST is as follows. The equation of interest

$$q_t + 6qq_x + q_{xxx} = 0 \tag{28}$$

is written as the integrability condition of two linear equations

$$(-L+\lambda)\phi \equiv \phi_{xx} + (\lambda + q(x,t))\phi = 0 \tag{29}$$

and

$$\phi_t = B\phi = -4\phi_{xxx} - 3q_x\phi - 6q\phi_x + C\phi \tag{30a}$$

$$= (q_x + C)\phi + 4(\lambda - q/2)\phi_x \tag{30b}$$

(where C is determined once a normalization is chosen for $\phi(x,t;\zeta)$). Then $q(x,0)$ is mapped into the scattering data $S(0)$ of (29). The evolution of $S(t)$ is simple and linear. From a knowledge of $S(t)$, we reconstruct $q(x,t)$. Schematically,

$$\begin{array}{ccc} q(x,0) & \xrightarrow{\text{direct transform}} & S(0) \\ & & \Big\downarrow \text{time evolution of Sc. data} \\ q(x,t) & \xleftarrow{\text{inverse transform}} & S(t). \end{array} \tag{31}$$

The procedure is completely analogous to the way in which one would solve the linearized version of (28)

$$q_t + q_{xxx} = 0 \tag{32}$$

by the Fourier transform. Here the direct transform is

$$b(k,t) = \frac{1}{2\pi}\int_{-\infty}^{\infty} q(x,t)e^{-ikx}dx, \tag{33}$$

and $b(k,0)$ is known once $q(x,0)$ is given; the time evolution of $b(k,t)$ is

$$b_t(k,t) = ik^3 b(k,t); \tag{34}$$

the inverse transform is

$$q(x,t) = \int_{-\infty}^{\infty} b(k,t)e^{ikx}dk. \tag{35}$$

Indeed, we will show that IST, in the linear limit, reduces to the Fourier transform.

We also know that we can interpret both equations (28) and (32) as infinite dimensional Hamiltonian systems; we may write each formally as

$$q_t = \frac{\partial}{\partial x}\frac{\delta H}{\delta q} \tag{36}$$

where $\delta/\delta q$ is the variational derivative of the Hamiltonian functional $H[q]$, i.e.,

$$\lim_{\epsilon\to 0}\frac{1}{\epsilon}\left(H[q+\epsilon\delta q] - H[q]\right) = \int_{-\infty}^{\infty}\frac{\delta H}{\delta q}\delta q dx\Big).$$

Equation (36) is analogous to the expression

$$z^{\cdot} = J\nabla H(z) \tag{37}$$

valid for finite dimensional systems. Here z is a $2N$-vector (e.g., $q_1, \ldots, q_N\, p_1, \ldots, p_N$), J a skew-symmetric matrix (e.g., $\begin{pmatrix} 0 & I_N \\ -I_N & 0 \end{pmatrix}$), and ∇ the gradient $(\partial/\partial q_1, \ldots, \partial/\partial p_N)$. In (36), $q(x)$ should be considered as an infinite dimensional vector, $\partial/\partial x$ a skew-symmetric operator instead of a matrix and $\delta/\delta q$ a variational derivative replacing the gradient. The corresponding two form $\Sigma\delta q_i \wedge \delta p_i$ which is preserved under the flow is

$$\frac{1}{2}\int_{-\infty}^{\infty}\delta q(x)\wedge\left(\int_{-\infty}^{x}\delta q(y)dy\right)dx. \tag{38}$$

For (1.28), the Hamiltonian $H = \int_{-\infty}^{\infty}(1/2\, q_x^2 - q^3)dx$; for (32), $H = \int_{-\infty}^{\infty} 1/2\, q_x^2\, dx$. The Fourier transform (33) is a canonical transformation which carries the old coordinates $(q(x), -\infty < x < \infty)$ to new ones $A = 2\pi|b|^2/k$, $\theta =$ Arg $b(k,t)$ in which the two form (38)

$$\frac{1}{2}\int_{-\infty}^{\infty}\left(\delta q\wedge\int_{-\infty}^{x}\delta q\right)dx = \int_0^{\infty}\delta A(k)\wedge\delta\theta(k)dk \tag{39}$$

is preserved. (The reader should prove (39) for himself; for those unfamiliar with the wedge notation, $\delta q \wedge \delta w$ means $\delta_1 q\delta_2 w - \delta_2 q\delta_1 w$ where δ_1 and δ_2 are independent variations.) Since $w_x = q$, one should not think of $q(x)$ and $w(x) = \int_{-\infty}^{x} q(y)dy$ as conjugate variables; rather one should read (38) as the continuous limit of $1/2\ \Sigma_i\delta q_i \wedge \Sigma_{j<i}\delta q_j$. On the other hand, the new coordinates A and θ are conjugate variables. From (34),

$$A_t = 0, \quad \theta_t = k^3$$

which are Hamiltons' equations

$$A_t = -\frac{\partial H}{\partial\theta}, \quad \theta_t = \frac{\delta H}{\delta A}$$

where $H = 1/2\int_{-\infty}^{\infty} q_x^2 dx = 1/2\int_0^{\infty} k^3A^2(k)dk$. In an exactly analogous way, IST is a canonical transformation which carries the old coordinates $(q(x), -\infty < x < \infty)$ to the new ones which are the scattering data S given by (27).

Gardner [13] was the first to note that the KdV equation could be written in a Hamiltonian framework. Later, Zakharov and Faddeev showed how it could be interpreted as a completely integrable Hamiltonian system. For a finite dimensional system of $2N$ dimensions, the term *completely integrable* means that the system possesses N independent constants of the motion $F_j(p,q)$ $(p = (p_1, \ldots, p_N), q = (q_1, \ldots, q_N)), j = 1, \ldots, N$ which are in involution with respect to the Poisson bracket. From this beginning, one can define N action variables (as functions of the F_j) and N corresponding angle variables. For infinite dimensional systems, things are more formal. In this context, we will use the term completely integrable to mean that an infinite number of new coordinates can be found analogous to action-angle variables such that the former are constants of the motion and the latter vary linearly with time. As the reader may have already guessed, the action coordinates are functions of the infinite set of conserved densities.

Let me make a further remark on the time dependence of the transformed variables and point out the sense in which the infinite line problem for (28), $(q(x,t) \to 0, x \to \pm\infty$, all $t)$ is simpler than the periodic problem $(q(x,t) = q(x+P,t)$ all x

Downloaded 02 May 2010 to 171.66.16.250. Redistribution subject to ASME license or copyright; see http://www.asme.org/terms/Terms_Use.cfm

and t). In the former, we know q at two points of the interval, namely $x = \pm\infty$, for all time. Indeed, the scattering data are a measure of how the asymptotic solutions of (29) ($e^{+i\sqrt{\lambda}x}$) change as x traverses the potential between $-\infty$ and $+\infty$. From (30), one can see that at $\pm\infty$, the time dependence of $\phi(\infty,t;\zeta)$ is independent of q as q and its derivatives are zero there. In the latter problem, the periodic problem, q is not known for all time at any point on the interval $[0,P]$. Consequently, the time dependence of the scattering data is much more complicated.

Both these cases contrast with the way in which Burgers' equation $u_t = u_{xx} + 2uu_x$ is linearized. There the equation can be written as the integrability condition of $\phi_x = u$ and $\phi_t = (u^2 + u_x)\phi$. Whereas it seems that the evolution of $\phi(x,t)$ depends on a knowledge of $u(x,t)$, this is not really the case as $(u^2 + u_x)\phi = \phi_{xx}$. Therefore, under the transformation $\phi_x = u\phi$, ϕ satisfies the linear heat equation. In the case of KdV on the infinite line, the equation for $\phi(x,t;\lambda)$ does not linearize; instead there is a free parameter λ and (28) is the integrability condition for (29) and (30) for all λ. So instead of knowing $\phi(x,t;\lambda)$ for all x and t, we know it for all t and λ at $x = \pm\infty$.

(F) The Lax Equation [14]

Despite the fact that the time dependence of the angle variable is more complicated, both the finite line and periodic problems show the key property that as $q(x,t)$ evolves according to (28) the spectrum of L of (29) (considered as an operator on $L^2(R)$ ($R = (-\infty, \infty)$ or $(0,P)$), does not change. This property was expressed in an elegant manner by Lax (1968) in the same paper in which he examined the two soliton interaction. He noted that if $L(t)$ (here self-adjoint) and $L(0)$ share the same spectrum, they are unitarily equivalent; that is, there exists a unitary operator U ($UU^* = U^*U = I$, the identity) such that

$$L(t)U(t) = U(t)L(0). \tag{41}$$

Thus if $\phi(x,0;\lambda)$ is an eigenfunction of $L = -d^2/dx^2 - q(x)$ at $t = 0$ with eigenvalue λ, then $\phi(x,t;\lambda) = U(t)\phi(x,0;\lambda)$ is the eigenfunction of $L(t)$ with the same eigenvalue. We see this directly from (41) since $L(t)U(t)\phi(x,0;\lambda) = \lambda U(t)\phi(x,0;\lambda)$. Differentiating (41) with respect to times gives us that

$$L_t = BL - LB = [B,L] \tag{42}$$

where $B = U_tU^*$ is skew-adjoint. Equation (42) is called Lax's equation and L and B are called a Lax pair. Note that B can be obtained by recognizing that $\phi_t(x,t;\lambda) = U_t\phi(x,0;\lambda) = U_tU^*\phi(x,t;\lambda)$ so in the case of KdV, from (30) we read off B as [recall $\lambda\phi_x = -\phi_{xxx} - (q\phi)_x$]

$$B = -4\frac{\partial^3}{\partial x^3} - 3\left(q\frac{\partial}{\partial x} + \frac{\partial}{\partial x}q\right) + C. \tag{43}$$

It turns out that all the solvable equations like KdV can be expressed in Lax form. Indeed Lax showed that there was an infinite sequence of B's, one connected with each odd order of $\partial/\partial x$, and therefore an infinite family of flows q_t under which the spectrum of L is preserved. Formulas for these are given in [12, 23]. The reader might verify directly that (42) is indeed equation (21).

(G) Simultaneous Developments in Nonlinear Optics and Bäcklund Transformations

At approximately the same time as these advances were being made, the soliton made its appearance in a totally new context, the propagation of ultrashort (10^{-12} sec) optical pulses in resonant media. In 1967, McCall and Hahn [15] discovered the phenomenon of self-induced transparency, an effect whereby the leading edge of a pulse is used to invert an atomic population while the trailing edge returns the population to its initial state by stimulated emission. This process is realizable if it takes place in a time short compared to the phase memory time of the medium and also if the pulse has sufficient intensity to cause the population inversion. If we assume a medium of nondegenerate two level atoms and neglect the effects of inhomogeneous broadening (the mismatch, due to Doppler shifting, between the carrier frequency of the incoming pulse and the energy difference of the two levels), then the process can be described in terms of a single field equation, the sine-Gordon equation

$$u_{xt} = \sin u, \tag{44}$$

where x measures distance from the beginning of the medium, t is the (retarded) time and the electric field envelope $E(x,t)$ is proportional to $\partial u/\partial x$.

This equation had been known for a long time. It had been studied long ago in connection with the theory of surfaces of constant negative curvature. In particular, A. V. Bäcklund (see [16]) had discovered that a new solution (or surface) $u_1(x,t)$ could be found in terms of an old one $u_0(x,t)$ by the transformation

$$u_{1x} - u_{0x} = 4i\zeta \sin\frac{u_1 + u_0}{2} \tag{45a}$$

$$u_{1t} + u_{0t} = \frac{1}{i\zeta}\sin\frac{u_1 - u_0}{2}. \tag{45b}$$

Such transformations are known as Bäcklund transformations (see [53] for a definition) and allow multisoliton solutions to be constructed in a fairly simple manner. For example, take $u_0 = 0$; then integrating (45) we find

$$u_1 = \pm 4\tan^{-1}\exp(-2\eta x - t/2\eta). \tag{46}$$

which describes a pulse u for which the corresponding electric field envelope E is equal to $4\eta\,\mathrm{sech}(2\eta x + t/2\eta)$ and the area $\int_{-\infty}^{\infty} E dx = u(\infty) - u(-\infty)$ is equal to 2π. These pulses are known as 2π pulses, and are called kinks (antikinks) if u increases (decreases) by 2π as x goes from $-\infty$ to $+\infty$. More complicated solutions can also be found by ladder process, a theorem of permutability attributed to Bianchi, which may be written

$$\tan\frac{u_3 - u_0}{4} = \frac{\zeta_1 + \zeta_2}{\zeta_1 - \zeta_2}\tan\frac{u_1 - u_2}{4}. \tag{47}$$

(I will leave the derivations of this as an exercise to the reader.) The more complicated solutions are known as $\underline{0\pi}$ (u goes from 0 at $-\infty$, to 2π and back to 0 at $+\infty$; this pulse is effectively a superposition of a kink and antikink) and $\underline{4\pi}$ (superposition of two kinks) pulses.

Just as in the case of the Korteweg-deVries equation, the sine-Gordon equation arises in a variety of contexts:

(1) as a model for dislocation in crystals (in which context Seeger, Donth and Kochendorfer [17] used the Bäcklund transformation to obtain the 2π pulse as early as 1953);

(2) as a model field theory (we have already referred to the work of Perring and Skyrme [18]); and

(3) in superconductivity where u describes the difference in the phases of the wave functions across a Josephson junction (see [19]).

It also describes a readily visualized mechanical model proposed by Scott which consists of a string of pendula suspended from and free to turn about a horizontal torsion wire. In this context $u(X,T)$ is the angle of twist measured from the vertical, and with $x = (X+T)/2$, $t = (X-T)/2$, (42) takes the form

Downloaded 02 May 2010 to 171.66.16.250. Redistribution subject to ASME license or copyright; see http://www.asme.org/terms/Terms_Use.cfm

$$u_{TT} - u_{XX} + \sin u = 0. \tag{48}$$

A kink is an anticlockwise twist of angle 2π; an antikink has the opposite orientation.

I do not want to leave the topic of the sine-Gordon equation without noting the important contributions that George Lamb has made to the subject. In a sequence of several papers, culminating with his 1971 article [20] in *Reviews of Modern Physics*, he elaborated on and discussed the physical relevance of the multisoliton and self-similar solutions of the sine-Gordon equation. He foresaw that the sine-Gordon equation was a sister under the skin to the Korteweg-deVries equation. Indeed, he independently discovered the inverse method for its solution. It is fitting, I think, to pay tribute to a modest man, a rare breed, a man who even resisted the urge to recount his accomplishments in his own book [47]. He only lists one of his own references.

(*H*) Soliton Factories and Later Developments of the 70s

With all the ingredients out on the table as early as 1967, it was somewhat surprising that it took five years to take the KdV equation out of its integrable isolation. Some felt that it was a fluke, a clever transformation somewhat akin to the Hopf-Cole transformation; see also Forsythe, Vol. 6, p. 100 where the linearization of Burgers' equation is given as an exercise. Then in 1972 (published in 1971 in the Soviet Union), Zakharov and Shabat [21] found the Lax pair for the nonlinear Schrödinger equation, another universal equation about which a lot more is written [50]. The Zakharov-Shabat result, the Potsdam conference of 1972, and the lectures of Kruskal on the sine-Gordon equation unleashed a great tide of energy on these problems. Wadati [22] discovered the setting in which to solve the modified Korteweg-deVries (MKdV) equation. Ablowitz, Kaup, Newell, and Segur (AKNS), [23] motivated by several key observations by Kruskal, solved the sine-Gordon equation (independently solved by Lamb and, a little later, by Faddeev and Takhtajan) and, soon thereafter, showed how to write the full set of equations (the AKNS hierarchy) solvable through the use of the Zakharov-Shabat eigenvalue problem

$$\begin{aligned} v_{1x} + i\zeta v_1 &= q(x,t)v_2, \\ v_{2x} - i\zeta v_2 &= r(x,t)v_1. \end{aligned} \tag{49}$$

By this time, it had become clear how to begin with any eigenvalue problem and write the evolution equations which kept its spectrum invariant. Soliton factories sprang up all over the world.

Tougher problems were handled. The Toda lattice (see [24]),

$$u_{ntt} = e^{u_{n+1}-u_n} - e^{u_n - u_{n-1}}, \tag{50}$$

was shown to be an intergrable model (Flaschka; Henon). It played the same seminal role for other classes of nonlinear partial difference equations which KdV did for partial differential equations.

The periodic problem for KdV was solved in several stages by several authors about and after 1976. The first discovery was the so-called finite-gap solution in which the periodic and antiperiodic spectrum of (29) with periodic potential $q(x)$ (Hill's equation) consists of $(2n + 1)$ simple eigenvalues λ_0, $\lambda_1, \ldots, \lambda_{2n}$ with remaining ones all double (McKean and van Moerbecke, [25], Novikov [26], Its and Matveev [27], and Kricever [28]). The infinite gap limit was treated by McKean and Trubowitz [29]. Many of the discoveries turned out to be rediscoveries of earlier work of Baker, Drach, Burchnall, and Chaundy [30].

Lax pairs were also found for problems with spatial dimension more than one. In particular we will discuss some results concerning the Kadomtsev-Petviashvili (KP) equation

$$\pm q_{yy} + (q_t + 6qq_x + q_{xxx})_x = 0 \tag{51}$$

(a weakly two-dimensional Korteweg-deVries equation). The initial value problem for this equation is very complicated and has only recently been solved (Manakov [31], Ablowitz, Fokas, Segur [32]). The instanton, the soliton of the self-dual Yang-Mills equations has also been found, and a construction of a k-parameter instanton solution has been given by Atiyah, Hitchin, Drinfeld, and Manin [33]. Several other field equations, important in nonlinear physics, have been found to be integrable.

Before I conclude this section, I want to tell you a bit about a giant in the field, V. E. Zakharov. He has contributed in so many areas, the Zakharov equations of plasma physics, his papers with Shabat outlining for the first time a general prescription for handling Lax pairs for equations with more than one spatial dimension, his work on the self-focusing singularity, and his paper in the Bullough-Caudrey volume (see references on the method of "dressing" (building hierarchies of solutions)). He seems to have the knack of getting to all of the good problems first. He is a genius, brilliant and intuitive. A wild bull of a man of great good humor and appetites, he has a deep and abiding love and need for poetry and literature as well as for physics. On one of our few meetings, he recited and acted out with great relish the opening scene from Macbeth. You will often come across his name.

(*I*) Soliton Miracles and the Need for a Unifying Point of View

A whole new world of integrable systems had been discovered together with constructive methods (IST, Bäcklund transformations, Hirota's method) for obtaining solutions. Hirota's method [34], which I have not yet mentioned, is quite ingenious. For the KdV equation, one sets

$$q(x,t) = 2\partial^2/\partial x^2 \ln \tau(x,t) \tag{52}$$

and obtains a quadratic equation for $\tau(x,t)$

$$\tau\tau_{xt} - \tau_x\tau_t + \tau_{xxxx} - 4\tau_x\tau_{xxx} + 3\tau_{xx}^2 = 0 \tag{53}$$

which Hirota rewrote in terms of a new differential operator which he introduced as

$$(D_tD_x + D_x^4)\tau\cdot\tau = 0. \tag{54}$$

See [34] for an explanation of the symbols. From (53), equation (54) N-soliton (and rational) solutions could be found simply by letting $\tau(x,t)$ be the sum of exponentials with phases linear in x and t and depending on arbitrary constants (which turn out to be the phase-shifts mentioned previously). For $N > 2$, the equations for the constants are overdetermined but consistent. What is it that brings about this consistency? The equaion $(D_xD_t + D_x^6)\tau\cdot\tau = 0$ has similar properties. But $(D_xD_t + D_x^8)\tau\cdot\tau = 0$ has only two-phase solitary wave solutions.

The Hirota method was once thought to be merely an ingenious device for finding solutions to soliton equations. In fact, the working definition of a system's integrability was taken to be: "send your equation to Hirota; if you get it back solved within three weeks, then it's integrable!" However, recent connections with quantum field theory and statistical mechanics indicates that Hirota's method plays a much more central role in the theory than heretofore believed. In [38], we indicate one way in which it ties in very naturally with the general theory. I believe it also clearly relates to the Painlevé property enjoyed by integrable systems. This property, which is discussed in [35], says that the only singularities of integrable systems which are not fixed, but depend on initial data, are poles. This is almost equivalent (not quite, since there are fixed singularities with ugly natures) to saying that

Downloaded 02 May 2010 to 171.66.16.250. Redistribution subject to ASME license or copyright; see http://www.asme.org/terms/Terms_Use.cfm

the Hirota $\tau(x,t)$ function is analytic in each of its variables. Certainly, for certain solution classes, it will be.

What, then, is the general theory? What is the unifying structure that ties all of the miracles that happen in soliton mathematics together? The miracles include: an infinite number of conservation laws, membership in an infinite family of commuting flows, a Hamiltonian structure, the Hirota formulation and the τ-function, the Painlevé property, the association with a linear eigenvalue problem, inverse scattering, isospectral, iso Riemann surface, isomonodromic deformations (see [26, 28, 37, 38, 39, 54]), and Bäcklund transformations.

The connecting link, I believe, comes from asking the question: given an evolution equation, how does one determine whether it is integrable and possesses all these remarkable properties? The first investigators to give a (reasonably) rational way of answering this question were Wahlquist and Estabrook [36]. In essence, they try to force the nonlinear equation of interest to be an integrability condition of two linear equations containing the unknown variable and its x derivatives as coefficients. In doing so, they obtain an infinite dimensional algebra or, to put it another way, a set of commutation relations that is not closed.

It is our contention (and my colleagues in these endeavors are Hermann Flaschka and Tudor Ratiu) that what the Wahlquist-Estabrook method is trying to tell us that the appropriate phase space on which all the flows live is an infinite dimensional Lie algebra, which for problems in one spatial dimension is isomorphic to a Kac-Moody algebra. This algebra can be written as a direct sum of two subalgebras, K and N. On the dual of N, a Poisson bracket and a Hamiltonian vector field can be defined. There is also a specific class of Hamiltonians which gives rise to an infinite set of commuting flows. From this starting point, many of the other features on the miracles list fall out as natural consequences. Our work is complementary to recent work by an active group at Kyoto (M. Sato, T. Miwa, M. Jimbo, Y. Sato, M. Kashiwara, and E. Date) and by G. Wilson and G. Segal at Oxford University.

(J) Small-Amplitude Long Waves in a Channel of Slowly Changing Depth. Equations of the KdV Type [41]–[43]

In this final section, we return to the model that started the whole business. The plan is to give a careful derivation of the KdV equation for the case or water waves. Following Johnson's derivation [44], we will also include the effects of a slowly varying depth and comment on how to attack the resulting perturbed KdV equation. Several remarks on the Boussinesq (bidirectional) equation and Kadomtesv-Petviashvili (weakly two-dimensional KdV) will close out the section.

Consider the following situation shown in Fig. 2. (The amplitude and horizontal length scales of the disturbance are greatly amplified and diminished, respectively, so that everything will fit in the picture.) Assume a two-dimensional, vorticity-free fluid with velocity field $\mathbf{u}(x,y,t)$ in a simply connected domain bounded by a time-independent lower boundary $y = -H(x)$ and a free boundary $y = h_0 + N(x,t)$. The conditions at the ends $x = -\infty, +\infty$ will be left unspecified for the moment but we will imagine that at these points the bottom boundary levels out to a constant depth. We introduce a velocity potential $\phi(x,y,t)$ given by $\mathbf{u} = \nabla\phi$.

We also assume that the disturbance in which we are interested has the following features. Its horizontal length l is large when compared to the average depth h_0; in fact $h_0^2/l^2 = \epsilon << 1$. Its amplitude a is small compared with the average depth h_0 i.e., $a/h_0 = \mu << 1$. The phenomena of interest to us occur when these two scales balance. The distance over which the bottom boundary changes significantly (by order one) is greater than l. With these rules in mind we scale the independent and dependent variables as follows:

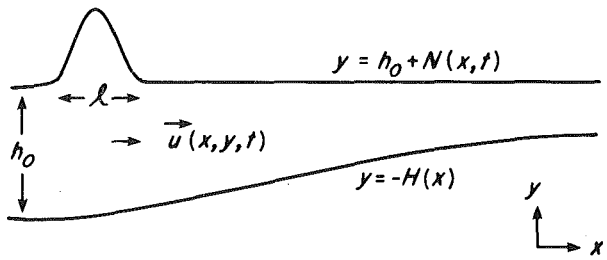


Fig. 2 Solitary wave propagating in a channel of changing depth

$$x \to lx, \quad y \to h_0 y, \quad t \to \frac{\sqrt{gh_0}}{l} t \tag{55}$$

$$H \to h_0 h, \quad N = a\eta, \quad \phi \to \frac{a}{h_0} l\sqrt{gh_0}\,\phi.$$

Here g is gravity and, consistent with the last sentence, we assume $h_x = \epsilon h_X$, $X = \epsilon x$ and h_X is at most order one. With these scalings, the equations of continuity, the boundary condition on normal velocity at $y = -h$, the continuity of normal stress (pressure) at the free surface (use Bernoulli's equation), and the free surface condition that equates the normal velocity of a particle at the surface with the normal velocity of the surface are (subscripts denote partial derivatives)

$$\phi_{yy} + \epsilon\phi_{xx} = 0 \tag{56}$$

$$\phi_y = -\epsilon^2 h_X \phi_x, \quad y = -h, \tag{57}$$

$$\phi_t + \eta + \frac{1}{2}\mu\phi_x^2 + \frac{1}{2}\frac{\mu}{\epsilon}\phi_y^2 = 0, \quad y = 1 + \mu\eta \tag{58}$$

$$\eta_t + \mu\phi_x\eta_x = \frac{1}{\epsilon}\phi_y, \quad y = 1 + \mu\eta. \tag{59}$$

The equations are solved by recognizing that (56) admits power series solutions in y (actually $y + h$ is more convenient) and we find, after using (57)

$$\phi(x,y,t) = F(x,t) - \frac{\epsilon}{2}F_{xx}(y+h)^2$$

$$+ \epsilon^2\left(\frac{1}{24}F_{xxxx}(y+h)^4 - h_X F_x (y+h)\right) + \ldots . \tag{60}$$

Let us first derive the shallow water equations which are found by letting $\epsilon \to 0$, μ finite. From (60)

$$\frac{1}{\epsilon}\phi_y = -F_{xx}(1 + \mu\eta + h) - F_x h_x$$

where we have written h_x for ϵh_X.

Now we can take limit $\epsilon \to 0$ and setting $\phi_x = u$, we have for (58) and (59)

$$\begin{aligned} u_t + \mu u u_x + \eta_x &= 0, \\ \eta_t + ((1 + h + \mu\eta)u)_x &= 0, \end{aligned} \tag{61}$$

the shallow water equations (in the lattice model, this limit corresponds to taking the distance between the masses to be zero). It is well known that, for most initial conditions, shocklike structures, where η_v and u_x become infinite in finite time, are encountered.

However the limit of interest to us is when nonlinearity measured by μ and dispersion measured by ϵ are both small and balance. Setting $\mu = \epsilon$ and expanding (58) and (59) about $y = 1$, we find,

$$\phi_t + \eta + \frac{1}{2}\epsilon\phi_x^2 = 0, \quad y = 1 \tag{62}$$

Downloaded 02 May 2010 to 171.66.16.250. Redistribution subject to ASME license or copyright; see http://www.asme.org/terms/Terms_Use.cfm

$$\eta_t + \epsilon(\phi_x \eta)_x = \frac{1}{\epsilon}\phi_y, \quad y=1, \tag{63}$$

where now

$$\frac{1}{\epsilon}\phi_y = -F_{xx}(1+h) + \frac{\epsilon}{6}F_{xxxx}(1+h)^3 - \epsilon F_x h_X.$$

The fundamental difference between the two limits is that dispersion in the form of higher order derivatives on F has been introduced at a level that can balance the tendency of the wave to break. Writing $u = F_x$ (u is only the horizontal component of velocity to leading order since $\phi_x = F_x - \epsilon/2 (y+h)^2 F_{xxx} + 0(\epsilon^2)$), we have after taking the x derivative of (62) and neglecting terms of order ϵ^2,

$$u_t + \eta_x = \epsilon\left(\frac{1}{2}D^2 u_{xxt} - uu_x\right), \tag{64}$$

$$\eta_t + (Du)_x = \epsilon\left(\frac{1}{6}D^3 u_{xxx} - (u\eta)_x\right). \tag{65}$$

(Remember $\phi_x(y=1) = u - \epsilon h^2/2\, u_{xx} + 0(\epsilon^2)$.) While these equations are the starting point for analyzing the flows that have both left and right-going components, one can obtain the simpler KdV limit by seeking solutions to (64) and (65), which are unidirectional, either right-going or left-going, waves. It is vital that we use the correct characteristics, which are

$$\theta_\pm = \mp t + \frac{1}{\epsilon}\int^X \frac{dx}{D^{1/2}} \tag{66}$$

where $X = \epsilon x$. We can make a single equation for F out of (64) and (65) by integrating (64) or solving (62)

$$\eta = -\phi_t - \frac{1}{2}\epsilon\phi_x^2.$$

Substituting (60) into (65), we obtain

$$F_{tt} - (DF_x)_x = -2\epsilon F_x F_{xt} - \epsilon F_t F_{xx} + \epsilon\frac{D^3}{3}F_{xxxx}. \tag{67}$$

It is now straightforward to derive the equation that describes the long distance behavior of F. As a first try, let us take $D = 1$. Then solve (67) iteratively in a manner akin to what was done in Section C. Let $F = f + \epsilon F_1 + \ldots$ where f is assumed to be a function of $\theta_+ = -t + x$ and $X = \epsilon x$. To suppress secular growth (proportional to $\theta = t + x$) in F_1, we must choose f as function of X and $\theta_+ = \theta$ to satisfy

$$2f_{\theta X} + 3f_\theta f_{\theta\theta} + \frac{1}{3}f_{\theta\theta\theta\theta} = 0. \tag{68}$$

Now if D is not constant but depends on $X = \epsilon x$, we proceed exactly as before except that it is crucial to use the correct characteristic coordinates Θ_+ and Θ_- as given by (66). I will leave it as an exercise to the reader to show that in order to suppress secular growth in F_1, where $F = f(\Theta_+, X) + \epsilon F_1 + \ldots$, we must choose

$$q_\tau + 6qq_\Theta + q_{\Theta\Theta\Theta} = -\frac{9}{4}\frac{D_\tau}{D}q \tag{69}$$

where we have written θ_+ as θ,

$$f_\Theta = \frac{2}{3}D^2 q, \tag{70}$$

and τ is a rescaled distance coordinate

$$\tau = \frac{1}{6}\int^X D^{1/2}\, dX. \tag{71}$$

We call (69) the perturbed KdV equation or PKdV.

Several remarks are in order. First, notice how we choose to write the equation as an evolution in x rather than t for a profile $q(\tau,\theta)$ which depends on the (negative) retarded time $\Theta = -t + 1/\epsilon\int^X dx/D^{1/2}$. If D were constant, it would have been equally convenient to use either t (as we did in Section C) or x in this role. Here, because the medium itself depends on x, it is necessary to use the latter. The particular problem we are going to analyze in some detail later is posed as follows: given q at $x = 0$ as function of t for all time and that $q \to 0$ as $t \to \pm\infty$, find $q(x,t)$ for all $x \geq 0$.

Second, we point out that to treat the term on the right-hand side of (69) as a perturbation, we must take D_X/D to be of order $\sigma << 1$. But, recalling that we have already omitted terms of order ϵ^2 from the equations (64) and (65) we insist that

$$\epsilon << \sigma << 1. \tag{72}$$

Third, let us look at the mass flux through a given station x for all time. From the equations themselves we know

$$\frac{\partial}{\partial x}\int_{-h}^{1+\epsilon\eta} \tilde{u}dy = -\eta_t \tag{73}$$

where $\tilde{u} = \phi_x$ is the true horizontal velocity. Thus if no net mass is added between $t = -\infty$ and $+\infty$, we have that

$$\frac{\partial}{\partial x}\int_{-\infty}^{\infty} dt\left(\int_{-h}^{1+\epsilon\eta}\tilde{u}dy\right) = 0 \tag{74}$$

and, to leading order, this means that

$$\frac{\partial}{\partial x}\int_{-\infty}^{\infty} Du dt = 0, \tag{75}$$

with $u = F_x$. Now note from (69) that

$$\frac{\partial}{\partial \tau}\int_{-\infty}^{\infty} D^{9/4} q d\theta = 0 \tag{76}$$

or, converting to x, t coordinates,

$$\frac{\partial}{\partial x}\int_{-\infty}^{\infty} D^{3/4} u dt = 0. \tag{77}$$

This means that PKdV does not conserve the total mass flux through a given station. What happens, of course, is that some water is reflected and so, to analyze correctly the influence of a change in depth, one must also look at the left-going flow. We will do this when we investigate the propagation of a solitary wave toward a shore.

Fourth, let us derive a law that has been around for 150 years, Green's law. Suppose we were just considering a linear wave propagating in a region of slow depth change. Then the equation describing the evolution of the amplitude q would be given by (69) without the two last terms on the left-hand side. The result is that $D^{9/4}q$ or $D^{3/4}u$ or $D^{1/4}\eta$ (recall $\eta \sim -\phi_t \sim D^{-1/2}\phi_x$) is a function only of Θ and is therefore constant along right-going characteristics.

We are now in a position to describe how to handle both (69) and the full bidirectional problem (64) and (65). Imagine the following situation. A solitary wave q_s with amplitude η arrives at $x = 0$ at time $t = 0$ at which point the unperturbed depth begins to change. The solitary wave will undergo an adiabatic change (its amplitude parameter will change slowly) to satisfy the conservation of energy law $\partial/\partial\tau\int q_s^2\, d\Theta = -9/2\, D_\tau/D\int q_s^2\, d\Theta$. However, the mass flux law $\partial/\partial\tau\int q d\Theta = -9/4\, D_\tau/D\int q d\Theta$ then fails to be satisfied. We therefore must add to the right-going flow a shelf of amplitude of order σ (relative to the solitary wave amplitude) which stretches between the point to which infinitesimal distances would have traveled $\Theta_+ = 0$ to the solitary wave, a distance of order σ^{-1} as measured in the units of the solitary wave width. Therefore it carries a mass flux of the same order as the solitary wave. Its amplitude in the immediate rear of the solitary wave is determined by the amount by which the local mass flux law fails to be satisfied. Its future evolution from that point is given by Green's law.

However, this is not enough because, as we have already noted, the mass flux law for the full bidirectional equation is

Downloaded 02 May 2010 to 171.66.16.250. Redistribution subject to ASME license or copyright; see http://www.asme.org/terms/Terms_Use.cfm

still unsatisfied. Therefore, we must add another component, a wave of reflection. This has an amplitude (relative to the solitary wave) of order $\sigma\epsilon$ and stretches over a distance $(\sigma\epsilon)^{-1}$ times the width of the solitary wave so that it, too, carries a mass flux of equal order to each of the right-going components. The velocity field of this reflected component is determined on the right-going characteristic at $\Theta_+ = 0$ by the amount by which the mass flux law of the PKdV equation fails to satisfy the exact mass flux law of the full bidirectional equation. Its behavior elsewhere is determined by solving the Goursat problem: given u on $\Theta_+ = 0$ and $\eta = u = 0$ on $\Theta_- = 0$, find u, η which satisfies the linearized version of the equations (64) and (65) in the quadrant $\Theta_+ < 0$, $\Theta_- > 0$. It turns out that Du and η are almost constant along the negative characteristics Θ_-. Green's law does not apply because the gradients of the field variables u and η are of the same order as the gradient in the undisturbed depth.

Using these ideas (which can probably be best characterized by the phrase "the judicious use of the conservation laws") we can find a completely consistent solution to the original problem. It is of interest to list the mass flux M (normalized by the factor $8/3\ \eta_0\rho\epsilon^{1/2}h_0^2$) associated with the three solution components ($4/3\ \eta_0^2\epsilon h_0$ is the amplitude of the incoming solitary wave, ρ is density, and h_0, $h(x)$, and h_f are the initial, local, and final undisturbed depths, respectively).

$$\text{Solitary wave:}\quad \frac{h}{h_0}$$

$$\text{Right-going shelf:}\quad \left(\frac{h}{h_0}\right)^{1/4} - \left(\frac{h}{h_0}\right)$$

$$\text{Reflected wave:}\quad \left(\frac{h_f}{h_0}\right)^{1/4} - \left(\frac{h}{h_0}\right)^{1/4}. \tag{78}$$

The sum of these three components is $(h_f/h_0)^{1/4}$ which is constant and equal to the right-going mass flux after the pulse has reached the new constant undisturbed depth and no further reflection need be accounted for. Note in particular, the interesting result that if $h_f << h_0$, most of the water is reflected. More details on these calculations and related results can be found in references [41–43].

We close this section with some comments on the roles of the exactly solvable "Boussinesq" and Kadomtsev-Petviashvili equations. The former is

$$v_{tt} - v_{xx} = v_x v_{xx} + v_{xxxx}. \tag{79}$$

We observe that the lattice equation (3) is exactly the same and, allowing ourselves a little latitude, namely replace F_t by $-F_x$ in the nonlinear terms, equation (67) is too. But in what sense is (79) a more accurate description of events than two uncoupled KdV equations? The answer is that it is no more accurate because if the right-hand side in (3), the nonlinear and dispersion terms, is to be of equal magnitude with the left-hand side then the terms we have ignored, $\epsilon^2 y_{xxxxxx}$ and nonlinear terms such as $\epsilon^2 y_{xx}y_{xxxx}$ are equally important. We may therefore ask: are there any circumstances in which (79) is the relevant canonical equation? The answer is yes. Recall that I pointed out that if in the first approximation the underlying system is hyperbolic with distinct characteristic velocities, then the slow distortion of the corresponding Riemann invariant about each characteristic direction is described by the Korteweg-deVries equation. However if two of these characteristic velocities are close, then one cannot separate the evolution along these two neighbors. It is a fairly simple exercise to show that the canonical equation describing the long-time behavior of solutions to

$$\left(\frac{\partial}{\partial t} + (c-\sqrt{\epsilon})\frac{\partial}{\partial x}\right)\left(\frac{\partial}{\partial t} + (c+\sqrt{\epsilon})\frac{\partial}{\partial x}\right) = \epsilon\sqrt{\epsilon}\frac{\partial u}{\partial x}\frac{\partial^2 u}{\partial x^2} + \epsilon\frac{\partial^4 u}{\partial x^4} \tag{80}$$

is indeed the Boussinesq equation. In the frame of reference traveling with the average velocity c, the slow evolution of the field u as function of $X = x - ct$ and $T = \sqrt{\epsilon}t$ is given by (79).

As a final remark to this section, consider what happens if a weak dependence on the other horizontal coordinate, which we will call z, is included in the model either for water or lattice waves. This gives rise to another term on the left-hand sides in equations (67) and (3) proportional to $-\epsilon F_{zz}$ or $-\epsilon c^2 y_{zz}$. It is a trivial matter to show that the canonical long-time equation corresponding to (6) will now be

$$f_{zz} + \frac{2}{c}f_{\xi T} + f_\xi f_{\xi\xi} + \delta^2 f_{\xi\xi\xi\xi} = 0$$

which can also be written as (set $f_\xi = 6u$, $\tau = c\,T/2$ and take $\delta^2 = 1$)

$$u_{zz} + \frac{\partial}{\partial\xi}(u_\tau + 6uu_\xi + u_{\xi\xi\xi}) = 0 \tag{81}$$

Equation (81) is known as the Kadomtsev-Petviashvili equation and it too, has many remarkable properties.

Acknowedgments

I would like to take this opportunity to thank my friends and colleagues Jerry Bona, Hermann Flaschka, John Greene, Robert Miura, and Norman Zabusky for their careful reading of this manuscript and valuable comments. The paper is dedicated to Martin Kruskal whose extraordinary scientific insight and unrelenting tenacity in pursuit of the understanding of the unusual has been a source of inspiration and learning to myself and many others.

Much of the material is based on the first few lectures in a series given in June, 1983 under the sponsorship of the National Science Foundation's Conference Board of Mathematical Sciences. The full set of lectures will be published as part of the CBMS series by SIAM [54]. I want to thank the Army Office of Research and the Air Force Office of Scientific Research for support of these and other studies.

References

1 Scott Russell, J., "Report on Waves," Rept. Fourteenth Meeting of the British Assoc. for the Advancement of Science, John Murray, London, 1844, pp. 311–390 + 57 plates.

2 Scott Russel, J., *The Modern System of Naval Architecture*, Vol. 1, Day and Son, London, 1865, p. 208.

3 Boussinesq, J., Théorie des Ondes et des Remous qui se Propagent le long d'un Canal Rectangulaire Horizontal, en Communiquant au Liquide Contenu dans ce Canal des Vitesses Sensiblement Pareilles de la Surface au Fond," *J. Math. Pures Appl.*, Vol. 17, No. 2, 1872, pp. 55–108; see also Vastano and Mungall, 1976.

4 Korteweg, D. J., and DeVries, G., "On the Change of Form of Long Waves Advancing in a Rectangular Canal, and on a New Type of Long Stationary Waves," *Phil. Mag.*, Vol. 39, 1895, pp. 422–443.

5 Fermi, A., Pasta, J., and Ulam, S., "Studies of Nonlinear Problems, I," Los Alamos Report LA 1940, 1955, *Lectures in Applied Mathematics*, Vol. 15, pp. 143–196. Newell, A. C., ed., American Mathematical Society, 1974.

6 Zabusky, N. J., and Kruskal, M. D., "Interaction of 'Solitons' in a Collisionless Plasma and the Recurrence of Initial States," *Phys. Rev. Lett.*, Vol. 15, 1965, pp. 240–243.

7 Kruskal, M. D., "Asymptology in Numerical Computation: Progress and Plans on the Fermi-Pasta-Ulan Problem," *PVOC. IBM Scientific Computing Symposium on Large-Scale Problems in Physics*, IBM Data Processing Division, White Plains, N.Y., 1965, pp. 43–62.

8 Kruskal, M. D., "The Korteweg-deVries Equation and Related Evolution Equations," *Lectures in Applied Mathematics*, Vol. 68, pp. 61–83, Newell, A. C., ed., American Mathematical Society, 1974.

9 Kruskal, M. D., and Zabusky, N. J., "Progress on the Fermi-Pasta-Ulam Non-Linear String Problem," Princeton Plasma Physics Laboratory Annual Rept. MATT-Q-21, 1963, Princeton, N.J., pp. 301–308.

10 Zabusky, N. J., "Computational Synergetics and Mathematical Innovation," *J. Comp. Phys.*, Vol. 43, 1981, pp. 195–249.

11 Miura, R. M., "Korteweg-deVries Equation and Generalizations. I. A. Remarkable Explicit Nonlinear Transformation," *J. Mathematical Phys.*, Vol. 9, 1968, pp. 1202–1204.

Downloaded 02 May 2010 to 171.66.16.250. Redistribution subject to ASME license or copyright; see http://www.asme.org/terms/Terms_Use.cfm

12 Gardner, C. S., Greene, J. M., Kruskal, M. D., and Miura, R. M., "Method for Solving the Korteweg-deVries Equation," *Phys. Rev. Lett.*, Vol. 19, 1967, pp. 1095-1097. "Korteweg-deVries Equation and Generalizations. VI. Methods for Exact Solution," *Comm. Pure Appl. Math.*, Vol. 27, 1974, pp. 97-133.

13 Gardner, C. S., "Korteweg-deVries Equation and Generalizations. IV. The Korteweg-deVries Equation as a Hamiltonian System," *J. Mathematical Phys.*, Vol. 12, 1971, pp. 1548-1551.

14 Lax, P. D., "Integrals of Nonlinear Equations of Evolution and Solitary Waves," *Comm. Pure Appl. Math.*, Vol. 21, 1968, pp. 467-490.

15 McCall, S. L., and Hahn, E. L., "Self-Induced Transparency by Pulsed Coherent Light," *Phys. Rev. Lett.*, Vol. 18, 1967, pp. 908-911. "Self-Induced Transparency," *Phys. Rev.*, Vol. 183, 1969, pp. 457-485.

16 Eisenhart, L. P., *A Treatise on the Differential Geometry of Curves and Surfices*, Ginn & Co., Reprinted by Dover, New York, 1960.

17 Seeger, A., Donth, H., and Kochendorfer, A., "Theorie der Versetzungen in Eindimensionalem Atomreihen," *Z. Phys.*, Vol. 134, 1953, pp. 173-193.

18 Perring, J. K., and Skyrme, T. H. R., "A Model Unified Theory," *Nucl. Phys.*, Vol. 31, 1962, pp. 550-555.

19 Scott, A. C., Chu, F. Y. F., and McLaughlin, D. W., "The Soliton: A New Concept in Applied Science," *Proc. IEEE*, Vol. 61, 1973, pp. 1443-1483.

20 Lamb, G. L., Jr., "Analytical Descriptions of Ultra-Short Optical Pulse Propagation in a Resonant Medium," *Rev. Mod. Phys.*, Vol. 43, 1971, pp. 99-129.

21 Zakharov, V. E., and Shabat, A. B., "Exact Theory of Two-Dimensional Self-Focusing and One-Dimensional Self-Modulation of Waves in Nonlinear Media," *Soviet Physics JETP*, Vol. 34, 1972, pp. 62-69.

22 Wadati, M., "The Exact Solution of the Modified Korteweg-deVries Equation," *J. Phys. Soc. Japan*, Vol. 32, 1972, p. 1681.

23 Ablowitz, M. J., Kaup, D. J., Newell, A. C., and Segur, H., "Method for Solving the Sine-Gordon Equation," *Phys. Rev. Lett.*, Vol. 30, 1973, pp. 1262-1264. "Nonlinear-Evolution Equations of Physical Significance," *Phys. Rev. Lett.*, Vol. 31, 1973, pp. 125-127. "The Inverse Scattering Transform—Fourier Analysis for Nonlinear Problems," *Studies in Appl. Math.*, Vol. 53, 1974, pp. 249-315.

24 Flaschka, H., "The Toda Lattice. I. Existence of Integrals," *Phys. Rev. B.*, Vol. 9, 1974, pp. 1924-1925. "On the Toda Lattice. II. Inverse Scattering Solution, *Prog. Theoret. Phys.*, Vol. 51, 1974, pp. 703-716.

25 McKean, H. P., and Van Moerbeke, P., "The Spectrum of Hill's Equation," *Invent. Math.*, Vol. 30, 1975, p. 217.

26 Novikov, S. P., "The Periodic Problem for the Korteweg-deVries Equation," *Funct. Anal. Appl.*, Vol. 8, 1974, pp. 236-246.

27 Its, A. R., and Matveev, V. B., "The Periodic Korteweg-deVries Equation," *Funct. Anal. Appl.*, Vol. 9, 1975, p. 67.

28 Krichever, I. M., and Novikov, S. P., *Mathematical Physics Reviews*, Vol. 1, Novikov, S. P., ed., Soviet Scientific Reviews, pp. 5-23.

29 McKean, H. P., and Trubowitz, E., "Hill's Operator and Hyperelliptic Function Theory in the Presence of Infinitely Many Branch Points," *Comm. Pure and Appl. Math.*, Vol. 29, 1976, pp. 143-226.

30 Burchnall, J. L., and Chaundy, T. W., "Commutative Ordinary Differential Operators I, II," *Proc. London Math. Soc.*, Vol. 21, 1922, pp. 420-440. *Proc. Royal Soc.*, London, Series A, Vol. 118, 1928, pp. 557-583.

31 Manakov, S. V., "The Inverse Scattering Transform for the Time Dependent Schrödinger Equation and Kadomtsev-Petviashvili Equation," *Proc. Joint US-USSR Symposium on Soliton Theory*, Kiev 1979, Zakkarov, V. E., and Manakov, S. V., eds., North-Holland, Amsterdam, 1981, pp. 420-427.

32 Fokas, A. S., and Ablowitz, M. J., "On the Inverse Scattering and Direct Linearizing Transforms for the Kadomtsev-Petviashvili Equation, to be published. Segur, H., "Comments on Inverse Scattering for the Kadomtsev-Petviashvili Equation," *Proc. La Jolla Workshop*, Dec. 1981.

33 Atiyah, M. F., Hitchin, N. J., Drinfeld, V. G., and Manin, Yu. I., "Construction of Instantons," *Phys. Lett.*, Vol. 65A, 1978, p. 285.

34 Hirota, R., "Direct Methods in Soliton Theory," *Topics in Current Physics*, Bullough, R., and Caudrey, P., eds., Springer-Verlag, Vol. 17, 1980, pp. 157-175.

35 Ablowitz, M. J., Ramani, A., and Segur, H., "Nonlinear Evolution Equations and Ordinary Differential Equations of Painleve Type," *Lett. Nuovo Cimento*, Vol. 23, 1978, pp. 333-338. "A Connection Between Nonlinear Evolution Equations and Ordinary Differential Equations of *p*-Type I, II," *J. Math. Phys.*, Vol. 21, 1980, pp. 715-721; pp. 1006-1015.

36 Wahlquist, H. D., and Estabrook, F. B., "Bäcklund Transformation for Solutions of the Korteweg-deVries Equation," *Phys. Rev. Lett.*, Vol. 31, 1973, pp. 1386-1390. "Prolongation Structures of Nonlinear Evolution Equations, *J. Mathematical Phys.*, Vol. 16, 1975, pp. 1-7.

37 Flaschka, H., and Newell, A. C., "Monodromy and Spectrum Preserving Deformations," *Comm. Math. Phys.*, Vol. 76, 1980, pp. 65-116.

38 Flaschka, H., Newell, A. C., and Ratiu, T., "Kac-Moody Algebras and Soliton Equations," II Lax Equation Associated With $A_1^{(1)}$. III Stationary Equation Associated With $A_1^{(1)}$, to appear, *Physica D.*, 1983.

39 Jimbo, M., Miwa, T., Mori, Y., and Sato, M., "Density Matrix of an Impenetrable Bos Gas and the Fifth Painleve Transcedent," *Physica D.*, Vol. 1, 1980, pp. 80-139.

40 Segal, G., and Wilson, G., "Loop Groups and Equations of KdV Type," to be published.

41 Miles, J. W., "The Korteweg-de-Vries Equation: A Historical Essay," *J. Fluid Mech.*, Vol. 106, 1981, pp. 131-147.

42 Miles, J. W., "On the Korteweg-deVries Equation for a Gradually Changing Channel," *J. Fluid Mech.*, Vol. 91, 1979, pp. 181-190.

43 Knickerbocker, C. J., and Newell, A. C., "Shelves and the Korteweg-deVries Equation," *J. Fluid Mech.*, Vol. 98, 1980, pp. 803-818. "Internal Solitary Waves Near a Turning Point," *Phys. Lett.*, Vol. 75A, 1980, pp. 326-330. "Reflections From Solitary Waves in a Channel of Varying Depth," to appear, *J. Fluid Mech.*.

44 Johnson, R. S., "On the Development of a Solitary Wave Moving Over an Uneven Bottom," *Proc. Camb. Phil. Soc.*, Vol. 83, 1973, p. 183.

45 Bullough, R., and Caudrey, P., eds., *Solitons: Topics in Current Physics*, Vol. 17, Springer-Verlag, 1980.

46 Ablowitz, M. J., and Segur, H., *Solitons and the Inverse Scattering Transform*, SIAM Studies in Applied Mathematics, 1981.

47 Lamb, G. L., *Elements of Soliton Theory*, Wiley-Interscience, New York, 1980.

48 Lonngren, K., and Scott, A. C., eds., *Solitons in Action*, Academic Press, New York, 1978.

49 Calogero, F., and Degasperis, A., and the *Inverse Spectral Transform*, Part I, North-Holland, 1982.

50 Eckhaus, W., and Van Harten, A., *The Inverse Scattering Transformation and the Theory of Solitons: An Introduction*, Mathematical Studies, Vol. 50, North-Holland, 1981.

51 Flaschka, H., and McLaughlin, D. W., eds., "The Theory and Application of Solitons," *Rocky Mountain Journal of Mathematics*, Vol. 8, 1978.

52 "Nonlinear Evolution Equations Solvable by the Spectral Transform," *Research Notes in Mathematics*, Vol. 26, Pitman, 1978.

53 Miura, R., ed., *Backlund Transformations*, Lecture Notes in Mathematics 515, Springer-Verlag, 1976.

54 Newell, A. C., *Nonlinear Wave and Solitons*, CBMS Lectures to be published.

55 Emmerson, G. S., *John Scott Russell a Biography*, John Murray, London, 1977.

56 Whitman, G. B., *Linear and Nonlinear Waves*, Wiley-Interscience, New York, 1971.

57 Remark: in actual fact, Boussinesq simplified the bidirectional equation (67) with $D = 1$ by setting $F_t = -F_x$ and $F_{xt} = -F_{xx}$ and thereby imposing the right-going solution on the water wave problem. It is thus with (79), which is bidirectional, but does not obtain for two directional water waves, that his name is associated.

Downloaded 02 May 2010 to 171.66.16.250. Redistribution subject to ASME license or copyright; see http://www.asme.org/terms/Terms_Use.cfm

N. Olhoff
Department of Solid Mechanics,
The Technical University
of Denmark,
DK-2800 Lyngby, Denmark

J. E. Taylor
Department of Aerospace Engineering,
The University of Michigan,
Ann Arbor, Mich. 48109

On Structural Optimization

This paper presents a survey of the field of optimal structural design, with the main emphasis laid on fundamental aspects. The basic concepts for structural optimization problems are outlined, and we discuss the mathematical formulation and the characteristic properties and features of such problems for both discrete and continuum structures. A picture of the present status of the field is given, and we present an assessment of areas that are currently of special importance and undergoing rapid development. Furthermore, we identify some types of problems that require particular care in their formulation, and we indicate issues for future research.

1 Introduction

Structural optimization may be defined as the rational establishment of a structural design that is the best of all possible designs within a prescribed objective and a given set of geometrical and/or behavioral limitations.

This topic is intellectually attractive as well as technically significant, and it has a quite long history; fundamental problems of optimal structural design attracted the interest of Galileo (1638), and later of, e.g., J. Bernoulli (1687), Newton (1687), D. Bernoulli (1733), Lagrange (1770), Saint-Venant (1864), Maxwell (1869), and Lévy (1873). Structural optimization combines mathematics and mechanics with engineering, and has now become a broad multidisciplinary field which finds applications in aeronautical, civil, mechanical, nuclear, and off-shore engineering, as well as in space technology. The development has particularly taken place over the last 20–25 years, and has been strongly boosted by the availability of large, high-speed digital computers.

Considerations of limited energy resources, shortage of economic and some material resources, strong technological competition, and environmental problems motivate the considerable current research going on in the field of structural optimization, and indicate increasing significance for the field in the future.

Taking the design criterion as minimum cost or weight of the structure for given performance, or taking the criterion as maximum performance for a bound on cost (thereby achieving maximum economy of the structural material), the relevance of structural optimization is obvious. As a few examples, let us mention the possibility of energy saving by decreasing the weight of space, aero, or land-borne structures and transportation systems; cost reduction of load-carrying structures for given capacity, strength, and/or stiffness requirements; increasing the efficiency of fibers in composite materials by optimizing their distribution and orientation; minimizing dynamic response (and hence noise and vibration) of rotating machinery or structures subjected to external excitation.

Current research in optimal structural design may very roughly be said to follow two main paths. Along the first, the research is primarily devoted to studies of *fundamental aspects of structural optimization*. Broad conclusions may be drawn on the basis of mathematical properties of governing equations for optimal design. These properties are not only studied analytically in order to derive qualitative results of general validity, but are also often investigated numerically via example problems. Along the other main path of research, the emphasis is laid on the *development of effective numerical solution procedures* for optimization of complex practical structures.

Notwithstanding the obvious significance of the latter line of research, the present paper will primarily be devoted to fundamental aspects and properties of structural optimization. First, we give an account of basic concepts and well-established areas of optimization in Section 2. In Section 3, we present a generalized formulation for optimal design, derive a formal set of governing equations by means of variational analysis, and briefly discuss commonly used solution techniques. This is followed up in Section 4 by an account of variational problem formulations for a large class of specific design objectives. These sections reflect current knowledge, while the subsequent sections give a picture of relatively new areas of research. Section 5 is devoted to the subject of multicriteria optimization, which is very important in practical design contexts, and Section 6 deals with shape optimization, a type of problem that also constitutes a significant extension. In Sections 7 and 8 we discuss two classes of problems for which it has recently been recognized that particularly careful formulation is required for correct optimal solution. These classes comprise, respectively, certain optimization problems involving eigenvalues, and problems concerning optimal design of, e.g., plates, shells, and composite materials. Fruitful directions for further work are indicated in the final section of the paper.

The constant flow of general reviews, surveys of subfields, conference proceedings, and new textbooks on optimal structural design testify the strong activity, recent advances,

Contributed by the Applied Mechanics Division for publication in the JOURNAL OF APPLIED MECHANICS.

Discussion on this paper should be addressed to the Editorial Department, ASME, United Engineering Center, 345 East 47th Street, New York, N.Y. 10017, and will be accepted until two months after final publication of the paper itself in the JOURNAL OF APPLIED MECHANICS. Manuscript received by ASME Applied Mechanics Division, April, 1983.

Copyright © 1983 by ASME
Downloaded 02 May 2010 to 171.66.16.250. Redistribution subject to ASME license or copyright; see http://www.asme.org/terms/Terms_Use.cfm

and increasing importance of the field. A selection of such recent publications is listed as references [1–26] at the end of this paper. We have tried to keep the reference list brief by drawing on the aforementioned literature as a source for additional bibliography. Thus, only a limited number of special papers and reports are included in the reference list.

The reviews in references [1–9] together make up a very exhaustive collection of optimal design literature, starting with Galileo and going up to 1981. The reviews by Wasiutyński and Brandt [1], Sheu and Prager [2], and Niordson and Pedersen [3], are all very broad in scope. Joint work under the auspices of the Structural Division of ASCE resulted in 1981 in a report edited by Lev [4], which contains a general review and offers the most up-to-date and comprehensive listing of the international literature on optimal structural design. A valuable review of the Chinese research efforts in the field from the end of the so-called "Cultural Revolution" and up to 1981 is given by Qian [5].

The increasing rate of publication in the field is illustrated by the fact that the authors of five recent reviews, Rozvany and Mróz [6], Venkayya [7], Schmit [8], Vanderplaats [9], and Haug [13, pp. 3–74], found it necessary to limit the scopes of their articles, but, nevertheless, a wealth of references are cited in these papers. Reference [6] reviews optimization problems (mainly for plastic design) that can be solved by analytical methods, while references [7–9] are devoted to the application of numerical methods for optimization of complex practical structures. Haug's paper in [13] gives an exhaustive account of various methods and classes of optimization problems for continuous structures.

The recent surveys [10, 11] are also devoted to special fields of optimization. Olhoff [10] considers optimal design with respect to structural eigenvalues, mainly for conservative problems in continuous formulation, while Ashley [11] presents an exhaustive survey of optimal design of discrete, highly complex, aeronautical structures.

The proceedings of specialty meetings on optimal structural design held in Warsaw in 1973 [12], Iowa City in 1980 [13], Liège in 1980 [14], Tucson in 1981 [15], and Siegen in 1982 [16] contain a considerable number of significant contributions and are the best sources for obtaining an idea of the current state of knowledge in the field.

Finally, mention should be made of excellent textbooks written within the last 10 years by Prager [17], Rozvany [18], Grinev and Filippov [19], Haug and Arora [20], Banichuk [21], Kirsch [22], Carmichael [23], Troitskij and Petuchov [24], Lepik [25], and by Lurie [26]. An extended listing of books is available in reference [4].

2 Basic Concepts and Well-Established Areas

In this section the distinctions between usual analysis, redesign or sensitivity analysis, and optimization of structures will be made clear, and the basic concepts pertaining to optimal design will be outlined. At the end of the section we will give a brief account of well-established subareas of structural optimization.

In a usual *analysis problem*, the structural design is given, together with relevant properties of the material(s) to be used and the support conditions for the structure. Also, one set or more of loading is specified, that is, completely specified in deterministic problems, or given in terms of probabilities in probabilistic problems. For each set of loading, the relevant set of equilibrium (or state) equations, constitutive equations, compatibility conditions, and boundary conditions, are then used for determining the structural *response*, e.g., the state of stress, strain and deflection, natural vibration frequencies, and load factors for elastic instability or plastic collapse.

Redesign (or *sensitivity analysis*) refers to the type of problem where some of the design, material, or support parameters are changed (or varied), and where the corresponding changes (or variations) of the structural response are determined via a repeated (or special) analysis.

It is worth noting that a conventional design procedure normally consists of a series of repeated changes of the structural parameters followed by analysis, i.e., a series of redesign analyses, which is carried out until a structure is found that fulfills the behavioral requirements and is reasonable in cost. If the changes of the structural parameters prior to a given redesign analysis are determined rationally from the earlier analyses as the best possible ones, the procedure would identify one of optimal design. However, usually the changes are only decided by guesswork based on information obtained from the previous analysis, and a structure obtained by the conventional procedure will not necessarily be better than other possible alternatives.

The label *structural optimization* identifies the type of design problem where the set of structural parameters is subdivided into so-called *preassigned parameters* and *design variables*, and the problem consists in determining optimal values of the design variables such that they *maximize* or *minimize* a specific function termed the *objective* (or *criterion*, or *cost*) *function*, while satisfying a set of *geometrical* and/or *behavioral requirements*, which are specified prior to design, and are called *constraints*.

Design Variables. The design variables used in various types of structural optimization problems may be categorized as follows:

Cross-sectional design variables describe properties of structural elements like cross-sectional area (of a bar, rod or beam), second area moment (of a beam, column or arch), or thickness (of a plate). Such design variables are usually assumed to be continuous, and very often they are considered a function of the spatial coordinate(s) of the element (see the following). However, cross-sectional design variables may also be discrete as, for example, in cases where uniform structural members are only available in distinct, standardized sizes.

The design variables describing the *layout* of a structure may be categorized as topological design variables and configurational design variables:

Topological design variables describe the number, spatial sequence, and mutual connectivity of members and joints in a structural system, and are integer variables.

Configurational (or *geometrical*) *design variables* may be coordinates of joints in structural systems, or the form of centerlines or midsurfaces of structural elements like bars, beams, arches, or shells. Usually they are represented by continuous variables.

Shape design variables describe the shape of external boundaries or interfaces of a structure. Examples are the cross-sectional shape of a rod, column, or beam; the boundary shape of a disk, plate, or shell; or the shape of interfaces in a three-dimensional structural element made of different materials. Design variables of this type are generally continuous; see Section 6.

Material design variables represent material properties, and are usually discrete. However, properties of fiber composite materials can often be described in terms of the concentration and direction of the fibers, and may then be considered as continuous design variables. As discussed in Section 8, anisotropic, composite materials may very well arise as a result of optimization.

Support or *loading design variables* describe the support (or boundary) conditions or the distribution of loading on a structure. Thus, either the location, number, and type of support or the external forces may be varied in order to yield a

Downloaded 02 May 2010 to 171.66.16.250. Redistribution subject to ASME license or copyright; see http://www.asme.org/terms/Terms_Use.cfm

more effective design, see, e.g. [6]. The design variables in this category may be continuous or discrete.

Continuous and Discrete Problems. According to the manner in which the *design variables* are assumed to *depend on the spatial variables*, optimal design problems may be roughly categorized as

(1) *Continuous* (or *distributed parameter*) optimization problems, and
(2) *discrete* (or *parameter*) optimization problems.

Usually the design variables of structural elements like rods, beams, arches, and plates are considered to vary continuously over the length or domain of the element, and such problems then fall into category (1), while problems of optimizing inherently discrete structures like trusses, grillages, frames, or complex practical structures belong to category (2). The governing equations of both types of problem (as well as mixed types) can be derived by variational analysis, see Sections 3 and 4.

Constraints. Any set of the design variables defines a design of the structure and may be represented as a point in the so-called *design space*. Many designs from among the totality of possible designs will generally not be acceptable in terms of various design and performance requirements. To exclude such designs as candidates for an optimal solution, the design and performance requirements are expressed mathematically in the form of constraints prior to optimization. These constraints directly or indirectly impose limits on the ranges of variation of the design variables. Relative to the design space, the constraints define hypersurfaces that encircle the set of acceptable, or so-called *feasible* or *admissible designs*. The constraints may be of two types: geometrical constraints and behavioral constraints.

Geometrical (or *side*) *constraints* are restrictions imposed explicitly on the design variables due to considerations such as manufacturing limitations, physical practicability, aesthetics, etc. Constraints of this kind are typically *inequality constraints* that specify lower or upper bounds on the design variables, but they may also be *equality constraints* like, e.g., *linkage constraints* that prescribe given proportions between a group of design variables.

Behavioral constraints are generally nonlinear and implicit in terms of the design variables, and they may be of two types. The first type consists of *equality constraints* such as state and compatibility equations governing the structural response associated with the loading condition(s) under consideration. The second type of behavioral constraints comprises *inequality constraints* that specify restrictions on those quantities that characterize the response of the structure. These constraints may impose bounds on *local* quantities like stresses and deflections, or on *global* quantities such as compliance, natural vibration frequencies, etc.

Objective Function. The *objective function*, which is also termed the *cost* or the *criterion function*, must be expressed in terms of the design variables such that its value can be determined for any point in the design space. It is this function whose value is to be minimized or maximized by the optimal set of values of the design variables within the feasible design space, and it may represent the structural weight or cost, or it may be taken to represent some local or global measure of the structural performance like stress, displacement, stress intensity factor, stiffness, plastic collapse load, fatigue life, buckling load, natural vibration frequency, aeroelastic divergence, or flutter speed, etc. In *single-criterion* problems (see Section 4), the objective function represents a single property that is of primary concern, but the objective function may, for example, also represent a weighted sum of a number of different properties, as may be the case in so-called *multicriteria optimization* problems (see Section 5).

Well-Established Areas. *Single-criterion* optimization problems have been studied in a high fraction of the total number of possible (and meaningful) combinations of design objectives, constraints, and design variables for different types of structures. Common fundamental features for problems with quite different design objectives were already discussed by Prager and Taylor in reference [28].

Considering objectives pertaining to *static loading*, particularly the areas of *design against plastic collapse* (limit load) and *elastic design* under *strength*, *stiffness*, or *stability requirement* are well established.

The first systematic theory of optimal plastic design was based on *uniform energy dissipation*, and introduced by Drucker and Shield [29] in 1956. However, the most general theory, based on the *cost gradient concept*, was initiated by Marcal and Prager [30] and further developed by Prager and Shield [31] in 1967. This so-called Prager-Shield theory has later been extended by, e.g., Save [32] and Rozvany [18]. It may be said that the major work in the area of optimal plastic design is due to Prager and coworkers, and optimal solutions are available for a multitude of structural elements and systems, see e.g. references [2, 3, 6, 18, 22]. Accounts of current trends are given by Rozvany [13, pp. 82–151; 16, pp. 103–110].

The area of elastic optimal design under static loading has been developed via the joint efforts of a much larger number of researchers, and a wealth of solutions are available in the literature, see e.g. [1–7]. Fundamental aspects in this area are discussed in depth later in this paper, so here only the papers by Keller [33] from 1960 and Masur [34] will be mentioned as examples of contributions that have had a considerable impact on the contemporary development of the area. It is worth noting that optimization of elastic structures is generally more difficult to cope with than optimization of plastic structures. Hence, except for special cross-sectional types, elastic design involves a nonlinear relationship between specific stiffness and mass in bending and torsion, and this is not the case under plastic collapse conditions.

Optimal layout of trusses (Maxwell, Michell et al.) and, in particular, grillages (Prager, Rozvany) constitutes a very well-developed area; see [6, 17, 18]. It is interesting to note that optimal layouts for trusses have been found to be the same for different types of design objectives, and the same is true for optimal grillage layouts. Recent extensions to new types of structures include optimal layout of archgrids [35] and cable networks, which have been termed Prager-structures, see Rozvany [16, pp. 101–110].

Optimal design under *dynamic loading* conditions was initiated by Niordson [36] in 1965. This area is already reasonably well established for single-criterion optimization, and many results are available for design under natural frequency requirements, forced steady state and transient response requirements, and for aeroelastic optimal design. The reader is referred to references [4, 7–11], [13, pp. 3–74], and [19] for elastic design and to reference [25] for inelastic design.

3 Mathematical Problem and Methods of Solution

Within the deterministic design philosophy, a problem of optimizing an inherently discrete structure, or an initially discretized continuum structure, may generally be stated in the mathematical form

Downloaded 02 May 2010 to 171.66.16.250. Redistribution subject to ASME license or copyright; see http://www.asme.org/terms/Terms_Use.cfm

$$\begin{aligned} &\text{Determine} \quad D_i, \quad i=1, \ldots, n, \text{ which} \\ &\text{minimize} \quad F(D_1, \ldots, D_n) \\ &\text{subject to} \quad h_j(D_1, \ldots, D_n) = 0, \quad j=1, \ldots, p, \\ &\quad \text{and } g_k(D_1, \ldots, D_n) \le 0, \quad k=1, \ldots, q. \end{aligned} \tag{1}$$

Here, D_i is the vector of n design variables, F is the objective function, and a number of p equality constraints and q inequality constraints are assumed to be specified. (Note that one may substitute $F = -G$ in (1) if an objective function G is to be maximized).

The functions F, h_j, and g_k depend both on design and state, and the equality constraints comprise the state equations. Assuming F, h_j, and g_k to be continuously differentiable functions of D_i, we may formally solve problem (1) using *the calculus of variations*. Based on F we form an augmented objective function F^* to be minimized,

$$F^* = F(D_1, \ldots, D_n) + \sum_{j=1}^{p} \lambda_j (h_j(D_1, \ldots, D_n) + \sum_{k=1}^{q} \mu_k [g_k(D_1, \ldots, D_n) + s_k^2], \tag{2}$$

where the equality and inequality constraints in (1) are adjoined by means of Lagrangian multipliers λ_j, $j=1, \ldots, p$, and μ_k, $k=1, \ldots, q$, respectively, after we have converted the inequality constraints into the equalities $g_k(D_1, \ldots, D_n) + s_k^2 = 0$, $k=1, \ldots, q$, by introducing the real slack variables s_k.

The conditions of stationarity of F^* with respect to arbitrary admissible variation of D_i, $i = 1, \ldots, n$, lead to a number of n so-called *optimality conditions*,

$$\frac{\partial F}{\partial D_i} + \sum_{j=1}^{p} \lambda_j \frac{\partial h_j}{\partial D_i} + \sum_{k=1}^{q} \mu_k \frac{\partial g_k}{\partial D_i} = 0, \quad i=1, \ldots, n, \tag{3}$$

and stationarity with respect to the Lagrangian multipliers λ_j, $j=1, \ldots, p$, recovers the equality constraints in (1),

$$h_j(D_1, \ldots, D_n) = 0, \quad j=1, \ldots, p. \tag{4}$$

Stationarity of F^* with respect to s_k, $k=1, \ldots, q$, yields the so-called *switching conditions* $\mu_k \cdot s_k = 0$, and the necessary conditions $\delta^2 F^*/\delta s_k^2 \ge 0$ for a minimum of F^* imply that the Lagrangian multipliers μ_k must be non-negative, i.e., $\mu_k \ge 0$, $k = 1, \ldots, q$. A combination of the latter result with the switching conditions and the defining equations for s_k yields the conditions

$$\left.\begin{aligned} &\mu_k = 0 \quad \text{if} \quad g_k(D_1, \ldots, D_n) < 0 \\ &\mu_k \ge 0 \quad \text{if} \quad g_k(D_1, \ldots, D_n) = 0 \end{aligned}\right\} k=1, \ldots, q, \tag{5}$$

which are seen to imply simplification in (3) if one or more of the inequality constraints are not tight.

Equations (3)–(5) constitute the formal set of governing equations for the structural optimization problem and are often called the *generalized Kuhn-Tucker conditions*. The preceding exposition is presented in terms of a discrete or discretized structure, but it is quite evident, or may easily be seen from Section 4, that the accommodation for a continuous optimization problem is fairly straightforward. Therefore, no a priori distinction will be made between continuous and discrete optimization problems in the discussion contained in the remaining part of this section.

The governing equations for specific problems are usually, as here, derived as *necessary conditions* for a local extremum, that is, the equations do not, in general, state sufficient conditions for global optimality. In fact, *sufficiency* can only be proven for *convex problems*, as in relatively simple cases where a linear relationship exists between the stiffness and the mass per unit length or area of the structure. In reference [28], Prager and Taylor have derived sufficiency conditions for a variety of such problems by making use of extremum principles of structural mechanics.

It is a characteristic feature that the governing equations can only be solved analytically for relatively small subclasses of problems within the two categories of (1) continuous and (2) discrete optimization problems mentioned in Section 2. This is because the optimality conditions are in general *nonlinear* both in the design and in the state variables, and the design variables generally also appear nonlinearly in the (stiffness) coefficients of the state equations in solid mechanics. Thus, for the vast majority of problems within the two categories, it is necessary to apply *iterative numerical methods* of solution. Note that this implies discretization in problems belonging to category (1), although not necessarily at the initial stage. The numerical methods commonly used for solution of problems where optimality conditions are contained in the discretized or initially discrete set of governing equations are usually termed *optimality criterion methods*. The reader is referred to, for example, references [7, 9, 14, 22] for more detailed description.

For complex practical structures in category (2), often the optimality conditions together with the state equations and other constraint conditions form such a large and complicated set of algebraic equations that it may be advantageous to apply a purely numerical solution procedure from the very outset. Direct procedures of this type are identified as methods of *mathematical programming*, such as *linear*, *nonlinear*, *geometric*, or *integer programming*. References [8, 9, 14, 22] contain accounts of these methods.

Recently, Fleury et al. (see, e.g. reference [14, chapter 10]) have developed a very powerful approach in which the initial problem is replaced by a sequence of simple explicit problems. Employing a dual solution scheme to solve each subproblem leads to a generalization of conventional optimality criteria techniques. Using a primal solution scheme gives rise to a mixed method which permits a gradual transition between a rigorous, but slow, mathematical programming approach and a rapid, but possibly unstable, optimality criteria procedure. This approach implies a reconciliation of optimality criteria and mathematical programming techniques.

4 Variational Analysis With Generalized Objectives

For simplicity, the presentation in this section is based on single-criterion, single-purpose design of continuum structures. We note, however, that the arguments and conclusions are directly applicable to discrete systems as well. Our goal is to demonstrate the means to perform variational analysis for a broad range of structural optimization problems. The application of control theory for the analysis of structural optimization is not covered here; a brief mention of this approach is given in [4, Chapter 9], and the subject is treated in detail in Carmichael [23] and Lurie [26]. The reader is referred to [4, Chapter 9] also for the discussion and listing of current literature on the many aspects of analysis in structural optimization that are not taken up in this section.

For the discussion of problems where the objective of minimization is given by some *global* measure[1] only, let us suppose that the measure is represented as $\int_\Omega f(D, y)dx$ for specified function f of design $D(x)$ and response (state) $y(x)$. Ω identifies the domain of the structure. The optimal design problem may be stated in the form:

[1] Mróz and Mironov [37] present a form of analysis for problems of this kind.

Downloaded 02 May 2010 to 171.66.16.250. Redistribution subject to ASME license or copyright; see http://www.asme.org/terms/Terms_Use.cfm

$$\min_{D(x)} \left(\int_\Omega f(D, y)\, dx \right)$$

$$\begin{aligned} \text{subject to:} \quad & \text{(state equations)} \\ & \text{(behavioral constraints)} \\ & D_{\min} - D(x) \le 0 \\ & \int_\Omega D\, dx - V \le 0. \end{aligned} \tag{6}$$

In static response problems, for example, the "state equations" constraint refers simply to the equilibrium boundary value problem statement. The behavioral constraints may reflect requirements or bounds on various measures of response and together with the last two constraints in the list define admissible designs.

If there are no behavioral constraints present, or if they are also expressed in global measure, then the analysis for problem (6) is conventional. That is, the Lagrangian may be formed for the problem in the usual way, and the generalized Kuhn-Tucker conditions apply.

The analysis is demonstrated via the example of Bernoulli-Euler beam design for the minimization of $\int_0^L \rho y\, dx$, where $\rho(x)$ is a specified weighting on beam displacement $y(x)$. The Lagrangian for this problem

$$\min_{D(x)} \left(\int_0^L \rho y\, dx \right)$$

$$\begin{aligned} \text{subject to:} \quad & (Sy'')'' - p = 0 \\ & D_{\min} - D(x) \le 0 \\ & \int_0^L D\, dx - V \le 0 \end{aligned} \tag{7}$$

may be written as

$$L = \int_0^L \rho y\, dx + \int_0^L \left[-\bar{y}\left((Sy'')'' - p \right) + \gamma (D_{\min} - D + s_d^2) \right] dx$$

$$+ \Gamma \left[\int_0^L D\, dx - V + s_v^2 \right]. \tag{8}$$

The bending stiffness is denoted by S for this example, and $p(x)$ represents the load distribution. In (8) $\bar{y}(x)$, $\gamma(x)$, and Γ are Lagrangian multipliers, and $s_d(x)$ and s_v are real slack variables. Stationarity of the Lagrangian L with respect to $y(x)$ (admissible $y(x)$ are identified via the kinematic boundary conditions) requires

$$(S\bar{y}'')'' - \rho = 0 \quad \text{(and } BC\text{'s)}, \tag{9}$$

which is called the *adjoint state equation*. Note that the weighting $\rho(x)$ has the role of a load in this equation. The remaining necessary conditions can be written in the form

$$\begin{gathered} \frac{dS}{dD} \bar{y}'' y'' + \gamma - \Gamma = 0 \\ (Sy'')'' - p = 0 \\ \gamma (D_{\min} - D) = 0; \quad \gamma \ge 0; \quad D_{\min} - D \le 0 \\ \Gamma \left[\int_0^L D\, dx - V \right] = 0; \quad \Gamma \ge 0; \quad \int_0^L D\, dx - V \le 0 \end{gathered} \tag{10}$$

after the slack variables have been eliminated.

The first of these equations is referred to as the *optimality condition*. The term $(dS/dD)\bar{y}''y''$ is the *gradient* of the objective function with respect to the design variable $D(x)$ and is seen to measure *specific mutual energy*, i.e., mutual between the original and the adjoint states. Note that over intervals where $D > D_{\min}$, we have $\gamma = 0$, that is, the optimality condition requires the gradient, or the specific mutual energy, to be of constant value.

If the weighting function $\rho(x)$ in the preceding example equals the primary load, i.e., if $\rho(x) = p(x)$, then in the solution $y(x) = \bar{y}(x)$. In this case, the design objective $\int_0^L py\, dx$ is the measure of *compliance*. Note also that since compliance equals twice the negative of *potential energy*, the extremum with respect to design of compliance corresponds to the extremum of potential energy. Whenever the objective of the optimization problem can be associated in this way with the governing functional of a *variational principle* in mechanics, the optimal design problem may be stated directly in terms of that governing functional. The problem statement for minimum compliance design, for example, is simply

$$\begin{aligned} & \min_D (-\text{Potential Energy}) \,\big|\, \text{Equilibrium} \\ & \text{subject to:} \quad \text{design constraints.} \end{aligned} \tag{11}$$

Clearly, the Lagrangian for this problem has a simpler form than the one for problem (6) since the state equation need not be adjoined, but will appear as a necessary condition of stationarity with respect to variation of $y(x)$. A similar interpretation may be made for the problems of design for maximum Euler buckling load, design for maximum first natural frequency, and design for maximum collapse load (see [3, 10, 28, 36], for example, and references cited there).

One should note that, in fact, the problem statement is generally not unique, i.e., most often *alternate equivalent forms are available for the variational statement of structural optimization problems*. For example, the problem "minimize compliance within an available resource of structural material" is equivalent to "minimize the amount of structural material for designs within a prescribed bound on compliance." With problems expressed in dimensional form, the equivalence may be verified to within a scale factor, i.e., the optimal designs for the alternate problems are similar.

Problems subject to behavioral constraints expressed in terms of some *local* measure may be represented formally using the same procedures as in the example. However, the results cannot generally be supported within simple analysis. The reason for this is that in cases where the (local) constraint is tight only at a point or at a set of points, the corresponding "adjoint load" is given by Dirac δ-functions. Haug [38] provides a description of the analysis that underlies such problems with singularities.

There are two distinct forms of optimization problem where the objective of minimization is itself expressed in terms of a *local* measure. One form is obtained in the case where the point at which a minimum is to be achieved is *designated*. To continue with the beam example, if the goal is to minimize with respect to design the value for displacement at location x_0, the design problem statement is:

$$\begin{aligned} & \min_{D(x)} \left(|y(x_0)| \right) \\ & \text{subject to:} \quad \text{constraints as in (6).} \end{aligned} \tag{12}$$

This problem also leads to singularities in the "adjoint load"; once again, an analysis to support the necessary conditions for the problem is given in [38].

In the second type of problem with local objective, the argument of the min problem is the maximum value, with respect to domain, of the local measure. As an example, suppose the purpose is to predict the beam design that minimizes the maximum value of $|y(x)|$, where $y(x)$ is the beam displacement as in the foregoing. For this objective, the design $D(x)$ must be determined according to:

Downloaded 02 May 2010 to 171.66.16.250. Redistribution subject to ASME license or copyright; see http://www.asme.org/terms/Terms_Use.cfm

$$\min_{D(x)} \left[\max_{x} \left(|y(x)| \right) \right] \tag{13}$$

subject to: constraints as in (6).

The familiar variational analysis is, in general, not directly applicable to such min-max problems. This can be explained on the basis of the following observation. If, in the neighborhood of the optimal solution, there is a trade-off between values of $|y(x)|$ at different points (i.e., one value increases while another decreases), then the argument $[\max_x |y(x)|]$ will have a *corner* at that point. In other words, the objective function is not differentiable in general for min-max problems.

Haug [38] proposes an alternative form for the problem as follows: $[\min_D |y(\hat{x})|]$ subject to the constraint $(dy/dx)_{\hat{x}} = 0$ in addition to the constraints of (6). Special care must be exercised in cases where the constraint equation on dy/dx has more than one root. In another approach, the minimization operates on a "p-norm" of the local measure. The problem may be stated (for the same example) as:

$$\min_{D(x)} \left[\int_{\Omega} |y(x)|^p dx \right]^{1/p} \tag{14}$$

subject to: constraints as in (6).

The peaks in $|y(x)|$ become emphasized as, in this expression, p grows large; the result for $p \to \infty$ solves the original min-max problem (13). While this approach is supportable in analysis, computational procedures based on the p-norm tend to be inefficient.

To describe another option, an approach is available whereby min-max design problems can be treated using the usual means of variational analysis. In this approach, a parameter β dependent on design is introduced as a bound on the local measure that appears in the argument of the max. Considering problems where the design depends on maximum value of stress, i.e., $\min_D[\max_x(|\sigma(x)|)]$ as an example, in terms of the bound formulation, the design is determined according to:

$$\begin{aligned} &\min_{D(x)}(\beta) \\ &\text{subject to:} \quad |\sigma(x)| - \beta \le 0 \\ &\qquad\qquad \text{constraints of (6).} \end{aligned} \tag{15}$$

This interpretation is supported by the fact that, from the necessary conditions of problem (15), the constraint on stress must be tight at least at a point, whereby $\beta = \sup_x |\sigma(x)| = \max_x |\sigma(x)|$ at that point. The necessary conditions for problem (15) are obtained via generalized Kuhn-Tucker conditions, just as was done for problem (6). Details of this analysis for min-max problems are presented in Taylor and Bendsøe [39].

5 Multicriteria Optimization

In contrast to problems where a single criterion governs, for *multicriteria optimization* the solution, i.e., the optimal design, reflects simultaneous minimization on two or more criteria. The labels *vector optimization* or *multiobjective optimization* are also used for such problems. Truss design to minimize weight and to achieve at the same time the lowest possible values for components of nodal displacement and/or member stress is an example. The design of the minimum weight elastic bar or plate for minimum values of stress and/or displacement at designated points is another. For the general multicriteria problem, each of the performance criteria might be expressed in terms of one or the other among global or local measures (including maximum with respect to domain) such as those described in Section 4.

Ordinarily in multicriteria optimization there exists a possibility for *trade-off among criteria*, i.e., a change in design may result in *improvement* according to one or more criteria but only at the expense of a *worsening* as measured by others. Thus, by the same argument as was employed in the discussion of min-max problems in Section 4, the analysis of scalar optimization is not directly applicable to multicriteria problems. One alternative is to derive the solution for the multicriteria problem through a process of reduction from its set of *Pareto solutions* (see the following). Otherwise, several options are available for the treatment of multicriteria optimization via interpretation into one or another *scalar form*. Generally the resulting scalar problem must be solved a number of times with this approach.

Several of the better known approaches for handling multicriteria design problems are described briefly in the following. For this purpose $g_i(D)$ is taken to represent the component criteria, where the aim is to minimize with respect to design D on the vector $\{g_1, g_2, \ldots, g_n\}$. It is assumed that the separate criteria g_i are conditioned to be consistent with direct minimization on each of them. As an example, where the objective is to minimize the difference between designated measures f_i and given goal values, say $\bar{f}_i$, for these, the g_i might be defined by $g_i(D) = |\bar{f}_i(d) - \bar{f}_i|$. Note that a decision on the choice of values $\bar{f}_i$ may itself comprise a part of the overall design process.

We first consider a few representative scalar interpretations for multicriteria problems. For the methods summarized in the table, weights $w_i \ge 0$ and constraint bounds $\epsilon_i \ge 0$ are specified. In practice, the choice of values for w_i and for ϵ_i may reflect the designer's judgment.

Method	Corresponding scalar problem
Weighted sum	$\min_D \left(\sum_i w_i g_i \right)$
Goal attainment or bound method	$\min_D (\beta)$ subject to $w_i g_i - \beta \le 0 \quad (i = 1, 2, \ldots n)$
Constraint method	$\min_D (g_k)$ subject to $g_i - \epsilon_i \le 0 \quad (i = 1, 2, \ldots n, i \pm k)$ $(i \quad k)$

With the constraint method the user also has the option of choosing which component is to appear as the argument of the min problem.

Multicriteria optimization may be expressed in the form of a min-max problem as well. For $g_i(D)$ and w_i as defined in the foregoing, the problem statement is: $\min_D[\max_i (w_i g_i)]$. We note that the bound method given in the table provides a means of solving such min-max problems. In fact, the bound method still applies in cases where components g_i are themselves identified with max with respect to domain of a local measure. The weighted sum and constraint methods are not directly applicable in this situation.

A design among admissible designs is identified as *Pareto optimal* if there is no other admissible design for which some criterion would be improved without simultaneous worsening of at least one criterion. A given multicriteria optimization problem may have anything from one to an infinity of Pareto solutions, and the solution to the multicriteria problem is included among them. In a strictly Pareto approach, the full set of Pareto solutions must be determined. Then the optimal design must be identified within this set. The latter step generally requires the application by the designer of judgment or some other basis of choice.

Downloaded 02 May 2010 to 171.66.16.250. Redistribution subject to ASME license or copyright; see http://www.asme.org/terms/Terms_Use.cfm

The full set of Pareto designs (see the table) can be generated by application of the bound method covering an appropriate range of values for weighting factors w_i. It may be appreciated in this way that a choice of values for w_i is related to the application of judgment in a Pareto approach. Thus it appears that in those multicriteria problems where means are available to support a sharp judgment, the bound method should prove more efficient than a problem-solving approach based strictly on the Pareto concept. Otherwise, the approaches are distinguished by whether the judgment is introduced at the beginning or at the end of the solution procedure.

Stadler has written major surveys on multicriteria optimization [40–42]. A concise statement of the various scalar interpretations of multicriteria problems is given by Osyczka and Koski [16, pp. 173–181]. Also Osyczka [16, pp. 169–174] discusses ideas related to numerical solution of multicriteria problems based on min-max interpretation. A variational analysis for min-max problems [39] is applied in Bendsøe et al. [43] to multicriteria design.

6 Shape Optimization

The determination of overall shape for a dam to minimize its weight, the design of a fillet in a bar or a shaft, or of a hole in a membrane to minimize stress concentration, and the prediction of cross-sectional shape of a torsion bar for minimum compliance – are representative examples taken from the literature on shape optimal design (see, e.g., references [16, pp. 233–241] and [44]). Our purpose in this section is to discuss in general terms the features of variational analysis applied to such shape design problems. The reader is recommended to resources in the literature for material on specific applications and for information about procedures for computational solution. A survey of developments in the subject is given in reference [4, Section 9.6]; the same survey, but this time including some details of analysis, appears in reference [14, Chapter 15].

Considering two or three-dimensional structural forms, the boundary or interface curves or surfaces that define shape (per the description of *shape design variables* given in Section 2) appear as limits of integration on integrals over the domain of the structure. Therefore a change of shape is reflected (in part) by variation of the limits of integration, and this is what distinguishes shape optimization compared with other categories of problems in optimal structural design. The implications of "variation in domain boundary" on the evaluation of "variation of state with respect to design change" is described qualitatively with the help of the sketch of *state* versus *domain* in Fig. 1. The total variation is expressed as $\delta_T z = \delta z + (\partial z/\partial x)\delta x$, and of course, the difference between $\delta_T z$ and δz reflects the contribution associated with "change of domain."

An analysis for shape optimization, presented in several separate papers by the authors Cea, Haug, Zolesio, and Rousselet (original papers are in reference [13]), produces an expression for the variation of an objective functional such as the one in problem (6), in terms of normal displacement of the boundary. The development is described using ideas from the kinematics for deformation of a continuum and in particular the concept of material derivative. A concise description of this analysis is given in reference [14, Section 15.3]. The result itself provides the means required for first-order computational methods, to evaluate the design derivative for a small change in the shape design. The set of cited papers includes a discussion of solution procedures and the treatment of example problems.

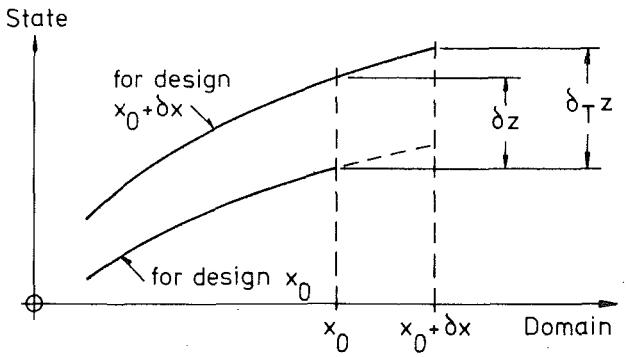


Fig. 1

In a conceptually different approach, the necessary conditions for optimal shape are generated directly from variational analysis expressed for variable domain (free boundary) problems. Examples of such analysis are provided for various planar problems in papers by the authors Haug, Rousselet, Banichuk, Cherkaev, Karihaloo, Gurvich, Onoprienko and Parbery (all cited with brief descriptions in reference [14, Section 15.2]), as well as in a series of papers by Mróz and Dems (their most recent paper appears in [16]). An exceptionally readable version of the variational treatment for maximum stiffness of a torsion bar is given in reference [14, Section 15.4].

The necessary conditions for shape design problems include a requirement (the optimality condition) that within the limitations of design constraints, specific energy or mutual energy has constant value over the optimum boundary. This corresponds to the similar result obtained in the material-placement design example described in Section 4. For the aforementioned torsion problem, the optimality condition is

$$\nabla z \cdot \nabla z = \text{const.} \tag{16}$$

on the optimal boundary. In equation (16), z represents the Prandtl stress function; torsional stiffness is given by $2\iint z\, dA$. As was indicated for other categories of structural optimization problems, the appropriate expression of specific energy provides a local measure of design sensitivity. In the torsion problem, the measure $\nabla z \cdot \nabla z$ reflects the change in stiffness per unit area of material added along the boundary. We note that the simplicity of form of the optimality condition tends to be misleading – generally it is not a simple matter to implement the condition in a procedure for computational solution.

The variational analysis has also been worked out for the design of optimal modification (remodel) of shape, see reference [16, pp. 216–223]. Not surprisingly the resulting optimality condition requires that specific energy have constant value over the optimally modified portions of the boundary. Also this value is an upper bound to the value of specific energy on other parts of the boundary.

In yet another approach, optimal shape may be predicted indirectly for two-dimensional problems by operating in an appropriate way with a model for material placement design. Consider as an example the material placement design of a membrane, where the design is represented by thickness $t(x, y)$, and suppose that the optimal thickness can be predicted within the constraint $t \geq \bar{t}$ over the domain Ω^* that covers admissible domains for the optimally shaped membrane. In terms of a sequence of solutions to this problem for decreasing value of the bound $\bar{t}$, the optimally shaped membrane is obtained from the limit solution for $\bar{t} \to 0$. An application of this method is described in [45].

7 Multimodality in Certain Problems Involving Eigenvalues

A large class of problems involves optimization with respect

Downloaded 02 May 2010 to 171.66.16.250. Redistribution subject to ASME license or copyright; see http://www.asme.org/terms/Terms_Use.cfm

to a *fundamental eigenvalue*, e.g., the fundamental natural vibration frequency, buckling load, or critical aeroelastic divergence or flutter speed, see references [10, 11, 19]. Since design changes involve changes in the entire spectrum of a given type of eigenvalue, one or more higher order eigenvalue may very well descrease during the process of optimizing with respect to the fundamental one. This may result in a *coalescence* of eigenvalues such that the fundamental eigenvalue of the optimized structure becomes *multimodal* (or *multiple*), i.e., associated with more than one *eigenmode* (deflection function).

Experience in recent years has revealed that generation of multimodality by optimization with respect to eigenvalues is not uncommon. It is an important as well as tricky issue, because possible multiplicity is generally not known a priori, but must, nevertheless, be appropriately allowed for in the mathematical formulation and solution procedure, in order that the correct optimal solution can be determined.

As an example; consider a thin, straight, elastic column that has geometrically similar (e.g., circular) cross sections of variable area $D(x)$, such that the area moment of inertia is $I(x) = c\,D^2(x)$, where c is a given constant for the cross-sectional geometry. The column has a given volume V,

$$\int_0^L D\,dx = V, \tag{17}$$

given length L and Young's modulus E, and is subjected to an axial compressive force, the value of which is P at buckling. If we assume that the deflection $y(x)$ is normalized by

$$\int_0^L y'^2 dx = 1, \tag{18}$$

then the critical value of P, i.e., the Euler buckling load, will be given by the potential energy in the buckled state,

$$P = \int_0^L \mathrm{E}cD^2 y''^2 dx. \tag{19}$$

The problem of determining the cross-sectional area function $D(x)$ that maximizes the Euler buckling load P for given values of V, L, E, and c may be stated as

$$\max_{D(x)} \left(P = \int_0^L \mathrm{E}cD^2 y''^2 dx\right) \tag{20}$$

subject to: the constraints of equations (17) and (18).

Here, no minimum constraint has been specified for the design variable $D(x)$. Following the procedure outlined in Section 4, we obtain by varying $y(x)$ and $D(x)$ the well-known buckling differential equation

$$(\mathrm{E}cD^2 y'')'' + Py'' = 0, \tag{21}$$

and optimality condition

$$Dy''^2 = k, \tag{22}$$

where k is a positive constant.

The coupled set of differential and integral equations (17)–(19), (21), and (22), together with appropriate boundary conditions, governs the optimization problem (20) if P is a simple eigenvalue. It constitutes the traditional formulation of the problem and will be referred to as the *single mode formulation*.

Note that within this formulation, if there is an inner point of zero bending moment, $\mathrm{E}cD^2y'' = 0$, according to the optimality condition (22), we will have $\mathrm{E}c\,k^{1/2}D^{3/2} = 0$, i.e., both the cross-sectional area D and the bending stiffness $\mathrm{E}c\,D^2$ will vanish. This means that a discontinuity of the slope y' of the deflection is possible at the point, which will actually correspond to an *inner hinge* of zero bending moment.

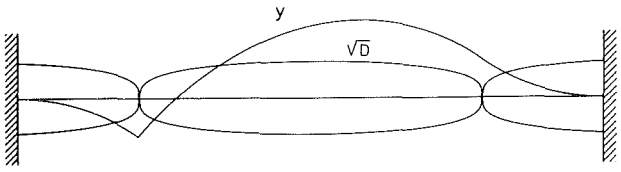


Fig. 2

Consider now the problem of optimizing a *doubly clamped column*. The solution that is *optimal within the single mode formulation* of the problem, see [46], is shown in Fig. 2 by design $\pm\sqrt{D}$ and corresponding fundamental mode y. It has inner hinges at distances $0.208 \cdot L$ from the clamped ends. The Euler buckling load of this column is $P = 42.91 \cdot c\,\mathrm{E}V^2/L^4$, which is 8.7 percent higher than for the corresponding uniform column.

However, the design shown in Fig. 2 is only optimal within the class of doubly clamped columns with *two inner hinges* [46]. It is quite obvious that the column would obtain a greater Euler buckling load for the same volume, length, cross-sectional shape, and material, if it were made to buckle in a symmetric fundamental buckling mode with a continuous slope throughout. This could easily be achieved by redistributing the given amount of material slightly so that the hinges became locked. However, as was discussed earlier, the problem is that the optimality condition (22) of the traditional, single mode formulation for optimal design *predicts* zero cross section and bending stiffness at points of vanishing bending moment, and two such points are necessarily present in a doubly clamped column whenever the single mode formulation is used. This clearly indicates that the *single mode formulation is inadequate* for the problem under consideration, which motivates a *reformulation* of the problem in [46].

The reformulation is based on the assumption that the fundamental buckling load of the optimal design may be a *double* (or *bimodal*) *eigenvalue*, i.e., that the optimal value of P may be associated with *two* linearly independent buckling modes, $y_1(x)$ and $y_2(x)$. The development is based on a functional formed as the bimodal potential energy of the column in its buckled state and terms that represent the volume constraint and conditions of normalization of the modes, respectively. By variational analysis of the functional, a set of *bimodal governing equations* is derived for the optimization problem. This set consists of (18), (19), and (20) expressed in terms of $y_1(x)$ and $y_2(x)$, together with (17) and a new, bimodal optimality condition of the form

$$D(x)\left[(1-\gamma)y_1''^2 + \gamma\, y_2''^2\right] = k. \tag{23}$$

Here γ, $0 \le \gamma \le 1$, is a Lagrangian multiplier and k a positive constant. We note that this optimality condition does not necessarily lead to vanishing column cross section at points of zero bending moment, as was the case with the earlier condition (22).

Indeed, solving the bimodal set of equations, which is done numerically in [46], the optimal design is found to have *finite* variable cross section throughout, with a minimum magnitude of $0.226 \cdot V/L$ attained at distances $0.247 \cdot L$ from the clamped ends.

This bimodal optimal design is symmetrical within double precision computational accuracy, and is shown to suitable scale in Fig. 3 by linear dimensions $\pm\sqrt{D}$. Figure 3 also shows modes y_1 and y_2 for the double optimal buckling eigenvalue. Purely symmetrical and antisymmetrical combinations of these modes can be constructed which satisfy the set of bimodal equations together with the same design $D(x)$, but a

Downloaded 02 May 2010 to 171.66.16.250. Redistribution subject to ASME license or copyright; see http://www.asme.org/terms/Terms_Use.cfm

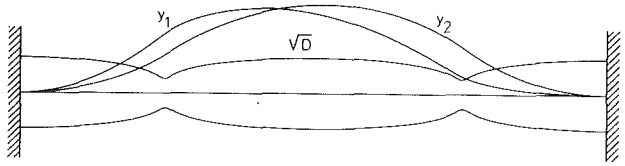


Fig. 3

different value of γ. The optimal, double buckling load is found to be $P = 52.3563 \cdot c\,EV^2/L^4$, i.e., 32.62 percent higher than the buckling load of a uniform, doubly clamped column of the same volume, length, and material. The numerical results have recently been confirmed by an exact analytical solution established by Masur [47] for the same problem, and the optimality condition (23) has been rederived via quite different approaches, see, e.g., detailed analyses by Masur [47] and Teschner [16, pp. 424–429].

In fact, great care must be exercised in applying traditional variational analysis to problems involving multimodal optimal eigenvalues. Hence, as was pointed out by Masur and Mróz [48] these problems are of the max-min type, and Haug and Rousselet [49] have shown that their solutions are generally not differentiable in the usual sense (Fréchet differentiable) with respect to all possible types of design changes. However, at least for the case of a doubly clamped column, the recent investigation [47] has shown that at a given bimodal point in the design space there is a subclass of feasible design variations, which involves no trade-off where one of the eigenvalues decreases, but these design variations ensure bimodality of the varied design. Within this relevant set of design variations the solution seems to be differentiable and stationary at its optimum.

Passing now to discuss future problems where optimal eigenvalues of any finite multiplicity may ocur, the aforementioned difficulties can be avoided by adopting a bound formulation of the type discussed in Sections 4 and 5. Let us use the previous Euler column equations for the purpose of illustration. The problem of maximizing the smallest eigenvalue is equivalent to maximizing a lower bound β on the set of eigenvalues P_i, $i = 1, 2, \ldots, \infty$, which, in a min format, may be stated as

$$\begin{aligned} &\min_{D(x)} \ (-\beta) \\ &\text{subject to:} \quad -(P_i-\beta) \le 0 \quad i=1,2,\ldots,\infty \\ &P_i = \int_0^L \mathrm{E}c\, D^2 y_i''^2\, dx \quad i=1,2,\ldots,\infty \qquad (24) \\ &\int_0^L y_i' y_j'\, dx - \delta_{ij} = 0 \quad i=1,2,\ldots,\infty, \quad j=1,\ldots,i \\ &\int_0^L D\, dx - V \le 0. \end{aligned}$$

Here, the entire set of modes y_i, $i=1, \ldots, \infty$, is orthonormalized in the equation where Kronecker's delta, δ_{ij}, appears.

The problem (24) may be interpreted as one of multicriteria optimization (see Section 5) and is treated in detail as an example in reference [43]. Using a variational approach, forming a Lagrangian based on the functional $-\beta$, with the constraints appended by means of Lagrangian multipliers, the Kuhn-Tucker condtions, $\eta_i = 0$ if $P_i > \beta$ and $\eta_i \ge 0$ if $P_i = \beta$, $i = 1, \ldots, \infty$, are obtained for the Lagrangian multipliers η_i associated with the inequalities $-(P_i-\beta) \le 0$, $i = 1, \ldots, \infty$, in (24). Assuming that a total number of N Lagrangian multipliers η_i are greater than zero, implying that at least N eigenvalues P_i are equal to the lower bound value β, or, in other words, that the fundamental eigenvalue is at least N-fold, we have

$$\begin{aligned} &\eta_n > 0, \quad P_n = \beta \quad n = 1, \ldots, N \\ &\eta_n = 0, \quad P_n \ge \beta \quad n = N+1, \ldots, \infty \end{aligned} \qquad (25)$$

after a convenient reindexing of variables. The condition of stationarity of the Lagrangian with respect to the bound β takes the characteristic form

$$\sum_{n=1}^{N} \eta_n = 1, \qquad (26)$$

and the optimality condition becomes

$$D(x) \sum_{n=1}^{N} \eta_n y_n''^2 = k, \qquad (27)$$

where k is a positive constant. Finally, after some manipulations (see [43]), the differential equations for the eigenmodes y_n are obtained in the well-known form

$$(\mathrm{E}c\, D^2 y_n'')'' + P_n y_n'' = 0, \quad n = 1, \ldots, N. \qquad (28)$$

Equations (25)–(28), together with the constraint equations in (24), which need only be considered for $i = n = 1, \ldots, N$, constitute the complete set of governing equations for our multimodal optimization problem. In a given problem, the appropriate value of N is generally unknown a priori and must be determined as the highest possible number of Lagrangian multipliers η_n, which, together with their linearly independent modes y_n, are admitted by the optimality condition (27).

In the derivation of the preceding equations in reference [43], no property of symmetry is assumed for the optimal design $D(x)$, and it is worth noting that no cross product terms appear in the optimality condition (27). This reflects the fact that the mutual energy is zero among the particular orthonormal set of modes y_n, $n = 1, \ldots, N$, which satisfies the governing equations and is associated with the multiple eigenvalue $P_n = \beta$.

We also note that the generalized, multimodal formulation for optimal design, illustrated in the foregoing for the case of column optimization, reduces to the single mode formulation and the bimodal formulation, respectively, for $N = 1$ and $N = 2$. In fact, the mathematical formulations for $N = 1, 2, \ldots, N^*$ are all contained as special cases in the formulation for a given $N = N^* + 1$, which means that the design spaces associated with the formulations for $N = 1, 2, \ldots, N^*$ are all contained as subspaces in the design space corresponding to the formulation for $N = N^* + 1$. Hence, allowance for a higher degree of multiplicity implies *an extension of the design space*.

Other examples that demonstrate necessity of an extended, multimodal formulation have already been found in several conservative problems involving design of arches and frames against vibration and instability, see, for example, work by Blachut, Gajewski, Zyczkowski, Plaut, and Olhoff reported in [16], and the issue has even manifested itself within the class of nonconservative (aeroelastic) problems, see Seyranian [50]. As is pointed out by Masur and Mróz [48], the necessity of applying a bi or multimodal formulation increases with the degree of statical indeterminacy and complexity of the structure to be optimized.

8 Regularization of Problems to Obtain Closure of the Design Space

In recent years it has become clear that in many continuous problems with structural response governed by *partial differential boundary value problems*, there need not exist an optimal design or optimal distribution of material properties

Downloaded 02 May 2010 to 171.66.16.250. Redistribution subject to ASME license or copyright; see http://www.asme.org/terms/Terms_Use.cfm

within some initial formulation of the problem. The typical problems in this category involve thickness optimization of plates and shells, optimization of nonhomogeneous materials, elastoplastic materials, and shape optimization problems where some global or local measure of the solution to a boundary value problem is to be extremized.

The reason for the lack of an optimal solution within an initial or "traditional" formulation is that the set of *feasible* (or *admissible*) designs, i.e., the *design space*, is *not closed* in the appropriate sense, which means that the problem is not well posed. The remedy for this is to ensure closure of the set of feasible designs via a *regularization* of the mathematical formulation of the optimization problem.

Mathematical indications of the need for regularization are generation of *anisotropy* in the design and the impossibility of satisfying the Weierstrass necessary condition for optimality in certain subregions of the structural domain; see Lurie [26]. Numerically, the need manifests itself by lack of convergence or by dependence of the designs on the size of the applied mesh. In particular, it is not possible to obtain a limiting, numerically stable design by consecutively decreasing the mesh size.

As an example, let us consider the problem of minimizing the compliance (maximizing the stiffness) of a thin, axisymmetric, solid elastic plate, using the plate thickness function $h(r)$ as the design variable. A given volume of isotropic material is specified for the plate, which we consider to be annular with given radii of inner and outer clamped edges. We assume an upper and lower bound to be prescribed for the plate thickness, i.e., we have $0 < h_{\min} \leq h(r) \leq h_{\max}$. The static load distribution on the plate is assumed to be given by $p = \text{const} \cdot \cos 4\theta$, i.e., it is independent of the radial coordinate r, but varies harmonically in the circumferential direction θ.

In the so-called "traditional formulation" of plate optimization problems, the optimal plate thickness function h is assumed to belong to the set of continuous functions or continuous functions with a *finite* number of discontinuities, and the plate bending rigidity D, which is proportional to h^3, is assumed to be *isotropic*, i.e., independent of orientation.

Figure 4 depicts some numerical designs obtained by Olhoff and Cheng (reference [13, pp. 278-303]) to our example problem when the traditional formulation is used. The figure shows radial sections through plate designs obtained by using (*a*) 150, (*b*) 200, (*c*) 250, and (*d*) 300 equally spaced mesh points to cover the interval of the radial distance from the inner to the outer plate radius, and it is seen that as the number of mesh points is increased, the rotationally symmetric plate forms an increasing number of thinner and thinner stiffeners to counteract the deflections caused by the circumferentially varying load distribution. At the same time, the plate compliances decrease; they are found to be (*a*) 53.6 percent, (*b*) 52.5 percent, (*c*) 43.3 percent, and (*d*) 42.8 percent, respectively, of the compliance of a uniform reference plate that has the same volume, inner and outer radii, boundary conditions, loading, and material.

The results clearly indicate that a limiting design cannot be obtained by continuously increasing the number of mesh points, i.e., an optimal design does not exist within the set of thickness functions considered in the "traditional formulation": the design space associated with that formulation is not closed.

To determine the optimal solution, it is necessary to extend the design space such as to include the limiting designs. In reference [51], this is done by constructing a new, *generalized plate model*, which covers geometrical anisotropy as well as isotropy, and which constitutes the basis for a regularization of the mathematical formulation of the optimization problem. The new, axisymmetric plate model consists of a

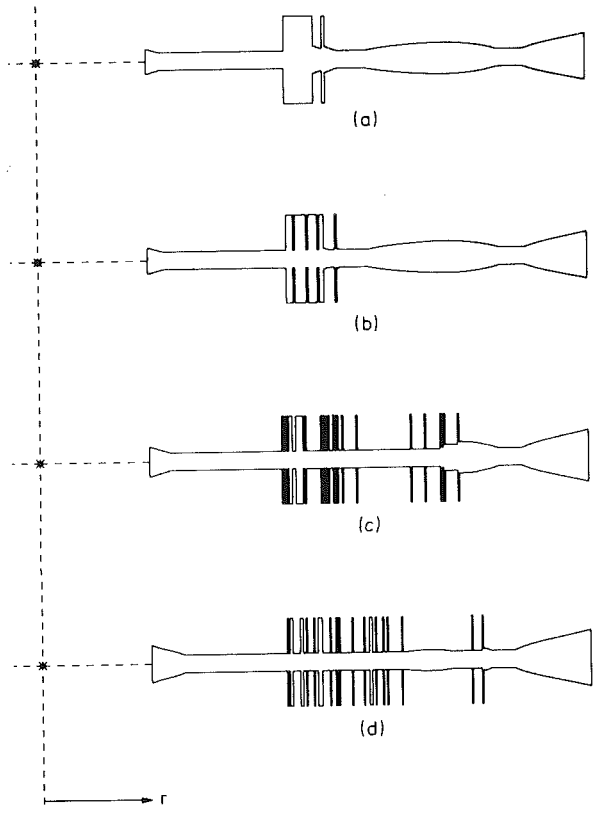


Fig. 4

solid part of variable thickness $h_s(r)$, $0 < h_{\min} \leq h_s \leq h_{\max}$, which is equipped with a system of infinitely thin integral stiffeners (or ribs) of variable *concentration* (or *density*) $\mu(r)$. Figure 5 shows a radial section through a small ring element of the plate. It has the radial extent Δr and a finite number of circumferential stiffeners of rectangular cross section of height $h_{\max} - h_s$. The concentration of the stiffeners is defined by

$$\mu(r) = \lim_{\Delta r \to 0} \frac{\sum_i \Delta c_i}{\Delta r}, \quad 0 \leq \mu(r) \leq 1, \tag{29}$$

where Δc_i is the width of the ith stiffener of the small element.

The regularized formulation in [51] involves the use of *two* simultaneous design variables, namely $h_s(r)$ and $\mu(r)$. Moreover, since the design is inherently *geometrically anisotropic* (cylindrically orthotropic) in subregions where $0 < \mu < 1$, it is necessary to consider the plate bending rigidity to be a *tensor*, i.e., to depend on orientation. The expressions for the components of this tensor are derived via two different *smear-out procedures* by Cheng in reference [13, pp. 304-332] and by Olhoff et al. in reference [52].

The optimal solution obtained in [51] to the regularized formulation of our example problem is shown in Fig. 6 (the scale is a little different from that used in Fig. 4). The unhatched area in Fig. 6 indicates the solid part of the plate, whose thickness is $h_s(r)$, and the sum of the extents in the normal direction of the hatched areas at a given value of the radial coordinate r represents $\mu(r) \cdot (h_{\max} - h_s(r))$. This function is plotted to the same scale as $h_s(r)$ in the figure, and illustrates the material consumption of the integral stiffeners by an equivalent thickness of purely solid material. The solid curve above the plate represents the θ-independent factorial $w(r)$ of the deflection function $W(r, \theta) = w(r) \cdot \cos 4\theta$. The compliance of the optimal design in Fig. 6 under the given load is only 36 percent of the compliance of the corresponding uniform plate of the same volume, and may be compared with the results stated earlier for the designs in Fig. 4.

Downloaded 02 May 2010 to 171.66.16.250. Redistribution subject to ASME license or copyright; see http://www.asme.org/terms/Terms_Use.cfm

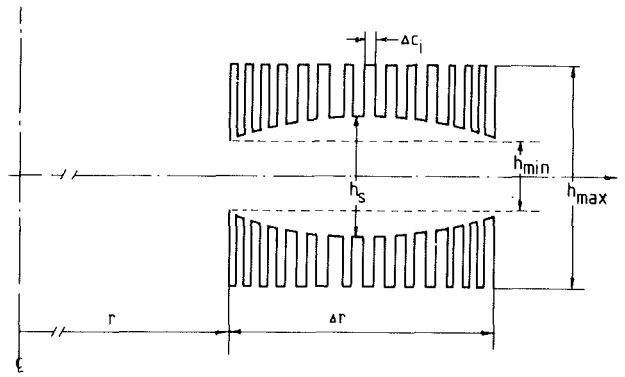


Fig. 5

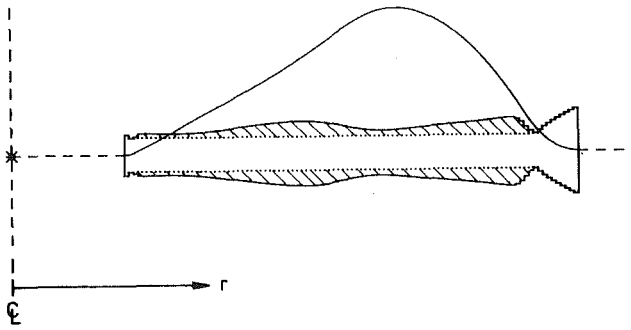


Fig. 6

The solution presented in Fig. 6 is numerically stable, which indicates closure of the design space by the regularized formulation, and the design must be expected to constitute the optimal solution within the type of plate topology considered. It is obvious, however, that a further extension of the design space by dropping the condition of axisymmetry of the plate, and allowing for an additional field of (radial) stiffeners, would lead to designs with even more optimal characteristics.

The regularized formulation of a *general* plate optimization problem is quite complex and involves four functions as simultaneous design variables: the thickness of the solid part of the plate, the concentrations of two mutually orthogonal fields of integral stiffeners, and the orientation of the stiffeners. This type of problem has only been studied very recently, see Rozvany et al. [53] for plastic plates and Bendsøe [15, pp. 13.29–13.34] for elastic plates, and up to now no optimal solutions are available for the general plate case.

Optimal designs of the type discussed in the foregoing must of course be considered as limiting designs from the point of view of practical application. In practice, the system of infinitely many, infinitely thin integral stiffeners may be lumped into a finite number of stiffeners of finite width (to meet stability requirements, for example), and it is worth mentioning that in [51] the efficiency of such a modified design is found to be reduced only very slightly relative to that of the optimal design.

Instead of using an extension as previously described, the set of feasible designs may as well be closed by a *restriction* of the design space. Dealing with optimization of axisymmetric plates, Niordson (see reference [16, pp. 380–386]) introduced a restriction on the set of designs considered feasible in the "traditional formulation" by specifying a constraint on the maximum absolute value of the slope of the plate thickness function. Such a constraint removes the anomalies of the traditional formulation described earlier, and has the advantage that the well-known theory of thin, *isotropic* elastic plates can still be used. But this is at the expense that the designs obtained are much less efficient than the geometrically anisotropic optimal designs determined via extension of the design space. Bendsøe, see reference [16, pp. 270–275], has shown mathematically that the restriction of the design space introduced via a maximum allowable value of the slope of the plate thickness function ensures the existence of solutions to a number of design objectives. Mathematical existence proofs are not available today for a general plate optimization problem involving extension of the design space, but have been given by Lurie et al. in references [54, 55] for some special cases.

The principal steps in the development of mathematical proofs of existence of solutions and closure of the design space for optimization problems involving a global or local measure of the solution to a boundary value problem, have, not surprisingly, many features in common with the approach described in the foregoing, and will be briefly outlined in a formal way in the sequel.

Consider the set of solutions (displacements) $z(D)$ to the boundary value problem consisting of the differential equation

$$L(D)z = 0 \tag{30}$$

and given boundary conditions, where $D \in \mathbf{D}$ represents a design or material distribution function belonging to the set $\mathbf{D}$.

Let $\{z_i\} = \{z(D_i)\}$ be some arbitrary, weakly convergent sequence of solutions. Denote by z^0 the weak limit of such a sequence,

$$z_i - z^0. \tag{31}$$

The function z^0 need not correspond to some design $D \in \mathbf{D}$.

Seek now, following, for example, reference [56], the so-called *G-closure* of the set $\mathbf{D}$. This problem consists in establishing a general description of the complete set of designs or material distributions that may be assembled from the given set of material(s). Physically, this usually involves processes of *mixing*, in which kinds of layered composites or other anisotropic designs (which need not correspond to a measurable partition of the structural domain), are considered. The problem of determining the G-closure is in this case mathematically similar to the problem known as *homogenization*, i.e., to determine the limit in some sense (here the G-limit) of a sequence of partial differential operators with rapidly varying coefficients, see e.g. Bensoussan et al. [27]. The homogenization has, in turn, its analogue in the smear-out process mentioned in connection with our example problem.

Now, if the G-closure problem can be solved, we obtain tensor functions $\bar{D}$ such that for any z^0 there will exist a $\bar{D}$ which can be set into correspondence

$$z^0 = z^0(\bar{D}) \tag{32}$$

with the element z^0. Then, the extended set of designs $\mathbf{D} \cup \bar{\mathbf{D}}$ (where $\bar{\mathbf{D}} = \{\bar{D}\}$) will be G-closed, and the problem of minimization of some weakly continuous functional $F(z)$ of the solution z will have its solution within this set. The minimum value $F(z^0)$ of the functional will then be the limit of some minimizing sequence $F(z_i)$,

$$F(z^0) = \lim_{i \to \infty} F(z_i). \tag{33}$$

The reader is referred to a recent paper by Armand [16, pp. 256–263] for an account of the types of problem for which G-closures of initially isotropic designs have been determined.

Some interesting examples from Lurie et al. [55] of numerical solutions obtained on the basis of G-closure developed as outlined in the foregoing, are illustrated in Figs. 7 and 8. These figures show, respectively, solutions to the problems of maximizing and minimizing the torsional rigidity of a bar that has a square cross section and is made of two elastic materials with different shear moduli. The modulus of

Downloaded 02 May 2010 to 171.66.16.250. Redistribution subject to ASME license or copyright; see http://www.asme.org/terms/Terms_Use.cfm

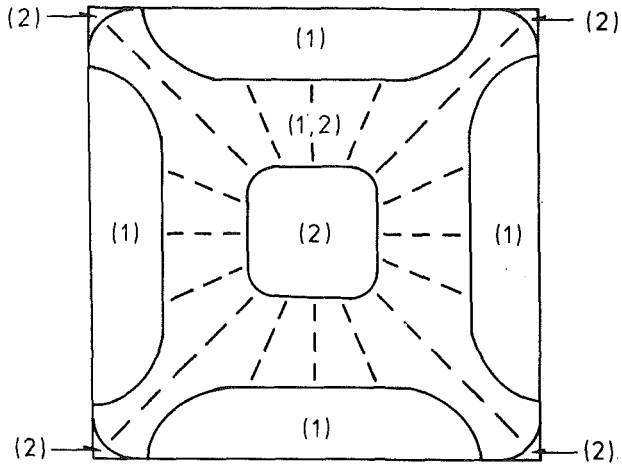


Fig. 7

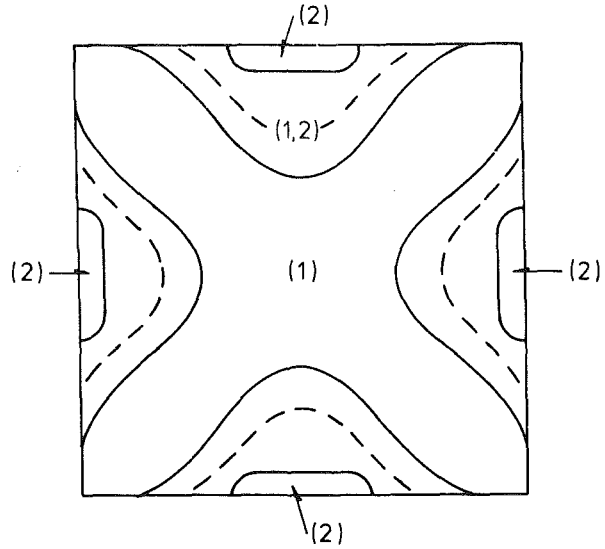


Fig. 8

the hard material indicated by (1) in the figures is taken to be three times that of the soft material (2), and four times as much hard material is available as soft material. In both optimal solutions there is a subarea, indicated by (1, 2), with *anisotropic* material between the subareas with isotropic, purely hard (1) and purely soft (2) materials. This anisotropic material is composed of consecutive, infinitely thin layers of hard and soft material, which constitute the G-closure for the problems in question. These layers follow the orientation of the contour lines of the Prandtl field, and are orthogonal to the dashed lines shown in the subareas (1, 2).

Solutions to problems of closure and regularization have yet to be obtained in a number of optimal design contexts, and lively activity is going on. In addition to the research cited earlier, mention should be made of very interesting work being carried out by Kohn, Strang et al. [57, 58]. In perfect agreement with the spirit of optimization, it is the principal task in all these investigations to seek, and to introduce into the analysis, new types of effective, generalized structures and composites, that can be constructed from some initial class.

9 Closure

A survey of the field of structural optimization from the point of view of fundamental aspects is attempted in this paper. The basic concepts of the field are reviewed and its main areas identified, and a variational approach is used as a means to illustrate quantitative features and properties and to facilitate our discussion of the state of the art in terms of current knowledge and areas of new development.

In optimization of structures, experience has shown that particular attention must be paid to the following five principal points in order that efficient and practical designs may be obtained:

(1) the objective or cost function must be taken to be as realistic as possible;
(2) the largest possible number of design variables of different types must be selected;
(3) as many realistic design requirements (behavioral constraints) as possible must be considered;
(4) the mathematical formulation must admit accommodation for unexpected properties of the optimal solution; and
(5) effective solution procedures are necessary.

These items are strongly interrelated. Item (1) is very important in practical design contexts, and it is recommended that more attention be paid to it in future research.

Item (2) implies enlargement of the design space, which opens the possibility of obtaining designs of increased efficiency. The fact that shape optimization introduces a new class of design variables in addition to types considered earlier explains the significance of this fruitful, relatively new area of research.

Item (3) is of major practical importance because optimization under few behavioral requirements will often weaken the structure drastically with respect to a type of failure that is not accounted for. This underscores the relevance of multicriteria optimization, and increased research efforts should be devoted to this area in the future.

The significance of Item (4) is due to the fact that optimization may generate unexpected features like multiple optimal eigenvalues and anisotropic designs or materials, which must be appropriately allowed for in the problem formulation as well as in the solution procedure in order that the correct solution may be obtained. Here, as well as in other contexts, it is important to note that even though most problems are eventually to be solved in *discretized* form, for most efficient treatment overall the *continuum problem* should be *analyzed* for as many *qualitative results* as possible *before* discretization. As is indicated in Section 7, much work remains to be done to gain a better understanding of multimodality in conservative and nonconservative problems involving eigenvalues, and the results discussed in Section 8 imply, for example, a need to revise a large number of smooth designs previously obtained for plastic as well as elastic solid plates and shells on the basis of traditional formulations.

The development of effective solution procedures (Item 5), in particular numerical methods for optimization of complex practical structures, constitutes a large and most important research area. The progress in this area has been discussed in excellent, recent reviews [4, 7, 8, 9, 11], and has therefore only been touched on in this paper. Also, the cited reviews discuss several applications of structural optimization.

References

Reviews and Surveys

1 Wasiutyński, Z., and Brandt, A., "The Present State of Knowledge in the Field of Optimum Design of Structures," ASME *Applied Mechanics Review*, Vol. 16, 1963, pp. 344–350.

2 Sheu, C. Y., and Prager, W., "Recent Developments in Optimal Structural Desiogn," ASME *Applied Mechanics Reviews*, Vol. 21, 1968, pp. 985–992.

3 Niordson, F. I., and Pedersen, P., "A Review of Opticmal Structural Design," in *Proc. 13th Int. Cong. Th. Appl. Mech.*, Becker, E., and Mikhailov, G. K., eds., Moscow, 1972; Springer-Verlag, 1973, pp. 264–278.

4 Lev, O. E., ed., *Structural Optimization, Recent Developments and Applications*, American Society of Civil Engineers, New York, 1981.

Downloaded 02 May 2010 to 171.66.16.250. Redistribution subject to ASME license or copyright; see http://www.asme.org/terms/Terms_Use.cfm

5 Qian, L., "Structural Optimization Research in China," in *Proc. Int. Conf. Finite Element Methods*, Shanghai, China, Aug. 1982, pp. 16-24.

6 Rozvany, G. I. N., and Mróz, Z., "Analytical Methods in Structural Optimization," ASME *Applied Mechanics Reviews*, Vol. 30, 1977, pp. 1461-1470.

7 Venkayya, V. B., "Structural Optimization: A Review and Some Recommendations," *Int. J. Num. Meth. Eng.*, Vol. 13, 1978, pp. 205-228.

8 Schmit, L. A., "Structural Synthesis—Its Genesis and Development," *AIAA Journal*, Vol. 19, 1981, pp. 1249-1263.

9 Vanderplaats, G. N., "Structural Optimization—Past, Present, and Future," *AIAA Journal*, Vol. 20, 1982, pp. 992-1000.

10 Olhoff, N., "Optimal Design With Respect to Structural Eigenvalues," in *Proc. 15th Int. Cong. Th. Appl. Mech.*, Rimrott, F. P. J., and Tabarrok, B. B., eds., Toronto, 1980; North-Holland, 1980, pp. 133-149.

11 Ashley, H., "On Making Things the Best—Aeronautical Uses of Optimization," *J. Aircraft*, Vol. 19, 1982, pp. 5-28.

Proceedings

12 Sawczuk, A., and Mróz, Z., eds., *Optimization in Structural Design*, Proc. IUTAM Symp., Warsaw 1973, Springer-Verlag, Berlin, 1975.

13 Haug, E. J., and Cea, J., eds., *Optimization of Distributed Parameter Structures*, Vol. 1 and 2, Proc. Nato ASI Meeting, Iowa City, 1980, Noordhoff, The Netherlands, 1981.

14 Morris, A. J., ed., *Foundations of Structural Optimization: A Unified Approach*, Proc. Nato ASI Meeting, Liege, Belgium 1980, Chichester, England, 1982.

15 Gallagher, R. H., ed., *Proc. Int. Symp. Optimum Structural Design*, University of Arizona, Tucson, Ariz., 1981.

16 Eschenauer, H., and Olhoff, N., eds., *Optimization Methods in Structural Design*, Proc. Euromech Colloquium 164, Siegen, FRG, 1982, Bibliographisches Institut, Mannheim, 1983.

Textbooks

17 Prager, W., *Introduction to Structural Optimization*, Int. Centre for Mech. Sci., Udine, No. 212, Springer-Verlag, Vienna, 1974.

18 Rozvany, G. I. N., *Optimal Design of Flexural Systems*, Pergamon Press, Oxford, 1976.

19 Grinev, W. B., and Filippov, A. P., *Optimization of Beams Governed by Eigenvalue Problems* (in Russian), Naukova Dumka Kiev, 1979.

20 Haug, E. J., and Arora, J. S., *Applied Optimal Design*, Wiley, New York, 1979.

21 Banichuk, N. V., *Optimization of the Shapes of Elastic Bodies* (in Russian), Nauka, Moscow, 1980. (English translation to appear.)

22 Kirsch, U., *Optimum Structural Design*, McGraw-Hill, New York, 1981.

23 Carmichael, D. G., *Structural Modelling and Optimization*, Ellis Horwood Ltd., Chichester, England, 1981.

24 Troitskij, W. A., and Petuchov, L. W., *Optimal Design of Elastic Bodies* (in Russian), Nauka, Moscow, 1982.

25 Lepik, Ü., *Optimal Design of Inelastic Structures Under Dynamic Loading* (in Russian; extended summary in English), Walgus, Tallinn, 1982.

26 Lurie, K. A., *Applied Optimal Control of Distributed Systems*, Plenum Press, New York (to appear).

27 Bensoussan, A., Lions, J. L., and Papanicolaou, G., *Asymptotic Analysis for Periodic Structures*, North-Holland, Amsterdam, 1978.

Papers and Reports

28 Prager, W., and Taylor, J. E., "Problems of Optimal Structural Design," ASME JOURNAL OF APPLIED MECHANICS, Vol. 35, 1968, pp. 102-106.

29 Drucker, D. C., and Shield, R. T., "Design for Minimum Weight," in *Proc. 9th Int. Cong. Th. Appl. Mech.*, Brussels, 1956, University of Brussels, 1957, Vol. 5, pp. 212-222.

30 Marcal, P. V., and Prager, W., "A Method of Optimal Plastic Design," *J. de Mécanique*, Vol. 3, 1964, pp. 509-530.

31 Prager, W., and Shield, R. T., "A General Theory of Optimal Plastic Design," ASME JOURNAL OF APPLIED MECHANICS, Vol. 34, 1967, pp. 184-186.

32 Save, M. A., "A Unified Formulation of the Theory of Optimal Plastic Design With Convex Cost Function," *J. Struct. Mech.*, Vol. 1, 1972, pp. 267-276.

33 Keller, J. B., "The Shape of the Strongest Column," *Arch. Rational Mech. Anal.*, Vol. 5, 1960, pp. 275-285.

34 Masur, E. F., "Optimum Stiffness and Strength of Elastic Structures," *J. Eng. Mech. Div.*, ASCE, Vol. 96, 1970, pp. 621-640.

35 Rozvany, G. I. N., and Prager, W., "A New Class of Optimization Problems: Optimal Archgrids," *Comp. Meth. Appl. Mech. Eng.*, Vol. 19, 1979, pp. 127-150.

36 Niordson, F. I., "On the Optimal Design of a Vibrating Beam," *Quart. Appl. Mech.*, Vol. 23, 1965, pp. 47-53.

37 Mróz, Z., and Mironov, A., "Optimal Design for Global Mechanical Constraints," *Arch. Mech. Stos.*, Vol. 32, 1980, pp. 505-516.

38 Haug, E. J., "A Unified Theory of Optimization of Structures With Displacement and Compliance Constraints," *J. Struct. Mech.*, Vol. 9, 1981, pp. 415-437.

39 Taylor, J. E., and Bendsøe, M. P., "An Interpretation for Min-Max Structural Design Problems Including a Method for Relaxing Constraints," *Int. J. Solids Structures*, to appear.

40 Stadler, W., "A Survey of Multicriteria Optimization or the Vector Maximum Problem, Part I: 1776-1960," *JOTA*, Vol. 29, 1979, pp. 1-52.

41 Stadler, W., "Applications of Multicriteria Optimization in Engineering and the Sciences (A Survey)," in *MCDM—Post Decade and Future Trends*, Zeleny, M., ed., JAI Press, Greenwich, Conn., 1983.

42 Stadler, W., "A Comprehensive Bibliography on MCDM," ibid.

43 Bendsøe, M. P., Olhoff, N., and Taylor, J. E., "A Variational Formulation for Multicriteria Structural Optimization," *J. Struct. Mech.*, Vol. 11, No. 4, 1983.

44 Pedersen, P., and Laursen, C. L., "Design for Minimum Stress Concentration by Finite Elements and Linear Programming," *J. Struct. Mech.*, Vol. 10, 1982, pp. 375-391.

45 Rossow, M., and Taylor, J. E., "An Optimal Structural Design Algorithm Using Optimality Criteria," *Int. J. Solids Structures*, Vol. 13, 1977, pp. 913-923.

46 Olhoff, N., and Rasmussen, S. H., "On Single and Bimodal Optimum Buckling Loads of Clamped Columns," *Int. J. Solids Structures*, Vol. 13, 1977, pp. 605-614.

47 Masur, E. F., "Optimal Structural Design Under Multiple Eigenvalue Constraints," *Int. J. Solids Structures* (to appear).

48 Masur, E. F., and Mróz, Z., "Singular Solutions in Structural Optimization Problems," in *Proc. IUTAM Symp. Variational Meth. in Mech.*, Evanston, Ill., 1978, Nemat-Nasser, S., ed., Pergamon Press, Oxford, 1980, pp. 337-343.

49 Haug, E. J., and Rousselet, B., "Design Sensitivity Analysis in Structural Mechanics, II. Eigenvalue Variations," *J. Struct. Mech.*, Vol. 8, 1980, pp. 161-186.

50 Seyranian, A. P., "Sensitivity Analysis and Optimization of Aeroelastic Stability," *Int. J. Solids Structures*, Vol. 18, 1982, pp. 791-807.

51 Cheng, K.-T., and Olhoff, N., "Regularized Formulation for Optimal Design of Axisymmetric Plates," *Int. J. Solids Structures*, Vol. 18, 1982, pp. 153-169.

52 Olhoff, N., Lurie, K. A., Cherkaev, A. V., and Fedorov, A. V., "Sliding Regimes and Anisotropy in Optimal Design of Vibrating Axisymmetric Plates," *Int. J. Solids Structures*, Vol. 17, 1981, pp. 931-948.

53 Rozvany, G. I. N., Olhoff, N., Cheng, K.-T., and Taylor, J. E., "On the Solid Plate Paradox in Structural Optimization," *J. Struct. Mech.*, Vol. 10, 1982, pp. 1-32.

54 Lurie, K. A., and Cherkaev, A. V., "G-Closure of Some Particular Sets of Admissible Material Characteristics for the Problem of Bending of Thin Plates," DCAMM Report No. 214, The Technical University of Denmark, June 1981.

55 Lurie, K. A., Cherkaev, A. V., and Fedorov, A. V., "Regularization of Optimal Design Problems for Bars and Plates," *JOTA*, Vol. 37 (Part 1), pp. 499-522, (Part 2), pp. 523-543, 1982.

56 Marino, A., and Spagnolo, S., "Un Tipo di Approssimazione dell' Operatore $\Sigma_{i,\,j}\ \mathfrak{D}_i(a_{ij}(x)\mathfrak{D}_j)$ con Operatori $\Sigma_j\ \mathfrak{D}_j b(x)\mathfrak{D}_j$, *Annali Scuola Normale Superiore di Piza, Scienze Fisiche e Matematiche*, Vol. 23, 1969, pp. 657-673.

57 Kohn, R. V., and Strang, G., "Structural Design Optimization and Relaxation of Variational Problems," in *Proc. Conf. Disordered Media*, New York 1981, Springer-Verlag, Berlin (to appear).

58 Kohn, R. V., and Vogelius, M., *A New Model for Thin Plates With Rapidly Varying Thickness*, Rept., Courant Institute of Mathematical Sciences, New York, 1982. (Submitted to *Int. J. Solids Structures*.)

Downloaded 02 May 2010 to 171.66.16.250. Redistribution subject to ASME license or copyright; see http://www.asme.org/terms/Terms_Use.cfm

Yih-Hsing Pao
Department of Theoretical and Applied Mechanics, Cornell University, Ithaca, N.Y. 14853
Fellow ASME

Elastic Waves in Solids

Research contributions over the past 50 years on the theory and analysis of elastodynamics are reviewed in this paper. Major topics reviewed are: general theories, steady-state waves in waveguides, transient waves in layered media, diffraction and scattering, and one and two-dimensional theories of elastic bodies. A brief discussion on the direct and inverse problems of elastic waves completes this review.

As a branch of the theory of elasticity, elastodynamics appears to be a rather new and recent topic in the literature of applied mechanics. Early issues of the JOURNAL OF APPLIED MECHANICS contained very few papers on the propagation of elastic waves. It was not until the 1950s that research articles on stress waves began to appear in the journal.

In fact, elastodynamics was the oldest subject of elasticity. It began with Navier's theory of motion of elastic bodies in 1821. His theory was soon adopted by A. L. Cauchy and S. D. Poisson to model light waves in ether. In fact, Cauchy's theory of elasticity, published in 1827–1828, was developed primarily to investigate the propagation of light as a transverse wave in an elastic solid (see Chapter 5 of reference [1]).

The publication of the monograph entitled "Stress Waves in Solids" by Kolsky in 1953 [2] marked the revival of research on elastic waves. Until that time, the main sources of reference on elastic waves in the English literature were Love's treatise on elasticity (Chapters 11, 12, reference [3]) and Rayleigh's *Theory of Sound* [4]. There were also a few books on theoretical seismology, especially that by Bullen [5], but they were not directed at engineering applications. Kolsky's monograph mainly reported the new developments in the 1940s on elastic waves, viscoelastic waves, and plastic waves related to dynamic loading on materials and structures.

Since then, the research activity on elastic waves has grown rapidly within the community of applied mechanics. By the 1970s, there appeared five reference-textbooks on elastodynamics: the one by Nowacki [6], Achenbach [7], Graff [8], Eringen and Suhubi [9], and Miklowitz [10]. In addition, there were many monographs on special topics of elastic waves published during this period, which will be discussed later.

The research on elastic waves was equally active in the field of geophysics. In chronological order we cite the monographs by Ewing, Jardetsky, and Press [11], Brekhovskikh [12], White [13], Aki and Richards [14], and Ben-Menahem and Singh [15]. Another field active on the subject is that of physical acoustics and ultrasonics. The monograph by Truell, Elbaum and Chick [16], and that by Auld [17] are representative.

The mathematical theory of elasticity is formulated in terms of body force $\mathbf{f}$, surface force (traction) $\mathbf{T}$, stress tensor τ, strain tensor ϵ, and displacement vector $\mathbf{u}$ of an elastic body. The material remains elastic during deformation. Isotropic materials are characterized by material constants, such as Young's modulus E, shear modulus μ, Poisson's ratio ν, and Lamé's constants λ and μ. Anisotropic materials are characterized by 21 independent stiffness coefficients c_{ijkl}. The theory of elastodynamics specializes in the case when all fields are time-dependent. Therefore, in addition to the displacement, $\mathbf{u}(\mathbf{x},t)$, the velocity and acceleration of a particle in the body are of interest. The mass density ρ becomes an important parameter in measuring the inertia.

The linear theory of elastodynamics is embodied in the following set of equations defined for a body of volume V enclosed by a surface $S = S_1 + S_2$:

Equations of Motion:

$$\nabla \cdot \tau + \rho\,\mathbf{f} = \rho\,\ddot{\mathbf{u}} \quad \mathbf{x} \text{ in } V \tag{1}$$

Constitutive Equation:

$$\tau_{ij} = c_{ijkl}(\partial\, u_1/\partial\, x_k) \quad \mathbf{x} \text{ in } V \tag{2}$$

Boundary Conditions:

$$\mathbf{u}(\mathbf{x},t) = \bar{\mathbf{u}} \qquad \mathbf{x} \text{ on } S_1$$
$$\mathbf{n} \cdot \tau(\mathbf{x},t) = \bar{\mathbf{T}} \qquad \mathbf{x} \text{ on } S_2 \tag{3}$$

Initial Conditions:

$$\mathbf{u}(\mathbf{x},0) = \mathbf{u}_0$$
$$\dot{\mathbf{u}}(\mathbf{x},0) = \mathbf{v}_0 \qquad \mathbf{x} \text{ in } V \tag{4}$$

where $\mathbf{u}_0$, $\mathbf{v}_0$, and $\bar{\mathbf{u}}$, $\bar{\mathbf{T}}$ are prescribed quantities.

Equations (1) and (2) can be combined into one vector equation for $\mathbf{u}(\mathbf{x},t)$

$$\frac{\partial}{\partial x_j}\left(c_{ijkl}\frac{\partial u_l}{\partial x_k}\right) + \rho f_i = \rho \ddot{u}_i \quad \mathbf{x} \text{ in } V \tag{5}$$

This is the celebrated Navier-Cauchy equation of motion for anisotropic, inhomogeneous, elastic solids (1821-1828).

For isotropic materials, we have

$$c_{ijkl} = \lambda \delta_{ij}\delta_{kl} + \mu(\delta_{ik}\delta_{jl} + \delta_{il}\delta_{jk}) \tag{6}$$

Equation (5) for isotropic and homogeneous materials is then expressed as

$$(\lambda + \mu)\nabla\,\nabla \cdot \mathbf{u} + \mu \nabla^2 \mathbf{u} + \rho \mathbf{f} = \rho \ddot{\mathbf{u}} \tag{7}$$

Contributed by the Applied Mechanics Division for publication in the JOURNAL OF APPLIED MECHANICS.

Discussion on this paper should be addressed to the Editorial Department, ASME, United Engineering Center, 345 East 47th Street, New York, N.Y. 10017, and will be accepted until two months after final publication of the paper itself in the JOURNAL OF APPLIED MECHANICS. Manuscript received by ASME Applied Mechanics Division, June, 1983.

Copyright © 1983 by ASME
Downloaded 02 May 2010 to 171.66.16.250. Redistribution subject to ASME license or copyright; see http://www.asme.org/terms/Terms_Use.cfm

Navier (1821) first reported this equation for the case of $\lambda = \mu$. Unless stated otherwise, we discuss the waves in isotropic and homogeneous media.

In this paper, we try to highlight some of the major progress made over the past 50 years on the analytical solutions to these equations. Since this is not meant to be a literature survey, we will frequently cite the aforementioned texts, other monographs, and review articles as sources of reference. An earlier review of the literature on elastic wave propagation was made by Miklowitz [18], and research articles from 1972-1977 were compiled in an annotated bibliography by Scott [19].

I Steady-State Waves in Media Free of Sources

The waves are said to be steady-state when the time dependence is harmonic; that is, $\mathbf{u}(\mathbf{x},t) = \mathbf{U}(\mathbf{x}) \exp(-i\omega t)$, and the media are *free* of sources if $\mathbf{f}$ in V and $\bar{\mathbf{T}}$ and $\bar{\mathbf{u}}$ on S vanish. The initial condition (4) is omitted.

Free steady-state waves in an infinite space, a half space, a plate, a circular cylinder, and a sphere have all been investigated prior to 1930. The propagation of two types of elastic waves, *P*-wave (primary, pressure, dilatational, irrotational, longitudinal) and *S*-wave (secondary, shear, rotational, distortional, tranverse) in isotropic media, and three types of elastic waves in crystals, one quasi-longitudinal and two quasi-transverse, were found by Cauchy and Poisson (1828). The surface wave in an isotropic halfspace was found by Lord Rayleigh (1887), and the phenomenon of reflection and refraction of elastic waves at a plane boundary was investigated by C. G. Knott (1899). Free waves in a plate were investigated by Lord Rayleigh (1888) and H. Lamb (1917), in a circular rod by L. Pochhammer (1876) and C. Chree (1889), and in a sphere (free oscillations) by Jaerisch (1880) and P. Lamb (1882).

Since then, there have been numerous additions to these topics. Here we discuss three topics: waveguides, waves in layered media, and anisotropic waves.

1 Dispersion and Waveguides. A waveguide is formed by a finite or infinite plate, or by a cylindrical surface. The wave is represented as

$$\mathbf{u}(\mathbf{x},t) = \mathbf{U}(x,y)e^{i(kz-\omega t)} \tag{8}$$

where the z axis is on the surface of the plate or along the axis of the cylinder. The apparent phase velocity is given by $c = \omega/k$ where k is the wave number (2π/wavelength), and ω the circular frequency.

In a waveguide, the *P* and *S*-waves are multiply reflected and the propagating wave mode as represented by the preceding equation is a result of interference of the reflected waves. The apparent wave speed c, which depends on the ratio of wavelength to plate thickness or cylinder radius, is not a constant. A wave is *dispersive* if the phase velocity is a function of wavelength, and the functional relation

$$f(c,k) = 0, \quad \text{or} \quad F(\omega,k) = 0 \tag{9}$$

is called the *dispersion relation*, or *frequency equation* [20].

The dispersion relation for waves in a plate bounded by two parallel planes was derived by Rayleigh and Lamb [21], and that for a circular cylinder by Pochhammer and Chree. Detailed analysis of these relations and calculation of the roots of the transcendental equations were not made until the 1950s. These topics were reviewed by Abramson, Plass, and Ripperger [22], Meeker and Meitzler [23], Pao and Kaul [24], and Thurston [25].

For elastic media, the frequency, ω, is always real, but imaginary and complex valued wave number, k, were found around the 1960s to exist for waves in plates and rods. The dispersion relations can then be mapped on an ω versus k plot in a multitude of branches of modes, each branch originating from $\omega = 0$ (real or complex k) and extending to infinity. Each point on the branch represents a mode of propagation with phase velocity $c = \omega/k$, and group velocity $c_g = d\omega/dk$.

The existence of the double-infinity of modes causes nearly intractable complexity of free waves in a plate bounded at all sides, or a rod of finite length. If any one of these plate-modes impinges on one edge of the plate, or any one of these cylinder-modes impinges on the end surface of the cylinder, all double-infinite modes are excited by reflection or refraction [26, 27]. The situation is even worse for waves in crystal plates or anisotropic rods. This has led to the development of approximate theories for plates and rods, which are discussed in Section *V*.

2 Layered Media. A layered medium is formed by many parallel planes S_1, S_2, . . . , or by a family of concentric cylindrical or spherical surfaces. At the interface S_i of two layers in contact, the boundary conditions (3) are replaced by the continuity condition,

$$\mathbf{u}_i = \mathbf{u}_{i+1} \quad \text{and} \quad \mathbf{n}\cdot\boldsymbol{\tau}_i = \mathbf{n}\cdot\boldsymbol{\tau}_{i+1} \text{ at } S_i \tag{10}$$

where the subscripts denote the ith medium and $(i+1)$th medium.

Elastic waves in a medium with parallel layers are classified according to their polarizations (the direction of the displacement vector). Those polarized in the plane of the layers are called *SH* waves (horizontal shear) or Love waves (1911), and those polarized in the plane perpendicular to the layer are called *P-SV* waves (pressure and vertical shear) or Rayleigh waves (1912). Both waves are dispersive.

At the interface, there exists another type of wave, known as the Stoneley wave (1924). Like the Rayleigh surface wave, it decays exponentially away from the interface. It exists only when the materials constants of adjacent media satisfy a certain condition [11].

Propagator Matrix. The dispersion relation for Love waves or Rayleigh waves is derived from solutions to equation (7), one for each layer, satisfying the boundary conditions (10) at each and every surface. The frequency equation in matrix form gets larger and larger as the number of layers increases (six more conditions for each additional interface). Computation of the roots of these equations becomes very difficult for a medium with many layers.

A major improvement was made by Thompson [28] and Haskell [29]. Their method essentially reduced one large matrix for a medium of n layers to a product of n small matrices, one for each layer. As a result, the task of calculating dispersion curves for a layered medium has been greatly simplified [30, 31]. A large number of layers is needed to model the earth's crust for seismic studies and for prospecting, and to model an inhomogeneous medium with rapid variation in material properties.

The Thompson-Haskell method was shown later by Gilbert and Backus [32] to be a special case of the propagator matrix introduced by Volterra (1887) to solve a system of differential equations with variable coefficients.

Free Vibration of a Layered Sphere. The propagator matrix method can be applied to a layered cylinder or sphere, stratified in the radial direction. The free vibration of the earth modeled by a layered sphere was analyzed by Alterman, Jarosch, and Pekeris [33], and the period of the lowest mode (spheroidal mode) was found to be 53.7 min. This was later confirmed by long-period seismograms of a Chilean earthquake in 1960.

The free vibration of a homogeneous sphere was first treated by Lamb (1882). He found the longest period of the spheroidal mode for the earth to be 66 min. if it is modeled by

Downloaded 02 May 2010 to 171.66.16.250. Redistribution subject to ASME license or copyright; see http://www.asme.org/terms/Terms_Use.cfm

an iron sphere (Section 196 of reference [3]). The solution was reformulated in spherical coordinates for the free and forced vibration of a sphere by Sato and Usami in a series of papers [34] (see Chapter 9 of reference [9]). The relation between normal modes (standing wave) of a sphere and progressing waves around a sphere was also established [35].

3 Anisotropic Waves. The development of electronic instruments since the 1940s has made possible the precise measurement of wave speeds in crystals to one part in 10^5 absolute value [36]. From the measured wave speeds and the density, which can often be calculated from atomic constants, one can measure the second-order elastic coefficients c_{ijkl} and even the third-order constants c_{ijklmn} [37].

Along with the experimental techniques, the theory of waves in crystals an anisotropic media was developed [38, 39, 40)].

This theory can also be applied to polycrystalline materials with texture and composite materials reinforced by continuous fibers, which are modeled as orthotropic media (orthorhombic symmetry) or transversely isotropic media (hexagonal symmetry).

An interesting development is the theory of wave surfaces in anisotropic media. A wave surface is the envelope of plane waves passing through the origin simultaneously in all directions. From the calculation of velocities in different directions, one can construct a velocity surface and a slowness surface (the reciprocal of velocity). The polar reciprocal of the slowness surface is the wave surface that is composed of three sheets, some having cusps. The direction of group velocity and energy propagation is, in general, different from that of the wave normal [41].

The Rayleigh and Stoneley type surface waves also exist in a crystal [42]. Waves in a layered anisotropic medium have also been investigated. In addition, an inhomogeneous medium composed of aligned inclusions (two-phase solids), such as cracks, pores, or elongated grains, can often be modeled as a homogeneous but anisotropic medium. A simple example is that a medium with periodic layers of two different materials behaves like a transversely isotropic solid when the wavelength is longer than the thickness of each layer. This and other recent developments on wave motion in anisotropic media were reviewed by Crampin [43].

Surface waves in piezoelectric crystals have been utilized for building delay lines and various surface acoustic wave (SAW) devices. This has been an active research area of electric communications in the 1970s [44, 45].

II Transient Waves in Layered Media

Transient waves are generated by the body force $\mathbf{f}(\mathbf{x},t)$ in equations (5) and (7), or the surface displacement $\bar{\mathbf{u}}(\mathbf{x},t)$ or traction $\bar{\mathbf{T}}(\mathbf{x},t)$ in equation (3). If the time function for these sources is exp $(-i\omega t)$ and the motion is observed long after the initiation of the source, the wave motion is also harmonic in time and is called steady-state. Otherwise, the wave motion is transient.

The free, steady-state waves discussed in the previous section are possible modes of time-harmonic waves propagating in a specific medium, and they may be excited by a particular type of source. Since the elastic wave of infinitesimal strain is linear, the transient wave solution can be obtained by superposing steady-state waves over the entire frequency spectrum (Fourier synthesis).

In an infinite medium, the transient wave field generated by a concentrated force of arbitrary time function was determined by G. Stokes (1849). To investigate the diffraction of light by inhomogeneities, Stokes assumed that the secondary sources emitting polarized light behaved like a concentrated force in an elastic ether. He constructed the general solution of the inhomogeneous equation (7) by what is now called the method of retarded potentials.

Next in mathematical complexity is the problem of transient waves in a half space. H. Lamb (1904) investigated this problem for an entirely different motivation. By then, the Rayleigh surface wave was confirmed from seismic records, and Lamb was interested in the relative magnitudes of surface tremors excited by a seismic source. Lamb applied essentially the method of Fourier transforms. The inverse transforms of the solutions, however, were not completed in Lamb's time. The "half space" and related problems have since become a focal point for many studies.

The solution is much more complicated when additional plane boundaries are introduced to form a layered half space. This is the basic model for theoretical seismograms, which has recently been a subject of intensive study.

1 Transient Waves in a Half Space. A half space bounded by one plane surface is the simplest model for observing elastic waves in solids. If any observation is to be made, the instrument must be placed on a surface that affects the transmission of elastic waves. Many applications of elastodynamics in seismic prospecting, underground nuclear testing, design of earthquake-resistant structures, dynamics of structural foundations, and development of electroacoustic devices, as well as basic studies on dynamics of material defects, begin with the model of a half space.

Lamb's Problem and Cagniard's Method. In 1904, Lamb formulated the solution to equation (7) for a line source (two-dimensional problem) or a point source in a half space ($z \geq 0$). A line source generates a semicylindrical P-wave, an S-wave, and a conical head wave (Mach wave) trailing the P-wave front. The Fourier time-transformed vertical displacement, $\bar{u}(x,z,\omega)$, of the P-wave may be expressed as

$$\bar{u}(x,z,\omega) = \frac{1}{2\pi}\int_{-\infty}^{\infty} \frac{A(h,k)}{R(h,k)}\, e^{-hz+ikx}\, dk \tag{11}$$

where $h^2 = k^2 - \omega^2/c^2$. The numerator depends on the frequency spectrum and wave number spectrum of the source, and $R(h,k)=0$ gives rise to the pole of Rayleigh's surface wave. Although Lamb indicated that the inverse Fourier transform could be obtained by a transformation of variable, he only derived asymptotic solutions for $u(x, z, t)$.

In the 1930s, Cagniard developed a general method to evaluate the inverse transforms (Cagniard used the Laplace transform, $\omega = is$) [46]. First, the wave number k is transformed to the horizontal wave slowness $p = k/\omega$,

$$\bar{u}(x,z,\omega) = \frac{1}{2\pi}\int_{-\infty}^{\infty} \frac{A(p)}{R(p)}\, e^{i\omega(px-qz)}\, dp \tag{12}$$

where $q^2 = c^{-2} - p^2$. It is seen that if a transformation is made from p to t by letting $t = px - qz$, the preceding integral can be changed to a Fourier integral in t, and the inverse transform is obtained "by inspection" [47, 48].

$$u(x,z,t) = H(t-t_0)\frac{A[p(t)]}{R[p(t)]}\frac{dp}{dt} \tag{13}$$

For a point source, the integrand involves Bessel functions $J_n(\omega pr)$. The solution for a vertical force was completed by Pekeris [49] and that for a horizontal force by Chao [50].

Green's Functions and Nuclei of Strains. The solutions derived by Stokes and Lamb are for a concentrated force represented by

$$\mathbf{f}_\delta(\mathbf{x},t) = \mathbf{f}_0\,\delta(\mathbf{x}-\mathbf{x}')\delta(t-t') \tag{14}$$

where δ is the delta function and $\mathbf{f}_0$ a constant vector. If $\mathbf{f}_0$ is a unit vector at $\mathbf{x}'$ in the direction of axis x_k, and the three displacement components at $\mathbf{x}$ are u_j $(\mathbf{x}-\mathbf{x}', t-t')$, the nine

Downloaded 02 May 2010 to 171.66.16.250. Redistribution subject to ASME license or copyright; see http://www.asme.org/terms/Terms_Use.cfm

quantities $G_{kj} \equiv u_j^{(k)}$ form a tensor of second rank, and G_{kj} is called the Green's function for the infinite or half space.

If the response $\mathbf{G}$ at $\mathbf{x}$ due to a concentrated force at $\mathbf{x}'$ is known, the general response $\mathbf{u}(\mathbf{x},t)$ due to a distribution of body force $\mathbf{f}(\mathbf{x},t)$ within a volume V is obtained by superposition

$$u_j(\mathbf{x},t) = \int_0^t dt' \int_V f_k(\mathbf{x}',t') G_{kj}(\mathbf{x}-\mathbf{x}', t-t') dV' \qquad (15)$$

Similarly, the response due to a source represented by the gradient of a concentrated force, $\nabla \mathbf{f}_\delta$, is given by $\nabla \mathbf{G}$ which is a third-rank tensor. The source $\nabla \mathbf{f}_\delta$ is called the *nuclei of strain* [3] or the *moment density* [14].

The moment density source has been proposed to model the slip motion of an earthquake fault, dislocations in a crystal, and cracks in a solid. Recent contributions on the moment sources and nuclei of strains are reviewed in an article by Pao and Gajewski [51] and in references [14, 15].

Moving Load. Waves generated by moving loads were investigated in the 1950s to analyze the effect of a blast wave on the surface of a half space. The early solutions were confined to the steady-state response of the medium when the wave field can be expressed in a moving coordinate system translating at constant speed with the blast front [52]. Transient response due to a concentrated force moving in an infinite medium (the "moving Stokes' problem") was determined by Payton [53] by applying a dynamic reciprocity theorem. The "moving Lamb's problem" was treated also by applying the reciprocity theorem or the method of integral transform [54] (Section 8.7 of reference [9]).

Contact Problems. In elastostatics, Boussinesque's solution for a concentrated force on a half space led to the solutions for contact problems developed by H. Hertz (1891). The analogous solution for dynamic contact problems has not yet been found because of the difficulty in treating the moving boundary conditions. Hertz's theory of impact (Section 139 of reference [3]) is still being applied to contact problems when the duration of impact is much longer than the fundamental period of the bodies [55].

Waves generated by the impact of a rigid indentor on a half space have also not been analyzed in detail because of the mixed boundary conditions (displacement prescribed over a portion of the surface and stresses over the rest). The indentation by a rigid wedge, however, can be analyzed by a similarity solution because there is no characteristic dimension for either the wedge or the half space [56, 57] (see Section 7.18 of reference [9]).

2 Transient Waves in Parallel Layers. Mathematical solutions of transient waves in a layered medium can be derived by Fourier transforms like those for the Lamb problem. For plane-strain problems, the vertical displacement $u^j(x,z,t)$ in the jth layer may be expressed as

$$u^j(x,z,t) = \frac{1}{4\pi^2} \int_{B_r} \int_{-\infty}^{\infty} \frac{N^j(\omega,p,q^j,z)}{D(\omega,p,q^j)} e^{i\omega(t-px)} |\omega| dp d\omega \qquad (16)$$

where B_r means the Bromwich contour slightly above the real ω-axis. The denominator D is the dispersion function for the layered medium (the wave number $k=\omega p$), and the numerator N^j contains the source function and the normal modes propagating in the jth layer. For a point source, the propagating factor $\exp(-i\omega px)$ is replaced by $J_n(\omega pr)$.

In the 1940s, equations like (16) were developed to investigate the propagation of sound waves in shoal water, which was modeled by two or three layers of fluid [58, 59]. The layered model was also applied to interpret complex seismograms, and around the 1950s much effort had been devoted to the analysis of the dispersion relation $D(\omega,p)=0$ [11]. Recent work on transient waves is discussed in reference [14] (Chapters 6–9) and reference [15] (Chapters 6, 7), and in a review article by Kennett [60].

Spectral Method and Method of Wave Slowness. Many methods have been developed to evaluate the integrals in equation (16). The methods may be divided into two classes. If the p-integral is evaluated first, we obtain a double summation of all normal modes, each for a frequency band $d\omega$. This intermediate result is also the complex Fourier spectrum of the transient wave $u^j(\mathbf{x},t)$, and the method is called the *normal mode method* or *spectral method.* If the ω-integral is evaluated first, the method is called the *slowness method.* Each method can further be subdivided depending on whether the slowness integral is evaluated with the original contour along the real axis or distorted into the complex plane.

The spectral method with a real contour for p is known as the *reflectivity method* [61, 62], and the method is suitable for numerical computation. The complex integral for p is used when various methods of complex analysis are applied to obtain approximate results [63].

The slowness method has not been as widely investigated as the spectral method. The method of generalized rays is a special case of the slowness method with a complex contour for p. A new slowness method using the real contour was recently proposed by Chapman [64]. Application of these two methods to waves in a plate was discussed by Miklowitz (Chapter 7 of reference [10]).

Method of Generalized Rays. The method of generalized rays is an outgrowth of research in geophysics from 1950 to 1970. It began with the expansion of the denominator function, $D^{-1}(\omega,p)$ in equation (16), into a series of exponential functions of the type $\exp(+i\omega q_j H_j)$ where H_j is the thickness of the jth layer [58, 65, 66]. Each term of the series is identified as a wave traveling along a specific ray path in the medium, and is called a generalized ray integral, the first being the wave from the source directly to the receiver, the second being reflected once, etc. Each ray integral can then be evaluated by Cagniard's method. Later, it was found that such an expansion of D from the general solution is not necessary. The ray integrals are constructed directly from the source function, the phase function, and the generalized reflection and transmission coefficients, which are the same as those for plane harmonic waves expressed in terms of the slowness variable [67].

As reviewed by Pao and Gajewski [51], the method of generalized rays unifies many different approaches to the exact solutions of transient waves in an infinite space, a half space, a plate, and layered media. The solution is exact because along each generalized ray, there is a minimum travel time. The waves that follow a ray with many reflections will arrive after those with a few reflections. By evaluating the ray integrals in order of their arrival times, the solution is exact up to the time of arrival of the next ray which is omitted in the calculation. The method, however, becomes impractical when a medium has three or more layers.

3 Waves in Wedges and Dipping Layers. If the two bounding surfaces of a layer are not parallel to each other, we have a structure of dipping layers, the simplest being a wedge of apex angle α. The case of $\alpha=\pi$ is a half space and that of $\alpha=\pi/2$ is a quarter space. The classical problem of waves in a quarter space, especially the question of how a Rayleigh surface wave turns around a corner, has not yet been answered to this day.

The Wedge Problem. As reviewed by Knopoff [68], *SH* waves (scalar waves) in a wedge can be analyzed by applying the Kantorovich-Lebedev transform, the method of

Downloaded 02 May 2010 to 171.66.16.250. Redistribution subject to ASME license or copyright; see http://www.asme.org/terms/Terms_Use.cfm

homogeneous functions (similarity solution), and others. All of these methods fail when applied to *P-SV* wave problems because of the coupling of *P* and *S*-waves at both boundaries. The singular behavior of waves at the apex presents another difficulty.

This difficulty can be illustrated by the plane-strain problem in a quarter space bounded by $x \geq 0$ and $y \geq 0$. If a solution is found by separation of variables or other equivalent methods that satisfies the boundary conditions at $x=0$ (prescribing τ_{xx} and τ_{xy}), the same solution cannot be made to satisfy exactly the boundary condition at $y=0$ (τ_{yy} and τ_{yx} prescribed). Although an iterative procedure can be developed to improve the solution in successive order [69], the convergence of the solution is not assured. If the homogeneous solutions are formulated for *P-SV* waves in a wedge, the matching of wave field in the elliptical zone to that in the hyperbolic zone is formulated in a pair of integral equations. These integral equations are also to be solved by iteration [70].

Recently, Miklowitz [71] applied the integral transform method to treat transient wave problems in a medium with two perpendicular boundaries (a quarter space or end surface of a plate). By carefully analyzing the poles and residues and the branch line integrals, he was able to determine the transient solution near the wave front.

Dipping Layers. When the apex angle of a wedge is small, approximate solutions for *SH* waves in the wedge, or a wedge overlaying a halfspace (a dipping layer), can be derived by analyzing the waves along the ray path of reflection [72, 73].

The solutions can be reformulated in terms of generalized ray integrals, using the local wave slowness along the horizontal or inclined surface. All local wave numbers can be transformed to a common wave slowness, which allows inverse transformation by the Cagniard method [74]. The transient *SH* wave solution so determined neglects the diffraction from the apex, and the solution obtained at a receiver is exact up to the time of arrival of the diffracted waves from the apex. This method can also be extended to a medium with several dipping layers and to *P-SV* waves.

III General Theory of Elastodynamics

The theory of elastodynamics was still developing at the time when Love made the last edition of his treatise in 1927. Since then, there have been several major additions to the general theorem and numerous mathematical methods developed for solving the elastodynamic equations. Some of them have already been discussed in previous sections. We discuss three more topics in this section: the elastic wave functions, the integral representation theorem, and the theorem of eigenfunction expansion.

The reformulation of variational principles of elastodynamics is another major addition. These principles are reformulated so that they are amenable for approximate solutions and numerical calculations. We will not, however, review them here. The principle formulated by Gurtin [75] is discussed in reference [9] (Section 5.18).

1 Elastic Wave Function. The special wave functions are the major tool of analysis for elastic waves in homogeneous isotropic media (two or three-dimensional problems), and for waves in a cylinder or a sphere. They are derived by separation of variables for scalar and vector wave equations in curvilinear coordinates. The difficulty of solving elastic wave equations for anisotropic and inhomogeneous media is caused by the inability to separate variables.

Resolution of Elastic Waves in Isotropic Media. The general solution to equation (7) is sought by resolving $\mathbf{u}$ into a dilatational field (irrotational) $\nabla\phi$, and a rotational (equivoluminal) field $\nabla \times \psi$

$$\mathbf{u} = \nabla\phi + \nabla \times \psi, \quad \mathbf{f} = \nabla b + \nabla \times \mathbf{B} \tag{17}$$

and ϕ and ψ satisfy the scalar and vector wave equation, respectively,

$$c_p^2 \nabla^2 \phi + b = \ddot{\phi} \quad c_p^2 = (\lambda + 2\mu)/\rho \tag{18}$$

$$c_s^2 \nabla^2 \psi + \mathbf{B} = \ddot{\psi} \quad c_s^2 = \mu/\rho \tag{19}$$

This decomposition was used by Poisson in the 1820s to determine the nature of light in the ether.

The question of completeness of this resolution, that is, whether every solution of the displacement equation (7) admits the representation (17), was raised by Clebsch (1863) and answered, in part, by Duhem (1898). A proof of the completeness theorem was given by Sterberg [76] (see Section 3.4.2, reference [7]).

Note that for sound waves in fluid or air, the velocity is $\mathbf{v} = \nabla\phi$ and the pressure is $p = -\rho\partial\phi/\partial t$ where ϕ satisfies the scalar wave equation (18). Therefore, the solution for sound waves in fluid is included in the dilatational part of elastic waves. The vector equation for the rotational part, equation (19), is the same as that for electromagnetic waves in vacuum (Chapter 8 of reference [1]).

Wave Functions in Curvilinear Coordinates. The next question to be answered is how to solve the scalar and vector wave equations. Fortunately, the same question arises in other branches of physics, and a comprehensive treatment of methods of theoretical physics was given by Morse and Feshbach (Chapters 11 and 13 of reference [77]).

There are 11 curvilinear coordinates formed by confocal quadric surfaces: rectangular; three cylindrical (circular, elliptic, parabolic); spherical; conical; ellipsoidal; paraboloidal; and three more coordinates by revolution (parabolic, prolate spheroidal, oblate spheroidal). For vector wave equations, only six coordinates (cartesian, spherical, conical, and three cylindrical) are separable.

For cartesian coordinates, each component $\psi_i (i = 1,2,3)$ in (19) satisfies a scalar wave equation, and they are related by the gauge condition $\nabla \cdot \psi = 0$ (Section 2.2.6, reference [10]).

For the other curvilinear coordinates, ψ may be decomposed into two parts: one is tangent to a particular coordinate surface, $\xi =$ constant, and the other is perpendicular to the first one. Equation (17) is thus replaced by

$$\boldsymbol{u} = \nabla\phi + \nabla \times (\mathbf{e}w\psi) + \nabla \times \nabla \times (\mathbf{e}w\chi) \tag{20}$$

where w is a scalar function of ξ, and $\mathbf{e}$ is a unit vector normal to the surface $\xi =$ constant. Both ψ and χ satisfy the same scalar wave equation as ϕ but with speed c_s. For the three cylindrical coordinates, we choose $\xi = z$, the axis of the cylinder, and $w = 1$; then $\mathbf{e}$ is parallel to z. For spherical or conical coordinates, we let ξ be the radial coordinate r and $w = r$, and $\mathbf{e}$ is normal to the spherical surface.

Solutions of the scalar wave equation for ϕ and ψ and χ obtained by separation of variables, each depending only on one coordinate, are called the scalar wave functions. The most familiar ones are

circular cylindrical(r,θ,z):

$$H_n^{(1),(2)}(kr)e^{in\theta}e^{i\gamma z}e^{i\omega t}$$

spherical(r,ϕ,θ):

$$h_n^{(1),(2)}(kr)P_n^m(\cos\theta)e^{im\phi}e^{i\omega t} \tag{21}$$

The other two cylindrical functions are the Mathieu functions for elliptical cylinder [78] and the Weber functions for parabolic cylinder [79]. The elastic wave functions are constructed from the scalar wave functions according to equation (20) and are tabulated in reference [80]. In addition to the six

Downloaded 02 May 2010 to 171.66.16.250. Redistribution subject to ASME license or copyright; see http://www.asme.org/terms/Terms_Use.cfm

separable coordinates mentioned previously, axially symmetric elastic waves in either prolate or oblate spheroidal coordinates can also be treated by separation of variables [81].

For the circular cylindrical and spherical coordinates, the angular parts of the wave functions, $\exp(in\theta)$ or $P_n^m(\cos\theta)\exp(im\phi)$, do not depend on the wave speed c_p or c_s. However, the angular parts of other wave functions such as the Mathieu functions, Weber functions, and spheroidal wave functions all contain the wave speed in their arguments. This makes it impossible to satisfy boundary conditions exactly at a coordinate surface because both P and S waves are always coupled (occurring simultaneously) at a boundary. Therefore, of 11 coordinates mentioned previously, only three systems, cartesian, circular-cylindrical, and spherical, can be treated by separation of variable for exact solutions to equation (7) and boundary conditions (3).

Anisotropic and Inhomogeneous Media. In general, waves in homogeneous anisotropic media cannot be represented by a $\nabla\phi$ and $\nabla\times\psi$ part as in equation (17). The general solutions are sought usually by superposing plane waves in all direction [82], or other methods [39, 43].

There is also no general theorem of resolution for waves in isotropic, inhomogeneous media. Elastic waves in an inhomogeneous medium are treated by various approximate methods such as an asymptotic expansion in inverse powers of frequency [83], a perturbation over the averaged material properties of a random medium [84], the parabolic approximation [85], or the geometric ray theory [86]. Some of these topics are discussed in reference [14] (Chapter 13), and reference [15] (Chapter 7).

2 Integral Representation Theorems. For scalar waves, there are two general integral representations for waves in a volume V bounded by a surface S: the Helmholtz theorem for steady-state waves (1860) and the Kirchhoff theorem for transient waves (1883). The latter as shown by Born and Wolf [87] can be derived from the former by a Fourier synthesis. These two integral theorems form the mathematical foundation for Huygens' principle [88].

Similar theorems exist for isotropic elastic waves. The Kirchhoff type theorem (general time function) was discussed by A. E. H. Love (1904). A detailed derivation of the integral formula was given by A. T. deHoop (1958) in his dissertation, and a precise statement of the theorem together with a proof was presented by Wheeler and Sternberg [89]. The Helmholtz type theorem (harmonic time function) was reported by Kupradze [90]. A different integral formula combining the one for a scalar wave, and another for a vector wave, was contained in the book by Morse and Feshbach (Chapter 13, reference [77]).

For anisotropic and inhomogeneous solids, the Green's function $\mathbf{G}(\mathbf{x}-\mathbf{x}',\ t-t')$ is defined as the solution of the following dyadic equations, analogous to equation (5)

$$\frac{\partial}{\partial x_j}\left(c_{ijkl}\frac{\partial G_{lm}}{\partial x_k}\right)+\delta_{im}\delta(\mathbf{x}-\mathbf{x}')\delta(t-t')=\rho\frac{\partial^2 G_{im}}{\partial t^2} \tag{22}$$

The exterior integral formula for anisotropic elastic waves in a volume V exterior to a surface S with outer normal $\mathbf{n}$ is [91]

$$\epsilon\mathbf{u}_m(\mathbf{x},t)=\int_V \rho f_i(\mathbf{x}',t)*G_{im}(\mathbf{r},t)dV'$$
$$-\int_S n_j' c_{ijkl}\left[G_{im}(\mathbf{r},t)*\frac{\partial u_l(\mathbf{x}',t)}{\partial x_k'}\right.$$
$$\left.-u_i(\mathbf{x}',t)*\frac{\partial G_{lm}(\mathbf{r},t)}{\partial x_k'}\right]dS' \tag{23}$$

where $\mathbf{r}=\mathbf{x}-\mathbf{x}'$ and the asterisk denotes a convolution integral

$$f(t)*g(t)\equiv\int_0^t f(t')g(t-t')dt' \tag{24}$$

The ϵ equals 1 if $\mathbf{x}$ is outside S and equals 0 if $\mathbf{x}$ is inside S. There is another formula for waves in a volume V interior to a surface S [91].

For steady-state waves, we omit the convolution, and the Fourier transform of $\mathbf{G}(\mathbf{r},t)$ should be used. Note that the factor $n_j' c_{ijkl}(\partial u_l'/\partial x_k')=n_j' c\tau_{ij}'$ is the traction on the surface S, and $n_j' c_{ijkl}(\partial G_{lm}/\partial x_k')$ is the dyadic traction. If S is a wave surface, the surface integral in the preceding formula is a mathematical representation of Huygens' principle for elastic waves.

Equation (23) states that the waves generated by a body force and surface sources, $\mathbf{u}(\mathbf{u}',t)$ and $\mathbf{n}'\cdot\tau(\mathbf{x}',t)$, are determined by the integral formula provided the Green's functions are known. Unfortunately, Green's functions for inhomogeneous media are unknown, and those for homogeneous but anisotropic media are expressed in the form of an integral [92]. The Green's function for an isotropic, homogeneous infinite medium, however, is expressible in terms of generalized functions, and it is precisely the solution determined by Stokes and discussed in Section *II*.

Using the Stokes' solution for an infinite medium as the Green's function in equation (22), one can form a vector integral equation for either $\mathbf{u}'$ or $\mathbf{n}'\cdot\tau'$ on the boundary S. Recent rapid advancement on the boundary integral equation (boundary element method) [93] has made it possible to numerically solve these boundary integral equations, at least for steady-state waves. Therefore, this integral representation formula, which has been a mathematical nicety for many years, suddenly has become an important ool for calculating elastic wave fields.

3 Solutions by Eigenfunction Expansions. One of the most elegant but least applied theorems of elastodynamics is the expansion of the transient wave function in a series of eigenfunctions. It is an extension of the Sturm-Liouville theorem of ordinary differential equations.

To solve the equation of motion (7) with body force $\mathbf{f}$, boundary conditions (3), and initial conditions (4), we first find the eigenfunctions, $\mathbf{u}^{(m)}(\mathbf{x})$, which satisfy the reduced elastic wave equations with homogeneous boundary conditions,

$$(\lambda+\mu)\nabla\nabla\cdot\mathbf{u}^{(m)}+\mu\nabla^2\mathbf{u}^{(m)}+\rho\omega_m^2\mathbf{u}^{(m)}=0$$
$$\mathbf{u}^{(m)}(\mathbf{x})=0\quad\text{on}\quad S_1,\quad \mathbf{n}\cdot\tau^{(m)}=0\ \text{on}\ S_2 \tag{25}$$

where $\tau^{(m)}$ is the corresponding stress tensor. The eigenvalues ω_m^2 are real and non-negative, and the eigenfunctions satisfy the orthonormal conditions:

$$\int_V \rho\mathbf{u}^{(m)}\cdot\mathbf{u}^{(n)}dV=\delta_{mn} \tag{26}$$

The expansion theorem states that the general solution to equations (7), (3), and (4) is (Section 5.17, reference [9])

$$\mathbf{u}(\mathbf{x},t)=\sum_m \phi_m(t)\mathbf{u}^{(m)}(\mathbf{x}) \tag{27}$$

The time function $\phi_m(t)$ is given by

$$\phi_m(t)=a_m\cos\omega_m t+(1/\omega_m)b_m\sin\omega_m t$$
$$-\omega_m\int_0^t \Phi_m(\tau)\sin\omega_m(t-\tau)d\tau \tag{28}$$

where a_m and b_m are determined from the initial conditions,

$$a_m=\int_V \mathbf{u}_0\cdot\mathbf{u}^{(m)}dV,\quad b_m=\int_V \mathbf{v}_0\cdot u^{(m)}dV \tag{29}$$

and the $\Phi_m(t)$ is determined from the body force and the boundary conditions:

Downloaded 02 May 2010 to 171.66.16.250. Redistribution subject to ASME license or copyright; see http://www.asme.org/terms/Terms_Use.cfm

$$\rho\omega_m\Phi_m(t) = -\rho\int_V \mathbf{f}\cdot\mathbf{u}^{(m)}\,dV$$

$$+\int_{S_1}\bar{\mathbf{u}}\cdot(\mathbf{n}\cdot\tau^{(m)})\,dS+\int_{S_2}\mathbf{T}\cdot\mathbf{u}^{(m)}\,dS \tag{30}$$

Although the orthogonality conditions for the eigenfunctions $\mathbf{u}^{(m)}(\mathbf{x})$ and real positiveness of ω_m^2 were analyzed in Love's treatise (Sections 124–127), the completeness of the orthonormal set of eigenfunctions was only treated in modern time by Gurtin [94], and the general solution was formulated by Reismann [95].

That this theorem is least applied is probably due to the difficulty of finding the eigenfunctions $\mathbf{u}^{(m)}$. For a body bounded on all sides, the only eigenfunctions that have been found explicitly are those for a layered sphere. However, Weaver and Pao [96] showed recently that this general solution can be applied to an infinite plate, the eigenfunctions being the propagating modes of the Rayleigh-Lamb waves. Therefore, almost all problems of transient waveguides can be solved directly by applying this theorem.

IV Diffraction and Scattering of Elastic Waves

One of the major applications of the theory of elastostatics is the determination of stress concentrations in a body with cracks, cavities, inclusions, or other types of discontinuities. Through many years' research, stress concentration factors (SCF) for various geometries have been found and compiled in handbooks. The question on whether these factors were applicable to dynamic loading was not answered until the late 1950s when dynamic stress concentration was recognized as a phenomenon of scattering of elastic waves.

The earliest investigation on the scattering of elastic waves was made by Clebsch [97]. He analyzed the scattering of elastic waves (vector waves) by a spherical inclusion for the purpose of understanding the scattering of light, a work predating Rayleigh's classical paper on scattering of light by nine years. Rayleigh's analysis of the scattering of scalar waves by a sphere and circular cylinder was later contained in his treatise, *Theory of Sound* [4]. A more comprehensive discussion was given by Lamb in connection with sound waves in fluids (Chapter 10 of reference [98]).

After Rayleigh's work, the scattering of sound, light and electromagnetic waves was an active research topic in physics, but the scattering of elastic waves drew little attention except for a small group of seismologists [99]. In the middle of the 1950s, two papers appeared on the scattering of elastic waves by a spherical inclusion, one by Nishimura and Jimbo [100] for studying the dynamic stress concentration around a cavity, and the other by Ying and Truell [101] for analyzing acoustic waves in polycrystalline solids.

Many investigations followed but the emphasis was on the low-frequency, long wavelength limit for steady-state waves [102] ($ka \leq 10$ where k is the incident wave number and a is the typical dimension of the scatterer), and the long-time response for an incident transient pulse [103]. These were summarized in the monograph by Pao and Mow [80].

At the start of the 1970s, the ultrasonic technique of nondestructive testing of materials (NDT) was advanced from the stage of detecting a crack to the stage of characterizing dimensions and properties of the crack or flaw (see the article by B. Thompson in this volume). This and other applications in geophysics and underwater acoustics have generated a great deal of interest in the high-frequency scattering of elastic waves and diffraction by a body with sharp edges.

1 Scattering by a Cylinder or Sphere. As in the case of scattering of sound, the scattering of elastic waves by a circular cylinder or a sphere can be analyzed by expanding the scattered field in a series of wave functions. The solutions thus obtained have wide applications in analyzing dynamic stress concentration and interactions of structures with ground waves and underwater sound.

Expansion in Wave Functions. Let ϕ_n, ψ_n, and χ_n be the vector elastic wave functions, equation (20),

$$\phi_n = \nabla\phi_n,\ \psi_n = \nabla\times(\mathbf{e}w\psi_n),\ \chi_n = \nabla\times\nabla\times(\mathbf{e}w\chi_n) \tag{31}$$

where ϕ_n, ψ_n, and χ_n are the scalar wave functions in cylindrical or spherical coordinates. The scattered wave $\mathbf{u}^{(s)}$ is expanded into an infinite series with unknown coefficients $\alpha_n, \beta_n, \gamma_n$,

$$\mathbf{u}^{(s)} = \sum_n (\alpha_n\phi_n + \beta_n\psi_n + \gamma_n\chi_n) \tag{32}$$

The incident wave is also expanded in a series of the regular part of these vector wave functions,

$$\mathbf{u}^{(i)} = \sum_n (a_n\hat{\phi}_n + b_n\hat{\psi}_n + c_n\hat{\chi}_n) \tag{33}$$

where $\hat{\phi}_n$ denotes the real part of ϕ_n etc. The coefficients a_n, b_n, and c_n can be calculated from $\mathbf{u}^{(i)}$ and the orthogonality conditions of the vector wave functions. The total wave outside the scatterer is

$$\mathbf{u} = \mathbf{u}^{(i)} + \mathbf{u}^{(s)} \tag{34}$$

For a circular cylinder or a sphere, the elastic wave functions form a complete orthogonal set. The unknown coefficients can be determined exactly from the prescribed boundary conditions for the total waves. Vector wave functions are also known for an elliptical cylinder and parabolic cylinder. The scattering coefficients, however, cannot be determined exactly because the angular parts of these functions contain two different wave speeds as discussed in Section *III*.1.

The convergence of these series depends on the wave parameter ka. For low frequencies ($\omega = kc_p$) or small inclusions, a few terms of the series are sufficient, as in the case of calculating stress concentration factors ($\omega = 0$ is the statical case). For high frequencies or large inclusions (such as the core of the Earth), the convergence is very slow and the number of terms needed (about equal to ka) becomes too large to be practical.

In the latter case, the series is converted to a sum of integrals by the Poisson sum formula [104] (Chapter 8 of reference [10]). Each integral can be evaluated either by the saddle point method or by the calculus of residues. The former gives rise to the reflected waves in the illuminated zone, and the latter gives rise to the diffracted waves in the shadow zone and the creeping waves around the inclusion [105].

Dynamic Stress Concentration and Resonance. Due to scattering, the stresses are raised around a cylinder or sphere. The ratio of the stress of the total wave at a point on or near the inclusion to that of the incident wave at the same point is defined as the dynamic stress concentration factor (DSCF). Around a spherical cavity or circular hole in a plate, the DSCF was found to be higher than the statical factor by 10–20 percent. This confirmed the experimental findings determined by dynamic photoelasticity techniques in the 1950s. Experiments were conducted then to determine the dynamic effect on underground structures due to blast waves on the surface. DSCF around a rigid and heavy inclusion, however, can be much larger than the statical factor [80].

The frequency spectrum of the scattered waves at near and far field are strongly affected by the resonance frequencies (complex-valued) of the inclusion. This was found first for a

Downloaded 02 May 2010 to 171.66.16.250. Redistribution subject to ASME license or copyright; see http://www.asme.org/terms/Terms_Use.cfm

circular fluid cylinder in an elastic solid [106] and an elastic sphere in a fluid. A general theory of resonance scattering and numerous recent contributions were reviewed by Flax, Gaunaurd, and Uberall [107]. The possibility of identifying an inclusion from the resonance frequencies is discussed in the review.

Interaction of Waves With Foundations and Underwater Structures. An underwater explosion generates a shock wave (discontinuity in velocity) in the water. At a certain distance from the source, the waves are attenuated to a weak shock (discontinuity in acceleration). The interaction of a weak shock with a submerged structure can be treated as the scattering of sound by an elastic body in fluid. Very active research on this topic was pursued in the post-World War II period. The results are summarized in a monograph by Junger and Feit [108]. More recent research contributions are reviewed by Uberall and Huang [109].

A similar problem occurs when a ground shock impinges on the foundation of a structure. At far field, the ground shock is in the form of an elastic wave. The motion of a large foundation is different from the incident wave motion because of scattering. An early investigation was made by Luko, who treated the foundation as a semicircular cylinder embedded in a half space, excited by an incident *SH*-wave [110]. This launched many investigations of the interaction of ground waves with foundations [111]. A new feature of this problem is that the motion of the foundation is also affected by the motion of the superstructure.

2 Diffraction by an Edge or a Crack. A semi-infinite strip (rigid or vacuous) is a degenerate case of a parabolic cylinder, and elastic waves scattered by a semi-infinite strip (a plane defined by $y=0$, $x\geq 0$) can be expressed in terms of the Weber functions (parabolic wave function) [79]. Similarly, the scattering of elastic waves by a finite strip ($y=0$, $-b \leq x \leq b$), which is a degenerate case of an elliptic cylinder, can be analyzed by applying the Mathieu functions [78]. The computations of these functions and the scattering coefficients are done approximately, and are feasible only for low frequencies.

A more general solution for the scattering by a semi-infinite strip is formulated by applying integral transforms and the Wiener-Hopf technique for steady-state waves. The two-dimensional problems were first treated by Maue [112] (see Chapter 9 of reference [7]), and the three-dimensional problem (incident plane wave oblique to the edge of the strip) was recently solved by Gautesen, Achenbach, and McMaken [113]. These solutions form the *canonical solution* for the geometric theory of diffraction.

Scattering of two-dimensional elastic waves by a finite strip is a typical mixed boundary value problem of elastodynamics. The solution can be formulated in terms of the unknown field quantities along the strip, which satisfy a pair of integral equations [114] (Chapter 9, reference [9]). The solutions for a vacuous strip (a crack of finite width) are of particular importance in the dynamic theory of fracture as reviewed by Sih [115] and Freund [116]. Other solutions for stationary or moving cracks are summarized in the volume edited by Sih [117].

Although the scattering of acoustic (scalar) waves by an exterior wedge has been solved by a similarity method and other methods, the wedge problem for elastic waves has not yet been solved. The closest solution found so far is the scattering by a quarter space [118]. The difficulty encountered for treating scattering is the same as that for treating the interior problems as discussed in Section *II*.3.

3 Diffraction by a Body of Arbitrary Shape. So far, we have discussed scattering of elastic waves by inclusions of special geometry – a sphere and a cylinder (strips as a limiting case). For the scattering of elastic waves by a body of arbitrary shape, other methods are required as discussed in this section. Many of these methods are extensions of the methods already being developed for acoustic waves or electromagnetic waves [105, 119].

Transition Matrix Method (T-Matrix). Following Waterman's original work for acoustic waves in 1969, the method of *T*-matrix for the scattering of elastic waves was developed simultaneously by Waterman [120] and Varadan and Pao [121], each based on a different representation theorem for steady-state elastic waves. A simpler derivation of the *T*-matrix was shown later by Pao [122], and that for transient waves has been formulated recently by Bostrom [123].

The method relates the unknown scattering coefficients in equation (32), $\boldsymbol{\alpha}(\alpha_n, \beta_n, \gamma_n)$, to the incident wave coefficients in equation (33), $\mathbf{a}(a_n, b_n, c_n)$, by an infinite matrix $\mathbf{T}$ such that

$$\boldsymbol{\alpha} = \mathbf{T} \cdot \mathbf{a} \tag{35}$$

The same basis wave functions in circular cylindrical or spherical coordinates, equation (21), are used for bodies of all shapes. The element of the *T*-matrix are integrals of the basis functions over the surface of a body.

The method is shown to be applicable to a large class of scattering problems. Recent developments of this method are reported in the proceedings of a special conference [124].

Geometric Ray Theory. The geometric ray theory for the scattering of acoustic waves by a smooth body and by a body with edges was developed by Keller [125] and Levy and Keller [126]. The theory was extended by E. Resende to two-dimensional elastic waves in an unpublished Ph.D. thesis in 1963. A full exposition of this method, including many recent contributions to the diffraction of elastic waves by a body with sharp edges, is contained in the monograph by Achenbach, Gautesen, and McMaken [127].

A geometric ray connects a source and a receiver by the path of minimum travel time of a wave (Fermat's principle). The amplitude of the wave decays as it radiates from the source, and the decay rate can be calculated, in the limit of high frequencies, in terms of the length of the ray. When the radiating ray is interrupted by an obstacle, the ray is bent around the obstacle, shedding additional energy into the obstacle and the surrounding medium. The amplitudes of the wave as the ray enters and leaves tangentially to the obstacle are determined by comparing the ray solution with the exact solution of a body with the same geometry and curvature at the point of tangency (the so-called *canonical solution*).

Although the geometric ray theory is valid in principle only for waves at very high frequencies (zero wavelength limit), it can actually be applied to frequencies at lower range. The method is also capable of handling the diffraction of pulses as shown in the case of sound [128]. The lack of canonical solutions for elastic waves (e.g., a body with two arbitrary Gaussian curvatures), however, imposes a serious limitation on this method.

Method of Integral Equation. The waves scattered by a body of arbitrary shape can be expressed by a surface integral and a volume integral by applying the integral representation theorem. For an inclusion of varying material properties, waves scattered by a region of inhomogeneity are expressed by a volume integral of equivalent body force multiplied by the Green's function for the surrounding medium. Since the volume integral contains the unknown total wave field in its integrand, we arrive at a volume integral equation for the scattered wave (body scattering). This integral equation can be solved by iteration, and the solution is called the Born approximation if the incident wave field is substituted for the

Downloaded 02 May 2010 to 171.66.16.250. Redistribution subject to ASME license or copyright; see http://www.asme.org/terms/Terms_Use.cfm

unknown total wave as the first trial [129], and called the static approximation if the statical field is used [130].

For an inclusion with constant material properties, the scattered waves are expressed as a surface integral of the sources $\mathbf{u}'$ and $\mathbf{n}' \cdot \tau'$ in equation (23). A boundary integral equation for the unknown surface sources is derived by letting the receiver approach the surface. This vector boundary integral equation is singular and can only be solved numerically.

The integral equation method seems to be most effective for two-dimensional steady-state waves [131] and transient waves [132]. The numerical results for three-dimensional scattering are currently being developed [133].

Other Methods. There are other methods developed for handling a special class of problems of scattering. The method of complex variables recently reported [134] offers a new approach to two-dimensional scattering. The method is an extension of the complex-variable method for elastostatics (Muskhelishvili's method). Despite the wave equation not being conserved by a conformal mapping, the transformed equation can nevertheless be solved by introducing the so-called zonal function, which can be treated numerically.

The method of matched asymptotic expansions has been recently applied to acoustic waves and elastic waves as reviewed by Datta [135]. The method matches the coefficients of the scattered wave at far-field to those at near field. The analytical results thus obtained provide an opportunity to study the effect of various parameters of the arbitrarily shaped body on scattering.

Finally, we mention the scattering of transient elastic waves (pulses). One general approach is to formulate the Kirchhoff-type integral equation for elastic waves derived from equation (23) and solve this equation numerically [132]. Another approach is to solve the steady-state problem, by whatever method, over a wide range of frequencies, and then perform the inverse Fourier transform by numerical methods (Fast Fourier Transform) [131].

For a few problems, the inverse transform can be performed analytically by applying the Cagniard method. This is shown for the diffraction of scalar waves by a semi-infinite screen [136], by a sphere [137], and by a circular cylinder [138].

V Two and One-Dimensional Theories of Elastic Bodies

Despite all the research efforts devoted to free waves and transient waves in layered media, we still do not have a solution for transient waves in a plate bounded on all sides (a rectangular block), or in a circular cylinder of finite length. The inherent difficulty of finding such a solution on the basis of a three-dimensional theory of elasticity was discussed in Sections *I* and *II*.

To analyze the free and forced motion of a finite plate or rod, various approximate theories were developed to capture the one or two-dimensional features of the motion. The most familiar ones are the Bernoulli equation of longitudinal motion of a thin rod, the Euler-Bernoulli beam theory, the Germain-Lagrange equation of a plate in flexural motion, and the Poisson equation for the extensional motion of a thin plate. All of these theories are limited to waves at low frequencies and long wavelength. Improvement on the range of frequency and wavelength can be made at the sacrifice of simplicity. We discuss a few theories which were developed in the 1950s and 1960s (Chapter 6, reference [7] and Chapter 7, reference [10]).

1 Approximate Theories for Plates. In the approximate theories the displacement $\mathbf{u}(x,y,z,t)$ is expanded into a series of the thickness coordinate of the plate, say z,

$$\mathbf{u}(x,y,z,t) = \sum_{n=0}^{\infty} \mathbf{u}^{(n)}(x,y,t) z^n \tag{36}$$

By truncating the series at various orders of n and averaging displacements and stresses over the thickness coordinate, z, one can derive a system of equations for the two-dimensional functions $\mathbf{u}^{(n)}(x,y,t)$ from the original system of equations (1), (2), and (3). This method, originally due to Cauchy and Poisson, was fully developed by Mindlin and his associates in the 1950s and is reviewed in reference [24].

Antisymmetric Motion. For an isotropic plate, the zeroth-order theory for antisymmetric motion is the Germain-Lagrange equation (1812) for the displacement $u_z^{(0)}(x,y,t)$. An improvement of the classical theory was made by Mindlin [139] to include the effect of shear and rotatory inertia.

Mindlin's theory extended the frequency range to the lowest frequency, ω_s, of the simple thickness shear modes of Rayleigh Lamb waves, and $\omega_s = \pi c_s/H$ where H is the plate thickness and c_s is the shear wave speed. The theory also eliminates the paradox of the classical theory that the phase velocity approaches infinity when the wavelength approaches zero.

By averaging the plate displacement $u_z^{(0)}(x,y,t)$ over the width coordinate y, the two-dimensional plate equation reduces to a one-dimensional beam equation for $\bar{u}_z^{(0)}(x,t)$. Thus, the Germain-Lagrange plate equation is reduced to the Bernoulli beam equation, and the Mindlin plate equation is the counterpart of the Timoshenko beam equation [140].

Symmetric Motion. The zeroth-order theory for symmetric motion is derived by retaining $u_x^{(0)}(x,y,t)$ and $u_y^{(0)}(x,y,t)$. This was derived by Poisson (1828), and is the dynamic counterpart of the generalized plane-stress theory of elastostatics (Section 314 of reference [3]). Again, by averaging over the width coordinate y, one obtains the classical one-dimensional wave equation for $\bar{u}_x^{(0)}(x,t)$ with wave speed $(E/\rho)^{1/2}$.

The Poisson theory was modified by Mindlin and Medick [141] to include the effect of stretching in the thickness direction z, and warping of cross sections. They retained terms $u_x^{(0)}, u_y^{(0)}, u_z^{(1)}$ and $u_x^{(2)}, u_y^{(2)}$ to obtain a system of five equations for extensional motion of a plate. The frequency range is extended to $2\pi c_s/H$.

Anisotropic and Composite Plates. Motion in anisotropic plates cannot always be decomposed into symmetric and antisymmetric motion about the midplane of a plate. Various orders of anisotropic plate equations were developed by Mindlin and associates to analyze the vibrations of piezoelectric plates as discussed in the book by Tiersten [142]. Piezoelectric materials like quartz were used as frequency standards and other devices in radio communications [143].

For higher order theories, the expansion in equation (36) is replaced by a series of Legendre polynomials or trigonometric functions [144]. The mathematics of averaging field quantities over the plate thickness and establishing boundary conditions for $\mathbf{u}^{(n)}$ is made precise when the variational equation of elasticity is used.

Such a technique of reducing a system of three-dimensional equations for $\mathbf{u}$ to a larger system of two or one-dimensional equations for $\mathbf{u}^{(n)}$ has also been applied to develop theories for composite materials and composite plates. A recent review is given by Ting [145].

2 Approximate Theories for Cylinders and Shells. For circular cylinders, the displacement $\mathbf{u}(r,\theta,z,t)$ in cylindrical coordinates is expanded into a series in the radial coordinate r,

$$\mathbf{u}(r,\theta,z,t) = \sum_{n=0}^{\infty} \mathbf{u}^{(n)}(z,\theta,t) r^n \tag{37}$$

Downloaded 02 May 2010 to 171.66.16.250. Redistribution subject to ASME license or copyright; see http://www.asme.org/terms/Terms_Use.cfm

or Jacobi polynomials in r. Various order theories may be derived by truncating the series and averaging displacements and stresses over the radius of the cylinder ($r=a$).

The zeroth-order axially symmetric motion is the classical Bernoulli theory (1741) for longitudinal waves in a thin rod, the wave speed being $(E/\rho)^{1/2}$. Based on this theory, waves are nondispersive, and a pulse of the form $u_z^{(0)}(z,t) = f(z-ct)$ will propagate without distortion in a rod. This contradicted experimental observation of a sharp impact on a rod (Hopkinson pressure bar), which led Davies [146] to reinvestigate the problem on the basis of Pochhammer-Chree theory (Chapter 3 of reference [2]).

Love modified the classical theory by considering the lateral inertia of the rod due to longitudinal motion (Section 278, reference [3]). The theory predicted dispersion but the range of frequency is still limited. Several other modifications were proposed, and the theory by Mindlin and McNiven [147] is valid for extensional waves in a rod for frequencies up to $4c_s/a$. This and other approximate theories were reviewed by McNiven and McCoy [148]. A comparison of exact solutions based on approximate theories with approximate solutions of the exact theory for waves in a finite rod was made recently by Hutchinson [149].

Improvements have also been made on approximate theories for thin-walled circular cylinders and shells of other geometries (Chapters 23 and 24 of reference [3]). A theory for circular cylindrical shells was developed by L. H. Donnel for investigating structural stability in 1938, and that for vibrations of shallow spherical shells was developed by E. Reissner in 1946. An extensive literature survey and a comprehensive summary of the theories for cylindical shells can be found in the monograph by Leissa [150].

VI Direct and Inverse Problems – Epilogue

Over the past 50 years, a wealth of knowledge on the propagation of waves in solids has been accumulated, mostly pertaining to waves in *elastic* solids as reviewed in this paper. Some of the theoretical results were confirmed by experimental observations, some were not. Some discrepancies were attributed to geometry (there is no such thing as a plate of constant thickness), boundary conditions (there is no rigid boundary), and loading conditions (it is very difficult to generate a concentrated force with a delta time function). Others were attributed to the inadequacy of instruments for measuring displacement, velocity, or strain at high frequencies (over 1 MHz) or short duration (less than 1 μsec). A major source of discrepancy is that actual materials do not behave as pure elastic solids at adiabatic or isothermal conditions, which is assumed in arriving at equations (5) and (7).

We cite here a few monographs or review articles on *inelastic* effects. Effect of temperature has been studied under the title of thermoelastic waves [151, 152], and that of viscosity under the title of viscoelastic waves [153]. Investigations have also been made on nonlinear elastic waves [154], on waves in porous media [155], on waves in prestressed media [156], and on the interaction of elastic waves with electromagnetic fields [157]. Each subject is accompanied by new methods of analysis and interesting results not predicted by the theory of elastodynamics.

Before we have another 50 years to perfect the theory of waves in solids, and to develop an all-inclusive mathematical method for solving anisotropic, inhomogeneous, vector wave equations, another challenge is thrust on us – the inverse problems of elastic waves. The topics reviewed in this paper are now labeled by many as the direct problems of elastic waves.

Let us call the body force $\mathbf{f}$ in equation (5) or (7), surface displacement $\bar{\mathbf{u}}$ and traction $\bar{\mathbf{T}}$ in (3), and initial displacement $\mathbf{u}_0$ and velocity $\mathbf{v}_0$ in (4) the *sources*, and the solutions for $\mathbf{u}(\mathbf{x},t)$ of equations (3), (4), and (5) the *responses*. The *property of the medium* is defined by the stiffness coefficients c_{ijkl} and the mass density ρ in (2) and (1). The *direct problems* are concerned with the determination of the response when the source and medium property are given. The inverse problems may be divided into two groups. The *inverse source problems* deal with the finding of the sources (any one or a combination of $\mathbf{f}$, $\bar{\mathbf{u}}$, $\bar{\mathbf{T}}$, $\mathbf{u}_0$, $\mathbf{v}_0$) from the response at a few locations over a limited time period, the property of the medium being given. *The inverse medium problems* deal with the determination of c_{ijkl} and ρ when the sources are known and some data of the responses are given.

Not much is known about the solutions for inverse problems of elastic waves. Interested readers may find an introduction to the subject in the monograph by Claerbout [158] and Chapter 12 of reference [14]. There are some inherent mathematical difficulties in solving the inverse problems as evidenced in the recent monographs [159, 160, 161].

We need not dwell on the importance of the inverse problems, as many interesting applications of the theory of elastic waves are inverse problems. They include the age-old problem of locating an earthquake source from seismograms, determining the nature of an earthquake source, determining the geometry and property of a material flaw from the scattering data (NDT), monitoring the safety of large structures from the signals emitted by microcracks (acoustic emission), finding the oil-trapping porous layer in the Earth (seismic prospecting), and determining the ocean bottom from reflection data. Above all, the problem itself is intellectually challenging. Looking ahead a little further, we believe the inverse problems of elastic waves in solids will be a good topic for a review article in the centennial volume of the JOURNAL OF APPLIED MECHANICS.

Acknowledgments

The author is indebted to Professor J. D. Achenbach who read the manuscript, and to Ms. Jennifer E. Michaels and Ms. Janice B. Conrad who assisted in preparing the manuscript. The research is supported by the National Science Foundation under grant No. MEA-8117988 and No. CEE-8206758.

References

1 Whittaker, E., *A History of the Theories of Aether and Electricity*, Vol. 1, Harper and Brothers, New York, 1960.

2 Kolsky, H., *Stress Waves in Solids*, Clarendon Press, Oxford, 1953.

3 Love, A. E. H., *A Treatise on the Mathematical Theory of Elasticity* (reprint of the 4th ed., 1927), Dover, New York, 1944.

4 Strutt, J. W. (Lord Rayleigh), *The Theory of Sound*, Vols. 1 and 2 (reprint of the 2nd ed., 1896), Dover, New York, 1945.

5 Bullen, K. E., *An Introduction to the Theory of Seismology*, 2nd Ed., Cambridge University Press, London, 1953.

6 Nowaki, W., *Dynamics of Elastic Systems*, Wiley, New York, 1963.

7 Achenbach, J. D., *Wave Propagation in Elastic Solids*, North Holland, Amsterdam, 1973.

8 Graff, K. F., *Wave Motion in Elastic Solids*, Ohio State University Press, Columbus, 1975.

9 Eringen, A. C., and Suhubi, E. S. *Elastodynamics*, Vol. 2, *Linear Theory*, Academic Press, New York, 1975.

10 Miklowitz, J., *The Theory of Elastic Waves and Wave Guides*, North Holland, Amsterdam, 1978.

11 Ewing, W. M., Jardetzky, W., and Press, F., *Elastic Waves in Layered Media*, McGraw-Hill, New York, 1957.

12 Brekhovskikh, L. M., *Waves in Layered Media*, 2nd Ed., Academic Press, New York, 1980.

13 White, J. E., *Seismic Waves: Radiation, Transmission, and Attenuation*, McGraw-Hill, New York, 1965.

14 Aki, K., and Richards, P., *Quantitative Seismology-Theory and Methods*, W. H. Freeman, San Francisco, 1980.

15 Ben-Menahem, A., and Singh, S. J., *Seismic Waves and Sources*, Springer-Verlag, New York, 1981.

Downloaded 02 May 2010 to 171.66.16.250. Redistribution subject to ASME license or copyright; see http://www.asme.org/terms/Terms_Use.cfm

16 Truell, R., Elbaum, C., and Chick, B. B., *Ultrasonic Methods in Solid State Physics*, Academic Press, New York, 1969.

17 Auld, B. A., *Acoustic Fields and Waves in Solids*, Wiley, New York, 1973.

18 Miklowitz, J., "Elastic Wave Propagation," ASME *Applied Mechanics Review*, Vol. 13, 1960, pp. 865–878.

19 Scott, R. A., "Linear Elastic Wave Propagation: An Annotated Bibliography, Parts I and II," *Shock and Vibration Digest*, 1977, p. 78.

20 Redwood, M., *Mechanical Waveguides*, Pergamon, New York, 1960.

21 Viktorov, I. A., *Rayleigh and Lamb Waves*, Plenum, New York, 1967.

22 Abramson, H. N., Plass, H. J., and Ripperger, E. A., "Stress Waves in Rods and Beams," in: *Advances in Applied Mechanics*, Dryden, H. L., Von Karman, T., eds., Vol. 5, 1958, pp. 111–194.

23 Meeker, R. T., and Meitzler, A. H., "Guided Wave Propagation in Elongated Cylinders and Plates," in: *Physical Acoustics*, Mason, W. P., ed., Vol. 1*A*, Academic Press, New York, 1964, pp. 111–167.

24 Pao, Y.-H., and Kaul, R. K., "Waves and Vibrations in Isotropic and Anisotropic Plates," in: *R. D. Mindlin and Applied Mechanics*, Herrmann, G., ed., New York, 1974, pp. 149–195.

25 Thurston, R. N., "Elastic Waves in Rods and Clad Rods," *Journal of Acoustical Society of America*, Vol. 64, 1978, pp. 1–36.

26 Mindlin, R. D., "Waves and Vibrations in Isotropic, Elastic Plates," in: *Structural Mechanics*, Goodier, H. N., and Hoff, N. J., eds., Pergamon Press, New York, 1960, pp. 199–232.

27 Zemenek, J., "An Experimental and Theoretical Investigation of Elastic Wave Propagation in a Cylinder," *Journal of the Acoustical Society of America*, Vol. 51, 1972, p. 265.

28 Thomson, W. T., "Transmission of Elastic Waves Through a Stratified Solid Medium," *Journal of Applied Physics*, Vol. 21, 1950, p. 89.

29 Haskell, N. A., "The Dispersion of Surface Waves on Multilayered Media," *Bulletin of the Seismological Society of America*, Vol. 43, 1953, p. 17.

30 Dunkin, J. W., "Computation of a Modal Solution in Layered, Elastic Media at High Frequencies," *Bulletin of the Seismological Society of America*, Vol. 55, 1965, p. 335.

31 Abo-Zena, A., "Dispersion Function Computations for Unlimited Frequency Values," *Geophysical Journal of the Royal Astronomical Society*, Vol. 58, 1979, pp. 91–105.

32 Gilbert, F., and Backus, G. E., "Propagator Matrices in Elastic Wave and Vibration Problems," *Geophysics*, Vol. 31, 1966, p. 326.

33 Alterman, A., Jarosch, H., and Pekeris, C. L., "Oscillations of the Earth," *Proceedings of the Royal Society*, London, Series *A*, Vol. 252, 1959, p. 80.

34 Sato, Y., Usami, T., Landisman, M., and Ewing, M., "Basic Study on the Oscillation of a Sphere, Part V," *Geophysical Journal of the Royal Astronomical Society*, Vol. 8, 1963, p. 44.

35 Press, F., "Long-Period Waves and Free Oscillations of the Earth," in: *Research in Geophysics*, Odishaw, H., ed., Vol. 2, MIT Press, Cambridge, Mass., 1964, pp. 1–26.

36 Papadakis, E. P., "Ultrasonic Velocity and Attenuation Measurement Methods With Scientific and Industrial Applications," in: *Physical Acoustics*, Mason, W. P., and Thurston, R. N., eds., Vol. 12, Academic Press, New York, 1976, pp. 277–374.

37 Thurston, R. N., "Wave Propagation in Fluids and Normal Solids," in: *Physical Acoustics*, Mason, W. P., ed., Vol. 1*A*, Academic Press, New York, 1964, pp. 2–167.

38 Kraut, E. A., "Advances in the Theory of Anisotropic Elastic Wave Propagation," *Review of Geophysics*, Vol. 1, 1963, p. 401.

39 Fedorov, F. I., *Theory of Elastic Waves in Crystals*, Plenum Press, New York, 1968.

40 Musgrave, M. J. P., *Crystal Acoustics*, Holden-Day, San Francisco, 1970.

41 Synge, J. L., "Elastic Waves in Anisotropic Media," *Journal of Mathematics and Physics*, Vol. 35, 1957, pp. 323–334.

42 Farnell, G. W., "Properties of Elastic Surface Waves," in: *Physical Acoustics: Principles and Methods*, Mason, W. P., and Thurston, R. N. eds., Vol. 6, Academic Press, New York, 1970, pp. 109–166.

43 Crampin, S., "A Review of Wave Motion in Anisotropic and Cracked Elastic Media," *Wave Motion*, Vol. 3, 1981, pp. 343–391.

44 Dransfeld, K., and Salzmann, E., "Excitation, Detection and Attenuation of High-Frequency Elastic Surface Waves," in: *Physical Acoustics: Principles and Methods*, Mason, W. P., and Thurston, R. N., eds., Vol. 7, Academic Press, New York, 1970, pp. 219–272.

45 L. T. Claiborne, Kino, G. S. and Stern, E., eds., "Surface Acoustic Wave Devices and Applications," *IEEE Proceedings*, Vol. 64, 1976.

46 Cagniard, L., *Reflection and Refraction of Progressive Seismic Waves*, English translation by E. A. Flynn and C. H. Dix, McGraw-Hill, New York, 1962.

47 Garvin, W. W., "Exact Transient Solution of the Buried Line Source Problem," *Proceedings of the Royal Society*, London, Series *A*, Vol. 234, 1956, p. 528.

48 deHoop, A. T., "A Modification of Cagniard's Method for Solving Seismic Pulse Problems," *Applied Scientific Research (B)*, Vol. 8, 1960, p. 349.

49 Pekeris, C. L., "The Seismic Buried Pulse," *Proceedings National Academy of Sciences of United States*, Vol. 41, 1955, pp. 629–639.

50 Chao, C.-C., "Dynamical Response of an Elastic Half-Space to Tangential Surface Loadings," ASME JOURNAL OF APPLIED MECHANICS, Vol. 27, 1960, pp. 559–567.

51 Pao, Y.-H., and Gajewski, R. G., "The Generalized Ray Theory and Transient Responses of Layered Elastic Solids," in: *Physical Acoustics*, Mason, W. P., and Thurston, R. N., eds., Vol. 13, Academic Press, New York, 1977, pp. 183–265.

52 Cole, J., and Huth, J., "Stresses Produced in a Half Plane by Moving Loads," ASME JOURNAL OF APPLIED MECHANICS, Vol. 25, 1958, pp. 433–436.

53 Payton, R. G., "An Application of the Dynamic Betti-Rayleigh Reciprocal Theorem to Moving Point Loads in Elastic Media," *Quarterly of Applied Mathematics*, Vol. 21, 1964, pp. 299–313.

54 Gakenheimer, D. C., and Miklowitz, J., "Transient Excitation of an Elastic-Half Space by a Point Load Traveling on the Surface," ASME JOURNAL OF APPLIED MECHANICS, Vol. 36, 1969, p. 505.

55 Goldsmith, W., *Impact*, Edward Arnold, London, 1960.

56 Kostrov, B. V., "Self-Similar Dynamic Problems of the Impression of a Rigid Die in an Elastic Half-Space," *Izv. Akad. Nauk SSSR Mekh. Mashinostr.*, No. 4, 1964, pp. 54–62.

57 Willis, J. R., "Self-Similar Problems in Elastodynamics," *Philosophical Transactions of the Royal Society of London*, Series *A*, Vol. 274, 1973, pp. 435–491.

58 Ewing, M., Worzel, J. L., and Pekeris, C. L., *Propagation of Sound in the Ocean*, Memoir 27, The Geological Society of America, New York, 1948.

59 Tolstoy, I., and Clay, C. S., *Ocean Acoustics*, McGraw-Hill, New York, 1966.

60 Kennett, B. L. N., "Elastic Wave Propagation in Stratified Media," in: *Advances in Applied Mechanics*, Yih, C.-S., ed., Vol. 21, 1981, pp. 79–169.

61 Fuchs, K., and Muller, G., "Computation of Synthetic Seismograms With the Reflectivity Method and Comparison With Observations," *Geophys. J. R. Astr. Soc.*, Vol. 23, 1971, pp. 417–433.

62 Kennett, B. L. N., and Clarke, T. J., "Seismic Waves in a Stratified Half-Space-IV. *P-SV* Wave Decoupling and Surface Wave Dispersion," *Geophys. J. R. Astr. Soc.*, Vol. 72, 1983, pp. 633–645.

63 Harkrider, D. G., "Surface Waves in Multilayered Elastic Media. Part II: Higher Mode Spectra and Spectral Ratios from Point Sources in Plane Layered Earth Models," *Bull. Seismol. Soc. Amer.*, Vol. 60, 1970, pp. 1937–1987.

64 Chapman, C. H., "A New Method for Computing Synthetic Seismograms," *Geophys. J. R. Astr. Soc.*, Vol. 54, 1978, pp. 481–518.

65 Pekeris, C. L., Alterman, Z., Abramovici, F., and Jarosch, H., "Propagation of a Compressional Pulse in a Layered Solid," *Review of Geophysics*, Vol. 3, 1965, p. 25.

66 Knopoff, L., Gilbert, F., and Pilant, W. L., "Wave Propagation in a Medium With a Single Layer," *J. Geophys. Res.*, Vol. 65, 1960, p. 265.

67 Muller, G., "Theoretical Seismograms for Some Type of Point-Sources in Layered Media, Part I, II, III," *Zeitschrift für Geophysik*, Band 34, s. 15–35 and 147–162, 1968, Band 35, s. 347–371, 1969.

68 Knopoff, L, "Elastic Wave Propagation in a Wedge," in: *Wave Propagation in Solids*, Miklowitz, J., ed., American Society of Mechanical Engineers, New York, 1969, pp. 3–43.

69 Lapwood, E. R., "The Transmission of a Rayleigh Pulse Round a Corner," *Geophysical Journal of the Royal Astronomical Society*, Vol. 4, 1961, pp. 174–196.

70 Achenbach, J. D., and Khehtan, R. P., "Elastodynamic Response of a Wedge to Surface Pressures," *Int. J. Solids Structures*, Vol. 13, 1977, pp. 1157–1172.

71 Miklowitz, J., "Wavefront Analysis in the Nonseparable Elastodynamic Quarter-Plane Problems, 1. Parts I and II," ASME JOURNAL OF APPLIED MECHANICS, Vol. 49, 1982, pp. 797–815.

72 Ishii, H., and Ellis, R. M., "Multiple Reflection of Plane *SH* Waves by a Dipping Layer," *Bulletin of the Seismological Society of America*, Vol. 60, 1970, pp. 15–28.

73 Hong, T.-L., and Helmberger, D. V., "Generalized Ray Theory for Dipping Structure," *Bulletin of the Seismological Society of America*, Vol. 57, 1977, pp. 995–1008.

74 Pao, Y.-H., and Ziegler, F., "Transient *SH* Waves in a Wedge-Shaped Layer," *Geophys. J. R. Astr. Soc.*, Vol. 73, 1982, pp. 57–77.

75 Gurtin, M., "Variational Principles for Linear Elastodynamics," *Archive Rational Mechanics and Analysis*, Vol. 16, 1964, pp. 34–50.

76 Sternberg, E., "On the Integration of the Equations of Motion in the Classical Theory of Elasticity," *Archive Rational Mechanics and Analysis*, Vol. 6, 1960, pp. 34–50.

77 Morse, P. M., and Feshbach, H., *Methods of Theoretical Physics*, McGraw-Hill, New York, 1953.

78 Harumi, K., "Scattering of Plane Waves by a Rigid Ribbon in a Solid," *Journal of Applied Physics*, Vol. 32, 1961, p. 1488.

79 Thau, S. A., and Pao, Y.-H., "Wave Function Expansions and Perturbation Method for the Diffraction of Elastic Waves by a Parabolic Cylinder," ASME JOURNAL OF APPLIED MECHANICS, Vol. 34, 1967, p. 915.

80 Pao, Y.-H., and Mow, C.-C., *Diffraction of Elastic Waves and Dynamic Stress Concentrations*, Crane and Russak, New York 1973.

81 Filipczynski, L., "Scattering of a Plane Longitudinal Wave on a Free Surface of a Disc in Solid Medium," *Proceedings of Vibration Problems (Warsaw)*, Vol. 2, 1961, pp. 41–56.

82 Buchwald, V. T., "Elastic Waves in Anisotropic Media," *Proceedings of Royal Society*, London, Series *A*, Vol. 253, 1959, pp. 563–580.

83 Karal, F. C., and Keller, J. B., "Elastic, Electrogmagnetic, and Other Waves in a Random Medium," *Journal of Mathematical Physics*, Vol. 5, 1964, pp. 537–547.

Downloaded 02 May 2010 to 171.66.16.250. Redistribution subject to ASME license or copyright; see http://www.asme.org/terms/Terms_Use.cfm

84 Karal, F. C., and Keller, J. B., "Elastic Wave Propagation in Homogeneous and Inhomogeneous Media," *Journal of the Acoustical Society of America*, Vol. 31, 1959, pp. 694–705.

85 McCoy, J. J., "A Parabolic Theory of Stress Wave Propagation Through Inhomogeneous Linearly Elastic Solids," ASME JOURNAL OF APPLIED MECHANICS, Vol. 44, 1977, pp. 462–468.

86 Cerveny, V., Molotov, I. A., and Psencik, I., *The Ray Method in Seismology*, Prague Charles University Press, 1978.

87 Born, M., and Wolf, E., *Principles of Optics*, 5th ed., Pergamon Press, New York, 1975.

88 Baker, B. B., and Copson, E. T., *The Mathematical Theory of Huygens' Principle*, 2nd ed., Oxford University Press, London, 1950.

89 Wheeler, L. T., and Sternberg, E., "Some Theorems in Classical Elastodynamics," *Archive for Rational Mechanics and Analysis*, Vol. 31, 1968, pp. 51–90.

90 Kupradze, V. D., "Dynamical Problems in Elasticity," in: *Progress in Solid Mechanics*, Sneddon, I. N., and Hill, R., eds., Vol. III, North Holland, New York, 1963.

91 Pao, Y.-H., and Varatharajulu, V., "Huygens' Principle, Radiation Conditions, and Integral Formulas for the Scattering of Elastic Waves," *Journal of the Acoustical Society of America*, Vol. 59, 1976, pp. 1361–1371.

92 Willis, J. R., and Bedding, R. J., "Transient Elastodynamic Fields in Anisotropic Plates and Layers," in *Modern Problems in Elastic Wave Propagation*, Miklowitz, J., and Achenbach, J. D., eds., Wiley, New York, 1978, pp. 347–371.

93 Banerjee, D. K., and Butterfield, R., eds., *Developments in Boundary Element Methods*, Vol. I, 1979, Vol. II, 1981, Applied Science, London.

94 Gurtin, M. E., "The Linear Theory of Elasticity," *Handbuch der Physik*, C. Truesdell, ed., Vol. VIa/2, 1972, pp. 1–295.

95 Reismann, H., "On the Forced Motion of Elastic Solids," *Applied Science Research*, Vol. 18, 1967, pp. 156–165.

96 Weaver, R., and Pao, Y.-H., "Axisymmetric Elastic Waves Excited by a Point Source in a Plate," ASME JOURNAL OF APPLIED MECHANICS, Vol. 49, 1982, pp. 821–836.

97 Clebsch, A., "Über die Reflexion an einer Kugelfläche," *Journal fur die reine und angewandte Mathematik*, Bd. 61, S. 195, 1863.

98 Lamb, H., *Hydrodynamics* (1st ed., 1879, 6th ed., 1932 Cambridge University Press), Dover, New York, 1945.

99 Sezawa, K., "Scattering of Elastic Wave and Some Allied Problems," *Bulletin of the Earthquake Research Institute*, Tokyo Imperial University, Japan, Vol. 3, 1927, p. 19.

100 Nishimura, G., and Jimbo, Y., "A Dynamical Problem of Stress Concentration—Stresses in the Vicinity of a Spherical Matter Included in an Elastic Solid Under Dynamical Force," *Journal of the Faculty of Engineering*, University of Tokyo, Vol. 24, 1955, p. 101.

101 Ying, C. F., and Truell, R., "Scattering of a Plane Longitudinal Wave by a Spherical Obstacle in an Isotropically Elastic Solid," *Journal of Applied Physics*, Vol. 27, 1956, p. 1086.

102 Pao, Y.-H., "Dynamical Stress Concentration in an Elastic Plate," ASME JOURNAL OF APPLIED MECHANICS, Vol. 29, 1962, pp. 299–305.

103 Baron, M. L., and Matthews, A. T., "Diffraction of a Pressure Wave by a Cylindrical Cavity in an Elastic Medium," ASME JOURNAL OF APPLIED MECHANICS, Vol. 28, p. 237, 1961.

104 Nagase, M., "Diffraction of Elastic Waves by a Sphere," *Journal of the Physical Society of Japan*, Vol. 11, 1956, pp. 279–301.

105 Hönl, H., Maue, A. W., and Westpfahl, K., "Theorie der Beugung," in: *Handbuch der Physik*, Band 25/1, Flugge, S., ed., Springer-Verlag, Berlin, 1961.

106 Pao, Y.-H., and Mow, C.-C., "Theory of Normal Modes and Ultrasonic Spectral Analysis of the Scattering of Waves in Solids," *Journal of Acoustical Society of America*, Vol. 59, 1976, pp. 1046–1056.

107 Flax, L., Gaunaurd, G. C., and Uberall, H., "Theory of Resonance Scattering," *Physical Acoustics*, Mason, W. P., and Thurston, R. N., eds., Vol. XV, 1981, pp. 191–294.

108 Junger, M. C., and Feit, D., *Sound, Structures, and Their Interaction*, MIT Press, Cambridge, Mass., 1972.

109 Uberall, H., and Huang, H., "Acoustical Response of Submerged Elastic Structures Obtained Through Integral Transforms," in: *Physical Acoustics*, Mason, W. P., and Thurston, R. N., eds., Vol. XII, 1976, pp. 217–275.

110 Luco, J. E., "Dynamic Interaction of a Shear Wall With the Soil," *Journal of Engineering Mechanics Division American Society of Civil Engineers*, Vol. 95, 1969, pp. 333–346.

111 Hall, W. J., ed., *Structural and Geotechnical Mechanics*, Prentice Hall, Englewood Cliffs, N. J., 1977.

112 Maue, A. W., "Die Beugung Elastischer Wellun an der Halbebene," *Zeitschrift für angewandte Mathematik und Mechanik*, B.33, S.1, 1953.

113 Gautesen, A. K., Achenbach, J. D., McMaken, H., "Surface-Wave Rays in Elastodynamic Diffraction by Cracks," *Journal of Acoustical Society of America*, Vol. 63, 1978, pp. 1828–1831.

114 Ang, D. D., and Knopoff, L., "Diffraction of Vector Elastic Waves by a Finite Crack," *Proceedings of the National Academy of Sciences*, Vol. 52, 1964, pp. 1075–1081.

115 Sih, G. C., "A Three-Dimensional Strain Energy Density Theory of Crack Propagation: Three-Dimensional Crack Problems," in: *Mechanics of Fracture II*, Sih, G. C., ed., Noordhoff International, Leyden, The Netherlands, 1975, pp. 15–53.

116 Freund, L. B., "The Analysis of Elastodynamic Crack Tip Stress Fields," in: *Mechanics Today*, Nemat-Nasser, S., ed., Vol. 3, Pergamon, New York, 1976.

117 Sih, G. C., ed., *Elastodynamic Crack Problems*, Vol. 1, Noordhoff International Publishing, Leyden, The Netherlands, 1977.

118 Kraut, E., "Review of Theories of Scattering of Elastic Waves by Cracks," *IEEE Transactions on Sonics and Ultrasonics*, Vol. SU-23, 1976, pp. 162–167.

119 Bowman, J. J., Senior, T. B. A., and Uslenghi, P. L. E., eds., *Electromagnetic and Acoustic Scattering by Simple Shapes*, North-Holland Publishing Company, Amsterdam, 1969.

120 Waterman, P., "Matrix Theory of Elastic Wave Scattering," *Journal of Acoustical Society of America*, Vol. 60, 1976, pp. 567–580.

121 Varatharajulu, V., and Pao, Y.-H., "Scattering Matrix for Elastic Waves, I. Theory," *Journal of Acoustical Society of America*, Vol. 60, 1976, pp. 556–566.

122 Pao, Y.-H., "Betti's Identity and Transition Matrix for Elastic Waves," *Journal of Acoustical Society of America*, Vol. 64, 1978, pp. 302–310.

123 Bostrom, A., "Time-Dependent Scattering by a Bounded Obstacle in Three Dimensions," *Journal of Mathematical Physics*, Vol. 23, 1982, pp. 1444–1450.

124 Varadan, V. J., and Varadan, V. V., eds., *Acoustic, Electromagnetic and Elastic Wave Scattering-Focus on the T-Matrix Approach*, Pergamon, New York, 1980.

125 Keller, J. B., "A Geometrical Theory of Diffraction," *Proc. Symposium on the Calculus of Variations and Its Applications* (Chicago, 1956), McGraw-Hill, New York, 1958, pp. 27–52.

126 Levy, B. R., and Keller, J. B., "Diffraction by a Smooth Object," *Communications on Pure and Applied Mathematics*, Vol. 12, 1959, pp. 159–209.

127 Achenbach, J. D., Gautesen, A. K., and McMaken, H., *Ray Methods for Waves in Elastic Solids*, Pitman Advances Publishing Program, Boston, 1982.

128 Friedlander, F. G., *Sound Pulses*, Cambridge University Press, Cambridge, 1958.

129 Gubernatis, J. E., Domany, E., Krumhansl, J. A., and Huberman, M., "The Born Approximation in the Theory of the Scattering of Elastic Waves by Flaws," *Journal of Applied Physics*, Vol. 48, 1977, pp. 2812–2819.

130 Mal, A. K., and Knopoff, L., "Elastic Wave Velocities in Two-Component Systems," *Journal of Institute of Applied Mathematics*, Vol. 3, 1967, pp. 376–387.

131 Kobayashi, S., and Nishimura, N., "Transient Stress Analysis of Tunnels and Caverns of Arbitrary Shape Due to Traveling Waves," in: *Developments in Boundary Element Methods—II*, Banerjee, P. K., and Shaw, R. D., eds., Applied Science, London, 1981, pp. 177–210.

132 Shaw, P. P., "Boundary Integral Equation Methods Applied to Wave Problems," in: *Developments in Boundary Element Methods-I*, Banerjee, P. K., and Butterfield, R., eds., Applied Science, London, 1979, pp. 121–153.

133 Seybert, A. F., Soenarko, B., Rizzo, F. J., and Shippy, D. J., "Application of the BIE Method to Sound Radiation Problems Using an Isoparametric Element," *ASME Paper No. 82-WA/NCA-1*, Presented at the ASME Winter Annual Meeting, Phoenix, 1982.

134 Liu, D., Gai, B., and Tao., G., "Applications of the Method of Complex Functions to Dynamic Stress Concentrations," *Wave Motion*, Vol. 4, 1982, pp. 293–304.

135 Datta, S. K., "Scattering of Elastic Waves," in: *Mechanics Today*, Nemat-Nasser, S., ed., Vol. 4, Pergamon, New York, 1978, pp. 149–208.

136 Felsen, L. B., "Propagation and Diffraction of Transient Fields in Non Dispersive and Dispersive Media," in: *Transient Electromagnetic Fields*, Felsen, L. B., ed., Springer-Verlag, Berlin, 1976, pp. 1–72.

137 Gilbert, F., and Helmberger, D. V., "Generalized Ray Theory for a Layered Sphere," *Geophysical Journal of the Royal Astronomical Society*, Vol. 27, 1972, pp. 57–89.

138 Chen, P. C., and Pao, Y.-H., "The Diffraction of Sound Pulses by a Circular Cylinder," *Journal of Mathematical Physics*, Vol. 18, 1977, pp. 2397–2406.

139 Mindlin, R. D., "Influence of Rotatory Inertia and Shear on Flexural Motions of Isotropic Elastic Plates," ASME JOURNAL OF APPLIED MECHANICS, Vol. 18, 1951, p. 31.

140 Timoshenko, S., "On the Correction for Shear of the Differential Equation for Transverse Vibration of Prismatic Bars," *Philosophical Magazine*, Vol. 41, 1921, p. 744.

141 Mindlin, R. D., and Medick, M. A., "Extensional Vibrations of Elastic Plates," ASME JOURNAL OF APPLIED MECHANICS, Vol. 26, 1959, pp. 561–569.

142 Tiersten, H. F., *Linear Piezoelectric Plate Vibrations*, Plenum Press, New York, 1969.

143 Bahadur, H., and Parshad, R., "Acoustic Vibrational Modes in Quartz Crystals: Their Frequency, Amplitude, and Shape Determination," in: *Physical Acoustics XVI*, Mason, W. P., and Thurston, R. N., eds., Academic Press, New York, 1982, pp. 38–171.

144 Lee, P. C. Y., and Nikodem, Z., "An Approximate Theory for High-Frequency Vibrations of Elastic Plates," *International Journal of Solids and Structures*, Vol. 8, 1972, p. 581.

145 Ting, T. C. T., "Dynamic Response of Composites," ASME *Applied Mechancis Reviews*, Vol. 33, 1980, pp. 1629–1635.

146 Davies, R. M., "A Critical Study of the Hopkinson Pressure Bar,"

Downloaded 02 May 2010 to 171.66.16.250. Redistribution subject to ASME license or copyright; see http://www.asme.org/terms/Terms_Use.cfm

Philosophical Transactions of the Royal Society of London, Ser. A, Vol. 240, 1948, p. 375.

147 Mindlin, R. D., and McNiven, H. D., "Axially Symmetric Waves in Elastic Rods," ASME JOURNAL OF APPLIED MECHANICS, Vol. 27, 1960, pp. 145–151.

148 McNiven, H. D., and McCoy, J. J., "Vibrations and Wave Propagation in Rods," in: *R.D. Mindlin and Applied Mechanics*, Herrmann, G., ed., Pergamon, New York, 1974, pp. 197–226.

149 Hutchinson, J. R., "Vibrations of Solid Cylinders," ASME JOURNAL OF APPLIED MECHANICS, Vol. 47, 1980, pp. 901–907.

150 Leissa, A., *Vibration of Shells*, National Aeronautics and Space Administration, Washington, D. C., 1973.

151 Nowacki, W., *Dynamic Problems of Thermoelasticity*, Noordhoff International, Leyden, The Netherlands, 1975.

152 Chadwick, P., and Smith, G. D., "Thermoelasticity, the Dynamical Theory," in: *Progress in Solid Mechanics*, Sneddon, I.N., and Hill, R., eds., Vol. I, North-Holland, Amsterdam, 1960, pp. 265–329.

153 Flugge, W., *Viscoelasticity*, Springer-Verlag, Berlin, 1975.

154 Bland, D. R., *Nonlinear Dynamic Elasticity*, Blaisdell Publishing, Waltham, Mass., 1969.

155 Biot, M. A., "Mechanics of Deformation and Acoustic Propagation in Porous Media," *Journal of Applied Physics*, Vol. 33, 1962, pp. 1482–1498.

156 Pao, Y.-H., Sachse, W., and Fukuoka, H., "Acoustoelasticity and Measurement of Residual Stresses," to appear in *Physical Acoustics*, Vol. 17, Academic Press, New York, 1983.

157 Moon, F. C., "Problems in Magneto-Solid Mechanics," in: *Mechanics Today*, Nemat-Nasser, S., ed., Vol. 4, Pergamon, New York, 1978, pp. 307–390.

158 Claerbout, J. F., *Fundamentals of Geophysical Data Processing*, McGraw-Hill, New York, 1976.

159 Sabatier, P. C., ed., *Applied Inverse Problems*, (Lecture Notes in Physics, No. 85), Springer-Verlag, Berlin, 1978.

160 Baltes, H. P., ed., *Inverse Source Problems in Optics*, Springer-Verlag, New York, 1978.

161 Baltes, H. P., ed., *Inverse Scattering Problems in Optics*, Springer-Verlag, New York, 1980.

Downloaded 02 May 2010 to 171.66.16.250. Redistribution subject to ASME license or copyright; see http://www.asme.org/terms/Terms_Use.cfm

J. L. Sanders, Jr.
Division of Applied Sciences,
Harvard University,
Cambridge, Mass. 02138
Fellow ASME

Analysis of Circular Cylindrical Shells

The paper is an account of the present state of the linear theory of circular cylindrical shells, problems of current interest, and in a broad sense the analytical methods that can be brought to bear on these problems.

Introduction

Circular cylindrical shells have attracted more attention than any other shape partly because of their technical importance and partly because the mathematical theory for them is relatively simple. This theory is more coherent and well developed than for any other special case. What has been done for circular cylinders provides hints at what might be done for shells of other geometries. This paper emphasizes ideas that have served to simplify and unify the subject.

General Linear Shell Equations

Let dimensionless stress and strain measures, displacements, stress functions, etc. (without a tilde) be given by

$$\tilde{N}_{\alpha\beta} = \sigma h N_{\alpha\beta}, \quad \tilde{M}_{\alpha\beta} = \sigma R h \epsilon^2 M_{\alpha\beta}$$

$$\tilde{E}_{\alpha\beta} = \sigma E^{-1} E_{\alpha\beta}, \quad \tilde{K}_{\alpha\beta} = \sigma (ER\epsilon^2)^{-1} K_{\alpha\beta}$$

$$(\tilde{u}_\alpha, \tilde{w}) = \sigma R E^{-1} (u_\alpha, \epsilon^{-2} w), \quad (\tilde{\chi}_\alpha, \tilde{\psi}) = \sigma R^2 h (\epsilon^2 \chi_\alpha, \psi)$$

$$(\tilde{p}_\alpha, \tilde{p}) = \sigma h R^{-1} (p_\alpha, p), \quad \epsilon^2 = hR^{-1}[12(1-\nu^2)]^{-1/2}$$

Here h is the (constant) shell thickness, R a reference radius of curvature, σ is a reference stress, E and ν are elastic constants, and ϵ is a small parameter. Coordinates on the shell middle surface are made dimensionless (if necessary) with reference to the length R. The negative of the second fundamental tensor of the middle surface is $R^{-1} b_{\alpha\beta}$. In shell theory a surface tensor $B_{\alpha\beta}$ defined by

$$B_{\alpha\beta} = \frac{1}{2} (\epsilon_{\alpha\gamma} b_{\gamma\beta} + \epsilon_{\beta\gamma} b_{\gamma\alpha}) \tag{1}$$

and a dual operation for any second-order tensor $T_{\alpha\beta}$ denoted by an overbar and defined by

$$\bar{T}_{\alpha\beta} = \epsilon_{\alpha\lambda} \epsilon_{\beta\mu} T_{\lambda\mu} \tag{2}$$

aid in writing the equations in a more compact form. Here $\epsilon_{\alpha\beta}$ is the two-dimensional permutation tensor. A cartesian tensor notation, appropriate for cylindrical shells in curvature coordinates, will be used but with a trivial reinterpretation the notation is also appropriate in general.

Contributed by the Applied Mechanics Division for publication in the JOURNAL OF APPLIED MECHANICS. Discussion on this paper should be addressed to the Editorial Department, ASME, United Engineering Center, 345 East 47th Street, New York, N.Y. 10017, and will be accepted until two months after final publication of the paper itself in the JOURNAL OF APPLIED MECHANICS. Manuscript received by ASME Applied Mechanics Division, March, 1983.

All two-dimensional thin shell theories are approximations. The present article will be devoted exclusively to what is called a "first approximation theory," i.e., a theory that is consistent with the Kirchhoff hypotheses. An account of the present status of the foundations of thin shell theory with extensive references to the literature can be found in a recent book by Dikman [1]. Suffice it to say that the approximations involved in a first approximation theory are traceable exclusively to the constitutive relations. As far as they go the remaining equations of the theory are exact. However, depending on how the dependent variables are defined, the equations can take different forms. The general equations given here were introduced practically simultaneously by Koiter [2] and the present author [3].

Equilibrium equations

$$N_{\alpha\beta,\beta} + \epsilon^2 b_{\alpha\gamma} M_{\beta\gamma,\beta} - \frac{1}{2} \epsilon^2 \epsilon_{\alpha\beta} (B_{\gamma\delta} M_{\gamma\delta})_{,\beta} + p_\alpha = 0$$

$$M_{\alpha\beta,\alpha\beta} - \epsilon^{-2} b_{\alpha\beta} N_{\alpha\beta} + p = 0 \tag{3}$$

Compatibility equations

$$\bar{K}_{\alpha\beta,\beta} - \epsilon^2 b_{\alpha\gamma} \bar{E}_{\beta\gamma,\beta} + \frac{1}{2} \epsilon^2 \epsilon_{\alpha\beta} (B_{\gamma\delta} \bar{E}_{\gamma\delta})_{,\beta} = 0$$

$$\bar{E}_{\alpha\beta,\alpha\beta} + \epsilon^{-2} b_{\alpha\beta} \bar{K}_{\alpha\beta} = 0 \tag{4}$$

Strain-displacement relations

$$E_{\alpha\beta} = \frac{1}{2} (u_{\alpha,\beta} + u_{\beta,\alpha}) + \epsilon^{-2} b_{\alpha\beta} w$$

$$K_{\alpha\beta} = \frac{1}{2} (\omega_{\alpha,\beta} + \omega_{\beta,\alpha}) + \epsilon^2 B_{\alpha\beta} \omega \tag{5}$$

$$\omega_\alpha = -w_{,\alpha} + \epsilon^2 b_{\alpha\beta} u_\beta, \quad \omega = \frac{1}{2} \epsilon_{\alpha\beta} u_{\beta,\alpha}$$

Stress-stress function relations (when $p_\alpha = p = 0$)

$$\bar{N}_{\alpha\beta} = -\frac{1}{2} (\zeta_{\alpha,\beta} + \zeta_{\beta,\alpha}) - \epsilon^2 B_{\alpha\beta} \zeta$$

$$\bar{M}_{\alpha\beta} = \frac{1}{2} (\chi_{\alpha,\beta} + \chi_{\beta,\alpha}) + \epsilon^{-2} b_{\alpha\beta} \psi \tag{6}$$

$$\zeta_\alpha = -\psi_{,\alpha} + \epsilon^2 b_{\alpha\beta} \chi_\beta, \quad \zeta = \frac{1}{2} \epsilon_{\alpha\beta} \chi_{\beta,\alpha}$$

Copyright © 1983 by ASME
Downloaded 02 May 2010 to 171.66.16.250. Redistribution subject to ASME license or copyright; see http://www.asme.org/terms/Terms_Use.cfm

Constitutive relations

$$E_{\alpha\beta} = N_{\alpha\beta} - \nu\bar{N}_{\alpha\beta}$$
$$M_{\alpha\beta} = K_{\alpha\beta} + \nu\bar{K}_{\alpha\beta} \tag{7}$$

The fact that Goldenveizer's well-known static-geometric analogy holds for this system of equations is evident. In the case of circular cylinders in (z, θ) curvature coordinates $b_{11} = b_{12} = 0$, $b_{22} = 1$, $B_{11} = B_{22} = 0$, $B_{12} = B_{21} = 1/2$. The preceding equations involve symmetric, modified stress and strain measures (except for $E_{\alpha\beta}$). A full discussion of these is out of place here but see [4]. The constitutive relations (7) have the same form as Love's uncoupled relations.

Because of the complexity of the system of shell equations and the approximate nature of the theory there was, in the early years of development, considerable uncertainty over what simplifications in the equations could be tolerated, particularly in the derivation of the constitutive relations.

Thus it was that a system of equations for circular cylindrical shells due to Love [5], entirely accurate by present day standards, was overlooked or ignored for at least 40 years. See [6] for a discussion. In the meantime a system of cylinder equations due to Flügge [7, 8] gained wide acceptance as a standard of accuracy. In a form applicable for arbitrary middle surfaces the theory has been called the Flügge-Lurie-Byrne theory. At least the beginnings of a proper error estimation procedure were introduced in the subject by Novozhilov [9]. The fundamental idea is that *relative* errors of order ϵ^2 are inherent in the theory due to the "neglect" of effects of transverse shear strains. Put another way a first approximation theory is one in which relative errors of order ϵ^2 are tolerated. Somewhat later, but independently, the same idea was developed by Koiter [2]. The idea has consequences for shell theory, rather more far-reaching than can be discussed here. For a recent survey of error estimation theory, pointwise and global, see [1].

One result of the Novozhilov and Koiter analysis is that certain terms can be deleted or added to the constitutive relations without impairing the accuracy of the system of equations. While uniqueness in the form of the equations might seem desirable, advantage can be taken of the permissible variability to construct the simplest possible system of equations for a particular form of the middle surface such as a circular cylinder.

Simplified Equations for Circular Cylindrical Shells

By exploiting the static-geometric analogy and the permissible variability in the constitutive relations Simmonds [6] reduced the system of equations for circular cylinders to a simple equation for a complex-valued variable $\Psi = w + i\psi$ which in the homogeneous case ($p_\alpha = p = 0$) reads

$$\nabla^4\Psi + \ddot{\Psi} - i\epsilon^{-2}(1 + i\epsilon^2 c)\,\Psi'' = 0 \tag{8}$$

where c is a real constant of order one. Dots and primes indicate differentiation with respect to θ and z, respectively, and ∇^4 is the biharmonic operator in z, θ coordinates. A system of auxiliary equations for the determination of stresses, strains, displacements, etc., in terms of w and ψ was also given in [6]. Equation (8) is simple but the major point at issue is that the reduction of the system to (8) does not entail any loss in accuracy over the system (3)–(7).

Because the shell equations for circular cylinders have constant coefficients in z,θ coordinates the system of equations can always be reduced by a straightforward elimination process to an eighth-order "characteristic" equation for, say, w. For the same reason any variable or combination of variables satisfies the same equation. The resulting characteristic equation depends on the system of shell equations used at the start and is generally not particularly simple. Simplification of the eighth-order equation by means of omitting inessential terms has proved to be an extremely difficult process to justify. The only result, at once simple and accurate, arrived at by this means seems to be that due to Morley [10]. If $c = 1$ and the imaginary part of Ψ is eliminated from (8) the result is Morley's equation. Since the characteristic equation has constant coefficients there must be exponential solutions of the form $w = e^{px}\cos n\theta$ or $w = e^{p\theta}\cos \alpha x$. Morley verified the accuracy of his results by comparing the numerical values of the "characteristic root" p to those obtained from the accurate Flügge equation for various integer values of n, and real values of α and ϵ. The characteristic roots are relatively easy to calculate because the eighth-degree equation for p is a sum of two squares and can be factored. Of course this is also the reason why the Morley equation can be put in Simmonds' complex form.

In [9] Novozhilov derived a system of complex equations for cylindrical shells (not necessarily circular) which he reduced to an equation of the fourth order for the scalar variable $N_{\alpha\alpha} - iK_{\alpha\alpha}$. Although for a different variable the equation (for circular cylinders) is the same as Simmonds' in the special case $c = 0$. A complex formulation of shell equations together with a reduction of the system to a scalar equation has obvious advantages even if the results apply only to special classes of solutions. The Reissner-Meissner equations and the linear shallow shell equations are cases in point.

Further significant developments with respect to the Morley equation were made by Koiter [11]. He constructed a strain energy function which reads as follows in the present notation.

$$\begin{aligned} V = {} & \frac{1}{2(1-\nu^2)}\left[E_z^2 + E_\theta^2 + 2\nu E_z E_\theta + 2(1-\nu)E_{z\theta}^2\right] \\ & + \frac{1}{2}\left[K_z^2 + K_\theta^2 + 2\nu K_z K_\theta + 2(1-\nu)K_{z\theta}^2\right] \\ & + \frac{1}{2}\epsilon^2\left[2(1-\nu)\,(E_z K_\theta - E_{z\theta}K_{z\theta})\right. \\ & \left. - 2E_\theta(K_z + K_\theta) + \epsilon^2 E_\theta^2 - \frac{3}{2}\epsilon^2(1-\nu)E_{z\theta}^2\right] \end{aligned} \tag{9}$$

The first two groups of terms are those corresponding to Love's constitutive relations. The third group of terms corresponds to a permissible variation of the constitutive relations according to the Novozhilov-Koiter arguments. Use of the strain-dependent relations (5) together with (9) in a variational principle leads (exactly) to what are undoubtedly the simplest possible set of accurate equilibrium equations in terms of displacements for a circular cylinder. These read as follows

$$\begin{aligned} & u'' + \frac{1}{2}(1-\nu)\ddot{u} + \frac{1}{2}(1+\nu)\dot{v}' + \epsilon^{-2}\nu w' = 0 \\ & \frac{1}{2}(1+\nu)\dot{u}' + \frac{1}{2}(1-\nu)v'' + \ddot{v} + \epsilon^{-2}\dot{w} = 0 \\ & \nu u' + \dot{v} + \epsilon^{-2}w + \epsilon^2(1-\nu^2)(\nabla^2 + 1)^2 w = 0 \end{aligned} \tag{10}$$

The following equations follow exactly from (10) and agree with equations given by Morley [10].

$$\begin{aligned} \epsilon^2\nabla^4 u &= -\nu w''' + \ddot{w}' \\ \epsilon^2\nabla^4 v &= -(2+\nu)\dot{w}'' - \ddot{w} \end{aligned} \tag{11}$$

The eighth-order characteristic equation satisfied by w is exactly Morley's. As reproduced here the load terms in Koiter's equilibrium equations have been dropped for reasons to be explained later. As Koiter and Morley note equations (11) are the same as for the Donnell equations.

Downloaded 02 May 2010 to 171.66.16.250. Redistribution subject to ASME license or copyright; see http://www.asme.org/terms/Terms_Use.cfm

Koiter's results are in real form, but they can be recast in complex form. Let Φ satisfy the complex Morley equation, (8), with $c=1$, and let $\Phi''=\epsilon^2\phi$. Put

$$w=\nabla^4\Phi \tag{12}$$

As defined here w is complex-valued. Here and in what follows expressions for displacements, stresses, and so forth will be left in complex form with the conventional understanding that the real parts have physical meaning. Equations (8), (11), and (12) lead exactly to the following expressions for the displacements

$$\begin{aligned}\epsilon^2 u&=\ddot{\Phi}'-\epsilon^2\nu\phi'\\ \epsilon^2 v&=-\ddot{\Phi}-\epsilon^2(2+\nu)\dot{\phi}\\ w&=-\ddot{\Phi}+i(1+i\epsilon^2)\phi\end{aligned} \tag{13}$$

From these relations complex strains can be calculated from (5) and then complex stress measures from the constitutive relations implied by (9). The stress-stress function relations (6) in z, θ coordinates are

$$\begin{aligned}N_z&=\ddot{\psi}-\epsilon^2\dot{\chi}_\theta,\quad M_z=\dot{\chi}_\theta+\epsilon^{-2}\psi\\ N_\theta&=\psi'',\quad M_\theta=\chi_z'\\ N_{z\theta}&=-\dot{\psi}'+\frac{3}{4}\epsilon^2\chi_\theta'-\frac{1}{4}\epsilon^2\dot{\chi}_z,\quad M_{z\theta}=-\frac{1}{2}(\dot{\chi}_z+\chi_\theta')\end{aligned} \tag{14}$$

The expressions for M_z, M_θ, and $M_{z\theta}$ in terms of ϕ and Φ can be used to solve for χ_z, χ_θ, and ψ by integration with no difficulty. Exact results are

$$\begin{aligned}\epsilon^2\chi_z&=-i\ddot{\Phi}'-i\epsilon^2\nu\phi'-\epsilon^4(1-\nu^2)\phi'\\ \epsilon^2\chi_\theta&=i\Phi+i\epsilon^2(2-\nu)\dot{\phi}+\epsilon^4(1-\nu^2)\dot{\phi}\\ \psi&=i\ddot{\Phi}+(1+i\epsilon^2)\phi\end{aligned} \tag{15}$$

Expressions for N_z, N_θ, $N_{z\theta}$ obtained via the stress functions agree with those obtained via the constitutive relations, as they must.

The Koiter equations are particularly interesting in that once the strain-displacement relations and the strain energy function are laid down the remaining equations of the system, which follow exactly, are not unduly complicated. However, compare equations (13) and equations (15). If in the latter the $\epsilon^4(1-\nu^2)$ terms were neglected then the static-geometric analogy, which lurks in the background, would become a feature of the theory. The Koiter equations favor simplicity in the real equilibrium equations which is especially desirable if one wishes to include inertia terms or perhaps use them as a starting point in the development of a nonlinear theory. Obviously a slightly different system of equations would emerge if one wished to obtain the simplest possible set of compatibility equations in terms of stress functions. In any case exactness and the ultimate in simplicity cannot be achieved simultaneously.

The possibility of writing the general linear shell equations in complex form has been examined by Novozhilov [9], Chernykh [12], Naghdi [13], Sanders [14], and perhaps others. The static-geometric analogy invites the attempt but satisfactory results have been achieved only for cylinders and spheres [14, 15]. However, see Simmonds [16], with references to the work if Libai, Wan, and others. In a complex formulation the stress functions, which are analogous to the displacements, play a role. Since stress functions cannot coexist with distributed loads provision has to be made for removing particular solutions. Since the object is to arrive at a simple theory it seems best to deal with the homogeneous equilibrium equations. In practical applications it usually is not difficult to reduce the problem beforehand.

A direct approach to complex shell equations [14] went through in the case of a circular cylinder [17]. The theory, like Koiter's, involved a strain energy function. However, the strain energy function gets lost as soon as the system of equations is simplified. A previously unpublished version consistent with Simmonds' characteristic equation is given here. Displacements and stress functions are given by the equations

$$\epsilon^2 u_\alpha=(\bar{b}_{\alpha\beta}-b_{\alpha\beta})\nabla^2\Phi_{,\beta}-\epsilon^2(1+\nu)\phi_{,\alpha} \tag{16}$$

$$w=-b_{\alpha\beta}\Phi_{,\alpha\beta}+i(1+i\epsilon^2 c)\phi \tag{17}$$

$$\epsilon^2\chi_\alpha=-i(\bar{b}_{\alpha\beta}-b_{\alpha\beta})\nabla^2\Phi_{,\beta}+i\epsilon^2(1-\nu)\phi_{,\alpha} \tag{18}$$

$$\psi=ib_{\alpha\beta}\Phi_{,\alpha\beta}+(1+i\epsilon^2 c)\phi \tag{19}$$

where $\bar{b}_{\alpha\beta}\Phi_{,\alpha\beta}=\epsilon^2\phi$ and both Φ and ϕ satisfy Simmonds' equation

$$\nabla^4\phi+b_{\alpha\beta}\phi_{,\alpha\beta}-i\epsilon^{-2}(1+i\epsilon^2 c)\bar{b}_{\alpha\beta}\phi_{,\alpha\beta}=0 \tag{20}$$

Stress and strain measures, which follow exactly from (16) to (20), are given by

$$\begin{aligned}\bar{N}_{\alpha\beta}&=[1+i\epsilon^2(c-2+\nu)]\phi_{,\alpha\beta}+i\epsilon^2\bar{b}_{\alpha\beta}\nabla^2\phi\\ &\quad+\frac{1}{2}i\epsilon^2(1-\nu)(\bar{b}_{\alpha\gamma}\phi_{,\gamma\beta}+\bar{b}_{\beta\gamma}\phi_{,\gamma\alpha})\end{aligned} \tag{21}$$

$$\begin{aligned}K_{\alpha\beta}&=-i[1+i\epsilon^2(c-2-\nu)]\phi_{,\alpha\beta}+\epsilon^2\bar{b}_{\alpha\beta}\nabla^2\phi\\ &\quad+\frac{1}{2}\epsilon^2(1+\nu)(\bar{b}_{\alpha\gamma}\phi_{,\gamma\beta}+\bar{b}_{\beta\gamma}\phi_{,\gamma\alpha})\end{aligned} \tag{22}$$

$$E_{\alpha\beta}=\overline{\phi_{,\alpha\beta}}-\nu\phi_{,\alpha\beta} \tag{23}$$

$$M_{\alpha\beta}=-i\phi_{,\alpha\beta}-i\nu\overline{\phi_{,\alpha\beta}} \tag{24}$$

Since displacements and stress functions are given the expressions (21) to (24) must satisfy the compatibility and equilibrium equations exactly. A set of real constitutive relations is implicit. They could be written out exactly but are not needed in applications. A relation (in z,θ coordinates) given here for the sake of a later discussion is

$$E_z=N_z-\nu N_\theta+\epsilon^2(c-2)K_\theta-\epsilon^2\nu cK_z+0(\epsilon^4) \tag{25}$$

The full set of constitutive relations differs from those of Love only by ϵ^2 and ϵ^4 terms, but no strain energy function exists for any value of c.

Global error estimates for shell theories with no strain energy function have been established by Simmonds [18]. For shells of *finite length* the Simonds result puts the cylinder equations just described at least partly on a firm foundation. Pointwise error estimates remain to be established.

It is an interesting fact that if all ϵ^2 terms are omitted in the right-hand side of equations (21) and (22) then what remains holds not only for the shallow cylinder but for any shallow shell with a quadratic middle surface except that equations (17) and (19) must be replaced by

$$w=i\psi=i\phi \tag{26}$$

and the characteristic equation must be made to read

$$\nabla^4\phi-i\epsilon^{-2}\bar{b}_{\alpha\beta}\phi_{,\alpha\beta}=0 \tag{27}$$

The shallow sphere and flat plate are exceptional cases where $b_{\alpha\beta}=\bar{b}_{\alpha\beta}=\delta_{\alpha\beta}$ and $b_{\alpha\beta}=0$, respectively.

In applications of a theory such as the one described where stress functions play a major role the expression of stress boundary conditions in terms of stress functions is particularly convenient. The statement of stress boundary conditions in such form, fully equivalent to Kirchhoff boundary conditions, is not very complicated. Results for shells of arbitrary middle surface were given in [19].

Point Loads, Dislocations, and Elementary Solutions

If a concentrated load is applied on the surface of a shell the

Downloaded 02 May 2010 to 171.66.16.250. Redistribution subject to ASME license or copyright; see http://www.asme.org/terms/Terms_Use.cfm

stress functions are multivalued with a branch point where the load is applied. The increase in the stress functions, $\Delta\chi_\alpha$ and $\Delta\psi$, following a simple closed circuit around the singular point must correspond to stress functions that produce no stresses because the stresses must be single-valued. Circuit relations, i.e., formulas for $\Delta\chi_\alpha$ and $\Delta\psi$ in terms of the components of the applied load have been worked out by Pietraszkiewicz [20]. They can also be obtained rather easily from results in [19]. For concentrated load solutions one must require $\Delta u_\alpha = 0$, $\Delta w = 0$ on the circuit in question along with some other conditions. There are six analogous Volterra-type dislocation solutions for which $\Delta u_\alpha \neq 0$, $\Delta w \neq 0$ but $\Delta\chi_\alpha = 0$, $\Delta\psi = 0$. In the complex formulation the concentrated load and dislocation solutions are closely related.

On the surface of a complete cylinder there are simple closed circuits which enclose the axis of the cylinder. The stress functions are single-valued provided no resultant force or couple acts on a cross section of the cylinder. Six elementary multivalued solutions are associated with the six beamlike solutions: axial tension and torsion, pure bending (two), and flexure (two). In these cases ϕ and Φ are expressible in closed form in terms of elementary functions. The displacements are single-valued and there are no singularities. There are six analogous dislocation solutions contained in the (complex) elementary beamlike solutions.

In connection with one of these dislocation solutions Buchwald [21] discovered a small flaw associated with the use of Morley's equation. Consider the problem of an infinite cylinder slit along a generator $\theta = 0$, and opened up by application of equal but opposing uniform loads acting normal to the two edges and tangent to the surface of the cylinder. This should be a one-dimensional problem in which the cylinder behaves as a cut circular ring under the same kind of loading. However, Buchwald found that the cylinder bends (according to the Morley equations). There is a term in w proportional to $\epsilon^2 z^2 \cos\theta$, which is negligible for $z = 0(1)$, but cannot be argued away because it becomes unbounded for $|z| \to \infty$. The cylinder can be straightened out by application of a small bending moment which produces stresses truly negligible compared to the other stresses involved. Nevertheless, for the sake of uniqueness one should be able to demand that absolutely no couple acts on a cross section of the cylinder, i.e., the stress functions must be single-valued. The solution to the unsimplified cylinder equations contains no such anomaly.

A simpler problem illustrates the same point. Let the slit cylinder be opened by uniform bending moments $M_\theta = -1$ applied on the cut edges. The exact solution according to the umsimplified cylinder equations is

$$u = 0, \quad v = \epsilon^{-2}(\pi - \theta), \quad w = 1, \quad N_z = 0, \quad M_\theta = -1$$

The real Koiter equations, and the complex equations in the case $c = 1$, both give exactly

$$v = \epsilon^{-2}[1 + \epsilon^4(1 - \nu^2)](\pi - \theta) \tag{28}$$

when the conditions $u = 0$, $w = 1$ are imposed for uniqueness. Both theories give

$$\begin{aligned} &E_z = K_z = 0, \quad K_\theta = -1 + 0(\epsilon^4) \\ &N_z = -\epsilon^2 + 0(\epsilon^6), \quad N_\theta = 0(\epsilon^6) \end{aligned} \tag{29}$$

The difficulty is that $N_z \neq 0$ and there is an axial compression acting on the cylinder. To remove it requires an additional displacement $u = \epsilon^2 z$ which is unbounded. The difficulty cannot be laid to the lack of a strain energy function in the complex equations because the Koiter equations yield the same result. The trouble is with small terms in the express or implied constitutive relations. In the case $c = 1$ equation (25) holds also for the Koiter equations. The K_θ term in (25) prevents N_z from vanishing. In other words the trouble is really due to a small anisotropy which makes the cylinder behave in an unexpected manner. Setting $c = 2 - 2\nu(2 + \nu)\epsilon^4$ (by an accurate analysis) removes the anomaly. Setting c exactly equal to two removes the anomaly in the remaining five elementary dislocation solutions.

To give correct results in the elementary cases seems to be an acid test for simplified cylinder theories. Simmonds [6] cites examples where the test fails. Other than in those cases noted the complex equations for any 0(1) value of c yield satisfactory results for the elementary solutions, including rigid body motions.

Asymptotic Methods

Since the characteristic equation contains the large parameter ϵ^{-2} attached to a term of lowest order derivatives the methods of singular perturbation theory apply. From that standpoint various specialized equations of cylindrical shell theory can be given a unified treatment. The brief account following is essentially a summary of results obtained by Novozhilov [9], Reissner [22, 23], and Simmonds [23].

The cylinder has a natural geometric orthotropy and, for the most part, results are clearest in terms of z,θ coordinates or scaled z,θ coordinates. There are three major cases and two minor cases to be considered. The classification into cases is made on the basis of how rapidly $\phi(z, \theta, \epsilon)$ varies as a function of z and θ. This is obviously a rather hazy concept and there is overlap among cases. However, the method of matched asymptotic expansions brings order to applications of the idea.

Suppose ϕ varies "rapidly" with z and θ. Introduce scaled independent variables ξ and η defined by $z = \epsilon\xi$, $\theta = \epsilon\eta$ and assume an asymptotic expansion of the form

$$\phi(\epsilon\xi, \epsilon\eta, \epsilon) = \phi_0(\xi, \eta) + \epsilon^2\phi_2(\xi, \eta) + \ldots \tag{30}$$

In ξ,η coordinates the characteristic equation becomes

$$\bar{\nabla}^4\phi + \epsilon^2\phi_{,\eta\eta} - i(1 + i\epsilon^2 c)\phi_{,\xi\xi} = 0 \tag{31}$$

where $\bar{\nabla}^4$ is the biharmonic operator in ξ,η variables. Formal substitution of the series (30) into (31) and separation of powers of ϵ^2 leads to a system of equations

$$\bar{\nabla}^4\phi_0 - i\phi_{0,\xi\xi} = 0 \tag{32}$$

$$\bar{\nabla}^4\phi_2 - i\phi_{2,\xi\xi} = -\phi_{0,\eta\eta} - c\phi_{0,\xi\xi} \tag{33}$$

etc. Since shell theory is an approximation in which there are relative errors of order ϵ^2 in the fundamental equations there is never any justification for retaining the ϕ_2 term in (30). As a matter of terminology a "shallow shell solution" to the full cylinder equation (20) *means* a solution for which the first term in an asymptotic expansion of the sort described satisfies the characteristic equation

$$\nabla^4\phi - i\epsilon^{-2}\phi'' = 0 \tag{34}$$

in terms of the original variables. The equation is a special case of the shallow shell equation, commonly called the Donnell equation in the case of circular cylinders. The form that the auxiliary equations for displacements, stress measures, etc., take has already been indicated.

Suppose ϕ varies slowly in the z direction but not too rapidly in the θ direction. Define scaled variables $\xi = \epsilon z$, $\eta = \theta$, put $\phi(\epsilon^{-1}\xi, \eta, \epsilon) = \phi_0(\xi, \eta) + \epsilon^2\phi_2(\xi, \eta) + \ldots$, and proceed as before. To be brief, a "semimembrane solution" to the full cylinder equations is one for which the first term in the asymptotic expansion satisfies the characteristic equation

$$(\ddot{\phi} + \phi)^{\cdot\cdot} - i\epsilon^{-2}\phi'' = 0 \tag{35}$$

in terms of the original variables. Novozhilov [9] attributes the equation to Vlasov. In z,θ coordinates the following simplified auxiliary formulas apply

Downloaded 02 May 2010 to 171.66.16.250. Redistribution subject to ASME license or copyright; see http://www.asme.org/terms/Terms_Use.cfm

$$u=\epsilon^{-2}\ddot{\Phi}'=i\chi_z,\quad v=-\epsilon^{-2}\ddot{\Phi}=i\chi_\theta,\quad w=-\ddot{\Phi}+i\phi=i\psi \tag{36}$$

$$N_z=\ddot{\phi}=iK_\theta,\quad N_\theta=\phi''+i\epsilon^2\ddot{\phi}=iK_z,\quad N_{z\theta}=-\dot{\phi}'=-iK_{z\theta}$$

Suppose ϕ varies rapidly in the z direction but not too rapidly in the θ direction. Appropriate scaled variables are $z=\epsilon\xi$, $\theta=\eta$. By the same process, and without loss in generality, the characteristic equation reduces to

$$\phi''-i\epsilon^{-2}\phi=0 \tag{37}$$

with solutions $\phi=G(\theta)\exp(\pm\sqrt{i}\epsilon^{-1}z)$. These are the common "edge-effect solutions." The Φ terms drop out of the formulas for u, v, and w, and there are other obvious simplifications.

The two minor cases follow from the scaling $z=\xi$, $\theta=\epsilon^{1/2}\eta$ and $z=\epsilon\xi$, $\theta=\epsilon^{1/2}\eta$. In these cases the asymptotic series proceed in powers of ϵ rather than ϵ^2. The first terms satisfy the equations

$$\ddot{\phi}''-i\epsilon^{-2}\phi''=0\quad\text{and}\quad\phi''-i\epsilon^{-2}\phi=0, \tag{38}$$

respectively. Except for a degenerate case (the flat plate equation, $\nabla^4\phi=0$) the foregoing exhausts the possibilities for simplified characteristic equations in z,θ coordinates. In each case $\Phi''=\epsilon^2\phi$ and Φ satisfies the same characteristic equation as ϕ.

There are two special classes of solutions that become combined in the complex formulation. These are, in real terms, membrane solutions for which $M_{\alpha\beta}<<N_{\alpha\beta}$, and inextensional bending solutions for which $E_{\alpha\beta}<<K_{\alpha\beta}$, provided those relations hold over a large part of the shell surface. In complex terms the stress and strain measures do not change phase. In the absence of distributed loads this can happen only if $\phi_{,\alpha\beta}$ is constant (possibly zero), or the "i" term in the characteristic equation for ϕ is missing (i.e., $\phi''=0$. These conditions with $\Phi''=\epsilon^2\phi$ lead precisely to what have been called the elementary solutions which do not follow accurately from a simplified characteristic equation.

One and the same solution to a shell problem can behave as a shallow shell solution over some limited region of the shell surface and perhaps as a semimembrane solution over the remainder, neither solution being valid over the whole surface. The method of matched asymptotic expansions furnishes a means for combining the results to obtain a uniformly accurate representation of the solution [24].

In other than z,θ coordinates there is a particularly interesting case Goldenveizer calls the "degenerate edge effect." This refers to the behavior of a solution in the neighborhood of a point where a boundary curve is tangent to a generator on the surface of the cylinder. In a local curvilinear and properly scaled coordinate system the characteristic equation takes a special simplified form. The nature of the solution in this case is in need of further investigation; see however, [25, 26].

A slightly modified form of the characteristic equation (35) for semimembrane solutions has proved to be useful in a variety of applications. The equation is

$$(\ddot{\phi}+\phi)^{\cdot\cdot}+\frac{1}{4}\phi-i\epsilon^{-2}\phi''=0 \tag{39}$$

The differential operator associated with (39) has two simple factors. Consider the one that leads to the equation

$$\phi'=-i^{3/2}\epsilon\left(\ddot{\phi}+\frac{1}{2}\phi\right) \tag{40}$$

On the complete cylinder (40) has Fourier series solutions in the form

$$\phi=\sum_2^\infty A_n\cos n\theta\exp\left[i^{3/2}\left(n^2-\frac{1}{2}\right)\epsilon z\right] \tag{41}$$

Compare this to solutions of (35)

$$\phi=\sum_2^\infty A_n\cos n\theta\exp[i^{3/2}n\sqrt{n^2-1}\,\epsilon z] \tag{42}$$

Provided (40) is used only for solutions that vanish as $z\to\infty$ (i.e., $n\neq0,1$) its solutions (41) are good approximations to (42) because $n^2-1/2$ is a good approximation to $n\sqrt{n^2-1}$ for all $n\geq2$. The errors involved are about 1 or 2 percent, independent of ϵ. Solutions corresponding to $n=0,1$ are, in any case, elementary solutions, and should be so represented. The usefulness of (40) lies in the fact that ϕ' is expressed in terms of ϕ and $\ddot{\phi}$, a fact that can be used to simplify the boundary conditions in problems of the semi-infinite cylinder [27, 28]. Solutions to (39) enjoy the same properties of matching with shallow shell solutions as do solutions to (35).

Application of Analytical Methods

Flügge's equations, Donnell's equations, and the JOURNAL OF APPLIED MECHANICS first appeared about 50 years ago. Conditions under which the Donnell equations are sufficiently accurate were settled by Hoff [29] almost 30 years ago. Sputnik went up in 1957. Koiter's fundamenetal paper on the theory of thin shells, an English translation of Novozhilov's book, and Morley's equation all appeared in 1959. That year marks something of a turning point in shell analysis for several reasons: intense renewed interest in the subject, firm foundations for the theory, and since then the rapid development of computers. Before 1959 the analysis of cylindrical shells was mostly a matter of Fourier series solutions for static, vibration, or buckling problems in the linear elastic case. The computer has opened the way for practical solutions to a host of new problems. The difficulties of nonlinear analysis can be bypassed and the range of application of linear analytical methods has been very much extended. Some examples in which a combination of analytical and numerical methods has proved effective are discussed in what follows.

The presence of an internal boundary characterizes a group of important problems in which the object is to determine the significant features of the stress field near the boundary given that the stress field far from the boundary is something simple. These are typically crack and cutout problems. Shell intersection problems are closely related. The literature on the subject is extensive and growing. Many of the results are already in handbooks [30, 31].

Problems of the sort described have been (or could be) formulated mathematically in terms of a system of integral equations. Such a formulation is usually more efficient computationally than a direct attack by finite element methods, provided of course, that the kernel functions in the integral equations are available and represented in a sufficiently simple form. The kernel functions required can be interpreted physically as concentrated loads or dislocations. Given the possibility of solving hundreds of simultaneous algebraic equations the determination of these kernel functions becomes much more than a problem of academic interest.

In the case of shallow spheres and cylinders complete results in closed form are available in the literature [32, 33]. These suffice provided the crack or cutout does not extend over too large a part of the shell surface. Similar solutions for other than spheres or cylinders is a subject of current research. Partial results are available [34].

Solutions to a large number of localized (or concentrated) load problems have been given in a recent treatise by Lukasiewicz [35]. For point loads on a cylindrical shell he, like Morley [36], presents results in the form of a modified Fourier series in which a singular term has been removed to

Downloaded 02 May 2010 to 171.66.16.250. Redistribution subject to ASME license or copyright; see http://www.asme.org/terms/Terms_Use.cfm

improve convergence. These forms do not take advantage of the known closed-form shallow shell solutions. Such representations are too cumbersome to be used as kernel functions in integral equations. Buchwald [37] (with references to Hoff) laid out a plan for solution of the normal load problem by the method of matched asymptotic expansions. The present author has obtained closed-form results for the semimembrane solution based on the approximate equation (39), which together with the shallow shell results furnishes a complete solution in closed form [38, 39]. Work is still in progress. Some closed-form solutions for the complete spherical shell are available [11], but here too more results are needed. The next logical step would seem to be to do similar things for shells of "slowly varying curvature." The theory for such shells was initiated by Lukasiewicz [40], and furthered by Koiter [41].

A cylindrical shell (a pipe) attached to a larger shell (a pressure vessel) is called a nozzle. An idealized nozzle is a semi-infinite cylindrical shell with a boundary $z=f(\theta)$ where f is a smooth periodic function of θ. The nozzle problem is to determine the relation between the forces and moments acting on the boundary and the displacements and rotations at the boundary. This is a problem which, in the author's opinion, is likely to yield to a combination of analytical and numerical methods, but for which a definitive solution has not yet appeared. For recent progress see [42].

Acknowledgment

First the author wishes to acknowledge the benefits of professional and personal associations with Eric Reissner, Jim Simmonds, and Warner Koiter over many years, and second the support of the Office of Naval Research under Contract N00014-81-K-0668, and the Division of Applied Sciences, Harvard University.

References

1 Dikman, M., *Theory of Thin Elastic Shells*, Pitman, 1982.

2 Koiter, W. T., "A Consistent First Approximation in the General Theory of Thin Elastic Shells," *Proceedings of the I.U.T.A.M. Symposium on The Theory of Thin Elastic Shells*, North-Holland, Amsterdam, 1960.

3 Sanders, J. L., "An Improved First-Approximation Theory for Thin Shells," NASA Report 24, 1959.

4 Budiansky, B., and Sanders, J. L., "On the 'Best' First-Order Linear Shell Theory," *Progress in Applied Mechanics—the Prager Anniversary Volume*, Macmillan, 1963, pp. 129–140.

5 Love, A. E. H., *A Treatise on the Mathematical Theory of Elasticity*, 3rd Ed., Cambridge University Press, 1920.

6 Simmonds, J. G., "A Set of Simple, Accurate Equations for Circular Cylindrical Shells," *Int. J. Solids Structures*, Vol. 2, 1966, pp. 525–541.

7 Flügge, W., "Die Stabilitat der Kreiszylinderschale," *Ing. Arch.*, Vol. 3, 1932, p. 463.

8 Flügge, W., *Stresses in Shells*, Chapter 5, Springer, 1960.

9 Novozhilov, V. V., *The Theory of Thin Shells* (English translation), Noordhoff, 1959.

10 Morley, L. S. D., "An Improvement on Donnell's Approximation for Thin-Walled Circular Cylinders," *Quart. J. Mech. Appl. Math.*, Vol. 12, 1959, pp. 89–99.

11 Koiter, W. T., "On the Simplest Possible Form of the Equations for Circular Cylindrical Shells in Terms of Displacements," Technological University of Delft, 1968.

12 Chernykh, K. F., *Linear Theory of Shells*, NASA Translation TT F-441, 1968.

13 Naghdi, P. M., "On the Differential Equations of the Linear Theory of Elastic Shells," *Applied Mechanics—Proceedings of the Eleventh International Congress of Applied Mechanics*, Springer-Verlag, 1964, pp. 262–269.

14 Sanders, J. L., "On the Shell Equations in Complex Form," *Proceedings of the Second I.U.T.A.M. Symposium on Thin Shells*, Springer-Verlag, 1969, pp. 135–156.

15 Koiter, W. T., "A Spherical Shell Under Point Loads at its Poles," *Progress in Applied Mechanics—The Prager Anniversary Volume*, Macmillan, 1963, pp. 155–169.

16 Simmonds, J. G., "Reduction of the Linear Sanders-Koiter Shell Equations for Nondevelopable Midsurfaces to Two Coupled Equations," ASME JOURNAL OF APPLIED MECHANICS, Vol. 42, 1975, pp. 511–513.

17 Sanders, J. L., "On the Novozhilov Circular Cylinder Theory" (in Russian), *Problems of the Mechanics of a Solid Deformed Body*, The Novozhilov Anniversary Volume, Sedov, L. I., ed., Izdatelstvo Sudostroenie, Leningrad, 1970.

18 Simmonds, J. G., "Extension of Koiter's L_2-Error Estimate to Approximate Shell Solutions With No Strain Energy Functional," ZAMM, Vol. 22, 1971, pp. 339–335.

19 Sanders, J. L., "On Stress Boundary Conditions in Shell Theory," ASME JOURNAL OF APPLIED MECHANICS, Vol. 47, 1980, pp. 202–204.

20 Pietraszkiewicz, W., "Multivalued Stress Functions in the Linear Theory of Shells," *Archiwum Mechaniki Stosowanej*, Vol. 20, 1968, pp. 37–45.

21 Buchwald, V. T., "Some Problems of Thin Circular Cylindrical Shells, II. The Infinite Crack," *J. of Math. and Phy.*, Vol. 47, 1968, pp. 57–66.

22 Reissner, E., "On Asymptotic Expansions for Circular Cylindrical Shells," ASME JOURNAL OF APPLIED MECHANICS, Vol. 31, 1964, pp. 245–252.

23 Reissner, E., and Simmonds, J. G., "Asymptotic Solutions of Boundary Value Problems for Elastic Semi-Infinite Circular Cylindrical Shells," *J. of Math. and Phy.*, Vol. 45, 1966, pp. 1–22.

24 Cole, J. D., *Perturbation Methods in Applied Mathematics*, Blaisdell, 1968.

25 Goldenveizer, A. L., *Theory of Elastic Thin Shells*, Pergamon, 1961.

26 Van Dyke, P., "Stress About a Circular Hole in a Cylindrical Shell," *AIAA Journal*, Vol. 3, 1965, pp. 1733–1742.

27 Sanders, J. L., "Closed Form Solution to the Semi-Infinite Cylindrical Shell Problem," *Contributions to the Theory of Aircraft Structures*, The Van der Neut Anniversary Volume, Delft Univesity Press, Rotterdam, 1972, pp. 229–237.

28 Chan, A. W., and Sanders, J. L., "Analysis of a Mitered Joint in a Cylindrical Shell in Bending," *Int. J. Mech. Sci.*, Vol. 22, 1980, pp. 621–636.

29 Hoff, N. J., "The Accuracy of Donnell's Equations," ASME JOURNAL OF APPLIED MECHANICS, Vol. 22, 1955, pp. 329–334.

30 Rooke, D. P., and Cartwright, D. J., *Compendium of Stress Intensity Factors*, Her Majesty's Stationery Office, London, 1976.

31 Sih, G. C., ed., *Plates and Shells With Cracks*, Noordhoff, 1977.

32 Lukasiewicz, S., "Concentrated Loads on Shallow Spherical Shells," *Quart. J. of Mech. and Appl. Math.*, Vol. 20, 1967, pp. 293–305.

33 Sanders, J. L., and Simmonds, J. G., "Concentrated Forces on Shallow Cylindrical Shells," ASME JOURNAL OF APPLIED MECHANICS, Vol. 37, 1970, pp. 367–373.

34 Simmonds, J. G., "The Fundamental Solution for a Shallow Shell With an Arbitrary Quadratic Midsurface," ASME JOURNAL OF APPLIED MECHANICS, Vol. 43, 1976, pp. 286–290.

35 Lukasiewicz, S., *Local Loads in Plates and Shells*, Sijthoff and Noordhoff, 1979.

36 Morley, L. S. D., "The Thin-Walled Circular Cylinder Subjected to Concentrated Radial Loads," *Quart. J. of Mech. and Appl. Math.*, Vol. 13, 1960, pp. 24–37.

37 Buchwald, V. T., "Some Problems of Thin Circular Cylindrical Shells, I. The Equations," *J. of Math. and Phys.*, Vol. 46, 1967, pp. 237–252.

38 Sanders, J. L., "The Cylindrical Shell Loaded by a Concentrated Normal Force," *Mechanics Today*, Vol. 5, Pergamon, 1980, pp. 427–438.

39 Sanders, J. L., "The Cylindrical Shell Loaded by a Concentrated Axial Force," *Developments in Theoretical and Applied Mechanics*, Vol. XI, University of Alabama in Huntsville, 1982, pp. 101–113.

40 Lukasiewicz, S., "On the Equations of the Theory of Shells of Slowly Varying Curvatures," *ZAMP*, Vol. 22, 1971, p. 6.

41 Koiter, W. T., "The Intrinsic Equations of Shell Theory With Some Applications," *Mechanics Today*, Vol. 5, Pergamon, 1980, pp. 139–154.

42 Steele, C. R., and Steele, M. L., "Stress Analysis of Nozzles in Cylindrical Vessels With External Load," ASME *Journal of Pressure Vessel Technology* (to appear).

Downloaded 02 May 2010 to 171.66.16.250. Redistribution subject to ASME license or copyright; see http://www.asme.org/terms/Terms_Use.cfm

R. T. Shield
Department of Theoretical and Applied Mechanics, University of Illinois at Urbana-Champaign, Urbana, Ill. 61801
Mem. ASME

Equilibrium Solutions in Finite Elasticity

Some areas in the theory of large deformations of elastic bodies are surveyed. Strain energy functions for isotropic materials are discussed, with emphasis on rubberlike materials, and exact and approximate solutions for equilibrium states are described. The applicability of the energy method for the determination of the stability of elastic systems is reviewed and applications are cited.

1 Introduction

This paper surveys some areas in the equilibrium theory of finitely deformed elastic bodies. A brief introduction to the basic equations is given in Section 2, and it is followed by a discussion of strain energy functions appropriate for isotropic materials, particularly for incompressible rubberlike materials. Exact solutions to problems or solutions close to exact for large deformations are surveyed in Section 4. Second-order effects are discussed in the next section, with emphasis on the use of the properties of the inverse deformation to simplify the determination of second-order solutions. Section 6 treats the theory of an infinitesimal displacement superposed on a large elastic deformation. The status of the energy stability criterion for continuous elastic systems under conservative loading is reviewed, and some stability results are discussed.

The coverage is not intended to be exhaustive and more attention is paid to those parts of the theory and the solutions to which I have made some contribution. Additional references for the topics discussed can be found in the books and papers listed in the references. Among the important areas in finite elastostatics that are not covered here are fiber-reinforced materials, finite element methods, conservation laws, rod and shell theories, material stability, and existence and uniqueness of solutions. Papers on these topics (and other topics) can be found in the proceedings [1, 2] of the two symposia on finite elasticity organized recently by Rivlin. Variational principles in finite elasticity are treated in [3].

2 Basic Equations

We use a fixed rectangular Cartesian coordinate system to describe the locations of particles in a body composed of elastic material. A particular state of the body is chosen as the reference or undeformed state B and we suppose that it occupies a region of space V. In a deformation of B into a body B^*, a typical particle initially at the point x_i moves to the point y_i. The coordinates y_i are then single-valued functions of x_i in V,

$$y_i = f_i(x_r). \tag{2.1}$$

Latin indices assume the values 1, 2, 3 and we use the notations

$$y_{r,s} = \frac{\partial y_r}{\partial x_s}, \quad x_{r;s} = \frac{\partial x_r}{\partial y_s}.$$

Conservation of mass requires

$$\det(y_{r,s}) = |y_{r,s}| = \rho/\rho^*,$$

where ρ and ρ^* are the densities for B and B^*, respectively. Throughout this paper, an asterisk (*) indicates that a quantity is associated with the deformed state.

The distance ds^* between neighboring particles in the deformed state is given by

$$ds^{*2} = dy_i dy_i = y_{i,r} y_{i,s} dx_r dx_s.$$

A repeated index implies summation over the values 1, 2, 3. The Cauchy strains C_{rs} defined by

$$C_{rs} = y_{i,r} y_{i,s} \tag{2.2}$$

therefore determine the changes in distance between neighboring particles. (We use the terminology of Prager [4], but Prager used $\bar{C}_{rs}$ for our C_{rs}.) An added rigid rotation of the deformed state B^* does not change the values of C_{rs}. The symmetric tensor C_{rs} has at least one system of principal axes at each point x_i, and the principal values of C_{rs} are λ_1^2, λ_2^2, λ_3^2, where λ_1, λ_2, λ_3 are the principal extension ratios. An infinitesimal cube of material at the point x_i with edges along the principal axes of C_{rs} is deformed into a rectangular parallelepiped with sides of lengths λ_1, λ_2, λ_3 times the side of the cube, centered at the point y_i, and rotated relative to the initial cube [5]. The edges of the parallelepiped are along principal axes of the strain tensor C_{rs}^* which arises if the initial distance ds between particles is expressed in terms of dy_i,

$$C_{rs}^* = x_{i;r} x_{i;s}.$$

Thus there is at least one triplet of orthogonal material directions at a typical particle that remains orthogonal after deformation. These principal directions of strain are unique if λ_1, λ_2, λ_3 are distinct.

A surface element with area dS and unit normal n_i in the reference state becomes an element with area dS^* and unit normal n_i^* in B^*. If the stress vector T_i^* is measured per unit

Contributed by the Applied Mechanics Division for publication in the JOURNAL OF APPLIED MECHANICS.
Discussion on this paper should be addressed to the Editorial Department, ASME, United Engineering Center, 345 East 47th Street, New York, N.Y. 10017, and will be accepted until two months after final publication of the paper itself in the JOURNAL OF APPLIED MECHANICS. Manuscript received by ASME Applied Mechanics Division, March, 1983.

Copyright © 1983 by ASME
Downloaded 02 May 2010 to 171.66.16.250. Redistribution subject to ASME license or copyright; see http://www.asme.org/terms/Terms_Use.cfm

area of the deformed state, then the infinitesimal force transmitted across dS^* is $T_i^*\, dS^*$ and we have

$$T_i^* = t_{ki} n_k^*,$$

where t_{ik} are the components of the Eulerian stress tensor, also known as the Cauchy stress or true stress. Balance of angular momentum requires that t_{ik} be a symmetric tensor but we shall see that the symmetry of t_{ik} also follows from the stress-strain relation. For many problems, it is more convenient to use the Lagrangian stress tensor T_{ik} which is defined so that the stress vector T_i, measured per unit area of the reference state, is given by

$$T_i = T_{ki} n_k.$$

The Lagrangian stress tensor is often called the first Piola-Kirchoff tensor; it is not symmetric in general. If we equate $T_i^* dS^*$ and $T_i dS$ and use the relation

$$n_k dS = |x_{s;t}|\, y_{r,k} n_r^* dS^*,$$

it follows that

$$t_{ik} = |x_{s;t}|\, y_{i,r} T_{rk}. \tag{2.3}$$

Kirchoff introduced a stress tensor S_{ik} related to T_{ik} through

$$S_{ik} = x_{i;r} T_{kr}, \quad T_{ik} = y_{k,r} S_{ri}. \tag{2.4}$$

With (2.3), it can easily be seen that S_{ik} is symmetric when t_{ik} is symmetric. The Kirchoff tensor is also known as the second Piola-Kirchoff stress tensor.

When the deformed body B^* is in equilibrium, the total applied force on a portion of the body that occupied a region V' with surface S' in the reference state is zero so that

$$\int_{S'} T_{ki} n_k dS + \int_{V'} F_i dV = 0, \tag{2.5}$$

where F_i are the components of the body force measured per unit volume of the reference state. Use of the divergence theorem and the arbitrariness of V' then gives the equilibrium equations

$$\frac{\partial T_{ki}}{\partial x_k} + F_i = 0. \tag{2.6}$$

For a motion of the body, the inertial term $\rho\, \partial^2 y_i / \partial t^2$ is added to the right-hand side of (2.6).

An elastic material is characterized by the existence of a strain energy W, measured per unit volume of the reference state B, which is a function of the deformation gradient $y_{r,s}$. In a quasi-static deformation of B^*, it is assumed that the rate of work of the applied forces is equal to the rate of change of the strain energy of the body, and this leads to the stress-strain relation

$$T_{ki} = \frac{\partial W}{\partial y_{i,k}}. \tag{2.7}$$

Some writers use "hyperelastic" to describe materials that have a strain energy and use "elastic" for materials for which the stresses are functions of the deformation gradient $y_{r,s}$ (see [6], for example). However, materials "elastic" in this broader sense are useful only if the degree of reversibility of strain is limited; unless T_{ik} are derived from a strain energy function, cycles of strain will exist for which mechanical work can be extracted from the material.

The strain energy W depends only on the changes in distance between neighboring particles and so depends on $y_{i,k}$ only through the Cauchy strains C_{rs} (material objectivity). Thus we have

$$W = W(C_{rs}), \tag{2.8}$$

and W also depends explicitly on x_i if the material is inhomogeneous. The restriction (2.8) on the form of W and (2.2) imply the symmetry relation

$$y_{r,m} \frac{\partial W}{\partial y_{s,m}} = y_{s,m} \frac{\partial W}{\partial y_{r,m}},$$

which in turn implies the symmetry of the Eulerian stress tensor t_{ik} through (2.3) and (2.7). From (2.4), (2.7), and (2.8) the Kirchoff stress S_{ik} is given by

$$S_{ik} = \frac{\partial W}{\partial C_{ik}} + \frac{\partial W}{\partial C_{ki}} = 2 \frac{\partial W}{\partial C_{ik}}, \tag{2.9}$$

where the last equality follows if W is written as a symmetric function in C_{ik} and C_{ki} (the differentiation with respect to C_{ik} treats C_{ki} distinct from C_{ik} for $i \pm k$).

When the deformation of the material is limited by a constraint such as incompressibility or inextensibility in the direction of fibers embedded in the material, the stress-strain relation (2.7) is modified by the addition of a constraint stress. Thus if the material is subject to the kinematic constraint

$$g(y_{i,k}) = 0,$$

then the constraint stress $\lambda \partial g / \partial y_{i,k}$ is added to the right-hand side of (2.7). For incompressible materials, deformations are restricted by

$$|y_{i,k}| = 1, \tag{2.10}$$

and this introduces a hydrostatic pressure p as the constraint stress. The stress-strain relation for the Lagrangian stress tensor is then

$$T_{ki} = \frac{\partial W}{\partial y_{i,k}} + p \frac{\partial x_k}{\partial y_i}. \tag{2.11}$$

3 The Strain Energy Function

The form of the strain energy W as a function of the strain components C_{rs} is restricted by any symmetry properties that the material may possess in the undeformed state. The restrictions on the form of W imposed by the various symmetries of the crystal classes have been determined by Smith and Rivlin, and a description of their results is given in [7].

An isotropic material has no preferred directions so that the form (2.8) for W does not depend on the orientation of the rectangular Cartesian coordinate system used to describe the initial locations x_i of the particles. If the coordinate directions are chosen in the directions of principal axes of C_{rs}, we see that W must be expressible as a function $F(\lambda_1^2, \lambda_2^2, \lambda_3^2)$ of the principal values λ_i^2 of C_{rs}. Moreover the value of F must be independent of the ordering of the principal values because any two of the values can be interchanged by a rotation of the coordinate system. Now the three values λ_i^2 are determined apart from order as the roots of the cubic equation

$$\Lambda^3 - I_1 \Lambda^2 + I_2 \Lambda - I_3 = 0,$$

where I_1, I_2, I_3 are given by

$$I_1 = \lambda_1^2 + \lambda_2^2 + \lambda_3^2, \quad I_2 = \lambda_2^2 \lambda_3^2 + \lambda_3^2 \lambda_1^2 + \lambda_1^2 \lambda_2^2, \quad I_3 = \lambda_1^2 \lambda_2^2 \lambda_3^2,$$

and it follows that for an isotropic material the strain energy W depends on C_{rs} only through I_1, I_2, I_3,

$$W = W(I_1, I_2, I_3). \tag{3.1}$$

The quantities I_i are three independent invariants of the strain tensor C_{rs} and we have

$$I_1 = C_{rr}, \quad I_2 = \frac{1}{2}(I_1^2 - C_{rs} C_{sr}), \quad I_3 = |C_{rs}| = |y_{r,s}|^2. \tag{3.2}$$

From (2.9) and (3.1), the Kirchoff stress components are

$$S_{ik} = 2\{(W_1 + I_1 W_2)\delta_{ik} - W_2 C_{ik} + I_3 W_3 C_{ik}^{-1}\}, \tag{3.3}$$

where $C_{ik}^{-1} = x_{i;r} x_{k;r}$ and we are using the notation

$$W_i = \partial W / \partial I_i, \quad i = 1,2,3.$$

Downloaded 02 May 2010 to 171.66.16.250. Redistribution subject to ASME license or copyright; see http://www.asme.org/terms/Terms_Use.cfm

The Eulerian or true stress t_{ik} is from (2.3), (2.4), and (3.3)

$$t_{ik} = \frac{2}{I_3^{1/2}} \{(W_1 + I_1 W_2)B_{ik} - W_2 B_{ir}B_{rk} + I_3 W_3 \delta_{ik}\}, \quad (3.4)$$

where B_{ik} is the Finger strain tensor defined by $B_{ik} = y_{i,r}y_{k,r}$ with principal values λ_i^2. The principal axes of B_{ik} and t_{ik} coincide and they are principal strain directions in the deformed body B^* which rotate with the body during an added rigid body rotation of B^*.

For materials such as rubber, which undergo little change in volume at stress levels that cause severe deformations, the material can be treated as incompressible and subject to the constraint (2.10) or $I_3 = 1$. The strain energy is then a function only of I_1 and I_2,

$$W = W(I_1, I_2), \quad (3.5)$$

and the term in W_3 in (3.4) is replaced by a hydrostatic pressure p (an arbitrary function of x_i to be determined for the deformation under consideration),

$$t_{ik} = 2(W_1 + I_1 W_2)B_{ik} - 2W_2 B_{ir}B_{rk} + p\delta_{ik}. \quad (3.6)$$

The form for W suggested by Mooney for rubber,

$$W = C_1(I_1 - 3) + C_2(I_2 - 3), \quad (3.7)$$

where C_1 and C_2 are constants, can be regarded as the first two terms in the expansion of W as a double power series about the values $I_1 = 3$ and $I_2 = 3$ for the undeformed state. It provides a complete second-order theory for small strains when terms above the second order in the strains are neglected in the stress-strain relation and in the governing equations (Rivlin [8]). When $C_2 = 0$, the material is called neo-Hookean by Rivlin [9] to reflect the simplest form for W that gives a linear stress strain relation for infinitesimal strains. The shear modulus G for small strains is $2(C_1 + C_2)$. Values of G for a rubber are around 5 kg/cm^2 (about 0.5 MPa).

The first term in (3.7) can be derived from a molecular theory for rubberlike materials with long-chain molecules and the Mooney form can provide a reasonable fit with experiment for rubberlike materials over a moderate range of strain (for references see [10, 11]). The experimental results of Rivlin and Saunders showed that W_1 is relatively constant for values of I_1 up to around 10 and they replaced the second term in (3.7) by a function of I_2. For larger ranges of strain more complex forms are needed. Moreover, while stress estimates depend on the values of W_1 and W_2, the analysis of the stability of a finitely deformed body can be quite sensitive to the values of the second derivatives of W with respect to I_1 and I_2.

If W is taken as a sum of a function of I_1 and a function of I_2, as suggested by Hart-Smith, then

$$W_1 = W_1(I_1), \quad W_2 = W_2(I_2). \quad (3.8)$$

Note that if W_1 depends only on I_1 then W_2 depends only on I_2 and vice-versa because W_1 and W_2 are derived from W by differentiation with respect to I_1 and I_2. Hart-Smith and Crisp [12] found that the forms

$$W_1 = K_1 \exp\{k(I_1 - 3)^2\}, \quad W_2 = K_2/I_2,$$

where K_1, K_2, and k are constants, gave very good agreement with experimental results of Treloar for the inflation of a plane circular rubber membrane, a problem for which the strain energy function suggested by Carmichael and Holdaway also gives good results [13]. Alexander [14] found that with the exponential form for $W_1(I_1)$ of the Hart-Smith theory, a fairly simple form for $W_2(I_2)$ provides a good fit with experimental results for neoprene film in simple tension and in equibiaxial extension over a wide range of strain. The two functions in (3.8) can be chosen to match experimental stress-strain data for two independent strain paths. In this way, values for W_1 and W_2 were determined in [15] from results of Treloar for a latex rubber in simple tension and in equibiaxial extension. The values obtained then provided good agreement with Treloar's results for simple shear. The expressions [16][1]

$$W_1/C_1 = 1 + 2.49 \times 10^{-7}(I_1 - 3)^4 \quad 3 \leqslant I_1 \leqslant 56$$

$$W_2/C_1 = \begin{cases} 0.376 + 1.32 \times 10^{-2}(4.928 - I_2)^{4.864} & \\ & 3 \leqslant I_2 \leqslant 4 \\ 0.77/I_2^{0.5} & 4 \leqslant I_2 \leqslant 200 \end{cases} \quad (3.9)$$

give a reasonable fit for the empirical values found in [15]. In contrast to the Mooney form, W_2 drops sharply as I_2 increases from the value 3 for the unstrained state and W_1 increases steeply at values of I_1 above 36, as required by the stiffening of rubber in simple tension at elongations greater than 500 percent. Other forms for W for incompressible isotropic materials can be found in the reviews by Treloar [10] and Ogden [11]. The deviation of the mechanical behavior of rubberlike materials from ideal elasticity is discussed in the review by Zapas ([2, pp. 445–455]).

Storakers [17] has shown how values for W_1 and W_2 can be derived from experimental values for the twisting moment M and axial force L in the extension and torsion of a circular cylinder of incompressible isotropic material. The solution derived by Rivlin shows that the strains depend on the radial distance r and the twist ψ only through the product $\xi = \psi r$. In the expressions for M and L, ψ occurs explicitly only in the upper limit and in factors multiplying the integrals. The derivatives $\partial M/\partial\psi$ and $\partial L/\partial\psi$ involve values of the shear stress and axial stress at the lateral surface of the cylinder and experimental values for M and L for varying ψ together with derived estimates for the derivatives $\partial M/\partial\psi$, $\partial L/\partial\psi$ can lead to values for W_1 and W_2 for a range of values of I_1 and I_2. A similar approach was used by Ludwik and Scheu [18] to obtain the shear stress-shear strain relation for plastic flow from experiments on torsion of a circular cylinder.

For incompressible materials in plane strain, $\lambda_3 = 1$, $\lambda_2 = 1/\lambda_1$ and each element is in pure shear. The invariants I_1, I_2 have a common value I and

$$t_{\alpha\beta} = H(I)B_{\alpha\beta} + p\delta_{\alpha\beta}, \quad H = 2(W_1 + W_2)_{(I_1 = I_2 = I)},$$

where Greek indices range over 1,2. The results of Treloar for a latex rubber in pure shear gave variations of only ± 7 percent in $H(I)$ for the range $5 < I < 35$, and Rivlin and Saunders found that $H(I)$ for a vulcanized rubber decreased by only 4.5 percent as I increased from 5 to 10. Thus the Mooney form (3.7) can give good estimates for stresses in plane strain deformations of a rubberlike material.

Much less attention has been given to the form of the strain energy function for *compressible* isotropic materials. Murnaghan [19] introduced three independent invariants J_i of the strain through

$$J_1 = I_1 - 3, \quad J_2 = I_2 - 2I_1 + 3, \quad J_3 = I_3 - I_2 + I_1 - 1,$$

and they have the advantage that J_1, J_2, and J_3 are of the first, second, and third order in the strains, respectively. If W is expanded in a power series in the invariants J_i and terms of the fourth and higher order are neglected, we obtain the form suggested by Murnaghan,

$$W = a_1 J_2 + a_2 J_1^2 + a_3 J_1 J_2 + a_4 J_1^3 + a_5 J_3, \quad (3.10)$$

where $a_1 - a_5$ are material constants (a linear term in J_1 is omitted in order to have zero stress in the undeformed state). The constants a_1, a_2 are determined by the first-order response of the material,

$$a_1 = -G/2, \quad a_2 = G(1 - \nu)/4(1 - 2\nu), \quad (3.11)$$

[1] There is a misprint in the last line of equations (43) of [16].

Downloaded 02 May 2010 to 171.66.16.250. Redistribution subject to ASME license or copyright; see http://www.asme.org/terms/Terms_Use.cfm

where G is the shear modulus and ν Poisson's ratio. The constants $a_3 - a_5$ can be chosen to fit data for large strains. The form (3.10) provides a general form for W for a second-order theory for isotropic materials.

Blatz and Ko [20] took W to be the sum of a linear form in I_1, I_2/I_3 and a function of I_3, and then chose the function of I_3 so that in simple tension the lateral extension ratio $\lambda_1 = \lambda_2$ is related to the axial extension ratio λ_3 by

$$\lambda_1 = \lambda_3^{-\nu},$$

where ν is Poisson's ratio for small strains, as before. This leads to the form

$$W = C_1\left\{I_1 - 3 + \frac{(1-2\nu)}{\nu}(I_3^{-\nu/(1-2\nu)} - 1)\right\}$$

$$+ C_2\left\{I_2/I_3 - 3 + \frac{(1-2\nu)}{\nu}(I_3^{\nu/(1-2\nu)} - 1)\right\}, \tag{3.12}$$

where C_1 and C_2 are constants and $2(C_1 + C_2)$ is the shear modulus G for small strains. For a limited range of deformation (up to an extension ratio of 2.4 in simple tension, for example), they found that experimental results for a polyurethane foam rubber with a 47 percent void content were in good agreement with $C_1 = 0$ and $\nu = 1/4$, so that for this material

$$W = \frac{1}{2} G(I_2/I_3 + 2I_3^{1/2} - 5). \tag{3.13}$$

Discussion of other work on the form of W for compressible isotropic materials can be found in [10, 11]. Soft biological tissues undergo considerable distension in the course of their natural functions and modeling them as elastic materials gives a simplified representation of their mechanical behavior. A discussion and references are given in [21].

4 Solutions to Problems

From (2.6) and (2.7), the equilibrium equations for an elastic deformation $x_i \to y_i$ with no body force are

$$\frac{\partial}{\partial x_k}\left(\frac{\partial W}{\partial y_{i,k}}\right) = 0. \tag{4.1}$$

For an incompressible material, the three equations

$$\frac{\partial}{\partial x_k}\left(\frac{\partial W}{\partial y_{i,k}} + p\frac{\partial x_k}{\partial y_i}\right) = 0 \tag{4.2}$$

together with the incompressibility condition (2.10) govern the four functions $y_i(x)$ and $p(x)$. Only a limited number of exact solutions to these equatinos have been found.

Homogeneous deformations for a homogeneous elastic material obviously satisfy (4.1) (or (4.2) with p constant). For incompressible isotropic materials, Rivlin showed that some exact solutions can be found in closed form for a general form $W(I_1, I_2)$ of the strain energy function for a homogeneous material. The solutions involve deformations for which the strains depend on a single spatial coordinate and appropriate choice of the pressure p as a function of this coordinate leads to satisfaction of the equilibrium equations. Thus if a circular cylinder of incompressible, isotropic material is first extended in simple tension and then subjected to pure torsion in which cross sections rotate relative to each other as rigid planes about the axis of the cylinder, the strains depend only on radial distance from the axis. Equilibrium is satisfied in the axial and circumferential directions and the pressure function p can be chosen, for any $W(I_1, I_2)$, so that equilibrium is satisfied in the radial direction and so that the outer surface is free from traction. This solution can be generalized to the inflation, bending, torsion, extension, and shearing of an annular wedge. Other "universal" solutions are the inflation of a spherical shell, the bending, stretching, and shearing of a rectangular block into an annular wedge, and the inverse of this deformation. Details of these solutions can be found in [6, 7, 22].

In 1955 Ericksen posed the problem of determining all universal deformations, those that can be produced in every homogeneous, isotropic, incompressible, elastic body by the application of surface tractions alone. He found that except for deformations in which the strain invariants were constant, the only universal deformations are those described in the preceding paragraph. In these solutions, the stresses depend on the particular material; Carroll [23] has shown that except for stress fields with constant invariants, there are no equilibrium Cauchy stress fields that can exist in every homogeneous, isotropic, incompressible, elastic body.

For a wedge subjected to uniform normal and tangential tractions on its faces, plane strain deformations can occur for which the stresses are functions only of the polar angle [24]. For a given form of the strain energy function for an isotropic material, the variation in the stresses with the polar angle can be found from the solution of an o.d.e. A particular solution was found to be valid for all incompressible materials and this led to a new universal solution with constant strain invariants in which radial lines become logarithmic spirals [25]. Fosdick and Schuler have shown that there are no other universal solutions for generalized plane strain and Fosdick has extended this result to axially symmetric deformations [26]. The question is still open on the existence of three-dimensional universal deformations with constant strain invariants [27].

The universal solutions for isotropic materials can be generalized to certain anisotropic incompressible materials depending on the symmetry exhibited by the solution (see [7]). For example, extension and torsion of a circular cylinder of material transversely isotropic with respect to the axis of the cylinder can be solved exactly for a general form for the strain energy. The solutions can also be modified to give solutions for compressible materials (see [7]). Thus in pure torsion of a circular cylinder of compressible isotropic material, cross sections remain plane and rotate relative to each other about the axis of the cylinder, but in addition, particle distances from the axis adjust to maintain equilibrium in the radial direction. If we denote by $R(r)$ the deformed distance R from the axis as a function of the initial radial distance r, for equilibrium $R(r)$ must satisfy a second-order o.d.e., and numerical integration can be used to derive the solution for a given form of the strain energy function W.

The large extension and twist of an elastic bar with slender section can be treated by an approach that treats the cylinder as a membrane of nonuniform thickness ([2, pp. 331—346]). The problem then reduces to a one-dimensional problem and the solution can be found for a particular strain energy by numerical integration of a second-order o.d.e. The solution is exact within the framework of the membrane assumption. For a section that is not symmetrical about the centroid, the location of the axis of torsion varies with the amount of torsion and is determined as part of the solution.

Other exact solutions of the equilibrium equations that have been obtained are valid only for particular forms of the strain energy function (called partial solutions by Hill [28]). Solutions for a Mooney material have been found [29] for the compression of a long rectangular block (plane strain) and of a circular cylinder (axial symmetry) between rough rigid plates. The solutions have the simplifying feature that material planes initially normal to the direction of loading remain plane, and with this assumption it is only possible to satisfy the zero traction condition on the lateral surface in an overall manner. Load-deflection curves for bonded rubber disks of neo-Hookean material in compression were found to be in good agreement with experimental results of Ghent and Lindley for compressions up to 25 percent.

Cylindrical shearing or antiplane shear is a deformation in

Downloaded 02 May 2010 to 171.66.16.250. Redistribution subject to ASME license or copyright; see http://www.asme.org/terms/Terms_Use.cfm

which the displacement of each particle is normal to a plane and independent of distance from the plane. It has application to the axial deformation of cylindrical rubber bush mountings. Finite antiplane shear is only possible without the application of body forces for particular forms of the strain energy [7, 30], which for incompressible materials, includes the Mooney form and strain energies dependent only on I_1. A review of work on antiplane shear fields near the tip of a crack (Mode *III* loading) has been given by Knowles ([2, pp. 257–268]).

The inflation of a thick-walled elastic torus has application to tire mechanics, and approximate solutions have been obtained under the assumption that the radii of the circles generating the torus are much smaller than the overall diameter of the torus (see Hill [2, pp. 211—236], and the references cited therein). Hill has also derived approximate solutions for cylindrical and spherical rubber bushings (see [28]).

For a plane sheet of neo-Hookean material in large extension in its plane, the transverse extension ratio $\lambda_3 = 1/\lambda_1\lambda_2$ is small compared to the inplane extension ratios λ_1, λ_2. If the contribution of λ_3^2 to W is neglected, the deformed locations y_α are then harmonic functions of the initial locations x_α and approximate solutions to problems can be found [31]. The solutions are asymptotic solutions for infinitely large strain for a neo-Hookean material. They are exact for a plane sheet with strain energy per unit area proportional to $\lambda_1^2 + \lambda_2^2$, but this material has all-around tension in the reference state so that solutions differ most from those for a neo-Hookean sheet near traction-free contours. The solution for a slit or crack in an infinite sheet under biaxial tension at infinity shows that the slit opens into an oval hole with a smooth contour, in agreement with experiments with rubber sheets. An elliptical hole in an infinite sheet subjected to biaxial tension at infinity becomes an elliptical hole with axes parallel to the principal directions of strain at infinity. Wu [32] has treated the closing of an elliptical hole in a stretched sheet by edge forces to model the suturing of a wound. The finite plane strain deformation for an infinite body containing a cylindrical hole, including the limiting case when the hole degenerates into a slit, has been treated by Varley and Cumberbatch ([1, pp. 41–64,] and [33]) for the so-called harmonic material. The principle of minimum potential energy was used by Feng and Tielking [34] to treat the stretching of a rectangular sheet with two edges clamped and two free.

The investigation of the singular local deformation near a crack tip in plane strain under Mode *I* loading was initiated by Knowles and Sternberg (for reviews see [1, pp. 23-40], and [35]), and behavior under Mode *II* loading has been treated by Stephenson [36]. Depending on the material, the governing equations can cease to be elliptic in the neighborhood of the crack tip (see [35]). Conditions for ellipticity of the equations for finite plane strain of incompressible isotropic materials and the related question of the existence of lines of discontinuity in the deformation gradients have been discussed recently by Abeyaratne [37]; the ellipticity conditions for three-dimensional deformations have been derived by Zee and Sternberg [38].

Problems involving elastic sheets are simplified by using the membrane approximation, which is a much better approximation for large strains than for small, in general. The theory was developed by Adkins and Rivlin (see [7]), who solved the axially symmetric problem of the inflation of a plane circular sheet by uniform pressure applied to one face of the sheet. The problem is one-dimensional and the solution can be found by numerical integration for particular forms of the strain energy. Comparison of the inflated profile of the sheet and the variation of the extension ratios in the sheet can then be made with experiment to test the suitability of strain energy functions [7, 12, 13].

The asymptotic analysis of the large deformation of a membrane of Mooney material was done by Isaacson, who showed that an inflated balloon that was initially axisymmetric approaches a spherical shape as the degree of inflation increases. When the membrane is deformed with no loading on its major surfaces, Wu showed that the limiting shape is a catenoid, a uniformly stressed minimal surface. References are given in the paper by Wu [39] which extends the asymptotic analysis. The approach used in [31] for plane sheets was used by Fenner and Wu [40] to treat out-of-plane deformations of plane membranes with rigid inclusions.

Problems involving contact of membranes with smooth surfaces as in the squashing of an inflated membrane between rigid plates have been treated by Feng et al. (see [41]) and by Callegari and Keller [42]. The wrinkling of membranes has been discussed by Wu and Canfield in [43], where references to other work of Wu on wrinkling can be found, and by Zak [44]. Yin [45] has considered the nonuniform inflation of a circular cylindrical membrane. References to other axisymmetric membrane solutions can be found in [39, 40]. Naghdi and Tang [46] have shown that the only universal solutions for membranes, deformations that can be maintained in every isotropic elastic membrane by edge loads and/or uniform pressure applied to one face, are those for which the deformed shape is plane, a right circular cylinder, a sphere, or a surface of constant mean curvature (see also Yin [47]).

5 Second-Order Effects

Because of the difficulty of obtaining exact solutions for large elastic deformations, methods of successive approximations have been developed (see [7]). A second-order theory is derived by assuming that the locations of particles in the deformed state admit expansions in the form

$$y_i = x_i + \epsilon\, u_i(x_r) + \epsilon^2\, v_i(x_r) + 0(\epsilon^3), \tag{5.1}$$

where ϵ is a dimensionless parameter that is a measure of the amount of deformation and which is involved in the description of the problem. Substitution of (5.1) into the equilibrium equations (4.1) gives partial differential equations for the first and second-order displacements u_i and v_i which are of the form

$$L_i(u_r) = 0, \quad L_i(v_r) = Q_i(u_r), \tag{5.2}$$

where L_i is a linear operator and Q_i is second order. The operator L_i is that appearing in the equilibrium equations for classical linear elasticity. The boundary equations are similarly split into two sets of conditions. When u_i are known, the determination of the second-order solution v_i corresponds to a problem in linear elasticity with body forces derived from u_i (see [7, 8]).

When the first-order solution is simple enough, the second-order solution can be determined by direct methods, and second-order effects have been determined for torsion and bending of isotropic cylinders, and complex variable methods have been developed for plane problems (see [7]). Selvadurai [48] has treated the torsion of a thick spherical shell using theory for axially symmetric deformations of incompressible materials developed in collaboration with Spencer. However for most problems, it is difficult to find analytical solutions for second-order effects because particular integrals for v_i for the second set of equations in (5.2) cannot be found in explicit forms in general. In some cases, the determination of second-order effects is simplified considerably by the use of properties of the inverse deformation.

The equilibrium equations (4.1) are the Euler differential equations for the functional F which is the total strain energy of the body given by

Downloaded 02 May 2010 to 171.66.16.250. Redistribution subject to ASME license or copyright; see http://www.asme.org/terms/Terms_Use.cfm

$$F=\int_V W\,dx_1dx_2dx_3. \tag{5.3}$$

If we express F in terms of the strain energy W^* measured per unit volume of the deformed body, then

$$F=\int_{V^*} W^*\,dy_1dy_2dy_3, \quad W^*=|x_{r;s}|\,W, \tag{5.4}$$

where V^* is the region of space occupied by the deformed body. For a homogeneous body, W does not depend explicitly on x_i so that W^* can be expressed as a function $G^*(x_{r;s})$. The Euler differential equations for the functional F in (5.4) are then

$$\frac{\partial}{\partial y_k}\left(\frac{\partial G^*}{\partial x_{i;k}}\right)=0 \tag{5.5}$$

and they are alternative forms for the equilibrium equations [49]. They can also be derived [50] by direct transformation of equations (4.1). Because (5.5) and (4.1) have the same form, we see that for an equilibrium deformation $x_i \rightarrow y_i$ of B, the *inverse deformation* $y_i \rightarrow x_i$ (of the body B^* into B) would be an equilibrium deformation for a material with strain energy $W^*=G^*(x_{r;s})$ per unit volume of B^*. A similar result holds for incompressible bodies and the pressure functions for the original and inverse deformations are related [50]. If the material of B is isotropic, W^* will be unchanged by a rigid rotation of B, and so for deformations of B^*, G^* will be a possible strain energy function for a real (isotropic) material obeying objectivity. Some of the conservation laws for finite elasticity can be interpreted in terms of resultant forces and moments for the inverse deformation ([1], pp. 1–10).

For plane strain deformations of an incompressible isotropic material, we saw in Section 3 that W is a function of a single invariant I and in this case W and G^* have the same functional form. Thus if a plane strain deformation is possible in homogeneous, incompressible, isotropic material without body forces, then the inverse deformation is also an equilibrium solution for no body force, a result first found by Adkins (see [7]). For a certain problem class and proper choice of the parameter ϵ, the inverse deformation is defined by the same boundary conditions as the original deformation but with ϵ replaced by $-\epsilon$. Thus for this class of problems in plane strain, equations (5.1) defining the original deformation will still hold if x_i and y_i are interchanged and ϵ is replaced by $-\epsilon$ ($x_3=y_3$ here). It can then be deduced that we must have [51]

$$v_\alpha=\frac{1}{2}\,u_\beta\frac{\partial u_\alpha}{\partial x_\beta}, \tag{5.6}$$

so that for this problem class, the second-order displacements can be derived by an automatic procedure when the classical solution to the problem is known. (Similarly the fourth-order solution can be found when the first, second, and third-order solutions are known, and so on.) In this way, second-order effects in a number of plane strain problems involving rigid inclusions were determined.

The strain energies W and G^* have the same functional form for three-dimensional deformations of an incompressible material if $W(I_1,I_2)$ is symmetric in I_1,I_2. The Mooney form (3.7) gives a complete second-order theory and when $C_1=C_2$, the inverse of an equilibrium deformation is possible in the same material. Chan and Carlson [52] applied this result to second-order torsion (see also Hill [53]).

For compressible materials, the inverse deformation can occur in the same material without body forces if [50]

$$W(I_1,I_2,I_3)=I_3^{1/2}\,W(I_2/I_3,I_1/I_3,1/I_3). \tag{5.7}$$

and this holds to third order in the strains for the Murnaghan form (3.10) for W if

$$a_3=2a_2-a_1/4, \quad a_4=-3a_2/4, \quad a_5=3a_1/2. \tag{5.8}$$

To second order, the inverse deformation is defined implicitly by interchanging x_i and y_i in (5.1), and if we solve for y_i we find that the first-order displacement for the inverse deformation is $-u_i(x_r)$, and the second-order term is $-v_i(x_r)+u_ku_{i,k}$. When (5.8) holds, the inverse deformation is also an equilibrium deformation so that if u_i and v_i satisfy (5.2), so do $-u_i$ and $-v_i+u_ku_{i,k}$ and we have

$$L_i(-v_r+u_ku_{r,k})=Q_i(u_r) \tag{5.9}$$

because Q_i is even in u_r. From (5.2), (5.9), and the linearity of L_i it follows that

$$L_i(u_ku_{r,k})=2\,Q_i(u_r).$$

Thus when u_i are known, a particular integral of the second of (5.2) is given by $u_ku_{i,k}/2$ [54]. This result applies also for incompressible materials (Hill [53]), the limiting case obtained when $\nu\rightarrow 1/2$.

The identation of an elastic half space by a smooth rigid punch and the problem of a rigid spherical inclusion in an infinite body with uniform stress at infinity were treated in [54] for a material with strain energy given by the Murnaghan form (3.10) with constants related by (5.8). In the indentation of a half space by a smooth rigid sphere, it was found that the second-order contact pressure vanishes to the same order as the first-order pressure as the edge of the contact region is approached (i.e., like $(a-r)^{1/2}$, where $r=a$ is the edge of the circular contact area). The second-order correction to the load is zero for incompressible materials because of the uncoupling of normal and tangential surface loadings in linear elasticity when $\nu=1/2$. In this problem, a convenient value for the parameter ϵ is a/S, where S is the radius of the indenting sphere. The Hertz solution for the pressure between two bodies in smooth contact is derived from the first-order solution to a half-space problem, and so ignores ϵ^2. As pointed out in [54], the Hertz solution can only be improved by taking into account second-order terms in the stress-strain relation as well as in the boundary conditions. Thus the Hertz solution for the contact pressure is exact within the framework of the classical theory of elasticity and attempts to improve the Hertz solution (see [55]) using linear elasticity are inadequate. For indentation by a flat-ended rigid circular punch, the singularity in the first-order solution at the edge of the punch generates a physically unacceptable singularity in the second-order solution [54], and a different approach is needed for this problem.

If a small twist is superposed on a uniform finite simple extension of an isotropic cylinder so that the state of strain is the same at each section, the solution to first order in the twist ψ per unit initial length can be found in terms of the St Venant warping function for the unextended cylinder (see [22]). The resultant load on each section reduces to an axial force L and a twisting moment M when the axis of torsion is the line of centroids of the cross sections. Because M is odd in ψ, the first-order value $\psi m(\lambda)$, where λ is the axial extension ratio, is in error by an $0(\psi^3)$ amount; the first-order solution determines $m(\lambda)$ for arbitrary λ and a general form for the strain energy function [22]. The axial force L is even in ψ and the second-order correction to L can be found if we use the relations

$$L=\frac{1}{l}\,\frac{\partial F}{\partial \lambda}, \quad M=\frac{1}{l}\,\frac{\partial F}{\partial \psi}, \tag{5.10}$$

where $F(\lambda,\psi)$ is the total strain energy of the cylinder and l is the initial length. Because M is $\psi m(\lambda)$ correct to second order, the second of (5.10) leads to

$$F=F_0+\frac{1}{2}\,l\psi^2 m(\lambda)+0(\psi^4),$$

where $F_0(\lambda)$ is the total strain energy for extension alone. From the first of (5.10) we now have

Downloaded 02 May 2010 to 171.66.16.250. Redistribution subject to ASME license or copyright; see http://www.asme.org/terms/Terms_Use.cfm

$$L = L_0(\lambda) + \frac{1}{2}\psi^2 \frac{dm}{d\lambda} + 0(\psi^4), \tag{5.11}$$

where $L_0(\lambda)$ is the axial force for simple extension. Thus the first-order solution has led to the value of L to second order because of the existence of a potential energy for the system, and a corresponding approach [16] applies for a mechanical system with several generalized forces derived from a potential energy. Assuming that the axial force L for simple tension increases with λ, from (5.11) we see that when the axial force is held constant the cylinder will tend to elongate or shorten on twisting according as $dm/d\lambda$ is negative or positive. Some results for rubberlike materials are given in [16].

6 Small Deformations on Large. The Energy Stability Condition.

If small deformations are superposed on a known finite deformation of an elastic body, a linear theory is obtained (see [22]) which is similar to the classical theory for infinitesimal deformations of an anisotropic inhomogeneous material. We suppose that the deformation $x_i \to y_i$ of B into B^* is an equilibrium deformation and suppose that the particles of B^* are given an additional infinitesimal displacement $w_i(x_r,t)$. The equations of motion are derived on the assumption that only linear terms in w_i need be retained. When the body force F_i for the deformation of B into B^* remains unchanged during the added infinitesimal motion, the equations of motion are found to be

$$\frac{\partial}{\partial x_k}(C_{ikrs} w_{r,s}) = \rho \frac{\partial^2 w_i}{\partial t^2}. \tag{6.1}$$

The coefficients C_{ikrs} are given by

$$C_{ikrs} = \frac{\partial^2 W}{\partial y_{i,k} \partial y_{r,s}} = C_{rsik}, \tag{6.2}$$

the derivatives of W being evaluated for the body B^*. (The incompressible case can also be treated.)

Equations (6.1) form the basis for the examination of the stability of the deformed state B^*. In general terms, an equilibrium state is said to be stable if in the motion following an arbitrary disturbance, the amplitudes of the additional displacements and velocities are vanishingly small whenever the disturbance itself is vanishingly small. For a conservative mechanical system with a finite number of degrees of freedom, it is well known (see [56]) that a necessary and sufficient condition for stability is that the total potential energy of the system has a relative minimum in the equilibrium configuration. This "energy method," which is equivalent to the "adjacent position of equilibrium method" (see [56]), is a static method in that arbitrary motions need not be analyzed to examine stability. It is natural to assume that the energy method for discrete systems applies also to the stability of continuous elastic bodies under conservative loading, and this ordinarily leads to the assumption that a locally positive-definite potential energy U measured from the equilibrium state is a sufficient condition for stability. In 1914, Hellinger remarked that the energy criterion cannot be applied directly to continuous systems of more than one dimension. Much later an example was given [57] to show that for small motions of two or three-dimensional elastic bodies, concentration or focusing of energy can occur even though the energy distribution is very flat at earlier times, and the discussion in [57] showed that existing proofs for the sufficiency of the energy criterion for continuous systems were deficient.

In [57], an equilibrium state was defined as *stable* whenever in the motion following any sufficiently small changes in the body and surface forces, made for a finite interval of time only, the displacements w_i and the velocities $\partial w_i/\partial t$ are everywhere arbitrarily small in magnitude. For usual structural materials it would also be realistic to include the requirement that the strains remain small during the motion in order to restrict damage to the material. It is clear from the example in [57] that the energy criterion for continuous systems can have meaning only for a more restricted class of disturbing forces than allowed in this definition of stability. The energy-focusing example in [57] involved arbitrarily small disturbing forces but their spatial and time derivatives were not small and it is unlikely that very small disturbing forces of this kind can originate from a natural event.

If a portion of the surface S_1^* is held fixed while the loading on the remainder S_2^* of the surface S^* of B^* does not vary (dead loading), then small disturbances of B^* will be governed by (6.1) together with the boundary conditions

$$w_i = 0 \quad \text{on} \quad S_1, \quad C_{ikrs} w_{r,s} n_k = 0 \quad \text{on} \quad S_2, \tag{6.3}$$

where S_1, S_2 are the portions of the surface of B corresponding to S_1^*, S_2^*. If we suppose that the disturbing forces act prior to $t=0$, then from (6.1) and (6.3) the total energy E_1 is conserved during the motion after $t=0$,

$$E_1 = U + T = (E_1)_{t=0}, \tag{6.4}$$

where U and T are the potential and kinetic energies,

$$U = \frac{1}{2}\int_V C_{ikrs}\, w_{i,k}\, w_{r,s}\, dV,$$

$$T = \frac{1}{2}\int_V \rho \frac{\partial w_i}{\partial t}\frac{\partial w_i}{\partial t}\, dV. \tag{6.5}$$

The body B^* is stable according to the energy criterion if U is positive definite for displacement fields w_i which vanish on S_1. Now differentiation of (6.1) and (6.3) with respect to the time t shows that the velocity $\partial w_i/\partial t$ satisfies the same equations and boundary conditions as w_i (C_{ikrs} are independent of t). Therefore a "second-order energy" E_2 is constant after $t=0$, E_2 being obtained by replacing w_i by $\partial w_i/\partial t$ in the form for E_1. Similarly the third-order energy E_3 obtained by using $\partial^2 w_i/\partial t^2$ instead of w_i in the functional E_1 is constant after $t=0$. In [58] it was shown that when U is positive definite for w_i zero on S_1, then for a small enough value of E_3 at $t=0$, the values of w_i, $w_{r,s}$, and $\partial w_i/\partial t$ will all be as small as desired in the motion after $t=0$. It was then shown that E_3 at $t=0$ will be small if certain integrals involving the second-time derivatives of the disturbing body force and the third-time derivatives of the disturbing surface force acting prior to $t=0$ are small. This result therefore gives restrictions, which if placed on the disturbing forces, will ensure the validity of the energy criterion as a *sufficient* condition for the stability of continuous systems. For one-dimensional problems, such as the Euler column, the restrictions are derived from the value of E_2 at $t=0$, and so involve one less time derivative of the disturbing forces [58].

That the energy criterion is a *necessary* condition for stability can be shown [59] by adapting the proofs of Liapounoff and Chetayev for discrete systems to conservative continuous systems to show that instability results when U can be negative. It can also be shown [59] that when dissipative forces linear in the velocities are present, the system is still unstable when U can assume negative values. Thomson and Tait [60] gave an argument to show that a discrete system with conservative and (completely) dissipative forces is unstable whenever U can assume negative values arbitrarily near the equilibrium state, and Koiter [61] has repeated the argument for both discrete and continuous systems. Despite the intuitive appeal of the arguments they are deficient because they assume that a negative total energy E that is nonincreasing must eventually fall below a given energy level.

The difficulty of using a realistic definition of stability for

Downloaded 02 May 2010 to 171.66.16.250. Redistribution subject to ASME license or copyright; see http://www.asme.org/terms/Terms_Use.cfm

continuous bodies has led to theories that define stability through the use of a norm, a quadratic functional used as a measure of "distance" from the equilibrium state (see [62-64] for example.) As emphasized in [57, 58], for approaches such as these it is necessary to relate the results to the behavior of bodies or structures under the action of disturbing forces, for which pointwise estimates of the displacements and strains are required in practice. It is incorrectly implied in [64] that a stability definition using a norm is equivalent to that used in [58].

When the unstrained body is homogeneous and isotropic and the known finite deformation is uniform with two equal extension ratios μ, the coefficients C_{ikrs} are constants and equations (6.1) are similar to those for the infinitesimal deformation of a homogeneous transversely isotropic material for which methods of solution have been developed for the equilibrium case [22]. The indentation of a half space with the equal extension ratios μ parallel to the traction-free plane boundary can be treated for axially symmetric rigid punches. The load on the punch can become negative for certain values of the extension ratio μ, depending on the material. For a Mooney material, the load becomes zero when μ is approximately two-thirds and this indicates that the half space becomes unstable when the compression parallel to the boundary reaches this amount. Solutions for a concentrated force at a point of the boundary applied perpendicular or parallel to the plane are given in [65]. Usmani and Beatty [66] consider an isotropic half space in a uniform state of plane stress with unequal values λ_1, λ_2 for the extension ratios parallel to the plane boundary and derive the condition on λ_1, λ_2 for stability of the half space.

In [67], solutions were found for the small bending by terminal couples or by a transverse end load of a circular cylinder of incompressible isotropic material that had been initially finitely extended or compressed, and numerical results were given for a Mooney material. The theory was used to examine the stability of a circular bar in compression and it was found that an extended Euler formula was in remarkably good agreement with the results for a Mooney material even for short bars that buckle at considerable amounts of compression. Beatty and Hook [68] found that the results of [67] and related work by Read and by Beatty were in general agreement with experimental data for the stability of thick circular rubber bars under compressive end loads. The radially symmetric buckling of cylinders in compression was studied by Wilkes [69] and by Vaughan [70], who also treated asymmetric buckling but did not take a general enough form for the perturbation. Beatty [1, pp. 125-150], has given a review of work on the stability of rubber bodies in compression. Green and Spencer [71] treated the stability of a circular cylinder under finite extension and torsion, again by assuming a small deformation superposed on the finite deformation. They found that for pure torsion with the length held fixed, a very long cylinder of neo-Hookean material is unstable for all values of the twist. This is to be expected because the axial force L is

$$L = 2C_1 \pi a^2 (\lambda - 1/\lambda^2 - \psi^2 a^2 / 4\lambda^2)$$

for a neo-Hookean circular cylinder, where λ is the axial extension ration, ψ is the twist per unit initial length, and a is the radius of the cylinder. L is compressive for $\lambda = 1$. For $\lambda = 1.2$, the cylinder became unstable at $\psi a/\lambda = 1.07$.

Some basic stability problems for finitely deformed membranes of isotropic elastic material were treated in [15] using the energy method. Stability conditions for a plane sheet of uniform thickness stretched uniformly in tension in its plane were determined for both dead loading and clamped edge conditions. For a Mooney material, the sheet with clamped edges is stable for all positive values of C_1 and C_2, but the sheet under dead loading becomes unstable at large enough extension ratios λ_1, λ_2; the smaller the ratio C_2/C_1 the larger is the stable region in the λ_1, λ_2 plane. For a sheet with the empirical values (3.9) for W_1, W_2, the ratio W_2/W_1 decreases fast enough as the extensions increase to keep the sheet stable under dead loading in the range of strain covered by (3.9). Recent results on the stability of thick plates of neo-Hookean material under inplane compression have been given by Sawyers [2, pp. 319-330], and Sawyers and Rivlin [72].

Stability conditions for a uniformly inflated and extended circular cylindrical tube have been found under the assumption that axisymmetric modes dominate the stability, and conditions to assure the validity of this assumption were obtained [15]. These conditions hold for a Mooney material and for the material for which (3.9) hold if the tube is not in overall compression, i.e., if the axial wall stresses is not less than the value produced by the pressure in a tube with a closed end. The stability of tubes with strain energies that model soft biological tissues and the effect of an internal fluid flow were considered in [21]. The stability of a uniformly inflated tube with closed ends and subjected to an compressive axial load was treated in [73]. The asymmetric mode corresponding to Euler buckling involves no change in volume to first order, and for long tubes the critical load can be expressed in terms of the Euler formulas using an equivalent Young's modulus for the finitely deformed tube. When the inflation induces very small strains, the internal pressure has no effect on the buckling load, as found previously by Haringx. Fourney and Stern [74] considered the stability of a finitely inflated and extended tube using a shell theory developed by Stern. Thick-walled tubes have been treated by Hill [75] and Haughton and Ogden [76].

A spherical membrane of uniform thickness when inflated uniformly by internal gas pressure p becomes unstable in the radially symmetric mode when $dp/d\lambda$ is less than $dp_G/d\lambda$, where p_G is the gas pressure for the mass of gas in the balloon and any attached reservoir and λ is the ratio of the inflated radius to the initial radius. For reservoir volumes very large compared to the balloon volume, the balloon is unstable when the $p - \lambda$ curve is falling. The values of the derivative of p_G lie between the values for the adiabatic gas law and the isothermal gas law, with the isothermal case more critical, and it is possible for the balloon to be stable under the adiabatic law and unstable under the isothermal law. The inflation pressure p is proportional to T/λ, where T is the tension in the membrane with equal extension ratios λ. Feodos'ev [77] showed that for a particular strain energy function instability occurs in the "$n = 1$" mode when $dT/d\lambda$ is negative, and the result holds generally [78]. The instability mode has the same normal displacement as an axial translation of the membrane but with zero tangential displacements. In [15] it was incorrectly stated that this mode did not lead to instability because of the failure to notice that when $n = 1$, the coefficients on both sides of the second of equations (6.11) in [15] vanish and the constants C, D are then arbitrary. (The same error occurs in [79]). For rubber balloons the nonspherical $n = 1$ mode does not appear, although for the material represented by (3.9), instability is very close around $\lambda = 2.5$. Alexander [80] has shown instability in the $n = 1$ mode experimentally for neoprene balloons, for which his strain energy function [14] predicts instability for $\lambda = 1.6$ to 4.3. Inequality (6.2) of [15] ensures that instability can only occur in the radial or $n = 1$ modes, and if the material is such that a plane sheet in tension under dead loading is stable, then it can be shown that the inequality is satisfied if $\lambda^{1/2} T$ is increasing. Thick-walled spherical shells have been treated by Hill [75] and Haughton and Ogden [76].

References

1 Rivlin, R. S., Ed., *Finite Elasticity*, AMD-Vol. 27, ASME, New York, 1977.

Downloaded 02 May 2010 to 171.66.16.250. Redistribution subject to ASME license or copyright; see http://www.asme.org/terms/Terms_Use.cfm

2 Carlson, D. E., and Shield, R. T., Eds., *Finite Elasticity*, Proc. IUTAM Symp., Lehigh Univ., Aug. 10–15, 1980, Martinus Nijhoff, The Hague, 1982.

3 Lee, S. J., and Shield, R. T., "Variational Principles in Finite Elastostatics," *J. Appl. Math. Phys. (ZAMP)*, Vol. 31, 1980, pp. 437–453. "Applications of Variational Principles in Finite Elasticity," ibid, pp. 454–472.

4 Prager, W., *Introduction to Mechanics of Continua*, Ginn & Co., Boston, 1961.

5 Love, A. E. H., *A Treatise on the Mathematical Theory of Elasticity*, Cambridge Univ., 4th ed., 1927; Rep. by Dover, New York, 1944.

6 Truesdell, C., and Noll, W., *The Non-linear Field Theories of Mechanics*, Hand. Phys., Vol. III/3, Springer, Berlin, 1965.

7 Green, A. E., and Adkins, J. E., *Large Elastic Deformations*, 2nd ed., Oxford Univ., 1970.

8 Rivlin, R. S., "The Solution of Problems in Second Order Elasticity Theory," *J. Rat. Mech. Anal.*, Vol. 2, 1953, pp. 53–81.

9 Rivlin, R. S., "Large Elastic Deformations of Isotropic Materials, I. Fundamental Concepts," *Phil. Trans. Roy. Soc.*, Vol. A240, 1948, pp. 459–490.

10 Treloar, L. R. G., "The Elasticity and Related Properties of Rubbers," *Rep. Prog. Phys.*, Vol. 36, 1973, pp. 755–826.

11 Ogden, R. W., "Elastic Deformations of Rubberlike Solids," in *Mechanics of Solids*, Hopkins, H. G., and Sewell, M. J., Eds., Pergamon, Oxford, 1982, pp. 499–537.

12 Hart-Smith, L. J., and Crisp, J. D. C., "Large Elastic Deformations of Thin Rubber Membranes," *Int. J. Eng. Sci.*, Vol. 5, 1967, pp. 1–24.

13 Klingbeil, W. W., and Shield, R. T., "Some Numerical Investigations on Empirical Strain-Energy Functions in the Large Axisymmetric Extensions of Rubber Membranes," *J. Appl. Math. Phys. (ZAMP)*, Vol. 15, 1964, pp. 608–629.

14 Alexander, H., "A Constitutive Relation for Rubber-Like Materials," *Int. J. Eng. Sci.*, Vol. 6, 1968, pp. 549–563.

15 Shield, R. T., "On the Stability of Finitely Deformed Elastic Membranes," *J. Appl. Math. Phys. (ZAMP)*, Part I, Vol. 22, 1971, pp. 1016–1028. Part II, Vol. 23, 1972, pp. 16–34.

16 Shield, R. T., "An Energy Method for Certain Second-order Effects with Application to Torsion of Elastic Bars Under Tension," ASME JOURNAL OF APPLIED MECHANICS, Vol. 47, 1980, pp. 75–81.

17 Storakers, B., "An Explicit Method to Determine Response Coefficients in Finite Elasticity," *J. Elasticity*, Vol. 9, 1979, pp. 207–214.

18 Ludwik, P., and Scheu, R., "Vergleichende Zug-, Druck-, Dreh- und Walzversuche," *Stahl u. Eisen*, Vol. 45, 1925, pp. 373–381.

19 Murnaghan, F. D., "Finite Deformation of an Elastic Solid," *Amer. J. Math.*, Vol. 59, 1937, pp. 235–260. *Finite Deformation of an Elastic Solid*, Wiley, New York, 1951.

20 Blatz, P. J., and Ko, W. L., "Application of Finite Elastic Theory to the Deformation of Rubbery Materials," *Trans. Soc. Rheol.*, Vol. 6, 1962, pp. 223–251.

21 Wong, J. S. K., and Shield, R. T., "The Stability of a Cylindrical Elastic Membrane of Biological Tissue and the Effect of Internal Fluid Flow," *Ing.-Arch.*, Vol. 49, 1980, pp. 393–412.

22 Green, A. E., and Zerna, W., *Theoretical Elasticity*, 2nd ed., Oxford Univ., 1968.

23 Carroll, M. M., "Controlled States of Stress for Incompressible Elastic Solids," *J. Elasticity*, Vol. 3, 1973, pp. 147–153.

24 Klingbeil, W. W., and Shield, R. T., "On a Class of Solutions in Plane Finite Elasticity," *J. Appl. Math. Phys. (ZAMP)*, Vol. 17, 1966, pp. 489–511.

25 Singh, M., and Pipkin, A. C., "Note on Ericksen's Problem," *J. Appl. Math. Phys. (ZAMP)*, Vol. 16, 1965, pp. 706–709.

26 Fosdick, R. L., and Schuler, K. W., "On Ericksen's Problem for Plane Deformations With Uniform Transverse Stretch," *Int. J. Eng. Sci.*, Vol. 7, 1969, pp. 217–233. Fosdick, R. L., "Statically Possible Radially Symmetric Deformations in Isotropic, Incompressible Elastic Solids," *J. Appl. Math Phys. (ZAMP)*, Vol. 22, 1971, pp. 590–607.

27 Marris, A. W., "Two New Theorems on Ericksen's Problem," *Arch. Rat. Mech. Anal.*, Vol. 79, 1982, pp. 131–173.

28 Hill, J. M., "A Survey of the Solved Problems for Rubber, Part II: Partial and Approximate Solutions," *Int. J. Mech. Eng. Ed.*, Vol. 10, 1982, pp. 153–168. "Partial Solutions of Finite Elasticity," *J. Appl. Math. Phys. (ZAMP)*, Vol. 24, 1973, pp. 401–408, 409–418, 609–618.

29 Klingbeil, W. W., and Shield, R. T., "Large-Deformation Analyses of Bonded Elastic Mounts," *J. Appl. Math. Phys. (ZAMP)*, Vol. 17, 1966, pp. 281–305.

30 Knowles, J. K., "On Finite Anti-Plane Shear for Incompressible Elastic Materials," *J. Austral. Math. Soc.*, Vol. 19*B*, 1976, pp. 400–415. "A Note on Anti-Plane Shear for Compressible Materials in Finite Elastostatics," ibid, Vol. 20*B*, 1977, pp. 1–7. "Universal States of Finite Anti-Plane Shear: Ericksen's Problem in Miniature," *Amer. Math. Monthly*, Vol. 86, 1979, pp. 109–113. See also Hill, J. M., "Generalized Shear Deformations for Isotropic Incompressible Hyperelastic Materials," *J. Austral. Math. Soc.*, Vol. 20*B*, 1978, pp. 129–141.

31 Wong, F. S., and Shield, R. T., "Large Plane Deformations of Thin Elastic Sheets of Neo-Hookean Material," *J. Appl. Math. Phys. (ZAMP)*, Vol. 20, 1969, pp. 176–199.

32 Wu, C. H., "Sutures in Stretched Membranes," *Quart. Appl. Math.*, Vol. 38, 1980, pp. 109–120.

33 Varley, E., and Cumberbatch, E., "Finite Deformations of Elastic Materials Surrounding Cylindrical Holes," *J. Elasticity*, Vol. 10, 1980, pp. 341–405.

34 Feng, W. W., and Tielking, J. T., "Large Plane Deformations of Rectangular Elastic Sheets," *J. Appl. Math. Phys. (ZAMP)*, Vol. 27, 1976, pp. 781–790.

35 Sternberg, E., "Some Recent Advances in the Application of Nonlinear Elastostatics to Singular Problems," in: *Trends in Solid Mechanics 1979*, Besseling, J. F., and van der Heijden, A. M. A., Eds., Proc. Symp. W. T. Koiter, Delft Univ., June 13–15, 1979, Delft Univ., 1979, pp. 225–234.

36 Stephenson, R. A., "The Equilibrium Field Near the Tip of a Crack for Finite Plane Strain of Incompressible Elastic Materials," *J. Elasticity*, Vol. 12, 1982, pp. 65–99.

37 Abeyaratne, R., "Discontinuous Deformation Gradients in Plane Finite Elastostatics of Incompressible Materials," *J. Elasticity*, Vol. 10, 1980, pp. 255–293. "Discontinuous Deformation Gradients Away from the Tip of a Crack in Anti-Plane Shear, ibid, Vol. 11, 1981, pp. 373–393.

38 Zee, L., and Sternberg, E., "Ordinary and Strong Ellipticity in the Equilibrium Theory of Incompressible Hyperelastic Solids," Technical Report No. 51 (N00014-75-C-0196), Calif. Inst. Tech., July 1982.

39 Wu, C. H., "Large Finite Strain Membrane Problems," *Quart. Appl. Math.*, Vol. 36, 1979, pp. 347–359.

40 Fenner, W. J., and Wu, C. H., "Large Plane to Surface Deformations of Membranes With Inclusions," ASME JOURNAL OF APPLIED MECHANICS, Vol. 48, 1981, pp. 357–360.

41 Feng, W. W., and Huang, P., "On the General Contact Problem of an Inflated Nonlinear Plane Membrane," *Int. J. Solids Struct.*, Vol. 11, 1975, pp. 437–448.

42 Callegari, A. J., and Keller, J. B., "Contact of Inflated Membranes With Rigid Surfaces," ASME JOURNAL OF APPLIED MECHANICS, Vol. 41, 1974, pp. 189–191.

43 Wu, C. H., and Canfield, T. R., "Wrinkling in Finite Plane-Stress Theory," *Quart. Appl. Math.*, Vol. 39, 1981, pp. 179–200.

44 Zak, M., "Statics of Wrinkling Films," *J. Elasticity*, Vol. 12, 1982, pp. 51–63.

45 Yin, W. L., "Non-Uniform Inflation of a Cylindrical Elastic Membrane and Direct Determination of the Strain Energy Function," *J. Elasticity*, Vol. 7, 1977, pp. 265–282.

46 Naghdi, P. M., and Tang, P. Y., "Large Deformation Possible in Every Isotropic Elastic Membrane," *Phil. Trans. Roy. Soc. Lond.*, Vol. *A*287, 1977, pp. 145–187.

47 Yin, W. L., "Universal Solutions for General and Area-Preserving Isotropic Elastic Membranes," *Arch. Rat. Mech. Anal.*, Vol. 77, 1981, pp. 37–46.

48 Selvadurai, A. P. S., "Second-Order Elastic Effects in the Torsion of a Spherical Annular Region," *Int. J. Eng. Sci.*, Vol. 12, 1974, pp. 295–310.

49 Carlson, D. E., and Shield, R. T., "Inverse Deformation Results for Elastic Materials," *J. Appl. Math. Phys. (ZAMP)*, Vol. 20, 1969, pp. 261–263.

50 Shield, R. T., "Inverse Deformation Results in Finite Elasticity," *J. Appl. Math. Phys. (ZAMP)*, Vol. 18, 1967, pp. 490–500.

51 Carlson, D. E., and Shield, R. T., "Second and Higher Order Effects in a Class of Problems in Plane Finite Elasticity," *Arch. Rat. Mech. Anal.*, Vol. 19, 1965, pp. 189–214.

52 Chan, C., and Carlson, D. E., "Second-order Incompressible Elastic Torsion," *Int. J. Eng. Sci.*, Vol. 8, 1970, pp. 415–430.

53 Hill, J. M., "Notes on a Paper by C. Chan and D. E. Carlson, Second-order Incompressible Elastic Torsion," *Int. J. Eng. Sci.*, Vol. 11, 1973, pp. 331–336.

54 Choi, I., and Shield, R. T., "Second-Order Effects in Problems for a Class of Elastic Materials," *J. Appl. Math. Phys. (ZAMP)*, Vol. 32, 1981, pp. 361–381.

55 Gladwell, G. M. L., *Contact Problems in the Classical Theory of Elasticity*, Sitjhoff & Noordhoff, Alphen aan den Rijn, 1980.

56 Ziegler, H., "Linear Elastic Stability," *J. Appl. Math. Phys. (ZAMP)*, Vol. 4, 1953, pp. 1–50.

57 Shield, R. T., and Green, A. E., "On Certain Methods in the Stability Theory of Continuous Systems," *Arch. Rat Mech. Anal.*, Vol. 12, 1963, pp. 354–360.

58 Shield, R. T., "On the Stability of Linear Continuous Systems," *J. Appl. Math. Phys. (ZAMP)*, Vol. 16, 1965, pp. 649–686.

59 Caughey, T. K., and Shield, R. T., "Instability and the Energy Criterion for Continuous Systems," *J. Appl. Math. Phys. (ZAMP)*, Vol. 19, 1968, pp. 485–492.

60 Thomson, W., and Tait, P. G., *Treatise on Natural Philosophy*, Cambridge Univ., 1879. Rep. by Dover, New York, 1962.

61 Koiter, W. T., "On the Instability of Equilibrium in the Absence of a Minimum of the Potential Energy," *Proc. K. Ned. Akad. Wet.*, Vol. *B*68, 1965, pp. 107–113. "The Energy Criterion of Stability for Continuous Elastic Bodies I, II," ibid, pp. 178–202.

62 Koiter, W. T., "The Concept of Stability of Equilibrium for Continuous Bodies," *Proc. K. Ned. Akad. Wet.*, Vol. *B*66, 1963, pp. 173–177.

63 Gilbert, J. E., and Knops, R. J., "Stability of General Systems," *Arch. Rat. Mech. Anal.*, Vol. 25, 1967, pp. 271–284.

64 Naghdi, P. M., and Trapp, J. A., "On the General Theory of Stability for Elastic Bodies," *Arch. Rat. Mech. Anal.*, Vol. 51, 1973, pp. 165–191.

65 Woo, T. C., and Shield, R. T., "Fundamental Solutions for Small Deformations Superposed on Finite Biaxial Extension of an Elastic Body," *Arch. Rat. Mech. Anal.*, Vol. 9, 1962, pp. 196–224.

Downloaded 02 May 2010 to 171.66.16.250. Redistribution subject to ASME license or copyright; see http://www.asme.org/terms/Terms_Use.cfm

66 Usmani, S. A., and Beatty, M. F., "On the Surface Instability of a Highly Elastic Half-Space," *J. Elasticity*, Vol. 4, 1974, pp. 249–263.

67 Fosdick, R. L., and Shield, R. T., "Small Bending of a Circular Bar Superposed on Finite Extension or Compression," *Arch. Rat. Mech. Anal.*, Vol. 12, 1963, pp. 223–248.

68 Beatty, M. F., and Hook, D. E., "Some Experiments on the Stability of Circular Rubber Bars Under End Thrust," *Int. J. Solids Structures*, Vol. 4, 1968, pp. 623–635.

69 Wilkes, E. W., "On the Stability of a Circular Tube Under End Thrust," *Quart. J. Mech. Appl. Math.*, Vol. 8, 1955, pp. 88–100.

70 Vaughan, H., "Axisymmetric and Asymmetric Instabilities in Elastic Solid Cylinders Under Finite Axial Strain," *J. Appl. Math. Phys. (ZAMP)*, Vol. 22, 1971, pp. 865–875.

71 Green, A. E., and Spencer, A. J. M., "The Stability of a Circular Cylinder Under Finite Extension and Torsion," *J. Math, Phys.*, Vol. 37, 1958, pp. 316–338.

72 Sawyers, K. N., and Rivlin, R. S., "Stability of a Thick Elastic Plate Under Thrust," *J. Elasticity*, Vol. 12, 1982, pp. 101–125.

73 Chen, L. Y., and Shield R. T., "The Stability of a Finitely Inflated Cylindrical Elastic Membrane under Axial Compression," *J. Elasticity*, Vol. 5, 1975, pp. 363–377.

74 Fourney, W. L., and Stern, M., "Further Results on the Stability of a Finitely Deformed Thin Cylindrical Shell," *Int. J. Eng. Sci.*, Vol. 10, 1972, pp. 613–622.

75 Hill, J. M., "Closed Form Solutions for Small Deformations Superimposed Upon the Simultaneous Inflation and Extension of a Cylindrical Tube," *J. Elasticity*, Vol. 6, 1976, pp. 113–124. "Closed Form Solutions for Small Deformations Superimposed Upon the Symmetrical Expansion of a Spherical Shell, ibid, pp. 125–136.

76 Haughton, D. M., and Ogden, R. W., "Bifurcation of Inflated Circular Cylinders and Elastic Material Under Axial Loading-II. Exact Theory for Thick-walled Tubes," *J. Mech. Phys. Solids*, Vol. 27, 1979, pp. 489–512. "On the Incremental Equations in Non-linear Elasticity-II. Bifurcation of Pressurized Spherical Shells," ibid, Vol. 26, 1978, pp. 111–138.

77 Feodos'ev, V. I., "On the Equilibrium Shape of Spherical Rubber Membranes Under Internal Pressure," *Prikl. Mat. Mekh.*, Vol. 32, 1968, pp. 339–344.

78 Chen, L. Y., and Shield, R. T., "On the Vibration and Stability of Finitely Inflated Spherical and Cylindrical Elastic Membranes," T. & A.M. Report No. 397 (UILU-ENG 74 6019), University of Illinois at Urbana-Champaign, Dec. 1974.

79 Zhong-Heng, G., "Problem of Spherical Membrane in the Theory of Large Deformation," *Arch. Mech. Stosow.*, Vol. 14, 1962, pp. 921–935.

80 Alexander, H., "Tensile Instability of Initially Spherical Balloons," *Int. J. Eng. Sci.*, Vol. 9, 1971, pp. 151–162.

Downloaded 02 May 2010 to 171.66.16.250. Redistribution subject to ASME license or copyright; see http://www.asme.org/terms/Terms_Use.cfm

R. I. Tanner
Professor of Mechanical Engineering,
University of Sydney,
Sydney, N.S.W. 2006,
Australia
Mem. ASME

Recent Progress in Rheology

Progress in fluid rheology is surveyed, including simple flows useful for stress measurements. The question of how to describe more complex flows is discussed in the light of knowledge of fluid microstructure, and several constitutive relations are exhibited. Finally, the need for numerical solutions to problems is emphasized.

1 Rheology and Continuum Mechanics

All real materials possess a microstructure at the molecular, crystal, or higher level. In applied mechanics, we are often anxious to avoid describing the material at such levels because the large-scale phenomena of interest usually involve the average behavior of a very large number of microstructural units. Thus it is often convenient to work with an idealized *continuum* model of the material, whose microstructure is not specified.

Continuum mechanics is the mathematical study of the response of such ideal bodies to applied forces and deformations. The early success of the theory of (small-strain) elasticity, which is largely a mathematical construction, raised considerable expectations from the methods of continuum mechanics. The only physical inputs to small-strain elasticity theory are the ideas in Hooke's law and the observation that most metals undergo only a fraction of a percentile strain before yielding. In fluid mechanics the success was almost as complete. In the isothermal case, only the Newtonian viscous law and a connection between density and pressure are needed as experimental inputs to the highly precise Navier-Stokes equations. These two examples are atypical and most other continuum mechanics descriptions cannot match the simplicity and elegance of these linear models. Thus the pure continuum approach becomes less and less useful as the complexity of material response increases. The response of polymer solutions and polymer melts is very complex and recent methods have tended to combine continuum mechanics with ideas obtained by thinking about the microstructure of the bodies under study. We shall term this study field, *rheology*.

Continuum mechanics principles were known in the nineteenth century: the conservation of mass, the stress principle, the conservation of linear momentum, and energy conservation are universally applicable. The balance of angular momentum yields, under certain constitutive assumptions, the symmetry of the stress tensor. We shall make the assumption that the stress tensor is symmetric here; it is not difficult to find examples of real materials (e.g., liquid crystals [1]) where the stress tensor is not symmetric. The kinematic analysis of bodies was also developed in the nineteenth century. Recently other additional principles or axioms have been announced [2] but often reliance on them is risky, except when some knowledge of the material microstructure leads one to believe that the particular axiom or principle is really relevant to the chunk of material being examined. When the microstructure is known, alternative procedures based on its analysis often give critical guidance in developing mechanical constitutive laws connecting stress and kinematics, as will be discussed in the following.

The term rheology was invented by E. C. Bingham in 1929; the original definition excluded classical elasticity and fluid mechanics. The definition thus makes rheology appear as a subset of continuum mechanics; I do not believe that this was the original intention of the founders of the science, they merely intended to focus attention away from the classical into new areas. Thus, if we ignore the specialization in materials, then continuum mechanics *is* rheology. Certainly rheologists use (or should use!) all the principles just mentioned, so the difference between the groups must be sought in attitudes and results rather than initial aims, and in particular in the methods used for the development of constitutive equations.

The emergence of rheology as a separate field occurred only in the 1920s when the mechanical behavior of important industrial materials like rubber, plastics, clays, paints, and many biological fluids began to attract increasing attention in the fields of physics, mechanics, and mathematics, in addition to the traditional interest from colloid chemists. The formation of the Society of Rheology in 1929 marks the start of international organizations in this newly recognized field. Thus the beginnings of rheology nearly coincide with the founding of this journal. The present paper seeks to show what recent progress has been made in the solution of simple flow problems, the development of constitutive models for more complex flows, and the implementation of these models for practical use using numerical methods.

2 Some Rheological Phenomena

It is well known that liquids with complex structure, such as macromolecular fluids, soap solutions, and suspensions behave in unexpected ways and are not described by the Navier-Stokes equations, which are for Newtonian liquids. The following describes some of the "non-Newtonian" effects which have been observed:

(*a*) Shear-Rate-Dependent Viscosity.
Most of these fluids display "shear thinning," that is

Contributed by the Applied Mechanics Division for publication in the JOURNAL OF APPLIED MECHANICS.
Discussion on this paper should be addressed to the Editorial Department, ASME, United Engineering Center, 345 East 47th Street, New York, N.Y. 10017, and will be accepted until two months after final publication of the paper itself in the JOURNAL OF APPLIED MECHANICS. Manuscript received by ASME Applied Mechanics Division, February, 1983.

Copyright © 1983 by ASME
Downloaded 02 May 2010 to 171.66.16.250. Redistribution subject to ASME license or copyright; see http://www.asme.org/terms/Terms_Use.cfm

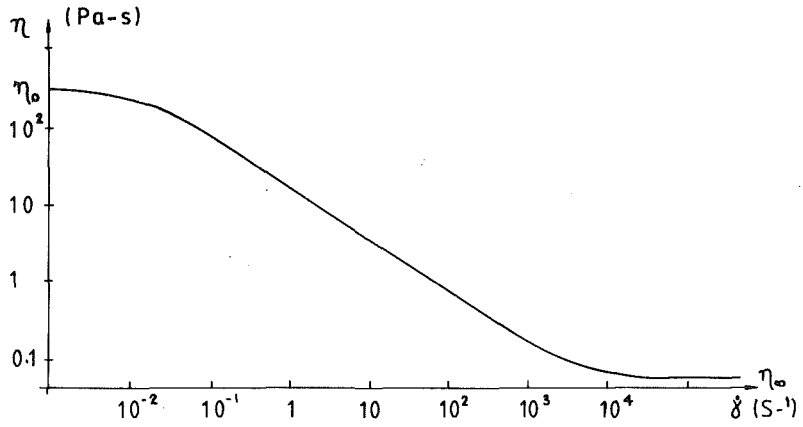


Fig. 1 A typical complete viscosity-shearing rate ($\eta - \gamma$) curve showing the zero shearing rate viscosity (η_0), the viscosity at very large shear (η_∞), and the intermediate "power-law" region

the viscosity decreases with increasing shear rate, sometimes reaching 10^{-3} or 10^{-4} of the zero-shear-rate viscosity. This factor is often the most important property for engineers (Fig. 1).

(*b*) **Normal-Stress Effects in Steady Shear Flows.** These fluids usually exhibit a number of second-order effects associated with the inequality of normal stresses in steady shear flow and related simple flows. These include: the "Weissenberg effect," in which a macromolecular fluid climbs up a rotating rod (see, e.g., Lodge [3], p. 232); the reversal of direction of the secondary-flow pattern when a sphere rotates in a liquid in a beaker; and the bulging of the surface of a liquid as it flows down a trough [4].

(*c*) **Transient Responses in Unsteady Shear Flows.** A wide variety of small-stain experiments, such as "dynamic testing" (i.e., oscillatory flows), stress relaxation, creep, and recoil have been used to obtain information on mechanical properties. In addition, some large-amplitude time-dependent experiments have also been performed: these include recoil ([3], p. 236, et seq.); shear flow with superposed oscillatory motion; the overshoot in stress at the starting up of a shear flow [5].

(*d*) **Other Phenomena.** The preceding examples involve shearing flows. In other flows there are additional phenomena, such as: swelling of extrudates issuing from a die [3]; development of a toroidal vortex in the inlet flow to a die; the "Uebler effect," which is the abrupt stopping of large bubbles in the accelerating velocity field where the fluid flows from a reservoir into a tube; the tubeless-siphon effect, in which a siphon continues to operate even though the upstream end has been withdrawn from the fluid; the unsteady-state behavior in elongational flow, in which apparently a steady-state elongational flow cannot be attained; "melt fracture" in which very irregular extrudates are produced; and the solid rubber-like behavior of polymeric liquids subjected to high-speed impact tests.

The literature references cited in the foregoing are generally books or review articles in which photographs are given or extensive data compilations are presented. The reader should especially consult the recent work of Bird, et al. [5].

To describe these various effects the Newtonian linear stress-strain rate relation must be replaced by another constitutive equation; alternative, less satisfactory names are "rheological equation of state," or "non-Newtonian model." The earliest attempts at writing such equations involved simple empiricism to describe some very limited class of flow phenomena; these included the "generalized Newtonian fluids" describing shear-thinning (Fig. 1), and the "linear viscoelastic models" describing transient phenomena in systems that undergo only very small strains, leading to the well-known integral form [5]. These are not adequate to describe most of the phenomena listed in the foregoing. Next, attempts were made to devise empirical "nonlinear viscoelastic models" which could describe and interrelate, at least qualitatively, a wide variety of phenomena. "Memory integral expansions" then were evolved, from which equations for special flows can be obtained as limiting cases. Finally, equations that take some account of microstructure have become popular. Generally speaking, the use of the constitutive relations in hydrodynamic problem solving has, not surprisingly, been (roughly) inversely proportional to the complexity of the constitutive relation. The result has been that for complex flows one usually used a generalized Newtonian fluid or some very simple nonlinear viscoelastic model, while elaborate equations were reserved for steady shearing and other simple flow patterns. Fortunately, with the development of advanced computational capabilities, this problem is now being solved.

Many useful results for *restricted flow classes* can be found without resort to a formal approach to constitutive equations. We discuss these next, together with relevant experimental work. Then we show how the older approaches to constructing constitutive equations approximate to these basic experimental results. Finally, attempts to seek the form of the response for general flows using microstructural arguments are outlined [6].

The discerning reader will note the absence of discussion on heat transfer, thermal effects and turbulence, and stability. Turbulence is judged to be of less importance in rheology than in classical fluid mechanics because often the viscosities of the fluids are high, velocities and length scales are low, and hence Reynolds numbers are low. It does present a significant challenge, however, and must be listed as a current research topic. Stability theory for non-Newtonian fluids is still developing, but slowly.

Thermal effects and heat transfer are of great importance in the practical application of rheology [5]. Generally speaking thermal effects are of quantitative importance and do not often lead to new phenomena which must be "explained." It is not really possible to make effective predictions in nonisothermal situations without effective computational ability, and hence we have preferred to leave this topic aside until there are more achievements to report and more space in which to report them.

Downloaded 02 May 2010 to 171.66.16.250. Redistribution subject to ASME license or copyright; see http://www.asme.org/terms/Terms_Use.cfm

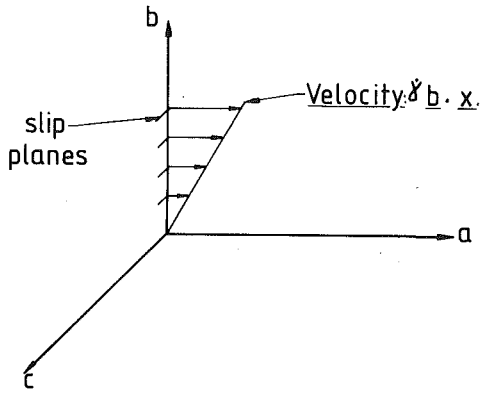


Fig. 2(*a*) Shear axes in simple shearing

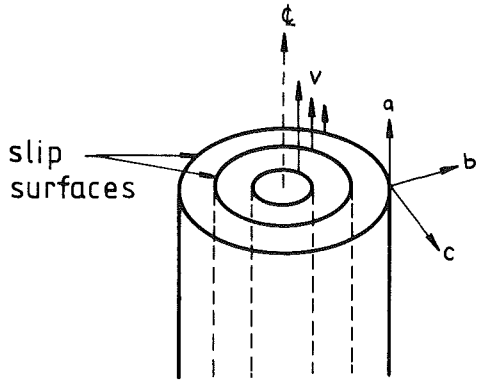


Fig. 2(*b*) Parallel flow

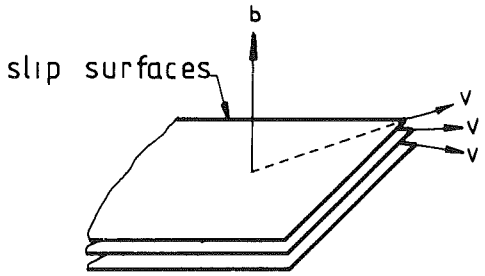


Fig. 2(*c*) Skew rectilinear flow

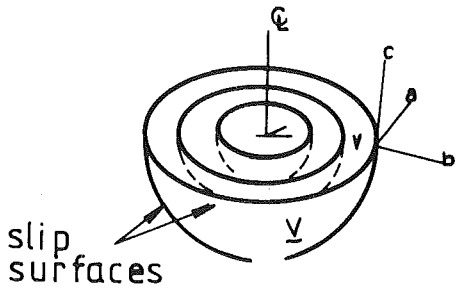


Fig. 2(*d*) Circular flow

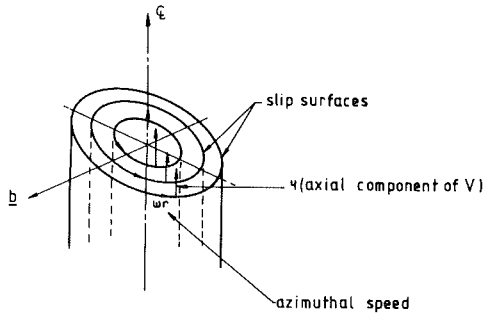


Fig. 2(*e*) Helical flow

Fig. 2 Kinematic details for viscometric flows

3 Viscometric and Other Simple Flows

In this section we consider some special, but very common, class of flows applicable to a very wide group of liquids. This approach contrasts with that used in the classical theory of linearly viscous (Newtonian) fluids, in which a special kind of fluid description is used to examine a very wide class of flow fields. We first discuss those motions called viscometric, which are motions substantially equivalent to steady simple shearing, such as Poiseuille and Couette flows, but we do not make any very restrictive prior assumption about the nature of the relation between stress and deformation in the fluids considered. We then consider unsteady shearing flows, again without much restriction on fluid response, and then finally a class of simple elongational flows, in which the stress system is easily deduced from symmetry. The fluids are supposed to be incompressible, and no thermal effects are considered. The viscometric motions discussed here can be visualized in terms of a sheaf of inextensible material surfaces in relative sliding motion, but the elongational flows are not so readily defined in geometrical terms. In Section 3.1 we give the kinematical definition of viscometric motions and describe the flows of this kind most frequently encountered in applications. The stress response of viscoelastic liquids in such motions is relatively simple because the shear rate at each particle is constant in time. We also describe some of the flows used in viscosity and normal stress measurements, and also mention other exact solutions of the dynamical equations which may be useful for such measurements. A review with a similar viewpoint to the present is given by Pipkin and Tanner [4].

3.1 Kinematics of Viscometric Flows. In viscometric fluid motions, each fluid element is undergoing a steady simple shearing motion, plus possibly a rigid translation and rotation. The primary example of such a motion is steady simple shearing itself, in which the velocity field has the form

$$\mathbf{v} = \dot{\gamma}(\mathbf{b}\cdot\mathbf{x})\mathbf{a}. \tag{1}$$

Here **a** and **b** are orthogonal unit vectors and $\dot{\gamma}$ is a constant, the shear rate. In such a motion, the fluid in a plane $\mathbf{b}\cdot\mathbf{x}$ = constant forms a material surface that is called a slip surface. Each slip surface moves as a rigid body, and the motion can be visualized as the relative sliding motion of a sheaf of slip surfaces. The vector **a** is tangential to the slip surface and represents the direction of relative sliding motion, while **b** is the direction normal to the slip surface. It is convenient to define a third unit vector **c**, orthogonal to **a** and **b** and thus tangential to the slip surfaces. We call **a**, **b**, and **c** the shear axes (Fig. 2(*a*)). The velocity field (1) is easily shown to be divergence-free, and hence it is possible in an incompressible fluid.

All viscometric flows can be visualized as the relative sliding motion of a sheaf of inextensible material surfaces [4]. In the examples most useful in practice, the slip surfaces move steadily as rigid bodies, and each slip surface occupies the same locus in space at all times. It is known from kinematical studies that the motion of two rigid bodies contacting over an area (a "lower pair") gives rise only to relative motion between the bodies described by sliding, turning, and screw actions. We can use this information in thinking about viscometric motions with rigid slip surfaces. In these kinds of viscometric motion the slip surfaces must be general cylinders, surfaces of revolution, or helicoids [4]. We can list the main categories of these restricted viscometric flows without

Downloaded 02 May 2010 to 171.66.16.250. Redistribution subject to ASME license or copyright; see http://www.asme.org/terms/Terms_Use.cfm

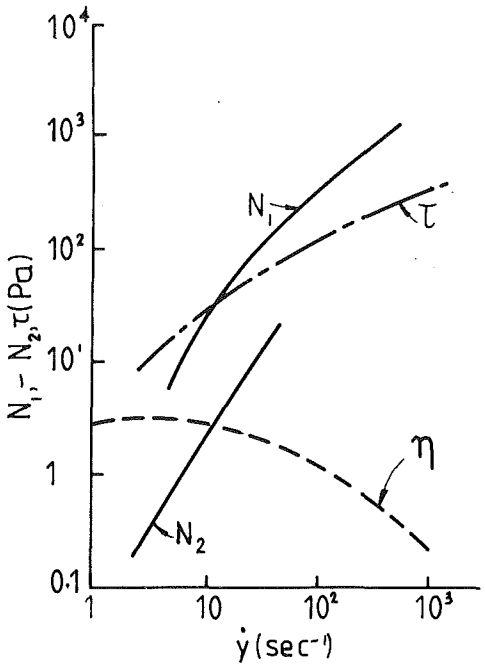


Fig. 3 The viscometric functions τ (shear stress), N_1 (first normal stress difference), $-N_2$ (magnitude of second normal stress difference) as functions of (steady) shearing rate ($\dot{\gamma}$) for a polyisobutyine solution. The viscosity ($\eta \equiv \tau/\dot{\gamma}$) is also shown.

considering the dynamical admissibility of any of them; the incompressibility condition is always satisfied.

Examples include steady parallel flows (Fig. 2(*b*)), skew rectilinear flows (Fig. 2(*c*)), steady circular flows (Fig. 2(*d*)), helical flows (Fig. 2(*e*)) and helicoidal flows. In the helical flow the streamlines have a rise per turn which is constant over each cylinder but may vary from one cylinder to another. If all helices have the same rise per turn, the slip surfaces need not be cylindrical but can be general helicoids. In these helicoidal flows, the velocity field has the form

$$\mathbf{v} = (r\mathbf{i}_r + c\mathbf{i}_z)\,\omega(r, z - c\theta) \tag{2}$$

The shear direction **a** is the same as the direction of motion, and the normal direction **b** is parallel to $\nabla\omega$, orthogonal to the helicoids ω = constant.

The preceding examples are of the kind that Lodge [3] calls steady curvilinear shearing motions. These examples include all viscometric flows that have so far proved to be of any practical interest, but they do not by any means exhaust the kinematical possibilities. For further discussion see reference [4].

3.2 Stresses in Steady Viscometric Flows. When a viscoelastic liquid is brought from rest into a state of steady shearing motion, the stress is time-dependent because of the transient effects of the past history of deformation. However, if the fluid is sheared at a constant rate, these transients die out in the course of time, and the shearing stress approaches a steady-state value that depends only on the shear rate. For the simplest special case, with a velocity field of the form $\underline{v} = \dot{\gamma}y\mathbf{i}$, the zx and zy-components of stress must be zero by symemtry, and the shearing stress σ_{xy} is some odd function of the shear rate,

$$\sigma_{xy} = \dot{\gamma}\eta(\dot{\gamma}), \quad \eta(-\dot{\gamma}) = \eta(\dot{\gamma}) \tag{3}$$

In drawing conclusions from symmetry as we have done here, we implicitly assume that the fluid is isotropic, so that any directional properties it may have are induced by the flow itself. The ratio $\sigma_{xy}/\dot{\gamma} = \eta$ is the viscosity function, or simply, the viscosity. In some older treatments it is called the apparent

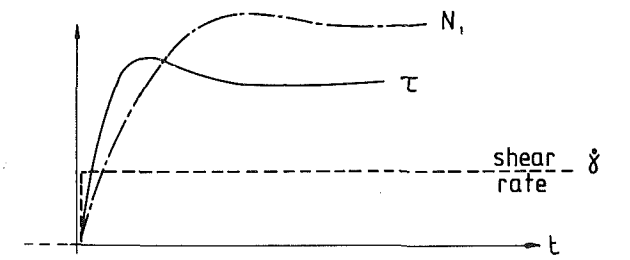


Fig. 4(*a*) Sudden imposition of strain-rate. The shear stress and normal stress difference curves may overshoot as shown at higher shear rates; at low enough shear rates no overshoot occurs and the curves rise smoothly to their steady-state values

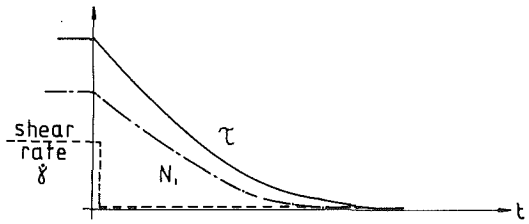


Fig. 4(*b*) Cessation of shearing. Usually N_1 vanishes faster than the shear stress. No undershoot has been observed.

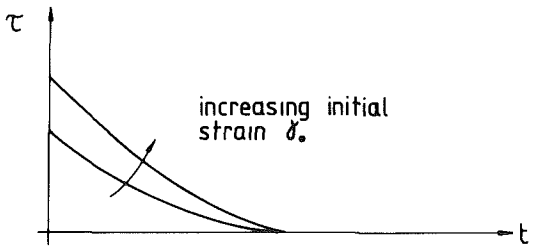


Fig. 4(*c*) Step of shear; here $\dot{\gamma}$ is an impulse function. The curves are proportional to the linear relaxation function $G(t)$ for small γ; at higher strains the function has a similar, but not identical shape, and the scale factor is not linear in γ.

Fig. 4

viscosity, but we shall not use this term. The normal stress components σ_{xx}, σ_{yy}, and σ_{zz} are even functions of the shear rate by a symmetry argument; reversal of shearing cannot affect these components. Consequently, the differences between these components must be zero in any theory depending linearly on shear rate; this does not apply to viscoelastic liquids. These symmetry arguments for deducing the form of the stress field in shear flows are due to Weissenberg [4].

The two independent differences,

$$\sigma_{xx} - \sigma_{yy} = N_1(\dot{\gamma}) \quad \text{and} \quad \sigma_{yy} - \sigma_{zz} = N_2(\dot{\gamma}) \tag{4}$$

are functions of the shear rate that vanish only when $\dot{\gamma} = 0$, so far as is known. We call these two functions of the shear rate the first and second normal stress differences. Under the classical conception of a fluid as a material that cannot indefinitely remain at rest when under the action of even a very small shearing stress, there can be no shearing stress on any surface element in the case $\dot{\gamma} = 0$, since here the statement that $\dot{\gamma}$ is zero means that the fluid has been at rest for so long that all transients have disappeared. This implies not only that σ_{xy} must vanish, but also that all normal stress components must be equal when $\dot{\gamma} = 0$. It is often convenient to make this explicit by writing

$$N_1 = \dot{\gamma}^2\nu_1(\dot{\gamma}) \quad \text{and} \quad N_2 = \dot{\gamma}^2\nu_2(\dot{\gamma}) \tag{5}$$

The functions ν_1 and ν_2 are even functions of the shear rate. We call them the first and second normal stress coefficients.

Downloaded 02 May 2010 to 171.66.16.250. Redistribution subject to ASME license or copyright; see http://www.asme.org/terms/Terms_Use.cfm

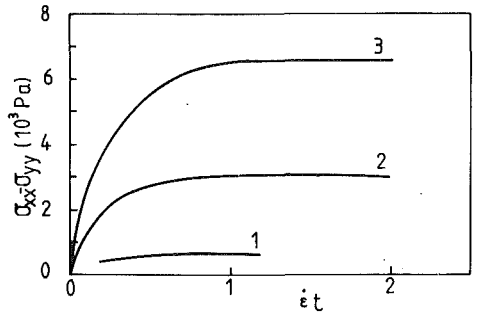


Fig. 5(*a*) Response of a rubbery liquid to a constant rate of elongation tensile test. Curves 1, 2, 3, were taken at elongation rates ($\dot{\epsilon}$) of 2.9 × 10^{-4}, 1.5 × 10^{-3}, and 2.8 × 10^{-3} s^{-1}, respectively. A steady stress state was reached in all cases.

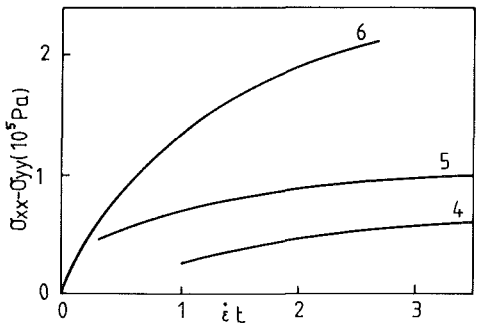


Fig. 5(*b*) Same sample as Fig. 6(*a*) at higher elongation rates, respectively, 2.5 × 10^{-2}, 4.5 × 10^{-2}, and 0.135 s^{-1}. The elongational stress difference has not reached a steady state.

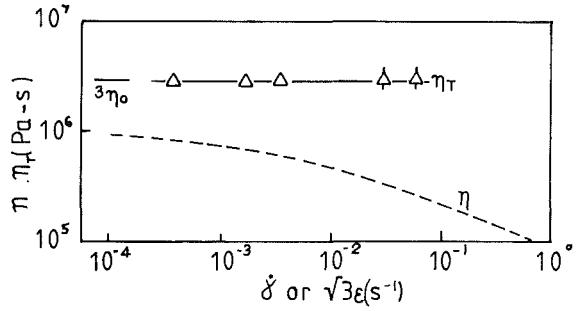


Fig. 5(c) Steady viscosities in elongation (η_T) and shear (η_S) for the rubber sample. The abscissa is proportional to the square root of twice the second invariant of rate-of-deformation tensor and equals $\dot{\gamma}$ in simple shearing. Note the large ratio η_T/η_S even at modest strain-rates. (Data of Stevenson, J. F., *A.I.Ch.E.J.*, Vol. 18, 1972, p. 540).

Fig. 5

3.3 Qualitative Behavior of the Viscometric Functions for Polymer Solutions. Figure 3 (full lines), shows the three viscometric functions for a 6.8 percent solution of a polyisobutylene (Oppanol B-100) in cetane at 24°C. The viscosity function typically decreases as the shear rate increases, from a limiting value η_0 at zero shear rate to a much lower value η_∞ in the limit of high shear rates. In Fig. 3, in contrast to Fig. 1 the region of η_∞ was not reached experimentally. An especially simple and useful form is the power-law approximation $\eta = k\dot{\gamma}^{n-1}$, with $n-1$ the slope of a doubly logarithmic plot (Fig. 1). This kind of approximation is useful for the region of intermediate shear rates in which the viscosity is dropping from η_0 toward η_∞. For shear-thinning (pseudoplastic) fluids the power n is less than unity. For any fluid, n must be greater than zero to satisfy the stability requirement that the shearing stress increases with the shear rate; occasionally (rheopectic) fluids have an n value greater than unity.

The first normal stress difference is positive, and the coefficient ν_1 has at least roughly the same form as η. The slope in the power-law region is generally greater than for η, and no limiting value at high shear rates has ever been reached to the author's knowledge. Some theoretical models based on microstructural ideas indicate that $\nu_1 \to 0$ as $\dot{\gamma} \to \infty$. The second normal stress difference is negative, according to the best available evidence. It appears that $-\nu_2$ is generally much smaller than ν_1, up to around 20 percent of ν_1. Partly for this reason, ν_2 is more difficult to measure than ν_1, and less is known about the form of this function. Weissenberg's hypothesis that $N_2 = 0$ is not correct, but for some purposes it is qualitatively adequate. In broadest terms, the effect of normal stress differences is that there is an extra tension N_1 in the direction of shearing, and this extra tension is not small.

3.4 Stress Fields. We are only considering situations in which the fluid can be treated as incompressible. The pressure is then a reaction to the constraint of no volume change, and it cannot be specified directly as a function of the shear rate. Instead, the momentum equation and the boundary conditions are used to determine the pressure required to enforce the constraint. Both because of this arbitrariness and because normal stresses in different directions are not equal, the term "pressure" must be used with great caution. In steady simple shearing motion, with $\mathbf{v} = \dot{\gamma}y\mathbf{i}$, the shear axes **a**, **b**, and **c** correspond to the Cartesian unit vectors **i**, **j**, and **k**. It is convenient to write the stress in dyadic notion as

$$\sigma = -p\mathbf{I} + \dot{\gamma}\eta(\mathbf{ab} + \mathbf{ba}) + \dot{\gamma}^2(\nu_1 + \nu_2)\mathbf{aa} + \dot{\gamma}^2\nu_2\mathbf{bb} \qquad (6)$$

In this case the pressure p represents the normal compressive force per unit area in the neutral direction, $-\mathbf{c}\cdot\sigma\cdot\mathbf{c}$.

In any viscometric flow, each fluid element is performing a steady simple shearing motion. Consequently, the stress in each element is given by an expression of the same form as that derived for steady simple shearing, with the same response functions η, ν_1, and ν_2, but with shear axes and shear rate appropriate to the particle considered. For the special flows considered in Section 3.1 we can immediately write expressions for the stress by substituting the expressions for the shear axes and shear rate found in those sections into equation (6) [4]. It remains to consider whether these flows are dynamically possible.

For the experimental determination of the viscometric functions η, ν_1, and ν_2 for a particular fluid, it is desirable to be able to set up experiments in which the velocity field is completely or at least partly known from the outset. The analysis of experimental data is then not complicated by the simultaneous determination of an unknown velocity field. A few specific velocity fields have such a high degree of symmetry that they satisfy the momentum equation exactly, or with neglect of inertia, no matter what forms the viscometric functions may take. We call such flows completely controllable. All such flows are known [4]. Homogeneous steady simple shearing, with a velocity field $\mathbf{v} = \dot{\gamma}y\mathbf{i}$, is a completely controllable flow. Since there is no acceleration, the momentum equations reduce to equilibrium equations. If the pressure p is uniform, then all stress components are independent of position, and the equilibrium equations are satisfied identically, no matter what forms the viscometric functions may have. Unfortunately simple shearing, because of edge effects, is in practice difficult to realize. Steady shearing between tilted plates [4] is also a completely controllable flow in which the shear rate varies with position.

One can write a complete list of completely controllable flows when inertia is present; it is a small list [4]. Since the Reynolds number is often extremely low in experiments on viscoelastic fluids, neglect of inertia is a good approximation, and we find there are two new kinds of flows that are controllable if inertia is neglected. One is an intrinsically unsteady motion with slip surfaces that curl up which appears to have

Downloaded 02 May 2010 to 171.66.16.250. Redistribution subject to ASME license or copyright; see http://www.asme.org/terms/Terms_Use.cfm

no experimental value. The other is the class of helicoidal flows with right helicoidal slip surfaces; the torsional flow is a special case of practical interest.

There are also partially controlled flows (e.g., Poiseuille flow) in which the main features of the flow are known, but which are not independent of the viscosity function. By using viscometric flows that are well understood kinematically, we can find η, ν_1, and ν_2 experimentally. Then we can compute stress and velocity fields in any other viscometric flow if we wish. We now turn to other flow classes.

3.5 Unsteady Shearing Flows. When one considers the kinematic aspects of the viscometric flows discussed in the foregong, there is no reason to restrict the motion to steady shearing rates. For example, it is perfectly easy to conceive an unsteady simple shearing motion in which $\dot{\gamma}$ is a function of time; the flow still continues to be described by the relative sliding of slip surfaces. If we confine our attention to the case of a sample that has been at rest long enough before testing so that stresses due to any previous motions have decayed, then the same stress symmetry occurs in both steady and unsteady shearing.

For inertialess unsteady shearing, the response functions $\tau(t)$, $N_1(t)$ and $N_2(t)$ define the situation completely for a given $\dot{\gamma}(t)$. Of the infinite number of possibilities for $\dot{\gamma}(t)$, the following are the main ones which have been tried experimentally [5].

(*a*) Oscillatory shear $\dot{\gamma} = \omega\hat{\gamma} \sin \omega t$

(*b*) Sudden imposition of shearing, $\begin{cases} \dot{\gamma}=0 & t\leqslant 0 \\ \dot{\gamma}=\dot{\gamma}_0 & t>0 \end{cases}$

(*c*) Cessation of shear (or stress relaxation) $\begin{cases} \dot{\gamma}=\dot{\gamma} & t\leqslant 0 \\ \dot{\gamma}=0 & t>0 \end{cases}$

(*d*) Step displacement of *shear*. If γ, a shear strain, is suddenly applied (or removed) at a certain time, then $\dot{\gamma}(t)$ is formally an impulse or delta function.

(*e*) Combinations of a steady shear with the foregoing.

Clearly in (*e*) the steady shear axes can be oriented parallel to the unsteady flow axes, or in some other direction. Most combined flows use the same axes but some experiments have superposed an oscillatory shear at right angles to a simple shear, thus producing an unsteady version of the skew motion shown in Fig. 2(*c*). Results for $\tau(t)$ and $N_1(t)$ are available, but none for $N_2(t)$. In addition to the preceding flows where $\dot{\gamma}(t)$ is imposed, it is also possible to perform creep and constrained elastic recovery tests where the shear stresses are imposed and the response is $\dot{\gamma}(t)$. Thus we can add to the preceding list

(*f*) Creep tests: $\begin{cases} \tau=0 & t<0 \\ \tau=\tau_0 & t\geqslant 0 \end{cases}$

(*g*) Constrained elastic recovery tests: $\begin{cases} \tau=\tau_0 & t<0 \\ \tau=0 & t\geqslant 0 \end{cases}$

Typical responses for $\tau(t)$ and $N(t)$ are shown in Figs. 4(*a*)-(*c*) for some of these tests.

3.6 Elongational Flows. Suppose that a rod of material is being extended homogeneously along its x-axis, so that each part of the rod is stressed uniformly. At each section we suppose that the rate of elongation $\partial u/\partial x$ ($\equiv \dot{\epsilon}$) is independent of x and is a function of time at most. Mass conservation and axial symmetry then demand that $\partial v/\partial y = \partial w/\partial z = -\dot{\epsilon}/2$. All shearing-stress components are zero and $\sigma_{yy} = \sigma_{zz}$, by symmetry. For an incompressible liquid the stress response is then completely defined by the dependence of $\sigma_{xx} - \sigma_{yy}$ on the rate of extension $\dot{\epsilon}$ and the time t elapsed since the stretching began:

$$\sigma_{xx} - \sigma_{yy} = \dot{\epsilon}\eta_T(\dot{\epsilon}, t) \tag{7}$$

where η_T is the stretching viscosity; generally it is a function of the rate of stretching $\dot{\epsilon}$ and time. The initial response of a polymer melt is elastic for many materials and might more appropriately be described in terms of the dependence of the stress on the strain ϵ. For this reason, the stress generally increases rapidly as time progresses during the initial stages of the motion (Fig. 5). If the rate of extension is large, this initial stage may end in fracture of the specimen. When rupture does not occur, the stretching viscosity η_T must eventually approach a limiting value, η_T ($\dot{\epsilon}$, ∞), which we will denote simply by $\eta_T(\dot{\epsilon})$. The limiting value is called the steady extensional viscosity, or Trouton viscosity; η_T has the value $3\eta_0$ for an incompressible Newtonian fluid with shear viscosity η_0.

The valuable compilation of material on elongational flows in the book by Petrie [7] should be consulted. Meissner [8] has drawn samples out to 90 times their original length and has achieved extension rates of 1 sec^{-1}.

To measure the steady-state viscosity $\eta_T(\dot{\epsilon})$, the fluid must be subjected to a constant rate of extension for so long that the stress reaches a constant value, or a constant stress for so long that the rate of extension becomes constant. All reported cases in which it is certain that a steady state was reached involve fluids of very high viscosity and rates of extension not greater than about 0.1 sec^{-1}. In this limited range, the Trouton viscosity has usually been found to be either nearly constant or, at the highest rates of extension, an increasing function of $\dot{\epsilon}$. Although these rates of extension are very low, the steady-shearing viscosities $\eta(\dot{\gamma})$ of the same materials are usually significantly lower at a shear rate $\dot{\gamma} = 0.1$ sec^{-1} than they are in the limit of zero shear rate. Consequently the ratio of the extensional viscosity to the shearing viscosity is an increasing function of the strain rate even when the Trouton viscosity is still constant, as in the data shown in Fig. 5(*c*). It is fairly easy to obtain much higher rates of extension, but the experiments in which this is done have always involved flows with a nonconstant rate of extension. Spinning experiments typically involve extension rates of the order of 0.1 to 10 sec^{-1}. Looking for a microstructural explanation of these facts, it is generally agreed that the observed increases in extensional viscosity are caused by alignment of the long-chain polymer molecules along the direction of stretching.

4 Constitutive Equation Development

The flows described in the preceding section are simple enough to be dealt with without explicit constitutive equations and they form a convenient basis for experimental work. In more complex flows it is essential to have a constitutive relation connecting the six components of the extra stress tensor τ_{ij} ($\equiv \sigma_{ij} + p\,\delta_{ij}$) with the kinematics. Two philosophies can be used:

(1) A global equation valid in principle for all flow patterns may be sought for a given substance;

(2) A more restricted equation valid only for certain types of flow field may be constructed.

A good example of the first type is the Newtonian fluid

$$\tau_{ij} = \eta\, A_{ij} = \eta\left(\frac{\partial v_i}{\partial x_j} + \frac{\partial v_j}{\partial x_i}\right) \tag{8}$$

where A_{ij} is the first Rivlin-Ericksen tensor and v_i is the velocity vector.

A restricted equation that is exact for viscometric flows is the *viscometric equation*

Downloaded 02 May 2010 to 171.66.16.250. Redistribution subject to ASME license or copyright; see http://www.asme.org/terms/Terms_Use.cfm

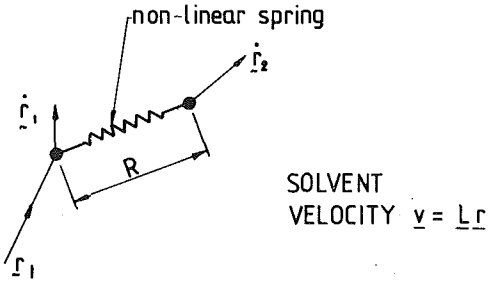


Fig. 6 The simplest "viscoelastic" microstructual model. The elastic dumbbell consists of two centers of Stokes viscous resistance (the spheres) joined by a linear (or nonlinear) law spring

$$\tau_{ij} = \eta\, A_{ij} + (\nu_1 + \nu_2) A_{ik}\, A_{kj} - \frac{1}{2}\nu_1\, B_{ij} \tag{9}$$

where

$$B_{ij} = \frac{\partial A_{ij}}{\partial t} + v_k \frac{\partial A_{ij}}{\partial x_k} + A_{ik}\frac{\partial v_k}{\partial x_j} + A_{jk}\frac{\partial v_k}{\partial x_i} \tag{10}$$

is the second Rivlin-Ericksen tensor. In (9) the positive functions η and ν_1 and the negative function ν_2 can be found from viscometric experiments and they depend on the generalized shear rate $\sqrt{\tfrac{1}{2} A_{ik} A_{ki}}$. Unfortunately (9) fails to give stability in unsteady flows and is also not accurate in elongational flows, so it can only be used confidently in flows that are close to viscometric. In this case, useful results can be found [4].

Attempts to derive approximate (global) constitutive equations without detailed physical insight into microstructure have not been very successful [2]. Several expansions in single and multiple-integral forms have not proved attractive due to the practical difficulty of finding the memory functions involved or due to the untypical response in, for example, steady elongation. Usually some restriction on strain size is needed to ensure that the response is relevant to experiment, and this is a severe restriction in flow problems. More successful have been the attempts to derive global constitutive models beginning from some reasonable conception of the fluid microstructure [6]. This active phase of rheology will now be briefly discussed.

One basically looks at (*i*) dilute solution theory, (*ii*) concentrated network theories, and (*iii*) suspension theory. The first two usually imagine a "springy" microstructure that can be extended under forces, while the suspension theory usually deals with rigid particles. We shall concentrate on the first two phases; for the latter see [9].

4 Dilute Solution Theory. In this case each element of the microstructure ("molecule") only interacts with the solvent itself. The large extensibility of the molecules is noted; they are deformed by hydrodynamic forces due to the macroscopic solvent motion and by the random input from the Brownian motion of solvent molecules. It is usual to simplify the molecular model to a simple mechanical model. Figure 6 shows the simplest possible scheme where the spring models the extensibility of the molecules and the interaction with the solvent is modeled by the two beads or points of hydrodynamic (Stokes flow) resistance. One can treat the problem as one of statistical mechanics and look for the probability function ψ for the bead separation (**R**). Usually the mass of the beads is ignored, and one works in configuration space (**R**); the possibility of using phase space ($\dot{\mathbf{R}}$, **R**) has also been explored [6]. Having determined $\psi(\mathbf{R}, t)$ for a given macroscopic flow field one can then compute the stress contribution τ_{ij} due to the molecules; the total stress is then given by

$$\sigma_{ij} = -p\,\delta_{ij} + \eta_s A_{ij} + \tau_{ij} \tag{11}$$

where η_s is the solvent viscosity. It is perhaps surprising that for a linear spring dumbbell (Fig. 6) an exact constitutive equation can be written for τ:

$$\lambda \frac{\Delta \tau_{ij}}{\Delta t} + \tau_{ij} = \eta\, A_{ij} \tag{12}$$

where the viscosity η is $\lambda\, n_0\, k\, T$; λ is a time constant, n_0 is the number of molecules per unit volume, k is Boltzmann's constant, and T is the absolute temperature.

The convected time derivative $\Delta/\Delta t$ is defined as

$$\frac{\Delta \tau_{ij}}{\Delta t} = \frac{\partial \tau_{ij}}{\partial t} + v_k \frac{\partial \tau_{ij}}{\partial x_k} - \tau_{ki}\frac{\partial v_j}{\partial x_k} - \tau_{kj}\frac{\partial v_i}{\partial x_k} \tag{13}$$

The nonlinear Maxwell model (12) can also be shown [7] to be exactly equivalent to the memory-integral relation

$$\tau_{ij}(x_i, t) = \int_{-\infty}^{t} \frac{\eta}{\lambda^2} \exp - \{(t-t')/\lambda\} \frac{\partial x_i}{\partial r_m}\frac{\partial x_j}{\partial r_m}\, dt' \tag{14}$$

where the particle that is at the place x_i in space at time t was at the place r_i at time t'. The quantity

$$\frac{\partial x_i}{\partial r_m}\frac{\partial x_j}{\partial r_m}\ (\equiv c_{ij}^{-1})$$

is a strain tensor; it is the inverse of the Cauchy-Green strain tensor [2] **C** using the present configuration **x** as a reference state. We shall denote this tensor by $\mathbf{C}^{-1}$. Apart from the substitution of this (nonlinear) strain tensor for the classical small-strain tensor, equation (14) is the well-known viscoelastic law of Boltzmann. One can compute various flows for (14) and one finds some lack of agreement with experiment – for example, a constant shearing viscosity and an extensional viscosity that becomes infinite as the rate of extension ($\dot{\epsilon}$) approaches $1/2\ \lambda$. The microstructure is too flexible and deforms too much; it permits the "spring" (Fig. 6) to become infinitely extended. We can improve the model by restricting the maximum spring length. An approximate constitutive model taking this factor into account [10] replaces the term $\lambda \Delta \tau_{ij}/\Delta t$ in (12) by

$$\lambda \frac{\Delta}{\Delta t}\left[\tau_{ij}/(1 + \tau_{ii}/3Mn_0 k\, T\right] \tag{15}$$

where M is a number (>1) which governs the ratio (maximum dumbbell length)/(mean dumbell length). This equation is fairly realistic and shows decreasing viscosity with shear rate and no singularity in extensional viscosity. One can also improve on the single exponential relaxation behavior of (14) by replacing $\eta/\lambda^2 \exp(-s/\lambda)$ by a spectrum of relaxation times:

$$\Sigma \frac{\eta_p}{\lambda_p^2} \exp(-s/\lambda_p) \tag{16}$$

or, rewriting (16) as a function $\mu(s)$ ($\equiv \mu(t-t')$) equation (14) can be replaced by

$$\tau_{ij} = \int_{-\infty}^{t} \mu(t-t')\, C_{ij}^{-1}\, dt' \tag{17}$$

Even though (17) is not very realistic it is much more realistic than the first approximation of the purely mathematical approach [2], which gives

$$\tau_{ij} = \int_{-\infty}^{t} \mu^{+}(t-t') C_{ij}\, dt' \tag{18}$$

(The second approximation involves double integrals over time and is little used). An obvious generalization of (17) and (18) is to replace **C** by some optimal strain measure, **H** say. If we assume **H** is an isotropic function of **C**, we can write, for an incompressible material [2]

Downloaded 02 May 2010 to 171.66.16.250. Redistribution subject to ASME license or copyright; see http://www.asme.org/terms/Terms_Use.cfm

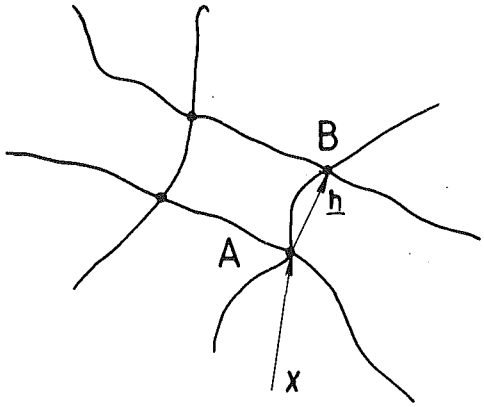


Fig. 7(*a*) Network concept for concentrated polymer solutions and melts [3]

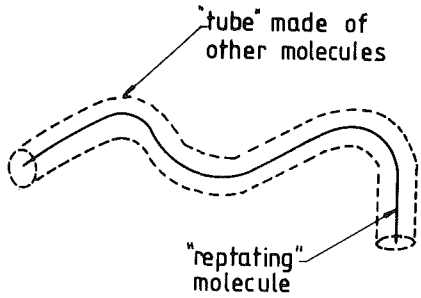


Fig. 7(*b*) Doi-Edwards concept of concentrated polymer solution and melt structure [11]

Fig. 7

$$H_{ij} = f_1 C_{ij} + f_{-1} C_{ij}^{-1} \tag{19}$$

where f_1 and f_{-1} are functions of the two invariants **tr C** and tr $\mathbf{C}^{-1}$. In that case one recovers

$$\tau_{ij} = \int_{-\infty}^{t} \mu(t-t') H_{ij}\, dt' \tag{20}$$

which is a very useful form akin to the Kaye-BKZ [6] model.

4.2 Theories for Molten Polymers and Concentrated Solutions. The theory of nondilute solutions is difficult and few successful attempts have been made to deal with rheological problems in the intermediate case of medium concentrations. For the high concentrations of greater interest in polymer engineering, the most successful basic ideas are the Yamamoto-Lodge network theory [3] (Fig. 7(*a*)) and the recent developments by Doi and Edwards [11] (Fig. 7(*b*)). In both cases the concentration is so high that gross interference between molecules is inevitable.

The simplest (Lodge) theory yields a constitutive equation identical in form to (17). Clearly this form has the same virtues and vices as the Maxwell form for dilute solutions, and the response is identical.

It is remarkable that two such diverse microstructural ideas arrive at the same constitutive model and we begin to see that the constitutive equation, in broad form, is relatively insensitive to details of the microstructural picture. This is fortunate, and gives confidence in the type of procedure being adopted.

Improvements in realism can be made; if one assumes longer strands disappear quicker, the results show decreasing viscosity and many other realistic features of real solutions. Approached in this way the theory is of course unwieldy but one can develop approximate approaches, following the dilute solution pattern, to yield a constitutive equation [6].

Table 1 *Various constitutive relations*

Constitutive Model	Small-Strain	Steady Viscometric			Steady Elongation	Start/Stop in Shearing Flow	Elongational Recoil	Single Shear Step	Double-Step Shear	Remarks
		η	N_1	N_2						
Newtonian Eqn. (8)	P	P	U	U	P	P	U	U	U	Infinite stresses in step strains
Criminale, Ericksen, Filbey *viscometric* Eqn. (9)	P	E	E	E	U-P	U	U	U	U	Useful for viscometric flows
Linear viscoelastic	E	P	U	U	P	P	P	P	P	No nonlinear effects
Nonlinear viscoelastic Eqn. (18)	E	P	P	P	P	M	P	P	P	Needs double integral which is hard to use
Lodge-Maxwell Eqn. (12, 17)	E	P	P	U	P	M	P	P	P	Useful for illustrative purposes
K-BKZ Eqn. (20)	E	E	G	G	G	G	M	E	G	Generally useful
Eqn. (15)	M	G	G	U	G	G	M	M-U	M-U	Dilute solution theory: unsuitable for large step strains

Despite the many attempts, the results of these efforts are not on the whole better than the Kaye-BKZ theory (a special case of equation (20)) and in some respects they are worse. For example, the single and double-step relaxation results described in Section 3 are very searching. Many of the models discussed here behave poorly in these tests.

4.3 Doi-Edwards Theory. Although the Yamamoto-Lodge concept of a network structure discussed in the foregoing has proved durable and useful, there have always been some problems with the junction concept. Recently an alternative view of the structure of entangled polymer fluids has been given [11]. The theory is based on the repeating chain model of de Gennes.

An essential idea in the Doi-Edwards theory is that the transverse segmental motions of each chain are impeded by the meshwork of strands from other chains in its neighborhood (Fig. 7(*b*)). Large-scale configurational rearrangement and diffusion are assumed to proceed mainly by repatition, i.e., by random snakelike motions of each chain parallel to its own contour. Each chain continually disengages itself from its current cage of strands, creating new cages and eventuallf a new configuration as its emerging end worms randomly through the mesh. Since the strands of the mesh are parts of chains that diffuse similarly, the lifetime of each cage constraint is itself comparable to the disengagement time for the entire chain. Thus, for chains that are long compared to the mesh size, the frequency of transverse jumps is small enough to make plausible the idea of a semipermanent cage and predominantly snakelike motion.

If the system is deformed the cages are distorted and the chains are carried into new configurations. Stress relaxation proceeds first by a relatively rapid equilibration of chain configurations within the distorted cages, then by a relatively slow diffusion of chains out of the distorted cages into random configurations.

Results have been obtained for several of the flows mentioned in the foregoing and it is possible to obtain from the theory a K-BKZ constitutive model of the form (20) as one special case.

Downloaded 02 May 2010 to 171.66.16.250. Redistribution subject to ASME license or copyright; see http://www.asme.org/terms/Terms_Use.cfm

5 Use of Constitutive Equations in Applied Mechanics

Except in the simplest continuum theories (elasticity, Newtonian fluids) it is normal and necessary to utilize various stages of approximation to real material behavior depending on the problem on hand. For example, in plasticity theory one might use elastic-plastic behavior, work-hardening theory, or simply rigid-plastic analysis depending on the problem being considered. The author believes that this must also be done in viscoelastic studies, and that it is wasteful and counterproductive to always insist on using the most realistic constitutive model for all purposes.

There are a number of classes of flow problems which arise in applications:

(1) Small strain behavior;
(2) Steady weak flows, of which simple shearing may be taken as an example;
(3) Steady strong flows, including simple elongation as a prime example;
(4) Weak flows with discontinuous velocity histories; this class includes stopping and starting shearing flows;
(5) Strong flows with discontinuous velocity history;
(6) Flows with single strain steps (it is not necessary to distinguish between the weak and strong cases here because a step-strain is necessarily finite);
(7) Flows with multiple strain jumps, especially jumps of varying sign.

The adjectives "weak" and "strong" here refer to the possible deformaton of the microstructure [12].

These seven categories form a hierarchy of hurdles of increasing difficulty on which constitutive equations can be tested. Results of calculations will show either

(*a*) No result or a physically impossible result; (*U*)
(*b*) A possible result but not in good agreement with typical experimental data on polymer fluids; (*P*)
(*c*) Moderate agreement with typical behavior; (*M*)
(*d*) Good agreement with experiments; (*G*)
(*e*) Exact agreement due to use of fitted data. (*E*)

These categories will be denoted by the letters (*U*) (unsuitable or useless), *P* (poor or possible), *M* (modest agreement meaning the sign and trend of the results are correct), *G* (good, meaning that the data are fitted within (say) ±20 percent in most places), and *E* (exact or excellent, meaning that the data are, or can be, fitted within a few percent). Table 1 shows the results of this exercise. Other models are given on pp. 444–445 of the book by Bird et al. [6] which should be consulted.

From Table 1 it will be clear that one should always avoid the cases where a *U* is indicaed for the class of response under consideration; generally one should also avoid the *P* cases.

The equations are roughly in order of increasing complexity as one goes down the Table, and the overall results get, on average, better as one moves down the Table. Nevertheless, one should not automatically choose the most complex equation (*K-BKZ*) if it is not required for accuracy.

Clearly, if step-strains occur, then the choice is limited if a moderate or better response is needed. For unsteady strong flows the choice is also limited, but otherwise a reasonable choice is available, especially if only illustrative problems are to be worked out. When the flow is steady but not nearly viscometric, one should beware of problems near points where large stresses occur and it may still be necessary to control the unbounded tensile stresses that occur with the Lodge and related Maxwell models. Finally, when the flow is nearly viscometric, then one can use the nearly viscometric methods developed in reference [4]. For illustrative cases, one often requires a simple model with a single time constant; in that case it may be possible to use the Maxwell model. When the flow is truly viscometric, we have no real need of a constitutive model as explained in Section 3.

For dilute solutions it is not possible to be so definite and further experimental work is needed in this area. Equation (15) avoids most of the obvious problems in this type of system. Thus it is to be expected that some judgment must be exercised in the choice of model for a particular situation.

Examples are given elsewhere [4]; these include lubrication and similar flows; purely elongational flows have been discussed by Petrie [7] and Denn [13]. We shall briefly study extrusion, which is a complex flow.

6 Application to Extrusion Studies Using Finite Elements

A stream of fluid emerging from a plain circular die does not usually have the same diameter as the die. With polymeric fluids the extrudate often has a diameter several times that of the tube, and we would like to understand this behavior.

There is of course an intrinsic interest in finding the mechanism of swelling and, more practically, the production of precision extrusions also needs an accurate predicton of swelling.

Two difficulties arise in a study of extrudate swell:
(*a*) Material nonlinearity;
(*b*) The free surface of the jet.

The first problem is common to all non-Newtonian flows; the second poses a special interest, quite separate from the first, involving mixed boundary conditions on the fluid. By mixed boundary conditions we mean that part of the fluid surface S_v has velocity (usually no-slip) boundary conditions and a part S_t has traction (or stress) boundary conditions. In addition, there may be thermal boundary conditions. Figure 8 shows a typical case.

Of the two difficulties just mentioned, the boundary condition problem is the more basic as free boundaries

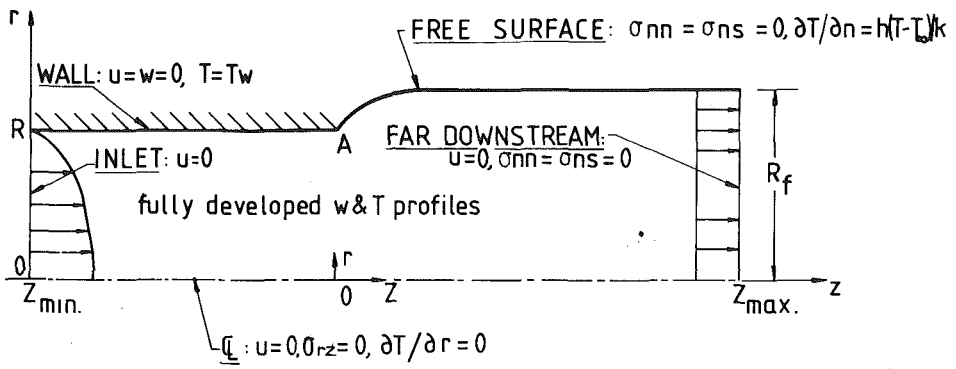


Fig. 8 Boundary conditions for extrusion problem

Downloaded 02 May 2010 to 171.66.16.250. Redistribution subject to ASME license or copyright; see http://www.asme.org/terms/Terms_Use.cfm

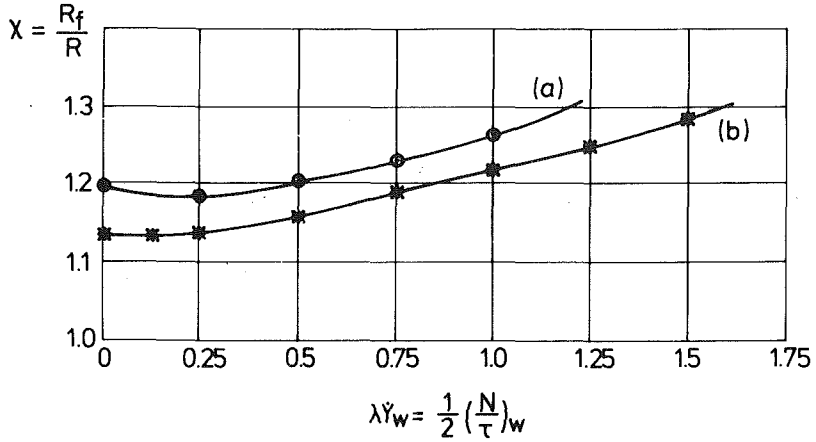


Fig. 9 Swelling ratio χ (final extrudate diameter/die diameter) for Maxwell fluid with relaxation time λ (Equation (12)); $\dot{\gamma}_W$ is shear rate at die wall for upstream. Curve (*a*) is for plane extrudates, curve (*b*) is for circular cross-section extrudates.

present fundamental difficulties even for simple material properties; only in 1972 was a creeping (inertialess) solution obtained for the basic extrusion problem. This solution [14] uses a finite element method and shows that at the point of exit where there is a sudden change in boundary condition there is a stress singularity. This singularity, compounded with the difficulty of locating the (unknown) free surface, argues against the possibility of finding a simple analytical method and suggests we commit ourselves to numerical methods for this class of problems. Available methods include finite differences, finite elements, and the so-called boundary element methods that rely on integral equation methods.

The presence of viscometric flow inside the die and a highly elongational flow at the exit shows that a fairly general model is needed; numerical (finite element) experiments with the viscometric equation (9) show that the reduction of viscosity near the lip is an incorrect modeling and yields a too low value of swelling. Maxwell-type models (12), (17) have also been used and further work is progressing. Some results giving the swelling ratio as a function of $\lambda\dot{\gamma}_w$, where λ is the relaxation time (12) and $\dot{\gamma}_w$ is the shear rate for upstream at the wall, are shown in Fig. 9. It is difficult to reach the high values of $\lambda\dot{\gamma}_w$ of practical processing interest with present numerical methods.

7 Future Directions

A personal assessment of the present position of the subject is

(1) Viscometric calculations are complete;
(2) Some new experimental methods for measuring the viscometric flow parameters ν_1 and ν_2 at high shear rates are needed;
(3) Nearly viscometric theory needs some further work, especially lubrication theory;
(4) Better experimental methods in elongational flow would be welcome;
(5) Much more work on the microstructural approach to developing constitutive equations is needed;
(6) Precise checking of the performance of constitutive models in the basic flows is needed; this is especially true in dilute solutions;
(7) For practical application, stable accurate numerical methods, much better than existing ones, need to be developed;
(8) The consideration of thermal effects and their proper integration with the foregong urgently needs work;
(9) Turbulent flows of viscoelastic fluids are still mysterious.

Most of these problems are especially acute with dilute solutions. The reader will be able to add many more problems without very great effort; there is still much to be discovered before the confident handling of the mechanics of rheological flows is possible.

References

1 de Gennes, P. G., *The Physics of Liquid Crystals*, Clarendon Press, Oxford, 1974.

2 Truesdell, C., and Noll, W., *The Nonlinear Field Theories of Mechanics*, Springer Verlag, Berlin, 1965.

3 Lodge, A. S., *Elastic Liquids*, Academic Press, London, 1964.

4 Pipkin, A. C., and Tanner, R. I., "A Survey of Theory and Experiment in Viscometric Flows of Viscoelastic Liquids," *Mechanics Today*, Vol. 1, 1972, pp. 262–318.

5 Bird, R. B., Armstrong, R. C., and Hassager, O., *Dynamics of Polymeric Liquids, Fluid Mechanics*, Vol. 1, Wiley, New York, 1977.

6 Bird, R. B., Hassager, O., Armstrong, R. C., and Curtiss, C. F., *Dynamics of Polymeric Liquids, Kinetic Theory*, Vol. 2, Wiley, New York, 1977.

7 Petrie, C. J. S., *Elongational Flows*, Pitman, London, 1979.

8 Meissner, J., "Development of a Universal Extensional Rheometer for the Uniaxial Extension of Polymer Melts," *Transactions of the Society of Rheology*, Vol. 16, 1972, pp. 405–420.

9 Herczyński, R. and Pieńkowska, I., "Toward a Statistical Theory of Suspension," *Annual Review of Fluid Mechanics*, Vol. 12, 1980, pp. 237–269.

10 Tanner, R. I., "Stresses in Dilute Solutions of Bead-Nonlinear-Spring Macromolecules. II. Unsteady Flows and Approximate Constitutive Relations," *Transactions of the Society of Rheology*, Vol. 19, 1975, pp. 37–65.

11 Doi, M., and Edwards, S. F., "Dynamics of Concentrated Polymer Systems, The Constitutive Equation," *Journal of Chemical Society, Faraday II*, 1978, pp. 1818–1832.

12 Pipkin, A. C., and Tanner, R. I., "Steady Non-Viscometric Flows of Viscoelastic Liquids," *Annual Review of Fluid Mechanics*, Vol. 9, 1977, pp. 13–32.

13 Denn, M. M., "Continuous Drawing of Liquids to Form Fibres," *Annual Review of Fluid Mechanics*, Vol. 12, 1980, pp. 365–388.

14 Nickell, R. E., Tanner, R. I. and Caswell, B., "The Solution of Viscous Incompressible Jet and Free Surface Flows Using Finite Element Methods, *Journal of Fluid Mechanics*, Vol. 65, 1973, pp. 201–208.

Downloaded 02 May 2010 to 171.66.16.250. Redistribution subject to ASME license or copyright; see http://www.asme.org/terms/Terms_Use.cfm

Quantitative Ultrasonic Nondestructive Evaluation Methods

R. B. Thompson
Ames Laboratory[1]
and Department of Engineering
Science and Mechanics,
Iowa State University,
Ames, Iowa 50011
Mem. ASME

Quantitative ultrasonic techniques for determining the serviceability of structural components are reviewed. Particular emphasis is placed on the use of forward and inverse elastic wave scattering theory as a fundamental foundation for predicting such engineering parameters as the probability of flaw detection and for developing improved techniques for flaw sizing. Ultrasonic measurement techniques for the determination of distributed failure-related properties such as residual stresses are discussed, and the status of the prediction of failure by the detection of acoustic emission precursors is reviewed.

1 Introduction

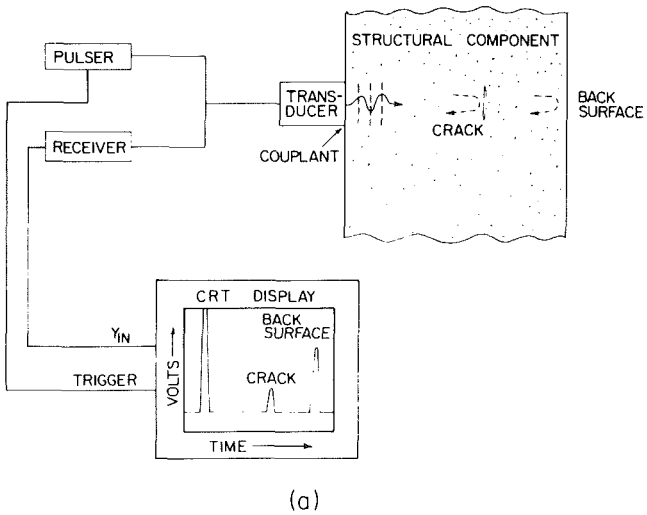
In deciding on the suitability of a structural component for further service, knowledge of material state, failure modes, and service conditions must be combined to make a prediction of the expected performance [1]. This prediction is inherently statistical because of the uncertainties in the foregoing information. When the prediction is combined with a benefits/risk analysis and an assignment of the penalties associated with decision errors, an optimum accept/reject decision can be made [2]. The role of quantitative nondestructive measurements is to assess the material state. Primary interest lies in identifying and sizing microscopic or macroscopic flaws that would ultimately lead to failure. It is also desirable to measure residual stresses and material properties such as fracture toughness so that actual, rather than average, values can be used in performance predictions.

Because of the ability to penetrate to the interior of metal, ceramic, or composite parts, elastic waves are one of the most important forms of probing energy. In addition, these waves exhibit rich propagation phenomena, which can be utilized in extracting a wide range of information about the structural integrity of a component. This paper reviews such uses of elastic waves. Primary attention is placed on techniques for detecting and sizing discrete flaws, with brief discussions of acoustic emission techniques and distributed property measurements also included.

2 Traditional Techniques

Ultrasonic inspection is most often accomplished in a pulsed mode in which short bursts of a few cycles of elastic wave energy, typically in the frequency range of 1–10 MHz, are injected into the part. A typical system is illustrated in Fig. 1. Flaws are indicated by a reflection of the energy (echoes) back to the same transducer (pulse-echo) as shown or to a second transducer (pitch-catch). In state-of-the-art systems, the signal processing takes the form of amplification followed by rectification [3]. Material discontinuities, which must be considered as candidate flaws, are detected when an echo appears that exceeds a preselected threshold. The size is then estimated based on either the peak value of this echo or the variation of the echo height as the probe is moved. Two examples will be given in this section. Approaches under development use more sophisticated signal processing based on a detailed understanding of the wave-flaw interaction, as will be discussed in the next section.

Consider first a relatively small flaw. For example, 1 mm or smaller flaws must be detected in materials used in certain aircraft turbine engines [4]. When the trasducer is positioned



(a)

Fig. 1 Schematic representation of ultrasonic pulse-echo system

[1]Operated for the U.S. Department of Energy by Iowa State University under contract No. W-7405-ENG-82.

Contributed by the Applied Mechanics Division for publication in the JOURNAL OF APPLIED MECHANICS.

Discussion on this paper should be addressed to the Editorial Department, ASME, United Engineering Center, 345 East 47th Street, New York, N.Y. 10017, and will be accepted until two months after final publication of the paper itself in the JOURNAL OF APPLIED MECHANICS. Manuscript received by ASME Applied Mechanics Division April, 1983.

Copyright © 1983 by ASME
Downloaded 02 May 2010 to 171.66.16.250. Redistribution subject to ASME license or copyright; see http://www.asme.org/terms/Terms_Use.cfm

such that the flaw signal is maximized, the strength of the signal may be taken as a first indication of the severity of the flaw. However, several phenomena in addition to the flaw size influence the signal strength. Included are the roughness, orientation, and shape of the flaw, the characteristics of the transducer and electronic instrumentation, the absorption of the wave in the material and changes in the ultrasonic beam intensity due to spreading during propagation, or as induced by focussing or defocussing effects as the beam passes through curved surfaces of parts. Some of these undesired influences can be experimentally reduced by comparing the signal to that produced by a reference flaw in the same material and measurement geometry. Unfortunately, this may require a large set of expensive calibration standards [5]. Alternatively, the transducer and measurement system can be calibrated on a single reflector, e.g., the back surface of a plate. The signals from flaws at different distances can then be compared by theoretically correcting for the effects of diffraction and/or attenuation. This is the basis for a system developed in Germany and known as the DGS technique [3,6]. However, a number of the abovementioned factors influencing echo height remain, and the most that can be learned is the minimum possible size of the flaw.

In sharp contrast is the fracture mechanics requirement to determine the largest possible flaw that could be present. Amplitude-based sizing approaches can only be used effectively when the flaw orientation and/or scattering characteristics are well understood from independent information so that suitable safety margins can be built into the accept-reject threshold.

When the flaw is comparable to, or larger than, the beam size, maps of the flaw can be deduced from measurements in which the transducer is scanned over the surface of a part. Figure 2 illustrates the inspection of a weld in a nuclear power plant, such as might be performed following the guidance of Section XI of the ASME Boiler and Pressure Vessel Code [7]. It is required that the weld, and adjacent base material, be ultrasonically inspected just prior to the beginning of service and periodically during its service life. Here the flaw size may be larger than the ultrasonic beam size so that the echo strength at a single probe position cannot be used to size the flaw. In general, the volumes are scanned by three separate pulse-echo beams, a straight beam propagating normal to the surface of the vessel and two angle shear beams, with nominal angles of 45 and 60 deg with respect to the surface normal. Echoes are considered to be recordable when they exceed a threshold, defined by the signal from a reference reflector. As the transducer is scanned, a map of the flaw shape is developed based on the transducer position and arrival times for recordable echoes. Idealized geometrical forms, e.g., ellipses, are then derived from the maps and used in fracture mechanics assessments of the serviceability of the structure.

As might be expected, the factors mentioned before, such as flaw orientation, roughness, and possible contacting of opposite faces, influence the result of this inspection. A series of recent round-robin tests have evaluated the reliability of this procedure [8], and as noted by Bush [9], "after examination of the data, one can understand the somewhat restrained comment from Europe that the conventional ASME Section XI ultrasonic techniques did not appear to be as good as might be desired." In fairness, it should be noted that the code arose when the major role of NDE was to control the overall weld quality, often on a sampling basis [10]. Under such conditions, flaws such as porosity and blowholes were sought, and the prescribed techniques were suitable. However, when seeking information for a fracture mechanics integrity assessment, the detection and sizing of sharp, planar, crack-like defects is the primary objective. Here more sophisticated approaches, based on the scattering characteristics of such flaws, are required. The scientific foundations of advanced techniques for these and other problems are reviewed in the next section.

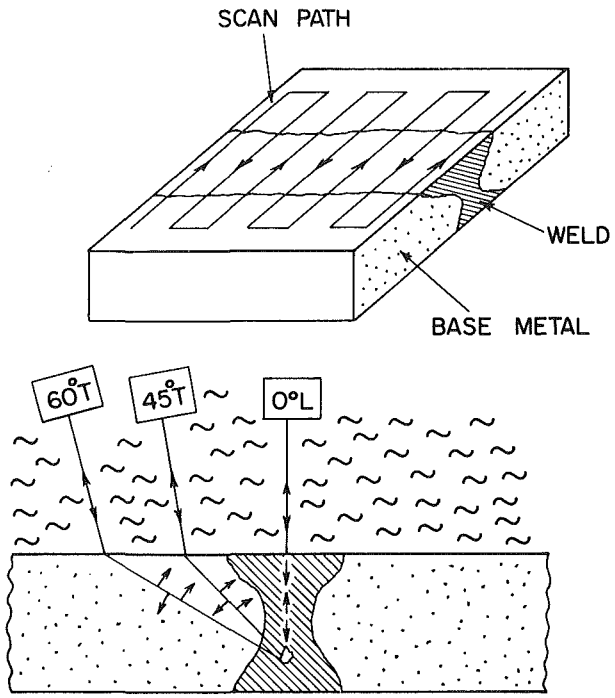


Fig. 2 Schematic representation of weld inspection following Section XI of the ASME Boiler and Pressure Vessel Code. Contact probes, *rather than the immersion coupled probe shown, are commonly employed.*

3 Advanced Techniques for Detecting and Sizing Flaws

The state of the art can be improved in two ways. Training and working conditions improvements can reduce errors due to human factors [11, 12]. Discussion of these steps is beyond the scope of the present paper. The physical factors can be addressed by improving the measurement techniques and data interpretation, keeping in mind the practical constraints of time limits, complex part geometries, and material anisotropy and heterogeneity that make the attainment of these goals difficult [1]. Three elements play and major role in the physical solutions: transducer improvements, high-speed digital processing, and elastic-wave scattering theory. Transducers will not be discussed in detail here [13]. However, it should be noted that, in practice, transducers often do not follow theoretical expectations [14,15]. Hence, their individual properties (radiation pattern, impulse response, etc.) must be measured and taken into account when interpreting experimental data. For example, deconvolution techniques are routinely used when experimentally studying the temporal or spectral properties of scattered ultrasonic signals [16–18].

The essential feature of improved interpretation of ultrasonic signals is a fundamental understanding of the elastic wave-flaw interaction. This subject has been under investigation for over 100 years, but progress has been accelerating recently because of the availability of high-speed digital computing and technological needs associated with seismology, nuclear test monitoring, structural response to high rates of loading, and nondestructive evaluation. By the mid-1970s, solutions had been developed for the scattering from three-dimensional objects such as spherical and cylindrical cavities and inclusions [19] as well as two-dimensional cracks [20]. These were primarily based on the classical techniques of wave-function expansions, integral

Downloaded 02 May 2010 to 171.66.16.250. Redistribution subject to ASME license or copyright; see http://www.asme.org/terms/Terms_Use.cfm

equations, and integral transform solutions. As an example of the integral equation approach [21, 22], the displacement fields, U_i^s, scattered when a volumetric flaw of constant density and elastic constants is illuminated by a plane wave, U_i^0, are given by the solution of the equation

$$U_i^s = \delta\rho\omega^2 \int_R dv' g_{im} U_m + \delta C_{jklm} \int_R dv' g_{ij,k} U_{l,m} \tag{1}$$

where the total field is $\mathbf{U} = \mathbf{U}^0 + \mathbf{U}^s$. Here R is the volume of the flaw, $\delta\rho$ and δC are the changes in density and elastic constants of the flaw with respect to the host medium, ω is the angular frequency, and g is the unbounded flaw free medium, elastic wave Green's function. For a crack, on whose faces stresses must vanish, equation (1) is often reexpressed as a surface integral of the form

$$U_i = C_{jklm} \int_\Sigma d\Sigma' N_k [-g_{li,m'} \Delta U_j] \tag{2}$$

where Σ is one surfaces of the flaw, $\mathbf{N}$ is the normal to that surface, and $\Delta\mathbf{U}$ is the discontinuity in the total displacement solution on the two faces of the crack.

A wide range of numerical and analytical techniques have recently been introduced, including moment, T-matrix, finite element, finite difference, boundary integral, perturbation, asymptotic, and ray solutions [23–32]. No attempt will be made at a detailed review of these solutions in this paper, and the reader is referred to the preceding general references for further citations. In the area of nondestructive evaluation, particular interest has been placed on approximate solutions that can be applied to complex shaped objects such as naturally occurring cracks and inclusions. The more exact techniques have provided the insight necessary to interpret and calibrate these solutions. Comparison to experiment has also been an essential element of the verification of the theories [24, 25, 27, 29, 33]. For example, Fig. 3(*a*) shows a comparison of the experiment and theory for the backscattering in titanium from a compound cavity nicknamed "Pinnochio," an 800 μm diameter head and a nose consisting of a 400 μm diameter cylinder capped by a hemisphere [34]. The theories presented are highly accurate computations based on the Method of Optimum Truncation (MOOT) [35, 36] and the more approximate prediction of the Distorted Wave Born Approximation (DWBA) [37]. Agreement is good to about 6 MHz for DWBA and at least to 12 MHz for MOOT for this complex shape. Figure 3(*b*) shows a comparable result for the pitch-catch (bistatic) scattering from an elliptical crack (2500) μm × 1250 μm major axes), also in titanium [38]. When the physical elastodynamic (elstodynamic Kirchhoff) approximation is corrected for attenuation, excellent agreement is obtained in this regime in which the wavelength is small with respect to the crack dimensions and the solution is dominated by waves diffracted by flashpoints at the crack edges.

These solutions are being applied in two areas of ultrasonic nondestructive evaluation: modeling the reliability of flaw detection and developing inverse scattering techniques for flaw sizing. These are discussed in greater detail in the following.

The reliability of flaw detection is receiving increasing attention in a number of industries, including nuclear power [9] and aerospace [39, 40]. The construction of major systems are often accompanied by costly demonstration programs to ensure that the reliability of nondestructive testing is adequate. Sufficiently accurate modeling would present an attractive alternative to the fabrication of numerous samples and could be used in extending the interpretation of existing tests.

In modeling the reliability of flaw detection, one must first

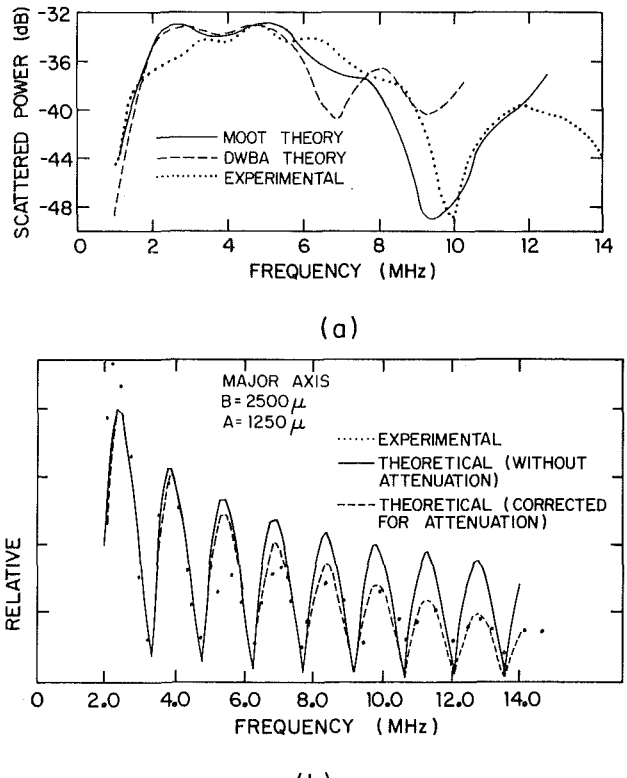


Fig. 3 Comparison of approximate theories to more exact calculations and to experiment. (*a*) distorted wave Born approximation for L→L pulse-echo scattering from "Pinnochio" defect viewed from the side. (*b*) Elastodynamic Kirchhoff approximation for L→L pitch-catch (60 deg) scattering from an elliptical crack (references [34] and [38])

determine the ratio of the flaw to noise signals. The latter can be produced by ultrasonic reflections from part surfaces, grain boundaries, pores, or the other benign discontinuities or by electronic sources in the receiving circuitry. Once signal-to-noise ratio has been specified over the bandwidth of interest, statistical techniques, such as are commonly used in radar and sonar [41], can be employed to compute the probability of detecting flaws as a function of the detection threshold.

Calculation of absolute levels of signal and noise requires direct inclusion of the measurement geometry in the computation. Reciprocity theorems [42, 43] have been shown to provide a convenient formalism for so doing. This approach, together with the elastodynamic Kirchhoff scattering model, has been used to predict the signal obtained when detecting cracks in welds of nuclear power plant pressure vessels with angle beam probes [44] and to evaluate proposed inspection techniques [45]. A somewhat similar scalar Kirchhoff scattering mode [46], which does not explicitly include mode conversion phenomena but which offers greater computational speed, has also been developed [47–49] and combined with experimentally determined statistical measures of operator variability to model the reliability of weld inspection [50, 51].

The foregoing applications are directed at modeling the inspection of welds in pressure vessels in which the flaws of interest are cracks that might be significantly larger than the ultrasonic beam size. Hence, the models explicitly include the beam profile. For simplicity and computational speed, the elastic wave-flaw interaction is treated by the Kirchhoff approximation, which is in its most favorable regime because of the large ratio of flaw size to wavelength.

At the other extreme is the modeling that has been performed to predict the reliability of detecting flaws in high-performance jet engine components. The critical flaw sizes are

Downloaded 02 May 2010 to 171.66.16.250. Redistribution subject to ASME license or copyright; see http://www.asme.org/terms/Terms_Use.cfm

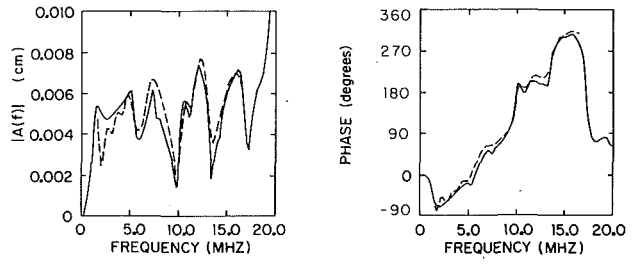


Fig. 4 Comparison of theory and experiment for absolute magnitude and phase of scattering amplitude of a 114 μm diameter tin-solder spherical inclusion in cast thermoplastic (reference [52])

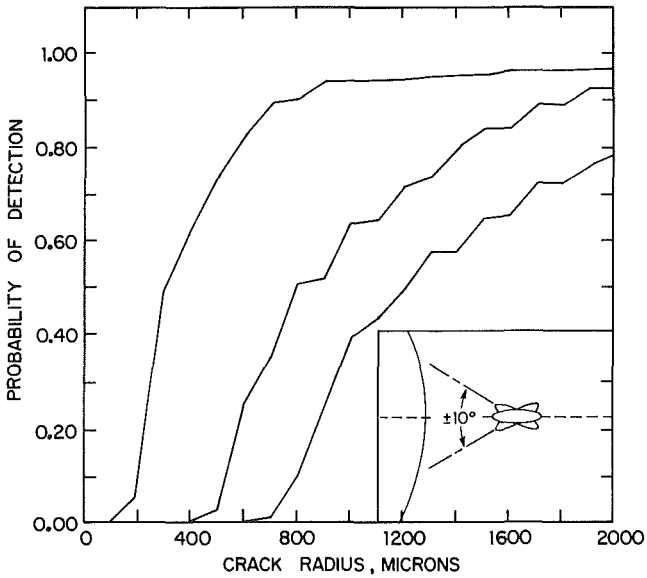


Fig. 5 Probability of detection of randomly oriented (within ±10 deg) circular cracks for three different detection thresholds (reference [58])

typically much smaller [4], often considerably less than the ultrasonic beam size. Models of the measurement process have been developed using the quasi-plane wave assumption that the beam intensity is slowly varying over the volume of the flaw [52]. These models make use of diffraction corrections which approximately account for the effects on refraction, mode conversion, or focussing at planar or cylindrically curved liquid-solid interfaces in immersion configurations such as shown in Fig. 2 [53]. Figure 4 illustrates the success of this approach by comparing the absolute value of the experimentally deduced scattering amplitude of a tin-lead solder spherical inclusion in cast thermoplastic to that predicted by an eigenfunction expansion [54].

This ability to predict absolute signal levels in realistic measurement geometries has been used as the basis for predicting the probability of detecting cracks in jet-aircraft engine component [55–58]. Figure 5 illustrates results of these calculations by plotting the probability of detecting cracks oriented nearly perpendicular to the surface of the web region of an IN100 turbine disk for three values of the detection threshold (signals are detected when their peak value exceeds the threshold). In this particular example, the noise is produced by scattering from microscopic pores in the material. It is found that, for a random crack misorientation of ±10 deg, the signal strength variations are sufficiently great that one cannot achieve a high probability of detection of a desired flaw size without significant probability of also rejecting smaller flaws. Modeling of such phenomena is essential to the design of inspection systems that minimize the false rejection and extra manufacturing cost that this implies.

One way of avoiding these false rejections is to apply scattering theory, in a second way, to characterize and size the previously detected material discontinuities. This requires a solution of "applied" inverse scattering problems. These are distinguished from the "pure" inverse scattering problems found in physics and mathematics by the presence of filtering, modeling inaccuracies, and computational errors [59, 60]. Because of these limitations, a unique solution to the applied problem may not exist, and some degree of a priori information must be utilized in characterization and sizing flaws from experimental data. The best one can expect is an estimate of the flaw parameters whose variance is related to the accuracy of a priori assumptions and the amount of information available. The greater the experimentally available information, the weaker the required assumptions. For example, using the DGS technique discussed in Section 2, the "size" is deduced from the absolute strength of a single backscattered signal. A literal interpretation of this size assumes that the flaw is a circular, smooth reflector, oriented perpendicular to the observer.

Imaging techniques are the most general ways of sizing flaws because of the large amount of information collected and processed. A crude example is an inspection performed in accordance with ASME Section XI, in the sense that the transducer is scanned over the surface of the part and a map of reflection versus position is formed. However, the map has a relatively low resolution due to the breadth of the ultrasonic beam, often 1.3 cm (0.5 in.) or greater. Significant improvement in resolution in the imaging mode can be acheived through a variety of techniques, as illustrated in Fig. 6. The most straightforward involves use of focussed transducers, which produce a focal spot size on the order of $F\lambda/a$, where F is the focal length, λ is the ultrasonic wavelength, and a is the radius of the transducer. An alternative way of forming a physical focus is through the use of phased arrays [61]. By varying the time delay or phase of the excitation pulse and of the reception amplification at each element of the array, a focussed beam with a resolution similar to that produced by a lens can be attained. This approach has the advantage that the beam can be rapidly scanned by electronically changing these delays or phase shifts. It suffers from the disadvantages the fields are excited and detected at discrete transducer elements rather than continuously over the full aperture. This leads to grating lobes and other degradations in performance [62].

Backward wave and holographic reconstruction techniques present computational algorithms for reconstructing flaw shapes, which have received considerable experimental and theoretical evaluation [63–66]. In these techniques, the flaw is illuminated by a quasi-monochromatic signal, and the amplitude and phase of the scattered fields are detected either by transducer arrays, a scanned single transducer, or optical pick-ups. The apparent sources of the scattered fields, located in the object, are determined by appropriately processing the signals to remove the effects of propagation to the receiving plane. Synthetic aperture imaging [67–71] represents a fourth imaging approach. Here broadband pulse-echo waveforms are recorded by a single transducer as it is scanned over the part surface, or by the elements of an array used one at a time. The flaw shape is computationally reconstructed by superimposing the returns with delays corresponding to the propagation time to various object points.

All of the foregoing imaging techniques depend critically on the phase of the received ultrasonic signals to accomplish the reconstruction of the flaw shape. The ALOK system [72] relies on correlations in plots of echo arrival time versus probe position to differentiate flaw signals from noise and to characterize and reconstruct the reflector.

Problems with imaging, such as experimental difficulties in obtaining the necessary information and degradation in this information due to part geometries or material anisotropy or

Downloaded 02 May 2010 to 171.66.16.250. Redistribution subject to ASME license or copyright; see http://www.asme.org/terms/Terms_Use.cfm

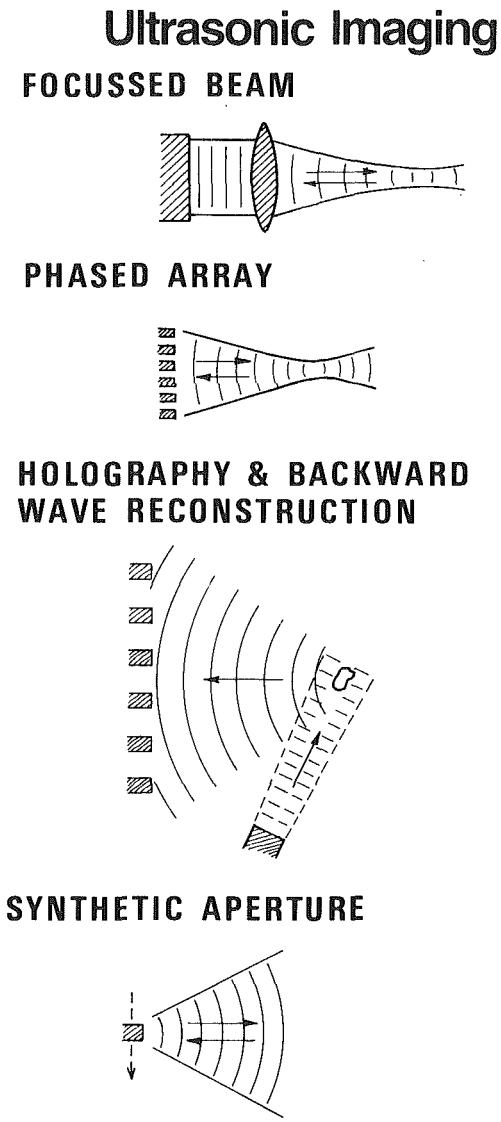


Fig. 6 Techniques for ultrasonic imaging

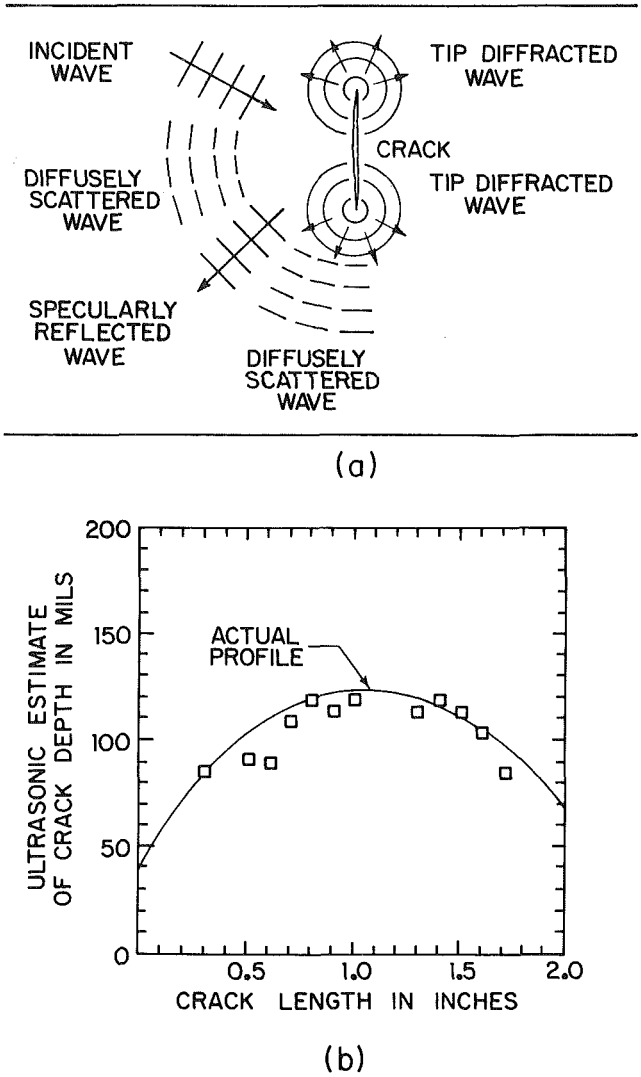


Fig. 7 Crack sizing based on tip diffacted waves. (*a*) physical principles, and (*b*) results of sizing fatigue crack (reference [77])

heterogeneity can limit the performance of an imaging system constructed with today's technology. Furthermore, the physical properties of the scattering process, such as internal reverberations of the flaw or scattering patterns that miss some or all of the receiving transducer, can also produce image degradations. Hence, considerable interest has evolved in viewing the ultrasound-flaw interaction as a scattering process and seeking inverse scattering solutions to determine the flaw's composition and dimensions [73, 74]. Often, the smaller amount of experimental information on which the decision is based requires that a priori assumptions be made about the flaw.

An important practical example is the sizing of a crack. From the fracture mechanics point of view, cracks, such as are induced by metal fatigue, are the most serious defects because of the stress intensification that occurs at their edges. When the ultrasonic wavelength is short with respect to the crack dimensions, the scattered fields may be thought to be composed of rays diffracted from the crack edges, superimposed on specular and diffuse reflections from the rough crack faces, Fig. 7(*a*). For maximum resolution, the imaging techniques just discussed require that each point in the receiving aperture be illuminated by scattered energy from all points on the crack. If this is not the case, or if the complexities of a complete imaging system are not appropriate, the waves diffracted from the tips can be used as the basis for sizing. For example, if a receiver is placed to the right of the crack shown in Fig. 7(*a*), the signal diffracted from the upper tip will arrive sooner than that from the lower tip, and the length of the crack can be computed from the time difference [75]. The same information can be recovered in the frequency domain by observing the constructive and destructive interferences of these two signals, such as was shown in Fig. 3(*b*). Comparisons of measured and actual sizes of a simulated crack based on interference frequencies have been found to have accuracies on the order of 5 percent under good conditions [38].

Similar concepts can be used if the crack breaks the surface of the part. In this case, the primary interference is between the signal diffracted from the crack tip and the corner reflection produced by sequential reflections from the crack face and the part surface [76]. Figure 7(*b*) shows the reconstruction of the edge of a fatigue crack in a simulated bore of a turbine rotor [77]. Other applications of the interference of tip-diffracted signals have been found in sizing cracks in weldments in nuclear power plant pressure vessels [78] and in laboratory studies of the growth of fatigue cracks in compact tension specimen [79].

The foregoing arguments have relied on a priori assumptions regarding the shape, and in some cases the orientation, of the crack. A more general approach involves an inverse

Downloaded 02 May 2010 to 171.66.16.250. Redistribution subject to ASME license or copyright; see http://www.asme.org/terms/Terms_Use.cfm

solution to equation (2). This has been recently accomplished based on both the Kichhoff approximation [80] and Fermat's principle [81]. Results have also been obtained for the case of slightly anisotropic media [82] and preliminary inversions of experimental data have been successful [83].

The preceding concepts have been presented for the case of examining cracks with longitudinal or transverse waves. The interference of Rayleigh wave signals diffracted from crack tips have also been used to size surface-breaking cracks [84]. In addition, the change in spectral content of a Rayleigh wave that has had the high-frequency (near-surface) components preferentially absorbed by propagating past a crack has been used effectively [85–87].

For volumetric flaws such as inclusions and voids, the short wavelength scattering can be considered to be the superposition of energy traveling along various ray paths. In measurements of the scattering from smooth objects it has been found that specular reflections, creep rays propagating around the periphery of the object, and rays propagating through the interior of the object make major contributions to the received signals and that the time and amplitudes of these rays can be used in sizing and identifying the material of the flaw [88–91]. Alternatively, the information can be deduced from the resonances produced by the interferences of these rays [88, 92–95]. However, experiments indicate that the creeping ray may be highly damped by the surface roughness of naturally occurring flaws [91], and the robustness of sizing techniques based on these ray paths may not be as great as desired for naturally occurring flaws.

Inverse scattering solutions have also been developed for reconstructing the shapes of volumetric flaws. The two that have received the most investigation are the Inverse Born Approximation (IBA) and the Physical Optics Far Field Inverse Scattering (POFFIS) algorithm. Although derived from significantly different physical models, the two approaches yield algorithms that have many similarities.

The IBA [96–105] was derived as an inverse solution to the elastic wave equation in the weak scattering limit. It is a reconstruction algorithm consisting of an inverse Fourier transform of the scattering amplitudes measured at appropriate angles and frequencies. Much attention has been given to the case of spherically symmetric objects, for which only a one-dimensional inverse transform is required [96, 97]. Despite the weak scattering assumption in the derivation, the algorithm has been found to accurately predict the size of voids and to be fairly robust in the presence of noise and limited bandwidth [98]. If the scatterer is an ellipsoid, the same one-dimensional algorithm has been shown to reconstruct the distance from the flaw centroid to the plane of tangency of the incident wave fronts [97]. Reconstruction of the shapes of ellipsoidal voids from experimental data has been successfully accomplished [99, 100], as illustrated in Fig. 8, and naturally occurring inclusions in aircraft engine turbine materials have been correctly sized [99]. Although difficulties can be encountered when the approach is applied to multiple, irregular, or highly resonant inclusion [101], a good under standing of the significant successes of this algorithm originally based on weak scattering assumptions, is emerging [102, 103].

The full three-dimensional form of the IBA has been studied less extensivley. However, it has been reported to be able to reconstruct shapes of complex defects such as cracks growing out of voids [104] and the effects of finite aperture have been identified [105].

POFFIS [106, 107] was derived as an inverse solution to the scattering from voids, as described by the physical optics approximation. The algorithm again consists of the evaluation of the inverse Fourier transform of measured scattered fields. However, instead of reconstructing the characteristic function of the flaw (defined to be unity on the interior and zero on the exterior) as in the IBA, the normal derivation of this function, i.e., the flaw edge, is reconstructed. In a recent comparison of inverse scattering algorithms based on synthetic data, POFFIS has been found to be applicable to a wide range of flaw shapes [108].

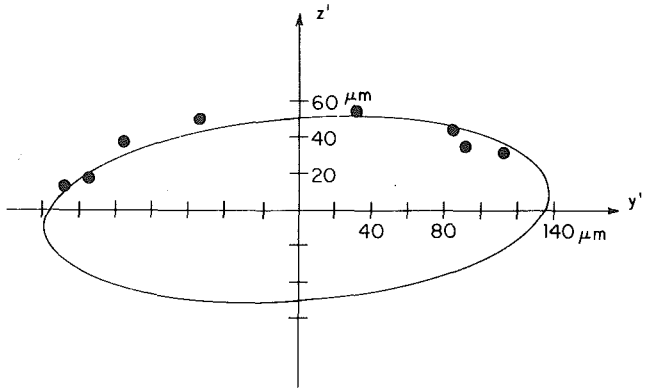


Fig. 8 Reconstruction of the size, shape, and orientation of a 47 μm × 96 μm (semiaxes) stainless steel ellipsoidal inclusion in plastic using the one-dimensional inverse Born approximation (reference [100])

There is a great deal of conceptual similarity between the processing employed in IBA, POFFIS, and synthetic aperture imaging [109, 110]. In the time domain, each can be qualitatively thought of as a procedure whereby the signals received at multiple transducer locations are superimposed with phase shifts chosen to produce constructive interference in the reconstruction plane when a scatterer is present at the corresponding position in the object plane. In synthetic aperture imaging, the detailed form of this superposition is based on time-of-flight arguments, while POFFIS is developed as a rigorous inverse solution of the physical optics scattering model. In each case, time is measured with respect to the excitation of the transmitting transducer. The IBA differs by the explicit utilization of low-frequency scattering information to determine the time at which the illuminating wave would reach the flaw centroid. All computations in the reconstruction are made with respect to this time [102]. For isotropic media, this approach has been shown to be equivalent to synthetic aperture imaging. However, it appears less sensitive to errors produced by anisotropic velocities [110]. This advantage is achieved at the expense of greater bandwidth requirements on the measurement.

A unique feature that distinguishes elastic wave scattering from acoustic scattering is the richness of information contained in the scattered fields when the wavelength is large with respect to the object size. A striking example is the direct relationship that has been observed between the amplitude of the long wavelength scattering and the maximum value of the reduced stress intensity factor on the periphery of an elliptical crack [111]. This result suggests that the strength of cracks in brittle materials could be directly deduced from a single nondestructive backscattering measurement made normal to the crack face. After extension of the theory to the case of illumination of surface-breaking cracks with elastic Rayleigh waves [42], the direct prediction of strength was confirmed in a set of destructive tests on pyrex [112], Fig. 9. It has also been found that long wavelength scattering measurements are strongly influenced by partial contact of the crack faces, such as would be produced by closure stresses. In the previously cited pyrex measurements, a slight preload was applied to the specimen to avoid this problem. For machining or indentation-induced cracks in silicon nitride, procedures have identified that correct for the closure and provided a conservative prediction of failure loads [113]. The sensitivity to partial contact has also been used as a tool study the closure phenomenon in fatigue cracks grown in aluminum [114, 115].

Downloaded 02 May 2010 to 171.66.16.250. Redistribution subject to ASME license or copyright; see http://www.asme.org/terms/Terms_Use.cfm

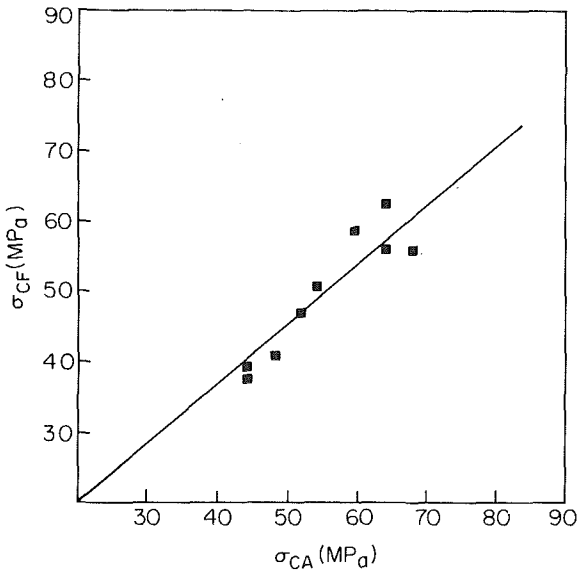


Fig. 9 Comparison of ultrasonically predicted failure stresses based on long wavelength scattering. σ_{cA}, with destructive test results, σ_{cF} (reference [112])

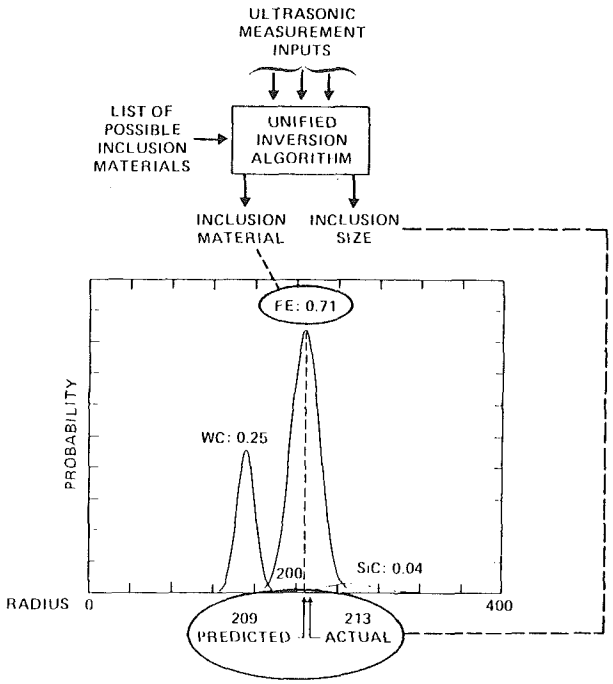


Fig. 10 Joint probability distribution of flaw size and material for inclusions in Si_3N_4 based on experimental measurements processed by probabilistic inversion algorithm. The probability of each flaw type is indicated above the curves (reference [125])

Application of the long wavelength scattering of SH waves to the problem of detecting and sizing cracks in butt weldments is also under investigation [116–118].

Scattering at long wavelength produces information regarding volumetric inclusions as well as cracks [119]. It has been found that, for a generalized flaw with possibly anisotropic elastic constants, up to 22 independent parameters can be extracted from measurements of long wavelength scattering at all angles [120, 121]. These are functions of the flaw's size, shape, orientation, and material parameters. Probabilistic inversion methods have been applied to experimental data [122] to determine the size, shape, and orientation of a spheroidal void in a titanium alloy. However, it should be noted that certain combinations of material parameters are not readily determined [123] from long wavelength scattering. Techniques have also been proposed to use the long wavelength scattering characteristics to differentiate cracks from inclusions [124].

As noted in the foregoing, no practical nondestructive measurement technique collects enough useful information to allow a totally general and unbiased reconstruction of the flaw and assumptions are explicitly or implicitly made in all sizing algorithms. For example, in the case of long wavelength scattering, this assumption takes the form of the implied statement, "If the discontinuity that has been detected is an elliptical crack normal to the measurement beam, then the maximum value of the reduced stress intensity factor must be . . .". In practice, the truth of such assumptions cannot be known absolutely. A probabilistic inversion technique has been developed that allows these assumptions to be introduced in a statistical way and has the additional advantage of assigning variances to the estimates of flaw parameters [125]. Figure 10 presents the result of determining the material and size of spherical inclusions in Si_3N_4 ceramic by this technique. Here estimates are obtained of $P(x,g\,|y)$, the probability that the flaw has a size x and composition g given the measurement result y. By integrating over x, $P(g\,|y)$, the probability of composition g, can be obtained. For the case presented, the correct flaw material, *Fe*, has the highest probability (71 percent) while the estimated flaw radius, 209 μm, is within 2 percent of the correct value.

The role of quantitative nondestructive evaluation does not end with a probabilistic assessment of the flaw state. This information must be combined with probabilistic failure models, loading and environmental information, and risk analysis to allow a final accept-reject decision to be made [2, 126].

4 Determination of Material Properties

The detection and sizing of discrete flaws has received by far the greatest attention in quantitative nondestructive evaluation because of the importance of this information in fracture mechanics or other failure modeling methodologies. Nondestructive techniques for measuring material properties such as fracture toughness, strength, fatigue damage, or residual stress would also be of great value in predicting the remaining lifetime or assessing other structural properties of components. In general, the microstructural changes that determine these mechanical properties also influence the ultrasonic velocity, scattering, or attenuation. Unfortunately, other microstructural changes not related to the mechanical property of interest modify these ultrasonic wave propagation parameters as well. The primary technical challenge lies in developing techniques to uniquely determine one mechanical property from the measurements. Success generally depends on a combined knowledge of material microstructure, elastic wave propagation and scattering, and measurement techniques.

The measurement of residual stress is a good example [127]. The application of a stress to a material and its subsequent deformation causes a shift in the ultrasonic velocity through a variety of mechanisms, including changes in the density, effective elastic constants, propagation distances, and dimensions [128]. For typical materials, velocity changes induced by stresses in the elastic range are linearly related to those stresses. If the acoustoelastic proportionality constants are known, simple stress fields can be measured. Figure 11 illustrates this for the case of the stresses surrounding a crack [129].

Although major progress has been made in the problem of measuring simple stress fields in materials of known acoustoelastic constants, the problem of measuring more complex, spatially varying stresses or stresses in materials with unknown microstructure requires considerably more

Downloaded 02 May 2010 to 171.66.16.250. Redistribution subject to ASME license or copyright; see http://www.asme.org/terms/Terms_Use.cfm

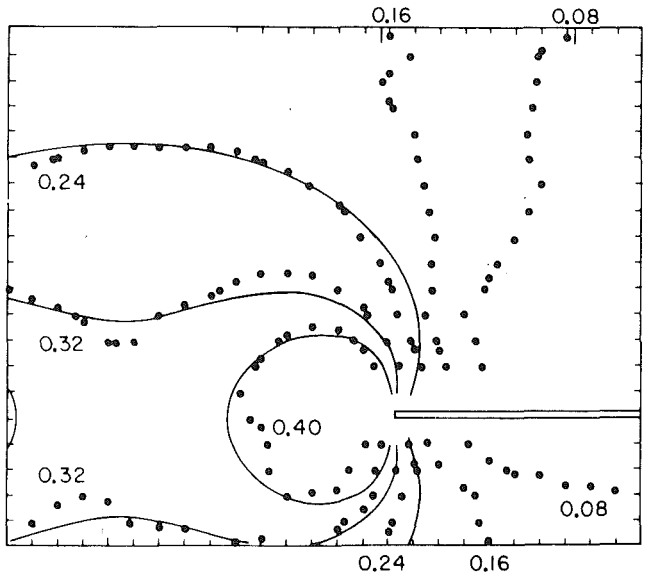


Fig. 11 Comparison of numerically predicted and ultrasonically measuring stress contours for 6061-T6 aluminum double edge notched panel (reference [129])

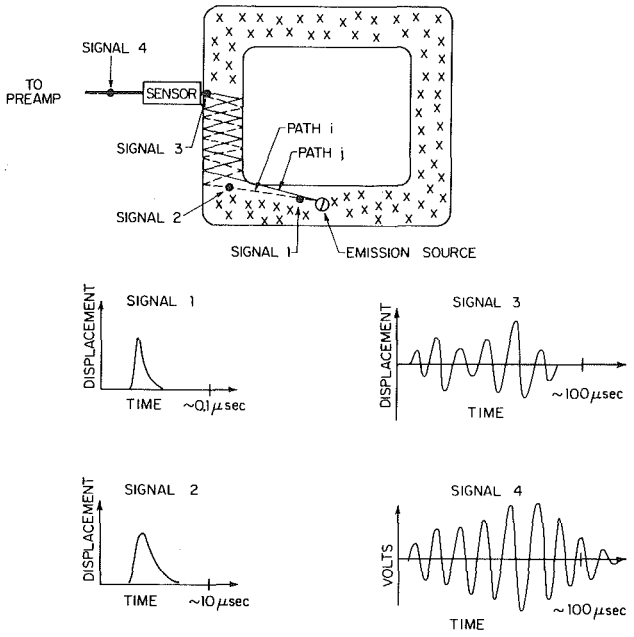


Fig. 12 Schematic representation of degradation of information during detection of acoustic emission signals including effects of material absorption, multiple reflections, and sensor filtering.

effort. Approaches under investigation in the latter area include the measurement of the velocities of horizontally polarized shear waves for several combinations of polarization and propagation directions, [130–132], which allows stress-induced changes in the wave velocity to be separated from changes due to anisotropic elastic constants, and measurements of the temperature dependence of the ultrasonic velocity [133], which also varies linearly with stress but appears to be less influenced by microstructural effects than the velocity itself.

The microstructurally induced shifts in ultrasonic velocity, which compete with stress-induced shifts, can be used to advantage in tests for other properties. For example, in cast iron, highest strength is produced when the carbon agglomerates into spheroidal particles, or nodules, during solidification (nodular cast iron) as opposed to forming much weaker graphite flakes (gray iron). The ultrasonic velocity has been shown to increase monatonically with nodularity, yield strength, and ultimate strength for the material [134, 135]. This effect is the basis of on-line techniques used, for example, by the automotive industry to ensure that their castings have the proper microstructure [136, 137].

A number of other material properties can also be sensed by ultrasonic attenuation and/or velocity measurements [137–141]. Included are grain size [142], fatigue damage [143], fracture toughness [144], and porosity [145]. Ultrasonic harmonic generation has also been found to be sensitive to fatigue damage [146]. The practical application of these techniques depends on a good theoretical understanding of the interaction, coupled with conditions in which microstructural variations are sufficiently controlled that competing effects are minimized.

5 Acoustic Emission

Acoustic emissions are transient elastic waves generated by the rapid release of energy during the deformation of a solid body. Under certain conditions, they are produced by failure related processes, such as the breaking of brittle inclusions during the propagation of fatigue cracks. They thus serve as an early warning of degradation of the structure. Since they are stimulated by the application of a load, rather than an illuminating ultrasonic beam, and since their radiation is often omnidirectional, a large structure can be monitored with just a few sensors, separated by distances on the order of meters.

Emission source location can often be determined by triangulation schemes based on the times of arrival of the signal at three distinct transducers. A typical example of acoustic emission testing occurs during the proof test of a pressure vessel. A load is applied somewhat in excess of the operating load. The absence of emissions is taken to signify that no significant crack extension or other failure related deformations occurred and hence that the vessel is suitable for a period of service defined by the detailed methodology of the proof test.

Considerable information concerning the deformation processes producing the emission are, in principle, contained in the temporal and angular distributions of the emissions. However, this is corrupted by two factors. First, competing operational noises, such as are produced by fluid flow in hydraulic systems, can mask low-level acoustic emissions. Hence, only a fraction of the true emissions can be detected. Second, material attenuation and component geometry can strongly modify the signals, as illustrated in Fig. 12. The time history of the emission will depend on the detailed microscopic process responsible for its generation. In general, one might expect a short-duration, broadband pulse with a rise time given approximately by the distance over which microscopic failure occurred divided by the speed of crack propagation. For example, in the failure of a brittle inclusion of 5 μm diameter occurring at 10 percent of the ultrasonic shear wave velocity (0.3mm/μsec), the rise time would be on the order of 17 nsec. Thus, spectral content up to 50 MHz would be anticipated. However, since the higher frequencies are preferentially absorbed by grain boundary scattering in polycrystalline metals, frequencies above a few MHz are generally not observed at the receiver location. Furthermore, since many parts have rather complex shapes and the receiver may be some distance away from the source location, the signal is further distorted by the interference of multiple arrivals. Finally, for sensitivity reasons, the sensor often has a narrow bandwidth, which again filters the "true" signal. The combination of these factors renders source identification from observed signals a challenging problem in real structures.

Downloaded 02 May 2010 to 171.66.16.250. Redistribution subject to ASME license or copyright; see http://www.asme.org/terms/Terms_Use.cfm

Because of the many successful applications and the tremendous potential of acoustic emission in the surveilance of large structures, considerable research is being performed to solve these problem [147–151]. Elements include the microstructural origins of the emissions, the radiation characteristics of these sources, and the filtering of this radiation by finite geometries such as plates. More details may be found in the reveiw article cited in the foregoing.

6 Future Directions

Despite the accomplishments represented by the research just discussed, further challenges remain before these approaches can be considered fully developed engineering tools. Some examples are discussed in the following.

Computational tools are available for treating scattering from single and multiple cracks of simple shape. However, this must be extended to the more complex flaw shapes found in practice. Examples include fatigue cracks in which closure stresses have produced multiple contact of asperities near the tip, intergrannular stress corrosion cracks with multiple facets and branches following grain boundaries, inclusions with irregular boundaries, and inclusions that are only in partial contact with the host material. The influences of complex-shaped part surfaces and anisotropic and inhomogeneous materials on ultrasonic beam propagation are important questions. Austenitic stainless steel welds and composite materials are good examples of the latter. In the areas of material property measurement and acoustic emission, considerable work also remains, as was indicated in the text.

Despite the magnitude of these remaining problems, the progress that has been made in the last decade suggests quantitative ultrasonic nondestructive evaluation will become an increasingly important engineering tool, standing side by side with fracture mechanics, in the future.

7 Acknowledgment

The preparation of this review was sponsored by the Center for Advanced Nondestructive Evaluation, operated by the Ames Laboratory, USDOE, for the Air Force Wright Aeronautical Laboratories/Materials Laboratory and the Defense Advanced Research Projects Agency under Contract No. W-7405-ENG-82 with Iowa State University.

References

1 Thompson, R. B., "Present Status and Future Needs for Quantitative Measurement Techniques," in *Review of Progress in Quantitative Nondestructive Evaluation 1*, Thompson D. O., and Chimenti, D. E., eds., (Plenum Press, New York, 1982), pp. 23–42.

2 Richardson, J. M., and Buckley, M. J., "Overview of Probabilistic, Failure Predictions and Accept-Reject Decisions," ibid, pp. 43–58.

3 Krautkramer, J., and Krautkramer, H., *Ultrasonic Testing of Materials*, Springer-Verlag, Berlin, 1977.

4 Salter, S. A., and Sundt, C. V., "Gas Turbine Engine Disk Cyclic Life Prediction," J. Aircraft, Vol. 12, 1975, pp. 360-365.

5 Berger, H., *Nondestructive Testing Standards-A Review*, ASTM STP 624, American Society for Testing and Materials, Philadelphia, 1977.

6 Krautkramer, J., "Determination of the Size of Defects by the Ultrasonic Impulse Echo Method," *Brit. Journal of Applied Physics*, Vol. 10, 1959, pp. 240–245.

7 *ASME Boiler and Pressure Vessel Code, An American National Standard, Section XI, Nondestructive Evaluation* (American Society of Mechanical Engineers, New York, 1977), revised periodically.

8 Caussin, P., Crutzen, S., Deuster, G., and Parry, G., "Analysis of PISC Trials Results for Alternative Procedures," *Nondestructive Evaluation in the Nuclear Industry–1980*, American Society for Metals, Metals Park, Ohio, 1981, pp. 345–360.

9 Bush, Spencer, H., "Reliability Strategies in Flaw Evaluation," in *Nondestructive Evaluation: Microstructural Characterization and Reliability Strategies*, Buck, Otto, and Wolf, Stanley M., eds., Metallurgical Society of AIME, Warrendale, Pa., 1981, pp. 65–80.

10 Nichols, R. W., "The State-of-the-Art of NDE as a Reliable Flaw Detector," in *Nondestructive Evaluation in the Nuclear Industry–1980*, American Society for Metals, Metals Park, Ohio, 1981, pp. 3–11.

11 *Nondestructive Evaluation: Reliability and Human Factors*, Fong, J., and Heddon, O., eds., NBS Special Publication, Gaithersburg, in press.

12 *NDE Education/Training for Engineers*, Thompson, D. O., ed., ASME Special Publication, New York, in press.

13 Sachse, Wolfgang, and Hsu, Nelson N., "Ultrasonic Transducers for Materials Testing and Their Characterization," in *Physical Acoustics*, Vol. XIV, Mason, W. P., and Thurston, R. N., eds., Academic Press, New York, 1979, pp. 277–406.

14 Posakony, G. J., "Engineering Aspects of Ultrasonic Piezoelectric Transducer Design," 1975 Ultrasonics Symposium Proceedings, IEEE, New York, 1975, pp. 1–9.

15 Papadakis, E. P., "Ultrasonic Transducer Evaluation in Five 'Domains': Time, Space, Frequency, Surface Motion, and Theory," 1977 Ultrasonics Symposium Proceedings, IEEE, New York, 1977, pp. 109–112.

16 Ahlberg, L. A., and Tittmann, B. R., "Measurement Techniques in Elastic Wave Scattering Experiments," 1980 Ultrasonics Symposium Proceedings, IEEE, New York, 1980, pp. 842–846.

17 Elsley, Dick, Richardson, John, and Addison, Bob, "Optimum Measurement of Broadband Ultrasonic Data," ibid, pp. 916–921.

18 Fitting, Dale W., and Laszlo, Adler, *Ultrasonic Spectral Analysis for Nondestructive Evaluation*, Plenum Press, New York, 1981.

19 Pao, Y. -H., and Mow, C. C., *The Diffraction of Elastic Waves and Dynamic Stress Concentrations*, Crane, Russak, and Company, New York, 1973.

20 Kraut, E. A., "Review of Theories of Scattering of Elastic Waves by Cracks," *IEEE Trans. on Sonics and Ultrasonics*, SU-23, 1976, p. 162.

21 Mal, A. K., and Knopoff, L., "Elastic Wave Velocities in Two-Component Systems," *J. Inst. Math. Appl.*, Vol. 3, 1967, pp. 376–387.

22 Gubernatis, J. E., Domany, E., and Krumhansl, J. A., "Formal Aspects of the Scattering of Ultrasound by Flaws in Elastic Materials," *J. Appl. Phys.*, Vol. 48, 1977, pp. 2804–2811.

23 *Modern Problems in Elastic Wave Propagation*, Miklowitz, J., and Achenbach, J. D., eds., Wiley-Interscience, New York, 1978, Part 2.

24 Elastic Waves and Non-Destructive Testing of Materials, Pao, Y. -H., ed., AMD-Vol. 29, American Society of Mechanical Engineers, New York 1978.

25 *Acoustic Electromagnetic, and Elastic Wave Scattering-Focus on the T-Matrix Approach*, Varadan, V. K., Varadan, V. V., eds., Pergamon Press, New York, 1980.

26 Achenbach, J. D., Gauteson, A. K., and McMaken, H., *Ray Methods for Waves in Elastic Solids with Applications to Scattering by Cracks*, Pittman, London, 1982.

27 *Elastic Wave Scattering and Propagation*, Varadan, V. K., and Varadan, V. V., eds., Ann Arbor Science Publishers, Ann Arbor, Mich. 1982.

28 *Review of Progress in Quantitative Nondestructive Evaluation 1*, Thompson, D. O., and Chimenti, D. E., eds., Plenum Press, New York, 1982.

29 *Review of Progress in Quantitative Nondestructive Evaluation 2*, Thompson, D. O., and Chimenti, D. E., eds., Plenum Press, New York, in press.

30 Gubernatis, J. E., "Elastic Wave Scattering Theory With Application to NDE," in *Fundamentals of Quantitative Ultrasonic Nondestructive Evaluation*, Thompson, D. O., and Thompson, R. B., eds., Springer-Verlag. Berlin, in press.

31 *Handbook on Acoustic, Electromagnetic, and Elastic Wave Scattering*, Vols. 1 and 2, Varadan, V. K., and Varadan, V. V. eds., North-Holland, Amsterdam, in press.

32 Pao, Y. -H., "Elastic Waves in Solids," ASME JOURNAL OF APPLIED MECHANICS, Vol. 50, 1983, pp. 1152–1164.

33 Tittmann, B. R., "Scattering of Elastic Waves From Simple Defects in Solids, a Review," *Wave Motion*, in press.

34 Tittmann, B. R., and Ahlberg, L., "Measurement of Scattering from Bulk Defects," in *Proceedings of the DARPA/AFWAL Review of Progress in Quantitative NDE*, Report AFWAL-TR-81-4080, Air Force Wright Aeronautical Laboratories, Dayton, Ohio, 1981, pp. 311–319.

35 Visscher, W. M., "Application of MOOT to Scattering of Elastic Waves From Compound Inclusions," ibid, pp. 287–291.

36 Opsal, J. L., "Calculation of Elastic Wave Scattering From Voids and Crack-Like Defects by the Method of Optimal Truncation," ibid, pp. 292–297.

37 Domany, E., Newman, K. E., and Teitel, S., "Elastic Wave Scattering by General Shaped Defects: The Distorted Wave Born Approximation," in, *Proceedings of the DARPA AFML Review of Progress in Quantitative NDE*, report AFWAL-TR-80-4078, Air Force Wright Aeronautical Laboratories, Dayton, Ohio, 1979, pp. 341–347.

38 Adler, L., and Achenbach, J. D., "Elastic Wave Diffraction by Elliptical Cracks: Theory and Experiment," *J. Nondestr. Eval.*, Vol. 1, 1980, pp. 87–100.

39 Moyzis, J. H., and Forney, D. M. Jr., "Increased Reliability, a Critical NDE Research Goal," *Review of Progress in Quantitative Nondestructive Evaluation 1*, Thompson, D. O., and Chimenti, D. E., eds., Plenum Press, New York, 1982, pp. 7–11.

40 Rummel, W. D., "Considerations for Quantitative NDE and NDE Reliability," *Review of Progress in Quantitative NDE 2*, Thompson, D. O., and Chimenti, D. E., eds., Plenum Press, New York, in press.

41 Whalen, A. D., Detection of Signals in Noise, Academic Press, New York, 1971.

42 Kino, G. S., "The Application of Reciprocity Theory to Scattering of Acoustic Waves by Flaws," *J. Appl. Phys.*, Vol. 49, 1978, pp. 3190–3199.

43 Auld, B. A., "General Electromechanical Reciprocity Relations Applied

Downloaded 02 May 2010 to 171.66.16.250. Redistribution subject to ASME license or copyright; see http://www.asme.org/terms/Terms_Use.cfm

to the Calculation of Elastic Wave Scattering Coefficients," *Wave Motion*, Vol. 1, 1979, pp. 3–10.

44 Chapman, R. K., "Ultrasonic Scattering From Smooth Flat Cracks, Summary Note on an Elastodynamic Kirchhoff Theory," Report No. NWR/SSD/82-0091/N, Central Electricity Generating Board, Northwestern Region Scientific Services Department, Manchester, England, 1982.

45 Coffey, J. M., Chapman, R. K., and Hanack, D. J., "The Ultrasonic Detectability of a Postulated Worst Case Flaw in a PWR Vessel," Report No. NWR/SSD/82/0045/R ibid, Apr. 1982.

46 Haines, N. F., and Langston, D. B., *J. Acoust. Soc. Am.*, Vol. 67, 1980, pp. 1443–1454.

47 Haines, N. F., "A Practical Model of Ultrasonic Refraction From Planar Surfaces," Report RD/B/N4995, Central Electricity Generating Board, Research Division, Berkeley Nuclear Laboratories, Berkeley, England, Jan. 1981.

48 Langston, D. B., "A Practical Model of the Ultrasonic Tandem Technique Used to Detect Through-Thickness Planar Defects," Report RD/B/5074N81, ibid, Aug. 1981.

49 Haines, N. F., and Green, A. J., "A Practical Model of Ultrasonic Reflection From Surface Breaking Planar Defects," Report RD/B/5073N81, ibid, Aug. 1981.

50 Haines, N. F., "A Method of Predicting the Reliability of Ultrasonic Crack Detection From an Analysis of PISC 1 data," Report RD/B/5209N81, ibid, Nov. 1981.

51 Haines, N. F., Langston, D. B., Green A. J., and Wilson, R., "Assessment of the Reliability of Ultrasonic Inspection Methods," Report TPRD/B/0064/R82, ibid, April, 1982.

52 Thompson, R. B., and Gray, T. A., "A Model Relating Ultrasonic Scattering Amplitudes to Measurements Through Liquid-Solid Interfaces," Submitted to *J. Acoust. Soc. Amer.*

53 Thompson R. B., and Gray, T. A., "Analytical Diffraction Corrections to Ultrasonic Scattering Measurements," *Review of Progress in Quantitative Nondestructive Evaluation 2*, Thompson D. O., and Chimenti, D. E., eds., Plenum Press, New York, in press.

54 Ying, C. F., and Truell, Rohn, "Scattering of a Plane Longitudinal Wave by a Spherical Obstacle in an Isotropically Elastic Solid," *J. Appl. Phys.*, Vol. 27, 1956, pp. 1086–1097.

55 Gray, T. A., and Thompson R. B., "Ultrasonic Flaw Detection in Turbine Rotor Components," *Review of Progress in Quantitative Nondestructive Evaluation 2*, Thompson, D. O., and Chimenti, D. E., eds., Plenum Press, New York, in press.

56 Addison, R. C., Jr., Elsley, R. K., and Graham, L. J., "Flaw Detection Below Curved Surfaces of Components," ibid.

57 Tittmann, B. R., Ahlberg, L., Cohen-Tenoudji, F., and Quentin, G., "Attenuation and Grain Noise Parameters in N_i-Base Alloys," ibid.

58 Fertig, K. W., Jr., and Richardson, J. M., "Computer Simulation of Probability of Detection," ibid.

59 DeFacio, Brian, "Rigorous Results on Inverse Source and Inverse Scattering Theory," *Review of Progress in Nondestructive Evaluation 1*, Thompson, D. O., and Chimenti, D. E., eds., Plenum Press, New York, 1982, pp. 219–226.

60 Lee, D. A., "Ill-Posed and Well-Posed Problems in Inverse Elastodynamic Scattering for Nondestructive Evaluation," *J. Nondestr. Evaluation*, Vol. 2, 1981, pp. 161–172.

61 Gebhardt, W., "An Ultrasonic Phased Array System for Defect Classification and Reconstruction," *New Procedures in Nondestructive Testing*, Springer-Verlag, Berlin, in press.

62 Aulenbacher, V., and Langenberg, K. J., "Analytical Representation of Transient Ultrasonic Phased-Array Near- and Far-Fields," *J. Nondestr. Eval.*, Vol. 1, 1980, pp. 53–66.

63 Lakin, K. M., and Landin, A. R., "Acoustic Imaging with Two-Dimensional Arrays," *Review of Progress in Nondestructive Evaluation 1*, Thompson, D. O., and Chimenti, D. E., eds., Plenum Press, New York, 1982, pp. 777–790.

64 Erhard, A., Wustenberg, H., Zimpfer, J., "Quasi-Two-Dimensional Holography as a Method for Flaw Size Determination," in *Proc. Int. Symposium on New Methods of Non-Destructive Testing of Materials and Their Application Especially in Nuclear Engineering*, German Society for Nondestructive Testing, Dortmund, Germany, 1980.

65 Berger, M., Bruck, D., Fischer, M., Langenberg, K. J., Oberst, J., and Schmitz, V., "Potential and Limits of Holographic Reconstruction Algorithms," *J. Nondestr. Eval.*, Vol. 2, 1981, pp. 85–112.

66 Aldridge, E. E., and Clement, M. J. -M., "Ultrasonic Holography" in *Ultrasonic Testing: Nonconventional Testing Techniques*, Szilard, J., ed., Wiley, Chichester, England, 1982, pp. 103–166.

67 Johnson, John, "Parameter Study of Synthetic-Aperture Focussing in Ultrasonics," *Review of Progress in Nondestructive Evaluation 1*, Thompson, D. O., and Chimenti, D. E., eds., Plenum Press, New York, 1982, pp. 735–752.

68 Barna, B. A., and Johnson, J. A., "The Effects of Surface Mapping Correction With Synthetic-Aperture Focussing Techniques on Ultrasonic Imaging," ibid, pp. 753–760.

69 Peterson, D. K., Baer, R., Liang, K., Bennett, S. D., Khuri-Yakub, B. T., and Kino, G. S., "Quantitative Evaluation of Real-Time Synthetic Aperture Acoustic Images," ibid, pp. 767–776.

70 Schmitz, V., "Classification and Reconstruction of Defects by Combined Acoustical Holography and Line-Saft (Holosaft)," in *New Procedures in Nondestructive Testing*, Springer-Verlag, Berlin, in press.

71 Seydel, J. A., "Ultrasonic Synthetic-Aperture Focussing Techniques in NDT," in *Research Techniques in Nondestructive Testing*, Vol. 6, Sharpe, R. S., ed., Academic Press, London, in press.

72 Grohs, B., Barbian, O. A., Kappes, W., Paul, H., Licht, R., and Hoh, F. W., "Characterization of Flaw Location, Shape, and Dimensions With the ALOK System," *Mater. Eval.*, Vol. 40, 1982, pp. 84–89.

73 Thompson, R. B., and Evans, A. G., "Goals and Objectives of Quantitative Nondestructive Evaluation," *IEEE Trans. on Sonics and Ultrasonics*, SU-23, 1976, pp. 292–299.

74 Thompson, R. B., and Thompson, D. O., "NDE Techniques for Quantitative NDE," in *Nondestructive Evaluation: Microstructural Characterization and Reliability Strategies*," Buck, O., and Wolf, S. M., eds., Metallurgical Society of AIME, Warrendale, Pa., 1981, pp. 33–51.

75 Silk, M. G., "Sizing Crack-Like Defects by Ultrasonic Means," in *Research Techniques in Nondestructive Testing*, Vol. 3, Sharpe, R. S., ed., Academic Press, London, 1977, pp. 51–100.

76 Achenbach, J. D., and Norris, A. N., "Interference of a Corner Reflected and Edge Diffracted Signals for a Surface Breaking Crack," *J. Acoust. Soc. Amer.*, Vol. 70, 1981, pp. 165–171.

77 Gruber, G. J., "Defect-Identification and Sizing by the Ultrasonic Satellite-Pulse Technique," *J. Nondestr. Eval.*, Vol. 1, 1980, pp. 263–276.

78 Nichols, Roy W., "NDE Effectiveness in Relation to RPV Integrity," *Quantitative NDE in the Nuclear Industry*, American Society for Metals, Metals Park, Ohio, 1983, pp. 6–11.

79 Golan, S., Adler, Laszlo, Cook, K. V., Nanstad, R. K., and Bolland, T. K., "Ultrasonic Diffraction Techniques for Characterization of Fatigue Cracks," *J. Nondestr. Eval.*, Vol. 1, 1980, pp. 11–20.

80 Achenbach, J. D., Viswanathan, K., and Norris, A., "An Inversion Integral for Crack Scattering Data," Wave Motion, Vol. 1, 1979, pp. 299–316.

81 Achenbach, J. D., and Norris, A., "Crack Characterization by the Combined Use of Time-Domain and Frequency-Domain Scattering Data," *Review of Progress in Quantitative Nondestructive Evaluation 1*, Thompson, D. O., and Chimenti, D. E., eds., Phenum Press, New York, 1982.

82 Norris, A. N., "Inverse Ray Tracing in Anisotropic Elastic Solids," *Review of Progress in Quantitative Nondestructives Evaluation 2*, Thompson, D. O., and Chimenti, D. E., eds., Plenum Press, New York, in press.

83 Achenbach, J. D., Norris, A. N., Ahlberg, L. A., and Tittmann, B. R., "Crack Mapping by Ray Methods," ibid.

84 Tittmann, B. R., Buck, O., Ahlberg, L., DeBilly, M., Cohen-Tenoudji, F., Jungman, A., and Quentin, G., "Surface Wave Scattering From Elliptical Cracks for Failure Prediction," *J. Appl. Phys.*, Vol. 51, 1980, p. 142.

85 Testa, A. J., and Burger, C. P., "Rayleigh Spectroscopy for Characterizing Surface Cracks," *Review of Progress in Quantitative Nondestructive Evaluation 1*, Thompson, D. O., and Chimenti, D. E., eds., Plenum Press, New York, 1982.

86 Singh, A., Burger, C. P., Schmerr, L. W., and Zachary, L. W., "Dynamic Photoelasticity as an Aid to Sizing Surface Cracks by Frequency Analysis," in *Mechanics of Nondestructive Testing*, Stinchcomb, W., ed. Plenum Press, New York, 1980.

87 Zachary, L. W., Burger, C. P., Schmerr, L. W., and Singh, A., "Surface Crack Characterization by Means of Dynamic Photoelastic Spectroscopy," *Exp. Mech.*, in press.

88 Sachse, W., "Ultrasonic Spectroscopy of a Fluid-Filled Cavity in an Elastic Solid," *J. Acoust. Soc. Am.*, Vol. 54, 1974, pp. 981–896.

89 Sachse, W., "The Scattering of Elastic Pulses and the Nondestructive Evaluation of Materials," *Mater. Eval.*, Vol. 35, Oct. 1977, pp. 83–89.

90 Pao, Y-H. and Sachse, W., "Interpretation of Time Records and Power Spectra of Scattered Ultrasonic Pulses in Solids," *J. Acoust. Soc. Am.*, Vol. 54, 1974, pp. 1478–1486.

91 Cohen-Tenoudji, F., Ahlberg, L., Tittmann, B. R., Opsal, J. L., Varadan, V. V., and Quentin, G., "The Role of Creep Rays in the Scattering From Spheroidal Cavities and Inclusions in Solids," *1981 Ultrasonics Symposium Proceedings*, IEEE, New York, 1981, pp. 853–858.

92 Gaunard, G. and Uberall, H., "Identification of Cavity-Fillers in Elastic Solids Using the Resonance Scattering Theory," *Ultrasonics*, Vol. 18, 1980, pp. 261–269.

93 Brill, D., Gaunard, G., and Uberall, H., "The Response Surface in Elastic Wave Scattering," *J. Appl. Phys.*, Vol. 52, 1981, pp. 3205–3214.

94 Brill, D., Gaunard, G. C., and Uberall, H., "Acoustic Spectroscopy," *J. Acoust. Soc. Am.*, Vol. 72, 1982, pp. 1067–1069.

95 Bolling, G., and Langenberg, K. J., "Ultrasonic Defect Classification Using the Singularity Expansion Method," *Review of Progress in Nondestructive Evaluation 2*, Thompson D. O., and Chimenti, D. E., eds., Plenum Press, New York, pp. 203–212.

96 Rose, J. H., and Krumhansl, J. A., "Determination of Flaw Characteristics from Ultrasonic Scattering Data," *J. Appl. Phys.*, Vol. 50, 1979, pp. 2951–2952.

97 Rose, J. H., Varadan, V. V., Varadan, V. K., Elsley, R. K., and Tittmann, B. R., "Inversion of Ultrasonic Scattering Data," *Acoustic, Electromagnetic, and Elastic Wave Scattering-Focus on the T-Matrix Approach*, Varadan, V. K., and Varadan, V. V., eds., Pergamon Press, New York, 1982.

98 Elsley, R. K., and Addison, R. C., Jr., "Dependence of the Accuracy of the Born Inversion on Noise and Bandwidth," *Proceedings of the DARPA/AF Review of Progress in Quantitative NDE*, Report AFWAL-TR-81-4080 Air Force Wright Aeronautical Laboratories, Dayton, Ohio, 1981, pp. 389–295.

99 Addison, R. C., Elsley, R. K., and Martin, J. F., "Test Bed for Quantitative NDE-Inversion Results," *Review of Progress in Nondestructive*

Downloaded 02 May 2010 to 171.66.16.250. Redistribution subject to ASME license or copyright; see http://www.asme.org/terms/Terms_Use.cfm

Evaluation 1, Thompson, D. O., and Chimenti, D. E., eds., Plenum Press, New York, 1982, pp. 251–261.

100 Hsu, D. K., Rose, James, H., and Thompson, D. O., "Quantitative Experimental Characterization of Inclusions in Solids by Inverse Born Algorithm," *Review of Progress in Nondestructive Evaluation 2*, Thompson, D. O., and Chimenti, D. E., eds., Plenum Press, New York, in press.

101 Thompson, R. B., and Gray, T. A., "Range of Applicability of Inversion Algorithms," *Review of Progress in Nondestructive Evaluation 1*, Thompson, D. O., and Chimenti, D. E., eds., Plenum Press, New York, 1982, p. 249.

102 Rose, J. H., and Richardson, J. M., "Time-Domain Born Approximation," *J. Nondestr. Eval.*, Vol. 3, 1982, pp. 45–54.

103 Rose, James H., and Opsal, Jon L., "The Inverse Born Approximation: An Exact Procedure for Determining Flaw Shape," *Review of Progress in Nondestructive Evaluation 2*, Thompson, D. O., and Chimenti, D. E., eds., Plenum Press, New York, in press.

104 Rose, J. H., and Opsal, J. L., "Inversion of Ultrasonic Data," ibid.

105 Kogan, V. G., and Rose, James H., "On the Effects of a Finite Aperture on the Inverse Born Approximation," ibid.

106 Bleistein, N., and Cohen, J. K., "The Singular Function of a Surface and Physical Optics Inverse Scattering," *Wave Motion*, Vol. 1, 1979, p. 153.

107 Bleistein, N., and Cohen, J. K., "Progress on a Mathematical Inversion Technique for Nondestructive Evaluation," *Wave Motion*, Vol. 2, 1980, p. 75.

108 Langenberg, K. J., and Bruck, D., "Inverse Scattering Algorithms," *New Procedures in Nondestructive Testing*, Springer-Verlag, Berlin, in press.

109 Lee, D. A., "Mathematical Principles of Data Inversion," *Fundamentals of Quantitative Ultrasonic Nondestructive Evaluation*, Thompson, D. O., and Thompson, R. B., eds., Springer-Verlag, Berlin, in press.

110 Thompson, R. B., Lakin, K. M., and Rose, J. H., "A Comparison of the Inverse Born and Imaging Techniques for Reconstructing Flaw Shapes," *1981 Ultrasonics Symposium Proceedings*, pp. 930–935.

111 Budianski, B., and Rice, J. R., "On the Estimation of a Crack Fracture Parameter by Long-Wavelength Scattering," ASME JOURNAL OF APPLIED MECHANICS, Vol. 45, 1978, p. 453.

112 Khuri-Yakub, B. T., Evans, A. G., and Kino, G. S., "Acoustic Surface Wave Measurements of Surface Cracks in Ceramics," *J. Am. Ceramic Soc.*, Vol. 63, 1980, pp. 65–71.

113 Tien, J. J. W., Khuri-Yakub, B. T., Kino, G. S., Marshall, D. B., and Evans, A. G., "Surface Acoustic Wave Measurements of Surface Cracks in Ceramics," *J. Nondestr. Eval.*, Vol. 2, pp. 219–229.

114 Resch, M. T., Shyne, J. C., Kino, G. S., and Nelson, D. V., "Long Wavelength Rayleigh Wave Scattering From Microscopic Surface Fatigue Cracks," *Review of Progress in Nondestructive Evaluation 1*, Thompson D. O., and Chimenti, D. E., eds. Plenum Press, New York, 1982, pp. 573–578.

115 Resch, M. T., Nelson, D. V., Shyne, J. C., and Kino, G. S., "Progress in the SAW NDE of Small Surface Fatigue Cracks," *Review of Progress in Nondestructive Evaluation 2*, Thompson, D. O., and Chimenti, D. E., eds., Plenum Press, New York, in press.

116 Datta, S. K., Fortunko, C. M., and King, R. B., "Sizing of Surface Cracks in a Plate Using Surface Waves," *Review of Progress in Nondestructive Evaluation 1*, Thompson, D. O., and Chimenti, D. E., eds., Plenum Press, New York, 1982, pp. 227–231.

117 Datta, S. K., Shah, A. H., and Fortunko, C. M., "Diffraction of Medium and Long Wavelength Horizontally Polarized Shear Waves by Edge Cracks," *J. Appl. Phys.*, Vol. 53, 1982, pp. 2895–2903.

118 Fortunko, C. M., King, R. B., and Tan, M., "Nondestructive Evaluation of Planar Defects in Plates Using Low Frequency Shear Horizontal Waves," *J. Appl. Phys.*, Vol. 53, 1982, pp. 3450–3458.

119 Gubernatis, J. E., Krumhansl, J. A., and Thomposn, R. M., "Interpretation of Elastic Wave Scattering Theory for Analysis and Design of Flaw Characterization Experiments: The Long Wavelength Limit," *J. Appl. Phys.*, Vol. 50, 1979, pp. 33–45.

120 Richardson, J. M., "The Inverse Problem in Elastic Wave Scattering at Long Wavelengths," *1978 Ultrasonic Symposium Proceedings*, IEEE, New York, 1978, pp. 759–766,

121 Kohn, W., and Rice, J. R., "Scattering of Long-Wavelength Elastic Waves From Localized Defects in Solids," *J. Appl. Phys.*, Vol. 50, 1979, pp. 33–53.

122 Tittmann, B. R., Morris, W. L., and Richardson, J. M., "Elastic Wave Scattering at Long Wavelengths," *Appl. Phys. Lett.*, Vol. 36, 1980, pp. 199–201.

123 Rose, J. H., "Inverse Scattering at Long Wavelength: $\delta\mu = 0$," *Review of Progress in Nondestructive Evaluation 1*, Thompson, D. O., and Chimenti, D. E., eds., Plenum Press, New York, 1982, pp. 131–136.

124 Gubernatis, J. E., and Domany, E., "Rayleigh Scattering of Elastic Waves From Cracks," *J. Appl. Phys.*, Vol. 50, 1979, pp. 818–824.

125 Fertig, K. W., and Richardson, J. M., "Inverse Scattering at Low and Intermediate Frequencies," in *Proceedings of the DARPA/AFML Review of Progress in Quantitative NDE*, report AFWAL-TR-80-4078 Air Force Wright Aeronautical Laboratories, Dayton, Ohio, 1980, pp. 528–540.

126 Richardson, J. M., and Evans, A. G., "Accept/Reject Decisions and Failure Prediction for Structural Ceramics: Application to Failure From Voids," *J. Nondestr. Eval.*, Vol. 1, 1980, pp. 37–52.

127 Allen, D. R., Cooper, W. H. B., Sayers, C. M., and Silk, M. G., "The Use of Ultrasonics to Measure Residual Stress," *Research Techniques in Nondestructive Testing*, Vol. 6, Sharpe, R. S., ed. Academic Press, London, in press.

128 Thurston, R. N., "Effective Elastic Constants for Wave Propagation in Crystals Under Stress," *J. Acoust. Soc. Amer.*, Vol. 37, 1965, pp. 348–356.

129 Kino, G. S., Barnett, D. M., Grayeli, N., Hermann, G., Hunter, H. B., Ilic', D. B., Johnson, G. C., King, R. B., Scott, M. P., Shyne, J. C., and Steele, C. R., "Acoustic Measurements of Stress Fields and Microstructure," *J. Nondestr. Eval.*, Vol. 1, 1980, pp. 67–77.

130 Thompson, R. B., Smith, J. F., and Lee, S., "Absolute Measurement of Residual Stress in Textured Materials," *Review of Progress in Nondestructive Evaluation 2*, Thompson, D. O., and Chimenti, D. E., eds., Plenum Press, New York, in press.

131 King, R. B., and Fortunko, C. M., "Evaluation of Residual Stress States Using Electromagnetic-Acoustic Transducers,' ibid.

132 King, R. B., and Fortunko, C. M., "Determination of In-Plane Residual Stress States in Plates Using Horizontally Polarized Shear Waves," *J. Appl. Phys.*, in press.

133 Salama, K., Wang, J. J., and Barber, G. C., "The Use of the Temperature Dependence of the Ultrasonic Velocity to Measure Residual Stress," *Review of Progress in Nondestructive Evaluation 2*, Thompson, D. O., and Chimenti, D. E., eds., Plenum Press, New York, in press.

134 Emmerson, P. J., and Simmons, W., "Final Report on the Evaluation of Graphite Form in Ferrite Ductile Irons by Ultrasonic Testing and on the Effects of Graphite Form on Mechanical Properties," *AFS Transactions*, Vol. 84, 1976, pp. 109–128.

135 Fuller, A. G., "Evaluation of the Graphite Form in Pearlitic Ductile Iron by Ultrasonic and Sonic Testing and the Effect of Graphite Form on Mechanical Properties, *AFS Transactions*, Vol. 85, 1977, pp. 509–526.

136 Kovacs, B. V., "Quality Control and Assurance by Sonic Resonance in Ductile Iron Casting," *AFS Transactions*, Vol. 85, 1977, pp. 499–508.

137 Papadakis, E. P., "Ultrasonic Velocity and Attenuation," in *Physical Acoustics*, Vol. XII, Mason, W. P., and Thurston, R. N., eds., Academic Press, New York, 1976, pp. 277–374.

138 Green, R. E. Jr., *Ultrasonic Investigation of Mechanical Properties, Treatise on Materials Science and Technology*, Vol. 3, Herman, H., ed., Academic Press, New York, 1973.

139 Papadakis, Emmanuel P., "Ultrasonic Velocity and Attenuation: Measurements Methods With Scientific and Industrial Applications," *Physical Acoustics Principles and Methods*, Vol. XII, Mason, W. P., and Thurston, R. N., eds., Academic Press, New York, 1976, pp. 277–374.

140 Vary, A., "Ultrasonic Measurements of Material Properties," *Research Techniques in Nondestructive Testing*, Vol. 4, Sharpe, R. S., ed., Academic Press, London, 1980, pp. 159–204.

141 Green, R. E. Jr., "Effect of Metallic Microstructures on Ultrasonic Attenuation," in *Nondestructive Evaluation: Microstructural Characterization and Reliability Strategies*, Buck, O., and Wolf, S. M., eds., Metallurgical Society of AIME, Warrendale, Pa., 1981, pp. 115–132.

142 Papadakis, Emmanuel P., "Ultrasonic Attenuation Caused by Scattering in Polycrystalline Media," *Physical Acoustics Principles and Methods*, Vol. IVB, Mason, W. P., and Thurston, R. N., eds., Academic Press, New York, 1968, pp. 269–328.

143 Joshi, N. R., and Green, R. E. Jr., "Ultrasonic Detection of Fatigue Damage," *Engineering Fracture Mechanics*, Vol. 4, 1972, pp. 577–583.

144 Vary, Alex, "Correlations Between Ultrasonic and Fracture Toughness Factors in Metallic Materials," *Fracture Mechanics*, Smith, C. W., ed., ASTM STP 677, American Society for Testing and Materials, Metals Park, Ohio, 1979, pp. 563–578.

145 Thompson, D. O., Wormley S. J., Rose, James H., and Thompson R. B., "Ultrasonic Scattering From Multiple Voids," *Review of Progress in Nondestructive Evaluation 2*, Thompson, D. O., and Chimenti, D. E., eds., Plenum Press, New York, in press.

146 Buck, O., Morris, W. L., and James, M. R., "Remaining Fatigue Life Prediction in the Initiation Regime Using SAW NDE," *J. Nondestr. Eval.*, Vol. 1, 1980, pp. 3–10.

147 *Fundamentals of Acoustic Emission*, Ono, K., ed., Proc. Joint Meeting of Acoust. Soc. Jpn. and Am., Honolulu, Hawaii, Dec. 1978, Materials Dept., UCLA.

148 Pao, Y-H., and Gajewski, R. R., "The Generalized Ray Theory and Transient Responses of Layered Elastic Solids," in, *Physical Acoustics Principles and Methods*, Vol. XIII, Mason, W. P., and Thurston, R. N., eds., Academic Press, New York, 1978.

149 Wadley, H. N. G., Scruby, C. B., and Speake, J. H., "Acoustic Emission for Physical Examination of Metals," *Intern. Metals Review*, 1980, pp. 41–64.

150 Lord, A. E. Jr., "Acoustic Emission — An Update," in *Physical Acoustics Vol. XI*, Mason, W. P., and Thurston, R. N., eds., Academic Press, New York, 1981, pp. 295–360.

151 Gerberich, W. W., and Jatavallabhula, K., "A Review of Acoustic Emission From Sources Controlled by Grain Size and Particle Fracture," in *Nondestructive Evaluation: Microstructural Characterization and Reliability Strategies*, Buck, O., and Wolf, S. M., eds., Metallurgical Society of AIME, Warrendale, Pa., 1981, pp. 319–348.

Downloaded 02 May 2010 to 171.66.16.250. Redistribution subject to ASME license or copyright; see http://www.asme.org/terms/Terms_Use.cfm

The Overall Elastic Response of Composite Materials

J. R. Willis
School of Mathematics,
Bath University,
Bath, BA2 7AY, England

If a composite is modeled as a randomly inhomogeneous medium, an "overall modulus operator" relates the ensemble average of the stress to that of the strain. This paper reviews methods for estimating the overall modulus operator when only a limited amount of statistical information on the composite is available. The most securely based estimates come from bounds on the energy. Such bounds induce bounds on the components of the overall modulus operator and have a precise status, independent of the pointwise quality of the approximating fields from which they are derived. Other approximations are also outlined, however; these include perturbation series, estimates obtained from making ad hoc closure assumptions, and self-consistent estimates. The paper concludes with a discussion of possible future developments.

1 Introduction

This paper intends to provide a review of methods for estimating the overall properties of random composites, with a particular emphasis on recent developments. Many comprehensive reviews of the subject exist already, for example, [1-4]. The present work is self-contained in the sense that it does not assume prior knowledge of the field, but it is brief, and original references are not always cited. It also tends to concentrate on methods and concepts rather than explicit results. Such results as are given are presented in their most general form; this has the advantage of demonstrating, reasonably concisely, what types of estimates can be given, but for more explicit formulas, applicable to particular media, as well as for proper attribution, the reader is referred to [1-4].

Earlier reviews by the writer [3, 4] have concentrated primarily on a definition of overall properties based on volume averages of nominally uniform fields. Here, both to avoid repetition and to accommodate a discussion of nonuniform fields, the discussion is phrased in terms of ensemble averages. Only static problems are considered, but the ensemble averaging approach can also be applied to dynamic problems, and all of the methods that are described have been generalized to the dynamic case.

The three principal methods for studying randomly inhomogeneous media are based, respectively, on perturbation theory, ad hoc closure assumptions to truncate a hierarchy, and variational principles. Perturbation theory works well for media whose properties vary only slightly from point to point, and it has the virtue of precision: the error involved in truncating a perturbation series can, in principle, be estimated exactly. Unfortunately, however, composites are strongly heterogeneous and recourse to other approximations is unavoidable in practice. Variational principles essentially bound the energy of the composite. If approximate fields are substituted into them, strict bounds for the energy result and induce bounds for components of the "overall modulus tensor." Their quality can be assessed from the difference between the upper and lower bounds, regardless of the pointwise accuracy of the approximate fields. Such bounds feature prominently in the text; they represent the most securely based aspect of "overall modulus" theory. A brief discussion of self-consistent methods is also presented.

The last section contains a discussion of prospects for future work. Some of this relates to extensions to dynamic problems but the paper concludes with an outline of a possible extension to a class of nonlinear problems, the implications of which have not so far been investigated.

2 Formulation

The basic problem to be considered is that of solving the equilibrium equations

$$\text{div } \sigma + f = 0 \tag{2.1}$$

for an elastic body occupying a domain Ω, subjected to body force f per unit volume and boundary conditions that either displacement or traction components, or some combination of these, are prescribed on the boundary $\partial\Omega$. The body is inhomogeneous, so that its tensor of elastic moduli L varies with position, x. Symbolically, stress σ is related to strain e by

$$\sigma = Le; \tag{2.2}$$

in components this would read $\sigma_{ij} = L_{ijkl}e_{kl}$. Components of strain are related to components of displacement by $e_{ij} = u_{(i,j)}$, the suffix j representing differentiation with respect to x_j and the bracket representing symmetrization.

It is convenient to introduce a "comparison" body, whose tensor of elastic moduli is denoted by L_0. Although this is not

Contributed by the Applied Mechanics Division for publication in the JOURNAL OF APPLIED MECHANICS.

Discussion on this paper should be addressed to the Editorial Department, ASME, United Engineering Center, 345 East 47th Street, New York, N.Y. 10017, and will be accepted until two months after final publication of the paper itself in the JOURNAL OF APPLIED MECHANICS. Manuscript received by ASME Applied Mechanics Division, March, 1983.

Copyright © 1983 by ASME
Downloaded 02 May 2010 to 171.66.16.250. Redistribution subject to ASME license or copyright; see http://www.asme.org/terms/Terms_Use.cfm

essential at present, L_0 will usually be taken as uniform over Ω, so that the corresponding boundary value problem for the comparison body is easier to solve than that for the original body. In any case, it is supposed that the problem for the comparison body generates the stress, strain, and displacement fields σ_0, e_0, u_0, and furthermore, that the associated Green's function for the displacement field is G_0; the slight complication in the definition of G_0 in the case of the traction boundary value problem is acknowledged here, but is not discussed in detail because it will be seen in the following that it causes no difficulty.

If σ, e represent stress and strain in the actual body, it follows that

$$\sigma = L_0 e + \tau, \tag{2.3}$$

where the "stress polarization" τ is given by

$$\tau = (L - L_0)e. \tag{2.4}$$

Substitution of (2.3) into (2.1) gives

$$\text{div}(L_0 e) + (\text{div } \tau + f) = 0 \tag{2.5}$$

and a representation for the strain field e can be found, using the Green's function G_0. This can be put in the form [3-5]

$$e = e_0 - \Gamma_0 \tau, \tag{2.6}$$

where Γ_0 is an operator whose kernel consists of derivatives of G_0; specifically, its components are given by

$$[\Gamma_0(x,x')]_{ijkl} = \partial^2 [G_0(x,x')]_{jk} / \partial x_i \partial x_l' |_{(ij)(kl)}. \tag{2.7}$$

It has a singularity of order $|x - x'|^{-3}$ which is to be interpreted in the sense of generalized functions [6]. The operator Γ_0 is uniquely defined even for the traction boundary value problem because it is associated with strain, whereas the nonunique part of G_0 is associated with a rigid body displacement.

Equations (2.4) and (2.6) may be combined to give operator equations for either e or τ. Eliminating τ gives

$$e = e_0 - \Gamma_0 [(L - L_0)e] \tag{2.8}$$

while eliminating e gives

$$(L - L_0)^{-1} \tau + \Gamma_0 \tau = e_0. \tag{2.9}$$

Equation (2.8) forms a natural starting point for a perturbation treatment, valid when $L - L_0$ is small. Equation (2.9) is useful for a different type of perturbation approach, applicable to a composite containing a dilute dispersion of inclusions. Both of these are discussed later, together with strict bounds that come from substituting simple forms for e or τ into variational principles. It may be noted in this context that (2.9) is self-adjoint, whereas (2.8) is not. The Hashin-Shtrikman variational principle [5, 7] states that

$$\delta \mathcal{H}(\tau) = 0, \tag{2.10}$$

where

$$\mathcal{H}(\tau) = (\tau, (L - L_0)^{-1} \tau) + (\tau, \Gamma_0 \tau) - 2(e_0, \tau) \tag{2.11}$$

and

$$(v, w) = (w, v) = V^{-1} \int_\Omega vw \, dx, \tag{2.12}$$

V denoting the volume of Ω. This principle follows directly from (2.9).

A further variant of (2.8) and (2.9) can be given by defining the tensor K so that $K^2 = L - L_0$. Then, with the notation $\rho = Ke = K^{-1}\tau$, $\rho_0 = Ke_0$, it follows that

$$\rho + (K\Gamma_0 K)\rho = \rho_0 \tag{2.13}$$

The symmetry of this form was exploited by Kantor and Bergman [8] to represent ρ as an expansion in the eigenfunctions of $(K\Gamma_0 K)$. This interesting development is not discussed further because it would entail too great a digression from the main line of presentation.

3 Mathematical Specification of a Composite

In this paper, a composite is modeled as a medium composed of several constituents or phases, firmly bonded together at their interfaces. Some composites (laminated media, for example) may have a regular structure, so that the tensor $L(x)$ is periodic in x. Others, for instance those comprising a matrix reinforced by aligned fibers, may not have a periodic structure but nevertheless, useful estimates of their properties might be obtained from analysis of a periodic model. There are also materials, however, for which it would be difficult to conceive a reasonable periodic approximation. Examples include composites containing chopped fibers and polycrystals: the latter, although not fabricated, are still media that display inhomogeneity on a microscale. The structure of such media is so complex that it is hardly feasible to define $L(x)$ at each point x. It is more likely, instead, that only a certain amount of statistical information is available, for instance, the volume concentration of each phase is likely to be prescribed.

A convenient way to describe the geometrical configuration of a composite is to introduce indicator functions that define the location of each phase of the composite. Thus, the indicator $f_r(x)$ takes the value 1 if x lies in phase r and zero otherwise. The functions $f_r(x)$ would be known exactly for a periodic composite but, for the less regular composites described in the foregoing, they are best considered as random fields, so that they also depend on a parameter α that belongs to a sample space $\mathfrak{A}$, over which a probability measure p is defined. This is equivalent to regarding the composite as one particular member, with label α, of an ensemble. For any given α, the functions $f_r(x,\alpha)$ are defined explicitly, in principle at least. In practice, however, only mean properties such as

$$P_r(x) = \langle f_r(x) \rangle = \int_{\mathfrak{A}} f_r(x,\alpha) p(d\alpha) \tag{3.1}$$

will be known (or, more strictly, will have been estimated). The function $P_r(x)$ represents the probability of finding phase r at x; it is equal to the volume concentration c_r of phase r (and so is independent of x) in the particular case of a statistically uniform medium. The next simplest statistic (and even this will not always be available) is

$$P_{rs}(x,x') = \langle f_r(x) f_s(x') \rangle = \int f_r(x,\alpha) f_s(x',\alpha) p(d\alpha). \tag{3.2}$$

This represents the probability of finding phase r at x and phase s at x'; in the case of a statistically uniform medium, it depends on x,x' in the combination $x\text{-}x'$ and can be estimated as the average of $f_r(x)f_s(x')$ over a large volume of one particular sample, with $x - x'$ fixed.

With these definitions, for a medium consisting of n phases, the rth phase having moduli L_r ($r = 1,2, \ldots n$), it follows that, in sample α,

$$L(x) = \sum_{r=1}^{n} L_r f_r(x,\alpha) \tag{3.3}$$

so that

$$\langle L(x) \rangle = \sum_{r=1}^{n} L_r P_r(x), \tag{3.4}$$

$$\langle L(x) X L(x') \rangle = \sum_{r=1}^{n} \sum_{s=1}^{n} L_r X L_s P_{rs}(x,x') \tag{3.5}$$

and so on.

For media with deterministic structure, the functions $f_r(x)$ are known with certainty so that, for example, $P_r(x)$ coincides with $f_r(x)$ and taking expectations has no effect. Only

Downloaded 02 May 2010 to 171.66.16.250. Redistribution subject to ASME license or copyright; see http://www.asme.org/terms/Terms_Use.cfm

random media will be considered in the sequel, because these present a challenge additional to that of solving a well-defined boundary value problem, but many of the methods, and even some of the results, apply to deterministic media if the relevant functions $P_r(x)$, $P_{rs}(x,x')$ etc., are employed. It is noted that a medium with periodic structure could still be random, in the sense described in the foregoing, if the precise location of a basic cell of the lattice were subject to uncertainty. This could lead to a situation, for example, in which $P_r(x)$ is uniform but $P_{rs}(x,x')$ is a periodic function of x-x'.

For composites consisting of a matrix containing a population of identical inclusions, an alternative characterization is obtained by specifying probability densities for the locations of the inclusions. For example, P_A is defined as the probability density for finding an inclusion centered at x_A, P_{AB} is the joint density for finding distinct inclusions centered at x_A, x_B, and so on. The probabilities $P_r(x)$, $P_{rs}(x,x')$ introduced in the foregoing can be found as integrals of these densities.

4 Perturbation Theory and Other Approximations

The elastic moduli $L(x)$ depend on the sample α. Correspondingly, the stress, strain, and displacement fields depend on α. If they could be found explicitly, their mean values and other statistics could be deduced directly. In particular, taking the expectation of (2.2) gives

$$<\sigma> = <Le> = \hat{L}<e> \tag{4.1}$$

the second equality providing a definition of the "overall modulus operator" $\hat{L}$.

A formal solution can be obtained by application of perturbation theory to (2.8). It is convenient to set

$$e = <e> + e', \tag{4.2}$$

with similar definitions for other fields. The solution is simplified by choosing $L_0 = <L>$. Then, taking the expectation of (2.8) gives

$$<e> = e_0 - \Gamma_0 <L'e'> \tag{4.3}$$

and, subtracting this from (2.8),

$$e' = -\Gamma_0 L'<e> - \Gamma_0(L'e' - <L'e'>). \tag{4.4}$$

If L' is small, then e' is small and can be expressed in terms of $<e>$ by iteration of (4.4). Thus,

$$e' = -\Gamma_0 L'<e> + \Gamma_0(L'\Gamma_0 L' - <L'\Gamma_0 L'>)<e> + \ldots . \tag{4.5}$$

Now from (4.1),

$$<\sigma> = \hat{L}<e> = <L><e> + <L'e'> \tag{4.6}$$

and so, from (4.5) and (4.6),

$$\hat{L} = <L> - <L'\Gamma_0 L'> + <L'\Gamma_0 L'\Gamma_0 L'> - \ldots . \tag{4.7}$$

The mean field $<e>$ is still unknown. It satisfies (4.3), however and this implies, with (4.6),

$$\mathrm{div}(\hat{L}<e>) + f = 0, \tag{4.8}$$

since $\mathrm{div}(L_0 e_0) + f = 0$. Equation (4.8) could also be obtained by taking the expectation value of (2.1). Once $<e>$ is determined, the actual field in any sample α follows from (4.5). It should be noted that (4.7) defines $\hat{L}$ as a nonlocal operator. For example, the second term in the series gives, with (3.5),

$$<L'\Gamma_0 L'><e> = \sum_{r=1}^{n}\sum_{s=1}^{n} L_r \int dx'\ \Gamma_0(x,x')[P_{rs}(x,x') - P_r(x)P_s(x')]L_s <e>(x'). \tag{4.9}$$

The term $P_{rs} - P_r P_s$ can usually be expected to decay to zero at large $|x-x'|$; the decay rate defines a correlation length l, which may be taken to define a microscale, much smaller than a typical macroscopic dimension of the body. Then, except when the distance of x from the boundary of the body is of order l, the kernel $\Gamma_0(x,x')$ in (4.9) can be approximated by the corresponding kernel for an infinite body. In the case where the mean field $<e>$ varies only slightly over distances of order l, $<e>(x')$ in (4.9) can be approximated by its value at x. The operator $\hat{L}$ then reduces to an ordinary tensor, and this is usually what is meant by the term "overall modulus." An alternative prescription for calculating this overall modulus can be developed directly, by subjecting a statistically uniform body to boundary conditions that will produce a uniform mean strain $<e>$ except, perhaps, in the "boundary layer" where $\hat{L}$ cannot be approximated by a constant tensor. For this special problem, the overall modulus can be taken as the tensor that relates the volume average of the stress to the volume average of the strain. This definition is independent of statistical assumptions but, when these are as described in the foregoing, it is at least very plausible that the definition based on volume averages reproduces the ordinary tensor to which $\hat{L}$ reduces when applied to slowly varying fields.

Now consider a matrix/inclusion composite. For ease of exposition, suppose that a matrix with moduli L_2 contains a single population of inclusions, all of the same shape, size, and orientation, with moduli L_1. The inclusions are labeled $A = 1, 2, \ldots N$ so that they are distributed at mean number density $n_1 = N/V$. If their distribution is statistically uniform, then $P_A(x) = n_1$. It is convenient to describe the deformation of such a composite in terms of (2.9) and (at least at present) to let $L_0 = L_2$. Then, τ is nonzero only over the inclusions and (2.9) gives

$$(L_1 - L_2)^{-1}\tau^A + \Gamma_0\tau^A + \sum_{B\neq A}\Gamma_0\tau^B = e_0, \quad x\in\Omega_A, \tag{4.10}$$

where Ω_A denotes the region occupied by inclusion A and τ^A is the restriction of τ to Ω_A. Now if (2.6) is averaged there results

$$<e> = e_0 - \int dx_A\,(\Gamma_0\tau_A^A)(x)P_A(x_A), \tag{4.11}$$

where x_A is the position of an agreed reference point, loosely called the center, of inclusion A, and τ_A^A is the expectation value of τ^A, conditional on inclusion A being centered at x_A. Next (4.10) is averaged, conditionally on inclusion A being fixed, and (4.11) is employed to eliminate e_0 in favor of $<e>$. This gives

$$(L_1 - L_2)^{-1}\tau_A^A + \Gamma_0\tau_A^A + \int dx_B\Gamma_0[\tau_{BA}^B P_{B|A} - \tau_B^B P_B] = <e>,\ x\in\Omega_A, \tag{4.12}$$

where τ_{BA}^B represents the expectation value of τ^B, conditional on both inclusions B and A being fixed, and $P_{B|A}$ is the probability density for finding inclusion B at x_B, conditional on inclusion $A\,(\neq B)$ being centered at x_A. It is related to P_{AB} since $P_{AB} = P_{A|B}P_B = P_{B|A}P_A$. The integral in (4.12) is expected to converge since, when x_B is far from x_A, the term in square brackets will usually tend to zero. The integral is therefore of the order of the volume concentration of the inclusions. If this is small, the lowest-order approximation is provided by neglecting the integral. Then, (4.12) reduces to

$$(L_1 - L_2)^{-1}\tau_A^A + \Gamma_0\tau_A^A = <e>,\ x\in\Omega_A, \tag{4.13}$$

which describes exactly the problem of a single inclusion perturbing a field $<e>$. Even if $<e>$ is not uniform over Ω, it is likely not to vary significantly over Ω_A. Also, except when the inclusion is close to the boundary, Γ_0 can be taken as the corresponding operator for an infinite body, since τ_A^A is zero outside Ω_A. With these restrictions, equation (4.13) describes

Downloaded 02 May 2010 to 171.66.16.250. Redistribution subject to ASME license or copyright; see http://www.asme.org/terms/Terms_Use.cfm

a single inclusion in an infinite body, perturbing a uniform field $<e>(x_A)$. This fundamental problem has been the subject of much attention. It has a simple solution, even when the matrix is anisotropic, when Ω_A is an ellipsoid; the problem is discussed in [3–5].

Once τ_A^A is expressed in terms of $<e>$, the expectation value of (2.3), with $L_0 = L_2$, gives

$$<\sigma> = \hat{L}<e> = L_2<e> + \int_{\Omega(x)} dx_A \tau_A^A(x) P_A(x_A), \quad (4.14)$$

where $\Omega(x)$ denotes the set $\{x_A : x \in \Omega_A\}$, that is, the set of positions x_A for the center of inclusion A such that the inclusion contains the point x. Equation (4.14) defines $\hat{L}$ as an ordinary tensor in the case of a dilute suspension, with $<e>$ varying only slightly over Ω_A.

Suppose now that the inclusions are distributed at a higher number density. The integral in (4.12) cannot be ignored and an estimate for τ_{BA}^B is required. One possible approach is to average (4.10), conditionally on two inclusions (A and B) being in fixed locations. This generates the equation

$$(L_1 - L_2)^{-1}\tau_{AB}^A + \Gamma_0 \tau_{AB}^A + \Gamma_0 \tau_{BA}^B + \int dx_C \Gamma_0 [\tau_{CAB}^C P_{C|AB} - \tau_C^C P_C] = <e>, \; x \in \Omega_A. \quad (4.15)$$

where τ_{CAB}^C is the expectation value of τ^C, conditional on inclusions A, B, and C being fixed, and $P_{C|AB}$ is the conditional density for finding inclusion C centered at x_C. There is a similar equation when $x \in \Omega_B$. Equation (4.15) is the next member of a hierarchy that never yields a closed equation for any conditional expectation of τ^A. A possible method for closing the hierarchy is to ignore the integral in (4.15). Its solution would then yield a zeroth-order estimate for τ_{BA}^B which could be substituted back into (4.12) to provide a first-order estimate for τ_A^A. This laborious procedure would have to be carried out to a higher order than the one described, to obtain a good estimate for $\hat{L}$ in the nondilute case. It would also confront the difficulty that probability densities such as $P_{C|AB}$ are unlikely to be known. Thus, it is reasonable to conclude that the problem is intractable and that an approximate solution should be sought. The simplest approximation procedure is to close the hierarchy at (4.12) by assuming that

$$\tau_{BA}^B = \tau_B^B. \quad (4.16)$$

This is likely to be true at large separations; it is also true exactly if the inclusions are arranged on a regular lattice, since the position of one inclusion fixes the positions of all inclusions. In the general case, equation (4.16) can either be regarded as a mathematical expedient, or perhaps, it might be justified by appeal to "physical intuition" at high densities of inclusions. In either case, it reduces (4.12) to a closed equation for τ_A^A and hence provides an estimate for $\hat{L}$, which contains information on the statistics of the composite only up to the one and two-point probability densities P_A and P_{AB}.

A similar procedure can, in fact, be applied to a general n-phase composite. If (2.9) is averaged, conditionally on finding phase r at x, there results

$$(L_r - L_0)^{-1}\tau_r^r + \sum_{s=1}^{n} \Gamma_0 [\tau_{sr}^s P_{s|r} - \tau_s^s P_s] = <e>, \quad (4.17)$$

where τ_r^r now represents the expectation value of $\tau(x)$, conditional on finding phase r at x, $\tau_{sr}^s(x', x)$ represents the expectation value of $\tau(x')$, conditional on finding phase s at x', and phase r at x and $P_{s|r}$ is defined so that $P_{sr} = P_{s|r}P_r$. The hierarchy of which (4.17) is a member can again be closed by adopting the approximation

$$\tau_{sr}^s = \tau_s^s. \quad (4.18)$$

The approximations (4.16) and (4.18) in fact have rather more than the ad hoc status suggested by their manner of introduction; this is explained in the section that follows.

5 Variational Principles and Optimal Approximations

The Hashin-Shtrikman variational principle has already been noted in Section 2. It is a stationary principle in the general case but L_0 can be chosen so as to make it either a maximum or a minimum principle. The best way to see this is to demonstrate connections between the Hashin-Shtrikman principle and the classical energy principles. First, the classical minimum energy principle can be given in the form

$$\mathcal{F}(u) \leq \mathcal{F}(u^*), \quad (5.1)$$

where u is the actual displacement field and u^* is any "trial" field that satisfies any given conditions on displacements. The functional $\mathcal{F}$ is defined by

$$\mathcal{F}(u^*) = V^{-1}\int_\Omega dx\{e^* L e^* - 2\sigma_0 e^*\} = (e^*, Le^*) - 2(\sigma_0, e^*), \quad (5.2)$$

where σ_0 satisfies $\mathrm{div}\sigma_0 + f = 0$ and any given traction boundary conditions; it can in particular be chosen as the stress generated in the comparison medium.

Suppose now that e^* is chosen as

$$e^* = e_0 - \Gamma_0 \tau^*, \quad (5.3)$$

where τ^* is arbitrary. Then, as shown by Willis [9] in a dynamical study whose static limit reproduces the present equations,

$$\mathcal{F}(u^*) = -\mathcal{K}(\tau^*) - (\sigma_0, e_0) + (\epsilon^*, (L - L_0)^{-1}\epsilon^*), \quad (5.4)$$

where

$$\epsilon^* = (L - L_0)e^* - \tau^*. \quad (5.5)$$

The term involving ϵ^* is negative definite when $L - L_0$ is negative definite at each point of Ω; furthermore, it is zero when τ^* is the actual polarization, τ. Thus, it follows that

$$\mathcal{F}(u) + (\sigma_0, e_0) = -\mathcal{K}(\tau) \leq -\mathcal{K}(\tau^*), \quad (5.6)$$

when $(L - L_0)$ is negative definite. A similar relationship can be generated between $\mathcal{K}$ and the complementary energy functional [9]; this shows that τ maximizes $(-\mathcal{K})$ when $L - L_0$ is positive definite at each point of Ω.

The result may therefore be summarized that

$$\mathcal{K}(\tau) \underset{(\geq)}{\leq} \mathcal{K}(\tau^*), \quad (5.7)$$

whenever $(L - L_0)$ is positive (or negative) definite at each point of Ω. The result (5.7) was derived under more restrictive conditions in [5, 7, 10]. It may be noted that the stationary value of $\mathcal{K}$ is attained when τ satisfies (2.9), so that $\mathcal{K}(\tau)$ reduces to

$$-(e_0, \tau) = (e_0, (L_0 e - \sigma)). \quad (5.8)$$

Elementary manipulation using Gauss' theorem gives

$$-(e_0, \tau) = (e_0, \sigma_0) - (e, \sigma) - 2(u_0 - u, f) \quad (5.9)$$

for the displacement boundary value problem,

$$-(e_0, \tau) = (e, \sigma) - (e_0, \sigma_0) \quad (5.10)$$

for the traction boundary value problem and

$$-(e_0, \tau) = (u - u_0, f) \quad (5.11)$$

when any homogeneous boundary conditions are applied; this last result can also be put in the form (5.10).

For a boundary value problem for a random medium, consider the proposition

$$\delta <\mathcal{K}(\tau)> = 0, \quad (5.12)$$

where τ is now regarded as a function of x and α, on $\Omega \times \mathfrak{A}$. The special choice

Downloaded 02 May 2010 to 171.66.16.250. Redistribution subject to ASME license or copyright; see http://www.asme.org/terms/Terms_Use.cfm

$$\delta\tau(x,\alpha)=\eta(x)f_r(x,\alpha) \tag{5.13}$$

with $\eta(x)$ arbitrary gives, on substitution into (5.13),

$$(L_r-L_0)^{-1}\tau_r^r(x)P_r(x)+\sum_{s=1}^{n}[\Gamma_0(\tau_{sr}^sP_{sr})](x)$$
$$=e_0(x)P_r(x) \tag{5.14}$$

since, by definition,

$$\int\tau(x,\alpha)f_r(x,\alpha)p(d\alpha)=\tau_r^r(x)P_r(x) \tag{5.15}$$

and

$$\int\tau(x',\alpha)f_r(x,\alpha)p(d\alpha)$$
$$=\sum_{s=1}^{n}\int\tau(x',\alpha)f_s(x',\alpha)f_r(x,\alpha)p(d\alpha)$$
$$=\sum_{s=1}^{n}\tau_{sr}^s(x',x)P_{sr}(x',x). \tag{5.16}$$

Equation (5.14) may be recognized as being identical to (4.17). Other members of the hierarchy are generated by taking

$$\delta\tau(x,\alpha)=\eta(x)f_r(x,\alpha)f_{r1}(x_1,\alpha)f_{r2}(x_2,\alpha)\ \ldots\ . \tag{5.17}$$

The variational principle (5.4) thus characterizes the problem for the random medium. Also, since taking expectations is a linear operation that does not disturb inequalities, $<\mathcal{H}(\tau)>$ is minimized by the actual $\tau(x,\alpha)$ when L_0 is such that L_r-L_0 is positive definite for each r, and is maximized when L_r-L_0 is negative definite for each r.

Now substitute into $<\mathcal{H}>$ the trial field

$$\tau^*(x,\alpha)=\sum_{r=1}^{n}\tau_r(x)f_r(x,\alpha) \tag{5.18}$$

to obtain

$$<\mathcal{H}(\tau^*)>=V^{-1}\int_\Omega dx\ \sum_{r=1}^{n}\Big\{\tau_r(L_r-L_0)^{-1}\tau_rP_r$$
$$+\sum_{s=1}^{n}\tau_r\Gamma_0(\tau_sP_{sr})-2e_0\tau_rP_r\Big\}. \tag{5.19}$$

This is stationary when

$$(L_r-L_0)^{-1}\tau_rP_r+\sum_{s=1}^{n}\Gamma_0(\tau_sP_{sr})=e_0P_r. \tag{5.20}$$

With τ_r chosen so that equations (5.20) are satisfied, let

$$e(x,\alpha)=e_0-\sum_{r=1}^{n}\Gamma_0(\tau_rf_r) \tag{5.21}$$

define an approximation for the actual strain in realization α. Taking the expectation of (5.21) generates the estimate

$$<e>=e_0-\sum_{r=1}^{n}\Gamma_0(\tau_rP_r) \tag{5.22}$$

for $<e>$; then, equations (5.20) and (5.22) give the equation that results from combining the closure approximation (4.18) with (4.17). The approximation (4.18) is optimal in this sense: it provides, for any chosen L_0, the closest approximation to the mean value of the energy that can be obtained, given only the one and two-point probabilities P_r and P_{rs}. The approximation (4.16) has a similar status, relative to the densities P_A, P_{AB}.

It may be noted that, whereas (4.12) or (4.17) give information only on the mean field $<e>$, the trial field (5.18) provides the estimate (5.21) for the field in any particular realization α. The accuracy of this estimate cannot be guaranteed but it is the best that can be provided, if only one and two-point probabilities are given. Usually, however, the trial field (5.18) will be used just to provide an estimate for $<\mathcal{H}>$.

This section concludes with a brief reference back to the classical energy principles. In particular, taking the expectation of (5.1) gives

$$<\mathcal{F}(u)>\le<\mathcal{F}(u^*)>. \tag{5.23}$$

A possible trial field u^* can be obtained from the polarization (5.18), the associated strain field $e^*(x,\alpha)$ being given by (5.21), except that the functions $\tau_r(x)$ are so far unrestricted. Evaluation of $<\mathcal{F}(u^*)>$ for such a trial field yields an expression that involves integrals of probabilities for up to three points and optimizing with respect to the functions τ_r gives the smallest upper bound for $<\mathcal{F}>$ that can be obtained, given statistical information up to this order. Substitution of the strain field

$$e^*=<e>-\Gamma_0[(L-L_0)e_1] \tag{5.24}$$

into (5.23) also generates a bound involving three-point probabilities. If e_1 is taken equal to $<e>$, equation (5.24) is the perturbation series expression for e, which was discussed in Section 4, truncated at the first nontrivial term. More generally, choosing $e_1(x)$ optimally produces an "optimal" bound of third order [11]; except in special cases, however, the bound obtained from (5.18) is better, because it includes the possibility (5.24) but contains additional flexibility. A corresponding approach can be based on the complementary energy principle; the result is that the energy can be bounded both from above and from below.

6 Bounds

Consider first the particular boundary condition

$$u_i(x)=\bar{e}_{ij}x_j,\quad x\in\partial\Omega, \tag{6.1}$$

in the absence of body force. It is easy to verify that the average of the actual strain e over Ω is $\bar{e}$ and it is reasonable to assume, if the body is statistically uniform and its dimensions are large relative to the microscale l, that $<e>=\bar{e}$, except in a boundary layer close to $\partial\Omega$, whose volume is a negligible fraction of V. Also, if L_0 is chosen uniform, $e_0=\bar{e}$. For this problem, the Hashin-Shtrikman principle in the form (5.12) gives

$$(\bar{e},L_0\bar{e})-<(e,Le)>\ \underset{(\ge)}{\le}\ -(\bar{e},<\tau^*>), \tag{6.2}$$

where τ^* is given by (5.18) and τ_r satisfy (5.20) or, equivalently,

$$c_r(L_r-L_0)^{-1}\tau_r+\sum_{s=1}^{n}\Gamma_0[\tau_s(P_{sr}-c_sc_r)]=c_r<e>. \tag{6.3}$$

Now by an application of Gauss' theorem,

$$<(e,Le)>=<(\bar{e},Le)>=(\bar{e},\hat{L}<e>), \tag{6.4}$$

the second equality following from the definition (4.1) of $\hat{L}$. The volume averages in (6.2) and (6.4) are unaffected (when V is large) by the nonuniformity in the boundary layer. Hence, considering only points x away from $\partial\Omega$, the functions $\tau_r(x)$ can be taken as constants, still called τ_r, which satisfy the algebraic equations

$$c_r(L_r-L_0)^{-1}\tau_r+\sum_{s=1}^{n}A_{rs}\tau_s=c_r\bar{e}, \tag{6.5}$$

where

$$A_{rs}=\int dx'\ \Gamma_0(x')[P_{rs}(x')-c_rc_s]. \tag{6.6}$$

Here, $\Gamma_0(x')$ denotes the kernel of the infinite-body form of the operator Γ_0 and the translation-invariance of both Γ_0 and P_{rs} has been exploited. $\Gamma_0(x')$ can be given explicitly for an isotropic medium and, even for a generally anisotropic

Downloaded 02 May 2010 to 171.66.16.250. Redistribution subject to ASME license or copyright; see http://www.asme.org/terms/Terms_Use.cfm

medium, a useful plane-wave decomposition can be derived [5]. Solving equations (6.5) gives

$$\tau_r = T_r \bar{e}, \tag{6.7}$$

say, and it follows from (6.2) and (6.4) that

$$\bar{e}\, L_0\, \bar{e} - \bar{e}\, \hat{L}\, \bar{e} \underset{(\leq)}{\leq} -\bar{e} < T > \bar{e}, \tag{6.8}$$

where

$$< T > = \sum_{r=1}^{n} c_r T_r, \tag{6.9}$$

having exploited that T_r and $<e>$ are uniform over Ω, except in the boundary layer, to remove the volume averages. It is convenient to express the result (6.8) in the compact form

$$\hat{L} \underset{(\leq)}{\geq} \tilde{L} \tag{6.10}$$

when $L_r \geq (\leq) L_0$ for each r, where

$$\tilde{L} = L_0 + < T >. \tag{6.11}$$

In (6.10), the inequalities represent order relations induced by the quadratic forms in (6.8).

The result (6.10) contains the classical Hashin-Shtrikman bounds, which arise as special cases when all of the functions $P_{rs}(x')$ depend on $|x'|$ only. The kernel $\Gamma_0(x')$ is a homogeneous (generalized) function of degree -3 and it can be shown that A_{rs} reduces to

$$A_{rs} = P c_r (\delta_{rs} - c_s), \tag{6.12}$$

where P is a constant tensor, given as the integral of $\Gamma_0(x')$ over a sphere of any radius; this is shown explicitly in [3-5]. When A_{rs} take the form (6.12), equations (6.5) can be solved explicitly and (6.11) reduces to

$$\tilde{L} = \{\Sigma\, c_r [I + (L_r - L_0)P]^{-1}\}^{-1} \Sigma\, c_s [I + (L_s - L_0)P]^{-1} L_s. \tag{6.13}$$

It is interesting that $\tilde{L}$ is expressed only in terms of volume concentrations. Information on the two-point probabilities P_{rs} is implicit, through the exploitation of their isotropy.

A similar reduction occurs for any statistically uniform two-phase composite since, for such a material,

$$P_{11} = c_1^2 + c_1 c_2 h,\ P_{12} = c_1 c_2 (1-h),\ P_{22} = c_2^2 + c_1 c_2 h, \tag{6.14}$$

where h depends on $x - x'$ only. The tensors A_{rs} retain the form (6.12) and the bounds given by (6.13) follow, if P is now defined as

$$P = \int dx' \Gamma_0(x') h(x'). \tag{6.15}$$

The foregoing estimates for $\hat{L}$ are useful for estimating $<e>$ for any boundary value problem, so long as $<e>$ varies slowly relative to the microscopic length scale l. More general, nonlocal estimates for $\hat{L}$ can be found but, for these, the displacement problem does not provide the best starting point.

It is useful, instead, to consider an infinite, statistically uniform medium, subjected to a field of body force $f(x)$ that decays sufficiently rapidly when $|x|$ is large. Then, using (5.11), the Hashin-Shrikman principle gives

$$(<u>, f) - (u_0, f) \underset{(\geq)}{\leq} -(e_0, <\tau^*>), \tag{6.16}$$

where the inner product (v,w) here denotes the integral of vw and not its volume average. The field u_0 is given by

$$u_0(x) = (G_0 f)(x) = \int dx' G_0(x - x') f(x'), \tag{6.17}$$

where G_0 is the infinite-body Green's operator and $G_0(x-x')$ is its kernel. The strain field e_0 is obtained by differentiating (6.17); it is convenient to put

$$e_0(x) = (E_0 f)(x). \tag{6.18}$$

The displacement field $<u>$ satisfies an equation like the one that determines u_0, but L_0 is replaced by $\hat{L}$. Correspondingly, let

$$<u> = (\hat{G} f)(x). \tag{6.19}$$

The operator $\hat{G}$ could be found if $\hat{L}$ were known. The polarization τ^* is still given by (5.18) and τ_r satisfy (5.20). Extending the notation used in (6.5), τ_r satisfy

$$c_r (L_r - L_0)^{-1} \tau_r + \sum_{s=1}^{n} A_{rs} \tau_s = c_r <e>, \tag{6.20}$$

where

$$<e> = e_0 - \Gamma_0 <\tau^*> \tag{6.21}$$

and A_{rs} now denotes the operator

$$A_{rs} : \tau_s \rightarrow \int dx' \Gamma_0(x - x') [P_{rs}(x - x') - c_r c_s] \tau_s(x'). \tag{6.22}$$

Suppose that solving equations (6.20) gives

$$\tau_r(x) = (T_r <e>)(x), \tag{6.23}$$

where T_r is now an operator. Then, by substitution back into (6.20)

$$<e> = [I + \Gamma_0 < T >]^{-1} e_0 \tag{6.24}$$

and

$$<\tau^*> = < T > [I + \Gamma_0 < T >]^{-1} e_0. \tag{6.25}$$

Here, I denotes the identity *operator*. Then, equation (6.16) gives

$$(f, \hat{G} f) - (f, G_0 f) \underset{(\geq)}{\leq} -(E_0 f, < T > [I + \Gamma_0 < T >]^{-1} E_0 f). \tag{6.26}$$

If the adjoint operator $E_0^\dagger$ is defined so that

$$(E_0 f, g) = (f, E_0^\dagger g), \tag{6.27}$$

then the result (6.26) can be put in the form

$$\hat{G} \underset{(\geq)}{\leq} \tilde{G}, \tag{6.28}$$

where

$$\tilde{G} = G_0 - E_0^\dagger < T > [I + \Gamma_0 < T >]^{-1} E_0, \tag{6.29}$$

the order relations in (6.28) again being induced by the quadratic forms in (6.26).

Note, now, that E_0 is the strain associated with G_0 and satisfies the equation

$$\operatorname{div}(L_0 E_0) + I = 0. \tag{6.30}$$

Let $\tilde{E}$ be the strain associated with $\tilde{G}$. Differentiating (6.29) gives

$$\tilde{E} = E_0 - \Gamma_0 < T > [I + \Gamma_0 < T >]^{-1} E_0 \tag{6.31}$$

since, from (2.7), Γ_0 is the strain associated with $E_0^\dagger$. Equation (6.31) can be rearranged to give

$$\tilde{E} = E_0 - \Gamma_0 < T > \tilde{E}. \tag{6.32}$$

Then, in view of the relation $\operatorname{div}(L_0 \Gamma_0 t) = \operatorname{div} t$, for any "polarization" t, it follows that

$$\operatorname{div}[(L_0 + < T >)\tilde{E}] + I = 0. \tag{6.33}$$

This demonstrates that $\tilde{G}$ is related in the expected way to the "overall modulus operator" $\tilde{L} = L_0 + < T >$. Also, it follows from (6.28) that

$$(v, \hat{G}^{-1} v) \underset{(\leq)}{\geq} (v, \tilde{G}^{-1} v) \tag{6.34}$$

Downloaded 02 May 2010 to 171.66.16.250. Redistribution subject to ASME license or copyright; see http://www.asme.org/terms/Terms_Use.cfm

for any vector field v. The term $\tilde{G}^{-1}v$ can be written $-\text{div}(\tilde{L}\epsilon)$, where ϵ is the strain associated with v. Therefore, by Gauss' theorem,

$$(\epsilon, \tilde{L}\,\epsilon) \underset{(\leq)}{\geq} (\epsilon, \tilde{L}\,\epsilon) \tag{6.35}$$

for any nonuniform strain field ϵ. Thus, the formal result (6.10) and (6.11) remains valid for nonuniform fields, when $\hat{L}$, $\tilde{L}$ are nonlocal operators. Even when the two-point probabilities are isotropic, the form (6.12) for A_{rs} applies only for uniform fields or, equivalently, in the "local" approximation. However, for any two-phase composite, equation (6.12) remains true, if P is defined as the operator

$$P:\tau \rightarrow \int dx'\ \Gamma_0(x-x')h(x-x')\tau(x'). \tag{6.36}$$

In this case, $\tilde{L}$ is given by (6.13), which now defines a nonlocal operator.

This discussion of bounds for the nonlocal operator $\hat{L}$ was motivated by recent work of Diener, Hürrich, and Weissbarth [12], who have produced bounds for the Fourier transform of $\hat{L}$ in the special case of an isotropic two-phase composite, with a particular form chosen for the two-point probabilities. These results could be reproduced by Fourier transforming (6.35), using the relation

$$(v,w)=(\bar{v},\bar{w})=(2\pi)^{-1}\int dk\ \bar{v}\,(-k)\ \bar{w}(k), \tag{6.37}$$

where $\bar{v}(k)$ represents the Fourier transform of $v(x)$. The general result (6.10) and (6.11) (together with the more explicit (6.13), which applies to any two-phase composite) is new.

The remark at the end of the preceding section, that the classical energy principles can be used to provide bounds of third order for the energy, can now be recognized to imply a method for bounding the tensor $\hat{L}$. Its "local" approximation, as a tensor of moduli, can be bounded by considering the boundary conditions (6.1); a general set of equations that define optimal bounds of third order have been given by Willis [4]. The topic is not pursued further because three-point probabilities are very seldom known in practice.

7 Self-Consistent Estimates

The long-established self-consistent estimates for overall moduli have taken as their starting point the solution to the problem of a single inclusion, embedded in "overall" material whose tensor of moduli is to be determined by one of several conditions for consistency. They are reviewed in [3, 4], for example. The fact that they take no account of statistics gives them the advantage of simplicity but also demonstrates an inherent limitation.

An alternative scheme of self-consistent type, which does take some account of statistics, is provided by noting that the Hashin-Shtrikman estimate $\tilde{L}$ given in the preceding section provides a variational approximation for $\hat{L}$, however L_0 is chosen and it might be suspected that $\tilde{L}$ would be closest to $\hat{L}$ if the comparison material could be chosen as identical with the overall material, so that $L_0=\tilde{L}$. The resulting self-consistent equation

$$\hat{L}=\tilde{L}(\hat{L}) \tag{7.1}$$

will not be exact, because the actual field in a composite will not generally be realized exactly by a polarization field of the form (5.18). It is, therefore, no more than an approximation, which at least is certain to lie between the Hashin-Shtrikman bounds, since these are generated by deliberately choosing L_0 too "soft" or too "hard." It has the virtue, however, that it is sensitive to two-point statistics. It has the additional feature that when the two-point probabilities are isotropic, it reproduces earlier self-consistent estimates obtained by solving spherical inclusion problems. Equation (7.1) is well suited to solution by iteration. This possibility has not been mentioned elsewhere, but there is no bar to choosing L_0 as a nonlocal operator, so that (7.1) could be used to estimate $\hat{L}$ for nonuniform fields.

A drawback of the scheme (7.1) is that the polarization τ is taken constant throughout any phase. *This is demonstrably incorrect, even for a dilute suspension of inclusions that have a shape other than ellipsoidal.* For a matrix containing inclusions, a slightly improved scheme could be devised by allowing the polarization over any inclusion to vary, but to be insensitive to the location of neighboring inclusions. The resulting functional $<\mathfrak{C}>$ involves only two-point statistics, so long as the polarization in the matrix is taken to be independent of the location of any inclusion.

The approximation just described has a variational foundation but it can also be generated directly, by ensemble averaging as in Section 4, this time with L_0 chosen different from the matrix tensor of moduli L_2. The closure assumption (4.16) is made for the inclusions and the conditional expectation of the matrix polarization is taken independent of the position of the fixed inclusion. If the polarization in the matrix is called τ^m, this amounts to making the additional assumption

$$\tau^m_{mA} = \tau^m_m. \tag{7.2}$$

After solving for τ^A_A in terms of τ^m_m and $<e>$, both are fixed by the requirement

$$(L_1-L_0)^{-1}\int dx_B\tau^B_B P_B+(L_2-L_0)^{-1}\tau^m_m P_m=<e> \tag{7.3}$$

which comes from averaging the equation $e=(L-L_0)^{-1}\tau$. Here, $P_m(x)$ represents the probability of finding matrix material at point x. Finally, L_0 is chosen so that

$$\int dx_B\tau^B_B P_B+P_m\tau^m_m=0, \tag{7.4}$$

which ensures that the overall modulus is estimated as L_0. In practice, of course, equations (7.3) and (7.4) do not have to be solved sequentially. Essentially this self-consistent scheme was proposed for dynamic problems by Devaney [13].

If the variational interpretation is sacrificed, it is in fact possible to proceed without making the approximation (7.2): this allows the matrix polarization to vary in the neighborhood of an inclusion and so might be expected to effect an improvement. If equation (2.9) is averaged, keeping inclusion A fixed, there result the two equations

$$(L_1-L_0)^{-1}\tau^A_A+\Gamma_0\tau^A_A+\int dx_B\,(\Gamma_0\tau^B_B)\,(P_{B|A}-P_B)$$
$$+\Gamma_0(\tau^m_{mA}P_{m|A}-\tau^m_m P_m)=<e>,\ x\in\Omega_A, \tag{7.5}$$

$$(L_1-L_0)^{-1}\int dx_B\tau^B_B p_{B|A}+(L_2-L_0)^{-1}\tau^m_{mA}P_{m|A}$$
$$+\Gamma_0\tau^A_A+\int dx_B(\Gamma_0\tau^B_B)(P_{B|A}-P_B)+\Gamma_0(\tau^m_{mA}P_{m|A}$$
$$-\tau^m_m P_m)=<e>,\ x\notin\Omega_A, \tag{7.6}$$

having made the approximation (4.16), but no other. These equations can be solved for τ^A_A and $\tau^m_{mA}P_{m|A}$, which tends to $\tau^m_m P_m$ when x is far from Ω_A.

It is a remarkable fact (that is to say, it surprised the writer), that solving (7.5) and (7.6) and imposing the self-consistency condition (7.4) always leads to the estimate $\tilde{L}$ which is obtained by taking $L_0=L_2$, the matrix moduli; the proof is not reproduced due to lack of space. It seems, therefore, that, for a matrix/inclusion composite, "self-consistent" methods as outlined are *unlikely to improve on the estimate* $\tilde{L}(L_2)$: systematic improvement could only be

Downloaded 02 May 2010 to 171.66.16.250. Redistribution subject to ASME license or copyright; see http://www.asme.org/terms/Terms_Use.cfm

made by relaxing the assumption (4.16) and allowing for interactions between neighboring inclusions. The omitted proof relies only on algebraic properties of the operators Γ_0 and $\hat{\Gamma}$ (defined from $\hat{G}$) and applies directly to the full dynamic problem, with suitable adjustment of the notation.

8 Prospects for Future Work

The estimation of overall moduli in terms of correlation functions is not likely to advance much further: calculations, for example, for particular shapes of inclusions and functions h could be performed but there remains the inherent problem that it is not always a practical proposition even to specify two-point probabilities. Of course, whether some other statistical characterization could be devised (perhaps, for instance, "small separations" of inclusions could be systematically defined) is an open question.

The study of nonlocal behavior of composites is largely academic in the static limit, because the most realistic way of generating rapidly varying fields is by ultrasound. The discussion of static nonlocal behavior was included to demonstrate, in a self-contained way, the type of response that is to be expected. The dynamics of composites is still a field of active research. It is impossible to give a full account here but all of the methods discussed for statics (perturbation theory, closure approximations, variational formulations) have been generalized to the dynamic case; for references, see [4, 9]. Even for isotropic composites, dynamic behaviour depends on the detailed form of the functions P_{rs} or P_{AB}; the static nonlocal operator $\hat{L}$ demonstrates this. Correspondingly, detailed calculations are only of value if this information is available. Conversely, there may be some hope of characterizing the statistics of a composite by experimental study of dispersion relations: one such attempt is reported in [14].

Very little attention has been paid to composites (or other random media) that are statistically nonuniform: it would be of great value for nondestructive evaluation if, for example, it proved possible to characterize regions of random inhomogeneity by the scattering of ultrasound.

Finally, reverting to statics, the estimation of nonlinear overall behavior in terms of statistics is completely unexplored: only "traditional" self-consistent schemes have been implemented. An observation, whose implications have not been investigated (so that it may turn out to be of no value) is now offered, for nonlinear elastic behavior. If the material is characterized by an energy function $W(e,x)$, description of the deformation relative to a linear comparison material provides the representation (2.6), where now

$$\tau = \sigma - L_0 e = \frac{\partial}{\partial e}\left\{ W(e) - \frac{1}{2} e L_0 e \right\}. \tag{8.1}$$

If this relation is invertible, the Legendre transformation

$$U(\tau) = e\tau - \left\{ W(e) - \frac{1}{2} e L_0 e \right\} \tag{8.2}$$

gives

$$e = \frac{\partial U}{\partial \tau}. \tag{8.3}$$

This implies, with (2.6),

$$\frac{\partial U}{\partial \tau} + \Gamma_0 \tau = e_0 \tag{8.4}$$

and this equation gives the variational principle

$$\delta\left\{ \int_\Omega dx (2U(\tau) + \tau\Gamma_0\tau - 2e_0\tau) \right\} = 0. \tag{8.5}$$

For simplicity, the description has been given for small strains and "physical" nonlinearity; generalization to large strains would require the use of suitable measures of stress and strain, as outlined by Ogden [15]. The point of greatest difficulty would probably be the question of invertibility of (8.1).

References

1 Hashin, Z., "Theory of Fiber Reinforced Materials," NASA Report No. CR1974, 1972.

2 Christensen, R. M., *Mechanics of Composite Materials*, Wiley-Interscience, New York, 1979.

3 Willis, J. R., "Variational and Related Methods for the Overall Properties of Composites," *Advances in Applied Mechanics*, Vol. 21, 1981, pp. 1–78.

4 Willis, J. R., "Elasticity Theory of Composites," *Mechanics of Solids*, the Rodney Hill 60th Anniversary Volume, Hopkins, H. G., and Sewell, M. J., eds., Pergamon Press, Oxford, 1982, pp. 653–686.

5 Willis, J. R., "Bounds and Self-Consistent Estimates for the Overall Moduli of Anisotropic Composites," *J. Mech. Phys. Solids*, Vol. 25, 1977, pp. 185–202.

6 Gel'fand, I. M., and Shilov, G. E., *Generalized Functions, Vol. I, Properties and Operations*, Academic Press, New York, 1964.

7 Hashin, Z., and Shtrikman, S., "On Some Variational Principles in Anisotropic and Nonhomogenous Elasticity," *J. Mech. Phys. Solids*, Vol. 10, 1962, pp. 335–342.

8 Kantor, Y., and Bergman, D. J., "Elastostatic Resonances—A New Approach to the Calculation of the Effective Elastic Constants of Composites," *J. Mech. Phys. Solids*, Vol. 30, 1982, pp. 355–376.

9 Willis, J. R., "Variational Principles for Dynamic Problems for Inhomogeneous Elastic Media," *Wave Motion*, Vol. 3, 1981, pp. 1–11.

10 Hill, R., "New Derivations of Some Elastic Extremum Principles," The Prager Anniversary Volume, MacMillan, New York, 1963, pp. 99–106.

11 Kröner, E., "Bounds for Effective Elastic Moduli of Disordered Materials," *J. Mech. Phys. Solids*, Vol. 21, 1977, pp. 9–17.

12 Diener, J., Hürrich, A., and Weissbarth, J., "Bounds on the Nonlocal Effective Elastic Properties of Composites," *J. Mech. Phys. Solids* to appear.

13 Devaney, A. J., "Multiple Scattering Theory for Discrete, Elastic, Random Media," *J. Math. Phys.*, Vol. 21, 1980, pp. 2603–2611.

14 Sayers, C. M., "Ultrasonic Velocity Dispersion in Porous Materials," *J. Phys. D. (Appl. Phys.)*, Vol. 14, 1981, pp. 413–420.

15 Ogden, R. W., "Extremum Principles in Non-Linear Elasticity and Their Application to Composites," *Int. J. Solids Structures*, Vol. 14, 1978, pp. 265–282.

Downloaded 02 May 2010 to 171.66.16.250. Redistribution subject to ASME license or copyright; see http://www.asme.org/terms/Terms_Use.cfm

The Generalized Finite Element Method—State of the Art and Future Directions

O. C. Zienkiewicz
Department of Civil Engineering,
University College of Swansea,
Swansea Wales, England

This contribution reviews the present status of computational procedures in mechanics and indicates some of the areas in which research is active. The generality of the finite element method is stressed as the all-embracing approximation procedure and attention is focused on the need for developing efficient measures of accuracy and adaptive procedures for achievement of a specified precision. Developments aimed at improving the overall efficiency of computation are highlighted and some new areas of application indicated.

Introduction

The 50th anniversary of the JOURNAL OF APPLIED MECHANICS provides a fitting opportunity for reviewing the status of computational mechanics and, in particular, of the finite element method which has made such important contributions to this field. The comparative facility with which solutions can today be obtained for previously intractable problems, such as large strain deformation of nonlinear solids, etc., has indeed provided an impetus to classical mechanics presenting new problems of constitutive modeling which now loom large in the practical applications domain.

At the outset of its introduction of the mid 1950s the finite element method presented a convenient, if somewhat crude, method of analysis of elastic continua by analogy with discrete structural problems for which the computer began then to provide a powerful vehicle. In those early days many considered that such alternatives as finite difference solutions, boundary integral equations, or series solutions had more mathematical respectability and generality.

Although such attitudes persist with some, the situation is generally reversed and, in the definition of the *Generalized Finite Element* method, we can today include all other procedures of approximation and discuss rationally their best field of application. Indeed the mathematical foundations available are now more firmly established for such a general statement than had previously existed. In a survey article written some years ago [1] the author traces some of the historical development and many other accounts of this exist, [2–4]. For completeness, in the first section of this paper we discuss the generalized finite element forms, demonstrate the relationship with other procedures of approximation, and discuss the way in which advantages of various forms may be combined.

All procedures of approximation introduce, by their very definition, the notion of errors and it is important, especially in application to mechanics and engineering design, to be able to assess what these errors are and how solutions with a given accuracy can be obtained economically. This aspect, somewhat neglected in the past, is in the forefront of current research and much in the way of new development is expected in the near future. Adaptive procedures of refinement thus will be focused on as one of the important "future directions."

While economics of finite element computation would appear to be less relevant with the decrease of computer costs, the interest in dynamics and nonlinear mechanics problems, previously prohibitively expensive, still requires the utmost efficiency for practical use. It is no wonder that much of the current research is directed here. In particular, development of efficient time stepping and iterative procedures is a thrust which may have a considerable impact on the practice, and we will devote a section to discussion of some possibilities.

It would seem inappropriate, in a survey of this nature, not to mention the impressive progress being made in the man-computer interface where the objectives are those of reducing the input effort and the tediousness of presenting and inspecting results. This area, however, presents a separate topic of research and activity not directly associated with present considerations; for this reason, as well as for space limitation, we will not discuss it further.

The areas of application of the generalized finite element processes are increasing daily since the realization of their general mathematical base. In computational solid mechanics, the "standard" versions of the finite element processes have the widest usage, though in linear problems of elasticity, particularly when infinite domains or singularities are involved, the boundary (integral) solution procedures present an economic alternative.

Detailed applications of the finite element method range from structural mechanics through metal forming processes

Contributed by the Applied Mechanics Division for publication in the JOURNAL OF APPLIED MECHANICS.

Discussion on this paper should be addressed to the Editorial Department, ASME, United Engineering Center, 345 East 47th Street, New York, N.Y. 10017, and will be accepted until two months after final publication of the paper itself in the JOURNAL OF APPLIED MECHANICS. Manuscript received by ASME Applied Mechanics Division, May, 1983.

Copyright © 1983 by ASME
Downloaded 02 May 2010 to 171.66.16.250. Redistribution subject to ASME license or copyright; see http://www.asme.org/terms/Terms_Use.cfm

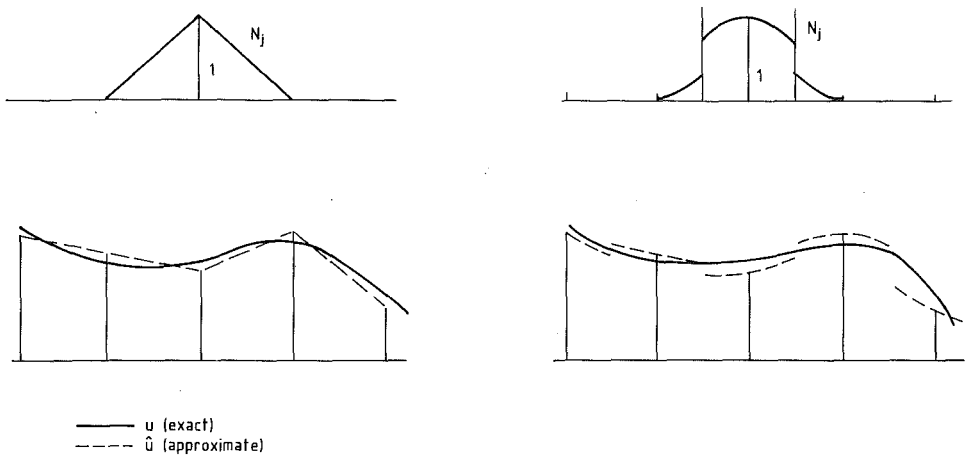


Fig. 1 Shape functions and weight (test) functions used in (*a*) Standard FE, (*b*) Standard FD in the solution of a simple one-dimensional problem

and from geomechanics to bioengineering. However, in fluid mechanics, where the need for a continuum-type solution appeared earlier than in solid mechanics, the "standard" finite difference procedures retain a large proportion of use, probably due to their earlier introduction. Here much effort is currently in progress to determine the "optimal approximation" method [5-7] and indications of extended finite element usage are evident.

Description of various fields of application are now textbook material [8-12] and will not be further enumerated. In passing we must remark that considerable effort is now being made to improve the procedures of approximation in hyperbolic, transport-type problems of greatest importance in fluid mechanics, despite the considerable progress already achieved.

2 The Generalized Finite Element Method (GFE)

All problems of mechanics (and indeed of many other areas of physics) can be cast in the form of differential equations (generally partial) which require satisfaction in a particular domain, together with their ancillary conditions on the boundary. Thus we require to solve

$$\mathbf{A}(\mathbf{u}) + \mathbf{q} = 0 \quad \text{in } \Omega \text{ (domain)} \tag{1a}$$

$$\mathbf{B}(\mathbf{u}) + \mathbf{b} = 0 \quad \text{on } \Gamma \text{ (boundary)} \tag{1b}$$

where $\mathbf{A}$ and $\mathbf{B}$ are appropriate operators, $\mathbf{q}$ and $\mathbf{b}$ known vector valued functions, and $\mathbf{u}$ the unknown (vector) function.

In the generalized finite element method, we approximate $\mathbf{u}$ by a trial expansion writing

$$\mathbf{u} \approx \hat{\mathbf{u}} = \sum_{i=1}^{n} \mathbf{N}_i \mathbf{a}_i \tag{2}$$

where $\mathbf{N}_i$ are prescribed trial (basic) functions and $\mathbf{a}_i$ are unknown parameters. *We note that if* $\mathbf{N}_i$ *does not depend on n* (the number of terms) *the foregoing is simply a series expansion*. This is not generally true for "standard" approximation procedures but is easily achieved if, for instance, hierarchical forms of expansion are used [13].

The approximating algebraic equations are obtained in the generalized finite element method by simply writing the weak (weighted residual) or variational forms

$$\int_\Omega \mathbf{v}_j^T (\mathbf{A}\mathbf{u} + \mathbf{q})\, d\Omega + \int_\Gamma \bar{\mathbf{v}}_j^T (\mathbf{B}\mathbf{u} + \mathbf{b})\, d\Gamma = 0$$

$$j = 1, 2, \ldots, n \tag{3}$$

where $\mathbf{v}_j$ and $\bar{\mathbf{v}}_j$ are suitable weighting (or test) functions. Clearly, many different possibilities exist for the choice of the shape functions $\mathbf{N}$ and the weighting functions $\mathbf{v}$ and $\bar{\mathbf{v}}$, and some restrictions are necessary for their definition if a convergent and accurate approximation is to be obtained. Such requirements (of completeness and integrability) are spelled out in detail in texts.

The weighting process of approximation was, it is believed, first proposed and used by Galerkin [14]. In his works he uses a variety of weight functions though at times the only possibility of $\mathbf{v}_j = \mathbf{N}_j$ is attributed to him. This widely used choice (called by some the Galerkin F.E. Method) is optimal in every sense for self-adjoint problems but not so generally.

The approximation of equation (3) reduces the problem to an algebraic equation system

$$\mathbf{P}(\mathbf{a}) = \mathbf{f} \tag{4a}$$

or, in linear situations, simply to the solution of

$$\mathbf{K}\mathbf{a} = \mathbf{f} \tag{4b}$$

from which, if the equations are not singular, a computer based solution is obtained.

"Standard" Finite Element Process (FE). Here invariably locally based trial functions are used with $\mathbf{a}$ usually (but not always) representing the local values of the function $\mathbf{u}$. This results in sparsely connected (banded) equation systems (4) and greatly facilitates the solution. Further, the property of integrals

$$\int_\Omega (\quad) d\Omega = \sum_e \int_\Omega e(\quad)\, d\Omega$$

$$\int_\Gamma (\quad) d\Gamma = \sum_e \int_\Gamma e(\quad)\, d\Gamma \tag{5}$$

where

$$\Omega = \sum_e \Omega^e, \quad \Gamma = \sum_e \Gamma^e$$

ensures that "elements" on which the local approximations are generally based can be treated in an analogous manner to "discrete structural elements" and assembled in a similar manner. Indeed this assembly process is characteristic of all finite element programs.

The "Galerkin" process applied to the equations guarantees their symmetry in self-adjoint problems and, after integration by parts, relatively low orders of continuity of trial functions is required.

What is too often missed in this procedure is that ap-

Downloaded 02 May 2010 to 171.66.16.250. Redistribution subject to ASME license or copyright; see http://www.asme.org/terms/Terms_Use.cfm

proximate analytical solutions (or indeed old-fashioned series solutions) are seldom included despite the fact that their use can often improve the accuracy substantially without increase of the solution cost.

"Standard" Finite Difference Approximation (FD). This can always be interpreted as a collocation solution in which the weighting function assume a Dirac form in equation (3). Here continuity requirement on the trial function can be considerably relaxed (by arguments of a "mollification" kind) and generally (C^{-1}) discontinuous approximations of an interweaving kind are used.

Figure 1(*a*, *b*) shows typical trial functions of both "finite element" and "finite difference" kind in solution of a triviel second-order equation

$$\frac{d^2u}{dx^2} = 0 \tag{6}$$

Boundary Solutions (BS). In these, the choice of the shape functions is limited to those satisfying the appropriate differential operator in the domain. Now, for linear operators **A** in equation (1*a*) (and limiting our attention to the homogeneous form) we take N such that

$$\mathbf{A}_i(\mathbf{N}_i) \equiv 0 \tag{7}$$

Clearly, the approximation $\hat{\mathbf{u}}$ also satisfies the appropriate equation and the approximating equations (3) reduce to an integral over the boundary

$$\int_\Gamma \bar{\mathbf{v}}_j^T(\mathbf{Bu}+\mathbf{b})d\Gamma = 0 \tag{8}$$

The dimensionality of the problem is altered since only the boundary needs to be considered. Once again various alternative weight-functions ranging from collocation to Galerkin procedures can be used but now, for obvious reasons, full connectivity always exists and the matrices (viz. equation (4)) are never sparse. Despite this obvious shortcoming the boundary solution methods require a smaller number of parameters for a given accuracy and, in some linear problems, lead to more economical solutions than the alternative.

The boundary solution methods originated by Trefftz [15] have been used extensively in aerodynamics since the 1930s (as so-called panel methods) and recently the integral equation form has gained popularity [16, 17]. As the use of exact solutions which approximately fit the boundary condition is natural here, this inherent advantage is frequently used. In the context of the various alternatives possible, it is worthwhile remarking that the singularities present in the integral equation form (using Green's functions) require the evaluation of difficult integrals. Recently much progress has been made in the use of other, complete expansions avoiding such problems [18, 19].

3 The Alternatives

Each of the subclasses of the GFE possess their relative merits, although standard FE are without a doubt the most popular. In the following we list some of the salient characteristics of each procedure:

(Standard) FE

1 Ease of dealing with nonhomogeneous situations by separate element considerations;

2 Ease of dealing with irregular domains and local refinement;

3 Natural incorporation of boundary conditions;

4 Ease of incorporating nonlinear behavior at element level;

5 Need for assembly of final equations;

6 "Average" rather than "pointwise" equation approximation;

7 "Mass" matrices of consistent nature require lumping for iterative or dynamic computation.

(Standard) FD

1 Regular meshes unless mapping of whole domain used;

2 No need for equation assembly;

3 "Pointwise" satisfaction of equations has merits in nonlinearity introduction;

4 "Mass" matrices naturally lumped;

5 Equation systems frequently nonsymmetric (unless energy type formulation used, which in fact returns to standard FE). Iterative solutions used largely for this reason.

(Standard) BS

1 Equation invariably full (not sparse as in preceding methods);

2 For given accuracy generally smaller number of variables, and integrals only evaluated on boundaries;

3 "Nonlinearity" in the problem domain can only be dealt with by using modified Newton Raphson processes, and reintroduces domain integrals;

4 Singularities and infinite boundaries treated "naturally" by introduction of exact solutions;

5 Equations generally nonsymmetric if boundary collocation used but can be cast symmetrically though at substantial cost;

6 Recovery of domain variations of stresses, etc. expensive.

It is no wonder that much research is being done to alter, where possible, specialized processes to avoid their limitation and more importantly, to link in unified systems the advantages of the specialized approaches.

In the context of such alteration we should mention some outstanding examples:

1 Generalization of the finite difference procedure to completely irregular meshes. Here the early work of Utku [20], and more recently that of Orkisz and his collaborators [21, 22], proceed to identify a set of associated nodes and, if necessary, subdomains (Fig. 2) arriving directly at a set of equations in an assembled form if collocation is used. Such procedures, to some extent, bridge the gap between FE and FD but while avoiding mesh generation introduce an equally expensive search computation.

2 Introduction of infinite domain mapping to the FE strategy to incorporate the advantages of BS into this process. Here so-called infinite elements should particularly be mentioned [23–25].

3 The use of global approximation functions in the

Downloaded 02 May 2010 to 171.66.16.250. Redistribution subject to ASME license or copyright; see http://www.asme.org/terms/Terms_Use.cfm

standard process introduced early by Mote [26] are recently gaining popularity.

The processes of linking subdomains in which alternative discretization approaches are used are equally important. Here much progress has been already achieved and, in particular, the simple processes of linking boundary solution domains to those in which standard FE approximations are used have much to commend them [27–30]. Indeed, such processes are by necessity used in purely boundary solution computations [31] to avoid the large full matrices, but in the future it is to be expected that standard finite element codes will incorporate boundary solution options in their repertoire.

Having established that all currently used approximation processes fall into the GFE class and that each has some possible merits, it is nevertheless our view that in the foreseeable future the generality of the "standard" finite element methodology presents such advantages over the alternatives that it will remain the unique tool for computational mechanics. However, three directions of change are evident and future codes will hopefully incorporate them to achieve the objective of maximizing the accuracy for a given computational cost. These are:

(*a*) Provision of a library of general solution of global nature which can, at users command, be used when desired;

(*b*) Addition of boundary solution "elements" which can be either incorporated in a general problem or used individually to solve the few simple linear problems for which such processes have a special efficiency;

(*c*) Abandoning the physical interpretation of "nodal variables" and the use of hierarchical variables in which a series form of expansion is used [13].

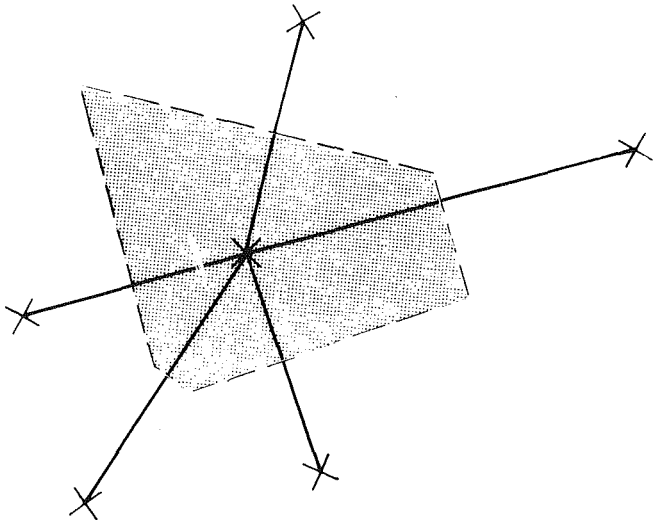


Fig. 2 Random mesh finite difference approximation

The last point is indeed implied if the use of global functions is introduced and, as will be seen in the next sections, leads not only to economy of computation but to better conditioning of equations thus reducing truncation errors.

4 Errors and Adaptive Processes

The characteristics common to all approximation methods is that at all times some error is introduced. Part of this is due to computer *roundoff* and inaccuracies in the solution of numerical equations, but the major contribution is involved in the *truncation* of the approximating sequences. While in the early days the user of the finite element (or of other numerical processes) was content to obtain answers by use of meshes similar to those in which satisfaction was obtained when test problems were solved, today attention is focusing on:

(*a*) reasonably accurate prediction of errors for any solution mesh used, and

(*b*) development of automatic processes by which a required accuracy can be most economically reached.

It is here that a very substantial research effort is currently directed and where, in the near future, practical results influencing the whole field of computational mechanics codes can be expected when the goals of this research are fully achieved. The choice between the various subclasses of the GFE or indeed the choice of elements used in a particular solution will then become purely a matter of economic consideration.

Without doubt, it is in this area that the contributions of those studying the mathematics of the GFE have been most substantial. From the early work of Fraeijs de Veubeke [32], who attempted to incorporate energy bounds in his solution, much progress has been achieved in estimating errors in a single finite element solutions. Here the work of Babuska and his coworkers on "a posteriori" estimates is seminal [33–37] and has laid the foundations for future research [38–40].

One of the simplest approaches to error estimation is presented through the consideration of a series-type solution

$$\mathbf{u} \approx \hat{\mathbf{u}} = \sum_{i=1}^{n} \mathbf{N}_i \mathbf{a}_i \tag{9}$$

when the functions $\mathbf{N}_i$ are so chosen that as the number of parameters is increased, e.g., n to $n+1$, the previous functions remain unchanged.

With such a formulation, which is "hierarchical" in the context of the standard finite element method, one can estimate the error

$$\mathbf{e} = \mathbf{u} - \hat{\mathbf{u}} \tag{10}$$

by considering the change of the solution as new degrees of

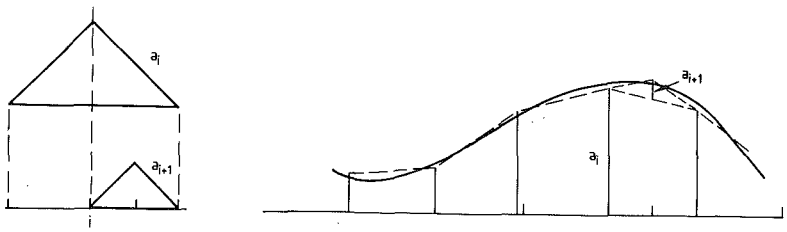


Fig. 3 Hierarchical element forms

Downloaded 02 May 2010 to 171.66.16.250. Redistribution subject to ASME license or copyright; see http://www.asme.org/terms/Terms_Use.cfm

freedom (i.e., new terms) are introduced in the approximation.

Consider, for instance, a hierarchically formulated subdivision into linear finite elements in a manner similar to that shown in Fig. (1*a*), which we now illustrate in Fig. 3. Here a_i $[i \leq n)$ is typically a parameter associated with the coarse mesh points and is a value of the unknown u at the node, but a_i $[n < i \leq m)$ are variables describing the difference of the fine mesh from the coarse mesh solution. The new variables are in a sense a measure of error present in the coarse mesh solution as

$$\mathbf{e}^m \approx \sum_{i=n+1}^{m} \mathbf{N}_i \mathbf{a}_i = \mathbf{N}^{(m)} \mathbf{a}^{(m)} \tag{11}$$

and can be readily evaluated in the solution.

Consider, for instance, a linear form of equation (1) with

$$\mathbf{A}(\mathbf{u}) = \mathbf{L}\mathbf{u} \tag{12}$$

The coarse mesh approximation gives

$$\mathbf{K}_n \mathbf{a}^{(n)0} = \mathbf{f}^{(n)} \tag{13}$$

while the introduction of hierarchical variables with the finer solution yields

$$\begin{bmatrix} \mathbf{K}_n & \mathbf{K}_{n,m} \\ \mathbf{K}_{m,n} & \mathbf{K}_m \end{bmatrix} \begin{Bmatrix} \mathbf{a}^{(n)} \\ \mathbf{a}^{(m)} \end{Bmatrix} = \begin{Bmatrix} \mathbf{f}^{(n)} \\ \mathbf{f}^{(m)} \end{Bmatrix} \tag{14}$$

The first approximation to $\mathbf{a}^{(m)}$ and hence to the error is simply obtained by putting $\mathbf{a}^{(n)} \approx \mathbf{a}^{(n)0}$ and writing

$$\mathbf{a}^{(m)} = \mathbf{K}_m^{-1}(\mathbf{f}^m - \mathbf{K}_{m,n}\mathbf{a}^{(n)0}) \tag{15}$$

Clearly, a similar approximation to the error can be obtained introducing the new degrees of freedom one by one and performing a quite trivial calculation

$$\mathbf{a}^{n+1} = (\mathbf{K}_{n+1,n+1})^{-1}(\mathbf{f}^{n+1} - K_{n+1,n}a^{(n)0}) \tag{16}$$

This, as is readily seen, does not involve the costly full solution of the fine mesh equations.

While the local estimate of error is useful, a more important measure is that in an energy norm defined as

$$\|\mathbf{e}\| = \left[\int_\Omega \mathbf{e}^T \mathbf{L} \mathbf{e} d\Omega\right]^{1/2} = \left[-\int_\Omega \mathbf{e}^T \mathbf{r} d\Omega\right]^{1/2} \tag{17}$$

in which

$$\mathbf{L}\,\mathbf{e} \equiv \mathbf{L}\,(\mathbf{u} - \hat{\mathbf{u}}) = -(\mathbf{L}\,\hat{\mathbf{u}} + \mathbf{q}) = -\mathbf{r} \tag{18}$$

where $\mathbf{r}$ is the "residual" showing how well the equations of the problem have been satisfied.

If we introduce a single degree of freedom hierarchically as in equation (16) and note that

$$(\mathbf{f}^{n+1} - \mathbf{K}_{n+1,n}\mathbf{a}^{(n)0}) \equiv \int_\Omega \mathbf{N}_{n+1} \mathbf{r} d\Omega \tag{19}$$

by the definition of the derivation of approximation equation, we can write an estimate of energy error

$$\|e\|_{n+1} \approx \int_\Omega [(\mathbf{N} \mathbf{r} d\Omega)/K_{n+1,n+1}]^{1/2} = \eta_{n+1} \tag{20}$$

This quantity can again be simply evaluated for each new degree of freedom whose introduction is possible and its summation will give a good estimate of the "energy" error.

While the expression [20] provides an excellent guide for adaptive refinement showing very accurately where new degrees of freedom are most effectively introduced, it is possible for the residual to be orthogonal to the new shape functions and thus an underestimate is only available. A safer error estimation can be obtained as

$$\bar{\epsilon}_{n+1} = \alpha\left[\int_\Omega N^2 d\Omega \int_\Omega r^2 d\Omega / K_{n+1,n+1}\right]^{1/2} \tag{21}$$

where α is empirically estimated as 0.75 [13].

Once reasonable error estimates are available the way is open to adaptive refinement and many techniques are under investigation. In all of these, after the current error has been estimated, a decision is taken to introduce additional refinements, followed by a complete reanalysis and a new error estimate. When the final error estimate is acceptable the process is completed. The optimal process is the one that accomplishes the final end with minimum cost. Two facts have to be taken into consideration

(*a*) that accuracy of error estimates improves with refinement and,

(*b*) that the hierarchical form of equations is rapidly convergent iteratively (see the next section) so that at intermediate stages of refinement the complete resolution could well be avoided and only a few iterations performed.

The process of error estimation given in the foregoing is valid in a wide range of formulation in the generalized FE method but to the writer's knowledge it has not yet been applied in the finite difference or boundary solution method. Its most fruitful application appears to be in the standard finite element approaches in which so-called *p*-refinement is used. Here the new degrees of freedom are not introduced by mesh subdivision (*h*-refinement), but simply by addition of higher order polynomial functions which allow an easy formulation to be achieved [13, 41, 42] with the final form of equation (14) having a strongly diagonal structure.

In Fig. 4 we show a refinement of a practical example proceeding automatically by introduction of higher order polynomials reaching a desired accuracy in five reanalysis steps. Note that in this simple elasticity example with displacement variables local refinements may be done independently in x and y displacement components.

Much effort is currently being devoted to extension of error estimation and adaptive refinement processes to nonlinear mechanics, and to transient processes where economy of solution is of utmost importance.

While in the foregoing we have mainly concentrated on the energy norm – its usefulness being in the prediction of overall stress accuracy for instance – it is possible to devise very much more precise computations of local stress (or stress intensity factors in fracture mechanics) in which the errors are proportional to energy norm squared. This work done recently by Babuska and his coworkers promises to open up new applications [43, 44].

5 Iterative Solution Processes and Time Stepping

Once the discretization of a continuum problem has been reached (viz., equation 4(*a*, *b*)), its solution is one involving purely algebraic procedures. It is curious to note here how different paths for this have been followed by different subclasses of the GFE.

In the standard finite element process, for instance, the great majority of programs are based on Gaussian elimination methods which, in linear problems with multiple load vectors, is undoubtedly advantageous. The same procedure is invariably used in boundary solution methods where the full matrix structure mitigates against the possibility of iterative methods.

In the standard finite difference methodology, on the other hand, iterative solution methods are the rule rather than the exception. Here the regular structure of the equations is particularly well suited to such processes.

When nonlinear situations are considered it is by no means clear that the direct solution techniques current in standard

Downloaded 02 May 2010 to 171.66.16.250. Redistribution subject to ASME license or copyright; see http://www.asme.org/terms/Terms_Use.cfm

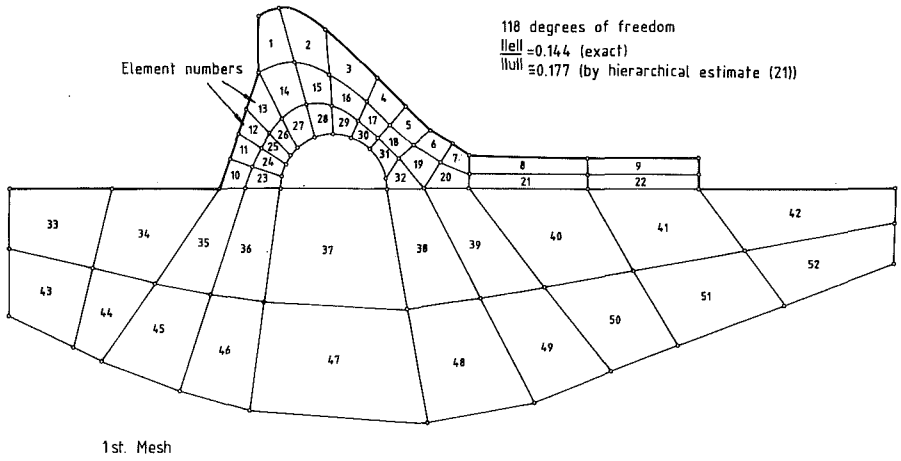


Fig. 4(*a*)

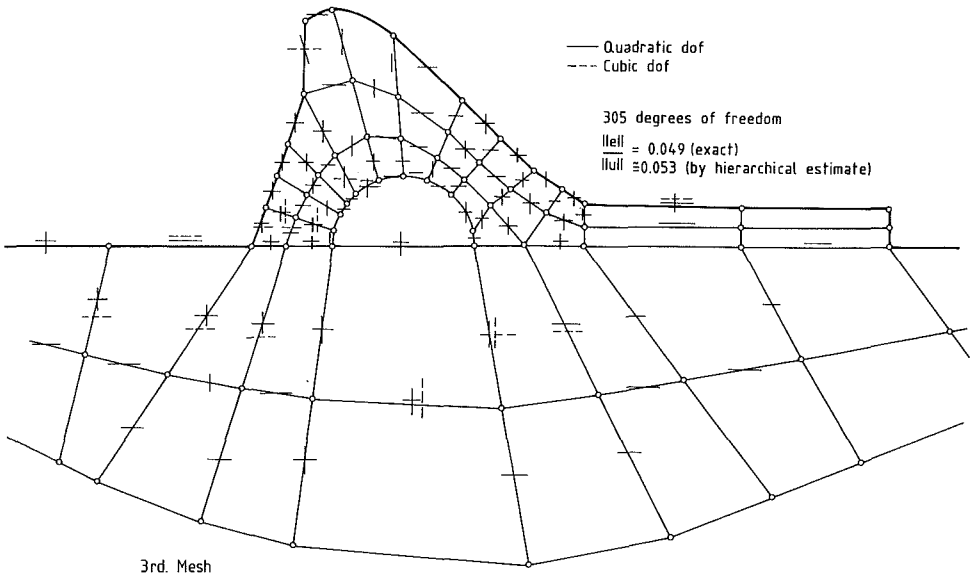


Fig. 4(*b*)

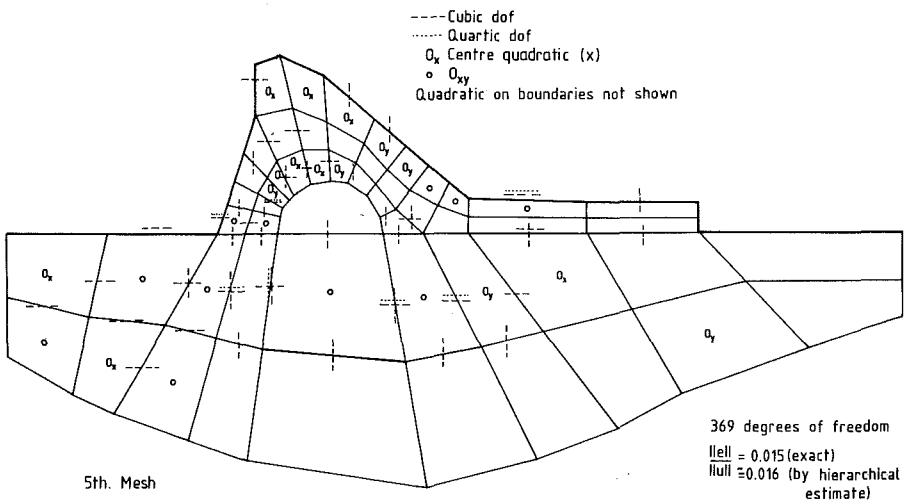


Fig. 4(*c*)

Fig. 4 A stress analysis with adaptive refinement

Downloaded 02 May 2010 to 171.66.16.250. Redistribution subject to ASME license or copyright; see http://www.asme.org/terms/Terms_Use.cfm

finite element approaches are optimal and, despite much recent progress in the treatment of nonlinear problems by the use of Quasi-Newton methods etc., [45, 46], it appears that iterative methods will enter the arena seriously, especially when large-scale three-dimensional situations are considered.

Here two directions will be noted. The first is the use of techniques similar to the Multigrid processes which were first introduced into the finite difference methods in the last decade [47–49], and which are today hailed as one of the most significant developments there [50]. The second is the revival of "dynamic relaxation" methods originally introduced in the early 1960s [51–56].

Turning to the first it is important to observe that standard, hierarchically formulated, finite elements present essentially a multigrid structure without any special treatment. If equations (13) and (14) are considered it is immediately evident that the first presents simply a coarse mesh solution, while the second of (14) is the projection of coarse mesh residual on to the "fine mesh" refinement.

If we proceed as in the standard multigrid processes by first solving the coarse mesh followed by a few iterations on $\mathbf{a}^m$, the fine hierarchical variables, and then resolve the coarse mesh solution (first of equation (14)) which represents projection of fine mesh residuals onto the coarse basis function), the convergence will be found to be rapid.

In the second, i.e., dynamic relaxation process the problem of solving equation (4*b*) (or the nonlinear form)

$$\mathbf{K}\mathbf{a} = \mathbf{f}$$

is sought as a steady state solution of a real or purely fictitious transient of the form

$$\mathbf{C}\dot{\mathbf{a}} + \mathbf{K}\mathbf{a} = \mathbf{f} \tag{22}$$

or

$$\mathbf{M}\ddot{\mathbf{a}} + \mathbf{C}\dot{\mathbf{a}} + \mathbf{K}\mathbf{a} = \mathbf{f} \tag{23}$$

The first possibility, which perhaps is better termed viscous relaxation, was introduced first by Oden [53] but has the disadvantage of converging in an overdamped manner to the static solution. However, acceleration processes this disadvantage can be overcome [56] and the time stepping algorithms of explicit nature allow linear and nonlinear solutions to be obtained with equal ease. Computer programs not involving the solution of simultaneous equations are much simpler than those in which elimination is used. Today the efficiency of such formation allows nonlinear steady state problems of computational mechanics to be solved routinely with such dynamic relaxation. The factor which still keeps the costs high is one associated with time step limitations of explicit calculations and many attempts are being made today to remedy the problem. Here again several avenues of approach are being investigated and hold much promise for the future.

One of these is to utilize the advantage of hierarchical formulation in which the coarse mesh advance can be made with fairly large explicit steps followed by smaller steps in hierarchical variables. In the context of the equivalent multigrid processes such techniques are already used with substantial economy of computation [50].

In the alternative a matrix splitting operation allows, at some expense of accuracy, unconditionally stable procedures to be used. Here a method originally proposed by Yanenko [57] and Marchuk [58] has recently been extended to the finite element process by Hughes et al. [59].

We will illustrate this on a simple example of solving equation (22). If a single step recurrence scheme is written, we have in the most general form

$$(\mathbf{C} + \theta\,\Delta t\,\mathbf{K})\mathbf{a}^{n+1} = (\mathbf{C} - (1-\theta)\,\Delta t\,\mathbf{K})\mathbf{a}^n + \mathbf{f} \tag{24}$$

or assuming a simple to invert, diagonal $\mathbf{C}$

$$(\mathbf{I} + \theta\,\Delta t\,\mathbf{A})\mathbf{a}^{n+1} = (I - (1-\theta)\,\Delta t\,\mathbf{A})\mathbf{a}^n + \hat{\mathbf{f}} \tag{25}$$

where $\mathbf{A} = \mathbf{C}^{-1}\mathbf{K}$ and $\hat{\mathbf{f}} = \mathbf{C}^{-1}\mathbf{f}$

If we expand the inverse in a series as

$$(\mathbf{I} + \theta\,\Delta t\,\mathbf{A})^{-1} = I - \theta\,\Delta t\,\mathbf{A} + \theta^2\,\Delta t^2\,\mathbf{A}^2 + \ldots \tag{26}$$

the solution to equation (25) can be written as

$$\begin{aligned}\mathbf{a}^{n+1} &= (\mathbf{I} + \theta\,\Delta t\mathbf{A})^{-1}(\mathbf{I} - (1-\theta)\,\Delta t\,\mathbf{A})\mathbf{a}^n \\ &\quad + (\mathbf{I} + \theta\,\Delta t\,\mathbf{A})^{-1}\hat{\mathbf{f}} = \\ &\quad (\mathbf{I} - \theta\,\Delta t\mathbf{A} + \theta^2\,\Delta t^2\mathbf{A}^2)\,\mathbf{a}^n \\ &\quad + (\mathbf{I} - \theta\,\Delta t\,\mathbf{A} + \theta\,\Delta t^2\,\mathbf{A}^2)\hat{\mathbf{f}}\,\Delta t + 0(\Delta t^3)\end{aligned} \tag{27}$$

Now if we divide the matrix $\mathbf{A}$ into parts $\mathbf{A}^e$ such that

$$\mathbf{A} = \sum_e \mathbf{A}^e \tag{28}$$

then a possible alternative algorithm of solution can be written as

$$\begin{aligned}\tilde{\mathbf{a}}^{n+1} &= [(\mathbf{I} + \theta\,\Delta t\mathbf{A}^1)^{-1}(\mathbf{I} + (1-\theta)\,\Delta t\,\mathbf{A}^1) \\ &\quad (\mathbf{I} + \theta\,\Delta t\mathbf{A}^2)^{-1}(\mathbf{I} + (1-\theta)\,\Delta t\,\mathbf{A}^2)\ldots]\mathbf{a}^n \\ &\quad + [(\mathbf{I} + \theta\,\Delta t\mathbf{A}^1)^{-1}(\mathbf{I} + \theta\,\Delta t\mathbf{A}^2)^{-1}\ldots]\hat{\mathbf{f}}\,\Delta t\end{aligned} \tag{29}$$

It is easily verified by multiplication that the preceding algorithm approximates the full inversion of equation (27) to $0(\Delta t^2)$ and that if the time interval is split into $t/2$, and in the second round the order of operation is reversed, the accuracy is increased to $0(\Delta t^3)$.

The algorithm when used with $\theta \geq 1/2$ is unconditionally stable and, when split, involves only inversion of matrices in which the nonzero part is small and the ease of computation approaches that of explicit ones. The most natural split is that to element size matrices, but this can lead to a substantial accuracy loss. Other possible splits into element groups or indeed into hierarchically defined parts of the matrices may be advantageous and current research is proceeding on these lines with much promise.

Similar, but not identical, procedures have been derived by Trujillo and others with the same objective of providing an unconditionally stable empirical form [60, 61].

Concluding Remarks

In the foregoing we have shown how much progress has been made in unifying the approximation concepts used today in computational mechanics and indicated some directions of current thought which, hopefully, will lead to a new generation of computer codes with improved efficiency and capacity for dealing with a variety of new problems.

Throughout, this paper focused on the numerical approximation aspects, but it is true in mechanics, as indeed in other fields, that progress can only be made when physical behavior is well understood and problems are well posed [62]. Superb computation with wrong constitutive relations will yield meaningless results, just as instability of the mathematical algorithm or lack of uniqueness (which could have been determined a priori) will prevent any results being obtained. For this reason interaction between those engaged in the study of physical phenomena and the analyst is much needed, and it is true to say many fundamental physical theories evolve today through numerical studies.

References

1 Zienkiewicz, O. C., "Finite Element Method—From Intuition to Generality," *Appl. Mech. Reviews*, 1970, pp. 249-256.

2 Williamson, C. F., Jr., "A History of the Finite Element Method of the Middle 60's," Ph.D. Thesis, Boston University, 1976.

Downloaded 02 May 2010 to 171.66.16.250. Redistribution subject to ASME license or copyright; see http://www.asme.org/terms/Terms_Use.cfm

3 Clough, R. W., Invited Lecture, International Conference on Engineering Application of the Finite Element Method, Høvik, Norway, 1979, Det Norske Veritas, Vol. 7, pp. 1-34.

4 Zienkiewicz, O. C., "The Finite Element Story," in *Twelve Notable Projects*, Levy, J. C., and Farvis, W. E. J., eds., 1982.

5 Gallagher, R. H., Oden, J. T., Taylor, C., and Zienkiewicz, O. C., eds., *Finite Elements in Fluids*, Vol. 1-2, Wiley, New York, 1975.

6 Gallagher, R. H., et al., eds., *Finite Elements in Fluids*, Vol. 3, J. Wiley, New York, 1978; Vol. 4, 1982.

7 Kawai, T., ed., *Finite Element Flow Analysis*, University of Tokyo Press, 1982.

8 Zienkiewicz, O. C., *The Finite Element Method*, 3rd ed., McGraw-Hill, New York, 1977.

9 Desai, C., and Abel, J., *Introduction to the Finite Element Method*, Van Nostrand-Reinhold, New York, 1971.

10 Gallagher, R. H., *Finite Element Analysis; Fundamentals*, Prentice-Hall, Englewood Cliffs, N.J., 1975.

11 Oden, J. T., and Reddy, J. N., *An Introduction to the Mathematical Theory of Finite Elements*, Wiley, New York, 1976.

12 Zienkiewicz, O. C., and Morgan, K., *Finite Elements and Approximations*, Wiley, New York, 1983.

13 Zienkiewicz, O. C., De S. R. Gago, J. P., and Kelly, D. W., "The Hierarchical Concept in Finite Element Analysis," *Computers and Structures*, Vol. 16, No. 1-4, 1983, pp. 53-65.

14 Galerkin, B. G., "Series Solution of Some Problems of Elastic Equilibrium of Rods and Plates, (Russian) *Vestn. Inzh. Tech.*, Vol. 19, 1965, pp. 897-908.

15 Trefftz, E., "Gegenstuck zum Ritz'schen Verfahren," *Proc. Soc. Int. Congress on Appl. Mech.*, Zurich, 1926.

16 Jaswon, M. K., and Symm, *Integral Equation Methods in Potential Theory and Elastostatics*, Academic Press, New York, 1977.

17 Banerjee, P. K., and Butterfield, R., *Boundary Element Methods in Engineering Science*, McGraw-Hill, New York, 1981.

18 Herrera, I., "Boundary Methods for Fluids," Chapter 19 in *Finite Elements in Fluids*, Gallagher, R. H., Norrie, D. H., Oden, J. T., and Zienkiewicz, O. C., eds., Wiley, New York, 1982, Vol. 4, pp. 403-432.

19 Herrera, I., "Trefftz Method," in *Progress in Boundary Element Methods*, Vol. 3, Brebbia, C. A., ed., Wiley, New York, 1983.

20 Nay, R. A., and Utku, S., "An Alternative for the Finite Element Method," *Int. Conf. Variational Methods in Engineering*, Southampton, 1972.

21 Liszka, T., and Orkisz, J., "The Finite Difference Method for Arbitrary Irregular Grids and its Application in Applied Mechanics," *Comp. and Structures*, Vol. 11, 1980, pp. 83-95.

22 Liszka, T., and Orkisz, J., "The Finite Difference Method for Arbitrary Irregular Meshes—A Variational Approach to Applied Mechanics," *Int. Congress on Comp. Methods in Engineering*, GAMNI, Paris, Dec. 1980.

23 Bettess, P., "Infinite Elements," *Int. J. Num. Meth. Eng.*, Vol. 11, 1977, pp. 53-64.

24 Bettess, P., and Zienkiewicz, O. C., "Diffraction and Refraction of Surface Waves Using Finite and Infinite Elements," *Int. J. Num. Meth. Eng.*, Vol. 11, 1977, pp. 1271-1290.

25 Zienkiewicz, O. C., Emson, C., and Bettess, P., "A Novel Boundary Infinite Element," *Int. J. Num. Meth. Eng.*, Vol. 19, 1983, pp. 393-404.

26 Mote, C. D., "Global-Local Finite Element," *Int. J. Num. Meth. Eng.*, Vol. 3, 1971, pp. 565-574.

27 Zienkiewicz, O. C., Kelly, D. W., and Bettess, P., "The Coupling of the Finite Element Method and Boundary Solution Procedures," *Int. J. Num. Meth. Eng.*, Vol. 11, pp. 355-375.

28 Zienkiewicz, O. C., Kelly, D. W., and Bettess, P., "Marriage a La Mode—the Best of Both Worlds (Finite Elements and Boundary Integrals)," *Proc. Int. Symp. Innovative Numerical Analysis in Applied Engineering Science*, Versailles, May 1977; also Chapter 5, *Energy Methods in Finite Element Analysis*, Glowinski, R., Rodin, E. Y., and Zienkiewicz, O. C., eds., Wiley, New York, 1979, pp. 81-106.

29 Katz, C., "Ein symmetrisches Verfahren zur Berechnung von Problemen mit Greenschen Funktionen," Techn. Universitat Munchen, 1982.

30 Kelly, D. W., Mustoe, G. G. W., and Zienkiewicz, O. C., "Coupling of Boundary Element Methods With Other Numerical Methods," Chapter 10, *Developments in Boundary Element Methods—1*, Banerjee, P. K., and Butterfield, R., eds., Applied Science, London 1979, pp. 215-285.

31 Watson, J. O., "Advanced Implementation of the Boundary Element Method in Two and Three-Dimensional Elastostatics," in *Developments in Boundary Element Methods*, Banerjee, P. K., and Butterfield, R., eds., Applied Science, London, 1979.

32 Fraeijs De Veubeke, B., "Displacement and Equilibrium Models in the Finite Element Method," Chapter 9, *Stress Analysis*, Zienkiewicz, O. C., and Holister, G. S., eds., Wiley, New York, 1965.

33 Babuska, I., and Rheinholdt, W. C., "Error Estimates for Adaptive Finite Element Computations," *Siam J. Num. Anal.*, Vol. 15, No. 4, 1978.

34 Babuska, I., and Rheinholdt, W. C., "A-Posteriori Error Estimates for the Finite Element Method, *Int. J. Num. Meth. Eng.*, Vol. 12, 1978, pp. 1547-1615.

35 Babuska, I., "Analysis of Optimal Finite Element Meshes," *Math. Comp.*, Vol. 30, 1979.

36 Babuska, I., and Rheinholdt, W. C., "Adaptive Approaches and Reliability Estimations in Finite Element Analysis," *Comp. Meth. in App. Mech. and Eng.*, Vols. 17/18, 1979, pp. 519-540.

37 Babuska, I., "The Self-Adaptive Approach in the Finite Element Method," in *MATELAP II*, Whiteman, J. R., ed., Academic Press, New York, 1975.

38 Zienkiewicz, O. C., Kelly, D. W., Gago, J., and Babuska, I., "Hierarchical Finite Element Approaches, Error Estimates and Adaptive Refinement," in *Mathematics of Finite Elements and Applications (IV)*, Whiteman, J., ed., Academic Press, New York, 1982, pp. 313-346.

39 Kelly, D. W., De S. R. Gago, J. P., Zienkiewicz, O. C., and Babuska, I., "A-Posteriori Error Analysis and Adaptive Processes in the Finite Element Method: Part I—Error Analysis," to be published, *I.J.N.M.E.*, 1983.

40 Gago, J., Kelly, D. W., Zienkiewicz, O. C., and Babuska, I., "A-Posteriori Error Analysis and Adaptive Processes in the Finite Element Method: Part II—Adaptive Mesh Refinement," to be published, *I.J.N.M.E.*, 1983.

41 Szabo, B. A., Basu, P. K., Rossow, M. P., "Adaptive Finite Element Analysis Based on *p*-Convergence," NASA Conference, pub. 2059, 1978, pp. 43-50.

42 Szabo, B. A., Dinavant, D. A., "An Adaptive Procedure Based on the *p*-Version of the Finite Element Method," Specialists Conf., University of Maryland, 1980.

43 Babuska, I., and Miller, A., "The Post Processing Approach in the Finite Element Method. Part 1: Calculation of Displacements, Stresses and Other High Derivatives of the Displacements," to be published, *I.J.N.M.E.*

44 Babuska, I., and Miller, A., "The Post Processing Approach in the Finite Element Method. Part 2: Calculations of Stress Intensity Factors," to be published, *I.J.N.M.E.*

45 Matthies, H., and Strang, G., "The Solution of Nonlinear Finite Element Equations," *Int. J. Num. Meth. Eng.*, Vol. 14, 1979, p. 1613.

46 Engelman, M. S., "Quasi-Newton Methods in Fluid Dynamics," in: *The Mathematics of Finite Elements Applications IV* [*MAFELAP 1981*], Whiteman, J. R., ed., Academic Press, New York, 1982, pp. 479-487.

47 Brandt, A., "Multi-Level Adaptive Solutions to Boundary Value Problems," *Math. Comp.*, Vol. 31, 1977, pp. 333-340.

48 Nicholandes, R. A., "On the Multiple Grid and Related Techniques for Solving Discrete Elliptic Systems," *J. Comp. Phys.*, Vol. 19, 1975, pp. 418-432.

49 Federenko, R. P., "A Relaxation Method for Solving Elliptic Difference Equations," *Z. Vvcisl. Mat. i. Mat. Fiz.*, Vol. 1, 1961, pp. 922-927.

50 MacCormack, R. W., "Status of Computational Fluid Dynamics and Prospects for Improved Numerical Methods," *The Influence of Computational Fluid Mechanics on Experimental Aerospace Facilities. A Fifteen Year Projection*. Nat. Acad. Press, Washington, 1983, pp. 79-93.

51 Otter, J. H., Cassell, A. C., and Hobbs, R. E., "Dynamic Relaxation, *Proc. Inst. Civ. Eng.*, Vol. 35, 1966, pp. 723-750.

52 Cassell, A. C., "Shells of Revolution Under Arbitrary Loading and the Use of Fictitious Densities in Dynamic Relaxation," *Proc. Inst. Civ. Eng.*, Vol. 45, 1970, pp. 65-78.

53 Oden, J. T., and Key, J. E., "Analysis of Static Nonlinear Response by Explicit Time Integration," *Int. J. Num. Meth. Eng.*, Vol. 7, 1973, pp. 225-240.

54 Pica, A., and Hinton, E., "Further Developments in Transient and Pseudo Transient Analysis of Mindlin Plates," *Int. J. Num. Meth. Eng.*, Vol. 17, 1981, pp. 1749-1761.

55 Underwood, P., "Dynamic Relaxation—a Review," to appear in *Computational Methods for Transient Response Analysis*, Belytschko, T., and Hughes, T. J. R., eds., North-Holland.

56 Zienkiewicz, O. C., and Löhner, R., "Accelerated Relaxation or Direct Solution to Future Prospects for FEM," to be published, *IJNME*, 1984.

57 Yanenko, N. N., *The Method of Frictional Steps*, Springer-Verlag, 1971.

58 Marchuk, G. I., *Numerical Methods in Weather Prediction*, Academic Press, New York, 1974.

59 Hughes, T. J. R., Levit, J., and Winger, J., *Unconditionally Stable Element by Element Implicit Algorithms for Heat Conduction Analysis*, 1981.

60 Trujillo, D. M., "An Unconditionally Stable Explicit Algorithm for Structure Dynamics," *IJNME*, Vol. 11, 1977, pp. 1579-1592.

61 Zienkiewicz, O. C., Hinton, E., Leung, K. H., and Taylor, R. L., "Staggered, Time Marching Schemes in Dynamic Soil Analysis and Selective Explicit Extrapolation Algorithms," *Proc. Conf. on Innovative Numerical Analysis for the Engineering Sciences*, Shaw, R., et al., eds., Univ. of Virginia Press, 1980.

62 Oden, J. T., and Bathe, K. J., "A Commentary on Computational Mechanics," *Applied Mechanics Reviews*, Vol. 31, 1978, pp. 1053-1058.

Downloaded 02 May 2010 to 171.66.16.250. Redistribution subject to ASME license or copyright; see http://www.asme.org/terms/Terms_Use.cfm